RIKEN Accelerator Progress Report 2012

vol. 46

BOOK & CD-ROM

独立行政法人理化学研究所　仁科加速器研究センター
RIKEN Nishina Center for Accelerator-Based Science

RIKEN Accelerator Progress Report 2012

***vol.* 46**

独立行政法人理化学研究所　仁科加速器研究センター

RIKEN Nishina Center for Accelerator-Based Science

Wako, Saitama, 351-0198 JAPAN

GRAVURE & HIGHLIGHTS OF THE YEAR

« Selection process of gravure and highlights »

Gravure and highlights will be selected by two-steps process. In the first step, referee will recommend manuscript for gravure or highlight. With the above recommendation, the editors will then give secondary recommendation.

After the following 1 and 2 are comprehensively considered, the editor-in-chief will draft a manuscript idea which will be thoroughly discussed by the editors for the final decision:

1. Approval based on the editor's judgment as an expert/non-expert in the field (thereby agreeing with the referee's recommendation)
2. Additional recommendation based on the editor's expertise.

GRAVURE HIGHLIGHT

New result in the production and decay of an isotope, $^{278}113$, of the 113th element

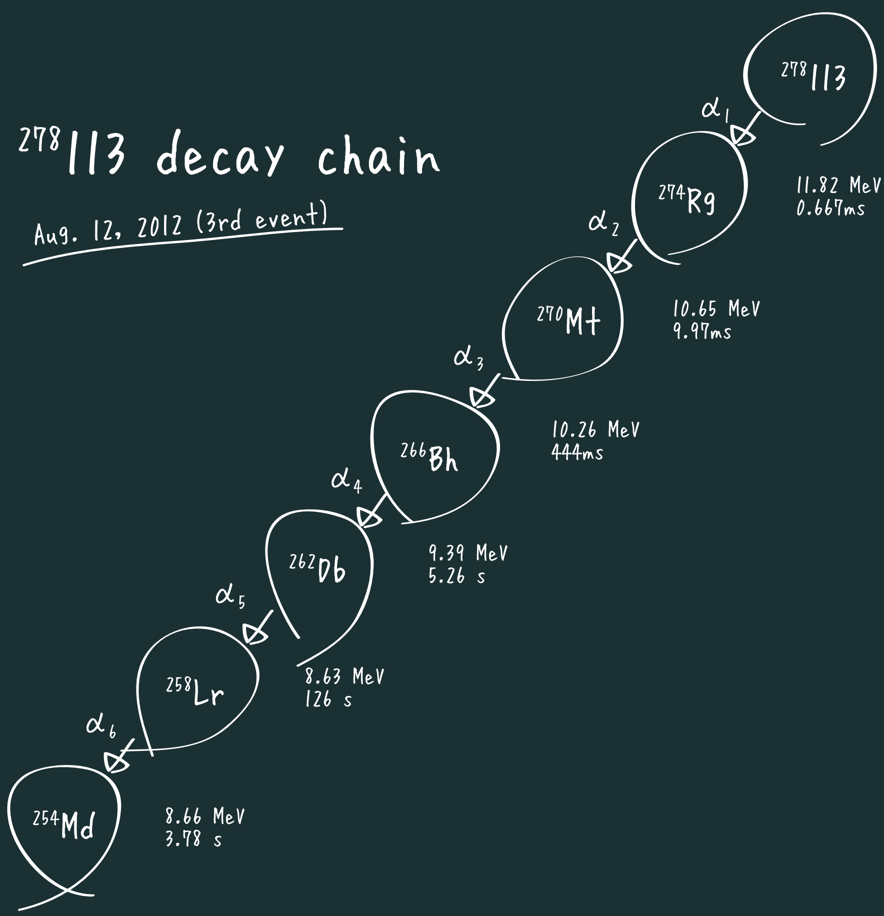

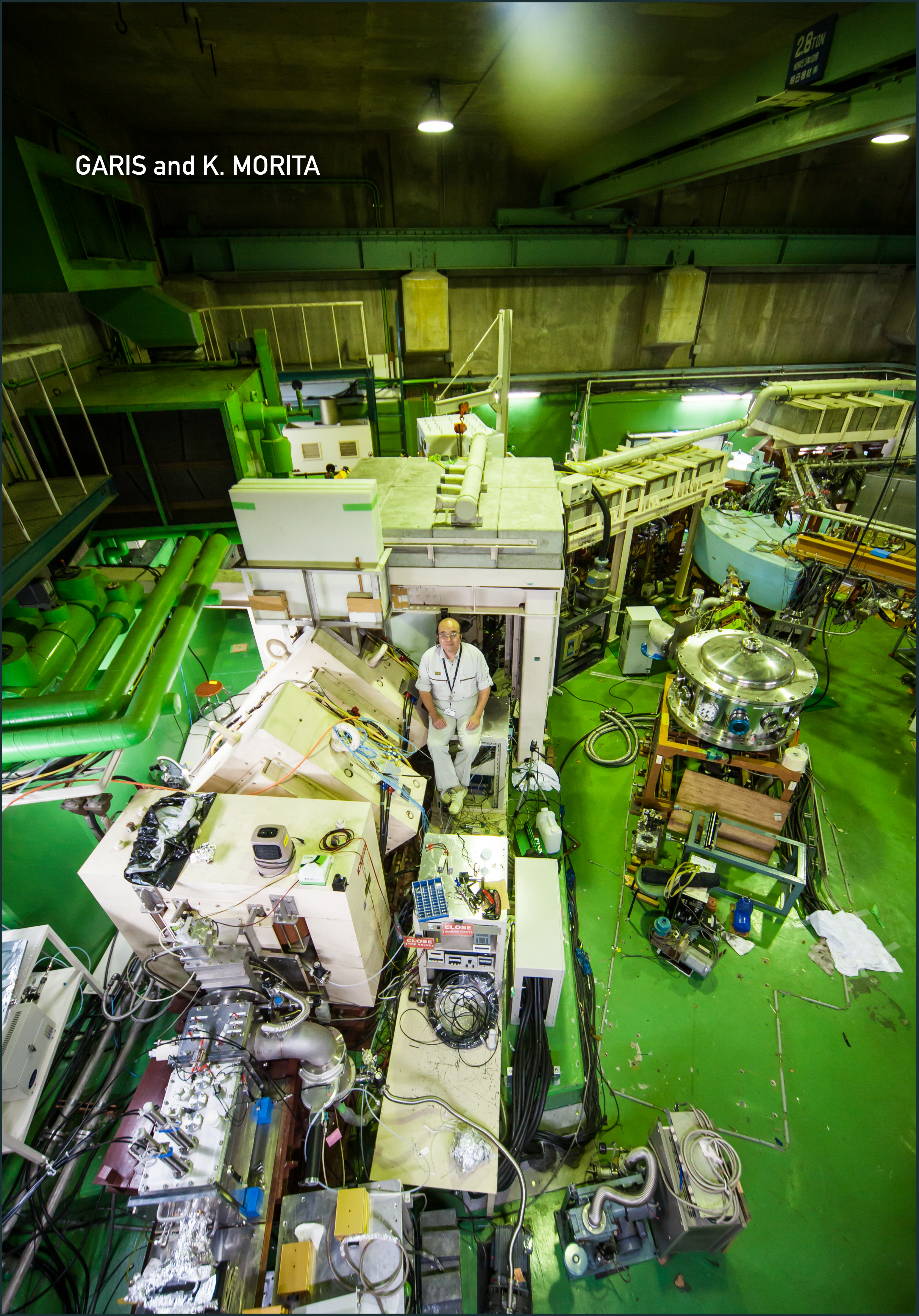

GARIS and K. MORITA

New result in the production and decay of an isotope, ^{278}113, of the 113th element[†]

K. Morita, K. Morimoto, D. Kaji, H. Haba, K. Ozeki, Y. Kudou, T. Sumita, Y. Wakabayashi, A. Yoneda, K. Tanaka, S. Yamaki, R. Sakai, K. Akiyama, S. Goto,[*1] H. Hasebe, M. Huang, T. Huang, E. Ideguchi,[*2] Y. Kasamatsu,[*3] K. Katori, Y. Kariya, H. Kikunaga, H. Koura, H. Kudo,[*1] A. Mashiko, K. Mayama, S. Mitsuoka,[*4] T. Moriya, M. Murakami, H. Murayama, S. Namai, A. Ozawa, N. Sato,[*4] K. Sueki, M. Takeyama, F. Tokanai, T. Yamaguchi, and A. Yoshida

In the experimental program aiming at confirming the existence of an isotope of the 113th element, i.e., ^{278}113, produced in the ^{209}Bi + ^{70}Zn $\to$ ^{278}113 + n reaction, we previously observed two convincing candidate events, both consisting of four consecutive α-decays followed by a spontaneous fission (SF) immediately after the implantation of a heavy particle in the semiconductor detector under a low-background condition of typically 5 s^{-1}.[1,2] We assigned the decay events to those originating from the primary products ^{278}113 and the sequential decays ^{278}113 (α_1) $\to$ ^{274}Rg (Z = 111) (α_2) $\to$ ^{270}Mt (Z = 109) (α_3) $\to$ ^{266}Bh (Z = 107) (α_4) $\to$ ^{262}Db (Z = 105)(SF).[1,2] These assignments were based on the fact that the chains were connected to the known sequential α-decays of ^{266}Bh and ^{262}Db as daughters of ^{278}113.[3,4] In the continuation of our research program, we observed a new decay chain consisting of six consecutive α-decays, i.e., ^{278}113 (α_1) $\to$ ^{274}Rg (α_2) $\to$ ^{270}Mt (α_3) $\to$ ^{266}Bh (α_4) $\to$ ^{262}Db (α_5) $\to$ ^{258}Lr (Z = 103) (α_6) $\to$ ^{254}Md (Z = 101), which allowed an unambiguous determination of the atomic number (Z) and mass number (A) of ^{278}113. Note that the α-decay branching ratio of ^{262}Db is 67%, a fact that led us to search for the α-decay of ^{262}Db in the present study.

The relevant series of experiments was performed at the RIKEN Nishina Center for Accelerator Based Science starting from September 5, 2003, and was tentatively completed on August 18, 2012. The net irradiation time was 553 days with a 1.35×10^{20} beam dose in total. The first and second events obtained in 2003–2004 and 2005–2006 were published in refs. 1 and 2, respectively.

A ^{70}Zn beam was extracted from the RIKEN Linear Accelerator. Other experimental details are described in the original article.

The α-decay mode was first observed for the fifth decay in the third (present) chain, while the modes observed in the first and second decay chains were of the SF decay type. The observed α-energy of E_α = 8.63$\pm$0.06 MeV is in good agreement with the adopted values for ^{262}Db: E_α = 8.450$\pm$0.020 MeV (I_α = 75%), 8.530$\pm$0.020 MeV (16%), and 8.670$\pm$0.020 MeV (9%).[5] The mean life obtained from the three decays (1 α-decay and 2 SFs) is 56^{+77}_{-21} s, which corresponds to the half-life of $T_{1/2} = 39^{+53}_{-14}$ s. The obtained $T_{1/2}$ value is also in good agreement with the adopted value of $T_{1/2} = 34 \pm 4$ s.[5]

In the present decay chain, the sixth α-decay (α_6) of $E_\alpha = 8.66 \pm 0.06$ MeV was also observed with a decay time of 3.78 s, which corresponds to $T_{1/2} = 2.6^{+12}_{-1.1}$ s. These decay properties are in good agreement with the adopted properties for the α-decay daughter of ^{262}Db; ^{258}Lr: 8.565 $\pm$ 0.025MeV (20%), 8.595 $\pm$ 0.010 MeV (46%), 8.621 $\pm$ 0.010 MeV (25%), and 8.654 $\pm$ 0.010 MeV (9%); $T_{1/2} = 3.92^{+0.35}_{-0.42}$ s; and b_α = 97.5%.[5]

The α-decay energies of ^{278}113, ^{274}Rg, ^{270}Mt, and ^{266}Bh show some discrepancies among the three chains. However, the observation in the rather widely distributed decay energies of the decay chains of odd-odd nuclei, for example, starting from ^{272}Rg,[6] is a natural feature caused by the decays to the many excited states in their daughters, and caused by the possible summing effect of the α-energy with a conversion electron or γ-ray energy, which is emitted simultaneously with the α-decay inside the detector.

Therefore, we could conclusively assign the sixth decay to that of ^{258}Lr. Consequently, we could unambiguously assign the third decay chain to ^{278}113 $\to$ ^{274}Rg $\to$ ^{270}Mt $\to$ ^{266}Bh $\to$ ^{262}Db $\to$ ^{258}Lr $\to$ ^{254}Md.

The total beam dose was 1.35×10^{20}. Combining all three events, the production cross section of ^{278}113 was determined to be 22^{+20}_{-13} fb (fb = 10^{-39} cm^2) with a 1σ error. The error includes only a statistical one. To deduce the cross section, the values of the transmission of the GARIS and the effective target thickness used were 0.8 and 450 μg/cm^2, respectively.

In conclusion, the isotope of the 113th element, i.e., ^{278}113, was produced in the ^{209}Bi(^{70}Zn, n)^{278}113 reaction and was unambiguously identified by the strong connection to the well-known daughter nuclides ^{266}Bh, ^{262}Db, and ^{258}Lr.

References
1) K. Morita et al., J. Phys. Soc. Jpn. **73**, 2593 (2004).
2) K. Morita et al., J. Phys. Soc. Jpn. **76**, 045001 (2007).
3) P. A. Wilk et al., Phys. Rev. Lett. **85**, 2697 (2000).
4) K. Morita et al., J. Phys. Soc. Jpn. **78**, 064201 (2009).
5) R. Dressler et al., Phys. Rev. C **59** 3433 (1999).
6) K. Morita et al., J. Phys. Soc. Jpn. **73**, 1738 (2004).

† Condensed from the article in J. Phys. Soc. Jpn. **81**, 103201 (2012).
*1 Department of Chemistry, Niigata University
*2 Research Center for Nuclear Physics, Osaka University
*3 Department of Chemistry, Osaka University
*4 Japan Atomic Energy Agency

Production of spin-controlled rare isotope beams†

Y. Ichikawa, H. Ueno, Y. Ishii, T. Furukawa, A. Yoshimi, D. Kameda, H. Watanabe, N. Aoi, K. Asahi, D. L. Balabanski, R. Chevrier,[*1] J. M. Daugas,[*1] N. Fukuda, G. Georgiev,[*2] H. Hayashi, H. Iijima, N. Inabe, T. Inoue, M. Ishihara, T. Kubo, T. Nanao, T. Ohnishi, K. Suzuki, M. Tsuchiya, H. Takeda, and M. M. Rajabali[*3]

The ability to control spin in a quantum system is a powerful tool in physics research, which holds true in the case of rare isotope (RI) beam experiments. It has been revealed that spin-oriented RI beams can be produced in the projectile fragmentation (PF) reaction[1)]. The study showed a unique relation between the spin orientation and the direction of the removed momentum of the nucleons abraded off through the reaction, suggesting that spin alignment is produced as a function of fragment momenta. Based on this technique, studies on nuclear structure through measurements of the nuclear moment have progressed. However, the spin orientation thus produced in the PF reaction tends to be partially or completely attenuated in cases where the RIs of interest need to be produced by removing a large number of nucleons from the projectile. Consequently, significant magnitudes of spin orientation have been obtained only in the vicinity of nuclear species for which a high-intensity primary beam is available. In this work, a novel technique, with which highly spin-aligned RI beams can be produced in a promising scheme independently of the mass difference between a projectile and a fragment, has been proposed, and the scheme involves a two-step PF method along with a technique of dispersion matching.

In the present method, a nucleus of interest is produced in the second PF reaction by one-nucleon removal from a secondary-beam particle so that the spin alignment can be high owing to the simplicity of the reaction[1)]. The idea of dispersion matching[2,3)] is combined with the two-step PF. By placing a secondary target in a momentum-dispersive focal plane and a momentum slit in the double-achromatic focal plane downstream, events with the same momentum change in the second PF reaction, which forms a decisive factor of the produced spin alignment, can be selected. The important point of this technique is that the reaction products that acquire equal amounts of momentum change at the second PF reaction are focused onto the same position in the double-achromatic focal plane. The application of this technique to PF-induced spin alignment can prevent loss of spin alignment owing to cancellation of opposite contributions from the higher and lower momentum components.

The validity of the method was demonstrated with BigRIPS[4)] at RIBF[5)]. The experimental scheme is shown in Fig 1. In the first reaction at F0, ^{33}Al was produced by a PF reaction of a 345-MeV/nucleon ^{48}Ca beam incident on a Be target with a thickness of 1.85 g/cm^2, chosen to provide the maximum production yield for the secondary ^{33}Al beam. The secondary ^{33}Al beam was introduced to a second wedge-shaped aluminum target with a mean thickness of 2.70 g/cm^2, placed in the momentum-dispersive focal plane F5. The ^{32}Al nuclei, including those in the isomeric state ^{32m}Al[6)], were produced through a PF reaction resulting in the removal of one neutron from ^{33}Al. The ^{32}Al beam was subsequently transported to F7, whereby the momentum dispersion between F5 to F7 was tuned to be with the same magnitude and opposite sign as that from F0 to F5 so as to cancel out the momentum dispersion from the site of the first PF reaction to F7. The slit at F7 was used to select a region of momentum change at the second PF within ±0.15% about the center of the distribution.

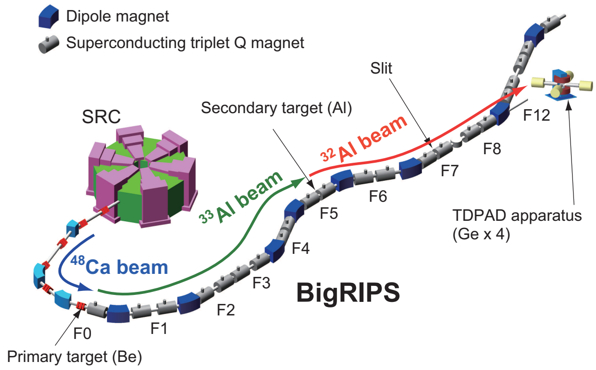

Fig. 1. Experimental scheme of the present method to produce ^{32}Al from ^{48}Ca via ^{33}Al at BigRIPS. The second PF reaction takes place at F5.

The ^{32m}Al beam was sent to an experimental apparatus placed in a focal plane after F7 for the time-differential perturbed angular distribution (TDPAD) measurement. ^{32m}Al was implanted into a Cu crystal with a thickness of 3.0 mm and an area of 30 × 30 mm^2, located between poles of a dipole magnet providing a static magnetic field B_0 of 0.259 T. The de-excitation γ rays emitted from ^{32m}Al were detected with four Ge detectors located at distances of 7.0 cm from the stopper and at angles of ±45° and ±135° with respect to the beam axis. The time-zero triggers for the TDPAD measurement were provided by signals from a beam-

† Condensed from the article in Nature Phys. **8**, 918 (2012)
*1 CEA, DAM, DIF, France
*2 CSNSM, IN2P3-CNRS, France
*3 Instituut voor Kern- en Stralingsfysica, KU Leuven, Belgium

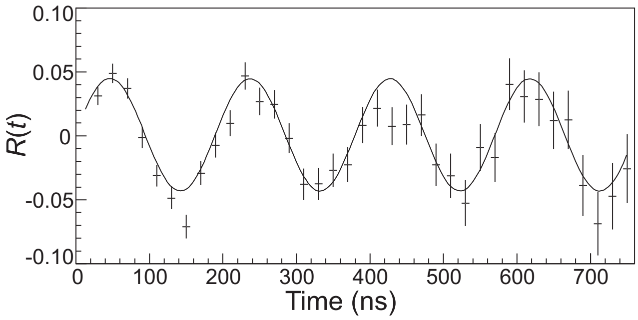

Fig. 2. $R(t)$ ratio evaluated according to Eq. 1. The solid line represents the $R(t)$ function after fitting to the experimental $R(t)$ ratio, according to Eq. 2.

particle counter of a plastic scintillator with a thickness of 0.1 mm placed upstream of the stopper. The TDPAD apparatus enabled us to determine the degree of spin alignment by observing the changes in the anisotropy of the de-excitation γ rays, emitted from spin-aligned ^{32m}Al in synchronization with the spin precession under the external magnetic field.

The degree of spin alignment in ^{32m}Al was determined from a ratio $R(t)$, defined as

$$R(t) = \frac{N_{13}(t) - \epsilon N_{24}(t)}{N_{13}(t) + \epsilon N_{24}(t)}, \quad (1)$$

where $N_{13}(t)$ and $N_{24}(t)$ are the sums of the photopeak count rates at the two pairs of Ge detectors placed diagonally to each other, and ϵ denotes a correction factor for the detection efficiency. Theoretically, the $R(t)$ ratio is expressed as a function of t as

$$R(t) = \frac{3A_{22}}{4 + A_{22}} \cos 2(\omega_{\mathrm{L}} t + \alpha), \quad (2)$$

in terms of the rank-two anisotropy parameter $A_{22} = AB_2F_2$, where A denotes the degree of spin alignment, B_2 is the statistical tensor for complete alignment, and F_2 is the radiation parameter. α is the initial phase of $R(t)$. The Larmor frequency ω_{L} is given by $\omega_{\mathrm{L}} = g\mu_{\mathrm{N}}B_0/\hbar$, where g is the g-factor of ^{32m}Al in units of the nuclear magneton μ_{N}.

The time variations $N_{13}(t)$ and $N_{24}(t)$ of the intensities for the 222-keV γ rays, emitted from the isomeric state ^{32m}Al, were obtained with detectors pairs Ge 1 - 3 and Ge 2 - 4, respectively. The $R(t)$ ratio, evaluated according to Eq. 1, is shown in Fig. 2. From the least χ^2 fitting to the experimental $R(t)$ ratio, according to Eq. 2, the degree of spin alignment was determined to be $A = 8(1)\%$.

A supplementary experiment was also carried out in order to compare the performance of the present method with that of the conventional single-step method, where ^{32}Al was directly produced in a PF reaction of a ^{48}Ca beam on a 4-mm thick Be target at F0. In this measurement, the degree of spin alignment

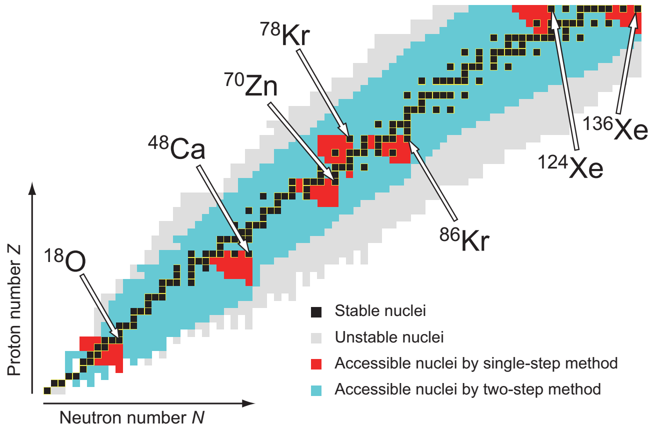

Fig. 3. Nuclear chart indicating "accessible nuclei." The criterion of accessibility is that the RI of interest is producible with its spin aligned and with the production yield sufficiently large in order to determine the g-factor with a 5σ confidence level in a one-day beam time.

was measured to be less than 0.8% in 2σ confidence level. The figure of merit (FOM) for the production of such spin-aligned RI beams is defined to be proportional to the yield and the square of the degree of alignment. Yield of ^{32m}Al at the final focal plane were 0.54(5) kcps and 0.87(6) kcps for the two-step and the single-step PF measurements, respectively. A primary beam whose intensity was deliberately attenuated by a factor of 1/100 was used in order to avoid saturation in the counting rate at the data acquisition system in the single-step PF measurement. Here, the FOM was compared based on the actual effectiveness without correction for the attenuation, in which the resulting FOM for the present method was found to be more than 50 times greater than that of the conventional method employing single-step PF reaction.

Figure 3 shows the result of numerical simulations for the accessibility of unstable nuclei, in terms of spin alignment, via the two-step and the single-step PF methods. In this simulation, primary beams are restricted to the typical species available with high intensity at RIBF[5]. The present method is expected to enable us to substantially broaden the accessible scope of spin-aligned RI beams. Such an ability to control spin, when applied to state-of-the-art RI beams, is expected to provide unprecedented opportunities for research on the nuclear structure of species situated outside the traditional region of the nuclear chart.

References

1) K. Asahi et al.: Phys. Lett. B **251**, 488 (1990).
2) B. L. Cohen: Rev. Sci. Instrum. **30**, 415 (1959).
3) H. G. Blosser et al.: Nucl. Instrum. Meth. **91**, 61 (1971).
4) T. Kubo: Nucl. Instrum. Meth. B **204**, 97 (2003).
5) Y. Yano: Nucl. Instrum. Meth. B **261**, 1009 (2007).
6) M. Robinson et al.: Phys. Rev. C **53**, R1465 (1996).

Recirculating He-gas stripper for high-intensity uranium beam

H. Imao, H. Okuno, H. Kuboki, O. Kamigaito, H. Hasebe, N. Fukunishi, Y. Watanabe, M. Fujimaki, T. Maie, T. Dantsuka, M. Komiyama, K. Kumagai, K. Yamada, T. Watanabe, M. Kase, and Y. Yano

Intensity upgrade of uranium beams is one of the main concerns at the RIKEN Radioactive Isotope Beam Factory (RIBF). A new injector, RILAC2, which includes a 28-GHz superconducting electron cyclotron resonance ion source[1)], has been successfully developed and became fully operational in fiscal year 2011. To further accelerate the uranium beams generated by this powerful injector, one of the highest priorities is to explore a new electron stripping method for the "destructive beams". Due to the high energy loss of uranium beams around 10 MeV/u (e.g., three thousand times larger than protons with the same energy), the lifetime problem of the conventional carbon-foil stripper was a principal bottleneck for the intensity upgrade in the present acceleration scheme. Developing the stripper for high-intensity uranium beams is a global challenge faced by other big heavy-ion projects such as the FAIR at GSI (Germany) and the FRIB at MSU/ANL (USA). In the present study, we developed a recirculating He-gas stripper characterized by basically infinite lifetime even for the irradiation of the world's most intense uranium beams at the RIBF.

Charge strippers using helium gas simultaneously provide durability, uniform thickness, and a high charge state equilibrium of the low-atomic number (Z) gas[2,3)]. The major technical challenges for our system were the windowless accumulation[3)] of thick He gas ($\leq$ 1 mg/cm^2) with large beam aperture diameters ($\geq$ ϕ10mm) and high-flow recirculation ($\sim$200 L/min) of pure He gas with low gas consumption rates ($\leq \sim$1%). The purity of the recirculating He gas, c_{He}, should be sufficient compared with the cross-section ratio for electron capture, $\sigma_{He}/\sigma_{imp}\sim {Z_{He}}^{4.2}/{Z_{imp}}^{4.2}$. All requirements were fulfilled by using an unprecedented scheme with a powerful multistage mechanical booster pump (MBP) array consisting of four foreline MBPs and three back MBPs with a total nominal pumping speed of 11,900 m^3/h. The system is designed to recirculate He gas with an efficiency of 99.5% and to reduce the pressure by nine orders of magnitude from the target pressure of $\sim$10 kPa to the beamline vacuum of $\sim$10^{-5} Pa with five-stage differential pumping systems including the MBP array.

The system was successfully installed at the A02 site in the RRC room. We verified that the basic performance was achieved in offline tests. Since April 2012, a series of beam irradiation tests was also performed. We confirmed that there is no evidence of target impurities, and no problems occurred when it was used with U^{35+} beams injected at 11 MeV/u with the intensity of up to 0.3 pμA . After the commissioning, the system was actually operated in user runs this fall with beam intensities of more than 1 pμA for the first time (Fig. 1). Electron-stripped U^{64+} beams were stably delivered to subsequent accelerators without any deterioration of the system for six weeks. The conversion efficiencies for U^{64+} with a typical operational target thickness of 0.6 mg/cm^2 are as high as 23% owing to the electron shell effect in the charge-exchange reactions. The temperature increase in the water-cooled tube orifices was tolerable ($\leq$150°C) with the transmission efficiency reaching about 80%. The reduction in the target density along the beam path owing to the heat load was not found to be large.

The new He gas stripper, which removed the primary bottleneck in the high-intensity uranium acceleration, and the success of some other remarkable accelerator upgrade performed in this year at the RIBF (e.g., ion source, high-power beam dump, K700-fRC, and 2nd rotating Be stripper) brought a tenfold increase in the average output intensity of the uranium beams compared to the previous year. Further sophistication of this new acceleration scheme for greater uranium beam intensities is in progress.

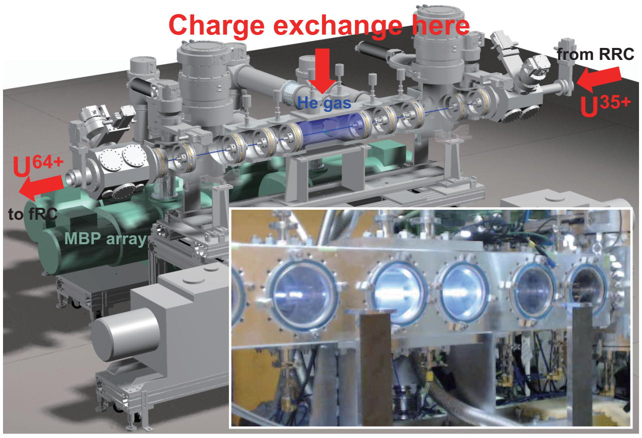

Fig. 1. Cross sectional view of the He gas stripper and picture of glowing 1-pμA uranium beams.

References
1) Y.Higurashi *et al.*: Rev. Sci Instr. 83, 02A308 (2012).
2) H. Okuno *et al.*: Phys. Rev. ST-AB **14**, 033503 (2011).
3) H. Imao *et al.*: Phys. Rev. ST-AB **15**, 123501 (2012).

Bending power upgrade for fRC

N. Fukunishi, M. Fujimaki, K. Kumagai, M. Kobayashi-Komiyama, and T. Maie

The RIKEN fixed-frequency Ring Cyclotron[1] (fRC) has been used as the third-stage accelerator in the fixed-energy acceleration mode of RIBF, which accelerates 345-MeV/nucleon xenon and uranium beams[2]. The fRC was originally designed to accelerate $^{238}U^{73+}$ ions using a 0.6-mg/cm^2-thick carbon foil stripper at 10.8 MeV/nucleon, just after the acceleration of the Riken Ring Cyclotron. Immediately after the start of beam commissioning of the fRC in 2006, we recognized that insufficient thickness uniformity in the used carbon foils produced a larger momentum spread than that accepted in the fRC. Hence, we decided to reduce the carbon foil thickness to 0.3 mg/cm^2 with a small modification of the injection radius of the fRC. The most probable charge state is 71+ in this case. This modification resulted in a satisfactory transmission efficiency of the uranium beams, i.e., 90%, which is close to the design value. One problem to be fixed is the short lifetime of each carbon foil used. It is about 12 hours for a uranium beam having an intensity of 15 pnA, which corresponds to 1% of the beam intensity expected after the scheduled intensity upgrade of RIBF, in which the new injector RILAC2[3] is constructed. To overcome the short lifetime problem, a helium-gas stripper system has been developed recently[4]. The most probable charge state expected for the helium gas stripper was 65+. Hence, the bending power of the fRC should be increased since it was limited to $^{238}U^{69+}$ ions.

In the design studies that started in May 2011 and completed in early July 2011, we made it clear that the following upgrades were necessary to realize $^{238}U^{65+}$ acceleration in the fRC. The power supplies exciting the fRC sector magnets should be upgraded since their operating currents were estimated to be at the 830 A level, well beyond the capacity of the original power supply (650 A). In addition, several original injection and extraction apparatuses used in the fRC were also insufficient in their maximum magnetic rigidities. Devices to be upgraded were the injection bending magnet, the magnetic inflection channel II and its power supply, and the extraction bending magnet. All these were newly constructed except for the extraction bending magnet, for which a replacement of its iron cores was sufficient to generate the required magnetic rigidity. A drawback of the new iron cores is a non-uniform magnetic field distribution, but it remains acceptable. Finally, two new beam steering magnets should be introduced in the beam injection line crossing the north valley chamber in order to compensate for the much stronger stray magnetic fields expected in $^{238}U^{65+}$ acceleration compared to those experienced in $^{238}U^{71+}$ acceleration. The details of the design studies are summarized in Ref. 5).

The manufacture of these devices was successfully completed at the end of FY2011. The installations were executed in the first three months of FY2012 intervening the tightly scheduled accelerator operations providing beams to users. The magnetic field measurements, in which we measured magnetic fields with various excitation currents but only along the centerline of each sector magnet, were also performed in a similar way. It is very challenging to skip the two-dimensional magnetic field mapping for big cyclotrons but we have experience doing this in the beam commissioning of the fRC in 2006. A one-night acceleration test for the $^{238}U^{65+}$ ions, using the upgraded fRC, was done from 14 - 15 July 2012. The $^{238}U^{65+}$ ions were successfully extracted from the fRC with a transmission efficiency of 80%.

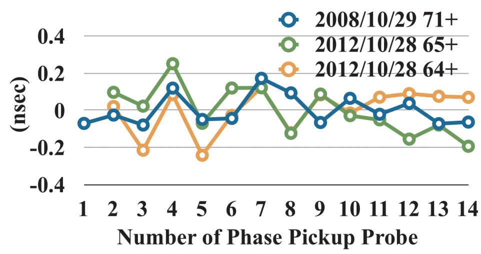

Fig. 1. Isochronous magnetic fields of the fRC.

Meanwhile, the newly developed helium gas stripper demonstrated that the stripping efficiency was higher (23%) for $^{238}U^{64+}$ than for $^{238}U^{65+}$ (15%) owing to the atomic shell effect of the uranium ion[4]. Therefore, we tried to accelerate the 64+ ions utilizing a design margin of one of the new power supplies. This was performed on 28 October, during the beam tuning time for the uranium beam service, scheduled in November and December 2012. The result was satisfactory. The obtained isochronous magnetic fields are shown in Fig. 1 for both the 64+ and 65+ uranium ions compared with the 71+ ions. Other quantities such as the transmission efficiency and the acceleration turn patterns exhibited no fRC performance decrement after the completion of the upgrade.

References
1) T. Mitsumoto et al.: Proc. 17th Int. Conf. on Cyclotrons and Their Applications, p. 384 (2004).
2) N. Fukunishi et al.: PAC09, Vancouver, Canada, MO3GRI01 (2009).
3) K. Yamada et al.: Proc. IPAC'10, Kyoto, Japan, MOPD046 (2010).
4) H. Imao et al.: Proc. IPAC'11, San Sebastian, Spain, TUPS088 (2011). H. Imao et al.: Proc. IPAC'12, New Orleans, Louisiana, USA, THPP084 (2012).
5) K. Kumagai, et al.: Proc. PASJ9, Osaka, Japan, WEPS055 (2012).

Observation of 18 new microsecond isomers produced by the in-flight fission of 345 MeV/nucleon ^{238}U[†]

D. Kameda, T. Kubo, T. Ohnishi, K. Kusaka, A. Yoshida, K. Yoshida, M. Ohtake, N. Fukuda, H. Takeda, K. Tanaka, N. Inabe, Y. Yanagisawa, Y. Gono, H. Watanabe, H. Otsu, H. Baba, T. Ichihara, Y. Yamaguchi, M. Takechi, S. Nishimura, H. Ueno, A. Yoshimi, H. Sakurai, T. Motobayashi, T. Nakao,[*1] Y. Mizoi, M. Matsushita,[*2] K. Ieki, N. Kobayashi, K. Tanaka,[*3] Y. Kawada,[*3] N. Tanaka,[*3] S. Deguchi,[*3] Y. Satou, Y. Kondo, T. Nakamura, K. Yoshinaga, C. Ishii,[*4] H. Yoshii,[*4] Y. Miyashita,[*4] N. Uematsu,[*4] Y. Shiraki,[*4] T. Sumikama, J. Chiba,[*4] E. Ideguchi,[*5] A. Saito,[*5] T. Yamaguchi, I. Hachiuma,[*6] T. Suzuki,[*6] T. Moriguchi,[*7] A. Ozawa, T. Ohtsubo,[*8] M. A. Famiano, H. Geissel, A. S. Nettleton,[*9] O. B. Tarasov, D. Bazin, B. M. Sherrill, S. L. Manikonda, and J. A. Nolen

In-flight fission with a high-energy ^{238}U beam provides the efficient means to produce neutron-rich nuclei far from stability over a wide range of the atomic number (Z) ranging from 30 to 60. To exploit this unparalleled advantage, we conducted comprehensive searches for new isotopes and isomers among neutron-rich nuclei with Z varying from 30 to 50 produced by the in-flight fission of a ^{238}U beam at 345 MeV/nucleon at RIBF. We separated and identified fission fragments by making full use of the BigRIPS separator[1)] which allows the efficient collection and separation as well as the particle identification of the fragments in flight. Isomeric γ-rays were detected by three clover-type HPGe detectors after ion implantation in an aluminum stopper at the focal plane. As a result we could unambiguously identify 45 new neutron-rich isotopes from Mn to Ba.[2)] At the same time we discovered 18 new isomers: ^{59m}Ti, ^{90m}As, ^{92m}Se, ^{93m}Se, ^{94m}Br, ^{95m}Br, ^{96m}Br, ^{97m}Rb, ^{108m}Nb, ^{109m}Mo, ^{117m}Ru, ^{119m}Ru, ^{120m}Rh, ^{122m}Rh, ^{121m}Pd, ^{124m}Pd, ^{124m}Ag, and ^{126m}Ag. Here, we briefly report on the new isomers.

Figure 1 shows all of the isomers observed in the present work as well as new isotopes in the nuclear chart. In general, new isomers are mainly observed around the mid-shell region between double closed-shell nuclei, ^{78}Ni and ^{132}Sn. This region is known to be a deformed region in which dramatic shape transitions occur. Intensive studies have been made in this region using conventional means with fission sources such as ^{252}Cf since 1970s.[3,4)] The present results allow further expansion of the study of neutron-rich exotic nuclei beyond the limits of the conventional means. A wealth of spectroscopic information obtained in this work such as of half-lives, γ-ray energies, γ-ray relative intensities, and $\gamma\gamma$ coincidences allows us to study the level schemes and isomerism in a highly systematic manner.

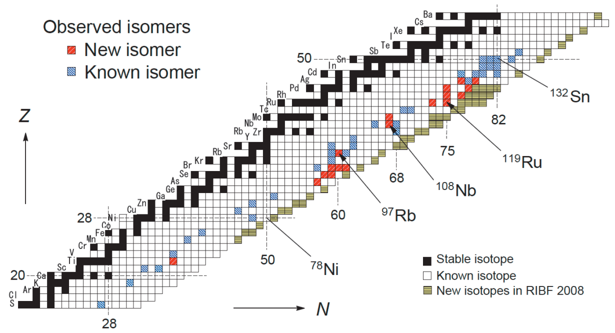

Fig. 1. Nuclear chart showing the isomers observed in the present work. (The neutron-deficient nuclei are omitted.)

We divided the mid-shell region into three parts with $N \sim 60$, 68, and 75. At $N \sim 60$, a sudden onset of the large deformation with the shape coexistence of spherical and prolate deformed shapes is known to occur. We proposed that ^{95m}Br, ^{97m}Rb, and ^{98m}Rb are shape isomers generated due to such shape coexistence. At $N \sim 68$, a variety of nuclear shapes, e.g., prolate, oblate, triaxial, and tetrahedral shapes as well as their coexistence are predicted to emerge. They are involved in the appearance of the isomers such as ^{108m}Nb and ^{109m}Mo. At $N \sim 75$, we observed several new isomers such as ^{119m}Ru in this unexplored region. The systematic appearance of isomers is similar to the case of $N \sim 60$. The systematics of two neutron separation energies predicted by the ETFSI-Q mass model[5)] exhibit the humps at $N \sim 75$ that are highly similar to those observed at $N \sim 60$. From these similarities, we speculate that these new isomers are generated by shape coexistence in a new deformed region.

References
1) T. Kubo et al.: Prog. Theor. Exp. Phys. 03C003 (2012).
2) T. Ohnishi et al.: J. Phys. Soc. Jpn. **79**, 073201 (2010).
3) E. Cheifetz et al.: Phys. Rev. Lett. **25**, 38 (1970).
4) M. Epherre et al.:Phys. Rev. C **19**, 1504 (1979).
5) J. M. Pearson et al.:Phys. Lett. B **387**, 455 (1996).

† Condensed from the article in Phys. Rev. C **86**, 054319 (2012).
*1 Department of Physics, The University of Tokyo
*2 Department of Physics, Rikkyo University
*3 Department of Physics, Tokyo Institute of Technology
*4 Department of Physics, Tokyo University of Science
*5 Center for Nuclear Study, The University of Tokyo
*6 Department of Physics, Saitama University
*7 Institute of Physics, University of Tsukuba
*8 Department of Physics, Niigata University
*9 NSCL, Michigan State University

In-beam γ-ray spectroscopy of ^{53}Ca and ^{54}Ca

D. Steppenbeck,[*1] S. Takeuchi, N. Aoi, P. Doornenbal, M. Matsushita,[*1] H. Wang, H. Baba, N. Fukuda, S. Go, J. Lee, K. Matsui, S. Michimasa,[*1] T. Motobayashi, D. Nishimura, H. Sakurai, Y. Shiga, P.-A. Söderström, T. Sumikama, H. Suzuki, R. Taniuchi, J. J. Valiente-Dobón,[*2] and K. Yoneda

Over recent years, the evolution of nuclear shell structure in exotic, neutron-rich nuclei has attracted much attention on both the experimental and theoretical fronts. In the neutron-rich fp shell, the onset of a new subshell closure at $N = 32$ was highlighted by structural characteristics along the Ca[1)], Ti[2,3)] and Cr[4,5)] isotopic chains, a feature that is reproduced well by several shell-model effective interactions, such as the GXPF1A[6)] and KB3G[7)] Hamiltonians. In the framework of the theoretical studies by Otsuka et al.[8)], the onset of the $N = 32$ subshell closure results as a direct consequence of a sizable $\nu p_{3/2} - \nu p_{1/2}$ gap, which presents itself as the $\nu f_{5/2}$ orbital shifts up in energy relative to the $\nu p_{3/2} - \nu p_{1/2}$ spin-orbit partners due to a weakening of the attractive proton-neutron $\pi f_{7/2} - \nu f_{5/2}$ interaction as protons are removed from the $\pi f_{7/2}$ orbital. One further important manifestation of the GXPF1A Hamiltonian is the prediction of a subshell gap at $N = 34$, which becomes significant if the $\nu f_{5/2}$ orbital lies sufficiently high in energy above the $\nu p_{1/2}$ orbital. In fact, it has already been shown that no $N = 34$ subshell gap exists along the Ti[3,9)] and Cr[4,5)] isotopic chains, and, therefore, the size of the energy gap in ^{54}Ca is an important structural characteristic that requires experimental input. Moreover, the single-particle states of ^{53}Ca may also reflect the nature of the $N = 34$ closure.

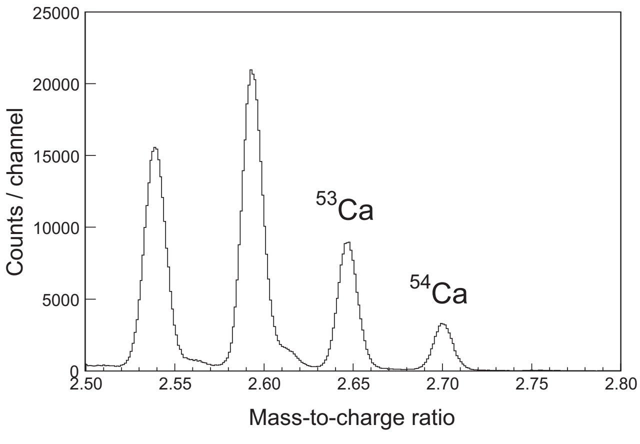

Fig. 1. Particle identification (A/q) for the Ca isotopic chain measured with the ZeroDegree spectrometer.

In the present work, the structures of ^{53}Ca and ^{54}Ca were investigated using in-beam γ-ray spectroscopy at the Radioactive Isotope Beam Factory to address this issue. A primary beam of ^{70}Zn at 345 MeV/u was delivered to the BigRIPS separator, where a radioactive beam containing ^{55}Sc and ^{56}Ti was produced and delivered to a 10-mm-thick Be reaction target located at the 8th focal plane. The DALI2 array was used to measure γ-ray transitions from excited nuclear states populated via nucleon knockout reactions. The reaction products were identified with the ZeroDegree spectrometer using standard $B\rho$-T-ΔE techniques; the particle identification for Ca isotopes is presented in Fig. 1. Several new γ rays have been identified in the present work for ^{53}Ca and ^{54}Ca. The spectrum for ^{53}Ca is displayed in Fig. 2 as an example of the quality of the data. The 1753-keV transition is reported here for the first time, while the line at 2227 keV is consistent in energy with a transition previously observed in a β-decay study[10)]. The results of the present work provide the first direct interpretation of the strength of the $N = 34$ subshell closure.

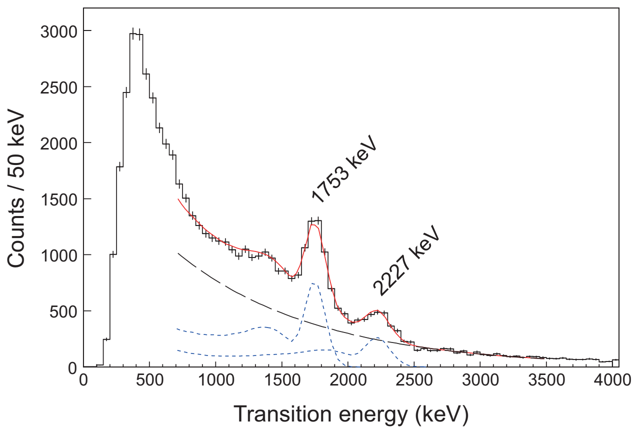

Fig. 2. (Colour) Doppler-corrected γ-ray spectrum for ^{53}Ca. The short-blue dashed lines are GEANT4 simulations.

References
1) A. Gade et al., Phys. Rev. C **74**, 021302(R) (2006).
2) R. V. F. Janssens et al., Phys. Lett. B **546**, 55 (2002).
3) D.-C. Dinca et al., Phys. Rev. C **71**, 041302(R) (2005).
4) J. I. Prisciandaro et al., Phys. Lett. B **510**, 17 (2001).
5) A. Bürger et al., Phys. Lett. B **622**, 29 (2005).
6) M. Honma et al., Eur. Phys. J. A **25**, 499 (2005).
7) A. Poves et al., Nucl. Phys. A **694**, 157 (2001).
8) T. Otsuka et al., Phys. Rev. Lett. **95**, 232502 (2005).
9) S. N. Liddick et al., Phys. Rev. Lett. **92**, 072502 (2004).
10) F. Perrot et al., Phys. Rev. C **74**, 014313 (2006).

*1 Center for Nuclear Study, University of Tokyo, Japan
*2 Legnaro National Laboratory, Italy

New-isotope search and production-cross-section measurement for neutron-deficient nuclei by using projectile fragmentation of 345-MeV/nucleon ^{124}Xe beam

H. Suzuki, T. Kubo, N. Inabe, N. Fukuda, H. Takeda, D. Kameda, K. Yoshida, K. Kusaka, K. Tanaka, Y. Yanagisawa, M. Ohtake, H. Sato, Y. Shimizu, H. Baba, M. Kurokawa, N. Iwasa, K. Ieki, S. Momota, D. Nishimura, S. Go, D. J. Morrissey, D. P. Bazin, A. Chiba, Y. Ohkoda, E. Ideguchi,[*1] R. Yokoyama,[*1] T. Fujii, D. Murai, H. Nishibata, M. Lewitowicz,[*2] G. DeFrance,[*2] I. Celikovic,[*2] and K. Steiger[*3]

In December 2011, we performed new-isotope search and production-cross-section measurement for highly neutron-deficient nuclei, which were produced by the projectile fragmentation of a primary beam of ^{124}Xe at 345 MeV/u using the BigRIPS separator[1]. The primary beam with an intensity of around 8 pnA was impinged on a 4-mm-thick Be target. Particle identification was performed in the second stage of the BigRIPS separator on the basis of the measured time of flight, energy loss, and magnetic rigidity.

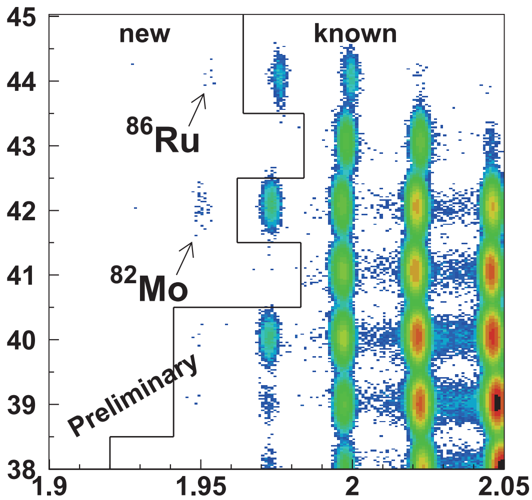

Fig. 1. Two-dimensional plots of Z vs. A/Q for new-isotope-search setting (Preliminary). ^{86}Ru and ^{82}Mo are the new isotopes.

We searched for the new isotopes near the proton-drip line around the atomic numbers $Z = 40 \sim 55$. Figure 1 shows a two-dimensional plot of Z versus mass-to-charge ratio (A/Q) of the Nb-Pd setting[2]. The solid lines indicate the limit of known isotopes. The new isotopes ^{86}Ru and ^{82}Mo are clearly identified on the left side of the limit lines. The relative root-mean-square Z and A/Q resolution are typically 0.40% and 0.061%, respectively.

We measured the production cross sections of the neuton-deficient isotopes including ^{100}Sn. The transmission was evaluated using the LISE++ with version 9.4.80. Figure 2 shows the obtained cross sections for Mo to Sb isotopes. The error bars are for the statistical and the couting method of the yield. The solid lines show the calculated value of EPAX3.01[3]. The production yield and cross section of ^{100}Sn are $(1.1 \pm 0.2) \times 10^{-4}$ cps/pnA and $(7.4 \pm 1.7) \times 10^{-1}$ pb, respectively. These experimental values are one-order of magnitude smaller than the values calculated with EPAX3.01. The discrepancy between the experimental data and the calculated values becomes significantly large in very neutron-deficient region, whereas it is relatively small around near stable region.

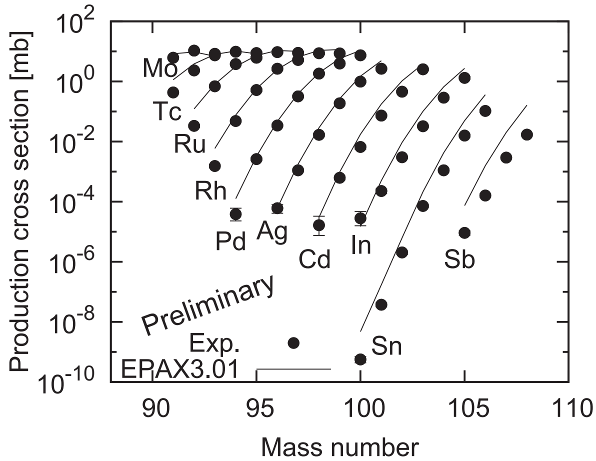

Fig. 2. Measured production cross section with the EPAX3.01 calculation (Preliminary).

Further analysis is now in progress. We are analyzing the momentum distribution of the fragments. They have a longer tail of the low-momentum side than that of the high-momentum side. The shape of such a low-momentum tail is important in estimating the purity of RI beams in the neutron-deficient region.

References
1) T. Kubo et al.: Nucl. Instr. and Meth. **B 204**, 97 (2003)
2) N. Inabe et al.: RIKEN Accel. Prog. Rep. **45**, 13 (2011)
3) K. Sümmerer: Phys. Rev. **C 86**, 140601 (2012)

*1 Center for Nuclear Study, University of Tokyo
*2 Grand Accelerateur National d'Ions Lourds, France
*3 Physik Department, Technische Universität München, Germany

A β-decay study of neutron-rich nuclei in the vicinity of ^{78}Ni

Z. Xu, S. Nishimura, G. Lorusso, P. Doornenbal, T. Sumikama, P.-A. Söderström, H. Watanabe, H. Baba, F. Browne, G. Gey, T. Isobe, P. John,[*1] H. S. Jung, Z. Li,[*2] K. Matsui, D. Mengoni,[*1] D. R. Napoli,[*3] M. Niikura, H. Nishibata, A. Odahara,[*4] E. Şahin,[*5] H. Sakurai, G. I. Stefan,[*6] J. Taprogge, Zs. Vajta, J. Wu, A. Yagi, K. Yoshinaga, and all the EURICA collaborators.

A β-decay experiment of neutron-rich nuclei around ^{78}Ni was performed as part of the EURICA campaign at the Radioactive Isotope Beam Factory (RIBF) at RIKEN in the end of 2012. The experiment aimed at exploring new isomers, half-lives, and β-decay spectroscopy of nuclei in the vicinity of the doubly magic ^{78}Ni. The results from this experiment serve as a benchmark for various theoretical models in the region far from stability.

The experiment used a high intensity ^{238}U beam from the RIBF facility with an energy of 345 MeV/u. The secondary beam was produced by in-flight fission of ^{238}U in a 3 mm-thick Be target and separated at BigRIPS.[1)] An event-by-event particle-identification (PID) was carried out at BigRIPS together with the ZeroDegree spectrometer, to obtain the atomic number Z and mass-to-charge ratio A/Q for fragments passing through the beam line. The resulting PID plot is shown as Z vs. A/Q in Fig. 1. An average beam intensity of 5 pnA was achieved during the 7.5 days of beam time, from which $\sim$4000 ^{78}Ni implantations were identified in the online data analysis.

A highly segmented silicon stopper array, WAS3ABi (wide-range active silicon strip stopper array for β and ion),[2)] was placed at the F11 focal plane for the implantation of heavy ions transported through the ZeroDegree. Eight layers of silicon strip detectors (DSSSD) were mounted inside the WAS3ABi chamber to fully cover the range of nuclei of interest in the secondary beam. Each silicon detector had a thickness of 1 mm and an active area of 60×40 mm^2, which segmented into 60 strips horizontally on the front side and 40 strips vertically on the back side. β-decay events detected by DSSSD, were associated with heavy-ion implantation within a time correlation window of 5 seconds as well as a three-dimensional position correlation window of $3 \times 3 \times 3$ pixels. The EURICA γ-ray detectors array was mounted around WAS3ABi with 84 HPGe crystals arranged into 12 clusters. The γ-ray detection efficiency for a 1 MeV γ-ray was measured to be around 8% with the γ source put inside the WAS3ABi chamber. A energy resolution of about 2.7 keV for the 1.3 MeV γ-ray was achieved before the experiment.

*1 Universita degli Studi di Padova, Italy
*2 Department of Physics, Peking University, China
*3 INFN, Italy
*4 Department of Physics, Osaka University, Japan
*5 University of Oslo, Norway
*6 IPN-Orsay, France

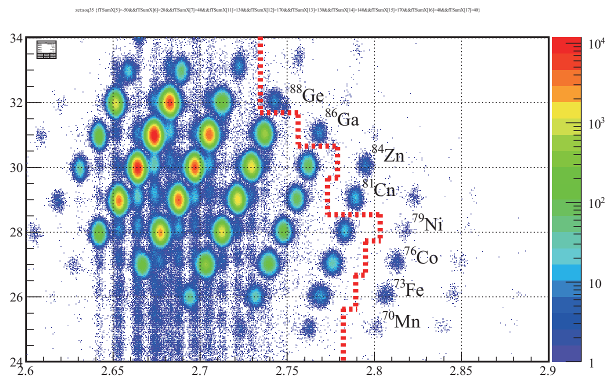

Fig. 1. *Particle-identification plot from the present experiment. The half-lives of the nuclei listed on the right side of red dotted line was measured for the first time in this work.*

The offline data analysis is still on-going. Half-lives of the nuclei located on the right side of the red dotted line in Fig. 1 have been measured for the first time, allowing for systematic studies and comparisons between different mass models and theoretical calculations around ^{78}Ni. It is also of great importance to study the low-lying states of odd Cu isotopes, because states with large collectivities as well as strong monopole migration have been experimentally observed in odd-mass Cu nuclides at $N > 40$.[3)] This has been interpreted as strong evidence of the erosion of the $Z = 28$ shell closure in this mass region. Level schemes of odd Cu isotopes built from the new data set will largely extend beyond the present knowledge of the evolution of the nuclear shell structure approaching ^{78}Ni.

References

1) T. Kubo: Nucl. Instrum. Methods Phys. Res., Sect. B **204**, 97 (2003).
2) S. Nishimura: Prog. Theor. Exp. Phys. **2012**, 03C006 (2012).
3) I. Stefanescu *et al.*: Phys. Rev. Lett. **100**, 112502 (2008).

Beta-decay spectroscopy below the doubly magic ^{132}Sn

G. Lorusso, H. Watanabe, S. Nishimura, Z.Y. Xu, H. Baba, F. Browne P. Doornenbal, G. Gey, T. Isobe, H.S. Jung, Y.K. Kwon,[*1] Z. Li,[*2] K. Moschner, H. Nishibata, A. Odahara,[*3] H. Sakurai, G. Simpson,[*4] P.-A. Söderström, T. Sumikama, J. Taprogge, Z. Vajta, J. Wu, A. Yagi, K. Yoshinaga, and the EURICA collaboration

The shell structure at $N = 82$ plays a crucial role for the rapid neutron capture (r-) process. For example, it determines the shape of the large $A \sim 130$ peak in the solar system abundance pattern, and affects the timescale of the r-process as well as the amount of neutrons available for fission[1]. However, below $Z = 50$, as the proton orbit $g_{9/2}$ is progressively emptied, all proton-neutron interactions become important and could modify the ordering of neutron orbits. The increasing surface diffuseness for large N/Z also modifies the energy of the orbits. Therefore, the evolution of the $N = 82$ gap is impossible to predict at present, and the prediction of neutron separation energies, half-lives, and neutron capture cross sections are unreliable, making the location and duration of the r-process uncertain. Clearly, more experimental data are needed to constrain the $N = 82$ shell structure and provide r-process calculations with experimental input.

To address these open questions, we have performed a decay-spectroscopy experiment at the RIBF facility in a very neutron-rich region below ^{132}Sn. The recent beam development at RIBF, along with the installation of the EUROBALL γ-ray detector has made this region accessible to decay-spectroscopy experiments. This region is not accessible in any other laboratory. The experiment was part of the EURICA uranium beam campaign in 2012.

In our experiment, the nuclei of interest were produced by fission of a $345A$ $\sim$-MeV ^{238}U primary beam colliding with a ^{9}Be target. Beam purification was provided by the BigRIPS fragment Separator. The fragments of interest were unambiguously identified, and their following β decays were recorded by the WAS3ABi[2] silicon stopper in conjunction with EURICA. Implantations were correlated with their subsequent β decays on the basis of position and time, enabling measurement of half-lives, β-delayed γ rays, and γ rays from the deexcitation of implanted microsecond isomers.

With three BigRIPS settings, we were able access very neutron-rich isotopes for more than 15 elements from Zr to Sn, measuring more than 30 new half-lives, including the two new r-process waiting points: ^{128}Pd and ^{127}Rh (see Fig. 1). New microsecond isomers were also identified. This large set of data will provide direct input for r-process calculations, new insights in the nuclear structure in this region, and will improve parametrization of mass formula, invaluable to model r-process nucleo-synthesis.

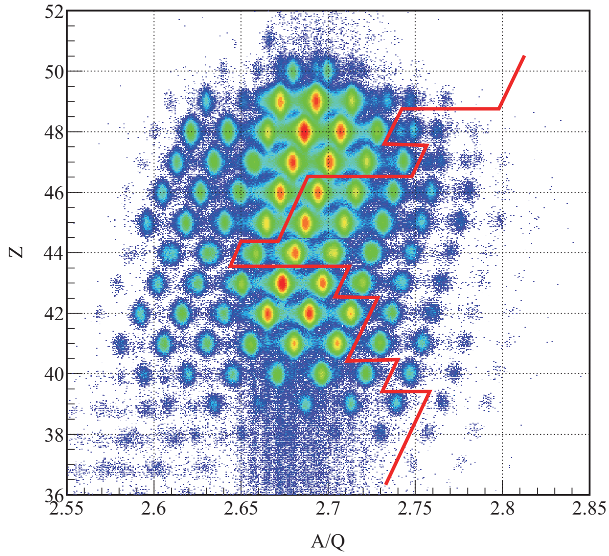

Fig. 1. Particle identification spectrum of nuclei transmitted throught the fragment separator BigRIPS. Red line indicate the limit of known half-lives previous to this experiment.

[*1] Institute for Basic Science, Republic of Korea
[*2] Department of Physics, Peking University, China
[*3] Department of Physics, Osaka University
[*4] LPSC, France

References
1) G. Martinez-Pinedo et al.: NUSTAR-THEORY-12 The role of fission in the r-process (2008).
2) S. Nishimura et al.: WAS3ABi in RIKEN Accel. Prog. Rep. 46 (2013).

Observation of Zeeman resonances of ^{84,85}Rb with OROCHI

T. Furukawa, T. Wakui, X.F. Yang, K. Imamura, T. Fujita, Y. Yamaguchi, H. Tetsuka, Y. Tsutsui, Y. Mitsuya, Y. Ichikawa, Y. Ishibashi, N. Yoshida, H. Shirai, Y. Ebara, M. Hayasaka, S. Arai, S. Muramoto, A. Hatakeyama, M. Wada, T. Sonoda, Y. Ito, T. Kobayashi,[*1] S. Nishimura, M. Nishimura, Y. Kondo, K. Yoneda, S. Kubono, Y. Ohshiro,[*2] H. Ueno, T. Shinozuka, [*3] T. Shimoda, [*4] K. Asahi, and Y. Matsuo

"OROCHI (Optical Radioisotope atom Observation in Condensed Helium as Ion-catcher)" is a new laser spectroscopy technique for low-yield exotic radioisotopes. In the OROCHI, we use superfluid helium (He II) as a stopping material for energetic RI beams produced in the projectile-fragment separators. The RI atoms stopped are subjected to in-situ laser spectroscopy in He II. The energetic ion beams introduced into He II can be stopped and trapped effectively because of the high stopping efficiency and small convection flow of He II. Thus, we can use most of the produced RIs for measurements. Furthermore, the characteristic features of the atoms immersed in He II[1], such as blue-shift and broadened absorption spectra because of the pressure of the surrounding helium liquid, enables us to reduce the detection of background photons originating from stray laser light.

Thus far, we have demonstrated successfully the feasibility of OROCHI to deduce the nuclear spins and moments with stable Rb, Cs, Ag, and Au isotopes introduced into He II by laser sputtering of sample materials[1]. In parallel to the off-line development, on-line experiments with accelerated beams of ^{85}Rb and ^{87}Rb ions (energy: both 66 MeV/u) have been performed. Recently, we have observed Zeeman resonances of introduced Rb isotopes for not only the primary ^{85}Rb (ground state, I^{π}=5/2$^-$) but also the radioactive ^{84}Rb (ground state, I^{π}=2$^-$) and ^{84m}Rb (isomer state, I^{π}=6$^-$) produced by the projectile fragmentation. In this paper, we report on the on-line experiment for measuring Zeeman resonances of Rb isotopes.

Figure 1-a) shows a schematic of our experimental setup in a superfluid helium cryostat. The ^{84,85}Rb beams from RIPS separator were injected into the cryostat filled in He II, respectively. In front of the cryostat, the injected ^{84,85}Rb were energy-degraded with two aluminum foils of various thickness for adjusting the stopping range in He II, and the number of injected ions were counted one by one with a plastic scintillator. Magnetic field of 0—5 Gauss are applied to the stopping position of ^{84,85}Rb with a set of coils ("B_0 coils" in Fig.1-a). The stopped Rb atoms were subjected to an irradiation of a CW pumping laser light (Ti:Sapphire laser; power: 100 mW; spot size: ϕ2 mm) and then optically pumped and polarized. The laser wavelength was tuned to the D1 absorption line of Rb atoms in He II (780 nm). The LIF photons from the laser-excited ^{84,85}Rb atoms were collected, wavelength-separated, and then detected with a photo detection system[2]. We apply a radio frequency wave (1 MHz) using a set of coils ("RF coils" in Fig.1-a) to the optically-pumped atoms by sweeping the magnetic field strength, and performed the laser-rf double resonance to observe the Zeeman splitting energies.

Figure 1-b) shows the time evolution of the observed photon intensity from ^{84}Rb atoms with sweeping the magnetic field strength. The horizontal axis indicates the variation in the applied field strength: B_0 = 3.4 Gauss at time t=500 ms gradually decreased to 0 Gauss at t=625 ms, and increased again to 3.4 Gauss at t=750 ms. We observed the laser-rf double resonance signals at t =580 ms and 670 ms, both corresponding to the same magnetic field strength. Note that the large peak at t=625 ms is the peak of B_0 =0

From the Zeeman resonance frequencies, we successfully deduced the nuclear spin values of ^{84,85}Rb. The beam intensity of the introduced Rb isotopes is typically 10^4 — 10^5 ions/s in both experiments. The typical yield required for OROCHI is estimated to be 10^3 ions/s with the present setup. This required yield is dominantly limited by the background counts on the photon detector owing to huge stray laser light. We plan to reduce the required yield to as small as 10 ions/s after the improvement of the setup through reduction of the stray laser light.

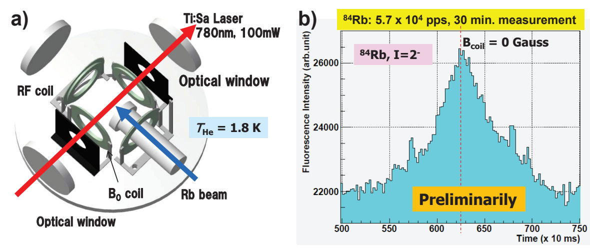

Fig. 1. a) Schematic of the experimental setup inside the cryostat. b) Laser-RF double resonance spectrum of ^{84}Rb. We can see the resonance peak at t=570 ms and 680 ms beside of the large peak of B_0=0 at 625 ms (see text).

References
1) T. Furukawa et al.: Hyp. Int. **196**, 191 (2010).
2) A. Sasaki et al.: RIKEN. APR. **44**, 204 (2011).

*1 Laser Technology Laboratory, RIKEN
*2 Center for Nuclear Study, University of Tokyo
*3 Cyclotron Radioisotope Center, Tohoku University
*4 Department of Physics, Osaka University

First online mass measurement with MRTOF mass spectrograph

Y. Ito, P. Schury, M. Wada, S. Naimi, T. Sonoda, H. Mita, F. Arai, A. Takamine, K. Okada, H. Wollnik, and A. Ozawa

Mass measurements of exotic nuclei, providing direct measure of the nuclear binding energy, are invaluable for nuclear structure and nuclear astrophysics. They require fast measurement time and high efficiency, because of their typically short lifetimes ($T_{1/2} < 100$ ms) and low production yields. As reported previously[1], there is great potential for using a multi-reflection time-of-flight mass spectrograph (MRTOF) for precision measurements of heavy, short-lived nuclei.

Recently, we performed the online commissioning experiment of MRTOF with unstable nucleus ^{8}Li, produced at RIPS and converted to a low-energy ion beam by the prototype SLOWRI, which was previously used for laser spectroscopy of Be isotopes[2]. Prior to being analyzed by the MRTOF, ions were prepared in a sequential pair of buffer gas-filled rf ion traps[3].

Ideally, an isobaric doublet measurement would be performed to determine the mass from the time-of-flight (ToF). In the case of ^{8}Li^{+}, however, the only

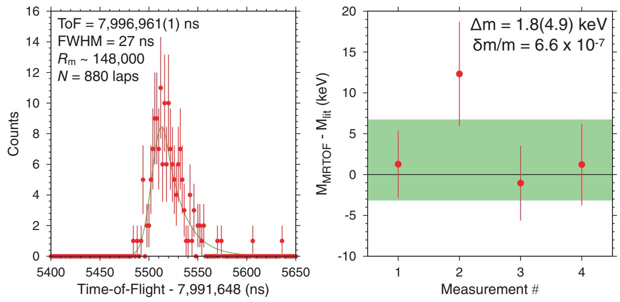

Fig. 1. Typical time-of-flight spectrum with a fit for ^{8}Li^{+} after 880 laps in the MRTOF (left) and the mass deviations from the literature value for each measurements (right). The green band shows the uncertainty of weighted averaged mass deviation. The mass resolving power, weighted mass deviation and mass precision are described in figures.

isobaric reference available was ^{4}He$_2^{+}$, the rate of which was too small to use as reference, so ^{12}C^{+} was used as a reference. Typical ToF spectra for ^{8}Li^{+} is shown in Fig. 1. The spectrum of ^{8}Li^{+} were each accumulated for 600 s, while ^{12}C^{+} only required 50 s. In order to properly take the tail into account, a Gaussian with exponential tail fitting function was used[4]. To compensate for ToF drift caused by slight voltage drifts, measurements of ^{8}Li^{+} interleaved those of ^{12}C^{+}. The ToF of ^{12}C^{+}, t_{12}, was determined by linear interpolation of ^{12}C^{+} ToFs, before and after each ^{8}Li^{+} measurement. In principle, the relationship of the mass to the ToF is given by $t = a\sqrt{m} + t_0$, where t_0 is a constant time offset. If $t_0 \ll t$, the mass of ^{8}Li^{+} can be calculated as

$$m_8 = (t_8/t_{12})^2 \cdot m_{12}. \quad (1)$$

In practice, constant time offset, measured to be t_0 = 199.0(1.3) ns, was subtracted from each ToF data prior to application of Eq. 1. Figure 1 shows the mass deviations of each ^{8}Li^{+}. In addition to the statistical uncertainties, $\delta t_0 = 10$ ns was added as the systematic uncertainty, considering 1.3 ns uncertainty and the estimated propagation time to pick up the switching noise in the t_0 measurement. The weighted average deviation of ^{8}Li^{+} was found to be $\Delta m = 1.8(4.9)$ keV, corresponding to a relative mass uncertainty of $\delta m/m = 6.6\times10^{-7}$. To confirm this method, the masses of ^{7}Li^{+} and ^{9}Be^{+} were similarly measured and found to deviate from known values by $\Delta m = 4.3(5.0)$ keV and $\Delta m = 4.2(5.1)$ keV, respectively.

An expansion of Eq. (1) up to the 1st order in (t_0/t_{12}), with t_0 accounted for, yields

$$m_8 = m_{12} \cdot \left(\frac{t_8}{t_{12}}\right)^2 + 2m_{12} \cdot \frac{t_8(t_8 - t_{12})}{t_{12}^3} \cdot t_0. \quad (2)$$

From Eq. 2, this ^{8}Li^{+} measurement truly represents a worst-case scenario for the MRTOF because of the large fractional mass difference between ^{8}Li^{+} and ^{12}C^{+}, which would not occur in any measurement of heavy nuclei. The systematic error from t_0 is maximal in this case. For measurement near $A/q \sim 100$ using a neighboring mass numbered reference, the systematic error would be reduced by an order of magnitude; for an isobaric reference, it would be negligibly small.

Despite this worst-case scenario, we achieve mass precision competitive with conventional PTMS of short-lived nuclei, but with shorter observation times. We have verified the accuracy of the technique online. For short-lived, heavy nuclei such as trans-uranium nuclei and nuclei important to r-process nucleosynthesis, we believe this new method will truly be a boon. We plan to begin measurements of trans-uranium elements and of r-process nuclei in FY2013.

References
1) P. Schury *et al.*: RIKEN Accel. Prog. Rep. **44**, 166 (2011).
2) M. Wada *et al.*: Phys. Rev. Lett. **101**, 212502 (2008).
3) Y. Ito *et al.*: RIKEN Accel. Prog. Rep. **45**, 149 (2012).
4) M. Koskelo *et al.*: Comp. Phys. Commun. **24**, 11 (1981).

First electron scattering off ^{132}Xe under the ERIS-SCRIT scheme

M. Wakasugi, T. Ohnishi, S. Wang, M. Togasaki, A. Ogawara, T. Amagai, T. Miyamoto, Y. Shimakura, K. Yanagi, T. Adachi, A.Enomoto, T. Yamaguchi, T. Hori, M. Hara, S. Ichikawa, K. Kurita, T. Tamae, and T. Suda

The SCRIT electron scattering facility[1)] is now under construction at RIBF in Nishina Center. The SCRIT device inserted in the electron storage ring (SR2) was connected to an ISOL system involving an RI target ion source, ERIS (Electron-beam-driven RI separator for SCRIT). Commissioning of the ERIS has been successfully curried out using stable Xe isotopes in last year.[2)] We conducted electron scattering experiments for ^{132}Xe isotope supplied by the ERIS in this year. In these experiments, ion-trapping properties in the SCRIT has been investigated and elastically scattered electrons from ^{132}Xe have been measured.

A pulsed ^{132}Xe ion beams containing $N_0 \sim 10^8$ ions/pulse with the duration of 300 μs was produced by beam chopping after mass separation in the ERIS. They were injected and trapped for appropriate trapping time in the SCRIT. Trapped ions were ejected form the SCRIT and transported to an analyzer to measure the number of total charge, Q, and the charge state distribution. On the other hand, the number of ions, N_{coll}, participating in collision with electron beam was measure by an electron beam loss monitor, which consists of a couple of plastic scintillators placed downstream of the SCRIT and is used as an online luminosity monitor. Observables Q and N_{coll} are expressed by $Q = \bar{q}\epsilon_t N_0$ and $N_{coll} = \epsilon_t \epsilon_0 N_0$, respectively, where is $\bar{q}$ an average charge state, ϵ_t is a trapping efficiency, and ϵ_0 is a geometrical overlap factor between the ^{132}Xe ion cloud and the electron beam. Assuming $\bar{q} \sim 1$ for short trapping time ($\sim$45 ms), ϵ_t is obtained from measured Q and N_0. Since the collision luminosity, L, the beam cross-section, a, and the electron beam current, I, were measured, N_{coll} is determined from the relation $L = N_{coll} I/a$.

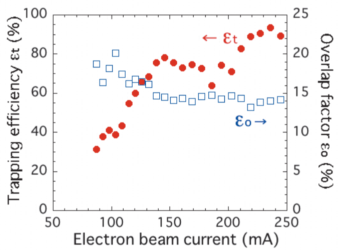

Fig. 1. Trapping efficiency ϵ_t (closed symbols) and overlap factor ϵ_0 (open symbols) as functions of the beam current.

Figure 1 shows the deduced trapping efficiency and the overlap factor as a function of the current. Most of injected ions, roughly 90%, were trapped and the overlap factor was about 15% at over 200 mA of the current. In this time the luminosity was reached to about 4×10^{26} /(cm^{2}s) as shown in Fig. 2 (a). The luminosity decays and the typical lifetime was τ=1.2 s (see Fig. 2 (b)). We found in this measurement that these trapping properties strongly depend on the electron beam instability,[3)] which is controllable by tuning an RF cavity condition. This suggests that there is possibility to control trapping properties by controlling beam instability.

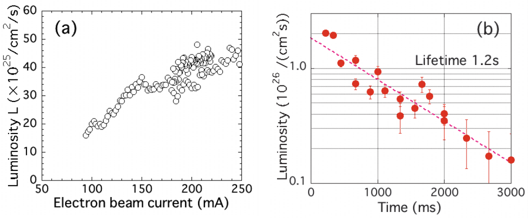

Fig. 2. The collision luminosity (a) and the decay of the luminosity (b).

At the current of 200 mA and the energy of 150 MeV for electron beams, we measured elastically scattered electrons from the ^{132}Xe trapped in the SCRIT. Electron detector is combination of a drift chamber and two calorie meters (CsI and BaF$_2$ crystal arrays). Scattering angle is covered from 25–45 degrees, and the solid angle is about 17 msr. We observed about 200 events of elastic scattering in a measurement for 4 hours. Preliminary obtained angular distribution of the elastic events is shown in Fig. 3. They are well agreement with cross section curve calculated using DRAPHA.[4)] Here we could confirm averaged luminosity during measurement to be about 4×10^{26} /(cm^{2}s).

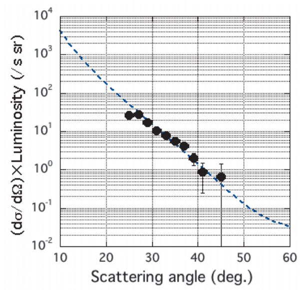

Fig. 3. Angular distribution of elastic scattering events.

References

1) M. Wakasugi et al., Phys. Rev. Lett. **100**, 164801 (2008).
2) T. Ohnishi et al., in this report.
3) R. Ogawara et al., in this report.
4) B. Dreper, DRAPHA, a phase-shift calculation code for elastic electron scattering.

Present status of the rare-RI ring construction

Y. Yamaguchi, M. Wakasugi, Y. Abe, T. Fujinawa, M. Kase, M. Komiyama, K. Kumagai, T.Maie, D. Nagae, J. Ohnishi, A. Ozawa, F. Suzaki, T. Uesaka, Y. Watanabe, T. Yamaguchi, H. Yamasawa, Y. Yanagisawa, J. Zenihiro, and Y. Yano

Construction of the rare-RI ring started in the beginng of April 2012. We report on its present status.

We first began construction of the infrastructure. Installation of an overhead traveling crane with transfer bridges[1)] was finished at the end of September 2012. Installation of a large stage was necessary to keep the beam level the same as SHARAQ. Construction of this stage, the height of which is 3.3 m, was completed at the end of November 2012. An AC power system[2)], the capacity of which is 3.2 MVA, was installed at the end of December 2012. Base line/point measurements and leveling for alignment of the devices were completed at the middle of January 2013. Installation of a water cooling system[3)] and a compressed air system was completed at the end of January 2013. Figure 1 shows the infrastructure at the K4 room. The construction of these infrastructures proceeded smoothly.

Recently, we decided the final placement of the injection line, the septums, the kicker, and the ring, as shown in Fig. 2. The injection line consists of ten quadrupole magnets and one dipole magnet with about 15.7 degrees bend. Two quadrupole magnets are located in the E20 room to transport a particle from the SHARAQ efficiently. The septum, which is operated as a DC magnet, is divided into two magnets (septum1 and septum2) to reduce the load exerted on it. The bending angles of septum1 and septum2 are 12.7 and 5.3 degrees, respectively. After passing septum magnets, a particle is injected into the ring from outside ($x = 90$ mm). The phase advance from the septum end to the kicker center is about $3\pi/2$. The injected particle is transported to the kicker with a betatron oscillation, and it is then kicked into the equilibrium ring orbit. The kicker is also used for extraction[4)], and the specifications of the septum for extraction are the same as those for injection. The ring consists of six magnetic sectors, and each magnetic sector consists of four dipole magnets. Some specifications for the ring are summarized in Table 1. This dipole is a rectangular bending magnet with a radially homogeneous magnetic field. We install ten trim coils in the two outer dipoles among the four dipoles in each magnetic sector to form a precise isochrnous magnetic field in the ring. According to our simulations, we can adjust an isochronism to within 3×10^{-6} for a momentum acceptance of $\pm 0.5\%$[5)]. The installation of the magnets, vacuum chambers, and power supplies will be completed by the end of March 2013.

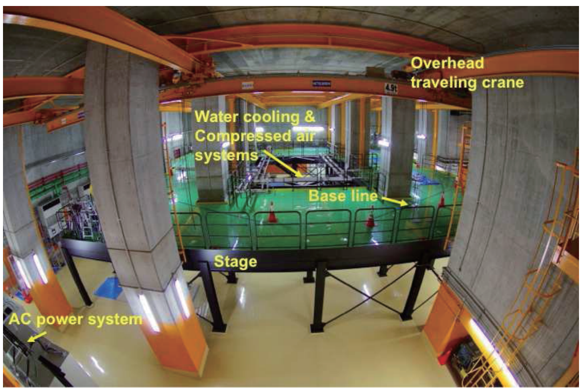

Fig. 1. Photograph of the completed infrastructure.

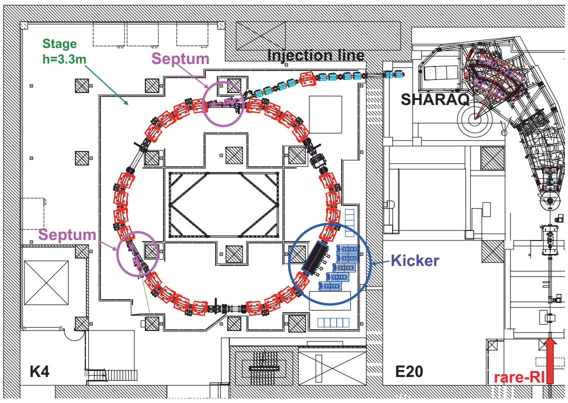

Fig. 2. Final placement of the injection line, septums, kicker, and ring.

Table 1. Specifications for the ring.

Circumference: 60.3507 m
Momentum acceptance: $\pm 0.5\%$
Revolution frequency (200 MeV/u): 2.82 MHz
Transition γ_{tr}: 1.2147
Tune: Q_x 1.25, Q_y 0.82
Max. β function: β_x 9.2 m, β_y 12.2 m
Dispersion of straight section: 66.9 mm/%

References
1) T. Fujinawa et al.: In this report.
2) T. Fujinawa et al.: In this report.
3) T. Fujinawa et al.: In this report.
4) Y. Yamaguchi et al.: In this report.
5) J. Ohnishi et al.: In this report.

Glauber-model analysis of total reaction cross sections for neutron-rich nuclei with Skyrme-Hartree-Fock densities†

W. Horiuchi, T. Inakura,[*1] T. Nakatsukasa, and Y. Suzuki

Advances in measurements of unstable nuclei have been providing information on exotic nuclei toward the neutron and proton driplines. Recently, total reaction or interaction cross sections were measured in pf-shell region[1)2)]. They exhibit interesting trends that indicate on exotic structure, for example, halos, skins, deformations etc., as the driplines are approached. Here, we focus on the nuclear deformation. If the intrinsic wave function shows some deformation, the nuclear radius becomes effectively large because the ground-state wave function is expressed as a superposition of the intrinsic wave functions with different orientations. Since the total reaction cross sections are closely related to the nuclear radius, it is interesting to investigate the relationship with the nuclear deformation.

In this work, we systematically analysed the total reaction cross sections, on a ^{12}C target, of unstable nuclei in the sd- and pf-shell region, focusing on nuclear size properties, especially radius and deformation, and their relationship with the cross section. We employ the Glauber model, which is widely used for analysing high energy nuclear reactions. In order to describe exotic deformations, input densities are generated from the wave functions obtained by the Skyrme-Hartree-Fock Method in a fully three-dimensional coordinate space. Both structure and reaction models employed here have no adjustable parameter.

Figure 1 presents the quadrupole deformation parameters β of Ne isotopes obtained from the Hartree-Fock solutions. The positive (negative) values of β indicate prolate (oblate) deformations. Beyond $N = 16$, we find a significant difference in the magnitude of β, between two types of interactions employed here, SkM* and SLy4. In the SkM* calculation, the deformation parameter β is positive and rapidly increases for $N > 18$. On the other hand, SLy4 predicts nearly spherical ground states (weakly oblate) for $N > 20$ and changes its shape into prolate for $N > 20$. The value of $|\beta|$ is always larger in SkM* for $18 < N < 24$.

This corresponds well with the observation of different behavior in the calculated total reaction cross sections of Ne isotopes incident on a ^{12}C target at 240 A MeV, shown in Figure 2, as a function of neutron number N. The agreement with recent data[2)] is very good. The slope of the curve in the figure changes at $N = 14$. The cross section increases gradually from $N = 10$ to 14 and shows a rapid rise above $N = 14$. The kink behavior can be explained by the onset of the deformation at $N > 20$, while the kink at $N = 14$ is due to the occupation of the $s_{1/2}$ orbitals at $N > 14$. The cross sections coincide again at $N = 24$, so do the predicted β values.

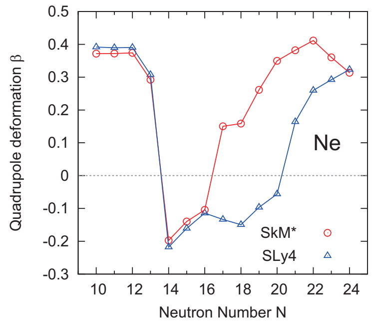

Fig. 1. Quadrupole deformation parameter β of Ne isotopes calculated with the SkM* and SLy4 interactions.

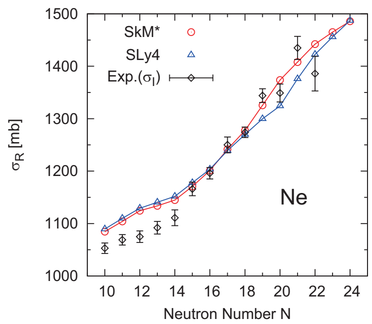

Fig. 2. Total reaction cross sections of Ne isotopes on a ^{12}C target at 240 AMeV. Experimental data are the interaction cross sections taken from Ref.[2)].

A similar trend in the total reaction cross sections is expected for Mg isotopes whose deformation behavior is similar to that of Ne isotopes. In Ref.[3)], we presented analysis for Mg isotopes as well as Si and S isotopes. The systematic measurements of σ_R (σ_I) for a long chain of isotopes may reveal the enhancement of the nuclear size, which can be a signature of the nuclear deformation.

References

1) R. Kanungo *et al.*: Phys. Rev. C **83**, 021302 (R) (2011).
2) M. Takechi *et al.*: Phys. Lett. **B707**, 357 (2012).
3) W. Horiuchi, T. Inakura, T. Nakatsukasa, and Y. Suzuki: Phys. Rev. C **86**, 024614 (2012).

† Condensed from the article in Phys. Rev. C **86**, 024614 (2012).
*1 Department of Physics, Chiba University

PHENIX silicon vertex tracker (VTX)

Y. Akiba, R. Akimoto, H. Asano, S. Bathe, S. Baumgart, K. Boyle, J. Bryslawskyj,[*1] C-H. Chen, L. Ding,[*2] A. Enokizono, S. Esumi,[*3] T. Hachiya, S. Horiuchi,[*3] J. Koster, K. Kurita,[*4] M. Kurosawa, A. Lebedev,[*2] M. McCumber,[*5] H. Nakagomi,[*3] R. Nouicer, C. Ogilvie,[*2] H. Sako, S. Sato, A. Shaver,[*2] M. Shimomura, M. Stepanov,[*6] A. Taketani, M. Wysocki,[*7] and the PHENIX VTX group

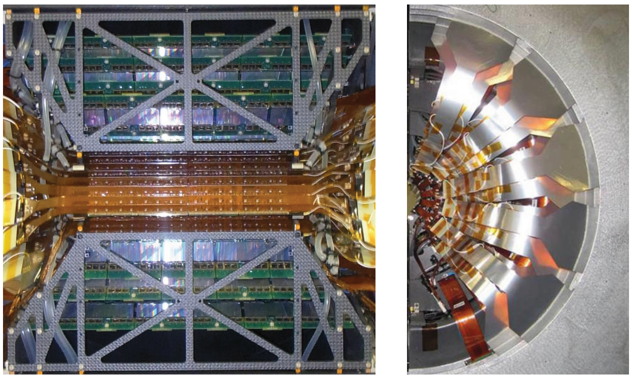

Fig. 1. A photograph of a half of the VTX detector. Left: side view. Right: Beam view.

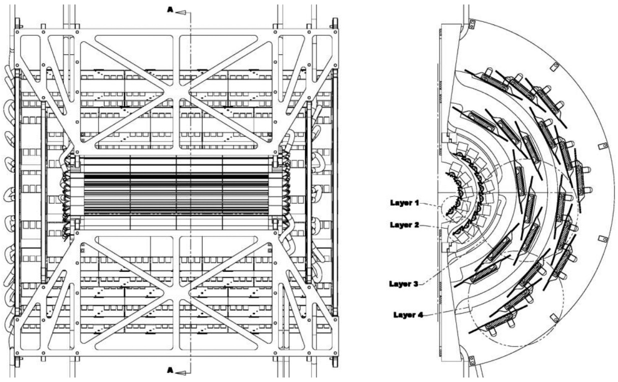

Fig. 2. A mechanical design drawing of the VTX

We have constructed a silicon vertex tracker (VTX) for the PHENIX experiment at RHIC. The primary purpose of the detector is to carry out precise measurements of heavy-quark (charm and beauty quarks) production in $A+A$, $p(d)+A$, and polarized $p+p$ collisions. The detector was jointly funded by RIKEN and the US-DOE.

The main topics in physics that can be studied using the VTX are as follows.

- Probing Quark Gluon Plasma (QGP) formed in collision of heavy nuclei such as Au+Au.
  - Energy loss of heavy quarks (charm and bottom quarks) in QGP
  - Elliptic flow of heavy quarks in QGP
  - Open charm and bottom production
  - Medium-induced modification of jets
- Study of the structure of the proton, in particular, that related to gluons.
  - Determination of gluon polarization $\Delta G(x)$ from heavy-quark measurements
  - Determination of $\Delta G(x)$ from γ-jet measurements
  - Measurement of transverse spin asymmetry A_N of charm and bottom production
- Nucleon structure in nuclei
  - Gluon shadowing over a broad x range

These measurements will be key measurements of RHIC programs in the next several years, for studying both QGP and the proton structure.

The VTX was constructed and was installed in PHENIX by the end of 2010. Fig. 1 shows a photograph of the VTX detector, and Fig. 2 is a corresponding mechanical drawing of the detector. The detector consists of four layers of silicon detectors. The inner two layers are pixel detectors (approximately 3.93M channels of 50μm $\times 425\mu$m pixels) and the outer two layers are strip detectors (approximately 344K channels of 80μm $\times$ 30mm strips).

The detector was successfully commissioned during

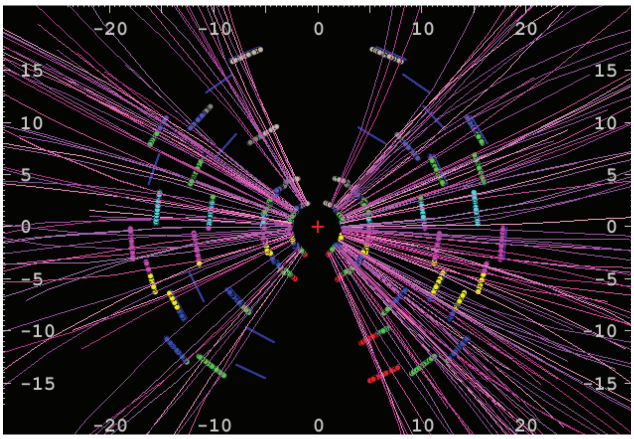

Fig. 3. Event display of VTX for a Au+Au collision.

*1 Baruch College, CUNY, USA
*2 Iowa State University, USA
*3 University of Tsukuba, Japan
*4 Rikkyo University, Japan
*5 University of Colorado, USA
*6 University of Massachusetts, USA
*7 Oak Ridge National Laboratory, USA

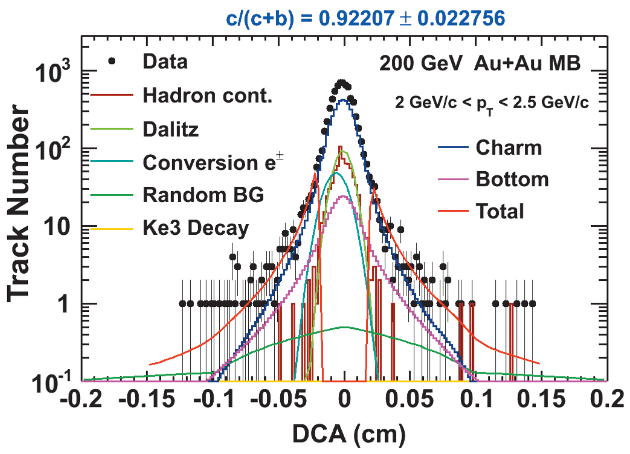

Fig. 4. DCA distribution of electrons for $2 < p_T < 2.5$ GeV/c in Au+Au collisions at $\sqrt{s_{NN}} = 200$GeV.

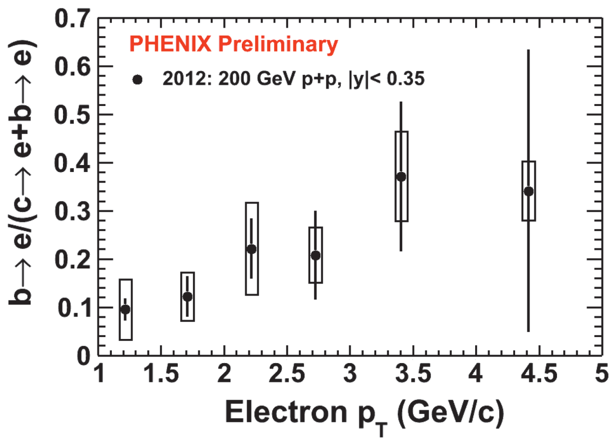

Fig. 5. $(b \to e)/(b \to e + c \to e)$ ratio in $p + p$ at $\sqrt{s} =$ 200GeV.

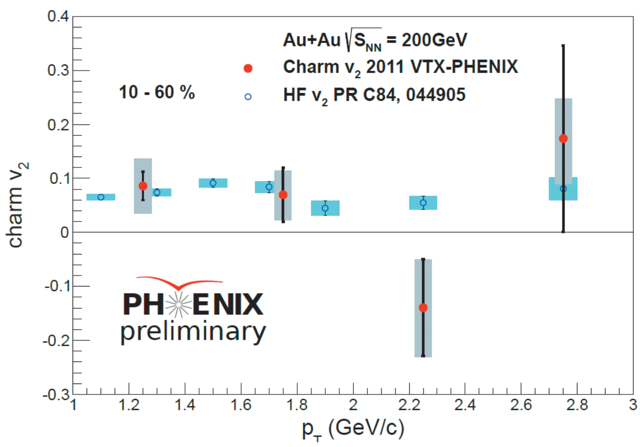

Fig. 6. Elliptic flow strength v_2 of charm decay electrons in 10-60% centrality of Au+Au collisions.

the 500 GeV $p + p$ run in RUN11 of RHIC. Subsequently, we collected 5 billion Au+Au events in RUN11. In RUN12, we obtained approximately 11/pb of p+p data at 510 GeV, 3/pb of p+p data at 200 GeV, 110/μb ($\simeq$ 6/pb of $N + N$) of U+U at 193 GeV, and 2.9/nb ($\simeq$ 36/pb of $N + N$) of Cu+Au at 200 GeV, within the VTX acceptance. Fig. 3 shows an event display of Au+Au collisions measured by the VTX detector.

We have developed the analysis code of the VTX[1]. A stand-alone tracking code for the VTX is used to reconstruct the collision vertex with high precision. Simulation studies show that a vertex position resolution of approximately 20 μm can be achieved.

One of the most important data analysis tasks is the precise alignment of the detector ladders[2]. A track from the PHENIX central arms is associated with the hits in VTX detectors, and the distance of closest approach (DCA) between the track and the collision vertex is measured. A DCA resolution of approximately 80 μm in the X-Y plane is achieved for $p_T > 1$ GeV/c for the RUN11 Au+Au data.

We have obtained several preliminary results of the VTX analysis in RUN11 Au+Au data and RUN12 p+p data at 200 GeV. By confirming a central arm track with hits in the VTX, we can eliminate the background of fake-high p_T tracks caused by decay-in-flight and photon conversions. This significantly improves the measurement of high p_T particles[3].

The main physics goal of the VTX detector is to measure nuclear modification factor R_{AA} and the elliptic flow v_2 of charm and bottom decay electrons separately in Au+Au collisions. Fig. 4 show the DCA distribution of electrons. The curves in the figure represents the decomposed contribution of charm, bottom, photonic background, and other sources. We have statistically separated electrons from bottom decays ($b \to e$) and charm decays ($c \to e$) from the difference of their DCA distributions. Fig. 5 show the fraction of $(b \to e)/(b \to e + c \to e)$ in $p + p$[4]. We have also obtained the first results of the v_2 of charm decay electrons[5]. These results were presented in Quark Matter 2012 international conference[6] in August 2012. We are working to finalize these results for publication.

References
1) T. Hachiya et al.: In this report (2013).
2) H. Asano et al.: In this report (2013).
3) C-H. Chen et al.: In this report (2013).
4) R. Akimoto et al.: In this report (2013).
5) M. Kurosawa et al.: In this report (2013).
6) http://qm2012.bnl.gov/; Nucl. Phys. A904-905, 1c-1092c (2013).

Measurement of A_L of $W^{\pm} \to \mu^{\pm}$ at forward rapidity with PHENIX

H. Oide, N. Amano, Y. Fukao, T. Iguri, Y. Imazu, M. Kim, T. Mibe, H. Murakami, T. Murakami, J. Murata, I. Nakagawa, K.R. Nakamura, S. Park, J. Seele, R. Seidl, N. Saito, K. Tanida, I. Yoon, K. Watanabe, and S. Yamashita

Production of $W^{\pm}$ bosons in longitudinally polarized $p+p$ collisions is a parity-violating process, and it produces finite longitudinal single spin asymmetry A_L. Measurement of A_L allows to probe sea quark polarized parton distribution functions (PDFs), and it has an advantage over existing semi-inclusive deep inelastic scattering (SIDIS) experiments for probing sea quark polarized PDFs in that the experimental result does not need to be interpreted with assumption of fragmentation functions. In the PHENIX experiment, $W^{\pm} \to \mu^{\pm}$ at forward rapidity is accessible as well as $W^{\pm} \to e^{\pm}$ at mid-rapidity. In 2011, we obtained longitudinally polarized $p+p$ collision data at $\sqrt{s} = 500$ GeV of about 25 pb^{-1} in total with operating a new muon trigger system[1]. This is the first set of data that enables measurement of the cross section and A_L of $W^{\pm} \to \mu^{\pm}$. The statistics will be improved up to ~ 300 pb^{-1} at $\sqrt{s} = 510$ GeV.

The signal of $W^{\pm} \to \mu^{\pm}$ events is to have a single reconstructed track in the event. According to the simulation, $W^{\pm} \to \mu^{\pm}$ is the dominant muon production process in $p_T^{\mu} \gtrsim 15$ GeV/c. The $Z \to \mu^{\pm}$ process, which has $O(10\ \%)$ contribution compared to $W^{\pm} \to \mu^{\pm}$, is an irreducible non-zero A_L process, and we also select this process as the signal. Other irreducible muon production background processes are open heavy flavor (charm and bottom), quarkonia, and Drell-Yan (γ^*). The dominant background events come from $p_T \lesssim 3$ GeV/c charged hadrons. Even though they are low p_T, there are small chances that they leave a high-p_T-like trajectory owing to the decay in the muon tracker volume. Because of the huge production cross section of charged hadrons, these events are ~ 100 times larger background in $p_T \gtrsim 15$ GeV/c compared to the $W^{\pm} \to \mu^{\pm}$ signal, without applying serious signal selection. The strategy of signal selection requires the consistency of high-p_T muons in various tracking parameters related with multiple scattering of particles with detector materials, quality of the track reconstruction (χ^2), bending of the track in the tracker, matching of the track with the collision vertex, and the timing of the track[2]. We determined the cut threshold to keep 90% of the $W^{\pm} \to \mu^{\pm}$ signal in $p_T^{\mu} \gtrsim 10$ GeV/c for each tracking variable using PYTHIA event generator and the full detector simulation. The remaining number of events for each p_T^{μ} bin is corrected by signal acceptance and efficiency to obtain p_T^{μ} spectrum. The signal-to-background (S/BG) ratio was estimated by comparing the obtained p_T^{μ} spectrum with the simulated $W^{\pm} + Z \to \mu^{\pm}$ spectrum in the NLO level. We conservatively assigned $\times 0.5$ - $\times 2.0$ S/BG ratio uncertainty for the preliminary A_L calculation. Figure 1 shows the preliminary result of A_L of muons from $W^{\pm}/Z$ in $18 < p_T^{\mu} < 60$ GeV/c. The current uncertainty of A_L is dominated by statistics, and thus far, the impact on sea quark polarized PDFs is not significant.

Toward the final result of the 2011 data, studies of crosschecks of signal efficiency, more efficient signal selection, and cross section measurement using likelihood fitting (which does not depend on the cross section prediction with event generator simulation) are ongoing. A paper reporting the final analysis result including the above improvements is forthcoming.

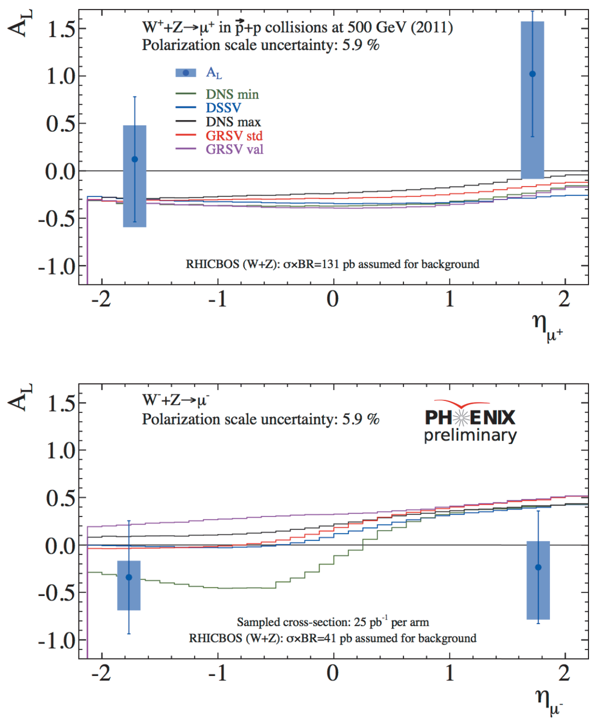

Fig. 1. Preliminary result of A_L of muons from W^+/Z (above) and W^-/Z (below) for 2011 data.

References
1) I. Nakagawa, et al.: RIKEN Accel. Prog. Rep. 45 63 (2012)
2) R. Seidl, et al.: RIKEN Accel. Prog. Rep. 45 58 (2012)

Towards understanding Kaon-induced mystery: current status and developments regarding J-PARC K1.8BR spectrometer†

Y. Ma, H. Ohnishi, Y. Sada, F. Sakuma, M. Tokuda

There are certain long-remaining puzzles regarding the hadron system containing K^- meson. Some particularly interesting topics concern the possible existence of the K^-N deeply bound state and the properties of the $\Lambda(1405)$ baryon. In order to address these questions, a carefully designed spectrometer has been constructed at the J-PARC K1.8BR beam line, where certain approved experiments (E15, E31, and E17) are to be carried out in order to understand the mystery induced by K^- meson. The details of these experiments are provided in the corresponding proposals and the full paper[1]. The present report focuses on the progress made last year in the commissioning of the K1.8BR spectrometer.

The secondary beam line, K1.8BR, is located in the Hadron Hall of the J-PARC 50-GeV proton synchrotron (PS) facility, which can provide various secondary beams with momentum up to 1.2 GeV/c. The schematic of the K1.8BR spectrometer is shown in Fig.1. The beam particles are measured and analyzed with the beam-line spectrometer located upstream of the target before its bombardment. A momentum resolution of $\sim 1\%$ has been achieved. The charged products from the reaction between the beam particles and target are measured using the cylindrical detector system (CDS) consisting of a solenoid magnet, a cylindrical drift chamber, and scintillators. The forward-flying neutrons are detected using a neutron counter (NC) constructed with plastic scintillators.

An engineering run to confirm the general performance of the spectrometer was carried out in June 2012. The results of particle identification with CDS tracking analysis are shown in Fig.2. A clear separation of π, K, p and d particles can be seen. The resolution of the CDS was estimated from the invariant mass distribution of the Λ hyperon via the $\Lambda \to \pi^- + p$ decay channel. A Gaussian resolution of $\sigma \sim 3.5$ MeV/c^2 has been obtained, which fully satisfies the designed value. An important feature of the current spectrometer is its ability to detect forward neutrons via the time-of-flight (TOF) method. The TOF spectrum obtained between a starting counter (T0) and the neutron counter is shown in Fig.3. A σ value of $\sim$150 ps corresponding to 9MeV/c^2 missing mass resolution has been obtained whereas the designed value is $\leq$10 MeV/c^2.

To summarize, the J-PARC K1.8BR spectrometer was tested during an engineering run in 2012. A satisfactory performance was obtained, and the spectrometer is currently operationally ready to under go a production run.

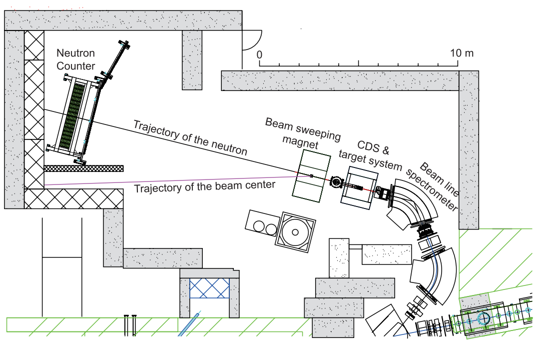

Fig. 1. Layout of K1.8BR spectrometer.

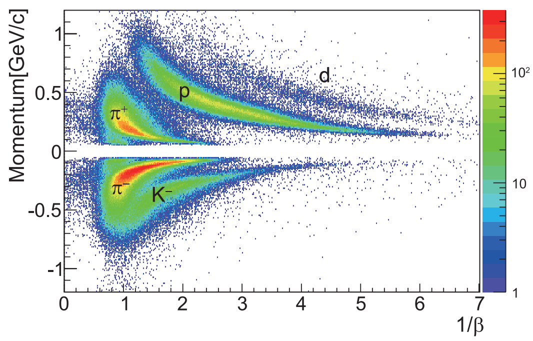

Fig. 2. Particle identification results.

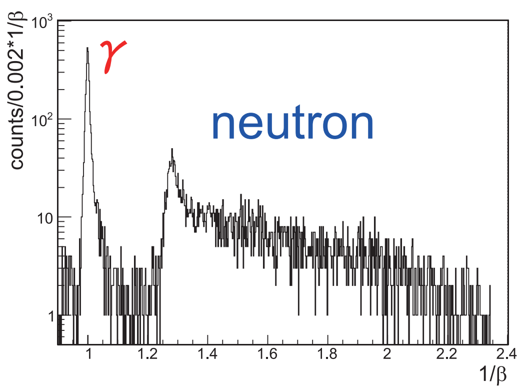

Fig. 3. Time of flight from neutron counter.

† Condensed from the article in Prog. Theor. Exp. Phys. 02B011 (2012)

References

1) F. Sakuma et al.: Prog. Theor. Exp. Phys. 02B011 (2012).

All QED contributions to lepton $g-2$ up to tenth order

T. Aoyama, M. Hayakawa, T. Kinoshita, and M. Nio

The anomalous magnetic moment of the electron, called $g-2$, plays a central role in testing the validity of quantum electrodynamics (QED). Now that we have succeeded in obtaining all QED contributions up to the tenth order of the perturbation theory, it becomes the most stringent test ever in physics.

A Harvard team measured the electron anomaly $a_e = (g-2)/2$[1]

$$a_e(\mathrm{HV}) = 1\ 159\ 652\ 180.73\ (0.28) \times 10^{-12} \quad (1)$$

with astonishing precision. The QED contributions to a_e depend on the fine-structure constant α, the coupling constant of QED, and the lepton-mass ratios between the electron and muon and between the electron and tau-lepton.[3] The value of α we used is determined by the measurement of h/m_{Rb}, the ratio of the Planck constant, and the mass of the Rb atom, combined with the very precisely known Rydberg constant and m_{Rb}/m_e[2,3]:

$$\alpha^{-1}(\mathrm{Rb}) = 137.035\ 999\ 049\ (90)\ . \quad (2)$$

With this α the theoretical prediction of a_e becomes

$$a_e(\mathrm{th}) = 1\ 159\ 652\ 181.78\ (6)(4)(2)(77) \times 10^{-12}, \quad (3)$$

which includes small but non-negligible hadronic and weak contributions. The uncertainties come from the calculated eighth-order QED term, the tenth-order QED term, the hadronic term, and the fine-structure constant, Eq. (2), from left to right. The theory, Eq. (3), is thus in good agreement with the experiment, Eq. (1), proving that QED is accurate even at this very high precision.

An alternative test of QED is to compare α of (2) with the value of α determined from the experiment and theory of $g-2$:

$$\alpha^{-1}(a_e) = 137.035\ 999\ 173\ (7)(5)(2)(34), \quad (4)$$

where the uncertainties come from the eighth-order QED term, the tenth-order term, the hadronic term, and the measurement of $a_e(\mathrm{HV})$, respectively. The fine-structure constant α is believed to be a universal constant. It is interesting to see what happens when the uncertainties of $\alpha^{-1}(a_e)$ and $\alpha^{-1}(\mathrm{Rb})$ are further improved.

There are 12672 vertex Feynman diagrams that contribute to the tenth-order $g-2$. They are divided into 32 gauge-invariant sets, as shown in Fig. 1. The contributions from the 17 sets, I(a–f), II(a,b), II(f), VI(a–c), VI(e,f), and VI(i–k), were determined previously.[4] The additional 14 sets have been also evaluated and

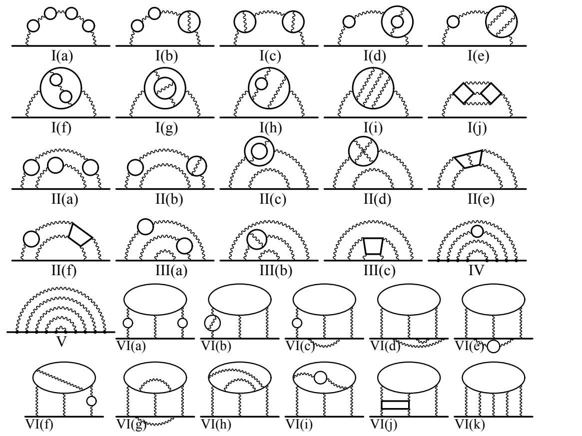

Fig. 1. Feynman diagrams contributing to the tenth-order lepton $g-2$. Typical diagrams from 32 gauge-invariant sets are shown.

reported.[5–7] The result for the final set, setV, consisting of 6354 diagrams, has been obtained recently.[8] The contribution from the eighth order has been reexamined and improved. All these achievements lead Eq. (3) and (4). As a byproduct, we evaluated all QED contributions to the muon g–2 up to the tenth order.[8] It now has a sufficiently small uncertainty to be ready for the new experiments of muon $g-2$ at J-PARC and fermilab.

References

1) D. Hanneke, S. Fogwell, and G. Gabrielse: Phys. Rev. Lett. **100**, 120801 (2008).
2) R. Bouchendira, P. Clade, S. Guellati-Khelifa, F. Nez, and F. Biraben: Phys. Rev. Lett.**106**, 080801 (2011).
3) P. J. Mohr, B. N. Taylor, and D. B. Newell: Rev. Mod. Phys. **84**, 1527 (2012).
4) T. Kinoshita and M. Nio: Phys. Rev. D **73**, 053007 (2006).
5) T. Aoyama, M. Hayakawa, T. Kinoshita, M. Nio, and N. Watanabe: Phys. Rev. D **78**, 053005 (2008).
6) T. Aoyama, K. Asano, M. Hayakawa, T. Kinoshita, M. Nio, and N. Watanabe: Phys. Rev. D**81**, 053009 (2010).
7) T. Aoyama, M. Hayakawa, T. Kinoshita, and M. Nio: Phys. Rev. D **78**, 113006 (2008); **82**, 113004 (2010); **83**, 053002 (2011); **83**, 053003 (2011); **84**, 053003 (2011); **85**, 033007 (2012); **85**, 093013 (2012).
8) T. Aoyama, M. Hayakawa, T. Kinoshita, and M. Nio: Phys. Rev. Lett.**109**, 113006 (2012); **109**, 113006 (2012).

Quarkonia spectral functions in hot matter: a study based on QCD sum rules and the maximum entropy method†

P. Gubler, K. Suzuki,*1 K. Morita, and M. Oka

The study of quarkonia in hot matter has, since the initially presented ideas[1)], evolved into a field with diverse activities in both experiment and theory. In particular, through the heavy-ion collision experiments at RHIC and LHC, a large amount of experimental data on quarkonium production in various reactions is now available, which can be compared with theoretical expectations. This task, however, has been identified as a very complex one, because a large number of competing effects need to be taken into account to describe the experimental results. The most basic inputs for these calculations are the quarkonia spectral functions, which include all the physically relevant information of the quarkonium states as well as their behavior at a finite temperature.

A useful approach for capturing information on quarkonia spectral functions at both zero and finite temperature is the QCD sum rules method. This method exploits the analytic properties of the two-point function of operators to derive certain integrals over the hadronic spectral functions (the "sum rules"), which, via the operator product expansion (OPE), can be related to a combination of perturbatively calculable quantities and non-perturbative condensates, containing information on the QCD vacuum. In the case of the quarkonia channels considered here, these are gluonic condensates, the most important one being the gluon condensate of mass dimension 4.

Recently, it has become possible to use the MEM technique to analyze QCD sum rules,[2)] which allows the most probable form of the spectral function from the OPE to be extracted without the need to use a specific functional form. This approach has since been applied to both charmonium[3)] and bottomonium[4)] channels and to summarize these results is the main goal of this article.

Let us first discuss the results of the charmonium channels. They are shown in the left-side plot in Fig. 1. By first focussing on the spectral functions at zero temperature, it is seen that clear peaks are generated, which represent the lowest state of each channel. The positions of these peaks reproduce the experimental values with a precision of about 50 MeV.

At finite temperature, we observe that the lowest peaks of all channels vanish slightly above the critical temperature T_c. The origin of this melting effect is a sudden change in the gluonic condensates around T_c, which can be related to the deconfinement transition of the gluonic matter.

† Condensed from references[3)] and[4)].

*1 Department of Physics, Tokyo Institute of Technology

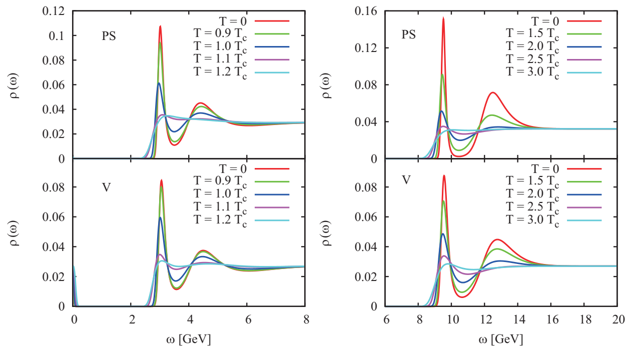

Fig. 1. Left (right) plot: Charmonium (bottomonium) spectral functions at zero and finite temperature in the pseudoscalar (top) and vector (bottom) channels, respectively.

Next, let us focus on the results for bottomonium. These are given in the right-side plot in Fig. 1. Here, as for charmonium, clear peaks are observed for each channel at zero temperature. At finite temperature, the bottomonium states are modified more gradually than their charmonium counterparts, which is in agreement with phenomenological expectations. Concretely, the spectral functions still exhibit a clear peak at $T = 2.0\,T_c$ which starts to dissolve at about $2.5\,T_c$. The reason for the robustness of the bottomonium states can be traced back to the fact that the gluon condensate terms in the OPE are proportional to $1/m_h^4$, with m_h being the quark mass. These are the driving terms for quarkonium melting and are therefore relatively suppressed for the bottomonium sum rules.

In summary, by combining the techniques of QCD sum rules and MEM, we have extracted the spectral functions from the OPE. As a result, it is found that the charmonium ground states dissolve into the continuum already existing at temperatures around T_c, while the bottomonium states are more stable and survive up to about 2.5 T_c.

References

1) T. Matsui and H. Satz: Phys. Lett. B **178**, 416 (1986).
2) P. Gubler and M. Oka: Prog. Theor. Phys. **124**, 995 (2010).
3) P. Gubler, K. Morita and M. Oka: Phys. Rev. Lett. **107**, 092003 (2011).
4) K. Suzuki, P. Gubler, K. Morita and M. Oka: Nucl. Phys. **A897**, 28 (2013).

Superconducting properties of $LaPt_3Si$ studied by μSR

I. Kawasaki, I. Watanabe, H. Amitsuka,[*1] K. Kunimori,[*2] H. Tanida, and Y. Ōnuki[*3,*4]

Since the discovery of the first heavy fermion noncentrosymmetric superconductor $CePt_3Si$,[1)] there has been considerable interest in superconductors that lack inversion symmetry. The superconducting (SC) order parameters in these superconductors cannot be classified in terms of parity, and the coexistence of spin-singlet and spin-triplet states is allowed.[2)] Therefore, unconventional SC properties are expected.

$LaPt_3Si$ (T_{sc}=0.65 K), which is isostructural with $CePt_3Si$, shows no sign of magnetic order or strong electronic correlation, and thus, it is expected to be an ideal system to study the effect of the lack of inversion symmetry on the SC state.[1)] A recent Josephson-effect study revealed an anomalous magnetic field dependence of the Josephson critical current that differs from the conventional Fraunhofer pattern and that breaks the time reversal symmetry.[3)] This suggests that $LaPt_3Si$ cannot be classified as a conventional s-wave superconductor.

In the present study, we performed zero-field and transverse-field μSR experiments on polycrystalline samples of $LaPt_3Si$ to investigate their SC properties. The μSR experiments were carried out at the RIKEN-RAL Muon Facility in the UK, where an intense pulsed muon beam is available.

Figure 1 shows the zero-field-μSR spectra measured at 60 and 870 mK, which are well below and above T_{sc}, respectively. These spectra were well fit by the following function: $P(t) = A_0 e^{-\lambda t} G_{KT}(t) + A_{bg}$, where A_0 is the initial asymmetry at t=0, λ is the electronic relaxation rate, and A_{bg} is the background signal. The function G_{KT} is the Gaussian Kubo-Toyabe relaxation function. As shown in Fig. 1, the observed relaxation spectra do not show any noticeable change below T_{sc} within the experimental accuracy, indicating that time reversal symmetry is conserved within the experimental accuracy of the μSR spectroscopy technique.

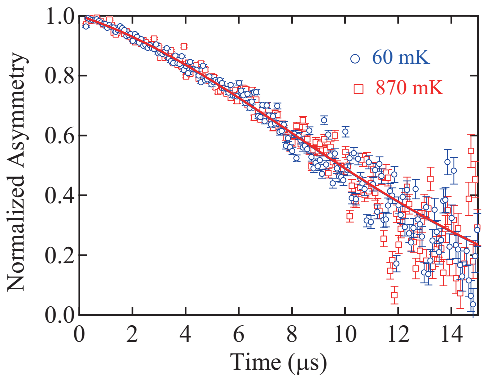

Fig. 1. Zero-field-μSR spectra measured at 60 and 870 mK.

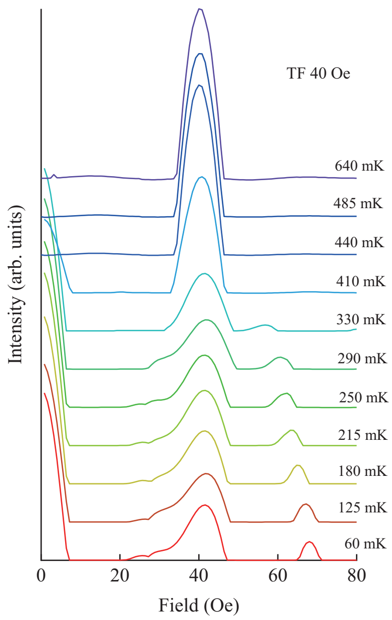

Fig. 2. Maximum entropy spectra of transverse-field-μSR data measured in a field of 40 Oe.

The transverse-field-μSR experiments were performed at a field of 40 Oe under field-cooled conditions. To analyze the spectra, we performed a Fourier transform using the maximum entropy technique; the obtained field distributions are shown in Fig. 2. In the high temperature, the spectra consist of a single peak. In contrast, in the low temperature range, where the sample is in the SC state, two additional components appear. These components are reminiscent of the intermediate state in a type-I superconductor[4,5)]. The component appearing in the lower field region arises from the Meissner state, and the higher field peak is attributed to the normal state of the sample. Therefore, this result suggests that $LaPt_3Si$ has a type-I character.

*1 Department of Physics, Hokkaido University
*2 Department of Quantum Matter, ADSM, Hiroshima University
*3 Advanced Science Research Center, Japan Atomic Energy Agency
*4 Graduate School of Science, Osaka University

References

1) E. Bauer *et al.*: Phys. Rev. Lett. **92** (2004) 027003.
2) L. P. Gor'kov and E. Rashba: Phys. Rev. Lett. **87** (2001) 037004.
3) Y. Aoki *et al.*: J. Phys. Soc. Jpn. **79** (2010) 124707.
4) V. K. Anand *et al.*: Phys. Rev. B **83** (2011) 064522.
5) A. J. Drew *et al.*: Physica B **374-375** (2006) 270.

μSR experiments on Al–Mg–Si alloys†

S. Wenner,[*1] K. Matsuda, K. Nishimura, T. Matsuzaki, D. Tomono, F. L. Pratt, C. D. Marioara,[*2] and R. Holmestad[*1]

Al–Mg–Si alloys are used extensively as structural materials due to their formability, mechanical strength, and corrosion resistance. They are heat-treatable, meaning that diffusion-controlled phase transformations are responsible for the most important hardening mechanisms. To enable substitutional diffusion in the Al matrix, a high concentration of vacancies is required. Mg–Si–vacancy clustering is the first step of the precipitation of hardening phases and happens even during storage at room temperature (RT). Muon spin methods are very sensitive to vacancies and can yield information about the environments around them.

We have applied muon spin relaxation to samples of Al–Mg–Si alloys with industrially relevant compositions and heat treatments. All samples were given a solution heat treatment (SHT) at 575°C for 1 hour before quenching and further heat treatments. Muon spin relaxation functions were measured at temperatures from 20 K to 300 K (achieved by helium cryostat cooling), as the kinetics of muons inside aluminium is heavily temperature-dependent.

To understand what factors influence the shapes of the relaxation functions, we simulate the muon kinetics with a Monte Carlo (MC) algorithm. The simulation includes muon trapping by defects, similar to improved Kubo–Toyabe methods.[1,2] Simulated relaxation functions are fitted to experimental ones, using physical quantities as fitting parameters. The resulting temperature variation of the muon trapping rate is shown for five selected samples in Fig. 1. We focus on the effects of RT storage in this report.

Muons are trapped by different defects at different temperatures, specifically defects of lower concentration at higher temperatures. The pure Al peak at 5–40 K has been observed earlier, for Al with 42 and 70 ppm Mn[3] and Al with 117 ppm Ag.[4] Its height was found to increase with the concentration of the trace elements. A peak is present at the same location in the alloy curves, showing muon trapping by Mg and Si atoms in solid solution. A saturation point is likely reached as the peak does not change upon altering the Mg and Si content.

Samples straight from quenching should include more vacancies than RT stored samples. In the 1.6% Mg_2Si samples, the only difference seen after RT storage is a decreased trapping at the highest temperatures. By *in situ* μSR studies of pure Al, vacancies were confirmed to trap muons at temperatures around 300 K.[5] While the as-quenched 1.6% Mg_2Si and ≈1.4% MgSi samples have almost identical muon kinetics, differences appear after RT storage. The muon trapping rate is lower for ≈1.4% MgSi in the range 140–240 K. The trapping site for this region is most likely also a vacancy, itself trapped in a beginning Mg–Si cluster. From the higher trapping in 1.6% Mg_2Si, we find either that (i) vacancies are more strongly bound in Mg-rich clusters than Mg-Si balanced ones, preventing their escape from the material, or (ii) muons are more strongly bound in vacancies with Mg-rich environments.

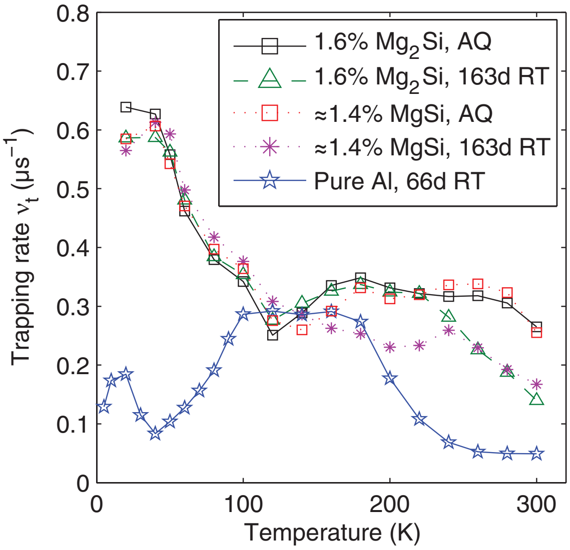

Fig. 1. Muon trapping rates for Al–Mg–Si alloys. The samples are either room temperature (RT) stored for many days (d) or as quenched (AQ) after SHT.

References
1) Hatano, T. et al.: Hyperfine Interact. **17**, 211 (1984).
2) Boekema, C. et al.: Phys. Rev. B **26**, 2341 (1982).
3) Niinikoski, T. et al.: Physica B+C **108**, 879 (1981).
4) Hartmann, O. et al.: Hyperfine Interact. **17**, 197 (1984).
5) Wenner, S. et al.: Proc. 13th Int. Conf. on Aluminium Alloys (2012), p. 37.

† Condensed from the article in Phys. Rev. B, Vol.86, 104201 (2012)
*1 Department of Physics, NTNU, Høgskoleringen 5, Trondheim NO-7491, Norway
*2 Materials and Chemistry, SINTEF, Box 4760 Sluppen, Trondheim NO-7465, Norway

High yield mutants of rice induced by C-ion beam irradiation

Y. Hayashi, R. Morita, H. Tokairin, S. Kogure, K. Ichinose, T. Wakana, T. Sato,*1 and T. Abe

Rice is a staple food for a majority of populations around the world. Increase in crop production is necessary to respond the global population growth. Development of high yield rice potentially contributes as the solution to the food problems faced by the world. Grain yield is one of the most important agricultural factors in the productivity of rice. We report on the high yield mutants of rice showing a tall phenotype with higher number of spikelets induced by C-ion beam irradiation (Fig. 1).

The imbibition seeds of rice (*Oryza sativa* L. cv. Nipponbare) were exposed to C-ions accelerated to 135 MeV/nucleon. M_1 plants were grown in a paddy field and M_2 seeds were harvested separately from each M_1 plant. Two tall mutants, 14-45 and 40-L, were isolated in the paddy field research. Then, 14-45 was selected from the M_2 populations of 20 Gy (37.4 keV/μm), and 40-L was selected from the M_3 populations of 40 Gy (22.5 keV/μm). In M_2 generation, 40-L was segregated into the dwarf and wild-type phenotypes. The M_3 population, which was segregated into the dwarf, wild type, and tall phenotypes, was derived from M_2 having the dwarf phenotype.

We conducted a yield survey for the tall mutant lines at the research paddy field of Tohoku University in Miyagi prefecture in 2011. Nipponbare was used as a control. There were 49 plants of each line, grown in one plot with 3 replications. To avoid the border effect, 25 plants from the inner plot (1.44 m^2) were collected. We measured the yield components (panicle number, panicle weight, panicle length, spikelet number, seed fertility, grain weight); plant height, and number of rachis branches per panicle. Most yield components were measured from the panicles on the main culms.

Results in terms of the plant height, yield, and components are presented in Tables 1 and 2. Specifically, 14-45 and 40-L showed a high plant height, about 1.2 times that of Nipponbare. Further, 14-45 and 40-L showed a high number of spikelets due to the high number of rachis branches per panicle and high number of spikelets per rachis branch (Table 1). Even though the seed fertility and grain weight of these mutant lines were relatively low, the grain yields per area were higher than Nipponbare (Table 2). As for the result of the yield survey in the saline paddy field conducted in 2010, there was no difference in the decrease ratio of the yield arising from the salinity stress between 14-45 and Nipponbare. However, 14-45 maintained higher yield than Nipponbare or other salt tolerant mutants in the saline paddy field.[1)]

Our results indicate that the mutation breeding technique using a heavy-ion beam will be more beneficial for developing a high yield rice variety through application to commercial varieties. In addition, high-yield mutants could be useful resources for the identification of quantitative trait loci (QTL) or genes affecting yield components.

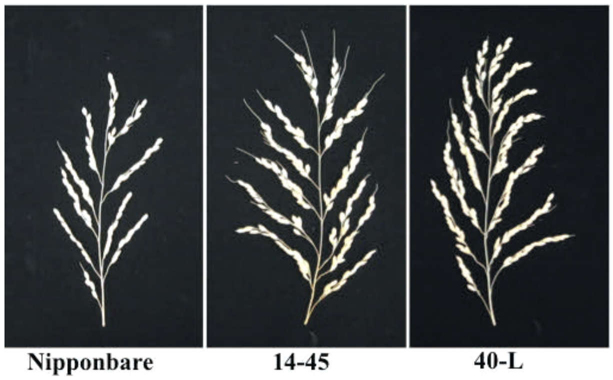

Fig. 1. Panicle structure of Nipponbare, 14-45, and 40-L.

Table 1. Comparison of Plant height and panicle structure between mutant lines and Nipponbare.

	Plant height (cm)	Rachis branch number	Spikelet number (/rachis branch)
Nipponbare	110.67±1.67	10.0±0.41	10.0±2.69
14-45	126.42±0.31	11.8±0.89	13.1±3.90
40-L	133.73±2.31	12.5±0.65	14.0±4.16

References
1) Y. Hayashi et al.: Jpn. J. Breed., **13** (suppl. 1), 205 (2011).

Table 2. Yield and yield components of mutant lines and Nipponbare.

	Panicle number	Panicle weight (g/panicle)	Panicle weight (g/plant)	Panicle length (cm)	Spikelet number (/panicle)	Fertility (%)	Grain weight (g/1000grains)	Yield (g/m^2)	Relative Yield*
Nipponbare	24.9±1.69	2.83±0.05	55.2±2.28	19.8±0.32	106.9±0.60	96±0.00	26.1±0.35	739.36±53.88	1.00
14-45	22.1±1.40	3.75±0.29	61.5±0.58	21.1±0.18	167.7±10.68	85±3.06	23.8±0.20	826.42±21.76	1.12
40-L	21.8±1.63	3.80±0.19	65.0±2.50	22.5±0.30	160.7±2.64	83±1.73	24.9±0.47	821.50±46.62	1.11

* Relative value of yield to Nipponbare

*1 Graduate School of Life Sciences, Tohoku University

C O N T E N T S

Page

2. Nuclear Physics (Theory)

3. Hadron Physics

4. Hadron Physics (Theory)

5. Particle Physics

8. Instrumentation

III. RESEARCH ACTIVITIES II (Material Science and Biology)

1. Atomic and Solid State Physics (Ion)

2. Atomic and Solid State Physics (Muon)

3. Radiochemistry and Nuclear Chemistry

4. Radiation Chemistry and Biology

I. PREFACE

Preface

On August 12th, 2012, Morita and his collaborators created the third atom of element 113. This long-awaited event was finally observed as six consecutive alpha decays connected to the well-known nuclides, unambiguous proof that the atomic number is 113 and the mass number is 278, as described in "Highlights of the Year" in this volume of the RIKEN Accelerator Progress Report (APR). This news was cited by hundreds of public articles worldwide. We, the Nishina Center, are proud of this great discovery, appreciate all participants engaged in this project, and hope to clinch our claim to naming rights for the 113th element.

The Radioisotope Beam Factory (RIBF) accelerator performance was greatly improved, in particular, by introducing the newly developed helium-gas-filled charge stripper and upgrading the fixed-frequency Ring Cyclotron. Descriptions of both developments are also featured in "Highlights of the Year." With this improvement, the RIBF is now at the forefront of global radioisotope beam production, and many new experimental results are being produced, as described in this APR. Moreover, hundreds of European nuclear physicists are visiting and collaborating with the Nishina Center for the EURICA (EUroball-RIKEN Cluster Array) Project to perform the world's first measurements of gamma rays and beta rays from very rare isotopes. Several experiments are being performed with SAMURAI, which was finally energized for such experiments.

Another significant achievement of the Nishina Center is the development of a new technique to produce spin-controlled rare isotopes, made available thanks to the great versatility of the BigRIPS isotope separator. The new technology provides unprecedented opportunities for research on the nuclear structure of species found outside the traditional region of the nuclear chart.

Another significant event was the construction of the Rare RI Ring. Operating in the isochronous mode, the ring can be considered RIKEN's 10th 24-sector ring cyclotron since the first Japanese cyclotron was built by Dr. Nishina in 1937. This ring does not accelerate but can measure the mass of rare isotopes at the PPM level.

We have also received supplemental funds for Slow-RI and the beam line from the Intermediate Ring Cyclotron to the old experimental halls. The former allows for RIs produced by BigRIPS to slow down for precision measurements such as nuclear magnetic moment measurements. With the latter, heavy-ion plant breeding will become more versatile with the use of beams with a higher penetrating power. All the experimental facilities planned at the launch of the RIBF project are now either realized or fully funded.

At the RIKEN-BNL Research Center, the newly installed silicon vertex detector exhibited the anisotropic flow of charm quarks in a quark–gluon plasma. With the improved muon arm, the first data on the asymmetries of W boson decay into muons were obtained. From the RIKEN RAL Muon Facility, two brand-new muon spin resonance (μSR) data were selected for "Highlights of the Year."

By 2012, RIKEN's five-year midterm was concluded. We have successfully completed almost everything we had planned to accomplish during this midterm with a special gift, element 113. As the saying goes, "Heaven helps those who help themselves."

Hideto En'yo
Director,
RIKEN Nishina Center for Accelerator-Based Science

II. RESEARCH ACTIVITIES I
(Nuclear-Particle Physics)

1. Nuclear Physics

New α-decay transitions of ^{217}U

Y. Wakabayashi, K. Nishio,[*1] S. Mitsuoka,[*1] K. Morita, K. Morimoto, D. Kaji, H. Haba, T. Sumita, A. Yoneda, and Y. Gono

Synthesis of neutron-deficient actinide nuclei close to the $N = 126$ shell closure is important for estimating the stability of the $N = 126$ closed shell[1] and the limit of existence for elements with $N = 126$. It is also interesting to study the structure of the actinide nuclei with a spherical shape. Actinide nuclei with $N = 126$ have been produced up to uranium (^{218}U), and ^{217}U is reported as the lightest uranium isotope produced thus far. The investigation on the nuclei in this region has been commenced. We chose the reaction ^{82}Kr + ^{138}Ba to produce a new isotope ^{216}U ($N = 124$) in the fusion-evaporation reaction as the first step. The cross section is important for evaluating cross sections of unknown nuclei such as ^{220}Pu with $N = 126$, for example, by using the reaction ^{82}Kr + ^{140}Ce, which would allow us to expand the scope our study. We have also attempted to find the isomeric states and new transitions for these actinide nuclei to study their nuclear properties.

An experiment using the ^{138}Ba + ^{82}Kr reaction was performed at the RIKEN Linear Accelerator (RILAC) facility. ^{82}Kr^{12+} beams of 384 and 397 MeV were used to bombard a rotating ^{138}BaCO$_3$ target foil having a thickness of about 430 μg/cm^2. The corresponding beam energies at the center of the target were 363 and 378 MeV, respectively. The bombarding energy of 378 MeV was chosen on the basis of the largest cross section for ^{216}U predicted by the code HIVAP[2]. We also used a beam energy of 363 MeV to examine the energy dependence of the cross section for other isotopes. ^{138}BaCO$_3$ targets were prepared by sputtering 99%-enriched ^{138}Ba on 1.5-μm-thick aluminum foils, and they were also covered with 65 μg/cm^2 of aluminum by sputtering. Evaporation residues (ERs) were separated from the beam particles by a gas-filled recoil ion separator (GARIS) and were implanted into a position-sensitive strip detector (PSD; 58 $\times$ 58 mm^2) at the focal plane. Two timing detectors were set in front of the PSD to obtain the time-of-flight (TOF) signal of the ERs. The timing information was also used to distinguish between the α-decay event in the PSD and recoil implantation. In this experiment, 4.3 $\times$ 10^{17} and 7.8 $\times$ 10^{16} beam doses were accumulated at 397 MeV and 384 MeV, respectively.

The isotope identification was performed by using an α-decay chain and recoil implantation in the PSD with the help of known α-decay properties (energy and lifetime) of the descendants and the position correlation between implanted ERs and subsequent α-decays. Figure 1 shows an α-α correlation spectrum obtained at both beam energies, 384 and 397 MeV. The decay chain that originated from ^{216}U could not be identified, and the upper limit cross section was determined to be 10 pb. Additional irradiation experiments are necessary to study the production of ^{216}U.

For investigating the α decay of ^{217}U, three decay energies of 8050±45, 8134±45, and 8243±45 keV with the intensities of 16±10%, 26±13%, 58±22%, respectively, were assigned temporarily, as shown in Fig. 1, because these values are consistent with the transition properties (intensity and energy spacing) of other N=125 isotones. For example, ^{215}Th (Z=90) has the α-decay energies of 7336±15, 7387±15, and 7520±15 keV with the intensities of 8±3%, 52±3%, and 40±3%, respectively. In the past, four events in total were reported for ^{217}U, with a decay energy of 8018±11 keV and a half-life of $15.6^{+21.3}_{-5.7}$ ms[3,4]. In our result, the energy of 8243 keV seems to correspond to a ground-state transition. This is different from the reported value. In contrast, the half-life of $23.7^{+7.3}_{-4.5}$ ms obtained in our experiment was consistent with the reported value. Further irradiation experiments are underway, which will help to gather more statistics and to perform the α-γ coincidence measurement, which will in turn help to identify new transitions and a new theoretical approach.

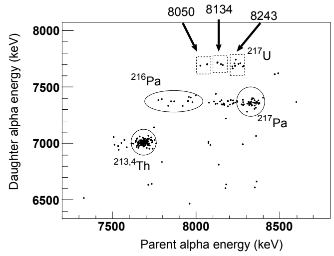

Fig. 1. An α-α correlation spectrum. The X and Y axis denote the α-decay energy of the parent and daughter nucleus, respectively. The time difference between implanted ERs and the parent α-decay and between the parent and the daughter α-decays was within 100 ms and 1 s, respectively. The horizontal and vertical position windows in the PSD were within the same strip (~3.6 mm width) and ±1.5 mm, respectively.

References
1) H. Koura and T. Tachibana: Butsuri (in Japanese), **60**, 717 (2005).
2) W. Reisdorf and M. Schadel: Z. Phys. A**343**, 47 (1992).
3) O.N. Malyshev et al.: Eur. Phys. J. A**8**, 295 (2000).
4) A.-P. Lappänen et al.: Eur. Phys. J. A**25**, s01, 183 (2005).

*1 Japan Atomic Energy Agency

Production of nuclear spin polarized ^{31,33}Cl

T. Nagatomo,Y. Ishibashi, Y. Abe, N. Yoshida, H. Shirai, T. Suzuki, T. Niwa, S. Fukuoka, N. Inaba, S. Okada, Y. Saito, T. Fujita, X.F. Yang, Y. Ichikawa, T. Furukawa, D. Nagae, A. Ozawa, D. Nishimura, M. Mihara, M. Fukuda, K. Asahi, K. Matsuta, S. Momota, T. Minamisono *1 and H. Ueno

Proton-odd nuclei located near the proton-drip line in the sd-shell have much smaller proton-separation energies compared with stable nuclei. In particular, ^{31}Cl ($I^{\pi} = 3/2^{+}$,[1] $T_{1/2} = 150 \pm 25$ ms) is known to have an extremely small separation energy of 290(50) keV. Thus, the nuclear structure of ^{31}Cl has attracted attention as a proton-rich loosely bound nuclear system. Recently, we reported the μ and Q moments of proton-rich nucleus ^{23}Al[2,3] that exhibits small proton separation energy. Despite the small separation energy, no significant signals of the exotic structure were found in the ^{23}Al structure. In the case of ^{31}Cl, because the valence proton is considered to be around ^{30}S (sub-shell closed nucleus), ^{31}Cl nucleus is considered to have a comparatively simpler configuration mixing than that of ^{23}Al.

The experiment was carried out by utilizing the RIKEN Projectile Fragment Separator RIPS. Nuclear spin-polarized ^{31,33}Cl nuclei were produced by the bombardment of ^{32}S ions on a 2.5-mm-thick ^{9}Be target. The ^{32}S^{15+} beam was delivered at $E = 100$ MeV/nucleon at a typical intensity of ~15 particle-nA on the target. The production process, $^{32}\mathrm{S} + ^{9}\mathrm{Be} \rightarrow ^{31,33}\mathrm{Cl} + \mathrm{X}$, is considered as a composite process of the pick-up and the projectile fragmentation processes. The fragments emitted at an angle from $-4.9°$ to $-0.8°$ with respect to the primary beam and at the momentum below 1.00 p_0, where $p_0 = 14.2$ GeV/c is the peak in the distribution, were selected by RIPS. A wedge-shaped degrader (145.2 mg/cm^2) was used for the momentum-loss analysis. Then, the ^{31,33}Cl ions were transported to a β-NMR apparatus and were implanted into a NaCl crystal (0.5-mm-thick) together with contaminating fragments as contaminants, which became low energy-β-ray emitters. The production cross sections of ^{31,33}Cl from ^{32}S were found to be significantly smaller than that expected from the similar processes such as ^{23,25}Al and ^{23}Ne produced from ^{24}Mg and ^{22}Ne.

First, β-NMR measurements by means of the adiabatic fast passage method (AFP) were conducted with ^{33}Cl nuclei, which were purely isotope-separated. The β-NMR spectrum of ^{33}Cl in NaCl at room temperature is shown in Fig. 1, together with the response curve where the effect of the frequency modulation width of the AFP magnetic field is shown as a dashed line. The amplitude of the NMR signal is proportional to the asymmetry change of β-ray emission with respect to the magnetic field. In Fig. 1, the maximum asymmetry change is normalized to be a product of the asymmetry parameters A and the polarization P. Since the asymmetry parameter of ^{33}Cl was estimated as $A = -0.39$, the degree of the polarization of ^{33}Cl was obtained as $P = 4.36(38)\%$. The obtained polarization was quite large compared with that of nuclei produced through the similar production process, which is typically $\sim 1\%$. From the results, the degree of polarization of ^{31}Cl is expected be similar or more than that of ^{33}Cl. It is quite interesting to understand the mechanism of the nuclear spin polarization process of ^{33}Cl. Further analyses are in progress.

In the case of ^{31}Cl, the contaminants in the secondary beam were unexpectedly large because the production cross section of ^{31}Cl was quite small. A measurement of the μ moment of ^{31}Cl under a well-separated ^{31}Cl beam with an improved β-NMR detection system is under preparation.

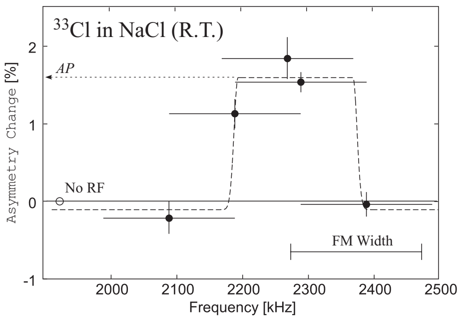

Fig. 1. Obtained NMR spectrum of ^{33}Cl in NaCl at room temperature.

References
1) A. Kankainen et al.: Euro. Phys. Jour. A **27**, 67 (2006).
2) A. Ozawa et al.: Phys. Rev. C **74**, 021301(R) (2006).
3) T. Nagatomo et al.: Hyperfine Interact. **198**, 103 (2010).

*1 Graduate School of Science, Osaka University

Complete set of deuteron-proton elastic scattering at 294 MeV/nucleon and three nucleon force

K. Sekiguchi, Y. Wada, J. Miyazaki, T. Taguchi, U. Gebauer,[*1] M. Dozono, S. Kawase,[*2] Y. Kubota,[*2] Y. Maeda,[*3] T. Mashiko, K. Miki, S. Sakaguchi, H. Sakai, N. Sakamoto, M. Sasano, Y. Shimizu, K. Takahashi, R. Tang,[*2] T. Uesaka, T. Wakasa,[*4]and K. Yako,[2]

Study of three-nucleon forces (3NFs) is important for clarifying nuclear phenomena. The first signature of the 3NF was found in the binding energies of ^{3}H and ^{3}He, and the significance of 3NFs has recently been pointed out in providing descriptions of discrete states in higher mass nuclei. Study of three-nucleon scattering at intermediate energies ($E/A \sim 200$ MeV) is a promising approach for investigating the dynamical aspects of 3NFs, such as momentum and/or spin dependence. A previous measurement of deuteron analyzing powers for deuteron–proton elastic scattering at 250 MeV/nucleon shows remarkably different features from those at lower energies ($E/A \sim 100$ MeV) in comparison between the data and the rigorous numerical 3N Faddeev calculations[1)]. In order to obtain a consistent understanding on the spin-dependence of 3NFs up to high momenta we have measured a complete set of deuteron analyzing powers (iT_{11}, T_{20}, T_{21}, and T_{22}) for deuteron–proton (dp) elastic scattering at 294 MeV/nucleon as the second experiment with polarized deuteron beams at RIBF.

A schematic diagram of the experimental setup has been provided in Ref. (1). First vector- and tensor- polarized deuteron beams were accelerated by the injector cyclotrons AVF and RRC up to 100 MeV/nucleon; subsequently, they were accelerated up to 294 MeV/ nucleon by the new superconducting cyclotron SRC. The polarization axis of each beam was rotated by using a Wien filter system prior to their acceleration[3)]. Therefore, single-turn extraction of the beams from all three cyclotrons, AVF, RRC, and SRC was required in order to maintain the polarization amplitudes during acceleration. The typical values of the beam polarizations determined by the experiment were 80% of the theoretical maximum values. The dp elastic scattering was performed by using a detector system, BigDpol, which was installed at the extraction beam line of the SRC. Polyethylene (CH_2) with a thickness of 330 mg/cm^2 was used as the hydrogen target. In BigDpol, four pairs of plastic scintillators coupled with photo-multiplier tubes were placed symmetrically in the directions of azimuthal angles to the left, right, up and down. Scattered deuterons and recoil protons were detected in the kinematical coincidence condition by each pair of detectors. The angles ($\theta_{\mathrm{c.m.}}$) measured in the center-of-mass system are in the range 40°–162°. In the experiment, the deuteron beams were stopped in the Faraday cup, which was installed at the focal plane F0 of the BigRIPS spectrometer.

Angular distributions of all deuteron analyzing powers iT_{11}, T_{20}, T_{21}, and T_{22} are represented by open circles in Fig. 1. The statistical errors are also shown. The dark (light) shaded bands in the figure represent the Faddeev calculations with (w/o) the Tucson-Melbourne99 3NF[4)] based on modern NN potentials, namely CDBonn[6)], AV18[7)], and Nijmegen I and II[8)]. The solid lines represent the results of the calculations with the Urbana IX 3NF[5)] based on the AV18 potential. Good agreements between the data and the calculations with the 3NFs are obtained at forward angles given by $\theta_{\mathrm{c.m.}} \leq 120°$; however, at backward angles, good agreements are not observed even when 3NFs are included. These results are highly similar to those obtained at 250 MeV/nucleon, indicating that some significant components are missing in the higher momentum transfer region.

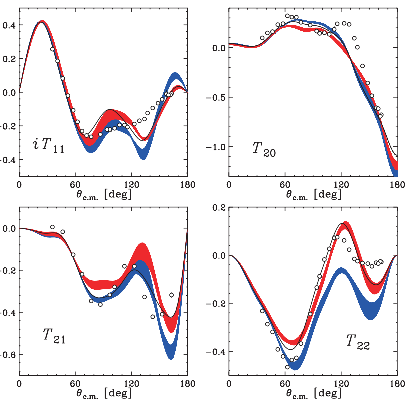

Fig. 1. Deuteron analyzing powers iT_{11}, T_{20}, T_{21}, and T_{22} for dp elastic scattering at 294 MeV/nucleon.

[*1] Department of Physics, Tohoku University
[*2] CNS, University of Tokyo
[*3] Faculty of Engineering, University of Miyazaki
[*4] Department of Physics, Kyushu University

References

1) K. Sekiguchi et al.: Phys. Rev. C **83**, 061001 (2011).
2) K. Sekiguchi et al.: RIKEN Accel. Prog. Rep. **42**, 27 (2009).
3) H. Okamura et al.: AIP Conf. Proc. **343**, 123 (1995).
4) S. A. Coon and H. K. Han: Few Body Syst. **30**, 131 (2001).
5) B. S. Pudliner et al.: Phys. Rev. C**56**, 1720 (1997).
6) R. Machleidt: Phys. Rev. C **63**, 024001 (2001).
7) R. B. Wiringa et al.: Phys. Rev. C **51**, 38 (1995).
8) V. G. J. Stoks et al.: Phys. Rev. C **49**, 2950 (1994).
9) K. Hatanaka et al.: Phys. Rev. C **66**, 044002 (2002).
10) Y. Maeda et al.: Phys. Rev. C **76**, 014004 (2007).

Spectroscopy of unbound oxygen isotopes using SAMURAI

Y. Kondo, T. Nakamura, N. Kobayashi, R. Tanaka, R. Minakata, S. Ogoshi, S. Nishi, D. Kanno, T. Nakashima, N. L. Achouri,[*1] T. Aumann,[*2] H. Baba, F. Delaunay,[*1] P. Doornenbal, N. Fukuda, J. Gibelin, J. W. Hwang, N. Inabe, T. Isobe, D. Kameda, S. Kim, T. Kobayashi, T. Kubo, S. Leblond, J. Lee, F. M. Marqués,[*1] T. Motobayashi, D. Murai, T. Murakami,[*3] K. Muto, N. Nakatsuka, A. Navin,[*4] N. A. Orr,[*1] H. Otsu, H. Sato, Y. Satou, Y. Shimizu, H. Suzuki, K. Takahashi, H. Takeda, S. Takeuchi, Y. Togano, A. G. Tuff,[*5] M. Vandebrouck,[*6] and K. Yoneda

The neutron-rich unbound oxygen isotopes ^{25}O and ^{26}O were studied in the first experimental campaign using a new spectrometer SAMURAI.[1)]

The limit of nuclear stability for neutron-rich oxygen isotopes is ^{24}O ($N = 16$), whereas ^{31}F, having 6 more neutrons, is bound. This sudden change in the drip line has not yet been understood. A recent shell-model study suggests that three-nucleon forces play an important role in explaining the drip line for oxygen isotopes.[2)] On the other hand, experimental information on the oxygen isotopes at $N > 16$ is limited because of the difficulty in producing extremely neutron-rich nuclei and observing unbound states. We performed an experiment to determine the masses and decay properties of unbound states of ^{25}O and ^{26}O by the invariant mass method using SAMURAI with intense RI beams provided by BigRIPS. The unbound nucleus ^{25}O (^{26}O) was produced using one- and two-proton removal reactions from ^{26}F (^{27}F) and ^{27}Ne (^{28}Ne), respectively, on a carbon target. Unbound states of ^{25}O and ^{26}O can be identified by the invariant mass spectrum reconstructed from the measured momentum vectors of the outgoing ^{24}O fragment and neutron(s).

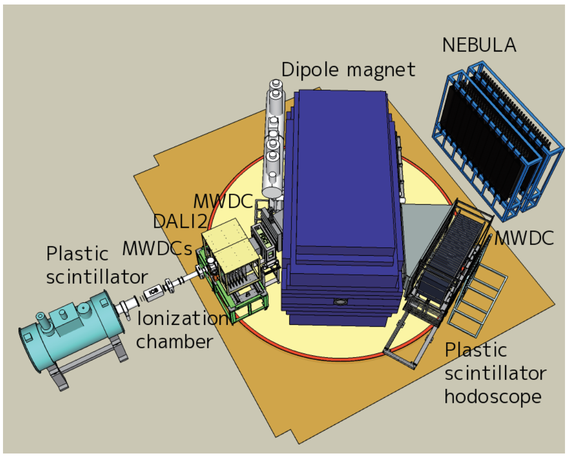

Fig. 1. Schematic view of the experimental setup.

Table 1. Energies and secondary beam intensities per 100-pnA ^{48}Ca beam. $\Delta P/P$ denotes the momentum acceptance using BigRIPS.

Beam	Energy (MeV/u)	$\Delta P/P$ (%)	Intensity (kpps/100 pnA)	purity (%)
^{27}F	212	±3	0.70	1.7
^{28}Ne	241	±3	10	25
^{26}F	212	±0.6	1.8	10
^{27}Ne	240	±0.6	9.4	54

Figure 1 shows a schematic view of the experimental setup. Secondary beams were produced by projectile fragmentation of a ^{48}Ca primary beam at 345 MeV/u with intensity of 110–200 pnA and separated by BigRIPS. ^{26}F and ^{27}Ne (^{27}F and ^{28}Ne) were obtained as a cocktail beam. Energies and intensities are summarized in Table 1. Secondary beams were monitored by plastic scintillators at the focal planes F3, F7, and F13, a MWPC at F5, and an ionization chamber at F13. Incident angle and position at the secondary target were measured by two MWDCs. The thickness of the secondary carbon target was 1.8 g/cm^2.

Outgoing charged fragments were detected by MWDCs placed at the entrance and exit of the SAMURAI dipole magnet,[3)] and a plastic scintillator hodoscope. Outgoing neutrons were detected by a large neutron detector array, NEBULA.[4)] A γ ray detector array DALI2[5)] was also installed at the target area to detect de-excitation γ rays emitted from excited outgoing charged particles.

Data analysis is currently in progress.

References

1) K. Yoneda et al.: RIKEN Accel. Prog. Rep. **45** , i, (2012).
2) T. Otsuka et al.: Phys. Rev. Lett. **105**, 032501, (2010).
3) H. Sato et al.: IEEE. Trans. Appl. Supercond. **23**, 4500308, (2013).
4) Y. Kondo et al.: RIKEN Accel. Prog. Rep. **44** , 150, (2011)., http://be.nucl.ap.titech.ac.jp/~nebula
5) S. Takeuchi et al.: RIKEN Accel. Prog. Rep. **41**, 149, (2008).

*1 LPC-Caen, ENSICAEN, Université de Caen, CNRS/IN2P3
*2 Institut für Kernphysik, Technische Universität Darmstadt
*3 Department of Physics, Kyoto University
*4 GANIL, CEA/DSM-CNRS/IN2P3
*5 Department of Physics, University of York
*6 Institut de Physique Nucléaire, Université Paris-Sud, IN2P3-CNRS

Structure of the most neutron-rich isotopes of Boron and Carbon studied via breakup and inelastic scattering at SAMURAI

T. Nakamura,[*1] N. A. Orr,[*2] Y. Kondo,[*1] J. Gibelin,[*2] N. Kobayashi,[*1] R. Tanaka,[*1] R. Minakata,[*1] S. Ogoshi,[*1] S. Nishi,[*1] D. Kanno,[*1] T. Nakashima,[*1] N. L. Achouri,[*2] T. Aumann,[*3] H. Baba, F. Delaunay,[*2] P. Doornenbal, N. Fukuda, J. W. Hwang,[*4] N. Inabe, T. Isobe, D. Kameda, S. Kim,[*4] T. Kobayashi,[*5] T. Kubo, S. Leblond,[*2] J. Lee, F. M. Marqués,[*2] T. Motobayashi, D. Murai,[*6] T. Murakami,[*7] K. Muto,[*5] N. Nakatsuka,[*7] A. Navin,[*8] H. Otsu, H. Sato, Y. Satou,[*4] Y. Shimizu, H. Suzuki, K. Takahashi,[*5] H. Takeda, S. Takeuchi, Y. Togano,[*9] A. G. Tuff,[*10] M. Vandebrouck,[*11] K. Yoneda

The investigation of the light neutron-rich dripline nuclei, including in particular those exhibiting halos, has been a central theme of nuclear structure physics over the last two decades. These studies have, however, been limited for the most part to the He, Li and Be isotopes. With the advent of the RIBF and intense energetic beams of ^{48}Ca the path has been opened to exploring structure of heavier neutron dripline nuclei. In the present work a series of measurements aimed at elucidating the structure of the two heaviest candidate two-neutron halo systems, ^{19}B and ^{22}C[1–3)], and the associated unbound sub-systems ^{18}B and ^{21}C, the level schemes of which are critical to the defining the ^{17}B-n and ^{20}C-n interactions for three-body models, has been undertaken. In addition to being of direct importance to halo physics, ^{18,19}B and ^{21,22}C are of considerable interest in terms of the evolution of shell-structure far from stability as they span the N=14 and 16 sub-shell closures below doubly-magic ^{22,24}O.

In order to explore the structure of ^{19}B and ^{22}C, reactions on a light (C) and heavy (Pb) target were investigated. In the former case, continuum states (core+n+n) were populated via inelastic scattering whereby it is hoped that ^{22}C(2_1^+) may be located and the corresponding transition strength determined. The neutron unbound ^{18}B and ^{21}C will be probed through the reconstruction of the core+n invariant mass spectra following single-neutron removal from ^{19}B and ^{22}C. Information on the angular momentum of the removed valence neutron will be obtained through the reconstruction of the ^{18}B and ^{21}C momentum distributions and the core+n angular correlations[4)]. In a complementary manner, single and two-proton removal from ^{19}C and ^{20}N, and ^{22}N and ^{23}O has also been employed to access ^{18}B and ^{21}C, respectively.

In the case of the Pb target, Coulomb dissociation is privileged and, for a well developed halo with a significant s-wave valence neutron configuration, strong low-lying E1 strength should be observed. Such enhancements are sensitive to the the spatial distribution of the valence neutrons and provide an independent means to determine their spectroscopic configuration. In addition, as has been shown for ^{11}Li[5)], the E1 strength function, when constrained by the total matter radius, may also be used to provide insight into the valence neutrons spatial correlations, which may be compared to those that will be deduced from the neutron-neutron relative momenta[6)].

The measurements outlined above were accomplished using the newly commissioned SAMURAI facility[7)], which comprised the superconducting 7 Tm spectrometer[8)] coupled to the large area neutron array NEBULA[9)] and the DALI2 γ-ray detector[10)], and were performed as part of the first phase of SAMURAI experiments. The setup was identical to that employed in our study of the most neutron-rich oxygen isotopes (Figure 1 of Ref.[11)]) and secondary beam intensities of up to some 100 and 20 pps of ^{19}B and ^{22}C at ∼240 MeV/nucleon were delivered by the RIBF. Preliminary analyses suggest that the main goals of the experiments will be achieved.

References
1) K. Tanaka *et al.*: Phys. Rev. Lett. **104**, 062701 (2010).
2) N. Kobayashi *et al.*: Phys. Rev. **C83**, 054604 (2012).
3) L. Gaudefroy *et al.*: Phys. Rev. Lett. **109**, 20503 (2012).
4) H. Simon *et al.*: Phys. Rev. Lett. **104**, 062701 (2010).
5) T. Nakamura *et al.*: Phys. Rev. Lett. **96**, 252502 (2006).
6) F.M Marqués *et al.*: Phys. Lett. **B476**, 219 (2000).
7) K. Yoneda *et al.*: RIKEN Accel. Prog. Rep. **45**, i (2012).
8) H. Sato *et al.*: IEEE. Trans. Appl. Supercond. **23** (2013) in press.
9) Y. Kondo *et al.*: RIKEN Accel. Prog. Rep. **45**, 131 (2012); http://be.nucl.ap.titech.ac.jp/˜nebula
10) S. Takeuchi *et al.*: RIKEN Accel. Prog. Rep. **41**, 149 (2008).
11) Y. Kondo *et al.*: in this report.

*1 Department of Physics, Tokyo Institute of Technology
*2 LPC-Caen, ENSICAEN, Université de Caen, CNRS/IN2P3, France
*3 Institut für Kernphysik, Technische Universität Darmstadt, Germany
*4 Department of Physics and Astronomy, Seoul National University, South Korea
*5 Department of Physics, Tohoku University
*6 Departiment of Physics, Rikkyo University
*7 Department of Physics, Kyoto University
*8 GANIL, CEA/DSM-CNRS/IN2P3, France
*9 ExtreMe Matter Institute (EMMI) and Research Division, GSI, Germany
*10 Department of Physics, University of York, UK
*11 Institut de Physique Nucléaire, Université Paris-Sud, IN2P3-CNRS, Orsay, France

Proton elastic scattering from ^{22}O and ^{24}O, drip-line nucleus, at RIBF

V. Lapoux,[*1] H. Otsu, S.Boissinot,[*1] H. Baba, R.J. Chen, E.C. Pollacco,[*1] Y. Blumenfeld,[*2] F. Flavigny,[*1] S. Franchoo,[*2] N. Fukuda, P. Gangnant,[*3] F. Hammache,[*2] Ch. Houarner,[*3] N. Inabe, D. Kameda, J.F.Libin,[*3] C. Louchart,[*1] A. Matta,[*2] M. Matsushita, T. Motobayashi, L. Nalpas,[*1] E. Yu. Nikolskii, M. Kurata-Nishimura, A. Obertelli,[*1] T. Onishi, E. Rindel,[*2] Ph. Rosier,[*2] H.Sakurai, F. Saillant,[*3] M.Takechi, S. Takeuchi, Y. Togano, K.Yoneda, A.Yoshida and K.Yoshida

Low-lying resonances or new magic shells represent stringent tests for the nuclear theories and their modeling of the nuclear interaction. These last years it was shown that several effects are playing a crucial role in the nuclear models, for the understanding of the location of the neutron drip-line and the spectroscopy of exotic nuclei: the inclusion of 3-nucleon forces[1], the influence of the proton-neutron interaction[2] and the continuum-coupling treatment. In this context, the excited states of the drip-line N=16 doubly-magic nucleus ^{24}O and the characteristics of the new magic shell gap[2] created at N=16 between the $2s_{1/2}$ and the $1d_{3/2}$ shells were intensively investigated. ^{24}O having no bound excited state, various particle spectroscopy techniques have been used. At MSU, via invariant mass method, possible states were indicated[3] above S_n =4.19 (14) MeV, around 4.5 and 5.3 MeV, but not clearly identified. Recently, at RIKEN, Tshoo et al. have confirmed the new excited states[4] and studied the deformation of the first 2^+ to establish the N=16 shell gap. In the same period, we used another technique, the missing mass method, to investigate the structure and the spectroscopy of ^{24}O via proton elastic and inelastic scattering.

The RIBF57 experiment was realized in the F8 area by combining the intense RIBF beams and the state-of-the-art particle detector array MUST2[5]. ^{24}O was produced in BigRIPS[6] at 263 MeV/n with unique mean intensities, 1760/s during ~7days, from the fragmentation on a Be target of the ^{48}Ca beam at 345 MeV/n. The (p,p') kinematics were obtained by the correlations of the proton energy with the scattering angle, and the incident and outgoing particles were identified in BigRIPS, and in the ZDS[7], respectively. The full experimental set-up was shown and explained in Ref.[8]. The excitation energy spectra (Ex) were extracted. The analysis method was checked on the (p,p') scattering of ^{22}O at 262.5 MeV/n, used as reference measurement. The Ex spectrum of ^{24}O was deduced but the excited states were not determined (except indications within maximum likelihood procedure) due to the very low statistics for the inelastic events (less than 100 counts for the whole data set) and the large background contamination due to the triton particles; the rate of ^{24}O was only 2.5 % of the total beam. For proton elastic scattering, we had enough statistics to obtain the angular distributions for $^{21\text{-}24}$O isotopes.

*1 CEA Saclay IRFU/SPhN, France
*2 CNRS-IN2P3, IPNO, France
*3 GANIL, France

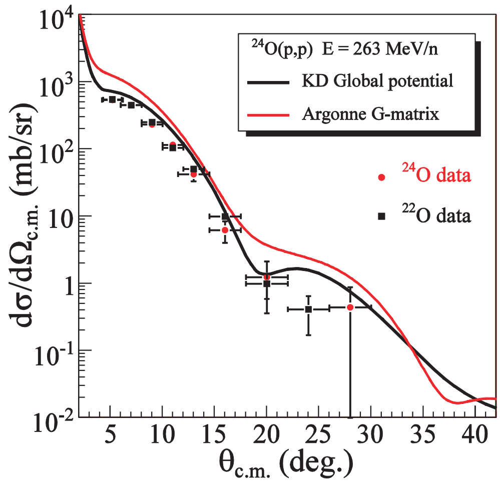

Fig.1. Elastic cross sections for ^{24}O(p,p)^{24}O at 263 MeV/n (exclusive data) compared to phenomenological (black curve) and to microscopic calculations (red). The data for ^{22}O(p,p) at 262.5 MeV/n are presented with black squares.

The ^{24}O(p,p)^{24}O elastic data were compared with calculations (Fig.1) done within the optical model potential (OMP) framework, using the ECIS06 code and KD[9] global nucleon-nucleus potential, and within G-matrix microscopic potential formalism[10]. From the $^{21\text{-}24}$O(p,p) elastic data, the matter density root mean square radii R_m can be extracted using microscopic density-dependent optical potentials: $R_m(^{22}O)$ = 3.0 ± 0.1, $R_m(^{24}O)$ = 3.25 ± 0.15 fm; full discussions are in progress, note that the ones from interaction cross sections[11] are 2.88(6) and 3.19(13) fm, respectively. These results constitute also a unique benchmark to explore the characteristics of the proton-nucleus interaction potentials around 260 MeV/n.

References

1) T. Otsuka *et al.,* Phys. Rev. Lett. 105, 032501 (2010).
2) T. Otsuka *et al*., Phys. Rev. Lett. **91**, 179202 (2003).
3) C.R. Hoffman *et al*., Phys.Lett.B **672**, 17 (2009).
4) K. Tshoo *et al.,* Phys. Rev. Lett. **109**, 022501 (2012).
5) E.C. Pollacco *et al.*, Eur. Phys. J. A **25**, 287 (2005)
6) T. Kubo *et al.*, NIM. in Phys. Res., B **204**, 97 (2003).
7) T. Ohnishi *et al.*, J. Phys. Soc. Jpn. **77**, 083201 (2008).
8) V. Lapoux *et al.*, RIKEN Accel. Prog. Report Vol **45** (2012) 7.
9) A. Koning and J. P. Delaroche, Nucl. Phys. ***A 713***, 231 (2003).
10) H. F. Arellano *et al.,* Phys. Rev. C **52,** 301 (1995).
11) A. Ozawa,T. Suzuki, I. Tanihata,, Nucl. Phys. ***A693***, 32 (2001).

Evidence for the significant d-wave component in the ^{12}Be ground state obtained in the $d(^{12}$Be,$t)^{11}$Be reaction

E. Yu. Nikolskii, A. A. Korsheninnikov, *[1] H. Otsu, H. Suzuki, K. Yoneda, H. Baba, K. Yamada, Y. Kondo, N. Aoi, M. S. Golovkov,*[2] A. S. Fomichev,*[2] S. A. Krupko,*[2] M. Kurokawa, E. A. Kuzmin,*[1] I. Martel,*[3] W. Mittig,*[4] T. Motobayashi, T. Nakamura, M. Niikura, S. Nishimura, A. A. Ogloblin,*[1] P. Roussel-Chomaz,*[4] A. Sanchez-Benitez,*[3] Y. Satou, S. I. Sidorchuk,*[2] T. Suda, S. Takeuchi, K. Tanaka, G. M. Ter-Akopian,*[2] Y. Togano, and M. Yamaguchi

At present, it is established that the shell closure at $N = 8$ disappears in light nuclei near the neutron drip line. In particular, studies[1,2] have revealed that the ^{12}Be ground state represents mixture of normal closed shell $(0p_{1/2})^2$ configuration with significant component of $(1s0d)^2$ orbitals relative to the ^{10}Be$_{g.s.}$ core. However, thus far only two experiments[3,4] have focused on quantitatively measuring the spectroscopic factors (SFs) for the corresponding configurations of valence neutrons in ^{12}Be$_{g.s.}$ via one-neutron knockout reaction with ^{12}Be. In a previous work[4], the deduced SFs showed a large admixture of the s and d-configurations.

In our R390n experiment at RIPS, the $d(^8$He,^{3}He$)^7$H, $d(^{12}$Be,^{3}He$)^{11}$Li, and $d(^8$He,$t)^7$He reactions were measured in order to extract information for the exotic ^{7}H, ^{11}Li, and ^{7}He systems[5,6]. Recently, we analyzed the data for the excitation energy spectrum of ^{11}Be* obtained in the same run and populated in one-neutron pickup reaction $d(^{12}$Be,$t)^{11}$Be at $E = 71A$ MeV and angular range of $\theta_{CM} \approx (2^0$–$7^0)$. These data have been previously reported[7]. In the spectrum measured up to $E^* \sim 5$ MeV, the low-energy excited states of ^{11}Be are not clearly resolved owing to insufficient energy resolution, FWHM $\approx$ 1.7 MeV. However, we applied decomposition analysis, assuming the contribution of the following states of ^{11}Be: $(1/2^-)$ 0.32 MeV, $(5/2^+)$ 1.78 MeV, $(3/2^-)$ 2.65 MeV, and some pseudo-state near $E^* \approx 3.8$ MeV that could be sum of three closed levels at 3.4, 3.89, and 3.96 MeV[8]. The intruder ground state $(1/2^+)$ of ^{11}Be was not included in the analysis because, according to DWBA calculations, the transfered momentum $L = 0$ should be considerably (about 5 times) suppressed at this energy and angular range.

In numerous variants of χ^2-minimization fittings the presence of $(5/2^+)$ state at 1.78 MeV was manifested. The cross sections for the states at 0.32, 1.78, and 2.65 MeV were evaluated to be 1.4 ± 0.5, 2.3 ± 0.8, and 2.4 ± 0.8 mb/sr, respectively. We attempted to estimate (very roughly) SFs for these states by performing DWBA cross sections calculations (the code DWUCK5[9] was used) based on two sets of optical potentials, which were determined for the ^{12}C$(d,t)^{11}$C reaction at 100 A MeV[10] and ^{12}C$(d,^3$He$)^{11}$B at 41 A MeV[11]. For the final estimation, the average cross sections for these two sets of potentials were taken. The estimated SFs together with ones deduced in[4] are presented in Table 1.

Table 1. The estimated spectroscopic factors for the low-lying excited states of ^{11}Be obtained in one-neutron pickup reaction $d(^{12}$Be,$t)^{11}$Be. The errors are statistical only. The last column presents SFs extracted in[4].

^{11}Be*	$< SF >$ (present)	SF Pain et al.[4]
0.00 $(1/2^+)$	—	0.56 ± 0.18
0.32 $(1/2^-)$	0.65 ± 0.24	0.44 ± 0.08
1.78 $(5/2^+)$	0.41 ± 0.14	0.48 ± 0.06
2.65 $(3/2^-)$	0.85 ± 0.30	0.40 ± 0.07

In spite of the rough estimation, the extracted SFs are in satisfactory agreement with results[4], exhibiting additional argument for the significant admixture of d-wave component in ^{12}Be$_{g.s.}$ and, therefore, for the melting of the magicity at $N = 8$ near the drip-line.

References
1) H. Iwasaki et al.: Phys. Lett. B **481**, 7 (2000).
2) H. Iwasaki et al.: Phys. Lett. B **491**, 8 (2000).
3) A. Navin et al.: Phys. Rev. Lett. **85**, 266 (2000).
4) S. D. Pain et al.: Phys. Rev. Lett. **96**, 032502 (2006).
5) E. Yu. Nikolskii et al.: Phys. Rev. C **81**, 064606 (2010).
6) E. Yu. Nikolskii et al.: RIKEN Accel. Prog. Rep. **43**, 8 (2010).
7) E. Yu. Nikolskii et al.: RIKEN Accel. Prog. Rep. **41**, 14 (2008).
8) J. H. Kelley et al.: Nucl. Phys. A **880**, 88 (2012).
9) P. D. Kunz: computer code DWUCK5 (1980), http://spot.colorado.edu/~kunz/DWBA.html.
10) J. Van de Wiele et al.: Phys. Rev. C **50**, 2935 (1994).
11) J.-P. Didelez et al.: Phys. Rev. C **13**, 1388 (1976).

*1 Kurchatov Institute, Russia
*2 Joint Institute for Nuclear Research, Russia
*3 Departamento de Fisica Aplicada, Universidad de Huelva, Spain
*4 GANIL, Caen Cedex, France

Well developed deformation in ^{42}Si†

S. Takeuchi, M. Matsushita,[*1] N. Aoi, P. Doornenbal, K. Li,[*2] T. Motobayashi, H. Scheit,[*3] D. Steppenbeck,[*1] H. Wang,[*2] H. Baba, D. Bazin, L. Càceres,[*4] H. Crawford,[*5] P. Fallon,[*5] R. Gernhäuser,[*6] J. Gibelin, S. Go, S. Grévy,[*4] C. Hinke,[*6] C. R. Hoffman,[*7] R. Hughes,[*8] E. Ideguchi,[*9] D. Jenkins,[*10] N. Kobayashi, Y. Kondo, R. Krücken,[*11] T. Le Bleis,[*6] J. Lee, G. Lee,[*12] A. Matta,[*13] S. Michimasa,[*1] T. Nakamura, S. Ota,[*1] M. Petri,[*4] T. Sako,[*12] H. Sakurai, S. Shimoura,[*1] K. Steiger,[*6] K. Takahashi,[*12] M. Takechi, Y. Togano, R. Winkler,[*14] and K. Yoneda

In this work, the first 2^+ and 4^+ excited states in ^{38,40,42}Si have been studied via in-beam γ-ray spectroscopy for assessing the validation of the nuclear quadrupole collectivity in the vicinity of the proton and neutron shell closures of $Z = 14$ and $N = 28$. Until now, the 2_1^+ excitation energies have been systematically measured for lighter nuclei[1–3] and, recently, also for the ^{42}Si nucleus[4–6], but there have been no data on higher excited states. Herein, we have successfully measured de-excitation γ-rays from excited states higher than the 2_1^+ state by employing nucleon removal reactions as a means to populate these states efficiently. Complementing the obtained energy levels of the 4_1^+ excited states with those of the 2_1^+ states, we have demonstrated a rapid development of nuclear deformation from $N = 24$ to $N = 28$.

The experiment was performed using intense radioactive beams of ^{40}S and ^{44}S obtained at the RIKEN Radioactive Isotope Beam Factory. The reaction channels were identified by measuring ^{40,44}S beams and ^{38,40,42}Si outgoing particles by BigRIPS and ZeroDegree, respectively. De-excitation γ rays were detected by the DALI2 array, which facilitates the efficient analysis of the γ–γ coincidence. A prominent γ line observed with an energy of 742(8) keV in ^{42}Si confirms the 2^+ state reported in an earlier study[6].

Among the γ lines observed in coincidence with the $2^+ \to 0^+$ transition in the ^{44}S to ^{42}Si reaction, the most probable candidate for the transition from the yrast 4^+ state was identified, thereby leading to a 4_1^+ energy of 2173(14) keV upon applying γ–γ coincidence analysis. As shown in Fig. 1, the energy ratio $R_{4/2}$ of 2.93(5) between the 2_1^+ and 4_1^+ states in ^{42}Si is fairly close to the rigid-rotor limit, 10/3. The 4_1^+ states in ^{38}Si and ^{40}Si were assigned to energies of 2239(25) and 2524(19) keV, respectively. The increase in the $R_{4/2}$ value in silicon isotopes from $N = 24$ to $N = 28$ shows a rapid development of deformation (see Fig. 1). Moreover, the large $R_{4/2}$ value of 2.93(5) for ^{42}Si, which is also the largest among the known $N = 28$ isotones, indicates that this nucleus has the characteristic of a well-deformed rotor despite the magic numbers $N = 28$ and $Z = 14$.

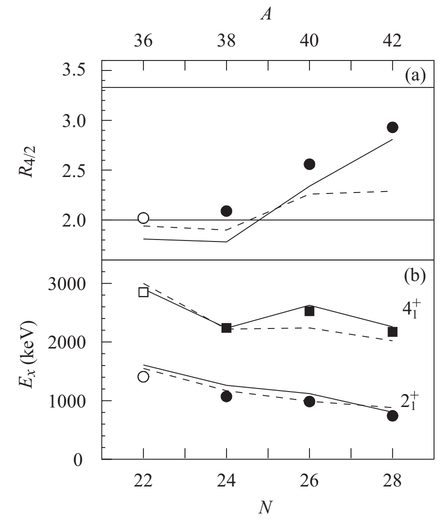

Fig. 1. (a) Ratios between the energies of the 2_1^+ and 4_1^+ states ($R_{4/2}$) for Si isotopes with harmonic vibration (2.0) and rigid-body rotation (10/3). (b) Excitation energies for 2_1^+ (circle) and 4_1^+ (square) states. The filled symbols indicate the results of the present study, and solid and dashed lines represent predictions by shell model calculations with the effective interactions of SDPF-MU[7,8] and SDPF-U-MIX[9], respectively.

References

1) R. W. Ibbotson et al.: Phys. Rev. Lett. **80**, 2081 (1998).
2) C. M. Campbell et al.: Phys. Rev. Lett. **97**, 112501 (2006).
3) C. M. Campbell et al.: Phys. Lett. B **652**, 169 (2007).
4) S. Grévy et al.: Phys. Lett. B **594**, 252 (2004).
5) J. Fridmann et al.: Phys. Rev. C **74**, 034313 (2006).
6) B. Bastin et al.: Phys. Rev. Lett. **99**, 022503 (2007).
7) T. Otsuka et al.: Nucl. Phys. A **805**, 127c (2008).
8) Y. Utsuno et al.: Phys. Rev. C **86**, 051301(R) (2012).
9) F. Rotaru et al.: Phys. Rev. Lett. **109**, 092503 (2012).

† Condensed from the article in Phys. Rev. Lett. **109**, 182501 (2012)
*1 Center for Nuclear Study, University of Tokyo
*2 State Key Laboratory of Nuclear Physics and Technology, Peking University
*3 Institut für Kernphysik, Technische Universität Darmstadt
*4 Grand Accélérateur National d'Ions Lourds, CEA/DSM-CNRS/IN2P3
*5 Lawrence Berkeley National Laboratory
*6 Physik-Department, Technische Universität München
*7 Physics Division, Argonne National Laboratory
*8 Department of Physics, University of Richmond
*9 Research Center for Nuclear Physics, Osaka University
*10 Department of Physics, University of York
*11 TRIUMF
*12 Department of Physics, Tokyo Institute of Technology
*13 Institut de Physique Nucléaire, IN2P3-CNRS,
*14 Los Alamos National Laboratory

Intermediate-energy Coulomb excitation of ^{104,112}Sn

P. Doornenbal, S. Takeuchi, M. Matsushita,[*1,2] D. Steppenbeck,[*1] H. Wang,[*3] N. Aoi,[*4] L. Audirac,[*5] H. Baba, P. Bednarczyk, S. Boissinot,[*5] M. Ciemala,[*6] A. Corsi,[*5] T. Isobe, A. Jungclaus,[*7] V. Lapoux,[*5] J. Lee, K. Matsui, T. Motobayashi, D. Nishimura, A. Obertelli,[*5] S. Ota,[*2] E. Pollacco,[*5] H. Sakurai, C. Santamaria,[*5] Y. Shiga, D. Sohler,[*10] and R. Taniuchi

In the tin isotopes between the $N = 50$ and $N = 82$ major shell closures, the 2_1^+ energies are well established and possess an almost constant value. This is the expected behavior of semi magic nuclei in the generalized seniority scheme. With the $E2$ excitation strength, the $B(E2)$ value, the robustness of the $Z = 50$ shell gap in the tin isotopes can be studied in great detail. From seniority truncated large scale shell model calculations, a parabolic pattern peaking at mid-shell is expected, reflecting the number of particles (p) times holes (h) available for pair breakup[1)].

In recent years, grand endeavors have been made to obtain the $B(E2)$ values for unstable proton-rich tin nuclei in Coulomb excitation experiments[1–4)]. For these nuclei, lifetime measurements from e.g. fusion evaporation reactions are impracticable due to higher lying isomeric states in the ns range. The resulting $B(E2)$ evolution for the tin nuclei indicated an unexpected enhancement towards the doubly-magic ^{100}Sn. In order to understand the underlying mechanisms for this enhancement, a Coulomb excitation measurement of ^{104}Sn was performed. A second isotope with known $B(E2)$ value, ^{112}Sn, was also inelastically scattered in order to extract the nuclear excitation contributions and potential from absolute cross-section measurements.

The experiment was performed at the Radioactive Isotope Beam Factory (RIBF). A ^{124}Xe primary beam was accelerated up to an energy of 345 MeV/u and impinged on a 3 mm thick Be production target at the F0 focus of the BigRIPS fragment separator[5)]. The $B\rho - \Delta E - B\rho$ method was applied to select and purify secondary beams of ^{104}Sn and ^{112}Sn in two subsequent measurements. Two wedge-shaped aluminum degraders of 3 mm thickness each were inserted at the F1 and F5 dispersive focal points, respectively. Particle identification was performed with the $B\rho - \Delta E -$TOF method. A sample spectrum for the ^{104}Sn setting is shown in Fig. 1.

The secondary beams were incident on a 557 mg/cm^2 Pb reaction target at energies around 150 MeV/u. In order to enhance the number of Sn fragments in the fully stripped charge state, a 6 mg/cm^2 thick Al foil was placed behind the reaction target. Scattering angles were determined by two double PPACs located 1430 and 930 mm upstream of the secondary target and one double PPAC located 890 mm downstream of the secondary target. To detect γ-rays from the $2_1^+ \rightarrow 0_{gs}^+$ transitions, the reaction target was surrounded by the DALI2 array[6)], consisting of 186 large-volume NaI(Tl) detectors at center-of-crystal angles from 19 to 150 degrees. An efficiency of 14 % and an energy resolution of 6 % (FWHM) for the 1.33 MeV γ-ray of the ^{60}Co stationary sources was measured for the DALI2 array. Reaction products behind the secondary target were identified by the ZeroDegree spectrometer, using again the $\Delta E - B\rho -$TOF method. Sufficient statistics for the $2_1^+ \rightarrow 0_{gs}^+$ transitions in ^{104}Sn and ^{112}Sn were collected, allowing for absolute cross-section measurements as a function of the scattering angle. The data is currently under analysis.

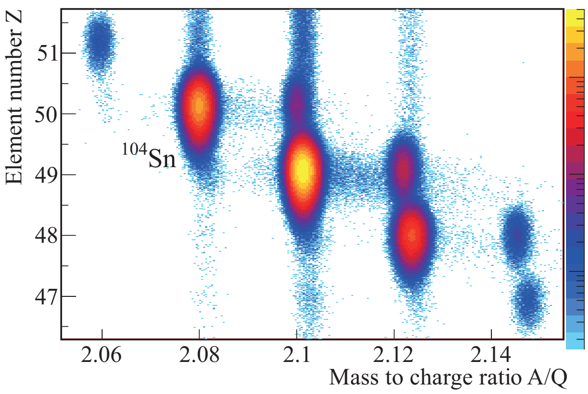

Fig. 1. Particle identification plot of the secondary beam in front of the Pb reaction target. The ^{104}Sn isotopes are labeled.

*1 CNS, University of Tokyo
*2 Department of Physics, Rikkyo University
*3 SKLNPT, Peking University
*4 RCNP, Osaka University
*5 CEA-Saclay, IRFU, SPhN
*6 IFJ Pan, Cracow
*7 CSIC Madrid
*8 Department of Physics, University of Tokyo
*9 Department of Physics, Tokyo University of Science
*10 MTA ATOMKI, Debrecen

References

1) A. Banu *et al.*, Phys. Rev. C **72**, 061305(R) (2005).
2) C. Vaman *et al.*, Phys. Rev. Lett. **99**, 162501 (2007).
3) J. Cederkäll *et al.*, Phys. Rev. Lett. **98**, 172501 (2007).
4) A. Ekström *et al.*, Phys. Rev. Lett. **101**, 012502 (2008).
5) T. Kubo *et al.*, Prog. Theor. Exp. Phys. 2012, 03C003 (2012).
6) S. Takeuchi *et al.*, RIKEN Acc. Prog. Rep. 36, 148 (2003).

In-beam γ-ray spectroscopy of ^{38,40}Si

M. Matsushita,[*1] S. Takeuchi, N. Aoi, P. Doornenbal, J. Lee, K. Li,[*3] T. Motobayashi, H. Scheit,[*4] D. Steppenbeck,[*1] H. Wang,[*3] K. Ieki, H. Baba, D. Bazin, L. Càceres,[*5] H. Crawford,[*6] P. Fallon,[*6] R. Gernhäuser,[*7] J. Gibelin, S. Go, S. Grévy,[*5] C. Hinke,[*7] C. R. Hoffman,[*8] R. Hughes,[*9] E. Ideguchi,[*2] D. Jenkins,[*10] N. Kobayashi, Y. Kondo, R. Krücken,[*11] T. Le Bleis,[*7] G. Lee,[*12] A. Matta,[*13] S. Michimasa,[*1] T. Nakamura, S. Ota,[*1] M. Petri,[*4] T. Sako,[*12] H. Sakurai, S. Shimoura,[*1] K. Steiger,[*7] K. Takahashi,[*12] M. Takechi, Y. Togano, R. Winkler,[*14] and K. Yoneda

Excited states in ^{38,40}Si nuclei have been studied using in-beam γ-ray spectroscopy with multi-nucleon removal reactions.[1)] The $N = 28$ isotope, ^{42}Si, can be regarded as a magic nucleus in the traditional shell model, because a large energy gap exists at $N = 28$ on account of the spin-orbit splitting. The enhanced collectivity in the vicinity of ^{42}Si, however, has been suggested by the recent studies,[2–5)] which show the lowering of the energies of the 2_1^+ state along the isotopic chain toward $N = 28$. In addition to such information on 2_1^+ states, the systematical data on higher-lying states, which may contribute valuable information on the nature of the nuclear collectivity and/or shell evolution, are required for further understanding the nuclear structure in this mass region.

In order to study such states, we performed multi-nucleon removal reactions with radioactive isotope beams of ^{40}S and ^{44}S at RIBF. BigRIPS and the ZeroDegree spectrometer were employed to identify secondary beams and reaction products, respectively. Deexcitaion γ-rays from the reaction products were measured by the DALI2 γ-ray detector array. Owing to the high intensity primary and secondary beams, several γ-ray lines were observed for the first time.

The Doppler-shift corrected γ-ray energy spectra obtained for ^{38}Si and ^{40}Si are shown in Fig. 1. Two γ-ray transitions with energies of 1168(22)- and 1284(26)-keV were newly obtained for ^{38}Si, whereas a 1539(16)-keV γ-ray line was observed for the first time in ^{40}Si. With an analysis on γ-γ coincidence and intensity for each peak, the 1168-keV and 1539-keV γ-ray lines were tentatively assigned to the $4_1^+ \rightarrow 2_1^+$ transitions in ^{38}Si and ^{40}Si, respectively. The energy ratio between the 2_1^+- and 4_1^+-state $R_{4/2}$, which reflects the nature of the nuclear collectivity, were obtained to be 2.09(5) and 2.55(3) for ^{38}Si and ^{40}Si, respectively. Considering the larger $R_{4/2}$ value (2.93) obtained for ^{42}Si[1)], these results indicate a rapid shape evolution from a spherical shape in the $N = 24$ isotope ^{38}Si to a well-deformed shape in the $N = 28$ isotope ^{42}Si. Further analysis concerning γ-γ angular correlations[6)] and/or momentum distributions of each state are expected to help the spin-parity assignments to the excited states.

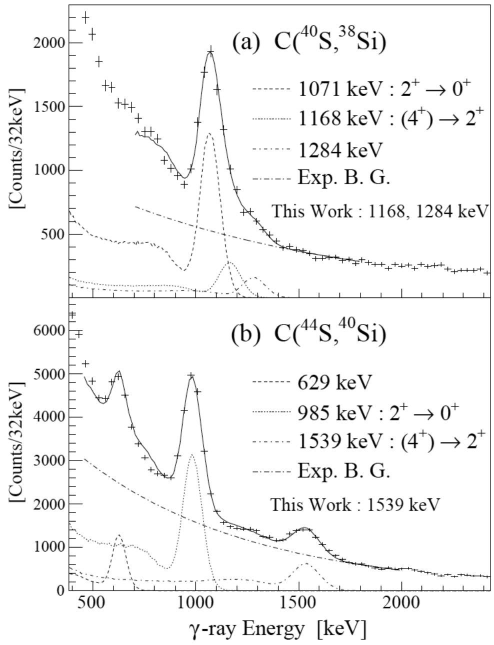

Fig. 1. Doppler-shift corrected γ-ray energy spectra obtained in coincidence with (a) C(^{40}S,^{38}Si) and (b) C(^{44}S,^{40}Si) reactions.

*1 Center for Nuclear Study, University of Tokyo
*2 Research Center for Nuclear Physics, Osaka University
*3 State Key Laboratory of Nuclear Physics and Technology, Peking University
*4 Institut für Kernphysik, Technische Universität Darmstadt
*5 Grand Accélérateur National d'Ions Lourds (GANIL)
*6 Lawrence Berkeley National Laboratory (LBNL)
*7 Physik-Department, Technische Universität München
*8 Physics Division, Argonne National Laboratory (ANL)
*9 Department of Physics, University of Richmond
*10 Department of Physics, University of York
*11 TRIUMF
*12 Department of Physics, Tokyo Institute of Technology
*13 Institut de Physique Nucléaire, IN2P3-CNRS
*14 Los Alamos National Laboratory

References

1) S. Takeuchi et al.: Phys. Rev. Lett. 109, 182501 (2012).
2) R.W. Ibbotson et al.: Phys. Rev. Lett. 80, 2081 (1998)
3) C.M. Campbell et al.: Phys. Rev. Lett. 97, 112501 (2006)
4) C.M. Campbell et al.: Phys. Lett. B 652, 169 (2007)
5) B. Bastin et al.: Phys. Rev. Lett. 99, 022503 (2007)
6) H. Oliver et al.: Phys. Rev. C 69, 024301 (2004)

Hindered proton collectivity in $^{28}_{16}S_{12}$†

Y. Togano, Y. Yamada,*1 N. Iwasa, K. Yamada, T. Motobayashi, N. Aoi, H. Baba, S. Bishop, X. Cai,*4 P. Doornenbal, D. Fang,*4 T. Furukawa, K. Ieki, T. Kawabata,*5 S. Kanno, N. Kobayashi, Y. Kondo, T. Kuboki,*6 N. Kume,*3 K. Kurita,*1 M. Kurokawa, Y. G. Ma,*4 Y. Matsuo, H. Murakami, M. Matsushita,*1 T. Nakamura, K. Okada,*1 S. Ota,*5 Y. Satou, S. Shimoura,*5 R. Shioda,*1 K. N. Tanaka,*2 S. Takeuchi, W. Tian,*4 H. Wang,*4 J. Wang,*7 and K. Yoneda

The reduced transition probability $B(E2; 0^+_{gs} \to 2^+_1)$ for ^{28}S was obtained experimentally using Coulomb excitation at 53 MeV/nucleon.

For the $Z \neq N$ nuclei, the collectivities of protons can be different from one of neutrons due to the neutron or proton structures. The difference of the collectivities can be evaluated using the ratio of the neutron transition matrix element to the proton one (the M_n/M_p ratio)[1]. M_p is related to $B(E2)$ by $e^2M_p^2 = B(E2)$. The M_n value can be deduced from the M_p value in the mirror nucleus by assuming the isospin symmetry. If collective motions of protons and neutrons have same amplitudes, the $|M_n/Mp|$ value is equal to N/Z. Deviation from $|M_n/M_p| = N/Z$ corresponds to a proton or neutron dominant excitation and should indicate a difference in the motions of protons and neutrons.

A ^{28}S beam was produced from 115-MeV/nucleon ^{36}Ar beam and separated by RIPS. The typical ^{28}S intensity was 120 s^{-1}, which corresponds to 1.9% of the total secondary beam intensity. A lead plate with a thickness of 348 mg/cm^2 was used as a secondary target. A scintillator array DALI2 was placed around the target to measure de-excitation γ rays from ejectiles. The scattering angle, ΔE, and E of the ejectiles were measured by using a silicon telescope located downstream of the target.

A 1.5 MeV peak was observed in the γ-ray energy spectrum obtained by DALI2. The peak corresponds to the de-excitation from the known 2^+_1 state in ^{28}S[2]. The $B(E2)$ value of ^{28}S was determined to be 181(31) e^2fm^4 by analyzing the angular distribution of ^{28}S* particle by DWBA calculation[3]. The $|M_n/M_p|$ ratio of ^{28}S amounts to $(1.9 \pm 0.2)N/Z$ by taking the present result and $B(E2)$ of mirror transition in ^{28}Mg[4]. The ratio is significantly larger than N/Z indicating the hindered proton collectivity. This hindrance can be understood if the proton collectivity in ^{28}S is reduced due to the magicity at $Z = 16$. Figure 1 shows (a) the $B(E2)$ values and (b) $|M_n/M_p|/(N/Z)$ ratios of $N = 12$ isotones and $Z = 16$ isotopes. As seen in the figure, the neighboring $N = 12$ isotones have larger $B(E2)$ values and $|M_n/M_p|/(N/Z) \sim 1$, supporting the $Z = 16$ magicity at ^{28}S. The double ratio of $^{30-36}$S are close to unity, indicating that the hindrance of proton collectivity does not appear in these nuclei. The large $|M_n/M_p|/(N/Z)$ at ^{38,40}S can be explained by the neutron skin effect by $Z = 16$ subshell closure[5]. The dotted lines in Fig. 1 show shell model predictions with the USDB effective interaction[6], which interprets the $N = 16$ magicity in neutron-rich nuclei with large $s_{1/2}$-$d_{3/2}$ gap, and the $Z = 16$ magicity in proton-rich nuclei is inherent in the model reflecting the isospin symmetry.

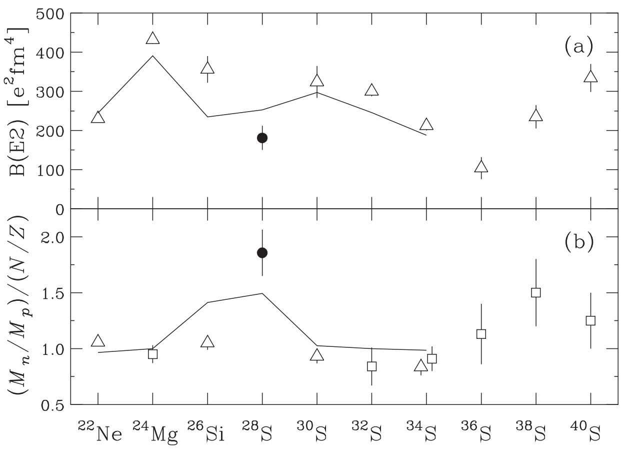

Fig. 1. $B(E2)$ (a) and the $|M_n/M_p|/(N/Z)$ ratios (b) of $N = 12$ isotones (^{22}Ne, ^{24}Mg, ^{26}Si) and $Z = 16$ isotopes.

References
1) A. M. Bernstein et al.: Phys. Rev. Lett. **42**, 425 (1979).
2) K. Yoneda et al.: Phys. Rev. C **74**, 021303 (2006).
3) J. Reynal, “Coupled Channel Code ECIS97” (unpublished).
4) S. Raman et al.: Nucl. Data Tables **78**, 1 (2001).
5) F. Maréchal et al.: Phys. Rev. C **60**, 034615 (1999).
6) B. A. Brown and W. A. Richter: Phys. Rev. C **74**, 034315 (2006).

† Condensed from the article in Phys. Rev. Lett. **108**, 222501 (2012)
*1 Department of Physics, Rikkyo University
*2 Department of Physics, TITECH
*3 Department of Physics, Tohoku University
*4 Shanghai Institute of Applied Physics, CAS
*5 Center for Nuclear Study (CNS), University of Tokyo
*6 Department of Physics, Saitama University
*7 Institute of Modern Physics, CAS

Investigation of shell evolution towards ^{78}Ni by decay spectroscopy

M. Niikura, Z. Xu, S. Nishimura, G. Benzoni,*1 F. Browne, P. Doornenbal, S. Franchoo,*2 G. Gey, T. Isobe, H. S. Jung, P. John,*3 Z. Li,*4 G. Lorusso, I. Matea,*2 K. Matsui, D. Mengoni,*3 P. Morfouace,*2 D. R. Napoli,*3 H. Nishibata, A. Odahara,*5 E. Sahin,*6 P.-A. Söderström, D. Sohler,*7 I. Stefan,*2 T. Sumikama, D. Suzuki,*2 R. Taniuchi, J. Taprogge, Zs. Vajta, V. Werner,*8 H. Watanabe, J. Wu, A. Yagi, for the EURICA collaboration

Considerable efforts have been made to experimentally reach the region in the closest vicinity of $^{78}_{28}$Ni$_{50}$ for studying the doubly-magic character of this very neutron-rich nucleus. Systematic studies of the excitation energy of the first 2^+ states and their reduced transition probability have been performed on even-even nuclei in this region, and they suggest the existence of shell gaps at $Z = 28$ and $N = 50$ in ^{78}Ni[1–4]. Despite this, the exact single-particle energy sequence and its evolution towards ^{78}Ni are still poorly revealed experimentally both for protons and neutrons.

Odd-mass nuclei provide unique tools for studying the single-particle evolution. For example in Cu isotopes, the proton $1f_{5/2}$ orbital is lowered in energy as the neutron number increases. It has been suggested in a recent work that this orbital lies even below the $2p_{3/2}$ one present between $N = 44$ and $N = 46$, implying a diminished gap at $Z = 28$[5]. For the neutron, some reduction of the single-particle energy gap between the $2d_{5/2}$ and $3s_{1/2}$ orbitals was deduced by β-delayed γ-ray spectroscopy[6–8]. Theoretical works that have attempted to extrapolate the single-particle energies at ^{78}Ni using different models predict different trends of single-particle evolution[9–11].

In order to extract single-particle energies by observing low-lying states in odd-mass nuclei close to ^{78}Ni, we performed a decay spectroscopy at the RIBF. Nuclei in this region were produced by in-flight fission of a 345-MeV/nucleon ^{238}U beam with an intensity of about 10 particle nA impinging on a 3-mm-thick Be target. Fission fragments were separated with the BigRIPS fragment separator and the ZeroDegree Spectrometer (ZDS)[12]. In order to reduce the background events in the β-ray spectra[13], the total beam intensity was kept below 100 particles per second at the end of the ZDS by selecting high-momentum fragments using slits at the momentum-dispersive focal plane F1. An unambiguous particle identification was achieved on an event-by-event basis by measuring magnetic rigidity ($B\rho$), time of flight (TOF), and energy loss (ΔE) of the fragment. They were measured using parallel-plate avalanche counters (PPACs) placed at F3, F5, and F7, with plastic scintillators placed at F5 and F7, and an ionization chamber placed at the end of the ZDS (F11).

The nuclei transported through the ZDS were implanted in a Wide-range Active Silicon Strip Stopper Array of Beta Ions (WAS3ABI) β-counting system[14] consisting of eight layers of double-sided silicon-strip detectors (DSSSDs) with a combined thickness of 8×1 mm. A 14.5-mm-thick aluminum degrader was placed upstream of the WAS3ABI chamber to implant all the ions in the 8-layer DSSSDs. The positions of the implanted nuclei as well as β rays from subsequent β decays were reconstructed using the deposited energy and the position in the DSSSD. The **EU**roball **RI**ken **C**luster **A**rray (EURICA)[15] was placed around the DSSSDs to detect γ rays originating from both the isomeric states and the β decays of the implanted ions. EURICA consists of 12 clusters, each composed of seven germanium crystals. The overall energy resolution is about 2.7 keV, and the total photo-peak efficiency of the array is about 7% at 1.3-MeV γ ray.

The data analysis is now in progress.

*1 Sezione di Milano, INFN, Italy
*2 IPN Orsay, IN2P3/CNRS, France
*3 Laboratori Nazionali di Legnaro (LNL), INFN, Italy
*4 Peking University, China
*5 Department of Physics, Osaka University
*6 Oslo University, Norway
*7 ATOMKI, Hungary
*8 WNSL, Yale University, USA

References

1) O. Sorlin and M.G. Porquet: Prog. Part. Nucl. Phys. **61** (2008) 602.
2) N. Aoi et al.: Phys. Lett. B **692** (2010) 302.
3) J. M. Daugas et al: Phys. Rev. C **81** (2010) 034304.
4) J. Van de Walle et al.: Phys. Rev. Lett. **99** (2007) 142501.
5) K. Flanagan et al.: Phys. Rev. Lett. **103** (2009) 142501.
6) O. Perru et al.: Eur. Phys. J. A **28** (2006) 307.
7) D. Verney et al.: Phys. Rev. C **76** (2007) 054312.
8) J. A. Winger et al.: Phys. Rev. C **81** (2010) 044303.
9) J. Duflo and A.P. Zuker: Phys. Rev. C **59** (1999) R2347.
10) K. Sieja et al., Phys. Rev. C **79** (2009) 064310.
11) A. F. Lisetsky et al., Phys. Rev. C **70** (2004) 044314.
12) T. Kubo: Nucl. Instr. and Meth. B **204** (2003) 97.
13) S. Nishimura et al.: Phys. Rev. Lett. **106** (2011) 052502.
14) S. Nishimura et al: in this report.
15) P.-A. Söderström et al.: in this report.

Neutron-knockout cross sections from light Sn isotopes

L. Audirac,[*1] P. Doornenbal, A. Obertelli,[*1] S. Takeuchi, N. Aoi, H. Baba, P. Bednarczyk, S. Boissinot,[*1] M. Ciemala,[*2] A. Corsi,[*1] T. Isobe, A. Jungclaus,[*3] V. Lapoux,[*1] J. Lee, K. Matsui, M. Matsushita,[*4,5] T. Motobayashi, D. Nishimura, S. Ota,[*5] E. C. Pollacco,[*1] H. Sakurai, C. Santamaria,[*1] Y. Shiga, D. Sohler,[*6] D. Steppenbeck,[*4] R. Taniuchi, and H. Wang[*7]

The robustness of shell closures away from stability is still an open question for nuclear shell structure. From this point of view, the region of ^{100}Sn, candidate for double magicity at $N = Z = 50$ situated at the proton drip-line, is of particular interest to study the evolution of single-particle energies, the residual interaction and the neutron-proton interaction in this mass region. On the experimental side, the systematics of the transition probability $B(E2; 0_1^+ \rightarrow 2_1^+)$ is shown to present an enhancement for light Sn isotopes as compared to shell-model predictions with a ^{90}Zr core[1–4]. The spectroscopy of ^{100}Sn produced by two-neutron removal reaction from ^{102}Sn could be foreseen in the future. The knowledge of neutron-removal cross sections in the ^{100}Sn mass region is of prior importance to show the feasability of such an experiment.

The present experiment was performed in July 2012 to measure neutron-removal cross sections from a beam of ^{104}Sn at the Radioactive Isotope Beam Factory (RIBF) of RIKEN. ^{104}Sn was produced and selected at the BigRIPS fragment separator[5] from the interaction of a primary beam of ^{124}Xe at 345 MeV/u with a 3 mm thick Be production target. ^{104}Sn interacted at about 150 MeV/u with a secondary target to produce ^{102}Sn. The reaction products were identified by the Zero Degree Spectrometer (ZDS) whereas the secondary target was surrounded by the gamma detection setup DALI2[6] to perform the spectroscopy of the residual nuclei. During the experiment, a second setting of selection of ^{112}Sn by BigRIPS was also used.

For the measurement of the production cross sections, identifications of the ions are requested at the entrance and the output of the secondary target. This is achieved by means of $B\rho - \Delta E - TOF$ method with the use of PPACs detectors, plastic detectors and MUSIC ionization chambers for beam position, time of flight and charge measurements, respectively. A first identification is made between the F5 and F7 focal planes for the incoming ^{104}Sn particles. The identification of the ions produced downstream the secondary target is achieved between the F9 and F11 focal planes.

Two types of secondary targets were used during the experiment: a carbon and a plastic target of CH_2. Data are under analysis; preliminary inclusive neutron-removal cross sections are obtained for carbon and for hydrogen by subtraction of the carbon background. Figure 1 shows the production of tin isotopes from incoming ^{104}Sn on a carbon target.

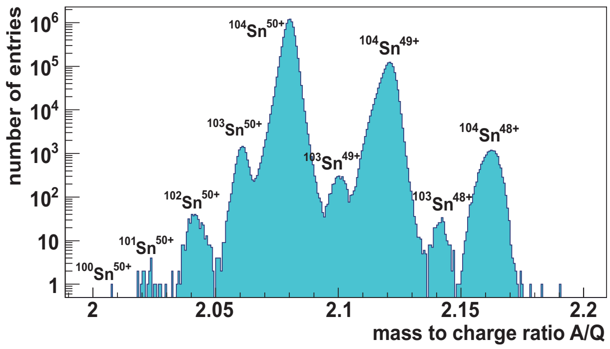

Fig. 1. Projection over the mass to charge ratio of the tin isotopes produced by ^{104}Sn interacting a carbon target. Isotopes and charge states are indicated.

These first direct reaction measurements in the vicinity of ^{100}Sn will be compared to state-of-the-art Shell-Model and eikonal formalism predictions. Moreover, a setting centered on the ^{112}Sn isotope has been measured and will allow us to extract the neutron-removal cross sections for this stable nucleus. They will be compared to the ones from ^{104}Sn, leading to a better understanding of the dependance of the cross section with the separation energy value. Finally, the gamma spectroscopy of the nuclei produced after the secondary target will be extracted. From the spectra, corrected with the detection efficiency of DALI2, the exclusive cross sections for the population of the bound excited states of ^{102}Sn and ^{103}Sn will be extracted.

[*1] CEA-Saclay, IRFU-SPhN
[*2] IFJ Pan Cracow
[*3] CSIC Madrid
[*4] CNS, University of Tokyo
[*5] Department of Physics, Rikkyo University
[*6] MTA ATOMKI, Debrecen
[*7] SKLNPT, Peking University

References
1) C. Vaman *et al.*, Phys. Rev. Lett. **99**, 162501 (2007).
2) A. Banu *et al.*, Phys. Rev. C **72**, 061305(R) (2005).
3) J. Cederkäll *et al.*, Phys. Rev. Lett. **98**, 172501 (2007).
4) A. Ekström *et al.*, Phys. Rev. Lett. **101**, 012502 (2008).
5) T. Kubo *et al.*, Prog. Theor. Exp. Phys. 2012, 03C003 (2013).
6) S. Takeuchi *et al.*, RIKEN Acc. Prog. Rep. 36, 148 (2003).

Production of ^{55}Sc and ^{54}Ca beams and measurement of yields and cross sections using projectile fragmentation of ^{70}Zn

N. Inabe, T. Kubo, H. Suzuki, N. Fukuda, H. Takeda, D. Kameda, K. Yoshida, K. Kusaka, K. Tanaka, Y. Yanagisawa, M. Ohtake, H. Sato, Y. Shimizu.

In July 2012, we delivered ^{55}Sc and ^{54}Ca beams produced by projectile fragmentation of ^{70}Zn of 345 MeV/u, which was the first ^{70}Zn beam from the SRC[1]. The RI beam productions were performed by the BigRIPS separator[2] through tuning with several settings. Herein, we report on yields and cross sections of not only ^{55}Sc and ^{54}Ca but also all isotopes produced during the BigRIPS tuning.

Table 1 lists the conditions of the BigRIPS required for productions of ^{55}Sc and ^{54}Ca beams and the conditions of an isomer tagging run using ^{54m}Sc for the confirmation of the particle identification (PID). Magnetic rigidity ($B\rho$) for the ^{54}Ca setting was set to obtain maximum yields but that for the ^{55}Sc setting was set at -1% lower than optimum value in order to mix ^{56}Ti. Slit widths were determined so as to maximize the purities of ^{54}Ca and ^{55}Sc+^{56}Ti. The conditions such as $B\rho$ and slit widths of ^{54m}Sc were determined so that yield of ^{54}Sc was large and neutron rich isotopes including ^{54}Ca, ^{55}Sc, and ^{56}Ti could be seen at the same time. A degrader at F1 was used for the separation of RI produced at a target and that at F5 was used for separation of contaminants produced at the F1 degrader. We used another setting that is A/Z=2.5 run for calibration of detectors. In the setting we didn't use degraders and set Be 10mm target, $B\rho$= 6.5559 Tm and momentum acceptance =±0.6%.

The PID is performed using the ΔE-TOF-$B\rho$ method, which allows the event-by-event determination of the atomic number Z and mass-to-charge ratio A/Q of fragments. The energy loss (ΔE) was measured by an ion chamber (MUSIC) at F7. The time-of-flight (TOF) between F3 and F7 was measured by using thin plastic scintillators. The fragment trajectory (positions and angles) was measured at F3, F5, and F7 by using PPACs in order to determine the $B\rho$ value of a fragment precisely.[3] A delayed γ-ray emitted from ^{54m}Sc was measured by four clover-type Ge detectors at F7.

Figure 1 shows PID plots of Z vs A/Q for ^{55}Sc and ^{54}Ca settings. The PID was confirmed very quickly by large counts of the γ-ray from ^{54m}Sc (~1counts/min) in the isomer tagging run. Intensity of the ^{54}Ca beam was 1.1 pps/pnA and the purity was 0.5%. Main contaminants were ^{55}Sc (6.1 pps/pnA) and ^{56}Ti (8.4 pps/pnA) that were isotones of ^{54}Ca. For the ^{55}Sc setting the intensities of ^{55}Sc and ^{56}Ti were 12.5 pps (purity; 5.5%) and 140 pps/pnA (purity 61%) , respectively, and the main contaminant was ^{57}V at 38.4 pps/pnA.

Cross sections were deduced using the transmission efficiency calculated by LISE++[4] for each setting. Figure 2 shows the obtained cross sections together with those calculated with EPAX3.01[5]. Both are found consistent over all the regions, although it appears that for Ca isotopes, measured cross sections are smaller than those calculated with EPAX3.01.

Table 1 Summary of the experimental conditions

		^{55}Sc	^{54}Ca	^{54m}Sc
Target		Be 10.0 mm		
Degrader (F1/F5)		Al 5.89 mm / Al 1.40 mm		
$B\rho$ (D1) (Tm)		6.8371	7.0100	6.9060
Momentum Acc. (%)		±3	±3	-0.47~3
Slit width (mm)	F2	±4	±4	-25~15
	F5	±120	±120	-60~120
	F7	±10	±5	-20~18

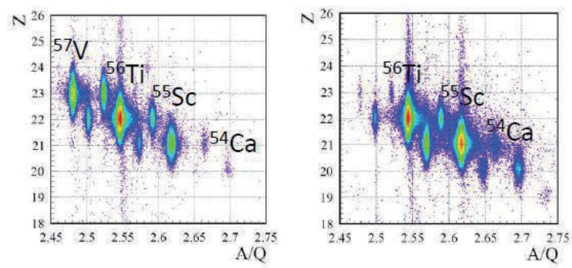

Fig. 1 Z vs. A/Q plots for the ^{55}Sc setting (left) and the ^{54}Ca setting (right).

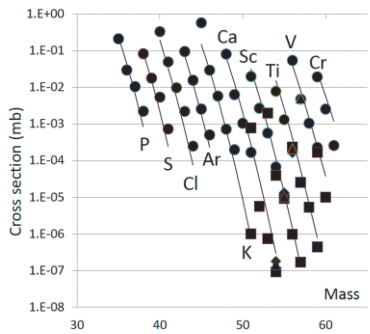

Fig. 2 Obtained cross sections for several settings. (Circle : A/Z=2.5, rectangle : isomer tagging run, triangle : ^{55}Sc setting, diamond : ^{54}Ca setting). Solid line shows cross sections calculated with EPAX3.01.

References
1)Y. Yano: Nucl. Instr. Meth. **B 261**, 1009 (2007).
2) T. Kubo: Nucl. Instr. Meth. **B 204**, 97 (2003).
3) T. Ohnishi et al.: Jpn. J. Phys. Soc. Jpn. **79**, 073201 (2010).
4) O. B. Tarasov and D. Bazin: a manual of the code LISE++ available at http://www.nscl.msu.edu/lise/.
5) K. Sümmerer: Phys. Rew. **C 86**, 014601 (2012).

Measurements of interaction cross sections for Na isotopes

S. Suzuki, M. Takechi, T. Ohtsubo,[*1] D. Nishimura, M. Fukuda, T. Kuboki, M. Nagashima, T. Suzuki,[*2] T. Yamaguchi, A. Ozawa, H. Ooishi, T. Moriguchi, T. Sumikama, H. Geissel, N. Aoi, Rui-Jiu Chen, De-Qing Fang,[*4] N. Fukuda, S. Fukuoka, H. Furuki, N. Inabe, Y. Ishibashi, T. Ito, T. Izumikawa,[*5] D. Kameda, T. Kubo, M. Lantz, C.S. Lee,[*2] Yu-Gang Ma,[*4] M. Mihara, S. Momota, D. Nagae, R. Nishikiori, T. Niwa, T. Ohnishi, K. Okumura,[*3] T. Ogura,[*1] H. Sakurai, K. Sato, Y. Shimbara,[*1] H. Suzuki, H. Takeda, S. Takeuchi, K. Tanaka, H. Uenishi,[*4] M. Winkler and Y. Yanagisawa

Interaction cross sections (σ_I) for Na isotopes from the stability line to the vicinity of the neutron drip line have been measured at around 240 MeV/nucleon. The σ_I values for $^{33\text{-}35}$Na were measured for the first time. The experiment was carried out at BigRIPS in RIBF.

The halo and skin structures at the nuclear surface have attracted much attention from physicists. These exotic structures were discovered by measurements of interaction cross sections.[1,2] Furthermore, the region of neutron rich Ne, Na, and Mg isotopes around N = 20, known as the "island of inversion" has been extensively studied, since the magic number vanishes in this region.[3] Recently, we measured σ_I for Ne isotopes, including for this region, and we suggested the neutron halo structures of ^{29}Ne and ^{31}Ne [4] from the detected enhancement in σ_I.

In this work, we measured σ_I for Na isotopes, including nuclei located in or near the "island of inversion." $^{22\text{-}35}$Na secondary beams were produced through the projectile fragmentation of a 345 MeV/nucleon ^{48}Ca primary beam on a Be target. We used the transmission method to measure σ_I. Figure 1 shows the mass number dependence of σ_I for $^{22\text{-}35}$Na isotopes on C targets. The gray line shows the systematic one for stable nuclei.[4] Enhancements in cross sections are already observed from the systematics of stable nuclei in lighter (A<24) and heavier (A>27) isotopes. From the known values of the nuclear deformation number β_2 of $^{22\text{-}31}$Na, these enhancements can be mainly ascribed to nuclear deformation. Large enhancements in heavier isotopes (A>32) suggest that these nuclei are strongly deformed.

From the present data, the root mean square (RMS) nuclear matter radii $\langle r_m^2\rangle^{1/2}$ were determined by using a Glauber-type calculation (Fig. 2). These $\langle r_m^2\rangle^{1/2}$ are almost in agreement with the theoretical calculation performed using the relativistic mean field model (RMF).[5]

From the comparison with the RMS nuclear proton radii $\langle r_p^2\rangle^{1/2}$, which are obtained using the RMS nuclear charge radii $\langle r_c^2\rangle^{1/2}$,[6,7] a monotonic growth of the neutron skin thickness has been observed as the neutron number increases in Na isotopes. Our results are consistent with the previous work conducted at GSI.[2] Moreover, the analysis of shell structure of neutron excess Na isotopes is currently in progress.

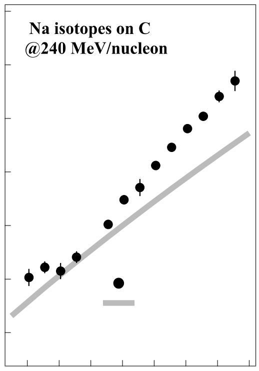

Fig. 1. The observed mass number dependence of interaction cross sections for Na isotopes on C targets. The open circles represent the present data and the gray line shows the systematics for stable nuclei.[4]

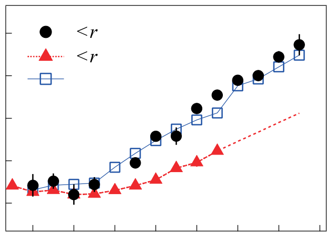

Fig. 2. The RMS nuclear matter radii deduced from present data [solid circles] and the RMS proton radii [solid triangles].[6] The broken line shows the RMS proton radii estimated using the empirical formula for the neutron rich region.[7] The open squares show the RMF calculation values of the RMS nuclear matter radii taken from Ref. 5.

*1 Graduate School of Science, Niigata University
*2 Department of Physics, Saitama University
*3 Institute of Physics, University of Tsukuba
*4 Shanghai Institute of Applied Physics, Chinese Academy of Sciences
*5 RI Center, Niigata University

References

1) I. Tanihata et al.. Phys. Rev. Lett. 55, 2676 (1985).
2) T. Suzuki et al.. Phys Rev. Lett. 75, 3241 (1995).
3) E. K. Warburton et al.. Phys. Rev. C 41, 1147 (1990).
4) M. Takechi et al.. Nucl. Phys. B 707, 357 (2012).
5) L. S. Geng et al.. Nucl. Phys. A 730, 80 (2004).
6) E. W. Otten. Treaties on Heavy-Ion Science 8, 517 (1989).
7) I. Angeli. At. Data Nucl. Data Tables 87, 185 (2004).

Production of radioactive ^{44}Ti beam

H. Ishiyama,[*1] Y.X. Watanabe,[*1] Y. Hirayama,[*1] N. Imai,[*1] Y. H. Kim,[*1] M. Mukai,[*1] M.Oyaizu,[*1] H. Miyatake,[*1] S.C. Joneg,[*1] H. Yamaguchi,[*2] D. Kahl,[*2] T. Nakao,[*2] Y. Wakabayashi, T. Hashimoto,[*3] P. Lee,[*4] G.W. Kim[*5] and T. Komatsubara

The ^{44}Ti ($T_{1/2}$ = 59 yr) nuclide has recently been observed as live radioactivity by γ-ray astronomy from the Cas A supernova (SN) remnant. The observed ^{44}Ti yield is larger by a factor of 2-10 than those calculated in current SN models. The ^{44}Ti yield strongly depends not only on current SN models but also on the astrophysical reaction rates in SN nucleosynthesis. The sensitivity study for the reactions concerned suggests that several key reactions can largely affect the ^{44}Ti yield, and the ^{44}Ti(α, p)^{47}V reaction has the highest sensitivity for the yield of ^{44}Ti, which directly destroys ^{44}Ti. Although the direct measurement of ^{44}Ti (α, p)^{47}V cross sections was performed at the Argonne National Laboratory[1)], this measurement did not cover the astrophysically interesting energy regime. Thus, we have proposed the direct measurement of the cross sections of ^{44}Ti(α, p)^{47}V in the energy regime of astrophysical interest. Further, a compound nucleus of the ^{44}Ti + α system is ^{48}Cr, in which ^{40}Ca + α + α three-cluster states were predicted to exist in almost the same energy regime of astrophysical interest[2)];however these states have not thus far been observed. These states can be accessible by the measurement of ^{44}Ti (α, α) resonant elastic scatterings. Therefore, in order to perform these measurements, we have attempted to produce a ^{44}Ti radioactive nuclear beam at the CRIB.

The production reaction for ^{44}Ti was selected to be the ^{3}He (^{42}Ca, ^{44}Ti) n reaction. The energy of the ^{42}Ca^{12+} primary beam was set at 5.92 MeV/u, which is the maximum value available at the AVF cyclotron. The pressure of the ^{3}He gas target with 2.5-μm-thick Havar windows was set to be 300 Torr at 90 K. The length of the ^{3}He gas target was 8 cm. The ^{44}Ti beam, in principle, can be separated from ^{42}Ca and other contaminants by using the in-flight technique at the CRIB. In order to measure the intensity and purity of the ^{44}Ti beam, an ionization chamber (IC) and a solid-state Si detector (SSD) were placed at F3(final focal plane) of CRIB, which can provide energy loss (ΔE) and residual energy (E) for particle identification.

Figure 1 shows the ΔE−E plots obtained from the IC + SSD at F3. The ^{42}Ca beam intensity was about 1 pnA. As shown in Fig. 1(a), when the Wien filter was not on, several contaminants, particularly ^{42}Ca with the highest intensity,

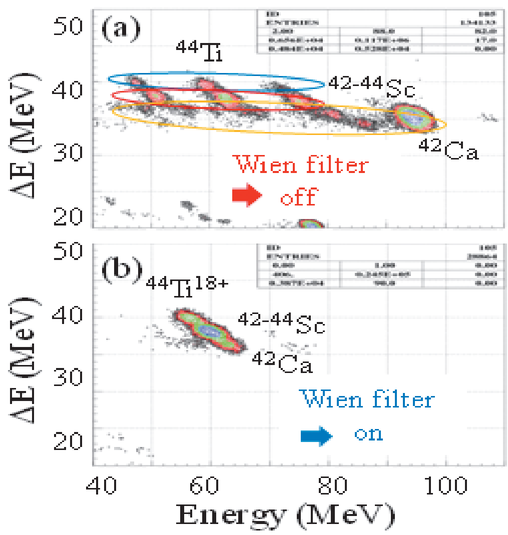

Fig. 1 ΔE−E plots at F3 of CRIB. The measurements shown in panels of (a) and (b) were obtained when the Wien filter was off with the CRIB optical parameters at A/q = 44/17+ and E = 110 MeV, and when the filter on at A/q = 44/18+ and E = 110 MeV, respectively. In Fig. 1(a), blue, red, and orange circles indicate ^{44}Ti, $^{42\text{-}44}$Sc, and ^{42}Ca with different charge states, respectively. Particle identification was carried out by obtaining the ΔE differences based on the elastic-scattered ^{42}Ca particles and from expected possible products from the production reaction.

were observed. When the Wien-filter was on (Fig.1(b)), most of these contaminants were removed. As the result, the observed intensity for ^{44}Ti was 130–350 pps (depending on the charge states)/1 pnA ^{42}Ca, corresponding to 0.9–2 × 10^4 pps/70 pnA ^{42}Ca, which is the maximum beam current for the ^{3}He gas target, and the beam purity was about 15%. A ^{44}Ti beam can now be generated with sufficient intensity to perform the abovementioned measurements. The particle identification for the beam contaminants can be performed using ΔE − E(TOF) measurements, in which the ΔE differences between different particles are the same as in Fig. 1 (b). After the construction of a new ionization chamber for ΔE measurement, which will be installed immediately in front of a secondary target (^{4}He), we plan to perform the abovementioned measurements.

References

1) A.A. Sonzogni et al.: Phys. Rev. Lett. 84, 1651 (2000).
2) P. Descouvemont : Nucl. Phys. A 709, 275 (2002).

*1 IPNS, KEK
*2 CNS, University of Tokyo
*3 RCNP, Osaka University
*4 Department of Physics, Chung-Ang University
*5 Department of Physics, Ewha Womans University,

Beam production of ^{22}Mg for studying alpha-scattering at CRIB

N. N. Duy, L.H. Khiem,[*1] S. Kubono, H. Yamaguchi,[*2] D. Kahl,[*2] T. Hashimoto,[*2] S. Ota,[*2] Y. Wakabayashi, T. Komatsubara, T. Teranishi,[*3] S. Kato,[*4] N. Iwasa, T. Yamada,[*5] Y. K. Kwon,[*6] A. Kim,[*7] Y. H. Kim,[*7] J. S. Song,[*7] J. Hu,[*8] and Y. Ito

Alpha-scattering and (α,p) reaction of the nucleus ^{22}Mg play important roles in explosive Hydrogen burning stage under high temperature and high density conditions such as X-ray bursts and type II supernovae. For nuclear structure, the experimental information of ^{26}Si above alpha threshold (9.17 MeV) is very limited. And its alpha cluster structure can be investigated via ^{22}Mg+α. Since the ^{22}Mg+α relates to astrophysical aspects, such as astronomical anomalies[1, 2, 3] and nuclear structure of ^{26}Si, it is necessary to produce a low-energy of radioactive ion beam of ^{22}Mg for direct measurement the ^{22}Mg+α system in invert-kinematics. We produced a ^{22}Mg to measure alpha-scattering and (α,p) of the nucleus ^{22}Mg at CRIB[4] (Center for Nuclear Study (CNS) low-energy RI Beam separator of the University of Tokyo) in October, 2011.

The radioactive ions are produced via ^{3}He(^{20}Ne,^{22}Mg)n reaction by bombarding a Havar-window with a thickness of 2.5 μm cryogenic gas target[5] of ^{3}He at 90 K with a length along the beam axis of 80mm, with the primary beam of ^{20}Ne . We optimized the intensity together with purity of ^{22}Mg^{12+} beam based on pressure of production target and current of primary beam of ^{20}Ne^{10+}. We tested four production target pressures up to 180 torr and searched the maximum yield of ^{22}Mg^{12+} at the interested energy E = 3.73 MeV/u. The RI beam was firstly purified between F0 and F2 using dipole magnets and identified by beam monitor PPAC[6].

The further purification of RI beam was performed by using the Wien Filter, achieving a high purity of ^{22}Mg on the experimental plane F3. Particle identification of different species from production reaction was carried out by time-of-flight (*ToF*) and energy E of particles measured by PPACs at F2, F3.

The results show that the average intensity of ^{22}Mg^{12+} at 3.73 MeV/u reaches to maximum value with the production target ^{3}He at 170 torr of pressure and 700 enA of ^{20}Ne^{10+}. In such condition, the ^{22}Mg^{12+} beam is 30% of purity and 1.2 x 10^3 pps of intensity on the active target at F3. The yield of ^{22}Mg^{12+} is not directly proportional to the intensity of the primary beam. As can be seen in Fig.1, at the same pressure of 170 torr of the gas target, although the ^{20}Ne^{10+} beam current is higher than 700 enA, the yield of ^{22}Mg^{12+} goes down. The phenomena should be caused by heating effect on the beam axis. Since a high current beam comes through, the gas will be expanded and density of the target along the axis will be decreased by heating power.

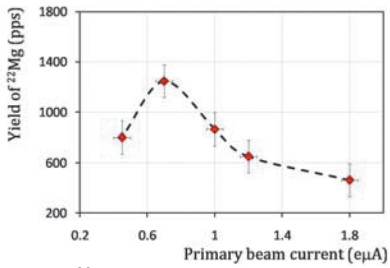

Fig.1. The yield of ^{22}Mg is as a function of the current of ^{20}Ne at 170 torr of target pressure.

Main contaminants are ^{20}Ne^{10+} and ^{21}Na^{11+}, as shown in Fig.2. The transmission of Wien Filter evaluated is 50% with a high voltage supply of ±65 kV. It is expected that the transmission and purity of the beam will be higher at higher voltage[7].

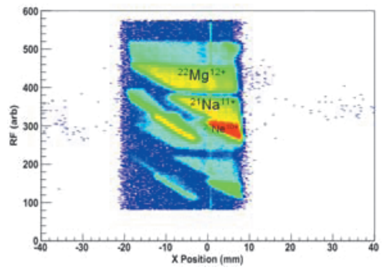

Fig.2. The main contaminants are only primary beam ^{20}Ne^{10+} and ^{21}Na^{11+}.

In general, the ^{22}Mg^{12+} beam is produced successfully for the measurement of the ^{22}Mg + α system at CRIB. The heating power in the gas along the beam axis affecting on the yield of the beam should be considered. The improvement of purity of the beam and transmission of Wien Filter gives an opportunity for a higher yield of RI beam production in future.

*1 Institute of Physics, Vietnam Academy of Science and Technology.
*2 Center for Nuclear Study, Graduate School of Science, Univ. of Tokyo.
*3 Department of Physics, University of Kyushu, Japan.
*4 Department of Physics, University of Yamagata, Japan.
*5 Department of Physics, University of Tohoku, Japan.
*6 Department of Physics, ChungAng University, Korea.
*7 Department of Physics, Seoul University, Korea.
*8 Institute of Modern Physics, Chinese Academy of Science.

References

1) J. C. Higdon et al., the Astrophys J, (1987) 317: 710-716.
2) M. Arnould et al., Astron. Astrophys. 64, (1978) 195-213.
3) W. Hillebrandt and F. K. Thielemann, the Astrophys. J, 255, 617-623, (1982) 15.
4) S. Kubono, Nucl. Inst. and Meth. A 539 (2005) 74–83.
5) H.Yamaguchi et al: Nucl.Instrum.Meth. A589(2008) 150.
6) H. Kumagai, A. Ozawa, et al. Nucl.Instrum.Meth. A470 (2001) 562-570.
7) H. Yamaguchi et al: CNS Report 2004 (2005) 69-70.

Discovery of 14 new isotopes and 19 new isomers around neutron-rich rare-earth isotopes produced by in-flight fission of 345 MeV/nucleon ^{238}U

D. Kameda, T. Kubo, N. Fukuda, H. Takeda, H. Suzuki, K. Yoshida, K. Kusaka, K. Tanaka, Y. Yanagisawa, M. Ohtake, N. Inabe, H. Sato, Y. Shimizu, H. Baba, M. Kurokawa, D. Nishimura, T. Ohnishi, N. Iwasa, A. Chiba, T. Yamada,[*1] E. Ideguchi,[*2] S. Go, R. Yokoyama,[*2] T. Fujii, H. Nishibata, K. Ieki, D. Murai, S. Momota, Y. Sato, J. Hwang, S. Kim, O. B. Tarasov, D. J. Morrissey, B. M. Sherrill, and G. Simpson[*3]

Neutron-rich nuclei with atomic number Z ranging from 57 to 71, which are called lanthanides or rare-earth isotopes, are of interest due to their large nuclear deformation. These nuclei are located around the double mid-shell region of the wide open shells characterized by the conventional magic numbers, i.e., $Z = 50$, 82 and neutron numbers $N = 82$, 126. A particularly large deformation is expected to occur around the double mid-shell nucleus $^{170}_{66}\mathrm{Dy}_{104}$ according to the largest value of the valence nucleon product N_pN_n.[1)] However, experimental difficulties in the production and identification of such neutron-rich rare-earth isotopes have prevented us from studying the shape evolution around this region since the first finding of the sudden onset of the large deformation at $N \sim 90$.[2)]

To expand the frontier of accessible neutron-rich rare-earth nuclei, we conducted a search for new isotopes and microsecond isomers by the in-flight fission of a 345-MeV/nucleon ^{238}U beam at the RIBF. In-flight fission is advantageous to both separation and identification of the products when compared with the ISOL system; fragments are immediately emitted from a target in a narrow cone with velocities similar to that of the projectile, regardless of the chemical properties. This allows one to utilize the in-flight separator for the efficient selection of the fragments as well as carry out particle identification in flight. Moreover, the fast physical process occurring within one microsecond allows the sensitive detection of isomeric decay with microsecond half-lives for the identified fragment by the particle-γ slow correlation technique.

We separated and identified fission fragments event by event using the BigRIPS separator. Particle identification was made by the TOF-$B\rho$-ΔE method for deducing the mass-to-charge ratio A/Q and Z. Isomeric γ-rays were detected by four clover-type HPGe detectors closely surrounding the stack of Si detectors at the focal plane in which fragments were implanted.[3,4)] Because of the excellent resolution achieved for A/Q, we identified a total of 14 new isotopes in the Z versus A/Q plot shown in Fig. 1; the dashed open circles indicate the new isotopes identified, namely, ^{153}Ba, ^{154,155}La, ^{156,157}Ce, $^{155\text{-}160}$Pr, ^{162}Nd, ^{164}Pm, and ^{166}Sm. At the same time we observed a total of 19 new isomers: ^{158m}Pm, ^{159m}Pm, ^{161m}Pm, ^{161m}Sm, ^{162m}Sm, ^{163m}Eu, ^{164m}Eu, ^{162m}Gd, ^{164m}Gd, ^{165m}Gd, ^{166m}Gd, ^{165m}Tb, ^{166m}Tb, ^{167m}Tb, ^{168m}Tb, ^{167m}Dy, ^{169m}Dy, ^{170m}Dy, and ^{171m}Ho as well as the previously reported isomers ^{152m}Pr, ^{153m}Nd, ^{154m}Nd, ^{156m}Nd, and ^{160m}Sm.

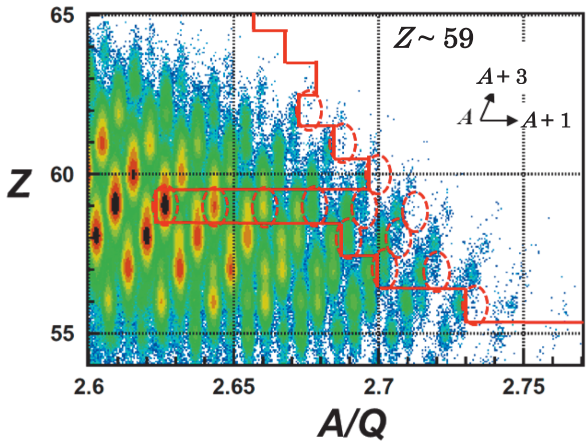

Fig. 1. Z versus A/Q PID plots of the fission fragments produced in the ^{238}U + Be reaction at 345 MeV/nucleon with the Z ~ 59 setting.[3)]

It is remarkable that the new isomers are observed in the localized area, for instance, in $N = 100$ isotones such as ^{162m}Sm, ^{163m}Eu, and ^{164m}Gd,[5)] and in the Tb isotopes.[6)] The K isomerism is one of the possible mechanisms for explaining the systematic appearance of isomers in this well-deformed region.[7)] The spectroscopic information obtained in this work, such as half-lives and γ-ray relative intensities, allows us to study the level schemes as well as the nature of nuclear isomerism around the double mid-shell region systematically for the first time. One of the interesting results is the finding of the isomeric state of the double mid-shell nucleus ^{170m}Dy. The systematic data of the production yields of isotopes and isomers identified in the present work are also invaluable for future experiments at RIBF. Detailed analysis is currently in progress.

References

1) R. F. Casten: Nucl. Phys. **A443**, 1 (1985).
2) P. Brix: Z. Phys. **126**, 344 (1949).
3) D. Kameda et al.: RIKEN Accel. Prog. Rep. **45**, 117 (2012).
4) D. Kameda et al.: RIKEN Accel. Prog. Rep. **45**, 120 (2012).
5) S. Go et al.: In this report.
6) R. Yokoyama et al.: In this report.
7) G. Simpson et al.: Phys. Rev. C **80**, 024304 (2010).

*1 Department of Physics, Tohoku University
*2 Center for Nuclear Study, University of Tokyo
*3 LPSC-IN2P3

Observation of new isomers in $N = 100$ neutron-rich rare-earth nuclei

S. Go, D. Kameda, T. Kubo, N. Inabe, N. Fukuda, H. Takeda, H. Suzuki, K. Yoshida, K. Kusaka, K. Tanaka, Y. Yanagisawa, M. Ohtake, H. Sato, Y. Shimizu, H. Baba, M. Kurokawa, D. Nishimura, T. Ohnishi, N. Iwasa, A. Chiba, T. Yamada,[*2] E. Ideguchi,[*1] R. Yokoyama,[*1] T. Fujii, H. Nishibata, K. Ieki, D. Murai, S. Momota, Y. Sato, J. Hwang, S. Kim, O. B. Tarasov, D. J. Morrissey, B. M. Sherrill, and G. Simpson,[*3]

Neutron-rich nuclei far from stability are fascinating since their isospin asymmetry sometimes gives rise to a drastic change in nuclear shapes and shell structure. In the double mid-shell regions, such as neutron-rich rare-earth region, nuclei are known to be well deformed, and K isomers are often observed systematically. Significantly hindered transitions could occur in the situation that the K quantum number is a good quantum number in the deformed system and the change in the K value exceeds the transition multipolarity[1)].

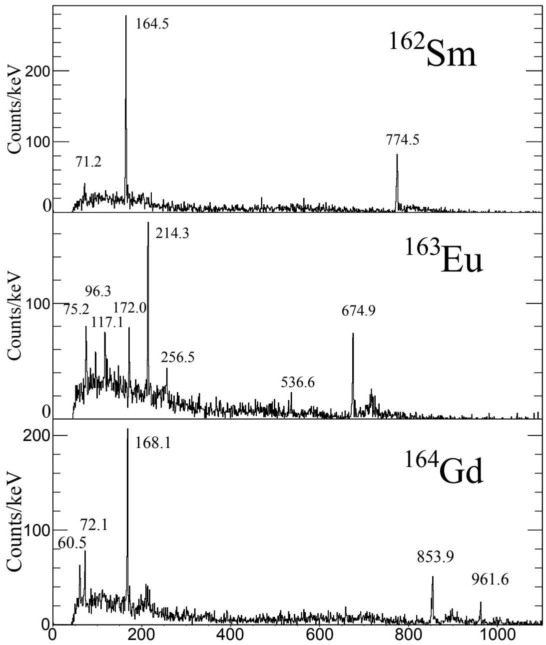

Fig. 1. Delayed γ-ray spectra for ^{162}Sm, ^{163}Eu, ^{164}Gd. The time gate is from 0.5 to 10 μs following ion implantation.

We observed new isomeric decays in the neutron-rich rare-earth isotopes, ^{162}Sm, ^{163}Eu, and ^{164}Gd, which have 100 neutrons, by means of the isomer spectroscopy at the RIKEN RI Beam Factory. In this experiment[2,3)], the nuclei were produced by the in-flight fission of ^{238}U at an energy of 345 MeV/nucleon with a ^{9}Be target of 4 g/cm^2 thickness. The intensity of the uranium beam was roughly 0.3 pnA. Fission fragments were separated using the BigRIPS separator according to the mass-to-charge ratio A/Q and energy loss. Particle identification was performed event by event by measuring the magnetic rigidity ($B\rho$), time of flight (TOF), and the energy loss (ΔE) of the particles that were stopped in the stack of Si detectors. The isomeric γ-rays were measured by four clover type Ge detectors closely surrounding the Si stack. Figure 1 shows the delayed γ-ray spectra of $N = 100$ isotopes.

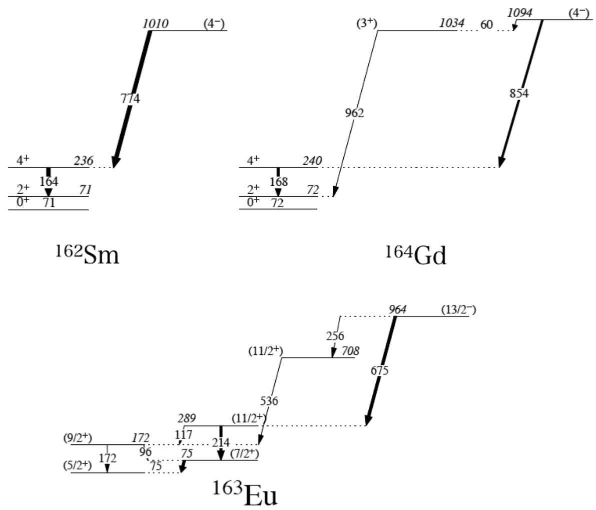

Fig. 2. Proposed level schemes of ^{162}Sm, ^{163}Eu, ^{164}Gd.

From the observed γ-ray energies and reduced transition probabilities as well as the systematics of heavier $N = 100$ isotones, level schemes of these isomers are proposed (Fig. 2). It is likely that these isomeric states are characterized by the two-quasineutron configuration as $[1/2[521] \otimes 7/2[633]]$ $K = 4^-$. Systematic studies of these new isomers in the deformed region with known K-isomers are currently in progress.

References
1) K. Lobner: Phys. Lett. B **26**, 369 (1968).
2) D. Kameda: *et al.*: RIKEN. Accel. Prog. Rep. **45**, 171 (2012).
3) R. Yokoyama *et al.*: RIKEN. Accel. Prog. Rep. **45**, 12 (2012).

*1 Center for Nuclear Study, University of Tokyo
*2 Department of Physics, Tohoku University
*3 LPSC-IN2P3

Yrast 6^+ seniority isomers of ^{136,138}Sn

G.S. Simpson,[*1] A. Jungclaus,[*2] G. Gey,[*1] J. Taprogge,[*2*3] S. Nishimura, H. Baba, S. Bönig,[*4] F. Browne, J.-M. Daugas[*5] P. Doornenbal, F. Drouet,[*1] N. Fukuda, R. Gernhäuser,[*6] S. Ilieva,[*4] N. Inabe, H.S. Jung, D. Kameda, T. Kröll,[*4] T. Kubo, G. Lorusso, A. Montaner-Piza,[*7] K. Moschner,[*8] D. Mücher,[*6] H. Nishibata, A. Odahara,[*9] R. Orlandi,[*10] P.-A. Söderström, K. Steiger,[*6] T. Sumikama, H. Suzuki, H. Takeda, Z. Vajta,[*11] H. Watanabe, A. Wendt[*8], J. Wu, Z. Xu, and A. Yagi

The even-A tin nuclei beyond N=82 are ideal candidates to make detailed tests of the predictions of shell-model calculations, due to their semi-magic nature and proximity to the doubly magic ^{132}Sn. The calculated energies of the excited states of the even-even Sn isotopes, made with different shell-model interactions, disagree[1–3]. Furthermore the role of three-body forces is unclear here, as is the evolution of nuclear structure in very neutron-rich regions. The isotopes ^{136,138}Sn are predicted to have isomeric 6_1^+ states[1–3], formed from the maximally aligned coupling of seniority 2, $\nu f_{7/2}$ orbits.

Excited states in the nuclei in the area of the nuclear chart south-east of ^{132}Sn are almost completely unknown. With the aim of testing shell-model predictions here, the nucleus ^{132}Cd has been studied for possible isomeric states and to observe its β decay.

The fission of a 345 MeV/nucleon ^{238}U beam from the RIBF facility, impinging on a 3-mm thick Be target was used to produce ^{132}Cd, ^{136,138}Sn and neighboring nuclei. The primary beam current was typically 8-10 pnA and the experiment ran for 5 days. Isotopes with mass-to-charge values near to, and including, ^{132}Cd, ^{136,138}Sn were selected, and identified, by the BigRIPS in-flight spectrometer, before being implanted into the WAS3ABI active stopper, situated at the BigRIPS focal point (F11). The EURICA spectrometer, which consisted of 12 Cluster Ge detectors, was used to detect γ rays emitted from isomeric nuclei stopped in WAS3ABI[4]. The WAS3ABI active stopper consisted of a stack of 8 double-sided, silicon-strip detectors and sat at the center of the EURICA array. Any γ rays detected up to a $\sim$100 μs after the implantation of an ion in WAS3ABI were recorded.

Excited states of the nuclei produced in the experiment, populated following β decay, can also be studied. The high granularity of the WAS3ABI array allows a spacial correlation between a detected β particle and the last implanted ion in that region of the detector.

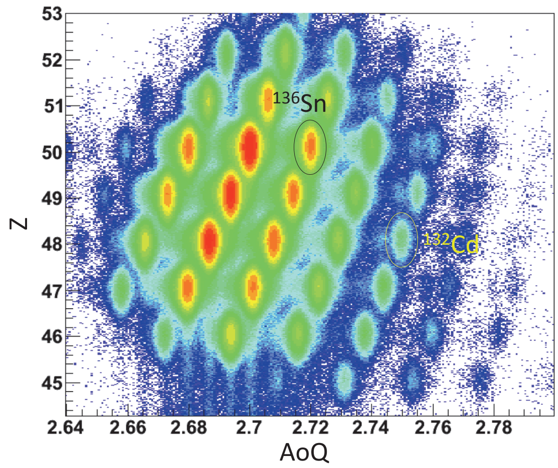

Fig. 1. Ions produced, identified and implanted into the WAS3ABI active stopper. The plot shows the Z of the identified fragment versus the mass-to-charge ratio (AoQ).

This correlation means that γ rays in coincidence with a detected β particle can be assigned to a parent nucleus.

A plot of the ions produced in this experiment are shown in Fig. 1. The combination of the unprecedented high intensity of the primary ^{238}U beam and the high efficiency of the detection setup, for both γ-rays and particles, allows detailed decay spectroscopy in a previously unaccessible region of the chart of nuclides. A preliminary analysis of the data shows that good candidates for isomeric cascades have been found in ^{136,138}Sn. The analysis of these data is currently on going, and includes a search for isomeric states in the other nuclei produced in the experiment. An examination of states produced following β decay will also be performed, along with a study of new the isotopes produced in this experiment.

References
1) M. P. Kartamyshev et al., Phys. Rev. C **76** 024313 (2007).
2) A. Covello et al., Journal of Physics: Conference Series **267**, 012019 (2011).
3) S. Sarkar et al., Phys. Rev. C **81** 064328 (2010).
4) S. Nishimura et al., in this report.

*1 LPSC, Grenoble, France
*2 IEM, CSIC, Madrid, Spain
*3 UAM, Madrid, Spain
*4 T.U. Darmstadt, Germany
*5 CEA Bruyères-le-Châtel, France
*6 T.U. Munich, Germany
*7 IFIC, CSIC-University of Valencia, Spain
*8 IKP, University of Cologne, Germany
*9 Osaka University, Japan
*10 IKS Leuven, Belgium
*11 ATOMKI, Debrecen, Hungary

Study of isomer and proton decays in N $\leq$ Z nuclei below ^{100}Sn

P. Boutachkov,[*1] K. Moschner,[*2] A. Blazhev,[*2] P. Davies,[*3] R. Wadsworth,[*3] F. Ameil,[*4] H. Baba, T. Bäck,[*5] M. Dewald,[*2] P. Doornenbal, T. Faestermann,[*6] A. Gengelbach[*7] J. Gerl,[*4] R. Gernhauser,[*6] S. Go, M. Górska,[*4] H. Grawe,[*4] E. Gregor,[*1] H. Hotaka, T. Isobe, D. G. Jenkins,[*3] J. Jolie,[*2] I. Kojouharov,[*4] N. Kurz,[*4] M. Lewitowicz[*8] G. Lorusso, L. Maier,[*6] E. Merchan,[*1] F. Naqvi[*9] H. Nishibata, D. Nishimura, S. Nishimura, N. Pietralla,[*1] H. Sakurai, H. Schaffner,[*4] H.S. Jung,[*11] P.-A. Söderström, K. Steiger,[*6] T. Sumikama, J. Taprogge,[*10] P. Thöle,[*2] H. Watanabe, V. Werner[*9] Z. Xu, A. Yagi, K. Yoshinaga, and Y. Zhu

In summer 2012 the first EURICA experiment took place. The aim of the RIBF83 experiment is to probe further the decays of known isomers in N=Z nuclei, in order to provide detailed tests of the shell model, as well as search for evidence of predicted, but as yet unobserved isomers in N $\leq$ Z nuclei. The EURICA setup utilizes the γ-ray efficiency of 12 EUROBALL HPGe cluster detectors in close geometry and an active stopper composed of a segmented Si-array. For this experiment we used a modified version of SIMBA[1)] active Si stopper for recording the implanted exotic nuclei and their subsequent particle decays, allowing also β-calorimetry measurements. The modifications allowed for β-calorimetry measurements of positrons emitted in decays with $Q_\beta \sim 10$ MeV. Prior to the experiment the detectors were setup and calibrated. A new DAQ for EURICA was set up, based on a multi-branch system, which uses time stamps to merge the data from different branches that belong to the same event.

To create the nuclei of interest, ^{98}In, ^{96}Cd and ^{94}Ag, projectile fragmentation of a 345 MeV/u ^{124}Xe beam on a ^{9}Be target was used. An identification plot of the nuclei separated in the BigRIPS spectrometer and implanted in the active stopper is shown in Fig. 1. The number of implanted ^{98}In, ^{96}Cd and ^{94}Ag nuclei is about 5000, 20000 and 50000, respectively. The number for ^{98}In is a factor of five less than expected in the proposal. For ^{96}Cd and ^{94}Ag the difference in production is about a factor of three less than expected. Although at the end of the beam time the primary beam intensity grew to more than 10 pnA (assumed in the proposal), the reduced rate in the first days and the more restrictive BigRIPS setting led to a reduction in yield compared to expectations for the isotopes of interest. All detector systems functioned well during the experiment. An example of part of the isomeric γ-decay spectrum of ^{96}Ag is shown in Fig. 2. The spectrum corresponds to a time range 0.1 to 20 μs after implantation and is background subtracted. It confirms the recently reported transitions in ^{96}Ag[2)] (strongest transitions marked in Fig. 2) and contains five times higher statistics compared to data from Ref.[2)]. This confirms the power of the EURICA setup when combined with the BigRIPS spectrometer at the RIKEN Nishina Center.

Further data analysis is on-going to search for unknown isomeric transitions and study the particle and particle-γ decays of the implanted nuclei. The particle-decay study relies on an implantation-decay-correlation procedure which maps the position where a nucleus is implanted in the active stopper and correlates a localized subsequent particle decay with the mapped nucleus.

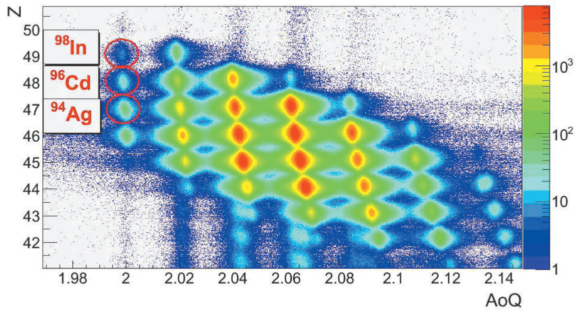

Fig. 1. BigRIPS identification plot.

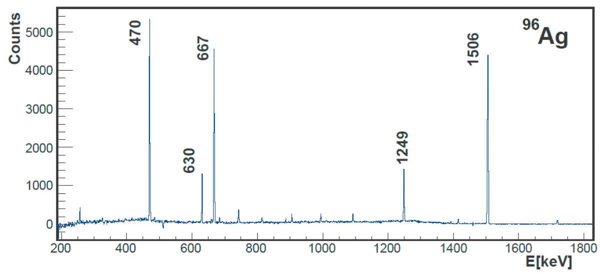

Fig. 2. Isomer γ-decay spectrum of ^{96}Ag.

*1 Technische Universität Darmstadt, Germany
*2 IKP, University of Cologne, Germany
*3 University of York, UK
*4 GSI, Darmstadt, Germany
*5 KTH, Stockholm, Sweden
*6 Technische Universität München, Germany
*7 Uppsala University, Sweden
*8 GANIL, France
*9 Yale University, USA
*10 Uni. Autnoma de Madrid and IEM, CSIC, Madrid, Spain
*11 University of Notre Dame, USA

References

1) Ch. Hinke, Dissertation TU München (2010)
2) P. Boutachkov et al.: Phys. Rev. C 84, 044311 (2011)

Observation of new isomers in neutron-rich deformed Tb isotopes

R. Yokoyama, [*1] D. Kameda, T. Kubo, N. Inabe, N. Fukuda, H. Takeda, H. Suzuki, K. Yoshida, K. Kusaka, K. Tanaka, Y. Yanagisawa, M. Ohtake, H. Sato, Y. Shimizu, H. Baba, M. Kurokawa, D. Nishimura, T. Ohnishi, N. Iwasa, A. Chiba, T. Yamada, [*2] E. Ideguchi, [*1] S. Go, T. Fujii, H. Nishibata, K. Ieki, D. Murai, S. Momota, Y. Sato, J. Hwang, S. Kim, O. B. Tarasov, D. J. Morrissey, B. M. Sherrill, and G. Simpson [*3]

In rare earth nuclei with $Z = 60-66$, it is known that there is a sudden onset of quadrupole prolate deformation at $N = 88-90$.[1)] It is interesting to examine how the nuclear shapes and shell structure change on the more neutron-rich side. However, little is known about the excited states of such neutron-rich nuclides due to experimental difficulties in their production and identification. In-flight fission of the ^{238}U beam at the RI Beam Factory (RIBF) in RIKEN enables us to produce beams of highly neutron-rich isotopes with a wide range of atomic numbers. This novel means provides us with the rare opportunity to study neutron-rich rare-earth nuclei far from stability, which have remain unexamined thus far.

Neutron-rich isotopes in the $Z \sim 60$ region were investigated using the in-flight fission of a 345 MeV/nucleon ^{238}U beam. Fission fragments were identified by measuring the time-of-flight (TOF) and $B\rho$ in the second stage of BigRIPS and measuring the ΔE-E by the Si stack at the last focal plane.[3)] The γ-rays from the isomeric states were detected by four clover-type HPGe detectors placed around the Si stack.[2)]

We have systematically observed new isomers in the neutron-rich Tb isotopes ^{165}Tb, ^{166}Tb, ^{167}Tb and ^{168}Tb. Total numbers of beam fragments were 1.3×10^5, 1.5×10^5, 1.2×10^5, and 6.0×10^4, respectively, over a period of 58 hours. The obtained energy spectra and decay curves are shown in Fig. 1. We have constructed the level schemes of ^{165}Tb and ^{167}Tb from the observed spectra and systematics of the lighter Tb isotopes, which are shown in Fig. 2. The γ rays around $\sim$50 and $\sim$ 75 keV are tentatively assigned as the cascading γ rays of the first and second excited states of the ground-state rotational band, by comparing them with those of the less neutron-rich odd-mass Tb isotopes.[4,5)] The strong peaks at 152.4 and 147.4 keV in ^{165}Tb and ^{167}Tb are respectively assigned as isomeric transitions, as shown in Fig. 2. The 75.9 and 73.6 keV γ rays could be assigned as doublets from the energy sum and intensity balance. The isomeric states may be interpreted to be one quasi-proton excitation to the 7/2[523] or 9/2[404] orbit on the basis of our proposed decay scheme and systematics of the lighter Tb isotopes. Further examination is in progress.

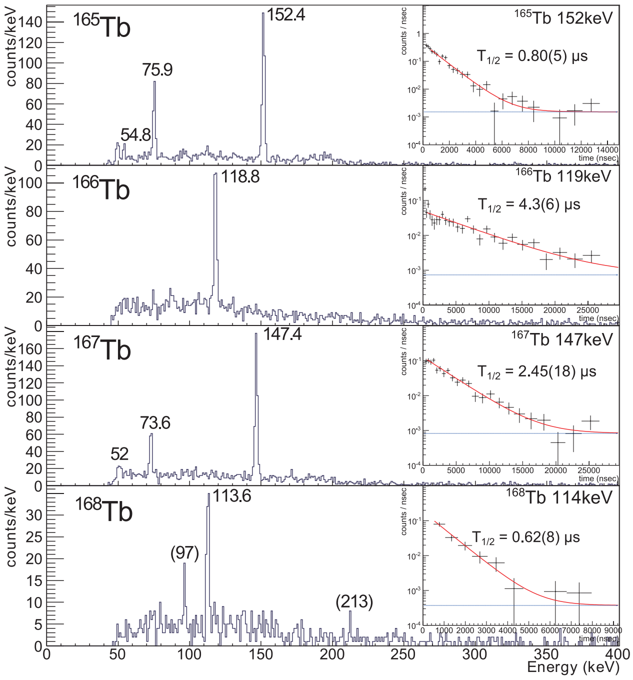

Fig. 1. γ-ray energy spectra for $^{165-168}$Tb isotopes.

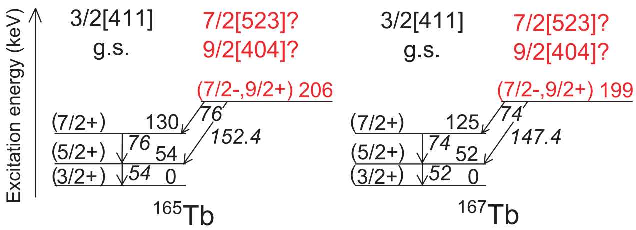

Fig. 2. Level schemes for ^{165}Tb and ^{167}Tb that are obtained for the first time in this study.

References

1) R. F. Casten *et al.*: Phys. Rev. Lett. **47**, 1433 (1981)
2) R. Yokoyama *et al.*: Riken Accel. Prog. Rep. **45**, 12 (2012)
3) D. Kameda *et al.*: In this report
4) P. Garrett *et al.*: Nucl. Phys. **A550**, 1 (1992)
5) G. Winter *et al.*: Nucl. Phys. **A176**, 609 (1971)

*1 Center for Nuclear Study, University of Tokyo
*2 Department of Physics Tohoku University
*3 LPSC-IN2P3

Study of spin-isospin responses via exothermic charge exchange reaction (^{8}He, ^{8}Li*(1$^+$))

H. Miya, S. Shimoura,[*1] K. Kisamori, M. Assié,[*2] H. Baba, T. Baba, D. Beaumel, M. Dozono, T. Fujii, N. Fukuda, S. Go, F. Hammache,[*2] E. Ideguchi,[*4] N. Inabe, M. Ito,[*5] D. Kameda, S. Kawase,[*1] T. Kawabata,[*3] M. Kobayashi,[*1] Y. Kondo, T. Kubo, Y. Kubota,[*1] C. S. Lee,[*1] Y. Maeda,[*6] H. Matsubara, S. Michimasa,[*1] K. Miki, T. Nishi, M. Kurata-Nishimura, S. Ota,[*1] H. Sakai, S. Sakaguchi, M. Sasano, H. Sato, Y. Shimizu, H. Suzuki, A. Stolz,[*7] M. Takaki, H. Takeda, S. Takeuchi, A. Tamii,[*4] H. Tokieda,[*1] M. Tsumura, T. Uesaka, K. Yako,[*1] Y. Yanagisawa, and R. Yokoyama,[*1]

We performed an experiment of the exothermic charge-exchange (CE) reaction of (^{8}He, ^{8}Li*(1$^+$)) at the RIKEN RIBF facility by using the BigRIPS, the High-Resolution beamline, and the SHARAQ spectrometer.[1)] Missing mass spectra for ^{4}He, ^{12}C(^{8}He, ^{8}Li*(1$^+$)) at the beam energy of 190 MeV/nucleon were measured. In this experiment, the spin-isospin response of a spin-dipole transition occuring as the result of a radioactive isotope beam induced CE reaction was studied. In order to identify ^{8}Li*(1$^+$), we searched for the 980-keV γ-ray corresponding to the $1^+ \rightarrow 2^+$ transition in ^{8}Li. The coincident detection of ^{8}Li and the 980-keV γ-ray can be considered clear evidence of the occurrence of the CE reaction. In this article, we report on the relevent experimental procedures and preliminary analysis.

Figure 1 shows the schematic view of the BigRIPS, the High-Resolution Beamline, and the SHARAQ spectrometer. A ^{8}He beam at 190 MeV/nucleon was produced via the projectile fragmentation reaction of the ^{18}O beam at 230 MeV/nucleon with a Be target at F0. The intensity of ^{8}He was approximately 2×10^6 cps at S0, where the secondary targets of solid ^{12}C and ^{4}He were installed. The target thicknesses of ^{12}C and liquid ^{4}He were 45 mg/cm^2 and 120 mg/cm^2, respectively. The liquid ^{4}He target was constructed with the system of CRYPTA.[2)] The beam trajectory was measured by low-pressure multi-wire drift chambers[3)] (LP-MWDCs) in the BigRIPS and the High-Resolution Beamline. The momentum of ^{8}He was measured at F6, which is the momentum dispersive focal plane, by using the LP-MWDCs. The scattered ^{8}Li was momentum analyzed with the SHARAQ spectrometer and detected by cathode readout drift chambers[4)] at S2. The 980-keV γ-rays emitted from ^{8}Li were detected by the NaI(Tl) detector array (DALI2[5)]) located near the secondary target.

Figure 2 shows the momentum correlation between ^{8}He and ^{8}Li in the ^{12}C(^{8}He, ^{8}Li)^{12}B reaction measurement. The horizontal and vertical axes represent the horizontal positions of ^{8}He at F6 and of ^{8}Li, respectively. Since the slope of the dashed line corresponds to the correlation of the dispersions at F6 (7.2 m) and S2 (5.8 m), the mometum spread at the S2 is canceled by tagging the momentum at F6. Therefore, the missing mass energy can be deduced. Further analysis is now in progress.

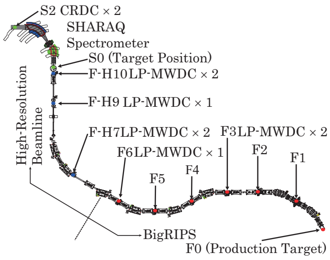

Fig. 1. Schematic view of BigRIPS, High-Resolution Beamline, and SHARAQ Spectrometer.

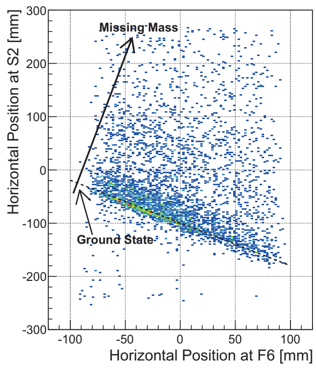

Fig. 2. Momentum correlation between ^{8}He and ^{8}Li in ^{12}C(^{8}He, ^{8}Li)^{12}B.

[*1] Center for Nuclear Study, The University of Tokyo
[*2] Institut de Physique Nucléaire, Orsay, France
[*3] Department of Physics, Kyoto University
[*4] Research Center Nuclear Physics, Osaka University
[*5] Cyclotron and Radioisotope Center, Tohoku University
[*6] Department of Applied Physics, University of Miyazaki
[*7] National Superconducting Cyclotron Laboratory, Michigan State University, USA

References

1) T. Uesaka *et al.*: Prog. Theor. Exp. Phys. (2012) 03C007.
2) H. Ryuto *et al*: Nucl. Instr. Meth. A 555, 1-5 (2005).
3) H. Miya *et al.*: CNS Ann Rep. 2011 (2013).
4) K. Kisamori *et al.*: CNS Ann Rep. 2011 (2013).
5) T. Takeuchi *et al.*: RIKEN Accel Prog. Rep. **36**, 148 (2003).

Measurement of the ^{8}He$(p,n)^8$Li reaction at 200A MeV in inverse kinematics

M. Kobayashi,*1 K. Yako,*1 S. Shimoura,*1 M. Dozono, S. Kawase,*1 K. Kisamori, Y. Kubota,*1 C.S. Lee,*1 S. Michimasa,*1 H. Miya, S. Ota,*1 M. Sasano, and M. Takaki

It is well-known that (p,n) measurements at intermediate energies are powerful tools to study the spin-isospin responses of nuclei. At RIBF, a facility for (p,n) measurements in inverse kinematics was constructed to extend the scope of spin-isospin studies to unstable nuclei. The first measurement was performed for the ^{12}Be(p,n) reaction at RIBF–SHARAQ in May 2011.[1] In April 2012, we performed a measurement for the ^{8}He$(p,n)^8$Li reaction as the second (p,n) measurement in inverse kinematics at RIBF. It was carried out as a parasite experiment on the missing mass spectroscopy of the $4n$ system via the ^{4}He$(^8$He$,^8$Be$)4n$ reaction.[2]

^{8}He is the heaviest of the bound He isotopes. It is expected to be described as a five-body $\alpha + 4n$ system and various configurations of these neutrons are proposed. A fundamental study on the structure of ^{8}He is its β–decay, where the Q-value is 10.7 MeV. In contrast to β–decay, charge-exchange reactions, such as (p,n) reactions, do not suffer from the Q-value limitation and can be used to study transitions to highly excited states.

The setup in this experiment is shown in Fig. 1. A primary ^{18}O beam of 230A MeV was used to bombard a Be target of 20 mm thickness, yielding a secondary ^{8}He beam of 200A MeV by projectile fragmentation. A typical intensity of the ^{8}He beam was 2 Mcps. Secondary targets of polyethylene $(CH_2)_n$ and carbon (C), with thicknesses of 0.39 and 0.46 g/cm^2, respectively, were employed. Runs with the C target were for evaluating the carbon contribution in the $(CH_2)_n$ target.

In this experiment, missing mass spectroscopy was employed. The excitation energy (E_x) of ^{8}Li and the scattering angle in the center-of-mass system ($\theta_{\rm cm}$) were constructed from the kinetic energy (T_n) and the scattering angle in the laboratory system ($\theta_{\rm lab}$) of a neutron produced by the (p,n) reaction. T_n was determined by measuring the neutron time-of-flight, for which the time references were taken from the plastic scintillator placed 10 m downstream from the secondary target and the neutron detector array (WINDS),[3] surrounding the target at a distance of 180 cm. $\theta_{\rm lab}$ was determined by the location of the scintillator bar in which the scattered neutron was detected.

Here, we focus on the decay channels to Li isotopes from excited states in ^{8}Li. The Li isotopes were tagged by using the energy-loss information of downstream detectors (a plastic scintillator and MWDCs).

Figure 2 shows a preliminary spectrum of the ^{8}He$(p,n)^8$Li reaction with tagging of the Li isotopes. Two loci are observed in this figure. The locus at low excitation energy is most likely to be an E_x = 0.98 MeV state with B(GT) = 0.24, which has been observed in β–decay studies. A region with a large transition strength is observed at around $E_x \sim 9$ MeV, which probably corresponds to the E_x = 9.3 MeV state. Further analysis is currently in progress.

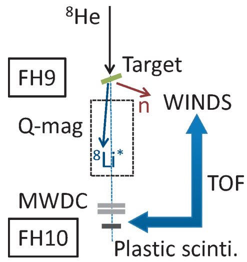

Fig. 1. Schematic view of the experimental setup.

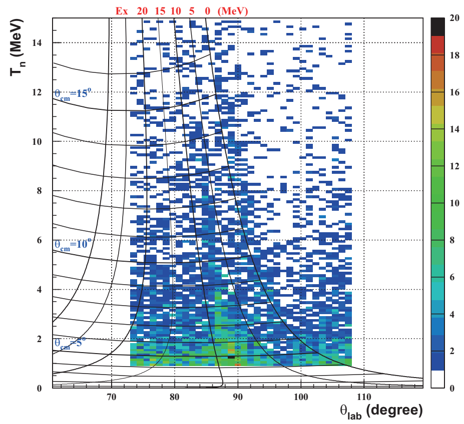

Fig. 2. Preliminary spectrum of the ^{8}He$(p,n)^8$Li reaction.

References
1) K. Yako *et al.*: RIKEN Accel. Prog. Rep. **45**, v (2012).
2) K. Kisamori *et al.*: in this report.
3) K. Yako *et al.*: RIKEN Accel. Prog. Rep. **45**, 137 (2012).

*1 Center for Nuclear Study, University of Tokyo

Missing-mass spectroscopy of the 4n system by exothermic double-charge exchange reaction ^{4}He(^{8}He, ^{8}Be)4n

K. Kisamori, S. Shimoura,[*1] H. Miya, M. Assie,[*2] H. Baba, T. Baba, D. Beaumel, M. Dozono, T. Fujii, N. Fukuda, S. Go, F. Hammache,[*2] E. Ideguchi,[*4] N. Inabe, M. Ito,[*5] D. Kameda, S. Kawase,[*1] T. Kawabata,[*3] M. Kobayashi,[*1] Y. Kondo, T. Kubo, Y. Kubota,[*1] M. Kurata-Nishimura, C. S. Lee,[*1] Y. Maeda,[*6] H. Matsubara, S. Michimasa,[*1] K. Miki, T. Nishi, S. Noji,[*7] S. Ota,[*1] S. Sakaguchi, H. Sakai, Y. Sasamoto,[*1] M. Sasano, H. Sato, Y. Shimizu, A. Stolz,[*7] H. Suzuki, M. Takaki, H. Takeda, S. Takeuchi, A. Tamii,[*4] L. Tang,[*1] H. Tokieda,[*1] M. Tsumura, T. Uesaka, K. Yako,[*1] Y. Yanagisawa, and R. Yokoyama,[*1]

Multi-neutron systems in nuclei have attracted considerable attention on both the experimental and theoretical fronts ever since candidates of bound tetra-neutron system were reported[1)]. However, later theoretical papers using ab-initio calculations[2)] suggest that bound tetra-neutron cannot exist.

We performed missing-mass spectroscopy of the 4n system via the exothermic double-charge exchange reaction ^{4}He(^{8}He,^{8}Be)4n. The experiment was carried out at the RI Beam Factory (RIBF) at RIKEN using the SHARAQ spectrometer and liquid He target system. In order to produce the 4n system with a small momentum transfer less than 20 MeV/c, the secondary beam of ^{8}He having a large internal energy was used at 190 A MeV. To obtain the missing-mass spectrum, we measured momentum of the ^{8}He beam with the High-Resolution Beamline and momentum of two alpha particles, which were the decay products of the ^{8}Be ejectile, with the SHARAQ spectrometer. If the spectrum has a resonance peak above the 4n threshold, it can be directly compared with theoretical predictions and information on the relevant interaction in the tetra-neutron system, such as the T=3/2 three-body force, can be obtained. Another interest is the possible correlations in sub-systems, such as di-neutron correlations in the four-body scattering state.

A primary beam of ^{18}O of 230 A MeV bombarded a target of 20-mm-thick Be at BigRIPS-F0 to produce the ^{8}He secondary beam. The typical ^{8}He beam intensity was 2×10^6 Hz. The ^{8}He beam was transported in High-Resolution-Achromatic mode to a liquid He target with thickness of 120 mg/cm^2 at the SHARAQ-S0. The momentum of ^{8}He was measured by Multi Wire Drift Chambers (MWDCs) at BigRIPS-F6. The SHARAQ spectrometer was operated to have a momentum acceptance about ±2.5% (considering momentum distribution ±0.74% of the two-alpha, and ±1% of the beam), and effective solid angle 4.3 msr, and satisfy momentum resolution 1/10000, which gives about 1 MeV missing-mass resolution. A Cathode Readout Drift Chamber (CRDC), which has no dead space and large effective area, was used as the detector for two-particle tracking[3)].

In the present analysis, a method for treating multi-hits in MWDCs under high beam rate condition was developed in order to achieve a large yield. At focal plane CRDC, ^{8}Be can identified by measuring the invariant mass of the coincident two-alpha particle with a good signal-to-noise ratio. Figure 1 shows a track of two-alpha particle of a candidate of the 4n event at CRDC. We identify about a few hundreds of events as candidates of 4n events, but still have to eliminate the back ground.

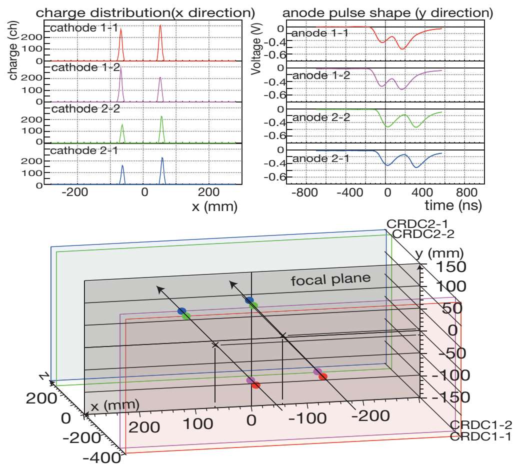

Fig. 1. The sample of an event snapshot. The vertical and horizontal positions of charged particles are determined by the center of the distribution of induced charges on the cathode pads and by measuring the drift time of electrons in the drift plane, respectively

References
1) F. Marques *et al.*: Phys. Rev. **C 65**, 044006 (2002)
2) S. Pieper: Phys. Rev. Lett. **90**, 252501 (2003)
3) K. Kisamori *et. al.*: CNS Ann. Rep. 2010 (2012)

*1 Center for Nuclear Study, the University of Tokyo
*2 IPN, Orsay, Fance
*3 Department of Physics, Kyoto University
*4 Research Center Nuclear Physics, Osaka University
*5 Cyclotron and Radioisotope Center, Tohoku University
*6 Faculty of Engineering, University of Miyazaki
*7 National Superconducting Cyclotron Laboratory, Michigan State University, USA

Heavy-ion double charge exchange reaction on ^{9}Be[†]

H. Matsubara, M. Takaki, T. Uesaka, S. Shimoura,[*1] N. Aoi, M. Dozono, T. Fujii, K. Hatanaka,[*2] T. Hashimoto,[*2] T. Kawabata,[*3] S. Kawase,[*1] k. Kisamori, Y. Kikuchi,[*1] Y. Kubota,[*1] C.S. Lee,[*1] H.C. Lee, Y. Maeda,[*4] S. Michimasa,[*1] K. Miki, H. Miya, S. Noji,[*5] S. Ota,[*1] S. Sakaguchi, Y. Sasamoto,[*1] T. Suzuki,[*2] L.T. Tang,[*1] K. Takahisa,[*2] H. Tokieda,[*1] A. Tamii,[*2] K. Yako,[*1] Y. Yasuda,[*2] N. Yokota,[*3] R. Yokoyama,[*1] and J. Zenihiro

The ^{9}He nucleus has a large A/Z ratio of 4.5. Although it is unbound, the first excited state of ^{9}He is reported to have a remarkably narrow width at a level of 100 keV[1)]. Most of the spin-parities and widths, however, are still scarcely known.

To study neutron rich nuclei, we have developed a new powerful probe, namely, the heavy-ion double charge exchange (HIDCX) (^{18}O, ^{18}Ne) reaction. This probe has noticeable advantages, *i.e.* (a) unstable nuclei can be investigated even by using stable nuclei for the target and for the beam, (b) missing mass measurement enables us to observe an excitation function both below and above the particle threshold, (c) out-going particles of ^{18}Ne can be clearly identified through the spectrometer because the ^{9}B nucleus is unbound, and thus, the A/Q=9/5 is unique for ^{18}Ne, and (d) the HIDCX transition rate between ^{18}O$_{\mathrm{g.s.}}$ and ^{18}Ne$_{\mathrm{g.s.}}$ is expected to be relatively large because of the overlapping of their wavefunctions in r-space, which arises from the fact that they are in the super-multiplet members.

The experiment was performed at the Research Center for Nuclear Physics (RCNP), Osaka University. A primary beam of ^{18}O was accelerated up to 80 MeV/nucleon with an intensity of 20 pnA. The beam bombarded a self-supporting foil target of ^{9}Be with an areal density of 5.0(1) mg/cm^2. The scattered particles were momentum-analyzed by the Grand Raiden (GR) spectrometer.

The particle identification to select ^{18}Ne was realized by using the time-of-flight information between RF from the accelerator and the triggering signals and by using its unique A/Q value.

An excitation energy spectrum of the ^{9}Be(^{18}O, ^{18}Ne)^{9}He reaction at 0−0.6° is compared with that of ^{12}Be(^{18}O, ^{18}Ne)^{12}Be reaction, as shown in Fig. 1. Although the same experimental setup analysis procedure was applied for both ^{9}Be and ^{12}C, only continuous increment caused by quasi-free scattering are seen in the spectrum of ^{9}He. There are no prominent structures. Coupled-channel calculations by the code ECIS[2)] were performed, where the microscopic form factors were obtained[3)] by folding the projectile and the target transition densities. The simplest transition path assumed for the calculation is double Gamow-Teller (GT) transitions from the ^{9}Be($3/2^-_{g.s.}$) to the ^{9}He($1/2^-_{g.s.}$) via the ^{9}Li($3/2^-_{g.s.}$). The calculation indicates that the differential cross section is less than 1 nb/sr owing to a tiny B(GT) value from the ^{9}Be($3/2^-_{g.s.}$) to the ^{9}Li($3/2^-_{g.s.}$). Because 10 nb/sr was the lower detection limit in the experimental condition, the cross section of the ^{9}Be(^{18}O, ^{18}Ne) reaction producing ^{9}He was too small to be observed owing to spatial deformation of ^{9}Be$_{\mathrm{g.s.}}$.[4)]

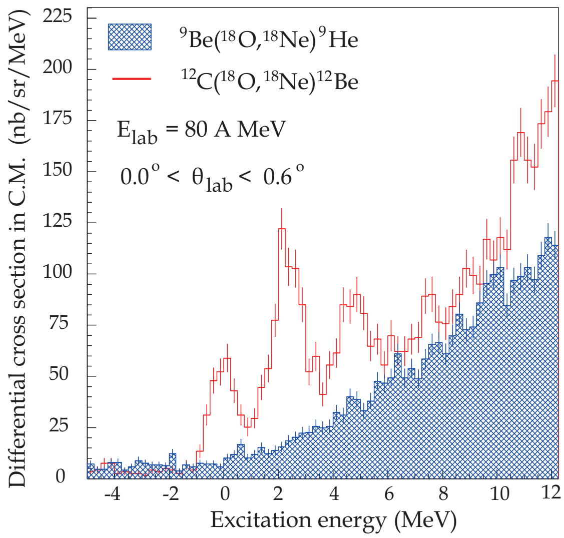

Fig. 1. Excitation energy spectra of ^{9}He and ^{12}Be.

We have established the HIDCX (^{18}O, ^{18}Ne) reaction with a stable beam as a spectroscopic tool. As a next step, we will propose the HIDCX (^{10}C, ^{10}Be) reaction with an unstable beam at the RIBF using the SHARAQ spectrometer for the search of double GT giant resonance.

† Condensed from the article in Few-Body Sys. (2013) in press

*1 Center for Nuclear Study (CNS), University of Tokyo
*2 Center for Nuclear Physics (RCNP), Osaka University
*3 Department of Physics, Kyoto University
*4 Department of Applied Physics, Miyazaki University
*5 National Superconducting Cyclotron Laboratory, USA

References

1) H.G. Bohlen *et al*: Prog. Part. Nucl. Phys. **42**, 17-26 (1999).
2) J. Raynal, program code ECIS-97.
3) J. Cook and J.A. Carr, computer program FOLD, Florida State University (unpublished); based on F. Petrovich and D. Stanley: Nucl. Phys. A275, 487 (1977); modified as described in J. Cook *et al.*: Phys. Rev. C 30, 1538 (1984); R.G.T. Zegers *et al.*: Phys. Rev. C **74**, 024309 (2006).
4) C. Scholl *et al.*: Phys. Rev. C **84**, 014308 (2011).

Study of low–lying states of ^{12}Be via the heavy–ion double–charge exchange ^{12}C(^{18}O, ^{18}Ne) reaction

M. Takaki, H. Matsubara, T. Uesaka, S. Shimoura,[*1] N. Aoi, M. Dozono, T. Fujii, T. Hashimoto,[*2] T. Kawabata,[*3] S. Kawase,[*1] K. Kisamori, C.S. Lee,[*1] J. Lee, Y. Maeda,[*4] S. Michimasa,[*1] K. Miki, H. Miya, S. Noji,[*5] S. Ota,[*1] M. Sasano, T. Suzuki,[*2] K. Takahisa,[*2] T.L. Tang,[*1] A. Tamii,[*2] H. Tokieda,[*1] K. Yako,[*1] N. Yokota,[*3] R. Yokoyama,[*1] and J. Zenihiro

The neutron-rich nucleus ^{12}Be provides the crucial evidence for the disappearance of the neutron magic number $N = 8$. Configurations of the ground (0_1^+) and 0_2^+ states in ^{12}Be are of considerable current interest. Previous studies highlighted that the normal $(0s)^4(0p)^8$ "$0\hbar\omega$" configuration mainly contributes to the 0_2^+ state, whereas the $(0s)^4(0p)^6(0sd)^2$ "$2\hbar\omega$" configuration mainly contributes to the 0_1^+ state. However, the levels of the contribution remain a subject of intense debate[1–5].

We measured the heavy-ion double charge exchange (HIDCX) ^{12}C(^{18}O, ^{18}Ne)^{12}Be reaction to study the low-lying states of ^{12}Be. The advantage of the (^{18}O, ^{18}Ne) reaction is that the transition probability between the ground states of ^{18}O and ^{18}Ne is expected to be large because the ground states are members of the same super-multiplet.

The HIDCX reactionexperiment was performed by using the Grand Raiden (GR) spectrometer at Research Center for Nuclear Study (RCNP), Osaka University. The ^{18}O beam with an energy of 79.6 MeV bombarded a natural carbon target with an areal density of 2.2(1) mg/cm^2. Scattering particles were momentum-analyzed by the GR. We obtained the excitation energy spectrum of ^{12}Be and angular distributions of the cross section for the low-lying states of ^{12}Be within the GR acceptance of 0.0°–2.5°.

Figure 1 shows the excitation energy spectrum of ^{12}Be. One can find three peaks with excitation energies of 0.0, 2.2, and 4.5 MeV, respectively. ^{12}Be has three states that can contribute to the 2.2 MeV peak: 2_1^+(2.11 MeV), 0_2^+(2.24 MeV), and 1_1^-(2.68 MeV). Figure 2 shows the angular distributions of differential cross sections for the ^{12}C(^{18}O, ^{18}Ne)^{12}Be reaction. The angular distributions show forward peaking shapes for the ground state and 2.2 MeV peak. In contrast, the 4.5 MeV peak has a flat shape. It has been suggested that ^{12}Be has the $J^\pi = 2^+$ state at an excitation energy of 4.56 MeV[6]. This resultsuggests that the HIDCX reaction at an intermediate energy has a sensitivity to multipolarities.

This experiment is the first case that has observed isolated peaks and obtained its angular distributions with the HIDCX reaction at an intermediate energy. Detailed analyses for the reaction process of the HIDCX and the configuration of the two low-lying 0^+ states in ^{12}Be are now in progress.

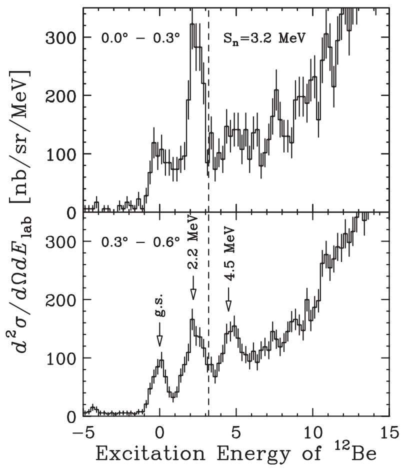

Fig. 1. Excitation energy spectrum of ^{12}Be.

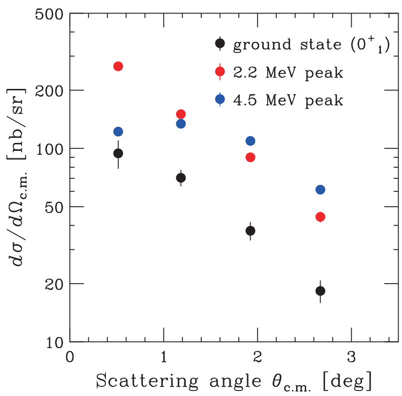

Fig. 2. Angular distributions of differential cross sections for the observed three peaks: the ground state (black), the 2.2 MeV peak (red), and the 4.5 MeV peak (blue).

References

1) F.C. Barker; J. Phys. G **2**, L45 (1976).
2) S. Shimoura *et al.*; Physics Letters B **560** (2003) 31; *ibid* **654**, (2007) 87.
3) H. Fortune and R. Sherr; Phys. Rev. C **74** (2006) 024301.
4) S.D. Pain *et al.*; Phys. Rev. Lett **96** (2006) 032502.
5) R. Meharchant *et al.*; Phys. Rev. Lett **108** (2012) 122501.
6) H. Fortune *et al.*; Phys. Rev. C **50** (1994) 1355.

*1 Center for Nuclear Study, University of Tokyo
*2 Research Center for Nuclear Physics, Osaka University
*3 Department of Physics, Kyoto University
*4 Department of Applied Physics, Miyazaki University
*5 National Superconducting Cyclotron Laboratry, Michigan State University

Spectroscopy of single-particle states in oxygen isotopes via (p, pN) reaction with polarized protons

S. Kawase,[*1] T. Uesaka, S. Shimoura,[*1] K. Yako,[*1] S. Ota,[*1] S. Michimasa,[*1] H. Tokieda,[*1] H. Miya, T. L. Tang,[*1] K. Kisamori, M. Takaki, Y. Kubota,[*1] C. S. Lee,[*1] R. Yokoyama,[*1] T. Fujii, M. Kobayashi,[*1] M. Sasano, J. Zenihiro, H. Matsubara, M. Dozono, J. Lee, H. Sakai, T. Kubo, K. Yoshida, N. Inabe, Y. Yanagisawa, H. Takeda, K. Kusaka, N. Fukuda, D. Kameda, H. Suzuki, T. Kawahara, T. Wakui, S. Sakaguchi, T. Noro,[*2] T. Wakasa,[*2] J. Yasuda, T. Fukunaga, Y. Maeda,[*3] W. Y. Kim,[*4] S. H. Hwang,[*4] S. Stepanyan,[*4] A. Obertelli,[*5] A. Galindo-Uribarri,[*6] E. Padilla-Rodal,[*7] and D. Beaumel

The (p, pN) reaction is an effective spectoroscopic tool to examine single-particle states. One can determine the spin-parity of single-particle states in nuclei from the momentum dependence of the cross section and the vector analyzing power without model dependence[1)].

We performed the SHARAQ04 experiment at RIKEN RIBF to measure single-particle spectra and to determine spin-orbit splitting in $^{14,22-24}$O. The beam including oxygen isotopes was produced via the projectile fragmentation of a primary ^{48}Ca beam that was accelerated upto 345 MeV/u by the SRC, and then achromatically transported into the high-resolution beamline. Particle identification was carried out by using time of flight (TOF) information between the F3-FH9 focal planes and light output information of the plastic scintillator at FH9. The beam bombarded a polarized proton target[2)] with a thickness of $\sim$100 mg/cm^2 placed at the S0 focal plane of the SHARAQ beam line. A schematic overview of the setup is shown in Fig. 1. Two low-pressure multiwire drift chambers (LP-MWDCs) were used to track beam particles to determine the reaction point on the target. Two sets of detectors were symmetrically placed on both sides of the beamline to detect the two nucleons scattered through the (p, pN) reaction. For scattered protons, two multiwire drift chambers (MWDCs) and two plastic scintillators were used to measure the scattering angle and the TOF, respectively. For neutrons, a pair of neutron hodoscopes consisting of 20 plastic scintillators each were used. The residual nuclei were analyzed by the quadrupole and dipole magnets, and detected by the plastic scintillator and the two MWDCs located downstream of the target. In addition, a carbon target ($\sim$130 mg/cm^2) was placed 15 cm downstream of the polarized target to simulteneously evaluate the background due to the carbon contained in the polarized target. The events in the carbon target were identified by the hit pattern of four plastic scintillators located right beside the carbon target. For the measurement of polarization of the target, the data for proton beam were also taken.

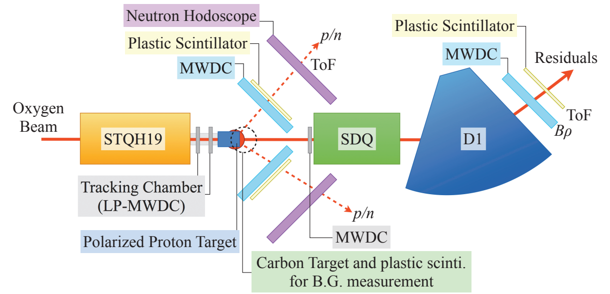

Fig. 1. Schematic overview of the setup of the SHARAQ04 experiment.

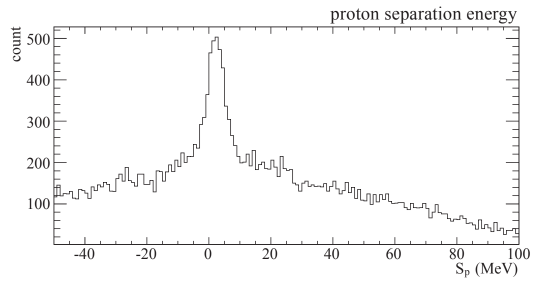

Fig. 2. Separation energy spectrum for pp elastic scattering

The separation energy is obtained from the scattering angles and the momenta of scattered nucleons. The momenta of scattered particles were determined from TOF measurements. Figure 2 shows the separation energy spectrum for the proton beam. The peak at 0 MeV corresponds to pp elastic scattering. The background is due to accidental coincidences and also from the proton knockout reaction in surrounding materials and in carbon nuclei contained in the polarized target. Gates on reaction points are not set in the analysis of the runs with the proton beam because of the lack of information on beam tracks. This lack of information is due to the low efficiency of LP-MWDC for protons.

The analysis for oxygen isotopes is in progress.

*1 Center for Nuclear Study (CNS), University of Tokyo
*2 Department of Physics, Kyushu University
*3 Department of Applied Physics, University of Miyazaki
*4 Department of Physics and Energy Sciences, Kyungpook National University, Korea
*5 CEA Saclay, France
*6 Oak Ridge National Laboratory, USA
*7 Instituto de Ciencias Nucleares, Universidad Nacional Autónoma de México, Mexico

References

1) G. Jacob, Th. A. J. Maris *et al.*: Nucl. Phys. A, 257(3), 517 (1976).
2) T. L. Tang *et al.*: in this report

Resonant scattering of ^{22}Na + p studied by thick-target inverse kinematic method

Y. B. Wang,[*1] S. J. Jin,[*1] J. Su,[*1] S. Q. Yan,[*1] Y. J. Li, [*1] B. Guo,[*1] Z. H. Li, [*1] W. P. Liu, [*1]
H. Yamaguchi,[*2] S. Kubono, D. Kahl,[*2] J. Hu, [*2,*3] H. S. Jung, J. Y. Moon,[*4] T. Teranishi,[*5] H. W. Wang,[*6]
H. Ishiyama,[*7] N. Iwasa, and T. Komatsubara

^{22}Na is one of the most important yet debatable cosmic γ-ray emitters. In 1972, Black found that in Orgueil meteorites the abundance ratio of ^{20}Ne/^{22}Ne is less than 1.5, which is much smaller than that of 9.8 on earth, this is the so-called Ne-Extraordinary problem[1)]. The excessive ^{22}Ne abundances are commonly explained as originated from the β^+ decay of ^{22}Na. The relative short half-life of ^{22}Na($T_{1/2}$=2.6 y) and the delayed 1.275 MeV γ ray indicate that ^{22}Na may be a very sensitive probe to the nova outburst, especially for the nearby ONe novae from the Sun[2)].

In a classic nova, there are two formation modes for the production of ^{22}Na depending upon the temperature[3)], *i.e.*

Chain I: ^{20}Ne(p, γ)^{21}Na(β^+)^{21}Ne(p, γ)^{22}Na,

Chain II: ^{20}Ne(p, γ)^{21}Na(p, γ)^{22}Mg(β^+)^{22}Na.

While the decay of ^{22}Na is delayed by its $T_{1/2}$=2.6 y half life, the ^{22}Na(p, γ)^{23}Mg reaction rates affect crucially the overall ^{22}Na abundance in the ejected shells. Due to the very complicated level structure of odd-mass ^{23}Mg close to the proton threshold, large uncertainties still exist on the ^{22}Na(p, γ)^{23}Mg reaction rates that attract intensive experimental investigations[4–7)]. In this report, the resonant scattering of ^{22}Na+p is studied by the thick-target inverse kinematic method, aiming to deduce the properties of relevant resonances in the compound ^{23}Mg.

The experiment was carried out at the **C**NS **R**adioactive **I**on **B**eam (CRIB) separator[8)], University of Tokyo. The ^{22}Ne^{7+} primary beam was provided by RIKEN AVF cyclotron with an energy of 6.0 AMeV. The ^{22}Na radioactive particles were produced by the ^{22}Ne(p, n)^{22}Na reaction. Nearly 100% pure ^{22}Na beam was delivered with an intensity of about 2.5×10^5 pps by the CRIB separator. The ^{22}Na beam particles went through two Parallel Plate Avalanche Counters (PPACs) before reaching the secondary proton target. The timing and position information from the two PPACs were used to determine the beam velocity vector on an event-by-event basis. The gas target chamber has an effective length of 300 mm, with the pressure of 310±2 Torr by a flow-gas system to fully stop the ^{22}Na particles. The lighter recoil particles coming out through the exit window of the gas target were detected by three silicon detector telescopes. Recoil protons were identified using the $\Delta E - E$, and the time-of-flight information.

The excitation function of ^{22}Na+p elastic resonant scattering from θ_0=0° silicon telescope is shown in Fig. 1.

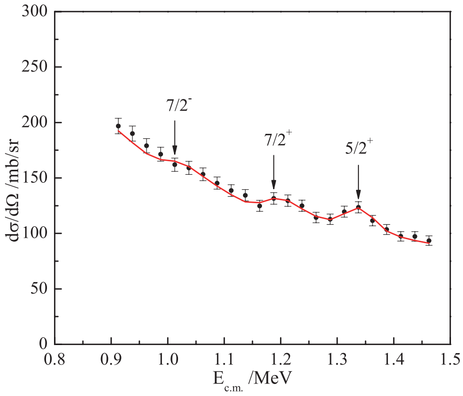

Fig. 1. Excitation function of the ^{22}Na+p elastic resonant scattering.

Three resonance-like signatures are seen at $E_{c.m.} \sim$ 1.03, 1.21, and 1.34 MeV in the excitation function. For the ^{22}Na+p elastic channel, there are two channel spins of $7/2^+$ and $5/2^+$, respectively. The largest orbital angular momentum is 1 for the measured $E_{c.m.}$ range, therefore only $l = 0, 1$ needs to consider in the R-matrix analysis. One set of spin and parity assignments is shown in Fig. 1. Shell model calculation of the ^{23}Mg level structure and the application of the new results to the astrophysical ^{22}Na(p, γ)^{23}Mg reaction rates are in progress.

References

1) D. C. Black, Geoch. Cosmochim. Acta **V36**, 347(1972).
2) A. F. Iyudin *et al.*, Astron. Astrophys. **300**, 422(1995).
3) J. José, *et al.*, Astrophys. J. **520**, 347(1999).
4) S. Kubono *et al.*, Z. Phys. **A348**, 59(1994).
5) D. G. Jenkins *et al.*, Phys. Rev. Lett. **92**, 031101(2004).
6) V. E. Iacob *et al.*, Phys. Rev. C **74**, 045810(2006).
7) A. L. Sallaska *et al.*, Phys. Rev. Lett. **105**, 152501(2010).
8) Y. Yanagisawa *et al.*, Nucl. Instr. Meth. **A539**, 74(2005).

*1 China Institute of Atomic Energy
*2 Center for Nuclear Study, University of Tokyo
*3 Institute of Modern Physics, Chinese Academy of Sciences
*4 Department of Physics, Chung-Ang University
*5 Department of Physics, Kyushu University
*6 Shanghai Institute of Applied Physics
*7 High Energy Accelerator Research Organization(KEK)

Investigation of the resonant scattering of ^{17}F+p

J. Hu,[*1] J.J. He,[*1] S.W. Xu,[*1] H. Yamaguchi,[*2] P. Ma,[*1] D. Kahl,[*2] J. Su,[*3] H.W. Wang,[*4] T. Nakao,[*2] Y. Wakabayashi, J.Y. Moon,[*5] T. Teranishi,[*6] H.S. Jung,[*5] T. Hashimoto,[*7] A. Chen,[*8] D. Irvine,[*8] and S. Kubono

X-ray bursts[1)] are likely to be an important source for the production of proton-rich nuclei via the high temperature rp-process,[2)] and the ^{14}O(α, p)^{17}F reaction is thought to be one of the crucial stellar reactions during the ignition phase of rp-process. Thus far, the reaction rate of this reaction remains unknown. Therefore, the studies of this waiting-point reaction are of great nuclear astrophysical importance to understand energy generation and nucleosynthesis in explosive stellar environments.

The ^{14}O(α, p)^{17}F reaction is mainly resonant, and its reaction rate depends on the resonant properties of those excited states that are above the α threshold in the compound nucleus ^{18}Ne. In this work, the proton resonant properties of ^{18}Ne were studied by the resonant elastic and inelastic scattering of ^{17}F+p resulting from a ^{17}F beam bombarding a thick H_2 gas target. The experimental goal was to determine the spin-parities and proton partial widths for those states that were above the proton threshold in ^{18}Ne.

The experiment was performed on CRIB.[3)] A 6.6 AMeV $^{16}O^{6+}$ primary beam with an average intensity of 560 enA was used to bombard a liquid-nitrogen-cooled D_2 gas target, where a secondary beam of ^{17}F was produced via the ^{16}O(d, n)^{17}F reaction. The D_2 gas at 120 Torr and 90 K was confined to a cell with a length of 80 mm. The cell was sealed by two Havar foils of 2.5 μm forming the entrance and exit windows, respectively. The ^{17}F beam was separated by the CRIB separator using the in-flight method. The average purity of the ^{17}F beams was about 98%. The ^{17}F beam, with a mean energy of 3.6 AMeV and an average intensity of 2.5×10^5 pps, was then delivered to F3 and used to bombard a thick H_2 gas target at which the beam was stopped. The experimental setup is shown in Fig. 1. The H_2 gas target chamber has a semi-cylindrical shape with a radius of 300 mm. The recoiled light particles were measured using three sets of ΔE-E Si telescopes at averaged angles of $\theta_{lab} \approx 3°$, 10° and 18°, respectively. Figure 2 shows the results of the particle identification performed using the ΔE-E method, wherein the recoiled protons can be clearly identified. The energy calibration for the silicon detectors was performed by using a standard triple α source. To compensate for the pulse height defect, a secondary proton calibration was performed using proton beams of different energies. In addition, at the secondary target position, an Ar gas target at 120 Torr was used in a separate run for evaluating the background contribution. We selected Ar gas because of its high Coulomb barrier for the ^{17}F + Ar interaction. The relevant data analysis is currently in progress.

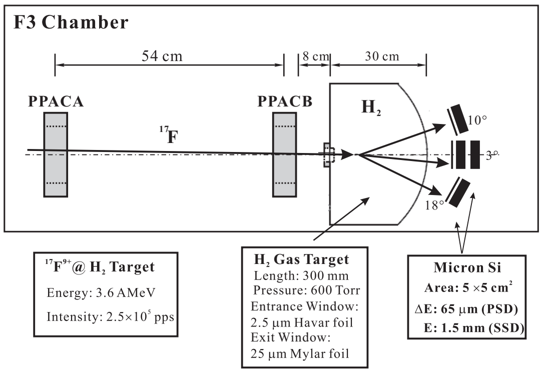

Fig. 1. Schematic diagram of the experimental setup at F3 chamber.

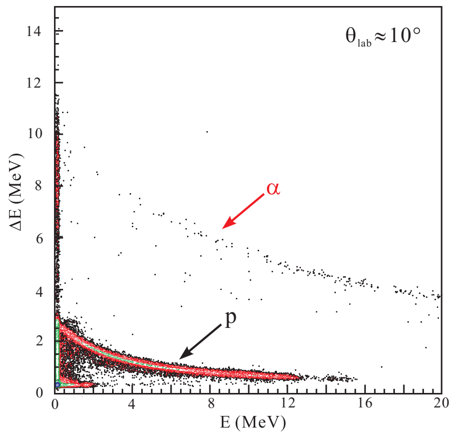

Fig. 2. Identification plot of the recoiled light particles.

*1 Institute of Modern Physics, Lanzhou, China
*2 Center for Nuclear Study, the University of Tokyo, Japan
*3 China Institute of Atomic Energy, Beijing, China
*4 Shanghai Institute of Applied Physics, Shanghai, China
*5 Department of Physics, Chung-Ang University, Korea
*6 Department of Physics, Kyushu University, Japan
*7 RCNP, Osaka University, Japan
*8 Department of Physics and Astronomy, McMaster University, Canada

References
1) W.H.G. Lewin, J.V. Paradijs, and R.E. Taam: Space Science Reviews **62**, 223 (1993).
2) R.K. Wallace and S.E. Woosley: Astrophys. J. Suppl. **45**, 389 (1981).
3) Y. Yanagisawa et al.: Nucl. Instr. Meth. **539**, 74 (2005).

Experiments for N/Z dependence of π^+ cross section in ^{129,132,136}Xe + CsI of 400 MeV/nucleon

M. Sako, T. Murakami,[*1] Y. Ichikawa,[*1] K. Ieki, Y. Ikeda,[*3] S. Imajo,[*1] T. Isobe, S. Ebesu,[*1] M. Matsushita,[*3] J. Murata, Y. Nakai, S. Nishimura, M. Nitta,[*3] H. Sakurai, R. Sameshima,[*1] E. Takada,[*2] and K. Yoshinaga

Information of the nuclear equation of state (EoS) within a broad density range is important for understanding the physics of neutron stars. The isospin-dependent term in EoS, i.e., the density dependence of the symmetry energy $E_{sym}(\rho)$, however, has large model dependence in the supra-normal density region ($\rho > \rho_0$, the saturation density $\rho_0 \cong 0.16 fm^{-3}$). As a result, the relationship between the radius and mass of a neutron star cannot be reliably calculated. According to a transport model calculation (IBUU04)[1)], detailed studies of the pion yield ratio, $Y(\pi^-)/Y(\pi^+)$, in central nucleus-nucleus collisions at intermediate energies would provide significant constraints on $E_{sym}(\rho)$ in the supra-normal density region.

The IBUU04 predicts that the beam energy dependence and the system-N/Z dependence of the pion yield ratio are strongly related to the behavior of $E_{sym}(\rho)$ in the supra-normal density region. We have already reported the beam energy dependence of the pion ratio in In(^{28}Si, $\pi^\pm$)X reactions for beam energies of 400, 600, and 800 MeV/nucleon[2)], and the system-N/Z dependence of the pion ratio in In(^{28}Si, $\pi^\pm$)X and In(^{132}Xe, $\pi^\pm$)X reactions for beam energies of 400 MeV/nucleon[3)]. A series of experiments was performed with a compact centrality filter and a pion range counter (RC)[4)] at Heavy Ion Medical Accelerator in Chiba (HIMAC). The total number of charged pions was estimated by using ΔE_i-ΔE_j (energy deposition at each layers of RC) correlations obtained experimentally for π^+ events, because we had demonstrated that π^+ events could be clearly identified by the $\pi^+ \rightarrow \mu^+ + \nu_\mu$ decay when π^+ stops in one of the elements of RC and in-flight energy depositions are same between π^+ and π^-.

We performed systematic experiments to investigate N/Z dependence of the pion yield ratio in further detail. We measured the pion yield ratio in CsI(^{129,132,136}Xe,$\pi^\pm$)X reaction for a beam energy of 400 MeV/nucleon at HIMAC. We configured the data acquisition system to perform high-statistics experiments and performed measurements at 45° and 90° in the laboratory system. We used Xe isotope beams to avoid the Z dependence between each reaction because the coulomb effect is different between π^+ and π^-. We use a CsI target whose average Z number is same as that of Xe in order to study the reactions between similar size of nuclei.

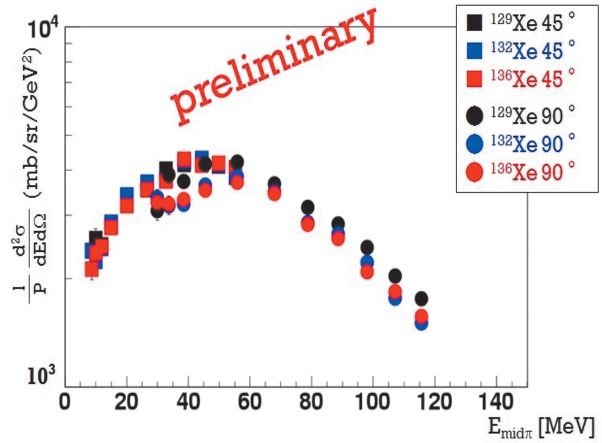

Fig. 1. Lorentz-invariant cross section of π^+ as a function of kinematic energy in the mid rapidity frame ($E_{mid\pi}$) for CsI(^{129,132,136}Xe,$\pi^\pm$)X reaction at 400 MeV/nucleon only with statistical errors.

Figure 1 shows lorentz-invariant cross section of π^+ as a function of the kinematic energy of the pions in a mid rapidity frame($E_{mid\pi}$). In the present analysis, statistical errors are only included although we roughly estimated systematic uncertainties as a few %. There is no clear difference in π^+ production cross sections between a series of experiments for Xe isotopes. The cross sections at 45° and 90° show smooth distribution though there may be a bump structure at about 40 MeV for 90° data. We consider that measured π^+ is mainly emitted from the reaction source at mid rapidity, and then, the pion ratio would also be a good measurement to discuss $E_{sym}(\rho)$.

Further analysis of the pion ratio and efforts to fix the systematic uncertainties are in progress.

References

1) Bao-An Li, Gao-Chan Yong, and Wei Zuo, Phys. Rev. C **71**, 014608 (2005).
2) M. Sako et al., RIKEN Accel. Prog. Rep. **44**, 20 (2011).
3) M. Sako et al., RIKEN Accel. Prog. Rep. **45**, 11 (2012).
4) T. Murakami et al., Nucl. Phys. A **834**, 593c (2010) (NN2009 proceedings).

*1 Department of Physics, Kyoto University, Kyoto, Japan
*2 Department of Accelerator and Medical Physics, NIRS, Chiba, Japan
*3 Department of Physics, Rikkyo University, Tokyo, Japan

Feasibility study for in-gas cell laser spectroscopy of indium

T. Sonoda, H. Mita, M. Wada, H. Iimura, H. Tomita, C. Sakamoto, T. Takatsuka, Y. Adachi, F. Arai, T. Furukawa, Y. Hirayama,[*1] H. Ishiyama,[*1] Y. Itou, S. Jeong,[*1] T. Kubo, Y. Matsuo, H. Miyatake,[*1] S. Naimi, T. Shinozuka,[*2] P. Schury, T. Wakui, Y. Watanabe[*1]

At RIKEN RIBF, RI-beams of highly exotic nuclei are available that have the highest intensity in the world. However, their usability is restricted to short periods of beam time owing to high demand and limited yearly operating hours due to the electrical cost required for accelerator operation. To bring about the most effective utilization for low-energy beam experiments in such a high-performance facility, we proposed a novel method, named PAratitic Laser Ion-Source(PALIS).[1)]

In the PALIS project, the first program for nuclear studies is to focus on laser spectroscopy by means of in-gas cell, in-gas jet laser spectroscopy.[2,3)] During the resonant ionization processes, the hyperfine splittings as well as the isotope shifts can be measured to determine the nuclear spins, moments, and charge radii.

Thus far, we have been investigating the resolution in the cases of the ionization inside the gas cell and inside the super-sonic gas jet for stable Cu, Fe, and Nb.[4)] The reduction of Doppler broadening can be observed in the case of the gas jet spectrum, although it predominantly includes intrinsic broadening due to the laser power and laser linewidth. For the improvement of the linewidth, we plan to install an injection locked Ti:Sapphire laser with a linewidth of 20 MHz in a PALIS laser system through collaboration with the Mainz University in FY2013.

In the present fiscal year, we have performed a feasibility study by the resonance ionization spectroscopy (RIS) of indium, which is one of candidates for PALIS experiments.

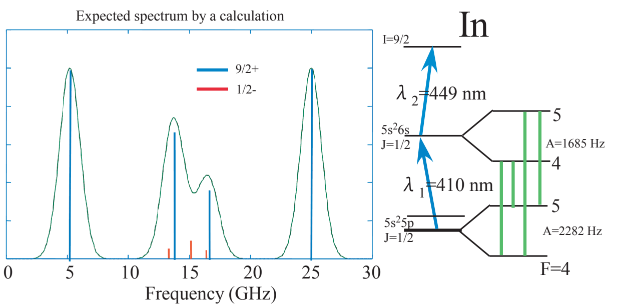

Fig. 1. The expected spectrum for indium ionization by scanning the first step in a calculation (left) and the tested ionization scheme (right).

The expected spectrum for indium ionization was derived by a calculation involving the ionization scheme that we plan to use. This calculation assumed the resolution of the linewidth of the laser as 2 GHz and the production ratio of nuclear spin, N ($\frac{9}{2}$+) / N ($\frac{1}{2}$-), as equal to 10. From the result shown in Fig. 1, we evaluated the hyperfine splittings in this ionization scheme considering that they are sufficiently separated, for extracting the nuclear magnetic moment.

In order to confirm the RIS of indium by experiment, we tested the ionization for a stable isotope in a gas cell by using the prototype PALIS system.[5)] The indium atoms were evaporated by a resistance heating transfer on the titanium crucible placed in the middle of the gas cell. They were transported by gas flow to the exit hole where the ionization occurs due to laser beam irradiation. The experimental setups and the ionization spectrum are shown in Fig. 2. The middle peak could not be resolved, as the intrinsic laser linewidth for the dye laser was about 5 GHz. However, for the measurement of nuclear magnetic moment, this can be ignored as the difference of the two side peaks is required.

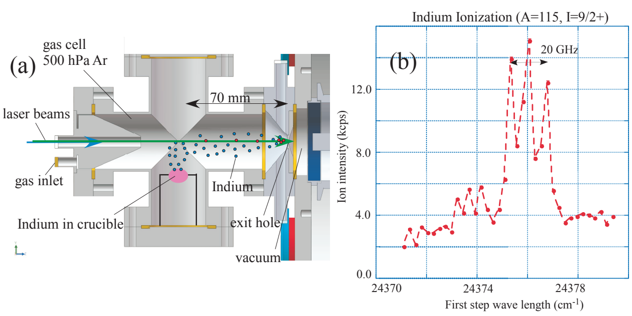

Fig. 2. (a) The experimental setups and (b) ionization spectrum by scanning the first step excitation in the experiment.

We performed a feasibility study of the in-gas cell laser spectroscopy of indium for a future PALIS experiment. The expected spectra were evaluated by a calculation and reproduced by the experiment. We plan to start the laser spectroscopy for neutron rich indium isotopes on day zero of the PALIS commissioning beam time.

References
1) T. Sonoda *et al.*: AIP Conf. Proc. **1104** 132 (2009).
2) T.E. Cocolios *et al.*: Phys. Rev. Lett. **103** 102501 (2009).
3) T. Sonoda *et al.*: Nucl. Inst. Meth. B **267** 2918 (2009).
4) C. Sakamoto: Master's thesis, Nagoya University (2013).
5) T. Sonoda *et al.*: Nucl. Inst. and Meth. B **295** 1(2013).

*1 High Energy Accelerator Research Organization (KEK)
*2 Cyclotron and Radioisotope Center, Tohoku University

2. Nuclear Physics (Theory)

Five-body resonances of ^{8}C using the complex scaling method†

T. Myo, Y. Kikuchi,*1 and K. Katō,*2

Recently, the new experiment on ^{8}C has been reported[1]. The ^{8}C nucleus is known as an unbound system beyond the proton drip-line and decays into many-body channels of ^{7}B+p, ^{6}Be+2p, ^{5}Li+3p and ^{4}He+4p.

In this report, we present our recent study on the resonance spectroscopy of ^{8}C. We employ the cluster-orbital shell model of the ^{4}He+p+p+p+p five-body system, and describe the many-body resonances under the correct boundary conditions by using the complex scaling method. We adopt the Hamiltonian, the nuclear part of which reproduces the ^{4}He-n scattering data and the ^{6}He energy[2,3]. The mirror nucleus of ^{8}C is ^{8}He, which is known as a neutron skin nucleus. It is interesting to examine the mirror symmetry between the protin-rich ^{8}C and the neutron-rich ^{8}He.

We show the level structures of ^{5}Li, ^{6}Be, ^{7}B and ^{8}C in Fig. 1. It is found that the present calculations agree with the observations and predict more energy levels. In Fig. 2, we compare the excitation energy spectra of proton-rich and neutron-rich sides. The good symmetry is confirmed between the corresponding nuclei. The differences of excitation energies for individual levels are less than 1 MeV.

We calculate the pair numbers of four valence protons in ^{8}C, which are defined by the matrix element of the operator $\sum_{\alpha\le\beta} A^\dagger_{J^\pi,S}(\alpha\beta)A_{J^\pi,S}(\alpha\beta)$. Here, α and β represent the single-particle orbits of protons and $A^\dagger_{J^\pi,S}$ ($A_{J^\pi,S}$) is the creation (annihilation) operator of a proton-pair with spin-parity J^π and the coupled intrinsic spin S. The total pair number is six for each state of ^{8}C. This quantity helps us to understand the pair coupling behavior of four protons. Figure 3 shows the pair numbers for ^{8}C ($0^+_{1,2}$). In the 0^+_1 state, the 2^+ neutron pair is close to five and the 0^+ pair is almost unity. This is obtained from a main configuration of $(p_{3/2})^4$ with the probability of 88% using CFP (1 and 5 for 0^+ and 2^+, respectively). The 0^+_2 state has almost two 0^+ proton pairs in addition to the 2^+ pairs. This is consistent with the $(p_{3/2})^2(p_{1/2})^2$ configuration with a probability of 93%; this configuration is decomposed into the pairs of 0^+, 1^+ and 2^+ with occupations of 2, 1.5, and 2.5, respectively. It is found that in the 0^+_2 state, the spin-singlet and the spin-triplet components are equally mixed in the 0^+ proton pair.

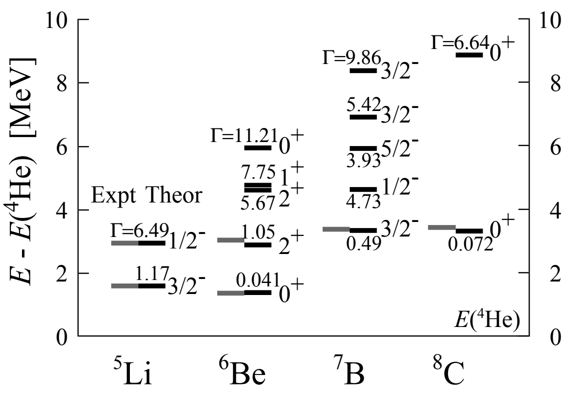

Fig. 1. Energy levels of ^{5}Li, ^{6}Be, ^{7}B and ^{8}C measured from the energy of ^{4}He. Units are in MeV. Black and gray lines are theory and experiments, respectively. Small numbers are theoretical decay widths.

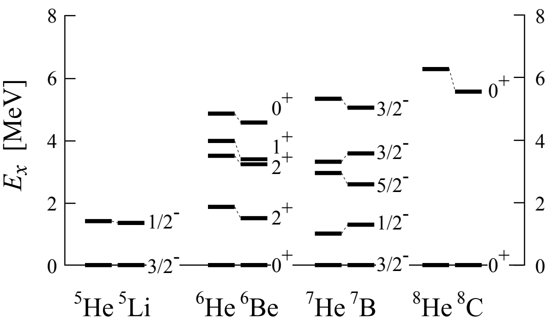

Fig. 2. Excitation energy spectra of mirror nuclei of $A = 5, 6, 7$ and 8 in the units of MeV.

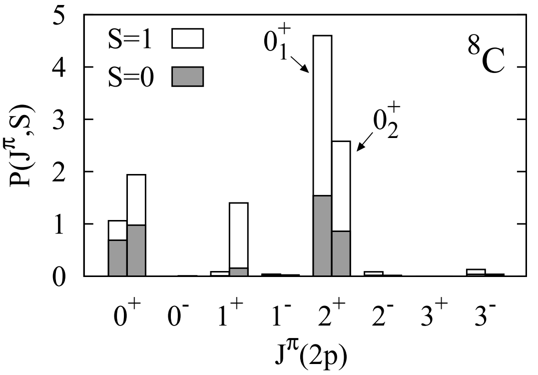

Fig. 3. Pair numbers of the $0^+_{1,2}$ states of ^{8}C.

† Condensed from the article in Phys. Rev. C**85**, 034338 (2012)

*1 Research Center for Nuclear Physics, Osaka University
*2 Graduate School of Science, Hokkaido University

References

1) R. J. Charity *et al.*: Phys. Rev. C**84**, 014320 (2011).
2) T. Myo, R. Ando and K. Katō: Phys. Lett. B**691**, 150 (2010).
3) T. Myo, Y. Kikuchi and K. Katō: Phys. Rev. C**84**, 064306 (2011).

Tensor-optimized shell model for the Li isotopes with a bare nucleon-nucleon interaction†

T. Myo, A. Umeya, H. Toki and K. Ikeda

The nucleon-nucleon (NN) interaction has strong tensor forces at long and intermediate distances caused by the pion exchange, which emerges large momentum transfer, and also strong central repulsions at short distance caused by the quark dynamics. It is important to investigate the nuclear structure by treating these characteristics of the NN interaction. Recently, we can express the strong tensor correlation in a reasonable shell model space[1]. We name this method as Tensor Optimized Shell Model (TOSM), in which the wave function is constructed with full optimization of the two particle-two hole ($2p2h$) states involving high momentum components induced by the tensor interaction[2]. The central Unitary Correlation Operator Method (UCOM) is used to treat the short-range repulsion[3]. We combine two methods, TOSM and UCOM to describe nuclei using bare interaction.

We have applied TOSM+UCOM to Li isotopes. The $0p0h$ configurations in Li isotopes are given in the $0s + 0p$ space with the $0\hbar\omega$ excitations. The obtained results using the bare AV8′ NN interaction are shown in Fig. 1. It is found that the excitation energy spectra are obtained consistent with the experimental results.

For comparison, we show the results using the effective Minnesota (MN) NN interaction, which does not have the tensor force, in Fig. 2. The MN interaction consists of the central and LS parts. The excitation energy spectra using the MN interaction show quite a large deviation from the experiment. The comparison of the results using AV8′ with those with MN makes it clear the role of the tensor force on the energy spectra of the p-shell nuclei. From these results, we have shown the reliability of TOSM+UCOM using the AV8′ interaction to investigate the structures of the Li isotopes.

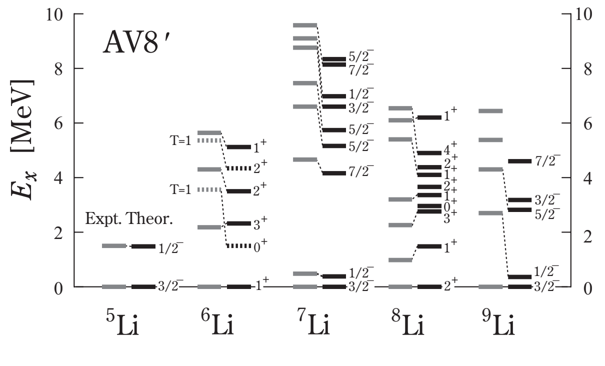

Fig. 1. Excitation energies of Li isotopes using AV8′ interaction with TOSM+UCOM.

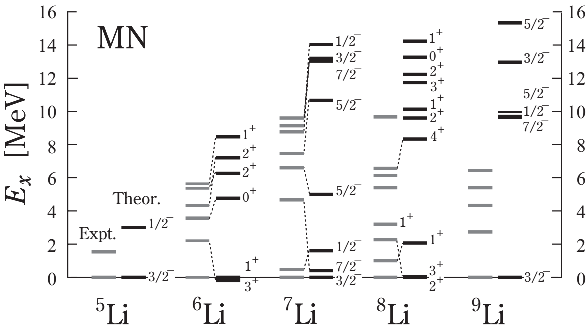

Fig. 2. Excitation energies of Li isotopes using MN interaction with TOSM.

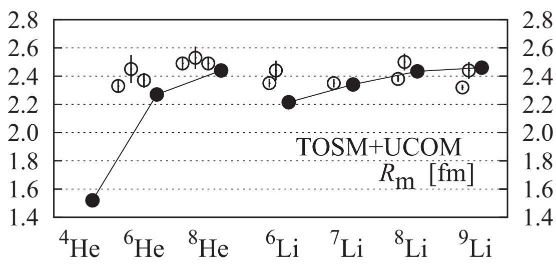

Fig. 3. Matter radii of He and Li isotopes in fm (solid circles) with the experiments (open circles).

The matter radii of He and Li isotopes are shown in Fig. 3 and the systematic trend agrees with the experiments. The value of ^{6}Li is smaller than the experiment, which is expected to be recovered including the asymptotic α+d clustering component in addition to the shell model basis states in TOSM.

References

1) T. Myo, H. Toki and K. Ikeda: Prog. Theor. Phys.**121**, 511 (2009).
2) K. Ikeda, T. Myo, K. Katō and H. Toki: Lecture Notes in Physics **818** "Clusters in Nuclei" Vol. 1, pp165-221, Springer, (2010).
3) H. Feldmeier, T. Neff, R. Roth and J. Schnack: Nucl. Phys. **A632**,61 (1998).
4) T. Myo, A. Umeya, H. Toki and K. Ikeda: Phys. Rev. C**84**, 034315 (2011).

† Condensed from the article in Phys. Rev. C**86**, 024318 (2012)

Formation of light p-shell Ξ^- hypernucleus via the (K^-, K^+) reaction

T. Koike and E. Hiyama

Due to the lack of experimental data, little is known about the nature of the ΞN interaction except that it could be weakly attractive. Therefore, an experimental search of Ξ^- hypernuclei via the ^{12}C(K^-, K^+) reaction is planned at J-PARC through the E05 experiment.[1] From the viewpoint of the theoretical few-body structure calculation, Hiyama et al. have predicted the possible existence of a Ξ^- hypernuclear bound state for several light p-shell nuclei,[2] although no reaction calculation has been performed for the corresponding Ξ^- hypernuclear formation. Hence, our purpose herein is to calculate the Ξ^- hypernuclear formation spectra via the (K^-, K^+) reaction on light p-shell targets and investigate the experimental feasibility of observing the Ξ^- hypernuclear bound state.

In this paper, we present the results of the ^{7}Li target case,[3] which can form the $^{7}_{\Xi}$H $= \Xi^- + {}^6$He bound state via the (K^-, K^+) reaction. The presence of the bound state peaks in the reaction spectra strongly depends on the Ξ^--^{6}He potential. In addition, since the ^{6}He core nucleus has the first excited 2^+ state only 1.8 MeV above the ground 0^+ state, it should be examined how the excited core nuclear state affects the shape of the spectrum. In order to investigate these issues, we calculate the ^{7}Li(K^-, K^+) reaction spectrum by employing various Ξ^--^{6}He potentials within the framework of the distorted wave impulse approximation (DWIA) using the $[\Xi^-$-^{6}He$(0^+)]$-$[\Xi^-$-^{6}He$^*(2^+)]$ coupled-channel Green's function approach.

Fig. 1 shows the calculated ^{7}Li(K^-, K^+) inclusive spectra for $p_{K^-} = 1.65$ GeV/c and $\theta_{K^+} = 0°$. Here, we use the effective Ξ^--^{6}He potentials in the Woods-Saxon form, which reproduce the binding energies and widths of $^{7}_{\Xi}$H calculated by Hiyama et al.,[2] with $\alpha + n + n + \Xi^-$ four-body cluster model using two types of the k_f-dependent ΞN G-matrix interaction: the Nijmegen hard core model D (ND) and the Nijmegen soft core model 04 (ESC). For each ΞN interaction, three values of the k_f parameter are selected in the unit of inverse femtometers.[2] Thus, we have six possible Ξ^--^{6}He potentials. In the case of ND, we can see two peak structures for every k_f number of parameters. The peaks in the $E < 0$ and $E > 0$ region correspond to the Ξ^--^{6}He(0^+) and Ξ^--^{6}He$^*(2^+)$ bound states, respectively. The contribution to the cross section from the ^{6}He$^*(2^+)$ core state amounts to about 1/3 of that from the ^{6}He(0^+) core state. In the case of ESC, the larger width compared to ND case makes the peak less visible. For ESC with $k_f = 0.9$ and 1.055, we can recognize only one peak corresponding to the Ξ^--^{6}He(0^+) bound state. For ESC with $k_f = 1.3$, we observe no peak structure, although the bound states are predicted in ref.[2]

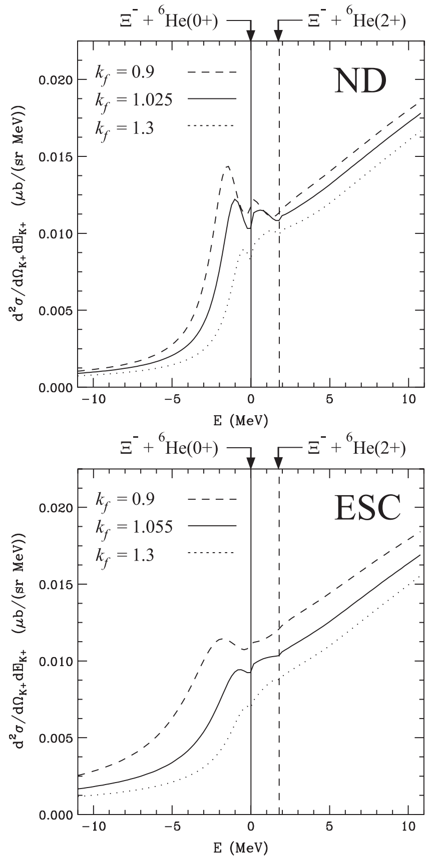

Fig. 1. Calculated ^{7}Li(K^-, K^+) inclusive spectra for $p_{K^-} = 1.65$ GeV/c and $\theta_{K^+} = 0°$. The top and bottom panels show the results corresponding to the case using potential ND and ESC with three k_f parameters, respectively. These spectra are smeared assuming 2 MeV detector resolution.

In conclusion, we can expect to observe the bound state peak of the Ξ^- hypernuclear state in the ^{7}Li(K^-, K^+) inclusive spectrum, except for the ESC with $k_f = 1.3$ case, including the 2 MeV detector resolution. In order to confirm the results more quantitatively, we plan to construct the realistic folding potentials instead of the Woods-Saxon potential used here. Further investigation in this regard is in progress.

References

1) T. Nagae et al.: Proposal for J-PARC 50 GeV Proton Synchrotron (2006).
2) E. Hiyama, Y. Yamamoto, T. Motoba , Th. A. Rijken and M. Kamimura: Phys. Rev. **C78**, 054316 (2008) .
3) T. Koike and E. Hiyama: Few-Body Systems (2013), DOI:10.1007/s00601-012-0538-4

Channel coupling effect on high-energy heavy-ion scattering

T. Furumoto and Y. Sakuragi*1

Recent developments in experimental facilities have enabled us to accelerate heavy ions, including unstable isotopes, at energies over a few hundreds of MeV per nucleon and to perform precise nuclear spectroscopy measurements of unstable nuclei through direct nuclear reactions. In this light, we recently proposed a microscopic nuclear reaction theory[1–3], based on the complex G-matrix interaction, called the CEG07[1].

In this report, we study the ^{12}C + ^{12}C scattering at $E/A = 100$–400 MeV, and we investigate the effect of inelastic excitations to the low-lying states of ^{12}C and incident energy dependence via the microscopic coupled-channel (MCC) method using the CEG07 interaction. In the MCC method, the diagonal and coupling potentials in the coupled-channel (CC) equations are calculated microscopically by the double folding of the CEG07 interaction with the diagonal and transition densities of the colliding nuclei. The details regarding the method are given elsewhere[3].

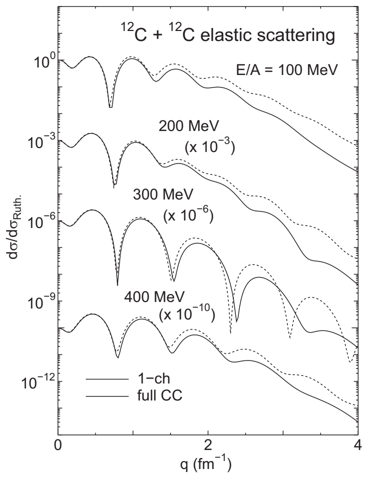

Fig. 1. Elastic cross sections calculated in the framework of the MCC method. The solid and dotted curves indicate the results with and without the channel coupling effects, respectively. This figure has been reproduced from a previous study[3].

We solve the CC equations at four incident energies and calculate the angular distributions of the ^{12}C + ^{12}C elastic cross sections as shown in Fig. 1. A sizable channel-coupling effect is clearly seen in the elastic cross sections at all incident energies. In the comparison of the single-channel calculation with the CC one, we notice that the diffraction pattern of the cross section slightly shifts backward and the cross

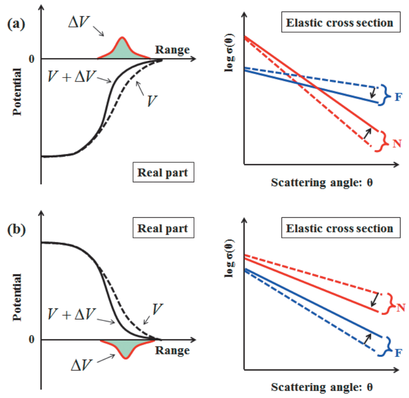

Fig. 2. Schematic of the relation between the potentials and the nearside/farside components of the cross section. This figure has been reproduced from a previous study[3].

section decreases at large angles due to the channel-coupling effect. Although the effect on the cross sections appears similar at all the incident energies, the contents of the effect are very different from each other as discussed below.

At the lowest energy $E/A = 100$ MeV, the real part of the bare folding potential in the elastic channel is strongly attractive[2,3] and the real part of the dynamical polarization potential (DPP) due to the channel coupling is found to have a positive sign (i.e. a repulsive nature)[3]. This leads to a decrease in the coherent sum of the nearside and farside scattering amplitudes accompanied by the slightly backward shift of the crossover point (upper panel in Fig. 2). The situation is completely opposite in the case of $E/A =$ 400 MeV, where the real part of the bare folding potential is strongly repulsive[2,3] while the real part of the DPP has a negative sign (i.e. an attractive nature)[3]. In such a situation, the dominant nearside component generated by the less repulsive potential slightly decreases, which again leads to a decrease in the coherent sum of the two amplitudes (lower panel in Fig. 2). This precisely explains what we have observed in Fig. 1 in terms of the drastic energy-dependence of the channel-coupling effects.

References
1) T. Furumoto, Y. Sakuragi, and Y. Yamamoto: Phys. Rev. C **78**, 044610 (2008); *ibid.* **80**, 044610 (2009).
2) T. Furumoto, Y. Sakuragi, and Y. Yamamoto: Phys. Rev. C **82**, 044612 (2010).
3) T. Furumoto and Y. Sakuragi: Phys. Rev. C **87** 014618 (2013).

*1 Department of Physics, Osaka City University, Osaka, Japan

RIKEN Accel. Prog. Rep. 46 (2013)

Localized versus non-localized clustering in nuclear structure

B. Zhou, Y. Funaki, H. Horiuchi,[*1] Z. Z. Ren,[*2] G. Röpke,[*3] P. Schuck,[*4] A. Tohsaki,[*1] C. Xu,[*2] and T. Yamada

Clustering is one of the most important features in light nuclei. Strongly correlated nucleons can compose a cluster subunit, typically, the alpha cluster. In the Brink model, the geometrical cluster structure can be obtained by the energy variational method without any a priori assumption. This description of the rigid, crystal-like structure in the Brink picture is based on the concept of localized clustering, which provides the traditional understanding of the cluster structure in nuclei.

The recently proposed THSR wave function[1)], based on the concept of non-localized clustering, is quite successful in describing the dilute gas-like states in light nuclei. The extension of this idea to address general cluster structures in nuclei also appears promising. In this work, we propose a hybrid wave function that includes the Brink wave function and the THSR wave function as special cases. As an example, we apply this new wave function to the study of the inversion doublet bands in ^{20}Ne. The intrinsic hybrid wave function can be written as,

$$\hat{\Phi}_{\rm Ne}(\beta,\boldsymbol{S}) \propto \mathscr{A}[\exp(-\frac{8(\boldsymbol{r}-\boldsymbol{S})^2}{5B^2})\phi(\alpha)\phi(^{16}{\rm O})]. \quad (1)$$

Here, $B^2 = b^2 + 2\beta^2$, $\boldsymbol{r} = \boldsymbol{X}_1 - \boldsymbol{X}_2$. The terms $\boldsymbol{X}_1$ and $\boldsymbol{X}_2$ represent the center-of-mass coordinates of the α and ^{16}O clusters, respectively. All calculations here are performed with restriction to axially symmetric deformation, that is, $\boldsymbol{S} \equiv (0, 0, S_z)$.

In this work, we adopt the same parameters as those used in a previous work[2)], that is, b is fixed at 1.46 fm and the nuclear interaction is the Volkov No.1 force. After making an angular momentum projection on the intrinsic hybrid wave function, we calculate the energies as a function of the two parameters β and S_z for the rotational bands of ^{20}Ne. The minimum points appear at $S_z = 0$ with different values of β. This indicates that the hybrid wave function is equivalent to the THSR wave function in the description of the inversion doublet bands in ^{20}Ne.

Moreover, the competition between the two parameters β and S_z leads to $S_z = 0$, which is relevant to clarify the concept of non-localized clustering in the typical case of ^{20}Ne. Figure 1 shows the energy curves of the $J^\pi = 0^+$, 1^- states with different values for the width of the Gaussian wave functions in the hybrid model. If β is fixed at 0, then the hybrid wave function becomes the Brink wave function. In this case, S_z denotes the inter-cluster distance parameter. For the ground state of ^{20}Ne, the minimum energy appears at $S_z = 3.0$ fm. For the $J^\pi = 1^-$ state, the optimum position appears at $S_z = 3.9$ fm. The non-zero values of S_z seem to indicate that the α + ^{16}O structure of ^{20}Ne favors localized clustering. This is just the traditional concept of localized clustering. However, we now have reason to believe that this argument is misleading. The non-zero minimum point S_z simply occurs because the width of the Gaussian wave function of the relative motion in the Brink model is fixed to a narrow wave packet. If β is adopted as 1.8 fm and 2.4 fm for $J^\pi = 0^+$, 1^-, respectively, according to the calculated minimum positions, namely, if we use a sufficiently broad width of the Gaussian wave packet for describing the relative motion, then we find that the minimum points appear at $S_z = 0$ as shown in Fig. 1. This result indicates that there is no localized clustering. Further, we have demonstrated for the $J^\pi = 0^+$, 1^- states in ^{20}Ne that the THSR wave functions at the minimum-energy points are 99.29% and 99.98% , respectively , being equivalent to the corresponding superposed Brink wave functions obtained by GCM calculations.

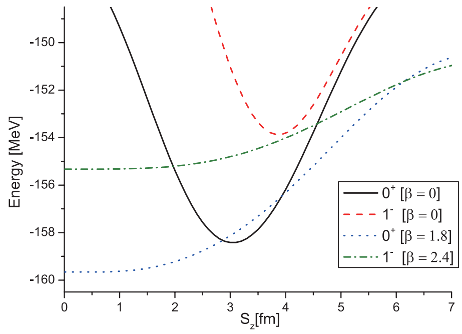

Fig. 1. Energy curves of $J^\pi = 0^+$, 1^- states with different widths of Gaussian relative wave functions in the hybrid model

In summary, the single projected THSR wave function accurately describes the inversion doublet bands in ^{20}Ne. We conclude that the THSR-type wave function goes beyond the traditional Brink wave function and that non-localized clustering is the essential characteristic of the cluster structures in nuclei.

*1 RCNP, Osaka University, Japan
*2 Department of Physics, Nanjing University, China
*3 Institut für Physik, Universität Rostock, Germany
*4 Institut de Physique Nucléaire, Université Paris-Sud, France

References
1) A. Tohsaki *et al.*: Phys. Rev. Lett. **87**, 192501 (2001).
2) Bo Zhou *et al.*: Phys. Rev. C, **86**, 014301 (2012).

Mean-field calculation including proton-neutron mixing

K. Sato, J. Dobaczewski [*1,*2], T. Nakatsukasa, W. Satuła,[*1]

In this study, we have developed a new code for mean-field calculation on the basis of the nuclear density functional theory (DFT), including an arbitrary mixing between protons and neutrons. This is the first step towards the density functional calculation including proton-neutron (p-n) pairing. The p-n pairing is a long-standing open problem in nuclear physics, and its possible relations to various phenomena in nuclei have been widely discussed.[1)] However, in spite of the recent impressive experimental progress and theoretical studies over the years, the understanding of the p-n pairing is still insufficient. To address this problem, we use the nuclear DFT approach. Our ultimate aim is to develop a DFT code including the p-n pairing and to apply it to various phenomena. To treat the p-n pairing within the DFT framework, one needs to generalize the quasiparticle states as mixtures of protons and neutrons. With this consideration, isospin is not a good quantum number for quasiparticles. In connection with this extension of quasiparticles, one also needs to extend density functionals to those with mixing between protons and neutrons. The density functionals should be extended in such a way that they are invariant under rotation in isospin space.[2)]

As the first step towards DFT calculation including p-n pairing, we consider the Hartree-Fock (HF) calculation without the pairing correlation, including the above-mentioned p-n mixing. We have developed a code for the p-n mixing calculation by extending the code "HFODD,"[3)] which solves the nuclear Skyrme-Hartree-Fock or Skyrme-Hartree-Fock-Bogolyubov problem by using the Cartesian deformed harmonic-oscillator basis. In this p-n mixing calculation, we have performed the so-called isocranking calculation by adding the isocranking term to the Hamiltonian:

$$\hat{H}' = \hat{H} - \vec{\lambda} \cdot \hat{\vec{T}}. \quad (1)$$

Here, $\hat{\vec{T}}$ is the total isospin operator. The isocranking term is analogous to that used in the standard tilted-axis-cranking calculations for high-spin states. By adjusting the isocranking frequency $\vec{\lambda}$, we can control the size and direction of the isospin of the system. Since the extended Skyrme energy density functionals including the p-n mixing are invariant under rotation in isospin space, the energy of the system should be independent of the direction of the isospin, if there is no Coulomb interaction. Therefore, we first performed isocranking calculations for $A = 14$ and $A = 48$ systems with the Coulomb interaction switched off, we also confirmed that our code is correctly implemented.

Next, we carried out calculations with the Coulomb interaction included. For $A = 14$ isobars, we calculated the energies of the well-known isobaric analogue states (IASs) with $T = 1$ in ^{14}C, ^{14}N, and ^{14}O. We found that the ground states of ^{14}C and ^{14}O (IASs with $T_z = 1$ and -1, respectively) are reproduced by normal HF states without the p-n mixing and that the excited 0^+ state of ^{14}N (the IAS with $T_z = 0$) is described well as a state consisting of single-particle states with the p-n mixing. In Fig. 1, we plot the energies of the IASs in $A = 48$ nuclei obtained by the isocranking calculation for ^{48}Cr. This figure shows that we can obtain states with different values of $\langle \hat{T}^2 \rangle$ and $\langle \hat{T}_z \rangle$ by varying the size and tilting angle of the isocranking frequency $\vec{\lambda}$. Note that, apart from the points at $T_z = 4$ and -4, the isospin projection on the z axis is not a good quantum number.

The isocranking calculation is a simple linear constraint method. We also implemented in our code an improved method for optimization with constraints, known as "the augmented Lagrange method,"[4)] which is widely used in quantum chemistry. This method can be employed, e.g., for the calculation of the excitation energies for high-isospin states in a single nucleus, from which we can evaluate the nuclear symmetry energy.

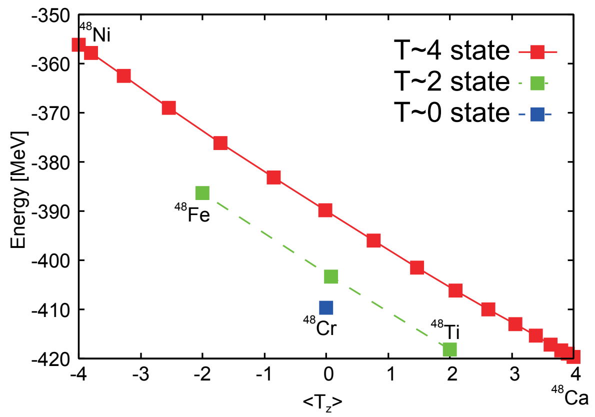

Fig. 1. Energies of $T \simeq 0, 2$ and 4 states in $A = 48$ isobars obtained by isocranking calculation as functions of $\langle \hat{T}_z \rangle$.

References
1) For a recent review, A. V. Afanasjev: arXiv:1205.2134.
2) E. Perlińska et al.: Phys. Rev. C **69**, 014316 (2004).
3) For the latest version, N. Schunck et al.: Comput. Phys. Commun. **183**, 166 (2012); See also http://www.fuw.edu.pl/ dobaczew/hfodd/hfodd.html.
4) A. Staszczak et al.: Eur. Phys. J. A **46**, 85 (2010).

*1 Institute of Theoretical Physics, Faculty of Physics,University of Warsaw
*2 Department of Physics, University of Jyväskylä

Regularized multi-reference energy density functional calculations with new Skyrme parametrizations

K. Washiyama, P.-H. Heenen,[*1] and M. Bender[*2]

Symmetry restoration and configuration mixing via the generator coordinate method (GCM), based on energy density functionals, are referred to as a multi-reference approach and have become widely used techniques for spectroscopic properties in low-energy nuclear structures.[1)] Recently, it has been indicated[2)] that these techniques are not well-defined for standard Skyrme energy density functionals and that multi-reference energy density functional calculations can exhibit discontinuities or even divergences in the energy when one of the collective coordinates is varied. Accordingly, a regularization procedure has been proposed to remove such spurious contributions to the energy.[3)] Although recent Skyrme parametrizations employ non-integer powers of the density for the density-dependent terms in energy density functionals in order to adjust the incompressibility of symmetric infinite nuclear matter to a realistic value, this regularization procedure imposes integer powers of the density. At present, only dated parametrizations such as SIII fulfill this condition.

Therefore, we have constructed new Skyrme parametrizations[4)] that have integer powers of density dependence for multi-reference energy density functional calculations with the regularization procedure. Compared to the widely used SLy5 and the SIII, which has integer powers of density dependence, a significant improvement in the reproduction of the experimental binding energies and charge radii for a wide range of singly magic nuclei is observed with the new parametrizations.[4)] It is shown that these constructed Skyrme parametrizations can be used to study correlations beyond the mean field in atomic nuclei.

With our new Skyrme parametrizations, we perform regularized multi-reference energy density functional calculations. Our method consists of (1) self-consistent Hartree-Fock-Bogoliubov (HFB) calculations with a constraint on the axial mass quadrupole moment as a generator coordinate to prepare HFB states for different deformations, (2) particle-number and angular-momentum projections for the obtained HFB states, (3) calculations of the Hamiltonian and norm kernels between the projected states, and (4) configuration mixing by solving the so-called Hill-Wheeler-Griffin equation. It is found that the regularization procedure removes the discontinuities that appeared in the non-regularized particle-number and angular-momentum projected deformation energy curves and that the regularization varies the energy by about 0.1 ∼ 1 MeV.

*1 PNTPM, Université Libre de Bruxelles, 1050 Bruxelles, Belgium
*2 Université Bordeaux, Centre d'Etudes Nucléaires de Bordeaux Gradignan, UMR5797, F-33170 Gradignan, France

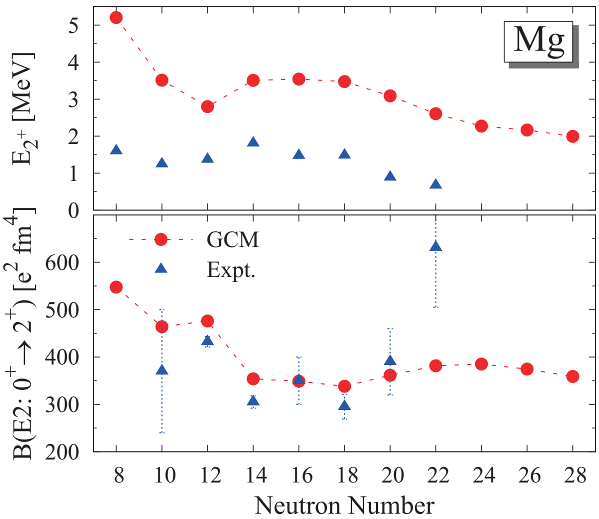

Fig. 1. Excitation energy of the first 2^+ state (top) and $B(E2: 0^+ \to 2^+)$ value (bottom) as a function of neutron number for Mg isotopes. The solid circles are the results of regularized GCM calculations, while the solid triangles are the experimental data.

Some of spectroscopic properties determined for Mg isotopes are shown in Fig. 1, where the first 2^+ energy and transition probability $B(E2 : 0^+ \to 2^+)$ are plotted and are compared with the available experimental data. A good description is obtained for the $B(E2)$ values. However, the first 2^+ energies are overestimated for all the isotopes. One of the reasons for this discrepancy may be the fact that the time-odd terms were neglected when calculating the Hamiltonian kernel in the multi-reference energy density functionals.

References

1) M. Bender and P.-H. Heenen: Phys. Rev. C **78**, 024309 (2008); J. M. Yao et al.: Phys. Rev. C **81**, 044311 (2010); T. R. Rodriguez and J. L. Egido: Phys. Rev. C **81**, 064323 (2010).
2) M. Anguiano et al.: Nucl. Phys. **A696**, 467 (2001).
3) D. Lacroix et al.: Phys. Rev. C **79**, 044318 (2009); M. Bender et al.: Phys. Rev. C **79**, 044319 (2009); T. Duguet et al.: Phys. Rev. C **79**, 044320 (2009).
4) K. Washiyama, K. Bennaceur, B. Avez, M. Bender, P.-H. Heenen, and V. Hellemans: Phys. Rev. C **86**, 054309 (2012).

Development of local energy density functional for description of pairing correlations in drip-line region†

M. Yamagami, J. Margueron,[*1] H. Sagawa, and K. Hagino

It is necessary to develop an effective interaction allowing one to predict the pairing properties of unstable nuclei in order to understand the nuclear dynamics in celestial bodies and in nuclear reactors. While extensive efforts have been made toward improving local energy density functionals, one of the bottlenecks stems from the pairing part represented by the pairing density function (PDF).

We proposed a new PDF in order to overcome the difficulty that the standard PDF with isoscalar density ($\rho = \rho_n + \rho_p$) term fails to reproduce the dependence of pairing on the mass number (A) and on the neutron excess ($\alpha = (N - Z)/A$).[1)] Our PDF $\tilde{h}_\tau(\mathbf{r}) = \frac{1}{2}V_0 g_\tau(\mathbf{r})\tilde{\rho}_\tau(\mathbf{r})$ includes the linear and quadratic terms of the isovector density ($\rho_1 = \rho_n - \rho_p$), in addition to the usual ρ term:

$$g_\tau(\mathbf{r}) = 1 - \eta_0\left(\frac{\rho}{\rho_0}\right) - \eta_1\left(\frac{\tau_3\rho_1}{\rho_0}\right) - \eta_2\left(\frac{\rho_1}{\rho_0}\right)^2.$$

Here, $\tau_3 = 1(-1)$ for $\tau = n$ (p) and $\rho_0 = 0.16$ fm^{-3}.

The parameters $(V_0, \eta_0, \eta_1, \eta_2)$ are determined so as to minimize the rms deviation $\sigma_{tot}^{(all)}$ between the experimental pairing gaps of even–even nuclei with $N, Z > 8$ and the results of the Hartree–Fock–Bogoliubov calculation with the particle–hole Skyrme force.[2)]

We found that the strong ρ dependence ($\eta_0 \approx 0.75$) is commonly required for the Skyrme parameterizations SLy4, SkM*, LNS, and SkP (see Fig. 1). We extracted an empirical correlation between V_0 and η_0 (the isoscalar part of PDF) and m_s^*/m (the isoscalar effective mass of the particle-hole Skyrme force) as $|V_0| = 260.58(\eta_0)^2 - 255.18m_s^*/m + 418.59$ MeV fm^{-3}. The curve expressed by this relationship is shown by dashed lines in Fig. 2. The change in $\sigma_{tot}^{(all)}$ is less than 0.05 MeV from the minimum value, if (V_0, η_0) satisfies two conditions: $\eta_0 \geq 0.75$ and $|V_0| \leq |V_{vac}|$ (the shaded region in Fig. 2). Here, an optimization was made to minimize the uncertainties in η_1 and η_2 for each (V_0, η_0). The pairing strength $V_{vac} = -458.15$ MeV fm^{-3} is determined from the neutron–neutron scattering length of the $^1S_0$ channel in vacuum.[2)]

We also discussed the effect of Coulomb force in the pairing channel. We showed that the linear ρ_1 term in the PDF can mimic the Coulomb effect in the pairing of neutron-rich nuclei. This local density approximation enables us to considerably reduce the computational effort.

† Condensed from the article in Phys. Rev. C **86**, 034333 (2012)

*1 Institut de Physique Nucléaire, Université Paris-Sud, IN2P3-CNRS, F-91406 Orsay Cedex, France

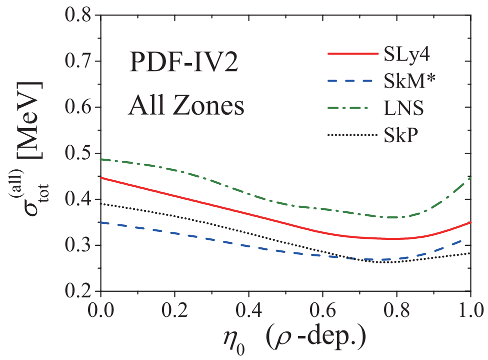

Fig. 1. Comparison of $\sigma_{tot}^{(all)}$ with SLy4, SkM*, LNS and SkP.

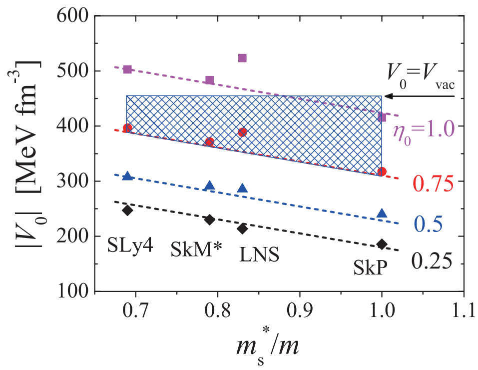

Fig. 2. The optimal values of V_0 at η_0 = 0.25, 0.5, 0.75, and 1.0 are shown as a function of m_s^*/m. The shaded region indicates the uncertainty of parameters. See the text for details.

Our PDF currently best describes the global properties of pairing correlations and pairing-sensitive observables. However, it is necessary to continue the analysis including newly obtained experimental data for more neutron-rich nuclei and also the excited states for the further improvement.

References

1) M. Yamagami, Y. R. Shimizu, and T. Nakatsukasa: Phys. Rev. C **80**, 064301 (2009).
2) M. Yamagami, J. Margueron, H. Sagawa, and K. Hagino: Phys. Rev. C **86**, 034333 (2012).

Neutron-skin thickness, pygmy dipole resonance, and $E1$ polarizability

S. Ebata,*1 and T. Nakatsukasa

Recent progress in radioactive beam facilities enables us to study unstable neutron-rich nuclei experimentally. To investigate the properties of nuclear system, we should find the elementary modes of unstable nuclei. The Pygmy dipole resonance (PDR) is known as a candidate of characteristic excited states of unstable neutron-rich nuclei. They appear in low energy region and are sometimes explained as a neutron-skin mode. Some previous studies indicate that there is a linear relation between PDR and neutron-skin thickness[1)] in isotope chains. On the other hand, it is reported that the correlation between PDR and the skin is small from a covariance analysis[2)]. Furthermore, Ref.2 indicates that the electric dipole ($E1$) polarizability is much more correlated to the neutron (N-) skin than PDR. Both previous studies are investigated in the limited region, i.e., $Z < 40$, with only one interaction parameter[1)], and special nuclei: ^{132}Sn, ^{208}Pb[2)]. In this report, we discuss our recent studies on the relation between these quantities and N-skin in neutron-rich unstable nuclei.

To study excited states in wide mass region, we had proposed the canonical-basis time-dependent Hartree-Fock-Bogoliubov (Cb-TDHFB) theory[3)]. We execute the linear response calculations with the Cb-TDHFB in a three-dimensional real-space. These calculations can describe any type of deformation effects on the excited states while treating the pairing correlation in the Bardeen-Cooper-Schrieffer-like approximation.

We systematically investigated of the $E1$ strength for Sn isotopes from N=50 to 90 with two Skyrme parameters (SkM* and SkI3). We solved the Cb-TDHFB equations in real time and computed the linear response of the nucleus. The procedure of linear response for $E1$ mode is the same as that in Ref.3. We obtained the strength function $S(E1;E)$ through the Fourier transformation of the time-dependent expectation value of $E1$ operator[3)]. To quantify the PDR, we used the ratio:

$$\frac{m_1(E_c)}{m_1} \equiv \frac{\int^{E_c} E \times S(E1;E)dE}{\int^{E_T} E \times S(E1;E)dE}, \quad (1)$$

where we adopt E_c=10 MeV and E_T=100 MeV in the present calculation. The $E1$ polarizability α_D is defined using the $E1$ strength function as,

$$\alpha_D \equiv 2\int^{E_T} \frac{S(E1;E)}{E} dE. \quad (2)$$

Figure 1 shows (a) the PDR ratio and (b) the $E1$ polarizability α_D as a function of N-skin thickness, which is defined by the difference between the root mean square radii of neutrons and protons for the Sn isotopes. In both panels, filled circle (square) symbols indicate the results obtained for SkM* (SkI3) Skyrme effective interaction. SkI3 parameter is revised to reproduce the ordering of single-particle states obtained by the relativistic mean field model on Pb isotopes. We can see, in panel (a), the different behavior of PDR ratio from N=50 (circle) to 82 (triangle) in the results of two interactions, but also recognize the linear relations over N=82. The change in relation indicates that the PDR reflects nuclear structure strongly. Further, the emergence of a linear relation shows that the PDR property changes from N=82. If the correlation between PDR and N-skin is robust "globally", it should not depend on the mass region and the interaction. In contrast, the relation between α_D and the skin is stable with respect to change in the neutron number and the interaction. However, the interaction dependence of the correlation in each nucleus is changing with the increase in the neutron number.

Currently, we are investigating the cases of other isotopes and interaction. We also plan to use this method for investigating other excitation modes.

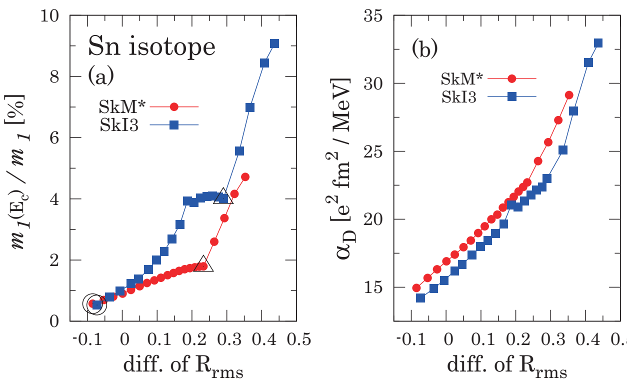

Fig. 1. (a) PDR ratio defined by Eq.(1). (b) α_D defined by Eq.(2) as a function of N-skin thickness for Sn isotopes with N=50−90. Filled circle (square) symbols indicate results in SkM* (SkI3) parameter set.

*1 Center for Nuclear Study, University of Tokyo

References

1) J. Piekarewicz: Phys. Rev. C **73**, 044325 (2006), T. Inakura, T. Nakatsukasa and K. Yabana: Phys. Rev. C **84**, 021302 (2011)
2) P.-G. Reinhard and W. Nazarewicz: Phys. Rev. C **81**, 051303(R) (2010).
3) S. Ebata *et al.*: Phys. Rev. C **82**, 034306 (2010).

Correlation between neutron skin thickness and pygmy dipole resonances

T. Inakura[*1]

Electric dipole ($E1$) excitation has been used as an important tool for investigating a nuclear structure. The low-lying $E1$ excitation, which is often called pygmy dipole resonances (PDR), is sensitive to nuclear properties at the nuclear surface and at a low density. Thus, the observed properties of the PDR may provide us with information on the neutron skin or halo.

The correlation between the PDR and neutron skin is one of the important subjects currently under dispute. If the strong correlation exists, the PDR may constrain skin thickness Δr_{np}. A calculation by Piekarewicz with the random-phase approximation (RPA) based on the relativistic mean-field model predicted a linear correlation for Sn isotopes[1)]. However, Reinhard and Nazarewicz performed a covariance analysis investigating the parameter dependence for the Skyrme functional models, which concluded that the correlation between the PDR strength and Δr_{np} is very weak in ^{68}Ni, ^{132}Sn, and ^{208}Pb[2)]. It should be noted that these conclusions, which seemed to contradict to each other, were drawn from RPA calculations for selected nuclei.

Recently, we performed a systematic RPA calculation on the PDR for even-even nuclei[3)] and found significant enhancement of the PDR strength in regions of specific neutron numbers. In this work, we perform an analysis similar to Ref.[2)] to investigate the Skyrme parameter dependence of the RPA results. The RPA equation is solved in fully self-consistent manner using a revised version of the RPA code in Ref.[4)] with the SkM* parameter set.

First, we define the PDR strength as

$$S_{\rm PDR}(E1) \equiv \sum_{n, E_n < \omega_{\rm cut}} B(E1; n)$$

with $\omega_{\rm cut} = 10$ MeV. In Figs. 1(a)-(c), the $S_{\rm PDR}$ for ^{68,78,84}Ni is shown as a function of the neutron skin thickness. The 21 plotted points are obtained by calculating Δr_{np} and $S_{\rm PDR}$ with the SkM* functional, and with slightly modified values of 10 Skyrme parameters. The scattered data points in Figs. 1 (a) and (b) suggest a weak correlation in ^{68,78}Ni. The calculated correlation coefficients are $r = 0.69$ and 0.76 for ^{68,78}Ni, respectively. In contrast, a strong linear correlation with $r = 0.94$ for ^{84}Ni is observed in Fig. 1 (c). It is apparent that the linear correlation is qualitatively different between ^{68}Ni and ^{84}Ni.

This qualitative difference of the linear correlation is associated with the neutron shell effect found in our previous study[3)]: In Ref.[3)], we found a strong

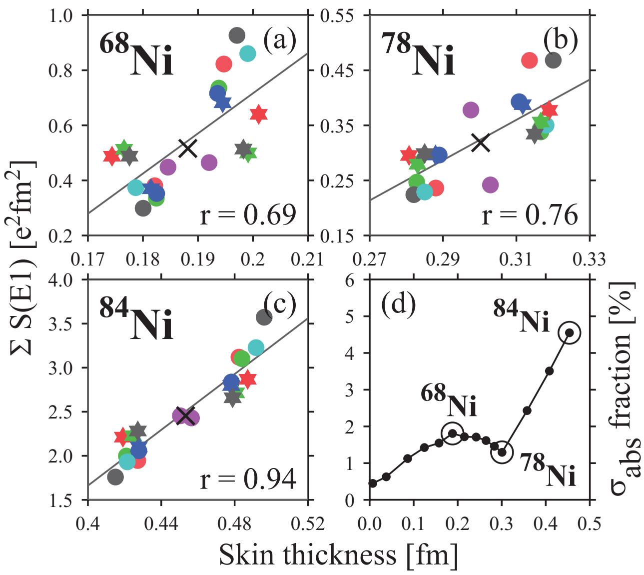

Fig. 1. (a)-(c) Correlations between $S_{\rm PDR}$ and Δr_{np} in ^{68,78,84}Ni. The cross denotes a result obtained with the original SkM* parameter set. Other symbols represent results with the modified parameter set. The solid line indicates a linear fit. Calculated correlation coefficients are also shown. (d) Photoabsorption cross section fraction as functions of Δr_{np} for even-even Ni isotopes.

linear correlation for the isotopic dependence of PDR strength and Δr_{np}, but only in restricted regions where the neutron Fermi levels are located at the weakly-bound low-ℓ shells, such as s, p, and d orbits. In Ni isotopes, this corresponds to the region with neutron number beyond 50, as illustrated in Fig. 1 (d). Thus, nuclei with a strong linear correlation in the isotopic dependence show a strong correlation in the parameter dependence as well. We confirm the same neutron shell effect on the correlation in O and Ca isotopes.

This result suggests that the observation of PDR could be a possible probe of the neutron skin in neutron-rich nuclei. The present result may provide a solution for the controversial issue on the correlation between the PDR and the neutron skin, for which different conclusions were reported previously[1,2)].

References

1) J. Piekarewicz: Phys. Rev. **C 73**, 044325 (2006).
2) P.-G. Reinhard and W. Nazarewicz: Phys. Rev. **C 81**, 051303(R) (2010).
3) T. Inakura et al.: Phys. Rev. **C 84**, 021302(R) (2011).
4) T. Inakura et al.: Nucl. Phys. A 768, 61 (2006).

*1 Department of Physics, Faculty of Science, Chiba University

Shell-model analysis of Gamow-Teller transition strength from ^{56}Ni

M. Honma,[*1] T. Suzuki,[*2,*3] and T. Otsuka,[*4,*5]

Gamow-Teller (GT) strength distribution provides us with various important information of the nuclear structure. Recently, the GT strength distribution was extracted for a double-magic nucleus ^{56}Ni[1)] from (p,n) charge-exchange reaction experiments and also for the neighboring nucleus ^{55}Co[2)]. In addition to the astrophysical interests[3)], these nuclei are of special importance from the viewpoint of the nuclear structure, because the measured data are directly related to the property of the $N = Z = 28$ closed shell.

In a naive picture, the GT($-$) transition from ^{56}Ni to ^{56}Cu should be dominated by a contribution of 1p-1h excitation between the fully occupied $\nu f_{7/2}$ orbit and the vacant $\pi f_{5/2}$ orbit. Therefore, it is expected that one can observe a single peak of the strength at the corresponding excitation energy. In reality, there should be some fragmentation of the strengths through the mixing with various minor excited configurations. However, it was predicted by the shell-model calculation[4)] using the effective interaction GXPF1J[5)] that the GT strength distribution in ^{56}Ni shows a "double-peak" structure, and in fact such a structure was observed by the recent measurement[1)].

It should be noted that the shell-model effective interaction KB3G[6)] predicts only one prominent peak in the GT strength distribution. In Ref.[1)], this discrepancy was explained as a result of the relatively weak spin-orbit and residual proton-neutron interactions in KB3G. This interaction successfully describes various nuclear properties of relatively light pf-shell nuclei. However, it predicts too high excitation energy of the lowest 2^+ state of ^{56}Ni, suggesting a problem in the description of the closed-shell structure[7)].

In order to analyze the difference between these two effective interactions in relation to the $(f_{7/2})^{16}$ core excitation, we have carried out shell-model calculations for the GT-strength distribution by gradually changing the restriction on the amount of such core excitation. In Fig.1, the case of $t = 0$ corresponds to the $(f_{7/2})^{16}$ closed-shell configuration for the parent ^{56}Ni, and in fact there is only one peak in the GT-strength distribution. In the results with GXPF1J, as the restriction is relaxed by increasing the truncation order t, the fragmentation of the strength becomes remarkable. The second peak appears at the level of $t = 2$ or higher, and it becomes comparable to the first one at $t = 4$, where the distribution looks converged and almost unchanged up to the level of $t = 6$. On the other hand, in the case of KB3G, the strength distribution shows only one peak for all truncation levels, and the fragmentation is not significant. Thus it is clear that the appearance of the "double peak" structure reflects the breakdown of the closed $f_{7/2}$ core.

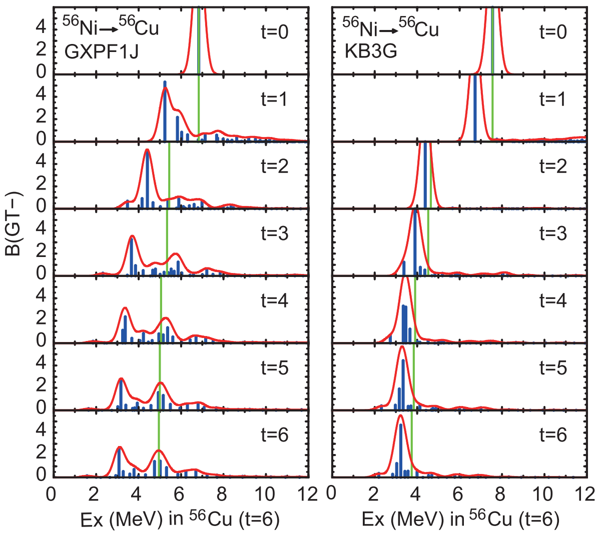

Fig. 1. Comparison of GT strength distribution between the shell-model results with two effective interactions GXPF1J (left) and KB3G (right). The truncation order t stands for the number of nucleons allowed to excite from the $f_{7/2}$ to higher orbits $p_{3/2}$, $f_{5/2}$ and $p_{1/2}$. The discrete strengths indicated by thick vertical bars are obtained by the prescription in Ref.[8)] through 100 Lanczos iterations, and they are folded by Gaussian of σ=0.5MeV as shown with a smooth curve. No quenching factor is considered for the purpose of comparison. A thin vertical line in each panel indicates the position of the centroid of the strength. The shell-model results are obtained by using the efficient shell-model code MSHELL[9)].

*1 Center for Mathematical Sciences, University of Aizu
*2 Department of physics, Nihon University
*3 National Astronomical Observatory of Japan
*4 Department of Physics, University of Tokyo
*5 Center for Nuclear Studies, University of Tokyo

References

1) M. Sasano et al.: Phys. Rev. Lett. **107**, 202501 (2011).
2) M. Sasano et al.: Phys. Rev. C **86**, 034324 (2012).
3) T. Suzuki et al.: Phys. Rev. C **83**, 044619 (2011).
4) T. Suzuki et al.: Phys. Rev. C **79**, 061603(R) (2009).
5) M. Honma et al.: J. Phys.: Conf. Ser. **20**, 7 (2005).
6) A. Poves et al.: Nucl. Phys. A **694**, 157 (2001).
7) M. Honma et al.: Phys. Rev. C **69**, 034335 (2004).
8) R. R. Whitehead: in *Moment Methods in Many Fermion Systems*, edited by B. J. Dalton et al. (Plenum, New York, 1980), p. 235.
9) T. Mizusaki: RIKEN Accel. Prog. Rep. **33**, 14 (2000).

Role of T = 0 pairing in Gamow-Teller states in N = Z nuclei†

C. L. Bai,*1 H. Sagawa, M. Sasano, T. Uesaka, K. Hagino, H. Q. Zhang,*2 X. Z. Zhang,*2 and F. R. Xu,*3

The strong attraction between nucleons is the basic factor responsible for the pairing correlations. So far, the pairing interaction of like-nucleons with the isovector spin-singlet (T = 1, S = 0) channel has mainly been discussed. In fact, the attraction between protons and neutrons is even stronger in the isoscalar spin-triplet (T = 0, S = 1) channel which gives rise to the deuteron bound state. However the role of T = 0 pairing is limited in nuclei because of large imbalance between neutron and proton numbers, and also the two-body spin-orbit interaction, which breaks the S = 1 pair more effectively than the S = 0 pair. In this contribution, Gamow-Teller (GT) states in N = Z nuclei with the mass number A from 48 to 64 are studied using the Hartree-Fock-Bogoliubov + quasiparticle random phase approximation (HFB+QRPA) with Skyrme interactionsThe isoscalar spin-triplet (T = 0, S = 1) pairing interaction is taken into account only in QRPA calculations, but not HFB. It is found in the context of SU(4) symmetry in the spin-isospin space that the GT strength of lower energy excitations is largely enhanced by the T = 0 pairing interaction, which works cooperatively with the T = 1 pairing interaction in the ground state. A two-peaked structure observed recently in a (p, n) reaction on ^{56}Ni[1)] can be considered as evidence of the role of T = 0 pairing in the GT collective states, as is seen in Fig. 1.

The peak ratio between the GT strength of the low energy region (below E_x = 20 MeV) and the high energy region (above E_x = 20 MeV) is plotted in Fig. 2 as a function of the mass number A. The ratio f between T = 0 and T = 1 pairing interactions is changed from f = 0.0, 0.5, 1.0, 1.5, and 1.7. In the cases of weak T = 0 pairing ($f \leq 1.0$), the high energy peak $B_{\rm high}$(GT) is larger than the low energy one $B_{\rm low}$(GT). With stronger T = 0 pairing ($f > 1.0$), the $B_{\rm low}$(GT) value becomes larger and dominates the GT strength distribution, especially in nuclei with $A \leq 56$. The low energy peak may appear as a single giant resonance peak in the strong T = 0 pairing limit. The empirical ratio of $B_{\rm low}$(GT) to $B_{\rm high}$(GT) in ^{56}Ni is obtained from the observed B(GT) strength distributions given in Ref.[1)]. This empirical ratio is consistent with the calculated ratio for the T = 0 pairing at $f \sim 1.5$.

References

1) M. Sasano et al.: Phys. Rev. Lett.**107**, 202501 (2011).

† Condensed from the article in Phys. Lett. B 719, 116 (2013)

*1 Department of Physics, Sichuan University, Chengdu 610065, China
*2 China Institute of Atomic Energy, Beijing 102413, China
*3 School of Physics, Peking University, Beijing 100871, China

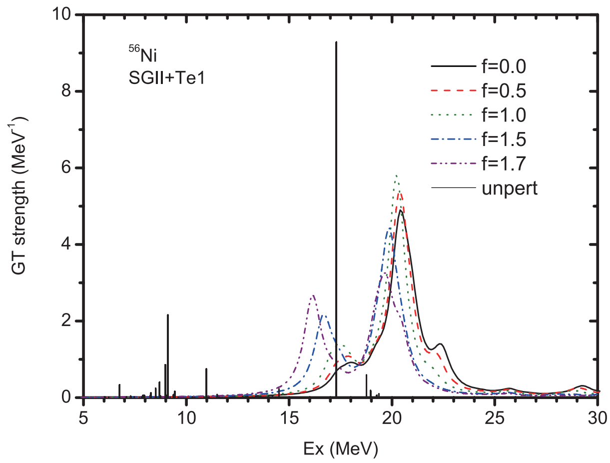

Fig. 1. (Color online) Gamow-Teller strength in ^{56}Ni obtained by HFB+QRPA calculations with the Skyrme interaction SGII+Te1. The excitation energy is referred to the ground state of ^{56}Ni. The T = 0 pairing interaction is included in QRPA by changing the ratio factor f between T = 0 and T = 1 pairing interactions as f = 0.0, 0.5, 1.0, 1.5, and 1.7. The solid lines show the unperturbed strength without RPA correlations. The QRPA strength is smoothed out by a Lorentzian function with a width $\Gamma = 1$ MeV.

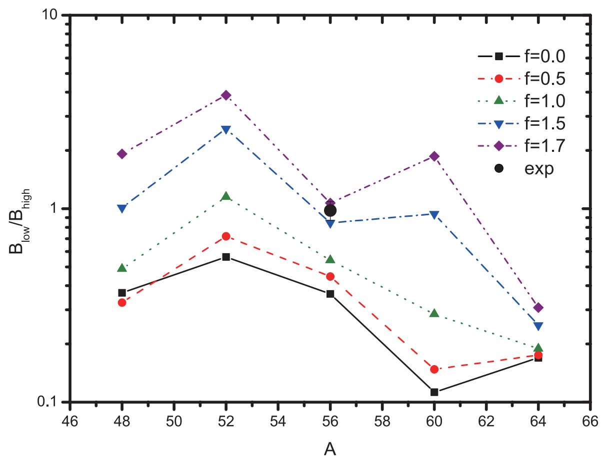

Fig. 2. (Color online) Ratio between Gamow-Teller peaks in the lower energy and higher energy regions as a function of the T=0 strength parameter, f, calculated with T21 interaction. The lower energy and higher energy regions are separated at E_x = 20 MeV. The experimental ratio in ^{56}Ni is obtained from observed B(GT) strengths in the lower and higher energy regions reported in Ref.[1)].

Competition between $T = 1$ and $T = 0$ pairing in pf-shell nuclei with $N = Z$

H. Sagawa, Y. Tanimura,*1 and K. Hagino

The isoscalar spin-triplet pairing interaction is known to be stronger than the isovector spin-singlet pairing interaction in the nuclear matter.Nevertheless, the nuclei are observed to favor the spin-singlet $T = 1$ pairing between identical particles. A straightforward explanation for this puzzle is that most stable nuclei have different numbers of neutrons and protons, and thus protons and neutrons occupy different single-particle orbits near the Fermi surface, which leads to the inhibition of a $T = 0$ pair. It has been suggested that the nuclear spin-orbit field largely suppresses the spin-triplet pairing much more than the spin-singlet pairing. In this paper, we study the quenching of two-body matrix elements for the $T = 0$ pairing interaction in the jj coupling scheme in comparison with that for the $T = 1$ pairing interaction. Especially, the effect of spin-orbit interaction on the isoscalar spin-triplet interaction is examined.[1)]

We adopt a separable form of the pairing interaction as

$$V^{(T=1)} = -G^{(T=1)} \sum_{i,j} P^{(1,0)\dagger}_{i,i}(\mathbf{r},\mathbf{r}') P^{(1,0)}_{j,j}(\mathbf{r},\mathbf{r}'), \quad (1)$$

where the pair field operator is defined as

$$P^{(T,S)\dagger}_{i,j} = \delta_{l_i,l_j}\sqrt{2l_i+1}[a^\dagger_i a^\dagger_j]^{(T,S)}\psi_i(\mathbf{r})^*\psi_j(\mathbf{r}')^*, \quad (2)$$

with a single-particle wave function $\psi(\mathbf{r})$. The spin-triplet $T = 0$ pairing is also given by a similar separable form, $V^{(T=0)}$, with a scaling factor f.

Figure 1 shows the pairing gain energies for the p-orbit ($l = 1$) and the f-orbit ($l = 3$) configurations as a function of the scaling factor f for the $T = 0$ pairing. The energies for both the $J^\pi = 0^+$ state with the isospin $T = 1$ and the $J^\pi = 1^+$ state with the isospin $T = 0$ are shown in the figure. To this end, we diagonalize the pairing Hamiltonian separately for the p- and f-orbit configurations in order to disentangle the role of the pairing and the spin-orbit interactions in a transparent way. For the $l = 1$ case, the $(2p_{3/2})^2$ and $(2p_{1/2})^2$ configurations are available for the $J^\pi = 0^+$ state, while the $(2p_{3/2}2p_{1/2})$ configuration is also available for the $J^\pi = 1^+$ state. In a similar manner, the $(1f_{7/2})^2$ and $(1f_{5/2})^2$ configurations participate in the $J^\pi = 0^+$ state in the $l = 3$ case, and the $(1f_{7/2}1f_{5/2})$ configuration is also involved in the $J^\pi = 1^+$ state.

For constructing the Hamiltonian, we use the spin-orbit splitting, parametrized as $\Delta\varepsilon_{ls} = -V_{ls}(\mathbf{l}\cdot\mathbf{s})$, where the strength is taken to be $V_{ls} = \frac{24}{A^{2/3}}$ (MeV).

As one can see in Fig. 1, the lowest energy state

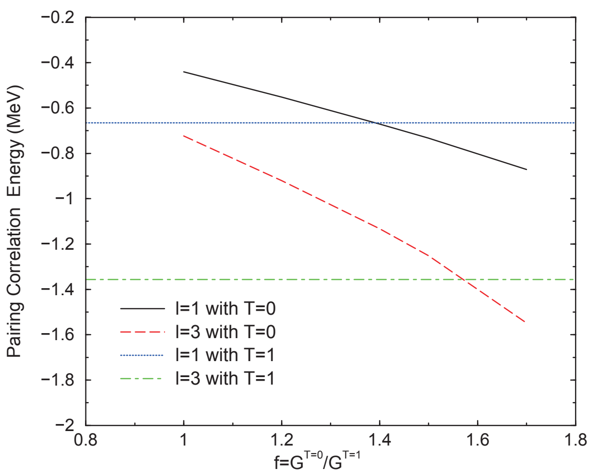

Fig. 1. The pairing correlation energies for the lowest ($J^\pi = 0^+$, $T = 1$) and ($J = 1^+$, T=0) states with the $l = 3$ and $l = 1$ configurations as a function of the scaling factor f for $T = 0$ pairing. The strength of the spin-singlet T= 1 pairing interaction is fixed to be $G^{(T=1)} = 24/$A MeV with a mass A = 56, whereas the strength for the spin-triplet $T = 0$ pairing, $G^{(T=0)}$, is varied with the factor f multiplied by $G^{(T=1)}$.

with $J^\pi = 0^+$ for the $l = 3$ case gains more binding energy than the $J^\pi = 1^+$ state for the strength factor $f < 1.5$. In the strong $T = 0$ pairing case, that is, $f \geq 1.6$, the $J^\pi = 1^+$ state gathers more binding energy than the lowest $J^\pi = 0^+$ state. These results are largely due to the quenching of the $T = 0$ pairing matrix element by the transformation coefficient from the jj to LS coupling schemes.This quenching never occurs for the $T = 1$ pairing matrix element, since the mapping of the two-particle wave function between the two coupling schemes is simply implemented by the factor $\sqrt{j+1/2}$. For the $l = 1$ case, the competition between the $J^\pi = 0^+$ and $J^\pi = 1^+$ states is also seen in Fig. 1. Because of the smaller spin-orbit splitting in this case, the couplings among the available configurations are rather strong, and the lowest $J^\pi = 1^+$ state gains more binding energy than the $J^\pi = 0^+$ state in the case of $f \geq 1.4$. These results are consistent with the observed spins of $N = Z$ odd-odd nuclei in the pf shell, where all the ground states have the spin-parity $J^\pi = 0^+$, except for $^{58}_{29}$Cu. The ground state of $^{58}_{29}$Cu has $J^\pi = 1^+$, since the odd proton and odd neutron mainly occupy the $2p$ orbits, in which the spin-orbit splitting is expected to be much smaller than that of $1f$ orbits.

References
1) H. Sagawa et al.: Phys. Rev. C**87**, 034310 (2013).

*1 Department of Physics, Tohoku University, Sendai 980-8578, Japan

Relativistic local density approximation for Coulomb functional of nuclei†

H.-Q. Gu,*1 H. Liang, W. H. Long,*1 N. Van Giai,*2 and J. Meng

The Coulomb interaction between protons is one of the most important building blocks in atomic nuclei. Nevertheless, its exchange term is considerably cumbersome to calculate because of the non-locality of the corresponding mean field. Thus far, in almost all of the non-relativistic self-consistent Hartree-Fock calculations, the Coulomb exchange term is evaluated within a local scheme by using the Slater approximation.[1)]

During the past decades, the nuclear covariant density functional theory (CDFT) has received widespread attention because it has successfully described many nuclear phenomena. In order to retain the simplicity of the relativistic Hartree (RH) theory, the non-local Coulomb exchange term is usually neglected, and its effects are assumed to be absorbed in the effective coupling strengths. However, in some cases neglecting the Coulomb exchange term may yield incorrect results. One example is the isospin symmetry-breaking corrections to superallowed β decays[2)], which are crucial for testing the unitarity of the Cabibbo-Kobayashi-Maskawa matrix.

The density-dependent relativistic Hartree-Fock (RHF) theory was recently developed.[3)] It has been shown that the meson exchange terms play very important roles in nucleon effective masses, symmetry energies, spin and pseudospin symmetries, the shell structure and its evolutions, deformations, spin-isospin resonances, etc. In this framework, for the first time, the non-local relativistic Coulomb exchange term is accurately taken into account.

With the simplicity of the local CDFT and its success in accurately treating Coulomb terms, it is worthwhile to explore the relativistic local density approximation (LDA) for the Coulomb functional of nuclei. This may be a simple approach to implement the missing Coulomb exchange effects in the RH theory, while retaining the merits of locality. This attempt is further supported by the recent success in incorporating the meson exchange terms into a local equivalent scheme.[4)]

Up to the next-to-leading order, the Coulomb exchange energy in the relativistic LDA is expressed as[5)]

$$E_{\rm Cex}^{\rm RLDA} = -\frac{3}{4}\left(\frac{3}{\pi}\right)^{1/3} e^2 \int d^3r \rho_p^{4/3}\left[1-\frac{2}{3}\frac{(3\pi^2\rho_p)^{2/3}}{M_p^2}\right],$$

where M_p (ρ_p) is the proton mass (density). The first and second terms correspond to the well-known Slater approximation and the corrections for the relativistic effects, respectively.

In Fig. 1, we show the systematics of the relativistic LDA results for the semi-magic Ca, Ni, Zr, Sn, and Pb isotopes from the proton drip line to the neutron drip line. The relative deviations $\Delta E_{\rm Cex}$ of the approximate Coulomb exchange energies from the relativistic Hartree-Fock-Bogoliubov[6)] (RHFB) results are defined as $(E_{\rm Cex}^{\rm LDA} - E_{\rm Cex}^{\rm RHFB})/E_{\rm Cex}^{\rm RHFB}$. By comparing these with the exact Coulomb exchange energies calculated using the RHFB theory, it is found that the relative deviations introduced by the relativistic LDA are less than 5% for these five semi-magic isotopes. In addition, the relativistic corrections to the LDA are found to play substantial roles in improving the results by 3% ~ 5%.

Therefore, the relativistic LDA for the Coulomb functional in nuclear CDFT is a very promising solution to ensure that the Coulomb terms are considered, and the relativistic corrections to the traditional Slater approximation are important.

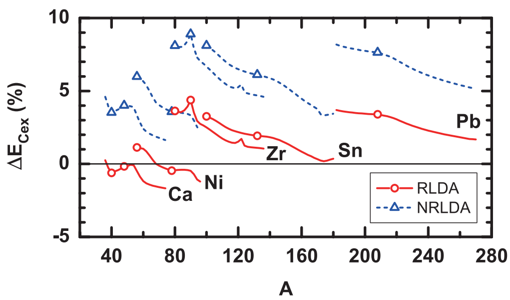

Fig. 1. Relative deviations of Coulomb exchange energies by the relativistic (solid lines) and non-relativistic (dashed lines) LDA for Ca, Ni, Zr, Sn, and Pb isotopes. Traditional doubly magic nuclei are denoted with open symbols.

References

1) J. C. Slater: Phys. Rev. **81**, 385 (1951).
2) H. Liang, N. Van Giai, and J. Meng: Phys. Rev. C **79**, 064316 (2009).
3) W. H. Long, N. Van Giai, and J. Meng: Phys. Lett. B **640**, 150 (2006).
4) H. Liang, P. Zhao, P. Ring, X. Roca-Maza, and J. Meng: Phys. Rev. C **86**, 021302(R) (2012).
5) E. Engel and R. M. Dreizler: *Density Functional Theory: an Advanced Course* (Springer-Verlag, Berlin, 2011).
6) W. H. Long, P. Ring, N. Van Giai, and J. Meng: Phys. Rev. C **81**, 024308 (2010).

† Condensed from the article in Phys. Rev. C **87**, 041301(R) (2013)
*1 School of Nuclear Science and Technology, Lanzhou University, China
*2 Institut de Physique Nucléaire, IN2P3-CNRS and Université Paris-Sud, France

Damping of giant dipole resonance in hot rotating nuclei†

N. Dinh Dang

At present, comprehensive experimental data on the dependence of the giant dipole resonance (GDR) width on temperature T and angular momentum J have been accumulated for a large number of medium- and heavy-mass compound nuclei starting from potassium up to lead isotopes. This systematics shows that the full width at half maximum (FWHM) of the GDR increases significantly with T at low and moderate T, but it seems to saturate at high T, above $T \sim 4-5$ MeV. At a given value of T, the GDR width also increases with J, but this increase is noticeable only starting from $J > 25\hbar$ for copper and heavier isotopes.

Among the theoretical approaches to the study of the hot GDR, the phonon damping model (PDM)[1) offers a microscopic mechanism of GDR damping via coupling of the GDR to noncollective particle-hole (ph) transitions, which exist already at $T = 0$, and particle-particle (pp) ones, which appear at $T \neq 0$ because of the distortion of the Fermi surface. This model is able to describe consistently both the increase in the GDR width at low and moderate T as well as its saturation at high T by using the single-particle energies, obtained in the Woods-Saxon potentials for protons and neutrons, and a set of three parameters, fixed at $T = 0$, which are the GDR energy and the ph and pp coupling constants. By including nonvanishing thermal superfluid pairing[2)], the PDM is also able to explain a nearly constant value of the GDR width at $T \leq 1$ MeV. In a recent development, the PDM was employed to calculate the ratio η/s of the shear viscosity η to the entropy density s directly from the GDR photoabsorption cross sections in medium and heavy spherical nuclei at $T \neq 0$. The results obtained show that this ratio decreases with increasing T to reach (1.3 – 4) KSS at $T = 5$ MeV. The quantity KSS $= \hbar/(4\pi k_B)$ has been conjectured by Kovtun, Son and Starinets (KSS) to be the lower bound for all fluids[3)]. A shortcoming of the PDM is that so far it does not include the dependence on angular momentum. The present work removes this deficiency by extending the PDM to finite angular momentum to make the model capable of describing the dependence of the GDR width on both T and J. The present extension will also be applied to examine the credibility of the preliminary analysis of the recent data[4)], according to which the GDR width extracted at the initial temperature $T \sim 4$ MeV and J $= 44\hbar$ of the compound nucleus seems to be smaller than that measured at the initial $T \sim 3$ MeV and $J = 41\hbar$ in ^{88}Mo (Fig. 1).

The formalism is based on the description of the noncollective (single-particle) rotation of spherical systems. This implies that the total angular momentum J can be aligned along the z axis, and therefore it is completely determined by its projection M on this axis alone. The numerical calculations were carried out for two spherical nuclei ^{88}Mo and ^{106}Sn. The analysis of the numerical results shows that the GDR width increases with M at a given value of T for $T \leq 3$ MeV. At higher T, the GDR width approaches a saturation at $M \geq 60\hbar$ for ^{88}Mo and $M \geq 80\hbar$ for ^{106}Sn. However, the region of $M \geq 60\hbar$ goes beyond the maximum value of M up to which the specific shear viscosity η/s has values not smaller than the KSS lower-bound conjecture for this quantity. This maximum value of M is found to be equal to $46\hbar$ and $55\hbar$ for ^{88}Mo and ^{106}Sn, respectively, if the value $\eta(0) = 0.6\times10^{-23}$ MeV s fm^{-3} for the shear viscosity at $T = 0$ is used. A check by using the KSS lower-bound conjecture for the specific shear viscosity and the same $\eta(0) = 0.6 \times 10^{-23}$ MeV s fm^{-3} also shows that the experimental data for the GDR line shape in ^{88}Mo at the the initial temperature $T \sim 4$ MeV and J $= 44\hbar$ of the compound nucleus leads to a violation of the KSS conjecture. This calls for the need of reanalyzing the recent experimental data reported in Ref.[4)] for the GDR in ^{88}Mo at these large values of temperature and angular momentum (Fig. 1).

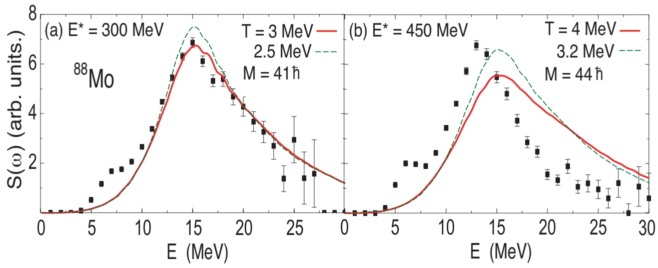

Fig. 1. GDR strength function for ^{88}Mo at $M = 41\ \hbar$ (a) and $M = 44\ \hbar$ (b) predicted by the PDM in comparison with the preliminary data from Ref.[4)].

† Condensed from the article in Phys. Rev. C **85**, 064323 (2012)

References

1) N. Dinh Dang and A. Arima, Phys. Rev. Lett **80**, 4145 (1998); N. Dinh Dang and A. Arima, Nucl. Phys. A **636**, 427 (1998).
2) N. Dinh Dang and A. Arima, Phys. Rev. C **68**, 044303 (2003).
3) P.K. Kovtun, D.T. Son, and A.O. Starinets, Phys. Rev. Lett. **94**, 111601 (2005).
4) M. Ciemala *et al.*, Acta Physica Polonica B **42**, 633 (2011).

Theoretical study of isovector spin monopole excitations by the (p, n) and $(^3\mathrm{He}, t)$ reactions on $^{90}\mathrm{Zr}$ and $^{208}\mathrm{Pb}$

C. L. Bai,[*1] H. Sagawa, K. Miki, M. Sasano, T. Uesaka, H. Q. Zhang,[*2] X. Z. Zhang,[*2] and F. R. Xu[*3]

The isovector spin monopole (IVSM) transition[1)] is one of the most important excitation modes in spin-isospin channels. The transition operator of this mode is given by $r^2\vec{\sigma}t_{\pm}$. The $\vec{\sigma}$ represents the Pauli spin matrices, wherea the t_- and t_+ indicate the isospin lowering and raising operators, respectively. Because of the r-dependence part, the IVSM mode involves the node-number change of $\Delta n = 1$ $(2\hbar\omega)$, corresponding to a "breathing" mode. Therefore, a study of the IVSM mode can provide insight into the incompressibility of nuclear matter with respect to spin and isospin densities.

The IVSM resonance can be observed by measuring charge-exchange (CE) reactions at intermediate energies, if the projectiles are strongly absorbed near the nuclear surface[2)]. The reaction mechanism of these CE reactions is becoming a hot topic, because a clear identification of the IVSM was recently reported by Miki *et al.* at the RIKEN RIBF[3)].

In this work, we theoretically evaluate the sensitivity of the CE (p, n) and $(^3\mathrm{He},t)$ reactions at 300 MeV per nucleon to probe the IVSM resonance. We calculate the cross sections for the IVSM mode in $^{90}\mathrm{Zr}$ and $^{208}\mathrm{Pb}$ by combining a sophisticated nuclear-structure model with nuclear-reaction calculations. For describing nuclear structures, we employ a self-consistent Hartree-Fock plus random phase approximation (HF+RPA) with eight parameter sets of Skyrme forces of the SGII and TIJ families. The reaction calculations are performed with a distorted wave Born approximation using the computer code FOLD[4)] with the effective nucleon-nucleon interaction at 325 MeV[5)] and the optical potential parameters[6)]. Here, the wave functions of the $^3\mathrm{He}$ and t particles are taken from Ref.[7)], and those of the p and n particles are assumed to be a delta function.

Figure 1 shows examples of the transition densities obtained for several IVSM states in $^{90}\mathrm{Zr}$, having bipolar shapes with a radial node around the nuclear surface. In the (p, n) reaction, the projectiles probe almost the whole part of the transition densities, and the scattering amplitudes are strongly canceled because of the sign difference between the inner and outer parts of the densities. In contrast, the $^3\mathrm{He}$ and t projectiles see the region only outside the node location, giving the large enhancement of the IVSM cross sections in the $(^3\mathrm{He},t)$ reaction. For further quantitative analysis, we will introduce the unit cross section for the IVSM mode in the same manner as for the GT mode[8)].

This work is being drafted with more detailed descriptions, and is to be submitted for publication soon.

*1 Department of Physics, Sichuan University, Chengdu 610065, China
*2 China Institute of Atomic Energy, China
*3 School of Physics, Peking University, Beijing 100871, China

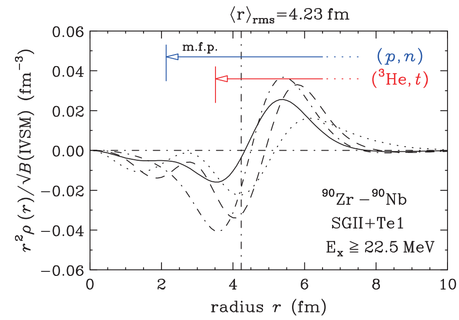

Fig. 1. Transition densities as a function of the radial coordinate for the IVSM excitations in $^{90}\mathrm{Zr}$, obtained from the HF+RPA calculation with the SGII+Te1 interaction and normalized by the square root of the strength. The r^2 is multiplied to take into account the volume term. The vertical dot-dashed line shows the mass root-mean-square radius, corresponding to the location of the nuclear surface. The horizontal arrows show the region where the projectile can penetrate taking into account the mean-free-path length estimated from the imaginary part of the optical potential.

References

1) N. Auerbach and A. Klein: Phys. Rev. C**30**, 1032 (1984); I. Hamamoto and H. Sagawa: Phys. Rev. C**62**: 024319 (2000).
2) N. Auerbach, F. Osterfeld, T. Udagawa: Phys. Lett. B**219**, 184(1989).
3) K. Miki *et al.*: Phys. Rev. Lett. **108**, 262503 (2012).
4) J. Cook and J.A. Carr: computer program FOLD, Florida State University (unpublished), based on F. Petrovich and D. Stanley: Nucl. Phys. A **275**, 487 (1977), modified as described in J. Cook *et al.*: Phys. Rev. C **30**, 1538 (1984) and R.G.T. Zegers, S. Fracasso and G. Colò: 2006 (unpublished).
5) M.A. Franey and W.G. Love: Phys. Rev. C **31**, 488 (1985).
6) T. Furumoto, Y. Sakuragi and Y. Yamamoto: Phys. Rev. C **82**, 044612 (2010).
7) S.C. Pieper and R.B. Wiringa: Ann. Rev. of Nucl. and Part. Sci. **51**, 53 (2001).
8) T.N. Taddeucci *et al.*: Nucl. Phys. A**469**, 125 (1987).

Nuclear Schiff moments of ^{129}Xe induced by time-reversal violating interactions

N. Yoshinaga and K. Higashiyama[*1]

The existence of a finite permanent electric dipole moment (EDM) of a particle or an atom indicates violation of time-reversal symmetry (T). It implies simultaneous violations of charge conjugation (C) and parity symmetry (P) through the CPT invariance. The standard model predicts tiny EDMs, which are extremely small and cannot be detected, given the present experimental accuracy. Thus, an experimental measurement of the EDM is one of the best probes for physics beyond the standard model. The EDM of a neutral atom with closed electron subshells is mainly induced by the nuclear Schiff moment, since the nuclear EDM is shielded by outside electrons owing to the Schiff theorem.[1)] Schiff moments for various nuclei have been calculated in terms of the various mean field approaches. However, no study has yet been undertaken that uses from the nuclear shell model point of view. Previously, we calculated the Schiff moment arising from the intrinsic nucleon EDM.[2)]

In this work, we calculate the Schiff moment arising from the P and T violating nucleon-nucleon interaction in terms of the pair-truncated shell model.[3)]

The Schiff moment operator may be written as[4)]

$$\boldsymbol{S} = \frac{1}{10}\sum_{i=1}^{A} e_i \left({r_i}^2 - \frac{5}{3}\left\langle r^2 \right\rangle_{\rm ch} \right) \boldsymbol{r}_i, \tag{1}$$

where $\langle r^2 \rangle_{\rm ch}$ is the mean squared radius of the nuclear charge distribution, $\boldsymbol{r}_i$ indicates the ith nucleon position, and e_i indicates the charge with $e_i = e$ for protons and $e_i = 0$ for neutrons. The Schiff moment for the $1/2_1^+$ states arising from the two-body interaction, which breaks P and T invariance, can be calculated through the first-order perturbation theory as

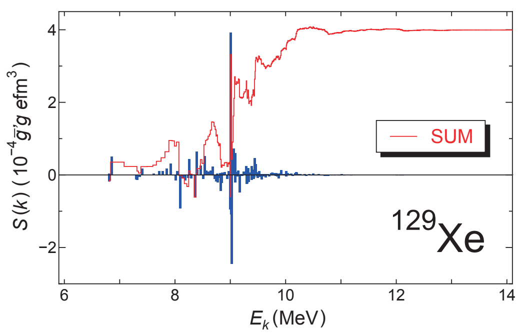

Fig. 1. Partial contribution to the Schiff moment as a function of excitation energy E_k.

[*1] Department of Physics, Chiba Institute of Technology

$$S_{\rm ch} = \sum_{k=1} \frac{\langle \frac{1}{2}{}^{+}_{1} | \hat{S}_z | \frac{1}{2}{}^{-}_{k} \rangle \langle \frac{1}{2}{}^{-}_{k} | V_{\pi}^{PT} | \frac{1}{2}{}^{+}_{1} \rangle}{E_1^{(+)} - E_k^{(-)}} + c.c., \tag{2}$$

where $\hat{V}_{\rm PT}$ represents the isovector interaction, and $\hat{S}_z$ is the third coordinate component of $\hat{\boldsymbol{S}}_{\rm ch}$. In this work, we adopt the two-body interaction $\hat{V}_{\rm PT}$, which is expressed as[5)]

$$\begin{aligned} \hat{V}_{\rm PT} = & -\frac{1}{16\pi}\frac{m_\pi^2}{M_N}\bar{g}'g\big[\,(\tau_{1z}+\tau_{2z})\,(\boldsymbol{\sigma}_1-\boldsymbol{\sigma}_2) \\ & +(\tau_{1z}-\tau_{2z})\,(\boldsymbol{\sigma}_1+\boldsymbol{\sigma}_2)\,\big]\cdot\boldsymbol{r}f(r), \end{aligned} \tag{3}$$

where

$$f(r) = \frac{\exp(-m_\pi r)}{m_\pi r^2}\left(1+\frac{1}{m_\pi r}\right) \tag{4}$$

with $\boldsymbol{r} = \boldsymbol{r}_1 - \boldsymbol{r}_2$ and $r = |\boldsymbol{r}|$. Here, g is the strong πNN coupling constant and $\bar{g}'$ is the strong πNN constant, which breaks P and T invariance. The calculated Schiff moment of the $1/2_1^+$ state in ^{129}Xe is

$$S = 3.99\times 10^{-4}\bar{g}'g\; e{\rm fm}^3. \tag{5}$$

To identify the microscopic origin of the nuclear Schiff moment, we calculate the partial contribution of the kth state $|\frac{1}{2}{}^{-}_{k}\rangle$, which is defined by

$$S(k) = \frac{\langle \frac{1}{2}{}^{+}_{1} | \hat{S}_{{\rm ch},z} | \frac{1}{2}{}^{-}_{k} \rangle \langle \frac{1}{2}{}^{-}_{k} | V_{\pi(I)}^{PT} | \frac{1}{2}{}^{+}_{1} \rangle}{E_1^{(+)} - E_k^{(-)}} + c.c.. \tag{6}$$

In Fig. 1, the calculated values of $S(k)$ are plotted against the excitation energy $E_k = E_k^{(-)} - E_1^{(+)}$. It is found that there are four large contributions around $E_k = 9.0$ MeV, one positive and others negative.

Making use of a relation between the EDM of the ^{129}Xe neutral atom and the nuclear Schiff moment:[6)]

$$d\left(^{129}{\rm Xe}\right) = 0.38\times 10^{-17}\left(\frac{S}{e\,{\rm fm}^3}\right)\; e\,{\rm cm}, \tag{7}$$

we can predict the atomic EDM:

$$d\left(^{129}{\rm Xe}\right) = 1.9\times 10^{-21}\bar{g}'g\; e\,{\rm cm}. \tag{8}$$

This will be tested in a future experiment.

References

1) L. I. Schiff: Phys. Rev. **132**, 2194 (1963).
2) N. Yoshinaga, K. Higashiyama, and R. Arai: Prog. Theor. Phys. **124**, 1115 (2010).
3) K. Higashiyama and N. Yoshinaga: Phys. Rev. C **83**, 034321 (2011).
4) V. F. Dmitriev and R. A. Sen'kov: Phys. Rev. Lett. **91**, 212303 (2003).
5) P. Herczeg: Hyperfine Interact. **75**, 127 (1992).
6) V. A. Dzuba et al.: Phys. Rev. A **66**, 012111 (2002).

Giant dipole resonance in ^{201}Tl at low temperature†

N. Dinh Dang and N. Quang Hung

Many experiments have been carried out in the last three decades to extract the giant width of the dipole resonance (GDR) and its line shape as functions of nuclear temperature T and angular momentum J. At present, the well-established systematics accumulated by measuring the γ decays of various hot compound nuclei formed in heavy-ion fusion reactions and inelastic scattering of light particles on heavy targets has shown that the GDR width increases with temperature T within the temperature region $1 \leq T \leq 3 - 4$ MeV. It has also been shown that the GDR widths increase with angular momentum J becomes noticeable only at $J \geq 27\hbar - 30\hbar$ in heavy nuclei, whereas its location remains mostly unchanged as T and J vary. Very recently, α-induced fusion reactions were used to measure the GDR width at low temperature[1,2]. The data extracted from these latest experiments for the GDR width in ^{119}Sb at $0.98 \leq T \leq 1.23$ MeV[1] are in good agreement with the prediction by the phonon damping model (PDM) for the GDR width in ^{120}Sn when thermal pairing is included[3]. These experiments also provided the data for the GDR width in ^{201}Tl[2], which were extracted within the temperature interval $0.8 < T < 1.2$ MeV. These values are significantly smaller than the prediction by the thermal shape fluctuation model (TSFM) for the GDR width in ^{208}Pb even after including the shell effect. The authors of Ref.[2] also made a comparison with the prediction by the PDM using the results for the GDR width in ^{208}Pb, where no pairing was taken into account. Because ^{201}Tl is an open-shell nucleus for both neutrons and protons, an adequate comparison should be made with the prediction within the PDM for the GDR width of the same ^{201}Tl nucleus, including the effects owing to thermal pairing of neutrons as well as protons. The aim of the present work is to make such a prediction.

We calculated the width and strength function of the GDR in ^{201}Tl at finite temperature within the framework of the quasiparticle representation of the PDM. Thermal pairing is taken into account by using the exact treatment of pairing within the canonical ensemble. This treatment allows us to calculate the exact equivalences to the pairing gaps for protons and neutrons in a nucleus neighboring a proton closed-shell one. Because of thermal fluctuations owing to the finiteness of the system, which are inherent in the canonical ensemble (CE), the exact CE thermal pairing gaps do not collapse at the critical temperature T_c of the superfluid-normal phase transition as in the case of infinite systems, but decrease monotonically as T increases and

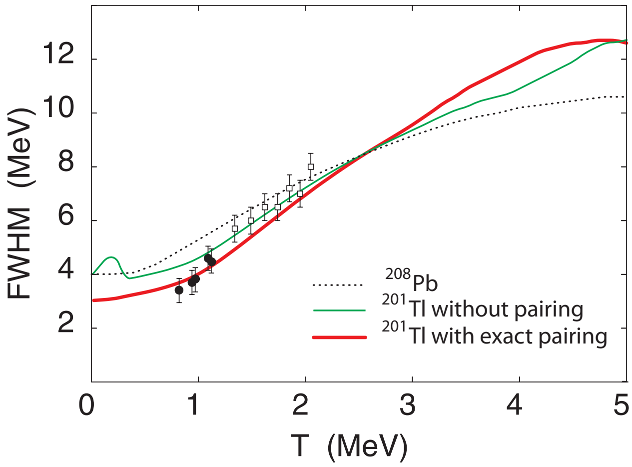

Fig. 1. GDR width as a function of T. The lines are PDM results for ^{208}Pb and ^{201}Tl without pairing and including exact CE thermal pairing gap as explained in the panel. The open and solid circles are experimental data for ^{208}Pb and ^{201}Tl, respectively.

remain finite up to T as high as 5 MeV. The theoretical predictions within the PDM are compared with the data of Ref. [2]. The good agreement between the PDM predictions including thermal pairing and the experimental data (Fig. 1) is a clear demonstration of the manifestation of the effect owing to thermal pairing, which plays a vital role in reducing the GDR width at low T in open-shell nuclei. Under the influence of thermal pairing, the GDR width in ^{201}Tl becomes as low as around 3.7 MeV at $T = 0.8$ MeV, and the width $\Gamma(0)$ of the GDR built on the ground state ($T = 0$) can be as small as 3 MeV, which is smaller than the GDR width in ^{208}Pb (4 MeV) at $T = 0$. The results obtained in the present work as well as the previous predictions for the GDR width in ^{120}Sn, where the important role of neutron thermal pairing has been shown to reduce the GDR width at $T \leq 1$ MeV[4], confirm that, in order to have an adequate description of GDR damping at low T, a microscopic model needs to take into account thermal pairing at least up to $T \sim 1.5$ MeV.

References

1) S. Mukhopadhyay *et al.*, Phys. Lett. B **709**, 9 (2012).
2) D. Pandit, S. Pal, A. De, and S.R. Banerjee, Phys. Lett. B **713**, 434 (2012).
3) N. Dinh Dang and A. Arima, Phys. Rev. C **68**, 044303 (2003).
4) P. Heckman *et al.*, Phys. Lett. B **555**, 43 (2003).

† Condensed from the article in Phys. Rev. C **86**, 044333 (2012)

Angular momentum dependence of moments of inertia due to Coriolis anti-pairing effect†

K. Tanabe and K. Sugawara-Tanabe

We have demonstrated that the angular momentum dependence (I-dependence) of the moments of inertia is essential to reproduce experimental energy levels along triaxial, strongly deformed (TSD) bands[1)].

We revisit the Coriolis anti-pairing (CAP) effect[2)] based on the mean-field theory, and we derive an explicit formula for the I-dependence of the moments of inertia. The effect of the pairing gap Δ on the moments of inertia $\mathcal{J}_x$ has been estimated by Bohr and Mottelson[3)] and by Bengtsson and Helgessen[4)], and the ratio $\mathcal{J}_x/\mathcal{J}_x^{\rm rig}$ is expressed as a function of $\xi = 2\Delta/\delta$, where $\mathcal{J}_x^{\rm rig}$ denotes the value of the rigid-body moments of inertia at $\Delta = 0$. In this estimate, the authors assume that only the large matrix elements of $(j_x)_{\alpha\beta}$ with common excitation energy of δ in $\varepsilon_\beta = \varepsilon_\alpha + \delta$ are important in the cranking formula for $\mathcal{J}_x$, where ε_α denotes the single-particle energy in the deformed field. Here, the x-axis is chosen as the rotational axis. On the other hand, the CAP effect was proposed by Mottelson and Valatin[2)], and further perturbation treatment has been carried out by Sugawara[5)] together with the blocking effect for the constrained HFB (CHFB) equation. Later, it was shown that the self-consistent CHFB calculation indicates that the phase transition from the super-state with a finite gap value ($\Delta \neq 0$) to the normal state with $\Delta = 0$ occurs gradually starting from the decrease in the gap in the unique-parity state with a large value of j (gapless superconductor)[6)]. Moreover, it has been shown that the projection of the particle number[7)] or that of the angular momentum[8)] prevents a rapid decrease in Δ and keeps its value finite even in high spin states.

We consider the case of an even-mass nucleus with axially symmetric deformation. Starting from the BCS solution, we solve the CHFB equation with second-order perturbation in the $-\Omega_x \hat{I}_x$ term, where the Lagrange multiplier (rotational frequency about x-axis) Ω_x is determined from the constraint for the total angular momentum operator $\hat{I}_x$[5)]. We estimate the Ω_x-dependent term in the gap equation by adopting an approximation similar to that used in Ref.[3)] for the case of $\Delta > 1/\rho$ with ρ denoting the level density in ε_α-space. According to the cranking formula and the method proposed previously[3)], we relate the average of the quantity $|(j_x)_{\alpha\beta}|^2$ to the rigid-body moment of inertia $\mathcal{J}_x^{\rm rig}$. Hence, in an analytic manner, we obtain the relation between Δ and the angular momentum I measured from its band-head value I_0 as

$$(I - I_0)^2 = \delta^2 \rho \mathcal{J}_x^{\rm rig} \ln \frac{\xi_0}{\xi} \times \Big[\Big(2 + \frac{17}{4}\xi^2\Big) \ln \frac{2}{\xi} - \frac{2111}{864}\xi^2 - \frac{125}{144}\Big]^{-1}, \quad (1)$$

where $\xi_0 = 2\Delta_0/\delta$ with Δ_0 obtained without rotation ($\Omega_x = 0$). Solving Eq. (1) with respect to ξ as a function of $I - I_0$, we determine the functional dependence of $\mathcal{J}_x/\mathcal{J}_x^{\rm rig}$ on $I - I_0$. We adopt $\rho = 2.5$ MeV^{-1}, $\delta = 2$ MeV, $\mathcal{J}_x^{\rm rig} = 68$ MeV^{-1}, and $\xi_0 = 1$. The result shows that $\Delta \sim 0$ and $\mathcal{J}_x \sim \mathcal{J}_x^{\rm rig}$ at around $I - I_0 \sim 17$.

Extending a similar treatment to the case of $\Delta < 1/\rho$ by employing the picket-fence approximation for level distribution, we obtain $\Delta \sim 0$ and $\mathcal{J}_x \sim \mathcal{J}_x^{\rm rig}$ at around $I - I_0 \sim 24$. We show the behavior of $\mathcal{J}_x$ (denoted J in the figure below) as a function of $I - I_0$.

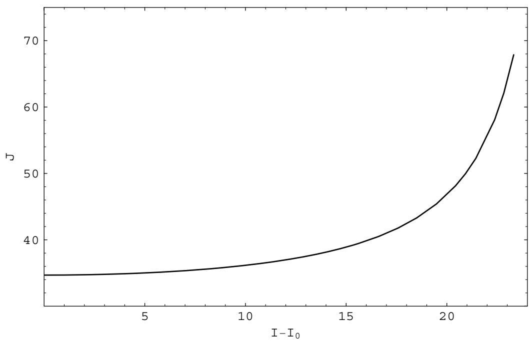

We can show that similar treatment is extensively applicable to the odd-mass nucleus, and also to the case of triaxial deformation.

References

1) K. Sugawara-Tanabe and K. Tanabe: Phys. Rev. C **82**, 051303(R)(2010).
2) B. R. Mottelson and J. G. Valatin: Phys. Rev. Lett. **5**, 511 (1960).
3) A. Bohr and B. R. Mottelson: *Nuclear Structure* (Benjamin, Reading, MA, 1975), Vol. II, p.82.
4) D. Bengtsson and J. Helgessen: Lecture notes in a summer school at Oak Ridge (1991).
5) K. Sugawara: Prog. Theor. Phys. **35**, 44 (1966).
6) B. Banerjee, H. J. Mang and P. Ring: Nucl. Phys. **A215**, 366 (1973).
7) J. L. Egido, P. Ring, S. Iwasaki and H. J. Mang: Phys. Lett. **154B**, 1 (1985).
8) Y. Sun and J. L. Egido: Phys. Rev. C **50**, 1839 (1994).

† Condensed from the article presented at the autumn meeting of Japan Physical Society, 11-14 Sep. 2012, Kyoto Sangyou University

Specific shear viscosity in hot rotating systems of paired fermions†

N. Quang Hung, N. Dinh Dang

The recent ultra relativistic Au-Au and Pb-Pb collisions at the Relativistic Heavy Ion Collider (RHIC)[1] and the Large Hadron Collider (LHC)[2] have revealed a strongly interacting matter that behaves like a nearly perfect fluid with extremely low viscosity η. This has generated a high interest in the study of viscosity in various systems of strongly interacting particles. In nuclear physics, although viscosity was theoretically calculated and experimentally extracted in 1970s, the calculations of the specific shear viscosity $\bar{\eta} = \eta/s$ (s is entropy volume density) in finite nuclei as a function of temperature T was reported very recently only in two papers[3),4)]. The results of these works, which have been carried out in two different approaches, show that $\bar{\eta}$ in hot nuclei at a temperature T as high as 5 MeV is actually very close to that obtained in the strongly interacting matter discovered at RHIC and LHC and $T > 170$ MeV. These works however considered only systems at finite temperature, whereas the effects of angular momentum or rotation were neglected. How the shear viscosity changes in a hot rotating finite system is an interesting question. The goal of present study is to study the specific shear viscosity of finite systems of paired fermions interacting via the monopole pairing force at finite temperature and angular momentum.

For this purpose, we employed two theoretical approaches, which has been proposed in Ref.[5)] and successful applied to study the pairing properties of hot rotating nuclei. The first one is the FTBCS1, which bases on the BCS theory at finite temperature and angular momentum, taking into account thermal fluctuations. The second one is the FTBCS1+SCQRPA, which is the FTBCS1 coupled to pair vibrations within the self-consistent quasiparticle random-phase approximation (SCQRPA). The numerical calculations are carried out for schematic models, which consist of Ω doubly folded equidistant levels interacting via a constant monopole pairing force G with different particle numbers $N = \Omega = 10, 20,$ and 100 as well as for several realistic nuclei such as ^{20}O, ^{44}Ca, and ^{120}Sn. The results of calculations have shown that (See e.g. Fig. 1) at a given temperature T, $\bar{\eta}$ increases with the angular momentum M; that is, a rotating system of paired fermions is more viscous. In medium and heavy systems, $\bar{\eta}$ decreases with increasing T at $T \geq 2$MeV and this feature is not affected much by angular momentum. However, in light systems, it increases with T at the values of angular momentum M close to M_{max}, which is defined as the limiting angular momentum for each system. Thermal fluctuations and coupling to the quasiparticle pair vibrations within the SCQRPA significantly increase $\bar{\eta}$ for small N systems with $N > 10$, whereas $\bar{\eta}$ decreases for large $N > 10$ systems. All the results of $\bar{\eta}$ obtained within the schematic models as well as realistic nuclei are always larger than the universal lower-bound conjecture $\hbar/(4\pi k_B)$ of the specific shear viscosity[6)] up to $T = 5$ MeV. Despite being illustrated by the results of calculations within nuclei, the present formalism can be applied to any finite system of fermions with discrete single-particle energies interacting via a monopole pairing force.

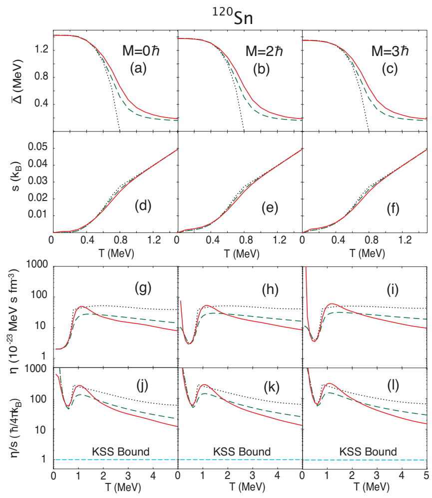

Fig. 1. Pairing gap $\bar{\Delta}$, density entropy s, shear viscosity η, and specific shear viscosity η/s obtained for ^{120}Sn isotope within the FTBCS (dotted line), FTBCS1 (dashed line), and FTBCS1 + SCQRPA (solid line) at different values of angular momentum M. The horizontal dashed lines in (j) − (l) denote the lower bound conjecture proposed in Ref.[6)].

References
1) K. Adcox et al. (PHENIX Collaboration): Nucl. Phys. A **757**, 184 (2005); B. B. Back et al.: *ibid.* **757**, 28 (2005); J. Arsene et al. (BRAHMS Collaboration): *ibid.* **757**, 1 (2005); J. Adams et al. (STAR Collaboration): *ibid.* **757**, 102 (2005).
2) K. Arnold et al. (ALICE Collaboration): Phys. Rev. Lett. **105**, 252302 (2010); G. Aad et al. (ATLAS Collaboration): *ibid.* **105**, 252303 (2010).
3) N. Auerbach and S. Shlomo: Phys. Rev. Lett. **103**, 172501 (2009).
4) N. Dinh Dang: Phys. Rev. C **84**, 034309 (2011).
5) N. Quang Hung and N. Dinh Dang: Phys. Rev. C **78**, 064315 (2008).
6) P. K. Kovtun, D. T. Son, and A. O. Starinets: Phys. Rev. Lett. **94**, 111601 (2005).

† Condensed from the article in Phys. Rev. C **86**, 024302 (2012)

Subroutine "kurotama" in PHITS

A. Kohama, K. Iida, K. Oyamatsu, H. Iwase,[*1] S. Hashimoto,[*2] and K. Niita[*3]

The total reaction cross section (σ_R) of nuclei is one of the most fundamental observables that characterize the geometrical size of nuclei. It is also important in numerical simulations in the fields of accelerator technology, particle therapy, and space radiation, as well as in many other fields that are related to particle and heavy-ion transport phenomena, because, in the codes for such simulations, one needs to estimate reaction rates systematically by using σ_R for various combinations of colliding particles over a wide energy range. The Particle and Heavy Ion Transport code System (PHITS)[1] is one of the most powerful codes designed for such simulations. There are several semi-empirical parameterizations of σ_R used in the codes. However, since they are too empirical in that they basically express σ_R in powers of $A^{1/3}$ with energy-dependent parameters determined in such a way so as to reproduce available data, the application of such parameterizations to unmeasured processes is accompanied by ambiguities. Thus, the aim of this study is to illustrate a practical formula based on systematics and motivated by a firm physics background.

In order to systematically estimate σ_R for nucleus–nucleus reactions, we apply the black-sphere (BS)-cross-section formula.[2] It was originally constructed for σ_R of proton–nucleus reactions in the framework of the BS approximation of nuclei, in which a nucleus is viewed as a "black" sphere of radius "a". In this formula, the geometrical cross section, πa^2, is expressed as a function of the mass and neutron excess of the target nucleus and of the proton incident energy, T_p, in a way free from any adjustable T_p-dependent parameter. We deduce the dependence of σ_R on T_p from a simple argument involving the nuclear "optical" depth for incident protons.[2] This formula can be easily extended to nucleus–nucleus reactions by using $\pi(a_P + a_T)^2$, where a_P (a_T) denotes the black-sphere radius of a projectile (target),[2,3] and can reproduce the empirical data remarkably well above 100 MeV/nucleon.[2,3] Note that no Coulomb effect is included.

Due to its suitability for systematics, the BS-cross-section formula ("kurotama" in Japanese) with its extension to energies of less than 100 MeV/nucleon is now officially incorporated into PHITS version 2.52. This extension is performed by smoothly connecting it with Tripathi's formula,[4] which is presently one of the most sophisticated empirical formulae, at E_{cut} = 115 MeV/nucleon. We call it "hybrid-kurotama" and the subroutine in PHITS "kurotama". It is to be noted that the absolute values of Tripathi's formula are renormalized to agree with the value of hybrid-kurotama at E_{cut}. In Fig. 1, we show the comparison of the formula values with the values of Tripathi's formula. The hybrid-kurotama values very precisely reproduce the empirical energy dependence of σ_R in such a wide energy region. In particular, they are consistent with the latest empirical data,[5] which are systematically most reliable.

The subroutine "kurotama" is to be revised by including the effect of the Coulomb dissociation relevant for reactions between heavy nuclei.[6]

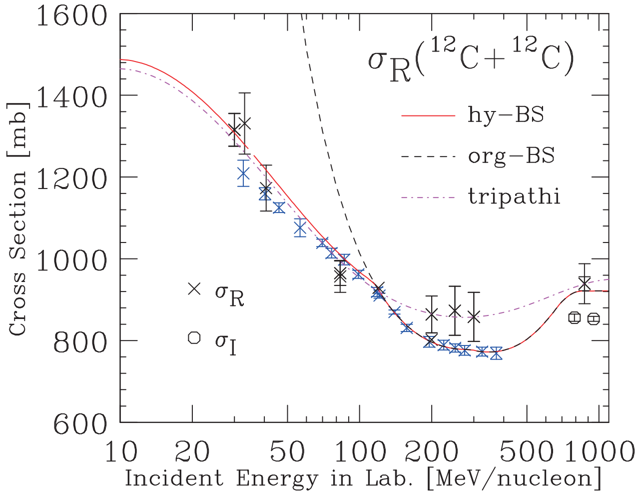

Fig. 1. Comparison of the BS-cross-section formula (hybrid: solid curve, original: dashed curve) with Tripathi's formula (dash-dotted curve)[4] for σ_R of ^{12}C + ^{12}C reactions as a function of incident kinetic energy per nucleon. We adopt the black-sphere radius, a_0, as 2.7 fm which is obtained from the measured peak angle of the first diffraction maximum of the proton elastic scatterings at 800 MeV. We also plot the measured values of σ_R and σ_I cited in Ref. 3). The crosses in blue indicate the data obtained by Takechi *et al.*[5]

*1 Radiation Science Center, KEK
*2 Nuclear Science and Engineering Directorate, JAEA
*3 Research Organization for Informa. Science & Technol.

References

1) K. Niita *et al.*: PHITS: Parti. and Heavy Ion Transport code Sys., Ver. 2.23, JAEA-Data/Code 2010-022 (2010).
2) K. Iida, A. Kohama, and K. Oyamatsu: J. Phys. Soc. Japan **76**, 044201 (2007).
3) A. Kohama, K. Iida, and K. Oyamatsu: Phys. Rev. C **78**, 061601(R) (2008).
4) R. K. Tripathi, F. A. Cucinotta, and J. W. Wilson: Nucl. Instr. Meth. B **117**, 347 (1997).
5) M. Takechi *et al.*: Phys. Rev. C **79**, 061601 (2009).
6) A. Kohama, K. Iida, K. Oyamatsu, H. Iwase, and K. Niita: RIKEN Accel. Prog. Rep. **44**, 47 (2011).

Compilation of the nuclear reaction data produced at RIBF

N. Furutachi,[*1] A. Makinaga,[*1] V. Devi,[*2] D. Ichinkhorloo,[*2] K. Katō,[*1] M. Odsuren,[*2] N. Otuka, K. Tsubakihara,[*2] and M. Aikawa,[*1]

Nuclear reaction data are essential for research and development in nuclear physics, astrophysics, nuclear engineering, and radiation therapy. These fields require a variety of nuclear reaction data in terms of, e.g., energies, cross sections, and reaction particles. The data must be compiled as a database and be accessible to nuclear data users. One such database is the EXFOR database maintained by the International Network of Nuclear Reaction Data Centres (NRDC) under the auspices of the International Atomic Energy Agency (IAEA). The Hokkaido University Nuclear Reaction Data Centre (JCPRG)[1)] is one of the nuclear data centers of the NRDC network, and has contributed about 10 percent of the data on charged-particle nuclear reactions in the EXFOR.

In addition to the collaboration of the NRDC network, the JCPRG established a collaborative research contract with the RIKEN Nishina Center in 2010, in order to advance the availability of the nuclear reaction data produced at RIBF. In this article, we report on our activities in 2012, concerning the compilation of the experimental nuclear reaction data produced at RIBF.

To make the nuclear data produced at RIBF available to users, we have registered them in the EXFOR database. We have identified the quality compilation of the RIBF data and smooth transition thereof into the database as one of the important tasks of this collaboration. We compile the data from peer-reviewed journals. From the papers published in 2011, we found 7 papers that contain RIBF data within the compilation scope of EXFOR, and all of them have already been registered in EXFOR. From the papers published in 2012, 13 papers were found, and 8 papers have been registered in EXFOR[2–9)] (Final update: Jan. 10, 2013). These data are available from the EXFOR search system[10)], and are easily accessed, using the accession numbers shown in Table 1. The list of RIBF data compiled into EXFOR is also available from our website[11)] with additional information. Apart from searching the published papers, we are also accumulating information about the forthcoming RIBF data. We participated in the 11th NP-PAC meeting, and checked the data to be compiled into EXFOR.

To improve the quality of the database, cooperation with authors has been advanced. We have asked authors to provide the original numerical data plotted in each figure to ensure the accuracy of data. We have been able to enter the original numerical data for almost all of the EXFOR entries with RIBF data. In addition, some EXFOR entries contain data or information about data corrections that are not provided in the papers (cf. E2368 and E2382). This information was provided by the authors. Furthermore, some of the EXFOR entries were proofread by the authors, and detailed descriptions of entries were corrected according to the authors' comments.

In November 2012, we held the RIBF ULIC mini-Workshop to discuss future RIKEN-JCPRG collaborative research and its related nuclear data activities. The compilation of electron scattering data, which is outside our compilation scope at present, is one of the tasks arising from the discussion. We are planning to compile the electron scattering data obtained with SCRIT[12)], and to enter them in EXFOR as a trial. Another topic is the compilation of nuclear reaction data not given in the paper. Sometimes nuclear reaction data can be entered in the database, even though they were omitted from the paper, since they were outside the purpose of that paper or unnecessary for the discussion. We are considering the compilation of such data through deeper collaboration with experimentalists.

Table 1. The numbers of compiled papers published in 2011 and 2012 and their accession numbers.

	2011		2012	
Entries	E2324	E2325	E2368[2)]	E2369[3)]
	E2327	E2346	E2370[4)]	E2371[5)]
	E2350	E2360	E2375[6)]	E2376[7)]
	E2364		E2378[8)]	E2382[9)]
Total	7		8	

References
1) JCPRG home: http://www.jcprg.org/
2) M. Takechi *et al.*: Phys. Lett. B **707** (2012) 357.
3) J. Chen *et al.*: Phys. Rev. **C 85** (2012) 015805.
4) Z. X. Cao *et al.*: Phys. Lett. B **707** (2012) 46.
5) H. Haba *et al.*: Phys. Rev. C **85** (2012) 024611.
6) N. Imai *et al.*: Phys. Rev. C **85** (2012) 034313.
7) L. H. Lv *et al.*: J. Phys. G: Nucl. Part. Phys. **39** (2012) 065102.
8) Y. Togano *et al.*: Phys. Rev. Lett. **108** (2012) 222501.
9) K. Miki *et al.*: Phys. Rev. Lett. **108** (2012) 262503.
10) EXchange FORmat (EXFOR) search system: http://www.jcprg.org/exfor/
11) RIKEN-JCPRG Nuclear data project: http://www.jcprg.org/riken/
12) M. Wakasugi *et al.*: Phys. Rev. Lett. **100** (2008) 164801.

*1 Faculty of Science, Hokkaido University
*2 Meme Media Laboratory, Hokkaido University

3. Hadron Physics

Data reconstruction and analysis framework for the PHENIX-VTX

T. Hachiya, Y. Akiba, R. Akimoto, H. Asano, S. Bathe, J. Bryslawskyj,[*1] C.-H. Chen, L. Ding,[*2] A. Enokizono, S. Esumi,[*4] S. Horiuchi, [*4] J. Koster, K. Kurita, [*3] M. Kurosawa, A. Lebedev, [*2] M. McCumber, [*5] H. Nakagomi, [*4] R. Nouicer, H. Sako, S. Sato, M. Shimomura, M. Stepanov, [*8] A. Taketani, M. Wysocki, [*9] and the PHENIX VTX group

A silicon vertex tracker (VTX)[1,2] was developed as a detector upgrade of the PHENIX experiment[3] and installed to the detector setup in December 2010. The primary purpose of the VTX is to separate the bottom and charm contributions by measuring the distance of the closest approach (DCA) of the electrons from semileptonic decays of heavy quarks (bottoms and charms). In high energy heavy ion collisions, heavy quarks are mainly produced in the early stage of the collisions and propagate through the hot and dense medium created by the collisions. Therefore, they are a clean probe for studying the property of the medium.

We successfully recorded the VTX data in $\sqrt{s_{NN}} =$ 200 GeV Au+Au and $p+p$ collisions in year 2011 and 2012 and analyzed them. The analysis procedure is subdivided into the six following tasks:

(1) Particle tracks were reconstructed using the VTX data together with the central arm spectrometer (CA)[4]. In the reconstruction, hit positions on the VTX were connected to tracks measured in the CA to identify electrons and to measure the DCA of these electrons. The three dimensional position of the primary vertex is also determined using the VTX.

(2) The calibration parameters such as the hot and dead channels and the aligned positions of the detector elements[5] are determined.

(3) The stability of the detectors was studied to maintain the quality of the data by checking the average hit rate of the VTX, the energy to momentum ratio measured in CA, etc., for each short period.

(4) Photon conversion, which is the largest background source of the single electron measurement, was rejected by requiring no nearby-hits in the VTX. Since the photon conversion produces e^+e^- pair with a small opening angle, the electron from the conversion often has an additional nearby hit made by its conversion partner.

(5) The detector acceptance and the efficiency were evaluated using the GEANT based detector simulation.

(6) The charm and bottom signals were extracted by comparing the DCA distribution of electrons between the data and simulation[6].

These tasks are described in more detail in the references.

We organized the analysis team composed of about 10 people to share these tasks. In order to maintain consistency of the analysis among the team, we developed a single integrated analysis code. To do this, we assigned a librarian who coordinate the code development and update the analysis code. This method was very successful for sharing the analysis tasks among the team and for quickening the analysis. In addition, the RIKEN CCJ[7] computing farm, which has a framework for high-speed scan of the data, enabled us to scan three billion events of Au+Au collision within a few days. Thus, we were able to optimize the analysis cuts and develop the analysis method by scanning the data several times and by making a feedback within a short period of time.

We obtained the first preliminary results of the separated charm and bottom production[6] and the charm flow[8] using the VTX detector. These results were presented in Quark Matter 2012 international conference. The further analysis is in progress to finalize these results for publication.

References

1) R. Nouicer et al.: Proc. of Sci. (Vertex 2007) 042 (2007).
2) T. Hachiya et al.: RIKEN Accel. Prog. Rep. **44**, 179 (2011).
3) K. Adcox et al.: Nucl. Instrum. Meth. A **499**, 469 (2003)
4) T. Hachiya et al.: RIKEN Accel. Prog. Rep. **45**, 156 (2012).
5) H. Asano et al.: RIKEN Accel. Prog. Rep. **45**, 159 (2012).
6) R. Akimoto et al.: RIKEN Accel. Prog. Rep. **46**, in this report (2013).
7) http://ccjsun.riken.jp/ccj/
8) M. Kurosawa et al.: RIKEN Accel. Prog. Rep. **46**, in this report (2013).

*1 City University of New York, USA
*2 Iowa State University, USA
*3 Department of Physics, Rikkyo University, Japan
*4 University of Tsukuba, Japan
*5 University of Colorado, USA
*6 Brookhaven National Laboratory, USA
*7 Japan Atomic Energy Agency, Japan
*8 University of Massachusetts, USA
*9 Oak Ridge National Laboratory, USA

Measurement of Invariant Yield for Heavy Flavor electron with Silicon Vertex Detector at RHIC-PHENIX

H. Asano, Y. Akiba, R. Akimoto, S. Baumgart, S. Bathe, J. Bryslawskyj,[*1] C-H. Chen, L. Ding,[*2] S. Esumi,[*3] T. Hachiya, S. Horiuchi,[*3] J. Koster, K. Kurita,[*4] M. Kurosawa, A. Lebedev,[*2] M. McCumber,[*6] H. Nakagomi,[*3] R. Nouicer, C. Ogilvie,[*2] H. Sako, S. Sato, M. Shimomura, M. Stepanov,[*5] A. Taketani, M. Wysocki,[*7] and the PHENIX VTX group

Heavy quark production has been studied by the PHENIX experiment at RHIC via measurements of single electrons from semi-leptonic decays at midrapidity ($|\eta| < 0.35$). The PHENIX experiment has been upgraded by installing a Silicon Vertex Tracker (VTX), and it obtained the first physics data of Au+Au collision in RUN 11 (RHIC experiment performed in 2011). The VTX has been developed for heavy flavor (charm and bottom) measurements and dedicated to the precise tracking of primary and secondary vertices.

The VTX has two advantages for heavy flavor electrons measurements. First, by selecting electrons with a distance of closest approach (DCA) to the primary vertex larger than several hundred microns, the photonic electron background is suppressed by orders of magnitude. Secondly, as the lifetime of mesons containing bottom quark is significantly longer than those containing charm quark, the detailed DCA distribution from the VTX allows separation of charm from bottom production statistically.[1)]

To obtain the heavy flavor electron spectrum with VTX, we need to calculate acceptance, track reconstruction efficiency, and the fraction of the background (mainly they are photon conversion electrons generated from the material).

The acceptance and track reconstruction efficiency, including the tracking efficiency in VTX, is calculated by a simulation. We used the same track selection cuts in the simulation as in the real data, and we applied hot and dead channel map that was made from real data. In the analysis, we applied a DCA $< 700\ \mu$m for inclusive electrons. This tight DCA cut effectively requires that the primary vertex was reconstructed by VTX. We corrected for the efficiency that the primary vertex is reconstructed. This efficiency is 90.1% per track for hadron and 90.7% for electrons in Minimum Bias event.

To obtain the heavy flavor electron spectrum from the inclusive electron spectrum, we need to estimate the fraction of conversion electrons. This fraction can be calculated by π^0 simulation.

After correcting for the acceptance, efficiency, and fraction of background, we have obtained the invariant yield spectra of heavy flavor electrons for Au+Au. The result is shown in Fig.1, and we compared the present spectra with published result for Minimum bias Au+Au. Since the published result has different p_T binning, we define a function to fit the published result, and then compared the ratio of that data to the fit curve. The measured spectrum is about 10 to 20% lower than the published one. This is because VTX has approximately 12% radiation length, and the electron track loses its energy by about 12% on average. Since the electron p_T spectrum decreases very rapidly with increasing p_T, an effective loss of electron yield is caused.

In conclusion, we obtained the first result of heavy flavor electron spectra. We are now trying to decompose charm and bottom yield from this result.

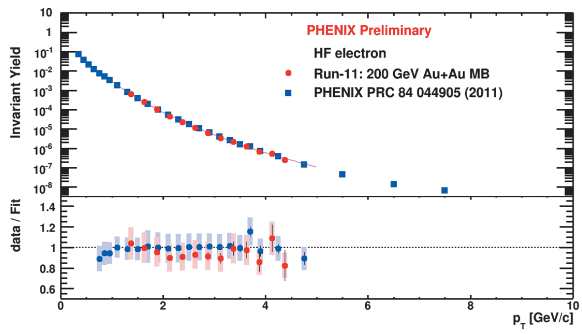

Fig. 1. Invariant yield of Heavy Flavor electon measured in Min-Bias (0-93%) Au+Au compared to PHENIX published results[2)] .

References

1) M.Baker et al.: Proposal for a Silicon Vertex Tracker (VTX) for the PHENIX Experiment, 2004 BNL-72204-2004, Physics Dept. BNL.
2) A.Adare et al.: (PHENIX Collaboration) Phys.Rev.C 84, 044905 (2011).

*1 City University of New York, USA
*2 Iowa State University, USA
*3 University of Tsukuba, Japan
*4 Department of physics, Rikkyo University, Japan
*5 University of Massachusetts, USA
*6 University of Colorado, USA
*7 Oak Ridge National Laboratory, USA

Measuring the Spectra of Inclusive Charged Hadrons in Au+Au Collisions at $\sqrt{s_{NN}} = 200$ GeV with Silicon Vertex Tracker at PHENIX

C.-H. Chen, Y. Akiba, R. Akimoto, H. Asano, S. Bathe, S. Baumgart, K. Boyle, J. Bryslawskyj, L. Ding, A. Enokizono, S. Esumi, T. Hachiya, S. Horiuchi, K. Kurita, M. Kurosawa, A. Lebedev, M. McCumber, H. Nakagomi, R. Nouicer, C. Ogilvie, H. Sako, S. Sato, A. Shaver, M. Shimomura, M. Stepanov, A. Taketani, M. Wysocki, and PHENIX VTX group.

When gold nuclei collide at $\sqrt{s_{NN}} = 200$ GeV at the Relativistic Heavy Ion Collider (RHIC) in Brookhaven National Laboratory, the energy density is high enough to deconfine the quarks within the nucleon and to create quark-gluon plasma (QGP). One way to study the properties of QGP is to understand the interaction between quarks and the medium. The most direct way to study the quark-QGP interaction is to study jets in QGP. However, direct jet reconstruction is difficult in the PHENIX experiment, since the current acceptance of PHENIX is not large enough. Instead, we can study particles with high transverse momentum (p_T) coming out from QGP, since most of high p_T particles come from jet fragments.

PHENIX measured the spectra of inclusive charged hadrons. The result indicates that in most central collisions, the nuclear modification factor R_{AA} is 0.2 at p_T larger than 5 GeV/c [1]. This means the production of high p_T particles in QGP is suppressed by a factor of 5 compared to the case where there is no medium, known as the 'jet quenching' effect. PHENIX also measured π^0 spectra up to $p_T = 20$ GeV/c [2], where R_{AA} is flat between 5 to 20 GeV/c, with a slight hint of increase in R_{AA} at the highest p_T. In order to understand the quark energy loss mechanism, it is important to extend the single particle spectra measurement to the highest possible p_T.

PHENIX installed and commissioned Silicon Vertex Tracker (VTX) in the 2011 run. VTX consists of two pixel layers and two stripixel layers, which provide excellent resolution on the position of the vertex. It can also provide precise measurement of track position. By measuring the DCA (distance of the closest approach) of the track and the vertex, the information can be used to separate the electrons coming from semi-leptonic decay of heavy flavor mesons from conversion electrons. This DCA distribution can also be used to separate charged hadrons from electrons, and to remove high p_T fake tracks, which mainly arise from conversion electrons and decay-in-flight particles.

Figure 1 shows the preliminary result of the inclusive charged hadron spectrum in minimum-bias Au+Au collisions measured with the VTX. The result is compared with the previously published PHENIX spectrum [1]. The two measurements agree very well up to $p_T = 8$ GeV/c, which is the highest p_T bin of the previous measurement. In order to compare these two spectra, a function is used to fit the new spectrum, and both spectra are compared with the fitted curve. The result is shown in the bottom panel of Fig. 1, which again shows a good agreement between the two results. The new measurement extends the p_T range to 10 GeV/c, and with a larger data set, the measurement may be significantly extended to higher p_T.

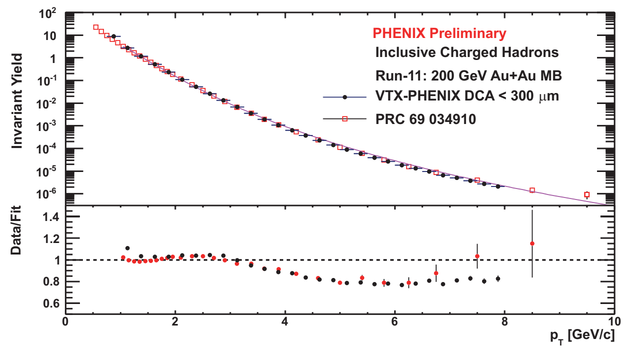

Fig. 1. Upper panel shows the spectrum of the inclusive charged hadron in minimum-bias Au+Au collisions (black points). The spectrum is compared with previous measurements (red points)[1]. The new measured spectrum is fitted with a function. The ratios between both spectra with the fitting function are plotted in the bottom panel.

References

1) S. S. Adler *et al.*: Phys. Rev. C **69**, 034910 (2004).
2) A. Adare *et al.*: Phys. Rev. Lett. **101**, 232301 (2008).

Heavy-quark measurement using distance of closest approach analysis

R. Akimoto, Y. Akiba, H. Asano, S. Bathe, S. Baumgart, K. Boyle, J. Bryslawskyj,[*1] C.-H. Chen, L. Ding,[*2] A. Enokizono, S. Esumi,[*3] T. Hachiya, S. Horiuchi,[*3] J. Koster, K. Kurita,[*4] M. Kurosawa, A. Lebedev,[*2] M. McCumber,[*5] H. Nakagomi,[*3] R. Nouicer, C. Ogilvie,[*2] H. Sako, S. Sato, A. Shaver,[*2] M. Shimomura, M. Stepanov,[*6] A. Taketani, M. Wysocki,[*7] and the PHENIX VTX group

Heavy quarks (charm and bottom) can be used as suitable probes to study the interaction between partons and the quark-gluon plasma (QGP). Heavy quarks are created mainly by initial hard scatterings, and thus, the changing of the four momenta when they pass through the QGP can be clearly evaluated from the final states. It is necessary to evaluate the changings to a variety of probes in order to determine QGP properties since they depend on several factors such as the equation of state or the initial condition.

The measurements of modifications for charm and bottom quarks separately are informative. The quark mass dependence of the modification can be evaluated from the measurements. They can be achieved by the analysis of the distances between the tracks and the beam collision vertex. The distance of the closest approach (DCA) to the collision vertex is evaluated for each track in the analysis. The DCA distributions of bottomed hadrons are wider than those of charmed hadrons since the lifetimes of bottomed hadrons are considerably longer than those of charmed hadrons. Therefore, the yields of charmed and bottomed hadrons can be evaluated from the difference in their DCA distributions.

Electrons and positrons from heavy quark decay were measured. The yields of charm and bottom quarks were evaluated by fitting the distribution of the DCA in the XY-plane[a] (XY-DCA) with the DCA templates of all sources. Electrons and positrons are mainly grouped into two types: non-photonic and photonic electrons. Non-photonic electrons are electrons and positrons from weak decay and they include heavy-quark electrons[b] and decay of kaons. Photonic electrons are electrons and positrons from photon conversion and Dalitz decays of neutral mesons. In addition, the signals with which hits created by other tracks are associated are required to be evaluated.

The templates of non-photonic electrons were made by single-track simulation without detector simulation. They were convoluted with a Gaussian whose RMS is equal to the DCA resolution. The templates of photonic electrons were made by single track simulation with detector simulation. The template of tracks with wrongly associated hits was evaluated by the XY-DCA distribution for the tracks with large absolute values of DCA along the Z-direction.

An isolation cut was applied to reject photonic electrons. A track was rejected by the cut if hits were found around the hits associated to it.

Figure 1 shows bottom fractions in heavy-quark electrons as a function of transverse momentum (p_T) of electrons for the measured data of $p + p$ collisions with $\sqrt{s} = 200$ GeV. The circles indicate the preliminary result from the DCA analysis. The triangles and stars indicate the results evaluated by the PHENIX and the STAR experiments, respectively, from the correlation between electrons and hadrons from heavy-quark decay.[1,2] The solid line indicates the result of FONLL calculation at rapidity $y = 0$, and the dashed lines indicate the boundaries of the error band for the calculation.[3] The bars and squares denote statistical and systematic errors, respectively. The result from the DCA analysis is consistent with the published results.

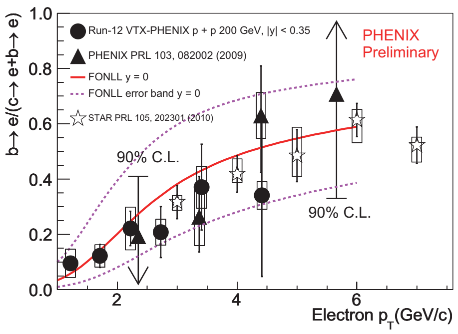

Fig. 1. Bottom fractions in heavy-quark electrons.

The bottom fraction in heavy-quark electrons was evaluated successfully from the DCA analysis for $p + p$ collision data and the result is consistent with the published results. The evaluation of Au + Au collision data is in progress.

*1 Baruch College, CUNY, USA
*2 Iowa State University, USA
*3 University of Tsukuba, Japan
*4 Department of Physics, Rikkyo University, Japan
*5 University of Colorado, USA
*6 University of Massachusetts, USA
*7 Oak Ridge National Laboratory, USA

a) The XY-plane is defined as the plane perpendicular to the beam axis and the Z-direction is defined as the direction along the beam axis.

b) Electrons and positrons from heavy-quark decay are called heavy-quark electrons.

References

1) A. Adare *et al.*: Phys. Rev. Lett. **103**, 082002 (2009).
2) M. M. Aggarwal *et al.*: Phys. Rev. Lett. **105**, 202301 (2010).
3) M. Cacciari *et al.*: Phys. Rev. Lett. **95**, 122001 (2005).

Flow measurement of heavy flavor electrons with PHENIX VTX

M. Kurosawa, Y. Akiba, H. Asano, R. Akimoto, S. Bathe, J. Bryslawskyj,[*1] C. Chen, L. Ding,[*2] S. Esumi,[*4] T. Hachiya, S. Horiuchi,[*4] A. Lebedev,[*2] J. Koster, M. Mccumber,[*3] H. Nakagomi,[*4] R. Nouicer, M. Shimomura, A. Taketani, M. Wysocki,[*3] and the PHENIX VTX group

The silicon vertex tracker (VTX) was installed into the PHENIX experiment in 2010, and it successfully collected approximately 5 billion events of Au+Au collisions at $\sqrt{s_{NN}} = 200$ GeV in the 2011 RHIC run. The main function of the VTX is the separation of heavy flavor (HF) hadrons, charm and bottom, with a measurement of Distance of Closest Approach (DCA) of single electrons from their decays.

Collective flow is one of the key measurements to study the hot and dense matter created in heavy ion collisions, because it is related to the early evolution of the matter. In particular, higher harmonic flow measurements play an important role in constraining theoretical model calculations describing the properties of the matter. In addition to the information from flow measurements of light flavors, heavy flavor measurements give us new information on the mass dependence of collective flow. Heavy flavors are produced in the initial parton interactions due to those large mass in heavy ion collisions at RHIC energies. This makes them a clean probe to study hot and dense matter since they experience the created matter.

The inclusive electron components include the photonic backgrounds from Dalitz decays and photon conversions, non-photonic background from hadronic decays, and non-photonic electrons from heavy flavor decays. The majority of background is Dalitz decay electrons and conversion electrons that are generated in VTX materials. Since the origins of conversions are not the primary vertex, they preferentially produce tracks with large DCA. Furthermore, the opening angle of Dalitz decay and conversions is very small for high momentum tracks. Thus, the majority of conversions can be removed by selecting tracks with $|DCA| < 200\ \mu$m and by requiring that there is no close-by hit associated with the track. By applying these cuts, 70% of the background can be removed.

After the removal of the background, the azimuthal anisotropy (v_2) of inclusive electrons was measured. It can be expressed as

$$v_2^{incl-e} = R^c \cdot v_2^c + R^b \cdot v_2^b + R^\gamma \cdot v_2^\gamma + R^h \cdot v_2^h \qquad (1)$$

where v_2^{incl-e}, v_2^c, v_2^b, v_2^γ, and v_2^h are v_2 of inclusive electrons, charm decay electrons, bottom decay electrons, photon conversions, and hadron backgrounds, respectively. R^c, R^b, R^γ, and R^h are the ratio of charm decay electrons, bottom decay electrons, photon conversions and hadron backgrounds, respectively. The ratio of each component was dependent on p_T and was derived from DCA fitting for each p_T region. The yields and shapes of the DCA distributions of non-HF components were derived from Monte Carlo simulations. The bottom fraction R^b was obtained from the fitting of the DCA distribution[1)].

The low production rates of bottom quarks make the extraction of bottom decay electron v_2 challenging with the current dataset, so our first result focuses instead on the extraction of the charm decay electron v_2. In order to study how much v_2^c is affected by v_2^b, we used three different v_2^b values (−0.2, 0, 0.2), and included it in the systematic uncertainty. The previous measurements[2)] were used for the v_2^γ and v_2^h from our data. Figure 1 shows the p_T dependence of the charm decay electron v_2 for 10−60% centrality. The obtained charm decay electron v_2 was consistent with previous results on heavy flavor v_2[2)]. This is not surprising since the fraction of bottom at low p_T is expected to be small.

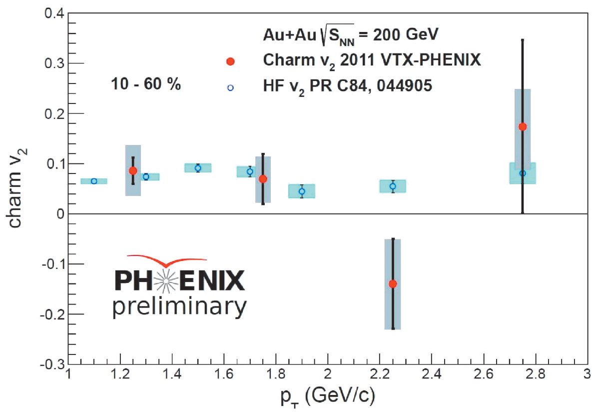

Fig. 1. p_T dependence of charm decay electron v_2 for 10−60% centrality. Open circled points indicate the previous data of heavy flavor v_2[2)].

In future, statical uncertainty can be improved by using remaining data and fine tuning the analysis. Bottom v_2 will be obtained by using more statistics.

References
1) R. Akimoto et al.: In this report (2013).
2) A. Adare et al.: Phys. Rev. C 84, 044905, (2011).

*1 Department of Physics, City Univ. of New York, USA
*2 Department of Physics and Astronomy, Iowa State Univ., USA
*3 Department of Physics, Univ. of Colorado, USA
*4 Department of Physics, Tsukuba Univ., Japan

High p_T hadron production in Au+Au collisions at $\sqrt{s_{NN}} = 200$ GeV

Y. Akiba, R. Akimoto, H. Asano, S. Bathe, S. Baumgart, K. Boyle, J. Bryslawskyj[*1] C-H. Chen, L. Ding,[*2] A. Enokizono,[*3] S. Esumi,[*4] T. Hachiya, S. Horiuchi,[*4] J. Koster, K. Kurita,[*3] M. Kurosawa, A. Lebedev,[*2] M. McCumber,[*5] H. Nakagomi,[*3] R. Nouicer, C. Ogilvie,[*2] H. Sako, S. Sato,[*6] A. Shaver,[*2] M. Shimomura, M. Stepanov,[*7] A. Taketani, M. Wysocki,[*8] and the PHENIX VTX group

One of the most significant discoveries at RHIC has been the suppression of high p_T hadrons in central Au+Au collisions[1)]. In pQCD models, the data constrains the transport coefficient, $\hat{q}$[2)].

However, pQCD models underestimate the path length dependence of energy loss[3)] and, when constrained by RHIC data, over-predict the energy loss at the LHC[4)]. This suggests that the mechanism of energy loss is not fully understood. More precise measurements are desirable.

Currently the best measurement at RHIC comes from neutral pions[5)]. For charged hadrons, the measurement is limited by a background from photon conversions and random tracks, both mimicking high transverse momentum tracks.

With the recent addition of a Silicon Vertexing Tracker (VTX)[6)] to PHENIX, it is possible to significantly reject this background and to extend the hadron measurement to higher p_T. One requires tracks to reconstruct with a small DCA (Distance of Closest Approach) of the track projection to the primary vertex. Real tracks reconstruct with zero DCA convoluted with the detector resolution, whereas fake tracks can have any DCA.

Figure 1 shows the raw DCA distribution in the transverse plane. One can see a peak around zero DCA, which is dominated by real tracks, on top of a background from random tracks and weak decays.

Figure 2 shows the transverse momentum distribution of tracks with and without the small-DCA requirement. At high p_T, the spectrum without the DCA requirement looks unphysically flat, whereas the spectrum with the requirement continues to fall. The observed behavior suggests that the DCA requirement successfully suppresses the background.

These plots indicate the potential of this method. The analysis is still in progress.

[*1] Baruch College, CUNY, USA
[*2] Iowa State University, USA
[*3] Rikkyo University, Japan
[*4] University of Tsukuba, Japan
[*5] University of Colorado, USA
[*6] Japan Atomic Energy Agency, Japan
[*7] University of Massachusetts, USA
[*8] Oak Ridge National Laboratory, USA

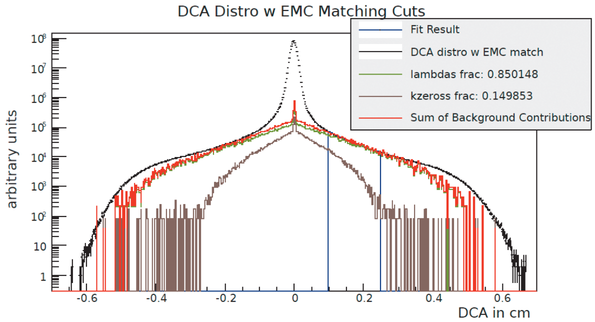

Fig. 1. Raw DCA distribution in the transverse plane. The peak around zero DCA is dominated by real tracks. The underlying background comes from random tracks and weak decays. The fall-off at ± 0.4 cm is an artifact of the tracking algorithm.

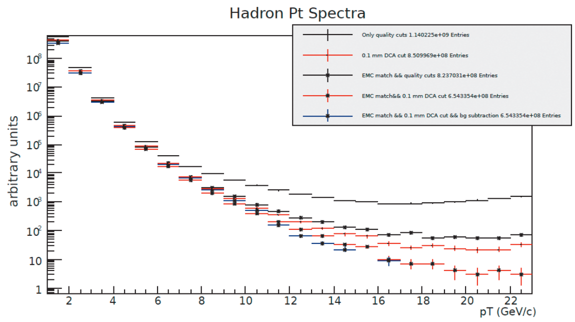

Fig. 2. Uncorrected hadron p_T spectra for different purity cuts. At high p_T, the spectrum without the DCA requirement looks unphysically flat while the spectrum with the DCA requirement continues to fall.

References

1) K. Adcox *et al.* [PHENIX Collaboration]; Phys. Rev. Lett. **88**, 022301 (2002) [nucl-ex/0109003].
2) A. Adare *et al.* [PHENIX Collaboration]; Phys. Rev. C **77**, 064907 (2008) [arXiv:0801.1665 [nucl-ex]].
3) A. Adare *et al.* [PHENIX Collaboration]; Phys. Rev. Lett. **105**, 142301 (2010) [arXiv:1006.3740 [nucl-ex]].
4) W. A. Horowitz and M. Gyulassy, Nucl. Phys. A **872**, 265 (2011) [arXiv:1104.4958 [hep-ph]].
5) A. Adare *et al.* [PHENIX Collaboration]; arXiv:1208.2254 [nucl-ex].
6) A. Taketani *et al.* [PHENIX Collaboration]; Nucl. Instrum. Meth. A **623**, 374 (2010).

PHENIX 2012 W Measurement and Fast Production Data Analysis

S. Park, N. Amano, Y. Fukao, T. Iguri, Y. Imazu, M. Kim, T. Mibe, H. Murakami, T. Murakami, J. Murata, I. Nakagawa, K.R. Nakamura, H. Oide, J. Seele, R. Seidl, N. Saito, K. Tanida, I. Yoon, K. Watanabe, and S. Yamashita

Measuring the parity violating single spin asymmetry of W boson production in longitudinally polarized proton collisions is one of the primary goals of the RHIC-PHENIX experiment[1]. PHENIX observes W bosons through their decays into a charged lepton and neutrino (not detected) at the central and forward/backward rapidity region. The production is described in the hard parton collision regime, and thus, its asymmetry measurement is sensitive to the helicity distributions of quarks and sea quarks.

PHENIX forward muon systems have been upgraded to achieve adequate trigger rejection power and improve backgrounds identification. New front-end electronics (MuTRG-FEE)[2] for fast online tracking of high momentum muons and Resistive Plate Chamber (RPC3) were installed in 2011. The combination of MuTRG-FEE, Muon Identifier (MuID) and Beam Beam Counter (BBC), so called SG1×MuID×BBC trigger[3], was operated as a physics trigger in 2011. However, the outcome of the analysis of 2011 data indicated that the MuID trigger efficiency drops rather significantly as the luminosity increases. This year, RPC3 was implemented instead of MuID as a new physics trigger (SG1×RPC3×BBC). In addition to the new trigger upgrade, Forward Vertex Detector (FVTX) is installed and operated to improve background identification using additional tracking information. In succession to the first measurement performed in 2011, PHENIX achieved integrated luminosity of 50 pb^{-1} with 52% polarization for a proton beam at a center of mass energy of $\sqrt{s} = 510$ GeV in 2012. The significant amount of statistics will come in 2013 to achieve the integrated luminosity goal 300 of pb^{-1}.

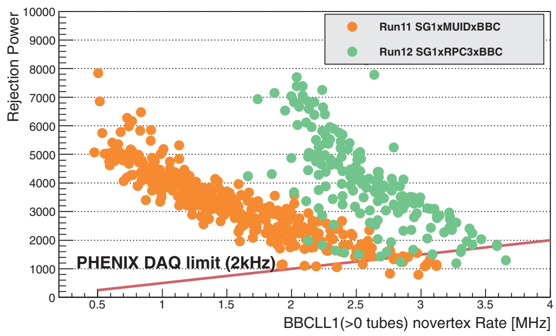

Fig. 1. Rejection power of SG1×MuID×BBC and SG1×RPC3×BBC trigger.

The new trigger provided higher rejection power in 2012 comparing with 2011. Figure 1 shows rejection power of SG1×MUID×BBC trigger and SG1×RPC3×BBC trigger with respect to BBC trigger rate. The conventional SG1×MUID×BBC trigger mix was kept in Run12 as well to check the consistency with new RPC trigger mix samples.

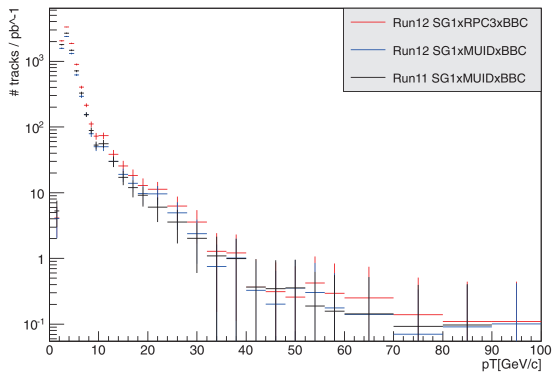

Fig. 2. The transverse momentum distribution of muon candidates. Each color indicates different data and triggers.

Figure 2 shows that the transverse momentum distribution of muon-like samples in 2011 and 2012. As shown in the figure, the momentum spectra of each trigger agree with each other. Trigger efficiency was not taken into account in Fig. 2. We expect higer trigger efficiency and background rejection in the new physics trigger. Further studies on the trigger efficiencies and estimation of signal to noise ratio are now underway.

References

1) R. Seidl et al.: RIKEN Accel. Prog. Rep. **45**, 58 (2012).
2) S. Adachi, et. al., Nucl. Inst. and Meth., **A703**, 114-132 (2013).
3) Y. Fukao et al.: RIKEN Accel. Prog. Rep. **44**, 188 (2011).

Measurements of the mid-rapidity parity violating spin asymmetries for $W^{\pm}$ bosons at PHENIX[†]

C. Gal, K. Okada, and M. Stepanov,[*1]

A great deal has been learned about the proton spin composition since the initial measurement of the contribution of the quarks to the spin of the proton. One particular area of further interest is the contribution coming from the anti-quarks ($\Delta\bar{u}$and $\Delta\bar{d}$). These polarized parton helicity distributions functions (PDFs) have been constrained so far only through semi-inclusive DIS (SIDIS) measurements (see the HERMES measurements[1)]). One weakness of this measurement method is the lack of prior knowledge about the fragmentation functions (FFs), making the end result a convolution of anti-quark PDFs and FFs. Using the parity violating $W^{\pm}$ boson coupling to quarks and anti-quarks, in polarized p+p collisions, we can circumvent this problem altogether[2)], giving us a cross-check of the SIDIS measurements.

Following a succesful feasibility run in 2009, PHENIX has continued the W program by performing measurements both at mid-rapidity and at forward/backward rapidities. We focus here on the midapidity measurement using the $W^{\pm} \to e^{\pm} + X$ decay channel. For this measurement the W^{+} (W) single spin asymmetry is a combination of the $\Delta\bar{d}$ and Δu ($\Delta\bar{u}$ and Δd) PDFs.

The PHENIX central arm detector has been described elsewhere[4)]. It consists of two spectrometers with tracking and electromagnetic calorimetry (EMCal) and covers a total area between -0.35 and 0.35 in η and $\Delta\phi = 2\pi/2$in azimuth. Due to the limited ϕ coverage we cannot calculate a p_T imbalance or detect both electron and positron from Z boson decays. Thus we employ a similar method to the one used by the UA1/2 experiments in the initial discovery of the W boson. We measure a transverse momentum (p_T) spectrum and identify W decays through the typical Jacobian peak at approximately 40 GeV/c. EMCal clusters were matched to tracks within 0.01 rad in ϕ. The bending of the tracks gave us the charge sign of the particle, while the positions in the EMCal and tracking system were used to reconstruct the primary interaction vertex. Only events that have a vertex with $|z| <$ 30 cm were used, making sure the resulting particles are within central arm acceptance. In order to decrease the level of the background, we use a relative isolation cut with a cone of $R = \sqrt{\Delta\eta^2 + \Delta\phi^2} = 0.4$. We accept only events in which the energy in the cone, excluding the candidate electron/positron divided by the candidate electron/positron energy is smaller than 10%. The isolation cut decreases the level of the background by a factor of ≈10 for both charges. The remaining background after all of our cuts was parametrized in order for us to be able to properly extract the asymmetries. We do this by fitting our spectrum with a power law plus a Jacobian peak obtained from PYTHIA simulation with a full GEANT reconstruction. The resulting fit together with the uncertainty band can be seen in figure 1.

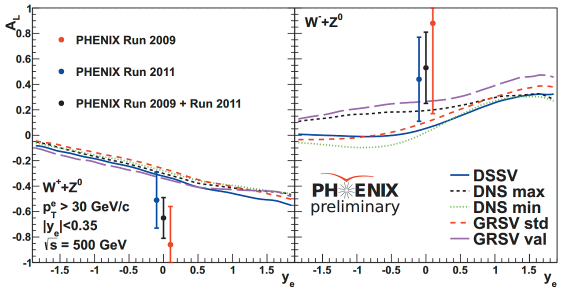

Fig. 1. Single spin asymmetry results for both W^{+} (left) and W (right).

Using the spin differentiated yields in the signal region (30 to 50 GeV/c) we have calculated the single spin asymmetries. The result for 2011, 2009 and the combination can be seen in figure 1. The deviation of the W^{+} asymmetry result from the theoretical cuves while still not statistically significant, would bring new constraints on the leading theories in the field if it remains with improved statistics.

In 2011 we have continued our midrapidity W program with more data than in 2009 and with better proton beam polarization. We developed new analysis tools to deal with a new detector configuration as well as to optimize our cuts. With the data already collected in 2011 and 2012 ($\approx 46pb^1$), and with an expected large dataset in 2013 ($\approx 160pb^1$) we will be able to have significant constraints on the polarized anti-quark PDFs.

References
1) Airapetian A. et al.: Phys. Rev. D **71**, 012003 (2005)
2) G. Bunce, N. Saito, J. Soffer, and W. Vogelsang: Ann. Rev. Nucl. Part. Sci. **50**, 525 (2000)
3) A. Adare et al.: Phys. Rev. Lett. **106**, 062001 (2011)
4) K. Adcox et al.: Nucl. Instrum. Meth. **A499**, 469 (2003)

† Condensed from the proceedings with the same title for SPIN2012 conference in Dubna

*1 Dept. of Physics, University of Massachusetts Amherst

Longitudinal double spin asymmetry of electrons from heavy flavor decays in polarized $p + p$ collisions at $\sqrt{s} = 200$ GeV†

K.R. Nakamura

For understanding of the proton spin structure, the PHENIX experiment at Brookhaven National Laboratory performs polarized $p+p$ collisions to study the gluon polarization in the proton. Determination of the gluon polarization distribution in the small Bjorken x region, $x \sim 10^{-2}$, is essential to reduce the current uncertainty on the total gluon polarization. To access the gluon polarization in such small Bjorken x, we performed the world's first measurement of double spin asymmetry of electrons from decays of hadrons containing heavy flavor quarks (heavy flavor electrons).

Figure 1 shows the measured double spin asymmetry. A constraint of the gluon polarization can be obtained from the measured spin asymmetry through a comparison with spin asymmetries calculated under various gluon polarization assumptions. The partonic interaction of the heavy flavor electron production has the following features: (1) gluon-gluon scattering is the dominant process in the heavy flavor production, and (2) the heavy flavor electrons are primarily produced by charm quarks. Therefore, we considered only charm quark production from gluon-gluon scattering, $gg \to c\bar{c} + X$, for the partonic interaction. Expected spin asymmetries were obtained from unpolarized and polarized cross sections of the gluon-gluon interaction calculated with leading-order perturbative QCD, and PYTHIA simulations for the hadronization of the charm quarks and the decay into electrons.

From the simulations, the Bjorken x distribution of gluons contributing to the heavy flavor electron production was obtained. By using the mean and RMS values of the distribution, the sensitive Bjorken x region of the measured double spin asymmetry of the heavy flavor electrons were determined to be $\langle \log_{10} x \rangle = -1.6^{+0.5}_{-0.4}$ ($10^{-2} \lesssim x \lesssim 8 \times 10^{-2}$).

From the comparison between the measured and expected asymmetries, a χ^2 curve as a function of $|\Delta g/g|^2$ was obtained, as shown in Fig. 2. The minimum value of χ^2, $\chi^2_{\rm min}$, located at $|\Delta g/g|^2 = 0$, which is the boundary of $|\Delta g/g|^2$. $\Delta\chi^2 \equiv \chi^2 - \chi^2_{\rm min} = 1$ and 9 were utilized to determine 1σ and 3σ uncertainties on the constraint of $|\Delta g/g|^2$. With these criteria, the upper limits were found to be $|\Delta g/g|^2 < 3.0 \times 10^{-2} (1\sigma)$ and $|\Delta g/g|^2 < 10.0 \times 10^{-2} (3\sigma)$ at Bjorken x of $\langle \log_{10} x \rangle = -1.6^{+0.5}_{-0.4}$ and a scale of $\mu = 1.4$ GeV. The constraints are consistent with the theoretical expectations of $|\Delta g/g|^2$ from gluon polarization distributions of DSSV[2] and GRSV[3] groups. The 1σ constraint on the integral of the gluon polarization was obtained to be $|\int_{0.01}^{0.08} dx \Delta g(x,\mu)| < 0.85$. From this result, large gluon polarization at the low Bjorken x region, e.g. $\Delta G[0.01, 0.08] \gtrsim 1$, is excluded.

† Condensed from an article[1] published in Phys. Rev. D.

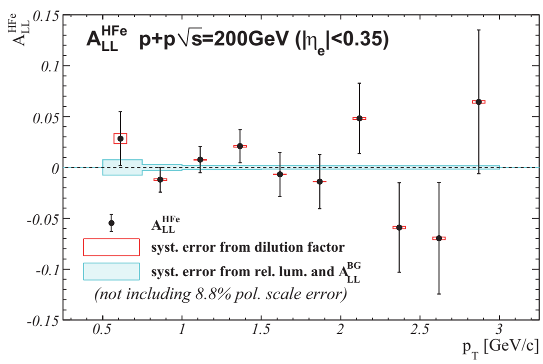

Fig. 1. Double spin asymmetry of the heavy flavor electron production. The red error bars represent scaling systematic uncertainties from dilution factor, and the blue error bands represent offset systematic uncertainties from relative luminosity and the background spin asymmetry.

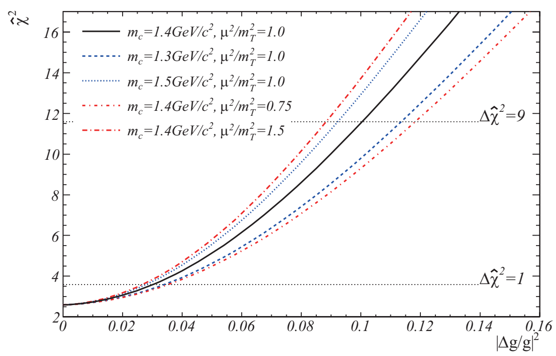

Fig. 2. $\hat{\chi}^2$ curves calculated from Fig. 1 and expected double-spin asymmetries as a function of assumed $|\Delta g/g|^2$ value. The black solid line is for default parameters of a charm mass $m_c = 1.4$ GeV/c^2 and a scale $\mu^2 = {m_T^c}^2$. The blue curves are after changing the charm mass m_c to 1.3 GeV/c^2 (dashed line) and 1.5 GeV/c^2 (dotted line) and the red curves are after changing the scale μ^2 to $0.75{m_T^c}^2$ (dashed dotted line) and $1.5{m_T^c}^2$ (long-dashed dotted line).

References

1) A. Adare et al.: Phys. Rev. **D87** (2013) 012011
2) D. de Florian et al.: Phys. Rev. **D80** (2009) 034030
3) M. Glück et al.: Phys. Rev. **D63** (2001) 094005

Status of π^0 pair A_{LL} analysis in RHIC-PHENIX experiment.

K. Hashimoto, R. Seidl, Y.Goto, and PHENIX Collaboration

The proton has a spin of 1/2 that originates from internal quarks and gluons. Results from Deep Inelastic Scattering (DIS) experiments show that the quark spin contribution to the proton spin is only about 25%. In the PHENIX experiment, the gluon-spin contribution to the proton spin has been studied for more than 10 years. In recent years, double helicity asymmetries, A_{LL} have been measured in several production channels ($\pi^0, \pi^\pm$, direct photon, etc). A_{LL} is defined as follos:

$$A_{LL} \equiv \frac{\sigma_{++} - \sigma_{+-}}{\sigma_{++} + \sigma_{+-}} \tag{1}$$

In this equation, $\sigma_{++(+-)}$ is the cross section in the same(different) helicity collision. and each signs represents bunch helicity signs.

One of the highest statistics channels is the measurement of A_{LL}[1] for inclusive π^0 production where the dominant hard sub-processes are quark-gluon and gluon-gluon scattering. Therefore, the π^0 production is a good channel as accessing the gluon spin.

Bjorken-x is defined as a fraction of a proton's longitudinal momentum and a patron's longitudinal momentum. If we select back-to-back hadron pair production at the mid-rapidity region, Bjorken x of two incoming partons should be almost balanced. If two Bjorken x are not balanced, the produced particles system is boosted, and these particles should move to the exterior of PHENIX central arm acceptance, where the rapidity region is $|\Delta\eta| < 0.35$. Thus, selection of back-to-back hadron pair production at a mid-rapidity region can suppress low Bjorken-x event.

Compared with single π^0, additional steps of π^0 pair A_{LL} analysis include 1) method of combination of data and 2) method for background subtraction. For further details, please see our previous report[3].

Fig 1 shows our preliminary result. The vertical axis is A_{LL} and the horizontal axis is the invariant mass of 2 π^0. In this plot, 8.8% uncertainty from the polarization measurement is not included. Our A_{LL} looks zero consistent due to large statistical uncertainty.

RHIC accelerator consist of 2 rings (called Blue ring and yellow ring). RHIC can store 120 bunches in blue and yellow rings and have 120 bunch crossings. A_{LL} of even number crossings should be the same that of odd number crossings. In 2009 data, A_{LL} with even crossing data and with odd crossing data have different value (In the past year, these values are consistent). Therefore, we include 2% uncertainty which comes from difference between even and odd crossing data. A preliminary result is zero consistent. Further, single spin asymmetry of the blue beam and yellow beams ware also calculated for cross checking. ($A_L \equiv \frac{\sigma_+ - \sigma_-}{\sigma_+ + \sigma_-}$, $\pm$ represents the bunch helicity sign for the blue and yellow beam). This asymmetry should be zero consistent and our result is zero consistent.

We need to develop different channel for improving the statistics. Back-to-back π^0 pair A_{LL} is the most simplest case of pair A_{LL} measurements but statistics is low. However, the measurement of π^0-$h^\pm$, π^0-jet or dijet production can increase statistics. If one of the gammas from π^0 fire trigger and charged hadron or jet is produced in the opposite direction, we can measure π^0-$h^\pm$ pair A_{LL} or π^0-jet pair A_{LL}.

The PHENIX collaboration plans to upgrade detecter systems. These new detecters will cover wider acceptance. This project is called sPHENIX. Long term future planning is single jet and di-jet measurements in sPHENIX. Especially, if sPHENIX full acceptance EM calorimeter can be obtained higher statistics. Moreover, with a hadron calorimeter, best kinematics sensitivity will be achieved in the jet measurement.

This analysis is being performed at CCJ[2], and we are grateful for its smooth operation.

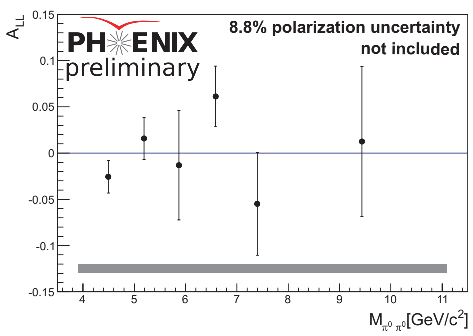

Fig. 1. Preliminary result of π^0 pair A_{LL}

References

1) A. Adare et.al.: Physical Review Letters 103 , 012003 (2009).
2) http://ccjsun.riken.jp/ccj/
3) RIKEN Accel. Prog. Rep. 45, P60 (2012).

Transverse single spin asymmetry measurement of muons from heavy-flavor decay at PHENIX

F. Wei[*1] and X. Wang [*1]

The measurement of transverse single-spin asymmetries (TSSAs) gives us the opportunity to probe the quark and gluon structure of transversely polarized nucleons. A number of pQCD-based models have been developed to explain TSSAs. Among them are the transverse momentum dependent (TMD) approach, which includes the Sieves effect[1)] and the Collins effect, [2)] and the higher twist mechanisms. [3)]

In the TMD approach, the determined TSSAs in D meson production can provide a clean measurement of the gluon Sivers distribution function, provided the kinematics are selected properly. D mesons, which predominantly originate from the c or $\bar{c}$ quarks, can be created either via an $q\bar{q} \to c\bar{c}$ or via a gluon fusion process $gg \to c\bar{c}$ at leading order. Since both processes result in unpolarized final c or $\bar{c}$ quarks, it is argued that the observed TSSAs for the process $p+p \to D+X$ can arise only because of the Silvers effect [4)] in transversely polarized $p+p$ collisions.

TSSAs in general can also be described using higher twist mechanisms. The TSSAs for open charm production in transversely polarized $p+p$ collisions are predicted by quark-gluon and tri-gluon correlations in the twist-3 contribution of the QCD collinear factorization approach, [5)] It has been predicted that the D and $\bar{D}$ meson production will have different A_N values. The measurement of TSSAs of a heavy flavor will allow us to better understand the TMD and tri-gluon collinear approach.

PHENIX has two spectrometers designed for measuring muon production over the pseudorapidity range $1.2 < |\eta| < 2.2$. The muon arms consist of thick hadron absorbers that reduce the hadronic background for muon measurements. muon trackers (MuTr) and muon identifiers (MuID). Prompt muons are produced from D or B meson through semi-leptonic decay. The main background source of prompt muons are punch through hadrons and muons from light hadron decay.

Preliminary results from the 2006 and 2008 datasets have been obtained as figures 1 and 2. The preliminary result of Run 2008 is consistent with that of Run 2006. The combined result indicates that the gluon Sivers effect is smaller than the sensitivity of the present measurement. During Run 2012, with the 200 GeV transverse polarized $p+p$ running, we implemented a new single muon trigger for enhancing our observation of medium p_T single muons. The preliminary result of Run 2012 will provide better constraints that can be applied to the current results. In addition, the forward silicon vertex (FVTX) detector was successfully installed in 2012. The FVTX detector covers same rapidity range as the muon arms. It will provide the forward muon system with a strong capability to reduce the hadron background and improve the current measurement significantly.

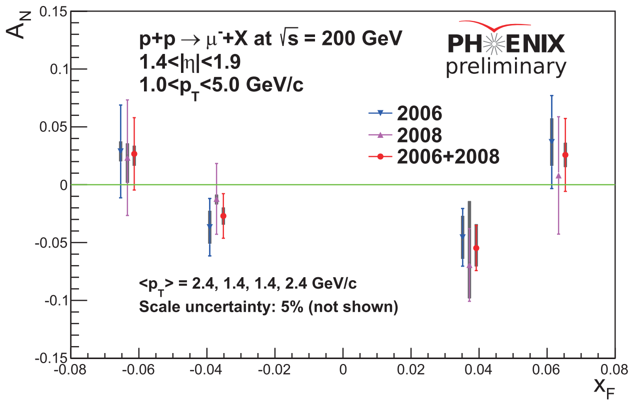

Fig. 1. x_F dependent PHENIX preliminary results in 2006 and 2008 and the combined results of 2006 and 2008.

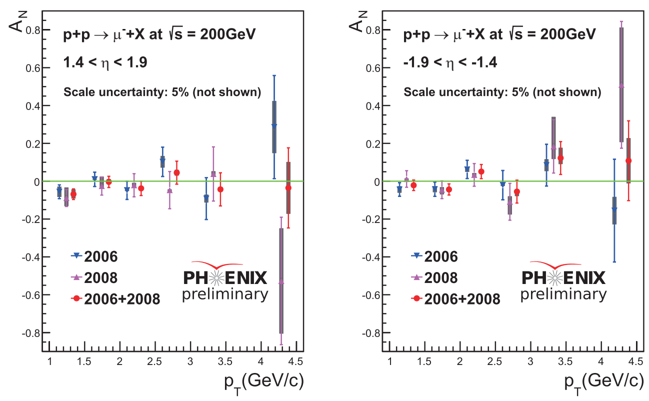

Fig. 2. p_T dependent PHENIX preliminary results at forward and backward rapidity in 2006 and 2008 along with the combined 2006 and 2008 results.

References

1) D. Sivers; Phys. Rev. D **41**, 83 (1990).
2) J.C. Collins; Nucl. Phys. B **396**, 161 (1993).
3) J. Qiu et al.; Phys. Rev. D **59**, 014004 (1999).
4) M. Anselmino et al.; Phys. Rev. D **70**, 074025 (2004), arXiv:hep-ph/0407100.
5) Z. Kang, J. Qiu et al.; Phys. Rev. D **78**, 114013 (2008).

*1 New Mexico State University, Las Cruces, NM 88003

Inclusive cross section and single transverse spin asymmetry for very forward neutron production in polarized $p+p$ collisions at $\sqrt{s}=200$ GeV†

Y. Goto for the PHENIX Collaboration

With the first polarized $p+p$ collisions at $\sqrt{s}=200$ GeV at RHIC, a large single transverse-spin asymmetry (A_N) for neutron production in very forward kinematics was discovered through a polarimeter development experiment[1]. The discovery of the large A_N for neutron production is also new important information to understand the production mechanism of the very forward neutron. The cross section of very forward neutron production was measured at ISR and Fermilab[2]. They measured a forward peak in the x_F distribution around $x_F=0.8$ and found only a small $\sqrt{s}$ dependence. The cross section was also measured at HERA in $e+p$ collisions[3]. They observed a suppression of the forward peak. In order to understand the production mechanism of the forward neutron, more data are necessary, and the asymmetry measurement gives new information.

At PHENIX, we measured the cross section and A_N of very forward neutron production in polarized $p+p$ collisions with a ZDC (Zero-Degree Calorimeter) by adding a position-sensitive SMD (Shower Maximum Detector)[4]. The detectors are located downstream of the RHIC-DX dipole magnet so that the charged particles from collisions are swept out. Beam Beam Counters (BBCs) are used as beam luminosity monitors. They are mounted around the beam pipe located ± 144 cm away from the collision point and cover $\pm(3.0$–$3.9)$ and 2π in pseudorapidity and azimuth spaces, respectively. The data were collected by two sets of triggers for the neutron measurement. One was the ZDC trigger for neutron inclusive measurements by requiring energy deposit on either side of the ZDC (the north side or the south side) above 5 GeV. The other was the ZDC⊗BBC trigger, a coincidence trigger of the ZDC trigger with BBC hits, which were defined as one or more charged particles on both sides of the BBCs.

The differential cross section, $d\sigma/dx_F$, in the integrated p_T region, $0<p_T<0.11\times x_F$ GeV/c for forward neutron production in $p+p$ collisions at $\sqrt{s}=200$ GeV was determined using two p_T distributions: a Gaussian form, as used in HERA analysis[3], and an exponential form, used for ISR analysis[2]. The results are plotted in Fig. 1. The measured cross section was consistent with the ISR result at $\sqrt{s}$ from 30.6 to 62.7 GeV, indicating that x_F scaling is satisfied at the higher center of mass energy.

The single transverse-spin asymmetry with the ZDC trigger was $A_N=-0.061\pm 0.010(stat)\pm 0.004(syst)$, and that with the ZDC⊗BBC trigger was $A_N=-0.075\pm 0.004(stat)\pm 0.004(syst)$. The x_F dependence of A_N of very forward neutron production is shown in Fig. 2. A significant negative A_N was seen in the positive x_F region, and there was no energy dependence within the errors in both trigger sets. No significant backward neutron asymmetry was observed.

† Condensed from the article in arXiv:1209.3283

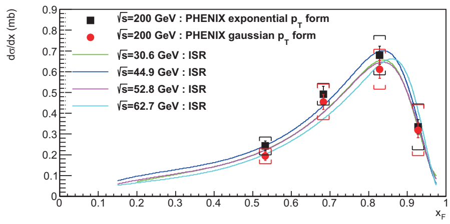

Fig. 1. The cross section results are shown. Statistical uncertainties are shown as error bars for each point, and systematic uncertainties are shown as brackets. Absolute normalization errors for the PHENIX and ISR are 9.7% and 20%, respectively.

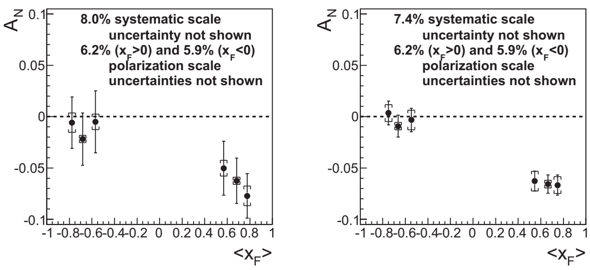

Fig. 2. The x_F dependence of A_N with the ZDC trigger (left) and with the ZDC⊗BBC trigger (right). The error bars show statistical uncertainties and brackets show p_T-correlated systematic uncertainties.

References

1) Y. Fukao *et al.*: Phys. Lett. **B650**, 325-330 (2007). [hep-ex/0610030].
2) J. Engler *et al.*: Nucl. Phys. **B84**, 70 (1975); W. Flauger, F. Monnig: Nucl. Phys. **B109**, 347 (1976).
3) S. Chekanov *et al.* [ZEUS Collaboration]: Nucl. Phys. **B776**, 1-37 (2007); F. D. Aaron *et al.* [H1 Collaboration]: Eur. Phys. J. **C68**, 381-399 (2010).
4) C. Adler, A. Denisov, E. Garcia, M. J. Murray, H. Strobele, S. N. White: Nucl. Instrum. Meth. **A470**, 488-499 (2001).

Advances in the PHENIX local polarimeter analysis in 2012

J. Koster, C. Gal, S. Park, and J. Perry,[*1]

The PHENIX experiment at the Relativistic Heavy Ion Collider (RHIC) observes high energy ($62.4GeV < \sqrt{s} < 510GeV$) collisions between polarized protons to study the spin structure of the proton. This report summarizes a recent and successful effort to greatly speed up the commissioning of longitudinally polarized beams at the RHIC.

The stable spin direction of circulating polarized beams at RHIC is the transverse spin direction. To enable studies utilizing longitudinally polarized proton, special "rotator" magnets are used to rotate RHIC's polarized beams from the transverse to the longitudinal direction just before the PHENIX experimental hall and then from the longitudinal to the transverse direction just after the beam has left the experiment. The Collider Accelerator Department already operates polarimetry equipment at RHIC to measure beam polarizations, but it does so in a separate area from the experiments. Therefore, it has no instrumentation to measure how successful their rotation from the transverse to the longitudinal spin has been. To solve this problem, accelerator experts rely on PHENIX's "local polarimeter" to help in tuning the rotator magnet currents and in tracking their performance.

The PHENIX "local polarimeter" utilizes a transverse spin asymmetry to quantify the direction of the beam polarization, i.e. what fraction of the beam is longitudinally polarized. Specifically, it uses a left-right single spin asymmetry, A_N, in neutron production at small scattering angles. Therefore, the analysis does not directly measure the longitudinal polarization. Instead it measures the residual transverse beam polarization. This transverse asymmetry is minimized by adjusting the rotator magnets until an acceptably small transverse asymmetry remains. The polarization can be measured by using the relation: $P = \epsilon_N / A_N$, where: P is the transverse beam polarization, ϵ_N is the measured asymmetry and A_N is the analyzing power.

In past years the analysis took days of expensive beam time to accumulate statistics since the analysis was performed using data on hard disk and it also required a special experimental setup incompatible with physics data-taking. The new analysis, using a field programmable gate array, takes only minutes to accumulate sufficient precision to tune the rotator magnets. Results from an eight-hour data-taking session, called a fill, are shown in figure 1. A summary of all data-taking in 2012 are shown in figure 2. These results were made available to accelerator experts within the RHIC-complex in real-time and enabled us and accelerator experts to quickly notice fills with too large residual transverse polarizations.

In summary, the new analysis sped up a process that previously took days thereby giving us additional days of physics data-taking and also allowed us to quickly identify problems in the RHIC accelerator.

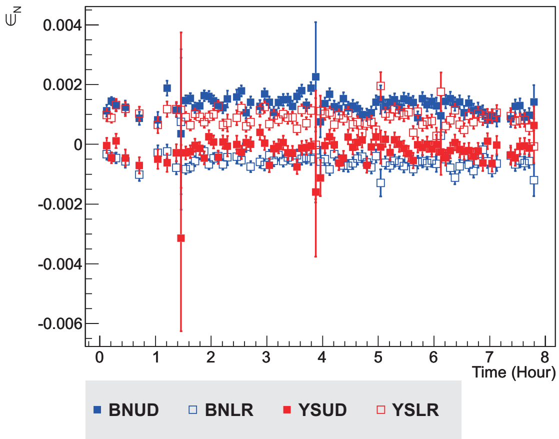

Fig. 1. Residual transverse polarization asymmetry (vertical axis) plotted versus the time within an experimental fill (horizontal axis) for a randomly chosen fill. The various types of asymmetry denoted BNUD, BNLR, YSUD and YSLR correspond to the two different beams (BN or YS) and to projections of the polarization in either the vertical or horizontal direction (LR or UD).

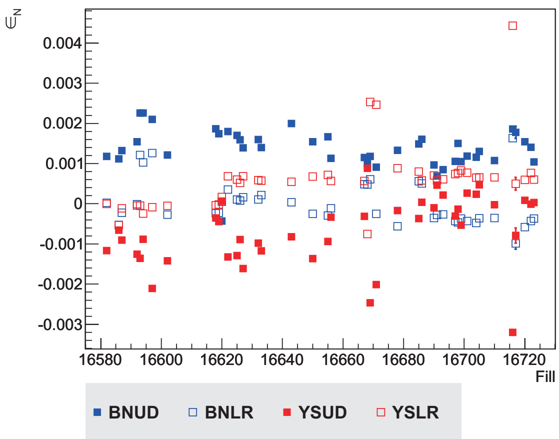

Fig. 2. A summary for all experimental fills of the residual transverse polarization asymmetry.

[*1] Iowa State University

Measurements of the beam path dependence of false double spin asymmetries in polarized $p+p$ collisions

K. Boyle and A. Manion,[*1]

A main goal of the RHIC Spin Program is to determine ΔG, the gluon spin contribution to the proton spin. At PHENIX, the double helicity asymmetry (A_{LL}) in π^0 production[1)] in longitudinally polarized $p+p$ collisions is the most sensitive measurement to ΔG due to the large statistical sample taken. In 2009, the systematic uncertainty from Relative Luminosity dominated the statistical uncertainty. Understanding and reducing this uncertainty is therefore very important to achieve the best determination of ΔG.

For longitudinal spin asymmetry measurements, luminosity normalization of the different spin orientations is required. The Relative Luminosity uncertainty quantifies how well this normalization is achieved, and consists of two contributions: 1) the accuracy of luminosity determination and 2) any asymmetry to which the luminosity detector is sensitive, and therefore could bias the π^0 A_{LL} measurement. For luminosity determination, event counts triggered in Beam-Beam Counters (BBC)[2)] by low momentum charged particle hits from $p+p$ collisions are used, and corrections due to rate and bunch width variations are applied[3)]. To determine if the BBC is sensitive to an asymmetry, the counts are compared to a second luminosity monitor, the Zero Degree Calorimeter (ZDC)[2)], which is triggered primarily by neutrons. In 2009, a ZDC to BBC asymmetry of $(1.2 \pm 0.2) \times 10^{-3}$ was measured, which was significantly larger than that of previous years.

With transverse spin, a forward neutron left-right asymmetry has been measured in the ZDC. During longitudinal running, small transverse spin components remain and are tracked using the remaining neutron asymmetry[4)]. We proposed that the luminosity asymmetry measured in 2009 was due to the remaining transverse component ($\sim 15\%$) coupled with a beam angle or offset of the beam path with respect to the ZDC. Such an offset or angle would modify the acceptance of the detector, and so increase or decrease the neutron yield depending on the polarization orientation. A toy Monte Carlo simulation of this effect was reported in[5)], and showed that such an effect could create a false asymmetry.

In the RHIC run at $\sqrt{s} = 200$ GeV in 2012, we proposed a study where the proton beams would be purposefully angled with respect to the nominal z-axis, while maintaining the two beam alignment so as not to reduce the luminosity. To reduce beam time used in this study, it was conducted during transverse running to maximize the effect. Data was recorded over several days at three different beam angles, as well as in

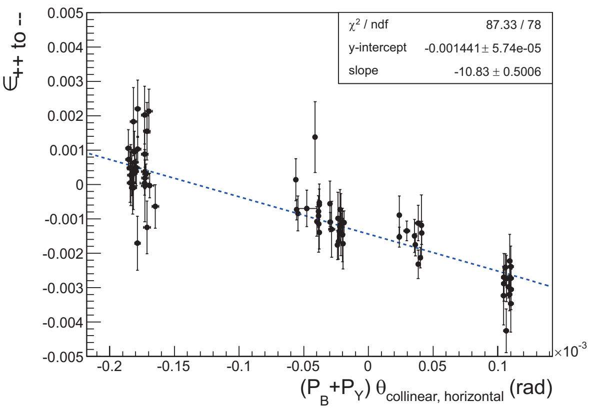

Fig. 1. False asymmetry $\epsilon_{++\text{to}--}$ vs beam angle with respect to nominal z axis. The effect is clearly visable. Also drawn is the result of a linear fit, which well describes the data.

the nominal settings. According to our hypothesis, this should induce an difference asymmetry, $\epsilon_{++\text{to}--}$, when comparing luminosity in two polarized up bunches and in two polarized down bunches, and this was in fact what was found. In Fig. 1, the results of this study are shown, and the linear dependence of the induced false double spin asymmetry as a function of the angle of the beams is clear from the fit. Here, the asymmetry is assumed to scale with polarization (P), like the transverse neutron asymmetry, and not with P^2, like A_{LL}, indicating it is indeed a single spin effect masquerading as a double spin effect.

To reduce this effect, we now keep the remaining transverse polarization components in longitudinally polarized $p+p$ collisions at $\sim 3-5\%$. We are also commissioning for the 2013 run a scaler readout for the ZDC shower maximum detector, which gives hit positions. This will allow us to mimic multiple beam angles and offsets during all running time, without requiring special beam conditions.

References

1) A. Manion [PHENIX Collaboration]: J. Phys. Conf. Ser. **295**, 012070 (2011).
2) K. Adcox, et al.: Nucl. Instr. Meth. **A499** 469-479 (2003)
3) A. Manion, et al: RIKEN Acc. Prog. Rep. **42**, 72 (2010)
4) C. Gal, K. Boyle, A. Deshpande: RIKEN Acc. Prog. Rep. **45**, 62 (2012)
5) K. Boyle, A. Manion: RIKEN Acc. Prog. Rep. **45**, 61 (2012)

*1 Department of Physics, Stony Brook University

Understanding of radial and elliptic expansion with blast wave model in AuAu $\sqrt{s_{NN}} = 200$ GeV at RHIC-PHENIX

Y. Ikeda

In non-central collisions, the initial geometry of the reaction zone is oval. A large azimuthal anisotropy of particle emission that depends on the initial geometry has been found. Experimentally, this azimuthal anisotropy is very important because it is related to the initial stage of collision. In particular, elliptical anisotropy, which is the second term of the Fourier series (v_2), is believed to carry information about the initial geometrical anisotropy. The large v_2 can be evidence for the short mean-free path of the particles in the hot dense medium. The measured v_2 increases with p_T in the low-p_T (soft) region, as shown by hydrodynamical calculations, in which fast thermalization is assumed in the initial stage and shear viscosity is thought to be small. The quark number scaling of v_2 suggests quark level collectivity in the hot dense matter and quark coalescence mechanism to form hadron from quark matter via quark-gluon phase transition.[1)2)3)4)]

The v_2 measurement in RHIC-PHENIX has so far been limited to particles of abundant yield because of the poor resolution of the reaction-plane detectors. A new reaction-plane detector RxP with higher resolution was installed to measure the elliptical flow in RHIC-PHENIX experiment.[5)] RxP allowed us to measure azimuthal anisotropy in higher p_T region, above 3 GeV/c.[6)] The hadron v_2 increase with p_T in the low momentum range ($p_T < 2$ GeV/c). Heavy particle has a smaller value of v_2 than light hadron for a given p_T. This can also be understood by shifting p_T towards higher p_T for heavier particles. This result agrees with the expectation that the heavy particle acquires larger transverse momentum via radial flow according to the hydro-dynamic model.

The Blast Wave model is a description of a fluid freeze-out state characterized by its temperature T_f and its radial flow velocity β_T.[7)] Following functions of Blast Wave describe the momentum spectra and the v_2 with T_f, β_T, and freeze-out eccentricity.

$$\begin{aligned}
\frac{dN}{p_T dp_T} &= \int dxdyW(Ax,y)K_1(\beta)I_0(\alpha) \\
v_2 &= \frac{\int dxdyW(x,y)K_1(\beta)I_2(\alpha)cos(2\phi_B)}{\int dxdyW(x,y)K_1(\beta)I_0(\alpha)} \\
\alpha &= \frac{p_T}{T}\sinh\rho = \frac{p_T}{T}\frac{e^{\rho}-e^{-\rho}}{2} \\
\beta &= \frac{m_T}{T}\cosh\rho = \frac{p_T}{T}\frac{e^{\rho}+e^{-\rho}}{2} \\
\tanh\rho &= \beta_T G(x,y)
\end{aligned}$$

where W(x,y) is density distribution of hot matter at freeze-out timing and G(x,y) is gradient of density distribution, which is calculated with W(x,y). The extracted freeze-out eccentricity by fitting of the function for p_T spectra and v_2 of six particles found to be smaller than the initial eccentricity estimated by Glauber Monte Carlo, but it still has the same orientation. The observation is consistent with the eccentricity extracted from HBT measurement that obtains system size of hot matter from two-hadron(π meson) interference[8)] (Fig. 1[9)]).

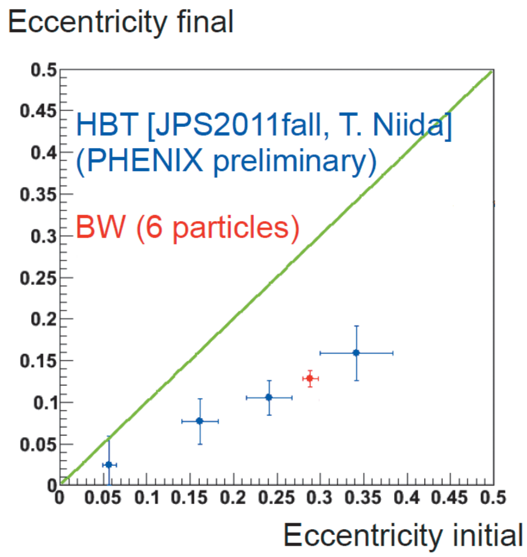

Fig. 1. Freeze out (final) eccentricity versus initial eccentricity. Red point shows the result of BW fitting. Blue points show results of the HBT analysis.

References
1) P. Houvinen, P.E. Kolb, U.W. Heinz, P.V. Ruuskanen, and S.A. Voloshin: Phys. Lett. B503, 58 (2001).
2) S. S. Adler et al.: (PHENIX Collaboration), Phys. Rev. Lett. 91, 182301 (2003).
3) R.J. Fries, B. Muller, C. Nonaka, S.A. Bass: Phys. Rev. Lett. 90, 202303 (2003).
4) R.J. Fries, B. Muller, C. Nonaka, S.A. Bass: Phys. Rev. C68, 044902 (2003).
5) E, Richardson et al.: Nucl. Intsr. And Mass. A vol636, 99, (2010).
6) Y.Ikeda: RIKEN Accel. Prog. Rep. 45, 52 (2011).
7) F. Retiere, and M. A. Lisa: Phys. Rev. C70, 044907 (2004).
8) T.Niida (PHENIX collaboration): arxiv1304.2876 (2013).
9) Y.Ikeda (PHENIX collaboration): CEJP, Vol 10, Issue 6, 1311(2012).

Measurement of higher harmonic flow of identified hadrons in Au+Au collisions at $\sqrt{s_{NN}} = 200$ GeV

S.Mizuno for PHENIX collaboration

Experimental studies using high-energy heavy-ion collisions has been performed for more than 10 years at the Relativistic Heavy Ion Collider (RHIC), in order to study properties of quark gluon plasma (QGP). A powerful tool for investigating the property of QGP is the azimuthal anisotropy of emitted particles.

To quantify the anisotropy, Fourier series is used for the azimuthal distribution of the number of emitted particles per event.

$$dN/d\phi = N_0[1 + \sum 2\nu_n cos\{n(\phi - \Psi_n)\}] \quad (1)$$

$$\nu_n = < \cos\{n(\phi - \Psi_n)\} > \quad (2)$$

where ϕ is azimuthal angle, ν_n and Ψ_n are the strength and direction of the n^{th}-order harmonic, respectively. ν_n is considered to carry information on the initial conditions and QGP viscosity. Because higher (n>2) order components are expected to be more sensitive to those effects, they have been studied actively.

In this analysis, azimuthal anisotropy of identified particles are studied. ν_n(n>2) are found to have similar dependence on mass and difference between meson and baryon to those seen in ν_2, as shown in Fig. 1.

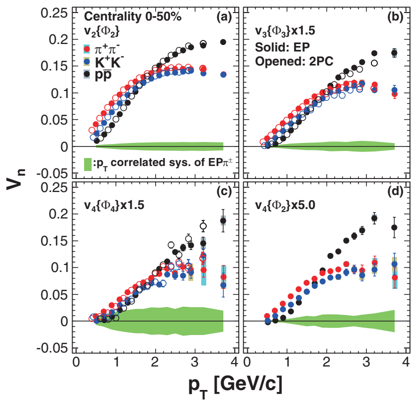

Fig. 1. $\pi^{\pm}$,$K^{\pm}$, and $p\bar{p}$ (a) v_2, (b) $v_3 \times 1.5$, (c) $v_4 \times 1.5$, and (d) $v_4(\Psi_2) \times 5.0$ as functions of p_T. Green band indicates p_T correlated systematic uncertainties.

Elliptic event anisotropy ν_2 at the low p_T region indicates that the system evolves hydrodynamically. Blast Wave functions (3),(4), which are inspired by hydrodynamical model, are used to fit the invariant yield[1] and ν_n in order to extract the freeze-out parameters.

$$\frac{dN}{p_T dp_T} \propto \int rdr \int d\phi m_T I_0(\alpha_t) K_1(\beta_t) \quad (3)$$

$$v_n(p_T) = \frac{\int rdr \int d\phi \cos(n\phi) I_n(\alpha_t) K_1(\beta_t) S(\phi)}{\int rdr \int d\phi I_0(\alpha_t) K_1(\beta_t) S(\phi)} \quad (4)$$

where $\alpha_t = (p_T/T_f)\sinh\rho$, $\beta_t = (m_T/T_f)\cosh\rho$, $\rho(\phi, r) = \rho_0(1 + 2\rho_n \cos(n\phi)) \times r/R_{max}$, and $S(\phi) = 1 + 2s_n \cos(n\phi)$. The parameters T_f, ρ_0, ρ_n, and s_n are temperature, surface average velocity, nth-order anisotropy of velocity, and spatial density anisotropy at freeze-out, respectively. Obtained parameters are shown in Fig.2. The radially averaged expansion velocity is presented as $< \rho >$.

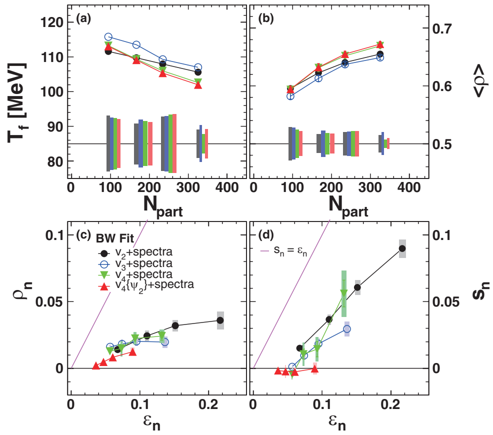

Fig. 2. (a) temperature, (b) spatially averaged velocity, (c) anisotropy of velocity and (d) spatial anisotropy at freeze-out. (a),(b) are functions of N_{part} and (c),(d) are functions of initial spatial anisotropy. Color bar located below each point in (a) and (b) are systematic uncertainties.

Freeze-out temperature and radially averaged expansion velocity are mostly constrained by the shape of the invariant yield. $< \rho >$ and s_n are plotted as a function of initial geometrical anisotropy ϵ_n calculated by Glauber Monte Carlo. Both anisotropy parameters ρ_n in velocity and s_n in spatial density have been found to behave similar to the centrality dependence of ν_n itself[2] and to scale with initial geometrical anisotropy. This indicates that the initial geometrical anisotropy is converted into the velocity anisotropy during the expansion resulting the reduced final geometrical anisotropy, which is also consistent with the final geometrical anisotropy extracted by HBT interferometry measurement.[3]

This results were presented as a poster in QM2012 and as a talk in ATHIC2012.

References

1) S. S. Adler et al.: Phys. Rev. C **69**, 034909 (2004).
2) A. Adare et al.: Phys. Rev. Lett. **107**, 252301 (2011).
3) J.Adams et al.: Phys. Rev. Lett. **93**, 012301 (2004).

Two particle correlations with respect to higher-order event planes in Au+Au $\sqrt{s_{NN}} = 200$ GeV collisions at RHIC-PHENIX

T. Todoroki for the PHENIX Collaboration

Quark gluon plasma (QGP) is a phase of nuclear matter where the existence is predicted by quantum chromodynamics at high temperature and high energy density, which is created by relativistic heavy ion collisions.

In previous measurements of di-hadron correlations in heavy ion collisions at RHIC[1)] and LHC[2)], near-side long range pseudo-rapidity correlations (ridge) and away-side double hump structures (shoulders) have been observed. These observations provide potential information to diagnose the mechanism of parton energy loss in QGP medium since those phenomena in correlations cannot be seen in p+p collisions, in which the QGP phase is not expected to be formed.

The higher-order flow harmonics, $v_n = \langle \cos n(\phi - \Psi_n) \rangle$ for $n>2$, anisotropy of emitted particle azimuth ϕ with respect to each harmonic event plane Ψ_n has been measured at RHIC and LHC[2)]. The higher-order flow harmonics are driven by hydrodynamics expansion from the fluctuations of initial participant density [3)] for odd harmonics, and from the fluctuations and elliptic shapes of nucleus-nucleus collisions for even harmonics. The observation suggests that v_n can reproduce the ridge and shoulder structure in the di-hadron correlations with rapidity gap $\Delta\eta>2$ between trigger and associate particle. However, the measurements of v_n and di-hadron correlations between trigger and associate particles with small $\Delta\eta$ gap at PHENIX[4,5)], where the contribution of jets is a large fraction of total correlation yields, again exhibited a shoulder structure in mid-central collisions centrality 20–50% even after subtraction of the contributions from v_n.

The results suggest that the shoulder emerges from the interplay between the hard scattered partons and the QGP bulk rather than simple collective expansion of QGP bulk. The data provide a possible discriminating power to the models of di-hadron correlations. Bulk of QGP contains the elliptic, triangular, and higher components in its shape, and the selection of the trigger particle with respect to each harmonic event plane enables us to control the parton path length in QGP bulk medium.

An extended measurement of correlations of intermediate momentum paris, with the selection of the trigger particle with respect to the second and third order event planes is performed to survey the origin of the shoulder structure in di-hadron correlations. The measurement results are shown in Figure 1. Transverse momentum ranges are $2<p_T<4$ GeV/c for trigger particles and $1<p_T<2$ GeV/c for associate particles. Each panel of the figure shows the correlation function of different $|\phi_t - \Psi_{2,3}|$ ranges. ϕ_t is the azimuthal angle of the trigger particle. Black data points show the correlations where $\phi_t - \Psi_{2,3} > 0$, and red data points show the correlations where $\phi_t - \Psi_{2,3} < 0$. Gray bands and red frames are systematics uncertainties coming from v_n measurements.

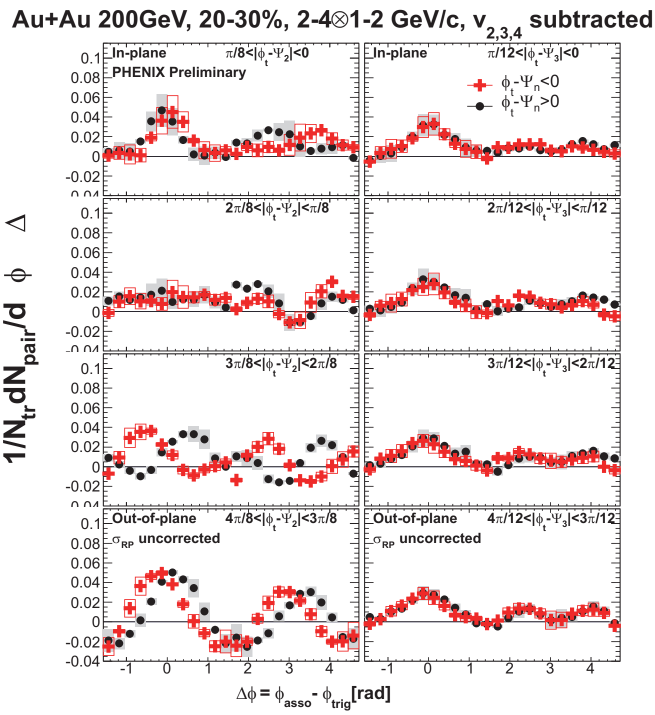

Fig. 1. Di-hadron correlations normalized to pair yield per a trigger with p_T selection $2<p_T<4$ GeV/c for trigger particles and $1<p_T<2$ GeV/c for associate particles in Au+Au $\sqrt{s_{NN}}$ =200 GeV collisions at centrality 20% to 30%. Contributions from v_2, v_3 and v_4 are subtracted.

The Ψ_3 dependent correlations in the right column of Fig.1 are almost consistent within systematic uncertainties, and the double hump structures in away-side stay in those correlations. In Ψ_2 dependent correlations in the right column of Fig.1, the shoulder structures are seen only in most top and bottom panels, wheras they are not seen in the middle two panels.

References
1) A. Adler *et al.*, Phys. Rev. C. **78**, 014901 (2008).
2) G. Aad *et al.*, Phys. Rev. C. **86**, 014907 (2012).
3) B. Alver *et al.*, Phys. Rev. C **81**, 054905 (2010).
4) A. Adare *et al.*, Phys. Rev. Lett. **107**, 252301 (2011).
5) T. Todoroki *et al.*, arXiv:1209.0044v2

Measurement of K_S in Au + Au collisions at $\sqrt{s_{NN}} = 200$ GeV at RHIC-PHENIX†

M. Nihashi for the PHENIX Collaboration

The fundamental theory of the strong interactions among quarks and gluons is quantum chromodynamics (QCD).

According to QCD, ordinary matter, which consists of protons and neutrons, undergoes phase transitions at extreme conditions, at temperature over 10^{12}K and/or at high densities over $10^{12}kgcm^{-3}$. High energy heavy-ion collision is a method to generate the hot matter. A RHIC-PHENIX experiment is studying this new phase of hot and dense matter, Quark Gluon Plasma, produced in heavy ion collisions.

In this report, I focus attention on the strange quarks to investigate properities of QGP at RHIC. Acquired knowledge about the properties of QGP from strange particles yield measurements are classified into four types here.

The first is from the total yield study. Particle ratios including multi-strange particles were reported as a signature of QGP at SPS. This is because if strangeness is only produced by hadronic interactions, multi-strange particles probably do not have enough time to reach chemical equilibrium owing to their small cross section in the medium. In recent years, it was reported that strangeness enhancement factors for central Cu+Cu collisions are higher than those for mid-central Au+Au collisions with similar number of participants at RHIC[1]. This report indicates that the total yield of the strangness may be likely related to initial geometry of the system of collision.

The second is from the radial flow study. The matter expands in all directions through all stages of fireball evolution. Accordingly, there is collective radial flow. The mT($m_T = \sqrt{m_0^2 + p_T^2}$) spectra of various speices provides us the information about freeze out temperature and radial flow velocity.

The third is from the intermidate $p_T(2 \leq p_T \leq 6GeV)$ study. In this region, strange-hadron production from both hard partons in minijets and soft partons in QGP is studied.

For instance, partons with $p_T \simeq$ 2GeV in y $\simeq$ 0 are the probe of the gluon distribution at x $\simeq$ 0.02 at RHIC energy. There is an important model, called the quark recombination/coalescence model, in which quarks and anti-qaurks of thermal and/or minijets are combined and form hadrons. We need to examine this model through systematic studies.

The last is from the high p_T study. Hard p_T strange-hadrons in mid-rapidiy region are from hard scattering, quark-jets and gluons-jets and this study indicates that flavour dependence in QGP, for example, energy loss by gluon radiations and jet-conversions[2].

The PHENIX detector consists of large-acceptance charged particle detectors. Charged Kaon in high p_T cannot be measured by Time of flight(TOF) particle identification method yet owing to finite timing resolution. On the other hand, 69.2% of the K_S mesons decay into charged pions (main branch) and K_S can be expected to be reconstructed and identified even for higher p_T.

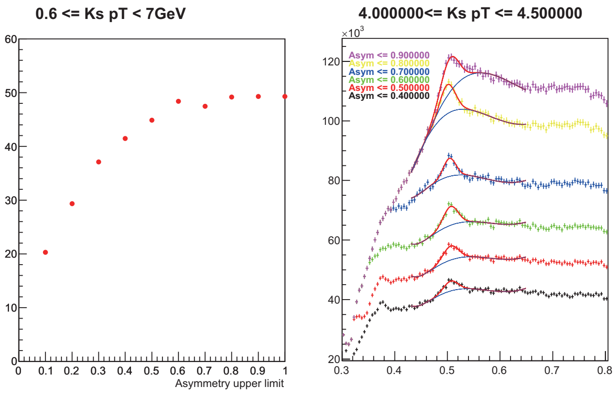

Fig. 1. Left figure is ratio of signal to statical errors$\sqrt{S+B}$ vs energy asymmetry upper limit. Right figure is the invariant mass distribution with various energy asymmetry cuts.

I reconstructed K_S from charged tracks of π^+ and π^- candidates by TOF PID. I used the TOF EAST detector and the PbSc sampling calorimeter as the timing device in order to obtain large acceptance. Invariant mass shape from K_S is distorted owing to mismomentum measurement from off-vertex effects, and K_S signal counting is sentitive to the correlated background shape. Energy asymmetry cut is known to increase the statistical significance of the signal ($\frac{S}{\sqrt{S+B}}$) in two-body decay and to change the corrlated background shape. Energy asymmetry scan results and the significance of the signal and invariant mass distributions are shown in fig. 1. At present, the estimation of systematic errors and improvement of counting technique are ongoing.

References
1) G. Agakishiev et al: Phys. Rev. Lett. 108, 072301 (2012).
2) W. Liu and R. J. Fries. Phys. Rev. C 77, 054902 (2008).

† Results from RHIC experimental operations in 2007

Study of background source of measurement of J/ψ photo-production at forward rapidity in Au+Au collisions at $\sqrt{s_{NN}}$ = 200 GeV

A. Takahara, Y. Akiba , E. T. Atomssa,[*2] M. Chiu,[*3] T. Gunji,[*1] H. Hamagaki,[*1] J. Nystrand,[*4] S. White,[*3] K. Skjerdal,[*4] Z. C. del Valle[*5]

The measurements of the photo-production of J/ψ at forward-rapidity($1.2 < |y| < 2.2$) in ultra-peripheral Au+Au collisions at $\sqrt{s_{NN}}$ = 200 GeV at RHIC-PHENIX was presented last year[1]. The Ultra-Peripheral Collision (UPC) is a collision whose impact parameter is greater than the sum of colliding nuclear radii. The measurement of $\gamma Au \rightarrow$J/$\psi + X$ in UPC plays an important role in determining the gluon density in nuclei at small Bjorken x, where the gluon density is expected to be suppressed due to the owing shadowing effect[2].

The requirements of UPC event selection at forward rapidity are that there are only two muon tracks at forward rapidity, at least one neutron is detected on both side of zero degree calorimeter, which is located 18.85 m forward and backward from interaction point and covers ± 2 mrad, and no other signal is detected by any other PHENIX detector. The left panel of Fig. 1 shows the invariant mass spectrum of dimuons at $1.2 < |y| < 2.2$ in the UPC event selection. In the measurements of J/ψ in UPC events, there are two expected non-negligible background sources. One is the direct dilepton production in UPC, $\gamma\gamma \rightarrow ll$. The other background source is the contamination of the most-peripheral collisions. It is necessary to quantitatively understand the contributions of these two background sources.

The right panel of Fig. 1 shows simulated $\gamma\gamma \rightarrow \mu\mu$ signal normalized to the luminosity, obtained in 2010[3]. The contribution of this process (0.1 event) is about 0.1% compared to measured J/ψ (74 events) shown in Fig. 1 (left). The red histogram in the left panel of Fig. 2 show charged particle multiplicity in mid-rapidity ($|y| < 0.35$), in the UPC events with J/ψ candidates in forward-rapidity without charged multiplicity cut in mid-rapidity. The blue histogram shows charged particle multiplicity in mid-rapidity ($|y| < 0.35$) in the p+p events, which corresponds to a limit of the peripheral collisions, with J/ψ candidate at $\sqrt{s_{NN}}$ = 200 GeV. It is seen that the multiplicities for the events with J/ψ in UPC and in $p+p$ collisions are very different; 39% of the J/ψ events in $p+p$ do not have any other tracks in mid-rapidity and that of UPC has 8 events more than 3 tracks.

Assuming that 7 events are from most-peripheral collisions, 7 × 0.39 J/ψ candidates are contaminated in the J/ψ candidates in UPC events. The right panel of Fig 2 shows the dimuon invariant mass spectrum in $p+p \rightarrow$ J/ψ+ X events, where the number of J/ψ are normalized to 2.8, 4% of UPC J/ψ. It is shown that the contribution from most-peripheral collisions is also negligible.

There are too low statistics to discuss background sources in further details .

*1 Department of Physics, University of Tokyo
*2 Stony Book University
*3 Brookhaven National Laboratory
*4 CERN
*5 Department of Physics, Lund University

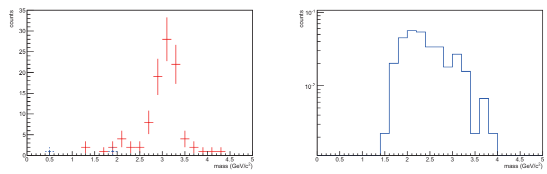

Fig. 1. Invariant mass distributions of dimuons at forward rapidity measured in 2010 in the UPC event selection (left). Crosses correspond to unlike-sign pairs and dashed crosses correspond to like-sign pair. Simulated $\gamma\gamma \rightarrow \mu^+\mu^-$ invariant mass distribution at forward rapidity normalized to luminosity in 2010 (right).

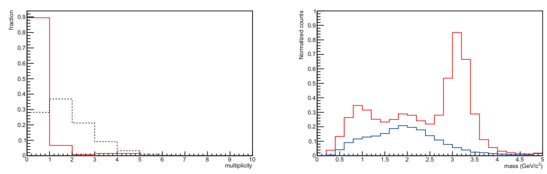

Fig. 2. Left: Red line corresponds to the multiplicity distribution of charged particles in mid-rapidity for the forward-rapidity UPC J/ψ events. Blue line corresponds to central multiplicity distribution of charged particles in mid-rapidity for 2009 $p+p$ forward-rapidity J/ψ. Right: dimuon invariant mass distributon of p+p collisions at $\sqrt{s}$ = 200 GeV in 2009 year. The distributions are normalized to have 2.8 J/ψ events.

References

1) A. takahara et al: RIKEN Accel. Prog. Rep. 45 (2012) 56
2) G. Baur, K. Hencken, D. Trautmann, S. Sadovsky, Y. Kharlov, Phys. Rept. 364 (2002) 359-450.
3) J. Nystrand; Nucl. Phys. A 752 (2005) 470c.

Estimates of statistical errors of π^0 v_2 in Pb-Pb collisions at $\sqrt{s_{NN}}$ = 2.76 TeV with ALICE at LHC

T. Tsuji, H. Hamagaki,*1 T. Gunji,*1 H. Torii,*1 for the ALICE collaboration

It has been observed in central Pb+Pb collisions at ($\sqrt{s_{NN}}$) = 2.76 TeV at the Large Hadron Collider (LHC) facility at CERN that the yield of charged particles at a high transverse momentum (p_T) is strongly suppressed as compared to the expected yield from p+p collisions, assuming the occurrence of scaling with the number of binary collisions. This suppression is attributed to the energy loss of hard scattered partons within quark-gluon plasma (QGP) created in heavy ion collisions. This phenomenon is called as jet quenching. A useful way to quantify the suppression of high-p_T hadrons is to introduce the nuclear modification factor (R_{AA}), where the $p+p$ cross section is scaled by the thickness function $\langle T_{AA}\rangle$ of the two nuclei

$$R_{AA}(p_T) = \frac{1}{< T_{AA} >}\frac{(1/N_{AA}^{evt})d^2N_{AA}/dp_Tdy}{d^2\sigma_{pp}/dp_Tdy}.$$

Experimental data can be well reproduced by multiple models with different approaches that calculate the energy loss of the hard scattered partons as they traverse the dense medium. To compare these models, we need to improve our experimental control of the path length L, since the energy loss of a high-p_T parton increases rapidly with the distance traveled through the medium.[1] Thus, the measurement of the energy loss with respect to the path length is expected to enable us to obtain detailed information about the mechanism of the parton energy loss. If R_{AA} is measured as a function of centrality ($cent$) and the azimuthal angle ($\Delta\phi$) with respect to the event plane, $R_{AA}(L)$ can be measured. Therefore, differential observable $R_{AA}(\Delta\phi)$ directly probes the path length dependence of the energy loss.

The $R_{AA}(p_T, cent, \Delta\phi)$ with respect to the azimuthal angle is factorized as

$$R_{AA}(p_T, cent, \Delta\phi) = F(\Delta\phi, p_T)\cdot R_{AA}(p_T, cent),$$

where $F(\Delta\phi, p_T)$ is ratio of the relative yield, given as

$$F(\Delta\phi, p_T) = \frac{N(\Delta\phi, p_T)}{\int d\phi N(\Delta\phi, p_T)},$$

and where $N(\Delta\phi, p_T)$ can be expressed in terms of a Fourier expansion with $\Delta\phi$.

$$N(\Delta\phi, p_T) \propto 1 + 2\sum_{n=1}^{\inf}(v_n\cos(n\Delta\phi)),$$

where v_n is the magnitude of the harmonics of the n-th order. The second harmonics, v_2, represents the strength of elliptic azimuthal anisotropy. The anisotropy v_2 at a low p_T is created by the collective flow, which is an origin of the background in measuring the $R_{AA}(p_T, \Delta\phi)$ for investigating the energy loss.

The statistical errors of $\pi^0 v_2$ were estimated. π^0 v_2 was extracted with the dN/dϕ method. In this method, v_2 is obtained by fitting the azimuthal angular distribution of π^0 with

$$N(\Delta\phi, p_T) = N(1 + 2v_2\cos(2\Delta\phi)).$$

π^0 values are reconstructed using the invariant mass method with reconstructed energy obtained by the photon spectrometer (PHOS) in the ALICE experiment. A statistical error of v_2 is inversely proportional to the one-half power of twice as much as the number of events. Figure 1 shows v_2 values as a function of p_T. Square points and circular points show v_2 values of the charged pion and the charged particle, respectively. In this figure, estimated amplitude of statistical errors from the half data of all high p_T triggered events in 2011 is shown using square bars. In these plots, the mean values of π^0 v_2 are conformed to those of the charged pion v_2 value. Therefore, statistical errors of π^0 v_2 are comparable in size to those of the charged pion, obtained from the 2010 run data. Calculations of $\pi^0 v_2$ are presently ongoing.

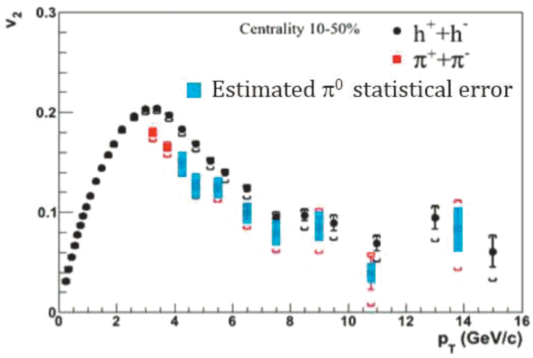

Fig. 1. v_2 values as a function of p_T. Square and circular symbols indicate v_2 values of the charged pion and the charged particle, respectively.[2] Square bars indicate the amplitude of statistical errors estimated from the half data of all high p_T triggered events in 2011.

References
1) A. Majumber: J. Phys. G. Nucl. Part. Phys. **34**, S377 (2007).
2) B. Abelev et al., for the ALICE Collaboration: Phys. Lett. **B719**, 18-28 (2013).

*1 Center for Nuclear Study, Graduate School of Science, University of Tokyo, Japan

Fragmentation function measurements with the Belle detector

R. Seidl, M. Leitgab,[*1] A. Vossen,[*2] F. Giordano,[*1] N. Kobayashi,[*3] M. Grosse-Perdekamp,[*1] A. Ogawa, C. Hulse[*4] and G. Schnell,[*4*5]

The Belle experiment at KEK has collected more than a 1 ab^{-1} of luminosity over the course of the data-taking which lasted until 2010. The analysis of that data is still continuing while preparations for the Belle II experiment are being ramped up. The initial goals of the Belle experiment are the exploration of CP symmetry breaking in the B meson sector for which it is designed to operate on the $\Upsilon(4S)$ resonance $\sqrt{s} = 10.58$ GeV. However, the majority of the cross section at that energy is due to open quark-antiquark production and thus it is possible to precisely study QCD physics in general and in particular the fragmentation process of how these quasi-free quarks fragment into final state hadrons. The published results on the spin dependent fragmentation function (FF) measurements of charged pions by the Collins effect or the interference fragmentation have already been reported previously[1)]. The inclusion of the analysis of pion-kaon and kaon-kaon pairs is ongoing and new results are expected soon.

The extraction of unpolarized FFs for pions and kaons has been finalized and has been submitted[2)]. As can be seen in Fig. 1 the measurement is very precise to almost the maximal fractional energy $z = 2E_h/\sqrt{s}$. Together with the previously existing world data from much higher energies it will allow to significantly decrease the uncertainties of the FFs of light quarks into pions and kaons and in particular enable a good determination of the gluon FFs which was previously poorly constrained due to the lack of data at energies significantly below the Z resonance. A global analysis by theorists including this new data set is expected to appear shortly after publication.

One addition on the extraction of unpolarized FFs is the measurement of hadron pairs. Those pairs could be detected in the same hemisphere which is the baseline to the interference FF measurements and also provides input to various resonance FFs such as those of the ρ^0, K^{*0}, Φ and other more exotic ones. The combination of two hadrons detected in opposing hemispheres gives additional information on favored versus disfavored fragmentation which is not accessible in inclusive measurements in e^+e^- annihilation. Favored (disfavored) here corresponds to the fragmentation of a quark into a hadron that does (not) contain that quark flavor as valence quark, such as $u \to \pi^+$ $(u \to \pi^-)$. An example of the expected yields from generic MC of uds and charm quark production is shown as a function of the fractional energies of the two particles in Fig. 2.

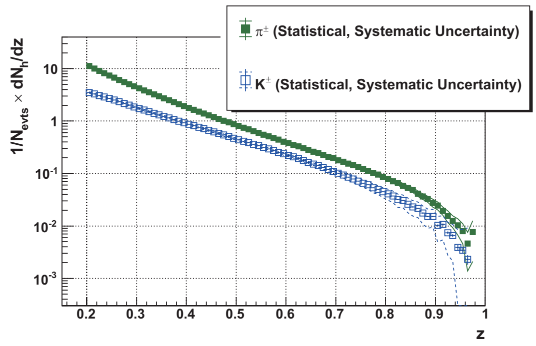

Fig. 1. Charged pion and kaon multiplicites as a function of the fractional energy z. The error bands describe the total systematic uncertainties.

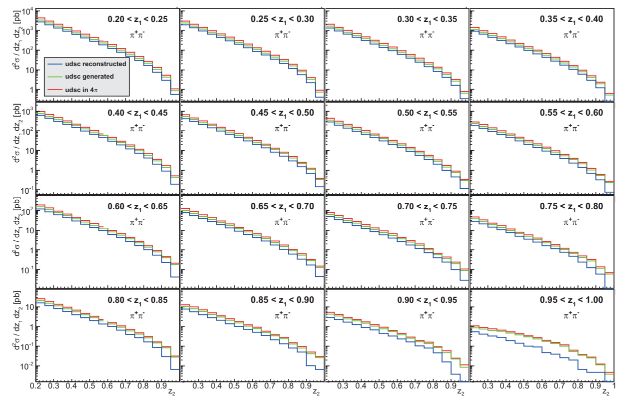

Fig. 2. Expected $\pi^+\pi^-$ multiplicites as a function of the fractional energy z_1, z_2 based on MC for uds and charm quark pair production with and without detector simulation and detector acceptance.

Furthermore the process of writing the Book on the physics of the B factories has been finished and will be published in 2013 including a chapter on the fragmentation function measurements which has been edited by the author of this article.

References
1) R. Seidl *et al.* [Belle Collaboration], Phys. Rev. Lett. **96**, 232002 (2006). R. Seidl *et al.* [Belle Collaboration], Phys. Rev. D **78**, 032011 (2008). A. Vossen *et al.* [Belle Collaboration], Phys. Rev. Lett. **107**, 072004 (2011).
2) M. Leitgab *et al.* [Belle Collaboration], arXiv:1301.6183.

*1 University of Illinois, Urbana, IL, U.S.A.
*2 University of Indiana, Bloomington, ID, U.S.A.
*3 Tokyo Institute of Technology, Japan
*4 University of the Basque Country, Bilbao, Spain
*5 Ikerbasque, Spain

Results of the commissioning run of E906/SeaQuest Drell-Yan experiment at the Fermilab

S. Miyasaka, Y. Goto, Y. Kudo,[*2] Y. Miyachi, K. Nagai,[*1] K. Nakano, S. Obata,[*1] F. Sanftl,[*1] S. Sawada, and T.-A. Shibata

The E906/SeaQuest experiment is a fixed-target experiment at the Fermi National Accelerator Laboratory (Fermilab). We, the SeaQuest group, measure a flavor asymmetry of antiquarks ($\bar{d}/\bar{u}$) in the proton and investigate how the asymmetry is changed when the proton is included in an atomic nucleus using the Drell-Yan process. In particular, we focus on the asymmetry at large Bjorken x, where the Bjorken x is a quark momentum fraction relative to the proton momentum. The Drell-Yan process occurs in hadron-hadron collision when a quark of one hadron and an antiquark of the other hadron annihilate into a virtual photon. Then, a muon pair is created as follows: $q + \bar{q} \rightarrow \gamma^* \rightarrow \mu^+ + \mu^-$. This process is a good tool to study antiquarks because the di-muon kinematics can be directly related to the quark and antiquark kinematics. In this experiment, a 120-GeV proton beam extracted from the Fermilab Main Injector is used. We use proton, deuteron, and atomic nuclei as targets. The ratio of $\bar{d}/\bar{u}$ is obtained by comparing the Drell-Yan events in $p + p$ and $p + d$ collisions.

The SeaQuest experiment began commissioning in February 2012. After a two-month commissioning period, the Fermilab accelerator complex was turned off for a planned year-long upgrade. A variation of several orders of magnitude in the beam intensity was observed at 360 Hz during this run. This variation was attributed to the Main Injector itself. The Fermilab Accelerator division is now investigating this problem and will resolve it during this shutdown. SeaQuest developed a veto trigger system based on the integral of the luminosity over approximately 200 ns in order to avoid large instantaneous luminosity. Using the veto system, SeaQuest succeeded in collecting valuable data during the lower luminosity parts of the beam cycle. Fig. 1 shows a typical di-muon event in the SeaQuest spectrometer. These data enabled testing of all the spectrometer devices, the data acquisition system, and the event reconstruction algorithms. A physics run is scheduled to start in June 2013. We are now modifying the PMT bases to accommodate high rates and zero-suppressed TDC to increase the life time of the data acquisition system toward the physics run. In addition, two new tracking drift chambers are being constructed to increase the acceptance of the SeaQuest spectrometer.

The Japanese group (RIKEN, KEK, Tokyo Institute of Technology, and Yamagata University) are in charge of one of the tracking drift chambers in the SeaQuest spectrometer. We have developed our local tracking code that reconstructs the tracks inside the drift chamber. The tracking code works well with the data accumulated in the commissioning run and gives us valuable reconstructed track information. With the help of the track information, a preliminary correlation function between the drift time and drift distance, which is a very important function for the drift chambers, is successfully extracted, as shown in Fig. 2. The function agrees with our simulation result. More precise analysis of this function and the other drift chamber-related analysis will be done before the physics run starts.

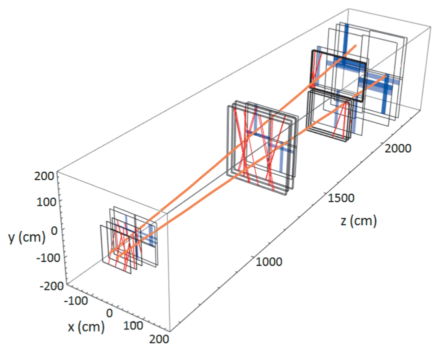

Fig. 1. Event display of SeaQuest. A typical di-muon event is shown. The 120-GeV proton beam comes from the left in this figure. Orange lines are muons. The red line and blue rectangle indicate the wire and hodoscope paddle that were fired by the muons.

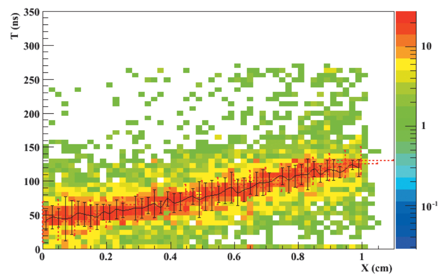

Fig. 2. The correlation function between the drift time and drift distance in one drift chamber. The drift distance is almost proportional to the drift time.

[*1] Tokyo Institute of Technology, Graduate School of Science and Engineering
[*2] Yamagata University, Faculty of Science

Feasibility study of deeply bound pionic atom spectroscopy in d(HI,^{3}He) reaction

K. Okochi, H. Fujioka, R.S. Hayano, K. Itahashi, S. Ito, T. Nishi, Y.K. Tanaka and Y.N. Watanabe

We have been working on the feasibility study of deeply bound pionic atom spectroscopy in the d(HI,^{3}He) reactions where HI denotes incident heavy ion beams. This study is expected to achieve pionic atom spectroscopy with unstable nuclei. It is known from previous experiments on deeply bound pionic atom spectroscopy with stable nuclei that the missing mass measurement in (d,^{3}He) reactions provides crucial information on the pion-nucleus interaction.[1,2] In the present study, we extend the scope of previous experiments and obtain the inverse kinematics of d(HI,^{3}He) reactions. As the first step, we set our goal as the establishment of the experimental method in the case of a stable nuclei beam of ^{124}Sn.

We consider an experimental setup that consists of an active target of a deuterium gas time projection chamber (TPC) and a full energy detector of silicon as shown in Fig. 1. In order to observe the forward scattering ^{3}He, we propose the application of the magnetic field and creating a dead region around the incident beam trajectory in case a beam intensity higher than $\sim 10^8$/s. The recoil angle of ^{3}He and the reaction point are measured in TPC and the kinetic energy of ^{3}He ($\sim$ 60 MeV) is measured in the full energy detector. We deduce the Q value of this pionic atom formation reaction from these observables.

In order to achieve a Q value resolution comparable to those of the previous experiments (400 keV(FWHM))[1], we need to estimate the reaction vertices within a 10 cm margin. However, it is difficult to determine the vertices in the case that the incident beam intensity is excessively high for performing event-by-event measurement. For the purpose of overcoming this difficulty, we formulated a vertex estimation method based on a proton emitted from pion absorption.

For the purpose of estimating the yield and the Q value resolution in this setup, we made a simulation by assuming the beam intensity and the detector performance as indicated in Table 1. In this simulation, the change of the trajectory radius due to the energy loss and the multiple scattering is ignored and the number of emitted protons per pionic atom is estimated from previous experimental results.[3] Consequently, the yield is estimated to be 3.1×10^4 /day. The Q value resolution is evaluated to be 6.0×10^2 keV (FWHM), as shown in Fig. 2. From these results, it is clear that this experimental method can ensure sufficient yield and about the same order of the Q value resolution as that of the previous results.

Table 1. Simulation Condition

Beam Intensity	10^9/s
Cross Section	2.54×10^{-1} μb
Position Resolution in TPC	500 μm
Dead Region of TPC	$\pm$7 mm
Energy Resolution of Si	0.1% at 60 MeV

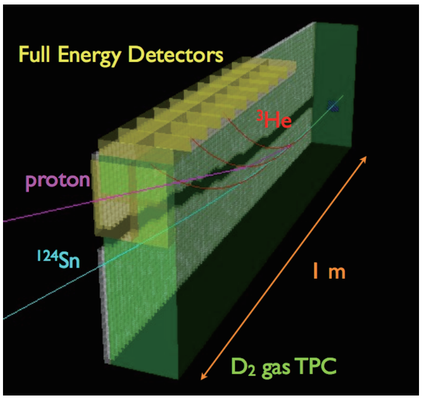

Fig. 1. Conceptual diagram of the experimental setup. In this figure, the green box is the TPC, the mesh-like structures are the readout pads of this TPC, and the yellow boxes are the full energy detectors. Red lines are the ^{3}He trajectories, the cyan line is the ^{124}Sn trajectory, and the magenta line is the proton trajectory.

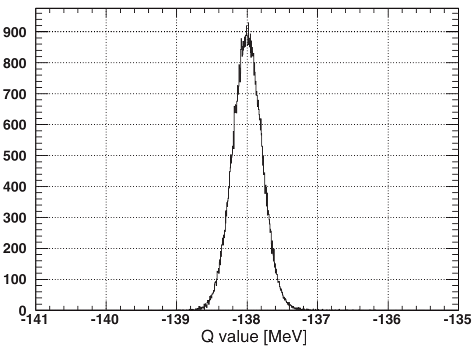

Fig. 2. Q value distribution with the closest distance < 1 mm.

References

1) K. Suzuki et al.: Phys. Rev. Lett. **92**, 072302 (2004).
2) T. Nishi et al.: Accel. Prog. Rep. **45**, iv (2012).
3) E. Gadioli and E. Gadioli Erba.: Phys. Rev. C **36**, 741 (1987).

4. Hadron Physics (Theory)

Matrix theory for baryons: an overview of holographic QCD for nuclear physics†

S. Aoki, K. Hashimoto, and N. Iizuka

We provide, for non-experts, a brief overview of holographic QCD and a review of a recent proposal of matrix-description[2)] of multi-baryon systems in holographic QCD. Based on the matrix model, we derive the baryon interaction at short distances in multi-flavor holographic QCD. We show that there is a very universal repulsive core of inter-baryon forces for generic number of flavors. This is consistent with a recent lattice QCD analysis for $N_f = 2, 3$ where repulsive core looks almost universal. We also provide a comparison of our results with the lattice QCD and the operator product expansion (OPE) analysis.

What is "M-theory" for nuclear physics? Although the "M-theory" stands for a theory of everything which unifies all string theories, one can generalize the use of the word "M-theory" not only for string theories but also for other subjects in physics. What is M-theory for nuclear physics, if exists?

This kind of question brings us to a bigger picture of relations between various subjects within physics, so it is not of no use. The question, however, sounds ridiculous, because the answer for it is obvious: The M-theory for nuclear physics is QCD, or more precisely, the Standard Model of elementary particles. Nucleons, which are the building blocks of nuclei, are bound states of quarks and gluons in QCD. Supposing that one could solve QCD completely, in principle one should be able to derive all the properties of nuclei, which is nothing but the nuclear physics. Therefore, in this sense, QCD is the M-theory for the nuclear physics. However, QCD is notorious as being difficult to solve, due to its strong coupling nature: the strong force makes quarks bound to each other. Therefore we need a new tool for solving QCD to "derive" nuclear physics.

Since this new tool has been missing for long years in research, apparently we have a hierarchical structure between studying perturbative QCD, nuclear physics and hadron physics. Standard nuclear physics starts with a quantum mechanics of multi nucleons, with inter-nucleon potential (nuclear force) given by experiments, or by hand to match phenomena. The quantum mechanics Lagrangian becomes

$$S=\int dt \left[\sum_{s=1}^{A}\frac{M}{2}\left(\partial_t x^M_{(s)}(t)\right)^2 - \sum_{s_1\neq s_2} V[x^M_{(s_1)} - x^M_{(s_2)}] + \cdots\right] \quad (1)$$

where we have A nucleons whose locations are given by $x^M_{(s)}(t)$ with $s = 1, \cdots, A$, $M = 1, 2, 3, 4$ ($M = 4$ being the holographic direction). The first term is the kinetic term of the nucleons with mass M, while the second term is the nuclear force. The problem lying in the unification of our concern is the fact that in nuclear physics the nuclear force V is given by experiments, and not by fundamental theory, *i.e.*, QCD. In principle, the potential should have been derived from QCD, as we all know that nucleons and hadrons are made of quarks and gluons — but it is very difficult.

It is very recent that the nuclear force was calculated from QCD with use of numerical methods: lattice QCD. The lattice QCD has accomplished a great success in hadron physics. In particular for hadron spectroscopy and hadron interactions, the lattice QCD is now very close to the physical parameters of QCD, the real world. Furthermore, there is a progress in this direction toward nuclear physics itself. Once the lattice QCD comes to deal with a system of multi-baryons, a part of nuclear physics becomes accessible directly from QCD. A huge number of quark contractions in large nuclei, which requires almost unrealistically high power of supercomputers, however, is a big obstacle in this direction. Furthermore, it is of course more ideal if we can understand physics without relying on the computers. Unfortunately we have not yet reached that stage. Therefore, we are facing at a situation where the hadron physics and the nuclear physics are disconnected from each other in a sense, due to a difficulty in solving the strongly coupled QCD.

At this occasion, the new tool using string theory comes into play. The renowned AdS/CFT correspondence[1)] makes it possible to solve a certain limit of QCD-like gauge theories, and it offers a certain direct path from QCD to nuclear physics. If one can derive an action like (1) from QCD, it can be regarded as an effective theory for nuclear physics derived from M-theory.

In this paper, we review the recent progress along this direction as an application of the AdS/CFT correspondence. In[2)], two of the present authors (K.H. and N.I.), together with Piljin Yi, derived an action of a multi-baryon system, by using the AdS/CFT correspondence applied to large N_c QCD. The action indeed has the form of (1), and it serves as a candidate for the bridge between QCD and nuclear physics.

References

1) J. M. Maldacena, Adv. Theor. Math. Phys. **2**, 231 (1998)
2) K. Hashimoto, N. Iizuka and P. Yi, JHEP 1010:003,2010.

† Condensed from the article in `arXiv:1203.5386`

Nucleon form factors in a covariant effective quark theory†

I. C. Cloët,*1 W. Bentz,*2 A. W. Thomas *1

[NUCLEON FORM FACTORS]

In order to describe the scattering of high energy electrons on nuclear targets in terms of quark degrees of freedom, the Nambu-Jona-Lasinio (NJL) model is often used as an effective theory of QCD. For example, this model was recently applied in Ref.[1] to describe quark distribution and fragmentation functions observed in deep inelastic electron-nucleon scattering. It is therefore of interest to investigate whether this model can also describe the spatial distribution of charge and magnetization density inside the nucleon. For this purpose, we show our results for the elastic nucleon form factors, and compare them to the empirical data.

We use a quark-diquark description of the nucleon based on the Faddeev framework. Details of this model description are explained in Ref.[2]. We include both the scalar and axial vector diquark channels, as well as the effects of the meson cloud around the constituent quarks in the framework of the NJL model. Our results for the nucleon Sachs form factors are shown in Figs. 1 - 4 as functions of the square of the momentum transfer (Q^2), and compared to the empirical form factors of Ref.[3]. The values of the magnetic form factors at $Q^2 = 0$ are $\mu_p = 2.78$ and $\mu_n = -1.81$ for the proton and neutron, respectively, compared to the experimental values $\mu_p^{\rm exp} = 2.79$ and $\mu_n^{\rm exp} = -1.91$. We see an overall good agreement between the calculated and empirical form factors. An extension of the model to describe the form factors of bound nucleons will also be discussed in our forthcoming article.

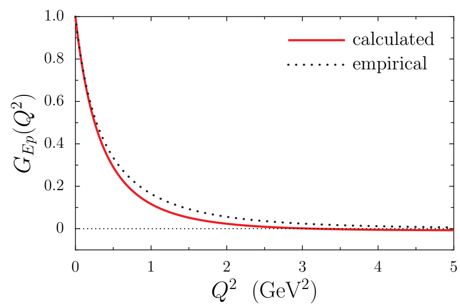

Fig. 1. Electric form factor of the proton. The sold line shows our calculated results, and the dotted line is the empirical curve from Ref.[3].

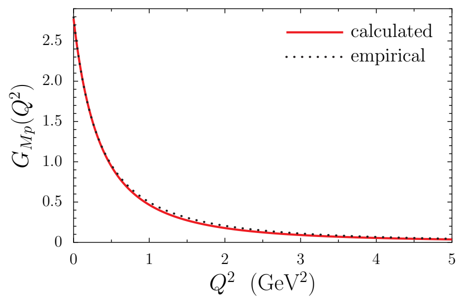

Fig. 2. Same as Fig.1 for the magnetic form factor of the proton.

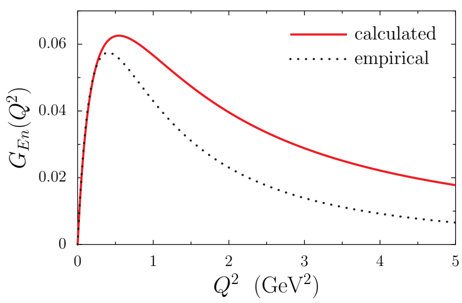

Fig. 3. Same as Fig. 1 for the electric form factor of the neutron.

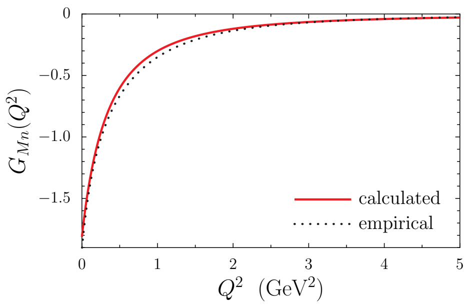

Fig. 4. Same as Fig. 1 for the magnetic form factor of the neutron.

References
1) H. H. Matevosyan, W. Bentz, I.C. Cloët, A.W. Thomas, Phys. Rev. **D 85** (2012) 014021.
2) T. Horikawa, W. Bentz, Nucl. Phys. **A 762** (2005) 102.
3) J. J. Kelly, Phys. Rev. **C 70** (2004) 068202.

† Condensed from an article by I. C. Cloët et al, to be published (2013).
*1 University of Adelaide, Adelaide, Australia
*2 Permanent address: Department of Physics, Tokai University, Kanagawa, Japan

KNO scaling and the effective action for small-x gluons

A. Dumitru

The color fields of highly boosted hadrons are very strong, parametrically of order $A^+ \sim 1/g$ where g is the coupling[1]. Collisions of such strong color fields release a large number of soft gluons. Due to non-perturbative dynamics of strong color fields a semi-hard "saturation scale" Q_s emerges; it corresponds to the transverse momentum where the phase space density of produced gluons is of order $1/\alpha_s$. We argue that in the strong field limit then a Gaussian effective theory leads to Koba-Nielsen-Olesen (KNO) scaling[2]. This relates the emergence of KNO scaling in $p_\perp$-integrated multiplicity distributions from high-energy collisions to properties of soft gluons around the saturation scale.

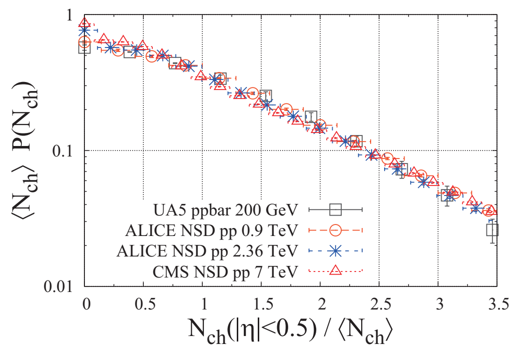

Fig. 1. KNO scaling plot of charged particle multiplicity distributions at midrapidity in non-single diffractive $pp\,/\,p\bar{p}$ collisions at various energies; data from refs.[3]. Note that we restrict to the bulk of the distributions up to 3.5 times the mean multiplicity.

KNO scaling conjectures that the particle multiplicity distribution in high-energy hadronic collisions is *universal* (i.e., energy independent) if expressed in terms of the fractional multiplicity $z \equiv n/\bar{n}$. This is satisfied to a good approximation in the central (pseudo-) rapidity region at C.M. energies of 200 GeV and above as shown in fig. 1. However, scaling is not perfect and the purpose of this contribution is to illustrate possible corrections.

In the strong field limit a semi-classical approximation applies and the soft gluon field (in covariant gauge) can be obtained in the Weizsäcker-Williams approximation from the source charge ρ which corresponds to the local color charge density per unit transverse area of the large-x "valence" sources which have been integrated out[4]. ρ is a random variable and color charge fluctuations are described by an effective action,

$$S[\rho] = \int d^2x_\perp \left[\frac{\rho^a\rho^a}{2\mu^2} + \frac{\rho^a\rho^a\rho^b\rho^b}{\kappa_4} \right] . \tag{1}$$

Aside from the standard ρ^2 operator which corresponds to Gaussian fluctuations[4] we have added here a quartic operator to illustrate possible corrections[6]. In the high-density limit the latter is assumed to be a small perturbation.

In fact, for a quadratic action ($\kappa_4 = \infty$) one obtains approximately a negative binomial multiplicity distribution (NBD)[5],

$$P(n) = \frac{\Gamma(k+n)}{\Gamma(k)\,\Gamma(n+1)} \frac{\bar{n}^n k^k}{(\bar{n}+k)^{n+k}} , \tag{2}$$

with a mean $\bar{n} \sim N_c(N_c^2-1)Q_s^2 S_\perp/\alpha_s$ and width $k \sim (N_c^2-1)\,Q_s^2\,S_\perp$; here, $S_\perp$ denotes a transverse area. Thus, $\bar{n}/k \sim N_c/\alpha_s \gg 1$ and it is in this "coherence" limit that the NBD exhibits KNO scaling.

NBD fits to multiplicity distributions in the central rapidity bin of p+p collisions from $\sqrt{s} = 200$ GeV to 7 TeV show that $\bar{n}/k$ is not constant but increases by about a factor of 3. This could be in part due to running of the coupling with the non-linear momentum scale $Q_s(\sqrt{s})$. Another source of corrections to asymptotic KNO scaling could be due to the presence of additional operators in the effective action at lower energies, such as $\sim \rho^4$. For $\kappa_4 < \infty$ we find that

$$\frac{\bar{n}}{k} \sim \frac{N_c}{\alpha_s} \left(1 - 3\beta\,(N_c^2+1)\right) \tag{3}$$

with $\beta \sim \mu^4/Q_s^2\,\kappa_4$. This illustrates that $\bar{n}/k$ increases as the contribution of the $\sim \rho^4$ operator decreases due to renormalization-group flow with energy towards a Gaussian theory[7].

References

1) A. H. Mueller, Nucl. Phys. B **558**, 285 (1999).
2) Z. Koba, H. B. Nielsen and P. Olesen, Nucl. Phys. B **40**, 317 (1972).
3) R. E. Ansorge *et al.* [UA5 Collaboration], Z. Phys. C **43**, 357 (1989); K. Aamodt *et al.* [ALICE Collaboration], Eur. Phys. J. C **68**, 89 (2010); V. Khachatryan *et al.* [CMS Collaboration], JHEP **1101**, 079 (2011).
4) L. D. McLerran and R. Venugopalan, Phys. Rev. D49 (1994) 2233, Phys. Rev. D49 (1994) 3352.
5) F. Gelis, T. Lappi and L. McLerran, Nucl. Phys. A **828**, 149 (2009).
6) A. Dumitru and E. Petreska, Nucl. Phys. A **879**, 59 (2012).
7) E. Iancu, K. Itakura and L. McLerran, Nucl. Phys. A **724**, 181 (2003).

Qaurk-gluon thermodynamics with the $\mathbb{Z}_3$ symmetry†

Y. Sakai, H. Kouno,*1 T. Sasaki,*2 and M. Yahiro,*2

Understanding the confinement mechanism is one of the most important subjects in hadron physics. According to lattice QCD,[3] the system is in the confinement and chiral symmetry breaking phase at a low temperature (T), but in the deconfinement and chiral symmetry restoration phase at a high T. Even then the confinement mechanism remains unclear for several reasons. The main reason is that the exact symmetry is not found for the deconfinement transition, and hence, the order parameter remains unknown. In the limit of zero current quark mass, the chiral condensate is an exact order parameter for chiral restoration. Contrastively, In the limit of infinite current quark mass, the Polyakov loop becomes an exact order parameter for the deconfinement transition, owing to the precise $\mathbb{Z}_3$ symmetry in this case. For the real world in which u and d quarks have small current quark masses, the chiral condensate is considered to be a good order parameter, but it is not clear whether the Polyakov loop is a good order parameter.

In order to solve this problem, we constructed a gauge theory invariant under the $\mathbb{Z}_3$ transformation, which is a gauge theory with three degenerate flavor quarks (q) with the twisted boundary condition (TBC) in the temporal direction[1]

$$q_f(\mathbf{x}, \tau = T^{-1}) = -\exp(-i2\pi(f-1)/3)q_f(\mathbf{x}, 0) \quad (1)$$

for flavors $f = 1, 2, 3$. This flavor-dependent boundary condition breaks the flavor symmetry explicitly. By the $\mathbb{Z}_3$ transformation, only the boundary conditions are changed to

$$q_f(\mathbf{x}, \tau = T^{-1}) = -\exp(-i2\pi(f-k-1)/3)q_f(\mathbf{x}, 0) \quad (2)$$

for integer k. The $\mathbb{Z}_3$ transformation changes f into $f-k$, but $f-k$ can be denoted as f since degenerate flavor quarks are being considered. In the $\mathbb{Z}_3$ symmetric gauge theory, the Polyakov loop becomes an exact order parameter of the deconfinement transition. The $\mathbb{Z}_3$-symmetric gauge theory then becomes a rather useful theory for understanding the confinement mechanism.

We have investigated the quark-gluon thermodynamics with $\mathbb{Z}_3$ symmetry using the Polyakov Nambu–Jona Lasinio (PNJL) model under the TBC, which we refer to as the TBC model.[4,5] It has $\mathbb{Z}_3$ symmetry, and hence, the Polyakov loop becomes an exact order parameter of the deconfinement transition. The Polyakov loop is zero up to some critical temperature T_c, but becomes finite above T_c. The $\mathbb{Z}_3$ symmetry is thus preserved below T_c, but spontaneously broken above T_c. Below T_c, the color confinement preserves the flavor symmetry. Above T_c, however, the flavor symmetry is broken explicitly by the TBC. We show[1] that the dynamics of the TBC model is similar to that of the PNJL model with the standard boundary condition below T_c. The similarity is relatively worse above T_c. One can then expect that QCD with approximate $\mathbb{Z}_3$ symmetry is similar to the quark-gluon theory with $\mathbb{Z}_3$ symmetry, and hence, $\mathbb{Z}_3$ symmetry is a good approximate concept in QCD, even when the current quark mass is small.

We have also investigated the quark chemical potential (μ) effect in the TBC model.[2] A current topic related to the confinement is the quarkyonic phase.[6] It is a confined phase with finite quark-number density. The concept of the quarkyonic phase was constructed in large N_c QCD, where N_c is the number of colors. In fact, the phase was first found at a small T and large μ in a large N_c QCD. We have investigated the interplay between the $\mathbb{Z}_3$ symmetry and the emergence of the quarkyonic phase in the TBC model. The quarkyonic phase factually exists at a small T and large μ. Although the $\mathbb{Z}_3$ symmetry is explicitly broken in the standard boundary condition, the quarkyonic-like phase with an extremely small value of the Polyakov loop and finite density exists at a small T and large μ. $\mathbb{Z}_3$ symmetry thus plays an essential role in the emergence and the location of the quarkyonic phase in the μ-T plane, and the quaryonic-like phase is a remnant of the quarkyonic phase in the TBC.

References
1) H. Kouno, Y. Sakai, T. Makiyama, K. Tokunaga, T. Sasaki, and M. Yahiro: J. Phys. G: Nucl. Part. Phys. **39**, 085010 (2012).
2) Y. Sakai, H. Kouno, T. Sasaki, and M. Yahiro: Phys. Lett. B**718**, 130 (2012).
3) M. Cheng, *et. al.*: Phys. Rev. D**81**, 054504 (2010); S. Borsanyi, *et. al.*: JHEP**09**, 073 (2010).
4) K. Fukushima: Phys. Lett. B**591**, 277 (2004); Phys. Rev. D**77**, 114028 (2008).
5) C. Ratti, M.A. Thaler, W. Weise: Phys. Rev. D**73**, 014019 (2006).
6) L. McLerran and R.D. Pisarski: Nucl. Phys. A**796**, 83 (2007).

† Condensed from the article.[1,2]
*1 Department of Physics, Saga University
*2 Department of Physics, Kyushu University

Relativistic hydrodynamics based on projection operator method†

Y.Minami and Y. Hidaka

We study relativistic hydrodynamics in the linear regime, based on Mori's projection operator method. In relativistic hydrodynamics, an ambiguity about the fluid velocity is considered to occur from choice of a local rest frame: the Landau and Eckart frames[1,2]. We find that the difference in the frames is not attributed to the choice of the local rest frame, but rather that of dynamic variables in the linear regime. We derive hydrodynamic equations in both frames by the projection operator method. We show that natural derivation gives the linearized Landau equation. We also find that, even for the Eckart frame, the slow dynamics is actually described by the dynamic variables for the Landau frame.

Relativistic hydrodynamics has been widely applied for studying relativistic nonequilibrium phenomena. For example, it describes hadron spectra and elliptic flow in the heavy ion physics[3], and jets in the astrophysics[4]. The hydrodynamic equations applied to these systems are mainly those for perfect fluids. One of reasons for this is that the dissipative effects in relativistic hydrodynamics are not fully understood, e.g, some pathological problems arise from the dissipative effects: the acausal propagation and the instability of the equilibrium state[5]. Although many hydrodynamic equations have been proposed to resolve these problems[6–11], it is not still obvious which equation describes the correct behavior of the relativistic dissipative fluid. Namely, even the basic equation has not been established in relativistic hydrodynamics.

In this report, we derive relativistic hydrodynamics by the Mori's projection operator method[12]. The projection operator method is a powerful tool for extracting slow dynamics without assuming microscopic details. This method is widely applied and successful in condensed matter physics. Furthermore, we here focus on linear fluctuations from the global equilibrium state at rest, the so-called the linear regime. Then, we need not bother about the local equilibrium and local rest for a relativistic fluid, in contrast to the earlier studies[6–11]. Therefore, our study is general and independent of details, such as the definition of the local rest frame. Instead, our study is restricted to the linear regime.

In the linear regime, the equations of motion for the slow variables are generally given as

$$\partial_0 \; A_n(t,\boldsymbol{x}) = \int d^3y i{\Omega_n}^m(\boldsymbol{x}-\boldsymbol{y})A_m(t,\boldsymbol{y}) - \int_0^\infty ds d^3y {\Phi_n}^m(t-s,\boldsymbol{x}-\boldsymbol{y})A_m(s,\boldsymbol{y}) + R_n(t,\boldsymbol{x}), \tag{1}$$

by the projection operator method[12]. Here, A_n are the slow variables, $i{\Omega_n}^m$ the frequency matrix, ${\Phi_n}^m$ the memory function, and R_n the noise term.

From the general expression (1), we can naturally derive the linearized Landau equation[1] by using the following three facts; (i) The slow variables of relativistic fluids are the conserved charge densities, which are the particle number, energy, and momentum densities, (ii) The particle number and energy are the thermodynamic variables, and the momentum density is related to the generator of Lorentz symmetry, and (iii) The hydrodynamics is a low energy effective theory, and then, the derivative expansion is applicable.

We can also derive the linearized Eckart equation[2] by choosing the particle current density in addition to the slow variables of the Landau frame. However, the important point is that the particle current is not essentially slow because it is not conserved. Then, the slow part of the current turns out to be determined by the actual slow variables, which is of the Landau frame[13]. Namely, the Landau frame is natural for the relativistic hydrodynamics.

† Condensed version of Y. Minami and Y. Hidaka, arXiv:1210. 1313 [hep-ph].

References

1) L. D. Landau and E. M. Lifshitz: *Fluid Mechanics* (Pergamon,New York, 1959).
2) C. Eckart: Phys. Rev. **58** (1940), 919.
3) U. W. Heinz and R. Snellings: arXiv:1301.2826 [nucl-th].
4) D. Mihalas and B. W. Mihalas: *Foundations of Radiation Hydrodynamics* (Dover Publications, 1999).
5) W. A. Hiscock and L. Lindblom: Phys. Rev. D **31** (1985), 725.
6) W. Israel, J.M.Stewart: Ann.Phys.(N.Y.) **118** (1979), 341.
7) G. S. Denicol, H. Niemi, E. Molnar and D. H. Rischke: arXiv:1202.4551 [nucl-th].
8) P. Van and T. S. Biro: Phys. Lett. B **709** (2012), 106.
9) A. Muronga: Phys. Rev. C **76**, 014910 (2007) [nucl-th/0611091].
10) K. Tsumura and T. Kunihiro: Prog. Theor. Phys. **126**, 761 (2011) [arXiv:1108.1519 [hep-ph]].
11) M. Natsuume and T. Okamura: Phys. Rev. D **77**, 066014 (2008) [Erratum-ibid. D **78**, 089902 (2008)] [arXiv:0712.2916 [hep-th]].
12) H. Mori: Prog. Theor. Phys. **33**, 423 (1965).
13) Y. Minami and Y. Hidaka: arXiv:1210.1313 [hep-ph].

The Chiral Magnetic Wave

H. -U. Yee

Triangle anomaly is a quantum mechanical violation of axial symmetry in the QCD of massless Dirac fermions,

$$\partial_\mu j^\mu_A = \frac{N_c e^2}{2\pi^2}\left(\sum_{F=u,d,s} q_F^2\right)\vec{E}\cdot\vec{B}\,, \tag{1}$$

in a P- and CP-violating environment $\vec{E}\cdot\vec{B}\neq 0$. Although its low energy consequences are completely accounted for by Wess-Zumino-Witten action, its possible effects in high temperature quark-gluon plasma that may be relevant in heavy-ion experiments are richer and less well understood. One such effect that has attracted recent interests from both theorists and experimentalists is Chiral Magnetic Effect (CME)[1,2], which dictates the existence of vector (axial) current in the presence of axial (vector) chemical potential and the magnetic field, $\vec{j}_{V,A} = \frac{N_c e}{2\pi^2}\mu_{A,V}\vec{B}$. Since a large magnetic field of strength $eB \sim 4m_\pi^2 \sim 10^{19}$ G along the perpendicular direction to the reaction plane is created in off-central heavy-ion collisions[1], the resulting charge separation induced by the CME may lead to non-zero electric charge dipoles on event-by-event basis, which may have an experimental signature in the two point correlation functions of charged particles, $\langle\cos(\phi_1+\phi_2)\rangle_{++,--} < 0$ and $\langle\cos(\phi_1+\phi_2)\rangle_{+-} > 0$[3].

The two versions of CME, $\vec{j}_{V,A} = \frac{N_c e}{2\pi^2}\mu_{A,V}\vec{B}$, naturally lead to the existence of gapless traveling waves of chiral charges, called Chiral Magnetic Wave (CMW)[4]. In the chiral basis, $Q_{L,R} \equiv \frac{1}{2}\left(\mp Q_A + Q_V\right)$, the dispersion relation of CMW is $\omega = \pm v_\chi k - iD_L k^2 + \cdots$ with the velocity v_χ given by $v_\chi = \frac{N_c e}{4\pi^2\chi}B$ (χ : susceptibility) and D_L is the diffusion constant. The sign in front of the first term that determines the direction of the CMW depends on the chirality of the traveling charges, so that left-handed chiral charges Q_L move to the direction opposite to that of the right-handed charges Q_R. Since the CMW describes universal hydrodynamic motion of charge fluctuations in the presence of magnetic field, its existence does not require a presence of background chemical potentials, which is an important difference from the CME.

The new charge transport induced by CMW may have important phenomenological implications in heavy-ion collisions. One possibility is a development of net electric quadrupole moment in the fireball created in off-central heavy-ion collisions[5]. The fireball initially has a net positive vector charge due to finite baryon stopping of the colliding nuclei. Since there is no net axial charge on average, we can think of the net vector charge as a sum of two equal amount of left-handed and right-handed chiral charges via the relation $Q_{V,A} = \pm Q_L + Q_R$. As each chiral charges move to the opposite directions dictated by CMW along the magnetic field which is perpendicular to the reaction plane, and since the total vector charge is a sum of the two chiral charges, there will be a net charge excess around the poles of the fireball whereas there will be a depletion of charges in the central region. The result is a net electric quadrupole moment. This electric quadrupole moment eventually leads to the charge dependent elliptic flow difference between negative and positive pions, $v_2(\pi^-) > v_2(\pi^+)$[5], which was indeed confirmed later by a recent **STAR** analysis[6].

Another effect from the CMW that is potentially important in heavy-ion experiments is the photon emission in the presence of magnetic field. Recent **PHENIX** analysis indicates a large elliptic flow of energetic photons of $p_T \geq 1$ GeV, which is at odds with previous theoretical predictions. One possible source for the observed large azimuthal asymmetry of the photon emissions, which has been neglected until recently, is the magnetic field. Based on the strong coupling computation in the Sakai-Sugimoto model, we have shown that the triangle anomaly which manifests itself as the CMW has a significant effect on the azimuthal pattern of the photon emission in the presence of the magnetic field[7]. The effect is pronounced especially at low energy $\omega \leq 1$ GeV, so it is not yet much relevant in explaining the current data, but it may become potentially important in the future experimental analysis.

As the physics of CMW is quite generic in the theory of chiral fermions, one can expect the same phenomenon appearing in many different situations, for example, in a finite density, low temperature regime. One can also study the CMW in the weak coupling regime using the framework of Boltzmann kinetic theory. Some progress in these directions is being made by the author.

References

1) D. E. Kharzeev, L. D. McLerran and H. J. Warringa, Nucl. Phys. A **803**, 227 (2008).
2) K. Fukushima, D. E. Kharzeev and H. J. Warringa, Phys. Rev. D **78**, 074033 (2008).
3) B. I. Abelev *et al.* [STAR Collaboration], Phys. Rev. Lett. **103**, 251601 (2009).
4) D. E. Kharzeev and H. -U. Yee, Phys. Rev. D **83**, 085007 (2011).
5) Y. Burnier, D. E. Kharzeev, J. Liao and H. -U. Yee, Phys. Rev. Lett. **107**, 052303 (2011).
6) G. Wang [STAR Collaboration], arXiv:1210.5498 [nucl-ex].
7) H. -U. Yee, arXiv:1303.3571 [nucl-th], accepted in Phys. Rev. D.

Interface tensions at deconfinement phase transition of large N matrix model

S. Lin, V. V. Skokov[*1] and R. D. Pisarski

$SU(N)$ gauge theory shows a deconfinement phase transition at $T = T_d$. In the temperature window $T \sim 1-2T_d$, a large deviation from classical conformality has been observed in lattice simulations. A matrix model has been developed to study the properties of the gauge theory in this region.[1)] In the deconfinement phase, the Polyakov loop gains a vacuum expectation value, which spontaneously breaks the center $Z(N)$ symmetry. This allows for the existence of N inequivalent vacua related by $Z(N)$ transforms. The purpose herein is to report the novel features of the topological objects that interpolate between two inequivalent vacua in the large N limit.

The large N limit of thermal vacuum was obtained in a previous work.[2)] The degrees of freedom of the matrix model are the eigenvalues of the time component of gauge field A_0. In the limit $N \to \infty$, the eigenvalues become continuous, $q_i \to q(x)$, with $x = \frac{i}{N}$. The eigenvalue distribution in thermal vacuum is characterized by the density function $\rho(q) = \frac{dx}{dq}$:

$$\rho(q) = 1 + b\cos dq, \quad -q_0 < q < q_0. \tag{1}$$

At $T = T_d^+$, $b = 1$, $d = 2\pi$ and $q_0 = 1/2$. The density vanishes at the end points $\rho(\pm q_0) = 0$. For $T < T_d$, the theory is in the confined phase with $b = 0$. b is a zero mode of the potential energy, which is an emergent feature of the large N limit. The solution corresponds to one vacuum. The other vacua can be obtained by $Z(N)$ transformations, which, in the large N limit can be expressed as

$$\begin{aligned} q(x) \to\ & q(x+1-\Delta) - 1 + \Delta,\ 0 < x < \Delta \\ & q(x-\Delta) + \Delta, \quad \Delta < x < 1. \end{aligned} \tag{2}$$

$Z(N)$ transforms preserve the potential energy, and thus, Δ is also an emergent zero mode of the potential energy.

The interface tension α is defined as the ratio of the effective action and transverse area $S_{eff} = K + V = \alpha A_\perp$. At T_d, there are two types of interfaces: order-order interfaces, which interpolate two deconfined vacua and order-disorder interfaces which interpolate between confined vacuum and deconfined vacuum. The case of the order-disorder interface is easy to construct. We can introduce a z dependence of b, whereby $b(z)$ interpolates between 0 for the confined and 1 for the deconfined phase. Since b is a zero mode for the potential energy, through an analogy with instanton physics, it can be surmised that the interface has equal kinetic and potential energies. Therefore, we conclude that the order-disorder interface tension vanishes. The case of the order-order interface is more interesting. Introducing a z dependence of Δ does not give the correct interface because the Δ mode would leads to divergent kinetic energy. A second possibility is to construct an order-order interface by joining two order-disorder interfaces, with one order-disorder interface obtained by a $Z(N)$ transform of the other. This leads to a vanishing interface tension.

At $T > T_d$, only order-order interfaces exist and their tensions are nonvanishing. We can envisage different scenarios in two limiting cases: $\Delta \to 0$ and $T \to T_d$. In the case of $\Delta \to 0$, we expect the eigenvalues in $0 < x < \Delta$ to shift by almost one period while the rest remain unshifted. Thus, we have both the kinetic and potential energy proportional to Δ. Detailed calculation shows $\alpha = \Delta\frac{d}{6\sqrt{3}}(1-2q_0)^3$. In the case of $T \to T_d$, we expect the interface to mimic the $T = T_d$ situation, namely, that of two vacua joined through a confining flat eigenvalue distribution. Considering that b is not a zero mode, each half of the interface gives a potential barrier $V \sim (1/2 - q_0)^2$. The kinetic energy $K \sim O(1)$. Through a balance between the kinetic and potential energies, a Δ independent interface tension is obtained $\alpha \sim (1/2 - q_0)$. This dictates the overall scaling in $(1/2-q_0)$. A more sophisticated ansatz gives a Δ dependent result. The results from both scenarios have been included in Fig.1

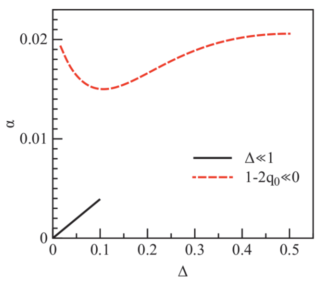

Fig. 1. Interface tension at $q_0 = 0.3$ in two scenarios.

References
1) A. Dumitru, Y. Guo, Y. Hidaka, C. P. K. Altes and R. D. Pisarski: Phys. Rev. D **86**, 105017 (2012)
2) R. D. Pisarski and V. V. Skokov: Phys. Rev. D **86**, 081701 (2012)

† Condensed from the article in Phys. Rev. D **87**, 105002 (2013)

*1 Department of Physics, Brookhaven National Laboratory, USA

Critical endpoint in matrix model for deconfinement and other effective models†

K. Kashiwa, R. D. Pisarski, and V. V. Skokov,*1

The investigation of the phase structure of Quantum chromodynamics (QCD) at finite temperature (T) and real chemical potential ($\mu_{\rm R}$) is one of the important subjects in particle and nuclear physics. If we obtain the QCD phase structure from a first principle calculation, there is no ambiguity. The first principle calculation, a lattice QCD simulation, has a sign problem at finite $\mu_{\rm R}$ and is not feasible. Because of this, effective model calculations are widely used to investigate the QCD phase diagram. Therefore, the construction of a reliable effective model is important.

In this paper, we investigate the properties of the deconfinement critical endpoint in the matrix model for deconfinement. This model is an extended version of the zero-parameter model proposed in Ref.[1] . This is a useful exercise, since the solution of the zero-parameter model does not agree with lattice data on the interaction measure of the pure SU(3) glue theory. Indeed, the matrix model for deconfinement[2,3] is tuned to give increasingly good agreement with the lattice QCD data than the zero-parameter model.

We calculated the Columbia plot as a function of m_l and m_s where m_l (m_s) is the light (strange) quark mass. In addition, the interaction measure, which is important to the QCD thermodynamics, was calculated. In both cases, we consider the heavy quark mass because we can then neglect spontaneous chiral symmetry breaking,which simplificies our calculation.

For the matrix model, and for models based upon polynomials of the Polyakov loop [4–7] , we find a heavy m^{de} , which is the critical point. Above m^{de}, a first order transition appears. We found that there is a large model dependence on m^{de} for the matrix and Polyakov-loop models [4–12] . In the matrix model, m^{de} is about 2.5 GeV for three degenerate quarks. For the polynomial and logarithmic Polyakov loop models, m^{de} becomes 3.5 and 1.0 GeV, respectively.

The above model dependence is a quantitative difference. A qualitative difference can be seen on the interaction measure defined as $(e-3p)/T^4$ where e, p, and T are the internal energy density, pressure, and temperature. In the matrix model for deconfinement has a two-peak structure on the interaction measure when it is plotted as a function of T . On the other hand, polynomial-type Polyakov-loop model [4–7] has a one-peak structure. The logarithmic-type Polyakov-loop model [8–12] provides a two-peak structure similar to the one of the matrix model.

The existence and computation of the deconfining critical endpoint is a well known problem. In this paper we have shown that its properties can be used to differentiate between different effective models. If the critical quark mass is very heavy, as in the matrix and polynomial Polyakov-loop models, the effects of lattice discretization for such heavy quarks will be severe. It may be useful instead to compute the background field at which the deconfining critical endpoint occurs, e. g. by adding a term proportional to $h({\rm tr}L + {\rm tr}L^\dagger)/2$ to the Yang Mills action, where h is the external field. Nevertheless, computing with a background field is elementary in numerical simulations on the lattice, and indicates if m^{de} is relatively light, ~ 1 GeV, or heavy, ~ 2 GeV.

References
1) P. N. Meisinger, T. R. Miller, and M. C. Ogilvie: Phys. Rev. D **65**, 034009 (2002).
2) A. Dumitru, Y. Guo, Y. Hidaka, C. P. K. Altes, and R. D. Pisarski: Phys. Rev. D **83**, 034022 (2011).
3) A. Dumitru, Y. Guo, Y. Hidaka, C. P. K. Altes, and R. D. Pisarski: Phys. Rev. D **86**, 105017 (2012).
4) R. D. Pisarski: Phys. Rev. D **62**, 111501 (2000).
5) O. Scavenius, A. Dumitru, and J. T. Lenaghan: Phys. Rev. C **66**, 034903 (2002).
6) A. Dumitru, D. Roder, and J. Ruppert: Phys. Rev. D **70**, 074001 (2004).
7) C. Ratti, M. A. Thaler, and W. Weise: Phys. Rev. D **73**, 014019 (2006).
8) K. Fukushima: Phys. Lett. B **591**, 277 (2004).
9) S. Roessner, C. Ratti, and W. Weise: Phys. Rev. D **75**, 034007 (2007).
10) T. Hell, S. Rossner, M. Cristoforetti, and W. Weise: Phys. Rev. D **81**, 074034 (2010).
11) D. Horvatic, D. Blaschke, D. Klabucar, and O. Kaczmarek: Phys. Rev. D **84**, 016005 (2011).
12) T. Hell, K. Kashiwa, and W. Weise: Phys. Rev. D **83**, 114008 (2011).

† Condensed from the article in Phys. Rev. D **85**, 114029 (2012)
*1 Department of Physics, Brookhaven National Laboratory

Finite-density dissipative hydrodynamic model for quark matter

A. Monnai

High-energy heavy-ion collisions can produce the quark-gluon plasma (QGP)[1], a deconfined quark matter which supposedly have filled the early universe. Experimental data from the Relativistic Heavy Ion Collider (RHIC) is found to be quantitatively well described in relativistic hydrodynamic picture, suggesting the hot medium is strongly coupled[2]. Detailed analyses have revealed viscosity would be indispensable in realistic description of the quark matter[3]. It is also note-worthy that the Large Hadron Collider (LHC) started to provide the data at higher energies.

In this study I focus on the net baryon number, to which most modern hydrodynamic studies are oblivious. It is conserved at forward rapidity where remnant of the nuclei is present. Baryon stopping has been used to quantify the extent of energy loss for the production of a hot medium at earlier mid-low energy collisions and can be important at RHIC and LHC when non-boost invariant expansion is taken into consideration. Development of a finite-density hydrodynamic scheme with off-equilibrium corrections would also be useful for beam energy scan programs which seeks to find a critical point on the phase diagram of quantum chromodynamics experimentally.

I estimate the effects of dissipative hydrodynamic evolution on the hot and dense matter at finite baryon density[4]. The relativistic dissipative hydrodynamic model is developed based on causal relativistic hydrodynamics extended for the particle number changing processes. Shear viscosity, bulk viscosity and baryon diffusion are taken into account. The initial conditions are employed from the color glass theory, a description of gluon saturation. The finite-density equation of state is constructed from the lattice QCD simulations with Taylor expansion method. The models for the transport coefficients are based on the Anti-de Sitter/conformal field theory correspondence. Here the evolution in the collisional axis is considered and the transverse dynamics is omitted for simplicity.

Figure 1 shows the net baryon distribution for Au-Au collisions with $\sqrt{s_{NN}} = 200$ GeV at RHIC and that for Pb-Pb collisions with $\sqrt{s_{NN}} = 2.76$ TeV at LHC. The data points are the scaled results of the net proton distribution from the BRAHMS Collaboration[5]. One can see that hydrodynamic convection widens the valleys of the net baryon rapidity distributions. It roughly reproduces the experimental data at RHIC. The effective reduction in baryon stopping could be a candidate explanation for the sudden enhancement of transparency at the collisions with higher energies[5]. Shear and bulk viscosities tend to reduce the hydrodynamic effect since the longitudinal pressure is decreased as responses to the expansion. Baryon diffusion also steepens the distribution since the net baryon dissipative current towards mid-rapidity is induced by the chemical gradients. Those results indicate that (i) the energy available for the production of a hot medium could be larger at the initial stage and (ii) finite-density dissipative processes could be observed in the analyses of the net baryon rapidity distribution. It is note-worthy that the viscous and the baryon diffusive effects might be larger since the transport coefficients chosen here are small and close to conjectured minimum boundaries. The results are also quantitatively sensitive to the choices of the initial conditions.

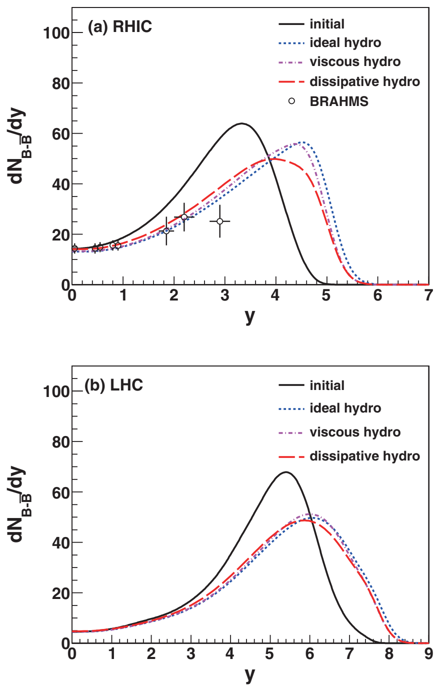

Fig. 1. Net baryon rapidity distributions of the initial state (solid lines) and after ideal (dotted lines), viscous (dash-dotted lines) and dissipative (dashed lines) hydrodynamic evolution at (a) RHIC and (b) LHC.

References

1) K. Yagi, T. Hatsuda and Y. Miake, *Camb. Monogr. Part. Phys. Nucl. Phys. Cosmol.* **23**, 1 (2005).
2) P. F. Kolb, P. Huovinen, U. W. Heinz and H. Heiselberg, *Phys. Lett. B* **500**, 232 (2001).
3) B. Schenke, S. Jeon and C. Gale, *Phys. Rev. Lett.* **106** 042301, (2011).
4) A. Monnai, *Phys. Rev.* C **86** 014908, (2012); arXiv:1301.2713 [nucl-th].
5) I. G. Bearden *et al.* [BRAHMS Collaboration], Phys. Rev. Lett. **93**, 102301 (2004).

Fluctuating hot QCD matter in heavy ion collisions

J. Liao

In high energy heavy ion collisions at the Relativistic Heavy Ion Collider (RHIC) and the Large Hadron Collider (LHC), a hot deconfined QCD matter (the quark-gluon plasm, or QGP) is created. In the past few years there appear convincing evidences for strong event-by-event fluctuations in the initial condition of such colliions, from the measured soft hadrons' azimuthal anisotropy, decomposed as various "harmonic flows", and its successful explanation via event-by-event hydrodynamic simulations. Naturally one expects such strong fluctuations in the initial condition also leave their imprints in other observables than just the bulk collective flows. Here we report our recent studies on two new aspects of the event-by-event fluctuations: the azimuthal anisotropy of jet quenching, and the azimuthal fluctuations of strong magnetic field.

1 Hard probe of geometry and fluctuations

The high energy jets from the initial hard scatterings provide the "imaging" tool of the created hot matter. Along the path through the medium, the jets will lose part of their energy (jet quenching) and as a result produce less high p_t hadrons as compared with the case without medium (as in pp collisions). The azimuthal anisotropy of jet quenching arises from the underlying hot matter's anisotropic distributions due to both geometry (in off-central collisions) and fluctuations in the initial condition. Such anisotropy can be quantified via azimuthal-angle ϕ-dependent nuclear modification factor $R_{AA}(\phi)$. The dominant component of this anisotropy is the $2nd$ harmonic (often called the elliptic) in the Fourier decomposition of $R_{AA}(\phi) \sim 1+v_2^J\cos[2(\phi-\Psi_2)]$. There are however also other harmonic components $v^J_{n=1,3,4,5,6,...}$ from fluctuations. Such anisotropy is sensitive to the jet energy loss mechanism and the initial fluctuations.

In a series of papers[1–3] we have systematically quantified the jet response v_n^J to the fluctuating initial condition using event-by-event simulations. We compare such response obtained from three energy loss models with differed in-medium path-length dependence as well as matter-density dependence. In particular for the elliptic one v_2^J, the comparison with data from RHIC to LHC in Fig.1 favors the NTcE model with quadratic path-length dependence and strong enhancement of jet-medium interaction near T_c.

2 Azimuthal fluctuation of magnetic field

Heavy ion collisions also produce very strong magnetic field $|\vec{B}|^2 \sim m_\pi^2$ at early times, and such $\vec{B}$ field leads to novel effects like the Chiral Magnetic Effect[4]

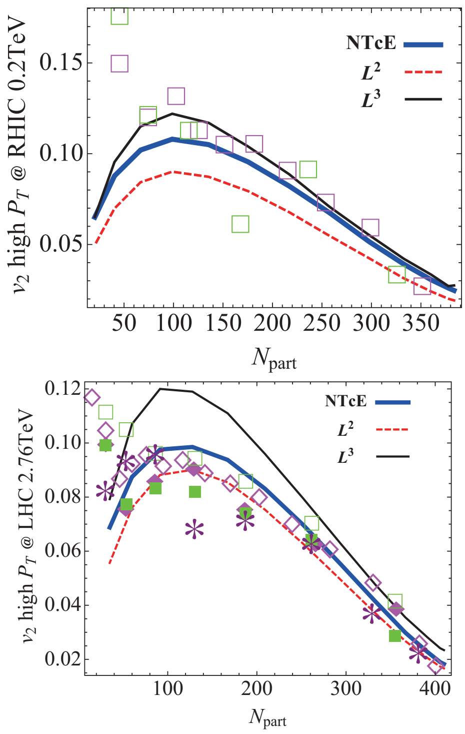

Fig. 1. Event-by-event modeling results for dominant azimuthal anisotropy of jet quenching from RHIC to LHC.

and the Chiral Magnetic Wave[5]. However the azimuthal fluctuations of such $\vec{B}$ field (with respect to also fluctuating matter geometry) have not been studied previously and they affect observables significantly. We have done a first detailed investigation of the event-by-event azimuthal correlations between the $\vec{B}$ orientation and the matter participant planes. Our results suggest that the azimuthal correlation is most strong in the mid-central to mid-peripheral events where the $\vec{B}$-induced effects can be best measured.

References

1) X. -L. Zhang and J. -F. Liao, Phys. Lett. B **713**, 35 (2012).
2) X. Zhang and J. Liao, arXiv:1208.6361 [nucl-th].
3) X. Zhang and J. Liao, arXiv:1210.1245 [nucl-th].
4) A. Bzdak, V. Koch and J. Liao, arXiv:1207.7327 [nucl-th].
5) Y. Burnier, D. E. Kharzeev, J. Liao and H. -U. Yee, arXiv:1208.2537 [hep-ph].
6) J. Bloczynski, X. -G. Huang, X. Zhang and J. Liao, Phys. Lett. B **718**, 1529 (2013).

Lattice calculation of nucleon electric dipole moment in $N_f = 2 + 1$ QCD

E. Shintani, T. Blum, T. Izubuchi

This is a status report of the lattice calculation of neutron and proton electric dipole moment (EDM) in $N_f = 2+1$ QCD. Here we focus on the determination of the first order of EDM with respect to θ-term, $d_N^\theta = d_N\theta + \mathcal{O}(\theta^2)$. In the Standard Model (SM), since the CKM phase contribution to nucleon EDM is started from 3-loop electroweak (EW) diagram[1,2], which is about 10^{-30}–10^{-33} e·cm, the θ-term contribution is expected to be the main effect. The tiny upper-bound from the experiment ($d_N^{\rm exp} < 2.9 \times 10^{-26}$ e·cm[3]) implies that θ-term is extremely small (strong CP problem). In fact, current algebra or chiral perturbation theory roughly suggests $\theta = d_N^{\rm exp}/d_N < 10^{-9}$–$10^{-10}$. Lattice QCD enables us to provide the theoretical value of d_N (and also θ) without any modeling. Furthermore, EDM is interesting for the supersymmetry model (SUSY) or other beyond the SM (BSM) for the constraint of its parameter for instance the CP-violating operator, which is expressed as the dimension-five operator (see Ref.[4,5] and references therein). The confirmation of the EDM lattice calculation in θ-term is a suitable test for the extension including higher dimensional operator.

There have been several attempts of lattice calculation in quenched QCD[6,8] and $N_f = 2$ QCD[7,9], but owing to large statistical fluctuation, these values still have large uncertainties including some systematic errors. To reduce the statistic and systematic uncertainties we attempt to employ the domain-wall fermion (DWF), which approximately realizes the chiral symmetry on the lattice to being under a few % of the violating effect, and furthermore, the use of the new algorithm developed to adequately use of machine resources, all-mode-averaging (AMA)[10]. This strategy advances the accuracy of neutron EDM calculation toward the 10% level with the present machine resource.

In this report, we present nucleon EDM calculation using dynamical DWF gauge ensemble of $24^3 \times 64$ lattice at $a^{-1} = 1.73$ GeV^{-1} generated by RBC/UKQCD collaboration[11]. We carry out the calculation of nucleon EDM form factor extracted from three-point function of (nucleon)-(electromagnetic current)-(nucleon), including leading order of θ-term following the reference[6]. In the AMA procedure, we define the improved correlator (two-point function and three-point function) as

$$\mathcal{O}^{(\rm imp)} = \mathcal{O}^{(\rm rest)} + \mathcal{O}_G^{(\rm appx)},\ \mathcal{O}^{(\rm rest)} = \mathcal{O} - \mathcal{O}^{(\rm appx)},$$
$$\mathcal{O}_G^{(\rm appx)} = N_G^{-1} \sum_{g \in G} \mathcal{O}^{(\rm appx),g}, \qquad (1)$$

with the original correlator $\mathcal{O}$ and approximation correlator $\mathcal{O}^{(\rm appx)}$. The last equation in Eq.(1) gives the average of N_G source location for $\mathcal{O}^{(\rm appx)}$. By using the relaxed CG for obtaining $\mathcal{O}^{(\rm appx)}$, the total computational cost is reduced to be 1/5 or less[10]. We use $N_G = 32$ source locations for $\mathcal{O}_G^{(\rm appx)}$ with relaxed stopping criteria under 0.003 for normalized residual norm. The original correlator $\mathcal{O}$ is obtained by the high-precision CG in which we use 10^{-8} stopping criteria. Low-mode, which is used in deflated CG, is computed by the Lanczos algorithm with the Chebychev acceleration of 4D even-odd preconditioner of DWF kernel, and we adopt 400 eigenmodes for quark mass $m = 0.005$ (which correspond to 300 MeV pion mass). Using 400 configurations, we obtain the result shown in Table 1. The nucleon EDM is the value of EDM form factor at physical kinematics ($q^2 = 0$), which is displayed in the first row in Table 1. We first obtain the finite value of neutron EDM over 1σ error in $N_f = 2+1$ QCD.

Table 1. Lattice results of neutron and proton EDM form factor at each squared transfer momenta. Using the linear fit function, we obtain EDM, which is the value of extrapolated form factor into zero momentum.

$m = 0.005$ $-q^2$ GeV^2	neutron (e·fm)	proton (e·fm)
0	−0.048(25)	0.019(39)
0.198	−0.049(21)	0.011(31)
0.382	−0.046(16)	0.028(23)
0.555	−0.047(20)	0.013(29)
0.721	−0.046(26)	0.029(35)

References

1) I. B. Khriplovich and A. R. Zhitnitsky, Phys. Lett. B **109**, 490 (1982).
2) A. Czarnecki and B. Krause, Phys. Rev. Lett. **78**, 4339 (1997).
3) C. A. Baker, *et al.*, Phys. Rev. Lett. **97**, 131801 (2006).
4) M. Pospelov and A. Ritz, Annals Phys. **318**, 119 (2005).
5) T. Fukuyama, Int. J. Mod. Phys. A **27**, 1230015 (2012).
6) E. Shintani, *et al.*, Phys. Rev. D **72**, 014504 (2005).
7) F. Berruto, *et al.*, Phys. Rev. D **73**, 054509 (2006).
8) E. Shintani, *et al.*, Phys. Rev. D **75**, 034507 (2007).
9) E. Shintani, S. Aoki and Y. Kuramashi, Phys. Rev. D **78**, 014503 (2008).
10) T. Blum, T. Izubuchi and E. Shintani, arXiv:1208.4349 [hep-lat].
11) Y. Aoki *et al.* [RBC and UKQCD Collaborations], Phys. Rev. D **83**, 074508 (2011).

Hadronic parity violation at next-to-leading order†

B. Tiburzi

Many corners of the Standard Model have been tested to very high precision through experiment. The hadronic neutral weak interaction, by contrast, is the least constrained of all Standard Model currents. Such an interaction is difficult to probe; because, even while largely shielded from electromagnetic contributions, it is easily overshadowed by dominant strong contributions. One must look to processes that violate strong interaction symmetries to isolate the hadronic weak interaction. Flavor-changing neutral currents are suppressed in the Standard Model due to the so-called GIM mechanism. To see the hadronic weak interaction through flavor-conserving neutral currents, one must look to isovector hadronic parity violation. Recent experimental advances[3,4] give reason for a concerted effort to study hadronic parity violation theoretically using QCD.

Lattice QCD computations can determine hadronic parity violation from first principles. Quite recently the first lattice QCD study of nuclear parity violation appeared[5]. In this pioneering work, the isovector channel was the focus, and a signal for the parity-violating pion-nucleon coupling, $h^{(1)}_{\pi N}$, was obtained. As with any lattice computation, there are a number of systematic errors which must be controlled to make contact with phenomenology. In particular, criticism has been raised about the ability to isolate pion-nucleon states convincingly in the above-mentioned calculation. As further refinements to the method are made, we can expect to see precision information about parity-violating hadronic couplings coming from lattice QCD computations. Complete information about hadronic parity violation in few-nucleon systems may not come solely from experiment or theory. A combination of the two will thus be essential to provide input for hadronic parity violation in nuclear few and many-body calculations. To this end, we study how well the sources of parity violation are known at hadronic scales. A leading-order QCD analysis was presented some time ago[6,7]. Since that work, better values for the bottom and charm quark masses are now known, as is the procedure for carrying out two-loop computations of the scale-dependence of parity-violating operators. We focus on both the isovector[1] and isotensor[2] parity-violating operators, and provide the complete next-to-leading-order analysis in QCD perturbation theory.

An example of our results is shown in Table 1. Using the QCD renormalization group to two-loop order, we determine the strength of the isotensor, parity-violating, four-quark operator at hadronic scales. At this order, results are renormalization scheme dependent, and we compare results in various renormalization schemes. The MOM and SMOM schemes will be particularly useful because these can be implemented in lattice QCD computations.

Table 1. Leading and next-to-leading order values of the Wilson coefficient of the $\Delta I = 2$ parity-violating operator, $C(\mu)$ scaled by its tree-level value $C^{(0)}$.

	$C(1\,\mathtt{GeV})/C^{(0)}$
Leading Order	0.70
't Hooft-Veltman	0.58
Naïve Dim. Reg.	0.74
RI/MOM	0.77
RI/SMOM($\gamma_\mu, \not{q}$)	0.67
RI/SMOM(γ_μ, γ_μ)	0.75
RI/SMOM($\not{q}, \not{q}$)	0.73
RI/SMOM($\not{q}, \gamma_\mu$)	0.81

Our next-to-leading order study of hadronic parity violation shows that QCD evolution generally suppresses the magnitude of the isotensor interaction at hadronic scales by about 1/4, with enhancements of some operators in the isovector channel up to a factor of 5. It will be interesting to see if hadronic matrix elements are small in the isotensor channel compared to the $\Delta I = 0, 1$ channels. If this were the case, hadronic parity violation would parallel the $\Delta I = 1/2$ rule, for which the maximal isospin changing channel is considerably suppressed. For this comparison, we must ultimately await the evaluation of non-perturbative physics from lattice QCD.

References
1) B. C. Tiburzi, Phys. Rev. D **85**, 054020 (2012), arXiv:1201.4852 [hep-ph].
2) B. C. Tiburzi, Phys. Rev. D **86**, 097501 (2012), arXiv:1207.4996 [hep-ph].
3) W. M. Snow, C. D. Bass, T. D. Bass, B. E. Crawford, K. Gan, B. R. Heckel, D. Luo and D. M. Markoff *et al.*, Phys. Rev. C **83**, 022501 (2011).
4) M. T. Gericke, R. Alarcon, S. Balascuta, L. Barron-Palos, C. Blessinger, J. D. Bowman, R. D. Carlini and W. Chen *et al.*, Phys. Rev. C **83**, 015505 (2011).
5) J. Wasem, Phys. Rev. C **85**, 022501 (2012); PoS LATTICE **2011**, 179 (2011), arXiv:1108.1151 [hep-lat].
6) J. Dai, M. J. Savage, J. Liu and R. P. Springer, Phys. Lett. B **271**, 403 (1991).
7) D. B. Kaplan and M. J. Savage, Nucl. Phys. A **556**, 653 (1993); Erratum-ibid. A **570**, 833 (1994); Erratum-ibid. A **580**, 679 (1994).

† Condensed from References[1] and[2].

Nucleon mass and strange content from (2+1)-flavor Domain Wall Fermion

Y. Aoki, T. Blum, T. Izubuchi, C. Jung, M. Lin, S. Ohta, S. Sasaki, E. Shintani and T. Yamazaki*1

Strange content of Nucleon ($\langle N|\bar{s}s|N\rangle$) and related quantities

$$f_{T_s} = \frac{m_s\langle N|\bar{s}s|N\rangle}{m_N} = \frac{dm_N}{dm_s}\times\frac{m_s}{m_N}, \qquad \sigma_s = m_s\langle N|\bar{s}s|N\rangle$$

has been drawing much attention in the last few years, due to its implications to the dark matter candidate search[1]. We measure $\langle N|\bar{s}s|N\rangle$ by applying Feynman-Hellman theorem $\langle N|\bar{s}s|N\rangle = dM_N(m_s')/(Z_m dm_s')$ to nucleon masses with reweighted sea strange mass $M_N(m_s')$. Strange quark reweighting has been successfully used to eliminate the systematic error from the discrepancy between dynamical strange quark mass (m_s) and the physical strange quark mass, and has shown to be usable in shifting m_s by up to $\sim 20\%$[2,3].

We used (2+1) dynamical flavor DWF with Iwasaki gauge action generated by RBC/UKQCD Collaborations with $a \sim 0.08$, 0.11fm[2], which we will refer to as DWF+I 0.08fm and 0.11fm ensemble respectively. We also measured nucleon mass and $\langle N|\bar{s}s|N\rangle$ on the DWF ensemble generated with Dislocation Suppressing Determinant Ratio(DSDR[4]) in addition to the Iwasaki gauge action (DWF+ID). Most of nulcleon propagators for DWF+ID ensembles were generated at RICC.

Figure 1 shows the nucleon mass as a function of pseudoscalar masses squared in physical units. The smallness of differences in masses between different ensembles suggests a^2 dependence of the nucleon mass is relatively small.

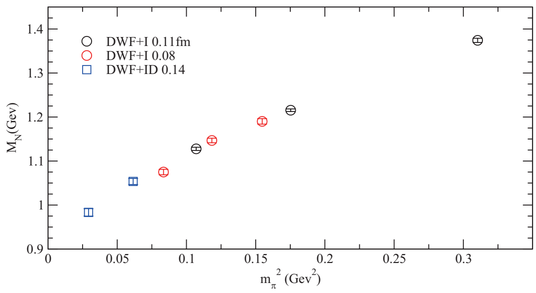

Fig. 1. Nucleon masses of the ensembles used in this analysis in physical units.

$\langle N|\bar{s}s|N\rangle$ for each ensemble($\langle N|\bar{s}s|N\rangle(m_l, a)$) and the continuum limit is calculated by fitting the rewighted nucleon masses $M_N(m_s', m_l, a)$ to

$$\begin{aligned} M_N(m_s', m_l, a) &= c_0' + \langle N|\bar{s}s|N\rangle(m_l, a)m_s', \\ \langle N|\bar{s}s|N\rangle(m_l, a) &= c_0 + c_1 m_l (+c_2 a^2). \end{aligned} \tag{1}$$

We used fits both with and without $c_2 a^2$ in Eq. (1), to estimate systematic error from the continuum extrapolation. A preliminary extrapolation to the continuum limit and physical pion mass gives $\langle N|\bar{s}s|N\rangle = 0.33(31)$ at 2Gev with $\overline{MS}$ while fitting without a^2 gives 0.09(16), which in turn gives

$$f_{T_s} = 0.035(33)(\text{with } a^2), \qquad 0.009(17)(\text{without } a^2).$$

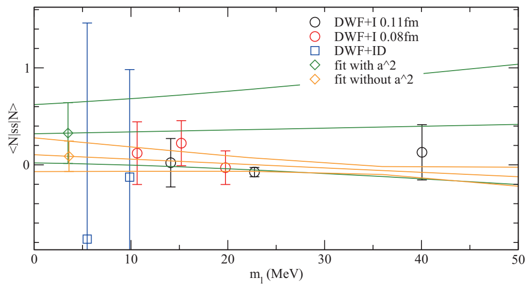

Fig. 2. Preliminary fits of nucleon strange contents calculated via Feynman-Hellman theorem and mass reweighting, renormalized at 2Gev.

While results with the currently available measurements on DWF+ID ensembles are still too noisy, it appears quite possible that further optimization of sources for the measurement of nucleon mass as well as increased statistics can improve the signal for $\langle N|\bar{s}s|N\rangle$ significantly without the need to extend the ensemble. Recent developments of various techniques such as EigCG[5] and Low/All mode averaging(LMA/AMA)[6] makes it possible to generate a large number of propagators per configurations at a numerical cost only a few times the cost for single propagator. Nucleon studies are particularly well suited to take advantage of this, as the correlation length for nucleons are much shorter than those for the light mesons. An exploratory study with AMA is in progress.

References

1) J. R. Ellis *et al.*, *Phys.Rev.* **D77** (2008) 065026,
2) Y. Aoki *et al. Phys.Rev.* **D83** (2011) 074508,
3) R. Arthur *et al.* `arXiv:1208.4412 [hep-lat]`.
4) D. Renfrew *et al.*, *PoS* **LATTICE2008** (2009) 048,
5) A. Stathopoulos *et al. SIAM J.Sci.Comput.* **32** (2010).
6) T. Blum *et al.*, `arXiv:1208.4349 [hep-lat]`.

*1 KMI, Nagoya University

Nucleon form factors with domain wall fermions on the lattice†

Y. Aoki, T. Blum, T. Izubuchi, C. Jung, M. Lin, S. Ohta, S. Sasaki, E. Shintani and T. Yamazaki

Understanding the internal structure of nucleons has long been a central mission of the theoretical and experimental nuclear physics research. The recent discovery of a "shrunk" proton[1)] makes first-principles high-precision calculations of observables pertinent to the nucleon internal structure using lattice QCD techniques both timely and essential. While in the past decade or so the numerical techniques of such calculations have been improved greatly, some results are still plagued with systematic errors that remain to be understood. Most notably, lattice results for the nucleon axial charge, g_A, are consistently lower than the experimental value by 10%-20%. Similar behavior has also been observed in the results for the isovector Dirac charge radius.

To tackle the systematic errors that may obscure the results, we performed lattice calculations in a large volume, with a sufficiently large source-sink separation and at pion masses as close to the physical point as possible. Specifically, we did our calculations on $32^3 \times 64$ lattices with 2+1 flavor domain wall fermions, generated by the RBC and UKQCD collaborations[2)]. These lattices have a physical spatial volume of about $(4.7\text{fm})^3$ and two pion masses of about 170 and 250 MeV (a physical pion mass is about 140 MeV). We set the source-sink separation to be about 1.3 fm, which is among the largest used in nucleon three-point functions in recent lattice calculations, to suppress excited-state contaminations. This report will focus on the calculation of the nucleon electromagnetic form factors which are directly related to the proton size. Other observables are reported by Jung[3)] and Ohta[4)].

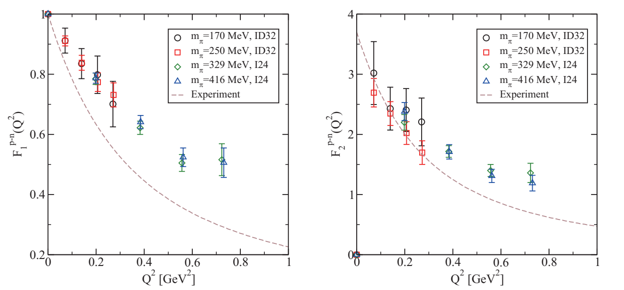

Fig. 1. The isovector nucleon Dirac (left) and Pauli (right) form factors. The results from current calculation are labeled as "ID32". Results labeled as "I24" are from earlier calculations[5)].

With 412 and 660 measurements for the pion mass of 170 MeV and 250 MeV, respectively, we obtained the isovector nucleon Dirac and Pauli form factors, $F_1^{p-n}(Q^2)$ and $F_2^{p-n}(Q^2)$ respectively. The results, along with earlier calculations[5)], are shown in Fig. 1. The pion mass dependence for $F_1(Q^2)$ is very mild for all the ensembles, and the Q^2 dependence is not as steep as the Kelly parametrization of the experimental data[6)], shown as the dashed lines in Fig. 1. The ID32 results for $F_2(Q^2)$, neverthelessly, seem to agree with the experimental curve at smaller Q^2 values.

The Dirac and Pauli charge radii, which are related to the proton and neutron radii, were determined from the dipole fits to $F_1(Q^2)$ and $F_2(Q^2)$. Our results, along with earlier calculations, are shown in Fig. 2. For $\langle r_1^2 \rangle^{1/2}$, all the results seem to fall on a straight line with respect to m_π^2, and can be linearly extrapolated to a value which is 20%-30% lower than the experiment. This, not-well-understood, behavior has been observed in other lattice calculations too, as summarized in[5)]. The results for $\langle r_2^2 \rangle^{1/2}$ approach the experimental value with some scatter. The two outliers may be suffering from larger finite volume effects compared to the rest. We plan to investigate this further by increasing the statistics and studying the finite volume effects.

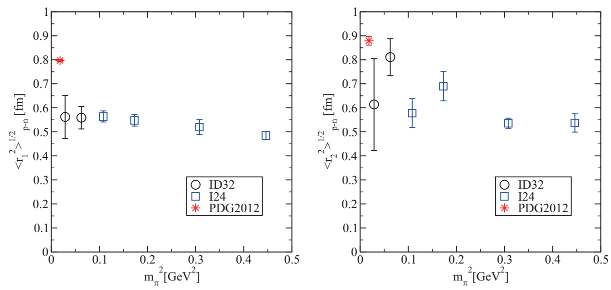

Fig. 2. Pion mass dependence of the isovector Dirac (left) and Pauli (right) r.m.s radii.

Part of this work was done on the RIKEN Integrated Cluster of Clusters (RICC) and the Teragrid/XSEDE computing resources supported by US National Science Foundation.

References

1) R. Pohl *et al.*, Nature **466**, 213 (2010).
2) R. Arthur *et al.*, arxiv:1208.4412 (2012).
3) C. Jung, PoS **LATTICE2012**, 164 (2012).
4) S. Ohta, PoS **LATTICE2012**, 171 (2012).
5) T. Yamazaki *et al.*, Phys. Rev. **D79**, 114505 (2009).
6) J. J. Kelly, Phys. Rev. **C70**, 068202 (2004).

† Condensed from PoS **LATTICE2012**, 172 (2012)

Finite-size scaling of nucleon axial charge in lattice QCD at nearly physical pion mass†

Y. Aoki, T. Blum, T. Izubuchi, C. Jung, M. Lin, S. Ohta, S. Sasaki, E. Shintani, and T. Yamazaki

Understanding nucleon structure is the main goal of RIKEN-BNL Research Center (RBRC). Nucleon is the main building block of baryonic matter that makes up ourselves and our environment, carrying the great majority of mass. Quantum chromodynamics (QCD), through its non-perturbative lattice numerical studies, provides a detailed account of how quarks and gluons, confined within nucleon, contribute such large mass despite their own lightness, which is not so different from electron or neutrino. By expanding the calculations we can account for nucleon structure, how the momentum, angular momentum, and electroweak currents are distributed within. We are leading the world in this field[1–3], distinguishing ourselves with almost exact chiral and flavor symmetries[4,5] of domain-wall fermions (DWF). In this article we report an aspect of the latest of such calculations[6], the finite-size scaling of the ratio of nucleon isovector axial vector and vector charges, g_A/g_V, with an unprecedented large lattice volume, about $(4.6\text{fm})^3$, and nearly physical pion mass values of about 250 and 170 MeV[5].

The lattice-QCD ensembles are generated jointly by the RIKEN-BNL-Columbia (RBC) and UKQCD collaborations: the strange-quark mass is set almost exactly at its physical value, and then reweighed to the exact value. The up- and down-quark mass are set degenerate and as light as practical, resulting in pion mass of about 250 and 170 MeV respectively[4,5]. We have accumulated about 1,500 gauge configurations for each ensemble, and are using one in eight of them for the present analysis. The nucleon mass is estimated as about 1.05 and 0.98 GeV respectively for the heavy and light ensembles. We are calculating all the form factors of the isovector vector and axialvector currents, some low-moments of the isovector unpolarized and polarized structure functions, and the strangeness content. We refer Refs.[1–3] for details of our analysis methods. Analysis for the heavy, 250-MeV, ensemble has been completed using the RIKEN RICC computers. That for the light, 170-MeV, ensemble is on-going using the US Teragrid/XSEDE computers.

From the calculated isovector vector charge, g_V, we confirm the chiral and flavor symmetries are very well preserved for the ensembles[6]. In Fig. 1 we summarize the calculations of the ratio, g_A/g_V, of the isovector axialvector charge, g_A, and vector charge. The ratio determines neutron life, among other things, and hence in turn nuclear isotope stability. It also determines the pion-nucleon coupling through the Goldberger-Treiman relation, and thus a major part of nuclear force, and in turn a major part of nuclear dynamics. Both the present (red) and previously published (blue)[1] calculations are plotted against a finite-size scaling parameter, $m_\pi L$, the product of the calculated pion mass, m_π, and the lattice spatial extent, L. The two calculations are very much different in their numerical sets up: a) the gauge actions are different, resulting in quite different momentum cuts off, $a^{-1} \sim 1.4$ GeV and 1.7 GeV, b) The up- and down-quark mass is set differently, so m_π are different, and c) L is set differently by almost a factor of two. Nonetheless the calculated values of the ratio, g_A/g_V, 1.15(5) in the present and 1.19(4) earlier, agree with each other very well at $m_\pi L \sim 5.8$. This confirms the deficit in the lattice calculations and supports our conjecture that the deficit arises from the small finite volume of the lattice that cannot contain virtual pion cloud surrounding the nucleon sufficiently well. We are increasing our statistics to understand this effect better, especially for the light ensemble. Momentum-transfer dependence of all the isovector form factors are being calculated as well.

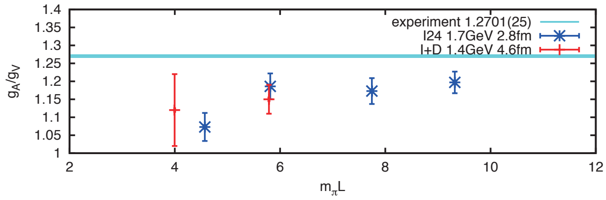

Fig. 1. Ratio g_A/g_V of isovector axial and vector charges, plotted against finite-size scaling parameter, $m_\pi L$, for the present (red) and published(blue)[1] calculations.

Further reducing the statistical error, especially for the light ensemble at m_π=170 MeV, is essential. We are actively pursuing this goal by improving our algorithms as well as computers.

† Condensed from the article in PoS Lattice2012 (2012) 171

References

1) T. Yamazaki *et al.*, Phys. Rev. Lett. **100**, 171602 (2008).
2) T. Yamazaki *et al.*, Phys. Rev. D **79**, 114505 (2009).
3) Y. Aoki *et al.*, Phys. Rev. D **82**, 014501 (2010).
4) Y. Aoki *et al.* Phys. Rev. **D83**, 074508 (2011).
5) R. Arthur, *et al.* arXiv:1208.4412 [hep-lat].
6) M. Lin *et al.* PoS LATTICE **2012**, 171 (2012).

Use of perturbative expansions in non-perturbative lattice computations – $\not{A}$-SeqSrc method in a QCD+QED system –

T. Izubuchi

We propose a perturbative series expansion with respect to the electric charge e, applied to a non-perturbative computation in lattice a QCD+QED system in a new way. As a concrete example, pion two pint Green's function in a QCD+QED system could be studied in fully non-perturbative ways[1)2)]. The quark propagators $S(x, y)$ in the background of $SU(3) \times U(1)$ gauge field, $U'_\mu(x) = U_\mu(x)e^{ieA\mu(x)}$, is computed by inverting the Dirac operator, $S(x, y) = [D(x, y)]^{-1}$, which is then contracted to make a pion propagator, $G(x, y) = -\mathrm{Tr}[S(x, y)S^\dagger(y, x)]$. Its large Euclidean time behavior will allow us to extract the pion mass as a function of input electric charge, $\sum_{\vec{x}} G(x, y) \sim C(e^2)\exp[-|x_4 - y_4|m_\pi(e^2)]$.

This fully non-perturbative treatment does not exploit the smallness of the QED coupling, $\alpha = e^2/4\pi \approx 1/137$. Alternatively, we could repeat the aforementioned standard procedure with a direct application of $e-$expansion at the quark level, $S = S|_{e=0} + e\partial_e S|_{e=0} + e^2/2!\partial_e^2 S|_{e=0} + \cdots$. From a matrix identity, $\partial_e S = \partial_e D^{-1} = -S(\partial_e D)S$, each term in $e-$expansion is easily evaluated, *e.g.* ($S^{(0)} = S|_{e=0}$)

$$\partial_e S = iS^{(0)} \not{A} S^{(0)} \quad , \tag{1}$$

$$\partial_e^2 S = -S^{(0)} \not{A} S^{(0)} \not{A} S^{(0)} - S^{(0)} \not{A}^{(2)} S^{(0)} \quad . \tag{2}$$

On la attice, the rhs of $\partial_e^2 S$ is computed using the sequential source method:

$$DX_0 = b, DX_1 = \sum_x \not{A}(x)X_0(x) \rightarrow X_1 = S^{(0)} \not{A} S^{(0)} b \quad . \tag{3}$$

Here, $\not{A} = -i\partial_e D = A_\mu(x)\mathcal{V}_\mu$ and $\mathcal{V}_\mu$ is nothing but the kernel of the conserved vector current $V_\mu^{(\mathrm{cons})} = \bar{q}\mathcal{V}_\mu q$ made of quark fields $q(x)$ by definition. In the continuum theory, $\mathcal{V}_\mu = \gamma_\mu$, and $\not{A}^{(2)}$ is the sea-gull type two photon vertex, which is a lattice artifact.

One could now extract pion's 2pt function in arbitrary order in e *separately*. As an example, $O(e^2)$ contributions for G are

$$\begin{aligned} G^{(2)} = &-(S^{(0)} \not{A} S^{(0)})(S^{(0)} \not{A} S^{(0)})^\dagger \\ &-1/2(S^{(0)} \not{A} S^{(0)} \not{A} S^{(0)})(S^{(0)})^\dagger \\ &-1/2(S^{(0)} \not{A}^{(2)} S^{(0)})(S^{(0)})^\dagger + \cdots \quad . \end{aligned} \tag{4}$$

When these $G^{(n)}$ are summed over the Boltzmann ensemble of the dynamical photon field, $A_\mu(x)$, the photon propagator, $\langle A_\mu(x)A_\nu(y)\rangle \sim \int dk e^{ik(x-y)}\delta_{\mu\nu}/k^2$, automatically connects pairs of $\not{A}$'s in (4) in all possible ways.

These are rather standard exercises of the perturbative expansion of the lattice field theory, but there are the following significant benefits when this $\not{A}$-SeqSrc method is implemented in the numerical simulation of lattice QCD+QED.

First, an arbitrarily high order of e contribution could be computed without larger statistical noise from the lower order contributions, and also each topologies of diagram could be separately obtained even within the same order in e.

For example, by taking the ratio of $O(e^2)$ to $O(e^0)$ contributions of pion propagators $G(x, y)$, one could extract the electromagnetic contribution for the pion masses : $G^{(2)}(x, y)/G^{(0)}(x, y) \sim 1 + \ln C(e^2)/C(0) - [m_\pi(e^2) - m_\pi(0)]|x_0 - y_0| + O(e^4)$. This capability of computing order-by-order and diagram-by-diagram is particularly useful for computing the important $O(e^6)$ hadronic contributions to the muon's anomalous magnetic moment. We could avoid a difficult subtraction by the $\not{A}$-method[3)].

Since we are computing each order of e^n, we could trivially change the value of electric charges. Thus, up-type quarks ($+2/3e$) and down-type quarks ($-1/3e$) could be computed by one same calculation when their masses are same.

Finally, the quark propagators $S^{(0)}$ used in (4) are the one only for $SU(3)$ background field, $U_\mu(x)$, without the photon fields, $A_\mu(x)$, whose effects are captured by $\not{A}$ vertices, not in the propagators. The most demanding part is the computation of the quark propagators and, by removing the $U(1)$ field from the propagator computation, the computational cost is significantly reduced. This is even more so when combined with recently proposed All-Mode Averaging (AMA)[4)], which reduces the computational costs by a significant factor, as much as $O(100)$, for light quarks and large lattice volumes in current state-of-the-art lattice computations.

References

1) T. Blum, R. Zhou, T. Doi, M. Hayakawa, T. Izubuchi, S. Uno and N. Yamada: Phys. Rev. D **82**, 094508 (2010) [arXiv:1006.1311 [hep-lat]].
2) T. Ishikawa, T. Blum, M. Hayakawa, T. Izubuchi, C. Jung and R. Zhou: Phys. Rev. Lett. **109**, 072002 (2012) [arXiv:1202.6018 [hep-lat]].
3) T. Blum, M. Hayakawa and T. Izubuchi: PoS LATTICE **2012**, 022 (2012) [arXiv:1301.2607 [hep-lat]].
4) T. Blum, T. Izubuchi and E. Shintani: arXiv:1208.4349 [hep-lat].

Lattice QCD studies of three-nucleon forces using the unified contraction algorithm †

T. Doi

Nuclear forces are fundamental quantities in nuclear physics, and it is of crucial importance to determine them from the underlying theory, QCD. Among others, the determination of three-nucleon forces (3NF) has a huge impact on not only nuclear physics but also astrophysics. In particular, recent observational data on the maximum mass of neutron stars triggered renewed interest in the nuclear equation of state at high density, where 3NF is considered to play a key role.

As for the first-principles determination of two-nucleon forces (2NF), a novel approach based on the Nambu-Bethe-Salpeter (NBS) wave function in lattice QCD has been recently proposed[1,2)], so that the potential is faithful to the phase shift by construction. The method has been successfully extended to various two-hadron interactions, such as hyperon interactions. Recently, the method itself has been generalized to the "time-dependent" HAL QCD method, so that the energy-independent (non-local) potential can be extracted without ground state saturation[3)]. See Refs.[2,4)] for recent reviews.

We perform the first lattice QCD study for 3NF[5)] by calculating the NBS wave function of three nucleons (3N) on the lattice, $\psi_{3N}(\vec{r},\vec{\rho},t)$, defined through the six-point correlator as

$$\begin{aligned}&\psi_{3N}(\vec{r},\vec{\rho},t-t_0)\times e^{-3m_N(t-t_0)}\\&\equiv \langle 0|(N(\vec{x}_1)N(\vec{x}_2)N(\vec{x}_3))(t)\ \overline{(N'N'N')}(t_0)|0\rangle, \quad (1)\end{aligned}$$

where $\vec{R}\equiv(\vec{x}_1+\vec{x}_2+\vec{x}_3)/3$, $\vec{r}\equiv\vec{x}_1-\vec{x}_2$, $\vec{\rho}\equiv\vec{x}_3-(\vec{x}_1+\vec{x}_2)/2$ are the Jacobi coordinates.

In the calculation of Eq. (1), one of the most challenging issues is the computational cost. Actually, it is well known that the cost of the contraction is exceptionally enormous for larger baryon number A, since (i) the number of quark permutations grows factorially with A and (ii) the contraction of color/spinor degrees of freedom becomes exponentially large for large A.

On this issue, we recently developed a novel algorithm, called "unified contraction algorithm"[6)]. Essentially, the idea is to consider the permutations and the color/spinor contractions simultaneously. In fact, if the quarks of the same flavor have the same space-time smearing function at the sink and/or source, a permutation of quark operators is equivalent to a permutation of color and spinor indices of the corresponding quark. Since color/spinor indices are dummy indices, we can carry out full permutations in advance of the lattice simulation. Thus, a significant reduction in the cost is achieved[6)], e.g., by a factor of 192 for ^{3}H/^{3}He nuclei, a factor of 20736 for the ^{4}He nucleus, and a factor of $\mathcal{O}(10^{11})$ for the ^{8}Be nucleus.

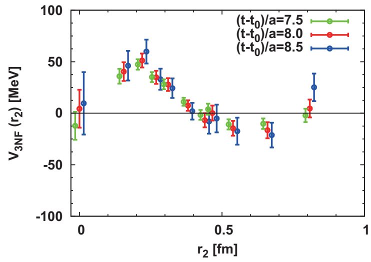

Fig. 1. The genuine 3NF in the triton channel with the linear setup, determined at each sink time.

This new algorithm enables calculation of the NBS wave function of 3N at each time slice. In Fig. 1, we show the results for 3NF in the triton channel for the "linear setup" with $\vec{\rho}=\vec{0}$, where 3N are aligned linearly with equal spacings of $r_2\equiv|\vec{r}|/2$. We employ $N_f=2$ dynamical clover fermion configurations generated by CP-PACS Collaboration, where $a^{-1}=1.269(14)$ GeV, $V=L^3\times T=16^3\times 32$, and $m_\pi=1.1$ GeV, $m_N=2.2$ GeV[8)].

The results shown here correspond to the update of those in Ref.[5)], where the method is improved from the original (time-independent) HAL QCD method to a time-dependent one, so that systematic errors from excited-state contaminations are suppressed. While 3NF are found to be small at large distances, in accordance with the suppression of two-pion exchange 3NF by the heavy pion, we observe an indication of repulsive 3NF at short distances. Note that a repulsive short-range 3NF is phenomenologically required to explain the properties of high density matter.

Further studies with finer lattices, lighter quark masses, and different geometries of 3N are in progress.

† Condensed from the article in Refs.[5–7)].

References
1) N. Ishii, S. Aoki and T. Hatsuda: Phys. Rev. Lett. **99**, 022001 (2007) [nucl-th/0611096].
2) S. Aoki, T. Hatsuda and N. Ishii: Prog. Theor. Phys. **123**, 89 (2010) [arXiv:0909.5585 [hep-lat]].
3) N. Ishii *et al.* [HAL QCD Collaboration]: Phys. Lett. B **712**, 437 (2012) [arXiv:1203.3642 [hep-lat]].
4) S. Aoki *et al.* [HAL QCD Coll.]: Prog. Theor. Exp. Phys. **2012**, 01A105 (2012) [arXiv:1206.5088 [hep-lat]].
5) T. Doi *et al.* [HAL QCD Collaboration]: Prog. Theor. Phys. **127**, 723 (2012) [arXiv:1106.2276 [hep-lat]].
6) T. Doi and M. G. Endres: Comput. Phys. Commun. **184**, 117 (2013) [arXiv:1205.0585 [hep-lat]].
7) T. Doi [HAL QCD Collaboration]: PoS LATTICE **2012**, 009 (2012) [arXiv:1212.1572 [hep-lat]].
8) A. Ali Khan *et al.* [CP-PACS Coll.]: Phys. Rev. D **65**, 054505 (2002) [E: D **67**, 059901 (2003)].

Lattice QCD with strong external electric fields†

A. Yamamoto

Quarks interact with gluons as well as photons. Generally, the electromagnetic interaction is neglected in most lattice QCD simulations since it is much weaker than the strong interaction. However, the electromagnetic interaction becomes important in several situations. For example, recent high precision simulations require the inclusion of the dynamical QED effect in order to reproduce isospin breakings correctly. Such simulations can reproduce the electromagnetic properties of hadrons. Further, strong background electromagnetic fields are important for QCD phenomenology. Even if the electromagnetic coupling is smaller than the QCD coupling, strong electromagnetic fields can drastically affect hadron properties. Physics in strong magnetic fields is a hot topic in lattice QCD.

Compared to strong magnetic fields, strong electric fields are not well studied in lattice QCD. This is due to some technical reasons. The lattice simulations with electric fields have been performed only in few exceptional situations.[1] In this study, we performed the two-flavor full QCD simulation with strong external electric fields.

What we expect in strong electric fields is as follows. When a strong electric field is applied, quark-antiquark pairs are produced from the vacuum by the Schwinger mechanism.[2] The quarks and the antiquarks flow along the electric field. However, we cannot observe such a nonequilibrium process, that is, we can observe neither the Schwinger mechanism nor the flowing electric current. In lattice QCD simulations, observables must be measured under equilibrium conditions. The equilibrium state in the electric field is the final state after the charged particles flow and stop. In a finite box, the highest and lowest voltage regions exist somewhere. Positive charged particles stop at the lowest voltage region and negative charged particles stop at the highest voltage region. As a consequence, a nonuniform charge density distribution appears.

In the confinement phase, we need to take into account color confinement. Charged particles are created by the Schwinger mechanism, but they cannot flow freely due to the confining force. There are two possibilities to separate the charged particles in the confinement phase. The first possibility is meson condensation. Charged mesons can be formed when the voltage difference exceeds twice the lightest charged meson mass. The charge generation occurs only above this threshold. Because the lightest charged meson is a pion, the threshold is twice the charged pion mass. The second possibility is deconfinement. The electric field tries to separate a pair of particles with opposite charges. When the electric field overcomes the confining force, the charged particles can be separated. The threshold of the voltage is the neutral pion mass. Note that, quantitatively, these thresholds can be shifted from the original pion mass by the effect of the electric field.

In Fig. 1, we show the numerical result of the charge density n_3 as a function of the applied voltage V. In the deconfinement phase, the charge density grows monotonically because the charged particles flow freely. In the confinement phase, the interpretation of the result is nontrivial. If the charge density were generated by the pion condensation, the charge density would be zero in $eV < 2m_\pi$. The charge density is non-zero in $aeV < 2am_\pi \simeq 0.52$. The charge density in $eV < 2m_\pi$ is generated not by the meson condensation but by the deconfinement in a finite volume. The charge density is non-zero even at $aeV = 0.24$, which is slightly below m_π. This is not surprising because the pion mass is shifted by the electric field. For a smaller voltage $eV \ll m_\pi$, the charge density is not generated. This is consistent with the expectation that the QCD vacuum is an insulator at zero temperature.

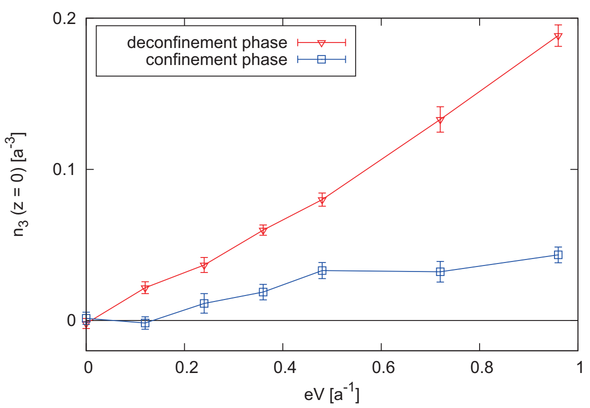

Fig. 1. Voltage dependence of the charge density.

† Condensed from the article in Phys. Rev. Lett. **110**, 112001 (2013).

References

1) H. R. Fiebig, W. Wilcox and R. M. Woloshyn: Nucl. Phys. B **324**, 47 (1989); J. C. Christensen, W. Wilcox, F. X. Lee and L. -m. Zhou: Phys. Rev. D **72**, 034503 (2005); E. Shintani *et al.*: Phys. Rev. D **75**, 034507 (2007); M. Engelhardt: Phys. Rev. D **76**, 114502 (2007); E. Shintani, S. Aoki and Y. Kuramashi: Phys. Rev. D **78**, 014503 (2008); W. Detmold, B. C. Tiburzi and A. Walker-Loud: Phys. Rev. D **79**, 094505 (2009); Phys. Rev. D **81**, 054502 (2010); M. D'Elia, M. Mariti and F. Negro: Phys. Rev. Lett. **110**, 082002 (2013).
2) J. S. Schwinger: Phys. Rev. **82**, 664 (1951).

5. Particle Physics

Automated lattice perturbation theory and relativistic heavy quarks in the Columbia formulation[†]

C. Lehner

The automation of lattice perturbation theory (LPT) was pioneered by Lüscher and Weisz in Ref.[1)], where lists were used to represent the information required to evaluate gluonic Feynman diagrams numerically. Using a similar data structure, these early results were extended in Ref.[2)] to the case of fermionic actions, enhanced in Ref.[3)] to also allow for complex smearing, and further refined in Refs.[4)] for various fermionic actions.

Here we propose to use a more general data structure and represent the gluonic and fermionic actions as well as operators and matrix elements in a symbolic manner using a computer algebra system (CAS). This approach has found wide use in the automation of continuum perturbation theory, where many high-loop calculations are preformed using FORM[5)]. Unfortunately, FORM lacks features to efficiently handle the complicated vertices that arise in lattice actions. In this work, we introduce a new CAS optimized for LPT. We present a flexible framework on top of said CAS that is capable of performing perturbative calculations using a lattice regulator as well as a continuum regulator and to generate contractions for non-perturbative computations.

The framework found its first applications within the heavy-quark physics project of the RBC and UKQCD collaborations that uses RHQ in the Columbia formulation to describe the heavy quarks. Recent results have been presented in Refs.[9,10)]. Relativistic heavy quarks, first proposed in Ref.[11)] and further refined in Refs.[6,12)], provide an effective heavy-quark action for large quark masses that is smoothly connected to a fully relativistic quark action as the quark mass becomes small compared to the lattice cutoff. The Columbia formulation[6)] corresponds to the lattice action

$$S = \sum_x \overline{Q}(x) \Bigg((\gamma_0 D_0 - \frac{1}{2} D_0^2) + \zeta \sum_{i=1}^{3} (\gamma_i D_i - \frac{1}{2} D_i^2) + m_0 + c_P \sum_{\mu,\nu=0}^{3} \frac{i}{4} \sigma_{\mu\nu} F_{\mu\nu}(x) \Bigg) Q(x) \qquad (1)$$

with heavy-quark fields Q. The parameters m_0, ζ, and c_P can be tuned to remove $\mathrm{O}(a\vec{p})$ discretization errors in on-shell quantities, where $a\vec{p}$ corresponds to the spatial momentum of the heavy quark in lattice units.

If we allow for a field rotation $Q'(x) = Q(x) + d_1 \sum_{i=1,2,3} \gamma_i D_i Q(x)$ with parameter d_1, we can match the quark fields Q' to continuum fields. Such a field rotation, however, leaves the mass spectrum of the theory invariant, and m_0, ζ, and c_P can be tuned non-perturbatively without knowledge of d_1. Figure 1 compares the perturbative and non-perturbative results for c_P and ζ on the 24^3 lattices of Ref.[13)].

In Ref.[10)] preliminary results for f_B and f_{B_s} were presented with light domain-wall fermions. A publication containing further details is in progress[8)].

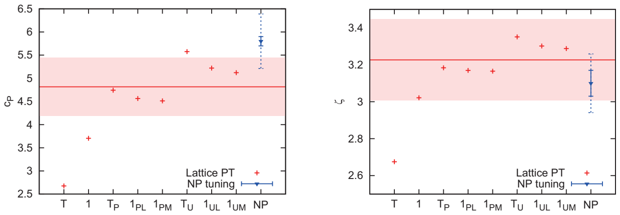

Fig. 1. Results for the perturbative tuning of parameters c_P and ζ on the 24^3 ensembles of Ref.[13)] for bottom quarks. We compare perturbative results with results of non-perturbative (NP) tuning. Perturbative results are given at tree level (T) or at one-loop level (1). The subscript P indicates that we use the average value of the plaquette for meanfield improvement, the subscript U indicates that the Landau gauge-fixed average link value was used for meanfield improvement. The subscript L denotes expansion in the bare lattice coupling, the subscript M denotes expansion in the $\overline{\mathrm{MS}}$ coupling constant at scale $1/a$, where a is the lattice spacing. The estimation of the errors is described in detail in Ref.[13)].

References

1) M. Luscher and P. Weisz, Nucl.Phys. **B266** (1986) 309.
2) A. Hart, G. von Hippel, R. Horgan and L. Storoni, J.Comput.Phys. **209** (2005) 340–353.
3) A. Hart, G. von Hippel, R. Horgan and E. Muller, Comput. Phys. Commun. **180** (2009) 2698–2716.
4) S. Takeda, Nucl.Phys. **B811** (2009) 36–65; D. Hesse, R. Sommer and G. von Hippel, PoS **LATTICE2011** (2011) 229.
5) J. A. M. Vermaseren.
6) N. H. Christ, M. Li and H.-W. Lin, Phys. Rev. **D76** (2007) 074505.
7) G. Passarino and M. J. G. Veltman, Nucl. Phys. **B160** (1979) 151.
8) C. Lehner, *In preparation*, 2012.
9) T. Kawanai, R. S. Van de Water and O. Witzel.
10) O. Witzel.
11) A. X. El-Khadra, A. S. Kronfeld and P. B. Mackenzie, Phys. Rev. **D55** (1997) 3933–3957.
12) S. Aoki, Y. Kuramashi and S.-i. Tominaga, Prog. Theor. Phys. **109** (2003) 383–413.
13) RBC Collaboration, UKQCD Collaboration, Y. Aoki *et al.*

† Condensed from the proceedings PoS LATTICE2012 (2012) 126

Neutral B meson mixing with domain-wall light and static b quark

T. Ishikawa, Y. Aoki, T. Izubuchi, and A. Soni*1 (for RBC Collaboration)

The Cabibbo-Kobayashi-Maskawa (CKM) matrix plays a key role in elementary particle physics. Constraints on the elements V_{ts} and V_{td} can be obtained from $B^0 - \overline{B^0}$ mixing. The mass difference between two neutral B mesons, which can be measured in experiments within 1% accuracy, is represented by

$$\Delta m_{B_q} = (\text{known factor}) \times |V_{tq}V_{tb}|^2\, m_{B_q}^{-1} \mathcal{M}_{B_q}, \quad (1)$$

where $q = \{d, s\}$, m_{B_q} and $\mathcal{M}_{B_q}$ denote B_q meson mass and mixing matrix element

$$\mathcal{M}_{B_q} = \langle \overline{B_q^0} | O^{\Delta B=2} | B_q^0 \rangle, \quad (2)$$

respectively. The ratio $|V_{ts}/V_{td}|$, which is powerful for constraining the CKM unitarity triangle, can be accessed through

$$\frac{\Delta m_{B_s}}{\Delta m_{B_d}} = \frac{|V_{ts}|^2}{|V_{td}|^2} \frac{m_{B_d}}{m_{B_s}} \frac{\mathcal{M}_{B_s}}{\mathcal{M}_{B_d}} = \frac{|V_{ts}|^2}{|V_{td}|^2} \frac{m_{B_s}}{m_{B_d}} \xi^2, \quad (3)$$

where ξ is called the $SU(3)$ flavor breaking ratio. By virtue of the ratio quantity, the theoretical uncertainties are mostly cancelled. All we need is a precise calculation of $\mathcal{M}_{B_q}$, which is highly non-perturbative, and the lattice QCD can access it, in principle.

The b quark on the lattice is, however, problematic, owing to large separation of energy scale between light and b quarks. Among several approaches, we use static approximation for the b quark, which is the leading order of the heavy quark effective theory (HQET). The static approximation is known to have $O(\Lambda_{\mathrm{QCD}}/m_b) \sim 10\%$ uncertainty. For a ratio quantity like ξ, however, the uncertainty is reduced to $O(m_s/m_b) \sim 2\%$. In addition, the static limit values are always important as an anchor point for other heavy quark approaches.

Our simulation is performed with domain-wall light quarks using 2+1 flavor Iwasaki gluon ensemble generated by RBC/UKQCD Collaborations[1]. In the static b quark action, two types of link smearing (HYP1, HYP2) are used for improving the S/N. Matching with continuum QCD is done by one-loop perturbation taking into account the $O(a)$ lattice discretization error.[2] Obtained results are extrapolated to physical quark mass point and continuum limit. Fig. 1 shows the chiral and continuum extrapolations for $(\mathcal{M}_{B_s}/\mathcal{M}_{B_d})^{1/2}$. The HYP1 and HYP2 data give consistent results with each other. We present a comparison of our results with other approaches in Figs. 2 and 3. Although the B meson decay constants f_{B_q} give $\sim 10\%$ difference from other groups, which can be understood owing to the static approximation, the ratio quantities f_{B_s}/f_{B_d} and ξ show good agreement with the other approaches, as anticipated.

*1 Brookhaven National Laboratory

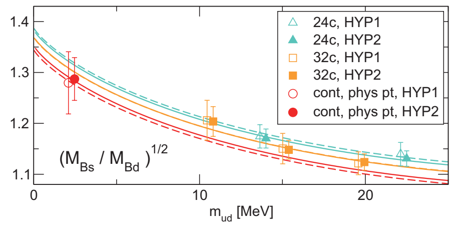

Fig. 1. Chiral and continuum extrapolations for $(\mathcal{M}_{B_s}/\mathcal{M}_{B_d})^{1/2}$. Fine (32c) and coarse (24c) lattices are used for obtaining the continuum results (red lines and symbols).

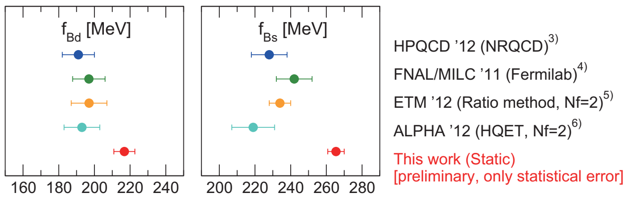

Fig. 2. Comparison of f_{B_d} and f_{B_s} with other groups' results. Only statistical error is included in our results, whereas systematic errors are taken into account in other group's ones.

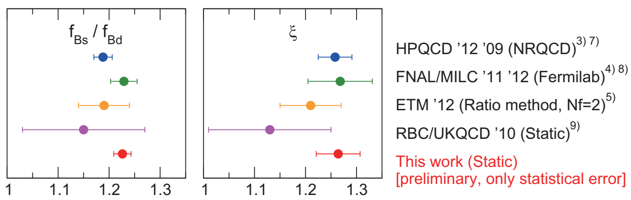

Fig. 3. Comparison of f_{B_s}/f_{B_d} and ξ with other groups' results.

Further study with an improved numerical method, such as all-mode averaging[10], is in progress in order to achieve substantial high precision.

References

1) Y. Aoki *et al.* [RBC and UKQCD Collaborations] : Phys. Rev. D **83**, 074508 (2011).
2) T. Ishikawa *et al.* : JHEP **1105**, 040 (2011).
3) H. Na *et al.* [HPQCD Collaboration] : Phys. Rev. D **86**, 034506 (2012).
4) A. Bazavov *et al.* [Fermilab Lattice and MILC Collaboration] : Phys. Rev. D **85**, 114506 (2012).
5) N. Carrasco *et al.* [ETM Collaboration] : PoS LATTICE **2012**, 104 (2012).
6) F. Bernardoni *et al.* [ALPHA Collaboration] : arXiv:1210.6524 [hep-lat].
7) E. Gamiz *et al.* [HPQCD Collaboration] : Phys. Rev. D **80**, 014503 (2009).
8) A. Bazavov *et al.* [Fermilab Lattice and MILC Collaboration] : Phys. Rev. D **86**, 034503 (2012).
9) C. Albertus *et al.* [RBC and UKQCD Collaborations] : Phys. Rev. D **82**, 014505 (2010).
10) T. Blum *et al.* : arXiv:1208.4349 [hep-lat].

QCD phase diagram with two-flavor lattice fermion formulations†

T. Misumi,*[1] T. Kimura, and A. Ohnishi*[2]

Quantum chromodynamics (QCD) under extreme conditions with temperature and density is one of the most challenging topics in hadron physics. In this report we propose a new framework of investigating the 2-flavor QCD with finite temperature and density by using the Karsten-Wilczek (KW) lattice fermion,[1,2] which possesses only two species doublers, i.e., minimally doubled fermion. This lattice formulation lifts degeneracy of 16 species without breaking its chiral symmetry by introducing a species-dependent imaginary chemical potential, instead of a species-dependent mass term introduced in the Wilson fermion formalism. Because of the chemical potential term, its discrete symmetry is not sufficient to be applied to fully Lorentz symmetric system, i.e., zero temperature and density, but enough to study the in-medium QCD.

The KW fermion is a kind of minimally doubled fermions, preserving its chiral symmetry and ultralocality, but breaking some of discrete spacetime symmetries. The Dirac operator in the momentum space yields

$$aD_{\rm KW}(p) = i\sum_{\mu=1}^{4}\gamma_\mu \sin ap_\mu + ir\gamma_4\sum_{j=1}^{3}(1-\cos ap_\mu). \quad (1)$$

In addition to this, we have to introduce dimension-3 and 4 counter terms, $i\mu_3\bar{\psi}\gamma_4\psi = i\psi^\dagger\psi$ and $id_4\bar{\psi}\gamma_4\partial_4\psi$, to take a correct Lorentz symmetric continuum limit. This has only two zeros at $p = (0,0,0,\arcsin(-\mu_3/(1+d_4))/a)$ when $-1-d_4 < \mu_3 < 1+d_4$ with $r=1$.

We study QCD phase diagram in the framework of the strong-coupling lattice QCD based on this KW-type minimally doubled fermion. The effective potential in terms of the meson field is obtained by performing the 1-link integral in the strong coupling limit ($g^2 \to \infty$), and then introducing auxiliary fields to eliminate the 4-point interactions. In the case with KW fermion, we have to consider both of the scalar $\sigma = \langle\bar{\psi}\psi\rangle$ and vector $\pi_4 = \langle\bar{\psi}i\gamma_4\psi\rangle$ condensates. Identifying $\bar{\psi}\gamma_4 = \psi^\dagger$, the latter corresponds to the imaginary density $i\langle\psi^\dagger\psi\rangle$. In the zero temperature case, we can solve the equilibrium condition analytically, and thus show the chiral phase transition is of 1st order because the order parameter σ changes discontinuously at the cricital chemical potential.

We can draw the phase diagram with respect to chiral symmetry by analyzing the effective potential $\mathcal{F}_{\rm eff}(\sigma,\pi_4)$ (Fig. 1). These results are qualitatively consistent with those with strong-coupling lattice QCD with staggered fermions, while there are some quantitative differences.[3] For example, the KW phase diagram is suppressed in T direction compared to that in staggered fermion. The μ_B dependence of σ and ρ_B seems to have some characteristics in Fig. 2. At $T = 0.3 > T^{\rm tri}$ with $m=0$, σ and ρ_B undergoes the 2nd-order phase transition at $\mu_B \simeq 0.5$, and at a larger μ_B ($\mu_B \simeq 1.15$), increasing rate of ρ_B as a function of μ_B becomes higher again. At lower temperature, $T = 0.2 < T^{\rm tri}$, partial restoration of the chiral symmetry is seen before the first order phase transition.

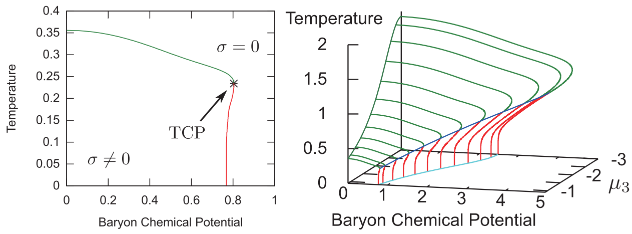

Fig. 1. (Left) Phase diagram for the chiral transition. The transition order is changed from 2nd (green) to 1st (red) at the tricritical point $(\mu_B^{\rm tri}, T^{\rm tri}) = (0.804, 0.234)$. (Right) Three-dimensional chiral phase diagram for T, μ_B and μ_3 for $m=0$.

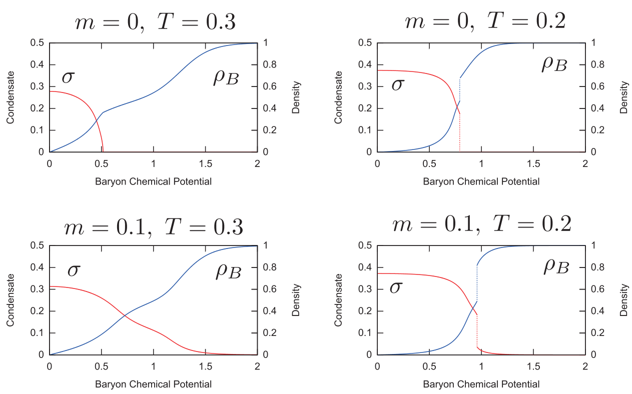

Fig. 2. Chiral condensate σ and the baryon density ρ_B for (left) $T=0.3$ and (right) $T=0.2$ with $d_4=0$. There are 1st and 2nd phase transitions for σ. In the case of $m \neq 0$, there appears the crossover behavior instead of the 2nd order transition.

References
1) L. H. Karsten, Phys. Lett. **B104** (1981) 315.
2) F. Wilczek, Phys. Rev. Lett. **59** (1987) 2397.
3) Y. Nishida, Phys. Rev. **D69** (2004) 094501.

† Condensed from the article in Phys. Rev. **D86** (2012) 094505.

*1 Physics Department, Brookhaven National Laboratory, USA
*2 Yukawa Institute for Theoretical Physics, Kyoto University

Strong-coupling analysis of parity phase structure in staggered-Wilson fermions†

T. Misumi,[*1] T. Z. Nakano,[*2,*3] T. Kimura, and A. Ohnishi[*3]

Since the dawn of lattice field theory, the doubling problem has been a notorious obstacle for lattice simulations. Recently, a new possibility of lattice fermion constructions was pointed out, which is called staggered-Wilson.[1)] It is constructed by introducing staggered versions of generalized Wilson terms[2)] into staggered fermions. As in the case of Wilson fermion, it is quite important to study the parity phase structure (Aoki phase)[3)] in staggered-Wilson fermions. In this report, we investigate strong-coupling lattice QCD with emphasis on parity phase structure for staggered-Wilson fermions.

We introduce "taste-dependent mass terms" which are generalizations of the Wilson term. There are two types of such terms, but we focus only on one of them, called Adams type. It is composed of four hopping terms,

$$M_{\mathrm{A}} = \epsilon \sum_{\mathrm{sym.}} \eta_1\eta_2\eta_3\eta_4 C_1C_2C_3C_4 = (\mathbb{1}\otimes\gamma_5)+\mathcal{O}(a) \quad (1)$$

with $\epsilon = (-1)^{x_1+\cdots+x_4}$, $\eta_\mu = (-1)^{x_1+\cdots+x_{\mu-1}}$, $C_\mu = (V_\mu + V_\mu^\dagger)/2$, $(V_\mu)_{xy} = U_{\mu,x}\delta_{y,x+\hat{\mu}}$. Added to usual staggered fermion actions, this term lifts the degeneracy of four tastes and ends up with two positive-mass flavors and two negative-mass flavors. The two branches correspond to $+1$ and -1 eigenvalues of γ_5 in the taste space. The Adams-type staggered-Wilson fermion action is given by

$$S_{\mathrm{F}} = \sum_{x,y} \bar{\chi}_x \left[\eta_\mu D_\mu + r(1+M_{\mathrm{A}}) + M\right]\chi_y, \quad (2)$$

with $D_\mu = (V_\mu - V_\mu^\dagger)/2$, where χ, r and M are the quark field, the Wilson parameter, and the usual taste-singlet mass, respectively. In lattice QCD simulations with these fermions, the mass parameter M has to be tuned to take a chiral limit as in the Wilson fermion.

In the strong-coupling limit we can drop the plaquette action. Then, by integrating out link variables in multi-hopping terms, the partition function for meson fields $\mathcal{M}_x(\chi_x\bar{\chi}_x)/N$ with the source J_x is given in the large N limit as

$$\mathcal{Z}(J) = \int \mathcal{D}[\bar{\chi},\chi,U]\,\exp\left[N\sum_x J_x\mathcal{M}_x + S_{\mathrm{F}}\right]$$
$$= \int \mathcal{D}\mathcal{M}\,\exp\left[N\left(\sum_x J_x\mathcal{M}_x + S_{\mathrm{eff}}(\mathcal{M})\right)\right]. \quad (3)$$

N is the number of color. We consider only scalar σ and pseudoscalar (pion) π condensates as $\mathcal{M}_x = \sigma + i\epsilon_x\pi = \Sigma\, e^{i\epsilon_x\theta}$. Then the effective action for the Σ and θ, up to $\mathcal{O}(\mathcal{M}^3)$, is factrized due to the translation invariance as $S_{\mathrm{eff}}(\mathcal{M}) = -V_4 V_{\mathrm{eff}}(\Sigma,\theta)$ with

$$V_{\mathrm{eff}}(\Sigma,\theta) = -\hat{M}\Sigma\cos\theta + \ln\Sigma + \left[f(\Sigma,\theta) - \ln\left[\frac{1+f(\Sigma,\theta)}{2}\right]\right] \quad (4)$$

where $f(\Sigma,\theta) = \sqrt{1-8\Sigma^2\sin^2\theta}$, and we denote $\hat{M}$ as the shifted mass parameter $\hat{M} = M + r$ with $r = 16\sqrt{3}$. Solving the saddle point conditions $\partial V_{\mathrm{eff}}(\Sigma,\theta)/\partial\Sigma = 0$ and $\partial V_{\mathrm{eff}}(\Sigma,\theta)/\partial\theta = 0$, the vacuum structure is determined. For $\hat{M}^2 > 4$, there is only the chiral condensate as

$$\frac{\langle\bar{\chi}\chi\rangle}{N} = \frac{1}{\hat{M}}, \qquad \frac{\langle\bar{\chi}i\epsilon_x\chi\rangle}{N} = 0\,. \quad (5)$$

On the other hand, for $\hat{M}^2 < 4$, a finite pion condensate appears and breaks the parity symmetry spontaneously,

$$\frac{\langle\bar{\chi}\chi\rangle}{N} = \frac{\hat{M}}{8-\hat{M}^2}, \quad \frac{\langle\bar{\chi}i\epsilon_x\chi\rangle}{N} = \pm\frac{\sqrt{2(4-\hat{M}^2)}}{8-\hat{M}^2}\,. \quad (6)$$

The sign of the pion condensate reflects the $\mathbb{Z}_2$ parity symmetry of the theory. The critical mass parameter is given by $\hat{M}_c^2 = 4$, or equivalently $M_c = -16\sqrt{3} \pm 2$. These results strongly suggest the existence of the parity-broken phase in the lattice QCD at least in the strong-coupling limit.

We can also derive the mass spectrum of the mesons by expanding the effective action $S_{\mathrm{eff}}(\mathcal{M})$ to the quadratic terms of the meson excitation field. The pion mass is derived from the corresponding propagator as

$$\cosh(m_\pi a) = 1 + 2\,\frac{\hat{M}^2-4}{5}. \quad (7)$$

The pion becomes massless at the critical mass $\hat{M}_c^2 = 4$, which indicates that a second-order phase transition occurs between the parity symmetric and broken phases in the strong-coupling limit.

References
1) D. H. Adams, Phys. Rev. Lett. **104** (2010) 141602; Phys. Lett. **B699** (2011) 394; C. Hoelbling, Phys. Lett. **B696** (2011) 422.
2) M. Creutz, T. Kimura, T. Misumi, JHEP **1012** (2010) 041; S. Durrand, G. Koutsou, Phys. Rev. **D83** (2011) 114512.
3) S. Aoki, Phys. Rev. **D30** (1984) 2653; M. Creutz, [arXiv:hep-lat/9608024]; S. Sharpe, R. Singleton. Jr, Phys. Rev. **D58** (1998) 074501.

† Condensed from the article in Phys. Rev. **D86** (2012) 034501.
*1 Physics Department, Brookhaven National Laboratory, USA
*2 Department of Physics, Kyoto University
*3 Yukawa Institute for Theoretical Physics, Kyoto University

Higgs mass in the Standard Model†

F. Bezrukov, M. Kalmykov,*1 B. Kniehl,*1 and M. Shaposhnikov*2

During the last year, the LHC revealed resonance at approximately 126 GeV, compatible with the Standard Model (SM) Higgs boson, and no observations of beyond SM physics.

If the only degrees of freedom are those of the SM, then the main concern at high energies becomes the renormalization group (RG) evolution of the Higgs boson self coupling λ. At one loop (leading) level, the fermionic (mainly top quark) contributions decrease λ, whereas the bosonic (from gauge bosons and Higgs boson itself) increase λ with energy. Thus, with all couplings of the SM fixed (keeping in mind the uncertainties in the top mass M_t and the strong coupling constant α_S), the situation depends on the value of λ, or equivalently on the Higgs boson mass M_h. For large M_h, the scalar sector enters strong coupling above some energy scale. At low M_h, the coupling constant λ becomes negative, leading to development of a new minimum in the Higgs effective potential $V(h) = \lambda(h)h^4/4$. The latter is not dangerous as it is, because the decay rate of the electroweak (EW) vacuum is exponentially suppressed. Only when the new minimum is sufficiently deep and appears at low field values, the decay rate becomes comparable with the age of the Universe[1)], making the model incompatible with observations. This bounds the pure SM Higgs boson mass to the region

$$111\,\mathrm{GeV} \lesssim M_h \lesssim 1\,\mathrm{TeV}.$$

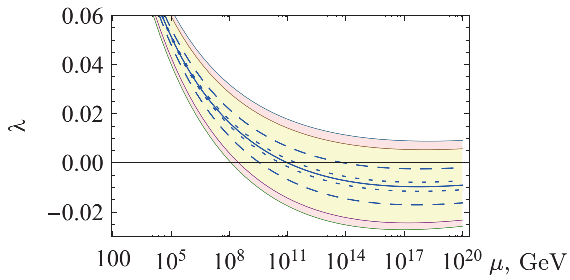

Fig. 1. Higgs coupling $\lambda(\mu)$ scale dependence for $M_h = 126\,\mathrm{GeV}$ with experimental and theoretical errors.

The Higgs boson mass corresponding to the boundary situation between these two regimes is unique for given values of all other SM parameters: Fermi constant, gauge couplings, and fermion masses. This is realized when the coupling constant only touches the zero axis, which gives two equations $\lambda(\mu_0) = d\lambda/d\log\mu|_{\mu_0} = 0$ determining two parameters—M_h and the scale μ_0, where λ vanishes (see Fig. 1).

† Based on article JHEP 1210, 140 (2012)
*1 II. Institut für Theoretische Physik, Universität Hamburg, Germany
*2 ITP EPFL, Switzerland

Conversion of this requirement into the physical values of the masses requires using three loop beta functions for the RG evolution between the EW scale and μ_0, and performing multiloop matching between the physical (pole) masses of the particles (Higgs boson and top quark, specifically) and the coupling constants in $\overline{\mathrm{MS}}$ scheme at the EW scale. The two-loop mixed electroweak-QCD corrections for this matching were obtained, improving the precision over the previous results. The resulting value of the critical Higgs boson mass is

$$M_h = 128.9\,\mathrm{GeV} + \frac{M_t - 172.9\,\mathrm{GeV}}{1.1\,\mathrm{GeV}} \times 2.2\,\mathrm{GeV} - \frac{\alpha_S - 0.1184}{0.0007} \times 0.6\,\mathrm{GeV} \pm 2\,\mathrm{GeV},$$

where the last term gives the theoretical uncertainties due to the higher loop contributions (coming mainly from the matching of the pole masses). This result is illustrated in Fig. 2. It is seen that with the current precision of the measurements of M_h, α_S, and M_t, it is impossible to ascertain whether the EW vacuum is stable, metastable, or the parameters correspond exactly to the borderline between the two cases.

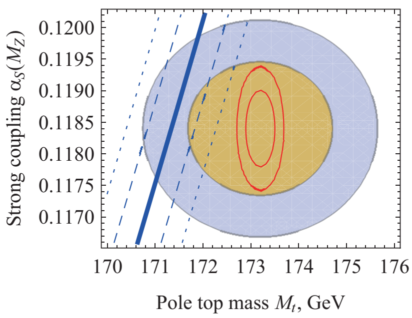

Fig. 2. Blue line corresponds to the critical Higgs mass of 126 GeV, with dashed lines indicating the theoretical error. Filled circles represent the experimental M_t and α_S precision, and red ellipses indicate the expected ILC precision.

Resolution of this question with more precise data may lead to exclusion of some of the extensions of the SM[2)], whereas others may be fully compatible with unstable EW vacuum[3)].

References

1) J. Elias-Miro et al.: Phys. Lett. B709, 222 (2012).
2) F. Bezrukov and M. Shaposhnikov: Phys. Lett. B659, 703 (2008).
3) D. Gorbunov and A. Tokareva: arXiv:1212.4466 [astro-ph].

Higgs, moduli problem, baryogenesis and large volume compactifications†

T. Higaki, K. Kamada,*1 and F. Takahashi*2

The energy density of baryons presently constitutes 4.6% of the total density of the universe[1]: $\Omega_B h^2 = 0.02223 \pm 0.00033$. $\Omega_B h^2$ is the energy density divided by the critical density that is measured by the expansion rate of the universe. The above equation can be translated as $n_B/s \approx 10^{-10}$, where n_B is the net number density of baryons and s is the entropy density in the universe. Furthermore, supersymmetry (SUSY) is one of the promising candidates for new physics. Hence, it is interesting to explain the baryon asymmetry in SUSY models, with which the 125 GeV Higgs-like particle discovered at the LHC can be realized in which flat directions suitable for the Affleck-Dine (AD) mechanism are present[2].

However, once SUSY-breaking is considered, moduli fields, which are the cause of the breaking, can produce a large entropy via their decays into the Standard Model radiation; consequently a baryon asymmetry much smaller than the observed one might be obtained. Therefore, one of the solutions is to produce a large asymmetry before the decays. For this purpose, we study the effect of a large coefficient c, which is inversely proportional to the cutoff scale M_* that is lower than the Planck scale $M_{\rm pl}$ (see Eq.(5)). A large c elongates the time scale of kicking the scalar quark (AD field) along the phase direction, thereby enhancing the asymmetry. This type of an elongated time scale can be realized by the string theory compactified on a large volume Calabi-Yau (CY) space via the volume moduli stabilization[3]:

$$K = -2\log\left[(T_b + T_b^\dagger)^{3/2} - (T_s + T_s^\dagger)^{3/2} + \xi\right], \quad (1)$$

$$W = W_0 + Ae^{-2\pi T_s}. \quad (2)$$

Here we used the Planck unit, i.e. $M_{\rm pl} = 2.4 \times 10^{18}\text{GeV} \equiv 1$. K and W are the Kähler potential and superpotential based on 4D $\mathcal{N} = 1$ effective supergravity, T_b and T_s are the overall volume and the hole size in a Swiss-cheese CY, $W_0 = \mathcal{O}(1)$ originates from closed string flux, and $\xi = \mathcal{O}(1)$ is dependent on the Euler number on the CY. The second term in the superpotential comes from an instanton on the small cycle; $A = \mathcal{O}(1)$. In the vacuum of the scalar potential, a large volume $\mathcal{V}$ of the CY is observed.

$$\mathcal{V} \sim (T_b + T_b^\dagger)^{3/2} \sim e^{2\pi T_s} \gg 1, \quad T_s \sim \xi^{2/3}. \quad (3)$$

As for the AD field localized on a singularity in the CY, the potential is given by

$$V = (m_0^2 - c^2H^2)|\phi|^2 + \frac{|\phi|^{2n-2}}{M_*^{2n-6}} + \left(A\frac{\phi^n}{M_*^{n-3}} + c.c.\right) \quad (4)$$

with the canonical kinetic term. Here, ϕ is the AD field, H is the Hubble scale coming from an inflaton, and c depends on $\mathcal{V}$.

$$c \equiv \frac{M_{\rm pl}}{M_*} \sim \mathcal{V}^{1/3} \gg 1. \quad (5)$$

For concreteness, we take $n = 6$, for example, the $\bar{u}\bar{d}\bar{d}$ flat direction as ϕ. Further it is noted that m_0 and A are soft SUSY-breaking terms dependent on $\mathcal{V}$: $m_0 = \mathcal{O}(\mathcal{V}^{-3/2} - \mathcal{V}^{-2}) \times M_{\rm pl} = \mathcal{O}(10^3 - 10^7)$GeV and $A = \mathcal{O}(\mathcal{V}^{-2}) \times M_{\rm pl} = \mathcal{O}(10^3)$GeV for $\mathcal{V} = \mathcal{O}(10^7)$ in the string unit. In such a case, the scalar top mass can be sufficiently heavy to realize the 125-GeV Higgs boson, and we hereafter consider $m_0 = 10^7$GeV for concreteness.

Before an estimation of the baryon asymmetry, we discuss the decay of $\Phi \equiv {\rm Re}(T_b)$, since it is lighter than T_s. The mass is then given by $m_\Phi \sim \frac{M_{\rm pl}}{\mathcal{V}^{3/2}} = \mathcal{O}(10^6)$GeV, and the decay into Higgs pairs reheats the universe at a temperature $T_{\rm dec}$ if kinematically allowed: $T_{\rm dec} \simeq \mathcal{O}(1) \times \left(\frac{m_\Phi}{10^6\text{GeV}}\right)^{3/2}$ GeV.

By solving the equation of motion of ϕ and considering a dilution by the modulus decay, the final baryon asymmetry can be determined[4]:

$$\frac{n_B}{s} \simeq 10^{-10} \times \delta_{\rm eff}\left(\frac{c}{10^2}\right)\left(\frac{T_{\rm dec}}{1\text{GeV}}\right)\left(\frac{m_0}{10^7\text{GeV}}\right)^{-1} \times \left(\frac{\phi_{\rm osc}}{10^{14}\text{GeV}}\right)^2\left(\frac{\Delta\Phi}{M_{\rm pl}}\right)^{-1} \quad (6)$$

Alternatively, $n_B/s \simeq \delta_{\rm eff}M_{\rm pl}/(\mathcal{V}^{5/3}\Delta\Phi)$. Here, $\delta_{\rm eff}$ is a CP phase factor and $\phi_{\rm osc} \simeq (M_*^3 m_0)^{1/4}$ is the value of the AD field at the beginning of its oscillation. Further, $\Delta\Phi \simeq (H_{\rm inf}^2/m_\Phi^2)M_{\rm pl} \leq M_{\rm pl}$ is an oscillation amplitude of the canonically normalized Φ, and $H_{\rm inf}$ is the Hubble constant during an inflation. In this way, it would be possible to obtain the moderate baryon asymmetry on account of a large c.

References
1) G. Hinshaw, D. Larson and E. Komatsu *et al.*, arXiv:1212.5226 [astro-ph.CO].
2) I. Affleck and M. Dine: Nucl. Phys. B **249**, 361 (1985); M. Dine, L. Randall, S. D. Thomas: Phys. Rev. Lett. **75** 398 (1995); Nucl. Phys. B **458**, 291 (1996).
3) V. Balasubramanian, P. Berglund, J. P. Conlon and F. Quevedo: JHEP **0503**, 007 (2005).
4) T. Higaki, K. Kamada and F. Takahashi: JHEP **1209**, 043 (2012).

† Condensed from the article in JHEP **1209**, 043 (2012)
*1 Deutsches Elektronen-Synchrotron DESY, Germany
*2 Department of Physics, Tohoku University, Japan

Dark radiation and dark matter in large volume compactifications[†]

T. Higaki and F. Takahashi[*1]

Recent observations of the cosmic microwave background suggest that there can be an extra component in the cosmic neutrino background. This component is called "dark radiation." The present dark radiation estimation by the WMAP and SPT teams are given in the respective studies[1,2)]

$$N_{\rm eff} = 3.84\pm0.40\ (68\%\mathrm{CL}),\ 3.71\pm0.35\ (1.9\sigma\ \mathrm{CL}). \tag{1}$$

This value should have been closer to three, which is the number of active neutrinos in the Standard Model. In this report, we estimate dark radiation using the string theoretic axion, which is an integrand of an RR 4-form potential on a 4-cycle on a Calabi–Yau (CY) space in the type IIB supergravity. The axion becomes ultralight because of the large volume extra dimensions.

For such an explanation of dark radiation, we consider a large volume scenario in string theory compactified on a CY space[3)], because the lightness is very robust in the large volume limit of the CY space. The effective action of the volume moduli based on 4D $\mathcal{N}=1$ effective supergravity is given by[4)]

$$K = -2\log\left[(T_b+T_b^\dagger)^{3/2} - (T_s+T_s^\dagger)^{3/2} + \xi\right], \tag{2}$$

$$W = W_0 + Ae^{-2\pi T_s} \tag{3}$$

Here, we used the Planck unit, i.e., $M_{\rm pl} = 2.4\times 10^{18}$ GeV $\equiv 1$, with K and W denoting the Kähler potential and superpotential respectively, T_b and T_s denote the overall volume and a hole one in a Swiss-cheese CY, $W_0 = \mathcal{O}(1)$ originates from the closed string flux, and $\xi = \mathcal{O}(1)$ is dependent on the Euler number on the CY. The second term in the superpotential comes from an instanton on the small cycle: $A = \mathcal{O}(1)$. Via the extremization of the above potential, we can find the large volume $\mathcal{V}$ of the CY as

$$\mathcal{V} \sim (T_b+T_b^\dagger)^{3/2} \sim e^{2\pi T_s} \gg 1, \quad T_s \sim \xi^{2/3} \tag{4}$$

in vacuum. The axion $a_b \equiv \mathrm{Im}(T_b)$ is almost massless because of the large value of $\phi \equiv \mathrm{Re}(T_b)$, even if $\delta W = Be^{-2\pi T_b}$ is included. Therefore, the axion becomes a possible candidate for the dark radiation.

Now, the modulus ϕ is the lightest modulus, whose mass is given by $m_\phi \sim \frac{M_{\rm pl}}{\mathcal{V}^{3/2}} = \mathcal{O}(10^6)$ GeV for $\mathcal{V} = \mathcal{O}(10^7)$ in string units, the decay of ϕ into Higgs bosons can finally reheat the universe at $\mathcal{O}(1)$ GeV in such a situation if kinematically allowed. In addition, the axion corresponding to dark radiation is also generated by the decay, and its fraction is comparable to that of Higgses:

$$\Gamma \simeq \frac{2z^2+1}{48\pi}\frac{m_\phi^3}{M_{\rm pl}^2}, \quad B_a \simeq \frac{1}{2z^2+1}. \tag{5}$$

Here, Γ denotes the total decay width of ϕ and B_a the branching fraction into the axions. We used the following interactions written by canonically normalized fields:

$$\mathcal{L} = \frac{z}{\sqrt{6}M_{\rm pl}}(\partial^2\phi)H_uH_d + \frac{2}{\sqrt{6}M_{\rm pl}}\phi(\partial_\mu a_b)^2, \tag{6}$$

where $H_{u,d}$ denote the Higgs fields in the minimal supersymmetric Standard Model localized on a singularity in the CY space. Thus, the moderate $N_{\rm eff}$ can be obtained for $z = \mathcal{O}(1)$ as below, while the Wino dark matter denoted as $\tilde{W}$ can be consequently obtained via the decay of the produced Higgs at a moderate branching fraction if kinematically allowed.

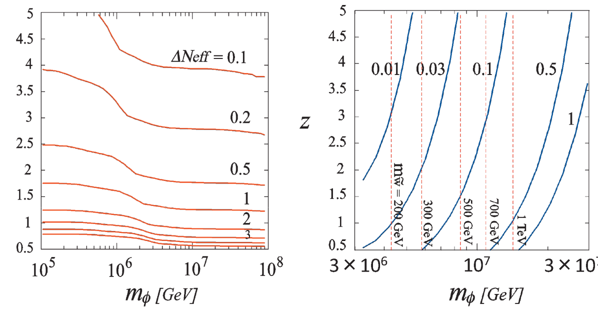

Fig. 1. Contours of $\Delta N_{\rm eff} \approx N_{\rm eff} - 3$ (left), and those of Wino dark matter abundance $\Omega_{\tilde{W}}h^2$ (bold lines in the right panel) and the mass $m_{\tilde{W}}$ (dotted lines in the right panel) as a function of z and m_ϕ. For $z \sim 1.5$, we find that $\Delta N_{\rm eff} \sim 1$ and $\Omega_{\tilde{W}}h^2 \sim 0.1$ with $m_{\tilde{W}} \sim (\log(\mathcal{V})\mathcal{V})^2)^{-1}M_{\rm pl} \sim 500$ GeV.

In this report, we considered an explanation to account for dark radiation in the cosmic neutrino background using the string theoretic axion, which is made ultralight by large volume CY.

References

1) G. Hinshaw, D. Larson, E. Komatsu, D. N. Spergel, C. L. Bennett, J. Dunkley, M. R. Nolta and M. Halpern *et al.*: arXiv:1212.5226 [astro-ph.CO].
2) Z. Hou, C. L. Reichardt, K. T. Story, B. Follin, R. Keisler, K. A. Aird, B. A. Benson and L. E. Bleem *et al.*: arXiv:1212.6267 [astro-ph.CO].
3) M. Cicoli, J. P. Conlon and F. Quevedo: arXiv:1208.3562 [hep-ph]; T. Higaki and F. Takahashi: JHEP **1211**, 125 (2012).
4) V. Balasubramanian, P. Berglund, J. P. Conlon and F. Quevedo: JHEP **0503**, 007 (2005).

† Condensed from the article in JHEP **1211**, 125 (2012)

*1 Department of Physics, Tohoku University, Japan

Hybrid inflation in high-scale supersymmetry†

T. Higaki, K.S. Jeong,*1 and F. Takahashi*1

LARGE volume scenario (LVS) of extra dimension in string theories[1)] is attractive because it can be naturally realized with only of O(1) parameters that TeV scale SUSY-breaking soft masses, baryogenesis, dark matter, dark radiation, and 125 GeV Higgs boson discovered at LHC[2)]. The model of volume moduli is given by the following effective potentials in 4D $\mathcal{N}=1$ supergravity

$$K_{\rm mod} = -2\log\left[(T_b+T_b^\dagger)^{3/2} - (T_s+T_s^\dagger)^{3/2} + \xi\right] \quad (1)$$

$$W_{\rm mod} = W_0 + Ae^{-2\pi T_s}. \quad (2)$$

Here, we took Planck unit, i.e., $M_{\rm pl} = 2.4\times10^{18}{\rm GeV} \equiv 1$, K and W are Kähler and super-potential, T_b and T_s are overall volume and a hole one in a Swiss-cheese Calabi-Yau (CY), $W_0 = \mathcal{O}(1)$ originates from closed string flux, and $\xi = \mathcal{O}(1)$ is dependent on Euler number on the CY. The second term in the superpotential comes from an instanton on the small cycle; $A = \mathcal{O}(1)$. Through the extremization of the above potential, one finds LARGE volume $\mathcal{V}$ of the CY space

$$\mathcal{V} \sim (T_b+T_b^\dagger)^{3/2} \sim e^{2\pi T_s} \gg 1, \quad T_s \sim \xi^{2/3} \quad (3)$$

in the vacuum. However, a flatness of an inflaton potential in this scenario may be an issue because the SUSY-breaking scale can be so high that the 125GeV Higgs boson is realized. However, an approximate no-scale structure due to LARGE volume not only realizes the dark radiation but also makes the scalar potential flat enough to realize an inflation in the early universe, while evading the decompactification problem by $\phi \equiv {\rm Re}(T_b)$. For the solution, the condition that $m_\phi \geq H_{\rm inf}$ is required, where $m_\phi \sim \frac{M_{\rm pl}}{\mathcal{V}^{3/2}}$ is the mass of ϕ and $H_{\rm inf}$ is the Hubble scale during the inflation.

Let us consider an F-term hybrid inflation[3)], because the model is simple, renormalizable, and hence, attractive. The potentials are given by

$$K_{\rm inf} = |\Phi|^2, \quad W_{\rm inf} = W_0 + \kappa M^2\Phi, \quad (4)$$

neglecting waterfall fields, because we are focusing on an inflationary era. With only these potentials, however, it is known that there is a dangerous SUSY-breaking tadpole $V_{\rm tadpole} = -2\kappa M^2 m_{3/2}(\Phi+\Phi^\dagger)$, which makes an unwanted local minimum or the inflationary period shorter. Here, $m_{3/2} \simeq W_0/M_{\rm pl}^2$ is the gravitino mass. Therefore, the parameter space can be constrained as shown in Fig.1[4)]. For instance, $H_{\rm inf} = \kappa M^2/M_{\rm pl}$ should be greater than of $\mathcal{O}(10^7)$GeV in the case that the tadpole $m_{3/2}$ is greater than $\mathcal{O}(1)$GeV.

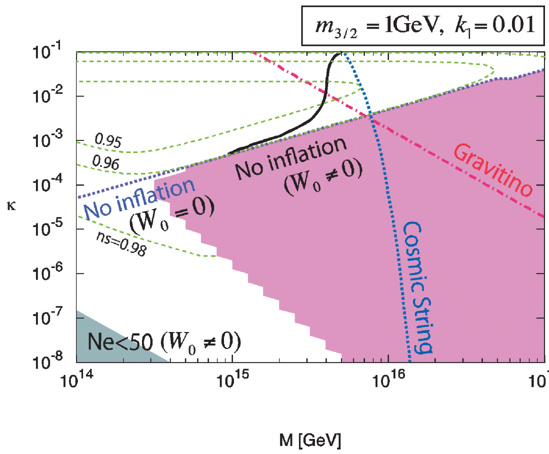

Fig. 1. Allowed parameter space in F-term hybrid inflation just with $K_{\rm inf}$ and $W_{\rm inf}$.

Getting back to LVS, $\Phi = \hat{\Phi}/(T_b+T_b^\dagger)^{1/2}$ is the canonically normalized inflaton on a singularity in the CY space. With $\hat{\Phi}$, the total Kähler potential can be rewritten similarly to the no-scale one: $K_{\rm mod}+K_{\rm inf} \approx -3\log(T_b+T_b^\dagger-|\hat{\Phi}|^2)+\mathcal{O}(\mathcal{V}^{-1})$. Note that there is no tadpole in the no-scale case, but the no-scale structure is now violated at $\mathcal{O}(\mathcal{V}^{-1})$, and hence the tadpole can be then estimated as[5)]

$$V_{\rm tadpole} = -2\zeta\kappa M^2\frac{m_{3/2}}{\mathcal{V}}(\Phi+\Phi^\dagger), \quad m_{3/2} \simeq \frac{W_0}{\mathcal{V}}. \quad (5)$$

Here, $\zeta \sim c/\log(\mathcal{V})$, and the tadpole is suppressed as $\zeta m_{3/2}/\mathcal{V}$ instead of $m_{3/2}$. Say, for $\mathcal{V} = \mathcal{O}(10^7)$ in the string unit, only tuning of c at ten percent level is necessary to elude the decompactification problem and the constraint on the inflation.

References

1) V. Balasubramanian, P. Berglund, J. P. Conlon and F. Quevedo: JHEP **0503**, 007 (2005).
2) T. Higaki, K. Kamada and F. Takahashi: JHEP **1209**, 043 (2012); M. Cicoli, J. P. Conlon and F. Quevedo: arXiv:1208.3562 [hep-ph]; T. Higaki and F. Takahashi: JHEP **1211**, 125 (2012).
3) E. J. Copeland, A. R. Liddle, D. H. Lyth, E. D. Stewart and D. Wands: Phys. Rev. D **49**, 6410 (1994); G. R. Dvali, Q. Shafi and R. K. Schaefer: Phys. Rev. Lett. **73**, 1886 (1994); A. D. Linde and A. Riotto: Phys. Rev. D **56**, 1841 (1997).
4) K. Nakayama, F. Takahashi and T. T. Yanagida: JCAP **1012**, 010 (2010).
5) T. Higaki, K. S. Jeong and F. Takahashi: JHEP **1212**, 111 (2012).

† Condensed from the article in JHEP **1212**, 111 (2012)
*1 Department of Physics, Tohoku University, Japan

Natural supersymmetric spectrum in mirage mediation†

M. Asano,*1 and T. Higaki

Low energy supersymmetry (SUSY) solves various issues in the Standard Model, and is one of the candidates for new physics. The naturalness discussion suggests that light SUSY particles exist not very far from the electroweak symmetry breaking (EWSB) scale. Otherwise, serious fine tuning would be needed to satisfy the EWSB conditions, which include the equation

$$-\frac{m_Z^2}{2} \sim |\mu_{\rm eff}|^2 + m_{H_u}^2. \tag{1}$$

Here, $m_Z \approx 91$GeV is the Z-boson mass, $\mu_{\rm eff}$ is the higgsino mass, and m_{H_u} is the SUSY-breaking soft term for the Higgs H_u coupled to the up quark sector. In contrast, the current SUSY search at LHC have already excluded the gluino and squarks lighter than 1.5 TeV, if their masses are nearly equal. Moreover, the recent discovery of the Higgs-like particle with a mass of around 125 GeV would imply the existence of the large radiative correction from heavy scalar top (stop).

For relaxing the tension between the soft mass scales and the EWSB scale, and for realizing 125GeV Higgs, we consider a TeV scale mirage mediation of the SUSY-breaking[1,2] in the Next-to-Minimal-Supersymmetric-Standard-Model (NMSSM)[3]. This mediation can have a TeV mirage messenger scale Λ, which reduces the cost of the fine-tuning because there exist only small quantum corrections running from the TeV scale Λ to the EWSB scale in the soft masses, whereas there is the additional contribution to the lightest Higgs mass in the NMSSM.

Furthermore, the soft masses are given by the pure moduli (gravity) mediation at Λ. This is because the renormalization group effect in soft masses and the anomaly mediation cancel each other at 1-loop level. The mass spectrum is controlled by the overall scale M_0 set to the TeV scale and by discrete parameters c_i in the string theory:

$$m_i^2(\Lambda) = c_i|M_0|^2, \quad M_a(\Lambda) = M_0. \tag{2}$$

Here, the gauge coupling unification has been assumed, m_i is a soft scalar mass for a visible field Φ_i, M_a ($a = U(1)_Y, SU(2), SU(3)$) is the gaugino mass, and the value of c_i depends on the origin of matter. When the Higgs sector arises from D-brane moduli, the coupling to closed string moduli is suppressed: $c_{H_u} = 0$. Then, the following is obtained at the EWSB scale

$$m_{H_u}^2 = -\mathcal{O}\left(\frac{|M_0|^2}{8\pi^2}\right) = -\mathcal{O}(100^2)\ \text{GeV}^2 \tag{3}$$

through a small quantum correction by stops. With the Eq.(1), $\mu_{\rm eff} = \mathcal{O}(100)$GeV is obtained even for $M_0 = \mathcal{O}(1)$ TeV: The tuning of $\mu_{\rm eff}$ can be relaxed to about 10%.

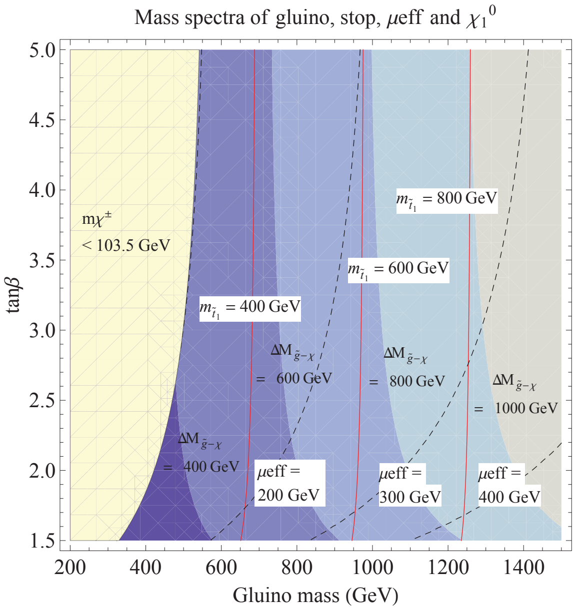

Fig. 1. Contours of $\mu_{\rm eff}$, the lightest stop mass $m_{\tilde{t}_1}$, and the mass difference between gluino and lightest neutralino $\Delta M_{\tilde{g}-\chi}$ in our model. Note that gluino mass $M_{SU(3)}$ is roughly given by M_0, whereas $\tan\beta = \langle H_u\rangle/\langle H_d\rangle$.

On the other hand, the lightest higgs mass m_h can increase owing the Yukawa coupling λ between the Higgses (H_u, H_d) and the singlet S in the superpotential $W_{\rm NMSSM} \supset \lambda S H_u H_d$ than in the case without it:

$$m_h^2 \approx m_h^2|_{\lambda=0} + \lambda^2 v^2 \sin^2 2\beta. \tag{4}$$

Here, $v \approx 174$GeV is the EWSB scale, and $\mu_{\rm eff} = \lambda\langle S\rangle$.

Thus, even for $M_0 = \mathcal{O}(1)$TeV, it is possible both to relax the SUSY little hierarchy problem and to realize the 125 GeV Higgs within the framework of the TeV scale mirage mediation in the NMSSM.

† Condensed from the article in Phys. Rev. D **86**, 035020 (2012)

*1 II. Institute for Theoretical Physics, University of Hamburg, Germany

References

1) K. Choi, A. Falkowski, H. P. Nilles and M. Olechowski: Nucl. Phys. B **718**, 113 (2005); K. Choi, K. S. Jeong and K. i. Okumura: JHEP **0509**, 039 (2005); M. Endo, M. Yamaguchi and K. Yoshioka: Phys. Rev. D **72**, 015004 (2005).
2) K. Choi, K. S. Jeong, T. Kobayashi and K. -i. Okumura: Phys. Lett. B **633** (2006) 355; R. Kitano and Y. Nomura: Phys. Lett. B **631**, 58 (2005).
3) M. Asano and T. Higaki: Phys. Rev. D **86**, 035020 (2012).

Supersymmetry, chiral symmetry, and the generalized BRS transformation in lattice formulations of 4D $\mathcal{N} = 1$ SYM†

H. Suzuki

It is widely believed that supersymmetry (SUSY) plays a fundamental role in particle physics beyond the Standard Model. A non-perturbative definition or formulation of supersymmetric theories is thus of great interest. Although the lattice formulation is the best developed non-perturbative framework for the quantum field theory, the spacetime lattice generally breaks the infinitesimal translation that is a part of the SUSY algebra. For this reason, SUSY can be realized only in the continuum limit in which the lattice spacing vanishes. Before investigating non-perturbative physical problems, therefore, we need to understand how SUSY (in addition to other symmetries that the lattice breaks) is restored in the continuum limit.

The four-dimensional $\mathcal{N} = 1$ supersymmetric Yang–Mills theory (4D $\mathcal{N} = 1$ SYM) is the simplest supersymmetric gauge theory in four dimensions, and we first need to understand the above issue of symmetry restoration in this simplest theory. Although the basic idea of the original proposal,[1] that the tuning of a single mass parameter restores all symmetries of 4D $\mathcal{N} = 1$ SYM, is natural, to show the validity of this idea in terms of the Ward–Takahashi (WT) relations—the basic characterization of the symmetry properties of a quantum field theory—is not as straightforward. In fact, the original analysis[1] was incomplete in that it neglected the contribution of gauge-fixing and ghost-anti-ghost terms. A later analysis[2] was also incomplete in that it did not adequately account for a possible operator mixing with a three-fermion operator.

A WT relation associated with the $U(1)_A$ symmetry of 4D $\mathcal{N} = 1$ SYM is found to be (when the point x stays away from a gauge invariant operator $\mathcal{O}$ by a finite physical distance; we denote this situation as $x \leftrightsquigarrow \operatorname{supp}(\mathcal{O})$)

$$\begin{aligned} \mathcal{Z}_A \left\langle \partial_\mu^S \operatorname{tr}[\bar{\psi}(x)\gamma_\mu\gamma_5\psi(x)]\mathcal{O}\right\rangle &= -\mathcal{Z}_{F\tilde{F}} \left\langle \left[F\tilde{F}\right]^L(x)\mathcal{O}\right\rangle \\ &\quad + 2\left(M - \frac{1}{2a}\mathcal{Z}_P\right)\left\langle \operatorname{tr}[\bar{\psi}(x)\gamma_5\psi(x)]\mathcal{O}\right\rangle, \quad (1) \end{aligned}$$

where $\mathcal{Z}_A$, $\mathcal{Z}_{F\tilde{F}}$, and $\mathcal{Z}_P$ are renormalization constants and M is the bare mass parameter of the gluino, the superpartner of the gauge boson in 4D $\mathcal{N} = 1$ SYM. This relation shows that, for the $U(1)_A$ symmetry to be restored and the axial vector current to be conserved up to the axial anomaly (∂_μ^S is the symmetric difference operator and $[F\tilde{F}]^L(x)$ denotes a lattice transcription of the topological density), we need to tune the parameter M such that

$$M - \frac{1}{2a}\mathcal{Z}_P = 0. \quad (2)$$

Further, a WT relation associated with SUSY is found to be (again when $x \leftrightsquigarrow \operatorname{supp}(\mathcal{O})$)

$$\begin{aligned} &\left\langle \partial_\mu^S \left[\mathcal{Z}_S S_\mu(x) + \mathcal{Z}_T T_\mu(x)\right]\mathcal{O}\right\rangle \\ &= \left(M - \frac{1}{a}\mathcal{Z}_\chi\right)\left\langle \chi(x)\mathcal{O}\right\rangle \\ &\quad - \mathcal{Z}_{3F}\left\langle \operatorname{tr}\left[\psi(x)\bar{\psi}(x)\psi(x)\right]\mathcal{O}\right\rangle, \quad (3) \end{aligned}$$

where $\mathcal{Z}_S$, $\mathcal{Z}_T$, $\mathcal{Z}_\chi$, and $\mathcal{Z}_{3F}$ are the renormalization constants and $S_\mu(x)$, $T_\mu(x)$, and $\chi(x)$ are some lattice operators. Thus, for the SUSY current in the left-hand side to be conserved without anomaly, we require

$$\mathcal{Z}_{3F} = 0, \quad (4)$$

in the continuum limit, and the mass parameter M to be tuned such that

$$M - \frac{1}{a}\mathcal{Z}_\chi = 0. \quad (5)$$

Since we have a common parameter M in Eqs. (2) and (5), for both SUSY and $U(1)_A$ to be restored simultaneously, we require

$$\mathcal{Z}_\chi = \frac{1}{2}\mathcal{Z}_P, \quad (6)$$

in the continuum limit.

In the present work, by extending the generalized BRS transformation developed in the continuum theory[3–5] to the lattice formulation and studying the consequence of a Wess–Zumino-like consistency condition, we validated Eqs. (4) and (6) for all orders of the perturbation theory. This result fills the gaps in the past studies and provides a theoretical basis for the lattice formulation of 4D $\mathcal{N} = 1$ SYM.

References
1) G. Curci and G. Veneziano: Nucl. Phys. B **292**, 555 (1987).
2) F. Farchioni *et al.*: [DESY-Münster-Roma Collaboration], Eur. Phys. J. C **23**, 719 (2002) [hep-lat/0111008].
3) P. L. White: Class. Quant. Grav. **9**, 1663 (1992).
4) N. Maggiore, O. Piguet and S. Wolf: Nucl. Phys. B **458**, 403 (1996) [Erratum-ibid. B **469**, 513 (1996)] [hep-th/9507045].
5) N. Maggiore, O. Piguet and S. Wolf: Nucl. Phys. B **476**, 329 (1996) [hep-th/9604002].

† Condensed from the article in Nucl. Phys. B **861**, 290–320 (2012)

Ferrara–Zumino supermultiplet and the energy-momentum tensor in the lattice formulation of 4D $\mathcal{N} = 1$ SYM†

H. Suzuki

Ideally, a non-perturbative formulation of a field theory with some symmetries should provide, as well as the definition of correlation functions, the definition of renormalized Noether currents that generate correctly normalized symmetry transformations on renormalized fields. This is expressed by renormalized Ward–Takahashi (WT) relations, and if these relations hold, it can be claimed with certainty that the symmetries are *actually* realized in quantum field theory.

Quite often, however, the regularization procedure breaks the preferred symmetries, and for this reason, it is generally very difficult to conclude even the existence of such renormalized Noether currents (especially when symmetry transformations are non-linear). In the lattice formulation of supersymmetric theories, one encounters such a situation, because in them almost all fundamental symmetries, such as translational invariance, supersymmetry (SUSY), and chiral symmetry, are broken by the lattice regularization.

In the present work, we propose a possible definition of the energy-momentum tensor—a Noether current associated with translational invariance—in the lattice formulation of the four-dimensional $\mathcal{N} = 1$ supersymmetric Yang–Mills theory (4D $\mathcal{N} = 1$ SYM). As noted above, since the lattice regularization breaks the translational invariance, any lattice energy-momentum tensor can be conserved only in the continuum limit, the limit in which the lattice spacing a vanishes. According to Ref. 1), in generic lattice gauge theories involving fermions, one has to (non-perturbatively) determine at least seven renormalization constants to construct a lattice energy-momentum tensor that is conserved in the continuum limit.

Further, it has been known for long time that Noether currents in 4D $\mathcal{N} = 1$ SYM, i.e., the $U(1)_A$ current, the SUSY current, and the energy-momentum tensor, form a multiplet under SUSY,[2)] called the Ferrara–Zumino (FZ) supermultiplet. Here, we define a lattice energy-momentum tensor by mimicking the structure of this FZ supermultiplet. That is, since the super transformation of the SUSY current is essentially the energy-momentum tensor in the classical theory of 4D $\mathcal{N} = 1$ SYM, we define a lattice energy-momentum tensor $\mathcal{T}_{\mu\nu}(x)$ as

$$\mathcal{T}_{\mu\nu}(x) = \frac{1}{2}\left[\Theta_{\mu\nu}(x) + \Theta_{\nu\mu}(x)\right] - c\delta_{\mu\nu}\,\mathrm{tr}\left[\bar{\psi}(x)(D+M)\psi(x)\right], \qquad (1)$$

where c is a constant and D is a lattice Dirac operator, and

$$\Theta_{\mu\nu}(x) \equiv \frac{1}{8}(\gamma_\nu)_{\beta\alpha}\frac{\partial}{\partial\xi_\beta}\left[\mathcal{Z}\bar{\Delta}_\xi\mathcal{S}_\mu(x)\right]_\alpha, \qquad (2)$$

where $\mathcal{Z}$ is a renormalization constant, $\bar{\Delta}_\xi$ is a renormalized, modified super transformation on lattice variables with the parameter ξ, and $\mathcal{S}_\mu(x)$ is a renormalized lattice SUSY current (α and β denote the spinor indices). An advantage of this definition of a lattice energy-momentum tensor is that the number of renormalization constants to be determined is four, which is almost half of the number required for generic lattice gauge theories. Although the lattice regularization also breaks SUSY, one can recover the breaking of SUSY by an appropriate tuning of the mass parameter M.[3,4)] Assuming that for this parameter, tuning has been performed, one can see that the lattice energy-momentum tensor (1) is conserved in the continuum limit:

$$\left\langle \partial_\mu^S \mathcal{T}_{\mu\nu}(x)\mathcal{O}\right\rangle \xrightarrow{a\to 0} 0, \qquad (3)$$

where ∂_μ^S is the symmetric difference operator; we assumed that the point x remains distant from a gauge-invariant renormalized operator $\mathcal{O}$ by a finite physical distance. The conservation law (3) is a minimal and fundamental requirement for any physical energy-momentum tensor, and the lattice energy-momentum tensor (1) may thus be used to measure physical quantities related with the energy-momentum tensor, such as viscosity, by numerical simulations.

According to our definition of the energy-momentum tensor, the trace anomaly in the energy-momentum tensor is directly related to the gamma-trace (or superconformal) anomaly in the SUSY current, as

$$\langle \mathcal{T}_{\mu\mu}(x)\mathcal{O}\rangle = \frac{1}{8}\left\langle \frac{\partial}{\partial\xi_\alpha}\left[\mathcal{Z}\bar{\Delta}_\xi\gamma_\mu\mathcal{S}_\mu(x)\right]_\alpha\mathcal{O}\right\rangle, \qquad (4)$$

where we have neglected disconnected parts. It is conceivable that a transparent understanding on the so-called anomaly puzzle can be obtained, provided the full structure of the FZ supermultiplet with corrections by the anomaly is realized in the lattice formulation, as given by Eq. (4).

References

1) S. Caracciolo, G. Curci, P. Menotti and A. Pelissetto: Annals Phys. **197** (1990) 119.
2) S. Ferrara and B. Zumino: Nucl. Phys. B **87** (1975) 207.
3) G. Curci and G. Veneziano: Nucl. Phys. B **292** (1987) 555.
4) H. Suzuki: Nucl. Phys. B **861** (2012) 290 [arXiv:1202.2598 [hep-lat]].

† Condensed from the article in Nucl. Phys. B **868**, 459–475 (2013)

Superconformal multiplets and Kohn-Rossi cohomology

J. Schmude

The representation theory of the superconformal algebra has been known since the '80s.[1] Each unitary irreducible representation (UIR) of the superconformal algebra – a supermultiplet – is composed of a finite number of UIRs of the the maximally compact subalgebra G_c of the bosonic subalgebra. For the case of $Osp(2|4)$ as relevant to three dimensional $\mathcal{N}=2$ theories,

$$\begin{aligned} G_c &= SO(2)_E \oplus SO(3)_S \oplus SO(2)_R \\ &\subset SO(2,3) \oplus SO(2) \subset Osp(2|4) \end{aligned} \tag{1}$$

Each of the UIRs of G_c – a particle state – is characterised by its energy E, spin S, and hyper- or R-charge R. The situation is very similar in other dimensions. The quantum numbers for representations of $SU(2,2|4)$ that characterise $\mathcal{N}=1$ theories in $d=4$ are energy, R-charge, and the spins j_1 and j_2.

Physical representations are further constrained by unitarity bounds.[2] Normalising highest weight states to unit-norm, the norm of a general descendant can be calculated using the superconformal algebra and expressed in terms of the above quantum numbers. It is consistent to remove all zero- and negative-norm states from a supermultiplet, which leads to multiplet shortening. Thus, the particle states of superconformal gauge theories (SCFTs) can be generally arranged in long, short, and massless multiplets.

Gauge/string duality relates d-dimensional SCFTs to string theories propagating on backgrounds of the form $AdS_{d+1} \times \mathcal{M}$, where $\mathcal{M}$ is a suitable compact manifold. A large class of examples is given by Freund-Rubin type compactifications where the internal manifold $\mathcal{M}$ is Sasaki-Einstein. Examples of this are given by

$$S^5, \quad T^{1,1}, \quad L^{a,b,c}, \quad S^7, \quad M^{1,1,1}. \tag{2}$$

The first three of these are $d=5$, $\mathcal{N}=1$, the final two $d=7$, $\mathcal{N}=2$.

Kaluza-Klein reduction of the relevant supergravity theory on $AdS_{d+1} \times \mathcal{M}$ yields a supergravity theory on AdS_{d+1}. The AdS/CFT dictionary relates the single particle states of this theory to gauge-invariant single trace operators of the dual SCFT, while also giving a precise map between the masses of the fields in AdS and the anomalous dimensions of the operators. It follows that the knowledge of the spectrum of differential operators $\Delta, \underline{\mathrm{D}}, \Delta_L$ on $\mathcal{M}$ is equivalent to knowing the anomalous dimensions of all gauge-invariant operators. Conversely, the Kaluza-Klein spectrum should reflect the multiplet structure of the superconformal algebra.

Kaluza-Klein spectroscopy for S^5 and S^7 is a relatively straightforward exercise; one can decompose all fields in spherical harmonics. For general quotient spaces G/H the spectrum has been computed using harmonic decomposition.[4] In the generic case however, the problem is considerably more difficult.

However, one can use the Sasaki-Einstein structure to recover the multiplet structure and gain a geometric understanding of multiplet shortening for generic manifolds.[5,6] In general, such manifolds are $U(1)$ fibrations over a local Kähler-Einstein base, with the $U(1)$ being generated by the Reeb vector η. The cotangent bundle decomposes thus as

$$\Omega^{(1,0)} \oplus \Omega^{(0,1)} \oplus \mathbb{C}\eta, \tag{3}$$

and it is possible to introduce a lift of the Dolbeault operators ∂ and $\bar\partial$ of the base – the "tangential Cauchy-Riemann operators" ∂_B and $\bar\partial_B$. In what follows, we restrict to the case of five-dimensional manifolds[5], the seven-dimensional case is in preparation[6].

One can show that the eigenvalues of scalar functions are bounded $\Delta \geq q(q+4)$. The bound is saturated if f is holomorphic, $\bar\partial_B f = 0$. Furthermore, one can use the Sasaki-Einstein structure given by the forms η, J, Ω to construct one- and two-forms that descend from f. As an example, table 1 shows one of the three vector multiplets. $\star$ denotes states that survive when f is holomorphic, $\Delta \equiv E_0(E_0+4)$.

Table 1. The "vector multiplet I"

holo.	wave func.	dim.	R
	$(f\eta)^-$	E_0+1	r
$\star$	f	E_0	r
$\star$	$(f\bar\Omega)^-$	E_0+1	$r-2$
	$(f\Omega)^-$	E_0+1	$r+1$
	$(f\bar\Omega^+).\Omega$	E_0+2	r

Using this method, it is possible to express the superconformal index[2] in terms of the Kohn-Rossi cohomology groups $H^{p,q}_{\bar\partial_B}(\mathcal{M})$,

$$1 + \mathcal{I}_{s.t.} \sum_{0 \leq p-q \leq 2} Tr t^{3R} \mu_a^{F_a} | H^{p,q}_{\bar\partial_B}(\mathcal{M}). \tag{4}$$

References

1) V. K. Dobrev and V. B. Petkova, Phys. Lett. B **162**, 127 (1985).
2) J. Kinney et. al., Commun. Math. Phys. **275**, 209 (2007) [hep-th/0510251].
3) H. Larsson, M.Sc. Thesis, (2004), http://fy.chalmers.se/~tfebn/LarssonMasterthesis.ps.
4) D. Fabbri et. al., Nucl. Phys. B **560**, 617 (1999) [hep-th/9903036].
5) R. Eager et. al., arXiv:1207.0573 [hep-th].
6) R. Eager and J. Schmude, work in progress.

$\mathcal{W}_3$ irregular states and isolated $\mathcal{N} = 2$ superconformal field theories†

H. Kanno,[*1] K. Maruyoshi,[*2] S. Shiba,[*3] and M. Taki[*4]

The compactification of the world-volume theory on M5-branes, known as the six-dimensional $\mathcal{N} = (2,0)$ theory, on a punctured Riemann surface $C_{g,n}$ leads to a large class of $\mathcal{N} = 2$ superconformal field theories (SCFTs) in four dimensions.[1)] These theories have exactly marginal gauge couplings, the space of which forms the moduli space $\mathcal{M}_{g,n}$ of the complex structure of $C_{g,n}$. The SCFTs S-duality group acts on this moduli space. The four-dimensional SCFTs tinclude another isolated class of SCFTs that do not allow marginal deformations. This class was originally found as a nontrivial infrared(IR) fixed point on the Coulomb branch of asymptotically free gauge theories and is the Argyres-Douglas type.[2)] The characteristic feature of these theories is that mutually non-local BPS particles simultaneously become massless at the superconformal point. Recently, it was shown that these isolated SCFTs can also be constructed by the compactification of the six-dimensional $\mathcal{N} = (2,0)$ theory on a sphere with an irregular puncture.[3)] This finding strongly suggests that the following AGT relation must be extended to this class of four-dimensional theories.

From the six-dimensional viewpoint, a remarkable correspondence has been uncovered:[4)] The instanton partition function of the four-dimensional $\mathcal{N} = 2$ gauge theory is exactly equal to the conformal block on $C_{g,n}$ of $\mathcal{W}$ algebra in two dimensions. This is the above-mentioned mentioned AGT relation between 4d and 2d theories. Further, an extension of the correspondence to isolated SCFTs has been proposed in[4)] based on the finding that the two-dimensional CFT counterpart of the irregular puncture is an irregular state that is a simultaneous eigenstate of the higher Virasoro generators. In this article, we explore this proposal for the irregular states of $\mathcal{W}_3$ algebra and isolated SCFTs with an $SU(3)$ flavor symmetry.

Our first nontrivial result is the irregular state conditions for the $\mathcal{W}(A_2, C_{0,1,\{3\}})$ theory:

$$W_2|I_2\rangle = \sqrt{\kappa}(3c_0^2c_2 + 3c_0c_1^2 - 3(\beta_3^2 + 5\beta^2)c_2$$
$$+3c_1c_2\partial_{c_1} + 3c_2^2\partial_{c_2})|I_2\rangle, \tag{1}$$
$$W_3|I_2\rangle = \sqrt{\kappa}\,\left(6c_0c_1c_2 + c_1^3 + 3c_2^2\partial_{c_1}/2\right)|I_2\rangle, \tag{2}$$
$$W_4|I_2\rangle = \sqrt{\kappa}\,\left(3c_0c_2^2 + 3c_1^2c_2\right)|I_2\rangle, \tag{3}$$
$$W_5|I_2\rangle = \sqrt{\kappa}\,3c_1c_2^2|I_2\rangle, \quad W_6|I_2\rangle = \sqrt{\kappa}\,c_2^3|I_2\rangle, \tag{4}$$

where W_n is the n-th generator of the $\mathcal{W}_3$ algebra. c_i and β_i are certain functions of quark masses and Higgs expectation value, respectively.

We also derive the irregular state conditions for generic $\mathcal{W}(A_2, C_{0,1,\{n+1\}})$ theories. The resulting conditions are slightly modified coherent state conditions for generators of conformal algebras; that is, that these conditions are not genuine eigenstate conditions but involve first-order differential operators of the parameters of the theory. This modified coherent state structure plays a key role in reproducing the non-trivial structure of the four-dimensional theory. We showed that the Seiberg-Witten curve of the $\mathcal{W}(A_2, C_{0,1,\{n+1\}})$ theory is recovered through the two-dimensional computation of the corresponding irregular state.

† arXiv:1301.0721

*1 Graduate School of Mathematics and KMI, Nagoya University
*2 California Institute of Technology
*3 High Energy Accelerator Research Organization (KEK)
*4 Mathematical Physics Lab., RIKEN Nishina Center

References
1) D. Gaiotto: JHEP **1208**, 034 (2012) [arXiv:0904.2715 [hep-th]].
2) P. C. Argyres, M. R. Plesser, N. Seiberg and E. Witten: Nucl. Phys. B **461**, 71 (1996) [hep-th/9511154].
3) S. Cecotti and C. Vafa: arXiv:1103.5832 [hep-th].
4) D. Gaiotto and J. Teschner: JHEP **1212**, 050 (2012) [arXiv:1203.1052 [hep-th]].

Universally valid Heisenberg uncertainty relation†

K. Fujikawa

A universally valid Heisenberg uncertainty relation is proposed by combining the universally valid error-disturbance uncertainty relation of Ozawa with the relation of Robertson. This form of the uncertainty relation, which is defined with the same mathematical rigor as the relations of Kennard and Robertson, incorporates both of the intrinsic quantum fluctuations and measurement effects.

The uncertainty relation forms the basis of entire quantum theory[1–3]. The original formulation by Heisenberg[1] is based on a gedanken experiment and emphasizes measurement processes. On the other hand, the formulations by Kennard[2] and Robertson[3] for generic variables A and B,

$$\sigma(A)\sigma(B) \geq \frac{1}{2}|\langle[A,B]\rangle|, \tag{1}$$

which are mathematically well-defined, but did not emphasize the measurement processes. In the spirit of the original formulation of Heisenberg, it may be desirable to express the uncertainty relation in terms of the measurement error $\epsilon(A)$ of the variable A and the disturbance $\eta(B)$ in the conjugate variable B, for example.

The recent experiment[4] provides a support for the idea of a universally valid error-disturbance uncertainty relation proposed by Ozawa[5,6] which is written as

$$\epsilon(A)\eta(B) + \sigma(A)\eta(B) + \epsilon(A)\sigma(B) \geq \frac{1}{2}|\langle[A,B]\rangle|. \tag{2}$$

In the relation (2), $\sigma(A)$ stands for the standard deviation $\sigma(A) = \langle(A - \langle A\rangle)^2\rangle^{1/2}$, and $\epsilon(A)$ stands for the measurement "error" of A defined by

$$\epsilon(A) = \langle(M^{out} - A)^2\rangle^{1/2}. \tag{3}$$

The quantity $\eta(B)$ stands for the "disturbance" of the conjugate variable B defined by

$$\eta(B) = \langle(B^{out} - B)^2\rangle^{1/2}. \tag{4}$$

We work in the Heisenberg picture and the variables without any suffix stand for the initial variables, and M^{out} and B^{out} stand for the meter variable and the variable B after the measurement of A, respectively.

In this notation, Ozawa proposes[5] to identify the Heisenberg's original uncertainty relation with

$$\epsilon(A)\eta(B) \geq \frac{1}{2}|\langle[A,B]\rangle| \tag{5}$$

which does not always hold[4,6]. This relation is not universally valid since we threw away two terms on the left-hand side in the relation (2).

We here suggest to combine the relation (2) with the standard Robertson's relation (1) in the form

$$\bar{\epsilon}(A)\bar{\eta}(B) \geq |\langle[A,B]\rangle| \tag{6}$$

where

$$\begin{aligned}\bar{\epsilon}(A) &\equiv \epsilon(A) + \sigma(A)\\ &= \langle(M^{out} - A)^2\rangle^{1/2} + \langle(A - \langle A\rangle)^2\rangle^{1/2},\\ \bar{\eta}(B) &\equiv \eta(B) + \sigma(B)\\ &= \langle(B^{out} - B)^2\rangle^{1/2} + \langle(B - \langle B\rangle)^2\rangle^{1/2}.\end{aligned} \tag{7}$$

The relation (6) is similar to (a modified form of) Arthurs-Kelly relation[7,8]

$$\begin{aligned}&\{\langle(M^{out} - A)^2\rangle + \sigma^2(A)\}^{1/2}\\ &\times\{\langle(B^{out} - B)^2\rangle + \sigma^2(B)\}^{1/2} \geq |\langle[A,B]\rangle|,\end{aligned} \tag{8}$$

and it emphasizes the repeated measurements of similarly prepared samples in quantum mechanics. We emphasize that the relation (6) is based on the positive metric Hilbert space and the natural commutator algebra, and thus its validity is at the same level as the standard Kennard[2] and Robertson[3] relations.

Our proposal is to identify the relation (6) as a *universally valid Heisenberg uncertainty relation* which incorporates measurement effects. Physically, we identify $\bar{\epsilon}(A)$ in (7) as the "inaccuracy" in the measured values of A and $\bar{\eta}(B)$ in (7) as the "fluctuation" of the conjugate variable B after the measurement of A. In this identification, the "good measurement" is defined by a small inaccuracy $\bar{\epsilon}(A) = \epsilon(A) + \sigma(A)$, namely, the measurement of a well-defined state with small $\sigma(A)$ by a detector with a small "error" $\epsilon(A)$. The measurement of a broad state with a small error does not constitute a good measurement.

It is gratifying that we can preserve Heisenberg's original idea in the form (6), by replacing $\frac{1}{2}|\langle[A,B]\rangle|$ with $|\langle[A,B]\rangle|$, which always holds as long as quantum mechanics is valid.

References
1) W. Heisenberg, Z. Phys. **43**,172 (1927).
2) E.H. Kennard, Z. Phys. **44**,326 (1927).
3) H.P. Robertson, Phys. Rev. **34**, 163 (1929).
4) J. Erhart, S. Sponar, G. Sulyok, G. Badurek, M. Ozawa and Y. Hasegawa, Nature Phys. **8**, 185 (2012).
5) M. Ozawa, Phys. Rev. A **67**, 042105 (2003).
6) M. Ozawa, J. Opt. B**7**, S672 (2005).
7) E. Arthurs and J.L. Kelly Jr, Bell. Syst. Tech. J. **44**, 725 (1965).
8) E. Arthurs and M.S. Goodman, Phys. Rev. Lett. **60**, 2447 (1988).

† Condensed from the article in Phys. Rev. A**85**, 062117 (2012).

Aspects of universally valid Heisenberg uncertainty relation†

K. Fujikawa and K. Umetsu*1

A universally valid Heisenberg uncertainty relation, which was proposed recently, is illustrated using the experimental data on spin-measurements by J. Erhart, et al.[Nature Phys. **8**, 185 (2012)]. This uncertainty relation is closely related to a modified form of the Arthurs-Kelly uncertainty relation which is also tested by the spin-measurements. The universally valid Heisenberg uncertainty relation always holds, but both the modified Arthurs-Kelly uncertainty relation and Heisenberg's error-disturbance relation proposed by Ozawa, which was analyzed in the original experiment, fail in the present context of spin-measurements, and the cause of their failure is identified with the assumptions of unbiased measurement and disturbance. It is also shown that all the universally valid uncertainty relations are derived from Robertson's relation and thus the essence of the uncertainty relation is exhausted by Robertson's relation, as is widely accepted.

Motivated by the past works by Ozawa[1,2] and the recent experiment at Vienna[3], a universally valid Heisenberg relation has been recently proposed[4], which assumes the form

$$\bar{\epsilon}(A)\bar{\eta}(B) \geq |\langle[A,B]\rangle| \tag{1}$$

where

$$\begin{aligned}\bar{\epsilon}(A) &\equiv \epsilon(A)+\sigma(A)\\ &= \langle(M^{out}-A)^2\rangle^{1/2}+\langle(A-\langle A\rangle)^2\rangle^{1/2},\\ \bar{\eta}(B) &\equiv \eta(B)+\sigma(B)\\ &= \langle(B^{out}-B)^2\rangle^{1/2}+\langle(B-\langle B\rangle)^2\rangle^{1/2}.\end{aligned} \tag{2}$$

We here work in the Heisenberg representation and those variables without any suffix stand for the initial variables. M^{out} stands for the meter variable after the measurement of A, and B^{out} stands for the conjugate variable after the measurement of A. It was suggested in Ref.[4] that $\bar{\epsilon}(A)$ is called the "inaccuracy" in the measured values of the variable A, and $\bar{\eta}(B)$ is called the inevitable "fluctuation" in the conjugate variable B after the measurement of A. The quantity $\epsilon(A) = \langle(M^{out}-A)^2\rangle^{1/2}$ is commonly referred to as "error" in the measurement of A, and $\eta(B) = \langle(B^{out}-B)^2\rangle^{1/2}$ as "disturbance" in the variable B after the measurement of A. $\sigma(A) = \langle(A-\langle A\rangle)^2\rangle^{1/2}$ is the standard deviation.

Relation (1) is a counter proposal to the naive Heisenberg-type error-disturbance relation[1,5]

$$\epsilon(A)\eta(B) \geq \frac{1}{2}|\langle[A,B]\rangle| \tag{3}$$

which was invalidated by the recent experiment[3]. The relation (1) is also closely related to a modified form of the Arthurs-Kelly relation[6,7],

$$\begin{aligned}&\{\langle(M^{out}-A)^2\rangle+\sigma(A)^2\}^{1/2}\\ &\times\{\langle(B^{out}-B)^2\rangle+\sigma(B)^2\}^{1/2} \geq |\langle[A,B]\rangle|.\end{aligned} \tag{4}$$

In terms of the actual experimental set up with $A=\sigma_x$ and $B=\sigma_y$, we have[3]

$$\epsilon(A) = 2\sin(\frac{1}{2}\phi), \qquad \eta(B) = \sqrt{2}\cos\phi \tag{5}$$

where ϕ in the interval $\frac{\pi}{2} \geq \phi \geq 0$ is called detuning angle, and $\sigma(A)=1$ and $\sigma(B)=1$ for the initial state $|\psi\rangle = |+z\rangle$. The relation (1) then becomes

$$(2\sin(\frac{\phi}{2})+1)(\sqrt{2}\cos\phi+1) \geq 2, \tag{6}$$

and (3) and (4) become, respectively,

$$\begin{aligned}&2\sqrt{2}\sin(\frac{1}{2}\phi)\cos\phi \geq 1,\\ &\{(4\sin^2(\frac{\phi}{2})+1)(2\cos^2\phi+1)\}^{1/2} \geq 2.\end{aligned} \tag{7}$$

One can easily confirm that the relation (6) is satisfied but both of the relations in (7) fail for all the values of ϕ, in agreement with experiment[3].

One can also confirm that Robertson's relation[8]

$$\sigma(M^{out}-A)\sigma(B^{out}-B) \geq \frac{1}{2}|\langle[M^{out}-A, B^{out}-B]\rangle|$$

gives (by assuming $[M^{out}, B^{out}]=0$)

$$\begin{aligned}&\sigma(M^{out}-A)\sigma(B^{out}-B)\\ &\geq \frac{1}{2}\{|\langle[A,B]\rangle| - |\langle[A,B^{out}-B]\rangle| - |\langle[M^{out}-A,B]\rangle|\}\end{aligned} \tag{8}$$

from which one can derive the relation (1) as well as the original relation of Ozawa[1], and thus all the universally valid relations are derived from Robertson's relation. By assuming the unbiased measurement and disturbance, one can also derive (3) from (8), and thus all the uncertainty relations from Robertson's relation.

References

1) M. Ozawa, Phys. Rev. A**67**, 042105 (2003).
2) M. Ozawa, J. Opt. B**7**, S672 (2005).
3) J. Erhart, et al., Nature Phys. **8**, 185 (2012).
4) K. Fujikawa, Phys. Rev. A**85**, 062117 (2012).
5) D.M. Appleby, Int. J. Theor. Phys. **37**, 1491 (1998).
6) E. Arthurs and J.L. Kelly Jr, Bell. Syst. Tech. J. **44**, 725 (1965).
7) E. Arthurs and M.S. Goodman, Phys. Rev. Lett. **60**, 2447 (1988).
8) H.P. Robertson, Phys. Rev. **34**, 163 (1929).

† Condensed from the article in PTEP 013A03 (2013).
*1 Maskawa Institute for Science and Culture, Kyoto Sangyo University

On neutrino masses via CPT violating Higgs interaction in the Standard Model†

M. Chaichian,[*1] K. Fujikawa, and A. Tureanu[*1]

The Lorentz invariant CPT violation by using non-local interactions is naturally incorporated in the Higgs coupling to neutrinos in the Standard Model, without spoiling the basic $SU(2)_L \times U(1)$ gauge symmetry. The neutrino–antineutrino mass splitting is thus realized by the mechanism which was proposed recently, assuming the neutrino masses to be predominantly Dirac-type in the Standard Model. The CPT violation such as the one suggested in this paper may open a new path to the analysis of baryon asymmetry since some of the Sakharov constraints are expected to be modified.

It has been recently shown that the non-local but Lorentz invariant and hermitian Lagrangain

$$
\begin{aligned}
S = &\int d^4x \Big\{ \bar{\psi}(x) i\gamma^\mu \partial_\mu \psi(x) - m\bar{\psi}(x)\psi(x) \\
&- \int d^4y [\theta(x^0-y^0) - \theta(y^0-x^0)]\delta((x-y)^2 - l^2) \\
&\times [i\mu\bar{\psi}(x)\psi(y)] \Big\}, \qquad (1)
\end{aligned}
$$

gives rise to a mass splitting between particle and antiparticle[1)]

$$
m_\pm \simeq m \pm 4\pi\mu \int_0^\infty dz \frac{z^2 \sin[m\sqrt{z^2+l^2}]}{\sqrt{z^2+l^2}}. \qquad (2)
$$

For the real parameter μ, the third term in the action has $C = CP = CPT = -1$ and thus no symmetry to ensure the equality of particle and antiparticle masses. The parameter l has dimension of length, and the mass dimension of the parameter μ is $[M]^3$.

To apply this mechanism to the Standard Model, we consider its minimal extension by incorporating the right-handed neutrino:

$$
\psi_L = \begin{pmatrix} \nu_L \\ e_L \end{pmatrix}, \quad \psi_R = \begin{pmatrix} \nu_R \\ e_R \end{pmatrix} \qquad (3)
$$

and the part of the Standard Model Lagrangian relevant to our discussion is given by

$$
\begin{aligned}
\mathcal{L} = &\ \overline{\psi}_L i\gamma^\mu(\partial_\mu - igT^aW^a_\mu - i\frac{1}{2}g'Y_LB_\mu)\psi_L \\
&+ \overline{e}_R i\gamma^\mu(\partial_\mu + ig'B_\mu)e_R + \overline{\nu}_R i\gamma^\mu\partial_\mu\nu_R \\
&- \left[\frac{\sqrt{2}m_e}{v}\overline{e}_R\phi^\dagger\psi_L + \frac{\sqrt{2}m_D}{v}\overline{\nu}_R\phi_c^\dagger\psi_L + \frac{m_R}{2}\nu_R^TC\nu_R\right] \\
&+ h.c. \qquad (4)
\end{aligned}
$$

with $Y_L = -1$, and the Higgs doublet ϕ and its $SU(2)$ conjugate ϕ_c. One may then add a hermitian non-local Higgs coupling, which is analogous to the last term in (1), to the Lagrangian (4),

$$
\begin{aligned}
&\mathcal{L}_{CPT}(x) \\
&= -i\frac{2\sqrt{2}\mu}{v}\int d^4y\delta((x-y)^2-l^2)\theta(x^0-y^0) \qquad (5) \\
&\times\big\{\bar{\nu}_R(x)\left(\phi_c^\dagger(y)\psi_L(y)\right) - \left(\bar{\psi}_L(y)\phi_c(y)\right)\nu_R(x)\big\},
\end{aligned}
$$

without spoiling the basic $SU(2)_L \times U(1)$ gauge symmetry. In the unitary gauge, we then find the neutrino and antineutrino mass splitting[2)]

$$
m_\pm \simeq m_D \pm 4\pi\mu \int_0^\infty dz \frac{z^2 \sin[m_D\sqrt{z^2+l^2}]}{\sqrt{z^2+l^2}}. \qquad (6)
$$

We have assumed Dirac-type neutrinos by setting $m_R = 0$, but this may not be unnatural in the present context since the notion of antiparticle is best defined for a Dirac particle. In other words, if the neutrino–antineutrino mass splitting is confirmed by experiments, it would imply that neutrinos are Dirac-type particles rather than Majorana-type particles. The remaining couplings of the Standard Model are very tightly controlled by the $SU(2)_L \times U(1)$ gauge symmetry, and one can confirm that only the neutrino mass terms allow the present non-local gauge invariant couplings without introducing Wilson-line type gauge interactions.

If such a neutrino-antineutrino masss splitting will indeed be observed by future experiments, the presented pseudo-Dirac scheme could be considered as an economical alternative to seesaw mechanism [3)], where at the same time an explanation for the mass splitting between the particle and its antiparticle is provided.

References

1) M. Chaichian, K. Fujikawa and A. Tureanu, Phys. Lett. B **712**, 115 (2012); "Lorentz invariant CPT violation", arXiv:1205.0152 [hep-th].
2) It is possible to assign a finite value to the last term in eq.(6) for $m_D \neq 0$.
3) P. Minkowski, Phys.Lett. B **67**, 421 (1977).
T. Yanagida, in Proceedings of Workshop on Unified Theory and Baryon Number in the Universe, ed. by O. Sawada and A. Sugamoto (KEK report 79-18, 1979) p. 95.
M. Gell-Mann, P. Ramond and R. Slansky, in *Supergravity*, ed. by P. van Nieuwenhuizen and D.Z. Freedman (North-Holland, Amsterdam, 1979), p. 315.
R. N. Mohapatra and G. Senjanović, Phys. Rev. Lett. **44**, 912(1980).

† Condensed from the article in Phys. Lett. B**718**, 178 (2012).

*1 Department of Physics, University of Helsinki, Finland

Electromagnetic interaction in theory with Lorentz invariant CPT violation[†]

M. Chaichian,[*1] K. Fujikawa, and A. Tureanu[*1]

An attempt is made to incorporate the electromagnetic interaction in a Lorentz invariant but CPT violating non-local model with particle-antiparticle mass-splitting, which is regarded as a modified QED. The gauge invariance is maintained by the Schwinger non-integrable phase factor but the electromagnetic interaction breaks C, CP and CPT symmetries. Implications of the present CPT breaking scheme on the electromagnetic transitions and particle-antiparticle pair creation are discussed.

A non-local but Lorentz invariant and hermitian Lagrangian, which gives rise to a mass splitting between particle and antiparticle, has been recently proposed[1)]. The application of this scheme to the neutrino–antineutrino mass splitting in the Standard Model has been discussed[2)]. It was emphasized there that only the neutrino mass terms in the Standard Model can preserve the basic local $SU(2)_L \times U(1)$ gauge symmetry in the Lorentz invariant non-local CPT breaking scheme without introducing non-integrable phase factors. From the point of view of particle phenomenology, this uniqueness of the neutrino mass splitting in the Standard Model is quite interesting[3)].

If one wants to accommodate the non-local Lorentz invariant CPT breaking mechanism in the couplings of general elementary particles, one needs to go beyond the conventional local gauge principle by incorporating the Schwinger non-integrable phase factor. To be specific, we study the simplest Lorentz invariant and non-local CPT breaking hermitian Lagrangian (a modified QED):

$$\begin{aligned} S = & \int d^4x \Big\{ \bar{\psi}(x) i\gamma^\mu D_\mu \psi(x) - m\bar{\psi}(x)\psi(x) \\ & - \int d^4y [\theta(x^0 - y^0) - \theta(y^0 - x^0)] \delta((x-y)^2 - l^2) \\ & \times i\mu\bar{\psi}(x) \exp\left[ie\int_y^x A_\mu(z) dz^\mu\right] \psi(y) \Big\} \\ & - \frac{1}{4}\int d^4x F_{\mu\nu}(x) F^{\mu\nu}(x), \end{aligned} \tag{1}$$

with $D_\mu = \partial_\mu - ieA_\mu(x)$. This action is invariant under the gauge transformation $\psi(x) \rightarrow e^{i\alpha(x)}\psi(x)$ and $A_\mu(x) \rightarrow A_\mu(x) + \frac{1}{e}\partial_\mu\alpha(x)$, and C=CP=CPT=-1 transformation property of the non-local term is the same as in the theory without the electromagnetic coupling. We thus have the particle-antiparticle mass splitting

$$m_\pm \simeq m \pm 4\pi\mu \int_0^\infty dz \frac{z^2 \sin[m\sqrt{z^2 + l^2}]}{\sqrt{z^2 + l^2}}. \tag{2}$$

It is interesting to examine the charged particle pair creation from a virtual photon $\gamma(k) \rightarrow e(p) + \bar{e}(\bar{p})$. We then obtain the current in momentum space

$$J^\mu(k) = e\bar{u}(p)\gamma^\mu v(\bar{p}) + e\mu\bar{u}(p) F^\mu(p, \bar{p}) v(\bar{p}) \tag{3}$$

where

$$\begin{aligned} F^\mu(p,\bar{p}) \equiv & (-i\frac{\partial}{\partial\bar{p}_\mu}) \int_0^1 d\eta [f_+(k(\eta - 1) + \bar{p}) \\ & - f_-(k(\eta - 1) + \bar{p})]|_{k=p+\bar{p}}, \end{aligned} \tag{4}$$

with the Lorentz invariant "form factor" defined by

$$f_\pm(p) = \int d^4z_1 e^{\pm ipz_1} \theta(z_1^0) \delta((z_1)^2 - l^2). \tag{5}$$

We have a small correction $F^\mu(p, \bar{p})$ to the electromagnetic current, which flips chirality (and thus it is similar to the Pauli term) and violates C, CP and CPT. Note that the first term in (3) alone is not conserved due to the mass splitting, but the first and second terms in (3) put together are conserved.

As for practical implications of CPT breaking in the present modified QED, the search for the mass splitting of particle and antiparticle, just as the search for the neutrino antineutrino mass splitting in oscillation experiments[4)], is interesting[5,6)]. In the atomic transitions of the matter or antimatter systems, the frequency differences caused by the small mass difference between the "electron" and "positron" such as in (2) will be important. Other possibilities are to look for the possible small C and CP breaking in electromagnetic interactions other than those caused by weak interactions.

References
1) M. Chaichian, K. Fujikawa and A. Tureanu, Phys. Lett. B **712**, 115 (2012).
2) M. Chaichian, K. Fujikawa and A. Tureanu, Phys. Lett. B **718**,178 (2012).
3) H. Murayama and T. Yanagida, Phys. Lett. B **520**, 263 (2001).
S. M. Bilenky, M. Freund, M. Lindner, T. Ohlsson and W. Winter, Phys. Rev. D **65**, 073024 (2002).
G. Barenboim and J. D. Lykken, Phys. Rev. D **80**, 113008 (2009).
4) P. Adamson *et al.* [MINOS Collaboration], Phys. Rev. Lett. **107**, 181802 (2011).
5) T. Aaltonen *et al.* [CDF Collaboration], Phys. Rev. Lett. **106**, 152001 (2011).
6) M. Hori *et al.* [ASACUSA Collaboration], Nature **475**,484 (2011).

† Condensed from the article in Phys. Lett. B**718**, 1500 (2013).

*1 Department of Physics, University of Helsinki, Finland

Euler products beyond the boundary

T. Kimura, S. Koyama,[*1] and N. Kurokawa[*2]

For the Riemann zeta and the Dirichlet L-functions, we investigate their behavior of the Euler products on the critical line. A refined version of the Riemann hypothesis, which is named "the Deep Riemann Hypothesis" (DRH), is examined.

Let χ be a primitive Dirichlet character with conductor N. The Dirichlet L-function is expressed by the Euler product

$$L(s,\chi) = \prod_{p} \left(1-\chi(p)p^{-s}\right)^{-1}, \tag{1}$$

where p runs through all primes. This product is absolutely convergent in $\mathrm{Re}(s) > 1$.[1,2] The (generalized) Riemann Hypothesis (GRH) for $L(s,\chi)$ asserts that $L(s,\chi) \neq 0$ in $\mathrm{Re}(s) > 1/2$. When $\chi \neq \mathbf{1}$, it is equivalent to the convergence of the Euler product for $\mathrm{Re}(s) > 1/2$. Here we examine a "deeper" conjecture in the sense that we dig into the line $\mathrm{Re}(s) = 1/2$: (Deep Riemann Hypotyesis (DRH)). If $\chi \neq \mathbf{1}$ and $L(s,\chi) \neq 0$ with $\mathrm{Re}(s) = 1/2$, we have

$$\lim_{n\to\infty} \prod_{p\le n} (1-\chi(p)p^{-s})^{-1} = L(s,\chi) \times \begin{cases} \sqrt{2} & (s=\frac{1}{2} \textit{ and } \chi^2 = \mathbf{1}) \\ 1 & (\textit{otherwise}) \end{cases}, \tag{2}$$

where the product is taken over all primes p satisfying $p \le n$.

We show some numerical datum which are admitted as evidence of this conjecture by introducing the partial Euler product

$$L_x(s,\chi) = \prod_{p\le x} (1-\chi(p)p^{-s})^{-1}. \tag{3}$$

In what follows we put χ_{7a} and χ_{7b} to be the character χ modulo 7 with $\chi^2 \neq \mathbf{1}$ and $\chi^2 = \mathbf{1}$, respectively. Namely, if we define the character χ modulo 7 by giving the value at the primitive root $3 \in \mathbb{Z}/7\mathbb{Z}$, we define $\chi_{7a}(3) = \exp(\pi\sqrt{-1}/3)$ and $\chi_{7b}(3) = -1$. We also denote by χ_3 the nontrivial character modulo 3, which satisfies $\chi_3^2 = 1$.

Denote by p_n the n-th prime number. Figures 1 and 2 show the datum for the values $L_x\left(\frac{1}{2}+it, \chi\right)$ for $x = p_{10}$ (green), $x = p_{100}$ (blue), $x = p_{1000}$ (yellow) and ∞ (red). This shows as $t \to 0$, we apparently see $L_x(1/2+it, \chi) \to L(1/2,\chi)$ for $\chi^2 \neq \mathbf{1}$, $L_x(1/2+it,\chi) \to \sqrt{2}L(1/2,\chi)$ for $\chi^2 = \mathbf{1}$. This supports the DRH (2).

We introduce the following error function in order

[*1] Department of Biomedical Engineering, Toyo University
[*2] Department of Mathematics, Tokyo Institute of Technology

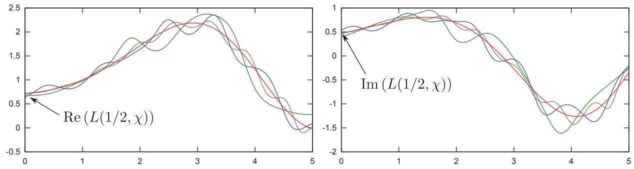

Fig. 1. Real part (left) and imaginary part (right) of $L_x(1/2+it, \chi_{7a})$

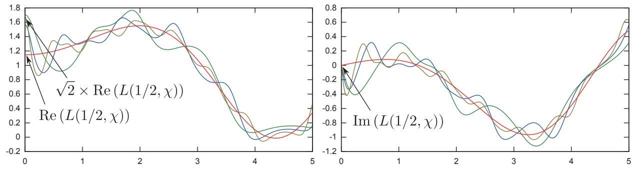

Fig. 2. Real part (left) and imaginary part (right) of $L_x(1/2+it, \chi_{7b})$

s	α (χ_{7a})	α (χ_{7b})
1/2	0.1167	0.1978
3/4	0.3814	0.3106
1	0.6389	0.6302

Table 1. Exponents of $\delta L_x(s,\chi) \sim x^{-\alpha}$ for χ_{7a} and χ_{7b}.

to estimate the speed of convergence for $L_x(s,\chi)$,

$$\delta L_x(s,\chi) = \begin{cases} \left|\frac{L_x(s,\chi)-\sqrt{2}L(s,\chi)}{\sqrt{2}L(s,\chi)}\right| & (s=1/2 \textit{ and } \chi^2 = \mathbf{1}) \\ \left|\frac{L_x(s,\chi)-L(s,\chi)}{L(s,\chi)}\right| & (\textit{otherwise}) \end{cases}$$

Figure 3 shows the values of $\delta L_x(s,\chi)$. When we approximate the error function as $\delta L_x(s,\chi) \sim x^{-\alpha}$, the exponents are determined by fitting the numerical results (Table 1). We see the speed of convergence becomes faster as the real part of argument gets larger.

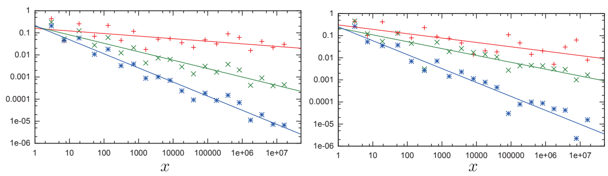

Fig. 3. $\delta L_x(s,\chi)$ for $s = 1/2$ (red), $s = 3/4$ (green) and $s = 1$ (blue) with χ_{7a} (left) and χ_{7b} (right)

References
1) F. Mertens, J. Reine Angew. Math. **78** (1874) 46.
2) E. C. Titchmarsh, Oxford University Press, 1987.

Hofstadter problem in higher dimensions

T. Kimura

The fractal structure of the energy spectrum for the two-dimensional magnetic lattice system, known as Hofstadter's butterfly,[1] is one of the most exotic consequences of the quantum property of the low-dimensionality. In this report we extend the Hofstadter problem, which is originally considered in two dimensions, to higher dimensions with not only Abelian, but also non-Abelian gauge field configuration.

We first consider the generic U(1) congifuration in $d = 2r$ dimensions

$$F_{2s-1,2s} = \omega_s, \quad F_{\mu\nu} = 0 \quad \text{for} \quad \text{otherwise}, \tag{1}$$

with $s = 1, \cdots, r$. When we put this on a lattice, it is realized as a link variable with the higher dimensional Landau gauge,

$$U_{2s-1}(x) = e^{-i\omega_s x_{2s}}, \quad U_{2s}(x) = 1. \tag{2}$$

In particular, the tight-binding model with the configuration satisfying

$$P_{\mu\nu}(x) = U_\mu(x) U_\nu(x+\hat{\mu}) U_\mu^\dagger(x+\hat{\nu}) U_\nu^\dagger(x) = -1, \tag{3}$$

is called the π-flux state,[2] since $\omega_s = \pi$ for $\forall s$. The configuration (3) is realized by $\mathbb{Z}_2 \subset$ U(1) link variables, $U_\mu(x) = \eta_\mu \equiv (-1)^{x_1 + \cdots + x_{\mu-1}}$. The Hamiltonian of the model is given by

$$\mathcal{H}_{\text{tight}} = \sum_{x,\mu} \eta_\mu c_x^\dagger (c_{x+\hat{\mu}} + c_{x-\hat{\mu}}). \tag{4}$$

Applying the transformation $c_x \to i^{x_1 + \cdots + x_d} c_x$, it is equivalent to the staggered fermion action, up to a trivial factor,[3]

$$S_{\text{staggered}} = \sum_{x,\mu} \frac{1}{2} \eta_\mu \bar{\chi}_x (\chi_{x+\hat{\mu}} - \chi_{x-\hat{\mu}}). \tag{5}$$

Although there is no spinor structure in this formalism, its spectrum is relativistic, because it is directly obtained from the naive Dirac fermion through the spin-diagonalization.

We consider another generalization of the Hofstadter problem in higher dimensions by applying a non-Abelian gauge field as a background configuration. We now concentrate on the four dimensional model with SU(2) gauge field for simplicity, whose configuration is given by $A_0 = 0$, $A_j = -\omega_j x_0 \sigma_j$ for $j = 1, 2, 3$ with σ_j being the Pauli matrix. The corresponding filling fraction is defined as $\omega_j = 2\pi n_j / L^2 \equiv 2\pi p_j / q_j$. The total background flux is given by

$$\frac{1}{16\pi^2} \int_{L^4} d^4x \, \epsilon^{\mu\nu\rho\sigma} \, \mathrm{Tr} \, F_{\mu\nu} F_{\rho\sigma} = 2\pi N, \tag{6}$$

with a field strength, $F_{0j} = -\omega_j \sigma_j$ and $F_{jk} = -\omega_j \omega_k x_0^2 \epsilon_{ijk} \sigma^i$. Here this integral is taken over the four dimensional hypercubic lattice of the size L^4, and we define the flux number $N = n_1 n_2 n_3$.

The link variable associated with this configuration is given by $U_0(x) = \mathbb{1}$, $U_j(x) = e^{-i\omega_j x_0 \sigma_j}$. In this case, the translation symmetry of the lattice system yields

$$x_0 \sim x + q_{\text{LCM}}, \quad x_j \sim x_j + 1, \tag{7}$$

where q_{LCM} is the least common multiple of q_1, q_2, q_3. This means that the unit cell of this system is also extended in only one dimension as well as the two dimensional case with U(1) magnetic field.

We numerically caluculate the spectrum of the lattice fermion with the configuration discussed above. The model defined in four dimensions is reduced to an effective one-dimensional model due to SU(2) $\cong S^3$ gauge symmetry. Fig. 1 shows the density of spectrum against ω_0, with homogeneous configuration $\omega_j = \omega_0$ for $j = 1, 2, 3$. Although its spectrum is not totally gapped, one can observe a hierarchical structure of the spectrum as well as the two dimensional case.[1] At the even fraction flux, e.g. $\omega_0/(2\pi) = 1/2, 1/4, \cdots$, we find a dip in the spectrum. Similar structure is discussed in the ordinary two dimensional Hofstadter problem at the gapless point of the filling fraction.

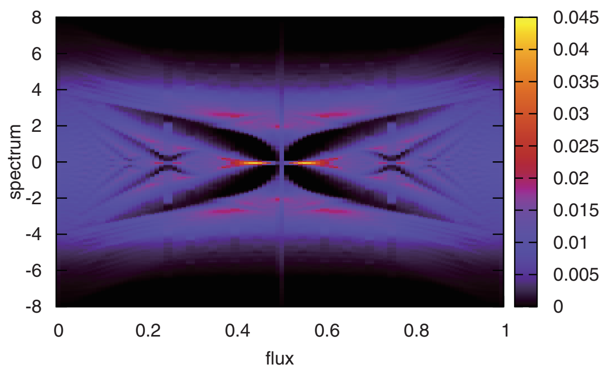

Fig. 1. Density of states for the Harper's equation for the homogeneous flux condition $\omega_{j=1,2,3} = \omega_0 \equiv 2\pi p/q$ with $q = 100$, $p = 0, \cdots, 99$.

References

1) D. R. Hofstadter, Phys. Rev. **B14** (1976) 2239.
2) I. Affleck, J. B. Marston, Phys. Rev. **B37** (1988) 3774; J. B. Marston, I. Affleck, Phys. Rev. **B39** (1989) 11538.
3) J. B. Kogut, L. Susskind, Phys. Rev. **D11** (1975) 395; L. Susskind, Phys. Rev. **D16** (1977) 3031.

Holographic entanglement entropy in topologically massive gravity†

N. Ogawa and T. Ugajin[1,2]

In understanding the quantum aspects of gravity, one promising method is to investigate some higher derivative gravity theories as the first steps. In this article, we focus on the well-known simplest higher derivative gravity, called *topologically massive gravity* (TMG)[1]). We attempt to test the AdS/CFT correspondence[2]) for TMG through the computation of *entanglement entropy* (EE).

1 TMG and dual CFT$_2$

TMG is defined by the action,

$$I_{TMG} = \frac{1}{16G_N}\left(I_{EH} + \frac{1}{\mu}\cdot I_{CS}\right),$$
$$I_{EH} = \int d^3x\sqrt{-g}\left(\mathcal{R} + \frac{2}{L^2}\right),$$
$$I_{CS} = \frac{1}{2}\int d^3x\sqrt{-g}\left[\epsilon^{\mu\nu\sigma}\Gamma^{\rho}{}_{\mu\lambda}\left(\partial_\nu\Gamma^{\lambda}{}_{\sigma\rho} + \frac{2}{3}\Gamma^{\lambda}{}_{\nu\kappa}\Gamma^{\kappa}{}_{\sigma\rho}\right)\right],$$

where I_{CS} denotes the gravitational Chern–Simons (CS) term. This theory adopts the usual AdS$_3$ and BTZ black–hole geometries as solutions, and the asymptotic symmetry analysis on them yields two sets of Virasoro symmetries with different central charges,

$$c_L = \left(1 - \frac{1}{\mu L}\right)\frac{3L}{2G_N}, \quad c_R = \left(1 + \frac{1}{\mu L}\right)\frac{3L}{2G_N}.$$

This result strongly suggests that the system is dual to a 2d asymmetric CFT with these central charges.

2 Formulas for EE on CFT and TMG

We consider the EE for an interval I_ℓ with length ℓ. The 2d CFT formula for the EE is already known as[3]),

$$S^{CFT}_\ell = \frac{c_L}{6}\log\left[\frac{\beta_L}{\pi}\sinh\left(\frac{\pi\ell}{\beta_L}\right)\right] + \frac{c_L}{6}\log(\epsilon) + (L \to R),$$

where $\beta_{L,R}$ denote the excitation temperatures of the left movers and right movers respectively, and ϵ denotes the UV cutoff.

On the gravity side, by considering a bulk conical deficit line Σ ending on the endpoints of I_ℓ on the boundary, corresponding to the *replica trick* for EE on field theories, we arrive at the formula,

$$S^{TMG}_\ell = \min_\Sigma\left(\frac{L_\Sigma}{4G_N} - \frac{1}{8G_N\mu}\int_\Sigma dl\,\omega_{ab\sigma}e^a{}_\alpha e^b{}_\beta\epsilon^{\mu\nu\sigma}N^\alpha{}_\mu N^\beta{}_\nu\right),$$

where $e^a{}_\alpha$, $\omega^{ab}{}_\alpha$, and $N_{\alpha\beta}$ denote the dribeins, spin connections and the binormal tensor to Σ, respectively. In the right hand side, the first term represents the famous Ryu–Takayanagi formula[4]) in Einstein gravity, and the second term represents the correction from the CS term. We can also derive simple relationships between $\beta_{L,R}$ of CFT and (M, J) of BTZ, which enables the comparison of S^{CFT}_ℓ and S^{TMG}_ℓ.

3 Numerical comparison for rotating BTZ

We now have all the necessary formulas to evaluate the entanglement entropy. However, we find that S^{TMG}_ℓ is too complicated and difficult to evaluate analytically. Instead, what we can do is to compute it numerically and compare it to the analytic value of S^{CFT}_ℓ. Although this would still involve some complicated procedure of numerically solving the EoMs, integrating the values, and finding the appropriate initial conditions, we can finally plot the results as displayed in Fig.1, showing the finite term of S_ℓ without $\log\epsilon$ divergences. This final result shows a good qualitative agreement of S^{TMG}_ℓ and S^{CFT}_ℓ, but we also find a disagreement of the order of $\sim 1\%$. This amounts to an order of $\sim 10\%$ of the CS contribution, and, hence this value is significant.

We do not thus far determined the origin of this unexpected disagreement, and it may provide some clue to a better understanding of this theory and holography.

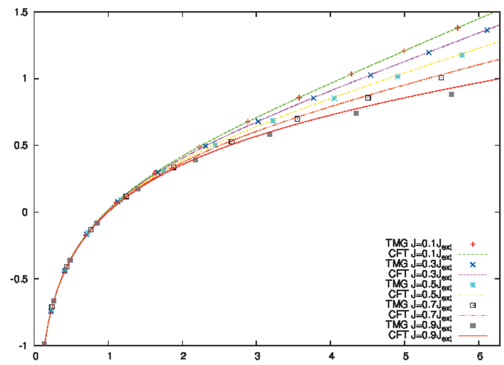

Fig. 1. Plot of (ℓ, S_ℓ) for $\mu L = 1$, called the *chiral point*.

References
1) S. Deser, R. Jackiw and S. Templeton: Phys. Rev. Lett. **48**, 975 (1982).
2) J. M. Maldacena: Adv. Theor. Math. Phys. **2**, 231 (1998) [hep-th/9711200].
3) V. E. Hubeny, M. Rangamani and T. Takayanagi: JHEP **0707**, 062 (2007) [arXiv:0705.0016 [hep-th]].
4) S. Ryu and T. Takayanagi: Phys. Rev. Lett. **96**, 181602 (2006) [hep-th/0603001].

† Condensed from the article in preparation, including tentative results.
*1 Kavli Institute for the Physics and Mathematics of the Universe, University of Tokyo
*2 Yukawa Institute for Theoretical Physics, Kyoto University

Viscoelastic-electromagnetism and Hall viscosity†

Y. Hidaka, Y. Hirono, T. Kimura, and Y. Minami

After Luttinger showed that the gravitational potential is essential for thermal transport,[1] it turns out that we can deal with thermal transport in a quite similar manner to the electric transport by introducing a kind of electromagnetism. In this formalism the gauge potential comes from some of the degrees of freedom in the spacetime geometry, and then the thermal gradient can be represented as the corresponding electric field. In this report, we explore the possibility of such an effective electromagnetic description of viscoelastic theory. We would like to show that the vielbein, introduced in Cartan's formalism for general relativity, can be interpreted as such a gauge potential describing viscoelastic theory, and then investigate some aspects of the corresponding electromagnetism, which we will call *viscoelastic-electromagnetism*.

The metric of the spacetime is generally written by using vielbein $e_\mu{}^a$, which connects the global curved spacetime coordinate with the locally flat coordinate, $g_{\mu\nu} = \eta_{ab} e_\mu{}^a e_\nu{}^b$, where $\eta_{ab} = \mathrm{diag}(-1, 1, 1, 1)$ is the locally flat Minkowski metric. We can provide a physical meaning for the vielbein in viscoelastic theory. The time component of the vielbein $e_\mu{}^0$ coincides with the gauge fields of gravito-electromagneticfields $e_\mu{}^0 = (e^\sigma, e^\sigma A_i$ describing the thermal transport. For the spatial component, introducing the displacement vector u_i, which is regarded as the 0-form, the vielbein can be expanded as $e_\mu{}^i = \delta_\mu{}^i + \partial_\mu u^i$ in the linear order. Here $\partial_\mu u^i \equiv u_\mu{}^i$ is the distortion tensor, which is just the 1-form with respect to the global coordinate. Thus, the vielbein plays essentially the same role as this distortion tensor. Therefore, we call the electromagnetism corresponding to this 1-form *viscoelastic-electromagnetism*.

The 2-form, obtained from the vielbein, yields the torsion tensor $T^a = de^a + \omega^a{}_b \wedge e^b$. In the following we assume that the spin connection is zero for simplicity, because it can be simply restored by replacing the derivative with the covariant one, $d \to d + \omega$. The field strength 2-form is given by $F_{\mu\nu}^{\ a} = \partial_\mu e_\nu{}^a - \partial_\nu e_\mu{}^a$. If this 2-form takes a non-zero value, the displacement vector, namely the vector potential for viscoelastic-electromagnetism, cannot be single-valued. In fact, the corresponding magnetic field is given by

$$B^{ia} = \epsilon^{ijk} \partial_j e_k{}^a, \tag{1}$$

and thus the magnetic flux $b^a = \int d\vec{S} \cdot \vec{B}^a$ is identified as the *Burgers vector*, which characterizes a lattice dislocation in a crystal. Similarly, the electric field yields

$$E_i{}^j \equiv F_{0i}^{\ j} = -\partial_i e_0{}^j \equiv -\partial_i v^j, \tag{2}$$

where we define the spatial derivative of the vielbein as the gradient of the velocity field due to the relation between the vielbein and the distortion fields. This shows that the velocity can be interpreted as the chemical potential for viscoelastic-electromagnetism, and also that we can formulate the momentum transport response by applying this viscoelastic-electric field.

We can show that the gauge transformation is consistent with viscoelastic theory. Taking the transformation for the 1-form, $e_\mu{}^a \to e_\mu{}^a + \partial_\mu w^a$, it does not affect the torsion tensor 2-form because we have $\epsilon^{\mu\nu}\partial_\mu \partial_\nu w^a = 0$. This symmetry comes from the conservation of energy and momentum, i.e., translation symmetry. Thus, we can derive the corresponding momentum current as Nöther's current.

Based on this formalism we derive the Středa formula[2,3] for the Hall viscosity, an anti-symmetric part of the viscosity tensor η_{ijab}, while the shear viscosity is given by a symmetric part. We start with the expression of the Hall current with the magnetization $\vec{M}$ as $\vec{J}_{\mathrm{H}} = \vec{\nabla} \times \vec{M}$. Since the gradient of the chemical potential yields the electric field $e\vec{E} = \vec{\nabla}\mu$ with the electric charge e, we have the relation between the current and the electric field,

$$\vec{J}_{\mathrm{H}} = \left(\frac{\partial \vec{M}}{\partial \mu}\right)_{T,B} \times \vec{\nabla}\mu = \left(\frac{\partial \vec{M}}{\partial \mu}\right)_{T,B} \times e\vec{E}. \tag{3}$$

Thus the Hall coefficient is given by

$$\sigma_{\mathrm{H}} = e\left(\frac{\partial M_z}{\partial \mu}\right)_{T,B} = e\left(\frac{\partial n}{\partial B}\right)_{T,\mu} \tag{4}$$

where we use the thermodynamic relation with the particle number density n. Applying this derivation to viscoelastic-electromagnetism, we have the following expression of the Hall viscosity,

$$\eta_{\mathrm{H},a}{}^b = \left(\frac{\partial M_a}{\partial v_b}\right)_{T,B} = \left(\frac{\partial P^b}{\partial B^a}\right)_{T,v}, \tag{5}$$

where the corresponding magnetization is given by $M_{ia} = \frac{1}{2}\epsilon_{ijk} x^j T^k_{\ a}$ and $v_b = e^0{}_b$ is the fluid velocity, which is conjugate to momentum P^b. Usually this part should be diagonal by assuming the isotropy, $\eta_{\mathrm{H},a}{}^b \propto \delta_a{}^b$. The formula derived above is written only in terms of thermodynamic quantities, which should be universal, and can be applied to generic systems.

† Condensed from the article in PTEP **2013** (2013) 013A02.

References

1) J. M. Luttinger, Phys. Rev. **135** (1964) A1505.
2) P. Středa, J. Phys. C: Solid State Phys. **15** (1982) L717.
3) A. Widom, Phys. Lett. **A90** (1982) 474.

Vortex counting from field theory†

T. Fujimori,[*1] T. Kimura, M. Nitta, and K. Ohashi[*2]

The gauge theory partition function plays an essential role in non-perturbative aspects of supersymmetric gauge theory. It is directly given by performing path integral for a certain supersymmetric theory, and correctly provides its low energy dynamics. Recently partition functions have been provided for the low dimensional gauge theories by performing vortex counting, where non-Abelian vortices in $\mathrm{U}(N)$ gauge theories play roles of instantons in two dimensions. In this report we apply the moduli matrix approach[1)] to study the vortex moduli space. The fixed points in the moduli space with respect to the isometry, which is coming from the symmetry of the gauge theory, are completely classified in terms of the moduli matrix. Thus we can write down the character for the tangent space through the moduli matrix method, and then obtain the vortex partition function.

We consider 2d $\mathcal{N}=(2,2)$ $\mathrm{U}(N)$ gauge theory with N fundamental chiral multiplets. The solution of the BPS equation can be written in terms of a holomorphic matrix $H_0(z)$, which we call the moduli matrix. $z = x1 + ix_2$ is the complex coordinate of the two dimensional space C. The rank of $H_0(z)$ is N for $\mathrm{U}(N)$ gauge theory. Remark the BPS state is invariant under the V-transformation, $H_0(z) \longrightarrow V(z)H_0(z)$ with $V(z) \in \mathrm{GL}(N, \mathrm{C})$ being holomorphic with respect to z.

In order to discuss the vortex moduli space volume by applying the localization formula, we have to study the fixed points with respect to the maximal torus of the symmetry of the theory. In this case it is given by $\mathrm{U}(1) \times \mathrm{U}(1)^{N-1} \subset \mathrm{SO}(2) \times \mathrm{SU}(N)$. Here $\mathrm{SO}(2)$ and $\mathrm{SU}(N)$ are the spatial rotation symmetry in two dimensions and the diagonal part of the color-flavor symmetry, respectively. The torus action on the moduli matrix is given by

$$H_0(z) \quad \longrightarrow \quad H_0(T_\epsilon z)T_{\vec{a}}, \tag{1}$$

where $T_\epsilon = e^{i\epsilon}$ and $T_{\vec{a}} = \mathrm{diag}(e^{ia_1}, \cdots, e^{ia_N})$. Letting $H_0^{\vec{k}}(z) = \mathrm{diag}(z^{k_1}, \cdots, z^{k_N})$ with $\vec{k} \in (\mathrm{Z}_{\geq 0})^N$, we can see it satisfies

$$H_0^{\vec{k}}(z) = V_{\vec{k}} H_0^{\vec{k}}(T_\epsilon z)T_{\vec{a}} \tag{2}$$

with

$$V_{\vec{k}} = \mathrm{diag}(e^{-i(k_1\epsilon + a_1)}, \cdots, e^{-i(k_N\epsilon + a_N)}). \tag{3}$$

Eq. (2) shows $H_0^{\vec{k}}(z)$ is invariant under the torus action up to the V-transformation given by (3).

In order to study the action of the torus action for the tangent space, let us consider the neighborhood around the fixed point parametrized by a small deviation $\delta H_0(z)$, which obeys the infinitesimal version of the equivalence relation $\delta H_0(z) \sim \delta H_0(z) + \delta V(z)H_0^{\vec{k}}(z)$. Since $\delta H_0(z)$ is an arbitrary $N \times N$ matrix whose components are polynomials of z, the vector space of all $\delta H_0(z)$ can be written as

$$\{\delta H_0\} \cong \mathrm{C}^N \otimes \underbrace{(\mathrm{C}[z] \oplus \cdots \oplus \mathrm{C}[z])}_{N} \tag{4}$$

where $\mathrm{C}[z]$ is the set of polynomials. The vector spaces C^N and $\mathrm{C}[z] \oplus \cdots \oplus \mathrm{C}[z]$ correspond to the rows and columns of $\delta H_0(z)$, respectively. On the other hand, the space of all infinitesimal V-transformation can be written as

$$\{\delta V H_0^{\vec{k}}\} \cong \mathrm{C}^N \otimes (I_{k_1}[z] \oplus \cdots \oplus I_{k_N}[z]) \tag{5}$$

where $I_k[z]$ is the set of polynomials which are multiples of z^k. Therefore the tangent space at the fixed point labeled by $\vec{k}$ is given by

$$T_{\vec{k}}\mathcal{M} \cong \mathrm{C}^N \otimes (P_{k_1}[z] \oplus \cdots \oplus P_{k_N}[z]) \tag{6}$$

where $P_k[z]$ is the set of polynomials whose degrees are less than k. Due to (2) the characters of the torus action on C^N and $P_{k_1}[z] \oplus \cdots \oplus P_{k_N}[z]$ are given by

$$\chi(\mathrm{C}^N) = \mathrm{Tr}\ [V_{\vec{k}}(z)] = \sum_l^N (T_\epsilon^{k_l} T_{a_l})^{-1}, \tag{7}$$

$$\chi(P_{k_1}[z] \oplus \cdots \oplus P_{k_N}[z]) = \sum_{l=1}^N T_{a_l} \sum_{i=1}^{k_l} T_\epsilon^{i-1}. \tag{8}$$

Thus the character of the torus action on $T_{\vec{k}}\mathcal{M}$ is

$$\chi(T_{\vec{k}}\mathcal{M}) = \sum_{l=1}^N \sum_{m=1}^N \sum_{i=1}^{k_m} T_{a_{ml}} T_\epsilon^{-k_l+i-1} \tag{9}$$

where we have denoted $a_{ml} = a_m - a_l$. Then the vortex partition function for $\mathrm{U}(N)$ gauge theory with N fundamental chiral multiplets is given by applying the localization formula:[2)] it can be found by replacing the sum by the producst over the weights as

$$Z_{\vec{k}} = \prod_{l,m}^N \prod_{i=1}^{k_m} \frac{1}{a_{ml} + (-k_l + i - 1)\epsilon}. \tag{10}$$

The number of products in this factor is Nk, which is just the dimension of the moduli space $\dim_{\mathrm{C}}\mathcal{M}_{N,k} = Nk$.

References
1) M. Eto *et al.*, Phys. Rev. Lett. **96** (2006) 161601.
2) U. Bruzzo *et al.*, JHEP **05** (2003) 054.

† Condensed from the article in JHEP **1206** (2012) 028
*1 Department of Physics, National Taiwan University, Taiwan
*2 Department of Math and Physics, Osaka City University

A comment on holographic Luttinger theorem†

K. Hashimoto, and N. Iizuka

Robustness of the Luttinger theorem for fermionic liquids is examined in holography. The statement of the Luttinger theorem, the equality between the fermion charge density and the volume enclosed by the Fermi surface, can be mapped to a Gauss's law in the gravity dual, *a la* Sachdev. We show that various deformations in the gravity dual, such as inclusion of magnetic fields, a parity-violating θ-term, dilatonic deformations, and higher-derivative corrections, do not violate the holographic derivation of the Luttinger theorem, as long as the theory is in a confining phase. Therefore a robustness of the theorem is found for strongly correlated fermions coupled with strongly coupled sectors which admit gravity duals. On the other hand, in the deconfined phase, we also show that the deficit appearing in the Luttinger theorem is again universal. It measures a total deficit which measures the charge of the deconfined fermions, independent of the deformation parameters.

The Luttinger theorem[1)]is one of the key fundamental relations in condensed matter physics and it states that the volume enclosed by the Fermi-surface is equal to the charge density. This theorem, which is originally derived by Luttinger and Ward for Landau's Fermi liquids, is non-trivial in the sense that this theorem is about the volume enclosed by the Fermi-surface. Remember that in the Landau's Fermi-liquid picture, we have a quasi-particle description for the spectrum near the Fermi-surface, but generically the quasi-particle description is not valid for the spectrum far away from the Fermi-surface, therefore the spectrum deep inside the Fermi-surface does not always allow the quasi-particle description generically.

It is widely known that the theorem holds for Fermi liquids having a Fermi surface, and there is a general non-perturbative proof of the Luttinger theorem for Fermi liquids[2)] (the original proof by Luttinger and Ward was with perturbation of Fermi liquids). On the other hand, in nature there are quite interestingly materials, such as high T_c superconductors or heavy fermions, where its normal phase shows non-Fermi liquid behavior, and in addition, the standard quasi-particle description breaks down. In such situations whether the theorem holds or not is to be better understood.

Recent progress in applications of string theory, the holographic principle[3)], to condensed matter systems brought an insight about the Luttinger theorem in strongly correlated fermion systems. In[4–6)], it was pointed out that a holographic system with a charged bulk fermion exhibits the Luttinger theorem of the boundary fermion theory. Furthermore, Sachdev clarified[7)] that in a simple holographic set-up for fermions with fermion-number chemical potential, the Luttinger relation follows simply from the Gauss's law in the bulk and that it holds in confined phase (thermal gas phase) but breaks down in deconfined phase (black hole phase). However it is also true that their argument uses a specific holographic setup like neglecting higher derivative corrections. So it is natural to ask how universal the non-perturbative Luttinger theorem is.

The holographic principle has been widely applied to various gravity setups, and robust correspondence has been thoroughly studied. Among many variations of the holographic models, some of the most popular and meaningful ones are: (i) higher-derivative corrections in the bulk gravity + Maxwell theory, (ii) inclusion of θ term and magnetic field, (iii) inclusion of a dilaton to have dilatonic gravity models.Each corresponds, in terms of condensed matter theory language, to: (i) Sub-leading terms concerning the strong coupling expansion, (ii) Parity-violating terms inducing quantum Hall effects under magnetic fields, and (iii) Drastically different infra-red behavior, for example having a Lifshitz-like scaling near quantum critical points, and more realistic systems with vanishing entropy at zero temperature.

We study whether the holographic derivation of the Luttinger theorem *a la* Sachdev can survive against the deformations, to find a universality of the holographic Luttinger theorem. We examine these deformations and show the Luttinger theorem to hold for all of these deformations, in the case of confining phases:

$$\langle \mathcal{Q} \rangle / q = \frac{qB}{2\pi} \sum_{l,n} \theta(-E_{l,n}) \,. \tag{1}$$

Here B is the magnetic field, q is the charge of the fundamental fermion, $\mathcal{Q}$ is the total charge and E is the energy levels.

References
1) J. M. Luttinger and J. C. Ward, Phys. Rev. **118**, 1417 (1960); J. M. Luttinger, Phys. Rev. **119**, 1153 (1960).
2) M. Oshikawa, Phys. Rev. Lett. **84**, 3370 (2010).
3) J. M. Maldacena, Adv. Theor. Math. Phys. **2**, 231 (1998)
4) S. A. Hartnoll, D. M. Hofman and D. Vegh, JHEP **1108**, 096 (2011)
5) S. A. Hartnoll, D. M. Hofman and A. Tavanfar, Europhys. Lett. **95**, 31002 (2011)
6) N. Iqbal, H. Liu and M. Mezei, JHEP **1204**, 086 (2012)
7) S. Sachdev, Phys. Rev. D **84**, 066009 (2011)

† Condensed from the article in JHEP 1207 (2012) 064.

Impurities in holography and transport coefficients†

K. Hashimoto, and N. Iizuka

We present a way to include impurities in AdS/CFT correspondence, in view of its application to condensed matter physics. Examples of these are the current impurity and spin impurity. We calculate electric conductivity and spin susceptibility of holographic superconductors, with doping of density/spin impurities.

Holography or AdS/CFT correspondence[1] is an extremely useful tool, in the sense that it gives a new view of strongly coupled limit of quantum field theories, from the gravitational viewpoint. Many of the transport coefficients in strongly coupled systems can be calculated by using holographic setting. In this paper we consider effects of generic impurities, including magnetic impurities.

Kondo effect is induced due to the quantum spin nature of magnetic impurities coupled to conducting electrons near their Fermi-surfaces. The spin operator of the impurity fermion $\psi_{\rm im}$[a] can be described by

$$\langle \psi^\dagger_{\rm im}\sigma^\mu\psi_{\rm im}\rangle \sim J^\mu\,. \qquad (1)$$

In this paper, treating J^μ as an external input, we consider the effects of the impurity J^μ to the transport coefficients in holographic settings. Our impurity is introduced by hand. For simplicity, we consider only homogeneous impurities which induce homogeneous source current J^μ. This naturally induces a bulk current $J^\mu(r)$, which is dependent only on the AdS bulk radial coordinates r.

Without the impurities, the conductivity (or the current correlator) is treated in the AdS/CFT correspondence as follows. Let us consider a strongly coupled fermion ψ in $1+2$ dimensions. The fermion number current is given by $\mathcal{O}^\mu \equiv \bar\psi\gamma^\mu\psi$. We weakly gauge this $U(1)$ symmetry, which is nothing but the electromagnetism, to have the coupling $\int d^3x A_\mu\mathcal{O}^\mu$. To derive the current correlator, in the gravity side, we upgrade the "source" $A_\mu(x^\mu)$ for the operator $\mathcal{O}^\mu$ to a bulk field $A_M(x^\mu, r)$ where r is the bulk coordinate along the AdS radial direction. According to the AdS/CFT dictionary, we demand that the bulk field approaches to the value of the boundary source, $\lim_{r\to\infty} A_{M=\mu} = A_\mu$. We solve the equation in the bulk, and substitute it to the bulk action, to obtain the classical bulk partition function which is a function of the boundary source A_μ. In the AdS/CFT this is equal to the boundary partition function with the source A_μ of the source term $\int d^3x A_\mu\mathcal{O}^\mu$.

Now, let us add the impurities. Suppose the impurity is giving the electric density and the electric currents only, then the impurity coupling at the boundary theory is the minimal coupling $\int d^3x A_\mu \mathcal{O}^\mu_{\rm imp}$, where the impurity operator would be given by the impurity fermion field $\psi_{\rm im}(x^\mu)$ as $\mathcal{O}^\mu_{\rm imp} \equiv \bar\psi_{\rm im}\gamma^\mu\psi_{\rm im}$. Let us treat the impurities as classical objects. Since we can distribute the impurity in an arbitrary manner in real-world experiments, we can take the vacuum expectation value of the current $\langle\mathcal{O}^\mu_{\rm imp}(x^\mu)\rangle$ to be an arbitrary function. That is, our impurity coupling is

$$\int d^3x A_\mu(x)\langle\mathcal{O}^\mu_{\rm imp}(x^\mu)\rangle. \qquad (2)$$

In going to the gravity side of the AdS/CFT correspondence, we upgrade this coupling (2) to the bulk coupling,

$$\int d^3x dr\ A_M(x,r) J^M(x^\mu, r). \qquad (3)$$

We propose that this is a generic effect due to the impurities in AdS/CFT correspondence. If one specifies the dynamics of the impurity, the configuration $J^M(x^\mu, r)$ is determined. Basically, the radial dependence of the bulk source field $J^M(x^\mu, r)$ represents how the impurity responds in different energy scales. Since the behavior of the impurities at different energy scale can be taken arbitrary as an external input, we take J^M as an input source to the bulk gravitational action.

A result of an explicit calculation of the conductivity, after the introduction of the charge density impurity, is presented in Fig.1. The calculation is the standard one in holography, in a AdS-Schwarzschild background. We see that the conductivity grows.

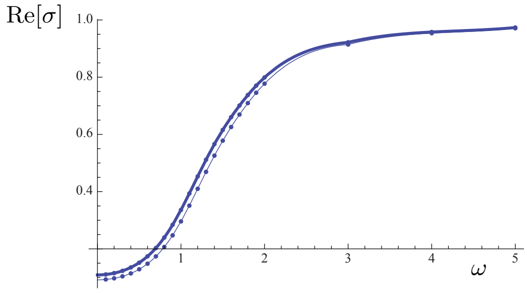

Fig. 1. The plot of the conductivity σ as a function of the frequency ω. Thick line: conductivity with the impurity $J^t = 0.1/r^6$. Thin line with dots: conductivity with no impurity.

References
1) J. M. Maldacena, Adv. Theor. Math. Phys. **2**, 231 (1998)

† Condensed from the article in arXiv:1207.4643.

a) This impurity fermion $\psi_{\rm im}$ should not be confused with conducting quasi-particle fermions, like electrons.

6. Astrophysics and Astro-Glaciology

Measurement of nitrogen and oxygen isotope ratios of nitrate in a shallow ice core drilled in the vicinity of Dome Fuji station, East Antarctica

S. Okamoto, K. Takahashi, H. Motoyama,[*1] A. Makabe,[*2] K. Koba,[*2] and Y. Motizuki

Ice core samples have been regarded as " time capsules " containing substantial information on the history of the earth, including information on climate change. They are also considered to have recorded astronomical events. In the event of extraterrestrial high energy radiation (e.g., supernova and solar proton events), the chemical composition of the atmosphere is changed. For example, γ-rays emitted by supernovae are absorbed into the atmosphere in the stratosphere to generate nitrogen compounds, including HNO_3. Therefore, nitrogen and oxygen isotope ratios ($\delta^{15}N$ and $\delta^{18}O$) of NO_3^- in ice core are expected to be used as archives of isotope fractionations by photochemical reactions in the stratosphere.

In 2010, a shallow ice core was obtained by drilling 10 km south of Dome Fuji station, East Antarctica, which is regarded as an ideal site for the research of atmospheric reactions because at this location, chemical components are directly transported from stratosphere. In this study, we analyzed $\delta^{15}N$ and $\delta^{18}O$ around two NO_3^- spikes (41.585–42.360 m, 45.335–46.530 m) in the Dome Fuji ice core using a denitrifier method.[1)] The method is based on the isotopic analysis of nitrous oxide (N_2O) generated from NO_3^- by denitrifying bacteria (*Pseudomonas aureofaciens*). The isotopic composition of N_2O is then measured on a mass spectrometer (SerCon Ltd.). Throughout the text, isotope ratios are reported using delta (δ) notation in units of "per mil" (‰): $\delta^{15}N_{\mathrm{sample}} = ((^{15}N/^{14}N)_{\mathrm{sample}}/(^{15}N/^{14}N)_{\mathrm{reference}} - 1) \times 1000$ ‰ and $\delta^{18}O_{\mathrm{sample}} = ((^{18}O/^{16}O)_{\mathrm{sample}}/(^{18}O/^{16}O)_{\mathrm{reference}} - 1) \times 1000$ ‰, where the $^{15}N/^{14}N$ reference is defined by the N_2 in air and the $^{18}O/^{16}O$ reference is defined by the Vienna Standard Mean Ocean Water (VSMOW). The reproducibilities of the $\delta^{15}N$ and $\delta^{18}O$ data were ± 0.39 ‰ and ± 0.71 ‰, respectively.

The $\delta^{15}N$ and $\delta^{18}O$ range from 142 ‰ to 279 ‰ and from 30.4 ‰ to 54.4 ‰, respectively (Fig. 1). This range is similar to that found in previous studies using snow pit samples from Dome C, inland Antarctica[2,3)]. In the upper part (41.585–42.360 m), $\delta^{15}N$ and $\delta^{18}O$ show highly significant correlation ($r = 0.88, p < 0.001$), while they show no correlation (r = -0.27) in the lower part (45.335–46.530 m). The $\delta^{15}N$ shows high values at the depth of NO_3^- spikes, while the values of $\delta^{18}O$ remain unclear. Previous studies inferred that $\delta^{15}N$ contains a NO_x source signature[4)] and that $\delta^{18}O$ is dependent upon the oxidation pathway that produces HNO_3 from NO_x in the atmosphere[4,5)]. Our results suggest that it should be possible to identify the source of NO_3^- spikes. Further measurements of the $\delta^{15}N$ and $\delta^{18}O$ of NO_3^- are expected to contribute in revealing hidden signatures through post-depositional processes of NO_3^- in inland Antarctica. Obtaining clearer results will require a better understanding of the possible fractionations associated with chemical reactions in the stratosphere.

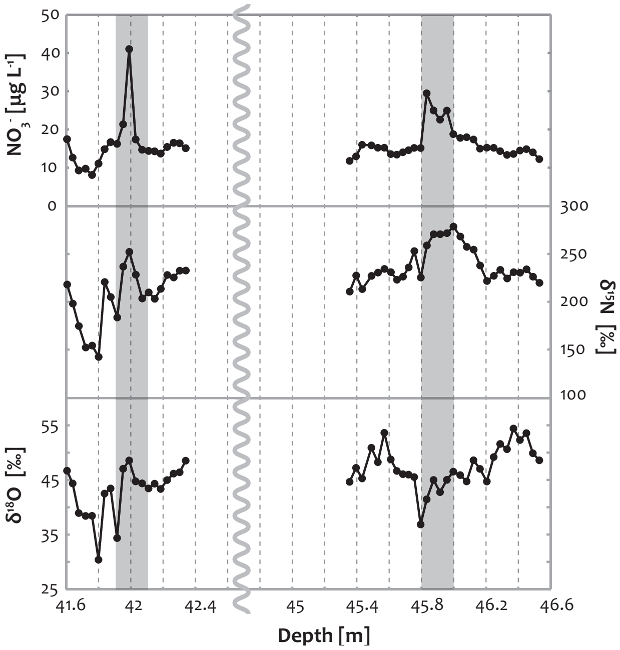

Fig. 1. Comparison of $NO_3{}^-$ concentration with the $\delta^{15}N$ (‰ versus N_2 in air) and $\delta^{18}O$ (‰ versus VSMOW) of NO_3^-.

References
1) K. Casciotti et al.: Anal. Chem. **74**, 19 (2002).
2) T. Blunier et al.: Geophys. Res. Lett. **32**, L13501 (2005).
3) M. M. Frey et al.: Atmos. Chem. Phys. **9**, 22 (2009).
4) M. G. Hastings et al.: J. Geophys. Res. **108**, D24 (2003).
5) G. Michalski et al.: Geophys. Res. Lett. **30**, 16 (2003).

*1 National Institute of Polar Research
*2 Faculty of Agriculture, Tokyo University of Agriculture and Technology

Modeling chemical reactions in the middle atmosphere induced by solar energetic particle events

K. Sekiguchi, Y. Nakai, T. Imamura,*[1] H. Akiyoshi, and Y. Motizuki

Influence of solar energetic particle (SEP) events in the atmosphere has attracted interest of researchers in atmospheric science. In SEP events, copious amounts of X-ray, γ–ray, and protons (also neutrons) come down to the stratosphere. They induce ionization and dissociation of molecules in the air, and subsequent chemical reactions result in changes in chemical compositions. In particular, the concentration changes in odd nitrogen species (NOx) and reactive nitrogen (NOy) are important because they affect short- and long-term change of stratospheric ozone concentration.

We started a simulation study to explicitly deal with many reactions of the chemical species, including ions, produced by protons in SEP events. In our approach, we use two kinds of chemical models. First we simultaneously solve differential equations for both the photochemical reactions and the proton induced reactions, where no transport processes are considered. (Hereafter, this calculation is referred to as BOX-model calculation.) After we estimate values of concentration changes of NOx from the BOX-model calculation, and we input them into a three-dimensional chemical climate model (CCM) for the instantaneous perturbation as the initial condition, where not only chemical reactions but also the transport of chemical species is included. In the CCM, however, the reactions induced directly by protons are not included. Based on the CCM results, we study the global influence of the SEP evens on the distribution of chemical composition on a time scale of several years. Here, we report the results of the BOX-model calculation.

We only took into account of the products from N_2 and O_2 for the interactions with the SEP protons. The G-values (amount of products per absorbed energy of 100eV) of radiolysis[1)] was used for estimating the yield of charged products (N^+, O^+, N_2^+, O_2^+, and e^-) and neutral atoms ($N(^4S)$,$N(^2D)$, $N(^2P)$, $O(^3P)$, and $O(^1D)$), under the reasonable assumption that the above products by radiolysis are defined only by the absorbed energy in the air.

By considering more than 200 chemical reactions (ion-molecule reactions and neutral chemical reactions including NOx, HOx, and ClOx cycles, etc.), we calculated of temporal variations in the concentrations using a commercial software for complex chemical kinetics (FACSIMILE, mcpa corp.). Fig. 1 shows the temporal behavior of concentrations of chemical species at geometric altitude of 25km. Temperature was set at 216 K during the calculation.

Furthermore, we performed a preliminary calculation for the SEP event that occurred in October 1989 (Fig. 2). The temporal absorbed-energy variation in the air was approximated by a rectangular function with its duration of 8 days[2)] and the SEP-proton fluence was estimated from the ion-pair production rates by the SEP protons[3)], W-value (average energy expended in ion-pair formation), and G-values of the air. Climatological temperatures and concentrations of chemical species were used for the initial condition at each geometric altitude between the lower stratosphere (25 km) and upper mesosphere (75 km). The temporal variation during the one-month run for 25km shows that the SEP protons increase the concentrations of NOx and NOy species more than 10 %.

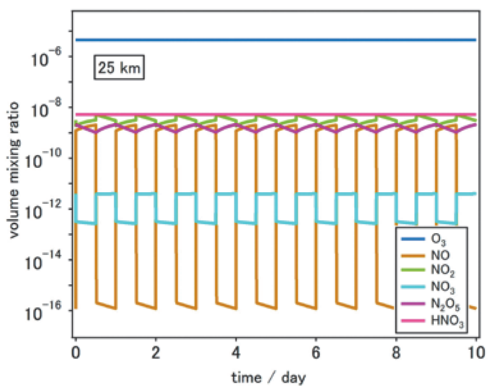

Fig. 1. Volume mixing ratio of chemical species in the stratosphere (25 km altitude) . Solar photolysis reactions run only during the daytime in this calculation.

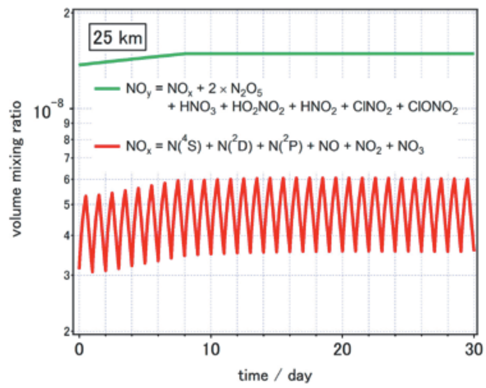

Fig. 2. Volume mixing ratio changes of NOx and NOy species for a month including the SEP event period (the first 8 days).

*1 National Institute for Environmental Studies, Japan

References

1) C. Willis and A. W. Boyd, *Int. J. Radiat. Phys. Chem.* **8**, 71 (1976).
2) *http://umbra.nascom.nasa.gov/SEP/*
3) C. H. Jackman et al., *Atmos. Chem. Phys.* **8**, 765 (2008).

Annually resolved water isotope measurements in a shallow ice core drilled in a vicinity of Dome Fuji station, East Antarctica

S. Kikuchi, S. Okamoto, K. Takahashi, Y. Nakai, and Y. Motizuki

Atmospheric temperature variation records in the past are necessary to investigate climate change. The historical air-temperature variation can be reconstructed from water isotope ratios in ice cores, $\delta^{18}O$ and δD. The relation- ship between the air temperature and water isotope ratios has been investigated, and further, it has been shown in glaciology that the water isotope ratios in ice cores are proportional to the atmospheric temperature around snowfall points.[1] We measured the water isotope ratios in a shallow ice core drilled in 2010 at a point 10 km south of Dome Fuji station, East Antarctica. Our measurement has been carried out with a temporal resolution of less than 1 year over a depth of 2 to 90 meters (~2600 samples in total).

The definition of $\delta^{18}O$ and δD is given as:

$$\delta^{18}O \text{ or } \delta D = (R_{processed} - R_{VSMOW})/R_{VSMOW}. \quad (1)$$

Here, $R_{processed}$ is isotope ratio ($^{18}O/^{16}O$ or D/H) calibrated by linear regression and R_{VSMOW} is the isotope ratio ($^{18}O/^{16}O$ or D/H) of Vienna Standard Mean Ocean Water. We used the liquid water isotope analyzer (Los Gatos Research, Inc.) based on off-axis integrated cavity output spectroscopy. The instrument is guar- anteed precision of 0.2‰ of $\delta^{18}O$ and 0.6‰ for δD (equivalent of 1σ for measurement error). We defined our original rule for evaluation considering the stability of the device and standard deviations of measured values. When a measurement did not meet our criterion, we conducted re-measurements as necessary.

Figure 1 shows the measured $\delta^{18}O$ values with the derived temperature deviation. To calculate the temperature deviation, we used the relationship between $\delta^{18}O$ and temperature, $\delta^{18}O/dT$ = 0.78‰/°C.[2] This relationship is consistent with those reported in previous studies, e.g, Masson-Delmotte et al., 2008.[1]

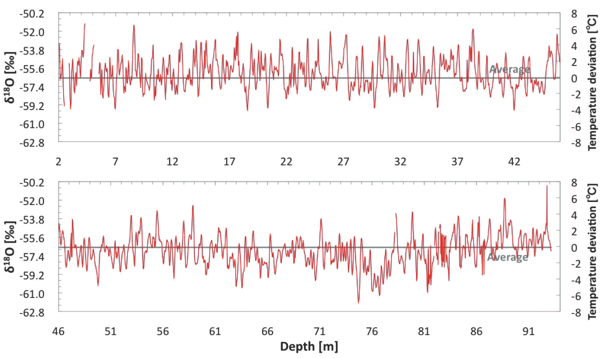

Fig. 1. Measured $\delta^{18}O$ values and temperature deviation.

Calibration was carried out by inter-/extrapolating a linear relationship between two working standards named DOME10 and DF Snow. The isotope ratios for these standard solutions are listed in Table 1. These working standard solutions comprise snowmelt water collected around Dome Fuji station. The reproducibility of this calibration method was confirmed by measurement including SLAP2, which is the primary (international) standard solution supplied by IAEA. Whether or not SLAP2 was included as one of the standards, the calibration lines did not widely vary (see Fig. 2). The error is sufficiently small in measurement values close to the standards. However, from Fig. 2, we also observe that more than half of the samples are measured by extrapolation outside DOME10. Although the extrapolation results in large errors of 1.6‰ for $\delta^{18}O$ and 3.9‰ for δD in the range of lower ratios, these errors are not large compared with the observed amplitudes in $\delta^{18}O$ or δD. Therefore, our measurements have sufficient precision and reproducibility for reconstruction of the air-temperature in the past. The annual temperature variation for the last 2,000 years will be constructed from our study.

Table 1. Isotope ratios of standard solutions

Name	$\delta^{18}O$ [‰]	δD [‰]
DOME10	-52.585	-406.605
DF_Snow	-48.894	-375.88
SLAP2	-55.5	-427.5

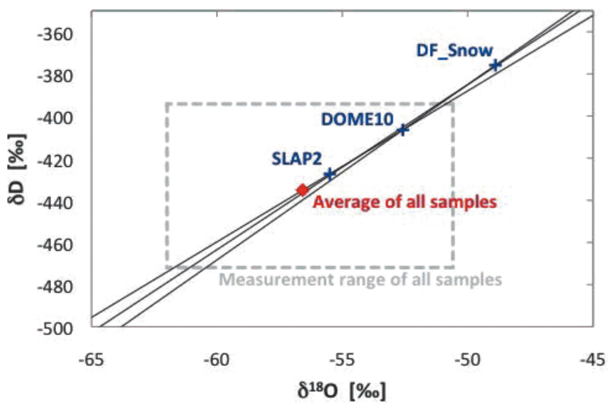

Fig. 2. Isotope ratios of standards and measurement range of all ice core samples.

References
1) V. Masson-Delmotte et al.: J. Clim. **21**, 13, 3359 (2008).
2) K. Fujita and O. Abe: Geophys. Res. Lett. **33**, L18503 (2006).

Dating of a Dome Fuji (Antarctica) shallow ice core by volcanic signal synchronization with B32 and EDML1/EDC3 chronologies

Y. Motizuki, Y. Nakai, K. Takahashi, M. Igarashi,[*1] H. Motoyama,[*1] K. Suzuki[*2]

Dome Fuji station is located in an inland site in East Antarctica, on a summit of Dronning Maud Land (DML) at an altitude of 3810 m a.s.l. (above sea level) (77° 19' 01" S, 39° 42' 12" E). The 10-m-depth mean snow temperature at Dome Fuji is −57.3°C, and the mean accumulation rate of ice is less than $\sim$ 30 mm water-equivalent yr^{-1}. Chronologies of shallow ice cores drilled at such low-accumulation sites are usually constructed by using known volcanic eruption dates as time horizon markers under the assumption that the accumulation rate between adjacent markers is constant. It is particularly difficult, however, to apply this method to date portions of shallow ice cores from before about AD 1260. From AD 1260 to the present, well-dated volcanic eruptions that can be correlated with volcanic sulfate spike signals in the core are used as time horizon markers, whereas the dates of earlier volcanic eruptions are highly uncertain, resulting in a correspondingly large dating uncertainty in the core before AD 1260.

Here we report extremely good synchronization of volcanic eruption signals between a shallow ice core drilled at Dome Fuji in 2001 (DF01 core) and the B32 shallow ice core from the site called DML05. We then applied volcanic signature matching to transfer the B32 chronology constructed by annual layer counting to a portion of the DF01 core for which annual layer counting was difficult because of the low precipitation rate. Matching was done by careful comparison of non-sea-salt sulfate (nssSO_4^{2-}) data, which have a temporal resolution of about 1 year, between the DF01 and B32 cores. The non-sea-salt sulfate is defined as

$$\mathrm{nssSO_4^{2-}} = [\mathrm{SO_4^{2-}}] - [\mathrm{SO_4^{2-}}/\mathrm{Cl^-}]_{seawater}[\mathrm{Cl^-}], \quad (1)$$

with $[\mathrm{SO_4^{2-}}\ /\mathrm{Cl^-}]_{seawater} = 0.140$ in units of μg L^{-1}.

The newly obtained chronology is called DFS1 (Dome Fuji Shallow ice core 1). In total, 31 volcanic eruptions were synchronized from AD 1900 back to AD 187, the earliest volcanic eruption date in the B32 core. We also used the B32-correlated EDML1/EDC3 chronology obtained from the top part of the EPICA Dronning Maud Land (EDML) deep ice core to date a portion of the DF01 core. This new chronology, called DFS2 (Dome Fuji Shallow ice core 2), uses the correlations between B32 and EDML1/EDC3 ages to date the DF01 core from AD 1900 back to AD 199; moreover, four volcanic eruption dates from the EDML1/EDC3 chronology were used to date the interval from AD 199 back to AD 1. Because the EDML1/EDC3 ages were determined by adopting the B32 chronology back to AD 1170, DFS1 and DFS2 dates are identical between AD 1170 and 1900. These two methods enabled us to obtain a detailed chronology of the DF01 core, in particular the part before the last millennium, which has been difficult before this.

The detailed peak-to-peak nssSO_4^{2-} synchronization between the two cores is shown in Fig. 1, where on the bottom horizontal axes not only the water-equivalent depth of the B32 core is shown, but also the water-equivalent depth of the DF01 core multiplied by α in each synchronized interval. The α values are straightforwardly derived by piecewise peak-to-peak matching. Each value of α means the inverse of the mean accumulation rate at Dome Fuji relative to that at DML05 in the synchronized interval in question. These α values fall within a very small range between 2.1 and 2.6, which supports our assertion that the overall synchronization presented here is extremely good.

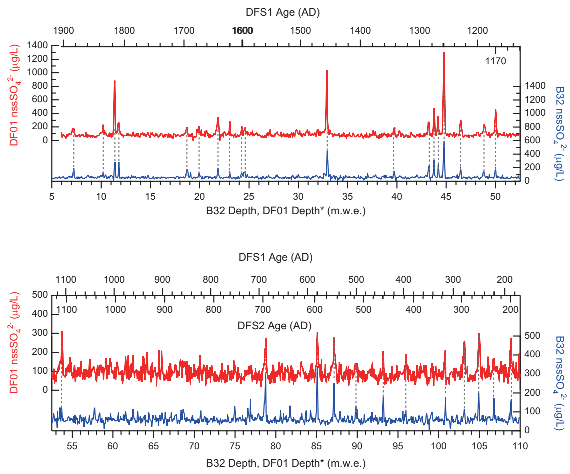

Fig. 1. Detailed volcanic signature matching between the DF01 and B32 cores, performed by using non-sea-salt sulfate records, from AD 1900 back to around AD 180. The bottom axis shows the water-equivalent depth in the B32 core, and that in the DF01 core multiplied by α (see in text) in each synchronized interval. The DFS1 ages are shown above the top axes, and the DFS2 ages are shown below the top axes where they deviate from the DFS1 ages (before AD 1170). Note the difference in the scale of the ordinate between the upper and the lower panel.

[*1] National Institute of Polar Research
[*2] Department of Environmental Sciences, Shinshu University

7. Accelerator

Recent developments in the RIKEN 28-GHz SC-ECRIS

Y. Higurashi, J. Ohnishi, K. Ozeki, H. Haba and T. Nakagawa

In 2012, we attempted to increase the intensity of highly charged uranium (U) ion beam produced from RIKEN 28-GHz SC-ECRIS[1], which can be operated at flexible axial field distributions from the so called "classical $B_{\min}$" to "flat $B_{\min}$"[2]. In the test experiments, we successfully increased highly charged U ion beam intensity using a pure aluminum (Al) chamber instead of a stainless steel (SS) one. We observed that the x-ray heat load for the cryostat of the ion source decreased when using the Al chamber. In this report, we present the experimental results described above in detail. We also discuss the plasma chamber surface effect on the beam intensity.

In this experiment, the maximum mirror magnetic field strength at the RF injection side (B_{inj}), minimum strength of the mirror magnetic field ($B_{\min}$), maximum mirror magnetic field strength at the beam extraction side (B_{ext}), and minimum magnetic field strength at the surface of the plasma chamber (B_r) were fixed at 3.2, 0.65, 1.8, and 1.85 T, respectively. The microwave frequency was 28 GHz generated by the gyrotron. We used the sputtering method to produce the U ion beam[3,4]. Under these conditions, we obtained ~110 eμA of U^{35+} at RF power of ~2 kW, which is almost twice that with the SS chamber. One of the possible explanations for the beam intensity enhancement may be the surface effect of the plasma chamber. It was observed that the intensity of highly charged heavy ion beam was strongly enhanced by a coating of Al_2O_3 on the plasma chamber surface[5]. The aluminum chamber also has the same effect as the Al_2O_3 coating because of the easy oxidation of the Al surface by air[6,7] . The detailed experimental procedure and results will be presented in another paper[8] . Figure 1 shows the charge state distribution of the U ion beams. The ion source was tuned to produce U^{35+} ion beam. We also measured the emittance of the highly charge U ion beams. We observed that the normalized root mean square emittance was ~ 0.06πmm mrad.

It was reported that the bremsstrahlung x-rays emitted from the plasma in the ion source add a heat load to the ion source cryostat[4] . A heat load of 6 W was observed at the microwave power of 6 kW with 28-GHz microwaves for the high performance SC-ECRIS at LBL (VENUS)[9] . When using small refrigerators for regenerating the liquid He in the liquid He vessel, the maximum cooling power will be limited with several W at 4 K. In this case, the beam intensity must be limited by the heat load. In the last year, to increase the cooling power, we installed a new GM-JT refrigerator, which has a maximum cooling power of ~4 W at 4.2 K. After installing the new refrigerator, we observed the total cooling power of 7.8 W at 4.2 K for x-ray heat load. When using the stainless steel chamber, the x-ray heat load was ~3.8 W at RF power of 2.1 kW. On the other hand, we observed the x-ray heat load of ~2 W with the Al chamber at the same RF power. This means that we can increase the RF power up to ~7.8 kW when using Al chamber at the present stage. In order to understand this result, we need further investigations. However, practically, the Al chamber has the important advantage of producing intense beams of highly charged U ion beams with limited cooling power compared to the stainless steel one.

In the autumn of 2012, we provided the U^{35+} ion beam to the accelerator using this method for the RIBF experiment. We successfully produced an average beam intensity of ~85 eμA for one month without break. The consumption rate of the metal U rod was ~5 mg/h.

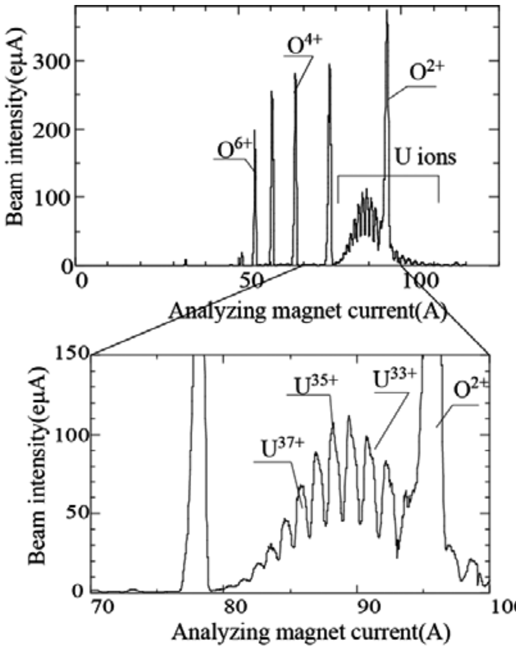

Fig.1 Charge state distribution of highly charged U ions.

References

1) T. Nakagawa et al: Rev. Sci. Instrum. 81, 02A320 (2010).
2) G. D. Alton and D. N. Smithe: Rev. Sci. Instrum. 65 , 775 (1994).
3) Y. Higurashi, et al: Rev. Sci. Instrum. 83, 02A333(2012).
4) Y. Higurashi et al: *Proceedings of the 8th Annual Meeting of Particle Accelerator Society of Japan* ,August 1-3, 2011, Tsukuba, Japan, p.185
5) T. Nakagawa: Jpn. J. Appl. Phys., Part 1 30, 930L (1991).
6) D. Hitz et al: Rev. Sci. Instrum. 67 ,883(1996).
7) T. Nakagawa et al: Jpn. J. Appl. Phys. 35, 4692 (1996).
8) Y. Higurashi et al: submitted to Jpn. J. Appl. Phys.
9) D. Leitner et al: *Proceedings 19th Int. Workshop on ECR ion sources*, 2010, Grenoble, France, p. 11

Operational test of micro-oven for ^{48}Ca beam

K. Ozeki, T. Kageyama, M. Kidera, Y. Higurashi, and T. Nakagawa

In the 18-GHz electron cyclotron resonance ion source (ECRIS)[1], the rod-insertion method has been used to supply the ^{48}Ca beam.[2] In this method, the ^{48}CaO rod is inserted directly into the plasma generated in the ECRIS. The rod is heated by the plasma, and the ^{48}Ca atoms are evaporated to be fed into the ECRIS. The typical beam intensity is about 18 electric μA for $^{48}Ca^{10+}$. However, frequent adjustment of the parameters of the ECRIS is needed to maintain a constant beam intensity. Therefore, we initiated operational testing of a micro-oven, which is already in practical use in several facilities,[3-6] with the goals of the enhancement and stable supply of the beam.

Figure 1 shows the structure of the micro-oven designed by us. The material is placed in the crucible, whose inner volume is about 0.7 cm^3. The crucible is heated by applying a current to the platinum wire, and the material is evaporated to be fed into the ECRIS.

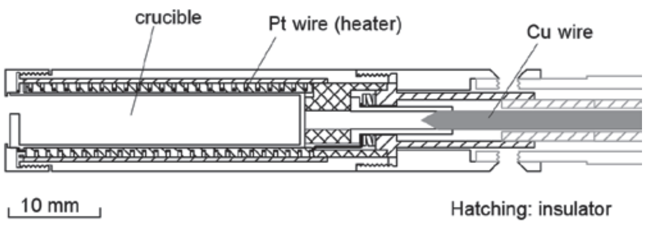

Fig. 1. Structure of the micro-oven. The micro-oven (black) is attached to the head of the support rod (gray). A current is applied to the heater via the support rod.

The test experiments were conducted using the 18-GHz superconducting ECRIS[7], because the 18-GHz ECRIS was being used for other experiments. The element ^{40}Ca was used as the material in these tests. Initially, $CaCO_3$ was reduced to CaO by heating above 900°C. A mixture of powders of CaO and aluminum was placed in the crucible.

When we supplied the ^{48}Ca beam using the rod-insertion method, it took a considerable amount of time and labor to start the ECRIS. In the course of supplying RF power to the ECRIS, runaway of the ECRIS occurred repeatedly due to a large amount of evaporation of water being adsorbed onto the CaO rod.

In contrast, in the oven method, the micro-oven can be heated independently. Therefore, the water adsorbed onto CaO can be evaporated without starting up the ECRIS. We confirmed that RF power was supplied to the ECRIS smoothly by preheating of the micro-oven. In the long-term sequence of experiments, midstream maintenances such as cleaning of the ECRIS and exchange of the material are necessary. The shortening of the time for restart of the ECRIS as in the case of our method leads to increase in the beam provision rate.

Metallic calcium is produced by following chemical reaction:

$$3CaO + 2Al \rightarrow 3Ca + Al_2O_3.$$

Using a Faraday cup installed at the exit of the analyzing magnet, we measured the beam intensity. The obtained charge distribution of Ca ions is shown in Fig. 2. Helium gas was used as a support gas to enhance the beam intensity.

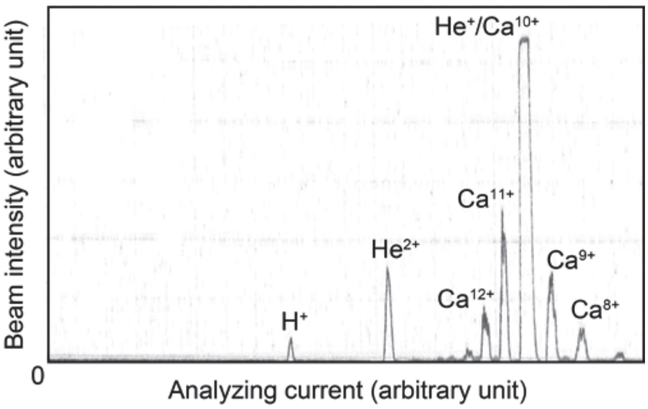

Fig. 2. Charge distribution of Ca ions.

The supplied RF power was 300 W. The typical and maximum beam intensities for Ca^{11+} were 25 and 38 electric μA, respectively. We also observed a stable beam intensity of 18 electric μA for several hours without performing any tuning of the ECRIS and the oven.

As the first step, we observed the production of a calcium beam using the micro-oven. In addition, we obtained basic information in operating the micro-oven. Hereafter, test experiments will be conducted using the 18-GHz ECRIS. Several relevant aspects such as the beam stability and the correlation between the beam intensity and the consumption rate of the material will be examined.

References

1) T. Nakagawa et al.: Nucl. Instrum. Methods B **226**, 392 (2004).
2) M. Kidera et al.: High Energ. Phys. Nucl. **31**, 97 (2007).
3) R. Harkewicz: Rev. Sci. Instrum. **67**, 2176 (1996).
4) V. B. Kutner et al.: Rev. Sci. Instrum. **71**, 860 (2000).
5) D. Wutte et al.: Rev. Sci. Instrum. **73**, 521 (2002).
6) R. Lang et al.: Proc. 15th Int. Workshop on ECR Ion Sources, Jyväskylä, Finland, 2002, p. 180.
7) T. Kurita et al.: Nucl. Instrum. Methods B **192**, 429 (2002).

Design of new 18-GHz ECRIS for RIKEN RIBF †

K. Ozeki, Y. Higurashi, J. Ohnishi, and T. Nakagawa

The RIKEN 18-GHz electron cyclotron resonance ion source (ECRIS)[1] has been used as an external ion source for the RIKEN linear accelerator (RILAC). The main function of this ion source is to produce an intense beam of multi-charged medium-heavy ions (e.g., $^{40}Ar^{8+}$, $^{48}Ca^{10+}$, $^{70}Zn^{15+}$, and $^{84}Kr^{18+}$) for the RIKEN radio isotope beam factory (RIBF) and the super-heavy element search experiment. Recently, we needed to develop new beams to meet the requirements for new beams and to extend the irradiation time (>1 month) of the heavy ion beam, particularly the metallic ion beam. To meet these requirements, we needed a new ion source. By equipping the RILAC with two ion sources, we could develop new ion beams while simultaneously producing a beam for the experiment. Furthermore, when faced with the problem of the ion source during beam production for the experiment, we could immediately switch to another ion source for producing the beam. This means that we would be able to extend irradiation time by using two ion sources. For these reasons, we started to design and construct the new 18-GHz ECRIS as an additional external ion source for the RILAC.

Figure 1 shows a schematic drawing of the new 18-GHz ECRIS. It consists of three solenoid coils that produce a mirror magnetic field along the axis. The main parameters of the solenoid coils are listed in Table 1. Maximum and minimum (B_{min}) intensities of the mirror magnetic field are >1.3 T and <0.5 T, respectively. Beam intensities of highly charged heavy ions strongly depend on B_{min}.[2-4] The optimum value of B_{min} to maximize the beam intensity is nearly constant (at 70%~80% of the magnetic field of electron cyclotron resonance).[2] On the other hand, the charge state in the plasma depends on the mirror ratio, because a longer confinement time for the plasma is obtained with a higher mirror ratio. By using this magnet system, the magnetic mirror ratio and B_{min} can be independently controlled to realize an optimum magnetic field distribution.

Table 2 lists the main parameters of the hexapole magnet. The radial magnetic field strength at the inner surface of the plasma chamber is ~1.3 T.

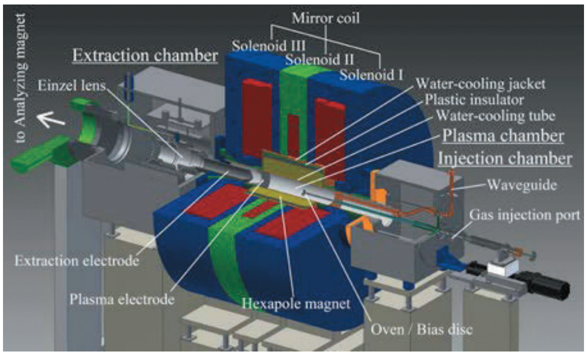

Fig. 1. Schematic drawing of the new 18-GHz ECRIS.

† Condensed from the Proc. 20th Int. Workshop on ECR Ion Sources.

Table 1. Specifications of the solenoid coils.

	Solenoids I & III	Solenoid II
Number of turns	296	60
Maximum current	660 A	300 A
Maximum voltage	105 V	10 V
Maximum intensity of the mirror magnetic field		>1.3 T
Minimum intensity of the mirror magnetic field		<0.5 T

Table 2. Specifications of the hexapole magnet.

Material	Nd-B-Fe permanent magnet
Inner diameter	85 mm
Outer diameter	186 mm (magnet only) 210 mm (including a holding jacket)
Length	250 mm
Number of divisions	36
Magnetic field intensity	~1.3 T at the inner surface

The plasma chamber consists of double-wall stainless steel tubing with a water cooling channel in the gap (~1 mm) to maintain the temperature against the heat load from the plasma, in order to prevent the demagnetization of the hexapole magnet. The flow rate and the temperature of the injected cooling water are ~6 L/min and 20°C, respectively. The inner diameter of the plasma chamber is 79 mm, which is slightly larger than that of the present 18-GHz ECRIS. There are two turbo-molecular pumps, ~500 L/s, placed at the RF injection side and beam extraction side to maintain a high vacuum in the plasma chamber (on the order of 10^{-8} Torr). The maximum extraction voltage is 20 kV. To maintain the high voltage for the plasma chamber, 3 mm thick plastic insulators are placed between the hexapole magnet, which is equipotential with the plasma chamber, and the solenoid coils. The high-temperature oven is inserted from the RF injection side. We also plan to install a movable negatively biased disc in the plasma chamber to increase beam intensity.

Recently, enhancement in the ECRIS performances by tuning of the microwave feed frequency was reported[5, 6]. We plan to use the travelling-wave tube amplifier for microwave generation to optimize the microwave frequency for the plasma chamber of the ion source. The frequency range is 17.2~18.4 GHz, and the maximum power is ~700 W.

References

1) T. Nakagawa: Nucl. Instrum. Methods B **226** (2004) 392
2) H. Arai et al.: Nucl. Instrum. Methods A **491** (2002) 9
3) H.W. Zhao et al.: Rev. Sci. Instrum. **79** (2008) 2A315
4) D. Leitner et al.: Rev. Sci. Instrum. **77** (2006) 3A302
5) L. Celona et al.: Rev. Sci. Instrum. **81** (2010) 02A333
6) D. Mascali et al.: Proc. 19th Int. Workshop on ECR Ion Sources, Grenoble, France, 2010, p. 165

Replacement of main coil of RRC-E sector magnet

Y. Watanabe, M. Kase, T. Maie, K. Kumagai, M. Nagase, N. Fukunishi, O. Kamigaito,
S. Fukuzawa,[*1] M. Hamanaka,[*1] S. Ishikawa,[*1] K. Kobayashi,[*1] Y. Kotaka,[*1] R. Koyama,[*1]
T. Nakamura,[*1] M. Nishida,[*1] M. Nishimura,[*1] J. Shibata,[*1] N. Tsukiori,[*1] and K. Yadomi,[*1]

The RIKEN Ring Cyclotron (RRC) has been in stable operation for over 26 years, and it is expected to work as a first-stage energy booster in any acceleration mode of the Radioactive Isotope Beam Factory (RIBF). The total operation time of the RRC is more than 4000 hours/year. However, recent problems arising from age-related deterioration have been occurring frequently in the RRC. Therefore, certain devices have been repaired, refabricated and/or replaced.[1-2)]

In May 2011, it was found that the upper main coil of the RRC-E sector magnet had undergone a layer shorting, and this was causing the RRC magnetic field to fluctuate by as much as ±20ppm. The upper main coil was examined between April and August of 2011. However, we were not able to find the shorted section, and we determined that it would be nearly impossible to repair the upper main coil and hence decided to fabricate a new main coil. In the summer of 2012, the old upper main coil was replaced by a new main coil fabricated in FY2011. Six months were required to fabricate the new main coil. Table 1 lists the replacement schedule of the main coil of the RRC-E sector magnet in 2012. Because this was the first time that the RRC main coil was being replaced, the task had been scheduled over a period of four weeks.

Table 1 Replacement schedule of main coil in 2012.

24-31 July	Preparatory work (removal of certain cables, pipes, decks, handrails, etc.)
1-4 August	Removal of upper yokes and main coil
1-7 August, 11-15 August	Setup/removal of iron plates, curing, etc., for carrying the main coils in and out
8-11 August	Carrying in and out of main coils
9-20 August	Installation of new main coil and restoration of upper yokes
15-24 August	Restoration of cables, pipes, etc.
23-31 August	Starting up of RRC (vacuum, cooling water, electrification, etc.)

There were three problems in this replacement task, and Fig. 1 shows photos of the concerned areas. 1) Carrying in and out of the main coils: the main coils carried in and out using a special jig located on the side of the second ion source room and on the third stage of the RRC room. 2) Removal of upper yokes: because we found that it would be difficult to remove some yokes with a crane only by magnetization and due to the presence of rust, each yoke was lifted up a few hundred μm with a hydraulic jack in advance. 3) Deposition and storage of removed upper yokes: because of their heavy weight and large size, the 12 removed yokes were carried and stored in three places–on the S sector magnet, in the south side of resonator No. 2, and in front of the shield door between the RRC room and the D room.

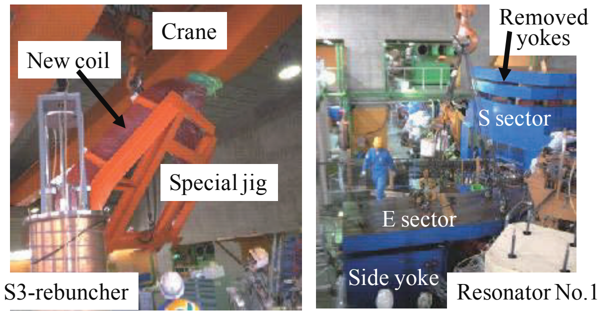

Fig. 1. Equipment used to carry main coil and yokes along with the locations relevant to the replacement.

We assumed at first that a layer short had occurred at a crossing area of the coil near the bus bar. However, the layer short had occurred at the pole side (inside) of the main coil far from the crossing area, as shown in Fig. 2. The resin of the main coil was carbonized by the layer short, and a scorch mark had appeared on the surface of the main coil.

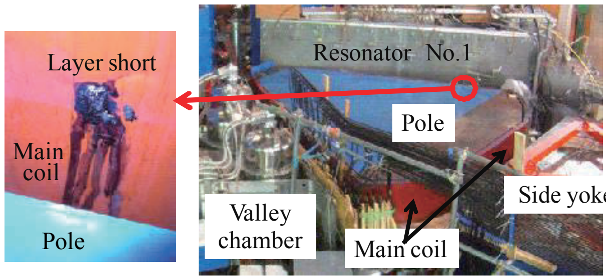

Fig. 2. Layer short of the main coil.

Furthermore, in June 2012, it was found that the lower main coil of the RRC-W sector magnet also showed signs of layer shorting, and this layer short also occurred at the same place as that occurring in 1999. Though the layer short was repaired again, we plan to replace the lower main coil (including the upper main coil) of the RRC-W sector magnet with a new main coil in FY2013. This task has been scheduled over a period of seven weeks.

References

1) Y. Watanabe et al.: Proc. IPAC 2012 (2012), p.433.
2) M. Hamanaka, et al.: RIKEN APR 2012, in this report.

[*1] SHI Accelerator Service Ltd.

New high-power beam dump for charge stripper at RRC

K. Yamada, M. Fujimaki, N. Fukunishi T. Maie, Y. Watanabe, and O. Kamigaito

A new high-power beam dump was developed and installed in the beam line downstream of the RIKEN Ring Cyclotron (RRC) in August 2012. In the RI-beam factory, very-heavy ions such as xenon and uranium are accelerated in combination with fixed-frequency Ring Cyclotron (fRC). For the acceleration mode, the charge state of beam particles accelerated by the RRC has to be multiplied by a charge stripping system before injecting to the fRC. The charge stripper is located in the RRC vault, and the location is named A02. The stripped beam including various charge states is separated by a set of two dipole magnets, called DAA1 and DMA1, just after the charge stripper. Until the summer of 2012, beam components with "un-selected" charge states were dumped by four sets of movable slits installed in the beam duct of DMA1. This old beam dump only allows a power dissipation of about 300 W on each slit. As described in Ref. 1, a new charge stripper system using helium gas was developped to enable further high-intensity beams by means of their durability, high-efficiency, and desirable influence on beam emittance. Consequently, a high-power beam dump was desired for continuous operation with a dump capacity up to 40 kW.

The high-power beam dump was built in newly fabricated chambers for the DAA1 and DMA1. The dump system consists of DAA1 inside dump, buffle slits at the exit of DAA1, DMA1 inside dump, and two sets of movable slits at the exit of DMA1. Each element is cooled by water with a total flow rate of 200 liter/minute. Figure 1 indicates the beam trajectory of different charge-state particles with respect to ^{238}U beam and ^{124}Xe beam. Major components of the beam are stopped by the DMA1 inside dump. The DMA1 dump has a wedge shape, and covers the entire lateral wall divided by seven blocks. Figure 2 shows a result of 3D heat transfer calculation assuming 12 mm $\times$ 24 mm uniform distribution of 10 kW heat load on the DMA1 dump (corresponding to ϕ6 mm spot size), and assuming turbulent forced convective heat transfer by cooling water. According to the calculation, the inner surface of the water channel heats over the saturation temperature of water at 0.5 MPa, indicating subcooled flow boiling. However, the heat flux on the surface is sufficiently lower than the critical heat flux of 11.2 MW/m^2 estimated by an approximation in pool boiling[2]. Comparing the degree of superheating, 38.9 K, at the critical heat flux with the result of 3D calculation, the surface temperature of beam spot may reach up to about 500 °C. Thus, a maximum 10 kW beam can be stopped at each spot on the DMA1 dump, indicating a total cooling power over 40 kW.

The beam dump functioned appropriately for a total 2 kW of ^{238}U beam during the RIBF experiment performed in the autumn of 2012. This will allow further upgrade of beam intensity in the near future.

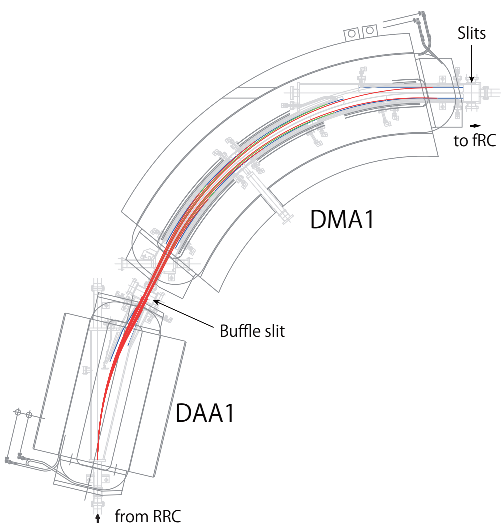

Fig. 1. Central trajectory of various charge-state particles in the beam dump setting for $^{238}U^{65+}$ beam (red line group) and $^{124}Xe^{46+}$ beam (green line group). Blue line indicates the stopping surface of the dump.

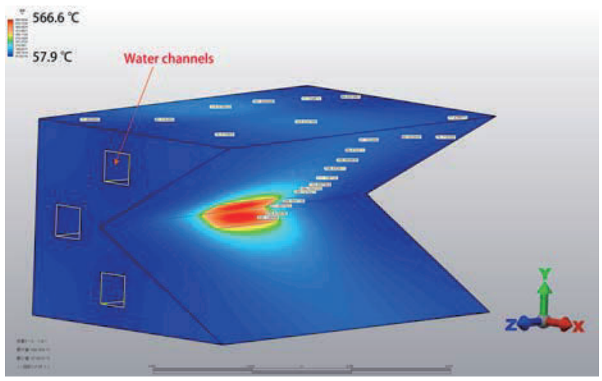

Fig. 2. Result of 3D heat transfer calculation in the vicinity of the beam spot.

References

1) H. Imao *et al.*: Phys. Rev. ST Acc. Beams **15**, 123501 (2012).
2) JSME Heat Transfer Handbook, Maruzen, 1993.

Measurement of magnetic field of fRC sector magnets for acceleration of $^{238}U^{64+}$ ions

K. Kumagai and N. Fukunishi

The fixed-frequency ring cyclotron (fRC) accelerated uranium beams with a charge state of 71+ from 11 MeV/u to 50 MeV/u. The $^{238}U^{71+}$ ions were converted from $^{238}U^{35+}$ using a carbon film charge stripper located downstream of the RIKEN ring cyclotron (RRC). A new He gas stripping system was developed, [1,2] which does not need to be exchanged, unlike a carbon film. The maximum yield of the charge state after stripping by the gas was 64+ and the 2nd yield was 65+. The fRC located after the stripper must be capable of accelerating uranium beams with a charge state of 64+ or 65+ accordingly.

To accelerate the $^{238}U^{64+}$ ions with the fRC, the magnetic field must be increased from 1.69 to 1.885 T at the central region of the sector magnet. Last year, we confirmed that the desired field distribution could be obtained only by increasing main-coil current, without modifying the magnet and its cooling system[3]. Based on those results, a new power supply was manufactured. Since this power supply also can be used as a power supply for RRC main coils, the maximum current and voltage was designed as 1080 A and 500 V, respectively. The power supply has four bypass circuits (50A-150V), which compensate for the variation in the magnetization of four sector magnets. The stability and the ripples of the power supply are designed to be less than ±3 ppm of the maximum current. Both coarse and fine current adjustment can be performed. A full-scale span can be adjusted by 16-bit resolution, and ±25A of preset value can be changed by 16-bit resolution. This means that a current can be set by the resolution below 0.001A. Manufacture of the power supply was completed in March 2012. Current stability over 8 hours was less than ±1ppm, excluding the initial drifts when the environmental temperature change was less than 2 °C as shown in Fig. 1.

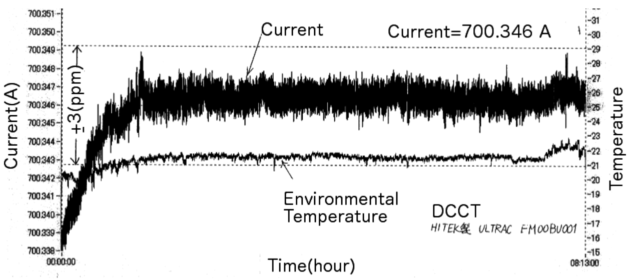

Fig. 1. Current stability of the main coil power supply over 8 hours.

We measured the higher magnetic field of the fRC to confirm magnetic field distribution of each sector magnet excited by the main coil and the 10 trim coils. A one-dimensional field measuring instrument manufactured in 2009 was used for the measurements[4]. The magnetic fields were measured by Hole Probe and NMR at the main-coil current between 650 and 860 A.

Figure 2 shows the magnetic field distributions along the centerline of the four sector magnets at a main coil current of 805A and 845A. The calculated field distribution for $^{238}U^{65+}$ and $^{238}U^{64+}$ acceleration obtained using TOSCA-3D is also shown. The B-H characteristic used in the calculations was fitted such that an actual field magnetized with the current below 650 A might be produced. As a magnetic channel for beam injection and a dummy channel composed of iron yoke are installed in the central part of SW sector and NE sector, the field distribution of the SW sector and the NE sector is lower than that in the NW and SE. Figure 3 shows an example of the magnetic field distribution produced by trim coils.

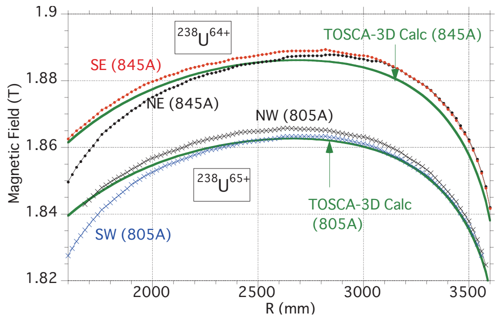

Fig. 2. Comparison of the field distributions of four sector magnets with the calculated distribution.

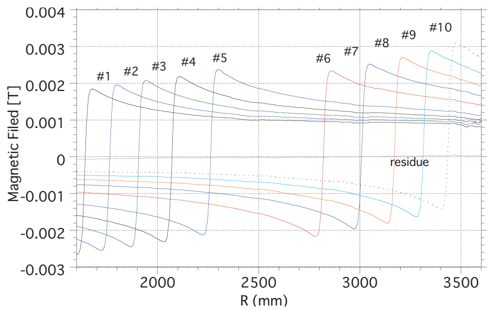

Fig. 3. SE trim-coil field distribution at a main-coil current of 845 A. The current of each trim coil is +100 A.

The first acceleration test of the $^{238}U^{65+}$ beam was done on July 14 and 15 [5]. The magnetic field required to accelerate $^{238}U^{65+}$ beam was generated and the beam was accelerated. The output efficiency from the fRC was about 85%. Just before the beam service time during the period in October to December, a test of the $^{238}U^{64+}$ acceleration was carried out satisfactorily. The beam intensity of more than 10 pnA extracted from the SRC was served for the users during the beam service time.

References
1) H. Imao et al.: Proc. IPAC'11, San Sebastian, Spain. TUPS088 (2011).
2) H. Imao et al.: Proc. PASJ9, Osaka, Japan, WELR02 (2012).
3) K. Kumagai et al.: RIKEN Accel. Prog. Rep. **45**, 111 (2011).
4) K. Kumagai et al.: RIKEN Accel. Prog. Rep. **43**, 131 (2009).
5) K.Kumagai, et al.: Proc. PASJ9, Osaka, WEPS055 (2012).

Beryllium rotating charge stripper for uranium acceleration at RIKEN RIBF

H. Hasebe, H. Kuboki, H. Okuno, H. Imao, N. Fukunishi, M. Kase, and O. Kamigaito

A charge stripper was used to strip uranium (U) beams to obtain U^{86+} at 50 MeV/nucleon in the acceleration chain at the RIKEN RIBF. A static-type carbon foil (C-foil) with a thickness of approximately 85 μm (17 $mg{\cdot}cm^{-2}$) has been used as a stripper. A rotating carbon disk (C-disk) stripper device was prepared at the E1 room in 2006 for high intensity U beam operation[1]. A C-disk with a diameter of 120 mm was installed and tested in 2007. However, the C-disk could not be used as a stripper because of the non-uniformity of thickness. Thus far, no C-disk commercially available or originally fabricated has met our requirements. Therefore, until 2011, we had no choice but to purchase polycrystalline graphite foils fabricated by Arizona Company[2] and attached to a small folder (an oval hole of 14 x 24 mm) to accomplish U beam time. However, the life-time of the foils decreased to nine hours with increased beam intensity. Thus, providing stable U beams became difficult.

In October 2012, we tried to use different disk materials of titanium (Ti) and beryllium (Be)[3] of disk diameters 120 mm. The thicknesses of the Ti and Be disks were 40 μm and 100 μm, respectively. A U^{64+} beam at 50 MeV/nucleon was irradiated on the rotating Ti/Be disk at 1000 rpm. Figure 1 shows the charge distributions of stripped U beam obtained with Ti and Be disks. The charge states at the peak were 82+ and 86+ for Ti and Be disk, respectively. It was found that a Be disk was suitable for practical usage. The beam width and longitudinal distributions of the stripped beam were monitored by profile monitors and plastic scintillators, respectively. The beam quality using Be disk was found to be the same as when using a static C-foil. In addition, the Be disk withstood U beam intensities twice as high as that in 2011.

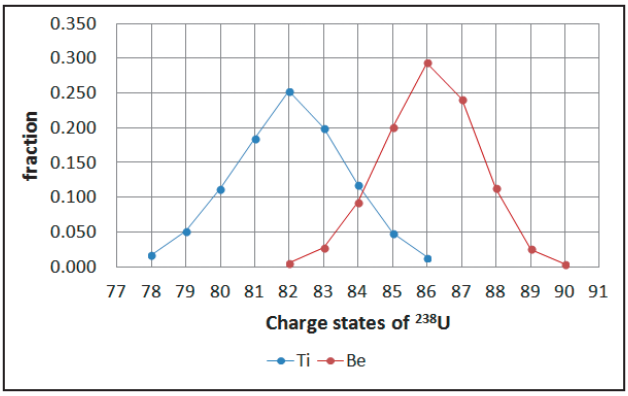

Fig. 1. Charge distributions using Be and Ti disk.

The Be disk was used for beam time from November to December 2012. The whole beam time was completed by only one disk with no exchange. Figure 2 shows the Be disk before installation. Figure 3 shows a photograph after the beam time. The outer circumference of irradiated positions (black band in Fig. 3) was deformed when the U beam intensity was increased to several electric μA. Moreover, many cracks were observed after the beam time. The cracks seemed to be produced just before the end of the beam time. However, these cracks did not affect the intensity of the stripped beam.

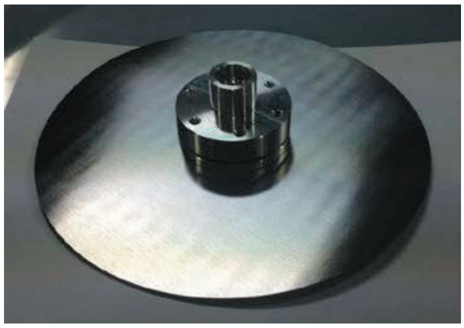

Fig. 2. New Be-disk.

Fig.3. Be-disk after use with many cracks.

The life-time of the stripper was drastically greater than the previous beam time. The total number of U particles irradiated per disk/foil were improved from 7.12×10^{15} (C-foil in 2011) to 1.18×10^{18} (Be-disk in 2012).

Finally, the most noteworthy fact is that the Be disk successfully provided stable U beam with great intensity for a long time. The thickness uniformity has to be improved in the future to improve the transmission efficiency of the subsequent cyclotrons IRC and SRC.

References

1) H.Ryuto et al.: Nucl. Instr. and Meth. A 569 (2008) 697.
2) ACF-Metals Arizona Carbon Foil Co. Inc., URL: http://www.techexpo.com/firms/acf-metl.html
3) Goodfellow Cambridge Ltd. URL:http://www.goodfellow.com/

Improvement of beam current monitor with high Tc current sensor and SQUID at RIBF†

T. Watanabe, N. Fukunishi, M. Kase, O. Kamigaito S. Inamori,[*1] and K. Kon,[*1]

The purpose of this study is to measure the DC current of high-energy heavy-ion beams non-destructively at high resolution. Therefore, a high critical temperature (HTc) superconducting quantum interference device (SQUID) beam current monitor has been developed for use in the radioactive isotope beam factory (RIBF) at RIKEN. Unlike at other existing facilities, a low-vibration, pulse-tube refrigerator cools the HTc fabrications, including the SQUID, in such a way that the size of the system is reduced and the running costs are lowered. As a result, by using a prototype of the HTc SQUID monitor, the intensity of a 1 μA Xe beam (50 MeV/u) was successfully measured with 100 nA resolution. Furthermore, since a higher resolution of 1 nA is required at the RIBF, development of an improved HTc current sensor has begun.

When a beam passes along the axis of the HTc current sensor, shielding current produced by the Meissner effect flows in the opposite direction along the wall of the sensor. Since the outer surface is designed to have a bridge circuit, the current generated by the beam is concentrated in the this circuit. The HTc SQUID is set close to the bridge circuit and can detect the azimuthal magnetic field with a high S/N ratio. To obtain higher resolution, a stronger magnetic field at the bridge circuit produced by the shielding current is necessary. Therefore, a new HTc current sensor with two coils was proposed (Fig. 1(a)), and a spraying machine was developed to fabricate the new HTc current sensor by dip-coating a thin layer of Bi_2-Sr_2-Ca_2-Cu_3-O_x (Bi-2223) onto a 99.6% MgO ceramic substrate (Fig. 1(b)). The spraying machine consists of a turntable that rotates the substrate and a spraying nozzle that moves vertically. Prior to coating the Bi-2223 materials onto the MgO substrate, we prepared only a test HTc bridge circuit in the form of a square disk with 5-cm-long sides for the cooling test. We confirmed that the bridge circuit had sufficient strength and that the Bi-2223 materials did not peel off when cooled by liquid nitrogen. Using three test pieces of MgO substrates (5 W x 50 D x 5 H (mm)) coated with the Bi-2223 materials, we analyzed the critical temperature (Tc), critical current density (Jc), and X-ray diffraction patterns. We obtained a critical temperature of 105 K and critical current density of 3250 A/cm^2. The X-ray diffraction patterns showed major peaks in the Bi-2223 phase. Since good results were obtained from the pre-test, we first attempted to spray and sinter the Bi-2223 materials onto the MgO substrate. However, the bridge circuit was prepared by a masking process, and a small crack was found after a cold isostatic pressing (CIP) process. Instead of using the masking process, by digging a thin groove on the bridge circuit and removing the Bi-2223 materials by hand, we could resolve this problem. However, the coated Bi-2223 material peeled off after sintering. The surface of the substrate is roughened with a blasting process[1]. Because the space inside the substrate is narrow, it is difficult to conduct a thorough blasting treatment. After removing the Bi-2223 material from only the inner side and repeating the blasting process, we were successful on the third attempt.

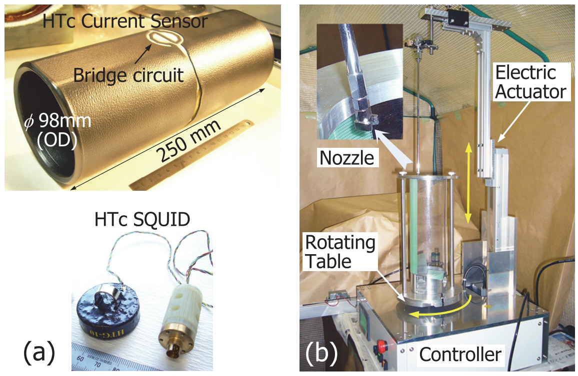

Fig. 1. (a) HTc current sensor and HTc SQUID and (b) spraying machine.

The old HTc tube already installed in the prototype of the HTc SQUID monitor was exchanged with the new one. We confirmed that the HTc current sensor was superconductive by using a current source. Unfortunately, the output voltage of the SQUID was one fourth that of the prototype. Previous investigations by Hao et al. showed that when the inductance of the bridge exceeds the inductance of the two-layer HTc current sensor, current will tend to flow up the inside surfaces of the HTc current sensor rather than through the bridge, thereby reducing the sensitivity. Results of finite element calculations in three dimensions Opera-3d indicate that the inductance of the HTc bridge circuit is 54.9 nH and the inductance of the two-layer current sensor is 8.2 nH. Despite these rather discouraging results, our efforts were devoted to understanding the mechanistic Meissner effect. In fact, this is a far more complicated problem and needs further study.

† Condensed from the article in J. Supercond. Nov. Magn. (2013) **26**, 1297-1300, DOI 10.1007/s10948-012-1943-0

*1 TEP Corporation

References

1) A. Ichinose, et al.: CRIEPI Rep. No. H09019 (2010).

Direct communication with EPICS control system from LabVIEW

R. Koyama,*[1] T. Watanabe, M. Komiyama, and H. Imao

Most of the RIKEN RI Beam Factory (RIBF) components are controlled using the Experimental Physics and Industrial Control System (EPICS)[1)]. The National Instruments (NI) LabVIEW is also widely used for the monitoring and control of accelerator devices in the RIBF. The LabVIEW can communicate directly with the EPICS by introducing NI's "LabVIEW EPICS Client I/O Server"[2)].

All control variables in the EPICS such as drive control instructions, measured values, and device statuses are passed to predefined Process Variables (PVs) in the input/output controllers. These PVs are directly bound to the Network Shared Variables predefined in LabVIEW by the LabVIEW EPICS Client I/O Server using the Channel Access protocol. These connections are schematically shown in the upper part of Fig. 1.

In the actual operation of the RIBF, the following parameters are acquired through the EPICS and are monitored using LabVIEW to use its excellent graphic-user interface: vacuum pressure of cyclotrons and beamlines, position of injection and extraction devices of cyclotrons, and current of magnet power supplies. In addition, we developed the LabVIEW program, which automates the charge-distribution measurement for the development of the gas stripper[3)], as shown in the lower part of Fig. 1. The program contains control of dipole and quadrupole magnets, control of Faraday cups, and data acquisition of beam currents. This program greatly improves the measurement efficiency when compared to manual measurement. We could easily obtain high-statistics data with less measurement time.

Last but not least, we are grateful to F. Nagahisa and N. Ikuta of NI Japan for their valuable advice.

References

1) M. Komiyama et al.: Proc. of ICALEPCS2009, Kobe, Japan, October 2009, TUP084, p.275 (2009).
2) http://joule.ni.com/nidu/cds/view/p/id/3180.
3) H. Imao et al.: Phys. Rev. ST Accel. Beams 15, 123501 (2012).

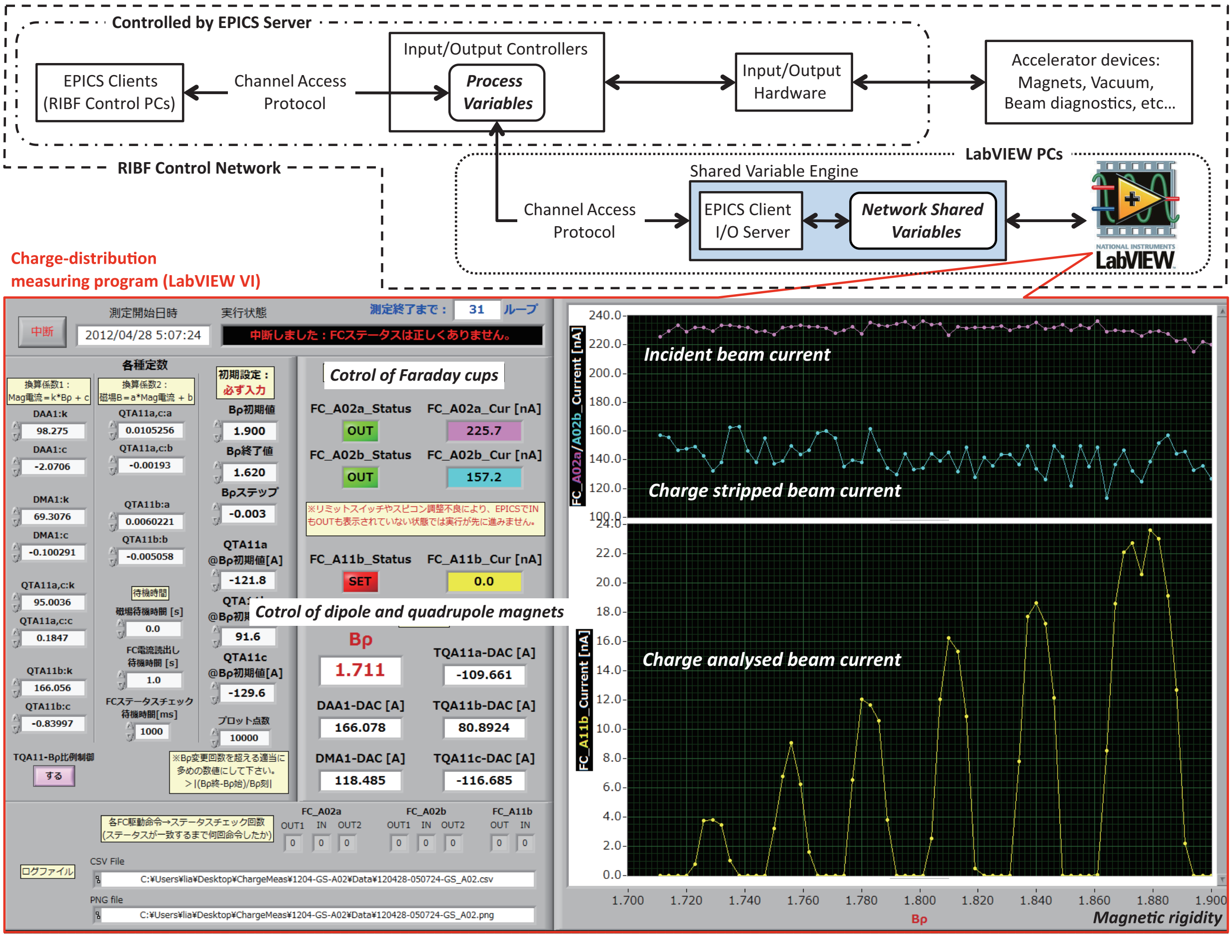

Fig. 1. Charge-distribution measuring program using LabVIEW EPICS Client I/O Server.

*1 SHI Accelerator Service, Ltd.

Updates on RIBF control system

M. Kobayashi-Komiyama, A. Uchiyama, M. Hamanaka,[*1] T. Nakamura,[*1] M.Fujimaki and N. Fukunishi

We report on two aspect of the RIBF control system. The first one concerns the upgrade of worn controllers used for old magnet power supplies. The second one is concerns the upgrades of the RIBF alarm system.

The RIBF facility and its control system consist of two parts. The old facility, once called the RIKEN Accelerator Research Facility (RARF), started its operation in 1986, wherein the control system was built on the CAMAC system with the device interface modules (DIMs) that are in-house controllers for devices such as magnet power supplies, beam diagnostic devices, and vacuum devices. The new facility became operational in 2006. In the new facility, the magnet power supplies are controlled by a new type of controller, the NIO, which is a commercial control board manufactured by the Hitachi Zosen Corporation. On the other hand, we have decided to use beam diagnostic devices that are similar to those used in the RARF in the new facility. In this case, there is one serious problem regarding the device controllers; maintaining DIMs becomes difficult year by year because the supply of several kinds of components used on the controller boards has been terminated and backup supplies have been nearly exhausted. Therefore, we have developed a succession controller named the network device interface module (N-DIM)[1], which is designed to be compatible with the DIM. Besides the development of the new facility, we have started replacement of DIMs by N-DIMs step by step since 2003. At the end of 2012, replacement of DIMs by N-DIMs has been completed for the old beam diagnostic and vacuum devices used for the ring cyclotrons and beam transport lines connecting the cyclotrons to each other.

At the same time, it is also required to investigate the possibility of applying N-DIMs to control magnet power supplies because about 80 DIMs still control 400 magnet power supplies in the old facility, and these have been in use for a long time. After we developed a new program executed on an EPICS I/O controller using N-DIM commands to control the old magnet power supplies, we have started various control tests using the N-DIM since this spring. We first conducted two kinds of basic validation tests on the N-DIM: controlling a power supply by switching its polarity and long-term operation testing by using an actual magnet power supply and a simulator, respectively. After we obtained satisfactory results for these tests, we investigated the radiation-hardness of a N-DIM by using it in the power supply of the injection-bending magnet II (BM2) of the RIKEN Ring Cyclotron (RRC) during actual beam service times because the old power supplies of the RRC are placed in the RRC room. As a result, the BM2 power supply has been controlled stably except for the occurrence of one accident during a two-month operation. The accident involved the excitation current of the power supply being suddenly set to be zero without any requests from the operators. We will decide whether N-DIMs are to be used under actual operation conditions after determining the reason for the accident by monitoring the control of the BM2 using various methods.

An alarm system to continuously survey the status of various devices and inform operators of their anomalous behaviors was implemented in the RIBF control system several years ago. The current system is based on the old version of the Alarm Handler[2] provided by the EPICS collaboration. We can use the alarm system to monitor vacuum systems along with the beam intensity measured by a selected Faraday cup installed in the beam transport lines; however, the system has not been optimized to set the alarm levels for the output current of the magnet power supplies because it is difficult to evaluate their instability. During our study of the alarm system, changes were repeatedly made to the system's alignment, and therefore, the alarm system information has not been properly updated. Furthermore, we found that the data format of the alarm history data was not a user-friendly one, such as the format of a relational database. Therefore, making improvements to of the alarm system is essential. Updating the version of the Alarm Handler and its setting files may have solved our problems, but we decided to introduce the alarm system based on the Control System Studio (CSS)[3] as a new alarm system because the CSS, which is an integrated development environment, is expected to be the next mainstream application in the EPICS collaboration. We have successfully set up CSS applications in two PCs. We have started monitoring the alarm information of almost all the vacuum systems of the beam transport lines in the RIBF, the rotating charge stripper at the E1 experimental vault, and nearly half of the magnet power supplies in the RIBF as a test operation. During two months of beam services, the system has been operating stably. Therefore, we have decided to extend the number of devices to be monitored to obtain all the information beneficial to stable operation of the RIBF accelerator complex.

In the near future, we plan to use the full functionality of the CSS including the GUI-based operator interface and data archive system. This will enable us to construct an integrated console. We will attempt to apply all the console functions to the control system of the AVF cyclotron as a first step.

References
1) M. Fujimaki, et al.: RIKEN Accel. Prog. Rep., 37, 279 (2004).
2) http://www.aps.anl.gov/epics/extensions/alh/index.php
3) http://cs-studio.sourceforge.net/

*1 SHI Accelerator Service Ltd.

Data Integration between EPICS-based System and Non-EPICS-based System by using MySQL

A. Uchiyama,*[1] M. Kobayashi-Komiyama, and N. Fukunishi

In RIKEN RI beam factory (RIBF), we constructed control systems based on the EPICS (Experimental Physics and Industrial Control System) for magnet power supplies, beam diagnostic instruments, vacuum control, ECR ion source control, etc.[1)] However, EPICS-based systems do not comprise the entire RIBF control system. For some of measurement instruments in the accelerator operation, non-EPICS-based systems, such as commercially available systems, are often used because of limited human resources. Furthermore, some users require integrating the data of the non-EPICS-based system and EPICS-based system because of the effectiveness of accelerator operation. In general, in order to integrate the commercially available system by EPICS, the EPICS driver/device support software is necessary for each device. However, the major source of complexity is caused by the costly development of EPICS driver/device support software.

In non-EPICS-based system, the administrators of each measurement instrument store the data in a MySQL database via MyDAQ2 system[2)], which is a simple data acquisition system developed by JASRI/SPring-8. The users of MyDAQ2 sent TCP socket messages to record their data in the MySQL database. At present, the data is stored in MySQL database by a wide variety of system, such as the temperature of water cooling system in RILAC/AVF/RRC, the vacuum system of 18GHz ECR Ion Source, the stability of RF [3)], and the temperature of magnet power supplies. If the EPICS Channel Access (CA) client can reach the data in the MySQL database, the data can be integrated between non-EPICS-based system and EPICS-based system. Therefore, we have developed an application to handle the data from the database of MySQL by using EPICS CA protocol. The structure of our system is as follows. (See Figure 1)

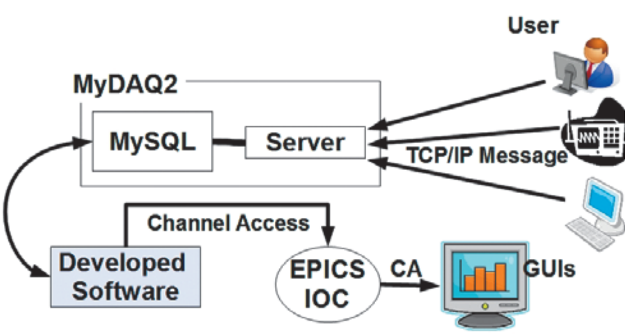

Figure 1: System chart showing the relation of developed software, EPICS and MyDAQ2

1. Each user stores the various kinds of the non-EPICS-based data in MySQL via MyDAQ2 server.
2. The latest data pass the values to EPICS IOC as records, such as analog input record or binary input record, every second in the same layer of the CA client.
3. The EPICS records made by the application are automatically named as follows regularly. 'MYDAQ2' : 'Signal name' : 'column number' (ex, MYDAQ2:DA100:c1)
4. Other EPICS CA clients, such as GUIs, are developed by using above EPICS records.

In slow-extraction line at J-PARC, MySQL is already used for system integration between especially for LabVIEW system and EPICS-based system [4)]. In this case, the system needs special EPICS record and the asynchronous device support software. However, to reduce the number of development process, the data is inserted to EPICS Input/Output Controller (IOC) from the application layer instead the low-level layer in our system.

In this system, only sending the message including the data to MyDAQ2 using socket program is sufficient to convert EPICS-compliant data from non-EPICS-compliant data. For storing the data to MyDAQ2, the socket program consist of simple coding written in C/C++, LabVIEW, Python, and bash. As a result, it is available to use the non-EPICS data from EPICS CA without development of the EPICS driver/device support software, which is expensive. Finally, we successfully developed some operator interfaces as EPICS CA client using EPICS record value obtained from MySQL database.

This system was already implemented for RIBF control system in order to integrate the numerical values between EPICS-based system, which does not require required fast scan time, and non-EPICS-based system. Currently, this system is used for GUIs in 18GHz ECR ion source control, RILAC vacuum control, BT-map[5)], etc. As a result of construction of the system, it was successful to provide the data integration service between EPICS and non-EPICS for accelerator operation without serious problem.

References

1) M. Komiyama et al.: Proc. ICALEPCS07, Knoxville, Tennessee, USA, (2007) P.187.
2) T. Hirono et al.: Proc. PCaPAC08, Ljubljana, Slovenia, (2008), P.55
3) R. Koyama et al.: RIKEN Accelerator Progress Report (2009)
4) Y. Sato et al.: Proc. ICALEPCS05, Geneva, (2005)
5) R. Koyama et al.: RIKEN Accelerator Progress Report (2011)

*1 SHI Accelerator Service, Ltd,.

NISHINA RIBF water-cooling system 2012

T. Maie, K. Kusaka, M. Ohtake, Y. Watanabe, E. Ikezawa, M Kase

Nippon Kucho Service Co., Ltd, SHI Accelerator Service Co., Ltd

The water-cooling systems located in the Nishina Building and RIBF Building, shown in Fig. 1, were operated for approximately 200 days in 2012. In this period, we did not meet any serious failures that stopped the beam service for more than two days, except for the following minor troubles. A mechanical seal of the water pump for the RRC was damaged during accelerator tuning. Flushing of the cooling pipes in the SRC-MDC1 was also carried out twice due to abnormal temperature-rise during the SRC operation.

Fig .1. Photographs of the water-cooling system in the Nishina Building (left) and that in the RIBF building (right).

We carried out two major construction concerning the cooling channels in 2012, as mentioned below, in addition to the annual maintenance efforts. One concerned the helium gas-stripper system, which was newly constructed in the RRC vault.[1] A new water channel was added for the stripper as shown in Fig. 2. We constructed a branch in the cooling channel for the injection/extraction devices of the RRC, which carries 130 L/min for the charge stripper. A new branch was also constructed in the channel for the beam transport magnets, which channel feeds cooling water at 200 L/min for a new beam dump in the analyzing magnet DAA1-DMA1,[2] as shown in Fig. 3. The other construction concerns a new cooling system for the Rare-RI Ring,[3] and the construction of this cooling system was begum in 2012. Stability of the system temperature is a crucial issue for the Rare-RI ring to achieve a high resolution of mass measurement with an accuracy of $\Delta M/M = 10^{-6}$. The main specifications of the new cooling-water system are summarized in Table 1.

Fig. 2. Photograph of the new water channels for the helium gas-stripper.

Fig. 3. Photograph of the water channels for the new beam dump in the DAA1-DMA1 magnet.

Table 1. Main specifications of the new water -cooling system of the Rare-RI Ring.

Cooling tower (low-noise, plume-abated type)	
Cooling capacity	2,000 kW
Circulating water	2,867 L
Heat exchanger (plate type)	
Exchangeable heat:	2,000 kW
Water pump	
Voltage	400 V (3 phase) - 4 pole
Power	55 kW
Water flow	2,370 L/min
Water temperature (design)	28 ℃ (out) / 38 ℃ (in)

References

1) H. Imao et al.: In this report.
2) K. Yamada et al.: In this report.
3) Y. Yamaguchi et al.: In this report.

Design study of the second superconducting ring cyclotron†

J. Ohnishi and H. Okuno

Uranium beams are accelerated by an RFQ, a DTL linac, and four ring cyclotrons (RRC, fRC, IRC, and SRC) at the RIBF, as shown in Fig. 1. U^{35+} ions extracted from the 28-GHz ECR ion source is converted to U^{64+} at the first charge stripper (CS) after the RRC and to U^{86+} at the second one after the fRC. The converting efficiencies of the two CSs are approximately 18% and 27%, respectively, and the total transmission efficiency from the ion source to the exit of the SRC is approximately 1/200, which is fairly low. Accordingly, in order to increase the beam current approximately tenfold, we have investigated the design of the second superconducting ring cyclotron (SRC2)[1)] instead of the fRC, which can accelerate U^{35+} without using the first CS.

The plan view and the parameters of the SRC2 are shown in Fig. 2 and Table 1, respectively. The acceleration RF frequency is fixed and the velocity gain is 2.06. The sector magnets use superconducting main coils and twenty normal one-turn trim coils, and the weight of the yokes of the one sector is approximately 1200 t. The parameters of the sector magnet are listed in Table 2. For comparison, the parameters for the superconducting dipole magnet for the SAMURAI spectrometer[2)] at the RIBF are also listed. Since the maximum magnetic field at the main coils is 2.53 T, which is low, and the magnetic force acting on the coils is also small, the superconducting coils can be of an epoxy-impregnated type and bath-cooled in liquid helium like the SAMURAI dipole magnet. Moreover, the support structure of the coils can be referred to the SAMURAI dipole magnet, and the refrigeration system can also be simplified by using several GM and GMJT cryocoolers instead of a large plant using the Claude cycle. In the beam injection and extraction, only one superconducting magnetic channel (sMIC2) must be used, whereas the other magnetic channels are of a normal conducting type and can be applied to the almost same design of those used for the SRC. Their parameters and the calculated beam envelopes in the injection and extraction orbit are given in Ref. 1.

The fundamental design of the SRC2, especially the magnet system, was successfully performed, but more investigations, such as the design of the RF cavities as well as the detail structure of the sector magnets and sMIC2 are required to evaluate the feasibility of the present design of the SRC2.

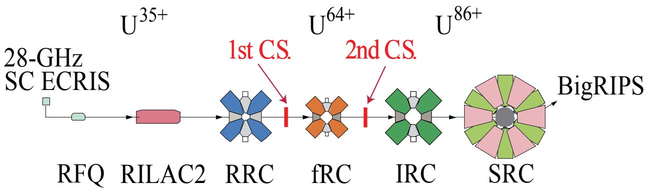

Fig. 1. The existing acceleration scheme for uranium

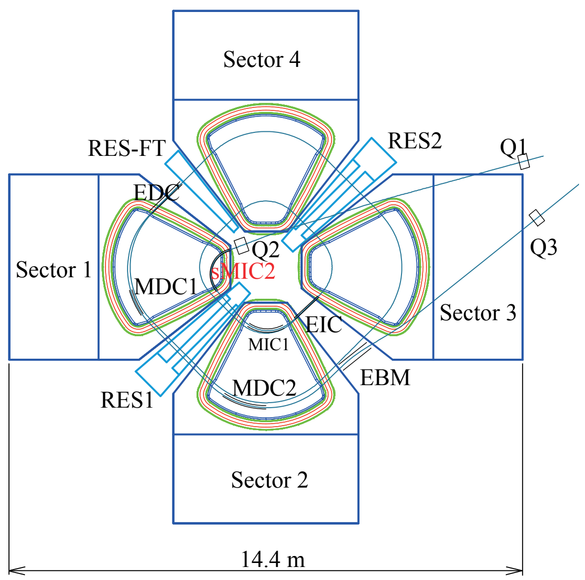

Fig. 2. Plan view of SRC2.

† Condensed from Ref. 1

Table 1. Parameters of SRC2.

K-value			2220
Energy	injection	MeV/u	10.8
	extraction	MeV/u	48
RF frequency		MHz	36.5 or 48.7
Harmonics			9 or 12
Average radii	injection	m	1.775
	extraction	m	3.65
Tune	νr		1.09~1.15
	νz		0.71~0.76

Table 2. Parameters of the SRC2 sector magnet and the dipole magnet for the SAMURAI spectrometer.

		One sector of the SRC2	SAMURAI
Weight of magnet	t	1200	566
Pole gap	mm	180	880
Magnetomotive force	MA	1.62	3.84
Max. magnetic field at orbit	T	3.2	3.1
Max. magnetic field at coils	T	2.6	5.4
Stored energy	MJ	11.3	27.4
Conductor		NbTi/Cu	NbTi/Cu
Current density	A/mm^2	81	66
Cu/NbTi ratio		10	5.5
Load factor		0.3	0.6

References

1) J. Ohnishi et al.: to be published in Proc. 9th ann. meeting of Accel. Soc Japan.
2) H. Sato et al.: RIKEN Accel. Rep. 45, 128(2012).

Test of differential pumping system with plasma window

H. Kuboki, H. Okuno, A. Hershcovitch, T. Dantsuka, H. Hasebe, K. Ikegami, H. Imao, O. Kamigaito, M. Kase, T. Maie, T. Nakagawa, and Y. Yano

A differential pumping system with a plasma window (PW)[1] has been developed for application to the charge strippers at the RIBF using high-density low-Z gas. We evaluated the differential pumping performances with Ar and He arc plasmas. Figure 1 shows a schematic of the pumping system. The system consists of a PW and two chambers. In our performance evaluation, the first chamber was evacuated by two mechanical booster pumps with a pumping rate of approximately 730 $m^3 \cdot h^{-1}$ in total. The second chamber was evacuated by a turbomolecular pump (TMP) with a pumping rate of 792 $m^3 \cdot h^{-1}$. The PW has a central bore of 2 mm in diameter, which isolates the atmosphere from the first chamber. The first chamber is connected to the second chamber via a flow constrictor having an inner diameter of 6 mm and length of 15 cm. The base pressure attained without gas flow was 9×10^{-2} Pa in the first chamber. At first, the PW was ignited and tested with Ar. Subsequently, we replaced Ar gas with He for PW operation with He.

The differential pumping efficiency was evaluated by measuring the pressures in the first chamber (P_1) and second chamber (P_2). The pressures P_1 and P_2 in the cases of Ar and He are plotted as a function of arc current in Figs. 2 (a) and (b), respectively. The solid circles and triangles denote Ar and He data obtained at RIKEN. The open circles and triangles denote Ar and He data obtained with the original PW at BNL[2]. The plotted data were corrected adequately depending on the gas species. We firstly measured P_1 and P_2 without PW operation and compared the results with those obtained with PW operation. The P_1 and P_2 values without PW are indicated by solid lines in the case of Ar in Fig. 2. Those of He are far above the vertical axis. The discrepancy between the RIKEN and BNL data can be explained by the difference in pumping rates; the pumping rates at BNL were 1073 $m^3 \cdot h^{-1}$and 1872 $m^3 \cdot h^{-1}$ for the first and second chambers, respectively. P_1 was reduced by a factor of 10 with PW operation for Ar, while this factor was more than 17 for He. P_2 was more drastically reduced by 100 and 5000 times for Ar and He, respectively. This high reduction factor for He is due to the extremely large P_2 value greater than 100 Pa in the case of no-PW operation. The TMP was almost useless in this pressure range, and hence, the second chamber had almost no evacuation. These reduction factors for P_1 and P_2 provide the advantage that at least one differential pumping stage can be removed by applying PWs to a conventional differential pumping system.

Measurements using a gas cell filled with Ar and He are planned in the near future. An improvement of enlarging central bore diameter from 2 mm to 4 mm is also planned for further developments.

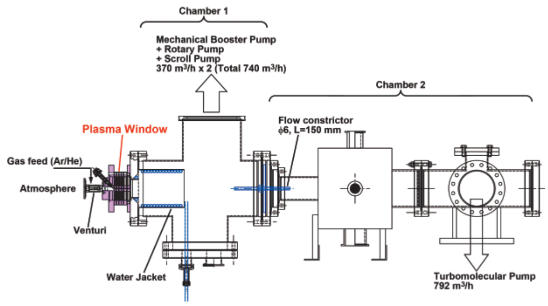

Fig. 1: Schematic of the differential pumping system with a PW.

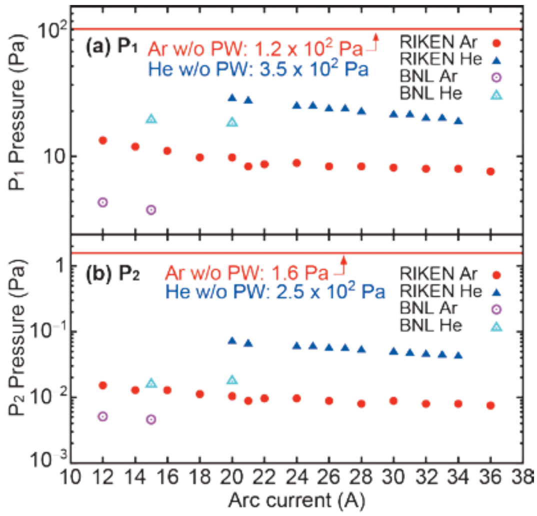

Fig. 2: Pressures (a) P_1 and (b) P_2 in cases of Ar and He plotted as a function of arc current. Please see the text for details.

References
1) A. Hershcovitch; J. Appl. Phys. **78**, 5283 (1995).
2) A. Hershcovitch; private communication (2011).

Design of cavity to recover energies of multi-charged uranium beams in ion-recycling ring

K. Suda

For the acceleration of the ^{238}U beam, two charge strippers are used to increase a charge state of the ions. The first stripper is placed downstream of the RRC, and it uses helium gas[1] as a material for the stripping. After a $^{238}U^{35+}$ beam with an energy of 10.75 MeV/nucleon passes through the stripper, multi-charged beams are generated. By using a bending magnet after the stripper, the beam with the charge of 64 is selected, and then transported to the fRC. A charge-stripping efficiency is around 15%. In order to increase the charge-stripping efficiency, a novel ring dedicated to recycle ions having other charge states, called an ion-recycling ring, is considered. The ring has two achromatic sections and two dispersive sections with a design dispersion of ~ 5 m. The stripper system is placed in one of the achromatic sections, through which ions are injected into the ring (charge-stripping injection). The ions with the required charge are only extracted by an extraction channel placed in one dispersive section, utilizing large spatial separations (~ 80 mm) between ion orbits having different charge states. The multi-charged ions lose their energies by about 2% per turn on account of the stripper. In order to recover the energies of ions, an energy-recovery cavity is installed in the other dispersive section. The charge-stripping efficiency with the ring is estimated to be improved up to around 70% under the condition that the circulated ions have charges between 58 and 70, and the helium gas with the thickness of 0.4 mg/cm^2 is used. In this report, the design of the cavity is presented.

The requirements of the cavity are as follows: (1) The accelerating electric field changes smoothly depending on the beam position, from 882 kV to 731 kV, corresponding to the ion charge states. (2) The power dissipation should preferably to be less than 100 kW, considering the cost of an rf amplifier. To realize condition (1), a half-wave resonator is considered, which is similar to the case of the RRC,[3] but without the movable box, as shown in Fig. 1. The design was performed by using a 3D-electromagnetic calculation software, CST Microwave studio 2012.[2] The resonant frequency is set to be the third harmonic (54.75 MHz) of the fundamental frequency (18.25 MHz), so that the height of the cavity became small, at about 1200 mm. The length of the dee is set to be 1100 mm. The small angle of the dee of 2° is to generate effective gap voltages that are required for multi-charged ions by changing the ion transit time through the cavity depending on their charges, where the gap voltages are assumed to be flat irrespective of the ion orbits. Two cavities are needed to achieve condition (2). The estimated power dissipation for each cavity is 41 kW to generate the required gap voltage for a charge of 58 (221 kV/gap). Figure 2 shows the gap voltage distribution, where the position is measured from the innermost circumference of the dee. The distribution is not flat as desired, and there are fluctuations at around the center of the dee (−18% at the maximum at 550 mm). Further calculations to improve the distribution are in progress.

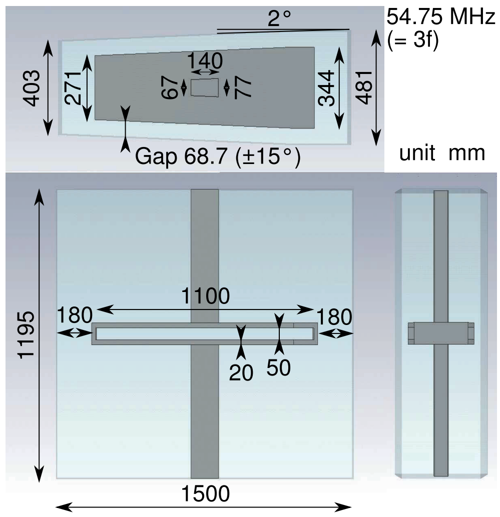

Fig. 1. Half wave resonator for the energy recovery of multi-charged ions in the ion-recycling ring.

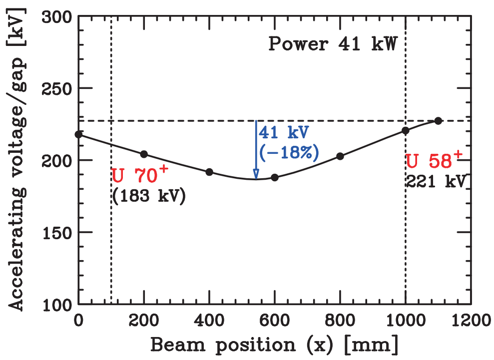

Fig. 2. Distribution of gap voltages.

References
1) H. Imao et al.: In this report.
2) http://www.cst.com.
3) T. Fujisawa et al.: Nuclear Instrum. Methods A292, 1 (1990).

Eeffects of grids in drift tubes

M. Okamura

A drift tube structure is commonly used in an ion linear accelerator and an RF buncher to induce a longitudinal electric RF field. To gain an efficient RF kick, an appropriate choice of the ratio of the gap length to the inner diameter of the drift tubes is important. A larger diameter of the drift tube elongates the effective electric field area penetrating the drift tubes. In particular in low-velocity regions, a phase change of the RF reduces the effective voltage in the gap. The ratio of the effective kick to induced voltage in the gap is called transit time factor (TTF). To prevent a low TTF, a grid structure has sometimes been used. In this report, we examine the field variation caused by a grid structure for a typical drift tube structure.

To obtain detailed 3D information of the field variation, we used the TOSCA-OPERA[1] assuming a static electric condition including fine structures of the grids. A cylindrical coordinate system is defined such that the z axis is the beam axis. Thus the field components are expressed as *Er*, *E θ* and *Ez*. The Fourier coefficients were derived from the field along the yellow circle indicated in Fig. 1. The radius of the circle is 7 mm from the beam axis, which is just inside of the apexes of the grid's pattern.

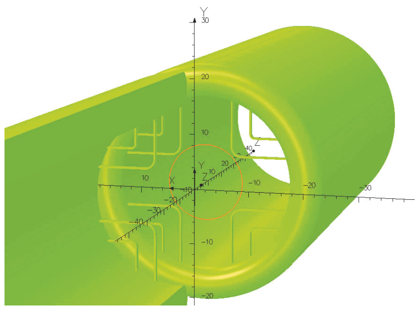

Figure 1: 3D model for OPERA

The inner diameter and gap length are 32 mm and 10 mm, respectively, in the assumed model. The edgse of the tube are rounded by a radius of r = 3 mm and the grid's face is fixed at the z = ±3.1 mm position. The grid consists of four quadrants and the width of the grid facing the beam direction is 0.2 mm. The grid length along the beam direction is 1.0 mm. The distance between two facing grids is 16.2 mm. In this analysis, the gap voltage is assumed to be 100 V.

Figure 2 shows the longitudinal electric field strengths at r = 7 mm, which is the *b0* component of *Ez* along the beam axis, with and without grids. The dotted lines include RF phase change assuming a 750-keV proton beam at 201 MHz. At the z = 0 position, the RF phase of *cosine* is zero. At the tail of the fields, the induced voltage has a negative value at around z = 15-30 mm.

The work was extracted from the presentation at IPAC12 in New Olreans, USA.

If the cavity employs a $\beta\lambda/2$ gap interval, these negative effects can be avoided, since $\beta\lambda/2$ = 30 mm.

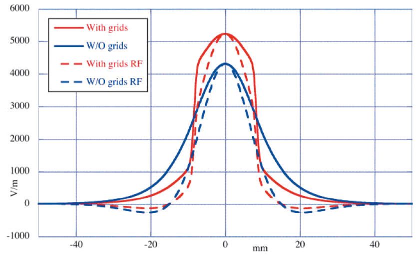

Figure 2: Longitudinal field strength (r = 7mm).

The TTF can be derived by comparing the solid and dotted curves at a certain phase (the graph shows zero phase angle). The obtained values are summarized in Table 1. The grids enhance the TTF by about 26%.

Table 1: Transit time factors

On axis	With grids	63.50%
	Without grids	50.14%
r = 7 mm	With grids	72.28%
	Without grids	57.03%

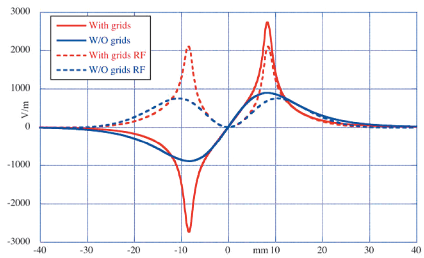

Figure 3: Transverse field strength (r = 7mm).

The *b0* component of *Er* represents the focusing and defocusing force. Figure 3 shows this component. The dotted lines indicate the field strengths with an RF phase angle of -90° at the z = 0 position. The integrated values along the axis with and without grids are 24.9% and 19.7% of the gap voltage respectively. The grids amplify the RF defocusing force by choosing a bunching RF phase.

In general, the grid structure is useful to obtain a better TTF. To investigate the nonlinear grid effects on a beam, detailed tracking simulation or experimental study is required.

References

1) OPERA-TOSCA, Vector Fields Software, Cobham http://www.cobham.com

Effect of solenoidal magnetic field on drifting laser plasma

M. Sekine, K. Takahashi,[*1] and M. Okamura

A laser ion source can provide various heavy ions using a simple apparatus. Although we can increase the ion beam current by increasing the laser power, this is usually not an option because other parameters, which includes the charge distribution will also change. Another way of increasing the current would be to suppress the three-dimensional expansion of the plasma. Applying a longitudinal magnetic field during the transportation of the plasma can limit the transverse expansion. Thus, we can extend the pulse length by increasing the drifting distance while maintaining a high current.[1),2)] If this technique is established, it can be used with various laser ion sources. However, the effect of the magnetic field on the laser ablation plasma is not well understood. We report on the stability and current decay of copper plasma confined by a solenoid.

A Nd:YAG laser was focused with lens with a focal length, f = 3000 mm, that irradiated a copper-plate target to create a plasma. The Nd:YAG laser (Brilliant, Quantel) produces infrared light with a 1064 nm wavelength and a 6 ns pulse length. The incident laser angle was 30^{o} relative to the normal of the target material. The laser energy and spot area measured at the target position were 490 mJ and 0.182 cm^2, respectively. According to the pulse length, energy, and spot size, the power density was estimated to be 3.3 × 10^8 W/cm^2. From previous work, it is expected that the most abundant charge state at this power density is one.[3)] Therefore the ion beam current density is just proportional to the particle number. This leads to a much simpler plasma for analysis of the effect of the solenoidal field. The vacuum was kept around 10^{-4} Pa. A Faraday cup (FC) used to measure the ion beam current was located at exit of the solenoid. The aperture size of the FC ranged from 0.5 to 10 mm. The suppressor voltage of the FC ranged from -2 to -10 kV. The length and inner diameter of the solenoid coil were 3 m and 72 mm, and it can give a magnetic field of 52 gauss/ampere at the center of the solenoid. The solenoid was located 315 mm from the target surface. Baffles with aperture sizes of 10, 20, and 30 mm were used to investigate how the diameter of the injected plasma affects its transport.

As shown in Figs. 1 (A) and (B), the pulse length of the ion beam was prolonged to ~100 μsec with the 3 m solenoid while maintaining a high current. However, we observed that the ion beam current fluctuated in some range of the magnetic field as shown in Fig. 1(B).

The baffles were used to improve the stability and control the current density. We compared the standard deviations of the current when using baffles. The deviation was smaller near the peak when baffles with 20 and 30 mm aperture were used as shown in Fig. 2.

[*1] Tokyo Institute of Technology

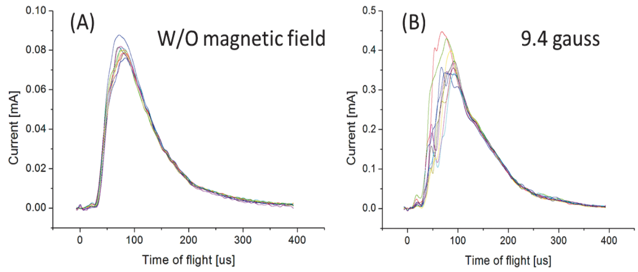

Fig.1 Stability of the current measured 10 times with the Faraday cup without magnetic field (A) and with the magnetic field (9.4 gauss) (B).

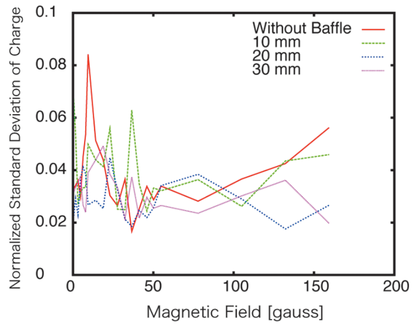

Fig.2 Dependence of the standard deviations of charge on the diameter of plasma injected into the solenoid.

We investigated how the current of the copper-ion beam was affected in three different ways: varying the magnetic field strength, the solenoid length, and the plasma diameter. As the magnetic field increases, the ion beam current increases. The pulse length of the ion beam was prolonged while maintaining a high current. However, we observed that the stability of the ion beam current could become worse in some range of the magnetic field. This means that the solenoidal field can disturb the plasma stability. The results also show that baffles with appropriate apertures improve the stability of the plasma transport. Although the plasma density decreases during drift in the solenoid, the decay rate is far less than without magnetic field due to the magnetic confinement. We need further experiments to understand the mechanism of magnetic guiding and the cause of the disturbance of the current.

References

1) M. Okamura, A. Adeyemi, T. Kanesue, J. Tamura, K. Kondo and R. Dabrowski, Rev. Sci. Instrum. **81**, 02A510 (2010)
2) J. Wolowski, J. Badziak, I. Ivanova-Stanik, P. Parys, W. Spepniewski and E. Woryna, Rev. Sci. Instrum. **75**, 1353-1359 (2004)
3) T. Kanesue, J. Tamura, and M. Okamura, Proceedings of EPAC08, Genoa, Italy, 2008, p. 421.

Emittance from laser ion source for RHIC and NSRL in BNL

M. Sekine

The Electron Beam Ion Source (EBIS) at Brookhaven National Laboratory (BNL) is a new heavy ion source for RHIC and the NASA Space Radiation Laboratory (NSRL)[1].

Laser Ion Source (LIS), which use a solenoid can supply types of ions from solid targets and is suitable for a long pulse length with low current, as ions provide for the fringe field of the solenoid. LIS was selected as an injector to EBIS, for which RMS emittance was required to be under 0.06 πmmmrad because LIS can provide several species every second and can result in low emittance. These species, namely, C, Al, Mg, Si, S, Ca, Ti, Cr, Fe, Cu, Ta, Au, etc., were required from the NSRL to simulate the influence of cosmic rays in the universe. Au and Cu beam were also required for RHIC. We have two ways by which the LIS current can be increased, that is, double pulse lasers and a solenoid magnetic field. Figure 1 shows experimental setup.

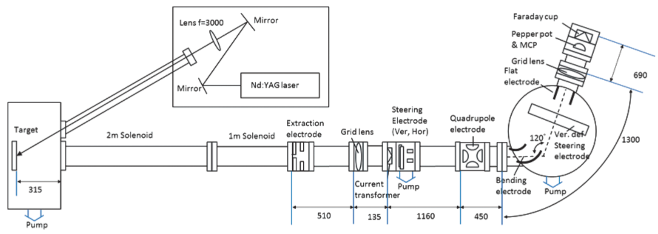

Fig.1. Experimental beam line

A Nd:YAG laser was focused by a lens with the focal length, f = 3000 mm, which irradiated C, Cr, Fe, and Cu target plates to create a plasma. The Nd:YAG laser (Brilliant, Quantel) produces infrared light with a 1064 nm wavelength and 6 ns pulse length. The incident laser angle was 30 degrees to the normal of the target material. The laser energy and spot area measured at the target position were around 490 mJ and 0.182 cm^2, respectively. According to the pulse length, energy, and spot size, power density was estimated to be around 3.3×10^8 W/cm^2. From a previous work, it is expected that the most abundant charge state at this power density is one.[2] Hence, it can be concluded that the ion beam current density is exactly proportional to the particle number.

The vacuum was maintained at around 10^{-4} Pa. The Faraday cup (FC) and pepper-pot (PP) were used to measure the ion beam current and emittance, which were located at end of the beam line where the simulated EBIS entrance was located. The FC aperture was 87 mm to collect the complete current. The suppressor voltage of the FC was around 140 V. The PP consisted of a copper mask (4 cm diameter), MCP (multi-channel plate) phosphor, and CCD camera. The length of the solenoid coil was 3 m. The beam extracted diameter was 15 mm. Voltages were at 20 kV between the target chamber and the extracted electrode, and after the extracted electrode where is ground voltages. This is one of the results used to measure Cr (q/A=22/52, laser energy at target; 490 mJ, target; 20 kV). The peak current was 186 μA and the normalized RMS emittance was x:0.062 πmmmrad and y:0.060 πmmmrad. Table 1 lists the required values and experimental results for the C, Cr, Fe, and Cu beam.

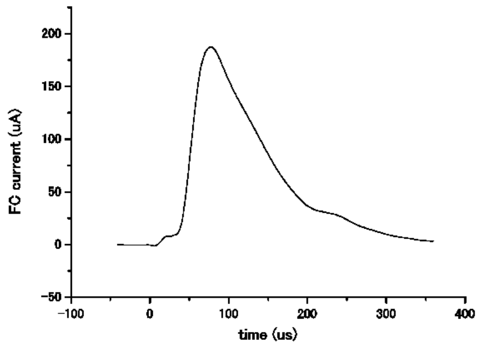

Fig. 2. FC signal for Cr (q/A=19/52)

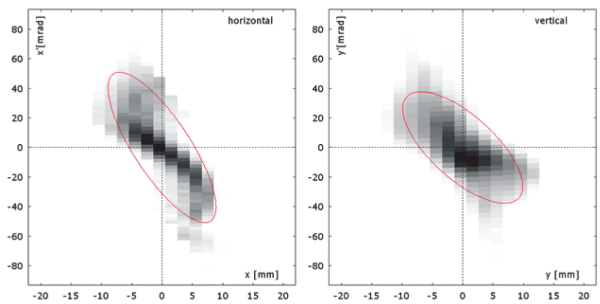

Fig. 3 Emittance of Cr (q/A=19/52)

Table.1. Required values and experimental results for the C, Cr, Fe, and Cu beam.

Species									
		C		Cr		Fe		Cu	
Mass of injected ion	AMU	6		52		56		63	
Required value									
charge state of interest	+	4	6	9	19	11	27	11	24
q/A		0.67	1.00	0.17	0.37	0.20	0.48	0.17	0.38
overall efficiency	%	50	50	50	50	50	50	50	50
injection time	μs	149.6	149.6	100.5	100.5	100.2	100.2	75.0	75.0
avg inj 1+ current	μA	294.0	196.0	194.5	92.1	159.6	76.5	213.3	90.4
total ion charge in species of interest	Coulomb	4.4E-08	2.9E-08	2.0E-08	9.3E-09	1.6E-08	7.7E-09	1.6E-08	6.8E-09
Experimental results									
Experimental result of injection time	μs	-	150	100	100	100	100	200	200
Experimental result of peak current	μA	-	663	310	187	285	154	332	142
Experimental result of total ion charge	Coulomb	-	4.6E-08	2.3E-08	1.4E-08	2.0E-08	2.1E-08	4.3E-08	2.0E-08
Nor RMS emittance X	πmmmrad	-	0.096	0.061	0.062	0.072	0.066	0.103	0.088
Nor RMS emittance Y	πmmmrad	-	0.117	0.072	0.06	0.077	0.058	0.069	0.06
solenoid	gauss	-	4.18	0	0	0	0	6.27	6.27
twin pulse	yes/No	-	Y	N	N	N	N	Y	Y

We have succeeded in producing several types of beams with the required emittance and current values.

References

1) https://www.bnl.gov/
2) T. Kanesue, J. Tamura, and M. Okamura, ; Proc. EPAC08, Genoa, Italy, 2008, p. 421.

8. Instrumentation

Curren Status of SAMURAI

K. Yoneda, T. Aumann,[*1] F. Delaunay,[*2] N. Fukuda, J. Gibelin, J. Hwang, N. Inabe, T. Isobe, N. Iwasa, S. Kim, N. Kobayashi, T. Kobayashi, Y. Kondo, T. Kubo, K. Kusaka, F.M. Marqués,[*2] Y. Matsuda, R. Minakata, T. Motobayashi, T. Murakami,[*3] T. Nakamura, S. Nishi, S. Ogoshi, J. Ohnishi, N.A. Orr,[*2] H. Otsu, T. Sako,[*4] H. Sakurai, H. Sato, Y. Satou, K. Sekiguchi, Y. Shimizu, H. Suzuki, K. Takahashi, H. Takeda, S. Takeuchi, R. Tanaka, T. Teranishi,[*5] Y. Togano, and K. Yoshida

This report describes the current status of a spectrometer constructed at the RIBF, called SAMURAI (Superconducting Analyzer for MUltiparticles from RAdio-Isotope beams with 7 Tm bending power). SAMURAI consists of a large superconducting dipole magnet[1)] and various types of particle detectors[2)]. It is characterized by large momentum acceptance and angular acceptance for particles emitted in fast RI beam reactions, and hence serves as a useful tool for experiments requiring multiparticle coincidence measurements. SAMURAI can be used in a variety of experimental studies such as breakup reactions, knockout reactions, polarized-deuteron-induced reactions, and multi-particle fragmentation. In our current plan, invariant-mass spectroscopy using breakup reactions is the most used during the early stages of operation, and SAMURAI's multiparticle detection capability is particularly suitable for this purpose. Combined with the high-intensity RI beams available at RIBF, SAMURAI facilitates studies on unbound states in unstable nuclei, thus enabling investigations that have previously been out of our experimental reach.

The construction of the magnet and detectors needed for coincidence measurements of heavy-ions (HIs) and neutrons completed in fiscal year 2011. This experimental setup includes detectors for incoming particles, detectors for neutrons emitted at forward angles, called NEBULA[3)], and detectors for HIs that are bent in the magnetic field. A commissioning experiment for this setup was carried out in March 2012, which was followed by the first series of physics experiments[4)] in May 2012.

The commissioning experiment aimed to confirm the performances of each experimental device, and to check the overall resolution and acceptance of SAMURAI as a spectrometer. The measurements were carried out with a primary beam of ^{18}O of 294 MeV/nucleon. The responses of detectors, mainly of drift chambers, were checked first, by using a mixed beam of particles with $Z = 3$–8. In this measurement, the optimal high voltages of the drift chambers were also examined.

Measurements were carried out to check the performance of NEBULA. In order to obtain the reference timing for the time-of-flight measurements, high-energy γ-rays generated in the reaction of ^{15}C on a thick Cu target at 247 MeV/nucleon were observed. Since the γ-ray energy spreads up to over 10 MeV, the data were also useful for the slewing correction. The detection efficiencies and resolutions were measured using quasi-monoenergetic beams of neutrons ($E_n \sim$ 200 MeV and 250 MeV) using a secondary proton beam and the ^{7}Li(p,n)^{7}Be reaction. The neutron beams were also employed to determiner the characteristics of cross talk in NEBULA as such events must be well understood in order to extract the true two-neutron events in breakup measurements with multi-neutron final states.

The performance of SAMURAI for the magnetic analysis of charged particles was examined by measuring their trajectories. The position and angle of the particles after passing through the magnet were measured with a secondary beam with a narrow momentum, i.e. with a well-determined $B\rho$. The measurements were carried out for three magnetic field settings (2.0 T, 2.5 T, and 3.0 T), and for ten $B\rho$ values ranging from 70% to 100% for each magnetic field, so that the trajectories were checked in various regions in the magnet.

In order to check the overall performance of SAMURAI, HI-neutron coincidence measurements were carried out by using breakup reactions. The invariant-mass resolution and acceptance should be obtained for reactions by ^{17}C, ^{15}C, and ^{14}Be beams with Pb and C targets. Data analysis is now in progress.

References
1) H. Sato et al.: RIKEN Accel. Prog. Rep. **45**, 128 (2012).
2) K. Yoneda et al.: RIKEN Accel. Prog. Rep. **43**, 178 (2010).
3) Y. Kondo et al.: RIKEN Accel. Prog. Rep. **44**, 150 (2011).
4) Y. Kondo et al.: In this report; T. Nakamura et al.,: In this report.

*1 GSI, Germany
*2 LPC CAEN, France
*3 Department of Physics, Kyoto University
*4 Department of Physics, Tokyo Institute of Technology
*5 Department of Physics, Kyushu University

Data acquisition for SAMURAI commissioning and day-one experiments

H. Otsu, T. Isobe, Y. Kondo,and T. Kobayashi

SAMURAI is a newly constructed spectrometer[1) for multiple particle coincidence measurements using a high intense RI beam at RIBF. It has been employed in physics experiments since it was commissioned in March 2012 and so-called "Day-one" experiments in May 2012. In the day-one experiments, measurements using invariant mass spectroscopy were performed by determining 4 momenta of neutrons coincident with heavy residuals. In the near future, the spectrometer will be employed for various experiments with various layouts of detector arrangement.

In the day-one experiments, data were obtained using the common trigger and event building mode in the BABIRL system[2)]. In order to reduce the dead time, we separated the data acquisition (DAQ) into 9 cpu ports with each VME controller, which is tabulated in table 1. Each port, except DALI and BigRIPS ports, consists of SBS 620 optical connection VME controller and (Slim size) PC with full height PCI card connection available. These configuration was not up-to-date because these modules were procured 4 years before in the period of the SAMURAI construction.

Trigger sources in the day-one experiments were 1) Beam downscaled (∼1/1000), 2) Beam × Neutron, 3) Beam × HODO, 4) Beam × DALI and 5) Beam × NEBULA(γ), which were selectable from a web console through a GTO circuit[3)]. The GTO circuit consists of programmable circuits with gated arrays. In the SAMURAI experiments, the GTO circuit acted as trigger source selector and DAQ latch arrays of communication between the circuit and DAQ PCs, which is schematically shown in Fig. 1. For the moment, the GTO circuit is programmed to be able to handle 8 trigger sources and 16 DAQ busy signals.

Table 1. List of data acquisition ports and their occupied period for 1 event processing during the Day-one experiments.

port name	dead time [μs]
Console/ Beam line plastics/ F5 MWPC	360
BDC/ICB (4×DC-TDC, 2× MADC32)	125
FDC1 (7×DC-TDC)	170
FDC2-1 (14×DC-TDC)	270
FDC2-2 (11×DC-TDC)	220
HODF (1×TDC V775, 1×QDC V792)	70
NEBULA (10×TDC V775, 10×QDC V792)	185
DALI (2×TDC V1190, 6×PHADC V785)	45
BigRIPS (1×TDC V1190, 1×TDC V1290	50

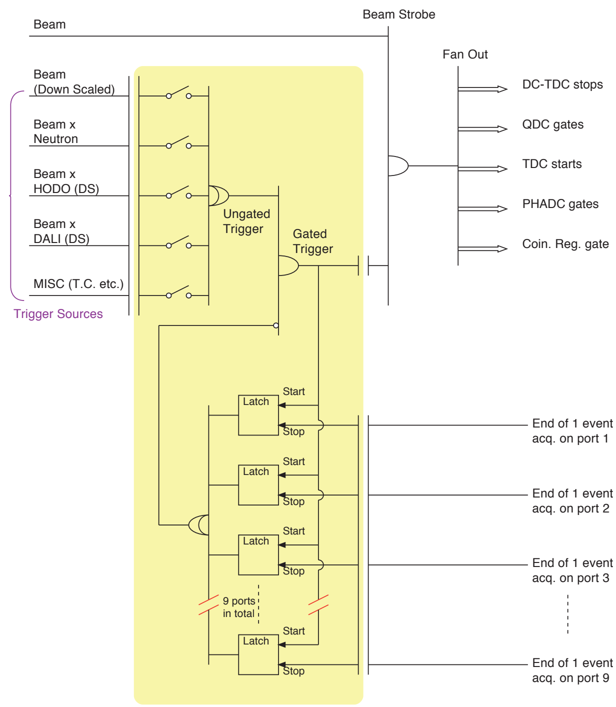

Fig. 1. Diagram for trigger source selection and latches for event handling in SAMURAI DAQ. A hatched region corresponds to the implemented circuits by the GTO module.

The DAQ system was successfully operated in the day-one experiment. We expect that the upcoming experiments, except the SAMURAI–TPC system, will be covered by the same DAQ system with minor updates. Interrupt occupied periods were measured in the environment of the day-one experiment and are listed in table 1 with typical modules for each DAQ port. Total dead time is determined by the longest occupied period, as that of the cpu port for the console, partly because the port contains the CAMAC module readout. Measured live time ratio was 75% for 0.7 kHz trigger, which is reasonably understandable with the 360 μs dead time.

In the near future, we plan to reduce the dead time down to the order of 200 μs (10% improvement expected) by rearranging the longer dead time ports as beam line detectors and FDC2 MWDC readout.

References
1) Y. Shimizu, et. al.: J. Phys.: Conf. Ser. 312 052022 (2011).
2) H. Baba, et. al.: Nucl. Instr. and Meth. A616 65 (2010).
3) H. Baba: private communication and his report in this volume.

Cryocooler overhaul of the SAMURAI superconducting magnet

H. Sato, K. Kusaka, M. Ohtake, K. Yoneda, Y. Shimizu, T. Motobayashi, and T. Kubo

The superconducting coils of the SAMURAI magnet are cooled by the liquid helium bath cooling method. Two GM/JT- and ten GM-cryocoolers are used to keep the coils at liquid helium temperature[1]. Operation of the magnet started in June 2011 and reached 10,000 hours in April 2012. An overhaul of the cryocoolers was carried out in October 2012, during an accelerator-maintenance period. According to the operation policy for the SAMURAI spectrometer, the temperature of the superconducting magnet should be kept at liquid helium temperature even during an overhaul. Thus, we introduced the same method as that for the cryocoolers on STQs in the BigRIPS, which is well established as "cold" maintenance[2,3].

Figure 1 shows the location of each cryocooler attached to the SAMURAI magnet. We prepared a maintenance cradle and a step with a stand, as shown in Fig. 2, for the cryocoolers located high above the ground. The overhaul included the following actions: (i) replacement of displacers, (ii) replacement of O-ring seals, (iii) cleaning of the inner wall of the cylinder, (iv) recharge of gaseous helium into the expander circuit line, (v) flushing of the JT circuit line (only for the GM/JT-cryocoolers), and (vi) cleaning of the compressor units. Actions (i), (ii), and (iii) were carried out in a bag containing gaseous helium, as shown in Fig. 3, in order to perform frost-free maintenance. The procedure of the overhaul in the gas bag is almost similar to that for the BigRIPS cryocoolers. However, special attention should be paid when the displacer, which consists of two separate parts not tightly fixed to each other, is re-installed into the cylinder. This is because the cryocoolers indicated as (3) and (4) in Fig. 1 are mounted horizontally to the cryostat.

After completion of the overhaul, the temperatures at the cold head decreased for 7 cryocoolers and increased for 5 cryocoolers. The temperature rise for 4 cryocoolers was lower than 2.6 K, which is within the allowable range. However, for the remaining GM for 20 K thermal shield, the temperature rise was 7.6 K, which is unacceptable. The displacer of this cryocooler was replaced for a second time, after which the temperature decreased successfully. We found that one of the O-ring seal on the displacer was distorted by an error in the replacement operation due to the above mentioned horizontal mount.

During the four-day maintenance period, the liquid helium level decreased from 91.5% to 84.1% for the upper coil, and from 88.4% to 82.4% for the lower coil. These correspond to 11.7 L and 9.7 L of liquid helium for the upper and lower coils, respectively. A total amount of 43 L was transferred in order to reach 95% level (227 L and 233 L for the upper and lower coils, respectively).

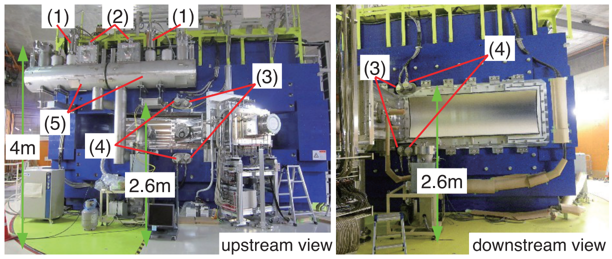

Fig. 1. Location of the cryocoolers: (1) GM/JT for 4.2 K; (2) GM for high-Tc power lead; (3) GM for 20 K thermal shield; (4) GM for 80 K thermal shield; (5) liquid helium reservoir vessels.

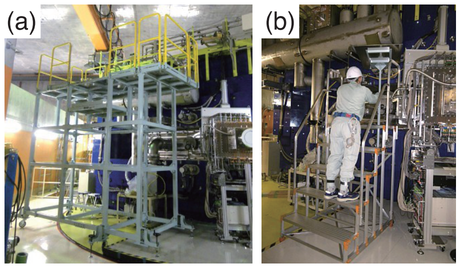

Fig. 2. (a) Maintenance cradle for cryocoolers mounted on the reservoir vessels. (b) Step with a stand for cryocoolers mounted on the upper coil.

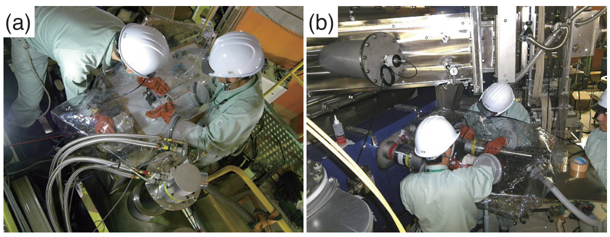

Fig. 3. The "cold" maintenance in the bag containing gaseous helium: (a) overhaul of the GM for power lead; (b) overhaul of the GM for 20 K thermal shield.

References

1) H. Sato et al.: IEEE Trans. Appl. Supercond. **23**, 4500308 (2013).
2) K. Kusaka et al.: RIKEN Accl. Prog. Rep. **45**, 235 (2012).
3) K. Kusaka et al.: IEEE Trans. Appl. Supercond. **23**, 4101305 (2013).

Large exit windows for the SAMURAI spectrometer

Y. Shimizu, H. Otsu, T. Kobayashi, T. Kubo, T. Motobayashi, H. Sato, and K. Yoneda

The first commissioning run of the SAMURAI spectrometer and its beam line was performed in March 2012[1]. Its vacuum system includes the beam line, magnet chamber, and two exit windows for outgoing neutrons and charged particles.

The neutron detector array NEBULA is located downstream of SAMURAI spectrometer. In order to minimize the reaction loss, the vacuum partition for neutrons should be as thin as possible. We set a large number of 10 for the safety factor against its possible destruction, because this window will be mounted almost permanently. The area to be covered is 2430×800 mm^2. The bend of the window caused by the pressure difference and the induced stress are calculated by the general purpose finite element analysis program code ANSYS[2]. If a flat plate of stainless steel (SUS304) is used for the window, the thickness must be larger than 25 mm to satisfy the safety condition. In order to reduce the effects of the reaction loss in retaining the safety factor, a partition was designed with the shape of a partial cylinder, resulting in a much smaller thickness of 3 mm. The calculated displacement by the atmospheric pressure at the central region and maximum stress are 173 μm and 44.1 MPa, respectively. The latter is about 1/12 of the tensile strength, 520 MPa. Figure 1 shows a photograph of the window for neutrons.

In order to measure the position and angle of the charged particles passing through the superconducting dipole magnet, a forward drift chamber (FDC2) was placed behind the SAMURAI spectrometer in the air partitioned with a thin foil window from vacuum. The window material deflects penetrating particles by multiple scattering and causes energy fluctuation by energy loss struggling. Required momentum resolution of 1/700 gives the upper limit of the amount of the material as radiation length of $L/L_R \sim 10^{-3}$. At the same time, the strength to hold the vacuum is needed. The vacuum partition is composed of a combination of a Kevlar textile for tensile strength and Mylar foil for vacuum seal, the thicknesses of which were 280 μm and 75 μm, respectively. The area to be covered by the window is 2800×800 mm^2. For the commissioning experiment, a window with a reduced area of 2800×400 mm^2, which is the maximum size that fulfilled the requirements at that time, was used. Figure 2 shows a photograph of this window. The maximum deflection around the center region was approximately 60 mm. The Mylar elongated by about 3.2% owing to air pressure, which was smaller than 1/3 of the tensile elongation at the break point. Since this window only achieved a safety factor of 3, the Kevlar and the Mylar will be removed from the window frame and new Kevlar and Mylar will be glued to the top of window frame every year for safety.

For experiments measuring heavy fragments and light charged particles in simultaneously, a full-size partition window is necessary, especially for detecting light charged particles. In the same manner as for the neutron window, a new partition with the vertical size of 800 mm is being designed with the same layer structure.

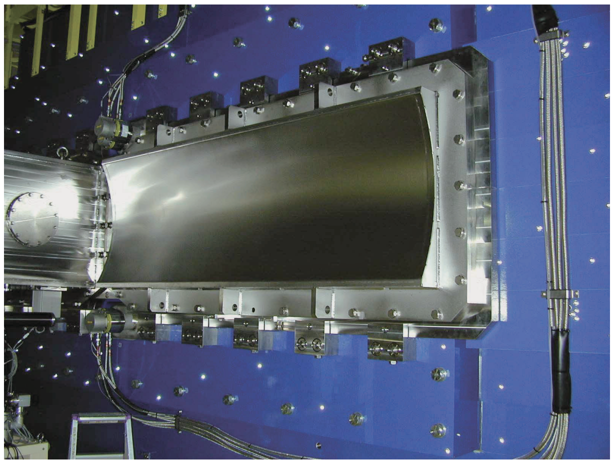

Fig. 1. Photograph of the window for neutrons.

Fig. 2. Photograph of the window for the charged particles.

References
1) K. Yoneda *et al.*: In this report.
2) http://www.ansys.com/

Precise position measurement of SAMURAI magnet and detectors

H. Otsu, Y. Shimizu, T. Isobe, Y. Kondo,and R. Minakata,

SAMURAI is a new spectrometer[1)] designed for multiple particle coincidence measurements using a high intensity RI beam at the RIBF. It has been employed in physics experiments starting from the commissioning experiment performed in March 2012, and the so-called day-one experiments in May 2012. In the day-one experiments, measurements using invariant mass spectroscopy were performed by determining 4 momenta of neutrons coincident with heavy residuals. In the near future, the spectrometer will be employed for various experiments with different arrangement of detector layouts.

In order to determine the physical quantities such as the momenta or scattering angles of particles, position detectors with high accuracy determination are placed upstream of the target for beam tracking (BDC1 and 2), upstream and downstream of the SAMURAI magnet for precise precession angle determination for reaction residues (FDC1 and 2). Scattering neutrons are detected by the neutron detector array NEBULA and their flight times are measured. In order to reflect the amount of physical precision without sacrificing the qualities of detector responses, installation position accuracies should be one or at least a half-order magnitude smaller than those of intrinsic resolutions. Based on these aspects, the required position accuracies are 50 μm(RMS) for position detectors and 1 mm(RMS) for timing detectors.

We introduced a photogrammetry system VSTARS/E5[2)] produced by Geodetic Systems Inc. for surveying the positions of the detectors using financial support from the RIKEN common usage instrument budget in FY2010. In this system, many numbers of target markers are fixed and/or pasted on the instruments. These markers are taken in photos from various aspects. From the markers' 2-dimensional positions on the pictures, 3-dimensional positions of each marker are reconstructed according to the relative position relation among the markers. By combining the position data of each marker, we can determine the position of each instrument with a precision of 50 μm (RMS) in a 5 m cubic region, which is the specification value of the system. Presently, we have succeed in reproducing the positions of each position sensitive detector (or its container box) within a margin of 100 μm (RMS).

Figure 1 shows a birds-eye view of the reconstructed target marker positions. Several marker positions form each of the surface planes of the detectors or the detector boxes. From the measurement, each position detector (BDC1,2 and FDC1,2) is well reproduced in a 3–dimensional manner. Table 1 lists values of the reconstructed positions of upstream detectors of the SAMURAI magnet, as examples. Those positions were obtained from the SAMURAI commissioning experiment in March 2012, and from the SAMURAI day-one experiment in May 2012. Around 1.5 or 1.6 mm differences were found for the beam tracking detectors along the beam direction from the comparison of the measurements. We interpreted that the difference is caused by a continuous force exerted by vacuum at the region between BDC1 and the SAMURAI magnet through the reaction target within 2 months. In the same manner, FDC2, located downstream of the magnet, was position-reconstructed within a 100 μm accuracy for a precise momentum analysis.

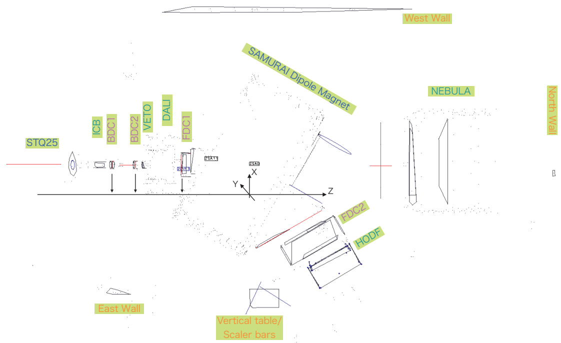

Fig. 1. Birds-eye view of reconstructed target marker positions and manually identified planes or lines that represent the real detector or magnet devices.

In the near future, we plan to employ the photogrammetry system at the other site of RIBF experimental instruments.

Table 1. Results of the position measurement as accurate positions and directions of BDC/FDC1

	[mm/mrad]	Comm. 2012/03	Day-one 2012/05	Diff.
BDC1	Z	−5950.94	−5949.40	−1.54
	X	−0.72	−0.74	0.02
	Y	−0.17	−0.17	0.00
	DX/DZ	0.32	0.74	−0.42
	DY/DZ	−0.43	−0.88	0.45
BDC2	Z	−4951.64	−4950.05	−1.59
	X	−0.23	−0.24	0.01
	Y	−0.88	−0.83	−0.05
	DX/DZ	1.09	1.10	−0.01
	DY/DZ	0.10	−0.29	0.39
FDC1	Z	−2889.08	−2888.85	−0.23
	X	−0.14	−0.02	0.12
	Y	–	0.05	–
	DX/DZ	–	−0.37	–
	DY/DZ	–	−0.38	–

References
1) Y. Shimizu et. al.: J. Phys.: Conf. Ser. 312, 052022 (2011).
2) URL: http://www.geodetic.com/products/systems/v-stars-e.aspx.

Current status of SAMURAI-TPC†

T. Murakami,[*1] R. Shane,[*2] A.B. McIntosh,[*3] W.G. Lynch,[*2] T. Isobe, J. Barney,[*2] Z. Chajecki,[*2] M. ElHoussieny,[*4] J. Estee,[*2] M. Famiano, G. Jhang, [*5] F. Lu,[*2] N. Nakatsuka, R. Olsen,[*2] W. Powell,[*6] H. Sakurai, A. Taketani, S. Tangwancharoen,[*2] M.B. Tsang,[*2] S.J. Yennello,[*3] and J. Yurkon,[*2]

Understanding the equation of state (EOS) for dense asymmetric neutron-rich matter has been identified as an important scientific objective in the Nuclear Science in the past decade. In order to extend constraints on the symmetric matter ($\rho_n \approx \rho_p$) EOS at supra-saturation densities, obtained from central nucleus-nucleus collisions, to the essential frontier of neutron-rich matter, a construction of SAMURAI-TPC for pion production and flow measurements at the RIBF was proposed to the U.S. DOE in the summer of 2008 as one of U.S.-Japan Collaborative Researches. Soon after an approval of the proposal in the fall of 2010 we started a R&D of the TPC based upon the design of EOS-TPC at LBL and now we are at a final stage of the construction. This report describes the current status of TPC construction.

The SAMURAI-TPC was designed to fit within the pole gap of the SAMURAI dipole magnet. In Fig. 1 an exploded view of the TPC is shown. The TPC consists of several main components, namely a front end electronics mounted on, a rigid top plate, a pad plane and three wire planes, a field cage, a voltage step-down, a thin-walled enclosure, a calibration laser optics, a target mechanism, rails, and so on. Details about a electronics for the SAMURAI-TPC including front end electronics are described in a separated report[1)].

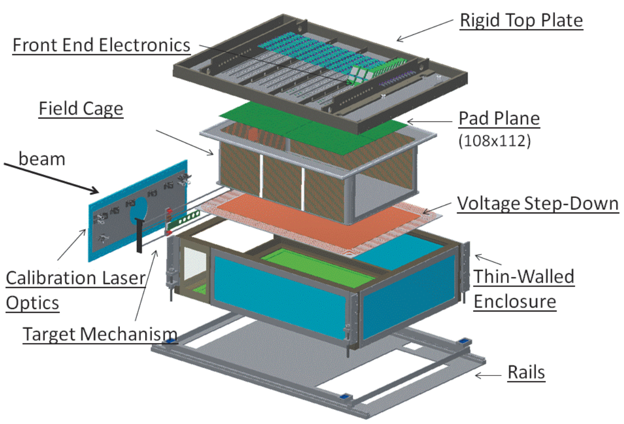

Fig. 1. Exploded view of SAMURAI-TPC.

† Supported in part by U.S. DOE
*1 Department of Physics, Kyoto University
*2 NSCL, Michigan State University, USA
*3 Cyclotron Institute, Texas A&M University, USA
*4 Department of Physics, Western University, USA
*5 Department of Physics, Korea University, Korea
*6 Physics Department, University of Liverpool, UK

The rigid top plate is a primary structural member of the TPC and reinforced with several ribs to hold a pad plane and three wire planes. Laser level measurements confirmed that the top plate was flat to within about 125 μm. The pad plane which consists of 108×112 pads of 12×8 mm^2 in size is mounted on bottom of the top plate. Each pad has capacitances of 12 pF to the ground and of 5 pF to adjacent pads. Cross talks between adjacent pads and non-adjacent pads are measured to be about 0.2% and less than 0.1%, respectively. Because of its large size the pad plane was fabricated in four pieces and glued to the top plane to form a single plane of 1.34×0.86 m^2 in size.

Wires for anode wire plane were wound on a frame in the detector lab of the NSCL/MSU and epoxied and soldered on a circuit board. Plans have been made to wind the ground plane and gating grid plane by the end of February. The field cage is mainly made of thin two layer PCB's so that reaction ejectiles could exit through it. Front window will be 12 μm PPTA and back window will be 125 μm Kapton, with evaporated aluminum electrodes. The cage is designed to be gas tight for separating detection gas volume from insulation gas outside the field cage.

In order to prevent sparking from cathode (20 kV) to ground the voltage step-down is situated about 6 mm below the cathode and glued to the bottom plate of the enclosure. The voltage step-down has 8 concentric copper rings which step the voltage down from cathode HV to ground. The thin-walled enclosure has a skeleton-structure of aluminum angle bars welded and polished for sealing. Its sides and down stream walls are made of framed aluminum sheet to minimize neutron scattering. The upstream plate will be modified to couple to the up stream beam-line. A motion chassis and hoist beams can be attached to the enclosure for lifting and/or rotating the entire TPC safely. We still need to work on the calibration laser optics, the target mechanism, and the rails, but those should be ready by the end of 2013. We plan to ship the TPC from MSU to RIBF in December of 2013.

References

1) T. Isobe et al.: RIKEN Accel. Prog. Rep. 46, in this report (2013).

Development of readout electronics for SAMURAI-TPC project

T. Isobe, H. Baba, N. Nakatsuka, T. Murakami,[*1] A. Taketani, W.G. Lynch,[*2] and E. Pollacco,[*3] for the SAMURAI-TPC Collaboration

Investigation of heavy-ion collision is one of the methods that can be used to study nuclear EoS. For performing a heavy-ion collision experiment at the Radioactive Ion Beam Facility (RIBF), a time projection chamber (TPC) will be installed in the SAMURAI superconducting dipole magnet. As the readout electronics for more than 12k channels in TPC, a novel readout system, GET[1)], is planned to be employed. GET stands for General Electronics for TPC, and has been developed mainly by France and USA collaboration. As shown in Figure 1, our GET system consists of ZAP, AsAd, CoBo, MUTANT and DAQ. The functionality of each component is summarized in Table 1. Although most components are provided by GET collaboration, each experimental group has to finalize their own system by developing some original components specialized for their experiment. In our case,we have developed the ZAP board, the updated DAQ, and an online software.

One of the main features of the SAMURAI-TPC readout system is the size of acquired data.

In spite of the data reduction and the limitation of the trigger rate, enormous amounts of data will be taken from the experiments using SAMURAI TPC because of the large number of readout channels. According to the simulation study, the most efficient way for the reduction is zero suppression, which will reduce the size by upto 90%. Drift time of an electron will limit the trigger to a rate between 200 and 500 Hz. In that case, the output data throughput is estimated to be 80∼300 MByte/sec, which corresponds to 100∼300 TByte per week. To handle such large amounts of data, the use of the RIKEN Integrated Computing Cluster (RICC) is considered for the data analysis.

The entire setup of the GET system for SAMURAI-TPC is supposed to be ready before the end of 2013. The SAMURAI-TPC is being constructed in the US and will be delivered to RIKEN at the end of 2013. The bunch of electronic boards will be mounted on the TPC and will be tested with cosmic rays. After that, the TPC will be mounted in SAMURAI magnet for the first experiment.

Table 1. Components of SAMURAI-TPC-GET readout system

TPC	Main detector. 108×112=12096 channels
ZAP	Adapter board to AsAd with protection from large signal. 1 ZAP for 1 AsAd.
AsAd	ASIC and ADC board. 4 AGET ASIC chips, FPGA and 4 ADCs (ADS6422) on 1 AsAd board. 64 channel readout with 1 ASIC (63 ch per AGET in our case). 512 samples at most. 1∼100 MHz sampling rate. Programmable gain. 192 AGET, 48 AsAd boards.
CoBo	Concentration board. DDRAM for event buffering. 4 AsAd per CoBo. Up to 10 CoBo can be mounted on 1 μ-TCA crate.
MUTANT	Trigger and time stamping module. 1 module per μ-TCA crate.
DAQ	Event building servers and computing farm for online/offline analysis.

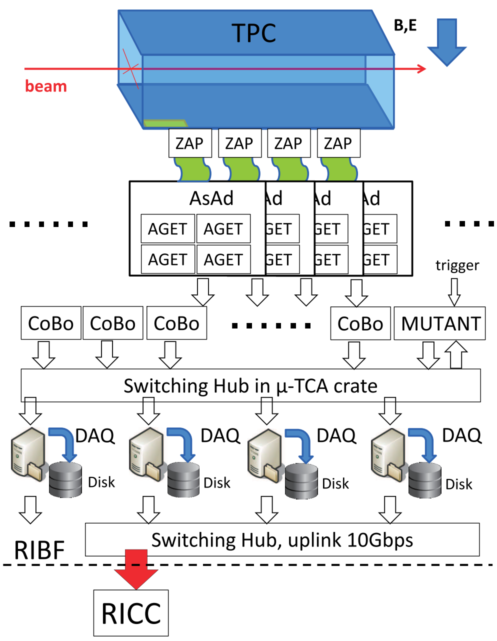

Fig. 1. Overview of readout system for SAMURAI-TPC

*1 Department of Physics, Kyoto University
*2 National Superconducting Cyclotron Laboratory, Michigan State University, United States
*3 CEA Saclay IRFU/SPhN, France

References

1) E. Pollacco et al.: Physics Procedia **37**, 1799 (2012).

Development of timing monitoring system for time projection chamber readout

K.Urano, A.Taketani, H.Baba, T.Murakami,[*1] T.Isobe, and K.Kurita[*2]

Construction of a large time projection chamber (TPC) is planned for experiments in order to study the equation of state (EOS) of nuclear matter. In order to determine the symmetry energy term of the EOS,[1)] it is necessary to measure multi particles and their momentum vectors simultaneously in the final state of heavy ion collisions over a large phase space.[2)] The TPC is a major part of the detector that is installed in the SAMURAI magnet gap.

The general electronics for the TPC (GET) is currently being developed[3)] by a collaboration among French, American, and Japanese institutions. The GET includes front-end preamplifiers, analog pipeline buffers, flash ADCs, trigger logics, a digital readout, a timing synchronization system, and a data acquisition system. In the GET system, 256 channels of preamplifiers, pipeline buffers, and flash ADCs are packed into one printed circuit board called AsAd. The timing signal sent from a master timing module tends to fluctuate on each AsAd board upon FPGA reprogramming. Up to 128 AsAd boards form a single GET system and they must be synchronized accurately to run with an approximately 100-MHz sampling clock. A timing monitoring system, called SPYBOX, plays an important role for this purpose. The SPYBOX is required to have:

(1) 128 input channels with LVDS signals from FireWire connectors.[4)]
(2) Capability to compare the timing difference between any two inputs.
(3) A timing resolution of less than 1 ns (FWHM).

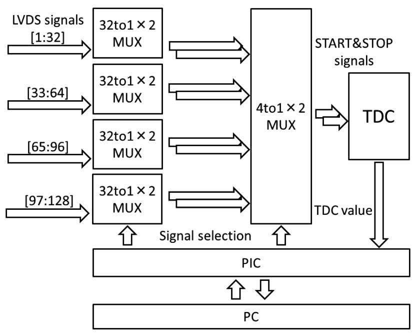

Fig. 1. Block diagram of the SPYBOX

Figure 1 shows the configuration of the SPYBOX. When the FireWire communication protocol is not employed, each AsAd board sends its reference timing signal to the SPYBOX through FireWire connections. Each timing signal is received by the LVDS receiver with a proper termination in order to isolate the AsAd circuits from the multiplexer circuits in the SPYBOX. The LVDS signals are fed into the multiplexers, and two signals are selected and transferred to a time-to-digital converter (TDC) that measures the time difference between the two signals. A CPU module controls the multiplexers and reads the data from the TDC. The CPU module also communicates with the rest of the PC.

We used Spartan3AN FPGAs as multiplexers and a converter. It supports 50 LVDS inputs. Four FPGAs were programmed to work as 32-to-1 $\times$ 2 MUX, and 2 signals were selected in each FPGA. Thus, total of 8 LVDS signals were chosen. They were fed to another FPGA and were further selected to be the start and the stop signals for the TPC. The last FPGA also worked as a LVTTL level adapter. The start and stop signals were fed to the ACAM TDC-GP21 through a coaxial cable. It had a timing resolution of 22 ps. For the CPU module, PIC18F4550 from Microchip Technology Inc. was used.

We checked the time differences among channels using the SPYBOX. The timing differences ranged over 1.5 ns before adjustments. Therefore we used buffer delays and look-up tables inside the FPGA chips to minimize the difference. Figure 2 shows the time difference among the signals after adjustments. The standard deviation was less than 0.12 ns. It found we can keep monitoring AsAd boards synchoronization upon FPGA reprogramming with a 100-MHz clock.

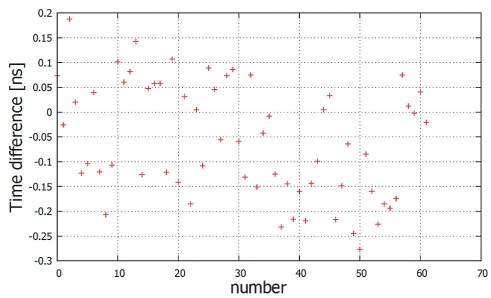

Fig. 2. Time difference of the signals passing through the FPGA

*1 Department of Physics, Kyoto University
*2 Department of Physics, Rikkyo University

References
1) L. W. Chen et al.: Phys. Rev. Lett. 94, 032701 (2005).
2) T. Isobe. RIKEN Accel. Prog.Rep. 45, 132 (2012).
3) http://www-actar-get.cea.fr
4) http://www.1394ta.org

Development of an Amplifier IC with Wide Dynamic Range for Si Detector in RIBF SAMURAI Spectrometer

A. Takuma, K. Kurita*[1], H. Murakami, A. Taketani, M. Kurokawa, M. Tanaka

A large acceptance and high magnetic rigidity spectrometer facility, SAMURAI,[1,2] is under construction at RIKEN. We plan to perform breakup reaction experiments that focus on the structure of proton rich nuclei. The Si tracker is required to have an amplifier with a wide dynamic range of more than 2500.

A dual gain amplifier that satisfies the requirement for a wide dynamic range has already been developed.[3] However, it requires twice as many channels for the readout electronics. To avoid this drawback, we proposed an integrated circuit(IC) amplifier, having an output (V_{out}) that is proportional to the square root of the input (V_{in}). We term it the square root amplifier. The square root gain response of this amplifier is the most suitable to equalize the Z resolution because the corresponding energy loss is proportional to Z^2.

Figure 1 shows the schematic diagram of the square root amplifier. An essential part of the square root amplifier is a variable gain amplifier. The inverter inverts the signal polarity, and the analog adder is used for DC offset corrections.

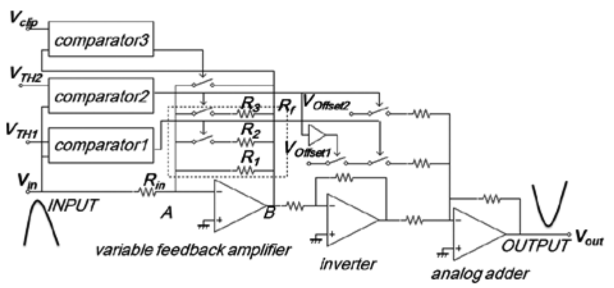

Fig.1. Diagram of square root amplifier

The behavior of this amplifier is described by the following three regions.

Region 1: ($0<V_{in}<V_{TH1}$) When the applied input voltage is less than the turn-on voltage of comparator1, the amplifier behaves as a high-resistance device. Thus, $R_f = R_1$ because R_2 and R_3 are disconnected.

Region 2: ($V_{TH1}<V_{in}<V_{TH2}$) When the applied forward voltage is more than the turn-on voltage of comparator1, the amplifier behaves as a lower-resistance device. In region 2, $R_f = R_1||R_2$ because only R_3 is disconnected. The symbol "||" indicates a combined resistance of the two resistors connected in parallel.

Region 3 : ($V_{TH2}< V_{in}$) In region 3, $R_f = R_1||R_2||R_3$, because both R_1 and R_2 are connected in parallel.

*1 Department of Physics, Rikkyo University

We resolved V_{out} discontinuity problem at the comparator transitions by inserting an inverter and an adder to correct the voltage gap. $V_{Offset1}$ and $V_{Offset2}$ are defined as the voltage values applied when the input voltage passes V_{TH1} and V_{TH2}, respectively. When the input signal is negative, V_{clip} clipping is effective in suppressing oscillation by lowering the gain.

We fabricated an application specific IC (ASIC) chip for the square root amplifier with TSMC 0.5μm technology and compared the measurements with the design values. The ideal values were calculated by the equation (1) below. Equations (2)-(4) describe the voltage relations.

$$V_{out} = -1.5\sqrt{V_{in}} \tag{1}$$

The design values were as follows.

Region 1 : ($0<V_{AB}<V_{TH1}$) $V_{out} = -6.3V_{in}$ (2)
Region 2 : ($V_{TH1}<V_{AB}<V_{TH2}$) $V_{out} = -1.2V_{in} + V_{Offset1}$ (3)
Region 3 : ($V_{TH2}< V_{AB}<2.5$) $V_{out} = -0.54V_{in} + V_{Offset2}$ (4)

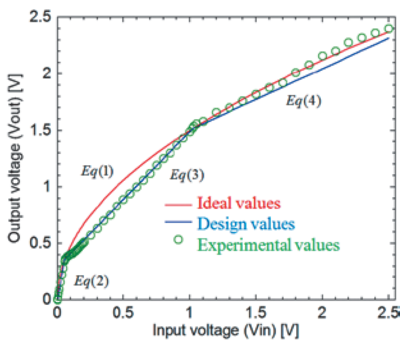

Fig.2. Comparison of ideal, design, and experimental values for input pulse

Figure 2 shows that the data taken are consistent with the design values and demonstrate that the fabricated ASIC has the suitable performance. We also confirmed that the output voltage signal, which corresponds to the input voltage of 0.25 mV, is distinguishable from the noise level. The dynamic range obtained was 10000.

In conclusion, we have developed a square root amplifier and achieved a dynamic range of ~10000. The achieved dynamic range exceeded our experimental requirement of 2500 for the SAMURAI Si tracker.

References

1) K. Yoneda et al.: RIKEN Acc. Prog. Rep. 43, 178 (2010).
2) Y. Togano et al.: RIKEN Acc. Prog. Rep. 44, 146 (2011).
3) M. Kurokawa et al.: RIKEN Acc. Prog. Rep. 43,182 (2010).

Present status of STQ system in BigRIPS and RI-beam delivery line

K. Kusaka, M. Ohtake, T. Kubo, K. Yoshida, Y. Yanagisawa, Y. Mori,[*1] M. Ohshima,[*1] T. Suzuki,[*1] K. Yamamoto,[*1] S. Watanabe,[*1] Y. Tezuka,[*1] A. Mikami,[*1] H. Hazama,[*1] H. Shiba,[*1] H. Ito,[*2] and T. Tsuchihashi[*2]

The BigRIPS in-flight separator and RI beam delivery line are characterized by superconducting triplet quadrupoles (STQs) with cryocoolers. Since the STQ with cryocoolers is a "stand-alone" superconducting magnet with a large cold mass but subject to small heat loads, [1] we adopt a unique thermal cycle operation in which we operate the cryocoolers continuously and never warm up the magnets[2].

Two cryocoolers maintain the liquid helium levels in the STQ cryostat. One is a Gifford–McMahon (GM) cooler that uses Joule–Thomson expansion (GM/JT) to cool the He vessel. The GM/JT cooler consists of two independent coolant helium circuits, designated as the expander- and JT-circuits. The expander-circuit is a two-stage GM cooler and it serves as a pre-cooler for the JT-circuit. The JT-circuit liquefies helium gas in the He vessel with the recondensing heat exchanger unit whose temperature can be tuned to around 4.3 K by controlling the JT-valve. The other is a GM cooler, which cools the shield surrounding the He vessel and power leads.

Most of the cryocoolers have been continuously operated since 2006, and the operation time of the cryocoolers is more than 65,000 h for STQ6-STQ15, and 55,000 h for STQ16-STQ23. The scheduled maintenance of the cryocoolers are performed yearly, and all the displacers of the GM/JT and GM coolers are replaced every 8,000 to 9,000 h of operation time, since the regenerator material in the displacer deteriorates in its performance with time. The degradation of the cooling capacity of the GM cooler appears as an increase in the GM head temperature. An example of the long-term trend of the GM head temperature is presented in prerevious studies. [3,4]

On the other hand, the pressure of the He vessel of the STQ is a good measure of the sound operation of the GM/JT cooler. Since the cooling capacity of the GM/JT cooler is 2.5 W and the total 4-K heat load of the cryostat is less than 2 W, we usually maintain the pressure of the He vessel in the range from 7 to 9 kPaG with on/off control of the 2-W heater power output. If the cooling capacity of the GM/JT cooler degrades, the He vessel pressure does not decrease to 7 kPaG and the heater does not turn on at first, and eventually the He vessel pressure begins to increase. If the pressure exceeds 20 kPaG, which is the cracking pressure of the safety check valve, the liquid He level starts decreasing.

We observe the temperature of the GM head and the pressure of the He vessel of all the STQs daily. We maintain the He vessel pressure in the designed range by controlling the JT-valve of the GM/JT cooler in order to excite the magnets safely in the beam-time periods.

Table 1. List of problematic GM/JT coolers.

	Date of Operation Stop	Total Operation Time	Time from Last Maintenance
STQ6	Apr 2	55,088 h	5,177 h
STQ8	Apr 9	52,958 h	5,377 h
STQ12	May 25	62,887 h	6,114 h
STQ13	Apr 13	61,213 h	4,940 h
STQ14	Apr 25	5,3776 h	5,680 h
STQ17	Jun 4	4,7913 h	6,722 h

Table 2. List of problematic GM coolers.

	Date of Operation Stop	Total Operation Time	Time from Last Maintenance
STQ6	Jan 26	55,917 h	3,567 h
STQ8	Apr 26	52,470 h	5,660 h
STQ14	May 25	62,887 h	6,114 h
STQ18	Feb 20	46,896 h	3,839 h
STQ22	July 7	52,272 h	5,680 h
STQ23	July 26	50,373 h	6,722 h

However, an unexpected rapid increase in the He vessel pressure of the STQs occurred many times from April to June in 2012. We were forced to stop beam time to replace the GM/JT coolers. The problematic STQs and the operation time of their GM/JT coolers are listed in Table 1. The degradation of cooling capacity of the GM/JT cooler was caused by the abnormal temperature (~15 K) of the second stage of the expander-circuit; this temperature should be normally below 14 K. After the replacement of the displacer, the expander head temperature reduced below 14 K, and the cooling capacity was recovered for all the problematic GM/JT coolers. In addition to the issues concerning the GM/JT coolers, rapid temperature increases in the head of the GM cooler and the power leads also occurred many times in 2012. We were forced to perform unscheduled maintenances wherein we replaced the displacer of the GM cooler with cryocooler maintainers on sites. Table 2 lists the problematic STQs and the operation time of their GM coolers.

We have thus far not been able to determine the reason for the degradation of the cooling capacity. The unexpected temperature rises of the GM head and the expander of the GM/JT cooler are still under investigation.

References

1) K. Kusaka et al.: IEEE Transactions on Appl. Supercond. 14, 310 (2004).
2) K. Kusaka et al.: RIKEN Accel. Prog. Rep. 41, 246 (2008).
3) K. Kusaka et al.: RIKEN Accel. Prog. Rep. 45, 235 (2012).
4) K. Kusaka et al.: IEEE Transactions on Appl. Supercond. 23, 4101305 (2013).

*1 Nippon Kucho Service Co., Ltd.
*2 Toshiba Corporation

Development of new ion-optics modes with high resolution at the second stage of BigRIPS separator

H. Suzuki, T. Kubo, N. Inabe, N. Fukuda, Y. Shimizu, H. Takeda, D. Kameda, H. Sato

We have developed new ion-optics modes with high $B\rho$ resolution at the second stage of the BigRIPS separator[1,2]. The resolutions of these new modes are calculated to be around 6600, which are double that of the original "standard mode" optics. The resolution of the standard mode is sufficient for the mass-to-charge ratio (A/Q) separation of the mid-heavy isotope beams produced at the BigRIPS separator. The new optics modes were developed for experiments such as mass measurements that require a greater resolution.

Two new ion-optics modes with high resolution ("high-resolution M-half mode" and "high-resolution D-double mode") were obtained by doubling the ratio of the dispersion to the magnification (D/M) from the focal planes F3 to F5 of the standard mode. The transfer matrix elements of each optics mode from F3 to F5 are summarized in Table 1. For the all optics modes, F3 and F5 are the achromatic and dispersive focal planes, respectively. The optical settings from F7 to F5 are mirror symmetries of those from F3 to F5, and thus, F7 is set as the achromatic focal plane.

The beam trajectories of the high-resolution modes are shown in Fig. 1 along with that of the standard mode. In the first mode, the high-resolution M-half mode, the magnification is half that of the standard mode (0.46), while the dispersion remains unchanged (31.7 mm/%). An advantage here is that the original F5 degraders can still be used because the wedge-anglesof the degraders depends on the dispersion value. In the other mode, the high-resolution D-double mode, the dispersion is double that of the standard mode (63.4 mm/%), while the magnification remains unchanged (0.92). In this case, the focus tuning is relatively easy because the magnification is not as small as that for the high-resolution M-half mode. For both modes, the angular and momentum acceptances are reduced from the standard mode because the beam envelopes are expanded.

In December 2012, we tested these high-resolution modes at the BigRIPS separator. The results are described in Ref.[3].

Table 1. Transfer matrix elements of high-resolution M-half mode (top row), high-resolution D-double mode (middle row), and standard mode (bottom row) from F3 to F5.

Optics mode	$(x\|x)$	$(a\|a)$	$(x\|\delta)$ [mm/%]
M-half	0.46	2.17	31.7
D-double	0.92	1.09	63.4
standard	0.92	1.09	31.7

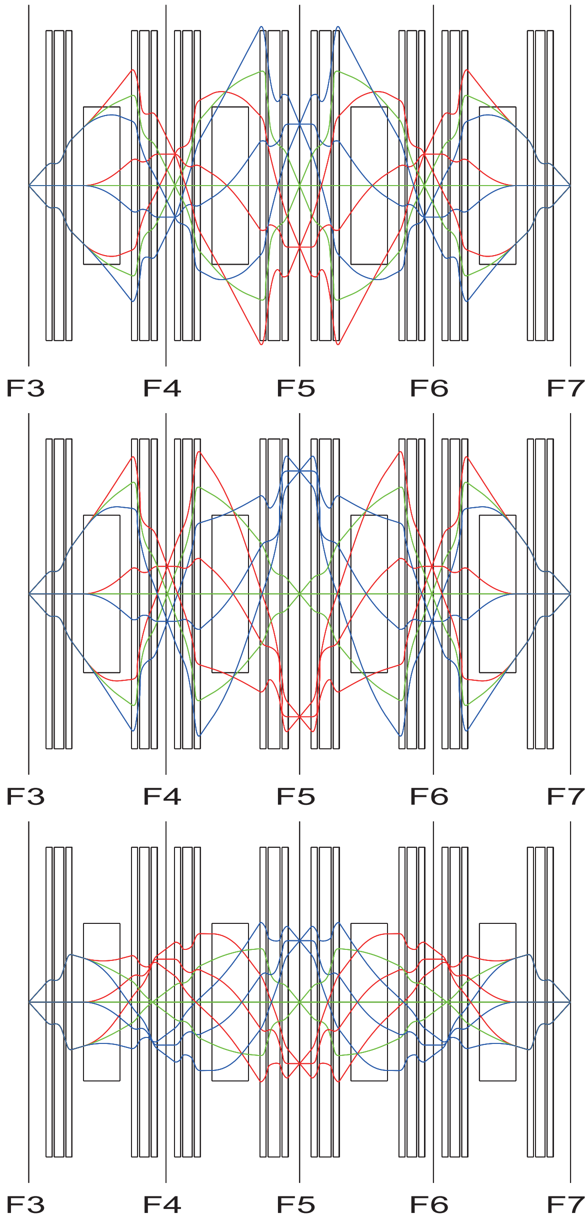

Fig. 1. Horizontal beam trajectories of high-resolution M-half mode (top panel), high-resolution D-double mode (middle panel), and standard mode (bottom panel) from F3 to F7. The horizontal angular spreads of ± 10 mrad at F3 and the momentum spreads of $\pm 1.5\%$ are shown.

References
1) T. Kubo: Nucl. Instr. and Meth. **B 204**, 97 (2003).
2) T. Kubo et al.: IEEE trans. Appl. Supercond. **17**, 1069 (2007).
3) N. Fukuda et al.: RIKEN Accel. Prog. Rep. **46**, (2012).

New high-resolution ion-optics modes at the second stage of BigRIPS separator

N. Fukuda, T. Kubo, N. Inabe, H. Suzuki, Y. Shimizu, H. Takeda, D. Kameda, and H. Sato

Two ion-optics modes[1)] were examined at the second stage of the BigRIPS separator[2,3)] to achieve higher $B\rho$ resolution compared to the standard mode. The first mode, which we call "high-resolution M-half mode", has half the magnification (M = 0.46) of the standard mode and leaves the dispersion unchanged (D = 31.7 mm/%). The second one, which we call "high-resolution D-double mode", has twice the dispersion (D = 63.4 mm/%) of the standard mode and the same magnification (M = 0.92). Both modes have been designed to have a resolution twice as high (~6600) as the BigRIPS standard mode by doubling the ratio of the dispersion to the magnification (D/M) from the achromatic focus F3 to the momentum-dispersive focus F5. The system from F7 to F5 is designed as a mirror-symmetric one, and thus, F7 is an achromatic focus.

The performance of new ion-optics modes were evaluated by using the fission fragments with Z ~ 50 produced in the ^{238}U + Be reaction at 345 MeV/nucleon. The first-stage settings of the BigRIPS were exactly the same for the three modes of the second stage, which allow us to directly compare the acceptances among the different modes. The tuning of ion optics, such as focusing and achromaticity, was performed prior to the main measurements.

The ion-optical matrix elements, $(x|x)$, $(x|a)$, $(a|x)$, and $(a|a)$, from F3 to F5 have been extracted from the position-position, position-angle, and angle-angle correlations of the ions between F3 and F5. The element $(x|\delta)$ has been obtained from the correlation between the position of F5 and the time of flight between F3 and F7 for the selected isotope, where δ is the relative $B\rho$ deviation. The matrix elements thus obtained experimentally are summarized in Table 1, along with the designed values[1)]. $B\rho$ was determined by trajectory reconstruction with the measured first-order matrix.

The A/Q spectra for Sn isotopes obtained for the three settings are shown in Fig. 1. The range of δ used in the analysis is set to be $|\delta| < 1\%$, which is supposed to be valid for the use of the first-order matrix. We also put a gate on the pulse heights of the plastic scintillators (timing counter) to achieve better timing resolution with minimum correction for the slewing effect. The improvement in A/Q resolution is confirmed for the D-double mode (0.028%) as expected, whereas the resolution for the M-half mode (0.035%) is comparable with that of the standard mode (0.035%). In order to properly evaluate the $B\rho$ resolution, we need to obtain the intrinsic resolutions of the detectors. A detailed analysis is currently in progress.

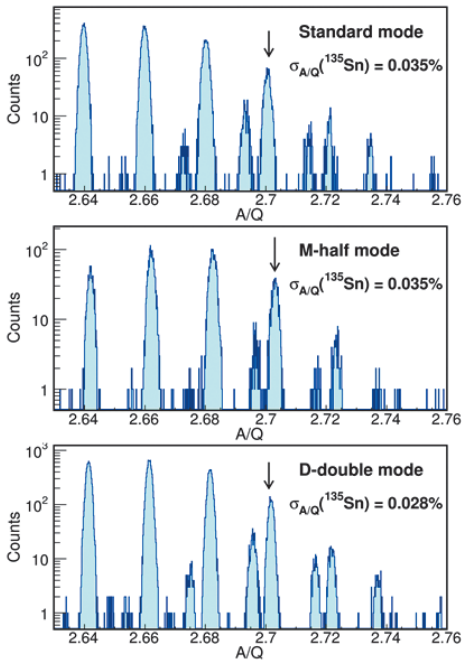

Fig. 1. A/Q spectra of Sn isotopes obtained with the standard mode (up), the high-resolution M-half mode (middle), and the high-resolution D-double mode (down). The A/Q resolution for $^{135}Sn^{50+}$ is shown for each mode.

References
1) H. Suzuki et al.: RIKEN Accel. Prog. Rep. **46,** (2012).
2) T. Kubo: Nucl. Instr. and Meth. **B 204**, 97 (2003).
3) T. Kubo et al.: Prog. Theor. Exp. Phys. **2012**, 03C003 (2012).

Table 1. Transfer matrix elements from F3 to F5 deduced for the high-resolution M-half mode, the high-resolution D-double mode, and the standard mode. The designed values[1)] are also shown.

Elements	M-half		D-double		Standard	
	Exp.	Design	Exp.	Design	Exp.	Design
$(x\|x)$	0.499±0.018	0.46	1.14±0.04	0.92	0.886±0.015	0.92
$(a\|a)$	2.38±0.02	2.17	1.10±0.01	1.09	1.13±0.01	1.09
$(x\|\delta)$ (mm/%)	31.8±0.1	31.7	60.2±0.1	63.4	30.8±0.1	31.7

Benchmark experiment for residual radioactivity for ^{124}Xe and ^{238}U beam irradiation on BigRIPS

K. Tanaka, N. Inabe, K. Yoshida, and T. Kubo

In the RIBF facility, intense heavy ion beams are irradiated on the target and beam dump of BigRIPS. To plan maintenance and improvement tasks in the high radiation environment, the estimation of long-term residual radioactivity is important. Particle and Heavy Ion Transport code System (PHITS)[1], which allows Monte-Carlo calculations, is useful for evaluating the future radioactivity at BigRIPS. In this study, benchmarks for the PHITS calculations are obtained for precise evaluation. The activation samples were irradiated using ^{124}Xe and ^{238}U beams, and their residual radioactivities were measured. The results were compared with those calculated by PHITS.

Figure 1 shows the experimental setup around the beam dump. The samples were located downstream of the beam dump. The primary ^{124}Xe and ^{238}U beams of 345 MeV/nucleon were injected into the copper beam dump. The primary beam and most of the charged particles generated by the nuclear reaction at the beam dump were stopped in the beam dump. Thus, the particles that irradiated and activated the samples were mainly secondary neutrons. The experimental method was the same as that in a previous study using a ^{48}Ca beam and details of the method are reported in that study[2]. The elements of the samples are Fe, Cu, Al, Ni, and Cr, which are widely used in the vacuum chambers, magnets, and other components of BigRIPS. The irradiation dose at the beam dump was 3.2×10^{13} (1.5pnA, 1h) for ^{238}U ions and 1.8×10^{14} (8pnA, 1h) for ^{124}Xe ions.

The γ-ray spectra from the activated samples were measured using a Ge detector. Figure 2 shows the preliminary results as the production ratios of the radioactive nuclei obtained by PHITS calculations to those obtained by measurements. Since the long-term radioactivity is the focus of this study, only the results of major long-lived radioactive nuclides are shown. To eliminate short-lived radioactivity, the cooling time for the measurement was between 120 and 140 days. Figure 2 shows the result of ^{48}Ca beam irradiation[2] for comparison purposes. In general, the results of PHITS calculation for ^{124}Xe and ^{238}U are in good agreement with the measurement. However, the calculated results for ^{48}Ca are 2 to 3 times higher than the measurements.

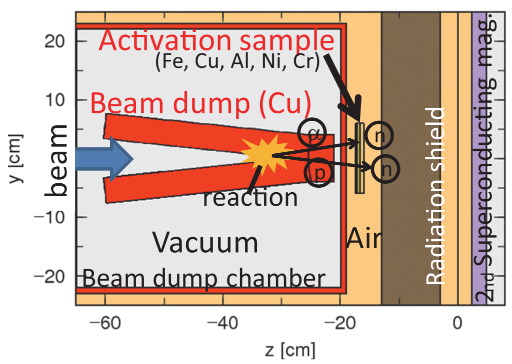

Fig. 1. Side cross-sectional view of the experimental setup. Detailed setup are shown in the previous study[2].

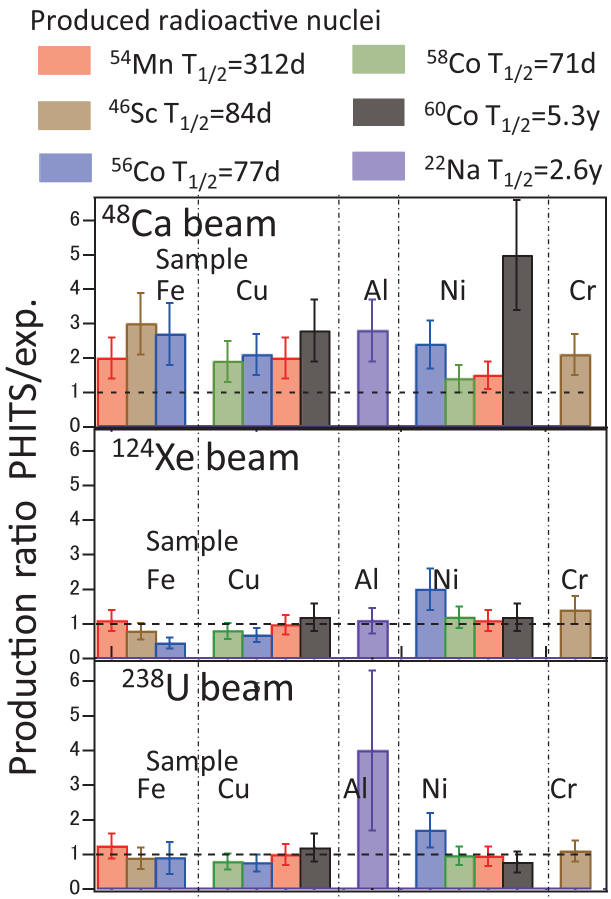

Fig. 2. Production ratios of radioactive nuclei in the samples (preliminary). Only long-lived nuclides are shown.

References
1) K. Niita, N. Matsuda, Y. Iwamoto, H. Iwase, T. Sato, H. Nakashima, Y. Sakamoto, and L. Sihver: JAEA-Data/Code **2010-022**, (2010).
2) K. Tanaka , N. Inabe, T. Ohnishi, and T. Kubo: Prog. Nucl. Sci. Technol. **2** (2011), p. 955.

Acceptance measurement of BigRIPS for spectroscopy of deeply bound pionic state in ^{121}Sn

Y.N. Watanabe, M. Dozono, H. Fujioka, N. Fukuda, T. Furuno, H. Geissel, R.S. Hayano, N. Inabe, K. Itahashi, T. Kubo, Y. Murakami, N. Nakatsuka, T. Nishi, K. Okochi, H. Suzuki, M. Takaki, H. Takeda, Y.K. Tanaka, H. Weick, H. Yamada, K. Yoshida

We report herein on the measurement and analysis of the acceptance of the BigRIPS when used as a high-resolution spectrometer. The momentum acceptance was measured in two different methods, and the consistency was confirmed. The angular acceptance was also measured near the central momentum value.

We have developed a new beam optics for the primary beamline and the BigRIPS to achieve the highest possible resolution by achieving a dispersion matching beam optics with the primary beam.[1] The newly developed beam optics is dedicated for use in our high-resolution measurement of deeply bound pionic atoms in the (d,^{3}He) reaction near the pion emission threshold.

The acceptance was used to obtain the excitation spectra in our experiment for the pionic atoms in the ^{122}Sn(d,^{3}He) reaction. We placed a strip of ^{122}Sn at the nominal target position of the BigRIPS and a set of multiwire drift chambers (MWDC) at the F5 dispersive focal plane to measure the ^{3}He tracks. We have successfully observed the deeply bound pionic states in ^{121}Sn and the angular dependence of the cross section, for the first time.[2]

We have considered two different methods for the estimation of the spectrometer acceptance near the forward zero degree. One is based on an assumption that the momentum acceptance has left-right symmetry referring to the beam axis of the BigRIPS. In the abovemensioned measurement of ^{122}Sn(d,^{3}He), we observed pionic atom formation spectra only in the lower energy side (left side) of the spectra and a structureless continuum at the higher energy side (right side) of the spectrum. The continuum is due to the nuclear excitation without pion production. Thus, we can deduce the acceptance for the entire region of interest by obtaining the reflection of the observed continuum with reference to the beam axis. The left panel of Fig. 1 shows the uncorrected spectrum for the reaction angle of $<1°$ with the acceptance obtained by the abovemensioned procedure and indicated by the red curve.

Another method is the direct observation of the momentum acceptance using a very wide momentum distribution of a mixture of fragments (mainly ^{12}N, ^{8}B, ^{10}C, and ^{14}O) produced in the reactions of the ^{18}O beam with the energy of 260 MeV/u on a ^{9}Be target with a thickness of 740 mg/cm^2. We measured the fragment momentum distributions at the focal planes from F1 to F5. Since the acceptance at F5 is much smaller than that at F1, we can conclude that the acceptance at F5 can be determined by measuring the transmission from F1 to F5. Thus by comparing the measured position spectrum at F1 and F5, the acceptance at F5 can be obtained. The measured acceptance and typical statistical errors are also indicated in the left panel of Fig. 1 by the blue line and the blue error bars. As seen, the F5 momentum acceptance is nearly flat within our ROI [-50 mm, 50 mm].

These results are consistent near the forward zero degree and we plan to apply the same methods to different angles (1°∼2°,2°∼3°).

In addition to the momentum acceptance of the spectrometer for different angles, we considered the angular acceptance near the central momentum value. The deduction is based on the p(d,^{3}He)π^0 reaction, which was measured for energy calibration. The angular differential cross section of this reaction is already known.[3] The right panel of Fig. 1 shows the angular dependence of the ratio of the measured ^{3}He at F5 and the calculated ^{3}He production. The fitted line is normalized to unity for the forward 0° direction. This line corresponds to the angular acceptance of our new optics.

We have deduced the momentum acceptance and angular acceptance of the BigRIPS used as a high-resolution spectrometer. The obtained acceptance will be used both in the analysis of the previous experiment and in future experiments.

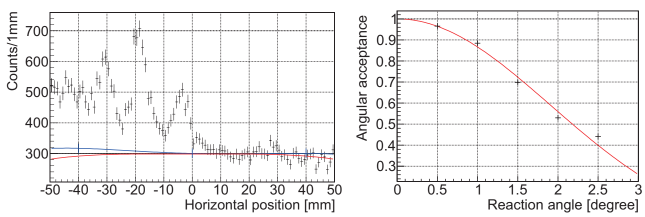

Fig. 1. (Left) ^{3}He horizontal position spectrum measured at F5 for the reaction angles $<1°$. The red curve represents the deduced acceptance by fitting the right-side region. The blue curve similarly represents the acceptance achieved from the comparison of the position spectrum at F5 with that at F1. (Right) Measured angular acceptance and fitted curve.

References
1) S. Itoh *et al.*: Accel. Prog. Rep. **44**, 221 (2011).
2) T. Nishi *et al.*: Accel. Prog. Rep. **45**, iv (2012).
3) M. Betigeri *et al.*: Nucl. Phys. A **690**, 473 (2001).

Energy resolution of ionization chamber for 345 MeV/nucleon heavy ions

Y. Sato, N. Inabe, D. Kameda, T. Kubo, Y. Shimizu, H. Suzuki, H. Takeda,
A.Taketani, D. Nishimura, N. Fukuda, M. Fukuda, H. Murakami, and K. Yoshida

Ionization chambers are used for the operation of the BigRIPS spectrometer and ZeroDegree spectrometer to identify the atomic number of particles in flight by measuring their energy deposition[1-3]. The configuration, manipulation, and performance of the ionization chambers have previously been reported[4,5]. However, the details of the relationship between the energy resolution for heavy ions and their atomic numbers are still unclear. Here, we report on the study of the energy deposition in the ionization chamber (effective gas length of 48 cm) installed at the F11 focal plane of the ZeroDegree spectrometer. The measured energy resolutions were compared with calculated values.

The energy depositions ΔE and their distributions Ω^2 by the heavy ions were measured via the new isotope search experiment conducted in 2008[6]. The energy resolution, $\Omega/\Delta E$, for fragments from the 345-MeV/nucleon-^{238}U improved with the atomic number Z of the fragments. This can be seen in Fig. 1 (plots); the A/Q values of fragments in the G1 (circles, Z: 21-39) and G2 (squares, Z: 36-51) settings in a previous study were 2.665 [6].

Simply stated, the energy resolution of the ΔE detectors is given by the average energy loss and fluctuation of the energy loss. The average energy loss ΔE of ions with charge Ze passing through a small thickness Δx with an electron density n_e can be expressed as[7,8]

$$\Delta E = \Delta x \left(\frac{4\pi Z^2 e^4}{m_0 V^2}\right) n_e \left\{\ln\left(\frac{E_M}{I}\right) - \beta^2 + \Delta L_{LS}\right\}. \quad (1)$$

Here, m_0 denotes the electron rest mass, V denotes the velocity of ions, $\beta = V/c$, and I denotes the mean ionization potential of the target electrons. The term E_M represents the maximum energy transferable to the target electrons. The parameter ΔL_{LS} denotes the correction term calculated by Lindhard and Sørensen[7]. It incorporates the Mott correction, the Bloch correction, and the nuclear size effect. The term for density effect correction is negligible.

In addition, the fluctuation of the energy loss Ω^2 due to electron collisions is given by

$$\Omega^2 = \Delta x \frac{2\pi Z^2 e^4}{m_0 V^2} n_e E_M X, \quad (2)$$

where the parameter X is calculated in LS theory[7].

However, in the gas ionization chamber, some generated δ-rays have a range exceeding the dimensions of the cavity. Therefore, in such a case, the energy deposition will be less than the energy loss, and the observed fluctuation of the energy deposition will differ from the energy straggling function of ions. This effect can be considered by using the truncated Bethe–Bohr model[8]. In this model, we define the cut-off energy of δ-rays E_d, and we assume that δ-rays ($E > E_d$) do not contribute to the energy deposition and its fluctuation. For a more exact calculation, we added the correction parameters, ΔL_{LS} and X, to this model. The mean energy deposition and its fluctuation are given by

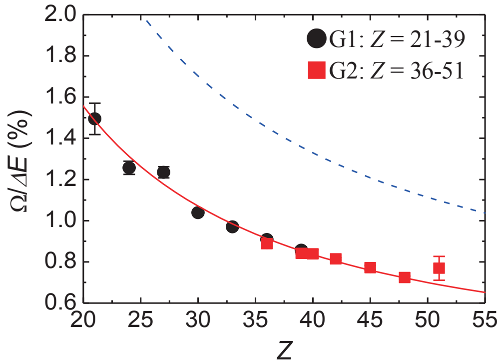

Fig. 1. Energy resolution vs. atomic number Z obtained for fragments of ^{238}U at 345 MeV/nucleon. The solid line indicates the result of fitting with $\Omega_{BB}/\Delta E_{BB}$ using the fitting parameter E_d. The calculation without considering the effect of δ-rays escaping, $\Omega/\Delta E$, is shown as a dashed line.

$$\Delta E_{BB} = \Delta x \left(\frac{4\pi Z^2 e^4}{m_0 V^2}\right) n_e \left\{\ln\left(\frac{\sqrt{E_M E_d}}{I}\right) - \beta^2 + \Delta L_{LS}\right\}, \quad (3)$$

$$\Omega_{BB}^2 = \Delta x \frac{2\pi Z^2 e^4}{m_0 V^2} n_e E_d X. \quad (4)$$

The experimental data is fitted to $\Omega_{BB}/\Delta E_{BB}$ using the fitting parameter E_d as shown in Fig. 1 (solid line). The fit shows good agreement with the experimental values. From the fit, the value of E_d is found to be 310 keV ($R \approx 55$ cm), where R denotes the effective range of the electrons in the gas. On the other hand, the dashed line indicates the result of the calculation without the effect of δ-rays escaping, i.e., the case of $E_d = E_M$. These results indicate the improvement in the energy resolutions due to the effect of δ-rays escaping from the cavity. The cut-off energy of electrons and its range reflect the cavity size. The effective gas length in our case is 1.2 times longer than that of the FRS in GSI, and the cut-off ranges measured in the FRS were 33-44 cm[8].

These results clearly show that the energy resolution of ionization chambers for heavy ions strongly depends on δ-rays escaping from the cavity. This fact provides useful information to optimize the composition and improve the performance of gas ionization chambers.

References

1) T. Kubo: Nucl. Instr. and Meth. Phys. Res. B 204, 97 (2003).
2) T. Kubo et al.: IEEE Trans. Appl. Supercond. 17, 1069 (2007).
3) T. Kubo et al.: Prog. Theor. Exp. Phys. 03C003 (2012).
4) K. Kimura et al.: Nucl. Instr. and Meth. Phys. Res. A 538, 608 (2005).
5) H. Otsu et al.: RIKEN Accel., Prog. Rep. 42, 163 (2009).
6) T. Ohnishi et al.: J. Phys. Soc. Jpn. 79, 073201 (2010).
7) J. Lindhard et al.: Phys. Rev. A 53, 2443 (1996).
8) M. Pfützner et al.: Nucl. Instr. and Meth. Phys. Res. B 86, 213 (1994).

Development of dispersion-matching transport for SHARAQ experiments

S. Michimasa,[*1] M. Takaki, M. Dozono, T. Nishi, S. Go, H. Baba, A. Stolz,[*2] S. Ota,[*1] K. Yako,[*1] H. Matsubara, H. Miya, H. Tokieda,[*1] S. Kawase,[*1] K. Kisamori, R. Yokoyama,[*1] T. Fujii, Y. Kubota,[*1] C.S. Lee,[*1] M. Kobayashi,[*1] T. Kawabata,[*3] T. Baba, M. Tsumura, R.G.T. Zegers,[*2] E. Ideguchi,[*4] H. Takeda, Y. Yanagisawa, T. Kubo, N. Inabe, N. Fukuda, D. Kameda, H. Suzuki, Y. Shimizu, H. Sato, T. Ichihara, H. Sakai, T. Uesaka, and S. Shimoura,[*1]

For high-resolution spectroscopy at SHARAQ[1)], we have provided beams with two ion-optical modes, depending on the required experimental design. These modes are Dispersion matching (DM) transport[2)] and High-resolution achromatic (HRA) transport[3)]. A beam study was performed to improve the momentum resolution of the DM transport and to implement and configure the new procedure to tune the DM transport. Here, we report the results of the beam study.

The DM mode is designed for high-resolution measurements of transfer momenta in a reaction by using the ion optics wherein the position and angle at the final focal plane of the spectrometer (S2) are independent of the beam momenta. The designed resolving power of the DM mode is $p/\delta p = 15000$. Further details concerning the DM mode are described in Ref.[2)]. The DM transport was performed in 2010, and we have simultaneously achieved lateral and angular dispersion matching conditions at SHARAQ with an RI beam of $\Delta p/p = 0.1\%$. The momentum resolution achieved at that time was $p/\delta p = 1800$ (FWHM).

The DM transport requires tuning before every physics measurement. In the previous procedure for tuning the DM optics, the SHARAQ spectrometer was firstly tuned by the HRA mode and the beamline optics was switched to the DM mode and tuned. In the present study, we primarily set the DM trajectory of the beamline by satisfying each focus condition in the beam transport sequence. In the last step, the SHARAQ spectrometer was iteratively tuned to reproduce the designed features of the secondary-target (S0) and S2 foci. This new procedure was very effective in terms of reducing the beam tuning time, because we did not have to tune the HRA transport. Consequently, we reduced the tuning time by 4 hours (1/3 of the original amount of time).

In the DM transport, the beam-momentum dependences on the horizontal position and angle at S2 were designed to be vanished. These features of the beam are shown in Figs. 1(a) and (b), which show the plots of the lateral and angular dispersion matching between the beamline and SHARAQ, respectively. In Fig. 1(c), the black histogram shows the horizontal spot size at S2. The width of this histogram represents the resolving power of the SHARAQ system, which was estimated to be $p/\delta p = 3000$ by considering the effects of multiple scattering in the tracking detectors positioned in the beamline. This resolution is due to the improvement in lateral dispersion matching between the beamline and spectrometer, and it is considered to be the result of iterative tuning in the present procedure. However, this width still suffered from different trajectories at BigRIPS-F3, where the beam spot size and angular spread were horizontally 3.9 mm and 14.8 mrad (FWHM), respectively. Consequently, we successfully achieved a resolving power of $p/\delta p = 8100$ by correcting the horizontal shifts at S2 calculated from the beam trajectories measured at F3 and the first-order transport matrix elements from F3 to S2. This improvement is indicated in red in Fig. 1(c). Data analyses of higher-order matrix elements and of the transport matrix related to the TOF between F3 and S2 are now in progress.

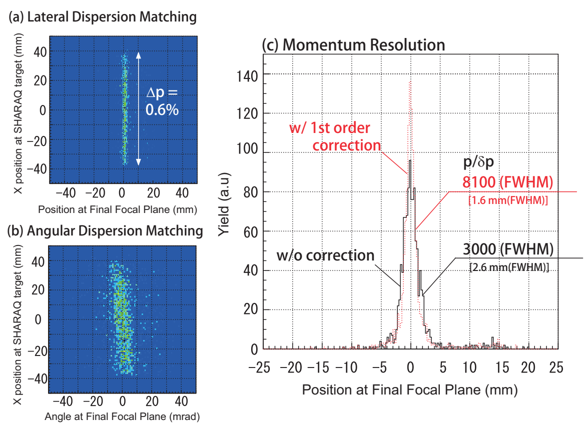

Fig. 1. Beam properties in the DM transport of SHARAQ. Figs. 1(a) and (b) show lateral and angular momentum matching plots at S2. Fig. 1(c) shows the achieved resolving powers without and with corrections made from the beam information at F3.

References

1) T. Uesaka, *et al.*: Prog. Theor. Exp. Phys., 03C007 (2012).
2) T. Kawabata *et al.*: Nucl. Instr. Meth. B **266**, 4201 (2008).
3) S. Michimasa *et al.*: RIKEN Accel. Prog. Rep. **45**, 136 (2012).

*1 Center for Nuclear Study, University of Tokyo
*2 NSCL, Michigan State University, USA
*3 Department of Physics, Kyoto University
*4 RCNP, Osaka University

A new neutron detector with a high position resolution for the (p, pn) reaction on rare isotopes

M. Sasano, Y. Kubota,[*1] T. Uesaka, S. Kawase,[*1] S. Ota,[*1] R. Tang,[*1] H. Tokieda,[*1] H. Miya, M. Kobayashi,[*1] H. Matubara, M. Dozono, C. Lee,[*1] T. Wakui, M. Itoh,[*2] K. Sekiguchi, and T. Taguchi

Nucleon-knockout (p, pN) reactions at intermediate energies (200–300 MeV) are a powerful probe for understanding the nature of single particle states (SPSs) in nuclei[1)]. Exclusive measurements of the (p, pN) reactions allow the determination of SPS properties such as separation energies, which has made them one of the hot topics discussed in studies on unstable nuclei.

The first goal of our (p, pN) studies is to measure SPS spectra for oxygen isotopes of $^{14-24}$O at the RIBF. For the $(p, 2p)$ reaction, we have performed an experiment on these isotopes at the RIBF (SHARAQ04). In the same experiment, we preliminarily measured the (p, pn) spectra using neutron detectors with a conventional design consisting of plastic scintillators with sizes of $6.5 \times 6.5 \times 220$ cm^3 with two photomultiplier tubes (PMTs, Hamamatsu H7195) at both ends. In this setup, only a poor resolution of about 5 MeV was achieved for the neutron SPS energy spectra, which was not sufficient for distinguishing between individual SPSs.

Herein, we present the development of a new neutron detector with a high position resolution better than 3 mm to measure neutrons with kinetic energies ranging from 50 to 200 MeV, emitted from the (p, pn) reactions at $200 - 300$ MeV. The opening angle θ between the beam-origin ejectile and knockout neutron predominantly determines the separation energies of SPS. The achievement of the position resolution of 3 mm in the direction of the opening angle is required for the separation-energy resolution of 500 keV, when the detector is placed at a distance of 2 m from the target.

Figure 1 shows a schematic view of the prototype detector, which has a total volume of $30.0 \times 30.0 \times 1000$ mm^3 of a highly segmented array consisting of 64 plastic scintillating fibers each with sizes of $3.75 \times 3.75 \times 1000$ mm^3. Scintillation photons generated in each fiber are read out using the multi-anode PMT (Hamamatsu H7546B), where photo-electron signals are independently multiamplified for each anode channel without losing the information on the fiber position at which the photon is generated.

In November 2012, a test experiment of the prototype detector was performed at the Cyclotron and Radioisotope Center (CYRIC), Tohoku University for examining the method to reconstruct the neutron hit position as well as to calibrate the detection efficiency. A preliminary analysis shows that the detection efficiency is about 2.0% and 1.6% for 68- and 50-MeV neutrons, respectively, when the threshold is set to the dynode signal of each PMT around 4 MeV electron-equivalent energy. Figure 2 shows a hit pattern of anodes of the PMT in the unit of QDC channels for a typical neutron-detection event. In this event, the fiber in which the reaction due to the incident neutron occurs can be easily identified, implying that an uncertainty of the detection position of ± 1.85 mm can be achieved. The detailed analysis for establishing the method of the hit-position reconstruction is under progress.

In summary, a prototype neutron detector with a high position resolution has been developed for measuring SPS energy spectra on oxygen unstable isotopes via the (p, pn) reaction with a high resolution in the separation energy of about 500 keV. By performing a test experiment using neutron beams at 68 and 50 MeV, we have obtained preliminary results of the detection efficiencies as well as the hit-pattern information needed for further analysis.

We acknowledge the staff at CYRIC for their efforts and support.

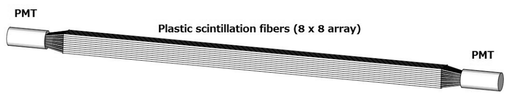

Fig. 1. A schematic view of the prototype detector. See text for details.

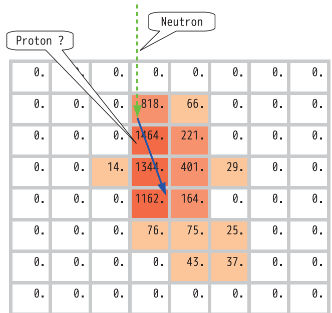

Fig. 2. An example of the hit pattern obtained for an event caused by a neutron at 70 MeV. See text for details.

*1 Center for Nuclear Study, University of Tokyo
*2 Department of Physics, Tohoku University

References

1) G. Jacob and TH. A. J. Maris: Rev. of Mod. Phys. **45**, 6 (1973).

The polarized proton target in SHARAQ04 experiment

T.L. Tang, T. Kawahara, T. Wakui, S. Sakaguchi, S. Kawase[1] and T. Uesaka,

The nucleon knockout reaction is used in SHARAQ04 experiment, which is performed in RIKEN RIBF. A polarized proton target was employed in the experiment for identifying the total angular momentum of knockout protons. The pulsed laser dynamic nuclear polarization [1) was used to polarize the target proton.

The principle of proton polarization is based on Hartman-Hahn theory [2) that the ESR (electron spin resonance) frequency of electrons in rotating frame matches the Larmor frequency of protons. In mathematical form,

$$\left(\Omega_S - \omega_{\mu w}\right)^2 + \Omega_{\mu w}^2 = \Omega_I^2 \qquad (1)$$

where Ω_S is the ESR frequency in lab frame, $\omega_{\mu w}$ is the microwave frequency, $\Omega_{\mu w}$ is the equivalent frequency by the microwave's magnetic field, and Ω_I is the proton Larmor frequency.

The system of polarized proton target included a target crystal, magnet, laser, microwave, magnetic field sweep, cooling chamber, and vacuum chamber. The target crystal was naphthalene doped with 0.05 mol% of pentacene, in which, the pentacene molecules are the polarizing agent. The ground state of pentacene is a spin-0 singlet state. Further, there are excited triplet states of spin-1 [3)]. The electron polarization was transferred to the proton owing to the hyperfine coupling between triplet state electrons and proton when equation (1) was satisfied. The magnetic field set the proton Larmor frequency. Two 514.5-nm continuous wave argon Lasers excited the pentacene into triplet states. The two lasers beams were chopped to form pulses. The microwave drove the electrons oscillating between triplet states $m = -1$ and $m = 0$. The magnetic field sweep swept through the ESR spectrum to make more electrons involved. The polarization direction can be adjusted by the phase of field sweep for cancellation of spurious asymmetry. The crystal was polarized under -160 ^{o}C for reducing the thermal depolarization. The settings of the polarization system are listed in Table 1.

The vacuum chamber contained the cooling chamber and it was connected to the beam pipe. A crystal holder, the crystal, microwave coil, magnetic field sweep coil, and NMR coil were placed inside the cooling chamber. The two laser beams were fed to the crystal through windows from outside. The chambers have arc openings that spanning 150^{o} horizontally and 20^{o} vertically along the beam line. 128-μm Kapton films covered the arc openings and allowed particles to go through and maintain vacuum pressure.

[1] Center of Nuclear Study, Tokyo University

Table 1. Settings of the polarization system.

Magnetic field [mT]	64.2 ~ 65.6
Vacuum [mbar]	7×10^{-2}
Temperature [^{o}C]	-160
Laser 1 power [W]	10.7
Laser 2 power [W]	11.1
Chopper frequency [kHz]	3.5
Laser pulse width [ns]	83.9
Microwave frequency [GHz]	2.695
Microwave power [W]	2.6
Microwave pulse width [ns]	15.9
Field sweep [mT]	± 3
Field sweep gate width [ns]	16.5
Field sweep Phase	0/180

The detection of polarization was done by two methods: proton-proton elastic scattering and NMR (nuclear magnetic resonance) detection. The elastic scattering can determine the absolute polarization, and the NMR signal provides a quick and easy way to monitor the relative polarization during the nuclear experiment. However, the NMR coil and the magnetic field sweep coil interfere each other. They have to be separated manually between polarization and polarization measurement. A 4~5 degree NMR pulse is used that it will not destroy the polarization. The crystal's polarization is then monitored by the NMR signal for every 2 hours on average. The relative polarization by NMR signal is shown in Figure 1. The absolute polarization by analyzing the proton-proton elastic scattering data is still underway.

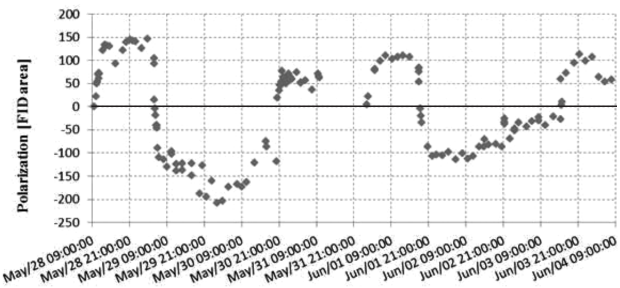

Figure 1. NMR signal of the polarized proton target.

In conclusion, the experimental conditions and setup were reported. Many improvements were suggested from this experiment. They can be employed in future experiments that use a polarized proton target as a standard tool.

References

1) M. Iinuma *et al.*: Phys. Rev. Lett. **84**, 171 (2000).
2) S.R. Hartmann, E.L. Hahn: Phys. Rev. **128**, 2042 (1962).
3) Sloop D *et al.*: J. Chem. Phys. **75** 3746 (1981).

Enlargement of solid polarized proton target for RI-beam experiment

S. Sakaguchi, T. Uesaka, T. Kawahara, T.L. Tang,[*1] and T. Wakui

The direct reaction with spin polarized light ions has been utilized as a powerful probe for investigating the nuclear structure, reaction mechanism, and interactions. For applying such method to studies of unstable nuclei, we have developed a solid polarized proton target system which can be operated in a low magnetic field of 0.1 T[1]. Measurement of the spin-asymmetry in the scattering of unstable nucleus has been realized for the first time by using this target[2]. The range of its application will be extended by enlarging the size of the target. The existent target has a diameter of 14 mm, which is smaller than the typical spot size of the RI-beams. To increase the target size, we improved three components as described below.

First, we prepared a large target material, which is a single crystal of naphthalene with a diameter of 25 mm. The crystal was fabricated by the vertical Bridgman method in cooperation with Ohyo Koken Kogyo Co., Ltd. The crystal is to be shaped into a disk with a thickness of 3 mm and a diameter of 24 mm.

Second, we modified the sizes and materials of the polarizing devices shown in Fig. 1(a). The crystal, mounted on a target holder, is surrounded by a loop-gap resonator (LGR) with a diameter of 28.2 mm for microwave irradiation. The LGR is installed in a NMR coil (30.4 mmϕ). For transmitting microwave to the LGR, we have another coil, called coupling coil (31.2 mmϕ). Position of the LGR and the NMR coil can be controlled by turning the shafts with metal gears. The angle of crystal holder can also be controlled with another shaft. By turning each shaft by 360 deg., one can move the LGR or the NMR coil by 17 mm, or rotate the crystal holder by 34.7 deg. Materials of the holders, gears, shafts, shaft holders, and a gear stage are diflon, brass (C3604), SUS304, brass (C5191), and SUS316L, respectively.

Finally, we developed the loop-gap resonator (LGR). It has a cylindrical shape, and generates an oscillating electromagnetic field along its axis. This field is required for transferring electron polarization to protons. As for the resonance frequency $f_{\rm MW}$, there are two requirements. First, the quarter wavelength $\lambda/4 \equiv c/4f_{\rm MW}$ should be sufficiently larger than the diameter of the LGR, 28.2 mm, for preventing the LGR from working as an antenna. From this requirement, $f_{\rm MW}$ should be lower than $\sim$1.9 GHz. The second requirement is concerned with the strength of static magnetic field, which defines the direction of polarizing axis. As high polarization requires stronger magnetic field and the field strength increases as $f_{\rm MW}$, $f_{\rm MW}$ should be higher than $\sim$1.3 GHz. Considering these requirements, the optimum microwave frequency is expected to be in a region of 1.5–1.8 GHz. We designed a trial LGR with a resonance frequency of 1.50 GHz in calculation which is known to be higher in actual cases by 0.3–0.7 GHz. The designed LGR has 19 plates of 4.4 μm-thick copper on both sides of a 25 μm-thick Teflon sheet as shown in Fig. 1(b). To cover the circumference of a LGR holder (88.67 mm), width of LGR is set to 89.60 mm. As the LGR sheet crinkles slightly, width of the overlap was $\sim$0.6 mm. We measured resonance pattern of the fabricated LGR, and found a sharp resonance peak at 2.15 GHz as shown in Fig. 2. The frequency will be retuned in the next version.

In summary, we have fabricated a new target crystal, device holders, moving system, and a microwave resonator for enlarging the size of the polarized proton target from 14 to 24 mmϕ. Other components such as coils for NMR and magnetic field modulation are under development. Upgraded polarized proton target, which are to be completed in near future, will expand the range of its application in RI-beam experiments.

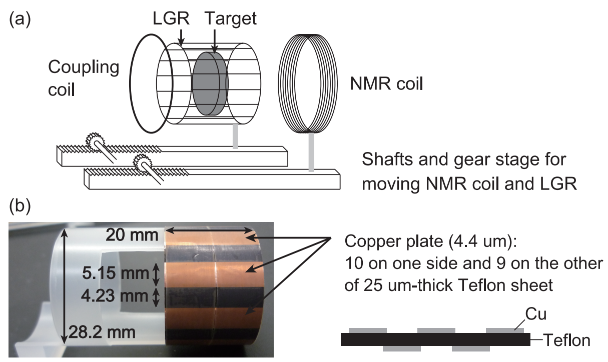

Fig. 1. (a) Target crystal and polarizing devices. (b) Loop-gap resonator (LGR) for MW irradiation.

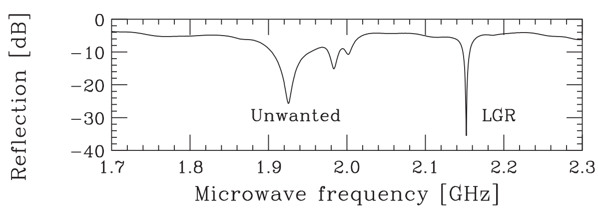

Fig. 2. Resonance pattern of the LGR.

*1 CNS, University of Tokyo

References

1) T. Wakui et al.: NIM A **550** (2005) 521.; T. Uesaka et al.: NIM A **526** (2004) 186.
2) T. Uesaka, S. S. et al.: PRC **82** (2010) 021602(R).; S. S. et al.: PRC **84** (2011) 024604.

Relaxation rate of proton polarization in p-terphenyl at room temperature

T. Kawahara, T. Uesaka, S. Sakaguchi, L. T. Tang,*1 and T. Wakui

A polarized-proton solid-target system constructed at the RIKEN RIBF and the Center for Nuclear Study, University of Tokyo, has a distinguished feature: a relatively high efficiency of 20% can be achieved with a low magnetic field of 0.1 T, which enables measurement of the reactions such as the $(\overrightarrow{p}$, 2p) reaction with RI beams at intermediate energies[1,2]. Up to now, however, the temperature of the target material is required to be around 100 K or lower, thereby limiting the application of this system. Thus, we are trying to achieve the same level of the polarization at room temperature, i.e. around 300 K. Once achieved, it would lead to new opportunities in measuring low-energy reactions such as the $(\overrightarrow{p}$, d) transfer reaction as well as many medical applications using polarized materials.

A straightforward approach to realize high polarization at room temperature is to increase the laser power to excite a maximum number of molecules to electron-spin triplet states. However, the temperature rise caused by laser irradiation can also increase the relaxation rate of the polarization, eventually degrading the polarization. Herein, we examine the method to overcome this problem.

Figure 1 shows the magnitude of proton polarization as a function of the average laser power.

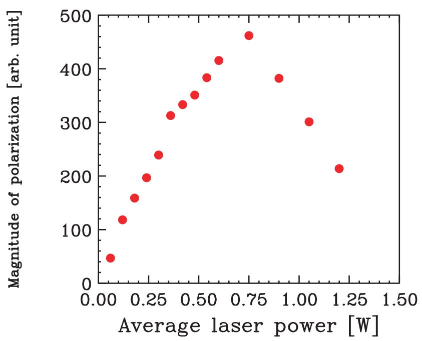

Fig. 1. The average laser power dependence of the magnitude of proton polarization.

Here, continuous wave (CW) light with a wavelength of 514 nm was provided by an Ar ion laser system (Coherent TSM25). The CW light was pulsed using a mechanical chopper, giving laser pulses each with a width of 50 μsec and with a repetition of 6.0 kHz. As shown in the figure, the polarization almost linearly increases with the increase in the average power up to 0.75 W, above which the polarization rapidly drops. This drop above 0.75 W can be considered to be the effect of the temperature rise. A similar trend is also reported in Ref. 3.

Figure 2 shows the polarization relaxation rate, Γ_{int}, as a function of the temperature in a region from 283 to 363 K.

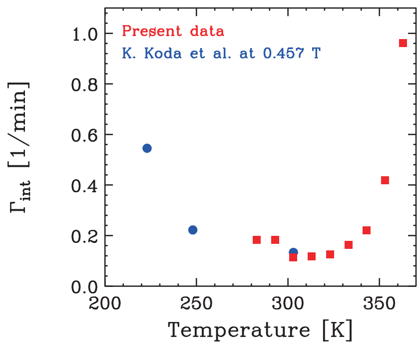

Fig. 2. The temperature dependence of relaxation rate of proton in p-tephenyl. The lower region was measured by K. Kohda *et al.*[4]

Here, N_2 gas, whose temperature was controlled by using liquid N_2 in conjunction with a heating system, was used for changing the temperature of a crystal with sizes of 1.5 $\times$2.0 $\times$11.0 mm^3. A thermometer was attached at the end of the crystal. As shown in the figure, as the temperature increases from 300 K to 360 K, the rate dramatically increases almost by a factor of 5, as expected from Fig. 1. For temperatures below 250 K, it is known that the relaxation rate deteriorates because of unfavorable change in the crystal structure[4]. Thus, keeping the crystal temperature around 300 K is crucial for achieving high polarization using high power laser. Further examination of the condition to achieve high room-temperature polarization is under progress.

References
1) T. Uesaka *et al.*: Eur. Phys. J. **150** , 71(2007).
2) T. Wakui *et al.*: Nucl. Instr. Meth. A **550**, 521(2005).
3) A. Kagawa *et al.*: Jour. Mag. Res. **197**, 9(2009).
4) K. Kohda *et al.*: J. Phys. Soc. Jpn. **51**, 3936(1982).

*1 Center for Nuclear Study (CNS),University of Tokyo

Technical knowledge about cooling of CRYPTA for liquid helium

M. Kurata-Nishimura, R. Yokoyama, K. Kisamori, H. Otsu and Y. Kondo

Dense and pure element target is one of the most important subject for increasing statistics of unstable nuclear experiment. For instance, since liquid helium has a density that is about 800 times higher than that of helium gas at room temperature, the reaction rate is expected to be increased proportionally to the density.

The CRYPTA[1] (cryogenic proton and alpha target system) has been used for a variety of experiments at RIBF. The system has been established well but it is still important to accumulate technical knowledge to be shared by others. In this paper, two findings about cooling of the CRYPTA for the liquid helium are introduced.

A structure of the CRYPTA for the liquid helium target is shown in Fig. 1. A 4K-Gifford-McMohon cycle refrigerator (RF704S) is mounted on top of a vacuum chamber and the first stage and the second stage of the refrigerator are connected to a heat shield and a target cell, respectively.

The system was operated for several years after a previous experiment without maintenance, and thus, the cooling problem has been observed, as shown in Fig. 2. The temperature of the heat shield suddenly increased from 20 K to 163 K in 30 min and 2.5 hours later, slowly dropped to the designated temperature. After eight hours, temperature oscillation was observed at the heat shield and the target cell. It continued until the cryogenic system was turned off. During the operation, the body of the refrigerator also cooled down.

This behavior was found to be caused by the damage of two insulators. The first and the second insulator isolate room temperature helium gas from the first stage helium gas and the first stage one from the second stage one, respectively. Because a small chasm developed between the insulator and a shrunken metal at the cryogenic temperature, mixing of two different temperature gases took place. The mixed helium gas increased temperature and when the chasm was occluded by restoring of the metal, the system operated normally. By replacing the insulator by a company, the CRYPTA was recovered.

In order to cool the target cell to the designated value of less than 4.2 K to liquify helium gas with 1 atmosphere, a heat shield that prevents thermal radiation from a vacuum chamber is necessary around the target cell. On the other hand, no material is preferable to avoid background reaction, and hence, there are 50 mmϕ holes at the entrance and exit along beam direction. In order to evaluate the effect of the hole at the heat shield, the reachable minimum temperature was compared by changing the material attached to the hole. The results are listed in the Table. 1. Without any material, the cell temperature was down only to 9.5 K, which is too high to liquify helium gas with 1 atmosphere. With 4 μm aluminized mylar foil, the temperature reached 4.4 K, which means that this foil is not adequate for absorbing thermal radiation. In contrast, the 12 μm aluminum foil and 0.11 mm aluminum tape worked as a thermal radiation absorber effectively, and the thickness of 12 μm was sufficient. The amount of the absorption depends on the physical properties, such as reflectance ratio and thermal conductivity of a material and surface area. Aluminum foil is one of the best choices, and thinner foils should be tested in further development.

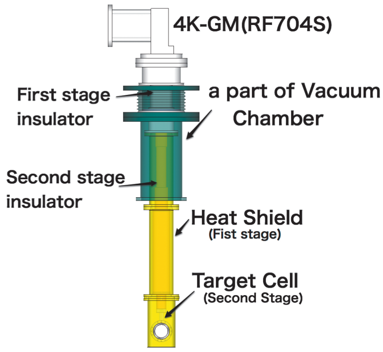

Fig. 1. Schematic drawing of the CRYPTA for liquid helium target.

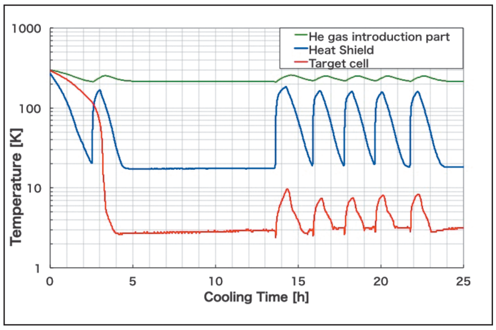

Fig. 2. Time variation of temperature for CRYPTA. Unexpected increase and decrease was observed periodically.

Table 1. Lowest temperature with material covering at holes of heat shield

Material	Thickness	Lowest Temperature [K]
No Material		9.5
Al Mylar	4 μm	4.4
Al foil	12 μm	3.6
Al Tape	0.11 mm	3.5

References

1) H.Ryuto et al.: Nucl. Inst. Meth. A555, 1 (2005).

Development of fast charging kicker system for Rare-RI Ring

Y. Yamaguchi, S. Sato,[*1] A. Tokuchi,[*1*2] W. Jiang,[*1] T. Kikuchi,[*3] A. Ozawa, and M. Wakasugi,

We use a kicker system for injecting a particle into the Rare-RI Ring as well as for extracting the particle from the ring. For this reason, a fast-response mechanism[1)] for the kicker power supply is indispensable to establish a self-trigger individual injection method, and a fast-charging mechanism for the kicker power supply is also necessary to extract a rare-RI from the ring.

The goal of shortening the charge time is defined based on the following conditions. The circumference of the ring is about 60 m. The revolution time of a particle is about 350 ns at the energy of 200 MeV/nucleon. To measure the flight time of the particle with an accuracy on the order of 10^{-7}, it is necessary to take at least 2000 revolutions corresponding to about 0.7 ms in flight time. Since the recovery time of a thyratron is typically less than 0.5 ms, the target charge time is 0.2 ms. Recently, we succeeded in shortening the charge time. In this paper, we report the results.

We have verified our results by using a model kicker system.[2)] The charge time of a model kicker power supply is about 100 ms, which is excessively long according to the requirements. Hence, we adopted a new charging mechanism, called the hybrid charging system. Figure 1 shows a schematic diagram of the hybrid charging system. The main part provides about 90% charging voltage, and the remaining 10% is supplied by a sub-part of the system. The main charge is completed in about 0.1 ms using a double forward converter composed of IGBTs and a pulse transformer. After the main charge was completed, the sub-part charge is immediately started. The sub-part charge is completed within 0.1 ms using a high-frequency (500 kHz) resonant circuit and a pulse transformer. In addition, when the charging voltage is attenuated, the sub-part operates to maintain the charging voltage level.

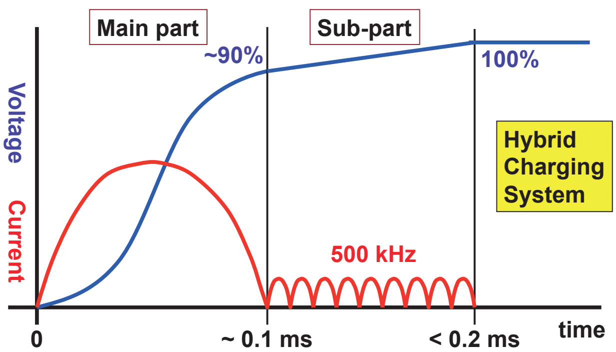

Fig. 1. Schematic diagram of the hybrid charging system. Blue and red lines show the voltage and current, respectively. The scaling is arbitrary.

By using the hybrid charging system, we achieved a charging time of 0.2 ms, which yields the shortest repetition time of about 0.7 ms, as shown in Fig. 2. We also confirmed that a rated charging voltage is possible up to 75 kV and that the fluctuation of the charging voltage was achieved to be less than ±1%. The sub-part of the system contributes to this small fluctuation.

New kicker power supplies with fast-response and fast-charging mechanisms are under construction, and we plan to test the performance of our new kicker power supplies in the fiscal year 2013.

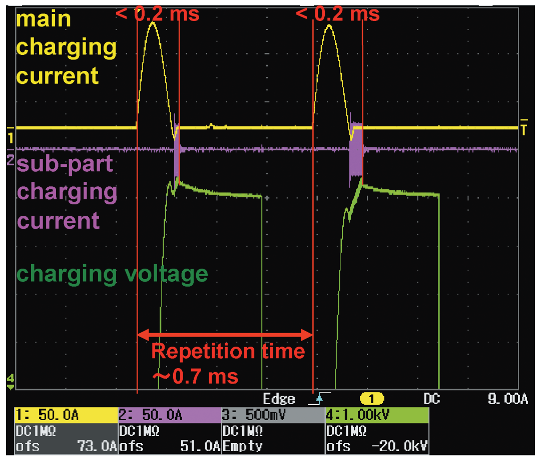

Fig. 2. Example measurement results. Yellow, red, and green waves show the main-charging current, sub-part charging current, and charging voltage, respectively.

References
1) Y. Yamaguchi et al.: RIKEN Accel. Prog. Rep. **44**, 157 (2011).
2) T. Ohkawa et al.: Nucl. Instrum. Meth. Phys. Res. A **547**, 287 (2005).

*1 Extreme Energy-Density Research Institute (EDI), Nagaoka University of Technology
*2 Pulsed Power Japan Laboratory Ltd.
*3 Department of Nuclear System Safety Engineering, Nagaoka University of Technology

Overhead traveling crane with transfer bridges for the Rare-RI Ring

T. Fujinawa, T. Maie, Y. Yamaguchi and M. Wakasugi

When construction of the Rare-RI Ring in the K4 room was being considered, one of most difficult obstacles to surmount was to carry out construction without disturbing the fifteen pillars in the room. The presence of the pillars makes the layout and overhead crane plan complicated. Even the purchase of many cranes will leave several narrow paths and unreachable places. As a solution to this problem, an overhead traveling crane with a transfer bridge system was designed and implemented. The system consists of three beams with two saddles, two transfer bridges (each 1.71 m in length) and only one suspension-type hoist motor. The hoist motor with heavy load is designed to move to any beam through the transfer bridge(s) and be able to carry the load to the destination without transshipment (the layout is shown Fig. 1).

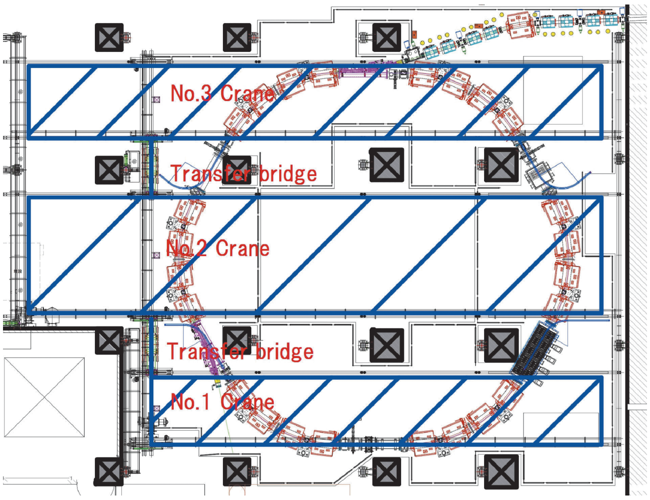

Fig. 1 System layout, Blue hatching line shows crane working area.

The specifications of the crane are listed in Table.1.
All the motors are equipped with an exclusive variable voltage variable frequency (VVVF) inverter speed control system. Further the hoist motor is a high-resistance basket-type induction motor. Both the VVVF and the high-resistance basket-type induction motor do not require special skills or training for operation.

The capacity of the hoist is designed to be 4.9 tons (t) because the system is controlled wirelessly.
The skill training course for crane operation is set to moving less than 5 t with radio control use; crane operation with more than 5 t requires a license. There are a few licensed operators in the RNC. The weight of the bending magnet for the ring is 8 t, and therefore, the separate top and bottom parts of the magnet can be hoisted by the 4.9-t crane, and using a 4.9-t crane is more economical than using a 10-t crane. When the hoist crosses over the bridge to the beam and vice versa, all the beams and bridges are positioned in a straight line, and they are locked by pneumatic control cylinders and pins (Fig. 2). During crossing, the crane speed is slowed down automatically. The crane's precision passion and speed are controlled by limit-switches located at both ends of the beams and bridges. The air compressor for pneumatic control is normally used for other pneumatic control systems of the Rare-RI Ring, this saves space and costs.

Fig. 2 Hoist, crane beams, and transfer bridge

This crane was commissioned at the end of September 2012, and it was useful in the construction of the stage for the ring and water cooling system. Further, from the New Year onwards, it will be used for installation of the ring and for hoisting the DC power sources. The contractor for crane construction has been given to Mitsubishi Electric FA Industrial Products Corporation.

Table 1 Technical specifications

	Hoist		No.1 Crane	No.2 Crane	No.3 Crane
Capacity	4.9 ton	Rail span	3.63m	6.08m	3.78m
Lifting Height	6.8m	Run	25.14m	31.19m	31.19m
Lifting Speed	0.9-8m/min	Control	Wireless	Wireless	Wireless
Traveling Speed	2.5-25m/min		2.4-24m/min	2.4-24m/min	2.4-24m/min

AC power system for Rare-RI Ring

T.Fujinawa, K. Kumagai, Y. Yamaguchi and M. Wakasugi

Rare-RI Ring[1)] is under construction. It requires an AC power system for magnet power supplies with capacity of 2.5 MW-415 V, and for the vacuum system needs 210 V. In 2012, the AC power source so-called metal clad switchgear for Rare-RI Ring was constructed, as shown in Fig.1.

The switchgear supplies five types of electricity, three phase 415 V, 210 V, single phase 240 V, 210 V, and 105 V. Such a combined system is a first for RIBF. For the magnet power supply, two dry-type transformers of 6.6 kV/415 V with delta-star and delta-delta connections are manufactured. For rectification power, these two types of windings can produce less harmonic currents with multiple rectifiers. The power capacity becomes 1.5 MVA for each, and this value is the largest in the RIBF for an MV/LV transformer. The delta-star 1.5 MVA transformer has a high efficiency rate of 99.40% and that of the delta-delta is 99.36%.

A Double-Power Transformer was newly introduced, which enables simultaneous supply of three phase 210 V and single phase 210/105 V from one transformer. Its capacity is 200 kVA. Compared to the normal case where two transformers are used, this system enable reduction of space and cost, and it needs only one vacuum circuit breaker (VCB). Its transformer is of a star-delta type, and its efficiency rate is 98.86%.

Two sets of air circuit breakers (ACBs) are lined up on the LV side. The DC output of the power source for main magnets in the Rare-RI Ring is more than 3500 A. A corresponding rated AC current of 2000A and breaking current of 65 kA are required for those ACBs. This is the first time ACBs are used in the RIKEN Wako campus. The transformers together with breakers of medium-voltage VCBs, ACBs, and low-voltage no-fuse-breakers with an earth leakage trip element (ELCB) are based on the Japan electrical manufacturers' standard (JEM) 1425 &1265 and IEC 62271-200. Such a switchgear is very safe for humans.

The switchgear is connected to the RIKEN Wako-No.2 high-voltage substation feeder No 52RF5 using a 6.6kV-triplex-type cable with an environmental management (EM) cross-linked polyethylene insulator and a polyethylene sheath (XLPE/PE). The size of the cable is 150 mm^2 and the allowable current is 286 A. The cable withstands a shortcut current of 22.43kA.[2)]

The feeder No 52RF5 was originally for the SHARAQ[3)], but it was transferred to No 52RF6, because the current transformers (CT) capacity of 52RF6 is not sufficient for 3.2 MVA but sufficient for SHARAQ. According to quotes given by the manufacturer, it would have been very costly to change the CTs.

The protection relays are installed on both the feeder side (52SRF5) and the incoming side (52SRF5R). The feeder side detects over current (50), short-circuit-current (51) and ground directional current (67), and the Rare-RI Ring side detects under voltage (27), 50 and 51.

The control system operates with DC110V and can work during an electrical power outage as well. It can be operated both locally and remotely. A remote control with a flat-panel display can be employed in the CGS center control room located in the NISHINA memorial building.

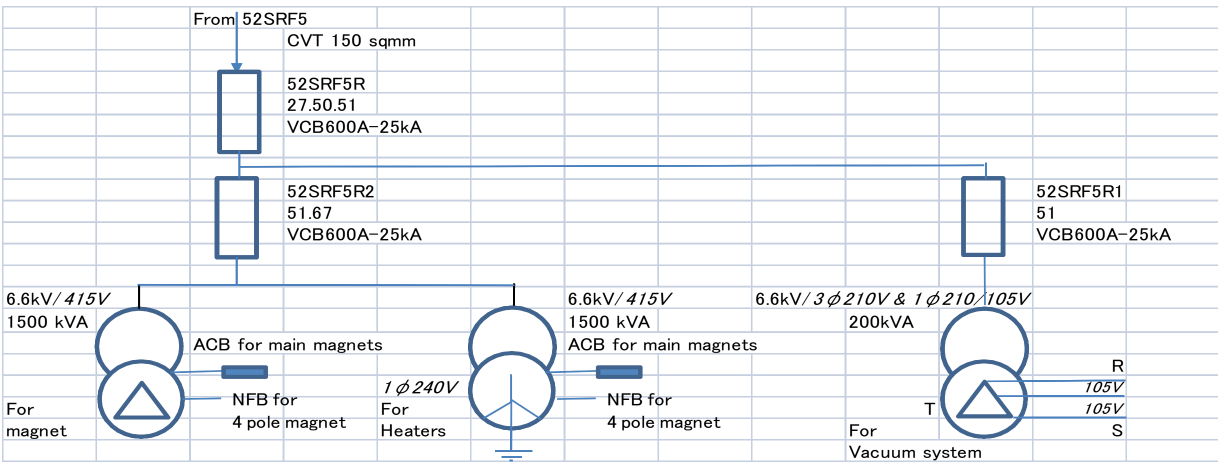

Fig.1. Single line diagram

References
1)Y.Yamaguchi et al.: Nucl.Instr.and Meth.in Phys.Res B266.4575-4578 (2008)
2) T.Fujinawa: Nihon Univ Cit. Vol 45. 91-97 (2008).
3) T.Fujinawa et al.: RIKEN Accel.Prog.Reo.41133-134 (2008).

Water cooling system for experimental facilities in the RIBF building

T. Fujinawa, T. Maie, Y. Yamaguchi and M. Wakasugi

In the RIBF building experimental facilities, development work for the water-cooling system for SHARAQ[1] was in the first stage in 2008 and that for SCRIT[2] was in the second stage in 2010 and has now reached the final stage. The third stage was signed in 2012, with NIPPONKUCHO SERVICE CO. LTD. which carried out the first stage successfully. The flow diagrams are shown in Fig.1.The specifications for the third stage is described in the following text. The primary pump with a capacity of 55 kW and 2370 ℓ/min and water pressure 784 kPa was installed in the pump room in the K4 basement together with 2 MW heat exchanger (HEX), ion-exchanger resin, and other components. The pump is composed of stainless steel. The electrical motor for the pump is of the 4 pole high-efficiency type with 93.7% efficiency at 75 - 100% load and 93.2% efficiency at 125% load. The current is 99.3 A, power factor is 82.2%, and slip is 0.99% at full load. The pump and motor in the pump room of K4 operate quietly. The motor is connected to the existing motor control center spear unit of RIBF water cooling system. The motor control center is in the accelerator building on the 1st floor. This ensures that there are no additional costs for the power supply of the cooling system. The capacity of the cooling tower for the third stage is 2 MW. The tower contains two high-efficiency 7.5 kW fans. It is located on the roof and connected with existing cooling towers. Presently, the total capacity of the cooling towers is 4 MW with 8,614 ℓ/min. The system for all stages is monitored and controlled remotely as well as locally. There is a flat display unit in the helium cryogenics control room, where operators work all year around. Rare-RI Ring uses SHARAQ as the BT line, and so the operation screen shows both SHARAQ and Rare-RI Ring together. The control power for all systems was changed from socket outlet of the commercial source to the existing metal-clad switchgear of MV/LV water-cooling system, which also connects to the CGS[3] bus. Through this modification, the reliability was improved. The primary cooling line is designed as a closed pipe line to avoid water evaporation. The system has a makeup water alarm device, which is sounded in the control room when a water leakage occurs.

Presently, the temperature is controlled by a three-way valve and the on-off action of cooling fans from the cooling tower. In the future, the unit-system of the temperature controller, which allows a permissible error of ±0.1 °C, will be connected without making any large modifications to the existing setup.

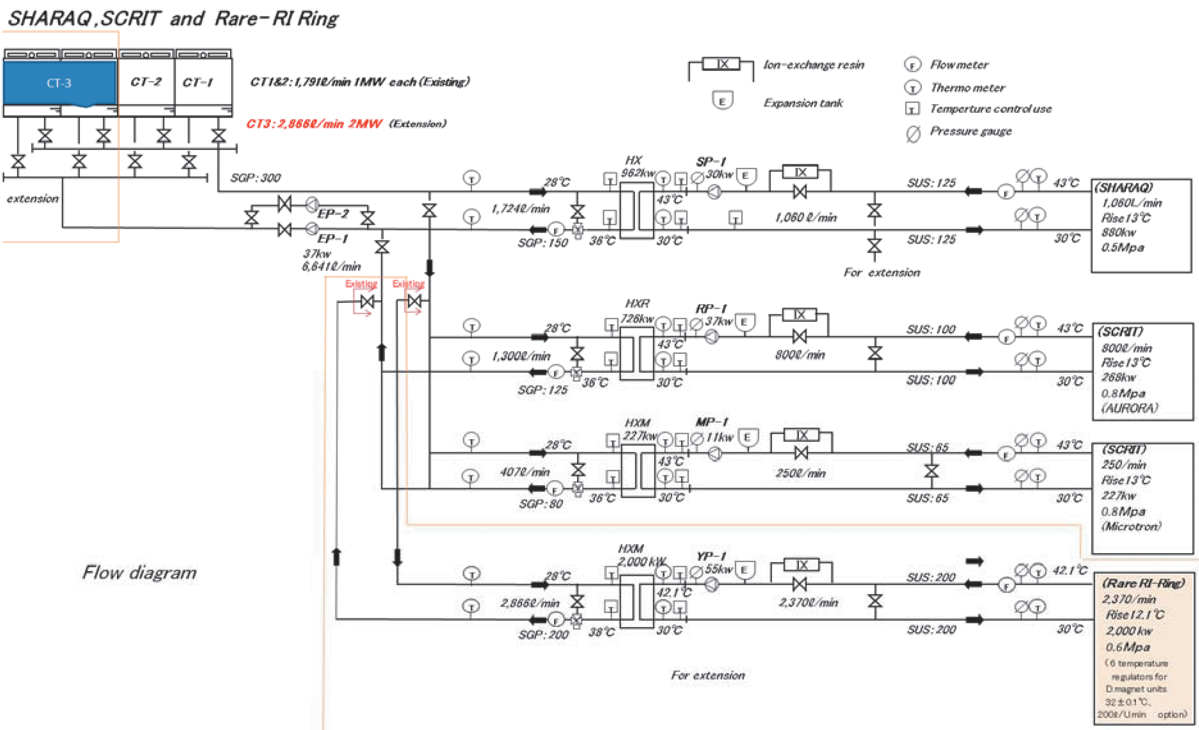

Fig.1 Flow diagram. The colored portion denotes the third stage.

References
1) T. Fujinawa et al.: RIKEN Accel. Prog. Reo. 41,133 (2008).
2) T. Fujinawa et al.: RIKEN Accel. Prog. Reo.43,142 (2010).
3) T. Fujinawa and Y.Yano: J. Part. Accel.Soc. Jpn .8, 18(2011).

Design of the trim coils generating the isochronous magnetic field for the rare-RI ring

J. Ohnishi, Y. Yano, Y. Yamaguchi, and M. Wakasugi

The rare-RI ring is a cyclotron-like storage ring with an isochronous magnetic field. The circumference of the ring is 60.35 m, and the momentum acceptance is ±0.5% for a standard beam with an energy of 200 MeV/nucleon and a magnetic rigidity of 6 Tm. Figure 1 shows the arrangement of a 1/12 unit cell of the entire ring. A total of 24 dipole magnets of the rectangular type are used. The length of the orbit, for which the deviation from the central orbit is x, is represented as $L = 60.35 + 24 \times 2 \times x \times \tan 7.5^\circ$, and Δx is ±34 mm for the beams with $dp/p = \pm 0.5\%$.

Figure 2 shows the average magnetic fields along the beam orbit in the 30° arc region of the unit cell. Three lines indicate the isochronous magnetic field for the mentioned standard beam and those calculated from a magnetic field map of the dipole. The isochronous magnetic fields are generated with ten one-turn trim coils attached on the pole faces of the dipoles. Figure 3 and 4 show the arrangement of the trim coils in a cross-section of the dipole and the calculated average magnetic field which each trim coil generates at a current of 300 A, respectively. A set of the trim coil currents can be calculated by the least square method using the average magnetic fields. The trim coil currents and fitting residuals for the standard beam are listed in Table 1 and shown in Fig. 5, respectively. Figure 5 shows that the accuracy of the isochronous magnetic field is within 3×10^{-6} in the orbit region of ±50 mm including the betatron amplitude. The real trim coils were fabricated as these designs and installed on the existing dipole magnets.

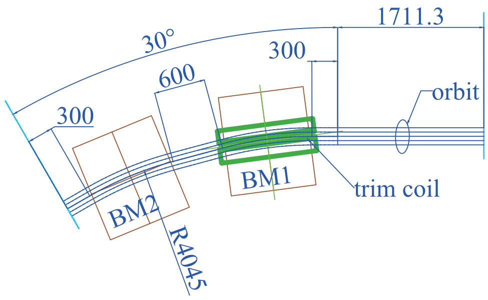

Fig. 1. 1/12 unit cell of the rare-RI ring.

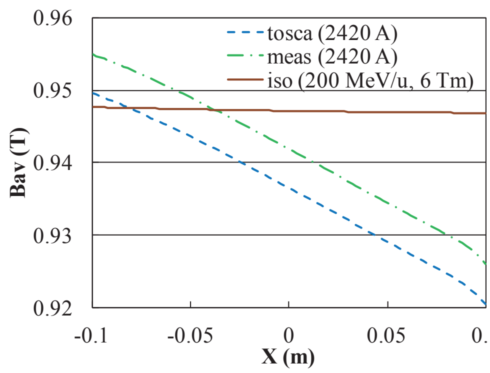

Fig. 2. The average magnetic field of the dipole and the isochronous magnetic field for the standard beam.

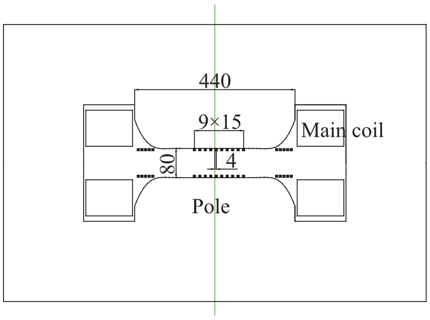

Fig. 3. Arrangement of the trim coils attached on the pole faces of the dipole.

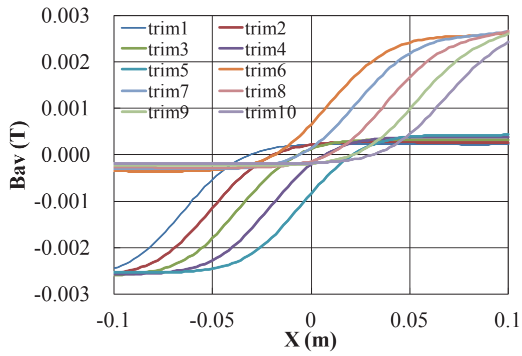

Fig. 4. The average magnetic field generated by each trim coil excited at 300 A.

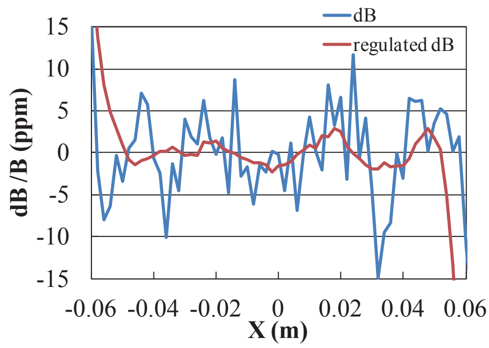

Fig. 5. Fitting of the residual error for the isochronous magnetic field. The red line denotes the regulated value in the width of 20 mm.

Table 1. Currents (A) of the main and trim coils for the isochronous magnetic field (200 MeV/nucleon, 6 Tm).

main	trim1	trim2	trim3	trim4	trim5
2433	419	212	114	222	301
trim6	trim7	trim8	trim9	trim10	
139	242	243	198	416	

Extremely fast, high-precision mass measurements with multi-reflection time-of-flight mass spectrograph†

P. Schury, F. Arai, Y. Ito, H. Mita, S. Naimi, T. Sonoda, M. Wada, and H. Wollnik

For offline testing of the MRTOF[1)], a thermal ion source capable of proving alkali element ions has been used to perform a doublet mass measurement of ^{40}Ca$^+$/^{40}K$^+$. The atomic masses of ^{40}Ca and ^{40}K differ by 1.311 MeV/c^2. An example spectrum is shown in Fig. 1 with 173 detected ions of ^{40}Ca$^+$ accumulated over the course of 2 hours. The FWHM of these ToF peaks was $\Delta t \approx 8.2$ ns – a mass resolving power of $R_m \approx 140{,}000$ achieved with a time-of-flight of $t \approx 2.3$ ms. An equivalent measurement by the popular method of Penning trap mass spectrometry would require a magnetic field strength of more than 170 T.

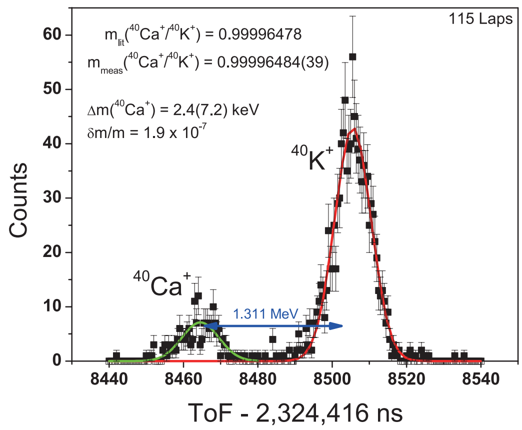

Fig. 1. Time-of-Flight spectrum of ^{40}Ca$^+$ and ^{40}K$^+$.

Furthermore, using this mass doublet, we were able to verify that the MRTOF-MS is capable of an extreme level of mass precision. Previous attempts to determine the absolute precision limit of the device using triplet measurements of ^{39,40,41}K$^+$ were stymied by slight drifts in the voltages between measurements, as the triplet could not be simultaneously measured due to a limited mass bandwidth of the device. Since this doublet is within the mass bandwidth of the device (roughly estimated as A/q divided by the number of reflections), the two experience the same drift and the affect of any such drift is cancelled out. To prevent excessive peak broadening from drifts, individual measurements were limited to 2 hours.

The mass of ^{40}Ca$^+$ can be determined from the times of flight by

$$m(^{40}\mathrm{Ca}^+) = m(^{40}\mathrm{K}^+) \cdot \frac{[t(^{40}\mathrm{Ca}^+)+t_0]^2}{[t(^{40}\mathrm{K}^+)+t_0]^2} \quad (1)$$

Generally, two species of reference ions are needed to determine t_0 – the delay between the TDC start signal and actual ion ejection from the ion trap – in Eq. 1. This delay has been measured to be $t_0 \approx 150$ ns. As such, neglecting it would introduce a systematic error of $\Delta m/m \leq 10^{-9}$, making it negligible in this case.

A set of 20 measurements of the ^{40}Ca$^+$/^{40}K$^+$ doublet were taken over the course of two days. In each, the peaks were fit by Gaussian functions to determine the ToF centers. The mass of ^{40}Ca$^+$ was then calculated using Eq. 1 with t_0 neglected. The resultant deviations from literature values are shown in Fig. 2. The weighted average deviation is Δm=-0.2(2.3) keV. From this we conclude that the fundamental accuracy limit of the MRTOF-MS is $\Delta m/m \ll 10^{-7}$.

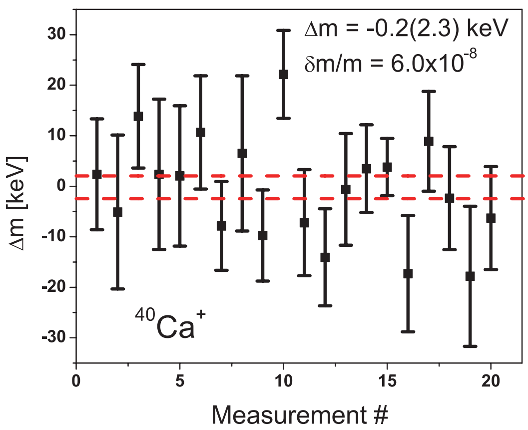

Fig. 2. Deviations of the measured mass of ^{40}Ca from the literature value[2)]. The red lines show the weighted average of the measurements.

The extremely fast nature of this measurement is particular favorable in light of a planned campaign to measure trans-uranium elements at the GARIS facility. Two of the desired first-round candidates are ^{256}Rf ($T_{1/2}$=6.5 ms) and ^{261}Bh ($T_{1/2}$=12 ms). As the required MRTOF-MS measurement time scales with the square-root of the mass, these extremely short-lived nuclei would each require merely $t \approx 5.9$ ms to achieve a similar resolving power to Fig. 1. In the future we hope to increase the resolving power while reducing the required number of laps to achieve even faster results with a wider mass bandwidth.

References

1) P. Schury et al.: RIKEN Accel. Prog. Rep. **45**, p.147 (2012)
2) G. Audi A.H. Wapstra and C. Thibault: Nucl. Phys. **A729**, p.129 (2003)

Development of an adiabatic field rotation system to measure spin polarization of unstable nuclei

Y. Ishibashi, N. Yoshida, H. Ueno, A. Yoshimi, Y. Ichikawa, Y. Abe, K. Asahi, M. Chikamori, T. Fujita, T. Furukawa, E. Hikota, D. Nagae, Y. Ohtomo, Y. Saito, H. Shirai, T. Suzuki, X.F. Yang, and N. Sakamoto

Ground-state nuclear moment measurements of unstable nuclei have been conducted by the β-ray detected nuclear magnetic resonance (β-NMR) method[1] by utilizing the fragmentation-induced spin-polarized radioactive isotope (RI) beams.[2] In this method, a resonance can be observed if both the conditions, namely production of a polarized RI beam and a resonant frequency scan of the oscillating magnetic field in β-NMR measurements, are simultaneously met, which makes the obtaining of β-NMR measurements complicated. In order to investigate the production of spin polarization separately from the resonance scan, a new adiabatic field rotation (AFR) system has been developed.[3] In this system, a static magnetic field $B_0 \sim 300$ mT is applied using a pair of permanent Nd magnets to preserve the polarization, and it can be adiabatically inverted in 150 ms by rotating the Nd magnets mechanically. Since the direction of RI spin is also inverted according to the B_0 rotation, the magnitude of spin polarization (or more correctly, the product of the spin polarization and the β-decay asymmetry parameter) can be determined through the change in the β-ray asymmetry, as done in conventional β-NMR measurements.

The performance of the system was studied with spin-polarized ^{20}F ($I^\pi = 2^+$, $T_{1/2} = 11.163$ s) nuclei produced in the ^{19}F($\vec{d}$,p)^{20}F reaction at $E/A = 7$ MeV at the RIBF facility. A spin polarized $\vec{d}$ beam was provided by a polarized ion source[4] and was accelerated by the AVF cyclotron. The $\vec{d}$ beams impinged on a CaF_2 crystal to produce polarized ^{20}F. The crystal was placed at the center of the AFR apparatus, as illustrated in Fig. 1, at room temperature. The up/down ratio R of β-rays emitted from ^{20}F nuclei was measured with a pair of plastic-scintillator telescopes positioned above and below the crystal.

Obtained ^{20}F spin polarization values with the $\vec{d}$ beams whose spin directions were “up” “down” and “unpolarized” with respect to the direction of the B_0 field, are plotted in Fig. 2. The obtained $P(^{20}\mathrm{F}) = -0.3(2)\%$ with the “unpolarized” $\vec{d}$ beam indicates a deviation from $P(^{20}\mathrm{F}) = 0$, caused by the effect of the B_0 field rotation on the efficiency changes of PMTs connected to the plastic scintillators. This effect can be reduced by placing the PMTs at a distance from the magnet. Further, corrected $P(^{20}\mathrm{F})$ values, calculated taking the $P(^{20}\mathrm{F}) = -0.3(2)\%$ effect as a common baseline shift, are also indicated by the values in red and expressed along the y-axis on the right in Fig. 2. From this analysis, we concluded that the system works as designed, despite the small baseline shift. We also note that the $\vec{d}$ beam delivered from AVF cyclotron at the RIBF facility was shown to be useful to produce spin-polarized RIs, and it was first applied in the present R&D study.

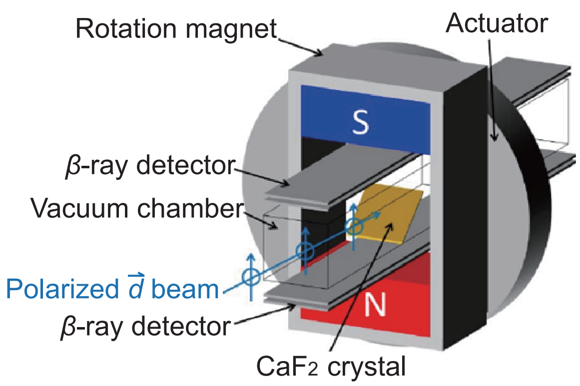

Fig. 1. A schematic layout of the adiabatic field rotation system.

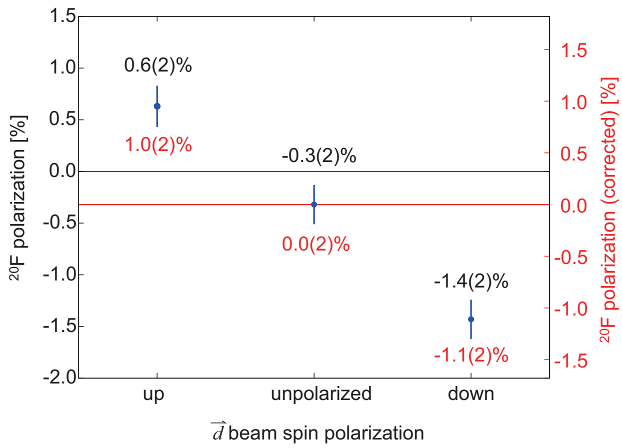

Fig. 2. Obtained polarization of ^{20}F. The values in black along the y-axis on the left are of uncorrected spin polarization, and those in red along the y-axis on the right are the corrected ones. For the correction factor, see the text.

References

1) K. Sugimoto et al.: Phys. Lett. **18**, 38 (1965).
2) K. Asahi et al.: Phys. Lett. B **251**, 488 (1990).
3) H. Ogawa et al.: Phys. Lett. B **451**, 11 (1999).
4) H. Okamura et al.: AIP Conf. Proc. **293**, 84 (1993).

Resistive surface current electrode for ion guide gas cell

H. Mita, T. Sonoda, M. Wada, H. Wollnik, S. Davila,*1 G.A. Eiceman,*1 H. Tomita, C. Sakamoto, T. Takatsuka, T. Noto, F. Arai, H. Iimura, Y. Itou, S. Naimi, P. Schury

An electric field guidance for high-energy radioactive ion thermalized in a gas cell is important for avoiding a long extraction time. A long extraction time causes severe ion losses not only due to the short life-time of radioactive nuclei, but also due to any loss processes in the gas cell, such as neutralization, molecular formation, and diffusion to the walls. Additionally, when using a large gas cell, ions are no longer efficiently directed to the small exit hole without proper electric field. Thus far, several techniques have been developed on this background, such as an rf-ion guide[1)], dc-ion guide[2)] and, recently, cyclotron-ion guide[3)]. To investigate the new technical challenge, we have developed a resistive surface current electrode for focusing ions towards the exit hole using just dc current.

Ion motion at the extraction stage near the exit in the gas cell strongly depends on the passage of ions through the small exit hole. If a simple static electric field exists, the ions follow the line of the electric force and the velocity is proportional to the electric field. In such case, for extracting ions from the exit hole to the vacuum side, it is necessary to create a line of the electric force that is terminated at the vacuum or at the region dominant by gas flow. This situation can be realized using a resistive surface current electrode, as represented by the following equation:

$$\phi = \frac{\rho i}{\pi r} \tag{1}$$

where ϕ, ρ, i, and r are the potential, electrical resistivity, surface current, and radius of the resistive surface current electrode. Since the potential is inversely proportional to the radius, the resistive surface current emulates the condition for ions swallowed up to the exit hole.

We have fabricated a resistive surface current electrode at NMSU (New Mexico State University). First we prepared a ceramic electrode whose diameter is 10 mm with a 1 mm exit hole at the center of electrode. A resistive layer and conductive layer were sprayed on the ceramic surface at the appropriate separated region.

In order to test the resistive surface current electrode, it was installed in the resonant laser ionization gas cell, which was developed for the prototype Parasitic Laser ion source (PALIS) system[4)]. In the present test, we evaluated the extraction time for the photo-ionized ions, with and without surface current on the resistive surface. The experimental setup is shown in the left side of Fig. 1.

The indium atoms are evaporated by resistance

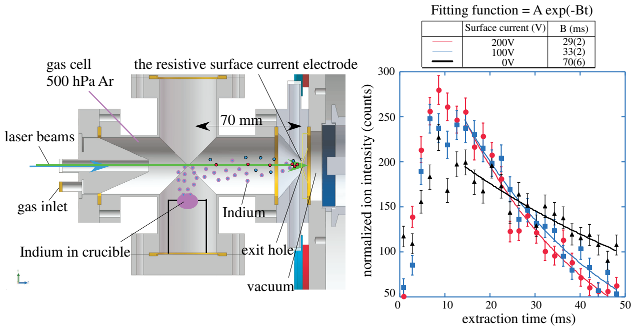

Fig. 1. The left figure shows the experimental set up for the test of the resistive surface current electrode, and the right graph shows the experimental data for the extraction time of photo ionized ions with and without the voltage for surface current.

heating transfer on the titanium crucible at the middle of the gas cell. They are transported by gas flow towards the exit hole. Two steps resonant laser ionization is performed for indium atoms. The laser beams are irradiated on the longitudinal axis of the cell, and in principle, the atoms that stay in the laser beam path are ionized anywhere inside the gas cell. However, the majority of atoms are ionized near the exit hole where they are gathered. The extraction time from the place where atoms are ionized to the vacuum where photo-ionized ions are detected was measured by recording the time period between the laser pulse and the ion detecting pulse. We clearly observed the effect of electric field on the resistive surface electrode, as shown in the right side of Fig. 1. Under higher gas pressure condition (500 hPa argon), the extraction time decreases compared to that of transported by gas flow, although there was no enhancement or reduction in ions intensity.

The resistive surface current electrode was developed for investigating a new electric field guidance in the gas cell. We will apply this new technique for future PALIS experiments.

References

1) M. Wada et al.: Nucl. Instr. Meth. B **204**, 570 (2003).
2) L. Weissman et al.: Nucl. Phys. A **746**, 655 (2004).
3) G. Bollen et al: Nucl. Instr. Meth. B **266**, 4442 (2008).
4) T. Sonoda et al.: Nucl. Inst. and Meth. B **295**, 1 (2013).

*1 New Mexico State University

An rf-carpet electrospray ion source to provide isobaric mass calibrants for trans-uranium elements

S. Naimi, S. Nakamura, Y. Ito, H. Mita, A. Ozawa, P. Schury, T. Sonoda, A. Takamine, M. Wada, H. Wollnik

As a preparation for superheavy elements mass measurement campaign at GARIS[1] with our multi-reflection time-of-flight mass spectrograph (MRTOF-MS)[2], we have build a molecular ion source to provide isobaric reference ions for all trans-uranium elements. This novel ion source is based on electrospray ionization combined with an rf-carpet[3] to collect molecular ions efficiently. The rf-carpet allows for simplification of the pumping system to transport ions from the source to the MRTOF-MS. The details of this ion source is shown in Fig. 1. To produce molecular ions a solution is prepared and then transported to the ESI capillary, where the ions experience a strong electric field resulting from the voltage difference between the latter and the transport capillary. This forms the Taylor cone, which forces the liquid to evaporate toward the capillary and allows for the formation of free molecular ions or their clusters. The ions are transported into the capillary by air flow to the rf-carpet, where they are stopped near the surface by a radiofrequency pushing rf field and driven by a dc field to the exit hole (0.5 mm diameter). The characteristics of the rf-carpet for different mass regions have been investigated[4]. High mass ions can be transported using considerably lower frequency, dc and rf amplitudes of the rf-carpet. Once extracted from the ions source the molecular ions are transported to the high vacuum region, where a quadrupole mass filter (QMS) is placed for initial mass selection. The selected ions are then send to the MRTOF-MS for analysis.

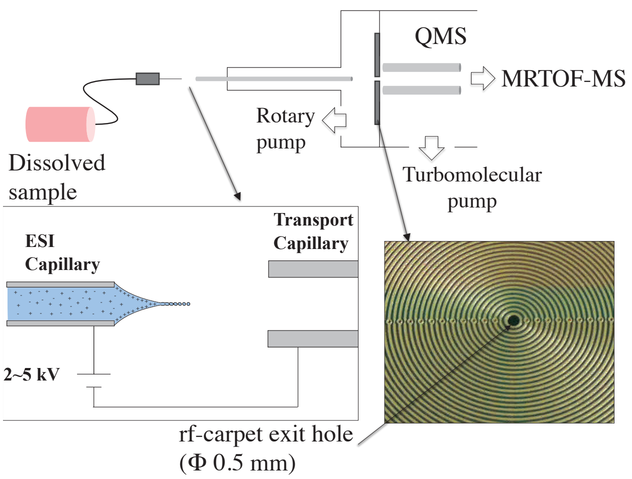

Fig. 1. Schematic overview of the new ion source, which consists of an electrospray ionization (ESI) system for ion production and an rf-carpet for ion collection. The typical distance between the two capillaries is about 2-3 cm and the diameter is about 0.25-0.5 mm.

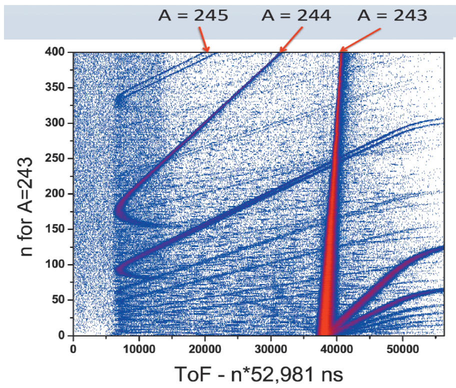

Fig. 2. Time-of-flight recorded with the MRTOF-MS for several number of reflections. At high number of reflections masses with $A = 243, 244$ and 245 were separated as well as their isobars produced with the molecular ion source. The color represents the ion intensity.

Molecular ions appropriate for isobaric references of trans-uranium elements, such as, $^{243-245}$Np, ^{243}Cf, $^{243-245}$Es, $^{243-245}$Fm and ^{245}Md, were efficiently extracted from the ion source and analyzed by the MRTOF-MS as shown in Fig. 2. We have also tested the performance of the MRTOF-MS, which could achieve 100,000 mass resolving power in only 20 ms (Table 1) for heavy masses making it the fastest and the most appropriate device for direct mass measurements of short-lived trans-uranium elements.

Table 1. Time-of-flight, peak width and the mass resolving power obtained for various molecules from the molecular ion source using 200 ppm of $C_6H_8O_7$ sample dissolved in methanol and traces of formic acid. The peak width Δt (ns) is the FWHM of the Gaussian fit.

m/z	Molecules	Time-of-flight (ns)	Δt	R_m
243	$C_{12}H_9N_3O_3^+$	20,493,142.0(0.5)	92	112,000
244	$C_{12}H_{10}N_3O_3^+$	20,482,317.1(1.8)	120	86,000
245	$C_{10}H_5N_4O_4^+$	20,469,137.7(1.4)	103	99,000
	$C_{12}H_{11}N_3O_3^+$	20,471,084.7(3.1)	138	74,000

References
1) K. Morita *et al.*, Eur. Phys. J. **A21**, 257 (2004).
2) P. Schury *et al.*, RIKEN Accel. Prog. Rep. **44**, 166 (2011).
3) M. Wada *et al.*, Hyperfine Interact. **199**, 269 (2011).
4) S. Naimi *et al.*, IJMS **337**, 24 (2013).

Investigation of the ion-surfing transport method with a circular rf carpet

F. Arai, Y. Ito M. Wada, P. Schury, T. Sonoda and H. Mita

High-energy radioactive isotopes produced in-flight can only be used in precision experiments after the decrease of their energy through collisions with a buffer gas in a gas cell. Such thermalized ions are extracted from the gas cell as a low-energy ion beam. In order to transport and extract ions quickly and efficiently, the guidance by electric fields is necessary. In this respect, an rf-carpet (RFC) method with a dc potential gradient is used as the standard technique[1]. For studies of more exotic nuclei, however, a larger RFC is required in turn requiring faster transport and simpler implementation to avoid discharge within the gas cell and mechanical complexity.

Recently, an alternative concept for ion transport by means of a traveling wave was proposed as illustrated in Fig. 1(a), called "ion surfing"[2]. This concept was experimentally realized and studied with a linear RFC[3]. An rf voltage applied to the electrodes

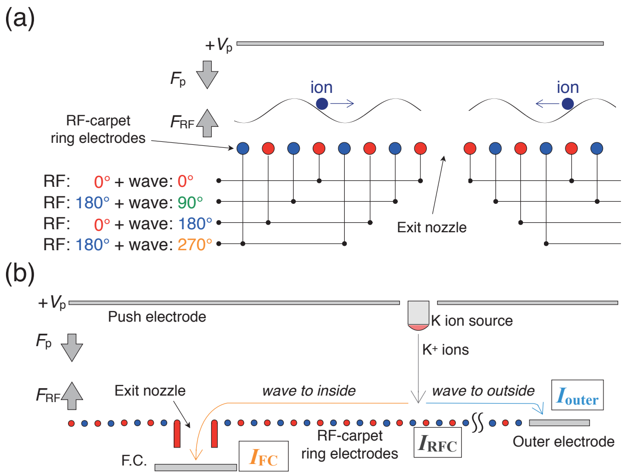

Fig. 1. (a) Concept of ion surfing with schematic of the applied rf and wave signal phases. (b) Sketch of the transport efficiency measurement method. An rf frequency f_{RF} of 9.8 MHz, AF frequency f_{AF} of 2 kHz, and helium pressure of 20 mbar were used.

with a 180° phase shift between adjacent electrodes creates an effective repelling force for the ions. In order to keep the ions just above the RFC surface, the repelling force F_{RF} needs to be balanced by a force opposite in direction, called the "push" force F_p, which can be provided by a static potential V_p. In the ion-surfing scheme, the confined ions are transported along the surface by superimposing a weak audio frequency (AF) signal that is phase-shifted by 90° on adjacent electrodes to form an overall traveling wave. Under optimal conditions, the speed of the ions approaches the wave's speed[3].

In the practical gas cell setup, the ions have to be extracted from a tiny exit nozzle. In this study, the transport and extraction of K^+ ions were tested with the experimental setup shown in Fig. 1(b), using a circular RFC with 0.5-mm-diameter nozzle; this setup has the same geometry as that used for an rf-carpet electrospray ion source[4]. The RFC consists of a planar printed circuit board with 54 ring electrodes, each 0.15 mm in diameter with 0.3 mm pitch. During the measurements, three currents were measured: the current striking the RFC electrodes I_{RFC}, the current reaching the outer electrode I_{outer}, and that of the RFQ rods behind the nozzle I_{FC}. The dc offset of the outer electrode was set to 0 V, which is the same as the RFC voltage offset, while that of the RFQ rods was floated on -55 V to extract the ions. The transport efficiency ε_{outer} was determined by the ratio I_{outer}/I_{RFC} and the transport efficiency including extraction ε_{ext} was determined by the ratio I_{FC}/I_{RFC}. The typical efficiency trends are shown in Fig. 2 as a function of the wave voltage V_{AF} at $E_p = 1$ V/mm for various rf voltages. For higher values of V_{AF}, the efficiency drops because the strong V_{AF} causes the ions to strike the RFC electrodes. The higher V_{RF} in turn leads to increase in F_{RF} and therefore, the efficiency reduction is rather suppressed. An efficiency of ~100% was obtained at $E_p = 1$ V/mm for both ε_{ext} and ε_{outer}, and at $E_p = 3$ V/mm for ε_{outer}.

We are planning to apply this method to the SLOWRI gas cell with improved geometry in FY2013.

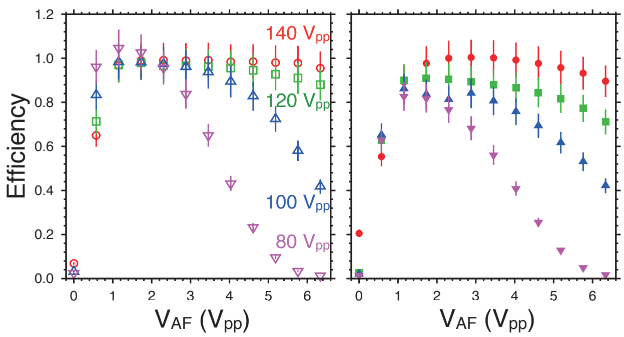

Fig. 2. Experimental results for ε_{outer} (left) and ε_{ext} (right) at $E_p = 1$ V/mm for each rf voltage V_{RF}.

References
1) M. Wada *et al.*: Nucl. Instr. Meth. **B204** 570 (2003).
2) G. Bollen: Int. J. Mass Spectrom. **299** 131 (2011).
3) M. Brodeur *et al.*: Int. J. Mass Spectrom. **336** 53 (2013).
4) S. Naimi *et al.*: Int. J. Mass Spectrom. **337** 24 (2013).

Development of the KISS gas cell

Y. Hirayama,[*1] N. Imai,[*1] H. Ishiyama,[*1] S.C. Jeong,[*1] Y.H. Kim,[*1] H. Miyatake,[*1] M. Mukai,[*1] M. Oyaizu,[*1] Y.X. Watanabe,[*1] Y. Matsuo, T. Sonoda, M. Wada, M. Huyse[*2], Yu. Kudryavtsev[*2], and P. Van Duppen[*2]

We have constructed the KEK Isotope Separation System (KISS) to study the beta-decay properties of neutron-rich isotopes with a neutron number around $N = 126$ from the astrophysical viewpoint.[1)] A gas cell filled with argon gas at a pressure of 50 kPa, which stops and collects unstable nuclei, is used in conjunction with a laser resonance ionization technique essential for selectively extracting isotopes of interest. We have reported the results of the offline and online tests to investigate the performance of the KISS gas cell.

We successfully extracted a stable nickel (which evaporated from a nickel filament placed in the gas cell) ion-beam, ionized using the laser resonance ionization technique at the offline test.[2)] By using an nickel beam with the energy of 28 kV, we optimized the RF and DC voltages of the SextuPole Ion Guide (SPIG) for cooling and extracting the beam, and obtained the mass-resolving power of 900, which is sufficient for selecting only ions having the mass numbers of interest to us.[3)]

Plasma induced by primary beam irradiation into the gas cell is supposed to reduce the ionization efficiency and selectivity. In order to measure the absolute extraction efficiency and selectivity of the KISS under the plasma induced by a primary beam, it was necessary to perform an online test and measure the efficiency and selectivity as a function of the primary beam intensity. For the online test using ^{56}Fe, we performed an offline test using an iron filament to identify the ionization scheme of the iron element and to measure the mass distribution.

We tried to identify a new efficient ionization scheme for the iron element. As a result, it was discovered that the transition of $3d^64s^2$ (J=4) $\rightarrow$ $3d^64s4p$ (J=5) (λ_1 =248.402 nm) $\rightarrow$ auto ionization state (λ_2 =423.784 nm) is an efficient ionization scheme. The strength of the transition to the excited state is one order of magnitude stronger than the early established ionization scheme. The saturation power for the 1st step laser (λ_1) was only 15 μJ/pulse, which was easily available in the present laser system.

We measured the mass-distribution in the region of A =40∼120 in the offline test, and found that the intensities of iron isotopes (A =54, 56, 57, and 58) were consistent with the natural abundances. An amount of 30% of iron isotopes formed hydrates such as $Fe(H_2O)_n$ (n =1, 2, and 3). In order to reduce the amount of the hydrates and improve the extraction efficiency, it was necessary to refrigerate the gas cell and argon gas down to ∼100 K for freezing water molecules. The design of a cryogenic gas cell is in progress.

We prepared two types of gas cells to study the plasma effect and determine the proportion of the primary beam that can be implanted into the gas cell. One is a simple "straight type" gas cell, which is affected by the plasma effect. The other one is a "bent type" gas cell, which is designed to reduce the plasma effect. In the first online test, we used the "straight type" gas cell, and in the next step, we plan to use the "bent type" gas cell.

We performed the first online test using ^{56}Fe with an energy of 90 MeV/nucleon and an intensity of 1 pnA. To implant the ^{56}Fe beam at the center of the gas cell, the energy of ^{56}Fe was degraded to about 1 MeV/nucleon at the entrance of the gas cell using aluminum degraders (2.65 mm in thickness). The beam intensity at the center of the gas cell was reduced to 0.2% of that upstream of the degraders.

The intensity of the extracted ^{56}Fe was measured with and without the irradiation of the ionization laser. However, the intensity was insensitive to the laser irradiation. This indicates that no neutral atom of ^{56}Fe was ionized by the laser. It was thought that the implanted ^{56}Fe atoms formed impurity molecules in the gas cell. In the mass distribution with the region of A =40∼250 measured in the online test, we observed intense peaks of impurity molecules at each mass number. We reproduced almost the same mass-distribution by irradiating the α-particles emitted from the ^{241}Am source in the offline test. It is supposed that the argon ions induced by the α-particles or ^{56}Fe beam combine with hydrocarbons and water molecules.

The reason for the observation of no ^{56}Fe ions is that during the neutralization process of the ^{56}Fe ion, this ion became a molecular ion combined with a hydrocarbon and/or a hydrate, and consequently, the molecular ion became neutralized. By baking the gas cell system and inserting an additional molecular filter in the gas supply line, we have cleaned the gas cell and the gas supply line in order to measure the ^{56}Fe ions ionized by the laser irradiation. The impurity level is expected to become about 0.1 ppb. After the cleaning, we plan to conduct the performance tests using "straight type" and "bent type" gas cells.

References
1) S.C. Jeong et al.: KEK Report 2010-2.
2) H. Ishiyama et al.: RIKEN Accel. Prog. Rep. **45** (2012) 151.
3) M. Huyse et al.: Nucl. Instru. and Method **B187** (2002) 535.

[*1] High Energy Accelerator Research Organization (KEK)
[*2] Instituut voor Kern-en Stralingsfysica, KU Leuven, Belgium

Improvement of the fluorescence detection system operation for laser spectroscopy of RI atoms in superfluid helium OROCHI

H. Tetsuka, T. Wakui, T. Furukawa, X. F. Yang, K. Imamura, Y. Yamaguchi, T. Fujita, Y. Tsutsui, Y. Mitsuya, Y. Ichikawa, Y. Ishibashi, N. Yoshida, H. Shirai, M. Hayasaka, Y. Ebara, S. Arai, S. Muramoto, A. Hatakeyama, M. Wada, T. Sonoda, Y. Ito, T. Kobayashi,[*1] S. Nishimura, M. Nishimura, Y. Kondo, K. Yoneda, H. Uemastu,[*2] H. Ueno, T. Shinozuka,[*3] T. Shimoda,[*4] K. Asahi, and Y. Matsuo

We have developed a new nuclear laser spectroscopic technique in superfluid helium (He II). We call this method OROCHI (which denotes optical radioisotope atom observation in condensed helium as ion-catcher). Owing to a considerable wavelength difference between the fluorescence and excitation wavelength in He II, the use of wavelength-separation filters can greatly reduce the background, which mainly originates from the excitation laser in the fluorescence detection system.[1)] We have succeeded in observing laser induced fluorescence (LIF) from ^{87}Rb (energy: 66A MeV) atoms stopped in He II.[2)] However, the reduction of the background due to stray laser light remains insufficient for the observation of low-yield radioactive isotopes (RIs). We report here two major revisions in the fluorescence detection system operation: (1) improvement of the laser beam shape and (2) optimization of the laser beam path.

Figure 1 shows a schematic diagram inside a 1.5-K bath of a helium cryostat.[3)] The distance between an RI-beam port and the laser beam path is 7.5 mm. Since the laser initially had poor beam quality, its outer lobe hit the port, producing intense stray light. In order to solve this problem, we adjusted a laser resonator to provide a laser light having a profile close to a Gaussian shape. Further, we covered the port with a shield made of black alumite, which has low reflectivity. As a result, the intensity of the stray laser light was reduced to 4.0×10^3 cps at 100 mW from 5.6×10^4 cps in the previous experiment, conducted in 2010.

The intensity of the stray laser light as a function of the laser position, measured after these improvements, is shown in Fig. 2. In spite of the improvements, two background peaks were still observed at $x = -5.0$ mm and -1.1 mm. The increase at $x = -5.0$ mm was found to originate from laser beam scattering at the port because the transmitted power was reduced. The increase at $x = -1.1$ mm was considered to be due to laser light reflection from optical windows because there was no indication of laser power loss. At the other laser position, the intensity remained reasonably small. This result enabled us to observe the Zeeman resonances of introduced Rb isotopes, not only the primary ^{85}Rb but also the radioactive ^{84}Rb in September 2012.[4)] The minimum beam intensity required for the measurement was estimated to be 10^3 pps.

To address the observed lower yield RIs, we plan to reduce the stray laser light by painting the inside of the 1.5-K bath black.

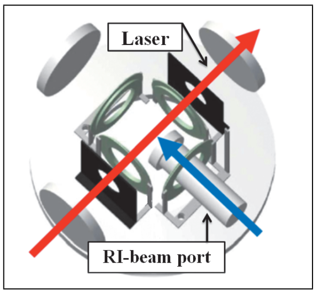

Fig. 1. Schematic diagram of 1.5-K bath. The RI beam is injected from the lower right. Laser light perpendicular to the RI beam passes through the bath. The diameter of laser beam is approximately 1.5 mm.

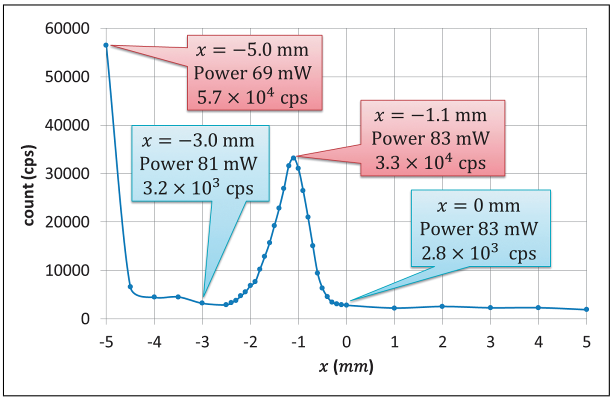

Fig. 2. Count of stray laser light as a function of the laser position along the horizontal direction. The position $x = -7.5$ corresponds to the center of the 1.5-K bath. The RI-beam port is located at $x = -7.5$ mm.

References
1) A. Sasaki et al.: RIKEN Accel. Prog. Rep. **44**, 204 (2011).
2) T. Furukawa et al.: J. Phys. Conf. Ser. **302**, 012054 (2011).
3) K. Imamura et al.: In this report.
4) T. Furukawa et al.: In this report.

*1 Laser Technology Laboratory, RIKEN
*2 Department of Physics, Tokyo Gakugei University
*3 Cyclotron Radioisotope Center (CYRIC), Tohoku University
*4 Department of Physics, Osaka University

Control of stopping position of Rb beam in superfluid helium for nuclear laser spectroscopy of RI atoms in OROCHI

X.F. Yang, T. Furukawa, T. Wakui, K. Imamura, H. Tetsuka, T. Fujita, Y. Yamaguchi, Y. Tsutsui, Y. Mitsuya, Y. Ichikawa, Y. Ishibashi, N. Yoshida, H. Shirai, Y. Ebara, M. Hayasaka, S. Arai, S. Muramoto, A. Hatakeyama, M. Wada, T. Sonoda, Y. Ito, T. Kobayashi, S. Nishimura, M. Nishimura, Y. Kondo, K. Yoneda, H. Ueno, T.Shinozuka,[*2] T. Shimoda,[*1] K. Asahi, and Y. Matsuo

In order to investigate the structures of exotic nuclei of extremely low yields by measuring nuclear spins and moments, our group has developed a new laser spectroscopy technique for the Optical Radioisotope atom Observation in Condensed Helium as Ion-catcher (OROCHI) system. Our technique has been demonstrated as feasible by means of a considerable amount of off-line and on-line R&D studies[1)2)].

In the online study, the stopping position of atoms in He II is crucial for the success of the experiment, because the maximum volume of the observation region for the photon detection system is only $5 \times 2 \times 2mm^3$. The degree of control should be sufficiently accurate to stop the atoms just on the line through which the laser passes, and this can be achieved by a system mainly comprising an degrader and two plastic scintillators, as shown in Fig.1a). The degrader used to control the energy of RI beams is made of aluminum foils whose thickness can be adjusted from 0 μm to 800 μm in steps of 12.5μm. One plastic scintillator with two PMTs (Tr-PL) placed in a pre-cryostat chamber is used to count the ions introduced into the chamber. Another one (He-PL) located at the center of the cryostat is used to check the stopping position of atoms. This system functioned as designed with respect to the stopping position of an ^{87}Rb beam (energy: 66MeV/u) directly introduced into He II in a previous experiment[2)].

In the comparison of the measured stopping range with that calculated using with the LISE++[3)], the Ziegler code is found to be more applicable for our beam energy[4)]. Based on the LISE++ calculation, we found that most of the unstable Rb isotopes produced by the projectile-fragment reaction of a ^{85,87}Rb beam at E/A = 66 MeV cannot reach the observation region in He II. Some upgrades of the setup were made to modify the length of the air gap from 75 *cm* to less than 40 *cm*, which can promise that the secondary beam of ^{84,85}Rb can reach the laser beam in He II.

The experiment was carried out for ^{84,85}Rb beams with RIPS, in which the performance of the stopping-position control system of Beams in He II was investigated. The actual procedure conducted with the ^{85}Rb beam was as follows: First, from a prior LISE++ calculation, we estimate the appropriate degrader thickness as 312.5 μm for stopping ^{85}Rb at the center of He II, where the Rb beam-path length was 7.5 mm; subsequently, during beam time, the relationship between the ratio of counts from He-PL (N_T) to Tr-PL (N_H) and the degrader thickness was obtained. From the measurement, the optimum Al degrader thickness fell in the range of 300 $\sim$ 350 μm; Finally, we counted the number of laser induced fluorescence (LIF) photons (N_L) from the stopped atoms to determine the stopping position. The peak position in Fig. 1b) yields a the degrader thickness of 337.5 μm, which corresponds to the thickness at which accelerated atoms are stopped at right position. For the isotope ^{84}Rb, we performed a similar procedure to obtain a degrader thickness value of 50 μm, which is fairly consistent with the LISE++ calculation result. Based on the exact determination of the stopping position, we performed the OROCHI experiment and succeeded in observing the polarization of ^{84,85}Rb atoms immersed in He II[5)].

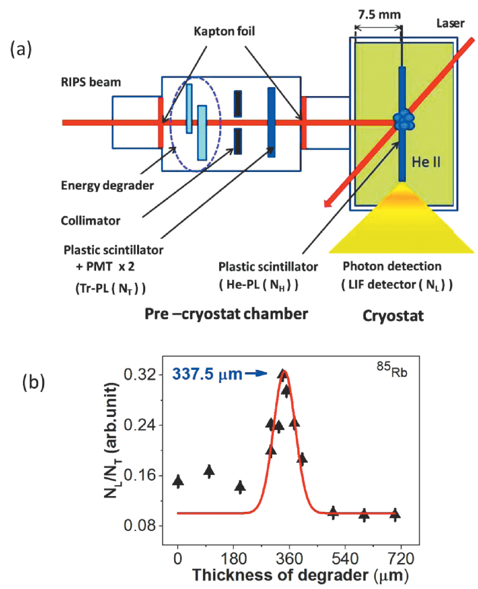

Fig. 1.: a) Schematic view of the system. b)Relationship between N_T/N_L and degrader thickness. The peak value provides gives the thickness corresponding to the stopping position of the control system for the online experiment

*1 Department of Physics, Osaka University
*2 Cyclotron Radioisotope Center, Tohoku University

References
1) T. Furukawa et al.: Hyp . Int. **196**, 191 (2010).
2) T. Furukawa et al.: J.Phys **302**, 012054 (2011).
3) O. Tarasov et al.: Nucl. Instr. Meth. B 266, 4657(2008).
4) J.F. Ziegler et al.: Pergamon Press, NY, 1985.
5) T. Furukawa et al.: submitted to RIKEN. Acc. Prog.

Development of a laser system towards optical pumping of various elements in OROCHI experiment

Y. Yamaguchi, H. Tomita, T. Furukawa, C. Sakamoto, T. Kobayashi, M. Tachikawa,*[1] K.D.A. Wendt,*[2] and Y. Matsuo

We are developing a laser system for OROCHI (Optical RI-atom Observation in Condensed Helium as Ion-catcher) experiment for the study of elements of unstable nuclei in superfluid helium (He II) using optical pumping and laser-radio frequency/microwave double resonance. In He II, the line width of excitation spectrum spreads by the effect of surrounding helium atoms and multiple energy levels of atoms are excited at the same time even with a single frequency laser. Using this feature, we succeeded in reproducing the nuclear magnetic moments and the spins of stable alkali atoms (Rb, Cs) in He II[1)] and also in generating the spin polarization of group 11 elements (Ag, Au)[2)]. We are now planning to generate spin polarization for multi-electron atoms like group 13 elements (Al, Ga, In) whose energy levels are complex[3)]. Output power of a few hundred mW is required to generate spin polarization in He II. For these purposes, we started to construct a new light source which can be operated within a wide wavelength range from visible to ultraviolet by a combination of Ti:Sapphire laser with intracavity Second Harmonic Generation (SHG).

As a first step, we built a laser cavity to obtain the excitation wavelength (370 nm) of indium (In) atom in He II. The basic design of a Ti:Sapphire laser is based on a group of Mainz University[4)]. Figure 1 shows the present laser cavity composed of a Ti:Sapphire crystal, a birefringent filter, a focusing lens and a SHG crystal (LBO). The operation scheme of this laser cavity oscillation is the following. Ti:Sapphire crystal is excited by a pulsed Nd:YLF laser (wavelength 527 nm, repetition rate 100 Hz-10 kHz, pulse width 200 ns) and a fluorescence from Ti:Sapphire crystal is amplified in the crystal during a round trip among mirrors M1 to M4. Amplified light passes through LBO crystal and the second harmonic light is generated. The second harmonic light is reflected out from the cavity by a dichroic mirror and we can obtain the second harmonic output.

We measured the power of the second harmonic when the wavelength was tuned from 740 nm to 770 nm with a birefringent filter at the input power of Nd:YLF laser of 5 mJ/pulse (Fig.2). We found the maximum power was 136 mW at 380 nm and the conversion efficiency of the output power to the pump laser power was in a range of 2.1-5.6%. The power at the excitation wavelength of In atom in He II (370 nm) was 93 mW, enough intense for our experiment.

*1 Department of Physics, University of Meiji
*2 Institute of Physics, Mainz University

In future, we are planning to conduct optical pumping of In atom in He II using this laser system. For this purpose, we are going to extend available wavelength range through the optimization of the laser cavity.

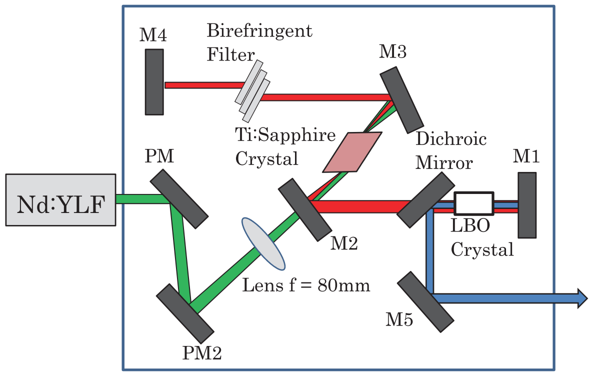

Fig. 1. The present setup of the cavity with Ti:Sapphire crystal and an intracavity SHG crystal (LBO).

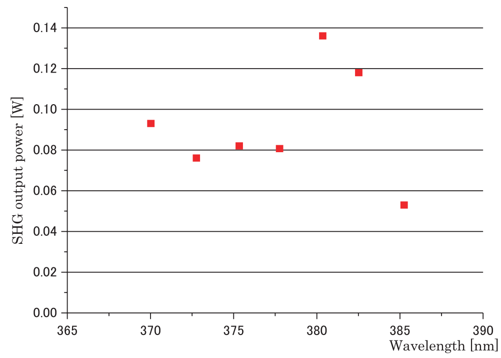

Fig. 2. Wavelength dependence of the output power of the second harmonic light.

References

1) T.Furukawa et al.: Phys.Rev.Lett. **96**, 095301 (2006)
2) T.Furukawa et al.: RIKEN Accel.Prog.Rep.42 194(2009)
3) Y. Kato et al.: RIKEN Accel. Prog. Rep. 44 242 (2011)
4) J.Yi et al.: Jpn. J. Appl. Phys. Vol. 42 (2003) pp5066-5070.

Development of a superfluid helium cryostat for OROCHI project

K. Imamura, T. Furukawa, T. Wakui, X. F. Yang, Y. Yamaguchi, H. Tetsuka, Y. Mitsuya, Y. Tsutsui, T. Fujita, Y. Ebara, M. Hayasaka, S. Arai, S. Muramoto, Y. Ichikawa, Y. Ishibashi, N. Yoshida, H. Shirai, A. Hatakeyama, M. Wada, T. Sonoda, Y. Ito, H. Odashima,[*1] T. Kobayashi,[*2] H. Ueno, T. Shinozuka,[*3] T. Shimoda,[*4] K. Asahi, and Y. Matsuo

We have been developing a new nuclear laser spectroscopic system for the Optical Radioisotope atom Observation in Condensed Helium as Ion-catcher (OROCHI)[1)] system that can be applied to the study of the nuclear structure of short-lived and low-yield unstable nuclei produced at accelerator facilities. OROCHI is based on a method combining superfluid helium and the laser spectroscopic technique. We use superfluid helium (He II) as a stopping material for an accelerated ion beam. We use the laser・radio frequency/microwave(RF/MW) double resonance method to measure Zeeman splitting and hyperfine structure splitting, and we determine the nuclear spin and moment that reflect nuclear structure. In OROCHI, the cryostat is a key apparatus not only for realizing a He II environment but also for performing laser spectroscopy experiments. Figure 1 shows the schematic layout of our cryostat.

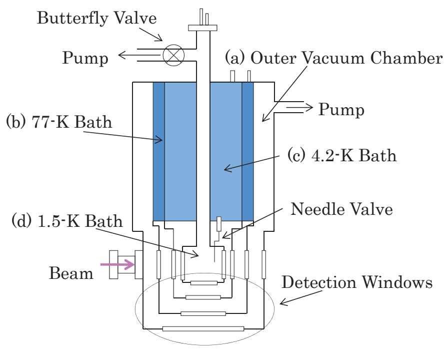

Fig. 1. Schematic layout of the cryostat of the OROCHI system

This cryostat consists of four baths. the basic structure of the cryostat consists of the following. (a) an outer vacuum chamber that prevents thermal radiation from the outer wall, (b) a liquid-nitrogen bath (77-K bath) filled with liquid N_2 to suppress the evaporation of liquid He, (c) a liquid-helium bath (4.2-K bath) that is filled with liquid He that also supplies liquid He to the superfluid helium bath, and (d) a superfluid helium bath (1.5-K bath), which is the most important part of our cryostat that acts as an observation region. Helmholtz coils and RF/MW antennas for the double resonance experiment are installed in the 1.5-K bath (Fig. 2).These instruments are located at positions such that they do not disturb the laser path in order to prevent the production of intense scatter light that can cause a large background signal.

For stable operation of the OROCHI system, it is important to a maintain stable environment in the 1.5-K bath and to keep He liquid for a long time in the 4.2-K bath. It is also necessary to keep detection windows clear in order to reduce the detection efficiency. To fulfill these requirements, the cooling procedure of the system was carefully followed step-by-step. After we archived the appropriate He II environment, we monitored the 1.5-K bath, the 4.2-K bath, and the outer vacuum chamber using GPIB-controlled measurement instruments. We were able to stabilize the 1.5-K bath environment using a GPIB-controlled needle valve and a butterfly valve. Consequently, we realized the experimental conditions described below: (a) Continuous operation time with a single liquid-He transfer after 19 h to obtain a stable He II condition in the 1.5-K bath. As regards the continuous operation time in this work, we successfully extended it to twice as long as that in our previous work[2)]. (b) Achievement of stable of temperature and pressure conditions at 1.79 ± 0.02 K, 12 ± 2 Torr in the 1.5-K bath, respectively. (c) Stable maintenance of the outer vacuum chamber pressure at 10^{-7} Torr. After these improvements, we could successfully measure the Zeeman splittings of ^{85,84}Rb using this cryostat.

For further stability of the system, an automatic controlling system for the cryostat and liquid helium transfer is under development.

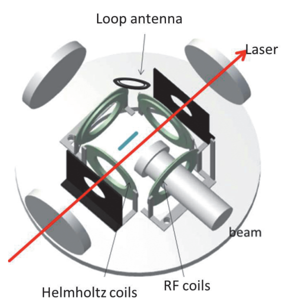

Fig. 2. Schematic of layout within the 1.5-K bath

*1 Department of Physics, Meiji University
*2 Laser Technology Laboratory, RIKEN
*3 Cyclotron Radioisotope Center (CYRIC), Tohoku University
*4 Department of Physics, Osaka University

References

1) T.Furukawa et al.: Hyp. Int. **196**, 191 (2010).
2) T.Furukawa et al.: J. Phys.: Conf. Ser. **302**, 012054 (2011).

In-beam commissioning of the EURICA array

P.-A. Söderström, S. Nishimura P. Doornenbal, G. Lorusso, T. Sumikama, H. Watanabe, Z.Y. Xu, H. Baba, F. Browne, S. Go, T. Isobe, H.-S. Jung, I. Kojouharov, N. Kurz, Z. Li,[*1] T. Nakao,[*2] H. Nishibata, M. Nishimura, A. Odahara,[*3] H. Sakurai, H. Schaffner, T. Shimoda,[*3] V. Werner,[*4] A. Yagi, and K. Yoshinaga

Spectroscopy experiments with both fast and stopped beams using the BigRIPS and ZeroDegree Spectrometer are well established at RIBF. To further increase the γ-ray detection efficiency in this kind of experiment, the EURICA (Euroball-RIKEN Cluster Array) project was proposed in 2011. Having one of the highest-efficiency γ-ray detectors existing coupled to the world's most intense in-flight radioisotope beams creates a unique opportunity for the worldwide nuclear physics community. At the end of 2011 and beginning of 2012 the EURICA array was assembled at RIKEN from twelve Euroball IV HPGe cluster detectors[1)], the RISING stopped-beam electronics and support structure[2)]. A fully automated filling system connected from the 7000 liter CE tank outside of the RIBF building to a new buffer tank at the F11 area, where EURICA is located, was constructed for the cooling of the EURICA array. A new high-voltage system, powered by an uninterrupted power supply, was installed, facilitating remote control of the high voltage to each individual crystal.

In-beam commissioning of the EURICA array and ancillary detectors was performed in March and April, 2012. In total, four days of beam time were devoted to the commissioning, using a primary beam of ^{18}O at an energy of 230 MeV/nucleon. Commissioning of the cluster detectors was carried out during one day out of the two-day beam-time starting in March. In this experiment a WAS3ABi (Wide-range Active Silicon Strip Stopper Array for β and Ion detection) prototype consisting of two double-sided silicon-strip detectors (DSSSD) was used to stop the beam. The main purpose of this commissioning was to verify that the cluster detectors were working for energy and lifetime measurements of isomeric states and that it was possible to correlate energies of γ rays to a preceding β decay in the DSSSDs. For this part, BigRIPS and the ZDS were tuned for the ^{16}N and ^{15}C nuclei following fragmentation of the primary beam.

Requested trigger was provided by silicon "OR" beam, only beam, and a 1 Hz clock for DAQ synchronization. The beam trigger was faster than a cluster self-trigger by $\sim$ 160 ns. The cluster self-trigger was faster than a DSSSD trigger by $\sim$ 400 ns. Difference in the trigger times are seen as a double prompt structure in the two-dimensional plot in Fig. 1 and can be used for fast verification that the triggering works as intended.

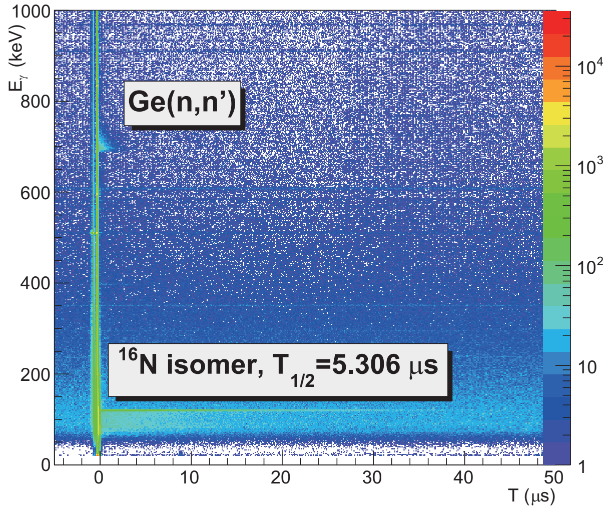

Fig. 1. Energy-time spectrum of the γ-rays from the commissioning experiment showing the $0^- \rightarrow 2^-$ transition in ^{16}N and neutron-scattering on the HPGe clusters.

The $0^- \rightarrow 2^-$ isomeric transition in ^{16}N, with an energy of 120.42 keV and a lifetime of 5.25(6) μs[3)], was selected to verify EURICA's ability to measure isomeric lifetimes. The lifetime was extracted from an energy-time matrix, shown in Fig. 1, constructed from the time difference between the clusters and the final ZDS scintillation detector. We derive a lifetime for the 0^- isomer in ^{16}N of 5.306(28) μs, in agreement with literature data.

References
1) J. Eberth et al.: Prog. Part. Nucl. Phys., **28**, 495 (1992)
2) S. Pietri et al.: Acta Phys. Pol., **B38**, 1255 (2007)
3) J. A. Beckeret al.: Phys. Rev., **155**, 1089 (1967)

*1 School of Physics and State key Laboratory of Nuclear Physics and technology, Peking University, China
*2 Center for Nuclear Study, University of Tokyo, Japan
*3 Department of Physics, Osaka University, Japan
*4 Wright Nuclear Structure Laboratory, Yale University, USA

WAS3ABi: The beta-counting system for the EURICA project

S. Nishimura, G. Lorusso, Z. Xu,[*1] J. Wu, R. Gernhäuser,[*2] H.S. Jung, Y.K. Kwon,[*3] Z. Li,[*4] K. Steiger,[*2] H. Sakurai

The new beta-counting system WAS3ABi (Wide-range Active Silicon-Strip Stopper Array for Beta and ion detection) has been developed and employed for β-decay spectroscopy of very neutron-rich nuclei in conjunction with the EURICA spectrometer. The system consists of eight double-sided silicon-strip detectors DSSSDs (Canberra Model PF-60CT-40CD-40*60) with sixty 1-mm strips and forty 1-mm strips in horizontal and vertical axes, respectively. Highly segmented position-sensitive DSSSDs with 14400 1-mm^2 pixels enable us to associate the implanted fragments and their subsequent β-decays precisely. Every two x-strips of the last four DSSSDs were combined owing to limited number of readout electronics. The DSSSDs were supported by four aluminum rods and stacked inside an aluminum chamber with a thickness of 0.2 mm located in the EURICA (See Figure 1). The WAS3ABi chamber was maintained at a temperature of 10 °C by injecting cooled dry-nitrogen gas for noise reduction in the DSSSDs. A scintillation detector (Bicron BC-400: dimension of 60 × 40mm ^{2}, 50 mm) was installed 3 mm downstream of the last DSSSD as Q_β calorimeter. The charge-sensitive preamplifier (Clear-Pulse CS-520) and shaping amplifier (CAEN N568B) were employed to achieve high detection efficiency of low energy β-rays below 100 keV[1)]. Inverted signals of the shaping amplifiers with shaping time of 0.2 μsec were fed into CAMAC leading-edge discriminators (LeCroy 3412, 4413) to obtain a β-decay trigger and timing information.

One of our challenges was to perform position reconstruction of fragments in the DSSSDs by selecting strips whose timing was faster than the expected time walk in the discriminators.

Figure 2 shows the hit distribution of the 2^{nd} DSSSD deduced by selecting the strip with the fastest timing in the horizontal and vertical axes after time-offset calibration. Timing of the neighboring strips show delayed timing as is expected owing to relatively lower energy deposited, although these strips had overflows in the ADC. The position reconstruction was confirmed by studying the correlations of timing and pulse height among the DSSSDs.

The first EURICA campaign with ^{238}U beam was conducted successfully with the new beta-counting system WAS3ABi in November-December 2012[2,3)]. Analysis of data is in progress.

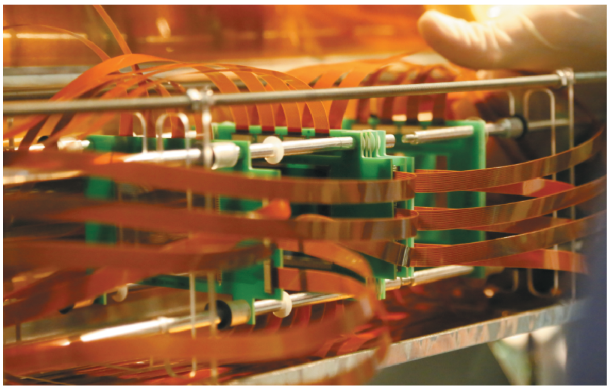

Fig. 1. Side view of WAS3ABi with eight DSSSDs. Aluminum rods were disconnected at the central position for the installation of the DSSSDs[4)].

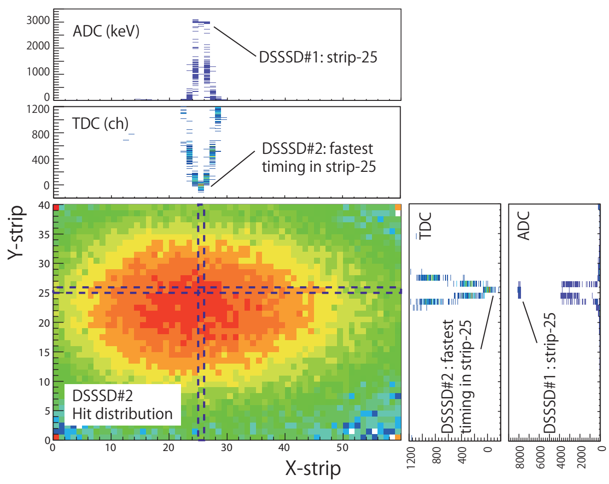

Fig. 2. Position reconstruction of heavy fragments in the WAS3ABi. The ADC and TDC values are presented as function of strip number for 1^{st} and 2^{nd} DSSSD, respectively. Maximum pulse-height is observed in the strip (strip 25) of 1^{st} DSSSD, when fastest timing is required in same position of the 2^{nd} DSSSD.

References

1) N. Uematsu and S. Nishimura: RIKEN Accel. Prog. Rep. **41**, 151 (2008).
2) Z. Xu et al, in this report.
3) G. Lorusso et al, in this report.
4) Four DSSSDs provided by the RISP Project at IBS.

*1 University of Tokyo, Japan
*2 Technische Universität München, Germany
*3 Institute for Basic Science, Korea
*4 Peking University, China

EURICA HPGe cluster array characterisation

F. Browne, P. Doornenbal, G. Gey, S. Nishimura, P.-A. Söderström, Zs. Vajta, H. Watanabe, Z. Y. Xu, H. Baba, I. Kojouharov, N. Kurz, T. Isobe, G. Lorusso, H. Sakurai, H. Schaffner, T. Sumikama, J. Taprogge, and J. Wu

Developments in high-resolution and -efficiency HPGe detector arrays in conjunction with increasingly sophisticated accelerator facilities elucidate ever further, through γ-ray spectroscopy, the structures of nuclei at the limits of stability. In recent years the RISING stopped beam campaign at GSI, Darmstadt, Germany has demonstrated the effectiveness of such configurations[1]. At the RIBF, 12 of the RISING cluster detectors are coupled to its world-leading accelerator and fragment separator facilities to measure isomeric and β-delayed γ radiation from exotic nuclei. Each of the Clusters comprises 7 individually encapsulated, tapered hexagonal crystals in a close-pack formation, where the face of each Cluster is $\sim$20 cm from the center of the Wide-range Active Silicon Strip Stopper Array for β and Ion (WAS3ABi) active stopper.

Advantages of a Cluster detector include, through the use of an add-back algorithm, the reconstruction of Compton scattered events between crystals. If multiple events are recorded in the same Cluster within a $\sim$400 ns time window the energies of the events are summed and treated as a single event, this increase the overall array efficiency, as shown in Fig. 2. The increase in efficiency arises through the improved peak-to-total performance facilitated by the add-back routine, the background suppression is shown in Fig. 1.

Efficiency measurements were carried out using a 19 kBq source placed at the center of the array. The acquisition trigger was provided by a 1 kHz clock, which opened a 110 μs gate. Deadtime effects were negated since the time difference between each trigger, 1 ms, was much greater than that of the measured deadtime of the system, $\sim$300 μs. Resolution and peak-to-background characteristics were determined using a ^{60}Co source.

At 1332.5 keV the individual Cluster FWHM was, on average, $\sim$2 keV, whereas the full array resolution was $\sim$3 keV. The peak-to-total ratio of the full-energy peaks at 1173 and 1333 keV relative to the total number of counts was 16.3%, after the add-back algorithm was implemented, this value increased to 25.8%. Figures 1 and 2 show the efficacy of the add-back routine in increasing the detection efficiency. It is obvious that at lower energies more total absorption will occur with no prior scattering, so if these absorptions were to be in coincidence with a low energy background then the add-back routine would determine the event as a higher energy γ ray, thus lowering efficiency, shown in Fig. 2.

Although the points in Fig. 2 were calculated without any form of stopper in place. Studies show that the efficiency reduction with WAS3ABi in place are $\sim$10% for E_γ < 100 keV, and $\sim$5% for energies between 244 and 488 keV, with no appreciable difference at the higher energies. However, even with WAS3ABi in place the array provides a ten fold increase of efficiency at an energy of 662 keV and 100 times the efficiency for γ-γ coincidences than the previous Clover array.

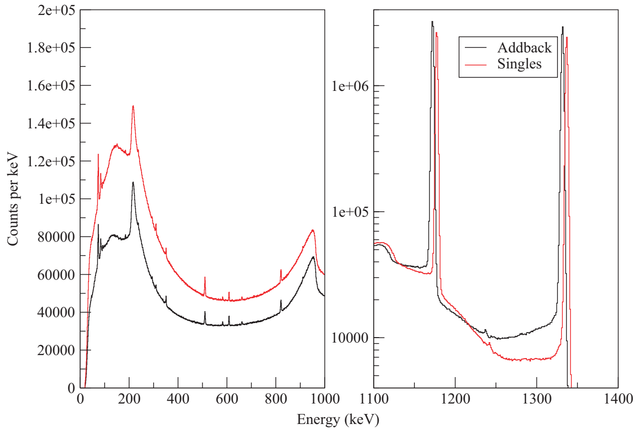

Fig. 1. Spectra from a ^{60}Co source. Left panel is Compton background, suppression due to add-back is evident. Right panel shows the 1173 and 13323 keV transitions, singles spectrum offset by +5 keV to accentuate the effect of add-back.

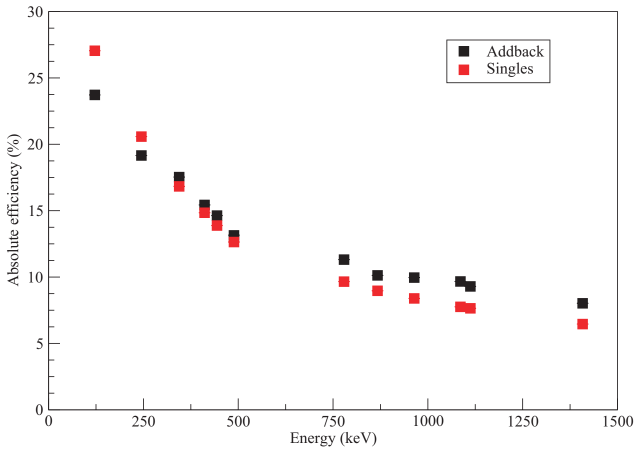

Fig. 2. Absolute efficiency of EURICA over a range of energies. Measured using an ^{152}Eu source placed at the center of the array.

References
1) S. Pietri et al: Acta Phys. Pol., B38 1255 (2007)

SCRIT electron spectrometer†

T. Suda, T. Adachi, T. Miyamoto, S. Wang, K. Yanagi, and T. Tamae

A magnetic spectrometer is being constructed for the world's first electron scattering experiments off short-lived nuclei at the SCRIT electron scattering facility. The spectrometer will enable us to measure the cross section for elastic electron scattering, from which we can determine the charge density distributions of unstable nuclei for the first time.

A reasonably good momentum resolution, $\Delta p/p \sim 10^{-3}$, is required for the spectrometer to resolve elastic and inelastic scattering. In addition, there are several requirements for the spectrometer as listed below, which are particularly important for low-luminosity electron scattering experiments. They include,

(1) a wide scattering angle coverage.
(2) a large azimuthal angle coverage.
(3) a long-target acceptance.

Requirement (1) is necessary to measure elastic cross section under a wide scattering angle at once, since the precise determination of angular dependence of the cross section is essential for this study. Requirement (2) is obviously important for low-luminosity experiments. Due to the fact that the SCRIT provides a long target of 40 cm, the spectrometer must accept scattered electrons from an extended target region. Considering these requirements, the spectrometer has been carefully designed[1]. Its construction started in the beginning of FY 2012.

The spectrometer employs a dipole magnet whose pole piece is rectangular in shape, and it is arranged so that the scattered electrons are bent horizontally. The magnet is of the window-frame type, which is known to provide homogeneous magnetic fields in the gap region. The dimensions of its gap are 170 cm (width) × 29 cm (height) × 140 cm (length), corresponding to a scattering angle coverage of 30-60 degrees and a solid angle of 100 msr, respectively. Two-layer field clamps are mounted on both sides of the magnet to reduce the field leakage. In addition to homogeneousness of the field, special attention has been paid to the magnet design to reduce the field leakage at the electron beam to less than a few gauss to avoid any serious effects on the circulating electron orbit in the storage ring. The total weight of the magnet is 45 tons.

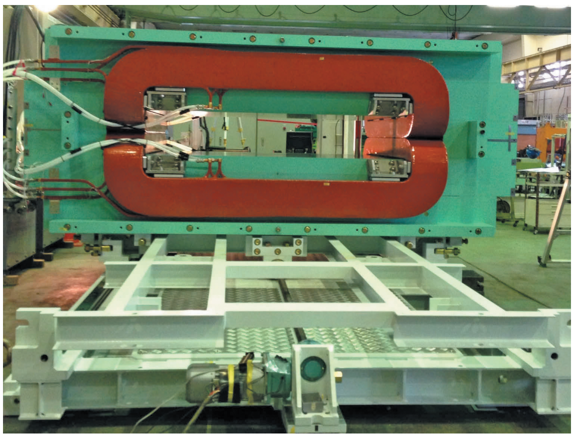

Fig. 1. The SCRIT magnetic spectrometer without the field clamps.

The construction of the magnet was completed, and it was successfully excited to the design value, $B_y^{max} = 0.8$ T. A series of magnetic field measurements followed at the NEC/TOKIN company using a magnetic-field mapping system with three-axis Hall probes.

A careful evaluation of the measured magnetic fields has currently begun, for which we are using the results of OPERA-3D calculations[2]. Figure 2 shows a snapshot of the first comparison of the vertical component of the magnetic fields measured along the z-axis (from the magnet center towards the center of the gap entrance) with those obtained by the OPERA3D calculation. The OPERA3D calculation is found to reproduce the measured field distribution reasonably well.

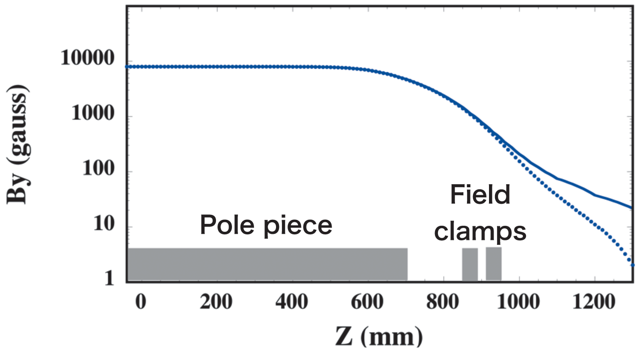

Fig. 2. Magnetic fields along the symmetric axis of the gap in the mid-plane. Solid circles indicate the measured data, and the solid line indicates the OPERA3D results.

The spectrometer is now ready to be transported to the SCRIT electron scattering facility at the RI Beam Factory. Its installation will be completed in FY2012, and its commissioning will be performed in FY 2013.

References
1) T. Adachi *et al.* Accel. Prog. Rep. **45**, 144 (2012).
2) OPERA Vector Field Code, http://www.cobham.com.

† Research Center for Electron-Photon Science (ELPH), Tohoku University

Current status of electron-beam-driven RI separator for SCRIT (ERIS) at RIBF

T. Ohnishi, S. Ichikawa, M. Togasaki, R. Ogawara, K. Kurita,[*1] and M. Wakasugi

To produce a low-energy RI (Radioactive Isotope) beam used for the electron scattering of unstable nuclei, the electron-beam-driven RI separator for SCRIT (ERIS) was constructed at the SCRIT (Self-Confining RI Ion Target) electron scattering facility[1)] in 2010. The commissioning of the ERIS was performed in 2011 and obtained results were reported in Ref. 2. During the present year, the preparation of uranium carbide target has been started in order to produce unstable nuclei. In addition, we have started supplying stable nuclei from the ERIS for the experiment. In this paper, we report the current status of the ERIS.

Uranium carbide is more suitable for a production target of unstable nuclei than uranium oxide, because its vapor pressure and density are lower and higher than those of uranium oxide, respectively. Uranium carbide is obtained by the carbothermal reduction of uranium oxide in presence of carbon at 1800 °C. There are two styles of mixing uranium oxide and carbon, related to shape of the production target. One is a pellet made of uranium oxide and graphite powders with bond, and the other is a graphite fiber impregnated with uranium oxide. One of the advantages in using the pellet is the easy control of the total amount of uranium and the density of the target, in comparison with the fiber. However, the process of preparing the fiber is easier than that of the pellet.

This year, we prepared a graphite fiber target with uranium oxide. Graphite fibers around 16 mm in length were put in the graphite tube, which had an inner length of 47 mm and an inner diameter of 13 mm until the graphite tube was filled. A uranyl nitrate solution was dropped and impregnated to graphite fibers. By heating up to 300 °C, the uranyl nitrate was oxidized under Ar-gas flow. Figure 1 shows the produced uranium oxide target with graphite fibers in the graphite tube. The total amount of uranium and graphite fibers were 4.8 and 1.5 g, respectively.

For the carbothermal reduction at 1800 °C or the heating of the target to 2000 °C, the cooling system of the ERIS was improved using simulations by ANSYS®, Release 13.0. The calculations were performed using the RIKEN Integrated Cluster of Clusters facility. Figure 2 shows an example of the calculated temperature distribution of the target chamber with the heater current of 600 A. The simulation included the effect of the heat contact between the tantalum heater and the copper current feedthrough, and the emission between the contents and the vacuum chamber. The comparison between the calculation and the measurement results showd that water channels were additionally processed in the wall of the vacuum chamber and the current feedthrough.

Fig. 1. Photograph of graphite fiber with uranium oxide in the graphite tube.

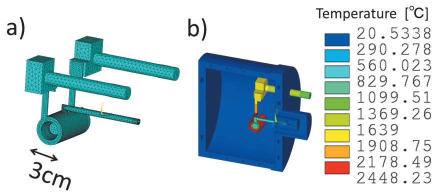

Fig. 2. Example of the simulation result calculated by the ANSYS code. a) Left figure shows the model of the target, heater, and feedthrough. b) Right figure shows the cross section of the calculated temperature distribution of the target chamber.

Besides preparation for the production of unstable nuclei, the ERIS has started supplying stable ion beams. The experiment of the elastic scattering for ^{132}Xe was performed as the first experiment using the ERIS, and the produced current of ^{132}Xe ions was around 200 nA at the exit of the ERIS. The operation of the ERIS was stable during the experimental period, which lasted for almost one month. The result of this experiment is reported in this progress report.

In summary, we have started the preparation of uranium carbide target and the supply of stable nuclei. The cooling system of the ERIS has been modified for high-temperature target operation. As a result these preparations, the production of unstable nuclei will be started soon.

References

1) M. Wakasugi et. al: RIKEN. Accel. Prog. Rep. **43**, 1(2010).
2) K. Koizumi et. al: RIKEN. Accel. Prog. Rep. **45**, 141(2012).

*1 Department of Physics, Rikkyo University

SCRIT luminosity monitor

T. Amagai, A. Enokizono, A. Enomoto, Y. Haraguchi, K. Kurita, T. Miyamoto, R. Ogawara, T. Ohnishi, Y. Shimakura, T. Suda, T. Tamae, M. Togasaki, M. Wakasugi, S. Wang, T. Yamaguchi, and K. Yanagi

A luminosity monitoring system is constructed for electron scattering experiments to be carried out for short-lived nuclei at the SCRIT electron scattering facility[1] of the RI Beam Factory. Its purpose is the precise monitoring of the collision luminosity, within a reasonably short time, between the stored electron beam and target short-lived nuclei. The monitoring system measures the number of bremsstrahlung photons produced during the collision between the electrons and the target nuclei trapped in the SCRIT device. Since the cross section of the bremsstrahlung process[2] is well known, the luminosity can be directly determined.

The system consists of a position detector and a calorimeter as shown in Fig. 1, which are used for the measurements of the spatial distribution and energy of the bremsstrahlung photons, respectively. It is placed at 670 cm downstream from the center of the SCRIT device.

The position detector consists of two identical fiber scintillation detectors, which are crossed each other and is placed in front of the calorimeter. Each detector has 16 optically isolated fiber scintillators (BFC-10) of 2×2 mm^2 cross-section areas with 2 mm spacing, and they are coupled to a 4×4 multi-anode PMT (Hamamatsu H6568).

The calorimeter is a Pb-glass Cerenkov detector. The size of the Pb glass is $100 \times 100 \times 300$ mm^3, and the glass is coupled to a 5" phototube (Hamamatsu R1250).

A full simulation was performed to determine the acceptance of this system for the bremsstrahlung process using GEANT4. The luminosity is, then, calculated based on the counting rate of the bremsstrahlung measured by the system.

Figure 2 shows the comparison between the two luminosities, determined by bremsstrahlung luminosity monitor and by the measurement of elastic scattered electron. Stable Xe ions are employed as targets, and the stored electron energy was 150 MeV. This result shows that two luminosities determined independently are consistent, and the bremsstrahlung monitor is a promising candidate as a luminosity monitoring system for future electron scattering experiments for short-lived nuclei.

The spatial distribution measured by the bremsstrahlung monitor revealed that the horizontal distribution was somewhat broader than expected, the reason for which is not yet clear. In the GEANT4 simulations, additional angular spread in the horizontal plane was considered so that the simulation could account for the measured distribution. A further detailed study of the entire SCRIT system is necessary.

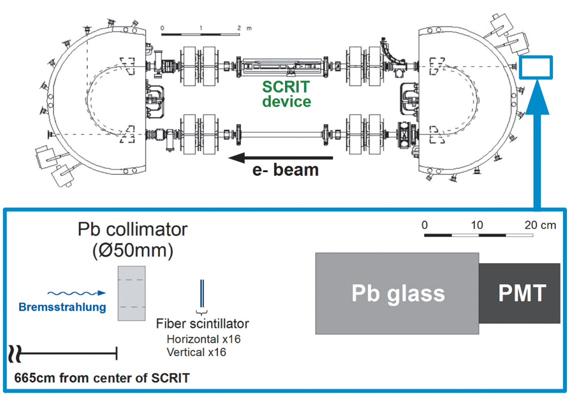

Fig. 1. Bremsstrahlung Luminosity Monitor.

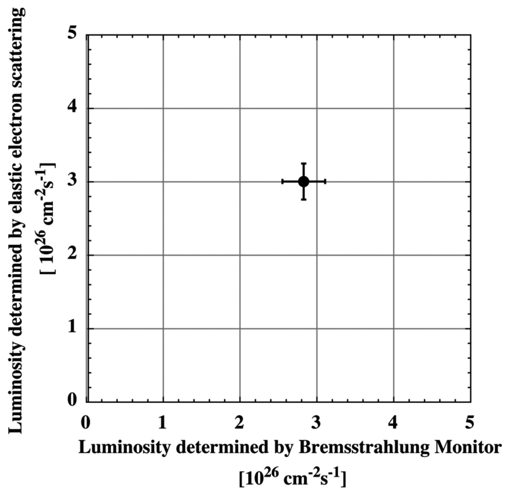

Fig. 2. Luminosities determined by bremsstrahlung luminosity monitor and elastic scattered electron measurement.

References
1) M. Wakasugi *et al.* Accel. Prog. Rep. **43**, (2009) 1.
2) H. Olsen and L. C. Maximon Phys. Rev. **114**, 887 (1959).

The Result of Xe Experiment at SCRIT Electron Scattering Facility

S. Wang, T. Amagai, M. Hara, T. Hori, S. Ichikawa, K. Kurita, R. Ogawara, T. Ohnishi, T. Suda, T. Miyamoto, T. Tamae, M. Togasaki, and M. Wakasugi

The SCRIT electron scattering facility[1)] has been constructed at RIBF since 2010. Becasue the RI (Radioative Isotope) beam, which will be used as the target nucleus for electron scattering experiment, is still under construction, natual Xe gas including nine stable Xe isotopes was used as the target to check the performance of the new ion transport line, such as transport efficiency and mass resolution since April, 2012. The energy of electron beam was set to 150 MeV with a lift-time around 150 minutes. Elastically scattered events from trapped ^{132}Xe ions were measured by the electron detection system[2)] and the vertex and energy spectra of those events are shown in Fig. 1. Elastic events are clearly seen from the target region during 4 hours measurement and the achieved mean luminosity is estimated to be around 3.5×10^{26} cm^{-2} s^{-1}.

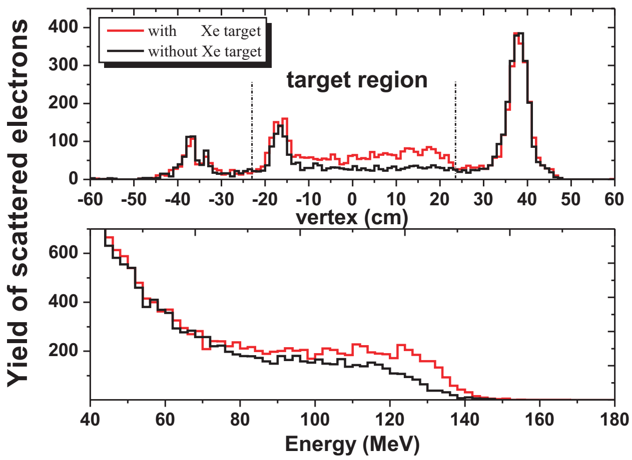

Fig. 1. The vertex and energy spectra of elastically scattered events from target nucleus ^{132}Xe.

Meanwhile an electron beam loss monitor[3)] was installed at downstream of the SCRIT device to measure scattered electrons, whose scattering angle was less than 1 degree. Due to the large cross section, the counting rate difference between with and without target was clearly observed in a short time and a linear relationship was found between the counting rate difference and the luminosity determined by electically scattered events. After being calibrated by luminosity, this loss monitor worked as an online luminosity monitor to optimalize the experiment condition. Achieved luminosity at different beam currents at KSR and SR2 experiments are shown in Fig.2. The maximun beam current at KSR experiment was round 80 mA. The number of injected ions in Xe experiment was nearly 1.0×10^8 ions/cycle as the similar number of RI ions in the future experiment, which is nearly a quarter of that in Cs experiment. It is clear that the beam current dependence of the luminosity is nonlinear to beam current, which suggests the ion trapping ability of electron beam is enhanced at larger beam current. The trend of three curves are almost same, when beam current is less than 130 mA. But the luminosity in the Cs experiment is still increased after 130 mA, while it was almost constant in the Xe experiment, which is due to the small number of injected ^{132}Xe ions. Due to the production rate of RI ions, increasing the number of injected RI ions seems impossible. To achieve a high luminosity for electron RI beam scattering experiment, a small beam size of RI beam and maximizing the overlap region between electron beam and RI beam are necessary.

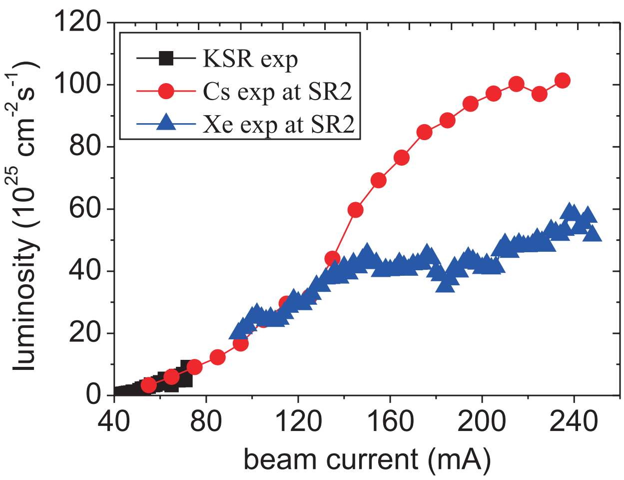

Fig. 2. Achieved luminosity at different beam currents. The black points are the result at KSR experiment and the red and blue points are the results about Cs and Xe experiment at SR2.

References
1) M. Wakasugi et al.: RIKEN Accel. Prog. Rep.**43**,(2010)1.
2) S. Wang et al.: RIKEN Accel. Prog. Rep.**45**,(2012)xx.
3) S. Tamaki et al.: RIKEN Accel. Prog. Rep.**45**,(2012)143.

Properties of trapped ions in the SCRIT device

R. Ogawara, T. Ohnishi, Y. Miyashita, S. Tamaki,[*1] M. Togasaki, H. Takehara,[*2] K. Koizumi,[*1] K. Kurita,[*1] T. Amagai, A. Enokizono, A. Enomoto, S. Ichikawa, T. Suda, T. Miyamoto, S. Wang, M. Hara, T. Hori, T. Tamae, Y. Shimakura, Y. Haraguchi, T. Yamaguchi, K. Yanagi, and M. Wakasugi

The SCRIT technique aiming at electron scattering off unstable nuclei is based on the ion-trapping phenomenon in an electron storage ring. Target ions trapped in SCRIT coexist with residual-gas ions. Trapping of residual gas ions is started at the moment of the target-ion injection. Residual-gas ions are continned to be created, whereas number of the target ion is strictly limited. Time evolution of both the target ion and the residual-gas ion are completely different. For evaluation of the SCRIT performance, it is, therefore, essential to understand behavior of trapped ions for a first few seconds after the target ion injection.
Time evolution of the total charge of trapped ions with and without target ions are compared in Fig. 1(a). Larger growth rate and lower equilibrium charge were observed with target ions. This suggests that a space charge effect due to charge state multiplication of initially existing ^{132}Xe ions makes trapping lifetime of residual-gas ions shorter, because the ion creation rate should be the same in both cases. Even at the same electron beam current, different lifetimes of target-ion trapping were observed as shown in Fig. 1(b). It was found in our measurements that an electron beam instability, especially for a coherent synchrotron oscillation (CSO), changes the trapping lifetime of target ions. This was confirmed in time-evolution measurements of residual gas ions with different amplitude of CSO as shown in Fig. 2. A CSO amplitude was controlled by tuning RF cavity condition and observed as synchrotron sidebands in revolution spectra of the electron beam, as shown in Figs. 2(a) and (b). Figure 2(c) shows the time evolution of relative abundance of trapped oxygen and hydrogen ions with the CSO amplitudes corresponding to cases shown in Figs. 2(a) and (b). The abundance of hydrogen ions for the case of larger CSO amplitude is one order less than that for the case with smaller CSO amplitude.

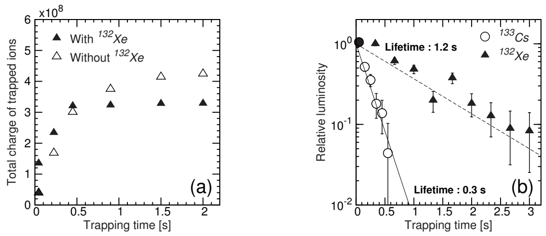

Fig. 1. (a) Time evolution of the total charge of trapped ions with and without target ^{132}Xe ion trapping. (b) Time evolution of relative luminosity for ^{133}Cs and ^{132}Xe.

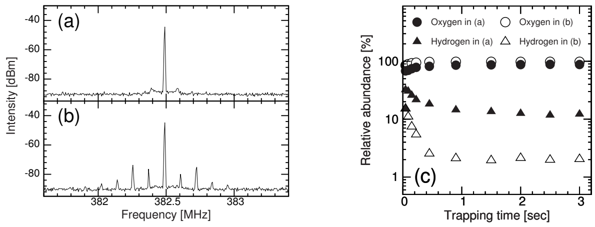

Fig. 2. (a, b) A CSO spectrum for electron beams in the vicinity of the second harmonic (382.488 MHz) of the RF frequency in this ring and (c) abundance of proton and oxygen ions with each beam conditions.

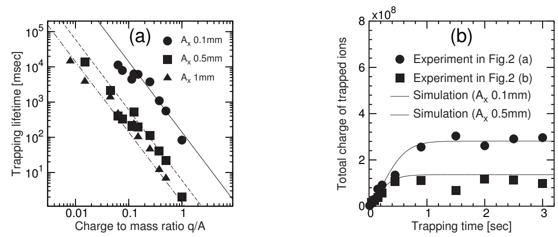

Fig. 3. (a) Trapping lifetime by the simulation of ion-trapping in SCRIT with CSO amplitude A_x of 0.1, 0.5, 1.0 mm. (b) A simulation of total charge time evolution including trapping lifetime and experimental resultfor the CSO spectrums shown in Fig. 2 (a, b).

From these measurements, we suppose that the trapping lifetime is strongly dependent on the space charge, the CSO amplitude, and q/A value. We calculated the trapping lifetime of ions having several q/A values considering the space charge and the CSO amplitude, and obtained lifetimes, as shown in Fig. 3 (a). We found that the computer simulation[2)] considering the calculated trapping lifetime well represents the time evolutions measured in the present experiments, as shown in Fig 3 (b).

References
1) M.Wakasugi et al.: Phys. Rev. Lett. 100, 164801 (2008).
2) M. Wakasugi, T. Suda, and Y. Yano: Nucl. Instrum. Methods Phys. Res., Sect. A 532, 216 (2004).

*1 Department of Physics, Rikkyo University
*2 Department of Electrical Engineering, Nagaoka University of Technology

GARIS-II commissioning #2

D. Kaji, K. Morimoto, H. Haba, Y. Wakabayashi, Y. Kudou, M. Huang, T. Sumita, K. Tanaka, M. Takeyama, M. Murakami, S. Yamaki, S. Goto,[*1] N. Goto,[*1] T. Koyama,[*1] N. Tamura,[*1] S. Tsuto,[*1] and K. Morita

A background evaluation and transmission measurement of a gas-filled recoil ion separator GARIS-II was studied by two reactions, namely, of ^{169}Tm(^{40}Ar,4n)^{205}Fr and ^{208}Pb(^{40}Ar,3n)^{245}Fm.

Projectiles of ^{40}Ar with a charge state of 11^+ were extracted from the 18-GHz ECR ion source and accelerated up to 197 MeV by the RILAC. The typical beam intensity incident on a target was 2.0×10^{12} s^{-1}. The $^{169}Tm_2O_3$ target was prepared by electrodeposition on a 3 μm titanium foil. The metalic ^{208}Pb target was prepared by vacuum evaporation on a 60 μg/cm^2 carbon foil. Target thicknesses were 250 μg/cm^2 for ^{169}Tm and 280 μg/cm^2 for ^{208}Pb (enrichment of 99.59%), respectively. Sixteen frames of the sector targets were mounted on a ϕ30 cm rotating wheel, which was rotated at 2000 rpm. The reaction products were separated in flight from projectiles and other by-products by GARIS-II, and guided into a focal plane detection system.[1)] The separator was filled with helium gas at a pressure of 80 Pa. The magnetic rigidity $B\rho$ was set to 1.64 T·m for the ^{205}Fr and 2.01 T·m for the ^{245}Fm measurement.

A cycle of the beam-on (5 s) and beam-off (15 s) measurements was repeated 237 times for ^{205}Fr and 616 times for ^{245}Fm. Total doses of 1.8×10^{15} for ^{205}Fr and 2.4×10^{16} for ^{245}Fm were accumulated. The products of ^{205}Fr and ^{245}Fm were clearly identified by a half-life analysis. Figure1 shows the energy spectra measured under the beam-on and beam-off conditions in the ^{245}Fm experiment. In order to compare the background suppression of GARIS-II with that of GARIS, data measured by GARIS is also given in figure panels (A) and (B). In GARIS's case, a total dose of 6.6×10^{16} ions was accumulated. Although no α-peaks are seen in the beam-on spectrum for GARIS, α-peaks of ^{245}Fm (4.2 s, 8.15 MeV) are clearly seen in the spectrum in panel (A) for GARIS-II. Then, the total counting rate of the detector at the typical intensity was approximately 6.5 cps, which is about 5 times lower than that for GARIS. The main components are arrival events due to target recoils, scattered beam particles, and light charged particles. The counting rate under beam-off conditions was approximately 0.09 cps in the energy range from 5 to 10 MeV. Although background α-peaks are almost not seen in the beam-off spectrum for GARIS, α-peaks due to transfer products of Po and At isotopes are seen in the spectrum in panel (C) for GARIS-II. This difference is caused by a difference of the deflecting angle between GARIS (45°+10°) and GARIS-II (30°+7°). Background particles such as those of Po and At isotopes are expected to be suppressed by using H_2 gas or He-H_2 mixed gas.[2)]

The transmission of GARIS-II was estimated to be 47% for ^{205}Fr and 71% for ^{245}Fm. The transmission values are plotted as a function of the recoil velocity v/v_0, expressed in the Bohr velocity unit, in Fig. 2, where the transmission curve of GARIS[3)] is also given for comparison. The obtained transmission and background suppression data of GARIS-II matched well the design values.

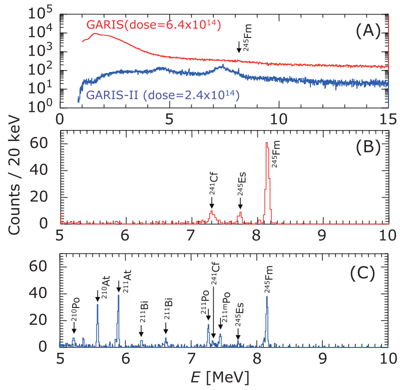

Fig. 1. Energy spectra measured in the ^{245}Fm experiment conducted using GARIS and GARIS-II. (A) Beam-on condition for both separators, (B) beam-off for GARIS, (C) beam-off for GARIS-II.

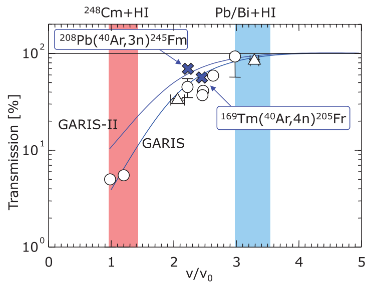

Fig. 2. Transmission curve. Velocity regions of interest for the reactions of both cold fusion and hot fusion are given by the blue and red stripes, respectively. ○, △: GARIS, ×: GARIS-II. Solid and dashed curves are estimated by considering multiple scattering with the filled gas.

*1 Department of Chemistry, Niigata University

References

1) D. Kaji et al.: in this report.
2) J. Khuyagbaatar et al.: GSI Sci. Rep. **2010**, 203 (2011).
3) D. Kaji et al.: Proc. Radiochim. Acta **1**, 105(2011).

Focal plane detector developed for GARIS-II commissioning #2

D. Kaji, K. Morimoto, F. Tokanai, Y. Fujimori, K. Mayama, S. Namai, M. Takeyama, A. Mashiko, and S. Yamaki

For the identification of evaporation residues (ERs) and their successive radioactive decays, a system of a time-of-flight (TOF) detector, a double-sided silicon detector (DSSD) array, and a VETO silicon detector array were installed at the focal plane of GARIS-II. A general drawing of the detection system is shown in Fig.1. After passing through a D_2 magnet of the separator, ERs transit the TOF detector and are later implanted into the DSSD array, 240 mm behind the TOF detector. The kinetic energy E of ERs are measured by the DSSD.

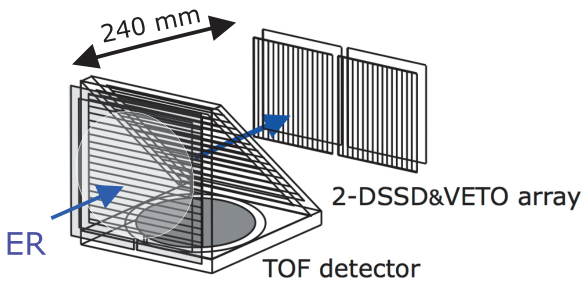

Fig. 1. Focal plane detection system of GARIS-II.

When ERs pass through an entrance foil of the TOF detector, secondary electrons are emitted. The effective area of the TOF detector is 140 mm in diameter. The entrance foil is made of a 1.1 μm self-supporting Mylar, which is covered by 19.3 $\mu g/cm^2$ gold and 20 $\mu g/cm^2$ CsI (cesium iodide) to enhance the numbers of the secondary electrons. The secondary electrons are immediately accelerated by an acceleration filed, bent downward by a mirror field, and carried out to a surface of micro-channel plate MCP assembly. The MCP assembly consists of two plates (PHOTONIS, 120-D-40:1-NR) assembled in a "chevron" configuration.

The DSSD array consists of two type of DSSDs (Micron, W1-1000 and W1-1500). The active area of the DSSD array is $2\times50\times50$ mm^2. The DSSD is divided in the horizontal and vertical direction into 16 strips. Information of energy, time, position, and strip's number are recorded for implanted nuclei to the DSSD as well as for the α particles emitted from their subsequent decay.

The VETO silicon detector (CAMBERRA, PF-16CT-58*58-300-EB) of almost the same size are installed 5 mm behind the DSSD, and used as a veto counter, which is quite effective for reducing backgrounds such as light charged particles passing through the DSSD. In order to obtain clean spectra of the subsequent α-decays, the pulses generated by reaction products or scattered projectiles are suppressed by an anti-coincidence condition between the DSSD, the TOF detector, and VETO-counter mounted downstream of the DSSD.

In GARIS-II commissioning #2[1)], this focal plane detection system was well calibrated by using ^{169}Tm(^{40}Ar,xn)$^{209-x}$Fr [x=4,5] reactions. For example of rough particle identification at the focal plane of GARIS-II, the $TOF-E$ scattered plot is shown in Fig. 2. It is found that ERs are separated from background particles owing to target-like particles, beam-like particles, and light charged particles. The typical energy resolution of the DSSD is 22 keV in FWHM for 6916 MeV α particles owing to ^{205}Fr.

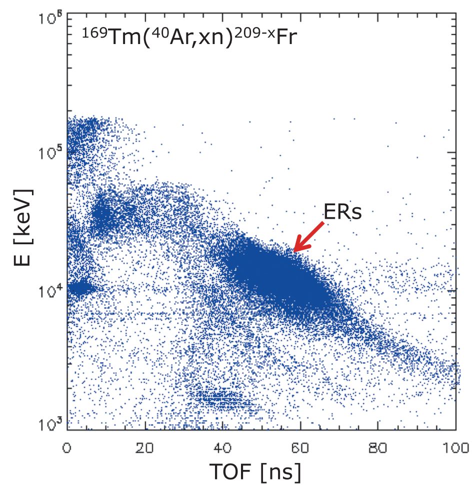

Fig. 2. Two-dimensional of energy measured by DSSD vs. TOF measured using timing counter.

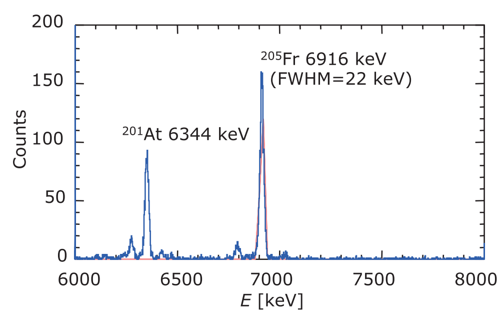

Fig. 3. Energy spectrum observed in the ^{40}Ar on ^{169}Tm irradiation.

References

1) D. Kaji et al.: in this reoport.

Development of a large area TOF detector for super-heavy element research

K. Morimoto, K. Mayama, D. Kaji, F. Tokanai, and Y. Fujimori

A new time-of-flight (TOF) detector with a large effective area has been developed for super-heavy element research. A focal plane image size of fusion products in an asymmetric fusion reaction such as hot fusion is larger than that in a symmetric reaction. In order to perform researches with the asymmetric fusion reaction, a new ToF detector was developed. The effective area of the new TOF detector is 120 mm in diameter. Figure 1 shows a comparison with a conventional TOF detector, and the new detector is shown on right side.

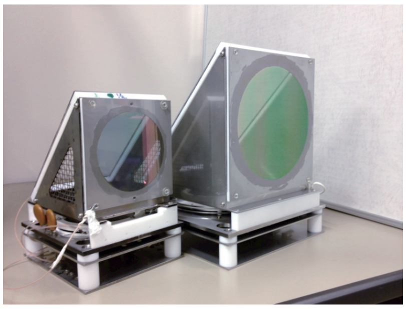

Fig. 1. Photograph of the TOF detectors. The detector to the left is a conventional detector with an effective area of 80 mm in diameter, and the detector to the right is newly developed with an effective area of 120 mm.

The detector consists of an entrance foil, three wire grids for formation of an electric field and a micro-channel plate (MCP) assembly. A Mylar film on which 19.3 μg/cm^2 gold and 20 μg/cm^2 CsI (Cecium iodide) is used as the entrance window. The gold is evaporated to be used as an electrode for producing an electric field and CsI is evaporated to enhance the number of secondary electrons. One wire grid is used for accelerating secondary electrons just emitted from the entrance film, and the other two sets of wire grids form a mirror field to deflect the electrons downward and introduce them to the MCP detector. All three wire grids are gold-plated tungsten wires with a diameter of 12 μm, stringed in 1 mm pitch. The MCP assembly consists of two plates (PHOTONIS 120-D). Figure 2 shows a schematic view of the TOF detector.

The detection efficiency and the time resolution of the detector were measured using an ^{241}Am alpha source. Figures 3 and 4 show results for the incident position dependences of time resolution and efficiency. Time resolution of 500 ps (FWHM) and detection efficiency of $> 80\%$ are achieved in the region of ± 50 mm from the center of the foil.

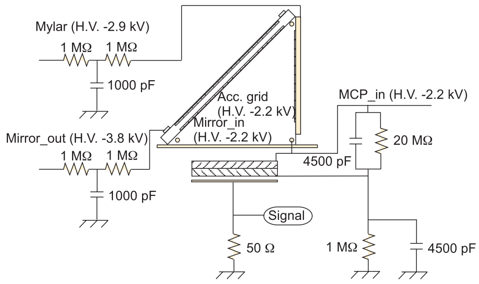

Fig. 2. Schematic view of the detector. Secondary electrons emitted from the entrance foil are accelerated by a 0.7 kV electric field. The electrons are then deflected downward by a mirror field, and finally introduced to the MCP.

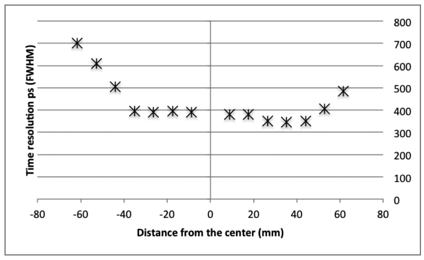

Fig. 3. Time resolution map on the entrance foil. The x-axis represents the incident position of alpha particle in horizontal space on the foil.

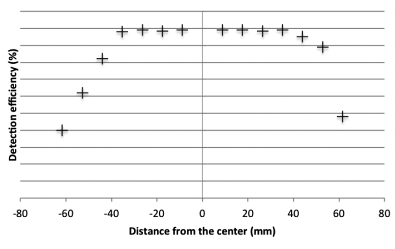

Fig. 4. Detection efficiency map on the entrance foil. The x-axis represents the incident position of alpha particle in horizontal space on the foil.

The new detector was used in a commissioning experiment of GARIS-II. The obtained data are described in Ref.[1)].

References

1) D. Kaji et al.: in this report.

Double-layered target developed for SHE search at GARIS

D. Kaji, K. Morimoto, T. Sumita, H. Hasebe Y. Kudou, and K. Tanaka

The development of a target system to withstand high-intensity beams is important for the superheavy element (SHE) search performed at the gas-filled recoil ion separator (GARIS). In particular, when using low melting point target substances such as Tl, Pb, and Bi, it is necessary to prevent melting of the target over a long duration of irradiation. Recently, we developed a double-layered target (Mode-B in Fig. 1) mounted on an existing rotating target wheel.[1)].

The basic idea of the double-layered target system is shown in Fig. 1. By dividing a conventional single-layered target foil into two layers, the energy loss in one target is reduced by half, and thus its temperature rise also reduces by half. Moreover, the total surface area of the target becomes double. Consequently, we can expect gas-cooling by the helium gas filled in the recoil separator to become more effective. Therefore, the acceptable beam intensity incident on the double-layered target is expected to be twice that of the single-target case. On the other hand, the angular spread of the beam on the target is almost same for both cased because the target thickness dose not change.

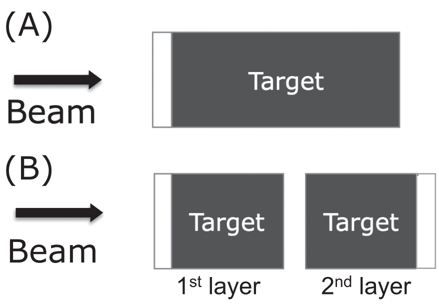

Fig. 1. A conventional single-layered target with backing foil (A) was separated into two layers of target (B).

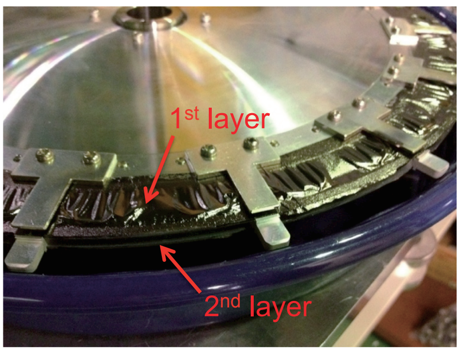

Fig. 2. Photograph of the double-layered target.

In May 2012, the performance of the double-layered target (Fig. 2) was investigated by measuring the yield of ^{254}No produced via the ^{208}Pb(^{48}Ca,2n) reaction at a focal plane of the GARIS. At first, we measured the yield of ^{254}No using the single-layered target and varying its thickness. Saturation of the ^{254}No yield was observed when the target thickness was more than 300 μg/cm^2. This saturation arises from the influence of the narrow width of the excitation function that is peculiar to cold-fusion reactions. Further, the increase in the multiple-scattering effect of ^{254}No in the thick target affects the saturation. Next, we used the double-layered target with layers of 560 and 540 μg/cm^2 in thickness. The obtained yield with the double-layered target showed a reasonable agreement with the expected value, which was extrapolated from the data points obtained by using the previous single-layered target. Thus, we decided to apply this double-layered target to the Z = 113 search experiment starting from Jul. 14, 2012. The 3rd decay chain of Z = 113 observed on Aug. 12, 2012 was the results obtained by using this double-layered target.[2)] The double-layered Bi target (380 + 380 μg/cm^2) withstood a strong ^{70}Zn beam of about 500 pnA over a duration of five days.

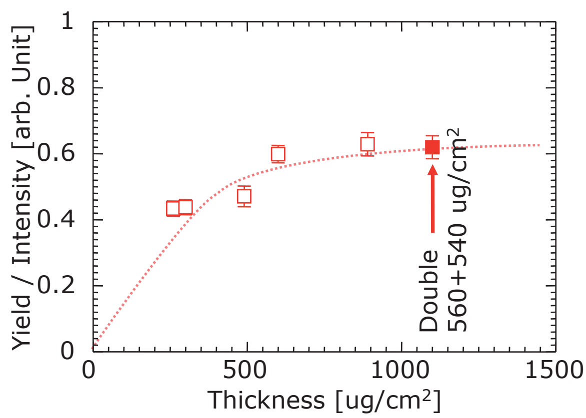

Fig. 3. Yield curve of ^{254}No as a function of target thickness. □: single-layered target, ■: double-layered target. The dashed line serves asa visual guide.

References
1) D. Kaji et al.: Nucl. Instr. and Meth. A **590**, 198 (2007).
2) K. Morita, K. Morimoto, D. Kaji et al.: J. Phys. Soc. Jpn. **81**, 103201 (2012).

Beam intensity monitor based on gas scintillation emitted from helium gas molecules in gas-filled recoil ion separator

D. Kaji, K. Morimoto, and F. Tokanai

We developed a new beam intensity monitor, which is based on gas scintillation emitted from helium gas molecules in a gas-filled recoil ion separator, in contrast to the conventional monitor measuring elastically scattered beams from a target.

Figure 1 shows the image of gas scintillation observed along the beam trajectory of ^{70}Zn, obtained using a CCD camera. It is found that the gas scintillation increases in strength with increasing beam intensity from 0.05 to 0.90 particle-μA (pμA). In this study, we first examined the origin of the gas scintillation, and subsequently, we investigated the intensity dependence of the scintillation as a function of the beam intensity.

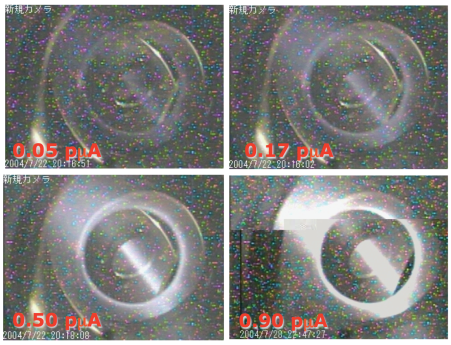

Fig. 1. Intensity dependence of gas scintillation.

The emission spectrum of the GARIS is measured by a monochromator system. The scintillation light is focused onto the input side of a light-guide fiber bundle through an acrylite vacuum window with a conventional UV lens. The fiber bundle transfers the light to a modified Czerny-Turner monochromator with a diffraction grating with 1200 lines/mm and a 400-nm braze. A photomultiplier tube (HAMAMATSU R928) is positioned for the detection of the grated light. In our study, spectral scans from 380 nm to 750 nm with a 1-nm step were performed using the monochromator, because the transmission of the acrylite window steeply decreases below 380 nm. The output current from the PMT anode is measured using a picoammeter controlled by LabVIEW software installed on a personal computer. All the observed peaks, as shown in Fig. 2, are in qualitative agreement with the atomic transitions from He gas excited by light charged projectiles[1]. However, the obtained intensity distribution is different from the reference value. To better understand this difference, further investigations require to be carried out.

The dependence of emission strength on beam intensity was studied (Fig. 3). Using a wavelength filter

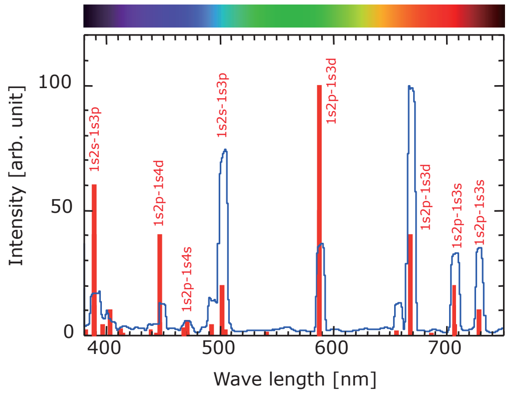

Fig. 2. Emission spectrum from He gas excited by a ^{70}Zn beam. Red bars indicate the proportion of the intensity profile of the atomic transitions from excited He molecules[1].

(Asahi Spectra Co. Ltd., MC -390J5), the peak of 389 nm was selected and its emission strength was measured. We used the short wavelength peak to avoid disturbance from visible light. The peak of 389 nm is convenient for measurement without the filtering out of visible light. We found that the emission strength has a linear correlation with the beam intensity in the range of 0.004-0.68 pμA. This result suggests the possibility of using the scintillation light as a beam intensity monitor.

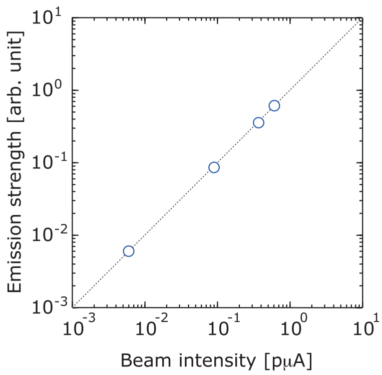

Fig. 3. Dependence of emission strength on beam intensity. The beam intensity was measured by the elastic beam intensity monitor. Data are normalized at 0.61 particle-μA.

References

1) http://physics.nist.gov/PhysRefData/ASD/lines_form.html

Development of large-area imaging detector for fast neutrons in MeV energy region

T. Hashiguchi, A. Taketani, K. Kino,[*1] H. Ota, K. Okada,[*2] S. Wang,[*1] K. Hirota,[*1] H. Baba,
Y. Yamagata,[*1] S. Tanaka,[*3] and Y. Otake

Neutrons with energies in the MeV region are suitable probes for the non-destructive inspection of large civil structures such as bridges because of high penetration even throguh thick concreate. We are aiming to develop a device non-destructivety to examine the inner structure of concreate. Our goal is to achieve a spatial resolution of a few cm for a concrete thickness of 50 cm. Along with the launch of the RIKEN Accelerator-driven Neutron Source (RANS)[1)] facility, we plan going to develop a detector for fast neutrons. Figure 1 shows an example of such a detector. The pixel size and thickness are most in need of optimization. The pixel thickness is associated with both the neutron reaction rate and the light collection efficiency of the MPPC. For a thicker scintillator, the neutron reaction rate is increased, but the rate of collection of the light sensor decreases due to the decreasing solid angle acceptance of the MPPC. The pixel thickness is determined by balance between both the parameters. The MPPC detection is set at a certain threshold in order to reduce unexpected dark count. We set this threshold between 15 to 50 photoelectrons. Figure 2 shows the optimized pixel thickness as a function of the pixel size. The pixel size is determined from both the magnitude of the crosstalk with the neighboring pixels and the spatial resolution requirement. For civil engineering requirements, the spatial resolution of imaging is less than or equal to 3 cm. We are currently attempting to optimize our detector for such a requirement.

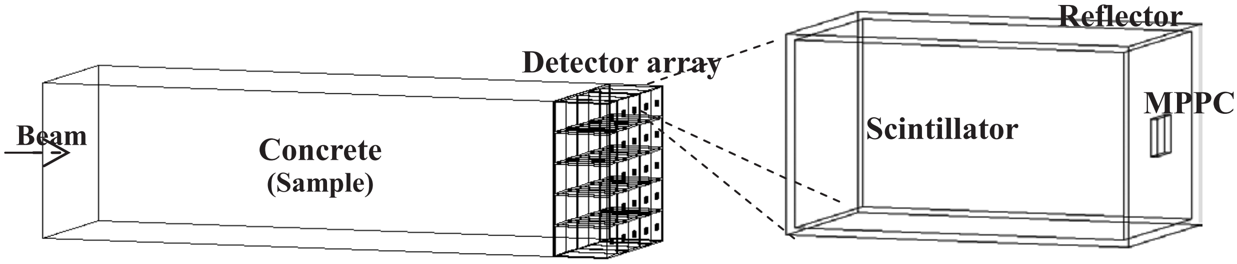

Fig.1 An example of geometry of sample and detector array.

The detctor is placed downstream of the object to be measured. The detector is composed of an array of plastic scitillators that are the equivalent of the BC-408. The injected fast neutrons make protons in the scitillator materials recoil, and the subsequently produced protons can generate scintillation light. The scintillation signal is detecetd by a multi-pixel photon counter (MPPC). The MPPC is a voltage of solid-state device with a realtive low operational volatge of ~ 100V, and it is intead of a photomultiplier, usually opetating at 1 kV. The pixelized scintillators are covered by removable reflectors.

The GEANT4 detector Mote Carlo simulator is used for optimizing the detector configuration. In the GEANT4, realistic physical processes are considered, such as the proton recoil process, electromagentic processes, and optical processes. The wavelegnth-dependent efficiency of the MPPC was measured by the manifacture and this value was used for the simulation. The neutron energy spectrum was calcurated by using the PHITS Monte Carlo simulation code.

Under these basic settings, we have currently optimized the detector for detection efficiency of fast neutrons and for minimizing crosstalk between adjacent pixels, which occurs due to elastic scattering of the neutrons in the scintillators.

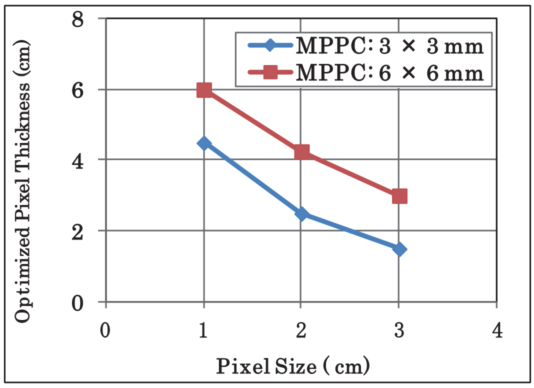

Fig.2 Pixel size as a function of pixel thickness.

*1 Advanced Manufacturing Metrology Laboratory, RIKEN
*2 Present Address : Spring 8, JASRI
*3 KEK, Tsukuba, Japan

References

1) RIKEN Symposium, Development of Small Neutron Imaging Devices for Industrial Application Integrating into VCAD System, (2009).

Magnetic lens for focusing pulsed white neutron beam using permanent magnet sextupole with modulation capability

M. Yamada, Y. Iwashita, Y. Otake, H. M. Shimizu, K. Hirota, Y. Seki, H. Tongu,*1 M. Ichikawa,*1 Y. Fuwa,*1 K. Mishima,*2 M. Hino,*3 M. Kitaguchi,*3 and P. Geltenbort,*4

Today, the next-generation neutron source, namely, the accelerator-based spallation neutron source, is taking the place of a nuclear fission reactor source, and most neutron optical devices use a pulsed beam with wide-wavelength-dispersion band. We developed a new magnetic neutron lens for focusing a pulsed wide-band neutron beam and named it the modulating permanent magnet sextupole, mod-PMSx.[1-2)]

This lens system is easy to handle and suitable for mass production, enabling it to be widely adopted in various neutron instruments. The image focused by a magnetic refractive lens of the same type as the mod-PMSx is clearer because there is no interaction between objects, such as absorption or scattering. Beam alignment precision has less stringent than reflective optics.

A refractive magnetic lens uses the interaction between a neutron's magnetic dipole moment and the magnitude of a sextupole magnetic field that is indicated by a positive constant value G_6.[3-4)] When a beam is pulsed, the Time-of-Flight method (ToF method) makes energy spectrometry possible; a neutron arriving at a time t at a distance from a start point L has a de Broglie wavelength λ given by

$$\lambda = h \cdot t / (m_n \cdot L) \,, \qquad (1)$$

where h and m_n are Planck's constant and the neutron mass, respectively.

Our lens system, mod-PMSx, can focus a beam over a wide-wavelength-band without any serious chromatic aberration effect, by the synchronized modulation of G_6 with a beam pulse. The sextupole magnet consists of a permanent magnet for generating the strongest magnetic field with compact volume without accompanying apparatus. The modulation scheme adopted the so-called rotating double ring structure shown in Fig. 1; a cylindrical permanent sextupole magnet is divided into two nested co-axial rings, where the inner ring is fixed and the outer ring can be rotated continuously. G_6 is modulated as a cosine function. The part of the descending slope of the cosine modulation is approximated and used as the ideal modulation that is proportional to t^{-2}.

A lens system with three-sextupole-magnet units was fabricated, whose unit effective length was 66 mm and bore diameter was ø15 mm. The sextupole field was generated by the so-called extended-Halbach configuration[5-6)] using a neodymium magnet and soft iron material, known as permendur. The maximum field gradients G^*_{6max}[T/m^2] of the three units are 5.8×10^4, 5.5×10^4, and 5.5×10^4. The averaged modulation width has the ability to focus a wide-wavelength-width of two (λ_{max} / λ_{min} = 2), which has never been achieved thus far.

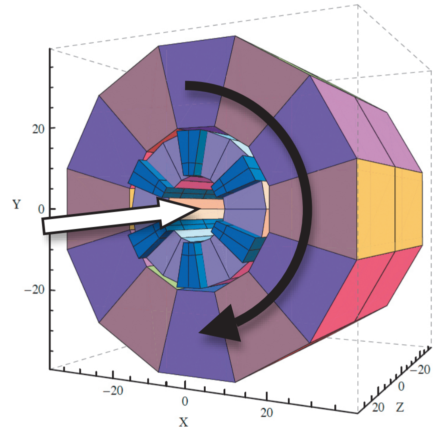

Fig. 1. The rotating double ring structure of mod-PMSx. The beam direction and outer ring rotation are indicated by the white and black arrows, respectively.

We performed a focusing experiment at a very cold neutron beam port (PF2-VCN) in Institut Laue-Langevin. The focused beam spot size defined by FWHM corresponded to a source aperture size (ø2 mm) over a wavelength band over 27 Å ≤ λ ≤ 55 Å (λ_{max}/ λ_{min} ~ 2) with a beam repetition rate of 30 Hz simply at a 1.84 m distance from the source aperture to the focus point. The neutron number per unit time and unit area was enhanced by 63 times as compared to an unfocused beam. Accordingly, demonstrations of magnified imaging for higher resolution measurement and focusing and polarized small angle neutron scattering experiment were performed successfully.

The mod-PMSx system can be applied to a shorter wavelength beam and the dynamic range of the wavelength band can be extended further. This device is expected to be used in neutron studies as an important tool because it not only has enhanced intensity but also has good instrumental performance.

*1 Institute for Chemical Research, Kyoto University
*2 International Center for Elementary Particle Physics, Tokyo University
*3 Research Reactor Institute, Kyoto University
*4 Institut Laue-Langevin, France

References

1) M. Yamada, et al.: Physica B, **404**, 2646 (2009)
2) M. Yamada, et al., Nucl. Inst. Meth. **A 634**, s156 (2011)
3) P. S. Farago: Nucl. Inst. Meth. **30**, 271(1964)
4) H. M. Shimizu, et al.: Nucl. Instr. and Meth. **A430**, 423 (1999)
5) K. Halbach: Nucl. Instr. and Meth. **A169**, 1(1980)
6) M. Kumada, et al.: IEEE, **12**, 129 (2002)

Preparation of the J-PARC E16 : An experiment to measure the mass modification of vector mesons in nuclei

S. Yokkaichi for the J-PARC E16 Collaboration

We have proposed the experiment E16[1] to measure the vector meson decays in nuclei in order to investigate the chiral symmetry restoration in dense nuclear matter. The experiment will be performed at the J-PARC Hadron Experimental Facility. The proposal of the experiment was granted scientific ("stage 1") approval by the PAC in March 2007. For the full approval, we need to establish the experimental feasibility as well as to show the prospects of acquiring sufficient funds and of beam-line construction.

The mass modification of vector mesons in hot and/or dense matter is predicted on the basis of the QCD because of the restoration of the chiral symmetry in such matter. Mass modifications in matter, however, due to hadronic many-body effects are also predicted. The predictions from these two viewpoints should agree in principle, however, still no clear connections are established between the two thus far.

Many experimental studies, including dilepton invariant mass measurements, have been conducted to approach the problem, and the mass modifications in hot and/or dense matter have been observed. However, the origin of the modification has not yet been confirmed; in other words, there is no consensus on the interpretations of the phenomena.

Among the experiments, the experiment KEK-PS E325[2], which was conducted by a collaboration including a part of the authors, measured the e^+e^- invariant mass spectra in 12-GeV p+A reactions and reported enhancements on the low mass sides of ω and ϕ mesons. These enhancements are consistent with the decrease in the mass of vector mesons predicted using the QCD sum rule[3]. The mass-shape modification of a narrow resonance, ϕ, can be observed only in E325, because it has the best mass resolution among the above-mentioned experiments, better statistics than the photon-induced experiment, and a better signal-to-noise ratio than the heavy-ion experiments.

The aim of the J-PARC E16 experiment is to perform a systematic study of the mass modification of vector mesons, particularly the ϕ meson, in nuclei, with statistics that are two orders larger in magnitude than those of the preceding E325 experiment. In other words, the aim is to accumulate 1×10^5 to 2×10^5 events for each nuclear target (H, C, Cu, and Pb), and deduce the dependence of the modification on the matter size and meson momentum, which have never been measured. Furthermore, the e^+e^- decays of the ρ, ω, and J/ψ mesons can be measured at the same time.

For this experiment, we plan to use a 10^{10}-pps, 30-GeV proton beam in the high-momentum beam line, which will be constructed in the J-PARC Hadron Experimental Facility. In order to increase the statistics by a factor of 100, the beam intensity should be increased by a factor of 10; the acceptance of the spectrometer, by a factor of 5; and the production cross section, by a factor of 2, by increasing the beam energy. In order to cope with the interaction rate at the target, which has increased by a factor of 10, to a value of 10^7 Hz, a new spectrometer based on a new technology needs to be built.

In 2009, we obtained a MEXT Grant-in-Aid[4] to develop and construct the spectrometer. Detector development is underway, as reported elsewhere[5–10]. To summarize, basic studies and beam tests of the two key detectors, the GEM Tracker[5] and HBD[6–8], have been performed. For the former, the required performance has almost been achieved and a detailed mechanical design is on-going. For the latter, performance improvement is in progress. The studies on the lead-glass calorimeter[9] and the read-out system[10] have been started and beam tests have also been performed.

Recently, a budget request by KEK to construct the high-momentum beam line has been approved and the construction is to commence in JFY 2013. The construction of the spectrometer magnet is planned in JFY 2014, and further details will be determined soon. After the completion of the magnet construction, we can start the installation of the detectors in the magnet. Due to the budgetary limiation, our first goal of the staged construction plan is to construct one-third of the spectrometer.

References

1) S. Yokkaichi *et al.*: J-PARC proposal No. 16 (http://j-parc.jp/researcher/Hadron/en/pac_0606/pdf/p16-Yokkaichi_2.pdf), Lect. Notes Phys. **781** 161 (2009).
2) M. Naruki *et al.*: *Phys. Rev. Lett.* **96**, 092301 (2006), R. Muto *et al.*: *Phys. Rev. Lett.* **98**, 042501 (2007).
3) T. Hatsuda and S. H. Lee: *Phys. Rev. C* **46**, R34 (1992), T. Hatsuda, S. H. Lee and H. Shiomi: *Phys. Rev. C* **52**, 3364 (1995).
4) Grant-in-Aid for Scientific Research on Innovative Areas 2104: "Elucidation of New hadrons with a Variety of Flavors", 2009–2013, http://www.hepl.phys.nagoya-u.ac.jp/public/new_hadron/index-e.html
5) Y. Komatsu *et al.*: in this report.
6) K. Aoki *et al.*: in this report.
7) K. Kanno *et al.*: in this report.
8) D. Kawama *et al.*: in this report.
9) Y. Aramaki *et al.*: in this report.
10) T. N. Takahashi *et al.*: in this report.

Construction and test of GEM tracker with ASIC for J-PARC E16 experiment

Y. Komatsu for the J-PARC E16 Collaboration

The J-PARC E16[1)] collaboration is preparing a tracking detector using a triple gas electron multiplier(GEM) to investigate the restoration of chiral symmetry in quantum chromo dynamics at the normal nuclear density. The tracking of charged particles is performed in a magnetic field and the momenta of e^+ and e^- are reconstructed. The position resolution of 100 μm is the goal of the tracker.

The GEM tracker is composed of a triple-GEM and a 2D readout board. The GEM tracker with the triple-GEM has also been constructed and tested in the COMPASS experiment[2)]. Ionized electrons are amplified by the triple-GEM foils when charged particles pass through the inner gas. The amplification gas is a mixture of Ar (70%) and CO_2 (30%), and the gain is of the order of several 10^4. The thin readout board has 2D ("X" and "Y") read-out strips, and details regarding these strips are reported elsewhere[3)].

The readout system employs an ASIC, the APV25-s1[4)], which has been developed at CERN for the SSD readout and also used for the GEM readout. We developed a small preamp board (57.8 mm $\times$ 68 mm) on which two APV chips are installed; thus, 256 channels of strips can be read. The advantages of using APV chips include 1) high density of channels, 2) rate capability (containing multiplexer and short shaping time) and 3) good S/N ratio.

The performance of the GEM tracker using the APV25 was evaluated in a test experiment at J-PARC K1.1BR beam line. The momentum of the beam was 1 GeV/c and π^-, e^-, and K^- were contained. The setup was equipped with five silicon strip setectors (SSDs) and three scintillation counters. The beam was triggered by the coincidence of two scintillation counters of dimensions of 3 $\times$ 3 cm^2 and other counters prepared in the upper stream of them. The position resolution is evaluated from the difference of the hit positions between the GEM tracker and the SSDs. The hit positions in the X and Y strips are measured simultaneously.

Figure 1 shows the plot of the position resolution in X vs. incident angle of the beam. The tracker is tilted so that the incident angle can be changed from 0° to 45°. The black points indicate the results of the past measurements with discrete amplifiers and FADCs. The red points indicate those measured this time with APV25 chips and APVDAQ modules. The position resolution is improved for the incident angles of 0°, 15°, and 30°. A resolution of 102 μm is achieved even for 30°. This improvement is thought to be due to the high S/N ratio of the APV25, and we are currently analyzing the reason for this improvement.

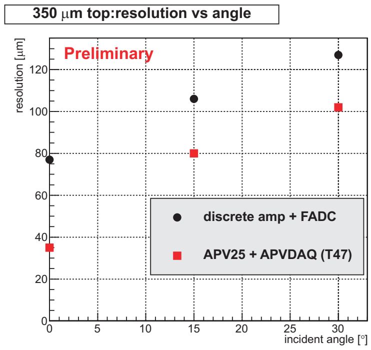

Fig. 1. Incident angle dependence of the position resolution. Black points indicate measurements made with discrete amps and FADC modules. Red ones indicate those made with APV-25 chips and APVDAQ (FADC).

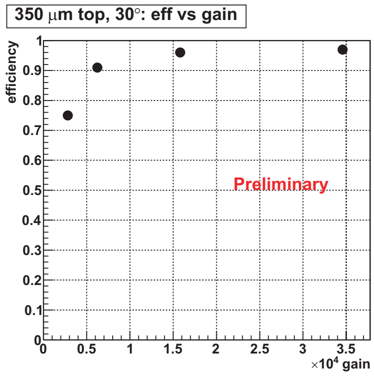

Fig. 2. Gain dependence of efficiency for the incident angle of 30°.

The gain dependence of the efficiency for the incident angle of 30° is shown in Fig. 2. A gain of 2 $\times$ 10^4 is required to obtain sufficient efficiency.

The GEM tracker has been constructed and tested with a new readout system, and it has shown good position resolution and efficiency. The next step is to carry out a test in a magnetic field, which is to be scheduled at J-PARC.

References
1) S. Yokkaichi et al.: in this report.
2) C. Altunbas et al.: Nucl. Instr. and Meth. A **490**, 177 (2002).
3) Y. Komatsu et al.: RIKEN Accel. Rep. **45** (2012).
4) M.J. French et al.: Nucl. Instr. and Meth. A **466**, 359 (2001).

Simulation of the behavior of photoelectrons in HBD for the J-PARC E16 experiment

D. Kawama for the J-PARC E16 collaboration

In the proposed J-PARC E16[1)] experiment, we are developping the Hadron Blind Detector (HBD)[2,3)], which uses CsI photocathode GEM detectors to detect Cherenkov photons produced by relativistic particles in a CF_4 radiator in order to separate electron/positron and other particles. The separation power of the HBD is directly affected by collection efficiency of the photoelectron (PE) which is the ratio of the detected PEs to the total PEs generated from the CsI. Although this value was studied by the PHENIX group[4)], we need much more understanding about the behavior of PEs in the electric filed of the GEM detectors and CF_4 gas. We studied the behavior by the Garfield[5)] (particle simulator in two- or three-dimensional electromagnetic field) with three-dimensional calculated electric fields by ANSYS/Maxwell[6)].

Fig. 1 shows a repetition unit of three-dimensional model of GEM foils for the HBD in the ANSYS. The boundary condition is that the electric field is parallel to the vertical symmetry plane, which is equal to the periodic boundary condition. In addition, arbitrary electric potential values are applied for the upper and lower surfaces. The arrows in the figure indicates the direction of the electric fields, namely, the inverse of the electron moving direction. The direction of the first arrow is opposite to that of the others in order to sweep out the electrons emitted by the ionization process before arriving at CsI. The geometrical parameter of the GEM foil is as shown in the figure with the mesh of the finite element method in ANSYS. The nominal hole diameter is 70 μm and the hole interval is 140 μm.

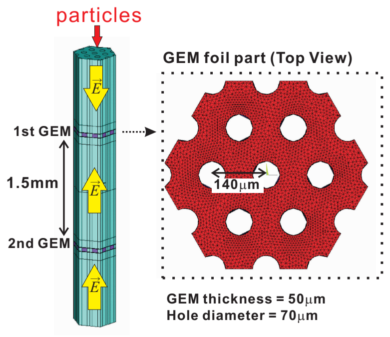

Fig. 1. Three-dimensional model used for electric field calculation in ANSYS.

Next, we performed the Garfield simulation with the calculated electric field and standard state CF_4 gas by setting the applied voltage across the GEM as 510 V. We studied the relationship between PE collection efficiency and hole diameter.

From this simulation, it was clarified that there are mainly two reasons for the inefficiency: the attachment of PEs to CF_4 gas and the back-scattering to the GEM. The attachment cross section is about 1×10^{-22} m^2 with a very sharp peak around the electron energy of 7 eV[7,8)]. In our GEM configuration, PEs have such energy just around the entrance of the GEM hole. The back-scattering is caused by the elastic process, whose cross section is on the order of 10^{-20} m^2. The PHENIX group[4)] measured the probability, and found it to be dependent on the electric field strength on the GEM surface. In this study, we used this value with the calculated electric field.

Considering these facts, we defined the figure of merit (FoM) for the collection efficiency as $FoM = \epsilon_{at} \cdot \epsilon_{bs} \cdot f_S$, where ϵ_{at} and ϵ_{bs} are the survival ratio for the attachment and back-scattering, respectively. The f_S value represents the ratio of the CsI effective area which determines the number of PEs generated from the CsI. The results are summarized in Table 1. The ϵ_{at} and f_S values increase for smaller hole GEMs, and ϵ_{bs} has opposite tendency affected by the electric field on the CsI. In total, the PE detection number is expected to be increased for smaller hole GEMs. Comparison with measured values is now in progress.

Table 1. Figure of merit for the collection efficiency changing the hole diameter. The ϵ_{bs} refer the PHENIX group result[4)]. For the smaller hole model, the stronger electric field makes it easier for PEs to reach to the energy to be attached to the CF_4 gas.

Diameter	60μm	70μm	80μm
ϵ_{at}	0.638	0.615	0.560
ϵ_{bs}	0.731	0.756	0.770
f_S	0.833	0.756	0.704
FoM	0.388	0.359	0.303

References
1) S. Yokkaichi *et al.*, in this report
2) K. Aoki *et al.*, in this report
3) K. Kanno *et al.*, in this report
4) B. Azmoun *et al.*, IEEE TRANSACTIONS ON NUCLEAR SCIENCE, VOL. 56, NO. 3, JUNE 2009
5) R. Veenhof, Garfield user guide, (http://garfield.web.cern.ch/garfield)
6) Ansys Maxwell Resource Center, ANSYS Inc., (http://www.ansys.com)
7) Y. Nakamura *et al.*, KTK Scientific, pp. 178-200, 1991
8) Electron scattering database, (http://www.lxcat.laplace.univ-tlse.fr/index.php)

Performance of a prototype hadron blind detector with cluster analysis for the J-PARC E16 experiment

K. Kanno for the J-PARC E16 Collaboration

A hadron blind detector (HBD) has been developed for the J-PARC E16 experiment.[1] The E16 experiment measures mass modification of light vector mesons in nuclei through e^+e^- invariant mass spectra. The HBD is used to identify electrons. The HBD identifies electrons by converting Čerenkov photons in CF_4 gas into photoelectrons with a CsI photocathode. Electrons can emit Čerenkov photons in our detector, while other charged particles do not; in the momentum region that we perform measurements for, 0.4–3 GeV/c. The number of charged particles, apart from electrons, that exceed threshold momenta for Čerenkov radiation is negligibly small in our experiment (the threshold for pions is 4.2 GeV/c in our detector). Converted electrons are amplified by a triple gas electron multiplier (GEM)[2] stack and then leave signals on readout pads. A sketch of the HBD is shown in.[3] A required property for the HBD is a hadron rejection factor of 100 with an electron detection efficiency of 80%. In order to evaluate both the hadron rejection factor (inverse of the fraction of pions identified as electron) and electron detection efficiency, we performed a beam test in Jan. 2013 at J-PARC K1.1BR with a 1 GeV/c beam of negative particles (mainly pions) containing a few tens of percent of electrons. Electrons can be distinguished from other charged particles by using other gas Čerenkov counters with dry air used as a radiator in the beam line.

The HBD for the beam test consists of a triple GEM stack and square pad readout. The size of square pads is 10 × 10 mm^2, resulting in 25 pads in the detector. We can identify electrons by applying a signal amplitude threshold since signal amplitudes induced by electrons are much larger than those induced by pions, due to Čerenkov photons. Furthermore, to improve the hadron rejection factor, we performed the cluster analysis as follows.

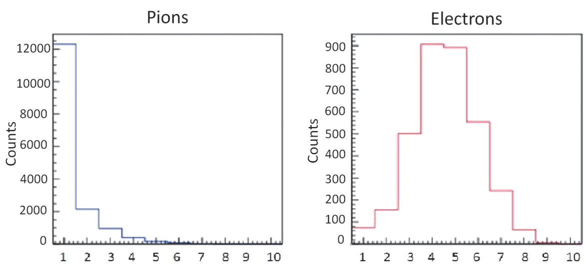

Fig. 1. The number of fired pads in a charge cluster with pions and electrons.

Čerenkov photons from an incident electron fire multiple pads, since the size of a Čerenkov blob in our detector is ∼35 mm while an incident pion mostly fires a single pad. We define a fired pad as a pad whose signal amplitude is greater than 3σ above its pedestal. The number of fired pads in a charge cluster produced by an incident charged particle is shown in Fig. 1. Pions generally fire a single pad, whereas electrons mostly fire four or five pads in an event. To suppress pion contamination, we require that electron candidates have more than three fired pads in a charge cluster.

Consequently, we achieve a hadron rejection factor of 100 with an electron detection efficiency of 70% when the signal amplitude threshold in units of primary charge is ∼3 e, as shown in Fig. 2. We observe 7 photoelectrons on average, while we expect 13 photoelectrons to be observed, based on a previous beam test. The lack of photoelectrons is considered to be caused by the low photoelectron-collection efficiency of the top GEM. We used a special GEM such that the distance between holes was twice the size of a standard GEM in order to enlarge the effective area of a CsI photocathode. The collection efficiency is expected to be improved by using a GEM with a regular hole/pitch ratio. With this configuration, we expect higher electron detection efficiency while retaining a good hadron rejection factor.

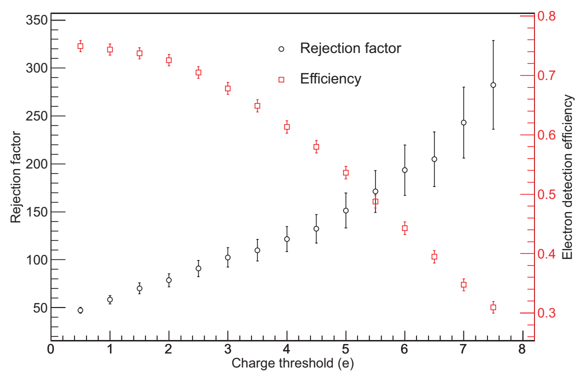

Fig. 2. Hadron rejection factor and electron detection efficiency as a function of the signal amplitude threshold in units of the primary charge.

References

1) S. Yokkaichi *et al.*: in this report
2) F. Sauli: Nucl. Instr. and Meth. A **386** (1997) 531
3) K. Aoki *et al.*: in this report

Performance test of electromagnetic calorimeters for J-PARC E16 experiment

Y. Aramaki, for the J-PARC E16 Collaboration

The electron trigger for J-PARC E16 experiment[1] is made by the GEM tracker (GT), the Hadron Blind Detector (HBD), and lead-glass calorimeter (LG). The requested e/π separation of the LG itself is a few percentage contamination of pion at an electron efficiency of 90% for the offline analysis, where the pion contamination is defined as the ratio of the pions survived at which electrons of 90% are kept for ADC distribution to the total amount of pions. It means that the performance of the LG is similar to that observed by the previous experiment, KEK-PS E325. Now we are designing the alignment of the LGs, and thus, we need to investigate the performance of the LG. We tested the incident angular dependence of the LG at J-PARC. The performance test of the LG used for the J-PARC E16 experiment is reported.

The LGs which were employed in the TOPAZ experiment at KEK-TRISTAN will be reused for the J-PARC E16 experiment. They have been kept in KEK after the deconstruction of the TOPAZ spectrometer. Most of the LGs are kept as the module construction, and thus, we disassembled them in April 2012. The number of LGs with PMT is 1517, and the number of the LG without PMT is 858. The physical properties and chemical components of the blocks are described in Ref.[2]. One LG is composed of five parts: a lead-glass block, light guide, flange, photomultiplier (PMT), and 2 mm-thick magnetic shield case made of PB permalloy. PB is a nickel iron soft-alloy containing 40–50% nickel. Both the lead-glass and light guide materials are made of SF6W.

We started designing the layout of the LGs last year. In order to choose the layout, a test was performed at J-PARC K1.1 beam line using the hadron beam of -1.0 GeV/c in January 2013. The hadron beam is composed mainly of pion. Electrons of the beam are mixed by about 30%. For the e/π separation, electrons and pions were detected and identified by two Gas Cherenkov detectors. The beam size focused on two scintillation counters was 1 cm. Figure 1 shows the definition of the incident angle and LG. The effective area of the LG is colored. The incident angle is defined as the angle formed by the beam direction and the photoelectric surface of the PMT of the LG. For example, if the incident angle is 180 °, the PMT is placed upstream of the beam.

The incident angular dependence of the LG has been tested. The typical ADC distribution of the LG inclined by 90 ° is shown in Fig. 2. The left panel shows the correlation of the ADC distributions for the upstream-sided Gas Cherenkov detectors (GCs), while the right panel shows the ADC distribution of the LG. For both of the panels, the black, red, and blue histograms are all events without any cut, electron, and pion events, respectively.

We evaluated the pion efficiencies with different incident angles at the threshold where the electron events of 90% are survived, and they are summarized in Table 1. For the incident angle of 90 ∘ and 180 °, pion efficiency is less than 5%, and thus, LGs must be inclined at 90 ° or 180 °.

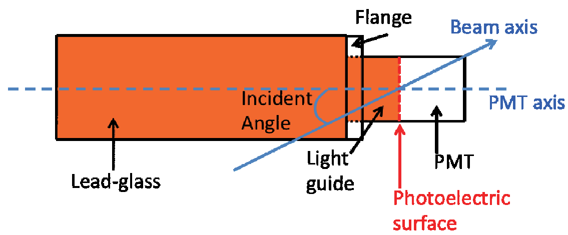

Fig. 1. The schematic of the inclined beam and the LG with PMT (Top view).

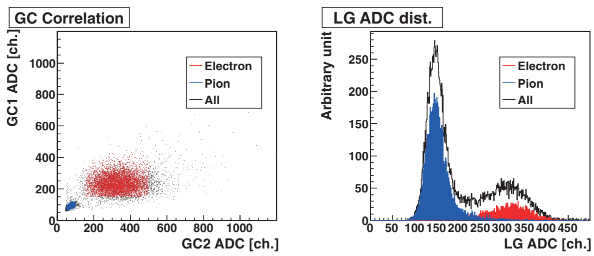

Fig. 2. Left: The correlation of the GC ADCs. Right: The ADC distribution of the LG.

Table 1. Pion efficiencies for the thresholds that yield 90% and 95% efficiency with different incident angles.

Ang. (deg.)	π eff. (%) @ e^-(90%)	π eff. (%)@ e^-(95%)
0	17.1 ± 0.2	26.1 ± 0.2
9.9	24.2 ± 0.3	32.0 ± 0.3
17	32.6 ± 0.3	47.5 ± 0.3
39	67.7 ± 0.2	79.2 ± 0.2
90	3.1 ± 0.2	6.9 ± 0.3
180	2.5 ± 0.1	6.5 ± 0.2

References

1) S. Yokkaichi *et al.*: in this report.
2) S. Kawabata *et al.*: Nucl. Instr. Meth., **A270**, 11 (1988).

Development of GEM tracker frontend electronics for the J-PARC E16 experiment

T. N. Takahashi, for the J-PARC E16 Collaboration

The proposed spectrometer for the J-PARC E16[1] consists of three kinds of detectors, GEM trackers, hadron blind Čerenkov detector (HBD) and leadglass electromagnetic calollimeter(LG), whose readout channels amount to ∼56000, ∼10000, and ∼1000, respectively. For such a large number of channels, dedicated electronics modules should be developed and tested. In 2012, a prototype of an analog frontend card for GEM tracker was developed.

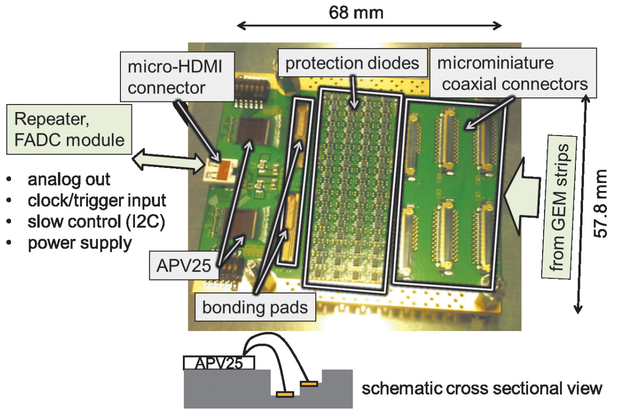

Fig. 1. Photograph of the APV25 hybrid card together with the schematic cross sectional view of the wire bonding area.

Figure 1 shows the prototype of the APV25 hybrid card. The APV25 hybrid card uses two APV25[2] chips on an area of 57.8×68 mm^2 and should cope with 256 readout channels per card. APV25 was basically designed as the frontend for silicon strip detectors, and therefore, its analog input section is vulnerable to the electrostatic discharge. In order to protect APV25 from sparks of the GEM detector, commercial transient voltage suppressor diode arrays are used. A pitch adapter made of an expensive material, such as ceramic or a flexible printed circuit, is not used in order to reduce the manufacturing cost. Instead, the bonding pads for the analog inputs are arranged in two layers on the PCB by using a milling machine. The bare APV25 dies are wire-bonded directly onto the PCB.

Figure 2 shows the GEM readout system for the test bench. As the backend readout electronics, we temporarily use an APVDAQ module and its repeater board, which was developed by the Belle-II silicon vertex detector (SVD) group[3]. The repeater board can drive the analog output signal of the APV25 chips upto 30 m. The APVDAQ is a VME-6U module. It features a 4-channel 10-bit Flash ADC (FADC) with

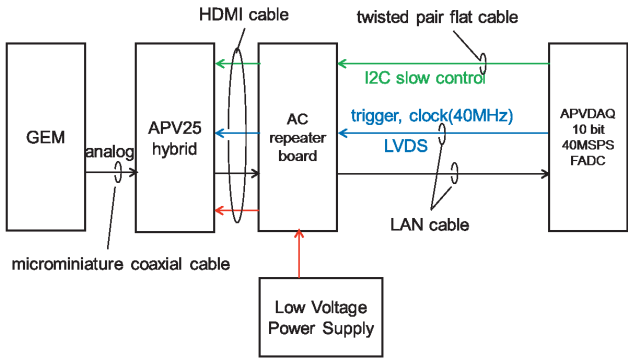

Fig. 2. Schematic view of the GEM readout system for the test bench.

40 MSPS to read multiplexed analog signals from 4 APV25 chips. For power supply, data and control signal transmission, HDMI cables, and category-7 LAN cables are used, considering the electrical performance and the cost. The former are used to connect the frontend hybrid and the repeater, whereas the latter are used between the repeater and APVDAQ module.

A beam test of the APV25 hybrid card prototype with a GEM tracker was performed at the J-PARC K1.1BR beam line from December 2012 to January 2013. The APV25 hybrid card almost worked well. The details of analysis status are reported elsewhere[4].

The next step is the improvement of the data acquisition rate. The raw data size of one APV25 chip is more than 3.7 kB per event because the long time window of ∼500 ns is needed for the charge collection under our experimental condition. In 2013, the system integration with the backend modules, which can be read via a gigabit ethernet port instead of the VME-bus and an online data reduction applying zero suppression algorithm on the FADC module, are planned.

References

1) S. Yokkaichi *et al.*: in this report.
2) M. Raymond *et al.*: Nuclear Science Symposium Conference Record, 2000 IEEE, vol.2, pp.0/113-9/118
3) M. Friedl and T. Tsuboyama: private communication.
4) Y. Komatsu *et al.*: in this report.

Study on the pion rejection factor of Hadron Blind Detector (HBD) for J-PARC E16 experiment

K. Aoki for the J-PARC E16 Collaboration.

The J-PARC E16 experiment[1] has been proposed to study the origin of hadron mass through mass modification of vector mesons in a nuclear medium. Vector mesons are produced in $p+A$ reactions and the invariant mass is reconstructed using e^+e^- decay. Therefore, electron identification is crucial to the experiment. We chose Hadron Blind Detector (HBD)[2], which is a mirrorless and windowless Cherenkov detector for electron identification. CF_4 is used as both the radiator and the amplification gas. A schematic of the photocathode of the HBD is shown in Fig. 1. We use a CsI-evaporated GEM as a photocathode. Three layers of GEMs work together to obtain sufficient gas gain to be readout with pads. A mesh is placed over the top GEM to manipulate the field of the drift gap, which is the area between the mesh and the top GEM. When in operation, a reverse bias field is applied so that most of the electrons from ionization at the drift gap are swept into the mesh. In contrast to ionization electrons, Cherenkov photons are converted into photoelectrons near the GEM surface where there is a field that extracts photoelectrons to GEM holes for amplification. Therefore, the HBD is sensitive to photoelectrons while it is blind to ionization electrons. The required rejection factor is 100 with an efficiency of more than 70%. To identify electrons from pions, we apply a certain charge threshold; however, some pions are misidentified as electrons due to the presence of a long Landau tail whose calculation is difficult. Ionization electrons that leave signal in the HBD, are generated close to the top GEM surface and at the transfer gap, which is the area between the top GEM and the second GEM. Ionization at the transfer gap undergoes only a two-stage amplification. To effectively suppress the effect of the transfer gap, the choice of gain of the top GEM is important. To evaluate the rejection factor of the HBD, we performed a test experiment at the J-PARC K1.1BR in Jan 2013. We used pion and electron beams with a momentum of 1 GeV/c. The GEMs used for the experiment have dimensions of 100 mm $\times$ 100 mm, with an insulating layer of 50 μm of kapton. We used GEMs without CsI evaporation this time and we focused on the rejection factors in this study. The readout pad dimensions were 20 mm $\times$ 20 mm. Three scintillation counters with dimensions of 10 mm $\times$ 10 mm were used to define the beam spot.

Figure 2 shows the rejection factors as a function of the drift gap field with a charge threshold at 10 primary electrons. The detection efficiency for electrons is considered to be 70% at this threshold since we observed 13 photoelectrons in a previous experiment with CsI-GEM. The transfer gap was 1.0 mm. The triangle, the square, and the diamond points in the figure were obtained for the configurations where applied voltages accross the top GEM (gas gain) were $\delta V_{\mathrm{GEM}} = 500$ V (15), 520 V (22), and 540 V (32) respectively. The rejection factor gradually increases as the applied voltages increases for a given drift gap field. This indicates that the amount of ionization at the transfer gap is significant. Therefore, reducing the transfer gap length and increasing the gain of the top GEM is effective in achieving a high rejection factor. Operation at 500 V or less is desiarble considering the GEM's operating life. A gas gain of 40 can be obtained with another type of GEM with a smaller hole size even when the applied voltage is 500 V. With such a GEM, we can expect a higher rejection factor than that obtained in the current test experiment. In addition, we can utilize the cluster size information when pads with finer segmentations are used. Combining these two factors, we can achieve the required rejection factor of 100 as described in[3].

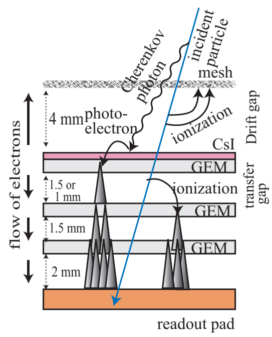

Fig. 1. Schematic of photocathode of HBD.

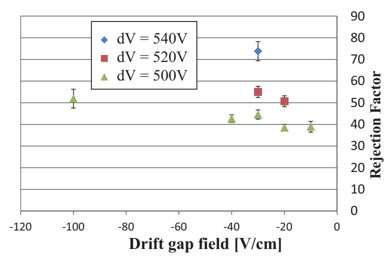

Fig. 2. Rejection factor obtained with a charge threshold at 10 primary electrons as a function of the drift gap field for different applied voltages across the top GEM.

References

1) S. Yokkaichi: in this volume.
2) A. Kozlov et al.: Nucl. Instrum. Meth. **A 523**, 345 (2004).
3) K. Kanno: in this volume.

The New PHENIX Analysis Train

J. Seele

The Relativistic Heavy Ion Collider[1)] is one of the most versatile particles colliders ever built having collided symmetric and asymmetric heavy ion species from a center of mass energy of 7.7GeV to 200GeV and polarized protons from a center of mass energy of 62.4GeV to 510GeV. PHENIX[2)] is one of two major experiments currently operating at RHIC. RHIC and PHENIX have been in operation for 12 years and through these years PHENIX has recorded data in nearly all of the collisional systems and energies.

In a given year, PHENIX records $\sim$1PB of raw experimental data. Currently, as there is no cheap, scaleable technology that would enable widescale analysis of all raw data by all of the PHENIX users in an on-demand fashion, PHENIX performs a physics-informed data compression by reconstructing the raw detector information into particle physics type primitives : charged particle tracks, energy deposits in calorimetry, etc. This reduces the data size to about 1/3 of its raw size and with this data size, PHENIX can store all the reconstructed data on its servers. PHENIX provides access to nearly all of the reconstructed data it has taken in the 12 years of operation. This large amount of varied information naturally necessitates a system of meta-data in order to track the data and ensure a high level of rigor and reproducibility in the analyses.

The PHENIX experiment possesses a large linux-based computing farm comprised of approximately 600 servers providing approximately 10,000 slots open to running user jobs. The farm is managed by using the condor batch computing system. This farm is the main tool for data analysis for the $\sim$400 PHENIX collaborators.

In order to meet the goals of efficient and reproducible analysis across the many disparate data sets, PHENIX built the Analysis Train (anatrain)[3)] system. The large amount of PHENIX data is broken up in smaller corpuscles, termed datasets, that represent a unique collisional species, energy, and data taking period. These datasets serve as the base organizing level for the anatrain. To give an idea of how the use proceeds. A PHENIX collaborator will develop an analysis aimed at a particular observable and dataset based on internal PHENIX software libraries. The user will then submit the analysis code to the manager of the anatrain who compiles the code and uses the anatrain to submit all the necessary jobs to the computing farm. In order to optimize the overall running time, many users' analysis jobs are submitted at a single time, grouped together, into what we term the monolithic running mode.

Early in the use of the anatrain, it was found one of the main time bottlenecks was the download time of the reconstructed data from servers where it resides to the computers where the analysis is done, thus it was decided that the system would only be able to cycle through the datasets once a week, which dictated then that the turnover in user analysis was also once a week, which in terms of analysis development is quite slow. Because of this, all the meta-tasks associated with analysis (debugging, compilation, etc) were also able to be slow. For example, the entire analysis code base was only compiled once a week before the next cycle began.

Recently, we became aware, through technological progress of our available computing power, that the bottleneck of moving the data from the server where it resides to the computer where the analysis will occur no longer exists. There were a number of paths to take forward in order to increase the speed and turnover of analysis in the collaboration. We could keep the same monolithic running mode where the data is cycled over, but at an increased frequency. This approach still suffered from its regimented nature that clashes with the way our collaborators worked. Thus an asynchronous, submit on request, model was identified as the best path forward.

In order to operate in the asynchronous mode, a number of the other meta-tasks needed modification. Instead of the simple single compile that was performed in the monolithic mode, a compile a request model was built in. Once the analysis passes a code test, the anatrain system submits the analysis jobs to the computing farm. The system monitors all the jobs as they download, run, and complete all the time analyzing the output for possible failure scenarios. Additionally, the system optimizes the download and running in multiple ways in real time so that extraneous downloading and running is not performed.

The anatrain provides PHENIX users with the capability to quickly and easily analyze one of many disparate datasets that the PHENIX experiment has recorded. The new anatrain is capable of a analysis turnover rate of 5-7 greater than the previous train system. This should allow the PHENIX users to quickly develop their analyses and lead to timely results for the PHENIX collaboration.

References

1) http://www.bnl.gov/rhic
2) http://www.phenix.bnl.gov/
3) C. Pinkenburg : J. Phys.: Conf. Ser. 331(2011)

Impact of circuit restoration on performance of PHENIX muon tracker

Y. Imazu, N. Amano, Y. Fukao, T. Iguri, M. Kim, T. Mibe, H. Murakami, T. Murakami, J. Murata, I. Nakagawa, K.R. Nakamura, H. Oide, S. Park, J. Seele, R. Seidl, N. Saito, K. Tanida, I. Yoon, K. Watanabe, and S. Yamashita

Investigation of the nucleon spin structure through measurement of W boson production in proton-proton collision recently commenced in 2011 in a PHENIX experiment. In the measurement, the PHENIX muon tracker (MuTr) plays a central role in both online and offline analyses to identify the muons decayed from the W boson[1–3].

MuTr is composed of strip-wire gas chambers with a cathode strip read-out. By weighting the read-out charge signals that spread over several cathode strips, we can determine the intersection position of a charged particle. In principle, lower noise, which is equivalent to the stability of the signals in the MuTr, provides better resolution. For effectively distinguishing muons from W bosons, which have a high momentum of typically >20 GeV, the MuTr must maintain its design resolution of $\sim$100 μm. To achieve this resolution, we need to exhaustively eliminate any possible source of noise/uncertainty in the MuTr that can cause any instability of the signals. Typically, the noise level of the MuTr needs to be limited to $\sim$1% for the typical size of the signals under the condition of an effective strip width of 1 cm.

However, an unexpected source of uncertainty was found to affect MuTr signals[4], which was the result of a cross-talk effect over read-out cathode strips through improperly grounded anode wires[5]. (By historical reasons, the improper ground state was kept unresolved for a long time and an easier solution to recover from it was lost during that time.) This effect created an unwanted, unstable baseline shift in the MuTr signals. As confirmed through dedicated measurements carried out in 2012, the noise level was found to become twice as bad as expected (Fig. 1). The noise level is expected to increase considerably as the collision rate increases.

To address the degradation in the MuTr performance resulting from the cross-talk effect, we conducted basic studies with test benches in RIKEN[5] to establish practical solutions of circuit restoration in order to ensure proper anode grounding. Then, we partially applied these solutions to the PHENIX MuTr starting from the 2011 operations. Through the data collected in the 2011 and 2012 operation, we were able to confirm that the solutions were effective for the suppression of the cross-talk effect over the entire MuTr acceptance region, as expected from the R&D studies[6], and suppress the noise level enough to achieve the requried resolution, even under high collision rate conditions (Fig. 1).

We finally completed full application of the grounding solutions to the entire MuTr acceptance by last autumn. In the upcoming 2013 operation, we will operate MuTr in the optimum condition for the W measuremnt for the first time. Final evaluation of the impact of the circuit restoration on the measurement will be obtained through the data that will be obtained soon.

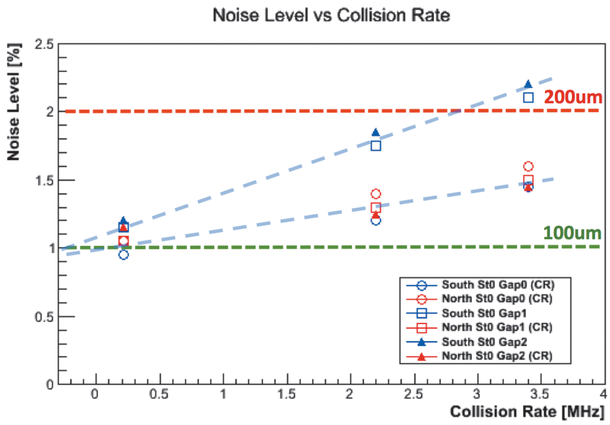

Fig. 1. Measured noise levels in several MuTr regions through the 2012 operation. The horizontal axis indicates various collision rates. Proportional behaviour of the noise level against the collision rate can be seen. The area denoted as “CR” corresponds to where we applied the circuit restoration. The MuTr resolutions expected from the noise level are shown also as a horizontal dashed lines.

References

1) Y. Fukao et al. *RIKEN Accel. Prog. Rep.*, 44, 2011.
2) R. Seidl et al. *RIKEN Accel. Prog. Rep.*, 45, 2012.
3) H. Oide et al. *RIKEN Accel. Prog. Rep.*, 45, 2012.
4) T. Mibe et al. *RIKEN Accel. Prog. Rep.*, 42, 2009.
5) Y. Imazu et al. *RIKEN Accel. Prog. Rep.*, 44, 2011.
6) Y. Imazu et al. *RIKEN Accel. Prog. Rep.*, 45, 2012.

Improvement of groval alignment of PHENIX muon tracker

T. Iguri, N. Amano, Y. Fukao, Y. Imazu, M. Kim, T. Mibe, H. Murakami, T. Murakami, J. Murata, I. Nakagawa, K.R. Nakamura, H. Oide, S. Park, J. Seele, R. Seidl, N. Saito, K. Tanida, I. Yoon, K. Watanabe, and S. Yamashita

The alignment of the tracking chamber is one of the long standing challenge for nuclear physics experiments. The PHENIX muon system measures the charged particle momentum with three tracking stations of cathode readout chambers, namely muon tracker (MuTr) impremented in a magnetic field volume. The precision of the relative alignment between the three tracking chambers directly affects the resolution of momentum measurment. Over the last a few years, PHENIX spin program has been focusing on the polarized sea quark measurements in protons through asymmetry measurement of W-boson production[1]. Because of the heavy mass of W-boson, decayed muon (which we detect) from W-boson has high transverse momentum on the order of 40 GeV. Such a high momentrum trajectory is barely bent in the magnetic field and its sagitta is on the order of several mm in the MuTr volume. The possible mis-aligment of MuTr chambers will result in further momentum smearing over its intrinsic resolution. The higher the momentum, the more serious side effect on the charge determination of the traversing particle. The possible charge mis-reconstruction is a fatal error for the asymmetry measurement, since the opposite charge (either W^+ or W^-) production is predicted to appear in opposite asymmetry.

PHENIX collaboration developed the global alignment program, which calculates the smallest χ^2 solution of actual hit locations when the straight tracks traverse the three MuTr stations keeping the relative location of chambers as free parameters. This way, the program will find the relative alignment of chambers to minimize the residuals, as defined in Fig. 1. The alignment parameters are limited to transverse shift and rotations. The deformation of the chambers is out of the scope of this research.

The consequence of the alignment optimization after analyzing magnetic field off data (all trajectories are straight) is presented in Fig. 2. The track samples used for the analysis is dominated by the low momentum hadrons punch through the muon tracker volume. Fig. 2 compares the residual distribution (x-axis) as a function of the distance from the beam center. The muon tracker on Station2 covers a range of 60 to 200 cm from the beam center. The black data points show the original residual distribution before the alignment optimization, while the red data points show the consequence of the optimization. As you can see, the optimized new alignment succsesfuly found the solution to shift the residual distributions around residual=0 compared to the original.

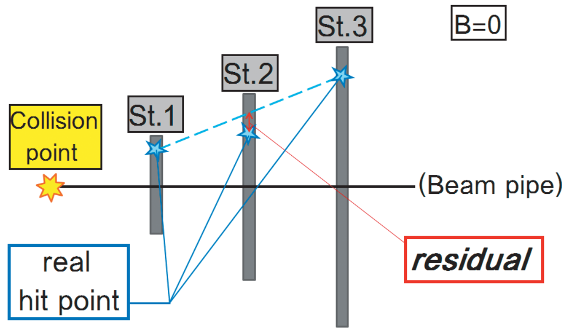

Fig. 1. Residual is defined as the distance between the linear interpolation of station-1 and station-3 hit locations at the station-2 and the actual hit in the station.

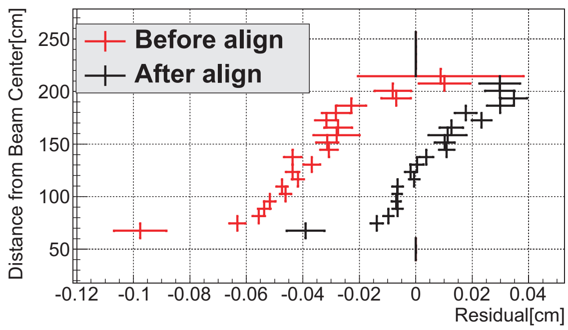

Fig. 2. Residual distribution plotted as a function of the distance from the beam center.

However, one notices that the optimized alignment is well centerized around zero only in the region closer to the beam center. The alignment is still not successful for the outer region. This is due to the statistical bias in the minimum χ^2 calculation. Because of the heavy weight of hadron production cross section towards the inner region (large rapidity), the impact of the mis-alignment of the outer region becomes weak. Furthermore, the residual distribution does not seem to be straight to the radial direction. We are investigating the further correction required to improve the alignment by introducing a work-around solution of the unwanted statistical weight of the track samples and possible internal alignement within the chamber to correct for non-linear relation of the residual towards the radial direction.

References

1) H. Oide: RIKEN Accel. Prog. Rep. **45** (2012).

Drift chamber construction for Drell–Yan measurement in SeaQuest experiment at Fermilab

K. Nagai,[*1] S. Obata,[*1] Y. Kudo,[*2] S. Miyasaka, Y. Goto, Y. Miyachi, K. Nakano, F. Sanftl,[*1] S. Sawada, and T.-A. Shibata

The proton consists of many partons, namely quarks, anti-quarks, and gluons. The parton distribution of the anti-quark $\bar{u}$ had been considered to be the same as that of $\bar{d}$ based on the SU(3) flavor symmetry. However, the NMC experiment at CERN revealed in 1991 that $\bar{u}$ and $\bar{d}$ are asymmetric. The SeaQuest collaboration at the Fermi National Accelerator Laboratory (Fermilab) aims to measure the flavor asymmetry between $\bar{d}$ and $\bar{u}$ in the region of Bjorken $x > 0.3$.

The Drell–Yan process, $q + \bar{q} \to \gamma^* \to \mu^+ + \mu^-$, is suitable for measuring anti-quarks in a proton because an anti-quark in a proton is always involved in this process. Thus the SeaQuest experiment measures momenta of muons created by the Drell–Yan process. The SeaQuest experiment uses a proton and deuteron as fixed targets and a 120-GeV proton beam with a typical intensity of 10^{13} in a 5-second pulse. The SeaQuest spectrometer has four tracking stations. We have constructed two operational drift chambers at Station 3: St. 3+ and St. 3− for the upper and lower halves respectively. Figure 1 shows the front view of the chamber. The outer dimensions of the chamber are

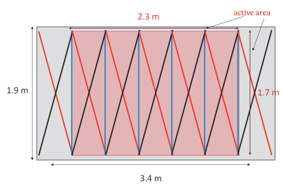

Fig. 1. Front view of the drift chamber. The outer dimensions of the chamber are 1.9 m × 3.4 m, and the active area is 1.7 m × 2.3 m.

1.9 m × 3.4 m, and the active area is 1.7 m × 2.3 m. There are six planes in each chamber and four planes out of six are tilted by 14° or by −14° from the vertical direction. The gas used for both chambers is a mixture of argon (86%), methane (10%) and CF_4 (4%). These chambers have two types of wires. One is named the "sense wire" and made of gold-plated tungsten of 30 μmϕ, and the other is made of gold-plated Be-Cu of 80 μmϕ. These wires form a cell structure. One sense wire is placed at the center of each cell and is surrounded by eight other wires. The distance between neighboring wires is 1 cm. The size of one cell is accordingly 2 cm × 2 cm. The number of readout channels is 768 in six layers.

*1 Tokyo Institute of Technology, Graduate School of Science and Engineering
*2 Yamagata University, Faculty of Science

We are constructing the new St. 3− chamber at Fermilab for the physics run that starts in June 2013. We started assembling the frame of the St. 3− chamber in June 2012. In July 2012, we set up an optimized procedure for stretching wires. We completed stretching 5,154 wires in two months. The wire tension is set to 75 gf for the sense wire and 130 gf for others. We loaded the wire with a weight of a metal block.

We have checked the tension of every wire stretched. Since the eigenfrequency of wire oscillation depends on the tension of the wire, we determined the eigenfrequency of each wire to measure the wire tension. We placed a magnet around the wire and injected a pulse current into the wire using a function generator. The wire was oscillated by the periodic Lorentz force due to the magnetic field and the pulse current. The frequency of pulse current was gradually changed. When it equaled the eigenfrequency of the wire, the amplitude of wire oscillation became maximum.

The requirement regarding the accuracy of the wire tension is better than ±10%. We re-stretched 21 wires whose tension was out of this range. We have currently achieved an accuracy of 5%.

Figure 2 shows the results of measurement of the tension of certain wires of a layer that were first stretched. We measured the tension of some wires of the layer

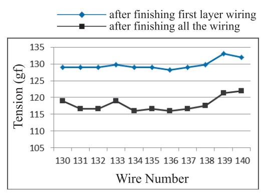

Fig. 2. Results of tension measurement. The blue line indicates the result of the tension measurement immediately after finishing the first layer wiring. The black one indicates that after stretching all the wires.

twice: immediately after finishing stretching wires of the first layer (the blue line in Fig. 2), and after stretching all the wires (the black line in Fig. 2). The wire tension decreased by about 9-10%. This result is consistent with our expectation based on the frame deformation.

In January 2013, we finished attaching windows to the chamber. We are currently pumping a dry gas into the chamber. This process will take about 40 days. When it is completed, we will begin a high voltage training for about one month and complete the construction of the new chamber in April.

Development of a wide-dynamic-range front-end ASIC for W + Si calorimeter for ALICE upgrade

S. Hayashi, H. Hamagaki,[*1] T. Gunji,[*1] M. Tanaka,[*2] and H. Ikeda[*3]

ALICE is one of the experiments at the CERN-LHC and it is dedicated for relativistic heavy-ion collisions. The study of the parton distribution function (PDF) in nuclei is essential to characterize the dense and hot medium properties generated in relativistic heavy ion collisions[1)]. However there are still large uncertainties regarding the gluon PDF at small values of *Bjorken-x* ($10^{-5} < x < 10^{-3}$) which is proportional to e^{-y} ,where y denotes rapidity, and small value of the momentum transfer scale Q^2 (∼a few GeV^2) in which region it is expected that the gluon density becomes extremely high and eventually saturates[2)3)].

The installation of an electromagnetic calorimeter (FOCAL) at forward rapidity ($2.5 < \eta < 4.2$) in the ALICE experiment is currently under consideration[4)]. FOCAL is intended to measure prompt γ and π^0 particles up to a transverse momentum of 50 GeV/c, covering the range of $10^{-5} < x < 10^{-3}$ and Q^2 = 1-1000 GeV^2. FOCAL consists of three longitudinal segments and each segment has seven layers of W + Si pad modules. The pad size is 1.1 cm × 1.1 cm and the thickness of the tungsten and Si pad is 3.5 mm ($\sim 1X_0$) and 525 μm. Si pixel layers are also placed at the first segment to identify $\pi^0 \to 2\gamma$ decay at high values of p_T. The signal from the Si pad is summed up longitudinally at each segment. The dynamic range of the signal varies from 50 fC to 200 pC and our ASIC is designed to cope with a wide dynamic range of the order of 10^4. As shown in Fig. 1, the first stage of our ASIC is composed of a current conveyor with four different gain outputs (1/512, 8/512, 64/512, and 256/512)[5)]. Another output with a gain of 128/512 is used to generate a fast trigger. Designing and simulation studies were carried out in the collaboration with the OpenIT project[6)]. The prototype chip (CALFE01) was fabricated with 0.25μm technology by UMC. The power consumption of the ASIC is 15 mW per channel for the analog part and 1.5 mW for digital part.

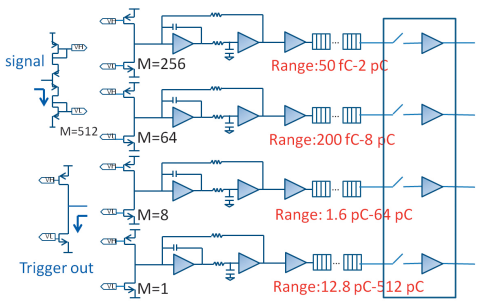

Fig. 1. Schematic of one readout channel for FOCAL.

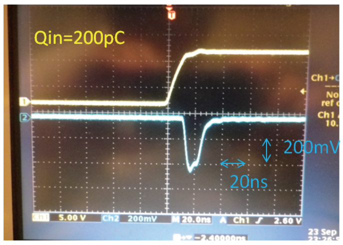

Fig. 2. Transient response of the trigger output when input charge is 200 pC. The upper line shows the input pulse. The lower line shows the pulse shape of the trigger output.

Figure 2 shows the transient response of the trigger output. The rising time of an output pulse is 10 ns which is equal to that of the input pulse. Figures 3 shows the pulse height and nonlinearity of the output for a given readout channel. The integrated nonlinearity is about 1% or less for all measured range. Further detailed studies will be carried out and the overall ASIC performance with a FOCAL detector will be checked.

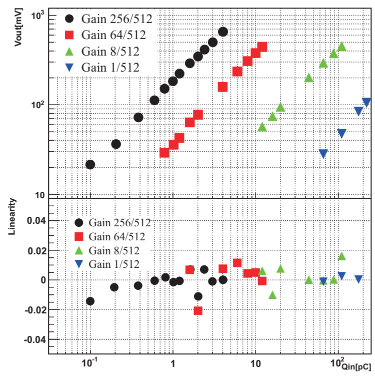

Fig. 3. Upper panel: Pulse height at AMC output. Lower panel: Non-linearity at AMC output.

*1 Center for Nuclear Study, Graduate School of Science, The University of Tokyo
*2 KEK, and Open-It
*3 JAXA, and Open-It

References

1) A. Adare, et al.: arXiv:1105.3928
2) L.D. McLerran and R. Venugopalan: Phys. Rev. D 49 2233 (1994)
3) K.J. Eskola, et al.: [hep-ph/0902415]
4) Y. Hori et al.: 2011 J. Phys.: Conf. Ser. 293 012029
5) K. Koli et.al.: Helsinki University of Technology Electronic Circuit Design Laboratory Report 30, Espoo 2000
6) http://openit.kek.jp/

Development of a polarized proton target with irradiated polyethylene

Y. Miyachi, K. Akasaka,[*1] S. Asaki,[*1] N. Doshita,[*1] Y. Fukao, Y. Goto, R. Hashimoto,[*1] S. Ishimoto, T. Iwata,[*1] H. Kobayashi,[*1] T. Kumada,[*3] H. Matsuda,[*1] I. Nakagawa, G. Nukazuka,[*1] K. Nakano, S. Sawada, T.-A. Shibata, S. Suzuki,[*2] K. Taketani,[*2] and Y. Tochigi[*1]

Spin polarized Drell-Yan (DY) is a long-awaited tool that can be used to explore the 3D internal structure of the proton, in terms of the transverse momentum dependent parton distribution functions. In contrast to pion-induced DY, whose observable will be measured with COMPASS at CERN in 2014, the measurement of the proton-induced DY, such as the E906/SeaQuest measurement at Fermilab, accesses anti-quarks inside the proton in the large Bjorken-x. In order to realize the measurement of the polarized-proton-induced DY, we have been developing a suitable polarized proton target.[1,2] Since a high cooling power is required to maintain polarization with a high-intensity beam, the use of a material with a large surface area, such as polyethylene powder or fiber, has some advantages over the use of solid NH_3 or LiH, which are present candidates for the polarized target material.

In order to create free electrons needed for dynamic nuclear polarization (DNP), we irradiated polyethylene samples with different form and crystallinity, including ethylene-octene copolymer (ENGAGE^{TM} 8003), which has a density of 0.87 g/cm^3, using a 2 MeV electron beam at the electron acceleration facility of the Takasaki Advanced Radiation Research Institute, Japan Atomic Energy Agency. It is known that the created free electrons recombine at a certain temperature above 77 K. The samples were placed on a copper plate, which was installed in a container with an oxygen absorber, and were indirectly cooled down to prevent the recombination by circulating liquid nitrogen through the plate. By using different beam conditions, we performed irradiation with 5 different doses of the electron beam, from 10^{14} to 10^{16} electrons/cm^2, for each material type.

We estimated the spin density of the irradiated ENGAGE^{TM} 8003 samples by measuring the ESR signal at 77 K. It should be noted that 2×10^{19} spins/g is the appropriate spin density for DNP. In Fig. 1, the measured spin densities are shown for the different electron doses. In general, a larger spin density was observed as the electron dose increased. It can be also seen that the spin density might become saturated above 10^{16} electrons/cm^2, as reported in a previous work.[3] Observed differences in the spin densities with the same electron dose might be caused by recombination during irradiation.

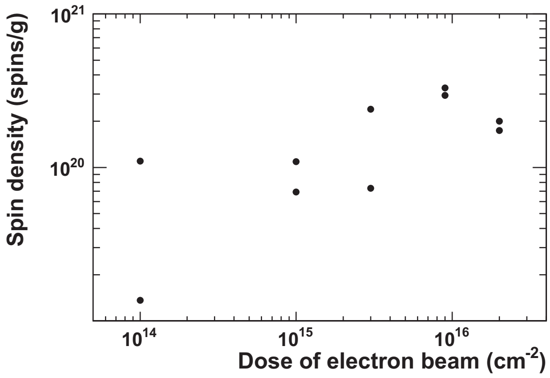

Fig. 1. Electron dose dependence of the electron spin density.

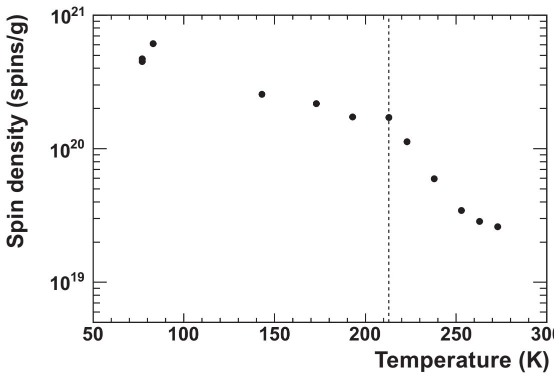

Fig. 2. Spin density development of the irradiated ENGAGE^{TM} 8003 sample with increasing temperature.

In order to determine the critical temperature of ENGAGE^{TM} 8003, we measured the spin density by changing its temperature from 77 K to 300 K. The results are shown in Fig. 2. It is clearly seen that the recombination of the created free electron occurred at the glass transition temperature, 213 K, which is indicated with a vertical dashed line.

*1 Yamagata University
*2 KEK
*3 Kansai Photon Science Institute, Japan Atomic Energy Agency

References

1) Y. Goto *et al.*: RIKEN. Accel. Prog. Rep. **45**, 167 (2012)
2) S. Ishimoto *et al.*: In this report.
3) T. Kumada *et al.*: J. Magn. Reson. **218**, 59 (2012)

Development of polarized proton target for SeaQuest experiment

S. Ishimoto, K. Akasaka,[*1] T. Asaki,[*1] N. Doshita,[*1] Y. Fukao, Y. Goto, T. Iwata,[*1] H. Kobayashi,[*1] H. Matsuda,[*1] Y. Miyachi, I. Nakagawa, K. Nakano, S. Sawada, T.-A. Shibata, S. Suzuki,[*2] K. Taketani,[*2] and Y. Tochigi,[*1]

We have been conducting the SeaQuest experiment with the aim of detecting muon pairs from the Drell–Yan process with a 120-GeV unpolarized proton beam extracted from the Fermilab Main Injector[1]. An extension of the SeaQuest experiment with a polarized proton target has been discussed for implementation in order to study the spin structure of the proton.

The polarized Drell–Yan experiment requires a polarized target with high resistivity to radiation damage. Solid NH_3 and LiH irradiated by electron beams are candidates of Dynamic Nuclear Polarization (DNP) target material. High cooling power at low temperature is required to maintain the target's polarization with a high-intensity beam.

We are developing a polarized proton target at KEK and Yamagata University[2] for use towards the polarized Drell–Yan experiment[3, 4]. The KEK target system is also to be used for the development of a neutron polarized filter and material research at J-PARC.

We have been developing an NMR system and along with the required software. Figure 1 shows the NMR Q-meter. It uses a radio frequency phase sensitive detection technique[5]. Figure 2 shows the proton thermal equilibrium (TE) signal in polyethylene at 2.5 T and 1.19 K recorded at Yamagata University. These data were obtained by the newly developed NMR system after averaging over 500 times. The strength of the signal indicates good S/N performance of our NMR system. The NMR TE signal S_0 at around 1 K will be used for the calibration of polarization. The accuracy of target polarization P_t depends on the uncertainty of S_0 and the temperature for the duration of obtaining the S_0 data.

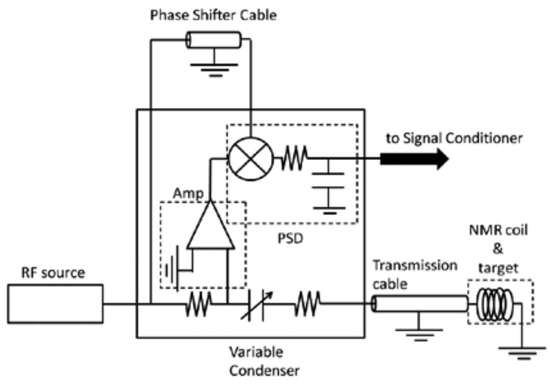

Fig. 1. Diagram of NMR Q-meter (106 - 213MHz)

*1 Department of Physics, Yamagata University,
*2 KEK,

The 1-K refrigerator and 5-T magnet have been originally developed at Michigan University[6] and they are presently located in the KEK-PS North Counter Hall.

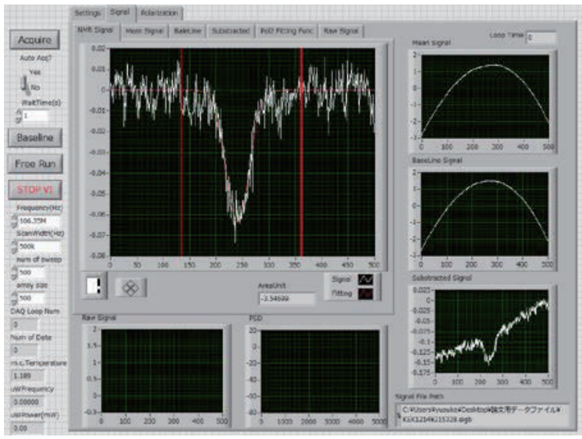

Fig. 2. Proton NMR in polyethylene at 2.5 T and 1.19 K, the polarization of TE signal was estimated as 0.21 %

Figure 3 shows the temperature record of the target as obtained by the Speer carbon resistor calibrated with helium pressure. We are planning to use a PID heater controller to keep the target temperature stable. A capacitance pressure sensor for evaporated helium will be used to obtain the target temperature with garter accuracy.

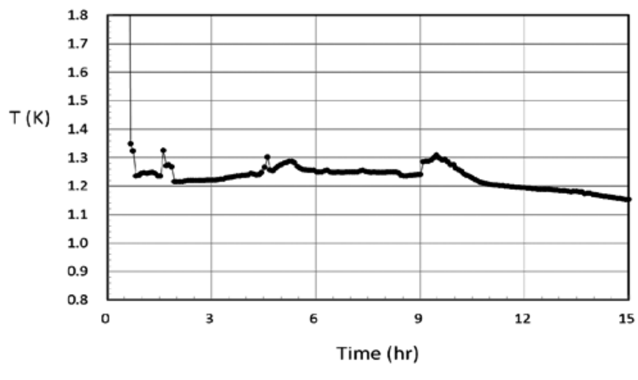

Fig. 3. Temperature record of target in the 1 K refrigerator

This research is supported by the JSPS Grant-in-Aid for Scientific Research (B) 22340070.

References

1) S. Noh and I. Yamaguchi: Jpn. J. Appl. Phys. **40**, L1299 (2001).
2) Y. Miyachi et al.: RIKEN. Accel. Prog. Rep. **46**, (2013).
3) Y. Goto et al.: RIKEN. Accel. Prog. Rep. **44**, 220 (2011).
4) Y. Goto et al.: RIKEN. Accel. Prog. Rep. **45**, 167 (2012).
5) G. Court et al.: Nucl. Instr. and Meth. **A 324**, 433(1993).
6) D. G. Crabb et al.: Phys. Rev. Lett. **64**, 2627 (1990).

Development of Time Projection Chamber for LEPS2

Y.Nozawa, M.Niiyama, M.Yosoi, Y.Kasamatsu,*[1] and H.Ohnishi

LEPS2 is a newly constructed beamline at SPring-8. We will study hadron photoproduction at this beamline. In the LEPS2 experiment, a Time Projection Chamber (TPC) will be installed in the solenoid magnet. The target will be installed inside the TPC, and the charged particles scattered at large angles will be detected by the TPC.

The position resolution is written with some parameters as follows.

$$\sigma_{xy}^2 = \sigma_{0,xy}^2 + \sigma_{\mathrm{W,P}}^2 \tan^2\alpha + \sigma_{D_\mathrm{T}}^2 L_D \quad (1)$$
$$\sigma_z^2 = \sigma_{0,z}^2 + \sigma_{\mathrm{dip}}^2 \tan^2\lambda + \sigma_{D_\mathrm{L}}^2 L_D. \quad (2)$$

Here, α is the angle between the track of charged particles and direction of wires (and pads); we call it as track-wire angle. λ is the angle between the track and the pad plane; we call it as dip angle. L is the drift length. We measured these coefficients using prototype TPCs for the electron beam at LEPS beamline. We also measured the performance by changing gases and preamps. By utilizing these coefficients, we estimated the mass resolution of Θ^+ and $\Lambda(1405)$. We obtained the masses of Θ^+ and $\Lambda(1405)$ from invariant mass of π^+, π^-, p, and missing mass of π^+, π^-, π^+ at the final state, respectively.

In order to reduce the multiple scattering, a neon-based gas mixture will be used in the TPC active volume. Therefore, we measured the performances with Ar-CH_4(90:10) gas (P10 gas), and Ne-CH_4(90:10) gas, which has less amount of material than P10 gas. We obtained a position resolution of 108 μm for P10 gas and 125 μm for Ne-CH_4 gas with 4 mm $\times$ 10 mm pads. The position resolution with Ne-CH_4 gas is lower than that with P10 gas. Since the number of ionized particles of Ne-CH_4 gas is less than that of P10 gas, the gain has to be obtained by avalanche. Therefore, the low position resolution with Ne-CH_4 gas may be caused by spatial broadening of the avalanche. The position resolution with Ne-CH_4 gas is lower than that with P10 gas. However, the mass resolution of Θ^+ and $\Lambda(1405)$ with Ne-CH_4 gas, which was obtained by simulation, was higher than that with P10 gas because the multiple scattering is dominant in the low momentum region. Therefore, we will use Ne-CH_4 for the gas of TPC.

Secondly, we measured the position resolution with 2 kinds of preamps. The position resolution decreased with increasing the track-wire angle for constant the sense wire voltage because the avalanche region on the sense wires widens with the track-wire angle. However, it was found that the position resolution improved with increasing sense wire voltage at larger track-wire angles, as shown in Fig.1. We think that the fluctuation in the charge amount of the avalanche in this region causes the deviation. In order to apply higher sense wire voltage while avoiding the overflow of ADC, we will use lower gain preamps. Therefore, we measured the position resolution with 1V/pC and 2V/pC preamps. The position resolution with 1V/pC preamp was higher than that with 2V/pC when the value of ADC of MIP was kept constant. The track-wire angle dependence with these preamps isshown in Fig.2. The position resolution at around 20° with 2V/pC was 907 μm, and that with 1V/pC was 844 μm. Therefore, 1V/pC preamps will be used for readout of the TPC.

We also measured the dip angle and drift length dependence, and using spatial resolutions obtained from these study, we estimated the invariant mass resolution of Θ^+ in its $K_\mathrm{S}^0\, p$ decay to be 6 MeV/c^2 from the simulation.

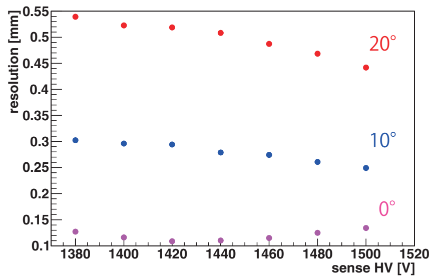

Fig. 1. The sense wire voltage dependence with P10 gas at 0°, 10°, and 20° in the track-wire angle.

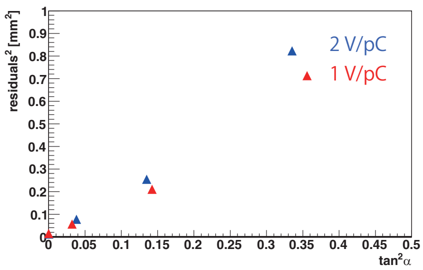

Fig. 2. The track-wire angle dependence with 1V/pC and 2V/pC preamps when the MIP peak is around 200 mV.

*1 Research Center for Nuclear Physics, University of Osaka

References

1) T. Lohse and W. Witzeling: The Time Projection Chamber, F. Sauli: Instrumentation in High Energy Physics, 1993, pp. 82-156

Performance study of a high-refractive-index aerogel Cherenkov detector for the spectroscopy experiment of η' mesic nuclei

Y.K. Tanaka, S. Friedrich,[*1] H. Fujioka, H. Geissel, R.S. Hayano, K. Itahashi, S. Itoh,[*3] V. Metag,[*1] M. Nanova,[*1] T. Nishi, K. Okochi, H. Outa, K. Suzuki, T. Suzuki, M. Tabata,[*4,*5] Y.N. Watanabe, and H. Weick

We have developed a high-refractive-index aerogel Cherenkov detector[1)] for the spectroscopy experiment of η' mesic nuclei at GSI.[2,3)] We have planned a missing-mass spectroscopy of the $^{12}C(p,d)\eta'\otimes^{11}C$ reaction near the η' emission threshold to search for η' mesic nuclei.[4)] A 2.5 GeV proton beam will be injected into a ^{12}C target, and the momenta of the ejectile deuterons will be measured using a fragment separator (FRS) as a spectrometer. At the downstream focal plane of the FRS, in addition to the signal deuterons (0.5 kHz, $\beta = 0.82$–0.85), a large number of background protons (50 kHz, $\beta = 0.94$–0.96) are expected to reach the detectors. The purpose of the Cherenkov detector is to reduce this background rate to the order of 100 Hz at the trigger level.

A schematic view of this detector is shown in Fig. 1. We used a 2 cm-thick silica aerogel, with a refractive index of 1.18, as a radiator.[5)] Behind the radiator, a mirror box was placed to guide the Cherenkov photons to the PMTs attached on the mirror box.

In November 2012, we tested this detector with deuteron beams at GSI. We employed deuteron beams of two velocities, $\beta = 0.843$ and $\beta = 0.944$, to evaluate the performance for both the background proton and the signal deuteron in the main experiment.

With the higher-velocity deuterons, a sufficient number of photoelectrons were observed. The red line in Fig. 2 shows the histogram of the total number of photoelectrons with the beam injected at the center of the radiator. From this histogram, the average number of photoelectrons was deduced to be 30.8, and the detection efficiency was evaluated to be higher than 99.9% even at a 9 photoelectron threshold. This efficiency was quite sufficient for background rejection in the main experiment.

In addition, the observed histogram with the lower-velocity deuterons is shown by the blue line in Fig. 2. A peak was seen at the pedestal position, as expected, but also a long tail of up to more than 10 photoelectrons was observed. This might be due to Cherenkov radiation in an ultraviolet region and/or Cherenkov photons from delta rays emitted in the aerogel, and would lead to a few percent of overkill of the signal deuterons (e.g., 3% at a 9 photoelectron threshold) in the main experiment.

From the test experiment, it was confirmed that this detector can be used for background rejection at the hardware level in the main experiment. As a future work, we plan to study a possible improvement to reduce the expected signal overkill, such as the lowering of the refractive index.

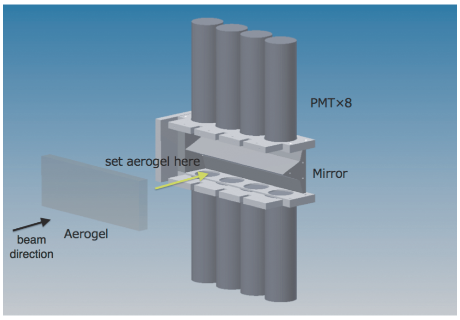

Fig. 1. Schematic view of the aerogel Cherenkov detector.

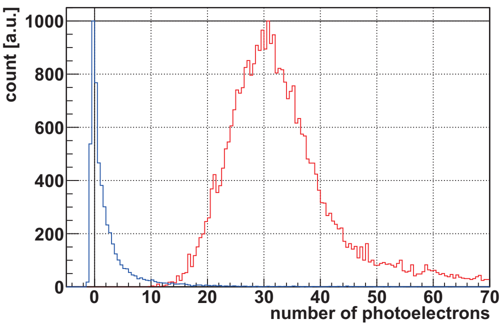

Fig. 2. Histograms of the total number of observed photoelectrons. Red indicates the higher velocity, $\beta = 0.944$. Blue indicates the lower velocity, $\beta = 0.843$.

References
1) Y.K. Tanaka *et al.*: Accel. Prog. Rep. **45**, 172 (2012).
2) K. Itahashi *et al.*: Letter of Intent for GSI-SIS (2011).
3) K. Itahashi *et al.*: Prog. Theor. Phys. **128**, 601 (2012).
4) D. Jido, H. Nagahiro, and S. Hirenzaki: Phys. Rev. C **85**, 032201(R) (2012).
5) M. Tabata *et al.*: Nucl. Instrum. Methods A **623**, 339-341(2010).

*1 Universität Gießen, Germany
*2 Department of Physics, University of Tokyo
*3 Japan Aerospace Exploration Agency
*4 Department of Physics, Chiba University

Development of new digital image analysis system for NEWTON experiment

K. Ninomiya, R. Kishi,[*1] H. Murakami,[*1] S. Saiba,[*1] T. Sakuta,[*1] A. Taketani, and J. Murata

According to ADD model[1)], extra dimensions are predicted to exist at below millimeter scale. In such a case, the observation of a deviation from Newton's inverse square law can be expected below millimeter scale. A modified gravitational potential is historically expressed in a Yukawa interaction form.

$$V(r) = -G\frac{mM}{r^2}\left(1+\alpha e^{-\frac{r}{\lambda}}\right), \qquad (1)$$

here, α is coupling constant and λ is the range of the new interaction. Numbers of experiments have been tested the inverse square law, excluding the non-zero value of α in various length scales. However, a high precision test of the Newtonian inverse square law is performed at astronomical scales. For this reason, we are test of the Newtonian inverse square law at below mm scale using torsion pendulum. An angular displacement of the torsion pendulum is measured as gravitational signal. In our experiment, the angular displacement is obtained using digital image analysis system. This analysis system is originally developed for PHENIX experiment, as an optical alignment system (OASys)[2,3)]. Applying this system, we developed digital analysis system using CCD camera. The motion of the torsion pendulum is captured with CCD camera, and stored as static sequence files. After then, image analysis is performed for all image files. The angle information of the torsion pendulum can be obtained by performed a linear least square fitting on the pixel intensity data[4)]. In this system, typical angular resolution of 100 micro degrees is achieved.

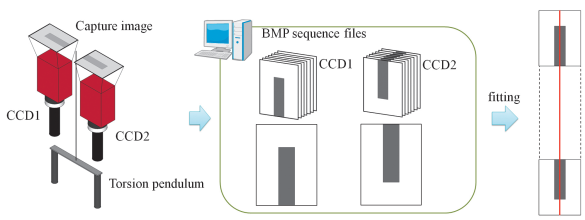

Fig. 1. 2CCD camera system.

Last year, we developed new experimental device(Newton IV) aiming to test the Newtonian inverse square law with the highest precision at below mm scale[5)]. As a result of the measurement, it became clear that the more precise position resolution was required. Therefore, in this year, we developed new image analysis system using microscope and two CCD cameras aiming to achieve the more precise angular resolution. The angular resolution is improved using CCD camera with microscope. However, if we capture only one side of the torsion pendulum using CCD camera, it would be difficult to distinguish the twisting motion from a parallel motion. Therefore, the parallel motion can become a systematic error. For this reason, we capture the both edges of the torsion pendulum using two CCD cameras. To capture the both ends of the torsion pendulum, it can be easy to distinguish the twisting motion from a parallel motion. Therefore, the new capture system can suppress the systematic error from the parallel motion. In addition, we can expect improvement of the angular resolution using new system by factor 1/10 comparing with a current analysis system.

We are now performing Newton IV experiment using new analysis system. Figure 2 shows an upper limit of the new Yukawa interaction.

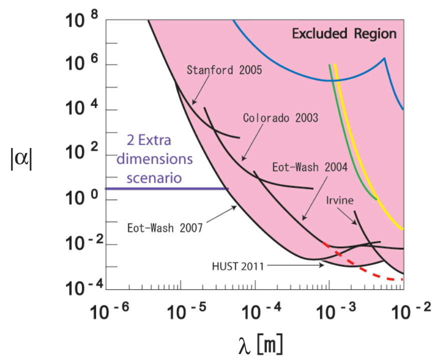

Fig. 2. Upper limit of the new Yukawa interaction at below centimeter scale.

The shaded area shows experimentally excluded regions. Red dashed line is expected area from our experiment. We will be able to achieve the most precise test of the inverse square law at below mm scale using new image analysis system in Newton IV experiment.

References

1) Nima Arkani-Hamed, Savas Dimopoulos, Gia Dvali, Phys. Lett. B 429 (1998) 263-272.
2) J. Murata, IEEE Nuclear Science Symposium Conference Record 675 (2005).
3) J. Murata et. al., Nucl. Instrum. Meth. A 500(2003) 309-317
4) K. Ninomiya et.al., Journal of Physics: Conference Series 189 (2009) 012026
5) H. Nishio, Master thesis, Rikkyo University (2011)

*1 Department of Physics, Rikkyo University, Japan

Development of the GTO module

H. Baba, T. Ichihara, T. Ohnishi, S. Takeuchi, K. Yoshida, Y. Watanabe, S. Ota,[*1] and S. Shimoura[*1]

We have developed the Generic Trigger Operator (GTO) module for nuclear physics experiments. This is a NIM module aimed at providing intelligent and remote trigger operations. In RIKEN RIBF, the beam line is very long and detectors are located at distant places. Signals are measured by a network-distributed data acquisition system[1]. Recently, FPGA-based modules of “Logic Unit for Programmable Operation” (LUPO) and “Mountable Controller” have been introduced[2,3]. FPGA is very powerful for constructing custom logical circuits. LUPO is a very successful VME/CAMAC module that provides the functions of time stamp, I/O and interrupt register, etc. The GTO module can be referred to as the NIM version of LUPO with the network interface. It enables us to change the connectivity of input and output signals like a multiplexer circuit by network commands. This feature is very useful for the long beam line in RIBF. In addition to the multiplexer function, GTO can have a variety of logical functions such as coincidence, veto, latch, gate, delay, clock, divider, selector, and fan-in/fan-out. These functions can be combined into the GTO module. The main components of GTO are shown in Figure 1. For logic signals, there are 24 NIM inputs and 8 NIM outputs connectors. To communicate with computers, GTO has Ethernet and USB2.0 interfaces. For Ethernet, we adopt Lantronix XPort, which works as a Ethernet to serial converter. The maximum data transfer rate is 920 Kbps. When more higher data transfer is required, USB2.0 is available through the FTDI FT2232H chip. The maximum data transfer rate is 320 Mbps.

It is possible to realize the function of delay generator in FPGA. Usually, it is implemented by a clock synchronized circuit. However, its time resolution is determined by the clock frequency. In usual FPGAs, the 200 MHz clock frequency (5 ns resolution) is maximum. To achieve the better resolution beyond the clock frequency, the propagation delay of logic elements can be used[4]. To pass though a look up table element in FPGA, only few pico seconds are required. In the case of the D-Flip Flop (D-FF) element, the time between input and output is about 1.2-ns. This 1.2-ns delay is useful to achieve longer delay with better time resolution. Here, we report the implementation of delay generator by using a 32 D-FF delay chain circuit. The delay time is given by the number of D-FF to be passed through, and it can be controlled by the preset counter and the multiplexer circuits (Fig. 2). The time jitter of this delay generator is shown in Fig. 3. Data are taken by Agilent Technologies U1050A-002 TDC, which has a very good timing resolution of 5-ps. The overall time jitter is about 0.06% in FWHM. This resolution can be applied to tune the coincidence timing in trigger circuit precisely.

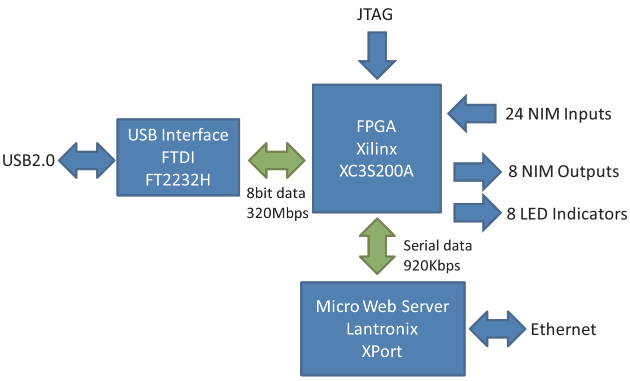

Fig. 1. The main components of GTO.

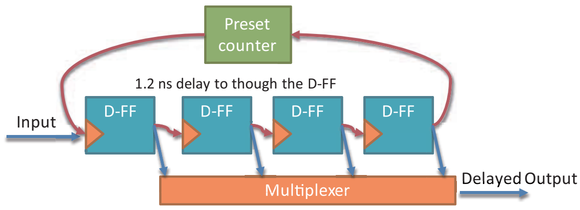

Fig. 2. The concept of delay chain by D-Flip Flop elements. In this delay generator, 32 D-FFs are connected.

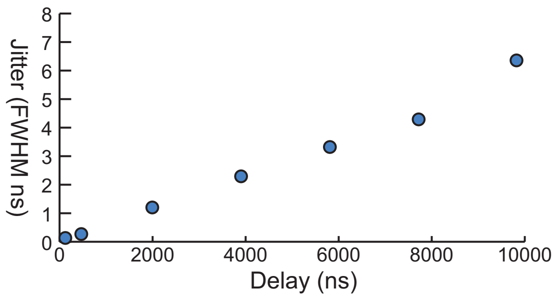

Fig. 3. The time jitter measurement of the delay generator.

*1 Center for Nuclear Study, University of Tokyo

References

1) H. Baba et al.: Nucl. Inst. Meth. A **616**, 65 (2010).
2) H. Baba et al.: RIKEN Accel. Prog. Rep. **44**, 213 (2011).
3) H. Baba et al.: RIKEN Accel. Prog. Rep. **45**, ix (2012).
4) H. Sadrozinski and J. Wu, *Applications of Field-Programmable Gate Arrays in Scientific Research*, CRC Press (2010).

Computing and network environment at the RIKEN Nishina Center

T. Ichihara, Y. Watanabe, and H. Baba

We are operating the Linux/Unix NIS/NFS cluster systems[1,2] at the RIKEN Nishina Center (RNC).

We have two server rooms for computers and network equipments. One is located at the Nishina Memorial Building, and the other is located at the RIBF Bldg. Both rooms are equipped with emergency power supply and UPS systems (20 kVA each). Since the UPS (20 kVA) in the Nishina Memorial Building was installed more than ten years ago, we replaced it during the three-day shutdown in the summer of 2012.

Figure 1 shows the current configuration of the Linux/Unix servers at the RNC. We are adopting Scientific Linux as the operation system. The host *RIBF.RIKEN.JP* is used as the mail server, NFS server of the user home directory /rarf/u/, and the NIS master server. Mailing list services are also supported. This is a core server for the RNC Linux/Unix cluster with approximately 600 user accounts registered.

The /rarf/w RAID has been used for the analysis of the experimental data. The size of the experiment data increases year by year. In addition, since the free space of the /rarf/w RAID became less than 30% and it reached the design life of six years, we replaced the RAID in the summer of 2012. As a result, the total size of the /rarf/w file systems was increased from 10 TB to 104 TB. The user disk quota of the /rarf/w space (default 100 GB) will be increased accordingly.

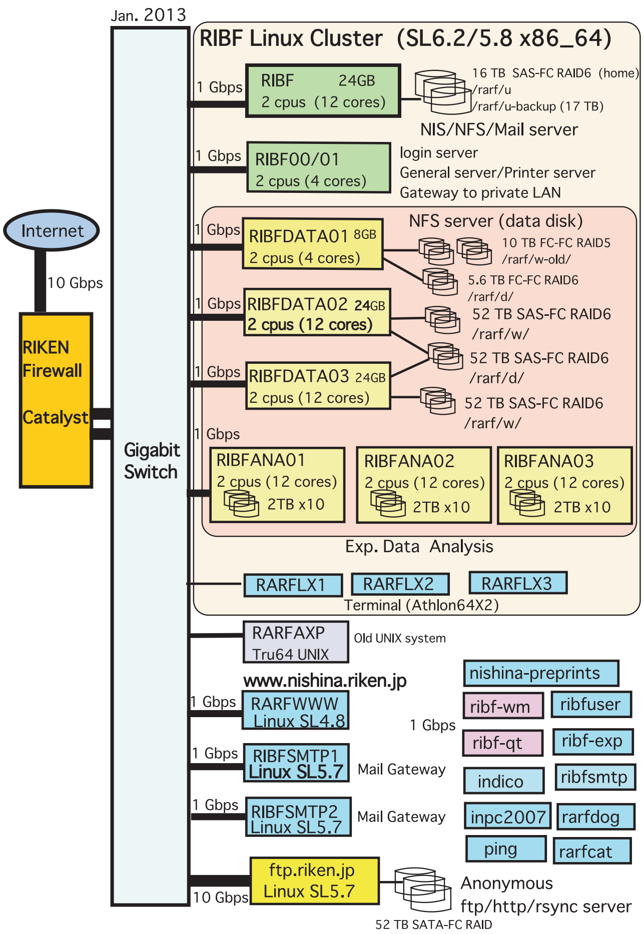

Fig. 1. Configuration of the RIBF Linux cluster.

New file servers *RIBFDATA02/03* were also installed. In addition, a new 52 TB RAID system (/rarf/d) was connected to the *RIBFDATA02/03* to store the new raw data obtained in the RIBF experiments.

Three dedicated data analysis servers *RIBFANA01-03*, which were installed in the spring of 2012, have been intensively used for the data analysis of the RIBF experiments.

The hosts *RIBF00/01* are used as ssh login servers to provide access to external users, and as general-purpose computational servers, printer servers, and gateways to the RIBF intranet.

The host *NISHINA-PREPRINTS* is an electric preprint server of the RNC. Several functions have been modified and added to the server for easy access and compilation of preprints and publications.

The hosts *RIBFSMTP1/2* are the mail front-end servers, and they are used for tagging spam mails and isolating virus-infected mails. The Sophos Email-protection advanced (PMX) has been newly installed on these servers in this year.

The Integrated Digital Conference (INDICO) system has been operated at the host *indico.riken.jp* since 2007. We are planning to replace this server early in 2013 in order to improve the function and reliability.

An anonymous ftp server, *FTP.RIKEN.JP*, is managed and operated at the RNC. Major Linux distributions including Scientific Linux, Ubuntu, Debian, etc. are mirrored daily at the ftp server for the convenience of their uses and facilitating their high-speed access.

We have been operating approximately 60 units of wireless LAN access points in the East Area of the RNC. Several access points for 2.4 GHz and 5.2 GHz have been added or replaced this year.[3] As a result, almost the entire radiation-controlled area of the East Area is covered by wireless LAN, for the convenience of experiments and maintenance work.

References

1) http://ribf.riken.jp/
2) T. Ichihara et al.: RIKEN Accel. Prog. Rep. 45, 174 (2012).
3) http://ribf.riken.jp/comp/net/wireless.html

CCJ operation in 2012

Y. Ikeda, H. En'yo, T. Ichihara, Y. Watanabe, and S. Yokkaichi

1 Overview

The RIKEN Computing Center in Japan (CCJ)[1) commenced operations in June 2000 as the largest off-site computing center for the PHENIX[2) experiment being conducted at the RHIC[3). Since then, the CCJ has been providing numerous services as a regional computing center in Asia. We have transferred several hundred TBs of raw data files and nDSTs, which is the term for a type of summary data files at the PHENIX, from the RHIC Computing Facility (RCF)[4) to the CCJ. The transferred data are first stored in a High Performance Storage System (HPSS)[5) before starting the analysis. The CCJ maintains sufficient computing power for simulation and data analysis by operating a PC cluster running a PHENIX-compatible environment.

A joint operation with the RIKEN Integrated Cluster of Clusters (RICC)[6) was launched in July 2009. Twenty PC nodes have been assigned to us for dedicated use, sharing the PHENIX computing environment.

Many analysis and simulation projects are being carried out at the CCJ, and these projects are listed on the web page `http://ccjsun.riken.go.jp/ccj/proposals/`. As of December 2012, CCJ has been contributed 30 published papers and more than 33 doctoral theses.

2 Configuration

2.1 Calculation nodes

In our machine room 258/260 in the RIKEN main building, we have 28 PC nodes[a)], and these nodes have been used for the analysis of the PHENIX nDST data. These nodes are operated by the data-oriented analysis scheme that carries out optimization using local disks[7) 8)]. The OS on the calculation nodes is Scientific Linux 5.3[9)], and the same OS works on the 20 nodes at the RICC. As a batch-queuing system, LSF 8.0.0[10) and Condor 7.4.2[11) were run on the CCJ and RICC nodes, respectively, as of Dec 2012.

Table 2 shows numbers of malfunctioned SATA or SAS disks in the HP servers (including NFS/AFS servers described in the next section).

2.2 Data servers

Two data servers (HP ProLiant DL180 G6 with 20 TB SATA raw disks) are used to manage the RAID of the internal hard disks, which contain the user data and nDST files of PHENIX. One old server (SUN Fire V40 with 10 TB FC-RAID) was terminated in March 2012. The disks are not NFS-mounted on the calculation nodes to prevent performance degradation by the congestion of processes and the network. These disks can be accessed only by using the "rcpx" command, which is the wrapper program of "rcp" developed at CCJ and has an adjustable limit for the number of processes on each server.

The DNS, NIS, NTP, and NFS servers are operated on the server ccjnfs20[b)] with a 10-TB FC-RAID, where users' home and work spaces are located. The home and work spaces are formatted with VxFS 5.0[12)]. The backup of home spaces on ccjnfs20 is saved to another disk server once a day and to HPSS once a week. The backups on HPSS are stored for 3 weeks.

Table 1. Limitation of number of job slots from LSF queue with cluster node.

	Nodes	Cores	Threads	Jobs
CCJ-hp1	18	144	144	180
CCJ-hp2	10	120	240	200
RICC	19	152	152	144
total	47	416	536	524

Table 2. Malfunctioned HDDs in 2012 and 2011

			Malfunctioned	
type	size	total	2012	2011
SATA	1 TB	192	20	9
	2 TB	120	5	4
SAS	146 GB	38	1	1
	300 GB	24	0	1

2.3 HPSS

Since Dec 2008, the HPSS servers and the tape robot have been located in our machine room, although they are owned and operated by RICC. The specifications of the hardware used can be found in the literature[13)]. The amount of data and the number of files archived in the HPSS were approximately 1.7 PB and 2.1 million files, respectively, as of Dec 2012.

2.4 PHENIX software environment

Two PostgreSQL[14) server nodes are operated for the PHENIX database, whose data size was 86 GB as of Dec 2012. The data are copied from The RCF everyday and are made accessible to the users. One

a) HP ProLiant DL180 G5 with dual Xeon E5430 (2.66 GHz, 4 cores), 16 GB memory and 10 TB local SATA data disks for each node, and HP ProLiant DL180 G6 with dual Xeon X5650 (2.66 GHz, 6 cores), 24 GB/20 TB as above, for each node

b) SUN Enterprise M4000 with Solaris 10

Table 3. DST and raw data files in HPSS on Dec 31, 2012

	DST		Raw data	
Run	size [TB]	cos	size [TB]	cos
1	4	2,3,100	3	3,205
2	24	2,3,4,100	36	1,3,5,205
3	10	2,3,6	46	100,205
4	14	2,3	11	205
5	287	2,3,6,100	292	5,205
6	92	3,6,100	339	11,100
8	22	3	128	12
9	106	3,7	13	
10	32	3	0	
11	142	3	0	
12	3	3	0	
total	736		854	

AFS[15] server node is operated for the PHENIX AFS. The size of the libraries for the PHENIX analysis setup was 2.5TB as of Dec 2012. The libraries are also copied from the RCF by afs everyday.

2.5 Network configuration

The topology of the network linking the CCJ, the RICC, and the RIKEN IT division was not changed in 2012. This topology was shown in the paper entitled "CCJ operation in 2011"[1].

2.6 Uninterruptible power-supply system (UPS)

The power consumption of the CCJ system, excluding the HPSS, is about 25 kW, and the power is supplied through five UPSs (10.5 kVA each) as of Dec 2012, after two old UPSs were replaced by a new UPS module in March 2012. For the HPSS, there is one 7.5-kVA UPS for 100 V and three 10.5-kVA UPSs for 200 V purchased by CCJ. For the latter three, batteries were changed by RICC in Oct 2012.

3 Data transfer from BNL

Data collected during the PHENIX experiment have been transferred from the RCF to the CCJ by grid-FTP[16] through SINET4 (maintained by NII[17]) with a 10 Gbps bandwidth. In 2012, 144 TB of nDSTs of the PHENIX Run-10AuAu (15 TB), Run-11pp (10 TB), Run-11AuAu (116 TB) and Run-12pp (3 TB) were sent from the RCF to the CCJ, and the data were stored in the the HPSS, and 100 TB of this data was moved to local disks on the HP calculation nodes. Files are transferred by grid-FTP at a maximum speed of 280 MB/s.

4 Issue with RAID controller

In the period Oct 2011–May 2012, a controller of the RAID disk connected to ccjnfs20 frequently displayed the "link down" error and stopped the operation of CCJ several times. Replacement of the RAID controller chassis and I/F card did not solve the problem. There was no error recurrence after the firmware of the RAID controller v3.63G.65 was updated to v3.73k.01 in June 11, 2012.

5 Lost data

In Oct 9, 2012, a file system of a user's home directory was damaged due to disk trouble and errors in operation when the ccjnfs20 was booted after a planned power outage. The data were recovered from the backup of Oct 5 (the day before the power outage).

6 Air-conditioners of server room

In Jan 2012, six air-conditioners operated in machine room (another one had malfunctioned). Three of them broke down and the temperature increased up to 28 °C on May (The normal temperature is about 22 °C through a year). Two of broken machines were restored and the temperature returned on June. Another was removed and five have been operational as of Dec 2012.

References

1) S. Yokkaichi et al.: RIKEN Accel. Prog. Rep. **44**, 228 (2011).
2) `http://www.phenix.bnl.gov/`
3) `http://www.bnl.gov/rhic/`
4) `https://www.racf.bnl.gov/`
5) `http://www.hpss-collaboration.org/`
6) `http://accc.riken.jp/ricc/`
7) T. Nakamura et al.: RIKEN Accel. Prog. Rep. **43**, 167 (2010)
8) J. Phys.: Conf. Ser. **331**, 072025 (2011).
9) `http://www.scientificlinux.org/`
10) `http://www-03.ibm.com/systems/technicalcomputing/platformcomputing/products/lsf/index.html`
11) `http://www.cs.wisc.edu/condor/description.html`
12) Veritas file system (Symantec Corporation).
13) S. Yokkaichi et al.: RIKEN Accel. Prog. Rep. **42**, 223 (2009).
14) `http://www.postgresql.org/`
15) `http://www.openafs.org/`
16) `http://www.globus.org/toolkit/docs/latest-stable/gridftp/`
17) `http://www.nii.ac.jp/`

III. RESEARCH ACTIVITIES II
(Material Science and Biology)

1. Atomic and Solid State Physics (Ion)

Reaction-rate measurements between slow velocity-selected polar molecules and a Ca^+ Coulomb crystal

K. Okada, T. Suganuma,[*1] T. Furukawa,[*1] H.A. Schuessler, M. Wada

Cold molecules and their ions have attracted research interest in the fields of fundamental physics and cold chemistry. In connection with cold chemistry, cold ion-molecule reactions play important roles in synthesis of interstellar molecules, and their reaction-rate constants are important information for studying the chemical evolution of interstellar clouds[1]. However, most measurements of ion-neutral reactions were only at room temperature or at a restricted range of temperatures near room temperature, even though the reactions occur at low temperatures in interstellar clouds. Therefore, we planned to experimentally determine the reaction rates between cold molecular ions and polar molecules using the ion trap technique under ultrahigh vacuum condition. In this project, we will perform reaction-rate measurements between the velocity-selected polar molecules and sympathetically cooled molecular ions cooled by a laser-cooled Ca^+ Coulomb crystal.

Recently, we developed a Stark velocity filter for performing the above reaction-rate measurements[2]. In fact, we confirmed the generation of slow ND_3, H_2CO, and CH_3CN molecules having thermal energies of a few Kelvin. Additionally, the number densities of the slow velocity-filtered polar molecules were determined to be in the range of $n = 10^4$–10^6 cm^{-3}. Here, we report the reaction-rate measurement between a Ca^+ Coulomb crystal and velocity-selected CH_3CN and ND_3 in order to check the reactivity between the slow polar molecules and cold Ca^+ ions.

Since the number density of the laser-cooled Ca^+ ions is considered to be constant as a first approximation, the relative number of ions can be determined from the volume of the Ca^+ Coulomb crystal, which can be determined by the size of the fluorescence image under the assumption of the cylindrical symmetry. Thus, in the present measurements, the relative number of Ca^+ ions is measured as a function of reaction time[3]. Figure 1(a) shows a plot of the relative number of ions in the Ca^+ Coulomb crystal as a function of time when irradiating with velocity-selected CH_3CN molecules. From the decay curve of the relative number, the reaction rate of γ=1.8(1.0)$\times10^{-5}$ s^{-1} is determined. The average collision energy of this reaction system is estimated to be lower than 10 K. We also show the corresponding fluorescence images of the Ca^+ Coulomb crystal, which was observed before and after a certain reaction time (Fig. 1(b)). A small dark region caused by the product ions was observed in the lower part of the fluorescence image after about 1 hour reaction time. In addition, the crystal became obscure owing to the increase in the number of product ions, which slightly heats the Ca^+ crystal. We have confirmed that the reaction rate of $Ca^+ + ND_3 \rightarrow$ *products* was also very slow[5]. It is conceivable that the loss of the number of the Ca^+ ions in these measurements is caused by the reactions with background H_2 molecules, i.e. $Ca^+(^2P_{1/2}) + H_2 \rightarrow CaH^+ + H$[3].

The observed reaction rates are on the order of 10^{-5} s^{-1}, which are much slower than typical reaction rates of molecular ion-polar molecule reactions at low temperatures[6]. Therefore, the present results confirm that, in principle, reaction-rate measurements between the velocity-selected polar molecules and sympathetically cooled molecular ions cooled by a laser-cooled Ca^+ Coulomb crystal can be performed. In the future, the present velocity-filter combined cryogenic trap apparatus should enable us to perform systematic measurement of cold ion-polar molecule reactions, which are important issues and will contribute to the progress of astrochemistry.

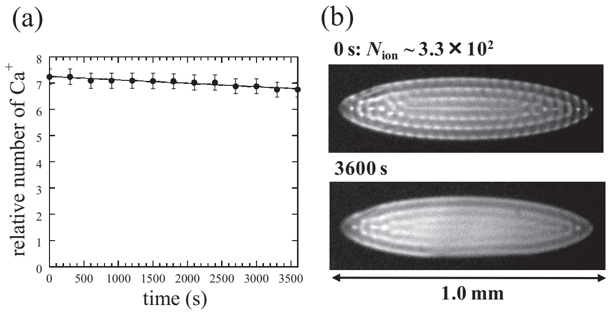

Fig. 1. An example of the reaction-rate measurement between a Ca^+ Coulomb crystal and the velocity-selected CH_3CN molecules under UHV condition[5].

References
1) E. Herbst *et al.*: Astro. Phys. J **185**, 505 (1973).
2) T. Suganuma *et al.*: RIKEN Accelerator Progress Report 44 (2011) 241.
3) N. Kimura *et al.*: Phys. Rev. A**83**, 033422 (2011).
4) K. Okada *et al.*: J. Phys. Conf. Ser. **388**, 102001 (2012).
5) K. Okada *et al.*: accepted for publication in Physical Review A.
6) T. Su, *et al.*: *J. Chem. Phys.* **76** 5183 (1982).

*1 Department of Physics, Sophia University

Formation of hydrogen-associated vacancy clusters in Nb as investigated from site occupancy change of hydrogen†

E. Yagi, N. Higami,*1 A. Takebayashi,*1 T. Hayashi,*1 Y. Murakami,*1 S. Koike,*2 and K. Ogiwara

The interaction of hydrogen with defects, especially vacancies, in metals is one of the fundamental problems on the properties of hydrogen and also in the research of fusion reactor materials, hydrogen embrittlement etc. It has been reported that hydrogen is trapped by vacancies. Such trapping affects various properties of hydrogen, such as hydrogen diffusion and hydrogen solubility, and is also related to the formation of superabundant vacancies. The recovery of the irradiation effect for high purity Nb and H-doped Nb was investigated by electrical resistivity and positron lifetime measurements. The recovery stage observed at around 250–270 K (stgeIII) in pure Nb, which was attributed to the free migration of monovacancies, was shifted by about 100–160 K to higher temperature in H-doped Nb, and it was interpreted to be a result of the trapping of hydrogen by vacancies.

The atomistic state of trapped hydrogen has not hitherto been studied, because of the experimental difficulties. Therefore, the channelling method utilizing a nuclear reaction of ^{1}H(^{11}B,α)$\alpha\alpha$ with a ^{11}B^{+} beam of about 2 MeV was developed. In this method hydrogen can be detected by measuring α particles. This method has been demonstrated to be very useful to locate hydrogen dissolved in metals.[1,2]

In previous study, the irradiation effect on Nb doped with hydrogen up to a concentration of 0.023 at a hydrogen-to-metal-atom ratio C_H=[H]/[M], $NbH_{0.023}$, was investigated by the channelling method at room temperature with a tandem accelerator. Irradiation was performed with an analysis beam of ^{11}B ions of energy of 2.03 MeV in the off-channelling direction (random direction). Irradiation introduces only defects nearly homogeneously in the depth region around ~200 nm where hydrogen is probed by the nuclear reaction, because the projected range of incident ^{11}B ions is 1.35 μm. By irradiation at room temperature up to a dose of 1.4×10^{16}/cm^2, a change of channelling angular profiles is completed. The lattice location of hydrogen changes from an original tetrahedral (T) site (T-1 state) to a T_{tr} site, which is displaced from a T site by 0.45–0.55 Å towards its nearest neighbour lattice point.[3] As channelling angular profile was obtained with much lower irradiation dose, less than 3.6×10^{14}/cm^2, at each angle, the effect of radiation damage by an analysis beam itself on the lattice location of hydrogen can be excluded.

In the present study, effect of post-irradiation annealing was investigated. First, the specimen was irradiated at room temperature up to about 3 times higher dose 4.2×10^{16}/cm^2. The site occupancy of hydrogen remained the same. On the subsequent annealing at 523 K for 1 h, the state of hydrogen changed from the T_{tr}-site occupancy to the occupation of (55–70)% of H atoms at T sites (T-2 state) and (30–45)% at random (R) sites. As described above, in H-doped Nb the stage III was shifted to higher temperature and, at this higher temperature, formation of vacancy clusters was observed. The annealing temperature of 523 K corresponds to the temperature for the vacancy clusters to be formed. Therefore, the irradiation-induced site change from the T site to the T_{tr} site is due to the trapping of hydrogen by vacancies, i.e., the formation of H-vacancy complexes (complex-1).

After the annealing, additional irradiation was performed at room temperature with a dose of about 1.4×10^{16}/cm^2, which is the same as that performed before the annealing. The site occupancy changed to (35–50)% at T + (50–65)% at R or (30–40)% at T + (10–20)% at T_{tr} + (50–60)% at R. This result indicates a difference in the state of hydrogen between the T-1 and T-2 states, because, if both states would be the same, most of the H atoms located at T sites after the annealing would become again located at T_{tr} sites. In the T-1 state, hydrogen is in the isolated state, i.e., free hydrogen, while, in the T-2 state, most of H atoms are associated with more vacancies. For this hydrogen-vacancy complex, a vacancy tetrahedron (tetravacancy composed of 4 vacancies) containing hydrogen inside at T site, H-4vac. (complex-2), is proposed. The R site occupancy corresponds to hydrogen in a larger vacancy cluster such as a void. Therefore, on annealing, large H-associated vacancy clusters, such as H-4vac. complex and H-associated voids, are formed. It is demonstrated that complex-1 does not act as a nucleus for the growth of a H-associated larger vacancy cluster, because, by irradiation up to 3 times higher dose, hydrogen site did not change as described above, whereas complex-2 acts as a nucleus and grows to a H-associated larger vacancy clusters by trapping still more irradiation-induced vacancies at room temperature.

† Condensed from the article in J. Phys. Soc. Jpn. **79**, 114601 (2010).

*1 School of Science and Engineering, Waseda University
*2 Department of Physics II, Tokyo University of Science

References

1) E. Yagi, T. Kobayashi, S. Nakamura, Y. Fukai, and K. Watanabe: J. Phys. Soc. Jpn. **52**, 84 (1983).
2) E. Yagi, T. Kobayashi, S. Nakamura, Y. Fukai, and K. Watanabe: Phys. Rev. B **31**, 1640 (1985).
3) E. Yagi, K. Sakuma, N. Higami, S. Hagiwara, K. Mori, M. Yoshii, S. Koike, T. Hayashi, and K. Ogiwra: J. Phys. Soc. Jpn. **77**, 124602 (2008).

Consideration of single-event gate rupture mechanism in power MOSFETs†

E. Mizuta,[*1] S. Kuboyama,[*1] N. Ikeda,[*1] T. Kambara, and T. Tamura[*1]

Power metal-oxide-semiconductor field -effect transistors (MOSFETs) are On/Off switching devices in a power circuit that are used to attain high efficiency and high speed. These power MOSFETs are widely used for the power handling portion of the electronic devices for space system as well as ground-based commercial devices. However, the catastrophic failure mode caused by a single-event gate rupture (SEGR) in space radiation environments remains a critical issue with these devices. The phenomenon of SEGR in power MOSFETs was reported for the first time in 1987.[1)] Over the past 20 years, the phenomenon was extensively characterized[2)] and several models have been proposed to describe their mechanism. In this paper, we report on the result of our SEGR test for MOSFETs of four structures and the observation of curious SEGR behavior that differed from the conventional behavior.

Figure 1 shows the structure models of MOSFETs used for the SEGR test. They include four types of structures: (A) normal one, (B) no source, (C) plain body, and (D) plain body and no source. Further, they are p-channel power MOSFETs having a rated drain voltage of -100 V. The SEGR test was performed at room temperature by irradiation with a Kr-ion beam of 713 MeV using the RIKEN RILAC + RRC. The applied gate voltage V_{GS} was increased from 0 to 15.0 V at intervals of 2.5 V for the rated drain voltage V_{DS} of -100 V. From the experimental results, SEGRs were observed only for the test structures A and B. SEGRs occurred at V_{GS} = +15.0 V, as shown Figure 2. In conventional studies, the SEGR defect point was generally found to be located on the oxide-faced upper region in the

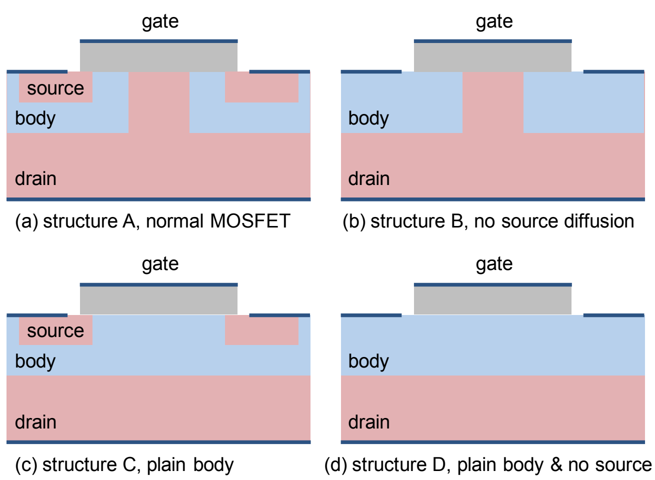

Fig. 1　Structure of SEGR testing.

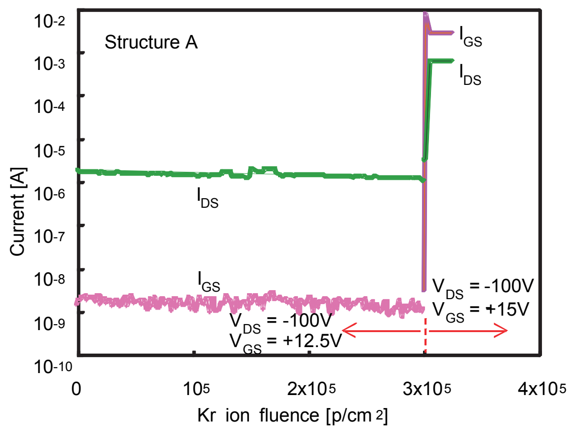

Fig. 2　Current monitor data during SEGR testing for p-MOSFET with the rated V_{DS} of -100 V.

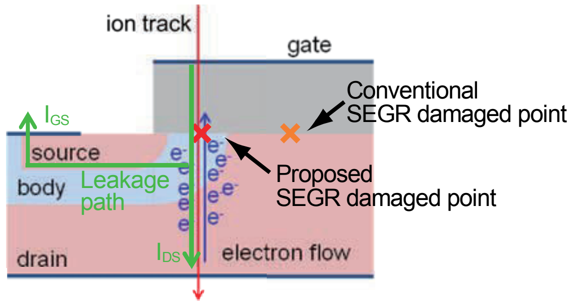

Fig. 3　Image of electron injection induced by ion strike in power MOSFETs.

drain region, where the drain bias was applied, because the highest electric field was generated by perpendicularly incident ions in the neck region (the region between body diffusions). However, the current increases might suggest that the gate oxide was damaged and that the current was injected from the gate, after which it flowed out to the drain and the source electrodes, because the current values of I_{GS} and I_{DS} were not identical. It was supposed that there were at least two current paths. If the SEGR defect point is located on the oxide-faced upper region, it can be used to explain the mechanism of the two current paths, as shown Figure 3. The electrons are generated along the ion track and accelerated by the electric field applied across the body-drain junction and injected into the gate oxide. The edge portion of the body might be more effective for the injection because of the reduced thickness of the diffusions. A further quantitative discussion will be included in the full paper for clarifying the mechanism†.

References
1) T. A. Fischer, et al.: IEEE Trans. Nucl. Sci. **NS-34**, 1786 (1987).
2) J. R. Brews, et al.: IEEE Trans. Nucl. Sci. **NS-40**, 1959 (1993).

† Condensed from the 12th European Conference on Radiation Effects on Components and Systems (RADECS 2011).
*1 Japan Aerospace Exploration Agency

Excitation density dependence of luminescence behavior in ion-irradiated α-alumina

M. Koshimizu,[*1] K. Kimura, and K. Asai[*1]

It has been well known that heavy ion irradiation in insulators leads to extremely high density electronic excitation around the ion trajectory. Heavy ion irradiation effects in insulators, in particular track formation, are strongly related to the relaxation of such excited states. However, little has been revealed on the relaxation dynamics and the interaction among the closely located excited states.

Measurement of time-resolved luminescence spectra is a powerful method to elucidate the relaxation dynamics and the interaction. The interaction among the excited states manifests itself in luminescence spectra, and the dynamics can be followed by the time-resolved measurement. In this report, the heavy-ion-induced luminescence of α-alumina is discussed with particular emphasis on the excitation-density dependence of the dynamics.

The measured sample was a single crystal of α-alumina. The sample was irradiated with N, Ar, and Xe ions at 2.0 MeV/nucleon obtained from the RILAC. The excitation density or linear energy transfer (LET) increased with the atomic number of the ion. Time-resolved luminescence spectra were obtained by a single-photon counting method. The arrival of a single ion was determined with a secondary-electron detector composed of a carbon foil and a multichannel plate. The luminescence from the sample was analyzed by a monochromator and detected with a MCP-mounted photomultiplier tube (PMT). In order to measure the luminescence in the vacuum ultraviolet wavelength region, the monochromator was evacuated, and a lens and PMT window made of MgF_2 were used. The time resolution of the measuring system was better than 100 ps.

Figure 1 shows the luminescence time profile at wavelength of 170 nm for each ion irradiation. This wavelength corresponded to the luminescence band observed under excitation by vacuum ultraviolet, and the band was ascribed to self-shrunk exciton.[1)] Based on the ascription, it is reasonable to consider that the heavy-ion-induced luminescence seen in Fig. 1 has similar origin. All the decay behavior cannot be represented with a single exponential decay component. The initial decay, on the time scale of a nanosecond, was much faster for Xe-ion irradiation than those of lower LET cases. In addition, the initial rise was faster for a higher LET. The observed luminescence dynamics at a high LET can be phenomenologically explained with following two hypothesis: enhancement of the radiative decay or quenching.

*1 Department of Applied Chemistry, Tohoku University

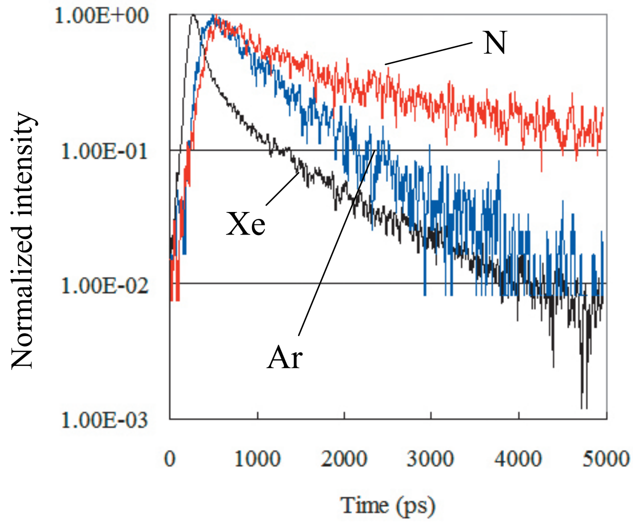

Fig. 1 Time profiles of heavy-ion-induced luminescence of α-alumina at 170 nm for different ions.

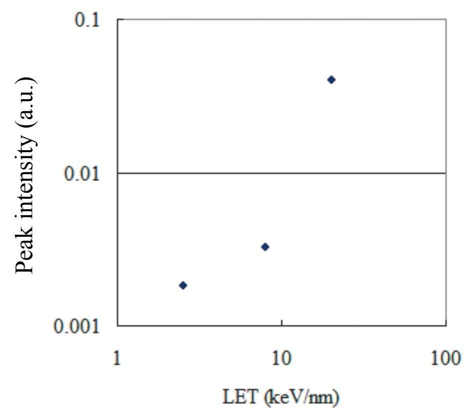

Fig. 2 Luminescence intensity at the peak of the time profile at 170 nm.

Figure 2 shows the LET dependence of the peak luminescence intensity of the time profile at 170 nm. The luminescence intensity increased sharply for Xe ion irradiation. This result clearly indicates that the fast rise and decay for Xe ion irradiation observed in Fig. 1 is not due to quenching, but is attributable to faster radiative decay at a higher excitation density. The faster radiative decay may be ascribed to the superradiance of the excited states having lattice distortions similar to the self-shrunk excitons.

References

1) M. Kirm et al.: Phys. Rev. B **60**, 502 (1999).

Effects of particle irradiations on vortex states in iron-based superconductors†

T. Tamegai,[*1,*2] Y. Nakajima,[*1,*2] H. Yagyuda,[*1] T. Taen,[*1] T. Kambara, and Y. Kanai

The discovery of superconductivity in LaFeAs(O,F) in 2008 has opened up a new era of research into superconductivity.[1] Following this discovery, the family members of iron-based superconductors have increased considerably. Although the superconducting mechanism for this new class of superconductors, including pairing symmetry, is still under intensive debate, iron-based superconductors have excellent basic properties for applications such as those requiring a large upper critical field and small electromagnetic anisotropy. Large critical current densities, J_c, have been reported for single crystals of iron-based superconductors.

Introduction of defects by various means using chemical or physical methods can enhance J_c. Heavy-ion irradiation, which produces columnar defects, is one of the most promising ways to achieve such enhancements.[2] We have shown that the heavy-ion irradiation is effective for introducing defects in iron-based superconductors by demonstrating a five-fold increase in J_c of a $Ba(Fe_{0.93}Co_{0.07})_2As_2$ single crystal using 200 MeV Au ions with a dose-equivalent matching field of B_ϕ = 20 kG.[3] Similar enhancements in J_c in iron-based superconductors have been reported for other ions with different energies, namely, 1.4 GeV Pb,[4] 2.6 GeV U,[5] and 800 MeV Xe.[6] Figure 1 shows the enhancement in the J_c of an optimally Co-doped $BaFe_2As_2$ at T = 10 K and H = 2 kOe by these irradiations as a function of B_ϕ. In all these irradiation experiments, energetic particles are introduced along the *c*-axis of the crystal. As expected, 2.6 GeV U induces the largest enhancement in J_c at higher defect densities.

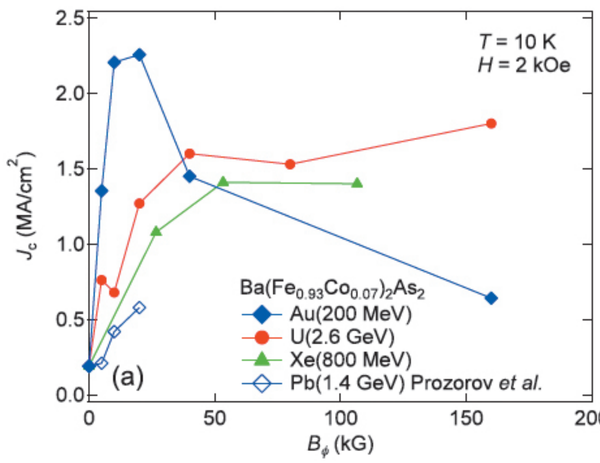

Fig. 1. Critical current density in heavy-ion irradiated optimally Co-doped $BaFe_2As_2$ single crystals at T = 10 K and H = 2 kOe as a function of defect density, which is measured by the dose-equivalent matching field, B_ϕ.

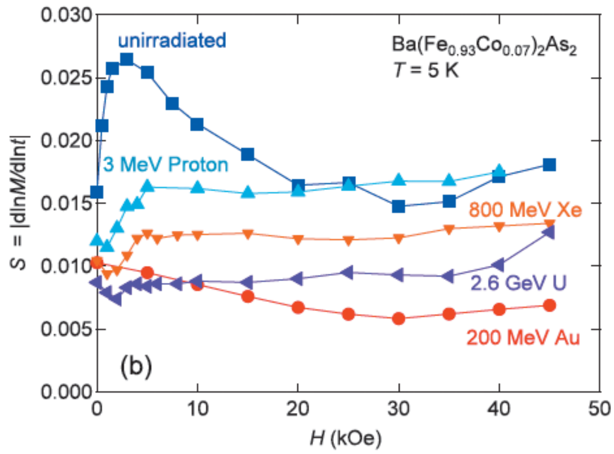

Fig. 2 Magnetic field dependence of the normalized relaxation rate S ($= d\ln M/d\ln t$) at 5 K in optimally Co-doped $BaFe_2As_2$ single crystals with B_ϕ = 20 kG.

Another approach to characterize the effect of introduced defects on the motion of quantized vortices in superconductors is to measure the temporal evolution of shielding current, which can be evaluated by monitoring the time-decay of irreversible magnetization in superconductors. Figure 2 shows the normalized relaxation rate of magnetization, $S = d\ln M/d\ln t$ for optically Co-doped $BaFe_2As_2$ single crystals with B_ϕ = 20 kG. The effect of proton irradiation at a dose of 1.2 × 10^{16} cm^{-2} is also compared. Except for the strong magnetic field dependence of S at low fields below 5 kOe, which is possibly due to the self-field effect, S is almost magnetic-field independent. The value of S is suppressed by introducing columnar defects, which is suitable for practical applications. It is also obvious that the suppression of S closely follows the enhancement in J_c on account of the introduction of columnar defects. In other words, samples having a small S show a large J_c.

References

1) Y. Kamihara *et al.*: J. Am. Chem. Soc. **130**, 3296 (2008).
2) L. Civale *et al.*: Phys. Rev. Lett. **67**, 648 (1991).
3) Y. Nakajima *et al.*: Phys. Rev. B **80**, 012510 (2009).
4) R. Prozorov *et al.*: Phys. Rev. B **81**, 094509 (2010).
5) H. Yagyuda *et al.*: Physica C **471**, 790 (2011).
6) T. Taen *et al.*: J. Phys.: Conf. Ser. **400**, 022119 (2012).

† Taken partly from Supercond. Sci. Technol. **25**, 084008 (2012)

*1 Department of Physics, The University of Tokyo
*2 JST-Transformative Research project on Iron-Pnictides

2. Atomic and Solid State Physics (Muon)

μSR study of the magnetism in the infinite-layer compound $LaNiO_{2+x}$

T. Adachi, T. Takamatsu,[*1] K. M. Suzuki, K. Naruse, M. Imaizumi,[*1] M. Kato,[*1] I. Kawasaki, I. Watanabe, and Y. Koike

The compound $LaNiO_2$ has attracted great interest as a promising candidate for the parent material of a new high-T_c superconductor since the first synthesis by Crespin *et al.* in 1983.[1)] $LaNiO_2$ consists of square-planar NiO_2 planes and La layers and is isostructural to the so-called infinite-layer compound $SrCuO_2$ which is a parent material of the high-T_c superconducting cuprates $Sr_{1-x}Nd_xCuO_2$[2)] with $T_c \sim 40$ K. Moreover, the $3d^9$ electronic configuration of Ni^+ in $LaNiO_2$ is the same as that of Cu^{2+} in the high-T_c cuprates.

The synthesis of $LaNiO_2$ by Crespin *et al.* was achieved by the reduction of the perovskite $LaNiO_3$ using H_2, but it was difficult to reproduce the synthesis well. A thin film of $LaNiO_2$ has successfully been synthesized by the reduction of a thin film of $LaNiO_3$ using CaH_2 at 280°C by Kawai *et al.*[3)] and using H_2 by Kaneko *et al.*[4)] The film made by Kawai *et al.* shows semiconductive behavior, while that made by Kaneko *et al.* shows metallic behavior in the electrical-resistivity measurements. This different behavior may be due to the difference of the oxygen content. However, it is hard to estimate the oxygen content and to study detailed magnetic properties in the films.

Recently, we have successfully synthesized bulk samples of $LaNiO_2$ by the low-temperature reduction of $LaNiO_3$ using CaH_2 at 300°C.[5)] Our sample is of almost single phase and the full widths at half maximum of peaks in the x-ray diffraction pattern are smaller than those for the samples formerly synthesized,[6)] indicating the higher crystallinity of our sample. Therefore, in order to investigate the magnetic properties, we have performed μSR measurements of $LaNiO_{2+x}$ with $x \sim 0$. Through the reduction process from $LaNiO_3$, tiny amounts of Ni metal and $LaNiO_{2+x}$ with $x \sim 0.5$ have been included in the sample. Zero-field (ZF) and longitudinal-field μSR measurements were carried out using a MiniCryo at temperatures down to ~ 7 K at RIKEN-RAL.

Figure 1 shows the ZF-μSR time spectra of $LaNiO_{2+x}$ with $x \sim 0$. Above 200 K, the spectra show slow depolarization due to randomly oriented nuclear spins. A fast depolarization of muon spins is observed below 200 K, followed by a muon-spin precession at 6.5 K, although the amplitude of the precession is quite small. The internal field at the muon site estimated from the precession frequency is ~ 270 G. This value is comparable with that reported for $LaNiO_{2+x}$ with $x = 0.5$ which is an antiferromagnetic insulator.[7)] Therefore, it is possible that the precession is originated from a tiny amount of $LaNiO_{2+x}$ with $x \sim 0.5$. That is, it is suggested that in $LaNiO_{2+x}$ with $x \sim 0$, the Ni-spin correlation is developed at low temperatures, while no long-range magnetic order is formed at 6.5 K. Accordingly, the ground state of $LaNiO_2$ is probably antiferromagnetic as in the case of the parent compound of the high-T_c cuprates.

In summary, we have found from ZF-μSR measurements that the Ni-spin correlation is developed at low temperatures in $LaNiO_{2+x}$ with $x \sim 0$. Therefore, the ground state of $LaNiO_2$ is probably antiferromagnetic as in the case of the parent compound of the high-T_c cuprates, suggesting possible appearance of the high-T_c superconductivity in suitably doped $LaNiO_2$.

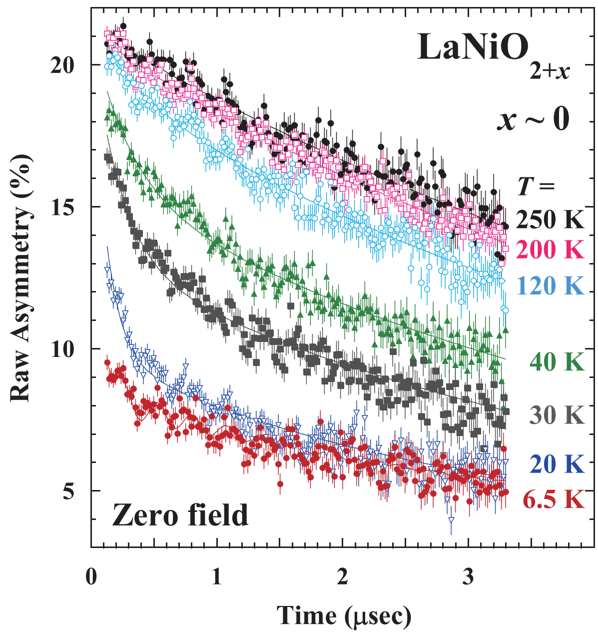

Fig. 1. Zero-field μSR time spectra of $LaNiO_{2+x}$ with $x \sim 0$.

*1 Department of Applied Physics, Tohoku University

References

1) M. Crespin et al.: J. Chem. Soc., Faraday Trans. II **79**, 1181 (1983).
2) M. G. Smith et al.: Nature (London) **351**, 549 (1991).
3) M. Kawai et al.: Appl. Phys. Lett. **94**, 082102 (2009).
4) D. Kaneko et al.: Physica C **469**, 936 (2009).
5) T. Takamatsu et al.: Jpn. J. Appl. Phys. **49**, 093101 (2010).
6) M. A. Hayward et al.: J. Am. Chem. Soc. **121**, 8843 (1999).
7) T. Moriga et al.: Bull. Chem. Soc. Jpn. **67**, 687 (1994).

Identifying muon sites in La_2CuO_4 using ab-initio and dipole field calculations

B. Adiperdana, I. A. Dharmawan, R. E. Siregar,[*1] S. Sulaiman, M. I. Mohamed-Ibrahim, I. Kawasaki, H. Guo, and I. Watanabe

In order to understand the interaction of positive muons with atoms or molecules in crystals we need to predict an ideal muon location. For this purpose, we are attempting to develop general-purpose software to predict the exact muon location in different materials. If we can successfully develop such software, the analysis process will become substantially faster compared with the speed of independently designed code. Hence, we first need to identify good prediction methods.

Many prediction methods have been developed, and muon sites have been most frequently predicted in La_2CuO_4 samples. In the last 13 years, prediction methods for muon sites have been developed using various approaches, but they have led to different results. This has caused confusion among theorists who want to clarify muon interactions. Figure 1 shows the predicted sites reported by previous studies.[1)] The main problem with previous methods was that they did not calculate the full trace potential map, under the restriction that the potential was calculated only within 1Å radius from each oxygen position, based on the hydroxide bond (OH^-) distance.

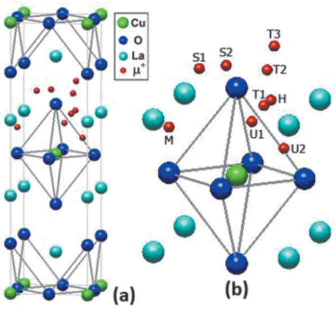

Figure 1. (a) La_2CuO_4 crystal structure; red spheres indicate muon sites previous studies, (b) magnified view of the crystal structure.

In the present study, as the first approach, we used ab-initio and dipole field calculations for an electronic dipole as well as nuclear dipole field. All of the calculations can be performed at a full trace potential, and hence all possible muon sites can be located.

The ab-initio calculation was performed with RIKEN integrated cluster of clusters (RICC) system using Vienna ab-initio simulation package (VASP)[2)] with projector augmented wave (PAW) in order to obtain the all electron wave functions. GGA PW91[3)] was used for the exchange and correlation functions, and the electrostatic potential was used to predict the muon site, using the ab-initio calculation.

The dipole calculation was performed using the spin structure data available in the work of Vaknin et al.,[4)] where the structure shows an antiferromagnetic behavior with a magnetic moment of about 0.5 μ_B/Cu. Upon expanding the size of the structure to a 50 Å spherical radius, the calculation was found to be converge.

The result obtained for the electrostatic potential is shown in Figure 2. It shows that there are two possible muon sites (M_1 and M_2). This result is in contradiction with those of previous studies on μSR spectroscopy that have indicated only show a single internal field between 410 and 425 G[5)]. To experimentally confirm the presence of multiple frequencies, we are now proposing that the internal field be re-measured using higher time resolution and single crystal samples of higher quality than those used 22-years ago for a-, b-, and c-crystal axis directions.

The dipole field calculation for the M_1 and M_2 positions indicated internal fields values to be 942 G and 192 G, respectively. When compared with experiment results, they are found to be twice and half times than the experimental value. We propose that there is a contribution in the form of a contact field from a muon, which makes the internal field larger or smaller than the experimental values. To calculate the contact field, we need to calculate the localized wave function. We plan to calculate this field in collaboration with the Universiti Sains Malaysia using spherical wave function approximations.

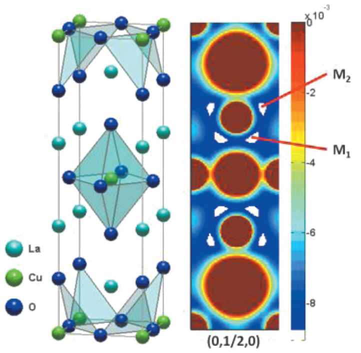

Figure 2. Electrostatic potential contour data for minimum potential for muon to be sit.

References
1) S. B. Sulaiman et al.: Phys. Rev B49, 9879 (1994).
2) G. Kresse and J. Futhmüller: Comput. Mater.Sci. 6, 15 (1996).
3) J. P. Perdew et al.: Phys. Rev. B 46, 6671 (1992).
4) Vaknin et al : Phys. Rev. Lett. 59, 2808 (1987).
5) Y. J. Uemura et al.: Physica C 153, 769 (1988).

*1 Department of Physics, Universitas Padjadjaran, Indonesia

Muon-spin-relaxation study of the Cu-spin dynamics in electron-doped high-T_c cuprates $Eu_{2-x}Ce_xCu_{1-y}Ni_yO_{4+\alpha-\delta}$

Risdiana, L. Safriani, T. Adachi, Y. Koike, I. Kawasaki, and I. Watanabe

The electron-hole doping symmetry in high-T_c cuprates has attracted great research interest in relation to the mechanism of high-T_c superconductivity. Some properties in both systems have been found to be similar. Phase diagrams of the hole- and electron-doped systems are very similar to each other, leading to the view of hole-electron doping symmetry. On the other hand, some properties have been found to be different from each other, leading to the view of hole-electron doping asymmetry. From inelastic neutron-scattering measurements, an incommensurate Cu-spin correlation corresponding to the so-called dynamically fluctuating stripes of spins and holes[1)] has been found in the hole-doped system,[2)] while a commensurate Cu-spin correlation corresponding to the simple antiferromagnetic correlation has been observed in the electron-doped system.[3)] From the viewpoint of effects of nonmagnetic impurities on the Cu-spin dynamics, we performed zero-field (ZF) muon-spin-relaxation (μSR) measurements in the hole-doped cuprates $La_{2-x}Sr_xCu_{1-y}Zn_yO_4$ [4-5)] and in the electron-doped cuprates $Pr_{1-x}LaCe_xCu_{1-y}Zn_yO_4$.[6)] It was found that in the hole-doped cuprates, Zn tends to induce the slowing down of the Cu-spin fluctuations in the entire superconducting regime, which can be attributed to the pinning and stabilization of the dynamically fluctuating stripes. Contrastively, in the electron-doped cuprates, the spectra were independent of the Zn concentration. That is, the Zn-induced slowing down of Cu-spin fluctuations that was observed in the hole-doped system was not observed in the electron-doped system.

We also performed ZF-μSR in the hole-doped cuprates $La_{2-x}Sr_xCu_{1-y}Ni_yO_4$ (LSCNO), in order to investigate the magnetic-impurity effects of Ni on the Cu-spin dynamics. Although a hole-trapping effect of Ni was clearly observed, the stripe-pinning effect of Ni was also observed in the underdoped LSCNO.[7)] To our knowledge, however, no one has reported on the effects of magnetic impurities on the Cu-spin dynamics in electron-doped cuprates thus far, which would allow a clear conclusion of the relation between the dynamical stripe correlations and the superconductivity in the electron-doped cuprates to be drawn.

We have succeeded in preparing the electron-doped cuprate $Eu_{1.85}Ce_{0.15}Cu_{1-y}Ni_yO_{4+\alpha-\delta}$ (ECCNO) for which the effects of Ni on the Cu-spin dynamics have been estimated, but not yet verified. Therefore, we performed zero-field μSR experiments of ECCNO with y = 0, 0.01, 0.02, and 0.05 in order to investigate the Cu-spin dynamics and possible existence of stripe correlations in electron-doped cuprates. α is the excess oxygen content at an apical site in the as-grown samples of $Eu_{1.85}Ce_{0.15}Cu_{1-y}Ni_yO_{4+\alpha}$. The values of δ, estimated from the weight change due to

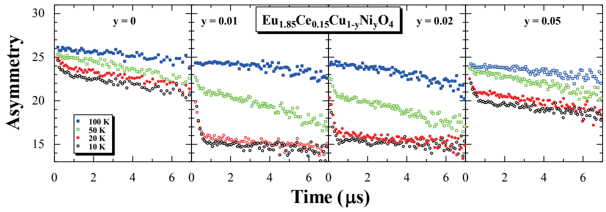

Figure 1: μSR spectra of $Eu_{1.85}Ce_{0.15}Cu_{1-y}Ni_yO_{4+\alpha-\delta}$ with y = 0, 0.01, 0.02, and 0.05 at various temperatures.

post-annealing, ranged from 0.02 to 0.09. The sample for which y = 0 shows superconductivity with T_c~11 K, while the samples for which y = 0.01, 0.02, and 0.05 do not exhibit superconductivity above 2 K.

Figure 1 shows the μSR time spectra of ECCNO with y = 0, 0.01, 0.02 and 0.05 at various temperatures. For all samples, the μSR time spectra show a Gaussian-type depolarization behavior at high temperatures above ~100 K due to the randomly oriented nuclear spin. For the sample for which y = 0, the spectrum changes from the Gaussian-type to the exponential-type depolarization behavior at low temperatures below ~50 K. However, there is no recovery of the asymmetry to 1/3 at 10 K in the long time region as observed for $Pr_{1-x}LaCe_xCuO_4$.[6)] Therefore, it remain unconfirmed whether the exponential-type depolarization without any recovery of the asymmetry in the long time regions is due to the slowing down of the Cu-spin fluctuations or due to the static magnetism of Eu.

One important result in the μSR time spectra of ECCNO is that the trace of the development of the Cu-spin correlation is observed at low temperatures for Ni-substituted samples. The muon-spin depolarization becomes fast for y = 0.01 and 0.02. This indicates that Ni tends to induce the slowing down of the Cu-spin fluctuations, as in the case of the hole-doped cuprates. As for y = 0.02, both a very fast depolarization in the short time region and a coherent-precession of muon spins are observed at 10 K, suggesting the existence of a static magnetic ground state. The depolarization becomes weak for y = 0.05 due to the destruction of the Cu-spin correlation by a large amount of Ni. The trace of the stabilization of the Cu-spin fluctuations by Ni indicates a possibility that the stripe model can globally explain the high-T_c superconductivity as in the case of hole-doped systems.

References

1) J. M. Tranquada *et al.*: Nature **375**, 561 (1995).
2) K. Yamada *et al.*: Phys. Rev. B **57**, 6165 (1998).
3) K. Yamada *et al.*: Phys. Rev. Lett. **90**, 137004 (2003).
4) T. Adachi *et al.*: Phys. Rev. B **69**, 184507 (2004).
5) Risdiana *et al.*: Phys. Rev. B **77**, 054516 (2008).
6) Risdiana *et al.*: Phys. Rev. B **82**, 014506 (2010).
7) Y. Tanabe *et al.*: Phys. Rev. B **83,** 144521 (2011).

μSR study of honeycomb-lattice system $Ba_3Co_2O_6(CO_3)_{0.7}$

T. Kawamata, H. Sudo,[*1] K. Naruse, T. Adachi, K.M. Suzuki, M. Imaizumi,[*1] I. Kawasaki, I. Watanabe, and Y. Koike

Geometrically frustrated spin systems have attracted interest because various magnetic phases appear to release the spin frustration in such systems. Both $BaCoO_3$ and $ACoX_3$ (A = Cs, Rb; X = Cl, Br) contain linear spin-chains of face-sharing $Co(O,X)_6$ octahedra running along the c-axis. The spin chains separated by Ba^{2+} or A^+ ions form an equilateral triangular lattice in the c-plane. Because of the strong frustration effect due to the triangular lattice, two successive magnetic phase transitions occur in these compounds.[1)]

The crystal structure of $Ba_3Co_2O_6(CO_3)_{0.7}$ is similar to that of $BaCoO_3$ and one-third of the spin chains of CoO_6 octahedra are replaced by CO_3 groups.[2)] Therefore, the spin chains form a honeycomb lattice in the c-plane, and it is expected that a long-range magnetically ordered state occurs because the honeycomb lattice has no geometrical frustration. However, no evidence of the magnetic phase transition has been observed at low temperatures down to 2 K from the susceptibility, specific heat and NMR measurements.[3)] On the other hand, the resistivity measurements exhibit a metal-insulator transition at $\sim$ 80 K. That is, a charge ordering, that the valence of Co ions changes from non-integer to mixed, may appear below $\sim$ 80 K. Therefore, a change of spin dynamics driven by the charge ordering at the metal-insulator transition is expected. In order to investigate the spin dynamics of $Ba_3Co_2O_6(CO_3)_{0.7}$, we performed μSR measurements which can probe higher-frequency spin fluctuations than NMR ones.

The μSR measurements were performed at the RIKEN-RAL Muon Facility. Single crystals of $Ba_3Co_2O_6(CO_3)_{0.7}$ were grown by the K_2CO_3-$BaCl_2$ flux method.[4)]

The μSR time spectra, $A(t)$, of $Ba_3Co_2O_6(CO_3)_{0.7}$ single crystals are shown in Fig. 1. It is found that there is no indication of the magnetically ordered state at low temperatures down to 6.5 K, for the time spectra are Gaussian-like. In order to see the change of the spin dynamics in detail, all of the time spectra were analyzed using the following function,

$$A(t) = A_0 \exp(-\lambda t) G_{\mathrm{KT}}(\Delta, t), \qquad (1)$$

where A_0 is the initial asymmetry, λ the depolarization rate of muon spins and $G_{\mathrm{KT}}(\Delta, t)$ the Kubo-Toyabe function.[5)] The best-fit results are shown by solid lines in Fig. 1. The parameters obtained from the best fit are shown in the inset of Fig. 1. It is found that A_0 is constant while λ increases and Δ decreases monotonically with decreasing temperature. That is, neither A_0, λ nor Δ show any anomaly at $\sim$ 80 K. In $Ba_3Co_2O_6(CO_3)_{0.7}$, accordingly, there is no change of spin dynamics within the time window of the μSR measurement.

*1 Department of Applied Physics, Tohoku University

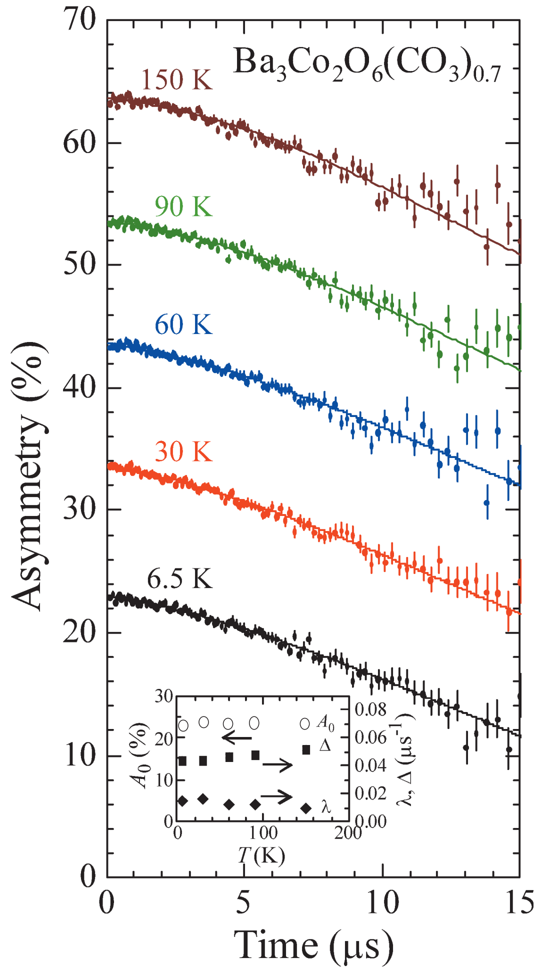

Fig. 1. μSR time spectra of $Ba_3Co_2O_6(CO_3)_{0.7}$. Each plot is shifted vertically by 10% for clarity. Solid lines are fitting results using Eq.(1). The inset shows the temperature dependence of A_0, λ and Δ obtained by the fitting.

References

1) M. F. Collins and O. A. Petrenko: Can. J. Phys. **75**, 605 (1997).
2) K. Boulahya *et al.*: Chem. Mater. **12**, 966 (2000).
3) K. Igarashi *et al.*: J. Phys.: Conf. Ser. **400**, 032024 (2012).
4) K. Iwasaki *et al.*: J. Appl. Phys. **106**, 034905 (2009).
5) R. Kubo and T. Toyabe: in *Magnetic Resonance and Relaxation*, edited by R. Blinc *et al.* (North-Holland, Amsterdam, 1967) p. 810.

Muon Spin Relaxation Studies on Pyrochlore Iridate $Nd_2Ir_2O_7$

H. Guo, K. Matsuhira,[*1] I. Kawasaki, M. Wakeshima,[*2] Y. Hinatsu,[*2] I. Watanabe, and Z.A. Xu

Pyrochlore iridates, $R_2Ir_2O_7$ (R = Y and lanthanide), are of great interest because of the interplay between relatively large spin-orbit coupling and electron-electron correlation, and novel phases are expected in the magnetic ordered state. Therefore, the identification of magnetic ordered states from experiments is essential for future investigations. We studied $Nd_2Ir_2O_7$, which resides on the ionic metal-insulator boundary.[1)]

The left panel of Fig. 1 shows the time dependence of asymmetry in ZF. The spectra show exponential-like depolarized behaviors above T_{MI}, and the muon-spin depolarization becomes faster with decreasing temperature. Significant loss of initial asymmetry is observed below T_{MI}. The right panel of Fig. 1 shows an early time region of the spectra. Below ∼30 K, the initial relaxation rate increases rapidly, and well-defined muon spin precession develops with further decrease in temperature, indicating the presence of a long-ranged magnetic ordered state. Therefore, we identify the magnetic transition temperature as T_{M} = 30 K. The spectra in Fig. 1 are fitted using the function of

$$A(t) = A_1\exp(-\lambda t)+A_2\cos(\gamma_\mu H_{\mathrm{int}}t+\phi)\exp(-\lambda_2 t),(1)$$

and A_2 is set to be zero when muon-spin precession is absent.

The extracted parameters are shown in Fig. 2. In Fig. 2(a), the internal field, H_{int}, at the muon site begins to increase below T_{M}, and saturates below 20 K. Below 9 K, H_{int} increases again, indicating occurrence of another magnetic ordering. Fig. 2(b) shows the temperature dependence of muon spin depolarization rate, λ. Upon cooling from 150 K, λ increases monotonically, and no anomaly was observed at ∼120 K, compared with a previous μSR experiment on Nd-227.[2)] With further decrease in temperature, the depolarization rate becomes larger when approaching T_{M}, and then decreases; however, no critical slowing down behavior is observed, unlike the usual spin-lattice relaxation process when the system undergoes a transition from paramagnetic to magnetic ordered state. We note that similar behavior is also observed in other pyrochlore iridates, and is attributed to the mean-field like transition with narrow critical width. Below about 20 K, λ continues to increase more quickly and exhibits a broad peak at ∼9 K, which is denoted as T_{Nd}, and then decreases at lower temperature.

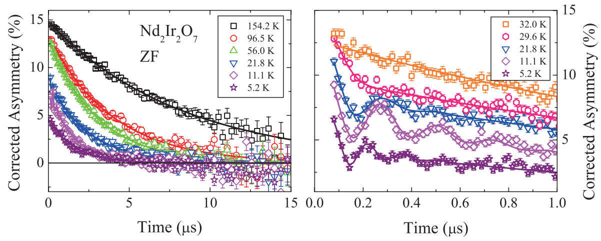

Fig. 1. (Color online) (Left) Typical time dependent asymmetry in zero field condition at different temperatures. (Right) An early time region shows the muon spin precession at low temperatures.

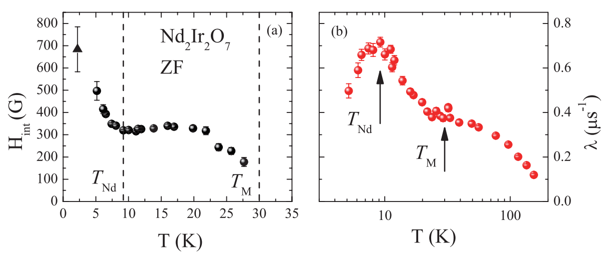

Fig. 2. (Color online) Temperature dependence of (a) internal field, H_{int}, at the muon site; (b) muon spin depolarization rate, λ.

Previous neutron experiment suggested a hidden Ir^{4+} moments ordering below T_{MI} = 33 K, and Nd^{3+} moments ordered below 15 ± 5 K. Our μSR results clearly show two magnetic transitions, i.e., the appearance of internal field below T_{M} = 30 K, and the further increase in internal field below ∼9 K. Combined with neutron experiment, these results indicate the ordering of Ir^{4+} moments below T_{M}, and the second increase in internal field below ∼9 K, reflecting the ordering of Nd^{3+} moments. The internal field at the muon site, ∼350 G, is much less than other pyrochlore iridates with insulating ground state, that is about 1100 G for Y-227 and Yb-227,[3)] suggesting a reduction of Ir^{4+} moment in Nd-227, assuming the magnetic structure and muon site are not changed drastically in the insulating phase.

References

1) K. Matsuhira *et al.*: J. Phys. Soc. Jpn. **80**, 094701 (2011).
2) S. M. Disseler *et al.*: Phys. Rev. B **85**, 174441 (2012).
3) S. M. Disseler *et al.*: Phys. Rev. B **86**, 014428 (2011).

*1 Facuty of Engineering, Kyushu Institute of Technology
*2 Division of Chemistry, Hokkaido University

μSR study of Heusler compounds $Ru_{2-x}Fe_xCrSi$

M. Hiroi, I. Watanabe, I. Kawasaki, and T. Suzuki

The magnetic properties of the Heusler compounds $Ru_{2-x}Fe_xCrSi$ have attracted considerable attraction. The Fe-rich compounds were found to be ferromagnetic,[1] and Ru_2CrSi was found to exhibit an antiferromagnetic transition at $T_N = 13$ K from specific heat and magnetic susceptibility measurements.[2] Whereas, in the Ru-rich compound $Ru_{1.9}Fe_{0.1}CrSi$ a peak in magnetic susceptibility was observed at $T_N^* \sim 30$ K, which appears to indicate an antiferromagnetic transition,[3] the absence of long-range order was suggested by a specific heat measurement.[4] Below T_N^* a strong irreversibility in magnetic susceptibility was observed; the onset temperature of the strong irreversibility is $T_g \sim 15$ K.[3] Our previous μSR measurements indicated that spin freezing occurs at T_g. Therefore, we concluded that spin-glass freezing occurs at T_g. On the other hand, in our μSR measurements, in the relaxation rates no anomaly that indicates phase transition or spin-freezing was found at around T_N^*. However, a large decrease in the initial asymmetry was observed, and the measurements of LF-μSR as a function of magnetic field indicated the appearance of a static internal field even around T_N^*. From these results, we assume that the formation of independent static magnetic regions begins around T_N^*, and with decreasing temperature toward T_g, the volume fraction of the static regions increases.

With decreasing Fe concentration, x, in $Ru_{2-x}Fe_xCrSi$ ($x \leq 0.1$), T_N^* decreases and appears to approach $T_N = 13$ K for $x = 0$, whereas T_g does not appear to vary significantly.[2] Consequently the relations of the antiferromagnetic transition in Ru_2CrSi to the anomalous behavior of slightly Fe-substituted samples around T_N^* and to the spin-glass freezing at T_g appear interesting. To investigate the connections in these anomalies, we performed μSR measurements for polycrystalline $Ru_{2-x}Fe_xCrSi$ with $x = 0$ and 0.01.

The measurements were carried out at the RIKEN-RAL Muon Facility using a spin-polarized pulsed positive surface muon beam. ZF-μSR, and LF-μSR in a longitudinal field, H_{LF}, of 100 Oe, were performed, and the time spectra of asymmetry $A(t)$ were measured at temperatures between 0.3 K and 50 K.

In Ru_2CrSi no precession signal was observed in the ZF-μSR time spectrum at 0.3 K despite the existence of the antiferromagnetic long-range order, probably because the internal field is too large to observe a precession signal. For Ru_2CrSi the relaxations of ZF-μSR and of LF-μSR at $H_{LF} = 100$ Oe, which was applied to reduce the influence of the background, were measured. These time spectra were mostly well fitted with a single exponential function:

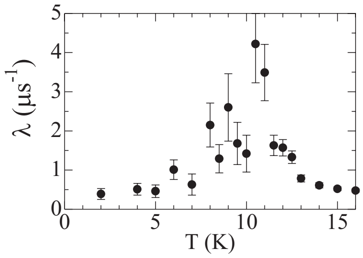

Fig. 1. Temperature dependence of the relaxation rate, λ, for LF-μSR at 100 Oe in Ru_2CrSi.

$$A(t) = A\exp(-\lambda t), \tag{1}$$

where A denotes the initial asymmetry and λ denotes the muon spin relaxation rate. Figure 1 shows the temperature dependence of λ for $H_{LF} = 100$ Oe in Ru_2CrSi. As shown in the figure, with decreasing temperature, λ increases, then exhibits a maximum at $\sim$11 K, and decreases. The initial asymmetry A decreases with decreasing temperature from $\sim$20 K, and stops decreasing at $\sim$11 K. These results suggest that a phase transition occurs at $\sim$11 K. Although this is consistent with the existence of the antiferromagnetic order, the peak of the specific heat was observed at a slightly higher temperature. The reason for this discrepancy is unclear at present.

For $x = 0.01$, in the magnetic susceptibility measurement, spin-glass-like behavior was observed, but antiferromagnetic nature may still be dominant. The time spectra for ZF-μSR and for LF-μSR at H_{LF}=100 Oe were measured and analyzed using Eq. (1). In this case, however, some of the time spectra were not well fitted with Eq. (1), possibly because of the increase in randomness brought about by Fe substitution. Nevertheless we can deduce the overall behavior from this analysis. For $x = 0.01$, although λ exhibits a maximum at $\sim$11 K as for $x = 0$, the temperature dependence of λ below 11 K appears more complicated. However, further study is needed to clarify the difference between these samples.

References

1) M. Hiroi et al.: Phys. Rev. B. **76** 132401 (2007).
2) M. Hiroi et al.: J. Phys.: Conf. Series **400** 032020 (2012).
3) M. Hiroi et al.: Phys. Rev. B. **79** 224423 (2009).
4) M. Ito et al.: Phys. Rev. B **82** 024406 (2010).

Drastic change in internal field in antiferromagnetic Kondo semiconductor $CeRu_2Al_{10}$ induced by small amount of Rh doping

H. Tanida, H. Guo, R. Kobayashi,[*1] I. Kawasaki, M. Sera,[*2] T. Nishioka,[*3] M. Matsumura,[*3] and I. Watanabe

The class of compounds denoted by CeT_2Al_{10} (T = Fe, Ru, and Os) with the orthorhombic $YbFe_2Al_{10}$-type structure can be categorized as Kondo semiconductors. Among these compounds, $CeRu_2Al_{10}$ and $CeOs_2Al_{10}$ exhibit a unique AFM order at the anomalously high transition temperatures of $T_0 = 27$ K and 29 K, respectively.[1,2] These two compounds are the first examples exhibiting AFM order among Kondo semiconductors. The AFM order was confirmed by neutron diffraction[3] and ^{27}Al NMR/NQR studies[4], wherein the ordered moment ($m_{\rm AF}$) is parallel to the c-axis. Zero-field μSR also revealed the existence of an internal magnetic field ($H_{\rm int}$) below T_0.[5] However, there remain many problems to be solved because the AFM order is very unusual. Anomalous magnetic anisotropy is one such example; $m_{\rm AF}\|c$ is unusual because the easy magnetization axis is the a axis, and the magnetic anisotropy is very large. Recently, it was reported that magnetic properties are drastically changed by doping $CeRu_2Al_{10}$ with only 10% Rh.[6] That is, χ along the a-axis shows a sudden drop at T_0 while those along the other axes are almost T-independent behavior, thereby suggesting that $m_{\rm AF}\|a$ is realized in Rh-doped $CeRu_2Al_{10}$.

In order to clarify the spin alignment and the critical Rh concentration x_c from the microscopic point of view, we carried out zero-field μSR on $Ce(Ru_{1-x}Rh_x)_2Al_{10}$ (x = 0.02, 0.03, 0.05, and 0.1). Since χ_a is considerably larger than χ_c, $H_{\rm int}$ is expected to be strongly enhanced if $m_{\rm AF}\|a$ is realized. Small single crystals were grown via an Al self-flux method, and these crystals were randomly mounted on silver plate.

The time spectra of $Ce(Ru_{0.98}Rh_{0.02})_2Al_{10}$ are shown in Fig. 1. Above T_0, the asymmetry is well explained by the Kubo−Toyabe function. Below T_0, clear oscillatory behavior is seen. As shown in the inset, the spectra exhibit fairly fast oscillations, thereby indicating the existence of at least two stopping sites. Similar behavior is also observed for x = 0.03, 0.05, and 0.1. We analyzed the data by assuming two precession frequencies (fast and slow frequencies), and the results are plotted in Fig. 2. For the slow component H_S, both the T dependence and the magnitude of $H_{\rm int}$ show similar behavior to those reported for x = 0, thereby indicating that $m_{\rm AF}\|c$ is realized. Since H_S is observed only for $x < 0.03$, x_c is considered to lie between x=0.02 and 0.03. On the other hand, for the fast component H_L, both the T dependence and the magnitude of $H_{\rm int}$ are drastically changed. $H_{\rm int}$ reaches about 800 Oe at low temperatures, which is about one order larger than that of H_S. As regards such a drastic change in $H_{\rm int}$, we hypothesize that $m_{\rm AF}\|a$ is realized in the Rh-doped alloys.

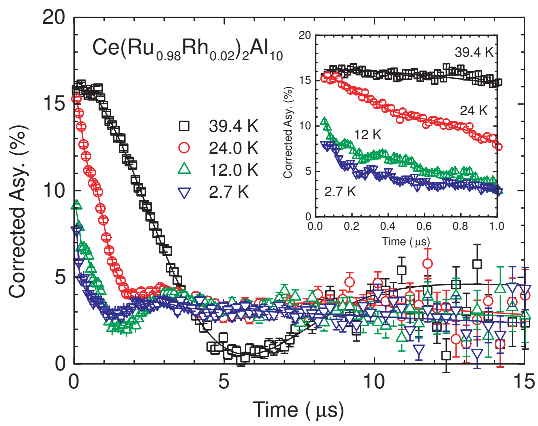

Fig. 1. Zero-field μSR spectra of $Ce(Ru_{0.98}Rh_{0.02})_2Al_{10}$. The inset shows the spectra for the initial time region.

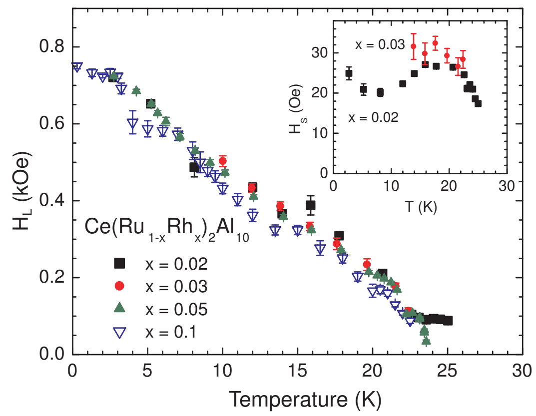

Fig. 2. T dependence of the internal magnetic field $H_{\rm L}$ of $Ce(Ru_{1-x}Rh_x)_2Al_{10}$ (x = 0.02, 0.03, 0.05, and 0.1). The inset shows the T dependence of $H_{\rm S}$.

*1 Quantum Beam Science Directorate, JAEA
*2 AdSM, Hiroshima University, Japan
*3 Graduate school of Integrated Arts and Science, Kochi University, Japan

References
1) A. M. Strydom: Physica B **404** 2981 (2009).
2) T. Nishioka *et al.*: J. Phys. Soc. Jpn. **78** 123705 (2009).
3) D. D. Khalyavin *et al.*: Phys. Rev. B **82** 100405 (2010).
4) H. Tanida *et al.*: Phys. Rev. B **84** 233202 (2011).
5) S. Kambe *et al.*: J. Phys. Soc. Jpn. **79** 053708 (2010).
6) R. Kobayashi: Thesis, Kochi University (2011).

μSR study of geometrical frustrated spin system in distorted triangular spin tubes

H. Manaka, I. Kawasaki, and I. Watanabe

The ground states of geometrically frustrated spin systems have attracted theoretical and experimental attention. Triangular spin tubes belong to a new category of one-dimensional Heisenberg antiferromagnets that have the tubes coexisting with geometrically frustrated spin systems in the triangular plane. [1] We succeeded in synthesizing high-quality single-phase polycrystalline $S = 3/2$ compounds with distorted triangular spin tubes (α-$KCrF_4$).[2] According to the magnetic susceptibility and heat capacity measurements, an antiferromagnetic long-range order occurred at $T_{N2} = 4.0(1)$ K and a magnetic phase transition occurred at $T_{N1} = 2.5(1)$ K.[2] In order to clarify the successive phase transitions at T_{N1} and T_{N2}, μSR measurements were performed on α-$KCrF_4$ at the RIKEN-RAL Muon Facility in U.K., and polycrystalline samples of α-$KCrF_4$ were prepared.

In fluorides, low-frequency oscillations due to the dipole-dipole coupling of F-μ^+-F states are generally observed. The observation of ZF-μSR time spectra at various temperatures revealed that typical F-μ^+-F states appeared above T_{N2}; however, below T_{N2}, these states disappeared because the antiferromagnetic phase transition occurred. The ZF-μSR time spectra below T_{N2} could be fitted well by the two components of muon spin relaxation, expressed by

$$A(t) = A_1 \exp(-\lambda_1 t) + A_2 \exp(-\lambda_2 t), \tag{1}$$

where A_1 and A_2 are the initial asymmetry, and λ_1 and λ_2 ($\lambda_1 > \lambda_2$) are the muon spin relaxation rates for fast and slow components, respectively. Figure 1 shows temperature dependence of the relative yield of volumetric fractional and relaxation rates of respective components. As can be seen in this figure, there is no anomaly that indicates the magnetic phase transition at T_{N1} within the experimental errors.

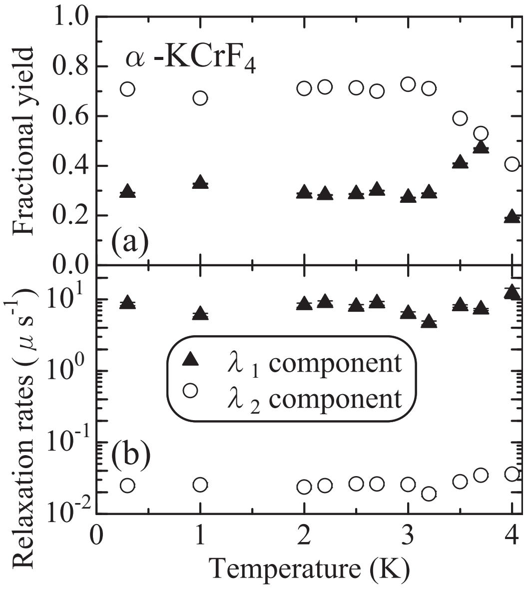

Fig. 1. Temperature dependence of (a) relative yield of volumetric fraction and of (b) two components of the relaxation rates given by Eq. (1).

Figure 2 shows the LF-μSR time spectra at 0.30 K. As can be seen in this figure, the decoupling behavior, i.e., the upward shift of the time spectra with increasing longitudinal magnetic fields (H_{LF}), indicates the existence of a static internal magnetic field at 0.30 K. This result agrees well with antiferromagnetic phase transition below T_{N2}. Further analyses of the μSR time spectra at various temperatures and longitudinal magnetic fields are necessary to clarify the antiferromagnetic ordered state observed at $T_{N1} < T < T_{N2}$ and the magnetic phase transition observed at T_{N1}.

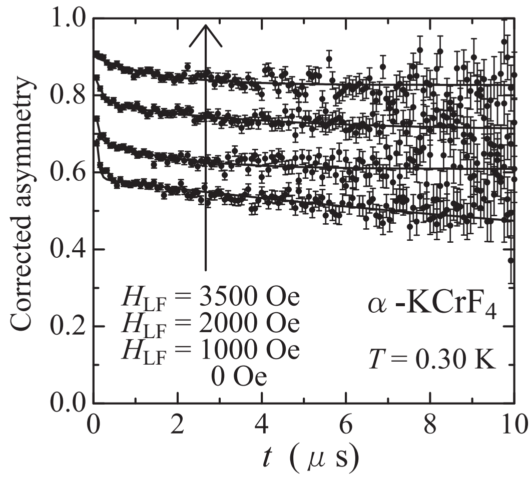

Fig. 2. μSR time spectra for various longitudinal magnetic fields (H_{LF}) up to 3500 Oe at 0.30 K. Solid lines are the best-fit lines given by Eq. (1).

References

1) H. Manaka *et al.*: J. Phys. Soc. Jpn. **78**, 093701 (2009).
2) H. Manaka *et al.*: J. Phys. Soc. Jpn. **80**, 084714 (2011).

μSR study of charge transport in organic semiconductor spiro-compound†

T. P. I. Saragi, Risdiana, L. Safriani, I. Kawasaki, J. Salbeck[*1] and I. Watanabe

Organic semiconductors have attracted so much attention from scientific and industrial community due to their interesting properties and huge potential applications in optoelectronics such as solar cells, light-emitting devices and field-effect transistors. Generally, there are two classes of active materials, namely conjugated polymers (for examples poly(*p*-phenylene vinylene) and poly(9,9'-dioctyl fluorene) and small molecules (for examples pentacene and tris(8-hydroxyquinoline) aluminum, Alq_3). However, understanding the charge transport properties in organic semiconductors is still need to be improved in particular the motion of carriers in organic conjugated molecules.

We have carried out the Longitudinal Field-μSR on small molecule crystalline 2',7'-bis(*N*,*N*-di-phenylamino)-2-(5-(4-*tert*-butylphenyl)-1,3,4-oxadiazol-2-yl)-9,9-spirobifluorene (Spiro-DPO), as displayed in Fig. 1. This compound belongs to the class of organic donor/acceptor dyads in which two different functional moieties (acceptor oxadiazole unit and donor bis(diphenylamino)biphenyl unit) are linked by a central spiro carbon atom[1,2]. It has been used as an efficient UV-sensitive material in a field-effect transistor that exhibited a responsivity of up to 6.5 A/W at a wavelength of 370 nm[2].

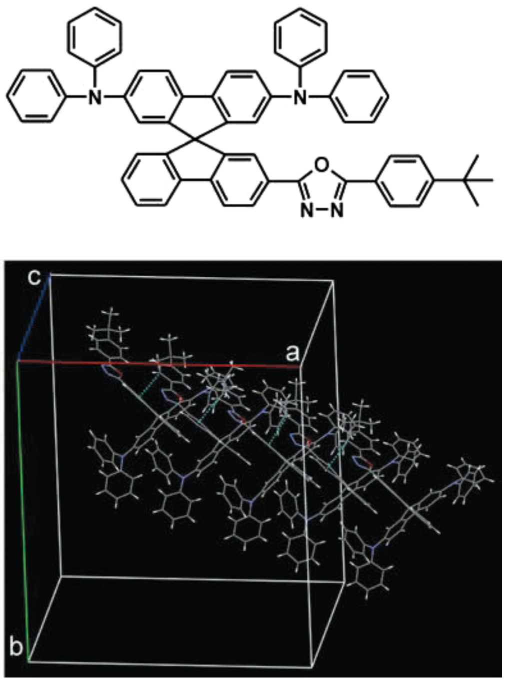

Fig. 1. The chemical structure of Spiro-DPO (top) and the structure obtained from X-ray diffraction analysis (bottom).

† Condensed from the article in Org. Electron. 14, 62 (2013).

*1 CINSaT, University of Kassel, Germany.

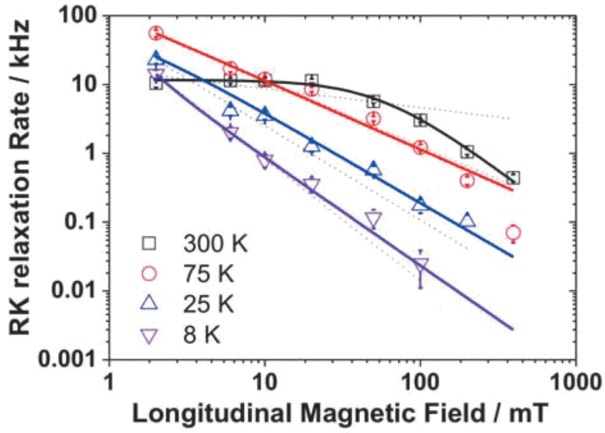

Fig. 2. RK relaxation rate Γ plotted versus longitudinal magnetic field at different temperatures. The solid lines show fits to Farazdaghi-Harris (FH) law $\Gamma(B) = A/(1+CB^n)$. The dotted lines show fits to power law $\Gamma(B) = CB^n$, whereas A and C are constants, B is longitudinal magnetic field and n is an exponent.

Our asymmetry data obtained from μSR experiment was fitted by using the general form for fluctuation of spin density with a muon relaxation function proposed by Risch and Kerr (RK):[3] $G(t)=\exp(\Gamma t)\mathrm{erfc}(\Gamma^{1/2}t)$ for $\lambda t_{max}>>1$, where erfc is the complementary error function, t_{max} is the experimental time scale and Γ is a relaxation parameter. Figure 2 shows the longitudinal field-dependent of the RK relaxation rate at different temperatures and the data was fitted by using FH and power law. However, our data was better fitted with FH law with respect to power law in particular at 300 K. We can see that at temperatures lower than 75 K the 1D regime of charge hopping holds down to below 2 mT, while at 300 K the regime only holds down to 100 mT. This indicates that at T ≤ 75 K the intrachain diffusion is probably much higher than the interchain one. The electron hopping takes place probably along the direction of (101), as displayed in Fig. 1. In contrast, interchain diffusion at 300 K increases significantly particularly at low fields, which means the electron hopping takes place not only along the direction of (101) but also in the other direction. Therefore, at 300 K the electron hopping is not 1D anymore, but rather 2D or 3D.

References

1) T. P. I. Saragi et al.: Chem. Rev. 107, 1011 (2007).
2) T. P. I. Saragi, R. Pudzich, T. Fuhrmann-Lieker, and J. Salbeck: Appl. Phys. Lett. 90, 143514 (2007).
3) R. Risch, and K. W. Kehr: Phys. Rev. B. 46, 5246 (1992).

μSR Study of Charge Carrier Motion in Active Layer P3HT:ZnO Hybrid Solar Cells

L. Safriani, Risdiana, A. Bahtiar,[*1] A. Aprilia[*1], R. Hidayat[*2], T. P. I. Saragi, I. Kawasaki and I. Watanabe

Solar power generation is a key method for generating electronic power. Several researchers have attempted to achieve higher performance of the solar cells and to find out more effective materials for use in solar cells. The discovery of conjugated polymers, such as Polythiophene (PT) and its derivatives, have attracted much attention owing to their chemical and thermal stability as well as their potential use as an absorbing solar spectrum material (active layer) in solar cells.

The most necessary property of these active layers is their ability to transfer the charge carrier resulting from the absorption of solar spectrum. In particular, poly (3-hexylthiophene) (P3HT) has considerable attracted research interest because P3HT shows the highest hole mobility among the series of poly(3-alkylthiophene)[1]. In our previous μSR study, we carried out ZF- and LF-μSR measurements in a P3HT sample. The charge carrier mobility was found to change from one-dimensional model (the charge transport is dominated by mobility along (intra) to the polymer chain) to a three-dimensional one (the charge transport is dominated by mobility perpendicular (inter) to the polymer chain), which is strongly dependent on their molecular structure and temperature[2,3].

Recently, the so-called hybrid (organic- inorganic) solar cell has been developed owing to the combined advantage between organic material (P3HT) and inorganic material such as zinc oxide (ZnO), which ensures better performance for practical application. It is well known that ZnO is an inorganic material with high electron mobility and can be easily prepared as electron acceptor to dissociate excitons formed in conjugated polymer as the active material of solar cells. ZnO also can be prepared as a nanoparticle that can resolve the problem of small diffusion range of P3HT[4]. Therefore, ZnO is the main candidate for the electron acceptor material in hybrid solar cells. However, a clear explanation about the effect of ZnO on the charge carrier mobility in P3AT has not yet been provided owing to their molecular structure and temperature dependence.

We have studied the microscopic intrinsic charge carrier motion in active material of P3HT:ZnO blend of hybrid solar cells along and perpendicular to the chain by using the longitudinal field (LF) μSR method. We also studied the effect of white light irradiation on the charge carrier generation and its dynamic motion in this sample.

[*1] Department of Physics, Padjadjaran University, Indonesia
[*2] Department of Physics, Bandung Institute of Technology, Indonesia

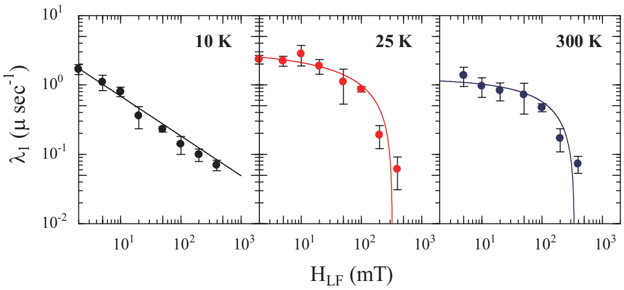

Fig. 1. Longitudinal field dependence of λ_1 in P3HT:ZnO.

Figure 1 shows the longitudinal field dependence of λ_1 in P3HT:ZnO. λ_1 is the corresponding depolarization rates associated with the fast component. We found that the charge carrier mobility changes from intrachain to interchain diffusion. One-dimensional intrachain diffusion is observed in the samples at low temperatures below 10 K, while three-dimensional interchain is observed at high temperatures above 25 K. Compared with μSR data of P3HT that shows dimensional crossover at 25 K[2], it is apparent that the dimensional crossover from one-dimensional to three-dimensional in P3HT:ZnO is observed at lower temperature. ZnO nanoparticles facilite electron transfer from P3HT in the blend more easily than in P3HT only.

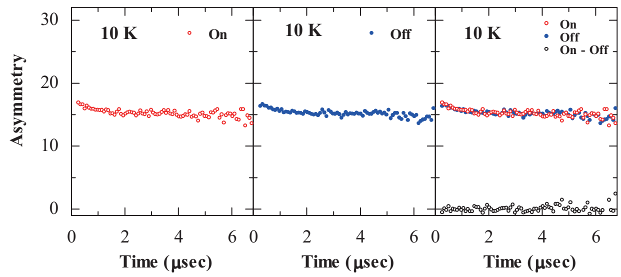

Fig. 2. Asymmetry spectra of P3HT:ZnO with (on) and without (off) light irradiation at 10 K.

Figure 2 shows the asymmetry spectra of P3HT:ZnO with and without light irradiation at 10 K. We did not observe any significant effect of light irradiation on the assymetry spectra. Some possible explainations are as follow: i) Excitons induced by light irradiation are generated only in the surface of sample ii) Transfer rate of excitons from P3HT to ZnO occur is slower owing to aggregation of ZnO nanoparticles.

References

1) A. Babel and S. A. Jenekhea: Synth. Met. **148**, 169, (2005).
2) Risdiana et al.: Journal of Physics Conf. Series **200**, 052024, (2010).
3) Risdiana et al.: Physica B **405**, S381, (2010).
4) L. W. Ji et al.: J Matter Sci. **45**, 3266, (2010).

Detection of Optically-Injected Spin-Polarized Conduction Electrons in Si by Muon Spin Relaxation

H.W.K. Tom, K. Nagamine,[*1,*2] K. Shimomura, K. Yokoyama, R. Kawakami, J. Muse,[*1]
K. Ishida, F.L. Pratt, I. Shiraki, A.D. Pant and E. Torikai

Silicon is the most important spintronics material; it is intrinsically favorable for spintronics applications because of its expected long spin lifetime and spin transport due to its low spin-orbit coupling and its embedded base in the existing electronics industry. However, Si has not been widely considered or studied in spintronics because there are no optical probes of spin-polarized conduction electrons in Si due to its indirect band-gap. A new muon-based probe for detection of spin-polarized conduction electrons in any semiconductor[1, 2] would advance spintronics development.

There is also an immediate impact—it is generally not accepted that spin-polarized conduction electrons can be optically injected in Si, due to the indirect band-gap of Si. However, near the band-gap (~3.5 eV, 354 nm) similar selection rules between J states occurs in Si as occur in direct band-gap semiconductors and ~30% spin-polarization is possible according to band-structure calculations.[3)]

The *n*-Si (100) sample with 10^{14} P doping was prepared with two electrodes; Au for the front electrode and ITO (optically transparent electrode) for the back one. These were biased with a pulsed voltage of ~40 V to carry the injected electrodes from the back electrode into the bulk Si. The muons were incident on the front surface at normal incidence and adjusted in energy to deposit in a broad distribution in the middle of the 300 micron thick sample.

The circularly polarized (CP) 355 nm (3.49 eV) UV light (6 ns pulse) was incident with a pulse timing to arrive 0.1 ~ 0.4 μs after the arrival of the muon pulse. The UV laser pulses were varied in a 4-pulse sequence that repeated every 4 muon pulses; 1 pulse off, 1 pulse on with CP helicity positive corresponding to optical spin parallel (P) case between muons and photon, 1 pulse off, and 1 pulse on with CP helicity negative with muon and photon spins antiparallel (A).. Thus, we obtained the μSR time spectrum with 1) laser Off, 2) Laser On (P+A) 3) Difference between P and A (P-A).

Typical μSR time spectra without lasers at 15 K under 20G LF were analyzed by taking the following assumptions based upon the present knowledge of the electronic states of the μ^+ in *n*-type Si; ① T-site muonium, ② BC-site muonium and ③ Mu^- at T-site. 1) Within some 0.1 T, both T-Mu and BC-Mu should take a typical LF decoupling pattern, while the T-Mu^- should not have a LF dependence. 2) Because of the exchange interaction with the dopant electrons, the T-Mu is subject to the depolarization at zero LF, while the BC-Mu takes visible relaxation in the range of $(\mu s)^{-1}$.

As seen in Fig. 1, ON-OFF effects were observed by laser injection for 100 G LF. As for the electronic states of muon responding to the laser electrons, the following conclusions were obtained at 10K.

1. In ON-OFF time spectrum for both 20 G and 40 G TF rotation, there was no corresponding μ^+ precession signal, suggesting the Mu^- at T-site does not respond to the electrons induced by the lasers.
2. In ON-OFF time spectrum for 2.3 G TF rotation, there was no corresponding muonium precession signal, suggesting the Mu at BC-site does not respond to the electrons induced by the lasers.
3. In LF decoupling, the difference in total asymmetry A(H) seems to follow the decoupling characteristics exhibited in $A_{T\text{-}Mu}$(H, OFF). Thus, the T-Mu seems to respond to the laser induced conduction electrons.

As for the most important spin-dependent PARA-ANTI effect, a high statics run of 200 M events run was conducted at 10 K under 100 G LF with 355 nm (3.49 eV) and 100% CP laser pulses. Although a clear ON-OFF effect of -1.953(21) % was observed, a non-significant PARA-ANTI effect of -0.006(30) % was observed. The result is suggesting a need of the measurement with a different photon wavelength (energy).

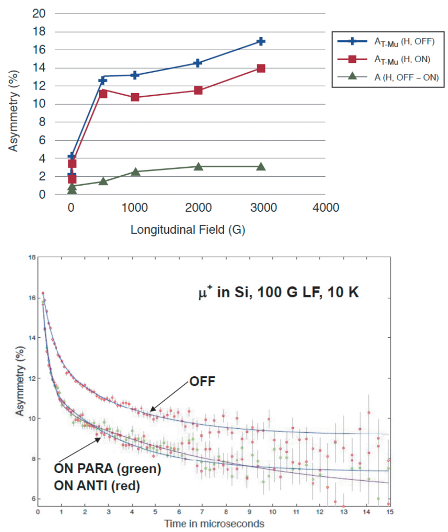

Fig. 1 (Upper) Typical example of laser irradiation effect in *n*-Si at 10 K under 20 G LF. PARA (ANTI) is the cases, where the laser electrons are polarized in parallel (anti-parallel) to the muon spin. (Lower) LF decoupling effect with laser off and on in *n*-Si at 10 K.

[*1] Physics & Astronomy, University of California, Riverside
[*2] Muon Science Laboratory, IMSS, KEK

References

1) E. Torikai *et al.*, *Physica B* **289-290**, 558 (2000).
2) K. Yokoyama *et al.*, *Physics Procedia* 30 (2012) 231.
3) F. Nastos et al., *Phys. Rev. B*76 (2007) 205113.

Muonium response to oxygen impurities in biological aqueous solution for hypoxia studies application

K. Nagamine,[*1,*2] J.S. Schultz,[*3] K.Shimomura,[*2] F.L. Pratt, K. Ishida, A.D. Pant, and E. Torikai

Hypoxia, or low oxygenation, is known as an important factor in tumor biology and in the response of tumors to treatment by radiation therapy. In cancer patients, an accurate measurement of hypoxia in specific regions may provide an important predictive value in the management of treatment and outcome of the disease[1)]. As regards hypoxia imaging techniques, improved O_2 detection methods form an important need. Several unsatisfactory trials have been conducted employing PET, MRI and EPR.

Here, we propose the use of the μ^+ as a new sensitive method to probe the existence of paramagnetic O_2 in the cancer of the human body. There have been experimental studies on the oxygen dissolving effects of the spin relaxation of muonium (Mu, $\mu^+ + e^-$) in pure water[2)]; the relaxation rate constant λ_{Mu} has been measured as 1.8 ± 0.1 l mol^{-1} s^{-1} due to electron spin exchange interactions with dissolved molecular O_2 in water. Since sensitivity range to the spin relaxation of a pulsed muon is 10^4 to 10^7 s^{-1}, the sensitivity for PO_2 (μ) becomes $0.5 \times 10^{-6} \sim 0.5 \times 10^{-3}$mol l^{-1}.

The solubility of O_2 in water at 23 C is 1.29×10^{-5} mol l^{-1}kPa^{-1}; under 1 atm, PO_2(s.l.) is 1.3×10^{-3} mol l^{-1}.Thus, PO_2(μ)/PO_2(s.l.) becomes 0.4×10^{-3} to 0.4, which value range perfectly corresponds to Hypoxia. A desirable feature of the muon method is its non-invasive and sensitive imaging; a spatial resolution at the mm level can be obtained at depths of up to 20 cm

However, the unsolved problem regarding the method is the background from other magnetic molecules, thereby providing the motivation of the present study.

Our experiment was conducted at Port 2 of the RIKEN-RAL in the UK using 60 MeV/c decay positive muons. The μ^+ in water take the states of a diamagnetic μ^+ fraction such as μ^+OH (60%), paramagnetic Mu fraction (20%) and a missing fraction (20%). In the Mu fraction, a half becomes an ortho state with spin 1, providing a spin rotation signal with a precession pattern that is 100 times faster than that of diamagnetic μ^+. Spin rotation and its relaxation were detected under 2.3 G transverse fields. All the measurements were conducted at room temperature. The O_2 concentration was controlled by changing the mixing ratio of N_2 gas and air; pure N_2 for 0% O_2 and air for 20.7% O_2 were used. In pure water, the Mu spin precession was found to undergo faster relaxation against increase in O_2, consistent with the existing data[2)].

Subsequently, tris-buffered saline (TBS), which is a buffer used in some biochemical techniques to maintain the pH, was introduced in pure water; the Mu signal was found to be essentially unchanged in 7.5 g of TBS solution in 1 liter of water. As shown in Fig. 1, Mu undergoes a relaxation change similar to pure water against O_2 increase.

Finally, 0.4 g of albumin was introduced in 1 liter of water with 7.5 g of TBS buffer and 10% O_2 impurities. Albumin, which generally refers to a water-soluble protein, is moderately soluble in concentrated salt solutions, and it experiences heat denaturation. As seen in Fig.1, a consistent relaxation was observed for controlled O_2 impurities. Upon increasing the albumin quantity to 4 g, the muonium signal was found to disappear.

Before the clinical application of the method to hypoxia studies, it is important to conduct systematic studies on the behavior of O_2 impurities in various biological aqueous systems. In this light, the present direct observation of muonium spin rotation in TBS and albumin water solution is quite encouraging. With the use of the buffer, a variety of biological solutes can be expanded.

At the same time, since Mu is a form of light hydrogen, hydrogen behavior in biological aqueous solution can directly be studied.

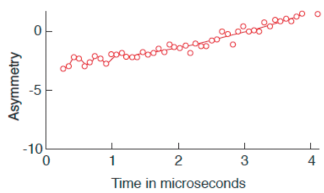

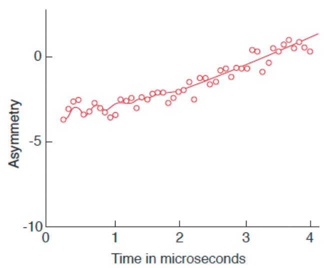

Fig. 1 (Upper) Muon spin rotation time spectrum in 7.5g of TBS water solution with O_2 concentration of 10% under 2.3 G transverse field (TF). (Lower) Muon spin rotation time spectrum in 0.4 g of albumin and 7.5g TBS water solution with 10% O_2 at room temperature under 2.3 G TF.

*1 Physics & Astronomy, University of California, Riverside
*2 Muon Science Laboratory, IMSS, KEK
*3 Bio-Engineering, University of California, Riverside

References
1) J.L. Tatum et al., *Int. J. Radiat. Biol.* **82**, 699 (2006).
2) E. Roduner et al., *J. Chem. Soc. Faraday Trans.* **91**, 1935 (1995).

Silica aerogel as a room-temperature thermal-muonium-emitting material for ultra-slow muon production

S. Okada, G. Beer, Y. Fujiwara, K. Ishida, M. Iwasaki, T. Mibe, Y. Oishi, N. Saito, M. Tabata,[*1*2] D. Tomono, K. Ueno, and K. Yokoyama

Positive muons with a few eV energy, so-called ultra-slow muons, can be produced by two-photon resonant laser ionization of thermal muonium atoms (μ^+e^-) in vacuum[1,2]. By accelerating the muons in an electrostatic field, variable-energy slow-muon beams with extraordinarily small energy spread can be realized. This will extend μSR (muon spin rotation and relaxation) studies to thin films, surfaces and interfaces, and nano-structures that have been impossible to investigate with the conventional μSR technique using surface muons. Moreover, this technique has attracted attention for use in the measurement of the muon anomalous magnetic moment g-2 and electric dipole moment at J-PARC[3], which requires μ^+ beam having extremely small transverse momentum.

For the slow muon production, it is essential to produce thermal muoniums in vacuum, which has been demonstrated previously with the following two approaches. One uses a tungsten foil heated to more than 2000 K, where muoniums are expected to be produced not inside the foil, but at the hot surface providing electrons. The other approach used silica (SiO_2) powder at room temperature, where muoniums formed in the silica are emitted from the silica powder particles and eventually from a layer of the material in vacuum.

The room-temperature target has several advantages. Firstly, it is experimentally easy to handle compared to the high-temperature target with a large radiant heat. Secondly, the lower energies of the produced muonium lead directly to a smaller emittance of the ionized source. Thirdly, the lower energy distribution results in a smaller spatial spread of muonium in vacuum and a smaller Doppler broadening of the resonant line for muonium excitation. These lead to the efficient use of the available laser power.

Thus far, although the silica powder has been the major candidate of the room-temperature target, powdery materials are not self-standing and thus incompatible with typical horizontal muon beams. Moreover, it is generally unfavorable to handle such powdery materials in the process of vacuuming.

A new candidate is silica aerogel, which has the same chemical composition as silica powder but is a solid with extremely low density. In the TRIUMF S1249 experiment[4], the muonium yield in vacuum has been investigated using silica aerogel as a thermal-muonium-emitting material. A preliminary result of the data analyses shows that muoniums produced near the surface in the aerogel (e.g., $\sim$100 μm below the surface for a 50 mg/cc density aerogel) are essential for vacuum emission. Based on this result, a simulation study of the diffusion process has been performed for increased surface area of the aerogel target. The result shows that the muonium yield in vacuum is much increased for the aerogel having 100-μm-notched surface.

As a part of the feasibility study of the optimization for higher muonium yield, we recently started investigating the production of the notched aerogel. There are two prominent ways to create the 100-μm-scale sub-structure. One is to produce the aerogel with a mold having the sub-structure from the beginning. The other is to notch the aerogel surface with a laser beam, electron beam, focused ion beam (FIB), etc. Figure 1 shows an SEM image of the first trial using FIB technology.

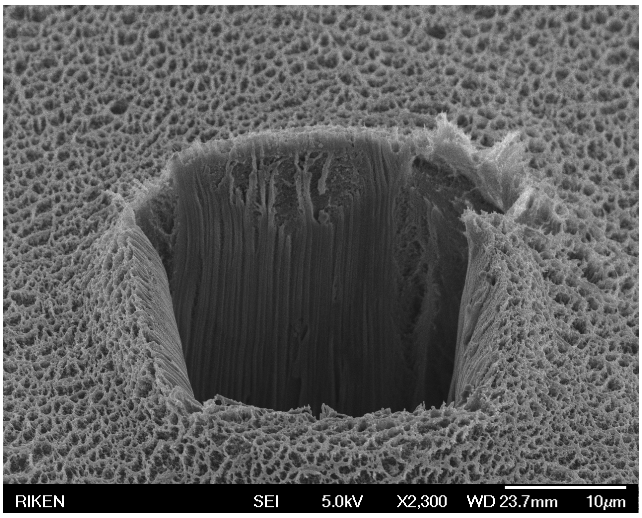

Fig. 1. An SEM image of the aerogel surface notched by FIB, taken at an angle of 45 degrees with respect to the surface with the support of Advanced Technology Support Division at RIKEN (D. Inoue).

References

1) K. Nagamine et al.: Phys. Rev. Lett. 74 (1995) 4811.
2) P. Bakule et al.: NIM. B 266, (2008) 355.
3) N. Saito, M. Iwasaki et al.: E34 proposal at J-PARC.
4) Y. Fujiwara et al.: RIKEN Accel. Rep. 45 (2011) 198.

*1 Dept. of Physics, Chiba University
*2 Japan Aerospace Exploration Agency (JAXA)

3. Radiochemistry and Nuclear Chemistry

Production of ^{256}Lr in the ^{248}Cm + ^{14}N reaction

N. Sato,[*1] T. K. Sato,[*1] M. Asai,[*1] A. Toyoshima,[*1] K. Tsukada,[*1] Z. J. Li,[*1] K. Nishio,[*1] Y. Nagame,[*1] M. Schädel,[*1,*2] H. Haba, S. Ichikawa, and H. Kikunaga

The study of the heaviest elements is an exciting and challenging endeavor in the field of nuclear chemistry. One atomic property that is most sensitive to changes in the electronic structure is the first ionization potential (IP). It is directly related to the stability of valence electrons in an atom. The ground-state electronic configuration of the last actinide, lawrencium (Lr), is predicted to be $5f^{14}7s^27p^1$.[1)] This configuration is different from that of the lanthanide homolog Lu ($4f^{14}6s^25d$) as the $7p$ orbital of Lr is stabilized below the $6d$ orbital by strong relativistic effects. The weakly bound outermost electron results in a significantly low IP for Lr as compared to the IPs for its neighboring heavy actinides.[1)] Owing to low production rates and short half-lives, the properties of Lr must be measured on an atom-at-a-time scale. The isotope ^{256}Lr, with a relatively long half-life of $T_{1/2} = 27 \pm 3$ s,[2)] is a suitable candidate for the IP measurement of Lr through the surface ionization method.[3)] In the present study, we measured the cross section of the ^{248}Cm(^{14}N, $6n$)^{256}Lr reaction to evaluate the production rate of ^{256}Lr.

A ^{248}Cm target with a 960 ± 60 μg/cm^2 thickness on a 1.86 mg/cm^2 Be backing foil was bombarded with a $^{14}N^{5+}$ beam extracted from the RIKEN AVF Cyclotron. The beam of 101.5 MeV ^{14}N ions passed through a 1.80 mg/cm^2 Be window, 0.09 mg/cm^2 helium cooling gas, and the Be backing foil, before entering the target material with 91 MeV remaining in the middle of the target. The average beam intensity was 1.2 particle-μA. The reaction products were transported to the rotating wheel α-particle detection system MANON (Measurement system for Alpha particle and spontaneous fissioN events ON-line) using a He/KCl gas-jet system. The KCl powder for the gas-jet transport was sublimated at 616 °C. The inner diameter and length of the Teflon capillary was 1.59 mm and 8.6 m, respectively. The helium gas flow-rate was 2.0 L/min. The gas-jet transport efficiency was estimated to be about (30 ± 8)%. The cycle time for collection and measurement with the MANON was 30 s. Alpha-particle energies were measured with two successively arranged planar silicon (PIPS) detectors (Canberra PD50-12-300AM) with an active area of 50 mm^2, providing a detection efficiency of (13 ± 3)% and an energy resolution of 13 keV (FWHM). Energy calibrations were performed using a standard ^{241}Am source and α-emitting by-products such as ^{151}Ho and ^{213}Fr.

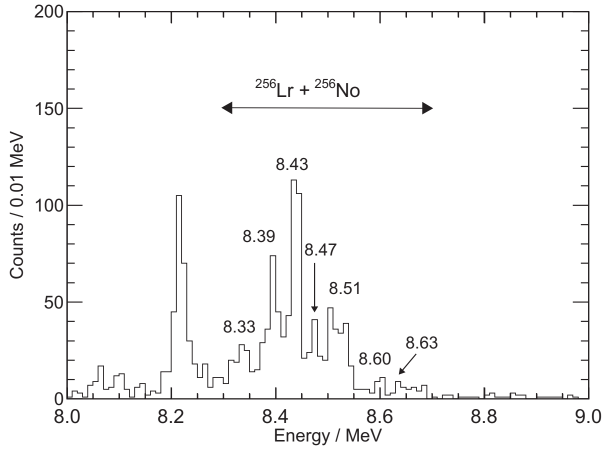

Fig. 1. Alpha-particle spectrum measured in the ^{248}Cm + ^{14}N reaction.

Figure 1 shows the α-particle spectrum measured in the time interval 0.5–61.0 s after the end of the collection. Several α-peaks of ^{256}Lr are observed in the α-particle energy (E_α) range from 8.3 to 8.7 MeV. The most intense peak at 8.43 MeV may include α particles of 2.91-s ^{256}No ($E_\alpha = 8.402$ and 8.448 MeV; α-decay branching ratio, $b_\alpha = 99.50\%$[4)]), which is the daughter of ^{256}Lr through electron capture decay. By counting both the α events of ^{256}Lr and ^{256}No, we can deduce the cross section of ^{256}Lr without requiring to consider the electron capture decay branch of ^{256}Lr. The measured half-life of 34 ± 4 s is in accordance with the literature.[2)] A 27 ± 10 nb cross section for ^{256}Lr was deduced based on the α-particle events between 8.3 and 8.7 MeV. The ^{256}Lr production rate, as obtained with the present target thickness and available beam intensity, is 1.3×10^3 ^{256}Lr atoms per hour.

References
1) A. Borschevsky et al.: Eur. Phys. J. D **45**, 115 (2007).
2) N. Nica: Nucl. Data Sheets **106**, 813 (2005) and references therein.
3) T. K. Sato et al.: Rev. Sci. Instrum. **84**, 023304 (2013).
4) D. C. Hofmann et al.: Phys. Rev. C **41**, 631 (1990).

*1 Advanced Science Research Center, Japan Atomic Energy Agency
*2 GSI Helmholtzzentrum für Schwerionenforschung

Extraction of molybdenum and tungsten by Aliquat 336 from HF and HCl solutions

Y. Komori, T. Yokokita, K. Toyomura, K. Nakamura, Y. Kasamatsu, H. Haba, J. Kanaya, M. Huang, Y. Kudou, A. Toyoshima,*[1] and A. Shinohara

Chemical studies of the transactinide elements ($Z \geq 104$) are interesting subjects. These heavy elements are expected to have chemical properties that cannot be simply deduced from the periodicity of the lighter homologues owing to the large relativistic effects on the valence electrons. We aim at performing extraction chromatographic experiments of element 106, seaborgium (Sg) using a liquid chromatographic system, ARCA[1)] to elucidate its complex formation with some ligands such as fluoride and chloride ions. In this study, we investigated the extraction behavior of molybdenum (Mo) and tungsten (W), the lighter homologues of Sg, on Aliquat 336-loaded resin (Aliquat 336/CHP20Y resin) from HF and HCl solutions. To avoid polymerization of Mo and W, carrier-free radioisotopes ^{90}Mo ($T_{1/2}$ = 5.7 h) and ^{173}W ($T_{1/2}$ = 7.6 min) were used because Sg cannot form the polynuclear species owing to its low production rates and short half-lives.

The short-lived isotopes ^{90}Mo and ^{173}W were simultaneously produced in the ^{nat}Ge(^{22}Ne, *xn*) and ^{nat}Gd(^{22}Ne, *xn*) reactions, respectively, using Gd/Ge mixed targets. The 140-MeV ^{22}Ne beam delivered from the RIKEN K70 AVF cyclotron passed through a beryllium vacuum window, the helium cooling gas, the beryllium target backing, and finally entered the target materials at an energy of 118 MeV. The typical beam intensity was approximately 300 particle nA.

Distribution coefficients (K_d) of ^{90}Mo and ^{173}W were obtained as functions of HF and HCl concentrations by a batch method. Reaction products transported by the He/KCl gas-jet system were deposited on a Naflon sheet for 1 or 5 min. The collected reaction products were dissolved in 240 μL of 0.1–10 M HCl (or 1–10 M HF) solution. A 10–20 mg of 51.9-wt.% Aliquat 336/CHP20Y resin, 100 μL of the HCl (or HF) solution containing ^{90}Mo and ^{173}W, 400 μL of a certain concentration of HCl (or HF) solution were mixed in a PP tube. These samples were shaken for 5 min at 25 ºC. Standard samples of ^{90}Mo and ^{173}W without resin were also prepared and were shaken together with the resin-containing samples. After centrifugation, the aqueous phase was pipetted into another PP tube that was subjected to γ-ray spectrometry using a Ge detector in order to determine radioactivities of ^{90}Mo and ^{173}W with 257 and 458 keV γ rays, respectively. Reaction kinetics was also investigated at 25 ºC by varying the shaking time to be 10 s, 5 min, and 10 min in 4 M HF and 2, 6, and 10 M HCl.

The on-line extraction chromatography of Mo and W was performed with ARCA. The 51.9-wt.% Aliquat 336/CHP20Y resin was filled into the 1.0 mm i.d. × 3.5 mm microcolumn of ARCA. The bottom of the microcolumn is plugged with a glass filter of approximately 1 mm thickness. The reaction products transported by the gas-jet system were deposited on the collection site of ARCA for 5 min. After the collection, the reaction products attached to the KCl aerosols were dissolved with 2, 4, 6, and 8 M HCl solutions and were subsequently fed onto the column at a flow rate of 1 mL /min. The effluents were collected in PP tubes for every 50 or 80 μL. Then, the remaining ^{90}Mo and ^{173}W in the column were eluted with 400–500 μL of 6 M HNO_3/0.01 M HF solution and were collected in another PP tube. These fractions of the effluents were assayed by γ-ray spectrometry with Ge detectors.

In the batch experiment, the K_d values of Mo and W were found to increase with increasing HCl in the concentration range of 1–6 M, as shown in Fig. 1. These increases are attributed to the formation of anionic chloride complexes. The K_d values of Mo are higher than those of W in the studied HCl concentrations. On the other hand, in the HF system, the K_d values of Mo and W decreased with increasing HF concentration and the K_d values of Mo were almost the same as those of W. The K_d values of Mo and W were almost constant with respect to the shaking time under the studied conditions. In the extraction chromatography with ARCA, the W species were eluted from the column without adsorption on the resin, whereas a portion of the Mo species was adsorbed on the resin in the studied HCl concentrations. This is consistent with the order of the K_d values obtained by the batch method.

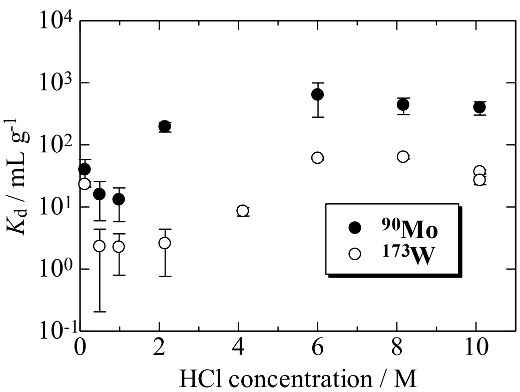

Fig. 1. Distribution coefficients of ^{90}Mo and ^{173}W as a function of HCl concentration.

References
1) M. Schädel et al.: Radiochim. Acta **48**, 171 (1989).

*[1] Japan Atomic Energy Agency

Solvent extraction of ^{93m}Mo using 4-isopropyltroplone (Hinokitiol) in the preparation of Sg reduction study

S. Miyashita,[*1] A. Toyoshima,[*1] K. Ooe, T. K. Sato,[*1] M. Asai,[*1] K. Tsukada,[*1] Y. Nagame,[*1] M. Schädel,[*1] Y. Kaneya,[*2] H. Haba, J. Kanaya, M. Huang, A. Wada, Y. Kitayama and A. Yokoyama

For the determination of the reduction potentials of Sg, we plan to carry out rapid continuous experiments using a new system combined with a flow electrolytic column[1)] and the rapid liquid-liquid extraction apparatus SISAK[2)]. The oxidation states of Sg chemically characterize its extraction behavior, and thus, rapid extraction enabling separation of Sg with different oxidation states is required. In our recent tracer-scale experiments, the extraction kinetics of ^{181}W as the lighter homologue of Sg into toluene containing 4-isopropyltropolone (Hinokitiol, HT) from 1.0 mol L^{-1} hydrochloric acid (HCl) was found to be sufficiently fast. In this present work, we examined the extraction behavior of ^{93m}Mo ($T_{1/2}$ = 6.9 h) under identical conditions.

^{93m}Mo was produced in the ^{93}Nb(*d*, 2n)^{93m}Mo reaction. ^{93}Nb metallic foils with thickness of 856 μg cm^{-2} were irradiated by a 24-MeV deuteron beam from the RIKEN K70 AVF cyclotron. The reaction products recoiling out of the target foils were transported with a He/KCl gas-jet to the chemistry laboratory. The transported products were subsequently collected on a PTFE sheet and dissolved by 1.0 mol L^{-1} HCl, which was used as an aqueous phase in all experiments. The organic phase was toluene containing a certain concentrations of HT. Seven hundred μL of each aqueous and organic phase was mixed in a vial and shaken for 10 to 600 s using a mechanical shaker. After shaking, the two phases were separated by centrifugation for 30 s. Five hundred μL of each aqueous and organic phase was taken into the vials. The presence of 263-keV γ-rays from ^{93m}Mo in the vials was detected by a Ge detector. The distribution ratio (*D*) was calculated by the ratio of radioactivity of ^{93m}Mo in the two phases.

Figure 1 shows the variation in the *D* values of ^{93m}Mo as a function of shaking time at the concentration of HT ([HT]) = 1.0 $\times 10^{-4}$ mol L^{-1}. For the comparison, our previous results of ^{176}W, obtained using the JAEA tandem accelerator, are also plotted in Fig. 1. The *D* of ^{93m}Mo and ^{176}W first increase with increasing shaking time and then reach an constant value. The extraction equilibrium of ^{93m}Mo is achieved within 3 min while that of W is achieved within 1 min. Figure 2 shows the variation in the *D* values of ^{93m}Mo and ^{176}W as a function of [HT] in the organic phase. The *D* of ^{93m}Mo and ^{176}W increase with increasing [HT] in the organic phase. The slopes of the *D* values of Mo and W against [HT] in the organic phase are 1.88 and 1.55, respectively in the log *D* vs. log [HT] plot. These results indicate that Mo and W are extracted into the organic phase with two HT molecules. Because the extraction kinetics of Mo and W using HT are sufficiently fast to use SISAK, we concluded that HT is a suitable extractant for the Sg reduction experiment.

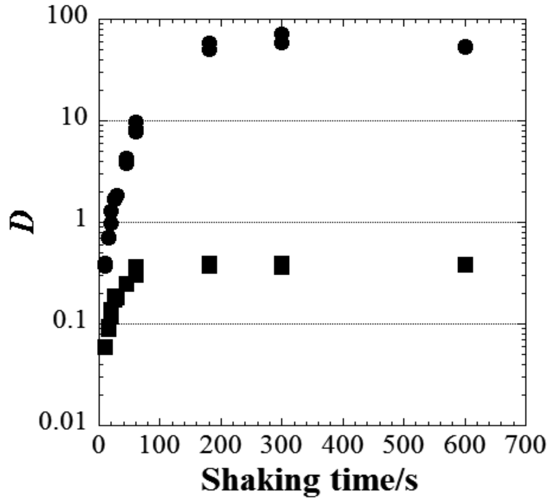

Fig. 1. Variation in distribution ratios(*D*) of ^{93m}Mo and ^{176}W as a function of shaking time. Closed circles and closed squares indicate the *D* values of Mo and W, respectively.

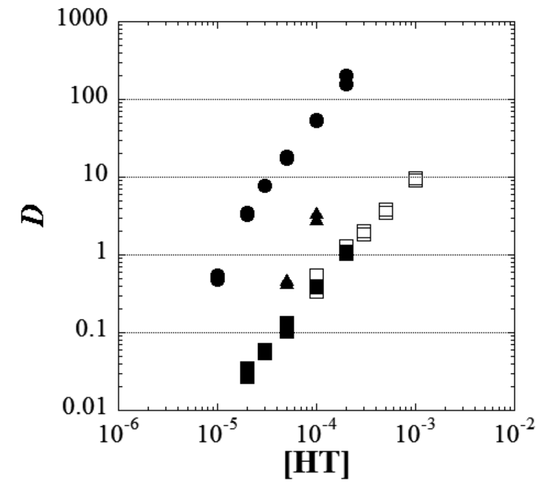

Fig. 2. Variation in distribution ratio (*D*) of ^{93m}Mo and ^{176}W as a function of [HT] in the organic phase. Closed circles and closed squares indicate the *D* value of Mo and W, respectively.

References

1) A. Toyoshima et al.: Radiochim. Acta **96**, 323 (2008).
2) J. P. Omtvedt et al.: Eur. Phys. J. D **45**, 91 (2007).

*1 Japan Atomic Energy Agency
*2 Graduate School of Science and Engineering, Ibaraki university

Anion-exchange behavior of Mo and W in HCl solution

A. Wada, Y. Oura, H. Haba, and J. Kanaya

For chemical studies of element 106, Sg, it is important to compare the chemical properties of Sg with those of its lighter homologues, Mo and W. Before performing an experiment on Sg chemistry, a separation condition using Mo and W radiotracers needs to be adequately considered. We attempted to prepare no-carrier-added radiotracers, ^{99}Mo ($T_{1/2}$ = 2.74 d) and ^{181}W ($T_{1/2}$ = 121.2 d), as well as to determine the cross sections of the ^{181}Ta(p, n)^{181}W reaction.[1)] In this study a preparation method for the ^{181}W tracer was improved and distribution coefficients (K_d) between the anion exchange resin and HCl solution were determined for W and Mo.

About 50 mg of dried anion exchange resin (DOWEX® 1X8, 100 - 200 mesh) were shaken for 20 min in 3 mL solution containing radiotracers. After centrifugation, γ -ray measurements were performed for 2 mL of solution. Distribution coefficients of W determined with the anion exchange resin and ^{181}W tracer prepared by the method described in Ref. 1 were systemically higher than the ones determined by Kronenberg *et al.*,[2)] as shown by Run 1 in Fig. 1. Since trace fluoride ions in the tracer solution were guessed to result in the higher K_d values, the preparation procedure of the ^{181}W tracer was improved to remove fluoride ions sufficiently from the final tracer solution. For Mo radiotracer, ^{93m}Mo ($T_{1/2}$ = 6.85 h), which was produced by the ^{93}Nb(d, 2n) reaction using the AVF cyclotron, was collected with a gas-jet system and dissolved in HCl solution with ^{181}W prepared by the improved method.

Three milliliters of no-carrier-added radiotracer solution in various HCl concentrations and about 50 mg of dried anion ion exchange resin (MCI® GEL CA08Y, 25μm) were shaken together for 30 min in Runs 2 and 3. After centrifugation, 1 mL of solution was subjected to γ-ray spectrometry with a Ge detector.

Distribution coefficients determined in this work for both W and Mo in HCl solution are shown in Figs. 1 and 2, respectively, together with those obtained by Kronenberg *et al.*[1)], who used carrier-added radiotracers (4×10^{-5} to 8×10^{-5} mol/L for W and 4×10^{-5} to 8×10^{-5} mol/L for Mo) and 1X8 anion exchange resin. The K_d values reported in this work and by Kronenberg *et al.* are almost consistent with each other. The ^{181}W tracer solution prepared by the improved method in this work was also confirmed to have a sufficiently low concentration of fluoride ions. Kronenberg *et al.* reported that the K_d value for W in 2 mol/L of HCl solution was the smallest, whereas the smallest K_d values for W were observed in 1 mol/L HCl concentration in this study. For Mo, K_d values in 1 mol/L HCL

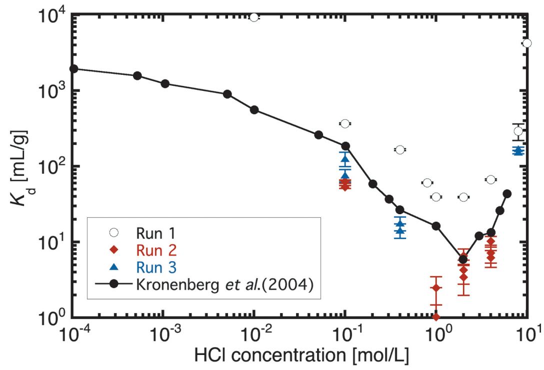

Fig. 1. Distribution coefficients of ^{181}W in HCl solution at room temperature. The radiotracer was prepared by the previous method[1)] in Run 1 and by the improved method in Runs 2 and 3.

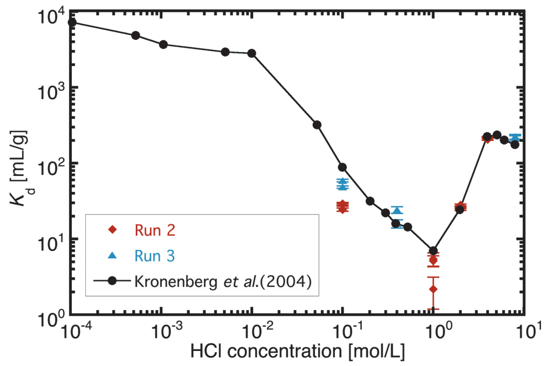

Fig. 2. Distribution coefficients of ^{93m}Mo in HCl solution at room temperature.

were the smallest in both this work and Kronenberg *et al.* Thus, the K_d value of W exhibited a dependency on the concentration of HCl, except for $\geq$ 4 mol/L, in this work is consistent with the dependency of the K_d value of Mo. It was found that for $\geq$ 4 mol/L of HCl concentration, K_d values for Mo were almost constant, whereas those for W seemed to increase with an increasing HCl concentration.

We hope that a suitable experiment for studying Sg chemistry will be performed in the near future and that subsequently, the chemical features of Sg will be revealed.

References

1) A.Wada, *et al.*: RIKEN Accel. Prog. Rep. **45**, 201 (2012).
2) A.Kronenberg *et al.*: Radiochim. Acta **92**, 395 (2004).

Development of an automatic and rapid solid-liquid extraction apparatus for on-line extraction of Rf

A. Kino, Y. Kasamatsu,[*1] K. Toyomura, Y. Komori, T. Yokokita, K. Nakamura, H. Haba,
J. Kanaya, M. Huang, Y. Kudou, T. Yoshimura, N. Takahashi,[*1] and A. Shinohara

The chemical properties of the transactinide elements ($Z \geq 104$) are expected to be characteristic owing to strong relativistic effects in their electronic shells. It is very difficult to perform chemical experiments on these elements because of their short half-lives and low production rates in nuclear reactions. On-line chemical experiments on a “one-atom-at-a-time” basis are required. Thus far, the complex formation with inorganic ligands in aqueous solutions have been investigated mainly for rutherfordium (Rf, $Z = 104$). In many cases, however, the behavior after a few-minute chemical separation was simply observed without confirming equilibration in the chemical reactions.

The purpose of the present study is to clarify the properties in the chloride complex formation of Rf, based on the data in equilibrium and further to investigate the time dependence of the chemical behavior of Rf for the first time. In our previous work, a solid-liquid extraction of Zr and Hf, the homologues of Rf, using triisooctylamine (TIOA) from HCl was performed by batch method. In this work, we developed an automatic apparatus to perform the batch-wise solid-liquid extraction of the transactinide elements rapidly and repeatedly. On-line experiments using this apparatus were conducted with Zr and Hf tracers at the AVF cyclotron in RIKEN. We investigated the equilibrium time of the extraction in several HCl concentrations by determining the time dependence of the K_d values.

A schematic view of the solid-liquid extraction apparatus is shown in Fig. 1. The nuclear reaction products, transported by the gas-jet system, are deposited on the collection site of the dissolution section and then dissolved with an aqueous solution. The solution sample passes through two valves and a slider, which moves horizontally to three positions, and then enters a Teflon reactor containing TIOA resin (reactor 1 in Fig. 1). After shaking the reactor using a vortex mixer, only the liquid phase is pneumatically pushed out of the reactor, and is subjected to the radiation measurement. To measure the radioactivity on the resin, a control experiment without resin is performed using reactor 2 in Fig. 1. The present apparatus is controlled by a computer through the LabVIEW system.

In the on-line experiment, ^{89g,m}Zr ($T_{1/2}$ = 3.27 d, 4.18 min) and ^{175}Hf ($T_{1/2}$ = 70 d) were produced in the ^{89}Y(p, n)^{89g,m}Zr and ^{175}Lu(p, n)^{175}Hf reactions, respectively. The TIOA resin (25–57 wt. % with the weights of 2.6–3.8 mg) and 6–11 M HCl (160–230 μL) containing the Zr and Hf radiotracers, transported by the gas-jet system from the irradiation chamber, were mixed and shaken for 10–120 s by the apparatus. The Zr and Hf remaining on the resin were eluted by washing three times with ca. 220 μL of a mixture of 5.1 M HNO_3 and 0.01 M HF. Subsequently, the resin was conditioned by HCl. The TIOA resin was reused 3–6 times. Each solution sample was assayed by γ-ray spectrometry using a Ge detector to obtain K_d values from the equation K_d (mL/g) = $[M]_{resin}/[M]_{soln}$.

Figure 2 shows the dependence of the K_d values of Zr and Hf on the shaking time using 8.0 M HCl and 31 wt. % TIOA resin. Figure 2 shows that the K_d values are roughly constant in the studied time range, and are consistent with those obtained in our previous batch experiment whereas errors are large. This suggests that the chemical reactions in the extraction reach the equilibrium within 10 s for ^{89m}Zr and ^{175}Hf. Similar results were observed in 7–11 M of HCl.

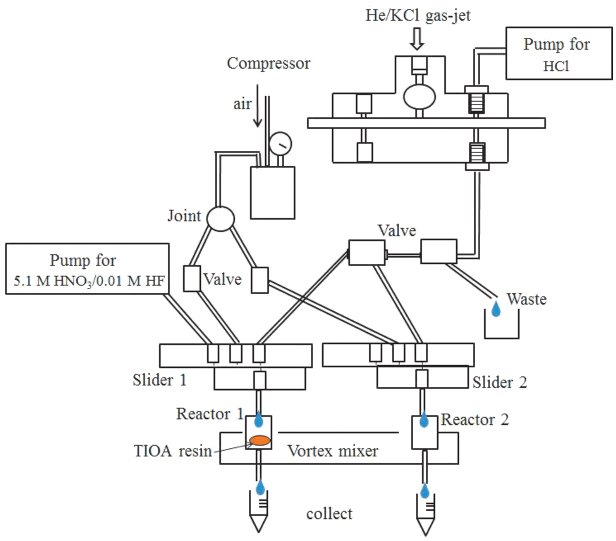

Fig. 1. Schematic view of the solid-liquid extraction apparatus.

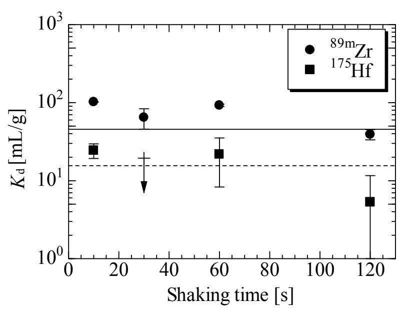

Fig. 2. Variations of the K_d values of ^{89m}Zr and ^{175}Hf with shaking time. The K_d values in equilibrium obtained previously using 7.9 M HCl are drawn by the solid line for Zr and dashed line for Hf.

[*1] Department of Chemistry, Graduate School of Science, Osaka University

Preliminary study on quadrivalent chemical species of rutherfordium in an aqueous solution by using TTA resin

A. Yokoyama, Y. Shigeyoshi, Y. Kitayama, A. Toyoshima,[*1] K. Tsukada,[*1] K. Ooe, E. Maeda, H. Kimura, H. Kikunaga, Y. Kudou, J. Kanaya, M. Huang, and H. Haba

Considerable research interest has been focused on Rutherfordium (Rf) when examining the chemical properties of superheavy elements. For speciation of Rf in an aqueous solution, we aim to observe its chemical behavior by means of reversed-phase chromatography with a chelate extractant of 2-thenoyltrifluoroacetone (TTA) as the stationary phase. Through this method, quadrivalent metal ions are extracted preferentially, unlike in previous studies using cation exchange resins, and hence, a specific complex formation constant of Rf can be determined. [1)]

Prior to the experiments with Rf, batch experiments of Zr and Hf were performed to determine the time required to attain chemical equilibrium on the TTA-resin and the eventual distribution ratios. The resin was brought into contact with ^{88}Zr and ^{175}Hf carrier-free atoms in acid solutions of $9.5\times10^{-5} - 0.10$ M HF/0.1 M HNO_3 and 1×10^{-4} M HF/0.01–0.1M HNO_3 allowed to attain equilibration in a polypropylene tube at room temperature.

An aliquot of the aqueous phase was subjected to γ-ray spectrometry using a Ge detector. Similarly, off-line reversed-phase extraction chromatography of ^{88}Zr and ^{175}Hf was also performed in a teflon tube column (1.6 mmØ) or a micro-column (1.6 mmØ×7 mm) into which the resin was filled. Then on-line reversed-phase extraction chromatography was performed with ^{89m}Zr and ^{175}Hf, which simultaneously produced in the ^{89}Y (*p*, *n*) and ^{175}Lu (*p*, *n*) reactions, respectively, at the RIKEN K70 AVF Cyclotron.

The chemical system for the Rf experiment with ARCA (automated rapid chemistry apparatus) with the micro-columns was connected to the automated rapid α/SF detection system at the AVF cyclotron and subjected to the experiment with ^{85}Zr ^{169}Hf, and ^{261}Rf isotopes produced in the ^{18}O-induced reaction with the targets of ^{nat}Ge, ^{nat}Gd, and ^{248}Cm, respectively.

The batch experiment demonstrated that the best performance in adsorption was obtained for TTA (octanol) resin on Kel-F resin and TTA (octanol) on CHP20/P20 resin. The equilibration was attained in less than 1 min. Besides, it was found that the results with TTA resin agree with the behavior of solvent extraction for Zr and Hf at lower acid concentrations in the results as well as those in previous report[1)].

Figure 1 shows an example of the obtained elution curves for the online experiment of TTA on CHP20/P20 resin with a ^{89m}Zr tracer. The tracer atoms are adsorbed on the resin although equilibration of the system is not observed, owing to the deviation from the behavior expected by the batch data.

Furthermore, we have succeeded in obtaining a preliminary α-spectrum of Rf nuclides transferred through a gas-jet system and passing through the ARCA system. The test run prior to the Rf experiment demonstrated a gas-jet efficiency of around 70%, dissolution efficiency of 49 %, and 36 % efficiency of detecting α particles. This indicated around 30 counts for 100 runs, but only 13 counts were observed for the actual experiment.

In conclusion, reversed-phase chromatography with TTA resin can be used for speciation of a Rf chemical species, although the resin preparation needs further improvement to optimize the experimental conditions for Rf.

Thus far, we have succeeded in obtaining a preliminary α-spectrum of Rf atoms transferred through a gas-jet system and passing through the ARCA system although an increase in Rf atoms introduced to the system could be expected.

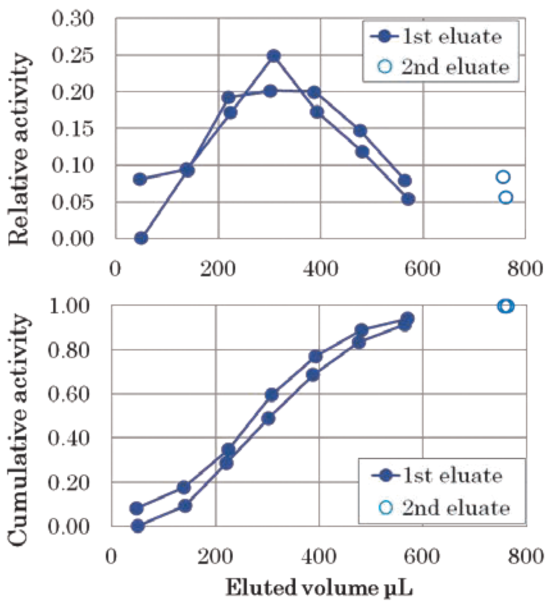

Fig. 1. An example of elution curve of Zr on the TTA resin. The conditions were 1.0×10^{-4} M in [HF], 0.01M in [HNO_3], and 0.1mL/min in flow rate.

Reference

1) M. Araki, T. Nanri., Y. Takeda, M. Nishio, M. Nishikawa, Y. Kasamatsu, Y. Ezaki, Y. Kudou, H. Haba, and A. Yokoyama: RIKEN Accel. Prog. Rep. **43**, 271 (2010).

*1 Japan Atomic Energy Agency

Extraction behavior of homologues of Rf into Tri-n-octylamine from HF/HNO_3 system

S. Sodaye,*[1] H. Haba, J. Kanaya, and M. Huang

Transactinide elements, also called superheavy elements (SHE) with atomic number $Z \geq 104$ are produced in heavy ion induced nuclear reactions at accelerators with low production rates. The low production rates and short-lived nature of these isotopes lead to a "one-atom-at-a-time" situation for chemical separation processes. Owing to the relativistic effects, the chemical properties of these SHEs deviate from those expected from simple extrapolations of the properties of their lighter homologues within the same group. Limited to the short-lived nature and low production rates, the experimental investigation to explore the chemical properties of these elements and to investigate the influence of the relativistic effects to electron shell still remains a challenge.

The search for a suitable chemical system to achieve fast and efficient separation of these elements still remains an open area of investigation. The first step in these studies is to choose a chemical system and study the chemistry of the lighter homologues of the SHE. Once found suitable for the lighter homologues, the system is tested for the rapid separation of the SHE.

^{104}Rf, the first transactinide element, is located in group 4 of the periodic table. Many systems have been studied for the aqueous chemistry of Rf and its homologues[1),2)]. Complex formation of Rf, with chloride, fluoride, nitrate, and sulfate in aqueous solutions has been studied[3)-8)] using ion exchange and solvent extraction methods.

With the objective to study the uptake of lighter homologues of Rf in tri-n-octylamine (TOA) from HNO_3/HF mixture, multitracers were produced by bombarding a ^{197}Au target with a 135 MeV/nucl. ^{14}N beam from the RIKEN Ring Cyclotron. After cooling the sample for a sufficiently long time, the target material was separated from the multitracers by solvent extraction with ethyl acetate. The multitracer solution was then brought into 0.1 M HNO_3/1×10^{-4} M HF system. For the solvent extraction experiments, the organic phase was fixed as 10% TOA solution in toluene and the aqueous phase was taken as 0.1 M HNO_3 mixed with varying HF concentration (from 0.1 M to 10^{-6} M).

For solvent extraction, the volume of the organic and aqueous phase was kept as 2 mL. After 30 minutes of equilibration at 20 ^{o}C, the samples were centrifuged to separate the two phases. After centrifugation, we took 1 mL aliquots of both phases and subjected them to gamma-ray spectrometry using HPGe detectors.

In this work, the radioactivity of the isotopes of various elements was seen in the organic phase, indicating complexation of those elements with the TOA. The distribution ratios (D) of ^{88}Zr and ^{175}Hf, which are lighter homologues of Rf, and those of ^{188}Pt are presented in Fig. 1 as a function of the HF concentration ([HF]) in the aqueous phase.

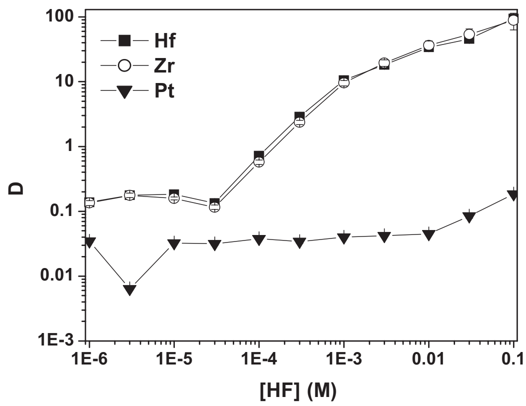

Fig. 1. Distribution ratios of ^{88}Zr, ^{175}Hf, and ^{188}Pt in the organic phase containing 10% tri-n-octylamine in toluene as a function of concentration of HF ([HF]) in the aqueous phase (0.1M HNO_3).

The results clearly show that the uptake of the lighter homologues of Rf increases with increasing HF concentration beyond 3×10^{-5} M, reflecting the formation of anionic fluoride complexes[6),7)]. At very low concentrations of HF, the uptake is nearly constant until [HF]= 3×10^{-5} M indicating that the F^- concentration was too low for the formation of strong anionic fluoride complexes. The uptake behavior of both Zr and Hf is very similar under the given condition. In addition, it can be seen from the figure that the noble metals such as Pt are poorly extracted in the organic phase and their uptake doesn't change much with the variation of the HF concentration in the organic phase. This indicates that the Pt group elements do not form anionic fluoride complexes under the given conditions.

References

1) J.V. Kratz: Radiochim. Acta **99**, 477 (2011).
2) Y. Nagame and H. Haba: *Production and Chemistry of Transactinide Elements* in *Radiochemistry and Nuclear Chemistry*, edited by S. Nagy, in *Encyclopedia of Life Support Systems (EOLSS),* Eolss Publishers, Oxford, UK, 2007.
3) H. Haba et al.: J. Nucl. Radiochem. Sci. **3**, 143 (2002).
4) H. Haba et al.: J. Am. Chem. Soc. **126**, 5219 (2004).
5) A. Toyoshima et al.: J. Nucl. Radiochem. Sci. **5**, 45 (2004).
6) A. Toyoshima et al.: Radiochim. Acta **96**, 125 (2008).
7) Y. Ishii et al.: Chem. Lett. **37**, 288 (2008).
8) Z.J. Li et al.: Radiochim. Acta **100**, 157 (2012).

*1 Radiochemistry Division, Bhabha Atomic Research Centre, Mumbai, India

Production of ^{88}Nb and ^{170}Ta for chemical studies of element 105

M. Huang, M. Asai,[*1] H. Haba, D. Kaji, J. Kanaya, Y. Kasamatsu,[*2] H. Kikunaga, Y. Kikutani,[*2] Y. Komori, H. Kudo,[*3] Y. Kudou, K. Morimoto, K. Morita, M. Murakami, K. Nakamura, K. Ozeki, R. Sakai, A. Shinohara, T. Sumita, K. Tanaka, A. Toyoshima,[*1] Y. Wakabayashi, and A. Yoneda

We plan to study the chemical properties of element 105, Db, which is produced in the ^{248}Cm(^{19}F,5n)^{262}Db reaction, using the gas-jet transport system coupled to the RIKEN GAs-filled Recoil Separator (GARIS) [1]. It is important to perform Db chemistry together with Ta and Nb under identical conditions to identify different chemical behavior among the homologues. In this work, we optimized the separation conditions of the isotopes of ^{170}Ta ($T_{1/2}$=6.76 min) and ^{88}Nb ($T_{1/2}$=14.55 min) produced in the ^{nat}Gd(^{19}F, xn)^{170}Ta and ^{nat}Ge(^{19}F, xn)^{88}Nb reactions, respectively, using the GARIS gas-jet system, as a preparatory step for the chemical studies.

A 106.4-MeV ^{19}F^{9+} beam was extracted from the RILAC. A ^{nat}Ge target of 0.29 mg/cm^2 thickness was prepared by vacuum evaporation on a 0.89 mg/cm^2 Ti backing foil, whereas a ^{nat}Gd$_2$O$_3$ target of 0.34 mg/cm^2 was prepared by electrodeposition on a 0.87 mg/cm^2 Ti. The two arc-shaped Ge and two Gd$_2$O$_3$ targets were mounted together with four 0.95 mg/cm^2 Ti blank foils on a rotating wheel having a 100-mm diameter, which was rotated at 1000 rpm. The beam energy was 103 MeV in the middle of the target and the typical intensity was approximately 3 particle μA (pμA). The working He pressure of GARIS was 33 Pa. At the focal plane of GARIS, a recoil transfer chamber (RTC) of 100-mm inner diameter and 100-mm depth was installed. The evaporation residues separated with GARIS were passed through a 0.5-μm Mylar window, and were transported by the He/KCl-aerosol-gas-jet system to a chemistry laboratory. The flow rate of the He gas was 2.0 L/min, and the inner pressure of the RTC was 47 kPa. After collection of the aerosols on a glass filter (ADVANTEC GB-100R) for 1 and 3 min for ^{170}Ta and ^{88}Nb, respectively, the filters were subjected to γ-ray spectrometry using a Ge detector. The magnetic setting of GARIS was varied in the magnetic rigidity (Bρ) range of 1.51–1.80 Tm for ^{170}Ta and 0.850–0.979 Tm for ^{88}Nb. In the GARIS separation of ^{88}Nb at low Bρ values, the beam particles with lower charge states broke the thin Mylar foil of the RTC. Thus, we installed a retractable Al shutter of 2-mm thickness and 30×100-mm^2 size at the focal plane to block the undesired beam particles. Furthermore, a 3-μm Al degrader was used to reduce the recoil range of ^{88}Nb before its entrance into the RTC.

Figures 1a and 1b show the γ-ray spectra observed for ^{170}Ta at 1.64 Tm and ^{88}Nb at 0.936 Tm, respectively. The desired peaks of ^{170}Ta and ^{88}Nb are clearly observed, as indicated in the figure. By following their decay curves, we confirmed that the 221.2-keV and 671.2-keV γ-rays are useful for performing the chemical studies of ^{170}Ta and ^{88}Nb, respectively.

Yield distributions of ^{170}Ta and ^{88}Nb related to Bρ are displayed in Fig. 2. The optimal Bρ of 1.64±0.01 and 0.936±0.001 Tm were determined for ^{170}Ta and ^{88}Nb, respectively. Under these experimental conditions, the production yields of ^{170}Ta and ^{88}Nb in the chemistry laboratory were evaluated to be 8.65±0.56 and 0.61±0.02 kBq/pμA after 1-min and 3-min long aerosol collection tasks, respectively. In this work, the gas-jet efficiency of ^{88}Nb was found to be 41±2%, while that of ^{170}Ta was 77±3%. Because the gas-jet efficiencies are very sensitive to the recoil ranges of the evaporation residues in RTC, we plan to optimize them during the next beam time by selecting suitable degraders.

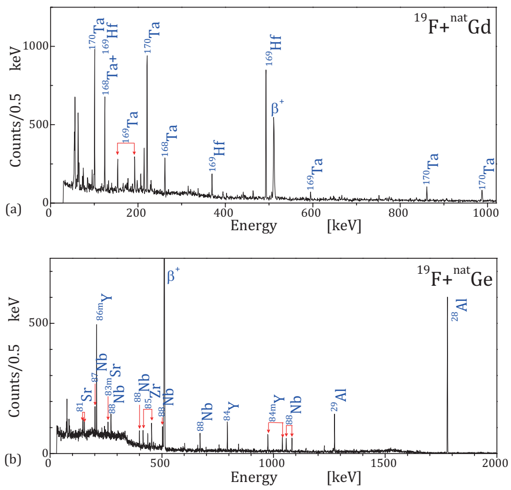

Fig. 1. γ-ray spectra obtained for (a) ^{170}Ta and (b) ^{88}Nb, respectively.

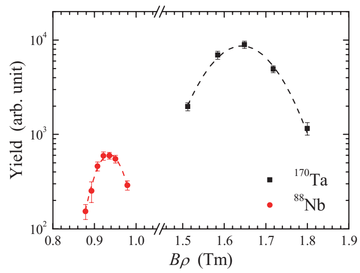

Fig. 2. Yields of ^{170}Ta and ^{88}Nb as a function of Bρ.

[*1] Advanced Science Research Center, JAEA
[*2] Graduate School of Science, Osaka University
[*3] Department of Chemistry, Niigata University

References

1) H. Haba et al.: Chem. Lett. **38**, 426 (2009).

Liquid scintillation measurement of ^{262}Db produced in ^{248}Cm(^{19}F,5n)^{262}Db reaction and pre-separated using GARIS gas-jet system

Y. Komori, K. Nakamura, M. Murakami, Y. Kasamatsu, H. Kikunaga, H. Haba, J. Kanaya, M. Huang, Y. Kudou, and A. Shinohara

In chemical experiments of the transactinide elements with atomic numbers Z ≥ 104, an automated and rapid chemistry apparatus coupled to an α-particle and spontaneous fission (SF) detection system is required. We have developed an online liquid scintillation detection system to detect α particles and fission fragments in solution samples eluted from the chemistry apparatus. To detect the α and SF events originating from the transactinide elements by liquid scintillation, a low-background condition is necessary due to problems such as relatively poor energy resolution and interference from β particles and γ rays. We are planning to remove radioactive by-products using the GARIS gas-jet system[1,2] to attain the low-background condition required for liquid scintillation measurement. In this work, we performed online liquid scintillation measurements of pre-separated ^{262}Db ($T_{1/2}$ = 34 s) with the GARIS gas-jet system to investigate the background count rate for the detection of time-correlated α–α events from ^{262}Db and the daughter nuclide ^{258}Lr ($T_{1/2}$ = 3.8 s).

The isotope ^{262}Db was produced in the ^{248}Cm(^{19}F, 5*n*)^{262}Db reaction.[3] The $^{19}F^{9+}$ ion beam was extracted from RILAC. The beam energy was 103 MeV at the middle of the $^{248}Cm_2O_3$ target. The average beam intensity was 2.6 pμA. The reaction products pre-separated with GARIS were attached to KCl aerosols and then transported through a Teflon capillary to a chemistry laboratory by the gas-jet system.

For the liquid scintillation measurements, the reaction products pre-separated and transported by the GARIS gas-jet system were deposited for 70 s on the collection site of a liquid chromatographic system, the ARCA.[4] The collected products were then dissolved in 0.1 M HNO_3/5 × 10^{-3} M HF mixed solution and the solution was transferred to a glass cell set in the detection chamber at a flow rate of 1 mL/min for 12 s. The solution was mixed with 4 mL of an emulsifier scintillation cocktail, Ultima Gold AB®, and subsequently, the liquid scintillation measurement was performed for 109 s. The measurement of the reaction products was started approximately 15 s after the end of collection. After the measurement, the solution in the cell was drained and 4 mL of Ultima Gold AB® was newly injected into the cell for the next measurement. Each measurement was performed alternately with two detection chambers. These procedures were automatically repeated. Energy calibration of the detectors was performed by using ^{226}Ra and ^{252}Cf as α and SF sources, respectively. The energy resolution of the detectors was approximately 580-keV FWHM for the 7.687-MeV α-peak of ^{214}Po. To evaluate the background count rate due to fast neutrons and γ rays generated by beam irradiation, blank samples were measured under the beam-on and beam-off conditions. The blank sample was prepared by mixing 200 μL of 0.1 M HNO_3/5 × 10^{-3} M HF solution with 4 mL of Ultima Gold AB®. The detection chambers were shielded with polyethylene blocks against fast neutrons that are observable in the α-event region. For data acquisition, a four-channel pulse shape discrimination module, the MPD-4, was used to discriminate α/β events and SF/β events. Both the amplitude (energy) and the time-to-amplitude converter (TAC) outputs of the MPD-4 were recorded with the A3100 via the list mode for two-dimensional analysis of TAC versus energy.

The count rates in the α- and β-event regions in the α-energy range of 7.5–9.7 MeV and those in the SF-event region are listed in Table 1. The count rates under the beam-on condition are larger than those under the beam off condition due to fast neutrons and γ rays. The count rates in the measurement of the reaction products are comparable to those of the blank samples under the beam-on condition, thereby indicating that α-, β-, and γ-emitting by-products were suppressed by the GARIS gas-jet system. In this experiment, time-correlated α–α events from ^{262}Db and ^{258}Lr, which were expected to be observed 1.5 correlations, were not observed. This is acceptable considering statistical fluctuations.

Table 1. Count rates in the α- and β-event regions in the α-energy range of 7.5–9.7 MeV and those in the SF-event region.

Sample	Beam	Count rate in α-event region [10^{-3} cps]	Count rate in β-event region [cps]	Count rate in SF-event region [10^{-3}cps]
Blank	off	0.10 ± 0.02	0.045 ± 0.001	0.011 ± 0.006
Blank	on	1.2 ± 0.1	0.40 ± 0.01	0.40 ± 0.04
Reaction products	on	1.2 ± 0.2	0.38 ± 0.01	0.46 ± 0.11

References

1) H. Haba et al.: Chem. Lett. **38**, 426 (2009).
2) H. Haba et al.: Phys. Rev. C **85**, 024611 (2012).
3) H. Haba et al.: submitted to RIKEN Accel. Prog. Rep. **46**.
4) M. Schädel et al.: Radiochim. Acta **48**, 171 (1989).

Production cross sections of (d,x) reactions on natural titanium†

M. U. Khandaker, H. Haba, J. Kanaya, and N. Otsuka

The method to obtain accurate knowledge of light charged particle-induced reaction cross sections has generated significant interest in nuclear data community because these reactions are being increasingly used in nuclear medicine, accelerator and nuclear technology, and the testing of nuclear reaction theories. Recently, we investigated the production cross sections of deuteron-induced radionuclides from various target elements, because the measured data of the (d,x) processes for different elements are scanty, relative to those of (p,x) processes. A general survey of previous reports shows that several investigations were carried out for the ^{nat}Ti(d,x) reactions, which led to the development of various applications. The formation of the ^{48}V radionuclide via the ^{nat}Ti(d,x) nuclear reactions can be advantageously utilized for the monitoring of deuteron beam parameters from the threshold to 50 MeV owing to its good physiochemical properties and large cross sections[1]. The International Atomic Energy Agency (IAEA) has already compiled and provided a set of recommended data[2] for some important monitor reactions including the ^{nat}Ti(d,x)^{48}V reactions. Moreover, ^{48}V is frequently used in nuclear medicine and for checking the sealing capability of used fuel storage tanks in nuclear power plants. ^{nat}Ti(d,x)^{48}V reactions also find applications in wear measurements of titanium-containing materials. ^{48}V is a well-known radiotracer in many research fields, ranging from biology to material sciences[3]. An accurate determination of the production cross sections for the ^{nat}Ti(d,x)^{48}V nuclear reactions, is therefore required, because it is of great importance in various practical applications, especially in nuclear medicine.

The objective of the present study was to validate the IAEA recommended cross sections of the ^{nat}Ti(p,x)^{48}V monitor reaction, and to report new cross sections for the ^{nat}Ti(d,x)^{43,44m,44g,46,47,48}Sc reactions with a high precision over the energy range of 2–24 MeV using the AVF cyclotron facility of the RIKEN RI Beam Factory, Wako, Japan. Details on the irradiation technique, the radioactivity determination, and the data evaluation procedures are available in Ref.[4]. A brief description of the used model codes that are relevant to this work is also available elsewhere[4]. Due to the space limitation of this report, only the ^{nat}Ti(d,x)^{48}V cross sections and the deduced yield have been presented in Figs. 1 and 2, respectively. Measured cross sections with an overall uncertainty of about 11% are available in Ref. [4] The shape of the IAEA recommended monitor cross sections for the ^{nat}Ti(d,x)^{48}V reaction was verified. It was found that the TALYS code could not reproduce the measured excitation functions properly. The present results would be considerably useful to probe and improve the predicting capabilities of the code.

† Condensed from the article in Nucl. Inst. Meths. B. **296**, 14 (2013).

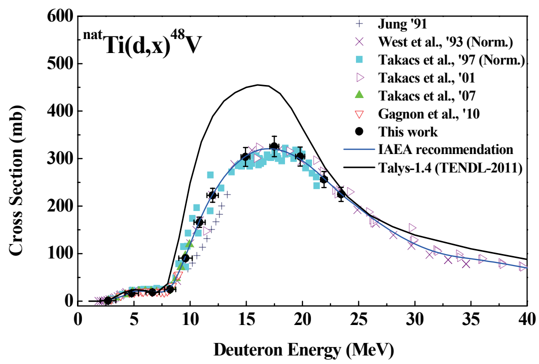

Fig. 1. Excitation function of the ^{nat}Ti(d,x)^{48}V reaction.

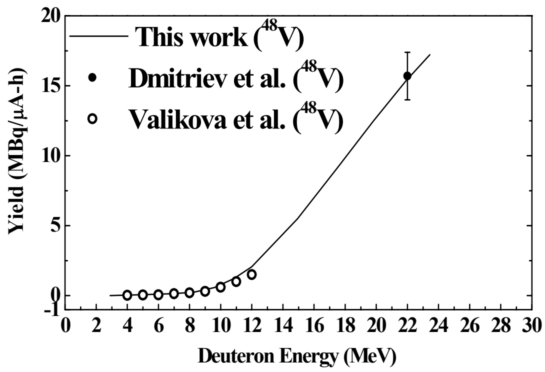

Fig. 2. Physical thick target yields for the ^{48}V radionuclide.

References

1) S. Takács, B. Király, F. Tárkányi and A. Hermanne: Nucl. Instrum. Methods Phys. Res. B **262**, 7 (2007).
2) S. M. Qaim, F. Tárkányi, P. Obložinský, K. Gul, A. Hermanne, M. G. Mustafa, F. M. Nortier, B. Scholten, Yu. Shubin, S. Takács, Y. Zhuang: Charged Particle Cross-Section Database for Medical Radioisotope Production: Diagnostic Radioisotopes and Monitor Reactions, IAEA-TECDOC-1211, Vienna, 2001. Data updated in January 2007 Available from: <http://www-nds.iaea.org/ medical/>.
3) J. M. L. Ouellet, K. Oxorn, L. A. Hamel, L. Lessard and C. Matte: Nucl. Instrum. Methods Phys. Res. B **79,** 579 (1993).
4) M. U. Khandaker, H. Haba, J. Kanaya and N. Otuka: Nucl. Instrum. Methods Phys. Res. B **296,** 14 (2013).

Excitation functions of Nb and Ta radioisotopes produced in ^{nat}Zr(p,x) and ^{nat}Hf(p,x) reactions up to 14 MeV

M. Murakami, H. Haba, J. Kanaya, S. Goto,[*1] and H. Kudo,[*1]

To perform chemical experiments of superheavy elements (SHE) effectively, the optimal conditions for the on-line experiments with SHE should be predetermined by off-line experiments using the homologues of interesting elements. Because SHE experiments are fundamentally performed on a single atom scale, carrier free radiotracers are desirable in off-line experiments. For the off-line experiment of element 105, Db, ^{95g}Nb ($T_{1/2}$ = 34.991 d) and ^{179}Ta ($T_{1/2}$ = 1.82 y) radiotracers are suitable. In this work, excitation functions of the ^{nat}Zr(p,x) and ^{nat}Hf(p,x) reactions were measured to determine the optimal conditions for the production of ^{95g}Nb and ^{179}Ta.

The excitation functions were measured using a stacked-foil technique. For the production of Nb isotopes, thin foils of natural Zr (20 μm thickness) and natural Cu (25 μm thickness) were stacked alternately and used as a target. The Cu foils were used to monitor both the beam current and beam energy. For the production of Ta isotopes, thin foils of natural Hf (25 μm thickness) and natural Cu (10 μm thickness) were stacked alternately. The size of all foils was 15 × 15 mm^2. Ten Zr foils and ten Cu foils were used in the Zr/Cu stack, whereas twelve Hf foils and twelve Cu foils were used in the Hf/Cu stack. The Zr/Cu and Hf/Cu stack were each irradiated by the 14.3-MeV proton beam supplied by the RIKEN AVF cyclotron for 30 min. The average beam currents were 0.53 μA for the Zr/Cu stack and 0.80 μA for the Hf/Cu stack. The proton energies in the individual target foils were calculated based on the stopping power formula[1]. After irradiation and proper cooling, γ- and X-ray measurements of each foil were obtained using Ge detectors.

The production cross sections were calculated by a well-known activation formula[2]. Nuclear data of the isotopes used in the calculation were taken from the NuDat 2.6 database[3]. A theoretical calculation was performed using the TALYS-1.4 code[4] to compare with the experimental results.

In this work, the production cross sections of ^{90g,91m,92m,95m,95g,96}Nb in the ^{nat}Zr(p,x) reaction and ^{175,176,177,178,179}Ta in the ^{nat}Hf(p,x) reaction were measured. Note that the independent cross section of ^{95m}Nb ($T_{1/2}$ = 3.61 d) was measured in addition to that of ^{95g}Nb. The maximum cross sections in the studied energy range were 8.5 ± 0.4 mb for ^{95m}Nb and 18.7 ± 0.8 mb for ^{95g}Nb, which were observed at 14.2 ± 0.1 MeV. The cross section ratio, $\sigma(^{95g}\mathrm{Nb})/\sigma(^{95m}\mathrm{Nb})$ was in the range of 1.3–2.2 and increased with the incident energy. Figure 1(a) shows the total cross section of ^{95m}Nb and ^{95g}Nb together with the data[5,6], which are available in the EXFOR database[7]. The measured cross sections of $^{95m+g}$Nb agree with those obtained by Levkovskij from the ^{96}Zr(p,$2n$) reaction[5], whereas they are lower than those given by Michel et al. from the ^{nat}Zr(p,x) reaction[6]. The measured cross sections of ^{179}Ta are reported for the first time and shown in Fig. 1(b). The maximum value was 304 ± 18 mb at 14.1 ± 0.2 MeV. In Fig. 1(b), predictions given by the TALYS code reproduce the measured data of $^{95m+g}$Nb and ^{179}Ta with relatively good accuracy.

Based on the cross sections measured in this work, thick target yields of ^{95m}Nb, ^{95g}Nb, and ^{179}Ta produced by the 14.3-MeV proton beam were 5.7 × 10^{-1}, 1.1 × 10^{-1}, and 4.6 × 10^{-2} MBq/(μA·h), respectively.

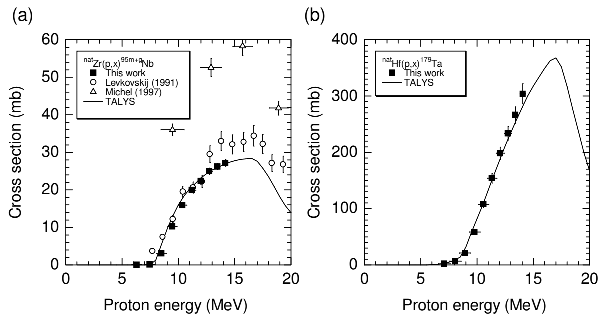

Fig. 1. Excitation functions of (a) ^{nat}Zr(p,x)$^{95m+g}$Nb reaction and (b) ^{nat}Hf(p,x)^{179}Ta reaction.

References
1) J. F. Ziegler et al.: *The Stopping and Range of Ions in Solids, Volume 1 of the Stopping and Ranges of Ions in Matter* (Pergamon Press, 1985).
2) M. S. Uddin et al.: Nucl. Instrum. Methods Phys. Res. B **258**, 313 (2007).
3) NuDat 2.6: http://www.nndc.bnl.gov/nudat2/.
4) A. J. Koning et al.: in *Proceedings of the International Conference on Nuclear Data for Science and Technology*, edited by O. Bersillon et al. (EDP Sciences, 2008), p. 211.
5) V. N. Levkovskij: *Activation Cross Section Nuclides of Average Masses (A = 40–100) by Protons and Alpha-Particles with Average Energies (E = 10–50 MeV)* (Moscow, 1991).
6) R. Michel et al.: Nucl. Instrum. Methods Phys. Res. B **129**, 153 (1997).
7) EXFOR: http://www.nndc.bnl.gov/exfor/exfor00.htm.

Optimizing production and purification method of zirconium-89 for medical use

A. Fukubayashi,[*1] F. Takenaka,[*1] T. Sasaki,[*1] T. Fukuchi,[*2] E. Matsuura,[*1] S. Kamino,[*2] H. Haba, and S. Enomoto[*1,*2]

Immuno-positron emission tomography (PET), which involves tracking and quantification of radiolabeled antibodies with PET *in vivo* imaging, is one of the advanced technologies used for characterizing, treatment planning, and treatment monitoring of cancer. Since antibody-based imaging agents have slow blood clearance, requiring multiple days to reach their optimal biodistribution, relatively long-lived positron emitters have been often employed as substituted. In the recent years, ^{89}Zr ($T_{1/2}$ = 78.4 h) has been a subject of focus in the field of nuclear medicine, because it has the physical and chemical properties that are suitable for immuno-PET.[1)] In order to perform efficient antibody radiolabeling and quantitative PET imaging with ^{89}Zr, the impurities, including the target material, should be removed. In the present study, we investigated production and purification procedures suitable for getting carrier-free ^{89}Zr for medical applications.

Zirconium-89 was produced by the (*p,n*) and (*d,2n*) reactions of yttrium foils with dimensions of 15 mm × 15 mm (chemical purity: 99.9%; natural abundance: ^{89}Y (100%); thickness: 0.127 mm) with 12.2-MeV proton, and 24-MeV deuteron beams supplied from the RIKEN AVF cyclotron. After the irradiations, 0.3–1 MBq of ^{89}Zr was chemically isolated from the ^{89}Y target using an anion-exchange and a hydroxamate column chromatography. First, the irradiated ^{89}Y target was dissolved in conc. HCl in the presence of H_2O_2 for the anion-exchange column chromatography. Zirmonium-89 was separated by conc. HCl through the anion-exchange column (Dowex1X8, 200–400 mesh; ø5 mm × 50-mm height). The hydroxamate resin was prepared from the reaction of the $-CO_2^-Na^+$ from a silica-based cation exchange resin with hydroxylamine hydrochloride, according to the previous report.[2)] For the hydroxamate column chromatography, the irradiated target was dissolved in 6 mol・L^{-1} HCl containing H_2O_2, and was then diluted with water to ensure the final concentration of 2 mol・L^{-1} HCl. After the ^{89}Zr adsorbed onto the hydroxamate column (ø5 mm × 50-mm height), the column was washed with 2 mol・L^{-1} HCl and water to remove ^{89}Y and other impurities. ^{89}Zr was finally separated with 1 mol・L^{-1} oxalic acid. The radioactivity in each fraction was measured with a Ge detector.

The γ-ray spectra of the ^{89}Y targets irradiated with the proton and deuteron beams are shown in Figs. 1A and 1B, respectively. The radioactive impurities of ^{88}Zr ($T_{1/2}$ = 83.4 d) and ^{88}Y ($T_{1/2}$ = 106.7 d) were observed in the target irradiated with a 24-MeV deuteron beam, while no radioactive impurity was observed in the case of proton irradiation. The chemical procedures for the separation of ^{89}Zr from ^{89}Y and other impurities were investigated using both anion-exchange column and hydroxamate column chromatography. With the anion-exchange column, the ^{89}Zr recovery was only 13%, which was less than in other studies performed on a larger scale.[3)] This was presumably because the trace amount of ^{89}Zr formed a radiocolloid without strong complexing reagents and showed an unexpected ion-exchange behavior. In contrast, when using the hydroxamate column, ^{89}Zr was recovered with a high radiochemical yield of > 95%. There was no detectable amount of ^{88}Y in the resultant ^{89}Zr solution (Fig. 1C), indicating that the target material was also efficiently removed from the Zr fraction.

The present study suggests that the production and purification of ^{89}Zr should be conducted with the proton beam and the hydroxamate column to avoid any contamination from ^{88}Zr and ^{88}Y, and to separate ^{89}Zr from the ^{89}Y target with high radiochemical yield, respectively. Furthermore, ^{89}Zr was produced with a yield of 12.7 MBq・μA^{-1}・h^{-1} by the irradiation of the 12.2-MeV proton beam, indicating that ^{89}Zr could be produced by using a small cyclotron in a regional hospital or pharmacy.

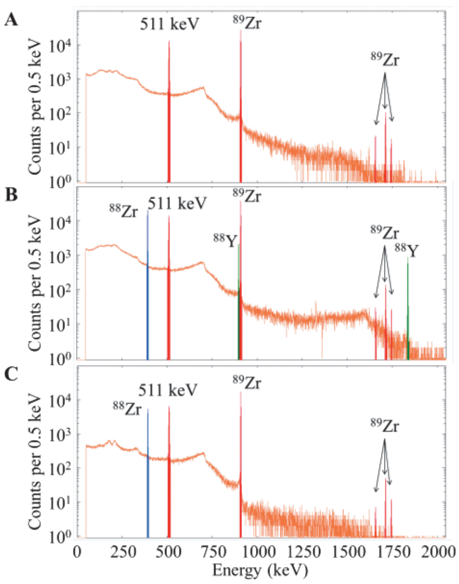

Fig. 1. Gamma-ray spectra of the solution of the ^{89}Y targets irradiated with the 12.2-MeV proton beam without any separation (A), and the deuteron beam without (B) and with (C) separation by hydroxamate column chromatography.

References

1) M. A. Deri et al.: Nucl. Med. Biol. **40**, 3 (2013).
2) J. P. Holland et al.: Nucl. Med. Biol. **36**, 729 (2009).
3) W. E. Meijis et al.: Appl. Radiat. Isotopes. **45**, 1143 (1994).

*1 Graduate school of Medicine, Dentistry, and Pharmaceutical Sciences, Okayama University
*2 RIKEN Center for Life Science Technologies

Production of ^{124}I radiotracer for positron emission tomography

T. Hanada,[*1] T. Fukuchi,[*2] S. Kamino,[*2] H. Haba, J. Kanaya, A. Shinohara, N. Takahashi,[*3] Y. Watanabe,[*2] and S. Enomoto[*1, 2]

Positron emission tomography (PET) has been widely used in nuclear medicine as a molecular imaging modality. Because PET utilizes the pairs of 511-keV γ rays produced by the annihilation of electron-positron pair, the probe used in PET imaging is a compound labeled by positron-emitting radioisotopes (e.g., ^{11}C, ^{18}F, and ^{64}Cu). Positron emitters generally used for PET imaging have relatively short half-lives (less than a few hours). Owing to their short half-life, the cyclotron needs to be nearby and prompt handling is required. On the other hand, PET imaging using antibodies usually needs a long time for biodistribution. Accordingly, a positron emitter ^{124}I, which has a relatively long half-life of 4.2 days, is useful for this kind of PET imaging[1]. Furthermore, the well-established chemistry of iodine helps the production of various PET radiotracers. We have attempted the production of ^{124}I as a PET tracer and evaluated its performance using the Planar Positron Imaging System (PPIS)[2] manufactured by Hamamatsu Photonics K.K.

The isotope ^{124}I was produced by the ^{124}Te(d,2n)^{124}I nuclear reaction using a 24 MeV deuteron beam delivered from the RIKEN AVF cyclotron. The production target was prepared by compressing 144.5 mg $^{124}TeO_2$ (isotopic purity of ^{124}Te: 99.9%) and 24.9 mg KCl into an 8 mm diameter pellet. The pellet was covered with 6 μm Al foil. The average deuteron-beam intensity was 3.3 μA, and the irradiation time was 3.25 hours. To separate the ^{124}I from the target material, we followed the procedure shown in Fig. 1. The irradiated target pellet was removed from the Al foil, and 2 mol/L NaOH was added to dissolve the target. Six mol/L H_2SO_4 and 0.1 mol/L KI were added to precipitate the TeO_2. After a centrifugation, the I^- in the supernatant was oxidized by 30% H_2O_2. Then, the I_2 was extracted with CCl_4, and the aqueous layer was discarded. Two mol/L NaOH was added into the organic layer for the back extraction of the ^{124}I. Finally, the ^{124}I-containing inorganic layer was neutralized by 2 mol/L HCl. The recovery of the ^{124}I in the final product was 54%. The γ-ray spectrum of the final purified product shown in Fig. 2 indicates the existence of contamination by ^{123}I. However, because of its shorter half-life ($T_{1/2}$ = 13.2 hours) and positron-less decay character, the PET imaging is not affected by this contamination.

In order to perform PET imaging, we transported the ^{124}I to the RIKEN Kobe institute. Then, the ^{124}I solution was diluted in isotonic saline, and 1.2 MBq of ^{124}I were administered to male Jcl:ICR mice (11 w.o.) under isoflurane anesthesia by intravenous injection. The ^{124}I imaging data were obtained within 1.5 hours by the PPIS. The imaging shown in Fig. 3 reveals specific accumulations of iodine in the thyroid, stomach, and bladder. Thus, we succeeded to produce ^{124}I as a PET radionuclide. We will develop ^{124}I-labeled compounds for further PET imaging.

This work was supported by the Japan Society for the Promotion of Science (JSPS) Grants-in-Aid for Scientific Research (KAKENHI) through Grant Number 22611018.

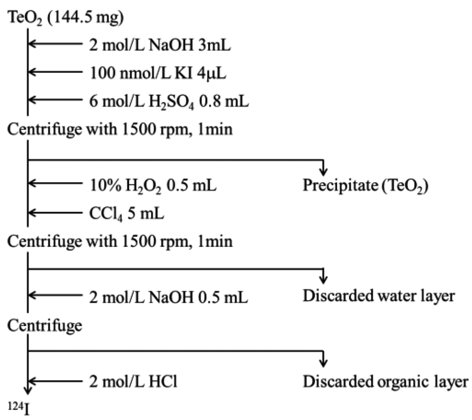

Fig. 1. Chemical separation procedure of ^{124}I from the TeO_2 target.

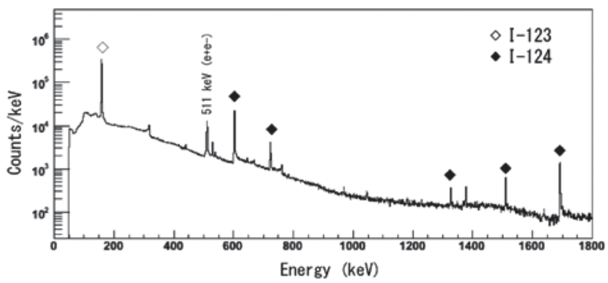

Fig. 2. γ-ray spectrum of the final product.

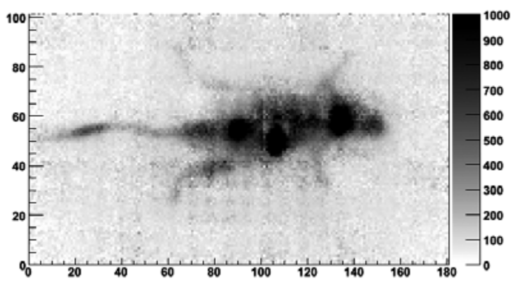

Fig. 3. The ^{124}I distribution image.

References
1) L. Koehler et al.: Molecules, **15**, 2686 (2010).
2) H. Uchida et al.: Nucl. Inst. and Meth., **A516,** 564 (2004).

*1 Department of Pharmaceutical Analytical Chemistry, Graduate School of Medicine, Dentistry, and Pharmaceutical Sciences, Okayama University
*2 Center for Molecular Imaging Science, RIKEN

Production of ^{65}Zn and ^{109}Cd using deuteron beam

J. Kanaya, H. Haba, M. Huang, M. Murakami, S. Shibata, Y. Wakitani, and S. Yamamoto

Since October 2007, we have distributed solutions of purified radioisotopes of ^{65}Zn and ^{109}Cd to the general public in collaboration with Japan Radioisotope Association.[1)] ^{65}Zn and ^{109}Cd have been produced through ^{65}Cu(p,n)^{65}Zn and ^{109}Ag(p,n)^{109}Cd reactions, respectively, using a 14-MeV proton beam delivered from the RIKEN AVF cyclotron. The typical intensity of the proton beam has been about 20 μA. Under our experimental conditions, the production yields of ^{65}Zn and ^{109}Cd have been 0.24 and 0.076 MBq μA^{-1} h^{-1}, respectively.[2)] In the literature survey on reaction cross sections for ^{65}Zn and ^{109}Cd,[3,4)] higher yields are expected using the deuteron-induced reactions, i.e., ^{65}Cu(d,2n)^{65}Zn and ^{109}Ag(d,2n)^{109}Cd. Thus, in this work, we tested the productions of ^{65}Zn and ^{109}Cd using a 24-MeV deuteron beam from the AVF cyclotron.

Zinc-65 and ^{109}Cd were produced by irradiating 24-MeV deuterons on metallic plates of copper (chemical purity: > 99.99%; thickness: 220 mg cm^{-2} × 3) and silver (> 99.99%; 260 mg cm^{-2} × 3) in a natural isotopic abundance. The average beam intensity was 147 nA for ^{65}Zn and 92.0 nA for ^{109}Cd. The number of incident deuterons was evaluated from the collected charge using a Faraday cup which was calibrated by the monitor reaction of ^{48}Ti(d,2n)^{48}V.[5)] After the irradiation for 1.0 h, the Cu targets were nondestructively subjected to γ-ray spectrometry with a Ge detector. On the other hand, the irradiated Ag target was put in a beaker containing 10 mg of Cd^{2+} carrier and dissolved with 1.5 mL of c. HNO_3. After evaporating the solution almost to dryness, the residue was diluted to 100 mL with H_2O. The pH of the solution was adjusted to 4 with aq. NH_3, and 2.5 mL of 2 M HCl was added to precipitate AgCl. The precipitate was discarded by the filtration. The pH of the filtrate was adjusted to 7 with aq. NH_3 and 1 mL of 1 M $(NH_4)_2HPO_4$ was added to precipitate $CdNH_4PO_4 \cdot H_2O$. The precipitate was filtered through the weighed filter paper and subjected to γ-ray spectrometry. Chemical yields were estimated by drying the samples at 110 °C until a constant weight was reached.

The thick-target yields of ^{65}Zn were determined to be 0.052 ± 0.004, 0.44 ± 0.03, and 0.73 ± 0.05 MBq μA^{-1} h^{-1} at 10.5, 18.2, and 24.0 MeV, respectively, whereas those of ^{109}Cd were 0.038 ± 0.003, 0.27 ± 0.02, and 0.38 ± 0.03 MBq μA^{-1} h^{-1} at 10.6, 18.1, and 24.0 MeV, respectively. In Figs. 1 and 2, the thick-target yields are shown as a function of the deuteron energy for ^{65}Zn and ^{109}Cd, respectively, together with those from the literatures.[3,4,6–8)] The thick-target yields of ^{65}Zn and ^{109}Cd were deduced from the excitation functions reported by Takács et al.[3)] and Uddin et al.,[4)] respectively, where the deuteron energy degradation with the thickness of stacked plates were calculated using the OSCER ver. 3.0 code.[9)] The thick-target yields of ^{65}Zn measured in this work are consistent with those of Takács et al.[3)] at 18.2 and 24.0 MeV, though that at 10.5 MeV is smaller by a factor of about 0.6. The yields of ^{109}Cd are consistent with those of Uddin et al.[4)] by considering their experimental uncertainties.

At present, we can use the 24-MeV deuteron beam with about 10-μA intensity to produce ^{65}Zn and ^{109}Cd. Thus, the production yields of ^{65}Zn and ^{109}Cd are expected to increase with the deuteron irradiation about 1.5 and 2.5 times, respectively, than those with the conventional proton.

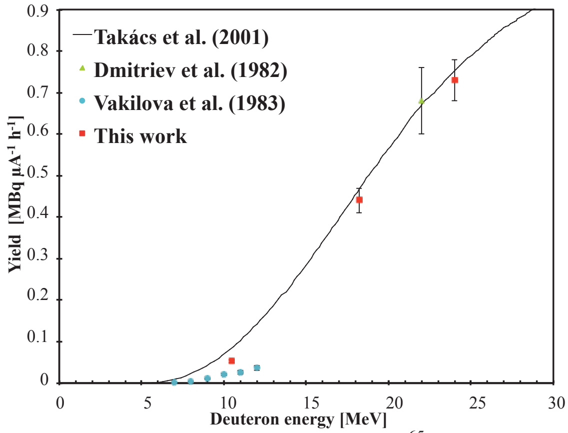

Fig. 1. Thick-target yields of ^{65}Zn.

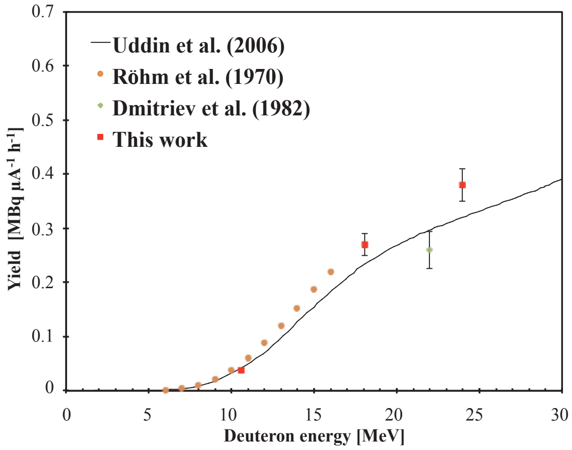

Fig. 2. Thick-target yields of ^{109}Cd.

References

1) T. Kambara et al.: RIKEN Accel. Prog. Rep. **42**, 295 (2008).
2) J. Kanaya et al.: J. Nucl. Radiochem. Sci. Suppl. **12**, 77 (2011).
3) S. Takács et al.: Nucl. Instrum. Meth. in Phys. Res. B **174**, 235 (2001).
4) M. S. Uddin et al.: Appl. Radiat. Isot. **64**, 1013 (2006).
5) IAEA Nuclear Data Services: http://www-nds.iaea.org/medical/.
6) G. Vakilova et al.: Sov. At. Energy **55**, 598 (1983).
7) H. F. Röhm et al.: J. Inorg. Nucl. Chem. **32**, 1413 (1970).
8) P. P. Dmitriev et al.: Vop. At. Nauki i Tekhn., Ser. Yad. Konst. Issue 4, 38 (1982).
9) K. Hata et al.: JAERI-M 63-247 (1988).

Application of ^{99}Ru Mössbauer spectroscopy to Ru-containing dilute f-electron lattice system

S. Tsutsui, Y. Kobayashi, M. Sera,[*1] T. Nishioka,[*2] M. Matsumura,[*2] H. Tanida, and R. Kobayashi[*3]

The dilute f-electron lattice system has recently attracted considerable interest in solid state physics. Recent works revealed the importance of d-electron contributions in series of compounds such as some filled skutterudites[1,2]. Observation of the hyperfine interactions at ligand sites other than the rare-earth ones in rare-earth intermetallics is also important when discussing the electronic states such as the hybridization between 4f and conduction electrons and magnetic structure. In this work, we carried out ^{99}Ru Mössbauer spectroscopy of novel rare-earth compounds RRu_2Al_{10} (R = La, Ce) to clarify the mechanism of the phase transition in $CeRu_2Al_{10}$[3–5].

Mössbauer spectroscopy is a complementary technique to nuclear magnetic resonance (NMR)/nuclear quadrupole resonance (NQR) and perturbed angular correlation (PAC) for investigation of hyperfine interactions. Unlike NMR/NQR and PAC, Mössbauer spectroscopy can detect isomer shift, a useful parameter for discussing the valence state at probe atoms and the hybridization between probe and surrounding atoms. On the other hand, locations for carrying out ^{99}Ru Mössbauer spectroscopy are very limited in the world. One of the reasons for this is preparation of ^{99}Rh γ-ray source. The ^{99}Rh γ-ray source for ^{99}Ru Mössbauer spectroscopy, whose half-life is 15 days, is produced by only the nuclear reaction of ^{99}Ru(p,n)^{99}Rh. Then, ^{99}Ru Mössbauer spectroscopy is carried out close to the accelerator that can provide the proton beam.

We prepared the γ-ray source for ^{99}Ru Mössbauer spectroscopy at the AVF cyclotron (K70-MeV) in RIKEN Nishina Center (RNC). The ^{99}Ru powder as a target is pressed and packed in an Al holder with a thin Al foil. The Al target holder with an attachment for cooling is installed to the end of beamline (C-03) connected to the AVF cyclotron. The target was irradiated with 15 A of 12 MeV proton beam for the ^{99}Ru(p,n)^{99}Rh reaction. ^{99}Ru Mössbauer measurements were carried out after irradiation of the ^{99}Ru target. The ^{99}Rh Mössbauer source was installed onto the Mössbauer velocity transducer. A NaI(Tl) scintillation detector was used for ^{99}Ru Mössbauer measurements. Doppler velocity was calibrated using the ^{57}Fe Mössbauer spectrum obtained at room temperature. Zero velocity was set by ^{99}Ru Mössbauer spectrum obtained at 77 K.

^{99}Ru Mössbauer spectra of RRu_2Al_{10} (R = La, Ce) were measured at 77 and 4.2 K. All the spectra obtained in the present work appear to be singlets, indicating the absence of nuclear magnetic or quadrupole interactions. The spectra of both compounds do not show temperature dependence. These facts demonstrate that the contribution of 4f electrons to the hyperfine interaction is too small to detect at ^{99}Ru nuclei.

Although $LaRu_2Al_{10}$ shows no phase transition above 4.2 K, $CeRu_2Al_{10}$ shows an antiferromagnetic ordering at 27 K[6]. Considering the magnetic structure[6], transferred hyperfine magnetic field at ^{99}Ru nuclei is expected owing to ferromagnetic ordering along a Ce-Ru-Ce zigzag chain. However, the results in the present work imply absence of the hyperfine magnetic field at ^{99}Ru nuclei either due to ordered Ru magnetic moments or transferred from ordered Ce magnetic moments.

The isomer shift also shows no rare-earth dependence between $LaRu_2Al_{10}$ and $CeRu_2Al_{10}$. This implies the absence of 4d-4f hybridization in $CeRu_2Al_{10}$, because hybridization effects are observed as a change in isomer shift values. This agrees with the recent results of electron density map obtained by synchrotron powder diffraction[7].

The precise analyses of the spectra are in progress.

References

1) R. Shiina: J. Phys. Soc. Jpn. **81**, 024706 (2012).
2) N. Kawamura, S. Tsutsui, M. Mizumaki, N. Ishimatsu, H. Maruyama, H. Sugawara and H. Sato: J. Phys.: Conf. Ser. **190**, 012020 (2009).
3) T. Nishioka, Y. Kawamura, T. Takesaka, R. Kobayashi, H. Kato, M. Muramatsu, K. Kodama, K. Matsubayashi and Y. Uwatoko: J. Phys. Soc. Jpn. **78**, 123705 (2009).
4) M. Matumura, Y. Kawamura, S. Edamoto, T. Takesaka, H. Kato, T. Nishioka, Y. Tokunaga, S. Kambe and H. Yasuoka: J. Phys. Soc. Jpn. **78**, 123713 (2009).
5) H. Tanida, D. Tanaka, M. Sera, C. Moriyoshi, Y. Kuroiwa, T. Takesaka, T. Nishioka, H. Kato and M. Matsumura: J. Phys. Soc. Jpn. **79**, 043708 (2009).
6) D. Khalyavin, A. Hiller, D. Adroja, A. Strydom, P. Manuel, L. Chapon, P. Peratheepan, K. Knight, P. Deen and C. Ritter: Phys. Rev. B **82**, 100405 (2010).
7) M. Sera, D. Tanaka, H. Tanida, C. Moriyoshi, M. Ogawa, Y. Kuroiwa, T. Nishioka, M. Matsumura, J. Kim, N. Tsuji and M. Takata: J. Phys. Soc. Jpn. **82** 024603 (2013).

*1 Advanced Science of Matter, Hiroshima University
*2 Faculty of Science, Kochi University
*3 Quantum Beam Science Directorate, Japan Atomic Energy Agency

Development of intense ^{7}Be beam for wear diagnostics of industrial materials

A.Yoshida, A. Nakao, T. Kambara, R. Uemoto,*1 H. Uno,*1 H. Yamaguchi,*2 T. Nakao,*2 and D. Kahl*2

The industrial cooperation team and SHIEI Ltd.*1 are developing a new method for wear diagnostics of industrial material using RI beams as tracers. RI nuclei are implanted in a near surface of the machine parts within depth of 10-100 μm, and its wear-loss is evaluated by the decrease in the measured radioactivity. Continuous γ-ray detection from the exterior of the machine enables real-time diagnostics of wear in running machines. For this purpose, RI nuclei having sufficiently long lifetime are desired. At present, we can provide an intense ^{22}Na ($T_{1/2}$ = 2.6y) beam at RIPS separator[1]. On the other hand, CNS*2 group has developed a cryogenic gas target system[2] at CRIB*3 separator and reported production of an intense ^{7}Be ($T_{1/2}$ = 53d) beam using the system. With the aim to utilize this intense ^{7}Be beam for the wear diagnostics, a beam study managed by industrial cooperation team was performed.

A primary beam of $^7Li^{2+}$ was accelerated by the AVF cyclotron up to 39.9 MeV (5.7 MeV/nucleon) with a maximum intensity of 1.2 particle μA (pμA). The ^{7}Be beam was produced via p(^{7}Li,^{7}Be)n reaction at the cryogenic gas target. The H_2 target gas was confined in a gas cell (8 cm long and 2 cm in diameter) sealed by 2.5-μm-thick Havar foils. The H_2 gas at a pressure of 760 Torr was cooled by liquid N_2 in a vessel at 90 K and circulated to the gas cell at a rate of 55 slm. The primary beam was focused on a Havar foil placed at entrance of the gas cell with the spot size of 1 mm in diameter. The target was very stable during this experiment. The produced ^{7}Be beam was introduced to the F2 focal plane without degrader foil at F1. In order to enable ^{7}Be implantation under air pressure condition, the vacuum chamber at F2 was modified so that a vacuum-separation foil could be attached. First, under a vacuum condition, the profiles of secondary beams were measured at F2 using a PPAC and a silicon detector. The energy and radius of the $^7Be^{4+}$ beam was 28.7 MeV (4.1 MeV/nucleon) and σ = 6.1 mm, respectively, with a momentum slit of ± 3.1% (± 50 mm) at F1. A contaminant nuclide of $^7Li^{3+}$ was observed with a fraction of 20% and energy of 18.8 MeV. Second, a Kapton vacuum-separation foil (50 μm thick and 5 cm in diameter) was assembled, and He gas at 1 atm was filled in the F2 chamber. The distance from the foil to the irradiation position was 14 cm. The ^{7}Li contaminant was stopped in the He gas, completely. The remainder of the ^{7}Be beam was 100% in purity and its peak energy was 13.5 MeV, with a width of σ = 1.6 MeV. The intensity of the ^{7}Be beam was 1.9 × 10^8 pps obtained by the following γ-ray measurement, which reproduced a reported value in the Ref.2.

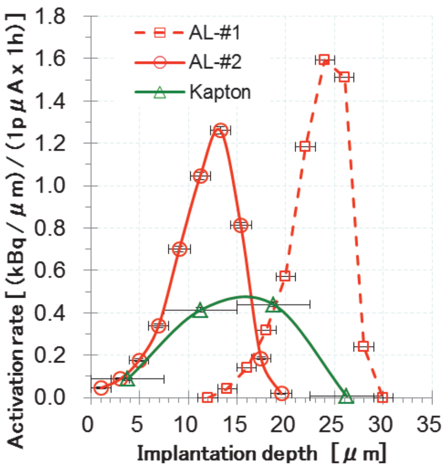

Fig. 1. Implantation-depth profile of thin-foil stacks.

To investigate the implantation-depth profile of ^{7}Be, two sets of thin-foil stack with a diameter of 16 mm were irradiated. One was a stack of 2-μm-thick aluminum foils and the other was a stack of 7.5-μm-thick Kapton foils. After irradiation, each stack was disassembled and the intensity of the γ ray (E γ = 478 keV) was measured using a Ge detector. First, the range profile of the above-mentioned ^{7}Be beam was measured using the aluminum-foil stack (AL-#1). Then, in order to control the implantation depth to near the surface, a rotating energy degrader was introduced. An 8-μm-thick aluminum foil was set on the beam path at 50° (corresponding to a thickness of 10.4 μm) and 90° , alternatively, relative to the beam axis with a time fraction of 5:1. The second aluminum-foil stack (AL-#2) and the Kapton-foil stack were irradiated under this condition. The obtained implantation-depth profiles are shown in Fig.1. In this figure, the ^{7}Be activation rate (kBq/μm) is normalized by the dose of the ^{7}Li primary beam (1 pμA × 1 h irradiation). X-error bars indicate the thickness of each foil, and Y-error bars indicate the statistical error in this measurement. From this result, we could achieve peak activity of 1.3 and 0.5 kBq/μm at depth of 13 and 15 μm from the surface of the aluminum and Kapton material, respectively. For example, when we measure the wear-loss of an aluminum machine part (case AL-#2), we can obtain peak activity density of 13 kBq/μm for 10-h irradiation. Since the best wear-loss sensitivity can be achieved near the depth of the maximum activity density, it would be required for actual applications to locate the peak of the activity distribution near the depth of interest for the wear-loss analysis.

*1 S.H.I. Examination and Inspection Ltd., http://www.shiei.co.jp/
*2 Center for Nuclear Study (CNS), University of Tokyo.
*3 CNS Radio Isotope Beam separator (CRIB).

References

1) T. Kambara et al.: AIP Conference Proceedings 1412, 423−429 (2011).
2) H. Yamaguchi et al.: NIM A589, 150−156 (2008).

4. Radiation Chemistry and Biology

Cell-killing effect of low dose of high-LET heavy ions (V)

M. Tomita, T. Tsukada, and M. Izumi

Non-DNA-targeted effects, which are not a direct consequence of radiation-induced initial lesions produced in cellular DNA, but rather an indirect consequence of intracellular and intercellular communications involving both irradiated and nonirradiated cells, have been observed over the past two decades, and the study of these effects is defining a new paradigm in radiation biology. These effects include low-dose hyperradiosensitivity (HRS), radiation-induced bystander response (RIBR), and so on.[1,2] The RIBR is generally defined as a cellular response that is induced in nonirradiated cells that receive bystander signals from directly irradiated cells within an irradiated cell population.[1,2] The heterogeneity of the absorbed dose within the irradiated tissues is more relevant for high-LET particle radiation than for low-LET photons. Therefore, RIBR induced by low doses of high-LET radiation is an important problem concerning the health of astronauts and in heavy-ion radiation therapy. In this study, we aim to clarify the molecular mechanisms and biological implications of RIBR induced by low doses of high-LET radiation. Previously, we showed that normal human fibroblasts that were irradiated with low doses of high-LET argon (Ar) and iron (Fe) ions induced HRS, thereby suggesting that bystander cell killing was induced.[3,4] In addition, nitric oxide (NO) was found to be involved in this process.[3,4]

First, we plot the revised clonogenic survival curve of normal human lung embryonic fibroblast WI-38 cells irradiated with Ar ions by adding newly obtained data to previous results[4] (Fig. 1). HRS could be clearly observed in the cells irradiated with Ar ions at doses lower than 0.1 Gy, and it was partly suppressed by pretreatment with carboxy-PTIO (c-PTIO), which is a scavenger of NO.

In the process of bystander response, it has been suggested that gap-junction intercellular communication (GJIC), reactive oxygen species (ROS), and the COX-2 (Cyclooxygenase-2) protein also play important roles along with NO.[2] Next, we examined the effects of the scavenger of ROS (DMSO), the inhibitor of GJIS (lindane), and COX-2 (NS-398). Lindane and NS-398 were dissolved in DMSO. As shown in Fig. 2, DMSO and lindane suppressed HRS to levels similar to that of c-PTIO, although the errors were large for the present results. These results suggest that ROS and/or GJIC are also involved in the process of bystander signal transfer along with NO. NS-398 showed the highest inhibitory effect. It has been speculated that NF-κB/Cox-2/prostaglandin E2 and NF-κB/iNOS/NO pathways play critical roles in α-particle-induced RIBR.[2] Currently, we are examining the roles of NF-κB and COX-2, which may be activated in bystander cells that have received ROS and NO, in HRS induced by high-LET radiations.

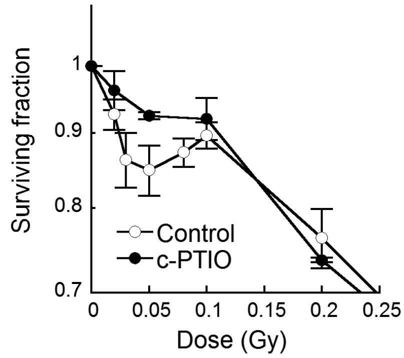

Fig. 1. Cell-survival curves of WI-38 cells. Confluent monolayers of WI-38 cells were irradiated with 95 MeV/u Ar ions (310 keV/μm) and some of the cells were pretreated with c-PTIO (20 μM). The surviving fraction was determined by a colony forming assay. The error bars represent the standard errors of the mean (SEM) (n = 3-5).

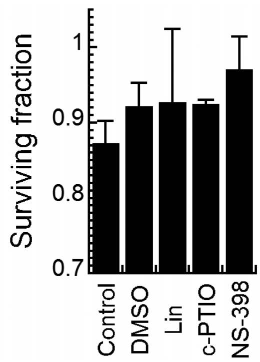

Fig. 2. Effect of inhibitors or scavengers. DMSO (0.1%), lindane (Lin, 50 μM), c-PTIO (20 μM) or NS-398 (50 μM) were added to the medium 2 h before irradiation. WI-38 cells were irradiated with 0.05 Gy of 95 MeV/u Ar ions (310 keV/μm). The error bars represent the standard errors of the mean (SEM) (n = 3).

References

1) K. M. Prise et al.: Radiat. Prot. Dosimetry **99**, 223 (2002).
2) T. K. Hei et al.: Curr. Mol. Pharmacol **4**, 96 (2011).
3) M. Tomita et al.: RIKEN Accel. Prog. Rep. **43**, 276 (2010).
4) M. Tomita et al.: RIKEN Accel. Prog. Rep. **45**, 207 (2012).

Effects of Trichostatin A on radiosensitivity to X-rays in mammalian cells with defects in DNA repair proteins

M. Izumi and T. Abe

In eukaryotes, DNA is packaged into nucleosomes, which are arranged in various higher order structures to form chromatin. The chromatin structure contributes to many aspects of DNA metabolism including replication, recombination, and transcription. However, it is not fully understood how repair reactions and checkpoint responses caused by heavy-ion irradiation are regulated by the chromatin structures. It is also unknown how the distribution of damage caused by ionizing radiation is different between euchromatin and heterochromatin. To investigate the roles of chromatin structures in DNA repair after heavy-ion irradiation, we have been focusing on the damage response observed after cells are treated with one of the potent histone deacetylase (HDAC) inhibitors, trichostatin A (TSA). HDAC inhibitors enhance radiosensitivity in mammalian cells[1,2], although the mechanism by which HDAC inhibitors enhance radiation sensitivity remains unknown.

In a previous study, we found that TSA exhibited different effects on sensitivity between X-rays and heavy ions in HeLa cells[3,4]. To analyze the roles of repair pathways in response to radiation after treatment with TSA, we investigated cell sensitivity to X-rays using the CHO cell and its mutant cell lines that have defects in DNA repair proteins. CHO cells or their derivatives were trypsinized and plated as single cells in TSA-free media. After allowing 24 h for attachment, cells were pre-treated with TSA (0.1 μM) for 10 h and irradiated with X-rays. Subsequently, the cells were cultured for an additional 14 h in the presence of TSA, and radiosensitivity was estimated by the colony-forming efficiency 14 days later.

As observed in HeLa cells, the treatment with TSA enhanced the sensitivity to X-rays up to 10 Gy (Fig. 1a). On the other hand, the treatment with TSA enhanced radiosensitivity to carbon ions at doses below 3 Gy (Fig. 1b). However, the survival rate did not change at doses over 3 Gy of carbon ions after treatment with TSA.

Next, we examined the cell sensitivity to X-rays using the CHO mutant cell lines that have defects in DNA repair proteins. Irs1SF cells lack XRCC3 (x-ray repair cross complementing 3) and exhibit defects in homologous recombination[5]. XRCC3 interacts with Rad51 and is necessary for the foci formation of Rad51. TSA enhanced the radioresistance to X-rays in irs1SF cells (Fig. 1a), thereby suggesting that the functional homologous recombination pathway is involved in the enhancement of radiosensitivity by TSA. On the contrary, TSA did not affect the survival of V3 cells as well as EM9 cells, which lack DNA-PK and XRCC1, respectively[6,7]. DNA-PK is necessary for non-homologous end-joining, whereas XRCC1 makes complex with ligase III and is involved in base excision repair. These results suggest that non-homologous recombination and base excision repair do not contribute to the enhancement of radiosensitivity by TSA. Currently we are investigating how TSA affects cell survival after heavy-ion irradiation in mutant cell lines.

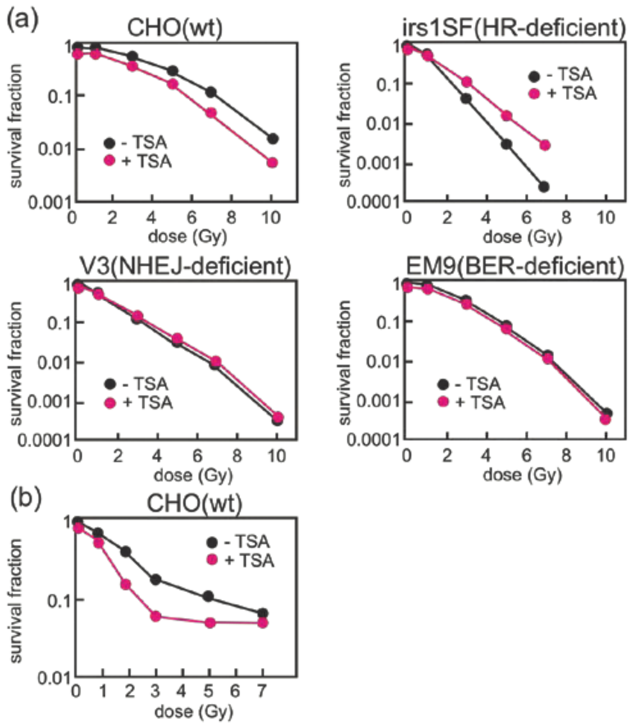

Fig. 1 The effects of trichostatin A (TSA) on radiosensitivity of CHO, irs1SF, V3, and EM9 cells. The black and red circles indicate cell survival in the absence and presence of TSA, respectively. Abbreviations: wt, wild type; HR, homologous recombination; NHEJ, non-homologous end-joining; BER, base excision repair.

References
1) Y. Zhang, et al.: Radiat. Res. **161,** 667 (2004).
2) K. Camphausen et al.: Clin. Cancer Res. **10,** 6066 (2004).
3) M. Izumi.: RIKEN Accel. Prog. Rep. **44,** 264 (2011).
4) M. Izumi, et al.: RIKEN Accel. Prog. Rep. **45,** 206 (2012)
5) R.S. Tebbs, et al.: Proc. Natl. Acad. Sci. USA **92,** 6354 (1995)
6) S.R. Peterson, et al.: Proc. Natl. Acad. Sci. USA **92,** 3171 (1995)
7) L.H. Thompson, et al.: Mol. Cell. Biol. **10,** 6160 (1990)

Examination of the balancer line towards construction of mutant isolation system in fruit flies

K. Tsuneizumi, and T. Abe

Heavy-ion beam mutagenesis is generally recognized as an effective method for mutation breeding[1, 2]. Although this method was greatly successful with a plant, it is still limited for animals. In order to extend the application to animals, we plan to acquire more basic data to set up the optimal condition of the irradiation system by heavy-ion beam using *Drosophila melanogaster* (fruit fly) as a useful model system.

In this technique, useful chromosomes, called balancers, can prevent crossing over between homologous chromosomes during meiosis. By using balancers, it is possible to make diploid chromosomes consistent, as shown in Fig.1. By using a double balancer line including two balancers for second and third chromosomes together, it is possible to obtain twice as many data as a single balancer line. Thus, we established the double balancer line to establish more variety of mutations that arise in second and third chromosomes before beginning the irradiation experiment.

From past research, an X-ray irradiation is known as mutagen to DNA damage[3, 4]. In multicellular organisms, an irradiation to the whole body is thought to affect various organs, with diverse effects. Therefore, we must distinguish between changes in body cells (somatic mutations) and changes in gametes (germline mutations). The former becomes a cause of death of the irradiated flies. The latter is passed on to the offspring. It is necessary to investigate the influence of the irradiation on survival rate, mating behavior, spermiogenesis, oogenesis, etc. Then, we conducted an exploratory experiment using X rays in order to acquire basic data.

Males and females were immediately separated after eclosion, and were bred for three days. These flies were respectively irradiated with different doses of X rays. The males were provided with fresh harems of virgin females every 2-3 days. The females were provided with males and were replaced to fresh medium every 2-3 days. The oviposited eggs were bred, the number of progeny that survived to adults was measured, and the reproductive abilities of the X-ray-irradiated individuals were assessed.

It was observed that mating behavior, spermiogenesis, and oogenesis of irradiated flies are sufficient for obtaining the next generation, as shown in Fig. 2. It is thought that the fall of reproductive ability of males is caused by aging, and not by the influence of irradiation. On the other hand, the reproductive ability of females did not change during the observation period, as shown in Fig.2. According to the observed results, data fluctuated up and down. We think that the instability of the system stems from the instability of the double balancer. Currently, we are establishing other balancer lines. This will help stabilize the mutant isolation system in the future.

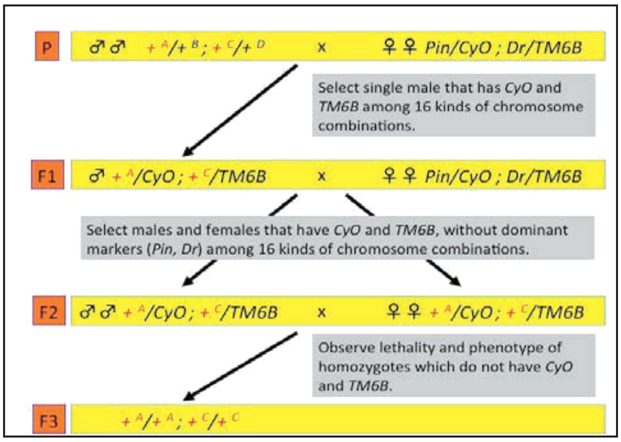

Fig. 1. A scheme of mutant isolation using a double balancer line. The irradiated genotype of the second chromosome and the third chromosome are written as $+^A/+^B$; $+^C/+^D$. Randomly selected single chromosomes ($+^A$, $+^C$) are amplified by a new crossing with the double balancer line. A mutant isolation is performed by mating with sisters and brothers, and homozygotes appear in the next generation. P : parental generation, F : filial generation, CyO : second chromosome balancer, and TM6B : third chromosome balancer.

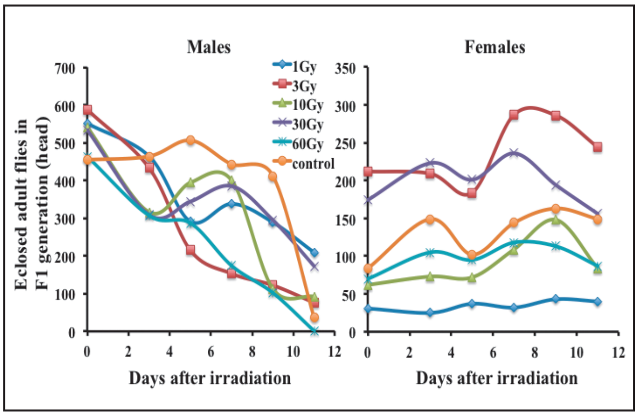

Fig. 2. Correlation between days after X-ray irradiation and changes in eclosed adult flies in F1 generation. Left panel shows the number of progeny from males irradiated with X rays. Right panel shows the number of progeny from females irradiated with X rays.

References

1) T. Abe et al.: Gamma Field Symp. **39**, 45 (2000).
2) A. Tanaka et al.: J. Radiat. Res. **51**, 223 (2010).
3) H. J. Muller: Science **66**, 84 (1927).
4) L. J. Stadler: Science **68**, 186 (1928).

Sperm abnormality resulting from DNA repair during pollen tube growth in *Cyrtanthus mackenii* †

T. Hirano,*1 K. Takagi, Y. Hoshino,*2 and T. Abe

The male gametophytes of plants are exposed to environmental stress and mutagenic agents during the double fertilization process, and therefore the gametophytes need to repair the DNA damage in order to transmit the genomic information to the next generation. However, our understanding of the DNA damage response in male gametes is still unclear. Therefore, we irradiated the bicellular pollen of *Cyrtanthus mackenii* with a heavy-ion beam and analyzed the DNA damage response in the male gametes during pollen tube growth using an *in vitro* culture system. In this study, we focus on sperm abnormality after DNA repair.

Anthers of *C. mackenii* in 1.5-ml tubes were irradiated with C ions (22.5 keV/μm) at doses of 10–80 Gy and then stored at -20°C. For pollen germination, pollen grains from the anthers were sown in 2 ml of liquid pollen culture medium[1] and cultured at 25°C in the dark. Male-gamete isolation from the pollen tube and immunocytochemical analysis were performed according to the protocol described previously.[2]

After the high-dose irradiation with doses of 40 Gy and 80 Gy, the cell cycle progression of generative cells was arrested at metaphase in pollen mitosis II (PMII) after 12 h of culture, and phosphorylated histone H2AX (γH2AX) foci, which are indicators of DNA double-strand breaks (DSBs), were detected in a majority of the arrested cells.[3] To analyze the behavior of the arrested cells, we investigated the cell cycle phase after 24 h of culture. During this culture period, most of the generative cells (92%) in non-irradiated pollen grains had formed pairs of sperm cells. The cell cycle in irradiated generative cells after 24 h of culture progressed in comparison with that after 12 h of culture, and the proportions of the generative cells that had completed metaphase after 24 h of culture were 87% at 40 Gy and 71% at 80 Gy. The cells passing through metaphase contained no γH2AX foci (Fig. 1). Therefore, it is suggested that the generative cells with chromosomal lesions, such as DSBs, were arrested in the cell cycle progression by the spindle assembly checkpoint until completion of chromosomal lesion repair.

After carbon-ion irradiation, sperm abnormalities such as lagging chromosomes and asymmetric division were observed. After 24 h of culture, the proportion of sperm cell pairs with lagging chromosomes in the PMII-completed male gametes was particularly high after irradiation with 10 Gy (22%). The male gametes from irradiated pollen grainscontained generative cell-like nuclei and sperm cell-like microtubule arrays (Fig. 1). The cells, which contained chromosomal bridges and did not show a clear chromosome separation, could progress into telophase. Therefore, this suggests that the cells with generative cell-like nuclei and sperm-cell-like microtubule arrays completed the PMII but failed in chromosome separation. We defined the cells as generative-cell-like sperm cells (GC-like SCs). The sperm cells connected by a chromosomal bridge and the GC-like SCs were observed after 12 h of culture, and male gametes in that category amounted to 24%, 74%, and 90% of the PMII-finished male gametes irradiated with 10 Gy, 40 Gy, and 80 Gy, respectively, after 24 h of culture. Both chromosomal and cell division abnormalities were observed in an irradiation dose-dependent manner in the PMII completed cells, thereby suggesting that error-prone DSB repair pathways such as non-homologous end-joining or single strand annealing were used for DSB repair in the generative cells.

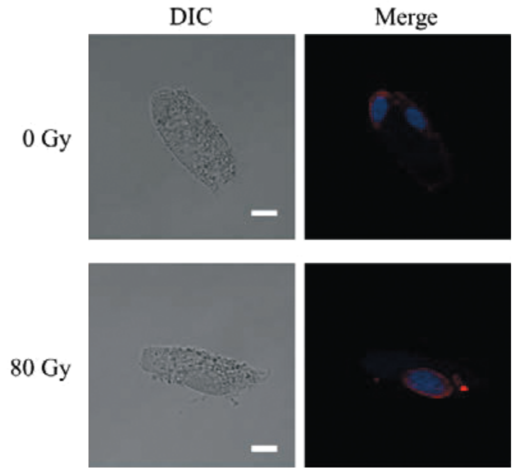

Fig. 1 Abnormalities in the sperm nuclei derived from irradiated pollen grains. We isolated cells as male germ units, in which the generative-cell or the sperm-cell pair was closely associated with the vegetative nucleus, from the pollen tubes cultured for 24 h. The merged images show nuclei stained with DAPI (pseudocolor: blue), γH2AX stained with anti-γH2AX antibody followed by secondary antibody (pseudocolor: green), and microtubules stained with anti-α-tubulin antibody followed by secondary antibody (pseudocolor: red). Bars = 10 μm.

† Condensed from the article in AoB PLANTS, **5**, plt004 (2013).
*1 Innovation Center, RIKEN
*2 Field Science Center for Northern Biosphere, Hokkaido University

References
1) T. Hirano and Y. Hoshino: J. Plant Res. 122, 225 (2009).
2) T. Hirano and Y. Hoshino: Sex. Plant Reprod. 23, 153 (2010).
3) T. Hirano et al.: RIKEN Accel. Prog. Rep. 45, 216 (2011).

Evaluation of LET-dependent effect in heavy-ion mutagenesis using rapid mutation detection system in *Arabidopsis thaliana*†

Y. Kazama,[*1] L. Ma, T. Hirano,[*1] S. Ohbu, Y. Shirakawa, S. Hatakeyama,[*2] S. Tanaka,[*2] and T. Abe

Heavy-ion irradiation is an excellent technology to induce mutations with high frequency. A notable physical characteristic of heavy-ion beams is that the accelerated particles deposit their energy densely in a localized region along the particle path. The degree of locally deposited energy is represented by linear energy transfer (LET; the energy transferred per unit length, keV μm^{-1}). We have been studying the effect of LET on mutation induction using the model plant *Arabidopsis thaliana*. In our previous study, we investigated the incidence of albino mutants in the M_2 generation of *Arabidopsis thaliana* after irradiation with LET of 22.5, 30.0, 61.5, 290, and 640 keV μm^{-1}.[1)] We found that irradiation with an LET of 30.0 keV μm^{-1} was the most effective for inducing mutations in the M_2 generation.

To determine the most effective LET to induce mutations, a more detailed examination of LET was required. However, analysis of the mutation frequency in the M_2 generation is expensive in terms of time and space requirements. Thus, we adopted a rapid method to detect the effects of LET on inducing mutations using a heterozygous mutant of the *Albino Pale Green 3* (*APG3*) gene.[2), 3)] The *APG3* gene is involved in chloroplast development. Homozygous mutants of *APG3* (*APG3*$^{-/-}$) show albino or pale-green leaves, whereas heterozygous mutants (*APG3*$^{+/-}$) and wild-type plants (*APG3*$^{+/+}$) have green leaves. In heterozygous plants in which intact alleles are mutated by mutagens, leaves show white sectors. This system allowed us to investigate the effect of LETs on inducing mutation in the M_1 generation.

Here, we investigated the effect of LETs on inducing mutations in the M_1 generation using the heterozygous *APG3* mutant. Seeds of *APG3* heterozygous plants (CS16118) were obtained from the Arabidopsis Biological Resource Center (Ohio State University). The CS16118 seeds were irradiated with $^{12}C^{6+}$ ions with a dose range of 100 to 450 Gy. The ions were accelerated up to 1.62 GeV, at which the LET of the $^{12}C^{6+}$ ions was 22.5 keV μm^{-1}. The LET of the $^{12}C^{6+}$ ions was adjusted to 30.0, 42.5, 50.0, or 61.5 keV μm^{-1} by reducing the ion velocity. As a negative control, seeds of wild-type plants were irradiated with $^{12}C^{6+}$ ions with an LET of 30.0 keV μm^{-1} at a dose of 300 Gy. The LET was measured at a point behind the seeds using an ionization chamber. Calculation of the mutation frequencies was performed as described previously.[3)]

The variation in LET clearly affected on the incidence of albino sectors (Fig. 1). The LET of 22.5 keV μm^{-1} was the least effective in inducing mutations, resulting in a frequency of only 3.08% white sectors, even at the most effective dose (450 Gy). In contrast, C ions with greater LET produced approximately double the frequency of white sectors, when compared with that induced by C ions with 22.5 keV μm^{-1} at a dose of 300 Gy. The low efficiency of C ions with 22.5 keV μm^{-1} was consistent with the results of previous studies on mutations in the M_2 generation.[1)] We also observed differences in mutation frequencies among the other LETs. At low doses (100–200 Gy), LETs of 50.0 and 61.5 keV μm^{-1} produced greater mutation frequencies than did LETs of 30.0 and 42.5 keV μm^{-1}. At these doses, C ions with LETs of 30.0 keV μm^{-1} and 42.5 keV μm^{-1} produced mutation frequencies similar to that of the LET of 22.5 keV μm^{-1}. At the 300 Gy dose, C ions with LETs of 30.0 or 42.5 keV μm^{-1} showed mutation frequencies similar to those produced by LETs of 50.0 and 61.5 keV μm^{-1}; these irradiation conditions (30.0, 42.5, 50.0, and 61.5 keV μm^{-1} at a dose of 300 Gy) were the most effective in producing high mutation frequencies in the M_1 generation. When we observed seed productivity under these conditions, 42.5–61.5 keV μm^{-1} severely affected the seed productivity. Therefore, we concluded that an LET of 30.0 keV μm^{-1} is appropriate for generating mutants that can produce an M_2 generation efficiently.

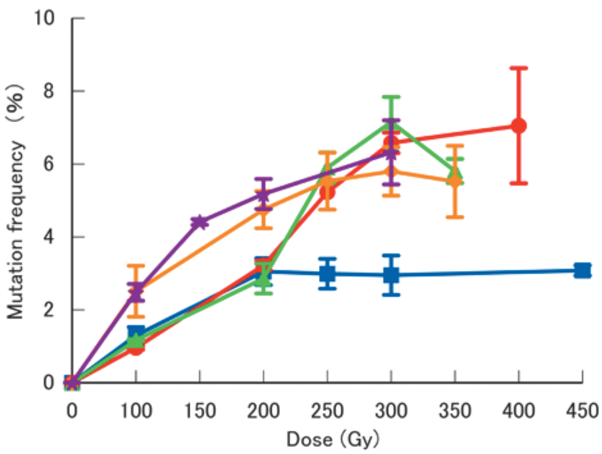

Fig. 1 Effect of LET on mutation induction in M_1 generation. Error bars indicate SE. Blue: 22.5 keV μm^{-1}; Red: 30.0 keV μm^{-1}; Green: 42.5 keV μm^{-1}; Orange: 50.0 keV μm^{-1}; Purple: 61.5 keV μm^{-1}.

References
1) Y. Kazama et al.: Plant Biotechnol. **25**, 113 (2008).
2) R. Motohashi et al.: Plant Mol. Biol. **64**, 481 (2007)
3) Y. Kazama et al.: RIKEN Accel. Prog. Rep. **44**, 267 (2011).

† Condensed from the article in Plant Biotechnol. **29,** 440 (2012)
*1 RIKEN Innovation Center
*2 Department of Regulatory Biology, Saitama University

Cyclopedic analysis of rice genes induced by heavy-ion beam irradiation

K. Ishii, R. Morita, S. Kogure, K. Ichinose, Y. Hayashi, T. Wakana, T. Hirano, T. Shibukawa,[*1] Y. Nagamura,[*1] and T. Abe

In plant mutagenesis by heavy-ion beam irradiation, the concept of the most effective linear energy transfer (LET_{max}) has been defined and reported. LET_{max} is dependent on the species being irradiated, for example, LET_{max} is 30 keV/μm for the dry seeds of *Arabidopsis thaliana*[1)] and 50 to 70 keV/μm for wet seeds of rice (*Oryza sativa* L. cv. Nipponbare).[2)] Because the type of mutation depends on the value of LET, it is possible that different DNA repair pathways work for different mutations, thereby showing different mutation rates.

To determine the LET_{max} value of rice, it was necessary to observe the mutation rate of the M_2 generation, which took 10 years. If a gene which is highly expressed specifically after irradiation at LET_{max} is isolated, the LET_{max} marker gene will enable the acceleration of mutation breeding. In this study, we attempted to isolate the LET_{max} marker gene in rice by both microarray and quantitative polymerase chain reaction (qPCR) analyses.

Imbibed seeds of rice were exposed to C-ion and Ne-ion beams accelerated to 135 MeV/u using the RRC. The dose was set to 15 Gy. The LET range of the C-ion beam was 22.5 to 50 keV/μm and that for the Ne-ion beam was 63 to 80 keV/μm. The LETs of the C-ion and Ne-ion beams were adjusted by a range filter that consisted of 12 energy absorbers.[3)] The values of LET were calculated at the surface of the seeds. Since Shibukawa et al. reported that the expression level of *OsRad51*, a recombinase of *O. sativa*, reduced 3 h after X-ray irradiation,[4)] we sampled embryos from seeds that had absorbed water at intervals of 0.5, 1, and 2 h after heavy-ion beam irradiation and isolated their RNA. The total RNA was labeled using the Quick Amp Labeling Kit (Agilent Technologies, Palo Alto, Calif.). Microarray analysis was conducted using the Rice Gene Expression Microarray, 4 × 44K (Agilent Technologies) and data were analyzed on the Subio Platform (Subio, Kagoshima, Japan). All experiments with C-ion and Ne-ion beams were conducted twice and thrice, respectively.

We filtered out 4,228 gene models that showed low signal intensity (raw signal intensity < 30) out of 45,221 gene models, and we further analyzed 40,993 gene models. The expression levels of 1,374 and 3,159 gene models when irradiated at 50 and 63 keV/μm of LET (LET_{max}) were significantly different from those when not irradiated (control), respectively ($p < 0.01$). The product set of the two sets consisted of 455 gene models. Out of the 455 gene models, the expression levels of 14 and 25 gene models when irradiated at 50 and 63 keV/μm of LET (LET_{max}) were at least twice as high as those at 22.5 keV/μm of LET, respectively. The sum set of the two sets consisted of 31 gene models. All the 455 gene models when irradiated at 22.5 keV/μm of LET did not show more than twice of the expression level than that at LET_{max}.

In this study, we isolated 31 gene models which showed at least two times higher expression when irradiated at LET_{max} than at lower value of LET. Further analysis including replication study by qPCR and functional analysis will enable us to identify the LET_{max} marker gene.

*1 Agrogenomics Research Center, National Institute of Agrobiological Sciences

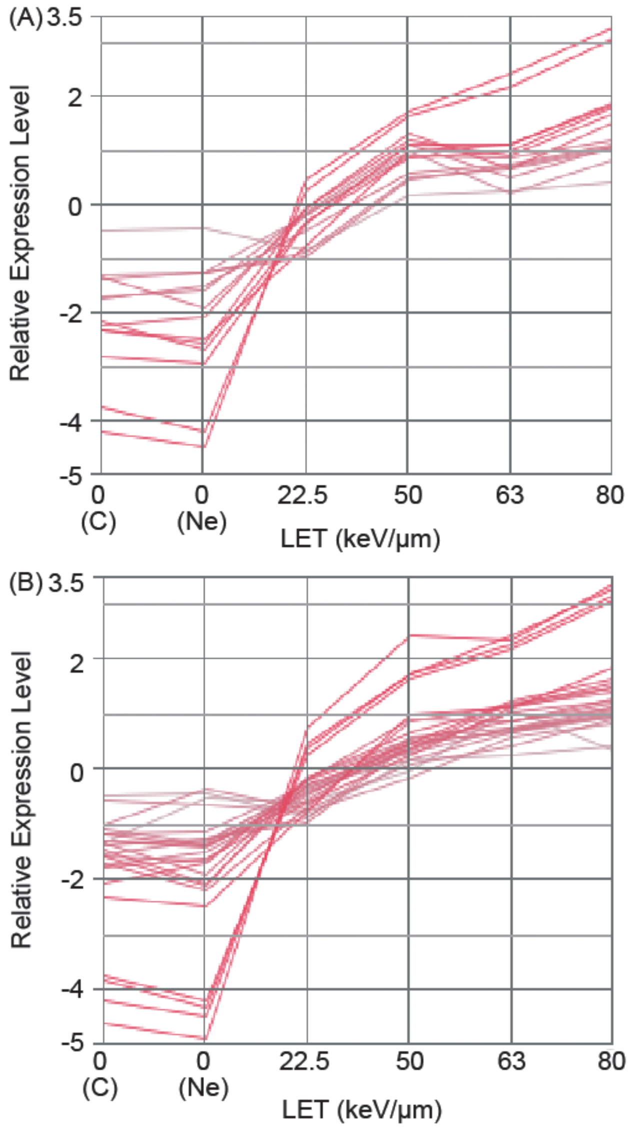

Fig. 1. Relative expression levels of gene models that showed higher expression levels when irradiated at 50 (A) and 63 keV/μm (B) of LET than at 22.5 keV/μm of LET.

References

1) Y. Kazama et al.: Plant biotechnology **25**, 113-117 (2008).
2) Y. Hayashi et al.: RIKEN Accel. Prog. Rep. **42**, 285 (2009).
3) H. Ryuto et al.: Plant Biotechnology **25**, 119 (2008).
4) Shibukawa et al.: RIKEN Accel. Prog. Rep. **43**, 280 (2010).

Genetic analysis of the rice 22-4Y mutant induced by heavy-ion beams

R. Morita, M. Nakagawa,[*1] S. Kogure, Y. Hayashi, H. Tokairin, H. Takehisa, T. Sato,[*2] and T. Abe

Many chlorophyll- and chloroplast-associated mutants that affect leaf coloration and/or plant viability have been identified and are referred to as albino, chlorina, stripe, and virescent. Among them, the virescent mutants produce chlorophyll (Chl)-deficient leaves during the early growth stages and develop mostly green leaves during the late growth stages. It is known that 13 virescent mutants exist in rice, and 4 of their causative genes are identified[1~3]. To understand the chlorophyll biosynthesis/chloroplast biogenesis, we screened the rice virescent mutants from the population generated by heavy-ion beam irradiation.

The 22-4Y has been obtained as a virescent mutant from rice (Oryza sativa L. cv. Nipponbare) by irradiating with a carbon-ion beam (20Gy, LET: 22.5 keV/μm). The 22-4Y shows a temperature-sensitive phenotype, i.e., it develops chlorotic leaves at a low temperature (20°C), but produce mainly green leaves at a high temperature (30°C). To measure the Chl content, we extracted Chl from the third leaf when the fourth leaf was still expanding (early growth stages). In the third leaf of 22-4Y, there was a trace amount of Chls compared with the wild type (WT) at 20°C. 22-4Y developed greener third leaves with much higher Chl concentration (about 35% of the WT) at 30°C. Next, we extracted Chl from a flag leaf (late growth stages). The 22-4Y accumulated almost the same amount of Chl as the WT in a flag leaf. These results suggest that 22-4Y is a temperature-sensitive virescent mutant.

Genetic mapping of the causative gene was performed using F_2 plants that were generated from a cross of 22-4Y and Kasalath (indica cultivar). Using Polymerase Chain Reaction markers, the causative gene was mapped to within 200 kb between two markers, E10886 and RM459, on the long arm of chromosome 5 (Fig. 1). There is another virescent gene, v10, which was mapped near the position of marker E10886. To verify whether the causative gene of 22-4Y is the v10 gene or not, an allelism test was performed using F_1 plants that were generated from a cross of 22-4Y and the v10 mutant. The F_1 plant developed normal green leaves at 20 °C, indicating that the causative gene of 22-4Y is not identical to the v10 gene. To clarify the causative gene of 22-4Y, we determined the DNA sequence of 16 genes existing within 200 kb of 22-4Y. We found that a deletion of 13095 base pairs (bp) occurred at the gene named LOC_Os05g34040. This gene encodes monooxygenase. It has been predicted that LOC_Os05g34040 generates two spliced variants, named LOC_Os05g34040.1 and LOC_Os05g34040.2. LOC_Os05g34040.1 encodes a 720-amino-acid (aa) polypeptide and LOC_Os05g34040.2 encodes a 583-aa-polypeptide. To determine the major spliced variants expressed in leaves, RT-PCR was performed. We used primer pairs to distinguish LOC_Os05g34040.1 from LOC_Os05g34040.2 by the sizes of the amplicons (345 bp for LOC_Os05g34040.1, and 278 bp for LOC_Os05g34040.2). When the RT-PCR was carried out using single-strand DNA, synthesized by total RNA extracted from Nipponbare leaves, as a template, only amplification of the 345 bp DNA fragment was observed, indicating that the major spliced variant expressed in leaves was LOC_Os05g34040.1. To confirm that the causative gene of 22-4Y is LOC_Os05g34040, we constructed transgenic 22-4Y mutants carrying the LOC_Os05g34040.1 cDNA driven by the maize ubiquitin promoter. One transgenic line grown at 20 °C developed normal green leaves, suggesting that LOC_Os05g34040 gene is the causative gene of 22-4Y mutant.

In this report, we isolated a virescent mutant, 22-4Y, and subsequently identified a novel virescent gene, LOC_Os05g34040, which encodes monooxygenase. The reason why the mutation involved in LOC_Os05g34040 causes a virescent phenotype is still unknown. To gain further insights into the function of the gene, gene expression and physiological analyses will be carried out.

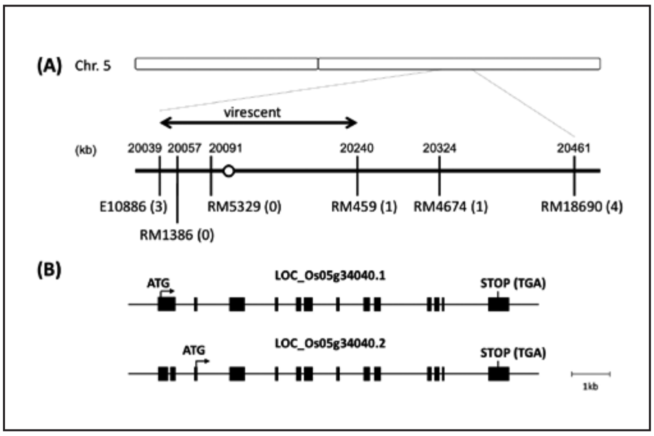

Fig. 1 (A) Chromosomal location of the mutation of 22-4Y. The number in the parenthesis indicates the number of recombinant plants. The white circle indicates the position of the gene LOC_Os05g34040. (B) Schematic representation of the genomic sequence of LOC_Os05g34040. Black boxes indicate exons. The initial codon (ATG) and the stop codon (STOP) are shown.

*1 Grad. Sch. Bioagric. Sci., Nagoya University
*2 Grad. Sch. Life Sci., Tohoku University

References

1) H. Sugimoto et al.: Plant J. **52**, 512 (2007).
2) SC. Yoo et al.: Plant Physiol. **150**, 388 (2009).
3) K. Kusumi et al.: Plant J. **68**, 1039 (2011).

Analysis of rice dwarf mutants induced by heavy ion beam

S. Kogure, R. Morita, Y. Hayashi, K. Ichinose, T. Wakana, H. Tokairin, K. Ishii, L. Ma, T. Sato,[*1] and T. Abe

Our team has studied the mutation induction in rice as an effect of heavy-ion beam irradiation. Rice is a model plant of monocots, which is useful in searching mutation sites because its entire genome sequences are available. In this study, we report the screening and analysis of dwarf mutants induced by heavy ion beam.

This year, 114 dwarf mutant lines were isolated by screening the 3824 lines of M_2 generation obtained by irradiation of imbibed rice seeds with a C-ion beam (15 Gy, LET 50 keV/μm) and Ne-ion beam (15 Gy, LET 63 keV/μm). There are various phenotypes in that dwarf mutants group. Four mutant lines showed the typical phenotype of rice gibberellin (GA) related mutants, severe dwarfness with wide leaf blades and dark green leaves[1]. Five mutant lines showed plastochron (PLA)-like phenotype, which mutants exhibit the rapid initiation of vegetative leaves without affecting phyllotaxy[2]. 46 were twisted, 12 showed premature death and 47 were of the other type (Fig. 1).

Three GA-type mutant lines were identified as mutated genes by sequence analysis. C-305 contained 2-bp deletion in KAO, and Ne-612 contained 12-bp deletion in GA3ox2 (Fig. 2), and both of their mutated gene were involved in GA biosynthesis[3]. C-1682 contained 72348-bp deletion, and it lacked whole GA positive regulator, GID2[1]. The last 1 GA-type mutant line is now being analyzed.

To identify more mutated regions of dwarf mutant lines, we classified "other type dwarf mutant lines" by height and fertility (Fig. 1). The mutant lines over 70% height of wild type were categorized as semi-dwarf, under 30% as severe dwarf, 30-70% as dwarf. One of the semi-dwarf mutant lines, Ne-1159, showed short grain. There are 3 causative genes already reported in that type of mutant. A sequence analysis revealed that Ne-1159 contained 3-bp deletion in D1[4] (Fig. 2). Next generation of other fertile semi-dwarf mutant lines will be grown to observe branching in order to judge *MORE AXILLARY BRANCHING* (*MAX*)[5] mutants.

Five PLA-like mutant lines did not contain any mutation in PLA genes. Some other unknown genes may have same the role, and research on this is ongoing.

It is necessary to identify more mutated regions of rice mutants for characterizing the mutations induced by heavy-ion beam irradiation. We have continued analysis, and some mutants will give us the deletion size, which is caused by heavy-ion beam irradiation, and new gene function. Furthermore, some semi-dwarf mutants may useful for breeding.

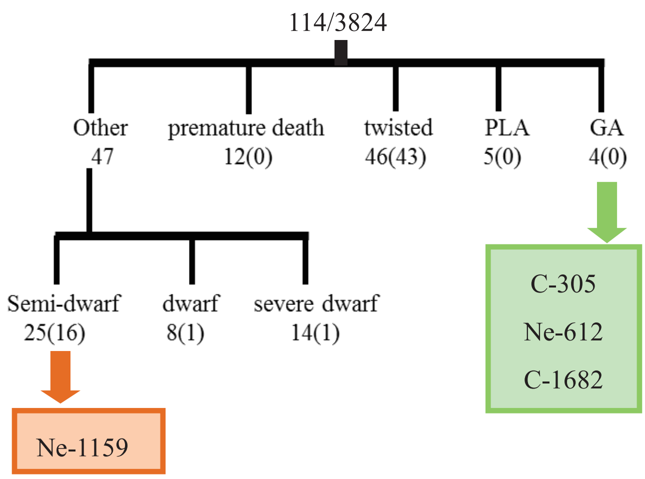

Fig. 1. Classification of rice dwarf mutant lines by typical appearance and height. The numbers in parentheses indicate the number of fertile lines. The mutant lines identified as mutation sites are shown.

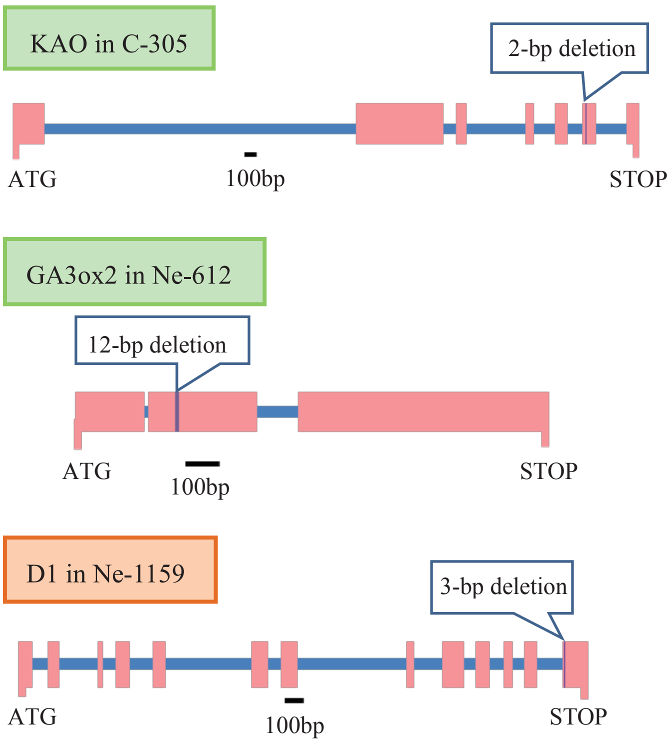

Fig. 2. Exon-intron structures of KAO, GA3ox2, and D1. Each mutation site of C-305, Ne-612, and Ne-1159 are shown.

References
1) A. Sasaki et al.: Science **299**, 1896 (2003).
2) K. Miyoshi et al.: Proc. Natl. Acad. Sci. USA **101**, 875 (2004)
3) T. Sakamoto et al.: Plant Physiol. **134**, 1642 (2004).
4) Y. Fujisawa et al.: Plant Cell Physiol. **42**, 789 (2001)
5) T. Arite et al.: Plant J. **51**, 1019 (2007)

*1 Graduate School of Life Sciences, Tohoku University

Effects of heavy-ion beam irradiation on *Brachypodium distachyon*

Y. Onda,[*1] Y. N. Tsuchiya,[*2] Y. Kazama,[*3] T. Abe, K. Mochida,[*1,*2,*4] and K. Shinozaki[*1,*2]

The grass family is one of the most widely distributed plant families and includes many agriculturally and economically important crops. *Brachypodium distachyon,* a temperate annual grass, belongs to the subfamily Pooideae, which also contains wheat, oats, and barley. Since *B. distachyon* is characterized by a small size, simple growth requirements, self-fertility, a short life cycle, and small genome size (approximately 272 Mb),[1)] this species has emerged as a new model system for research on cereals and grasses. Moreover, *B. distachyon* is the first member of the Pooideae subfamily with a sequenced genome[2)] and is, therefore, an ideal system for functional genomic studies on cereal and bioenergy crops.

We initiated studies on heavy-ion-beam-irradiated mutants of *B. distachyon* with an aim of understanding the molecular mechanisms underlying crop quality and productivity. Heavy-ion beams are accelerated ions produced by an accelerator, such as a cyclotron or synchrotron, and induce double-strand DNA breaks more effectively than other mutagenic techniques. For the beam experiments at the RIKEN RI Beam Factory, we irradiated dry seeds of the genome-sequenced accession Bd21 with the 50-keV μm^{-1} carbon ions at doses of 100–175 Gy. The germination and survival rates of the irradiated M_1 seeds decreased with increasing heavy-ion beam dose (Fig. 1). The survival rate declined sharply between 100 and 125 Gy. In the M_2 generation, the frequency of albino plants (ratio of number of albino individuals to the total number of germinated seedlings) was 1.1% at 100 Gy. These results suggest that the 50-keV μm^{-1} carbon ions at doses of 100–125 Gy effectively induce DNA alterations in the dry seeds of *B. distachyon*.

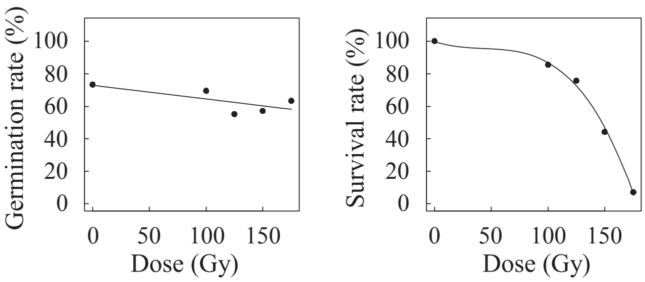

Fig. 1. Germination and survival rates of seeds after heavy-ion beam irradiation. Dry seeds were sown on wet filter paper and germinated at 25°C. Seedlings were transferred into soil and grown at 22°C.

*1 Biomass Engineering Program, RIKEN
*2 Plant Science Center, RIKEN
*3 Innovation Center, RIKEN
*4 Kihara Institute for Biological Research, Yokohama City University

Further, we irradiated dry seeds with the 22.6-keV μm^{-1} carbon ions at doses of 100–300 Gy. The progeny of heavy-ion-beam-irradiated seeds showed a variety of visible phenotypic differences. We measured several morphological phenotypes in the M_3 generation. (*e.g.*, leaf width) (Fig. 2). Then, we screened for 3 different types of mutants: mutants with narrower and longer leaf blades, which shows abnormal root development (Fig. 3A), mutants with a dwarf phenotype, and mutants with longer spikelets and more florets (Fig. 3B).

In this study, we carried out morphometric measurements of heavy-ion-beam-irradiated mutants. Our phenotyping data in the M_3 generation showed various visible phenotypes. The heavy-ion beam irradiation could be an efficient method to develop mutant resources for gene discovery by a forward genetics approach in the model grass.

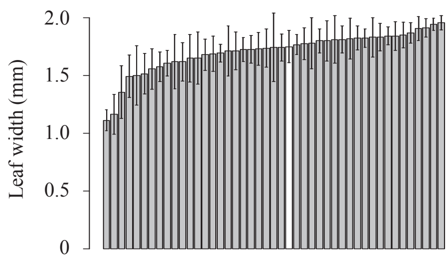

Fig. 2. The difference in leaf width among heavy-ion-beam-irradiated mutant lines in the M3 generation. Each of gray bar represents the mean value ± SD (n = 6–8, average = 7.91) for each mutant line. The white bar represents the mean value ± SD (n = 8) for WT.

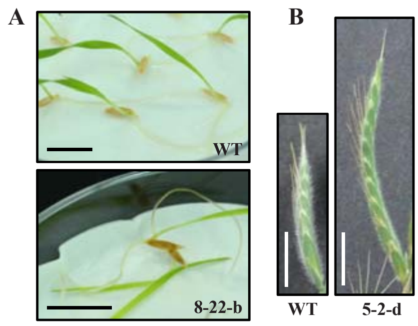

Fig. 3. Visible phenotypic differences between wild type and mutants in the M_3 generation. (A) Mutants show abnormal root development. Primary roots developed along a surface of filter paper (WT) or developed crookedly (8-22-b). Bars = 1 cm. (B) Mutants with longer spikelets and more florets. Bars = 1 cm.

References

1) J. Brkljacic et al.: Plant Physiol. 157, 3-13 (2011).
2) International Brachypodium Initiative. Nature 463, 763-768 (2010).

Effect of heavy-ionbeam irradiation on survival rates in sorghum

N. Satoh-Nagasawa,[*1] K. Asari,[*1] R. Itoh,[*1] N. Nagasawa,[*1] K. Yasuda,[*1] Y. Kobayashi,[*1] H. Takahashi,[*1] K. Sakurai,[*1] A. Watanabe,[*1] H. Akagi,[*1] Y. Hayashi, and T. Abe

Sorghum is the fifth most important grain crop worldwide based on tonnage, and it will continue to be of increasing importance because of the increased demand for limited freshwater supplies coupled with global climatic trends and expanding populations. This crop has extreme tolerance to low input levels, which is an essential trait for agriculture in hot and dry areas of the world. Moreover, the genome size of sorghum is relatively small, and its entire genome sequencing has recently been completed[1-3].

Agricultural field contamination with heavy metals is one of biggest issues worldwide. Previous studies have reported that sorghum (*Sorghum bicolor* L. Moench) is one of the species that is useful for phytoextraction because of its relatively high ability to absorb heavy metals along with its high biomass[4-6]. Phytoextraction refers to the uptake of contaminants from the soil by plant roots and their translocation to any harvestable plant part. The plant used for phytoextraction is one of the keys for its success[7, 8]. Thus, we are planning to create hyper heavy metal accumulator sorghum, which can uptake a considerable amount of heavy metals from the soil and translocate them from root to shoot by screening mutants.

In rice, several genes have been identified as important factors for uptake or translocation of heavy metals. Among them, *Oryza sativa* heavy metal P-type ATPase 3 (*OsHMA3*) is one of the most essential genes for cadmium translocation [9, 10]. In sorghum, homologous genes of *OsHMA3* have duplicated during evolution, and these genes can exist in tandem. Therefore, we have chosen heavy-ionbeams as the mutagen because of their ability to mutate relatively large regions in the genome.

Here, we report the effect of heavy-ionbeam irradiation on survival rates in the sorghum variety, BTx623. Dry seeds of BTx623 containing around 10% of water were irradiated by C-ion beams over a dose range of 75 to 125 Gy (LET: 22.6 keV/μm) and Ar-ion beams over a dose range of 5 to 25 Gy (LET: 283.9 keV/μm). The effect of each ion beam was observed 3 weeks after sowing by measuring the seed survival rates (Figs. 1, 2). From the obtained survival curves, the lethal dose 50 (LD_{50}) for dry seeds was estimated as approximately 80 Gy of C-ion irradiation and 16 Gy of Ar-ion irradiation. The Ar-ion beam had a stronger effect on the seeds than the C-ion beam possibly because the LET of Ar ions is higher than that of C-ions.

We will continue mutant screening for the abovementioned purpose along with checking the frequency of induced mutations.

*1 Department of Biological Production, Akita Prefectural University

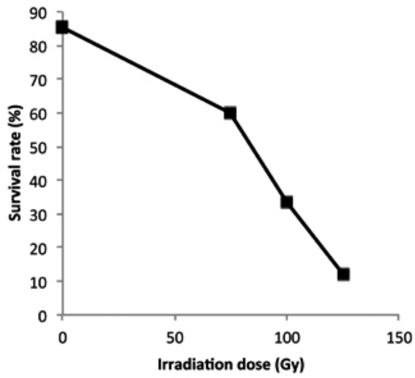

Fig. 1 Effect of C-ion beams on survival rate in BTx623, sorghum. (n = 4000 for 75 Gy and 100Gy, n = 3000 for 125 Gy)

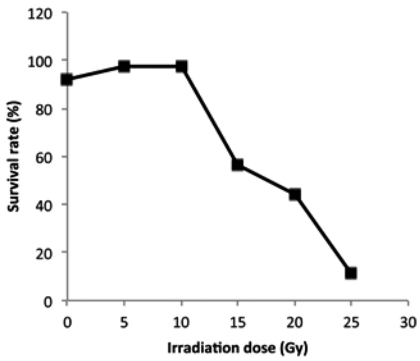

Fig. 2 Effect of Ar-ion beams on survival rate in BTx623, sorghum. (n = 72)

Acknowledgement

This work was supported by the Naito Foundation (N. S.-N.).

References

1) K. Arumuganathan and E.D. Earle: Plant Mol. Biol. Rep. **9**, 229 (1991).
2) A. H. Paterson et al.: Genome Research 15, p. 1643-1650 (2005).
3) A. H. Paterson et al.: Nature **457**, 551 (2008).
4) Y. J. An: Environ. Pollut. **127**, 21 (2004).
5) D. M. Kumawat and P.S. Dubey: Current Science **61**, 47 (1991).
6) L. Marchiol et al.: Plant Physiol. Biochem. **45**, 379 (2007).
7) A. Bhargava et al.: J. of Environ. Manage. **105**, 103 (2012).
8) U. Kraemer: Curr. Opin. Biotech. **16**, 133 (2005).
9) H. Miyadate et al.: New Phytol. **189**, 190 (2011).
10) D. Ueno et al.: Proc. Natl. Acad. Sci. **107**, 16500 (2010).

Deletion mapping of apomixis genomic region using irradiation with heavy-ion beams

M. Takahara,[*1] M. Ebina,[*1] R. Morita, Y. Kazama,[*2] T. Abe, T. Takamizo,[*1] and H. Nakagawa[*3]

Apomixis is an asexual mode of reproduction through seeds. It is widely observed among wild plant species but is almost completely absent among major crop species. Apomixis has the potential to provide great benefits through fixing hybrid vigor permanently in many crops such as maize. Therefore, we aimed to isolate the gene(s) controlling apomixis for application in major crops. Guinea grass (*Panicum maximum* Jacq.), a major tropical forage grass, has certain characteristics suitable for the study of apomixis. However, recombination is suppressed at the apomixis-controlling locus in guinea grass. To narrow down the apomixis-controlling genomic region, we have developed deletion mutants for this region by using irradiation with heavy-ion beams.[1), 2)] In the present study, we analyze deletion mutants with apomixis-specific sequence-tagged site (STS) markers, which were expected to be located in the apomixis-controlling genomic region.

Dry seeds of guinea grass (an apomictic cultivar "Natsukaze") were irradiated with $^{12}C^{6+}$ (23 keV/μm) ions at 300 and 400 Gy, $^{20}Ne^{10+}$ (63 keV/μm) ions at 150 and 200 Gy, and $^{56}Fe^{24+}$ (624 keV/μm) ions at 20 and 40 Gy.[2)] The M_2 plants generated from the seeds of M_1 plants were grown in a field. DNA was extracted from leaves, and subjected to the polymerase chain reaction (PCR) and amplified fragment length polymorphism (AFLP) analysis.

The mode of reproduction (apomixis or sexual) of each mutant line was analyzed by AFLP fingerprinting. In 22 lines (AM-1–22), all M_2 plants within a line showed the same AFLP pattern (Fig. 1A). This result indicated that these lines had maintained the apomixis mode of reproduction, although they had lost some apomixis-specific markers (Fig. 2). In contrast, two lines (SM-1, 2) showed different AFLP patterns between M_2 plants within a line (Fig. 1B), thereby suggesting that these two lines propagated with the sexual mode of reproduction. This result suggested that these sexual mutant lines lost the gene(s) crucial to apomixis. PCR analysis revealed that SM-1 lost two markers, and SM-2 lost only one marker (Fig. 2). However, it is possible that another deletion(s) that has not been detected is critical to the loss of the apomixis trait. Therefore, PCR analysis using more (over 100) STS markers co-segregated with apomixis is in progress. Moreover, the complete sequencing of this region by using a next-generation sequencer will reveal the exact deletion size for each mutant.

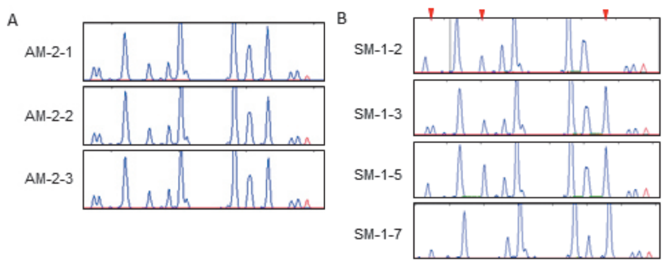

Fig. 1. AFLP patterns of three M_2 plants in the apomixis marker deletion line AM-2 (A) and four M_2 plants in the sexual mutant line SM-1 (B) detected by the ABI 3130xl capillary sequencer. The red arrows indicate different peaks between individuals. The vertical axis represents the intensity of the peaks, and the horizontal represents the relative size of the peaks.

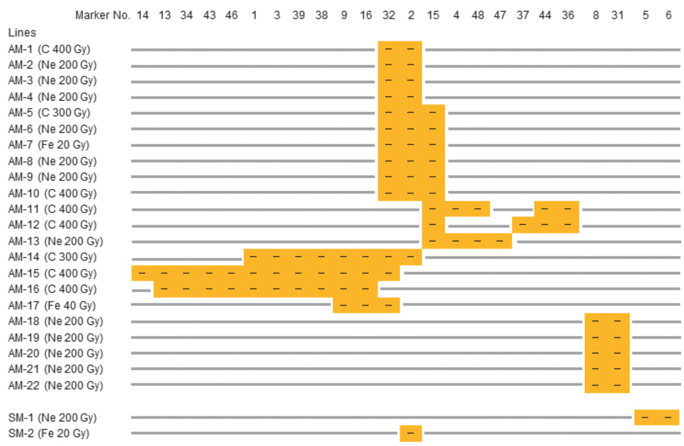

Fig. 2. Schematic results of PCR analysis using STS markers co-segregated with apomixis. The boxes with the minus symbols indicate the loss of markers in each mutant line.

*1 National Agriculture and Food Research Organization (NARO) Institute of Livestock and Grassland Science
*2 RIKEN Innovation Center
*3 Japan International Research Center for Agricultural Sciences (JIRCAS)

References

1) M. Takahara et al.: RIKEN Accel. Prog. Rep. **44,** 273 (2011).
2) M. Takahara et al.: RIKEN Accel. Prog. Rep. **45,** 215 (2012).

A DFR-deficient mutant of *Nicotiana tabacum* induced by C-ion beam irradiation†

Y. Kazama,*1 M.T. Fujiwara, H. Takehisa, S. Ohbu, H. Saito, H. Ichida, Y. Hayashi, and T. Abe

Tobacco (*Nicotiana tabacum* L.), a natural allotetraploid, is derived from the interspecific hybridization of ancestral *N. sylvestris* and *N. tomentosiformis*. Thus, at least two copies of every gene exist in the *N. tabacum* genome. In general, it is difficult to induce null mutants of tobacco owing to its amphidiploidy. Nevertheless, we have isolated three white flower mutants, *BY-4 white flower 1* (*bwf1*), *Xanthi white flower 1* (*xwf1*), and *Xanthi white flower 2* (*xwf2*). To reveal the mutation (s) induced in the allotetraploid genome, we have investigated one of the white flower mutants, *xwf1* (Fig. 1), which was induced by $^{12}C^{6+}$-ion beam irradiation (135 MeV/nucleon, 23 keV/μm) at a dose of 20 Gy.[1)]

To identify the gene(s) responsible for the white flower phenotype of *xwf1*, we utilized the information of the relevant genes of the anthocyanin biosynthetic pathway. We previously revealed that the petals of *xwf1* did not contain cyanidin, but instead contained the cyanidin precursors quercetin, kaempferol, and dihydrokaempferol. The data suggested that dihydroflavonol 4-reductase (DFR), anthocyanidin synthase (ANS), or flavonoid 3-O-glucosyltransferase (3GT) may be defective in the *xwf1* mutant. Southern blot analysis revealed that the *xwf1* mutant has a large deletion in one of the DFR gene (*DFR2*).[2)] Sequence analysis demonstrated that one copy of the DFR gene (*NtDFR2*) was absent from the genome of the *xwf1* mutant. The other copy of the DFR gene (*NtDFR1*) contained a single-base deletion resulting in a frameshift mutation, which is a spontaneous mutation in cv. Xanthi. These results revealed that both DFR genes were mutated in *xwf1*.

To examine if *NtDFR1* and *NtDFR2* were responsible for the white-flowered phenotype of *xwf1*, we performed transient transformation assays. *NtDFR1* and *NtDFR2* genes were introduced into the *xwf1* mutant by particle bombardment, and pigmentation in the petal cells was observed during the transient overexpression of these genes. The full-length cDNAs of *NtDFR1* and *NtDFR2* of cv. Xanthi were inserted downstream of the CaMV35S promoter. The resulting constructs (p35S-NtDFR1, p35S-NtDFR2) and p35S-YFP as an internal transformation control were co-coated onto gold particles and bombarded into petal limbs of *xwf1*. p35S-YFP-coated particles were also bombarded as a transformation control. After 72 h of incubation, we observed at least 1,000 epidermal cells in each bombarded petal limb, and successfully detected more than 100 YFP signals in all of at least 1,000 epidermal cells in each bombarded petal limb under a fluorescence microscope. Among them, pink spots were detected in every YFP-positive cell of the p35S-NtDFR2-introduced petal limbs (Fig. 2). In contrast, p35S-NtDFR1-introduced petal limbs did not show a pink color.[3)] These results indicate that anthocyanin formation in the *xwf1* mutant was complemented by the ransient expression of *NtDFR2* cDNA, but not by the transient expression of the spontaneously mutated *NtDFR1* gene. We also confirmed that the introduction of non-mutated *NtDFR1* successfully resulted in a pink color in petal limbs.[3)] These results suggested that the *NtDFR1* cDNA of cv. Xanthi encodes a non-functional protein.

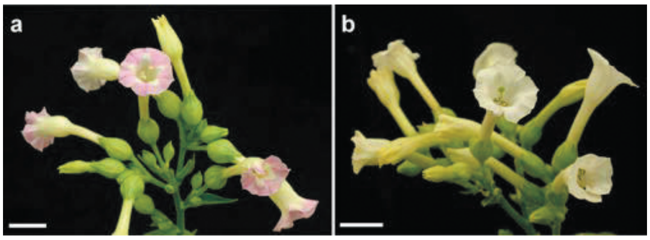

Fig. 1 Photographs of wild type tobacco cv. Xanthi (a) and white flower mutant (*xwf1*) (b). Bars = 1.5 cm.

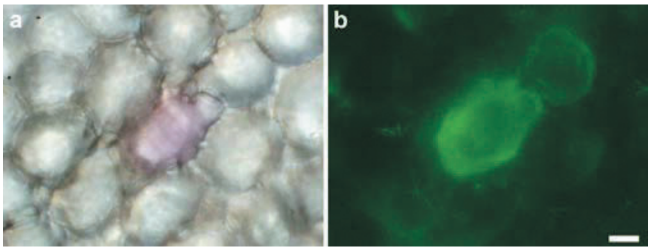

Fig. 2. Complementation test of *NtDFR2* gene in petal limbs of *xwf1* by particle bombardment. *NtDFR2* gene under the control of the CaMV35S promoter was introduced into the *xwf1* petal cells with an internal transformation control, that is, the *YFP* gene under the control of the CaMV35S promoter. After 72 h of incubation, the petal limb cells were observed under both the bright-field (a) and the fluorescence microscope (b).

References

1) Y. Kazama et al.: Plant Biotechnol. **25**, 105 (2008).
2) Y. Kazama et al.: RIKEN Accel. Prog. Rep. **42**, 280 (2009)
3) Y. Kazama et al.: Plant Cell Rep. **32**, 11 (2013).

† Condensed from the article in Plant Cell Rep. **32**, 11 (2013)
*1 RIKEN Innovation Center

A new early-flowering mutant line of strawberry cultivar ‘Satsumaotome’ induced by C-ion irradiation

Y. Takenoshita,[*1] M. Takemure,[*1] H. Saito and T. Abe

In modern Japan, the demand for strawberries increases sometime around Christmas. Although the strawberry cultivar ‘Satsumaotome’, which was developed in Kagoshima Prefecture, has large fruits and is of good quality, it is classified as a late-harvesting cultivar and cannot be harvested during the period of high demand. Therefore, we aimed to develop early-flowering mutants derived from ‘Satsumaotome’ by ion-beam irradiation. We estimated suitable doses of C-ion beams for irradiation on multiple-shoot cultures,[1)] and selected an early-flowering mutant line B0518.[2, 3)] We confirmed that B0518 was an early-flowering line whose fruits retained the excellent characteristics of ‘Satsumaotome’.[4)] Since we want to obtain mutants flowering earlier than B0518, we attempted individual selection and line selection from the population irradiated with ion beams in 2007.

In 2007, we irradiated C-ion beams (LET 23 keV/μm) at doses up to 40 Gy, targeting in-vitro cultured multiple buds derived from the shoot apex of ‘Satsumaotome’. After the irradiation, we cultured the multiple buds for mutant screening and finally obtained 384 nursery plants. In 2008, we selected 22 individuals from the 384 plants based on their flowering and fruiting habits. In 2009, we propagated the selected 22 individuals to 8 stocks respectively, and planted them in a field for line selection. We investigated the plant habits, day of flowering, size and shape of the fruits, and color of the fruit peel and flesh, and selected one promising line (B0701). From 2010 to 2011, we investigated the flowering and fruiting habits and yield of B0701 and B0518.

During the two-year observation from 2010-2011 in a greenhouse at Minamisatsuma in Kagoshima, the terminal inflorescence of B0701 flowered 6 days earlier than that of ‘Satsumaotome’, and 2 days earlier than that of B0518. The primary axillary inflorescence flowered 20–28 days earlier than that of ‘Satsumaotome’ and 1–4 days later than that of B0518 (Table 1). These characteristics of flowering showed similar tendency over the two years; therefore, we concluded that the early flowering characteristics of B0701 were stable.

The terminal inflorescences of B0701 were harvested earlier than that of ‘Satsumaotome’ and B0518 during the two years; as a result, the fruit yield of B0701 by December 31 increased by 7–30 kg/a than that of ‘Satsumaotome’, and increased by 12 kg/a than that of B0518. The fruit yield by February 29 increased 30–38 kg/a than that of ‘Satsumaotome’ and increased by 0–11 kg/a than that of B0518 (Tables 1 and 2).

In terms of the shape of the fruit, color of the peel, and color of the flesh, B0701 was identical to ‘Satsumaotome’ (data not shown).

From the results of this study, we confirmed that B0701 was an early-flowering and high-yielding line whose fruits retained the excellent characteristics of ‘Satsumaotome’. Thus far, we have obtained several early-flowering lines, and therefore, we concluded that ion beam breeding is effective for developing early-flowering mutant lines of the strawberry cultivar ‘Satsumaotome’.

Currently, we are conducting a performance test for the commercial production of B0701 in the production regions.

Table1. Flowering and harvest date of B0701 and B0518 in 2010-2011

Line・Cultivar	Terminal inflorescence				Primary axillary inflorescence			
	Flowering date[a]		Harvest date[b]		Flowering date[a]		Harvest date[b]	
	2010	2011	2010	2011	2010	2011	2010	2011
B0701	Nov.11	Nov.2	Dec.17	Dec.8	Dec.21	Dec.8	Feb.7	Jan.30
B0518	Nov.13	Nov.4	Dec.24	Dec.13	Dec.20	Dec.4	Feb.14	Feb.1
Satsumaotome	Nov.17	Nov.8	Dec.27	Dec.9	Jan.18	Dec.28	Feb.28	Feb.15

[a] Flowering date:50% of plants at first flower [b] Harvest date:20% of plants at first harvest

Table2. Fruit yield of B0701 and B0518 by December 31 and by February 29 in 2010-2011

Line・Cultivar	Fruit yield by December 31(kg/a)		Fruit yield by February 29(kg/a)	
	2010	2011	2010	2011
B0701	48±6.2	33±3.8	177±8.5	147±10.8
B0518	36±3.2	21±4.5	166±5.3	147±6.6
Satsumaotome	18±2.0	26±4.2	147±11.2	109±14.2

Values are means±S.D. (n = 20)

References

1) M.Ooe et al.: RIKEN Accel.Prog.Rep.**42**, 286 (2009)
2) Y.Takenoshita et al.: RIKEN Accel.Prog.Rep.**42**, 287 (2009)
3) Y.Takenoshita et al.: RIKEN Accel.Prog.Rep.**43**, 288 (2010)
4) Y.Takenoshita et al.: RIKEN Accel.Prog.Rep.**45**, 220 (2012)

*1 Kagoshima Prefectural Institute for Agricultural Development

Effects of heavy-ion beam irradiation on survival and growth rates in *Parachlorella kessleri*

S. Ota,[*1] T. Matsuda,[*1] T. Takeshita,[*1] T. Yamazaki,[*1] Y. Kazama,[*2] T. Abe and S. Kawano[*1]

Chlorella and *Parachlorella* species are freshwater unicellular algae belonging to Chlorophyta (green algae). Microalgae offer potentially renewable sources of biofuel that can be produced without compromising on the production of food[1)]. The *Chlorella* and *Parachlorella* species are characterized by their high growth rate, and thus, they are candidates for renewable sources for producing biodiesel[2)].

In our study, we tried to breed *P. kessleri* via heavy-ion beam irradiation. Very little is known about the effects of heavy-ion beam irradiation on microalgae. Thus, it may be important to report the survival curves and the effect on growth rates under heavy-ion beam irradiation. In this study, we plot the survival curves and study the growth of heavy-ion-beam-irradiated *P. kessleri* cells.

First, the survival rates were determined by a colony-forming unit (cfu) assay. Cells were irradiated by C ions (LET: 22.6 keV/μm), Ne ions (LET: 105 keV/μm), Ar ions (LET: 308 keV/μm) and Fe ions (LET: 788 keV/μm) with a dose range from 0 to 300 Gy. The heavy-ion-irradiated cells were spread onto TAP-agar plates in a petri dish (8.5 cm in diameter), and 1-2 week(s) later, the formed colonies were counted. Subsequently, the relative survival rates were calculated. The experiments were repeated three to five times. Among the heavy ions, Ar ions exhibited the most lethal activity (Fig. 1). At a dose of 100 Gy, the cfu dropped to nearly 0%, thereby indicating that the irradiated cells were lethally damaged by the Ar-ion beam. The Ne-ion beam also exhibited high lethal activity second only to the Ar-ion beam.

In the case of C- and Fe-ion beams, the survival curves exhibited gentler slopes than that those obtained with Ne/Ar ions (Fig. 1). Further, 17% and 31% of the irradiated cells still survived when subjected to a dose of 100 Gy of Fe and C ions, respectively. For irradiations stronger than 200 Gy, the cfu dropped to nearly 0% for C ions; however, in the case of Fe ions, some cells still survived at high doses. This result shows that the killing effect seems to be dependent on the beam's LET. However, the killing effect of the Fe-ion beam was less than that of the Ar-ion beams. One possible explanation for this result is the overkilling effect, and further studies are required to determine whether it is indeed overkilling.

Second, we employed a high-throughput screening method using 96-well microplates and a microplate reader (Viento nano; DS Pharma Biomedical, Tokyo, Japan). We spread the irradiated cells onto TAP-agar plates and extracted early-forming and/or large colonies and transferred them to a 96-well microplate (first plate screening efficiency: 10^{-2}). Next, potential mutants of high-growth were screened by optical density or visual inspection (second plate, screening efficiency: 10^{-2}). Finally, we determined the high-growth mutant from the second plate.

[*1] Department of Integrated Biosciences, Graduate School of Frontier Sciences, University of Tokyo
[*2] RIKEN Innovation Center

We compared the growth rate between the 0-Gy control and the C-ion 50-Gy irradiated strains after the first screening. We used the parameter μ to evaluate the growth rate, which is expressed as $\mu = \ln(OD_2/OD_1)/(T_2 - T_1)$[3)]. The parameter denotes the growth rate determined by optical density at 600 nm (OD_{600}) in a log-phase cell-cultivation time scale (T_2 - T_1 (days)). In this time interval, we measured the OD_{600} values of two-to-four-day-old cultures.

In the 96-well microplate assay, the heavy-ion beam irradiated population (C ion, 50 Gy) and the control population exhibited significantly different growth rates (Fig. 2). The irradiated population growth rate was overall faster than that of the control population, thereby indicating that heavy-ion-beam irradiation leads to a somewhat effective growth rate after the screening.

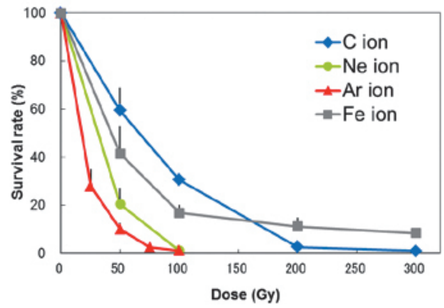

Fig. 1 Survival curves of *Parachlorella kessleri*. Cells were irradiated with C, Ne, Ar, and Fe ions, and colony formations were counted 1-2 weeks after spreading.

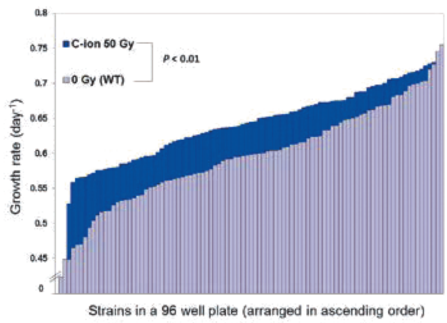

Fig. 2 Growth rate of non-irradiated (0-Gy control) and 50 Gy C-ion-beam-irradiated populations after the first screening. The p value was determined using the student's t test.

References

1) Chisti: Biotechnol. Adv. **26**, 126 (2007).
2) Přibyl et al.: Appl. Microbiol. Biotechnol. **94**, 549 (2012).
3) Levasseur et al.: J. Phycol. **29**, 587 (1993).

Effects of heavy-ion beam irradiation on gametophyte survival and sporophyte formation in *Undaria pinnatifida*

Y. Sato,[*1] T. Hirano,[*2] M. Yamaguchi,[*3] Y. Hayashi, N. Fukunishi, T. Abe

Undaria pinnatifida, called wakame in Japan, has a life cycle with alternating gametophytic and sporophytic generations (Fig.1). Since its full-scale cultivation occurred after 1955 and the methods progressed, the yield has increased rapidly.[1] Recently, however, the yield has been decreasing.[2] This decrease may be attributed to complex factors: changing environmental conditions, decreasing population of fisherman, unimproved productivity, etc. Consequently, the quality and price of *U. pinnatifida* have not been stable, and these situations have also decreased its market value. We think that breeding new cultivars with properties, such as high yield, high environmental adaptability, or high concentration of available contents for human health, is effective for improving the yield of *U. pinnatifida*.

RIKEN has developed a unique technology for mutation induction by heavy-ion beams.[3] In seaweed, red and green mutant strains of *Porphyra yezoensis* were established by heavy-ion irradiation to the gametophytic blades,[4] suggesting that heavy-ion mutagenesis will be an effective tool for genetic research and breeding in algae. Therefore, we started studying mutation breeding in *U. pinnatifida* by heavy-ion beams. As the first step, we irradiated the sporophylls with C-ion beams and analyzed the effects on gametophyte survival and sporophyte formation.

Sporophylls of *U. pinnatifida* were collected from Utatsu-Minato of Minami-Sanriku Cho in Miyagi prefecture. The pieces (3 cm × 3 cm) were excised from the sporophylls, cleaned by sterilized seawater and kept in a paper towel at 5°C for induction zoospores. After 12 hours, the pieces were packed in plastic dishes and irradiated with $^{12}C^{6+}$ ions at a dose of 0.5–25 Gy. After each dose of irradiation, the pieces were set on plastic dishes with sterilized seawater, and zoospores were induced. The zoospores were collected using a micropipette under a microscope and placed into the other plastic dishes with 30 ml sterilized seawater. The dishes were incubated at 20°C, photoperiod of 12 h/12 h (light/dark), and a light intensity of 20 µmol photons m^{-2} s^{-1}. Numbers of the germinated male and female gametophytes were counted after 2 weeks and 6 weeks of culture, and survival rate of the gametophytes was calculated by using eq. (1). The male and female gametophytes irradiated at a same dose were crossed, and formation rate of sporophytes was calculated by using eq. (2).

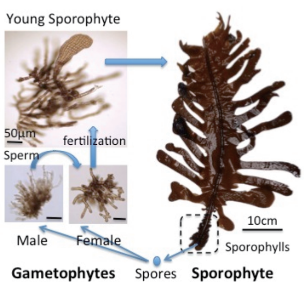

Fig.1 Annual life cycle of *U. pinnatifida*

Survival rate of male or female gametophytes = (number of gametophytes incubated after 6 weeks)/(that after 2 weeks) (1)

Formation rate of sporophytes after 6 weeks = (number of sporophyte)/(number of all female gametophytes) (2)

Most zoospores germinated by 2 weeks of culture but some germinated between 2 weeks and 6 weeks. Therefore, the survival rate of gametophytes at 5 Gy and less was occasionally over 100% (Fig. 2A). The survival rates of gametophytes decreased above 5 Gy: the survival rates of male gametophytes at 12.5 Gy and 25 Gy were 87.3% and 8.8%, respectively, whereas those of female gametophytes at 12.5 Gy and 25 Gy were 65.3% and 42.9%, respectively. The sporophyte formation in the female gametophytes showed higher sensitivity to the dose than the gametophyte survival (Fig. 2B). The formation rates were 53.3% at 5 Gy and 6.4% at 12.5 Gy. Moreover, there was no sporophyte at 25 Gy although the survival rate of female gametophytes was over 40%. These results indicate that in case of C-ion irradiation to the sporophyll, suitable dose for mutant screening in the sporophyte was less than 25 Gy. This range of dose is less than the suitable dose for *P. yezoensis* (25–150 Gy).[4] Currently, the sporophytes derived from the irradiated sporophylls are being cultured in a tank (patent pending) for mutant screening in M_1 generation and will be maintained until sporophyll formation to obtain zoospores for M_2 screening.

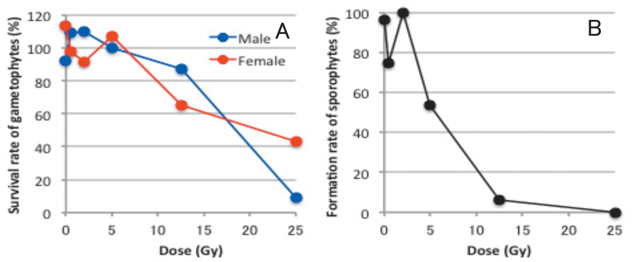

Fig.2 Survival rates of male and female gametophytes derived from sporophylls irradiated with C-ion beams (A). Formation rate of sporophytes in female gametophytes derived from sporophylls irradiated with C-ion beams (B).

References
1) R. Yamanaka and K. Akiyama: J. App. Phycol. 5, 249 (1993)
2) MAFF, Annual Statistics of Fishery and Fish Culture (2012)
3) T. Abe *et al.*: Plant Mutation Breeding and Biotechnology, edited by Q.Y.Shu, B.P.Forster, H.Nakagawa (Wallingford, Oxfordshire, 2012), p. 99.
4) K. Niwa *et al.*: Phycological Research 57(3),194–202 (2009)

*1 Riken Food Co.,Ltd
*2 Innovation Center, RIKEN
*3 Iwate Fisheries Technology Center

Verification of carbon ion dose distribution using VIPAR polymer gels

T. Maeyama, N. Fukunishi, K. L. Ishikawa,[*1] T. Furuta,[*2] K. Fukasaku,[*1,*3] S. Takagi,[*1] S. Noda,[*1*2] and R. Himeno[*1,*2]

An energetic heavy-ion beam has the advantages of a localized dose distribution and an enhanced radiobiological effectiveness in the Bragg peak region compared with X-rays and gamma rays. Exploiting these features, heavy-ion cancer therapy has established its effectiveness for solid cancers. For further sophistication of heavy-ion therapy, more accurate dose estimation methods than the pencil beam approximation now widely used are required to avoid unnecessary damage to healthy surrounding tissues. Particle transport simulations based on the Monte Carlo (MC) method are major candidates. We have developed a dose simulation code dedicated for medical use based on the particle transport code PHITS[1,2), and the accuracy of this MC method should be verified by experiments such as 3-dimensional (3D) gel dosimetry.

Gel dosimeters, including radiation sensitive chemicals, are nearly tissue-equivalent and are capable of imaging 3D dose distributions by using MRI because radiation-induced chemical products shift the relaxation time of proton nuclear magnetic resonance in gels. To verify the accuracy of dose distributions given by PHITS, a series of verification experiments was performed. VIPAR polymer gels were prepared following the prescription given by a Greece group[3)], and 135 MeV/u carbon beams accelerated by RIKEN Ring Cyclotron were used. MRI images of irradiated gels were obtained by 1.5-T MRI (Philips).

The experiment performed in April 2012 investigated the basic characteristic of PHITS by measuring one dimensional dose distributions, i.e. the Bragg curves, for chemically well-known tissue-equivalent phantoms (Kyoto Kagaku Co., Ltd.) and the gel dosimeters. Doses just behind the phantoms or the gels having different thickness were measured using a calibrated ionization chamber. We confirmed that, as expected, PHITS reproduced the measured Bragg curves well, and the peak position differences between the measured and the simulated Bragg curves were within 1 or 2 mm. In this experiment, the basic characteristics of gel dosimeters were also investigated. We confirmed that R_2 value, the inverse of the proton relaxation time (T_2) determined by MRI imaging, were precisely proportional to an irradiation dose up to 20 Gy for a given beam energy. Another important issue is the linear energy transfer (LET) dependence of R_2. As LET increases, radicals produced by heavy-ion irradiation contribute less effectively to R_2 because of enhanced recombination of radicals caused by increasing local ionization density. Hence, the LET dependence of R_2 should be calibrated. We measured a calibration curve of the dosimeter and found that R_2 for a given dose decreased to 30% of its low-LET value at the Bragg peak of carbon ions. This R_2 response as a function of LET was used to create R_2 maps in the following experiments.

In this experiment, gel dosimeters placed just behind complexly combined bone- and water-equivalent phantoms were also irradiated by $^{12}C^{6+}$ to investigate whether PHITS precisely predicted such geometrically complex dose distributions. The measured R_2 map shown in Fig. 1(a) was compared with the simulation shown in Fig. 1(b), in which the same horizontal and vertical scales were used. We found that a typical difference of R_2 was within 10%, and the differences in ion ranges were also less than 2 mm.

In the next experiments performed in September 2012 and January 2013, we examined the 3D dose distributions under a more complex condition. We set fowl meat in front of gel dosimeters as an example of a biological material and evaluated the dose distributions in the gels. Since the densities and chemical compositions of the biological material are unknown in this case and they were required in the dose simulation as input parameters, the prescriptions given by Shneider *et al.*[4)] were adopted. This relates the Hounsfield unit of biological material measured by X-ray CT to its chemical composition and density. Results of the comparison between the measured and simulated doses gave certain level of agreement, especially in the prediction of the ion ranges. The simulation reproduced the measured ranges within 2 mm.

Although more detailed investigations in the last experiment are required, the accuracy of the ranges confirmed in our experiments (1–2 mm) is much better than that of present radiotherapy[5)] (3 mm) and is close to the present high-definition MRI resolution (0.7 mm).

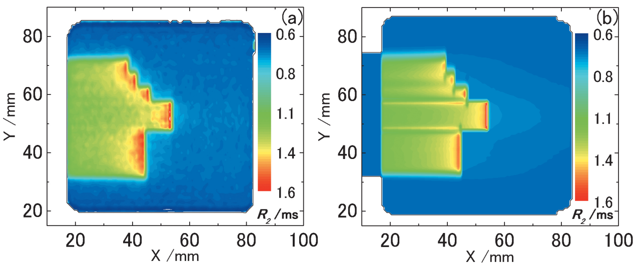

Fig. 1. Measured (a) and simulated (b) R_2 maps after irradiation of 20 Gy of $^{12}C^{6+}$ 135 MeV/u.

References

1) K. L. Ishikawa et al.: Prog. Nucl. Sci. Tech. 197 (2011).
2) T. Furuta et al.: IFBME Proceedings 39 (2012).
3) L. Petrokokkinos et al.: J Instrum. 4 (2009).
4) W. Schneider et al.: Phys Med Biol. 45 (2000).
5) O. Jakel et al.: Phys Med Biol. 46 (2001).

*1 RIKEN Computational Science Research Program
*2 RIKEN Advanced Center for Computing and Communication
*3 Dept. of neurosurgery, Himon'ya Hosapital

IV. OPERATION RECORDS

Program Advisory Committee meetings for nuclear physics and for material and life science

H. Ueno, K. Ishida, and H. Sakai

Two Program Advisory Committees (PACs) are responsible for reviewing the submitted proposals in the fields of nuclear physics (NP-PAC) and material and life science (ML-PAC). The NP-PAC is co-organized by the RIKEN Nishina Center (RNC) and the Center for Nuclear Study (CNS), the University of Tokyo. The NP-PAC reviews experimental programs at RIBF, whereas the ML-PAC reviews those at RAL and RIBF.

NP-PAC

The 11th NP-PAC meeting was held on June 18 and 19, 2012.[1] Two PAC members have been replaced after the previous meeting. At the meeting, nine new proposals and five re-submissions of previously discussed proposals that had been received were reviewed. In addition, a new experimental program to use CRIB was also described by the CNS director in accordance with a new guideline adopted after the suspension of the acceptance of CRIB proposals. Table 1 summarizes the outcome of the 11th NP-PAC meeting.

The 11th NP-PAC members are R. Tribble (Texas A&M, the chair), R.F. Casten (Yale Univ.), H. Emling (GSI), T. Glasmacher (MSU), M.N. Harakeh (KVI), M. Huyse (KU Leuven), T. Kishimoto (Osaka Univ.), M. Lewitowicz (GANIL), C.J. (Kim) Lister (UMass Lowell), T. Nakamura (Tokyo Tech.), T. Nakatsukasa (RNC), A. Ono (Tohoku Univ.), C. Scheidenberger (GSI), T. Shimoda (Osaka Univ.), F.-K. Thielemann (Univ. of Basel), M. Yahiro (Kyushu Univ.), and Y. Ye (Peking Univ.).

Table 1. Summary of the outcome of the 11th NP-PAC meeting. The sum of the proposals ranked with S and A is listed in the "approval" columns.

	11th NP-PAC (June 18–19, 2012)			
	proposal number		beam time (days)	
	request	approval	request	approval
GARIS (RILAC)	1	1	6	6
RIPS (RRC)	0	0	0	0
BigRIPS/ZDS	7	2	45.5	15
SHARAQ	0	0	0	0
SAMURAI	5	5	37.3	24.8
Construction	1	1	–	–
Total	14	9	88.8	45.8

ML-PAC

The 9th ML-PAC meeting was held on September 4 and 5, 2012.[2] The term of the ten PAC members were ended after the previous meeting, and nine members have been newly appointed. At the meeting, twenty-three RAL proposals and seven RIBF proposals received were reviewed. The summary of the outcome of the meeting is given in Table 2.

The 9th ML-PAC members are J.-M. Poutissou (TRIUMF, the chair), A. Amato (PSI), T. Azuma (RIKEN), S. Giblin (ISIS, RAL), R. Kadono (KEK), A. Kawamoto (Hokkaido Univ.), N. Kojima (Univ. of Tokyo), K. Kubo (ICU), D.E. MacLaughlin (UC Riverside), S. Maekawa (JAEA), P. Mendels (Univ. Paris-Sud Orsay), H. Yamase (NIMS), S. Yoshida (Yokohama City Univ.), and X.G. Zheng (Saga Univ.).

Table 2. Summary of the outcome of the 9th ML-PAC meeting.

	9th ML-PAC (September 4–5, 2012)			
	proposal number		beam time (days)	
	request	approval	request	approval
RAL	23	23	114	62
RIBF	7	6	52	26.5
Total	30	29	166	88.5

References
1) http://www.nishina.riken.jp/RIBF/NP-PAC/index.html
2) http://www.nishina.riken.jp/RIBF/ML-PAC/index.html

Beam-time statistics of RIBF experiments

H. Ueno and H. Sakai

This report describes the statistics of the beam times (BTs) utilized at the RIBF facility. In the following discussion, the BTs are categorized into two groups: high-energy-mode and low-energy-mode BTs. In the former, beams were delivered in the acceleration scheme of AVF, RILAC, or RILAC2 → RRC → (fRC → IRC →) SRC, where the accelerators in parentheses can be skipped in the cascade acceleration, depending on the beam used. In the latter, the acceleration scheme is AVF or RILAC (→ RRC).

BTs in the high-energy mode were scheduled for April–July and November–December in FY2012 considering the restriction of utility-power use, budgetary constraints, maintenance schedule of the accelerator system and the co-generation system and other constraints. In these BTs, the primary beams of ^{18}O, ^{48}Ca, ^{124}Xe, ^{70}Zn, and ^{238}U were delivered to users for $T_{\rm BT}$ = 77.7 days to conduct 14 experimental programs approved by the RIBF Program Advisory Committees[1]. In particular, the first SAMURAI[2] experiments, and the first and the following EURICA[3] experiments were performed as part of these BTs. It is noteworthy that $T_{\rm BT}$ = 77.7 days in FY2012 exceeds the 71.5 days achieved in FY2010. This improvement is due to the considerably improved stability of the accelerator system and an efficient BT schedule. Including $T_{\rm BT}$ = 20.2 days used by RIKEN for facility development programs, defined as machine study (MS) experiments, $T_{\rm BT}$ = 97.8 days was used in total for the experiments in the high-energy mode. The data summary of the high-energy mode BTs utilized in FY2012 is shown in Fig. 1 as a bar chart, where the total BTs provided for the users' experiments and those provided for the MS experiments are indicated by blue and orange bars, respectively.

The data summary of FY2012 BTs conducted in the low-energy mode is shown in Fig. 2. The BTs are classified by the accelerator operation modes AVF, RILAC, and RRC. Experiments in which the AVF or RILAC were operated in the stand-alone mode were conducted in parallel with the high-energy mode BTs. As seen in Fig. 2, the total low-energy mode BT in FY2012 was reduced by ~100 days compared with that in FY2011. This reduction is simply due to the fact that a series of long-term BTs on the Z = 113 experiment conducted under the RILAC stand-alone operation was completed on October 1, 2012. Except for this experiment, $T_{\rm BT}$ = 89 days was used for 68 experiments, which is more than $T_{\rm BT}$ = 75 days in FY2011.

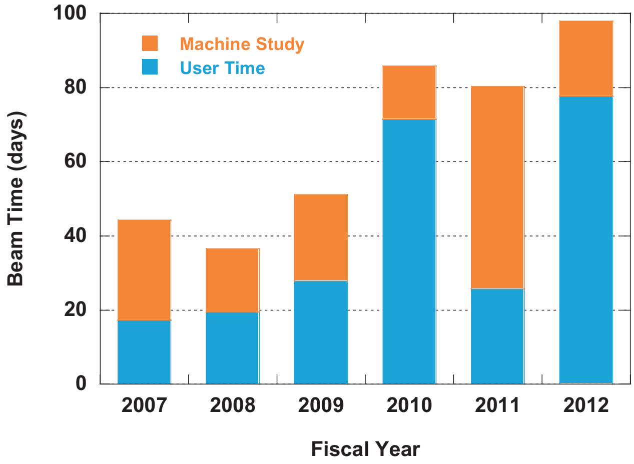

Fig. 1. Bar chart showing the BT statistics for high-energy-mode experiments from FY2007 to FY2012. The statistics of accelerator tuning time are not included. For details, see the text.

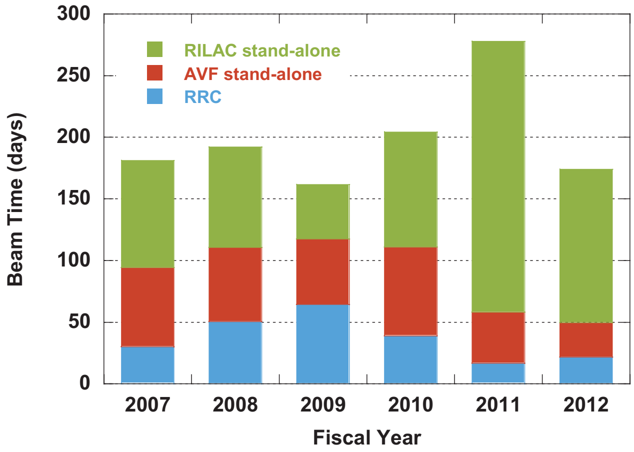

Fig. 2. Bar chart showing the BT statistics for low-energy-mode experiments from FY2007 to FY2012.

References

1) H. Ueno, K. Ishida, and H. Sakai: In this report.
2) K. Yoneda *et al.*: RIKEN Accel. Prog. Rep. **45**, i (2012).
3) S. Nishimura *et al.*: RIKEN Accel. Prog. Rep. **45**, x (2012).

Fee-based distribution of radioisotopes

T. Kambara, A. Nakao, A. Yoshida, H. Haba, J. Kanaya, Y. Wakitani, S. Yamamoto, and A. Ohtsubo

RIKEN distributes radioisotopes (RIs) produced at RIBF to users in Japan for a fee. This project was started in October 2007 in collaboration with the Japan Radioisotope Association[1)] (JRIA), which is an organization that has been established in order to support the utilization of RI in Japan. According to a material transfer agreement drawn between JRIA and RIKEN, JRIA mediates the transaction of the RIs and distributes them for a fixed fee to users. The distributed RIs are ^{65}Zn ($T_{1/2}$ = 244 days), ^{109}Cd ($T_{1/2}$ = 463 days), and ^{88}Y($T_{1/2}$ = 107 days).
The RIs have been produced by the RI Applications Team with 14-MeV protons from the AVF cyclotron. The ^{65}Zn, ^{109}Cd, and ^{88}Y nuclides are produced through the (p,n) reactions with natural Cu, Ag, and SrO targets, respectively. Recently, we examined nuclear reactions of ^{109}Ag$(d,2n)^{109}$Cd and ^{65}Cu$(d,2n)^{65}$Zn to produce ^{109}Cd and ^{65}Zn with a 24-MeV deuteron beam and found that the $(d,2n)$ reactions are more efficient and that the produced RIs have almost the same specific activities compared with the conventional (p,n) reactions.[2)] The RIs thus produced have sufficiently high quality for the fee-based distribution and both the reactions are currently being used for their production.

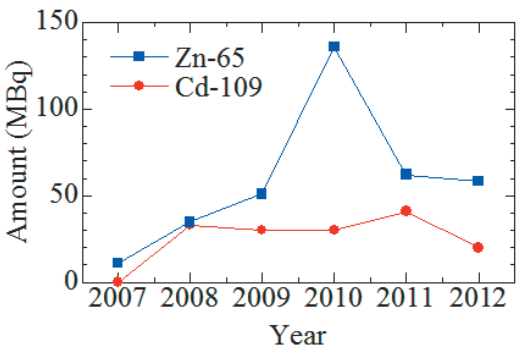

Fig. 1. Amounts of ^{65}Zn and ^{109}Cd distributed yearly from 2007 to 2012.

In 2012, we delivered two shipments of ^{109}Cd with a total activity of 20 MBq and 12 shipments of ^{65}Zn with a total activity of 58.4 MBq. The final recipients of the RIs were six universities and two research institutes. Compared with 2011, the amount of ^{109}Cd distributed in 2012 was about half (41 MBq in 2011) and the amount of ^{65}Zn was lower by about 6 % (62.1 MBq in 2011). Figure 1 shows the yearly trends in the amounts of the distributed RIs. Data on ^{88}Y have not been included because we have not accepted any relevant orders as yet.

The amount of distributed ^{65}Zn decreased after the earthquake that occurred on March 11, 2011, and it did not recover in 2012. The amount of ^{109}Cd that was distributed also decreased in 2012. We can speculate that the decrease in the demand is related to the Fukushima Dai-ichi Nuclear Power Plant accident that occurred after the earthquake, subsequent to which some of the user groups began to work on new projects and caused a decrease in the use of the RIs from RIKEN.

Information on the RIs can be obtained from JRIA through their dedicated website (https://www.j-ram.net/jram/DispatchTopPage.do; in Japanese), FAX (03-5395-8055), or E-mail (gyomu1@jrias.or.jp).

References
1) http://www.jrias.or.jp/ (Japanese), http://www.jrias.or.jp/e/ (English).
2) J. Kanaya et al.: in this report.

Electric power condition in Wako campus in 2012

T. Fujinawa, M. Kato, E. Ikezawa, H. Yamasawa and M. Kase

The monthly power consumption data for RIKEN Wako campus and RNC (RIKEN Nishina Center) and the energy supply by CGS[1] (Co-Generation System) are shown in Fig.1. The total annual data are listed in Table1. The total power consumption of RIKEN Wako campus in 2012 was 165,960 MWh, which was higher than that in 2011 by 10%. On the other hand, the total power consumption of RNC in 2012 was 82,599 MWh, which was higher than that in 2011[2] by 23%. The maximum power supply to Wako campus from TEPCO (Tokyo electric power corporation) reached 21.24 MW with a CGS output of 6.39 MW on June 28, 2012, when the RIBF experiments using the uranium (^{238}U) beam were conducted. The increased price of electricity, which was about 30% higher compared to of the previous year, resulted in a shortage of operation budget of RIBF accelerators.

We experienced instant voltage drops seven times: once in January due to trouble with TEPCO transmission lines, three times in April, and three times in September due to thunderbolts. The RIBF operations were not affected by the instant voltage drops.

We experienced earth-leakages thirty times of which three were in the RIBF building, and were a result of the contractor using poor electrical tools. The remaining were in the RING-LINAC substation with many ELBs trips. The causes are still under research by utility maintenance section.

According to the special offer by TEPCO, which aimed to reduce power consumption by no less than 30% between the hours of 13:00 to 17:00 on specific days. When the general power consumption was predicted to be very high, RIKEN successfully managed to reduce power consumption by 48% on average in the corresponding slots. There were 68 specific days in 2012 (before 2011, it was only 16 days), resulting in a large profit for RIKEN.

After March 11, the day of the earthquake, CGS continued nonstop operation till the end of the year. The periodic inspection of 8,000 hours scheduled in January 2012.The full overhaul of the gas turbine after 24,000 hours of operation is scheduled in the spring of 2013.

The performances of the absorption chillers are becoming worse year after year. The investigation was carried out in the spring and showed that repairs are necessary. One chiller was fully overhauled for renewal. Repair works for the remaining chillers are in progress by the manufacturer and will require time for completion.

Two sets of new CGSs in south area commenced commissioning test on November 2012. The CGS central control room of Nishina Center can monitor the electric output (MW) of new CGSs on time, but cannot evaluate the integrated value of electric energy (MWh). This makes it difficult for the RNC to know the total consumption of Wako campus

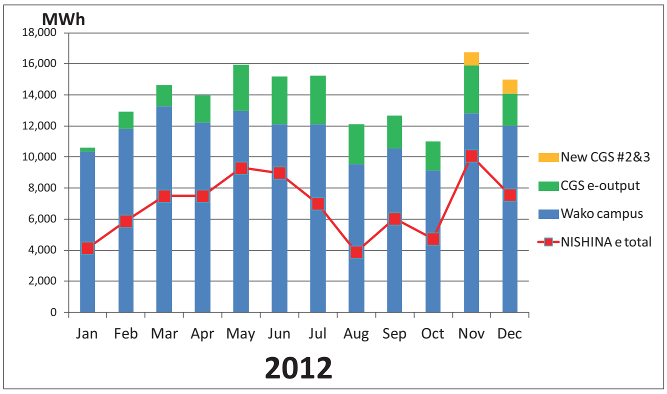

Fig.1 Electrical consumption in 2012

Table 1 Energy supply and consumptions in 2012

2012	Total	Unit	Note	% of 2011
Wako purchase	138,822	MWh	All Wako-campus electric power from TEPCO	120 %
Wako total	165,960	MWh	CGSs+TEPCO	110 %
RNC ele.	57,261	MWh	RNC electric power from TEPCO	178 %
CGS e-output	25,338	MWh	CGS electrical power output	72 %
RNC e total	82,599	MWh	RNC total electric power	123 %
CGS thermal	44,208	tons	RNC thermal power	98 %

Reference
1) T. Fujinawa and Y. Yano: Jpn. J. Particle Accel Society Vol.8, No.1, (18-25) 2011.
2) T. Fujinawa et. al : RIKEN Accel.Prog.Rep.45 (232) 2012.

Radiation safety management at RIBF

Y. Uwamino, H. Sakamoto, R. Hirunuma-Higurashi, H. Mukai, K. Tanaka, A. Akashio, T. Okayasu, H. Fukuda, S. Hashiguchi, S. Fujita, T. Yamaki, K. Nakano, H. Aiso, K. Igarashi and S. Iizuka

Residual radioactivity at the deflectors of the cyclotrons at RIBF (AVF, RRC, fRC, IRC, and SRC) has been measured regularly since 1986 when maintenance work was carried out, and the variations in the dose rates are shown in Fig. 1. The beam intensity of AVF has been increased since 2006 for radioisotope production, and the dose rate has also increased. Although the dose rate at RRC was usually around 20 mSv/h for 13 years after 1994, it has changed largely between 4 and 100 mSv/h since 2007. The dose rate of SRC rose in 2011, and it attained a value similar to those of AVF and RRC. The dose rates of IRC and fRC were measured in 2012, and they were found to be 0.7 mSv/h and 0.2 mSv/h, respectively.

The residual radioactivity was measured along the beam lines after almost every experiment. Points 1–23, marked with solid circles in Fig. 2, indicate the locations at which high dose rates were observed. Table 1 lists these dose rates and the measurement dates, beam conditions, and the decay periods after the end of facility operation. The maximum dose rate was found to be 90 mSv/h at location 21, which denotes the surface of the first quadrupole magnet after the BigRIPS target.

We continuously monitor the radiation in and around the RIBF facility by using neutron and gamma area monitors. It has been very difficult to measure the environmental gamma-ray dose because of the fallout due to the accident at the Fukushima Dai-ichi power station. The natural background radiation of gamma rays at the site boundary near the BSI East Bldg. was 0.039 μSv/h in January, 2011. It rose to 0.14 μSv/h on April 1, 2011, and decreased to 0.070 μSv/h on January 1, 2012, and to 0.062 μSv/h on January 1, 2013.

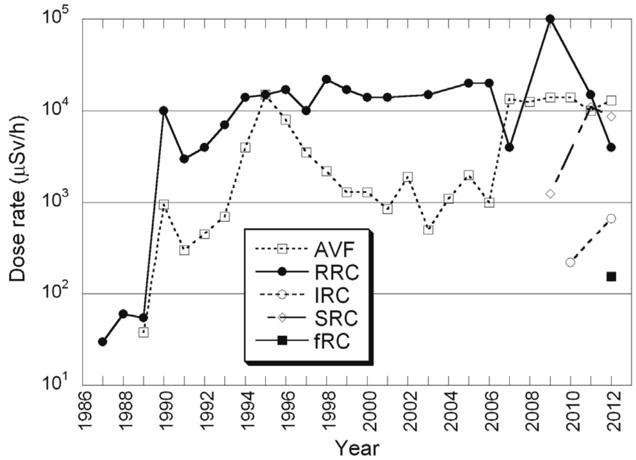

Fig. 1. Dose rates at the deflectors of five cyclotrons at RIBF.

Only the RIKEN linear accelerator, RILAC, was operated in August, 2012, and its contribution to the dose rate at the site boundary and at other facilities is negligibly small. Therefore, dose rates at this period were assumed to be due to natural background radiation at locations excluding the RILAC. The net accumulated dose, i.e., the dose excluding that of the background, at the site boundary was smaller than the detection limit, which was assumed to be 2 μSv/y for neutrons. The gamma-ray dose has always been smaller than the detection limit, which is about 8 μSv/y, if the neutron dose is not detected. The annual dose for 2012 was thought to be less than 10 μSv/y, which was considerably lower than the allowable limit (1 mSv/y).

Three monitors are placed at the boundary of the radiation-controlled area. One is positioned in the computer room of the Nishina building, and the other two are positioned on the roofs of the IRC and BigRIPS vaults of the RIBF accelerator building. The highest radiation dose value in 2012 was observed on the IRC roof as a result of beam loss at the transport line between the SRC and BigRIPS. The neutron dose was 42 μSv/y. The dose in the computer room was 4.1 μSv/y for neutrons. The dose on the BigRIPS roof was below the detection limit of 3 μSv/y for neutrons. The annual neutron dose at these locations since 1999 is shown in Fig. 3.

Table 1. Dose rates measured at beam lines in 2012. Points 1−23 indicate measurement locations shown in Fig. 2.

Point	Dose rate (μSv/h)	Date (M/D)	Particle	Energy (MeV/u)	Intensity (pnA)	Decay period (h)
1	310	1/4	Ne-22	110	1000	373
2	450	8/1	Rb-85	3.8	16	51
3	150	2/27	d	294	100	8
4	190	2/27	d	294	100	8
5	1700	4/20	O-18	230	500	18
6	250	2/27	d	294	100	8
7	90	1/4	Ne-22	110	360	376
8	880	1/4	Ne-22	110	360	376
9	250	2/27	d	294	100	8
10	250	2/27	d	294	100	8
11	85	7/25	U-238	50	39	199
12	600	4/20	O-18	230	430	17
13	700	4/20	O-18	230	430	17
14	3100	4/20	O-18	230	430	17
15	9000	7/25	Zn-70	345	100	293
16	160	7/25	Zn-70	345	100	293
17	90	7/25	Zn-70	345	100	293
18	130	4/20	O-18	230	430	18
19	360	7/25	Zn-70	345	100	293
20	85	1/4	Xe-124	345	10	388
21	90000	7/25	Zn-70	345	100	293
22	800	7/25	Zn-70	345	100	293
23	85	7/25	Zn-70	345	100	293

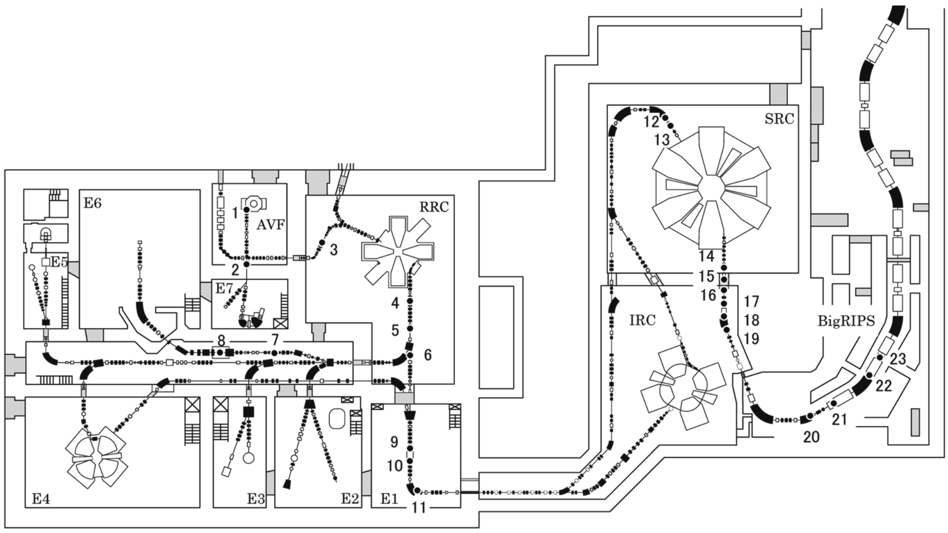

Fig. 2. Layout of beam lines at RIBF. Locations at which high dose rates were observed are indicated by solid circles labeled 1–23.

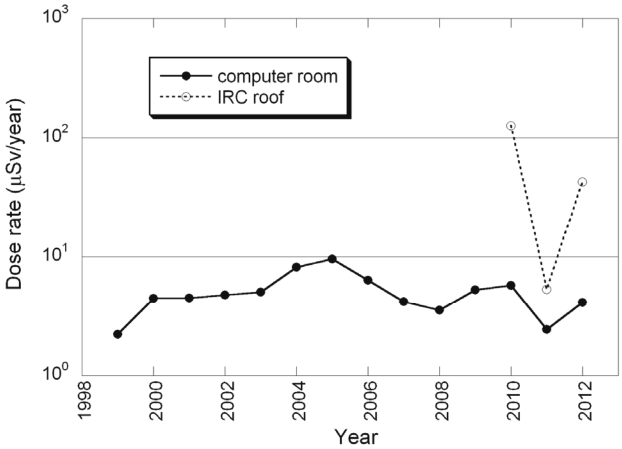

Fig. 3. Accumulated leakage radiation at the boundary of the radiation-controlled area.

The water used in the closed cooling systems at BigRIPS was sampled twice; the first sampling was carried out after facility operation with a 345-MeV/u 200-pnA (in average) ^{48}Ca beam in May and June, 2012, and the second sampling was carried out after facility operation with a 345-MeV/u 6.7-pnA ^{238}U beam in November and December, 2012. Radionuclide concentrations were measured by using a liquid-scintillation counter and a Ge detector. The results are shown in Tables 2 [A] and [B]. After facility operation with the intense ^{48}Ca beam, the summation of the ratios of the radionuclide concentrations to the prescribed limits for the drain water of all the radionuclides at the BigRIPS side-wall beam dump became larger than 1/10, and the water was dumped into the drain tank. This policy has been implemented to prevent contamination of the room in case of water leakage. The water in the drain tank, which contains drain water from other facilities, is released after confirming that the concentration of radionuclides is lower than the prescribed limit. This confirmation is required by law.

We are also responsible for safety at the Radioisotope Center, which is used not only by the personnel of the Nishina Center for Accelerator-Based Science but also by any researcher in the Wako campus. Researchers from the Brain Science Institute (BSI) are relocating to the Radioisotope Center, since the radioisotope handling facility of the BSI east building has been closed. The interiors of several rooms have been refurbished to accommodate these new researchers.

Table 2. Radionuclide concentrations in cooling water of BigRIPS, and the allowable limits for drain water, and the ratio of the concentration to the allowable limit.

[A] Water was sampled on June 24, 2012.

Cooling water	Nuclide	Concentration[a] (Bq/cm^3)	Limit[b] (Bq/cm^3)	Ratio to limit [a/b]
BigRIPS F0 target	H-3	3.6	60	6.0e-2[1)]
	Be-7	4.1e-3	30	1.4e-4
	Co-58	6.3e-4	1	6.3e-4
			summation	6.1e-2
BigRIPS exit beam dump	H-3	5.6	60	9.4e-2
	Be-7	2.6e-2	30	8.7e-4
			summation	9.4e-2
BigRIPS side-wall beam dump	H-3	8.6	60	1.4e-1
	Be-7	7.8e-3	30	2.6e-4
			summation	1.4e-1

[B] Water was sampled on January 9, 2013.

Cooling water	Nuclide	Concentration[a] (Bq/cm^3)	Limit[b] (Bq/cm^3)	Ratio to limit [a/b]
BigRIPS F0 target	H-3	3.3	60	5.5e-2
			summation	5.5e-2
BigRIPS exit beam dump	H-3	2.0	60	3.3e-2
	Be-7	7.6e-3	30	2.5e-4
	Co-57	1.2e-3	4	3.1e-4
	Co-58	2.7e-3	1	2.7e-3
	Co-60	5.7e-4	0.2	2.8e-3
	Mn-54	6.0e-3	1	6.0e-3
			summation	4.5e-2
BigRIPS side-wall beam dump	H-3	3.3	60	5.4e-2
	Co-57	3.5e-4	4	8.8e-5
			summation	5.4e-2

1) read as 6.0×10^{-2}

RILAC operation

E. Ikezawa, T. Ohki,*[1] M. Kase, T. Nakagawa, N. Sakamoto, H. Okuno, N. Fukunishi, M. Fujimaki, M. Nagase, T. Kageyama, M. Kobayashi-Komiyama, M. Kidera, Y. Higurashi, T. Watanabe, K. Yamada, T. Maie, H. Hasebe, H. Kuboki, K. Suda, Y. Watanabe, H. Imao, K. Ozeki, T. Aihara,*[1] H. Yamauchi,*[1] A. Uchiyama,*[1] K. Oyamada,*[1] M. Tamura,*[1] and O. Kamigaito

The RIKEN heavy-ion linac (RILAC) has been operating steadily throughout the reporting period and has been supplying various ion beams for various experiments. Some statistics regarding the RILAC operation from January 1 to December 31, 2012, are given in Table 1. The total beam-service time of the RILAC accounted for 91.6% of its operation time. The two operation modes of the RILAC, namely, the stand-alone mode and the injection mode, in which the beam is injected into the RIKEN Ring Cyclotron (RRC), accounted for 78.1% and 21.9% of the total beam-service time of the RILAC, respectively.

For the beam experiments of the RI Beam Factory (RIBF), a 2.695-MeV/nucleon ^{48}Ca-ion beam accelerated by the RILAC was injected into the RRC between April and June 2012.

Table 2 lists the beam-service times in the stand-alone mode of the RILAC allotted to each beam course in the RILAC target rooms in 2012. The e2 beam course in target room No. 1 was used in the machine study of a new gas-filled recoil ion separator (GARIS-Ⅱ). The e3 beam course in target room No. 1 was used in research experiments involving the heaviest elements and the study of the physical and chemical properties of these elements with the GARIS. The e4 beam course in target room No. 1 was used for radiation chemistry studies. The beam dump (DMe1) in target room No. 1 was used in a periodic inspection of the radiation facility.

This year, research experiments on the heaviest elements were carried out for 27 days from January through February, 36 days from March through April, 21 days from June through July, and 81 days from July through October.

Table 3 lists the operation time of the 18-GHz ECR ion source (18G-ECRIS) in 2012. Ion beams of the seven elements listed in the table were used for various experiments.

Table 1. Statistics on RILAC operation from January 1 to December 31, 2012.

Operation time of RILAC	5043.5	h
Mechanical trouble	250.3	h
Stand-alone RILAC	3608.4	h
Injection into RRC	1013.2	h
Total beam service time of RILAC	4621.6	h

Table 2. Beam service time of the stand-alone RILAC allotted to each beam course in target rooms No. 1 and No. 2 in 2012.

Beam course	Total time (h)	%
e2	58.0	1.6
e3	3431.5	95.1
e4	98.1	2.7
Beam dump (DMe1)	20.8	0.6
Total	3608.4	100.0

Table 3. Operation time of the 18G-ECRIS in 2012.

Ion	Mass	Charge state	Total time (h)
O	16	5	72.0
F	19	6	335.8
Ar	40	11	120.0
Ca	48	10, 11	1209.0
Zn	70	15	4404.8
Kr	86	16, 18	207.3
Xe	136	27	148.8
Total			6497.7

*[1] SHI Accelerator Service Ltd.

We carried out the following improvements and overhauls during the reporting period.

1) A data station system that was used as the front-end controller to remotely control the power supplies of RF systems No. 1, No. 2, No. 3, and No. 4 was replaced with a programmable logic controller.
2) In the RF systems, the power supplies that were in their final and intermediate stages of operation were subjected to annual inspection. In addition, the major components of mechanical parts were subjected to simple inspection.
3) Two water pumps of the water-cooling system for the RILAC cavities and vacuum pumps were overhauled. The other water pumps were subjected to simple inspection.
4) All cooling towers were subjected to monthly inspection and annual cleaning.
5) In the vacuum system of the RILAC cavities No. 3 and No. 4, a turbomolecular pump with a pumping speed for nitrogen of 2400 l/s located in each cavity was replaced with a cryogenic pump with a pumping speed for nitrogen of 5000 l/s. In addition, the vacuum control systems of these cavities were replaced with new ones.
6) All the turbomolecular pumps were subjected to annual inspection. The cryogenic pumps used for the FC-RFQ and the CSM cavities were overhauled.

We experienced the following mechanical problems during the reporting period.

1) In the No. 5 RF system, the contact fingers of the coaxial line supplying radio frequency (rf) power from the final amplifier to the power feeder had melted due to excessive rf current; therefore we repaired the coaxial line. In addition, the faulty part was replaced with a newly manufactured part.
2) Water was found to have splashed in the CSM-A4 cavity because of leakage from a cooling pipe on the outside wall of the cavity; therefore we repaired the pipe with a repair material as a stopgap measure.
3) A section of the cooling pipe of stem-2 in the FC-RFQ cavity had a vacuum leak; therefore we repaired the pipe with a repair material as a stopgap measure. In addition, the faulty part was replaced with a newly manufactured part.

Real time radiation monitoring of RIBF operations using ionization chambers

M. Nakamura, K. Yamada, A. Uchiyama,[*1] H. Okuno and M. Kase

In recent years, we have attempted to detect beam loss at the RIBF by using self-made ionization chambers (ICs).[1),2)] We input an alarm signal from the IC to the RIBF beam interlock system (BIS) and confirmed that this system can monitor the RIBF operations.[3)] However, there are some problems regarding selection of the alarm level.[3)] For selecting the level, we have to examine the calibration tests[2)] for every ion used in the RIBF. Such tests are rather consuming and now we are under investigation. Hence, from a different viewpoint, we propose that the IC signals can be applied for "real-time monitoring" of the RIBF operations.

In this report, we investigated seven ICs in SRC and one IC near the EDC in RRC. The position, size and experimental conditions of these ICs have been described in the previous reports.[1),2)] The input resistances of the AMPs for ICs in SRC and RRC were set at 1 GΩ and 10 GΩ, respectively. Yokogawa MX100 and MW100 data-loggers were used for monitoring the signal of the ICs in SRC and RRC, respectively. Assuming a quick response in the rapid RIBF operations, we collected ten data values in 1 s. The data loggers were fixed with 10 Hz noise filters. The signals from the loggers were sent to PCs in the RIBF control room. We investigated the monitoring of RRC and SRC operations, in which a $^{238}U^{86+}$ ion beam was accelerated at 345 MeV/nucleon.

A screenshot of the real-time monitoring of 7 ICs in SRC is shown in Fig. 1.

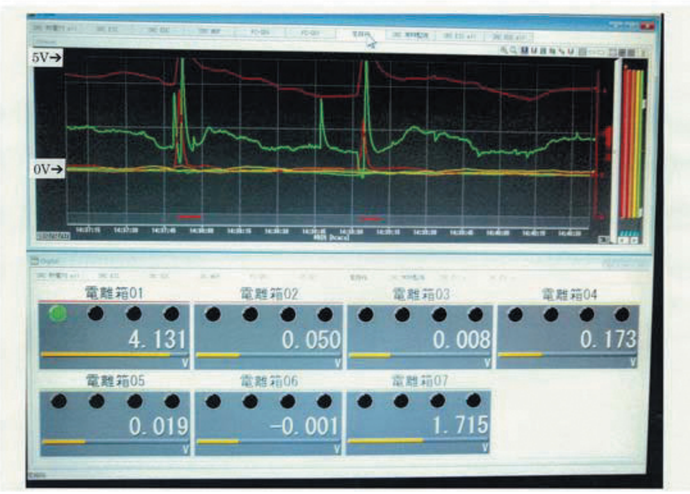

Fig. 1 A screenshot from one monitor in the RIBF control room, showing SRC operations.

In this screenshot, the upper part shows the time-profile of the 7 ICs signals and the lower part shows the real-time signal values. The maximum voltage in this profile was 5 V and the measurement time scale was 210 s. The signal intensity of the IC near the EDC was the strongest and these values sometimes exceeded 5 V. According to the GL800 data-logger[1)-3)], the maximum value of this signal was about 8−8.5 V. Other ICs signals were observed in the range of this picture. Through a comparison with the SRC operations in the RIBF control room, we confirmed that these data well reflected the SRC operation conditions.

Fig. 2 Screenshot from one monitor in the RIBF control room, showing RRC operations.

Figure 2 shows a screenshot of the real-time monitoring of the IC near EDC of RRC. The right side of this screenshot shows the time-profile of the IC signal and the left side shows the real-time signal value of the IC. The range of signal intensity was ±6 V and the time scale was 160 s. The maximum signal intensity was about 1.4 V. As shown in the figure, we observed a curve that occasionally fell below 0 V. This signal is assumed to contain certain unidentified noises from the RRC components, resulting in such a curve. However, through a comparison with the RRC operations in the RIBF control room, we could confirm that these data well reflected the RRC operation conditions.

These results indicate that many issues in the RIBF can be avoided by employing such real-time monitoring. Furthermore, we have incorporated the data for these ICs into the MyDaq system. Hence, we can compare data, such as, the intensity of magnetic fields, beam currents and voltages and can simulate the conditions in the RIBF.

References

1) M. Nakamura et al.: RIKEN Accel. Prog. Rep. 43, 138 (2009)
2) M. Nakamura et al.: RIKEN Accel. Prog. Rep. 44, 293 (2010)
3) M. Nakamura et al.: RIKEN Accel. Prog. Rep. 45, 228 (2011)

*1 SHI Accelerator Service Ltd.

Operation of SRC cryogenic system

H. Okuno, T. Dantsuka, Y. Mori,*[1] M. Ohshima,*[1] H. Hazama,*[1] A. Mikami,*[1] H. Shiba,*[1] T. Suzuki,*[1] K. Tezuka,*[1] K. Yamamoto,*[1] and S. Watanabe*[1]

The SRC cryogenic system, which consists of three compressors, a He refrigerator, and four He buffer tanks for cooling the 240-MJ superconducting magnets used for the SRC, has a cooling capacity of about 1 kW at 4.5 K and an inventory of 5000 l of liquid He. The cooling system was operated for around 8 months in 2012, with a three-month maintenance shutdown in summer (July–September) and a shutdown to conserve electrical power in January, as shown in Fig. 1. The trend observed for the main coil current of the SRC sector magnet is also shown in this figure. During system operation, no trouble was sufficiently major to stop the He refrigerator and the compressor. However, we continued operation despite the following problem. The cryogenic system had been suffering from a continuous helium gas leak since autumn, 2011. Figure 2 shows the total helium gas volume in the the buffer tank. The trend graph clearly shows its reduction in volume until the time of summer maintenance in 2013. The leak rate was about 300 m^3/month, and therefore, we needed to refill the helium gas once in two months. Despite our intensive hunts for the leak in the summer maintenance we could not find the leaks. However, we found the location of the leak whose rate increased immediately after we started making He gas flow in the current leads. The leak corresponding to the flow in the current lead led to the formation of a considerable amount of cold water vapor. Further investigation revealed that the O-rings containing indium (Fig. 3) were the reason for the leak. The system's heat cycle had caused the indium sealing to become loose. Torque checks of the bolts revealed that the bolts had come loose by about 0.5 mm. We have had no trouble in the operation of the He cooling system (Fig. 2) after we tightened the bolts using a torque wrench. We inferred that we could not find the leak during the summer maintenance because this leak does not appear when the current lead is warm.

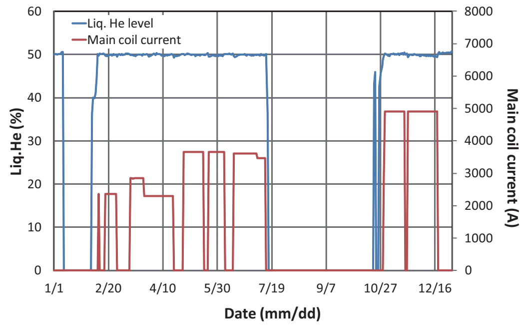

Fig. 1. Trend observed in liquid He level in the dewar and main coil current for the SRC superconducting sector magnet.

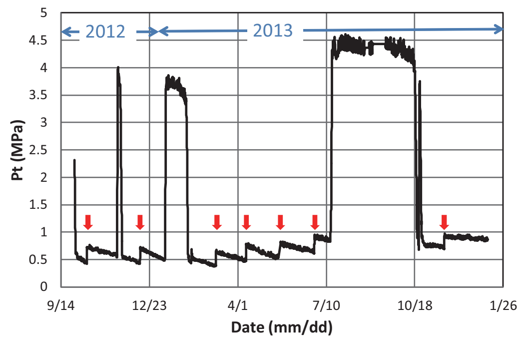

Fig. 2. Total helium gas volume in the buffer tanks. A pressure of 1 MPa corresponds to a volume of about 100 m^3. The red arrows indicate dates when the He gas was refilled to the He cooling system.

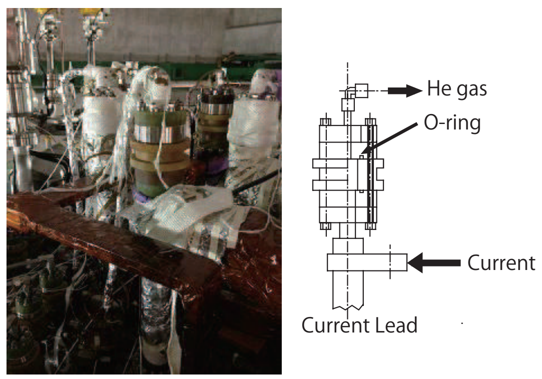

Fig. 3. Photograph and structural schematic of the current leads at which the leak occurred.

*[1] Nippon Kucho Service Co., Ltd

Present status of liquid-Helium supply and recovery system

T. Dantsuka, H. Okuno, M. Nakamura, T. Maie, K. Ikegami, M. Kase, S. Tsuruma,
M. Ohshima,[*1] Y. Tezuka,[*1] H. Hazama,[*1] and H. Shiba,[*1]

The liquid-helium supply and recovery system[1)], which can produce liquid helium at a rate of 200 L/h from pure helium gas, has been stably operated since the beginning of April 2001. The volumes of liquid helium supplied each year from 2001 to 2011 are shown in Fig. 1. The volume gradually increased from 2001 to 2008 but sharply increased in 2010, before decreasing sharply in 2011.

We extended the recovery pipe in the system at three places. First, a new recovery pipe was connected to the existing pipe at the Laser Science Laboratory at 1F and B1F. Next, new recovery pipes were connected to the existing pipe in the Main Research Building at B1F.

The purity of helium gas recovered from laboratories gradually improved once the construction of the system was completed. Currently, the impurity concentration in the recovered gas is rarely more than 200 ppm. The volume of helium gas recovered from each building in the Wako campus and the volume transported to the liquid-helium supply and recovery system were measured. The recovery efficiency, which is defined as the ratio of the amount of recovered helium gas to the amount of supplied liquid helium, was calculated. The recovery efficiency for the buildings on the south side of the Wako campus, such as the Cooperation Center building of the Advanced Device Laboratory, the Chemistry and Material Physics building, and the Nanoscience Joint Laboratory building, increased to more than 90%. The average recovery efficiency from January 2008 to July 2012 is shown in Fig. 2. This value also increased to over 90%.

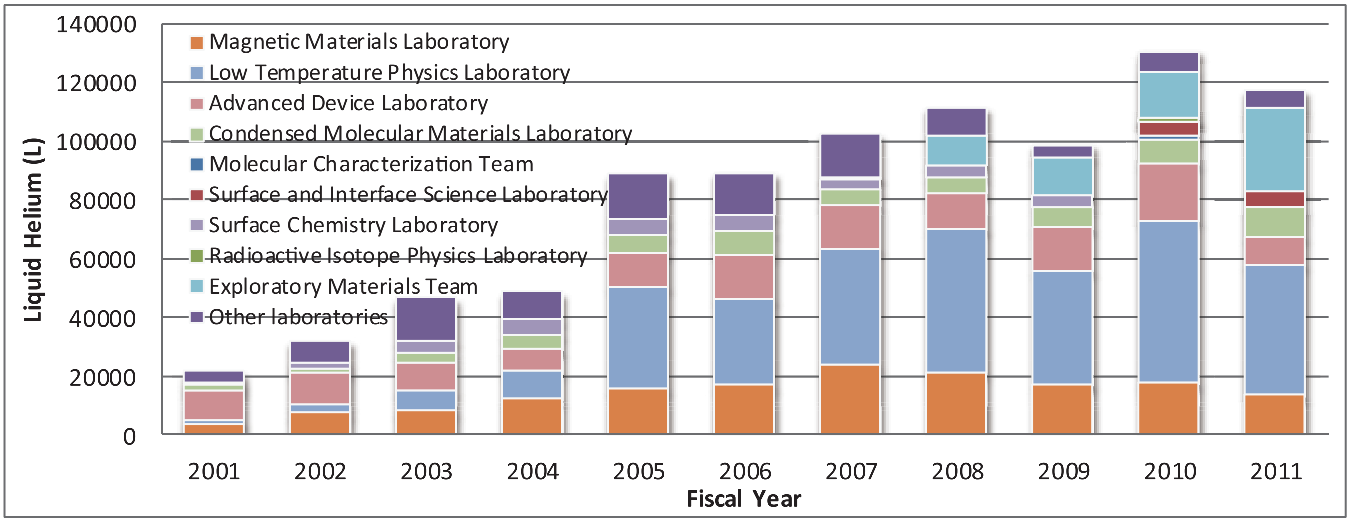

Fig.1. Volumes of liquid helium supplied to laboratories for each fiscal year from 2001 to 2011

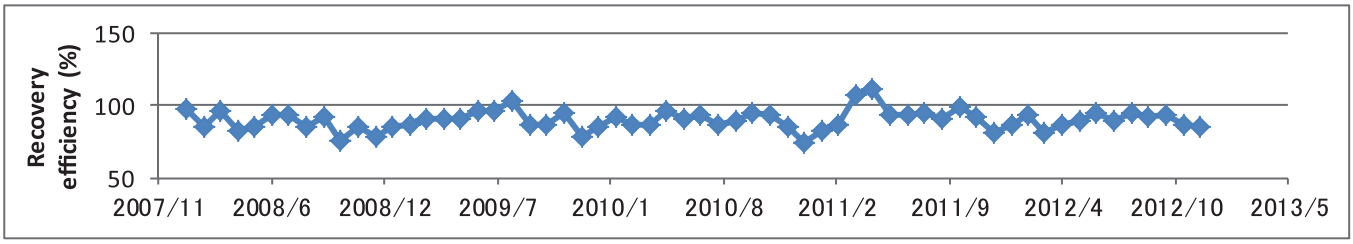

Fig.2. Average recovery efficiency measured from January 2008 to July 2012

*1 Nippon Air Conditioning Service K.K.

References

1) K. Ikegami et al.: RIKEN Accel. Prog. Rep. 34, 349 (2001).

V. ORGANIZATION AND ACTIVITIES OF RIKEN NISHINA CENTER (Activities and Members)

As of March 31, 2013

Organization Chart of Nishina Center for Accelerator-Based Science

- 理事長　野依 良治 / President RIKEN Ryoji Noyori
  - 理研仁科センターアドバイザリーカウンシル / Nishina Center Advisory Council
    - 理研BNLセンター評価委員会 / RBRC Scientific Review Committee (SRC) Meeting
    - RAL支所評価委員会 / Advisory Committee for the RIKEN-RAL Muon Facility
  - 理研BNLセンター管理運営委員会 / RBRC Management Steering Committee(MSC)
- 和光研究所長　小川 智也 / Director RIKEN WAKO Institute　Tomoya Ogawa
  - 基礎基盤研究推進部 / Advanced Research Promotion Division
    - 加速器研究推進課 / Accelerator-based Research Promotion Section
- 仁科加速器研究センター　延與 秀人 / Nishina Center for Accelerator-Based Science　Hideto En'yo
  - 理論研究担当　Theoretical Research
    - 副センター長：初田 哲男 / Deputy Director:Tetsuo Hatsuda
  - RIBF研究担当　RIBF Research
    - 副センター長：ウォルター・ヘニング / Deputy Director:Walter F. Henning
  - RIBF 施設共用コーディネーター：本林 透 / RIBF synergetic-use coordinator:Tohru Motobayashi
  - 特別顧問：矢野 安重 / Senior Advisor:Yasushige Yano
  - 特別顧問：石原 正泰 / Senior Advisor:Masayasu Ishihara
  - 共用促進委員会 / Scientific Policy Committee
  - 実験課題採択委員会 / Program Advisory Committee
  - 運営調整会議 / Coordination Committee
  - 安全審査委員会 / Safety Review Committee
  - マシンタイム委員会 / Machine Time Committee
  - 広報委員会 / Public Relations Committee

理論研究部門 / Theoretical Research Division

- 初田量子ハドロン物理学研究室　初田 哲男 / Quantum Hadron Physics Laboratory　Tetsuo Hatsuda
- 中務原子核理論研究室　中務 孝 / Theoretical Nuclear Physics Laboratory　Takashi Nakatsukasa
- 肥山ストレンジネス核物理研究室　肥山 詠美子 / Strangeness Nuclear Physics Laboratory　Emiko Hiyama
- 橋本数理物理学研究室　橋本 幸士 / Mathematical Physics Laboratory　Koji Hashimoto

素粒子物性研究部門 / Sub Nuclear System Research Division

- 延與放射線研究室　延與 秀人 / Radiation Laboratory　Hideto En'yo
- 岩崎先端中間子研究室　岩崎 雅彦 / Advanced Meson Science Laboratory　Masahiko Iwasaki
- 理研BNL研究センター　ニコラス・サミオス / RIKEN BNL Research Center　Nicholas P. Samios
  - 理論研究グループ　ラリー・マクラレン / Theory Group　Larry McLerran
  - 計算物理研究グループ　出渕 卓 / Computing Group　Taku Izubuchi
  - 実験研究グループ　秋葉 康之 / Experimental Group　Yasuyuki Akiba
- RAL支所　フィリップ・キング / RIKEN Facility Office at RAL　Philip KING

RIBF研究部門 / RIBF Research Division

- 櫻井RI物理研究室　櫻井 博儀 / Radioactive Isotope Physics Laboratory　Hiroyoshi Sakurai
- 上坂スピン・アイソスピン研究室　上坂 友洋 / Spin isospin Laboratory　Tomohiro Uesaka
- 森田超重元素研究室　森田 浩介 / Superheavy Element Laboratory　Kosuke Morita
- 玉川高エネルギー宇宙物理研究室　玉川 徹 / High Energy Astrophysics Laboratory　Toru Tamagawa
- 望月雪氷宇宙科学研究ユニット　望月 優子 / Astro-Glaciology Research Unit　Yuko Motizuki
- 加速器基盤研究部　上垣外 修一 / Accelerator Group　Osamu Kamigaito
  - 副部長：奥野 広樹（大強度化担当）/ 福西 暢尚（高安定化担当） / Deputy Director: Hiroki OKUNO (Intensity Upgrade), Nobuhisa FUKUNISHI (Stable and Efficient Operation)
  - 加速器高度化チーム　奥野 広樹 / Accelerator R&D Team　Hiroki Okuno
  - イオン源開発チーム　中川 孝秀 / Ion Source Team　Takahide Nakagawa
  - リニアックチーム　池沢 英二 / RILAC Team　Eiji Ikezawa
  - サイクロトロンチーム　坂本 成彦 / Cyclotron Team　Naruhiko Sakamoto
  - 運転技術チーム　福西 暢尚 / Beam Dynamics & Diagnostics Team　Nobuhisa Fukunishi
  - 低温技術チーム　奥野 広樹 / Cryogenic Technology Team　Hiroki Okuno
  - 加速器施設業務チーム　加瀬 昌之 / Infrastructure Management Team　Masayuki Kase
- 実験装置開発室　若杉 昌徳 / Instrumentation Development Group　Masanori Wakasugi
  - 低速RIビーム生成装置開発チーム　和田 道治 / SLOWRI Team　Michiharu Wada
  - 偏極RIビーム生成装置開発チーム　上野 秀樹 / Polarized RI Beam Team　Hideki Ueno
  - 短寿命核質量測定装置開発チーム　若杉 昌徳 / Rare RI-ring Team　Masanori Wakasugi
  - RI・電子散乱装置開発チーム　若杉 昌徳 / SCRIT Team　Masanori Wakasugi
- 実験装置運転・維持管理室　久保 敏幸 / Research Instruments Group　Toshiyuki Kubo
  - 超重元素分析装置チーム　森本 幸司 / GARIS Team　Kouji Morimoto
  - RIビーム分離生成装置チーム　吉田 光一 / BigRIPS Team　Koichi Yoshida
  - 多種粒子測定装置開発チーム　本林 透 / SAMURAI Team　Tohru Motobayashi
  - 情報処理技術チーム　市原 卓 / Computing and Network Team　Takashi Ichihara
  - 計測技術チーム　竹谷 篤 / Detector Team　Atsushi Taketani
- 応用研究開発室　阿部 知子 / Accelerator Applications Research Group　Tomoko Abe
  - 生物照射チーム　阿部 知子 / Radiation Biology Team　Tomoko Abe
  - RI応用チーム　羽場 宏光 / RI Applications Team　Hiromitsu Haba
- 共用促進・産業連携部　酒井 英行 / User Liaison and Industrial Cooperation Group　Hideyuki Sakai
  - 副部長：上野 秀樹（共用促進担当） / Deputy Director: Hideki UENO(User Support)
  - 共用促進チーム　上野 秀樹 / User Support Office　Hideki Ueno
  - 産業連携チーム　吉田 敦 / Industrial Cooperation Team　Atsushi Yoshida
- 安全業務室　上蓑 義朋 / Safety Management Group　Yoshitomo Uwamino

Members of Nishina Center for Accelerator-based Science

Executive Members

Hideto EN'YO (Director)
Walter F. HENNING (Deputy Director)
Tohru MOTOBAYASHI (RIBF synergetic-use coordinator)
Yasushige YANO (Senior Advisor)
Masayasu ISHIHARA (Senior Advisor)
Minami IMANISHI (Secretary)

Research Promotion Section Members

Shigeki ASAKAWA (Manager, Head of Accelerator-based Research Promotion Section)
Kyoji YAMADA
Hayato NISHIMURA
Yukari ONISHI
Masatoshi MORIYAMA
Yukiko SATO
Rie KUWANA
Yuko OKADA

Nishina Center's Committee Members

Nishina Center Advisory Council (NCAC) Members

not held

(Chair) Sydney GALES (GANIL, FRANCE)
Angela BRACCO (University of Milan, ITALY)
Wit BUSZA (MIT, USA)
Makoto INOUE (Kyoto University Research Reactor Institute)
Alexey KORSHENINNIKOV (Kurchatov Institute, RUSSIA)
Karlheinz LANGANKE (GSI, GERMANY)
Richard MILNER (MIT, USA)
Shoji NAGAMIYA (J-PARC Center)
Jean-Michel POUTISSOU (TRIUMF, CANADA)
WenQing SHEN (SINAP, P. R. CHINA)
Bradley SHERRILL (MSU, USA)
Tadashi SHIMODA (Osaka University)
Andrew TAYLOR (ISIS, UK)
Hiroshi TOKI (RCNP of Osaka University)
Robert TRIBBLE (Texas A & M University, USA)

Scientific Policy Committee Members

September, 2012

(Chair) Hirokazu Tamura (Tohoku University)
Yasuhiko FUJII (Comprehensive Research Organization for Science and Society)
Yoshiyuki FUJII (National Institute of Polar Research)
Shoji FUTATSUGAWA (Japan Radioisotope Association)
Ryutaro HIMENO (RIKEN)
Yujiro IKEDA (J-PARC)
Ryosuke KADONO (KEK)
Tadafumi KISHIMOTO (RCNP of Osaka University)
Tomofumi NAGAE (Kyoto University)
Hitoshi NAKAGAWA (National Agriculture and Food Research Organization)
Hideo OHNO (JASRI)
Takaharu OTSUKA (CNS)
Kazuo SHINOZAKI (RIKEN)
Hirohiko TSUJII (NIRS)
Akira UKAWA (University of Tsukuba)
Kazuyoshi YAMADA (KEK)
Masanori YAMAUCHI (KEK)

Program Advisory Committee meeting for Nuclear Physics Experiments at RI Beam Factory (NP-PAC) Members

June, 2012

(Chair) Robert TRIBBLE (Texas A & M University, USA)
Rick F. CASTEN (Yale University, USA)
Hans EMLING (GSI, GERMANY)
Thomas GLASMACHER (NSCL, MSU, USA)
Muhsin N. HARAKEH (KVI, NETHERLANDS)
Mark HUYSE (Instituut voor Kern- en Stralingsfysica, BELGIUM)
Tadafumi KISHIMOTO (RCNP, Osaka University, JAPAN)
Marek LEWITOWICZ (GANIL, FRANCE)
Christopher J. (KIM) LISTER (University of Massachusetts, Lowell, USA)
Takashi NAKAMURA (Tokyo Institute of Technology, JAPAN)
Takashi NAKATSUKASA (RIKEN, JAPAN)
Akira ONO (Tohoku University, JAPAN)
Christoph SCHEIDENBERGER (GSI, GERMANY)
Tadashi SHIMODA (Osaka University, JAPAN)
Friedrich-K. THIELEMANN (University of Basel, SWITZERLAND)
Masanobu YAHIRO (Kyushu University, JAPAN)
Yanlin YE (Peking University, P. R. CHINA)

Program Advisory Committee meeting for Materials and Life Science Researches at RIKEN Nishina Center (ML-PAC) Members

September, 2012

(Chair) Jean-Michel POUTISSOU (TRIUMF, CANADA)
Alex AMATO (PSI, SWITZERLAND)
Toshiyuki AZUMA (RIKEN, JAPAN)
Sean GIBLIN (RAL, STFC, UK)
Ryosuke KADONO (KEK, JAPAN)
Atsushi KAWAMOTO (Hokkaido University, JAPAN)
Norimichi KOJIMA (University of Tokyo, JAPAN)
Kenya KUBO (ICU, JAPAN)
Douglas E. MACLAUGHLIN (University of California, Riverside, USA)
Sadamichi MAEKAWA (JAEA, JAPAN)
Philippe MENDELS (Laboratorie de Physique des Solides - Universite Paris-SUD, FRANCE)
Hiroyuki YAMASE (NIMS, JAPAN)
Shigeo YOSHIDA (Yokohama City University, JAPAN)
Xu-Guang ZHENG (Saga University, JAPAN)

Industrial Program Advisory Committee (In-PAC) Members

June, 2012

(Chair) Akihiro IWASE (Osaka Prefecture University)
Toshiyuki AZUMA (RIKEN)
Kenya KUBO (International Christian University)
Toshinori MITSUMOTO (Sumitomo Heavy Industries, Ltd.)
Hitoshi NAKAGAWA (Japan International Research Center for Agricultural Science)
Nobuhiko NISHIDA (Tokyo Institute of Technology)

Theoretical Research Division
Quantum Hadron Physics Laboratory

1. Abstract
Atomic nuclei are made of protons and neutrons bound by the exchange of Yukawa's pion and other mesons. Also, protons and neutrons are made of quarks bound by the exchange of gluons. These strong interactions are governed by the non-Abelian gauge theory called the quantum chromodynamics (QCD). On the basis of theoretical and numerical analyses of QCD, we study the interactions between the nucleons, properties of the dense quark matter realized at the center of neutron stars, and properties of the hot quark-gluon plasma realized in the early Universe. Strong correlations common in QCD, graphene and cold fermionic atoms are also studied theoretically.

2. Major Research Subjects
(1) Origin of the nuclear force
(2) Theory of spontaneous symmetry breaking
(3) Non-perturbative study of supersymmetric quantum field theories
(4) Physics of particles with resonant interactions
(5) QED calculation of the lepton anomalous magnetic moments

3. Summary of Research Activity

(1) Lattice Nuclear Force

Three-nucleon forces (3NF) have been studied in lattice QCD. The enormous computational cost is drastically reduced (by a factor of 192) by developing a new algorithm (the unified contraction algorithm). The results with time-dependent HAL QCD method indicates that repulsive 3NF exists at short distance in the triton channel.

(2) Theory of spontaneous symmetry breaking

Generalization of the Nambu-Goldstone theorem The general counting rule for Nambu-Goldstone modes is derived using Mori's projection operator method in non-Lorentz invariant systems at zero and finite temperatures. The number of Nambu-Goldstone modes is equal to the number of broken charges, Qa, minus half the rank of the expectation value of [Qa; Qb].

(3) Non-perturbative study of supersymmetric quantum field theories

Although the supersymmetry is widely believed to play a fundamental role in elementary particle physics beyond the standard model, non-perutbative formulation of supersymmetric field theories remains quite difficult. On this long-standing problem in theoretical elementary particle physics, I made the following contribution In this fiscal year: (1) By using the generalized BRS transformation, I clarified a mechanism that forbids the appearance of a cubic-fermion anomaly in the supersymmetic Ward-Takahashi relation in lattice formulations of the four dimensional N=1 supersymmetric Yang-Mills theory. (2) On the basis of the structure of the Ferrara-Zumino supermultiplet, I constructed the energy-momentum tensor in lattice formulations of the four dimensional N=1 supersymmetric Yang-Mills theory that is conserved in the quantum continuum limit. It is expected that physical quantities in the four dimensional N=1 supersymmetric Yang-Mills theory, which are related to the energy-mementum tensor, can be computed by using this non-pertubative construction.

(4) Physics of particles with resonant interactions

The Efimov effect that arises for three particles with resonant interactions has been investigated numerically for atoms. The three-body parameter that characterizes the Efimov effect has been shown to originate from a nonadiabatic deformation of the three-atom system near their van der Waals radius. This explained the observed relation between the Efimov three-body parameter measured in ultra-cold atomic experiments and the van der Waals radius.

(5) QED calculation of the lepton anomalous magnetic moments

All QED contributions up to the tenth order of perturbation theory to the anomalous magnetic moments of electron and muon have been determined. The contribution from the tenth-order diagrams without a fermion loop has been finally determined after serval years of extensive numerical work on RIKEN's supercomputer systems. This leads the best precise values of theoretical predictions of the muon and electron anomalous magnetic moments and the fine structure constant.

Head
Tetsuo HATSUDA

Members
Hiroshi SUZUKI
Takumi DOI
Yoshimasa HIDAKA
Pascal Raphaël Gabriel NAIDON

Special Postdoctoral Researchers
Daisuke KADOH
Arata YAMAMOTO
Kanabu NAWA
Yuji SAKAI

Foreign Postdoctoral Researchers
Michael Gordon ENDRES
Gergely Peter FEJOES

Contract Researchers
Makiko MATSUKAWA
Yoichi IKEDA

Visiting Scientists
Motoi TACHIBANA (Faculty of Science and Engineering, Saga University)
Toichiro KINOSHITA (Physics Department, Cornell University)
Sinya AOKI (Center for Computational Sciences, University of Tsukuba)
Taichi KAWANAI (Graduate School of Science, University of Tokyo)
Ryoichi SEKI (Physics Department, California State University)
Masahito UEDA (Graduate School of Science, University of Tokyo)
Tatsuyuki TAKATSUKA (Faculty of Humanities and Social Science, Iwate University)
Hong MAO (Hangzhou Normal University, China)
Sho OZAKI (Yonsei University, Korea)
Takashi OKA (Graduate School of Science., University of Tokyo)
Shoichi SASAKI (Graduate School of Science, Tohoku University)
Andreas IPP (Vienna University of Technology, Austria)
Keitaro NAGATA (Information Media Center, Hiroshima University)
Takashi INOUE (College of Bioresource Science, Nihon University)
Yoshitaka HATTA (Graduate School of Pure and Applied Science, University of Tsukuba)
Teiji KUNIHIRO (Graduate School of Science, Kyoto University)
Kenji MORITA (Yukawa Institute for Theoretical Physics, Kyoto University)
Kazuyuki KANAYA (Graduate School of Pure and Applied Science University of Tsukuba)
Makoto TAKIZAWA (Showa Phamaceutical University)
Sachiko TAKEUCHI (Faculty of Social Welfare, Japan College of Social Work)

Visiting Researcher

Takashi SANO (Japan Society for the Promoation of Science)

Research Consultant

Hiroshi TOKI (RCNP, Osaka University)

International Program Associates

Nino BRATVIC (Phys. Dep., Technical Univ. Munich)
Fukun XU (Chinese Academy of Science)

Student Trainees

Bruno CHARRON (Graduate School of Science, University of Tokyo)
Akihiko MONNAI (Graduate School of Science, University of Tokyo)
Yasufumi ARAKI (Graduate School of Science, University of Tokyo)
Yuji HIRONO (Graduate School of Science, University of Tokyo)
Yusuke HAMA (Graduate School of Science, University of Tokyo)
Tomoya HAYATA (Graduate School of Science, University of Tokyo)
Yasuki TACHIBANA (Graduate School of Science, University of Tokyo)
Koichi MURASE (Graduate School of Science, University of Tokyo)
Kota MASUDA (Graduate School of Science, University of Tokyo)
Masaru HONGO (Graduate School of Science, University of Tokyo)
Yuya TANIZAKI (Graduate School of Science, University of Tokyo)
Ryuichi KURITA (Graduate School of Science, University of Tokyo)
Sho KAMATA (Graduate School of Science, Rikkyo University)
Masanori YAMADA (Graduate School of Pure and Applied Science, University of Tsukuba)

Secretaries

Yoko FUJITA
Yuri TSUBURAI
Kayo YAMAJI

Theoretical Research Division
Theoretical Nuclear Physics Laboratory

1. Abstract

Nuclei are finite many-particle systems composed of protons and neutrons. They are self-bound at the femtoscale (10^{-15} m) by the strong interaction (nuclear force), the study of which was pioneered by Hideki Yukawa. The uncommon properties of the nuclear force (e.g., repulsive core, spin–isospin dependence, tensor force) prevent complete microscopic studies of nuclear structure. A number of unsolved problems remain even at present. In addition, radioactive beam facilities reveal novel aspects of unstable nuclei. We are tackling these old problems and new issues in theoretical nuclear physics, developing new models and pursuing large-scale calculations of quantum many-body systems. We are also strongly involved in research on other quantum many-body systems to resolve mysteries in quantum physics

2. Major Research Subjects

(1) Nuclear structure and quantum reaction theories
(2) First-principle calculations with density functional theory (DFT) for many-fermion systems
(3) Computational nuclear physics

3. Summary of Research Activity

(1) Regularized multireference energy density functional calculations with new Skyrme parametrizations

Symmetry restoration and configuration mixing using the generator coordinate method based on energy density functionals, referred to as the multireference approach, has become widely used in studies of low-energy nuclear structure. It was recently pointed out that these techniques are ill defined for standard Skyrme energy density functionals, and the results can exhibit discontinuities or even divergences in the energy. Thus, a regularization procedure has been proposed to remove such spurious contributions to the energy. This regularization procedure, however, imposes the use of integer powers of the density for the density-dependent terms in the energy density functionals.

Therefore, we constructed new Skyrme parametrizations that have integer powers of the density dependence for multireference energy density functional calculations with the regularization procedure. The reproduction of the experimental binding energies and charge radii for a wide range of singly magic nuclei is significantly improved. With our new Skyrme parametrizations, we performed regularized multireference calculations for a systematic study of the spectroscopic properties of Mg isotopes. A good description of the $B(E2:0^+ \rightarrow 2^+)$ values was obtained. However, the first 2^+ energies are overestimated for all the isotopes. One of the reasons for this overestimation could be the neglect of time-odd terms when calculating the Hamiltonian kernel.

(2) Mean-field calculation including proton–neutron mixing

We have been developing a new code for Hartree–Fock (HF) calculation based on nuclear DFT including arbitrary mixing between protons and neutrons. This is a first step toward DFT calculation including proton–neutron (p–n) pairing. To treat the p–n pairing within the DFT framework, one needs to generalize the quasiparticle states as mixtures of protons and neutrons. In connection with this extension, the density functionals should also be extended to those with mixing between protons and neutrons. As a first step toward p–n pairing, we performed HF calculations (without pairing correlation) including p–n mixing. The isospin of the system is controlled by a linear constraint on the isospin (called the isocranking term). We made test calculations for A = 14 and 48 isobars. For A = 14 isobars, we calculated the energies of the well-known isobaric analog states (IASs) with T = 1 in ^{14}C, ^{14}N, and ^{14}O. We found that the IAS with T_z = 0 is described well as a state consisting of single-particle states with p–n mixing. For A = 48 isobars, we found that we can obtain states with different values of T and T_z by adjusting the isocranking frequency. We also implemented in our code an improved method for optimization with constraints, known as the augmented Lagrange method, which is widely used in quantum chemistry. This can be used, e.g., for calculating the excitation energies for high-isospin states in a single nucleus, from which we can evaluate the nuclear symmetry energy.

(3) Microscopic study of the shape transition in chromium isotopes around N = 40

We investigated the nature of the quadrupole collectivity in the low-lying states of neutron-rich chromium isotopes, $^{58–66}$Cr, by solving the five-dimensional (5D) collective Schroedinger equation. We determined the vibrational and rotational inertial functions and the collective potential in the 5D quadrupole collective Hamiltonian microscopically derived using the constrained Hartree–Fock–Bogoliubov plus local quasiparticle random phase approximation (RPA) method, which we proposed recently. The results of the calculation are in good agreement with the available experimental data and suggest that remarkable prolate deformation develops in the chromium isotopes around N = 40. However, the results also indicate that they still possess transitional characteristics, and large-amplitude shape fluctuations dominate in their low-lying states. We also discussed the similarities and dissimilarities of the quadrupole shape transition near ^{64}Cr with $N = 40$ and that near ^{32}Mg with $N = 20$.

(4) Relativistic Slater approximation for Coulomb exchange effects
The relativistic local density approximation (LDA) for the Coulomb exchange functional in nuclear systems is presented. This approximation consists of the well-known Slater approximation in the non-relativistic scheme and the corrections due to the relativistic effects. The validity of the relativistic LDA in finite-nuclei calculations is examined by comparing it with the results of the relativistic Hartree–Fock–Bogoliubov theory, where the non-local Coulomb exchange term is treated exactly. The relative deviations of the Coulomb exchange energies in the relativistic LDA calculations are in general less than 5% for semi-magic Ca, Ni, Zr, Sn, and Pb isotopes from the proton drip line to the neutron drip line. It is also worth emphasizing that the relativistic corrections to the LDA are found to play substantial roles in improving the agreement with the exact results by 3%~5%.

(5) Feasibility of the finite amplitude method in covariant density functional theory
The finite amplitude method in covariant density functional theory (CDFT) was developed, including both the so-called iterative finite amplitude method (i-FAM) and matrix finite amplitude method (m-FAM). A benchmark test was performed with the conventional RPA code for the isoscalar giant monopole resonance in ^{208}Pb. The feasibility of the FAMs for CDFT was proven. Furthermore, the calculated results in this study show that the existence of a Dirac sea does not introduce additional difficulties for the present FAMs in the relativistic scheme, and the effects of a Dirac sea can be included implicitly and automatically in the coordinate space representation. In addition, the rearrangement terms can be calculated implicitly without extra computational costs in both m-FAM and i-FAM.

(6) Subroutine “kurotama” in PHITS
The total reaction cross section (σ_R) of nuclei is one of the most fundamental observables that characterize the geometrical size of nuclei. It is also important in numerical simulations in the fields of accelerator technology, particle therapy, and space radiation, as well as in many other fields that are related to particle and heavy-ion transport phenomena. The reason is that, in the codes for such simulations, one needs to estimate the reaction rates systematically by using σ_R for various combinations of colliding particles over a wide energy range. The Particle and Heavy Ion Transport code System (PHITS) is one of the most powerful codes designed for these simulations. To systematically estimate σ_R for nucleus–nucleus reactions, we apply the black sphere (BS) cross section formula. Owing to its suitability for systematics, the BS cross section formula (“kurotama” in Japanese) with its extension to energies of less than 100 MeV/nucleon is now officially incorporated into PHITS version 2.52.

(7) Black sphere approximation of deformed nuclei
Following the success of the BS approximation of spherical nuclei for systematic analyses of the total reaction cross sections (σ_R), we extend this framework to reactions involving deformed nuclei. Instead of starting with the Fraunhofer diffraction from a circular disk for spherical nuclei, we adopt the Fraunhofer diffraction from a spheroid for deformed nuclei as the starting point. The study is now in progress.

(8) Low-energy electric dipole strength and dipole polarizability
We have shown that the low-lying electric dipole strength in neutron-rich isotopes is correlated with the neutron skin thickness. However, this correlation is robust only for specific nuclei. In contrast, the dipole polarizability has a universal correlation with the neutron skin thickness, especially when we subtract the contribution from the giant dipole resonance (GDR). These studies were conducted using the canonical-basis time-dependent Hartree–Fock–Bogoliubov theory that we proposed earlier.

(9) Extension of the phonon damping model to non-zero angular momentum
The phonon damping model (PDM) is extended to include the effect of angular momentum at finite temperature. The formalism is based on the description of the non-collective (single-particle) rotation of spherical systems. This implies that the total angular momentum J can be aligned along the z axis; therefore, it is completely determined by its projection M on this axis alone. Numerical calculations were performed for two spherical nuclei, ^{88}Mo and ^{106}Sn. The analysis of the numerical results shows that the GDR width increases with increasing M at a given value of T for $T < 3$ MeV. At higher T, the GDR width approaches saturation at $M > 60$ for ^{88}Mo and $M > 80$ for ^{106}Sn. However, the region of $M > 60$ goes beyond the maximum value of M up to which the specific shear viscosity η/s has values not smaller than the Kovtun–Son–Starinet (KSS) lower-bound conjecture for this quantity. This maximum value of M is found to be equal to 46 and 55 for ^{88}Mo and ^{106}Sn, respectively, if the value $\eta(T = 0) = 0.6 \times 10^{-23}$ MeV s fm^{-3} for the shear viscosity at $T = 0$ is used. A check using the KSS lower-bound conjecture for the specific shear viscosity and the same $\eta(0) = 0.6 \times 10^{-23}$ MeV s fm^{-3} also shows that

the experimental data for the GDR line shape in ^{88}Mo at the initial temperature of $T \sim 4$ MeV and angular momentum of $J = 44$ of the compound nucleus leads to violation of the KSS conjecture. This calls for a reanalysis of the recent experimental data for GDR in ^{88}Mo at these large values of temperature and angular momentum.

(10) Description of the width of giant dipole resonance in ^{201}Tl measured at low temperature
We calculated the width and strength function of the GDR in ^{201}Tl at a finite temperature within the framework of the quasiparticle representation of the PDM. Thermal pairing is taken into account by using the exact treatment of pairing within the canonical ensemble (CE). This treatment allows us to calculate the exact equivalences to the pairing gaps for protons and neutrons in a nucleus neighboring a proton closed-shell one. Because of thermal fluctuations owing to the finiteness of the system, which are inherent in the CE, the exact CE thermal pairing gaps do not collapse at the critical temperature T_c of the superfluid–normal phase transition, as in infinite systems, but decrease monotonically as T increases and remain finite up to T as high as 5 MeV. The good agreement between the PDM predictions including thermal pairing and the recent experimental data clearly demonstrates the manifestation of the effect owing to thermal pairing, which plays a vital role in reducing the GDR width at low T in open-shell nuclei. Under the influence of thermal pairing, the GDR width in ^{201}Tl becomes as low as around 3.7 MeV at $T = 0.8$ MeV, and the width $\Gamma(0)$ of the GDR built on the ground state ($T = 0$) can be as small as 3 MeV, which is smaller than the GDR width in ^{208}Pb (4 MeV) at $T = 0$. The results obtained in the present work as well as the previous predictions for the GDR width in ^{120}Sn, where the important role of neutron thermal pairing has been shown to reduce the GDR width at $T < 1$ MeV, confirm that, to yield an adequate description of GDR damping at low T, a microscopic model needs to take into account thermal pairing at least up to $T \sim 1.5$ MeV.

(11) Specific shear viscosity in hot rotating systems of paired fermions
The Green–Kubo relation is used to calculate the specific shear viscosity from the retarded Green's function that describes the propagation of quasiparticles within the quasiparticle mean field of a classically rotating system of nucleons that interact via a monopole interaction. Thermal fluctuations are included within the improved version of the finite-temperature BCS theory (called FTBCS1), whereas coupling to monopole pair vibrations is taken into account within the self-consistent quasiparticle random phase approximation (SCQRPA). The general features of the specific viscosity η of this system can be summarized as follows. At a given temperature T, η increases with increasing angular momentum M; that is, a rotating system of paired fermions is more viscous. In medium-weight and heavy systems, η decreases with increasing T at $T > 2$ MeV, and this feature is not greatly affected by the angular momentum. However, in light systems, it increases with increasing T at values of M close to M_{max}, which is defined as the limiting angular momentum for each system. At $T < 2$ MeV, local minima and/or a local maximum appear because of the significant change in the curvature of the temperature dependence of the thermal pairing gap. Thermal fluctuations and coupling to the quasiparticle pair vibrations within the SCQRPA significantly increase η for small-N systems ($N < 10$), whereas η decreases for large N (>10) systems. All the results of η obtained within the schematic model as well as realistic nuclei are always larger than the universal lower bound of the specific shear viscosity up to $T = 5$ MeV.

Head

Takashi NAKATSUKASA

Members

Akihisa KOHAMA

Special Postdoctoral Researchers

Wataru HORIUCHI

Tsunenori INAKURA

Kouhei WASHIYAMA

Postdoctoral Researcher

Koichi SATO

Contract Researcher

NguyenDinh DANG

Research Associate

Guo LU

Senior Visiting Scientists

Kenichi MATSUYANAGI
Hiroyuki SAKURAGI

Research Consultants

Kiyomi IKEDA
Kosai TANABE

Visiting Researcher

Haozhao LIANG

Visiting Scientists

Takashi ABE (Univ. of Tokyo)
Yasuhisa ABE (RCNP)
Anatolijs AFANASJEVS (Mississippi State Univ.)
Yoshihiro ARITOMO (JINR)
Paolo AVOGADRO (Univ. of Milan)
Simone BARONI (Univ. of Washington)
Carlos BERTULIANI (Texas A&M Univ.)
Satoshi CHIBA (Japan Atomic Energy Agency)
Elisabeth ELSTER (Ohio Univ.)
Yoshiko ENYO (Yukawa Inst. Theoretical Phys.)
Shuichiro EBATA (Univ. of Tokyo)
Hubert FLOCARD (INP-Orsay)
Shinichiro FUJII (CNS)
Koichi HAGINO (Tohoku Univ.)
Ikuko HAMAMOTO (Lund Univ.)
Koji HIGASHIYAMA (Chiba Institute of Technology)
Nobuo HINOHARA (Univ. of North Carolina)
Michio HONMA (Aizu Univ.)
Takatoshi HORIBATA (Aomori Univ.)
Kei IIDA (Kochi Univ.)

Akitsu IKEDA (Shizuoka Inst. Sci. Tech.)
Naoyuki ITAGAKI (Univ. of Tokyo)
Makoto ITO (Kansai Univ.)
Akira IWAMOTO (Japan Atomic Energy Agency)
Kaori KAKI (Shizuoka Univ.)
Kiyoshi KATO (Hokkaido Univ.)
Toshitaka KAJINO (NAOJ)
Masaaki KIMURA (Hokkaido Univ.)
Wenhui LONG (Peking Univ.)
Takuma MATSUMOTO (Hokkaido Univ.)
Jie MENG (Peking Univ.)
Peter MOLLER (Los Alamos National Lab.)
Takayuki MYO (Osaka Institute of Technology)
Kazusuke OGATA (Kyushu Univ.)
Makito OI (Univ. of Surrey)
Akira ONO (Tohoku Univ.)
Kazuhiro OYAMATSU (Aichi Shukutoku Univ.)
Nguyen Hung QUANG (Tan Tao Univ.)
Badawy SARHAN (Cairo Univ.)
Ryoichi SEKI (California Univ.)
Yoshihumi SHIMIZU (Kyushu Univ.)
Kosuke SUMIYOSHI (Numazu National College of Technology)
Yasuyuki SUZUKI (Niigata Univ.)
Naoki TAJIMA (Univ. of Fukui)
Masatoshi TAKANO (Waseda Univ.)
Masaaki TAKASHINA (RCNP)
Kazuo TAKAYANAGI (Sophia Univ.)
Noboru TAKIGAWA (Tohoku Univ.)
Kazuko TANABE (Otsuma Women's Univ.)
Yasutaka TANIGUCHI (Univ. of Tsukuba)
Jun TERASAKI (Univ. of North Carolina)
Yutaka UTSUNO (Japan Atomic Energy Agency)
Takahiro WADA (Kansai Univ.)
Gentaro WATANABE (POSTECH)
Kazuhiro YABANA (Grad. Sch. of Pure and Applied Sci., Univ. Tsukuba)
Taiichi YAMADA (Kanto Gakuin Univ.)
Masayuki YAMAGAMI (Aizu Univ.)
Kenichi YOSHIDA (Niigata Univ.)

Naotaka YOSHINAGA (Saitama Univ.)

Yumin ZHAO (Shanghai Jiao Tong Univ.)

Students

International Program Associate

Jia-Jie SHEN (Shanghai Jiao Tong Univ.)

Part-time Staff (Research Assistance)

Kiyomi ARAI

Miki KANO

Noriko OKAYASU

Yoko OZAWA

Tsuneyo SUZUKI

Secretaries

Noriko KIYAMA

Keiko SUZUKI

Theoretical Research Division
Strangeness nuclear physics Laboratory

1. Abstract

We proposed accurate few-body calculational method called "Infinitesimally shifted Gaussian lobe method". Recently, we developed this method to four-body systems and five-body systems. For example, we applied it to hypernuclear physics and clarified what is important and impressed. In fact, we applied this method to three kinds of hypernuclear experiments (KEK-E419, BNL-E930, and -E929) in the past, and we contributed to these experiments by discussing with experimentalists, analyzing the data, and interpreting the data. And we applied the method double Λ hypernucleus, ${}^{11}\mathrm{Be}_{\Lambda\Lambda}$ within the framework of $\alpha+\alpha$+n+$\Lambda+\Lambda$ five-body problem to identify the state of HIDA event which was observed recently by emulsion experiment (KEK-E373).

2. Major Research Subjects

(1) Hypernuclear structure from the view point of few-body problem
(2) Ultra clod atom
(3) Baryon-baryon interaction based on lattice QCD
(4) Clustering structure for ^{12}C and ^{16}O

3. Summary of Research Activity

(1) The structure of the isodoublet hypernuclei , ${}^{10}\mathrm{B}_{\Lambda}$ and ${}^{10}\mathrm{Be}_{\Lambda}$ within the framework of an $\alpha+\alpha+\Lambda$+N four-body cluster model is studied. The Λ binding energies of ${}^{10}\mathrm{B}_{\Lambda}$ and ${}^{10}\mathrm{Be}_{\Lambda}$ are 8.70 MeV and 8.94 MeV, respectively. The energy splitting of 1^- and 2^- does not contradict with the observed data of BNL-E930.

(2) By the quenched lattice QCD simulation for two nucleons with finite scattering energy, validity of the derivative expansion of the general nucleon-nucleon potential is studied. The leading-order potentials obtained at different energies (E ～0 MeV and 45 MeV) show no difference within statistical errors, which validated the local approximation of the potential up to E=45 MeV for the central and tensor potentials.

Head

Emiko HIYAMA

Foreign Postdoctoral Researchers

Pascal NAIDON (After April, researcher of Hatsuda Lab.)
Ang LI
Philipp GUBLER

Special Postdoctoral Researchers

Takenori FURUMOTO (After November, Visiting Scientist)

Contract Researchers

Yasuro FUNAKI
Takahisa KOIKE
Keiko MURANO
Ying ZHANG
Jinjiu HU(After July, Visiting Scientist)
Kenji FUKUKAWA
Hiroya SUNO

Visiting Scientists

Takayuki MYO (Osaka Institute of Technology)
Taiichi YAMADA (Kanto Gakuin University)
Tetsuo HYODO (Tokyo Institute of Technology)
Makoto OKA (Tokyo Institute of Technology)

Tomokazu FUKUDA (Osaka Electro-Communication University)
Daisuke JIDO (YITP, Kyoto University)
Hidekatsu NEMURA (University of Tsukuba)
Soichi ISHIKAWA (Hosei University)
Atsushi HOSAKA (RCNP, Osaka University)
Shoji SHINMURA (Gifu University)
Akinobu DOTE (KEK)
Thomas RIJKEN (Radboud University Nijmegen)
Kazuma NAKAZAWA (Gifu University)
Atsushi UMEYA (Nihon Institute of Technology)
Yoichi IKEDA (After September, contract researcher of Hatsuda Lab.)
Toru SATO (Osaka University)
Satoru HIRENZAKI (Nara Women's University)
Masayuki ASAKAWA (Osaka University)
Masakiyo KITAZAWA (Osaka Univeristy)
Wolfram WEISE(Technical University of Munich)
Yoshikazu FUJIWARA (Kyoto University)

Research Consultants
Yasuo YAMAMOTO
Kiyomi IKEDA

Junior Reserch Associate
Shota OHNISHI

Student Trainees
Simpei ENDO (Graduate School of Science, University of Tokyo)
Akira YOKOTA(Graduate School of Science and Engineering, Tokyo institute of Technology)
Saori MAEDA(Graduate School of Science and Engineering, Tokyo institute of Technology)

Secretary
Yoko FUJITA
Yuri TSUBURAI
Kayo YAMAJI

Theoretical Research Division
Mathematical Physics Laboratory

1. Abstract

The aim of mathematical physics laboratory is to apply mathematical scheme to resolve long-standing issues in various subjects of physics. Mathematics, in particular that originates in superstring theory, has universal feature which is common to wide range of physics. This covers elementary particle physics, hadron physics, nuclear physics, cosmology, general relativity and condensed matter physics. We apply mathematical scheme such as superstring theory, D-branes, AdS/CFT correspondence, solitons, statistical mechanics and integrable systems. Topics which the laboratory covers currently include non-perturbative analysis of quantum chromo-dynamics, superstrings, and models beyond the standard model of particle physics, and soliton physics.

2. Major Research Subjects

(1) Application of Superstring Theory
(2) Non-perturbative analyses of strongly-coupled gauge theories
(3) Physics of Black Holes and Cosmology
(4) Solitons physics
(5) Condensed matter theory
(6) Transport phenomena

3. Summary of Research Activity

Interplay between mathematics and physics is indispensable, as any physics law is described in terms of mathematics. However, the present status of various theoretical physics does not fully appreciate the usefulness of mathematics, as each topics goes into details and has less interaction with other subjects even nearby. We integrate various subjects of physics, by applying recent development of mathematics and mathematical physics, to solve long-standing issues in physics. In particular, mathematical methods in superstring theory has been developed and is mature enough to be applied to other physics. We put efforts on the application as described below, in addition to some other mathematical techniques such as numerical simulations, solitons and integrable systems.

(1) Application of superstring theory

AdS/CFT correspondence and nuclear physics
The renowned AdS/CFT correspondence, which was initiated in superstring theory, is a useful and powerful tool for analyzing strongly-coupled gauge theories. This has been applied to QCD, the dynamics of quarks. We studied how this powerful tool can have an impact on nuclear physics. We computed an effective action of multi-baryon systems, which should serve as a basic quantum action for nuclear physics. This turned out to reproduce nicely nuclear forces and baryon spectrum. In addition, three-body nuclear force was computed.

(2) Theoretical condensed matter theory

The AdS/CFT correspondence can be also applied to condensed matter physics, in particular strongly correlated electron systems. Our application lead to, for example, an analysis of a non-perturbative Luttinger theorem. In addition, various symmetry-based arguments can facilitate nontrivial universal consequences, including for example counting of Nambu-Goldstone modes in the Lorentz-violating systems. We explored spin-singlet fractional quantum Hall states and also ultrasoft modes in transport phenomena, and viscoelastic electromagnetism and Hall viscosity. Relativistic hydrodynamics from projection operator method was studied.

(3) String phenomenology and cosmology

We have studied large-volume compactification scenario in string cosmology, in particular the moduli problem and the baryogenesis. In addition, dark radiation and the dark matter problem are studied extensively. When the supersymmetry breaking scale is high, we studied high-scale supersymmetry in the hybrid inflation scenario.

(4) Lattice QCD

So-called Aoki phase was studied, with staggered-Wilson fermion formulation at the strong coupling of QCD. QCD phase diagram with 2-flavor QCD was also studied. Together with them, Strong-coupling analysis of parity-phase structure was investigated.

Head

Koji HASHIMOTO

Special Postdoctoral Researchers

Masato TAKI

Postdoctoral Researchers

Yuki MINAMI

Masaki MURATA

Noriaki OGAWA

Johannes Walter SCHMUDE

Contract Researcher

Tetsutaro HIGAKI

Yoshimasa HIDAKA

Research Consultant

Keiji IGI

Yoshio YAMAGUCHI

Senior Visiting Scientist

Koichi YAZAKI

Visiting Researcher

Taro KIMURA (JSPS PD)

Visiting Scientists

Tatsumi AOYAMA (Nagoya Univ.)

Kazuo FUJIKAWA（Nihon Univ.）

Masanori HANADA

Hideaki IIDA

Norihiro IIZUKA (CERN)

Nobuyuki ISHIBASHI (Univ. of Tsukuba)

Hiroshi ITOYAMA (Osaka City Univ.)

Friedrich LENZ

Yu MAEZAWA

Shoichi MIDORIKAWA (Aomori Univ.)

Muneto NITTA (Keio Univ.)

Kazutoshi OHTA

Makoto SAKAGUCHI (Keio Univ.)

Norisuke SAKAI (Tokyo Women's Christian Univ.)

Yuuichirou SHIBUSA (Nagasaki Inst. Of Applied Science)

Asato TSUCHIYA (Shizuoka Univ.)

Tamiaki YONEYA (The Open Univ. of Japan)

Secretary

Noriko KIYAMA

Keiko SUZUKI

Sub Nuclear System Research Division
Radiation Laboratory

1. Abstract

Nucleons, such as protons and neutrons, are a bound state of constituent quarks glued together with gluons. The detail structure of nucleons, however, is not well understood yet. Especially the mechanism to build up the spin of proton, which is 1/2, is a major problem in physics of the strong force. The research goal of Radiation Laboratory is to solve this fundamental question using the world first polarized-proton collider, realized at RHIC in Brookhaven National Laboratory (BNL) in USA. RHIC stands for Relativistic Heavy Ion Collider, aiming also to create Quark Gluon Plasma, the state of Universe just after the Big Bang. RIKEN-BNL Research Center (RBRC) directed by N. Samios carries our core team at BNL for those exciting researches using the PHENIX detector. We have found that the proton spin carried by gluons is indeed small, which is a very striking finding beyond our expectations. Recently we successfully identified W boson both in the electron/positron and muon decay channel, with which we established the method to determine how much anti-quarks carry the proton spin. Other than the activities at RHIC we are preparing new experiments at SPring-8, J-PARC and Fermilab to study the nature of hadron. We are also performing technical developments such as novel ion sources, fine pitch pixel detectors and neutron optical devices.

2. Major Research subjects

1) Spin physics with relativistic polarized-proton collisions at RHIC
2) Study of nuclear matter at high temperature and/or at high density
3) Technical developments on radiation detectors and accelerators

3. Summary of Research Activity

(1) Experimental study of spin structure of proton using RHIC polarized proton collider

[See also RIKEN-BNL Research Center Experimental Group for the activities at BNL]

In order to understand the spin-structure of the proton, we are currently studying the contributions from gluon and antiquark spin, and orbital angular motion of quarks and gluons to the nucleon. We have been measuring quark and antiquark spin contributions to the proton with W bosons produced in polarized-proton collisions by observing decay electrons in the central detector and decay muons in the forward detector of the RHIC-PHENIX experiment. The majority of the data is expected to be taken in 2013-2015 for this program. To study orbital motion of quarks and gluons in the proton, one of the key measurements is the Drell-Yan process (quark-antiquark annihilation) with polarized beams and/or targets. We are considering to perform such measurements at RHIC by upgrading the PHENIX detector with forward-going electron/positron and muon detection capability. As a pilot for the fixed-target experiment, some of us are participating in the SeaQuest experiment using 120-GeV unpolarized protons at Fermilab. One of the goals of the experiment is to measure the flavor asymmetry of the antiquark distributions in unexplored kinematic regions. Furthermore, measurements of azimuthal distribution of muon pairs with respect to the transverse vector of virtual photon allow us to study the orbital motion of quarks in the nucleon with unpolarized beam and target.

(2) Experimental study of quark-gluon plasma using RHIC heavy ion collider

[See also RIKEN-BNL Research Center Experimental Group for the activities at BNL]

In Wako we are operating a cluster computer system specialized to analyze huge data sets taken with the PHENIX detector. In the cluster, 380 jobs can run simultaneously reading out 380 TB of local data storage under a house-made job control system. The system was used extensively to analyze the first PHENIX VTX detector data in RUN11 AuAu and RUN12 200GeV pp to get the first physics results from the detector. The first results of VTX on heavy flavor measurement were presented in Quark Matter 2012 conference. We also support students who are working on ALICE heavy ion experiment at LHC.

(3) Study of properties of mesons with domestic accelerators

Preparation of the experiment E16 at J-PARC Hadron Experimental Hall is underway with the Grant-in-Aid for Scientific Research on Innovative Areas (MEXT, No. 21105004). The experiment aims to perform the systematic study of the mass modification of low-mass vector mesons in nuclei to explore the chiral symmetry in nuclear matter, i.e. the mechanism to create the mass of hadrons. The development of Gas Electron Multiplier (GEM) tracker using Ar/CO_2 gas was completed. A detailed mechanical design for the installation is ongoing. Newly made preamp board for the tracker using the APV25 chip (CERN-made ASIC for Si vertex readout) is tested and the chip is found to be applicable to our purpose. The design of the production type board is started. For the Hadron-blind Cherenkov detector (HBD: CsI coated GEM with CF4 gas radiator) we achieved the pion-rejection power of 99% with keeping the electron efficiency of 70% as required for the experiment. This performance was observed with a small-size test GEM ($10x10cm^2$)with smaller-size readout pad than the conventional one, so that the confirmation using the large size GEM($30x30cm^2$) is yet to be done. Front-end electronics and trigger system is under development, by learning from the Belle-II experiment and by collaborating with domestic groups in J-PARC and LEPS-2. The high-momentum beam line, where this experiment will be performed, is finally approved for the construction and the funding is secured in KEK. The first beam will be in JFY 2015. The spectrometer magnet construction is scheduled at the end of JFY 2014, and the detector installation is expected at the middle of JFY 2015.

(4) Detector development for PHENIX experiment

The silicon vertex tracker (VTX) which was installed in December 2010, has demonstrated excellent performance in determining the track information around a collision point. We found, however, several ladders of silicon detectors malfunctioned due to the electric contact problem. Since the summer 2011, we have been reworking on those ladders and successfully fixed large fraction of them on time for the data taking in 2012. We have also completed the momentum-sensitive trigger system for the PHENIX forward muon arms under the collaboration with KEK, Seoul National University, Kyoto and Rikkyo University. The new trigger system has demonstrated a satisfactory performance in taking data of polarized proton collisions at energy of 500GeV, providing the first sea-quark polarization measurements via W-boson production at forward rapidity. The entire trigger upgrade project has been completed by integration of newly-installed resistive plate chambers.

(5) Neutron optics

Cold or thermal neutron beam is a high-sensitivity probe to study not only the structure of condensed matter, but also fundamental physics. We have been successful in developing of an interferometer using multilayer mirrors, which is useful to test quantum mechanics and other fundamental physics, and of differential phase imaging to see an internal structure of a bulk materials. Based on these activities, Social Infrastructure Technology Development Program in RIKEN Innovation Center has established a new program and RANS(Riken Accelerator-driven compact Neutron Source) has been constructed at the K1 space in the RIBF building. This year thermal neutron imaging is successfully observed, and fast neutron with the energy over 1 MeV has also been detected by new detector system with plastic scintillators. This activity completed its development stage and will be transferred to Neutron beam technology team of RIKEN Center for Advanced Photonics from the next fiscal year.

(6) Development of beam source

Under the collaboration with BNL and KEK, we are developing two types of laser ion sources (LIS) to produce high brightness versatile heavy-ion beams. The first is to provide highly charged high current beams. Using a sub nano-second laser system, we induce fully stripped carbon beams and highly charged gold beams those will be used in an induction based synchrotron in KEK. The second project is to supply singly charged very low emittance heavy ion beams to NASA space radiation laboratory in BNL. The new source engages with an electron beam ion source and covers wide variety of species to represent cosmic rays.

Head

Hideto EN'YO

Members

Yasuyuki AKIBA
Yuji GOTO
Itaru NAKAGAWA
Yoshie OTAKE
Ralf SEIDL
Yasushi WATANABE
Satoshi YOKKAICHI

Special Postdoctoral Researchers
Yoshichika SEKI

Foreign Postdoctoral Researcher
Stephen BAUMGART

Contract Researchers
Yoshinori FUKAO
Tomohiro NISHITANI
Takashi HACHIYA

Postdoctoral Researcher
Kazuya AOKI
Yoki ARAMAKI
Yoshimasa IKEDA
Yoshimitsu IMAZU
Kohei SHOJI
Tomonori TAKAHASHI

Contract Technical Scientist
Yohei NAKATSUGAWA

Senior Visiting Scientists
Ken-ichi AOKI (Grad. Sch. of Sci., Kanazawa Univ.)
Takashi NAKANO (RCNP, Osaka Univ.)
Toshiaki SHIBATA (Grad. Sch. of Sci. and Eng., Tokyo Inst. of Tech. Sch. of Sci.)
Hirohiko SHIMIZU (Inst. of Materials Structure Sci., KEK)

Visiting Scientists
Tomohiro ADACHI (DAI-ICHI KIDEN CO.,LTD)
Christine A.AIDALA (Univ. Massachusetts, Amherst, USA)
Ryoji AKIMOTO (CNS, Univ. Tokyo)
Alexander BAZILEVSKY (BNL, USA)
Wolfgang BENTZ (Tokai Univ.)
Mickey CHIU (Univ. of Illinois at Urbana, USA)
Ondrej CHVALA (Univ. of California at Riverside)
Takumi DOI (University of Kentucky)
Dipanwita DUTTA (Nuclear Physics Division, Bhabha Atomic Research Centre)
Hirotsugu FUJII (Grad. Sch./College of Arts and Sciences, Univ. of Tokyo)
Kenji FUKUSHIMA (YITP, Kyoto Univ.)
Haruhiko FUNAHASHI (Grad. Sch. of Sci., Kyoto Univ.)
Yuji HASEGAWA (Wien Inst. Tech.)
Tetsuo HATSUDA (Grad. Sch. of Sci., Univ. of Tokyo)
Toshiyuki HATTORI (Res. Lab. for Nuclear Reactors, Tokyo Inst. of Tech. Sch. of Sci.)
Masanori HIRAI (Grad. Sch. of Sci. and Eng., Tokyo Inst. of Tech.)
Kensuke HOMMA (Grad. Sch. of Sci., Hiroshima Univ.)
Takuma HORAGUCHI (Grad. Sch. of Sci., Hiroshima Univ.)
Ryo ICHIMIYA (KEK)

Katsuya ISHIGURO (Grad. Sch. of Natural Sci. & Tech., Kanazawa Univ.)
Noriyoshi ISHII (Grad. Sch. of Pure and Applied Sci., Univ. of Tsukuba)
Hirokazu ISHINO (Tokyo Inst.Tech.)
Robert JAMESON (Goethe Universitat Frankfurt, Germany)
Takeshi KANESUE (Kyushu Univ.)
Hirotsugu KASHIWAGI (Takasaki Advanced Radiation Res. Inst., JAEA)
Hiroyuki KAWAMURA (The Univ.of Liverpool)
Yuji KOIKE (Grad. Sch. of Sci. & Tech., Niigata Univ.)
Yoshiaki KOMA (Numazu National College of Technology)
Kotaro KONDO (Grad. Sch. of Sci. and Eng., Tokyo Inst. of Tech.)
Shunzo KUMANO (Inst. of Particle and Nuclear Studies, KEK)
Teiji KUNIHIRO (Grad. Sch. of Sci., Kyoto Univ.)
Makoto KUWAHARA (Nagoya Univ.)
Yoshikazu MAEDA (RCNP , Osaka Univ.)
Yajun MAO (Peking Univ., China)
Tsutomu MIBE (KEK)
Liu MING (LANL)
Kenji MISHIMA (KEK)
Yoshiyuki MIYACHI (Tokyo Inst. Tech.)
Yoshihiro MORI (Grad. Sch. of Sci., Kanazawa Univ.)
Norihito MURAMATSU (RCNP, Osaka Univ.)
Ryotaro MUTO (KEK)
Katsuro NAKAMURA (Grad. Sch. of Sci., Kyoto Univ.)
Tompfumi NAGAE (Grad.Sci.of Sci.,Kyoto Univ.)
Yoshifumi NAKAMURA (DESY, Germany)
Atsushi NAKAMURA (Information Media Center, Hiroshima Univ.)
kenichi NAKANO (Tokyo Inst. Tech.)
Megumi NARUKI (KEK)
Masayuki NIIYAMA (Grad. Sch. of Sci., Kyoto Univ.)
Munehisa OHTANI (Inst. fuer Theoretische Physik, Universitact Regensburg, Germany)
Hiromi OKADA (KEK)
Masahiro OKAMURA (BNL, USA)
Kyoichiro OZAWA (Grad. Sch. of Sci., Univ. of Tokyo)
Petra RIEDLER (CERN, Switzerland)
Naohito SAITO (J-PARC, KEK)
Hiroyuki SAKO (JAEA)
Murad SARSOUR (Georgia State University)
Shoichi SASAKI (Grad. Sch. of Sci., Univ. of Tokyo)
Susumu SATO (JAEA)
Shin-ya SAWADA (Inst. of Particle and Nuclear Studies, KEK)
Michiko SEKIMOTO (Inst. of Particle and Nuclear Studies, KEK)
Kenta SHIGAKI (Grad. Sch. of Sci., Hiroshima Univ.)
Prashant SHUKLA (Nuclear Physics Division, Bhabha Atomic Research Centre)
Kazutaka SUDO (Inst. of Particle and Nuclear Studies, KEK)
Toru SUGITATE (Grad. Sch. of Sci., Hiroshima Univ.)
Mizuki SUMIHAMA (RCNP , Osaka Univ.)
Tsuneo SUZUKI (Grad. Sch. of Sci., Kanazawa Univ.)
Taneja SWADHIN (SUNY at Stony Brook)

Masao TABUCHI (Nagoya Univ.)
Junpei TAKANO (KEK)
Kiyoshi TANIDA (Seoul National Univ.)
Hisayuki TORII (Grad. Sch. of Sci., Hiroshima Univ.)
Xiaorong WANG (New Mexico State University)
Shizui WATANABE (Tokyo Metropolitan College of Aeronautical Engineering)
Satoru YAMASHITA (ICEPP)
Imuran YOUNUS (Univ. of New Mexico, USA)

Students

Junior Research Associate

Hidemitsu ASANO (Fac. of Sci., Kyoto Univ.)
Shinichi HAYASHI (Fac. Sci. , Univ. Tokyo)
Yusuke KOMATSU (Fac. Sci. , Univ. Tokyo)
Shinichi MASUMOTO (Fac. Sci. , Univ. Tokyo)
Sanshiro MIZUNO (Univ. Tsukuba)
Masaya NIHASHI (Grad. Sch. of Sci., Hiroshima Univ.)
Megumi SEKINE (Tokyo Inst. Tech.)
Dosatsu SAKATA (Univ. Tsukuba)
Takahito TODOROKI (Univ. Tsukuba)
Tomoya TSUJI (Fac. Sci. , Univ. Tokyo)

International Program Associate

Ryu Sunyoung (RCNP,Osaka Univ.)
Park SANGHWA (Seoul National Univ.)

Student Trainees

Nobuaki AMANO (Grad. Sch. of Sci., Kyoto Univ.)
Atsushi ERA (Nagoya Univ.)
Ciprian GAL (Dept. of Physics , SUNY at Stony Brook)
Masayasu HASEGAWA (Grad. Sch. of Sci., Kanazawa Univ.)
Kimiaki HASHIMOTO (Fac. of Sci., Rikkyo Univ.)
Kazuya HAYASE (Tokyo Univ. of Science)
Seiko HIROTA (Fac. Sci. , Univ. Tokyo)
Tomoya HOSHINO (Grad. Sch. of Biosphere Sci., Hiroshima Univ.)
Shouyang HU (China Inst. Atom. Energy)
Sotaro KANDA (Fac. Sci. , Univ. Tokyo)
Kouki KANNO (Fac. Sci. , Univ. Tokyo)
Paul KLINE (Dept. of Physics , SUNY at Stony Brook)
Yukiyoshi KON (RCNP , Osaka Univ.)
Andrew MANION (Dept. of Physics , SUNY at Stony Brook)
Shou MIYASAKA (Tokyo Inst. Tech.)
Shinji MOTOKI (Grad. Sch. of Biosphere Sci., Hiroshima Univ.)
Yoshihide NAKAMIYA (Grad. Sch. of Sci., Hiroshima Univ.)
Wataru NAKAI (Fac. Sci. , Univ. Tokyo)
Shoichiro NISHIMURA (Fac. Sci. , Univ. Tokyo)
Hideyuki OIDE (Fac. Sci. , Univ. Tokyo)
Takahiro SAWADA (RCNP, Osaka Univ.)

Atsuko TAKAGI (Fac. Sci. , Univ. Tokyo)
Hisayuki TAKAHARA (CNS)
Yuki WATANABE (Tokyo Univ. of Science)
Yosuke WATANABE (Fac. Sci. , Univ. Tokyo)
Ruizhe YANG (UIUC)

Intern

Inseok YOON (Seoul National Univ.)
Masako YAMADA (Grad. Sch. of Sci., Kyoto Univ.)
Takayuki YAMAMOTO (Waseda Univ.)

Part-time Staff (Research Assistance)

Takeru IGURI (Rikkyo Univ.)
Ryota MATSUBARA (Rikkyo Univ.)
Haruna MURAKAMI (Rikkyo Univ.)
Kentaro WATANABE (Rikkyo Univ.)

Secretaries

Noriko KIYAMA
Keiko SUZUKI

Sub Nuclear System Research Division
Advanced Meson Science Laboratory

1. Abstract

Particles like muons, pions, and kaons have finite lifetimes, so they do not exist in natural nuclei or matters. Implanting these particles into nuclei/matters, exotic phenomena in varieties of objects can be studied from a new point of view.

Kaon is the second lightest meson which has strange-quark as a constituent quark. It is expected that if one embed a kaon into nuclei, the sizes of the nuclei become smaller and forms a high density object beyond the normal nuclear density. Study of this object could lead to better understanding of the origin of the mass of the matter, and may reveal the quark degree of freedom beyond the quark-confinement. Those properties can be studied by precise heavy pionic atom research in different angle. The other example is the weak interaction in nuclear matter. It can only be studied by the weak decay of hypernuclei, which have lambda particle in the nuclei.

Muon provides even wider variety of study ranging from particle physics to condensed matter and life sciences. For instance, stopping positively charged muon in a material, we obtain information on the magnetic properties or the local field at the trapped site. Injecting negatively charged muon to mixture of deuterium and tritium, muon attracts surrounding atoms and trigger nuclear fusions between deuterium and tritium. Ultra-slow muon beam can be used for the material surface studies and also as a source of ultra-cold muon beam for precise muon g-2 measurement.

As is already clear, in our research we introduce different kind of impurities into nuclei/matters, and study new states of matter, new phenomena, or the object properties.

2. Major Research Subjects

(1) Study of meson property and interaction in nuclei
(2) Origin of matter mass / quark degree of freedom in nuclei
(3) Condensed matter and material studies with muon
(4) Nuclear and particle physics studies via muon catalyzed fusion and ultra cold muon beam
(5) Non-perturbative aspects of string theory

3. Summary of Research Activity

Hadron physics at J-PARC and RIKEN-RIBF

Kaon and pion will shed a new insight to the nuclear physics. The recent discovery of deeply bound pionic atom enables us to investigate the properties of mesons in nuclear matter. At RIKEN-RIBF, we have carried out the first precise experimental study of the pionic atom. We have prepared another next generation kaon experiments (E15, E17 and E31) at J-PARC and is ready for the first physics run in 2013. In these experiments, we are aiming at precise determination of the KN interaction, and clarify the nature of kaon in nuclei and $\Lambda(1405)$. By these experiments, we aim to be a world-leading scientific research group using these light meta-stable particles.

1) Deeply bound kaonic nuclei

We have performed experimental exploration of theoretically predicted deeply bound kaonic nuclear states in ^{3}He nucleus K^-ppn and K^-pnn. Akaishi and Yamazaki first calculated large binding energy and narrow width for the K^-ppn state. One of the most interesting features of the kaonic nucleus is that the strong attraction of the kaon is expected to contract the surrounding nucleons resulting in extremely high density of several times larger than normal nuclear density. Measurement of the kaon properties at such high energy density will provide precious information on the origin of hadron masses and the chiral symmetry breaking and its partial restoration.
The experimental principle adopted uses stopped K^- on suprefluid helium target, and we focus on emitted nucleon momenta measurement by Time-of-Flight (TOF) method. The last orbit of kaonic ^{4}He atom is 2p and the branching ratio from the last orbit to the nuclear kaon bound state accompanied with a nucleon emission was estimated to be 1 % at minimum.
The exploration was performed from 2002/September till 2005/December as series of experiments at the KEK-PS (E471, E549, E570) with almost common experimental setup. The obtained spectral shape was rather smooth and elaborate analysis showed upper limit of the kaonic nucleus formation for both K^-ppn and K^-pnn states.
After the completion of above series of experiments, the KEK-PS was shut down to switch to a new facility J-PARC. At the J-PARC, we are focusing on the experiment to search for the simplest kaonic nucleus, K-pp bound state, via in-flight (K-,n) reaction on liquid ^{3}He target (J-PARC E15). For this experiment, new experimental apparatus, new liquid ^{3}He target, large cylindrical detector system to detect/identify decay products of K-pp bound state and large volume neutron counter to measure momenta of the emitted neutron on the reaction by TOF method. The first engineering run of data taking has been

performed during year 2012. Now we are waiting first physics data taking which is planned in March 2013.

2) Deeply bound pionic atoms
We have made precision spectroscopy of pionic lead and tin atoms, and extracted information on the in-medium interaction between pion and nucleus, which leads to the exclusive quantitative evaluation of the chiral symmetry restoration in the nuclear matter.
Our collaboration which mainly consists of the RIKEN and the University of Tokyo group conducted throughout the experiments starting from R&D of pionic atom formation in nuclear reactions to its application to the precision spectroscopy.
The experiment was carried out in GSI, Darmstadt. Our first discovery was pionic 2p state in the lead 207 nucleus where the negative pion is accommodated in a delicate balance between the Coulomb attraction and the strong repulsion.
Following the discovery, we have performed experiments to measure 1s pionic lead 205 and ^{115}Sn, ^{119}Sn and ^{123}Sn isotopes.
We have analyzed the experimental spectra elaborately and extracted in-medium isovector interaction between pion and nucleus. In combination with experimental information on the pionic hydrogen and deuterium which gives the interaction in vacuum, we have accomplished evaluation of the in-medium interaction modification. The modification is originating in the partial restoration of the chiral symmetry in the nucleus, and we have quantitatively evaluated for the first time the reduction of the chiral order parameter in the nuclear matter to be 33 %, which is consistent with theoretical prediction of 30 %.
Presently, we have been preparing for a sophisticated experimental setup of the pionic atom spectroscopy at the RIBF in RIKEN and recently successfully observed pionic ^{121}Sn atom for the first time. We expect about twice better experimental resolution with much smaller systematic errors.

3) Precision X-ray measurement of kaonic atom
Simultaneously with the above experiment (1), we have performed an X-ray spectroscopy of atomic $3d \rightarrow 2p$ transition of negatively charged K mesons captured by helium atoms. Many kaonic atoms are known to be measured with various elements, however, there are very large deviations in the measured energy levels for the helium (and the oxygen) from the systematic expectations. The deviation originates in technical issues in old experiments, and new and high precision data have been long awaited for. Also, wave functions of the kaonic atoms are expected to reflect the information on the existence of the inner structure, namely deeply bound kaonic states. As a result of the experiment, we have succeeded in performing the spectroscopy and achieved the shift of 2 ± 2(stat.) ± 2(syst.) eV. The obtained results reject older data without any doubt, and the above deviation is dissolved. Presently, aiming at the determination of the level width and yield, we are analyzing the data. To clarify the KN interaction strength, we are preparing another x-ray measurement of the kaonic helium-3 atom, which is another day-one experiment at J-PARC.

Muon science at RIKEN-RAL branch
The research area ranges over particle physics to condensed matter studies and life science. Our core activities are based on the RIKEN-RAL Muon Facility located at the Rutherford Appleton Laboratory (UK), which provides intense pulsed-muon beam. We have variety of important research activities such as muon-catalyzed fusion (μCF) and condensed matter physics by muon spin rotation / relaxation / resonance (μSR).

(A) Condensed matter/materials studies with μSR
An new international collaboration with Universiti Sains Malaysia (USM) on the muon science has been established on Nov. 1st in 2012 in order to enhance the scientific activity on the muon-site estimation. The main purpose of this collaboration is to study muon sites in materials and hyperfine interactions at the muon sites. The RIKEN side will provide μSR experimental data which have been obtained at the RIKEN-RAL Muon Facility (RIKEN-RAL) and the USM side will act on theoretical and computational analysis by using those data. For speedy and effective progress of the collaboration activities, RIKEN also provides the computation atmosphere by using the RIKEN Integrated Cluster of Clusters (RICC). The construction of a general program with user friendly front-end functions is being discussed to estimate the muon site. Such a program is important for general researchers to enhance the understanding of their experimental results by using the μSR technique.
In 2012, some important scientific achievements for the material science have been obtained at the RIKEN-RAL on the basis of μSR collaborations as follows.
1) A magnetically ordered state has been confirmed in the pyrochlore iridate, $Nd_2Ir_2O_7$ just below the metal-insulator transition. This observation proves an important role of a hybridized state between Ir 5d and O 2p electrons for the electro-magnetic state of the pyrochlore iridate.
2) The Li and Na diffusion behavior in candidate materials for the next generation of the battery have been investigated. Diffusion constants of both atoms were quantitatively determined. This result has given a new scheme of the atomic diffusion of the battery material which is important to design new materials which have higher performance as battery

materials.
3) The electron diffusion in some organic solar-cell materials has been probed by using the μSR technique. The dimensionality of the diffusion behavior has been clarified to be changed from the 3D- to 1D-like motion. The hopping frequency has been numerically obtained.

(B) Nuclear and particle physics studies via muon catalyzed fusion and ultra-cold muon beam
1) Muon catalyzed fusion (μCF)
We are studying the muon catalyzed fusion (μCF) processes in a wide range of hydrogen target conditions such as isotope mixture, temperature, density and phase. We are continuing the study of the new high pressure and high density solid D_2 target system. Now we have confirmed the formation of solid D_2 at 33.6 K and 790 bar.

2) Generation of ultra-slow positive muon beam
Low energy muon beam, whose kinetic energy is variable from a few keV to a few tens of keV, will be useful for μSR as well as for the source of a very sharp beam for precision measurement of muon's anomalous gyro-magnetic ratio (g-2). Progresses were made in several key techniques to produce low energy muons. We almost finished the analysis of the muonium emission measurement from material surface of several silica aerogel samples done at TRIUMF. Based on that information, we are planning schemes to increase the muonium emission rate. A new laser system is developed at RIKEN Wako campus to increase the laser intensity and the ionization efficiency by 100 times. First Lyman-alpha was generated in February 2013. Further study to increase and stabilize the laser power is in progress.

Theoretical Researches

1) Non-perturbative aspects of string theory
One of the most promising approach toward the understanding of the non-perturbative aspects of string theory is that through matrix models. We have found a new dynamics in one of those matrix models. We have shown that one of matrix models which related to non-critical string theory with the central charge one exhibits a novel critical behavior through the phenomenon stems from the very quantum nature of the system, the tunneling phenomenon. We have pointed out that if the potential of the model is set properly, there should occur certain tunneling called resonant tunneling put the system to certain singular behavior, before the system reached the well-known criticality, where the Fermi surface reached the ridge of the potential valley. The precise nature of this novel critical behavior is yet to be uncovered but this phenomenon will likely to shed lights on non-perturbative aspects of string theory through its matrix model dynamics.

2) Physics of Quantum Hall system
We have investigated the interlayer phase coherence and the Josephson currents in the bilayer quantum Hall system based on the noncommutative geometrical approach. We have demonstrated that the Josephson inplane current provokes anomalous behaviors in the Hall resistance in counterflow and drag experiments. Furthermore, we investigate the condition on the input current for the tunneling current to be coherent and dissipationless. Our results explain quite well the experimental report on the input current due to the von Klitzing group. We have predicted also how the condition changes when the sample is tilted in the magnetic field.

Head

Masahiko IWASAKI

Members

Katsuhiko ISHIDA
Kenta ITAHASHI
Yoshio KOBAYASHI (After August, Visiting Scientist)
Yue MA
Hiroaki OHNISHI
Haruhiko OUTA
Fuminori SAKUMA
Tsukasa TADA
Isao WATANABE

Special Postdoctoral Researchers

Ikuto KAWASAKI
Kazuki UENO (After September, Visiting Scientist)

Contract Researchers

Yu OISHI
Shinji OKADA
Dai TOMONO
Koji YOKOYAMA

Special Temporary Employee

Teiichiro MATSUZAKI

Senior Visiting Scientist

Kazuhiro TANAKA (IPNS, KEK)

Visiting Scientists

Tadashi ADACHI (Grad. Grad. Sch. Eng., Tohoku Univ.)
Jun AKIMITSU (Coll. Sci. Eng., Aoyama Gakuin Univ.)
Kunio AWAGA (Grad. Sch. Sci., Nagoya Univ.)
Pavel BAKULE (IPS AS CR, Czech)
George BEER (Univ. of Victoria, Canada)
HyoungChan BHANG (Seoul Natl Univ., Korea)
Graeme BLAKE (Univ. of Groningen, Netherlands)
N. Ludmila BOGDANOVA (ITEP, Russia)
Lee CHOW (UCF, USA)
Catalina CURCEANU (INFN, Italy)
Prasad Tara DAS (SUNY, USA)
Irwan DHARMAWAN (UNPAD, Indonesia)
Yasuaki EINAGA (Fac. Sci & Tech., Keio. Univ.)
Masaya ENOMOTO (Fac. Sci., Tokyo Univ. of Sci.)
Zyun Francis EZAWA (Grad. Sch. Sci., Tohoku Univ.)
Mark FAYFMAN (Kurchatov Inst., Russia)
Donald FLEMING (Univ. of British Columbia/TRIUMF)
Yutaka FUJII (Fac. Eng., Fukui Univ.)
Hiroyuki FUJIOKA (Grad. Sch. Sci., Kyoto Univ.)
Masaki FUJITA (IMR, Tohoku Univ.)
Hideto FUKAZAWA (Grad. Sch. Sci., Chiba Univ.)
Nobumasa FUNAMORI (Grad. Sch. Sci., Univ. of Tokyo)
Yukio FURUKAWA (Fac. Sci. & Eng., Waseda Univ.)
Takayuki GOTO (Fac. Sci. & Tech., Sophia Univ.)
Masashi HARADA (Toyota Central R&D Labs.)
Kazuo HAYAKAWA (Fac of Sci. & Tech., Shizuoka Inst. Sci. & Tech.)
Ryugo S. HAYANO (Grad. Sch. Sci., Univ. of Tokyo)
Wataru HIGEMOTO (ASRC, JAEA)
Satoru HIRENZAKI (Fac. Sci., Nara Women’s Univ.)
Masahiko HIROI (Fac. Sci., Kagoshima Univ.)

Hiromi IINUMA (IPNS, KEK)
Masami IIO (CSC, KEK)
Susumu IKEDA (IMSS, KEK)
Yutaka IKEDO (IMSS, KEK)
Rintaro INOUE (ICR, Kyoto Univ.)
Takayuki ISHIDA (Grad. Sch. Infor. & Eng., Univ. Elect. Commu.)
Yasuyuki ISHII (Dept. Phys., Tokyo Medical Univ.)
Fumihiro ISHIKAWA (Grad. Sch. Sci. & Tech., Niigata Univ.)
Shigeru ISHIMOTO (IPNS, KEK)
Tomoichi ISHIWATARI (SMI, Austria)
Takashi ITO (ASRC, JAEA)
Ryosuke KADONO (IMSS, KEK)
Koichi KAGESAWA (Grad. Sch. Arts & Sci., Univ. of Tokyo)
Kazuya KAMAZAWA (Toyota Central R&D Labs.)
Toshiji KANAYA (ICR, Kyoto Univ.)
Motomi KATADA (Grad. Sch. Sci. & Eng., Tokyo Met. Univ.)
Mineo KATO (IMSS, KEK)
Roland KAWAKAMI (UC Riverside, USA)
Takayuki KAWAMATA (Grad. Sch. Eng., Tohoku Univ.)
Naritoshi KAWAMURA (IMSS, KEK)
Seiko KAWAMURA (J-PARC, JAEA)
Kenji KAWASHIMA (Coll. Sci. Eng., Aoyama Gakuin Univ.)
Hikomitsu KIKUCHI (Grad. Sch. Eng., Univ. of Fukui)
Yasushi KINO (Fac. Sci., Tohoku Univ.)
Wataru KOBAYASHI (Grad. Sch. Pure & Applied Sci., Univ. of Tsukuba)
Akihiro KODA (IMSS, KEK)
Masahito KODERA (Fac. Sci. & Eng., Doshisha Univ.)
Yoh KOHORI (Fac. Sci., Chiba Univ.)
Yoji KOIKE (Grad. Sch. Eng., Tohoku Univ.)
Kenji KOJIMA (IMSS, KEK)
Norimichi KOJIMA (Grad. Sch. Arts & Sci., Univ. of Tokyo)
Kenya KUBO (Grad. Sch. Sci., ICU)
Shoko KUME (Grad. Sch. Sci., Univ. of Tokyo)
Yoshitaka KUNO (Grad. Sch. Sci., Osaka Univ.)
Takuya KURAHASHI (IMS, NINS)
Haruhiko KUROE (Fac. Sci. & Tech., Sophia Univ.)
Guido LANGOUCHE (NVAO, Netherlands)
Shunsuke MAKIMURA (IMSS, KEK)
Hirotaka MANAKA (Grad. Sch. Sci. & Eng., Kagoshima Univ.)
Kenji MATSUDA (Grad. Sch. Sci. &Eng. for Edu., Univ. of Toyama)
Yasuyuki MATSUDA (Grad. Sch. Arts & Sci., Univ. of Tokyo)
Tsutomu MIBE (IPNS, KEK)
Mototsugu MIHARA (Grad. Sch. Sci., Osaka Univ.)
Yasuhiro MIYAKE (IMSS, KEK)
Hitoshi MIYASAKA (Grad. Sch. Sci., Tohoku Univ.)
Jun MIYAZAKI (Fac. Sci. Div., Nihon Univ.)
Soichiro MIZUSAKI (Coll. Sci. & Eng., Aoyama Gakuin Univ.)
Tomoyuki MOCHIDA (Grad. Sch. Sci., Kobe Univ.)

Mohamed Ismail MOHAMED IBRAHIM (USM, Malaysia)
Kazuhiko MUKAI (Toyota Central R&D Labs.)
Yujiro NAGATA (Coll. Sci. Eng., Aoyama Gakuin Univ.)
Takashi NAGATOMO (IMSS, KEK)
Hiroyuki NAKAMURA (Grad. Sch. Eng., Kyoto Univ.)
Jin NAKAMURA (Grad. Sch. Infor. & Eng., Univ. Elect. Commu.)
Kazutaka NAKAHARA (Univ. of Maryland. USA)
Satoshi NAKAMURA (Grad. Sch. Sci., Tohoku Univ.)
Takashi NAKAMURA (Grad. Sch. Sci. & Eng., Tokyo Tech.)
Takayoshi NAKAMURA (RIES, Hokkaido Univ.)
Takehito NAKANO (Grad. Sch. Sci., Osaka Univ.)
Saburou NASU (Grad, Sch. Eng. & Sci., Osaka Univ.)
Kazuhiko NINOMIYA (Grad. Sch. Sci., Osaka Univ.)
Nobuhiko NISHIDA (Fac. Sci., Tokyo Tech.)
Katsuhiko NISHIMURA (Grad. Sch. Sci.&Eng. for Edu., Univ. of Toyama)
Kusuo NISHIYAMA (IMSS, KEK)
Tatsuo NORITAKE (Toyota Central R&D Labs.)
Hiroyuki NOUMI (RCNP, Osaka Univ.)
Hiroshi NOZAKI (Toyota Central R&D Labs.)
Yasuo NOZUE (Grad. Sch. Sci., Osaka Univ.)
Agung NUGROHO (ITB, Indonesia)
Kazuki OHISHI (CROSS Tokai)
Yoshitaka OHKUBO (KURRI, Kyoto Univ.)
Atsushi OKAZAWA (Grad. Sch. Arts & Sci., Univ. of Tokyo)
Vassili PEREVOZCHIKO (VNIEF, Russia)
ROGER PINK (SUNY at Albany, USA)
Leonid PONOMAREV (Kurchatov Institute, Russia)
Francis PRATT (RAL, UK)
Risdiana (UNPAD, Indonesia)
Lusy SAFRIANI (UNPAD, Indonesia)
Naohito SAITO (IPNS, KEK)
Shin-ichi SAKAMOTO (J-PARC, JAEA)
Tobat SARAGI (Univ. of Kassel, Germany)
Kazuhiko SATO (Grad. Sch. Sci. & Eng., Saitama Univ.)
Masaharu SATO (Grad. Sch. Sci., Univ. of Tokyo)
Tomoko SATO (Grad. Sci., Hiroshima Univ.)
Wataru SATO (Inst. Sci. & Eng., Kanazawa Univ.)
Ralph SCHEICHER (Michigan Tech. Univ., USA)
Ryoichi SEKI (California State Univ., Northridge, USA)
Kouichirou SHIMOMURA (IMSS, KEK)
Ichiro SHIRAKI (Grad. Sch. Medi. & Eng. Sci., Univ. of Yamanashi)
Patrick STRASSER (IMSS, KEK)
Hiroyuki SUGAI (ASRC, JAEA)
Jun SUGIYAMA (Toyota Central R&D Labs.)
Shukri SULAIMAN (USM,, Malaysia)
Hiroyuki SUZUKI (AKTD, NIMS)
Ken SUZUKI (SMI, Austria)
Soh SUZUKI (CRC, KEK)

Takao SUZUKI (Shibaura Inst. of Tech.)
Takatoshi SUZUKI (Grad. Sch. Sci., Univ. of Tokyo)
Yoshikazu TABATA (Grad, Sch. Eng. & Sci., Kyoto Univ.)
Shigeru TAKAGI (Grad, Sch. Sci., Tohoku Univ.)
Kazuyuki TAKAI (Grad. Sch. Sci. & Eng., Tokyo Tech.)
Nao TAKESHITA (NeRI, AIST)
Yoichi TANABE (WPI, Tohoku Univ.)
Manobu TANAKA (IPNS, KEK)
Hiroshi TANIDA (Grad. Sch. Adv. Sci. Matter, Hiroshima Univ.)
Akihiro TANIGUCHI (KURRI, Kyoto Univ.)
Harry TOM (UC Riverside, USA)
Eiko TORIKAI (Grad. Sch. Medi. & Eng. Sci., Univ. of Yamanashi)
Akihisa TOYODA (IPNS, KEK)
Kyo TSUKADA (Grad. Sch. Sci., Tohoku Univ.)
Satoshi TSUTSUI (JASRI)
Masatomo UEHARA (Grad. Sch. Eng., Yokohama Natl.Univ.)
Izumi UMEGAKI (Toyota Central R&D Labs.)
Helmut WEICK (GSI, Germany)
Zhuan XU (Zhejiang Univ. China)
Eiichi YAGI (Fac. Sci. & Eng., Waseda Univ.)
Yasuhiro YAMADA (Fac. Sci., Tokyo Univ. of Sci.)
Toshimitsu YAMAZAKI (Grad. Sch. Sci., Univ. of Tokyo)
Yutaka YOSHIDA (Fac of Sci. & Tech., Shizuoka Inst. Sci. & Tech.)
Masaru YOSOI (RCNP, Osaka Univ.)
Arkady YUKHINCHUK (VNIIEF, Russia)
Johann ZMESKAL (SMI, Austria)

Visting Technicians
Shinji KAI (Tanaka Kikinzoku Kogyo K.K.)
Jumpei NAKAMURA (IMSS, KEK)
Kazuo OOYAMA (JOHO com.)
Kunihiro SHIMA (Tanaka Kikinzoku Kogyo K.K.)

Research Consultants
Yoshinori AKAISHI
Atsuko ITO
Masayasu KAMIMURA
Hironari MIYAZAWA

Junior Research Associates
Yuya FUJIWARA (Grad. Sch. Sci., Univ. of Tokyo) (After April, Student Trainee)
Yuki NOZAWA ((Grad. Sch. Sci., Kyoto Univ.)
Yuta SADA (Grad. Sch. Sci., Kyoto Univ.)
Makoto TOKUDA (Grad. Sch. Sci. & Eng., Tokyo Tech.)
Tadashi HASHIMOTO (Grad. Sch. Sci., Univ. of Tokyo) (After April, Student Trainee)

International Program Associates

Budi ADIPERDANA (UNPAD, Indonesia)
Hanjie GUO (Zhejiang Univ., China)

Student Trainees

Yuki AKIYAMA (Grad. Sch. Sci. & Eng., Shizuoka Inst. Sci. & Tech.)
Ryo DEGAWA (Grad. Sch. Sci., Tokyo Univ. Sci.)
Shun ENOMOTO (Grad, Sch. Sci., Osaka Univ.)
Jafar ESMAILI (Isfahan Univ. Tech., Iran)
Tatsuya FURUNO (Grad. Sch. Eng., Kyoto Univ.)
Daisuke FURUSAWA (Grad. Sch. Eng., Kyoto Univ.)
Maryam HASSANVAND (Isfahan Univ. Tech., Iran)
Masatoshi HIRAISHI (Grad Sch. High Enegy Acce. Sci., Sokendai)
Suguru IGARASHI (Grad. Sch. Sci. & Eng., Aoyama Gakuin Univ.)
Masato IMAIZUMI (Grad. Sch. Eng., Tohoku Univ.)
Takuya INABE (Grad. Sch. Eng., Tohoku Univ.)
Kentaro INOUE (Grad. Sch. Sci., Osaka Univ.)
Miho ITO (Grad. Sch. Sci. & Eng., Saitama Univ.)
Satoshi ITOH (Grad. Sch. Sci., Univ. of Tokyo)
Takuya KAKURAI (Grad. Sch. Sci., Univ. of Tokyo)
Richika KATO (Grad. Sch. Sci., ICU)
Yuka KAWAHARA (Grad. Sch. Sci., Tokyo Univ. Sci.)
Akio KAWASAKI (MIT, USA)
Hiroaki KOBAYASHI (Grad. Sch. Arts & Sci., Univ. of Tokyo)
Jun KOBAYASHI (Fac. Sci., Saitama Univ.)
Hiroshi KOU (Grad. Sch. Sci. & Eng., Tokyo Tech.)
Hiroto KUMABE (Grad. Sch. Sci. & Eng., Shizuoka Inst. Sci. & Tech.)
Kazuya MAE (Grad. Sch. Sci, ICU)
Tatsuya MATSUE (Fac. Sci., Tokyo Univ. Sci.)
Ryo MIYATANI (Fac. Sci., Tokyo Univ. of Sci.)
Masanori MIYAZAKI (Grad Sch. Phys. Sci., Sokendai)
Yohei MURAKAMI (Grad. Sch. Sci., Univ. of Tokyo)
Masaki NAKAMURA (Grad. Sch. Sci. & Eng., Tokyo Tech.)
Noritsugu NAKATSUKA (Grad. Sch. Eng., Kyoto Univ.)
Koki NARUSE (Grad. Sch. Eng., Tohoku Univ..)
Yugo NINOMIYA (Grad, Sch. Eng & Sci., Osaka Univ.)
Takahiro NISHI (Grad. Sch. Sci., Univ. of Tokyo)
Ayumi OCHIAI (Fac. Sci., Tokyo Univ. of Sci.)
Noriaki OKABE (Grad. Sch. Sci. & Eng., Saitama Univ.)
Kota OKOCHI (Grad. Sch. Sci., Univ. of Tokyo)
Yusuke ONODERA (Grad. Sch. Sci. & Eng., Saitama Univ.)
Kaori OTAKE (Coll. of Liberal Arts, ICU)
Anba Datt PANT (Grad. Sch. Sci. & Eng., Yamanashi Univ.)
Manami SATAKE (Grad. Sch. Sci. & Eng., Tokyo Tech.)
He Xi SHI (Grad. Sch. Sci., Univ. of Tokyo)
Kazuma SHIGA (Fac. Sci., Tokyo Univ. of Sci.)
Ryo SHIMIZU (Fac. Sci., Tokyo Univ. of Sci.)
Takaaki SHINKAWA (Grad. Sch. Sci. & Eng., Saitama Univ.)

Edi SUPRAYOGA (ITB, Indonesia)
Wayan Gede SUHARTA (ITSNS, Indonesia)
Kensuke SUZUKI (Grad. Grad. Sch. Eng., Tohoku Univ.)
Yoshiki TANAKA (Grad. Sch. Sci., Univ. of Tokyo)
Kazuhiro TAKAHASHI (Grad. Sch. Sci., Univ. of Tokyo)
Hiroki TAKEDA (Grad. Sch. Sci. & Eng., Aoyama Gakuin Univ.)
Koichi TODOROKI (Grad. Sch. Sci., Univ. of Tokyo)
Natsuki TOMIDA (Grad. Sch. Sci., Kyoto Univ.)
Yoshinori TSUKAMOTO (Fac. Sci. & Eng., Shizuoka Inst. Sci. & Tech.)
Yoshiko TSUKIYAMA (Grad. Sch. Sci. & Eng., Saitama Univ.)
Tomotaka UEHARA (Fac. Sci., Saitama Univ.)
Ryo USUI (Fac. Sci., Tokyo Univ. of Sci.)
Yuni WATANABE (Grad. Sch. Sci., Univ. of Tokyo)
Riku YAMAGUCHI (Fac. Sci., Tokyo Univ. Sci.)
Hiroyuki YAMADA (Grad. Sch. Sci., Univ. of Tokyo)
Noyuri YAMAMURA (Grad. Sch. Sci, ICU)
Mamoru YASUIKE (Fac. Sci., Tokyo Univ. Sci.)
Tomohiro YASUNAGA (Fac. Sci. & Eng., Doshisha Univ.)
Junya YOSHIDA (Grad. Sch. Arts & Sci., Univ. of Tokyo)

Part-time Staff

Toshihiko HIRAIWA (Grad. Sch. Sci., Kyoto Univ.)

Assistants

Yoko FUJITA
Yuri TSUBURAI

Sub Nuclear System Research Division
RIKEN-BNL Research Center

1. Abstract

The RIKEN BNL Research Center was established in April 1997 at Brookhaven National Laboratory. The Center is dedicated to the study of strong interactions, including spin physics, lattice QCD and RHIC physics through the nurturing of a new generation of young physicists. The Center has three research groups: Theory Group led by L. McLerran, Experimental Group led by Y. Akiba, and Computing Group led by T. Izubuchi. In addition to the strong research program in these three groups, we have a joint-fellowship program with other Universities. The fellowship program enables a talented researcher to maintain a tenure track position at his/her university as well as a Fellow position at RBRC for a certain period of time.

2. Major Research Subjects

Major research subjects of the theory group are
(1) Perturbative QCD
(2) Phenomenological QCD

Major research subject of the experimental group are
(1) Experimental Studies of the Spin Structure of the Nucleon
(2) Study of Quark-Gluon Plasma at RHIC
(3) PHENIX detector upgrades

Major research subject of the computing group is
(1)Lattice QCD numerical research

3. Summary of Research Activity

Summary of Research Activities of the three groups of the Center are given in the sections of each group.

Director
Nicholas P. SAMIOS (Ph.D)

Administrative Staff / RIKEN Japan
Shigeki ASAKAWA (Administration Manager, Accelerator-based Research Promotion Section)
Kazunori MABUCHI (Deputy Administration Manager, RBRC)
Keiko SUZUKI (Japan)

Sub Nuclear System Research Division
RIKEN-BNL Research Center
Theory Group

1. Abstract

The RIKEN BNL Research Center (RBRC) was established in April 1997 at Brookhaven National Laboratory in New York, USA. The Center is dedicated to study of strong interactions, including hard QCD/spin physics, lattice QCD and RHIC physics through nurturing of a new generation of young physicists. The Theory Group activities are closely and intimately related to those of the Nuclear Theory, High Energy Theory and Lattice Gauge Theory Groups at BNL. The RBRC theory group carries out research in three areas: numerical lattice QCD, perturbative QCD and phenomenological QCD. It pioneered the use of the domain-wall fermion method in lattice QCD and has investigated various aspects of hadron physics including the calculation of neutral Kaon CP-violations that is relevant for checking the Cabibbo-Kobayashi-Maskawa theory. The perturbative QCD effort has developed various new methods required for studying hadron structures, especially in spin physics research. The group has pioneered phenomenological QCD researches of color superconductivity, isospin density, and small-x phenomena in extreme hadronic matters.

2. Major Research Subjects

(1) Perturbative QCD
(2) Phenomenological QCD
(3) Lattice QCD numerical research (From 2011, also at RBRC's Computing group)

3. Summary of Research Activity

The RIKENBNL Research Center (RBRC) was established in 1997 to support the RIKEN activities at RHIC in BNL, and also to promote theoretical studies related to RHIC, i.e. theories of strong interaction. The center's first director was T. D. Lee (Columbia University), and in October 2003, the former director of BNL, N. P. Samios, succeeded to the post of director. H. En'yo, Chief scientist of RIKEN in Wako, is also associate director of RBRC. The center consists of a theory group lead by L. Mclerran (BNL), an experimental group lead by Y. Akiba of RIKEN, currently resident at BNL, and a computing group lead by T. Izubuchi (BNL&RBRC).

Research in the RBRC theory group focuses on a wide variety of phenomena caused by the strong interaction, one of the four fundamental interactions in nature. The strong interaction is described theoretically by Quantum Chromodynamics (QCD), and the research projects in the RBRC theory group aim to elucidate various phenomena brought about by the strong interaction from the principles of QCD. Major subjects of our research include studies (a) based on lattice QCD, (b) on spin physics based on perturbative QCD, and (c) on QCD in extreme conditions such as high temperature, high density or high energy. RBRC offers RHIC Physics Fellowships, allowing joint appointments with universities. These Fellowships enable a talented researcher to maintain a tenure track position at his/her university as well as a Fellow position at RBRC for a certain period of time. This system was established in order to increase the research potential of RBRC and to disseminate its research activities and results.

At present, RBRC has cooperative agreements with Arizona State University, the City University of New York, University of Connecticut, Pennsylvania State University, the State University of New York at Stony Brook, Texas A&M University, as well as with BNL and with Lawrence Berkeley National Laboratory.

(1) Perturbative QCD and spin physics

The ongoing RHIC spin experiments have motivated much of the parallel theoretical developments at RBRC. In the area of transverse spin physics, novel predictions have been obtained for the single transverse-spin asymmetry in open charm production in pp collisions at RHIC. This asymmetry probes three gluon correlations in polarized proton. In addition, radiative QCD corrections to single-spin observables were investigated, providing the relevant evolution equations. Further work focused on hyperon production at RHIC, and on azimuthal asymmetries in the Drell-Yan process.

In the spin and perturbative QCD program, a major contribution from the hadronization process to the single transverse spin asymmetry in inclusive hadron production was obtained, which is likely to explain the recent experimental anomaly between the eta and pi mesons. In addition, the evolution and the universality properties of the so-called naive time-reversal odd fragmentation function has been obtained. Other work includes the investigation of the universality properties of the unintegrated gluon distribution a small x .

(2) Phenomenological QCD -- QCD under extreme conditions --

To establish a detailed picture of relativistic heavy ion collisions, QCD-based theoretical approaches are in progress. Especially the idea of "color glass condensation (CGC)" can be a key to understand the initial condition of the heavy ion collision. Other phenomenological approaches are in progress to understand the characteristics of strongly interacting quark gluon plasma. A recent effort has been initiated to understand heavy ion elliptic flow in term s of viscous hydrodynamics. A new finite temperature effective field theory is being developed for the strongly interacting quark gluon plasma to explain the suppression of sheer viscosity in the region of the phase transition.

Efforts on RHIC phenomenology proceed on a broad front. Recent efforts include improving hydrodynamic computations using state of the art equations of state derived from lattice gauge theory. Understanding the nature of matter at high baryon number density has generated the idea of Quarkyonic Matter, that may have implications for an upcoming low energy run at RHIC and eventual experiments in the future at FAIR and NICA. An issue being studied is the nature of mass generation and the breaking of translational invariance. A central focus of work at RBRC, the Color Glass Condensate and the Glasma, matter that controls the high energy limit of QCD, is being realized in experiments at RHIC. A workshop held in May 2010 summarized activity in this field, and proceedings will come out as a special edition of Nuclear Physics A. Much activity focuses on the relation between observations at LHC and the implications made at RHIC.

Group Leader

Larry McLERRAN

Deputy Group Leader

Robert PISARSKI

Members

Derek TEANEY *2
Adrian DUMITRU *2
Cecilia LUNARDINI *2
Anna STASTO *2
Jinfeng LIAO *2
Fedor BEZRUKOV *2
Ho-Ung YEE *2
Zhongbo KANG *3
Adam BZDAK *3
Shu Lin *3(RIKEN FPR)
Koji KASHIWA *4

Visiting Members

Miklos GYULASSY (Columbia Univ., USA)
Robert L. JAFFE (Massachusetts Inst. Technol., USA)
Edward SHURYAK (State Univ. New York, Stony Brook, USA)
Testufumi HIRANO (U. Tokyo)
Feng YUAN (LBNL)

Secretarial Staff

Kerry KIRCHHOFF (Secretary to Director N. P. Samios)
Pamela ESPOSITO (Theory and Computing Group Secretary)
Taeko ITO (Experimental Group Secretary and Assistant to Account Manager for Administration)

****1 RIKEN BNL Fellow *2 RHIC Physics Fellow,***
****3 Research Associate, *4 Special Postdoctoral Researcher, *5 RHIC visiting***

Sub Nuclear System Research Division
RIKEN BNL Research Center
Computing Group

1. Abstract

The Computing Group at the RIKEN BNL Research Center (RBRC) was split from the Theory Group at the RBRC in October 2011.

The main mission of the group is to provide important numerical information that is indispensable for theoretical interpretation of experimental data using the theories of particle and nuclear physics. Their primary area of research is lattice quantum chromodynamics (QCD), in which the strong interactions between quarks and gluons are simulated from first principles on large-scale computers.

A unique feature of their studies is the use of quark fields on lattices with *chiral symmetry*, called domain-wall quarks, which has been extensively developed in the RBRC since 1996. The Computing Group has strong ties to the High Energy Theory, Nuclear Theory, and Lattice Gauge Theory Groups at BNL as well as with theory groups at other US universities such as Columbia University and the University of Connecticut. As part of their activities, they form one of the largest lattice QCD collaborations, the RIKEN BNL Columbia (RBC) Collaboration, which began in 2000 and was extended in 2005 to include another active collaboration, the UKQCD collaboration, based primarily at the University of Edinburgh and the University of Southampton.

2. Major Research Subjects

(1) Search for new law of physics through tests for Standard Model of particle and nuclear physics, especially in the framework of the Cabibbo–Kobayashi–Maskawa (CKM)
(2) Dynamics of QCD and related theories
(3) Theoretical and algorithmic development for lattice field theories

3. Summary of Research Activity

In 2011, QCD with Chiral Quarks (QCDCQ), a third-generation lattice QCD computer that is a pre-commercial version of IBM's Blue Gene/Q, was installed as an in-house computing resource at the RBRC. The computer was developed by a collaboration among RBRC, Columbia University, the University of Edinburgh, and IBM. Two racks of QCDCQ having a peak computing power of 2 × 200 TFLOPS are in operation at the RBRC. In addition to the RBRC machine, one rack of QCDCQ is owned by BNL for wider use for scientific computing. In 2013, 1/2 rack of Blue Gene/Q is also installed by US-wide lattice QCD collaboration, USQCD. The group has also used the IBM Blue Gene supercomputers located at Argonne National Laboratory and BNL (NY Blue), and the cluster computers at RIKEN (Japan), Fermi National Accelerator Laboratory , the Jefferson Lab, and others.

Such computing power enables the group to perform precise calculations using up, down, and strange quark flavors with proper handling of the important symmetry, called chiral symmetry, that quarks have. Several projects are ongoing: flavor physics in the framework of the CKM theory for kaons and B mesons; the electromagnetic properties of hadrons; hadronic contributions to the muon's anomalous magnetic moment; the proton's and neutron's electric dipole moments; proton decay; nucleon form factors, which are related to the proton spin problem; and QCD thermodynamics in finite temperature/density systems such as those produced in heavy-ion collisions at the Relativistic Heavy Ion Collider. Major breakthroughs on important problems such as the direct CP violation process ($K \to \pi\pi$, ε'/ε) will be attempted using this computer.

Group Leader
Taku IZUBUCHI *1

Members
Tomomi ISHIKAWA *1
Brian TIBURZI *2
Eigo SHINTANI *3
Christoph LEHNER *3(RIKEN FPR)

Visiting Members

Yasumichi AOKI (Nagoya Univ.)
Robert MAWHINNEY (Columbia Univ., USA)
Shigemi OHTA (KEK)
Thomas BLUM (University of Connecticut)
Chulwoo JUNG (BNL)
Meifeng LIN (Yale Univ.)
Yusuke TANIGUCHI (Tsukuba Univ.)
Takeshi YAMAZAKI (Nagoya Univ.)

Secretarial Staff

Kerry KIRCHHOFF (Secretary to Director N. P. SAMIOS)
Pamela ESPOSITO (Theory and Computing Group Secretary)
Taeko ITO (Experimental Group Secretary and Assistant to Account Manager for Administration))

****1 RIKEN BNL Fellow *2 RHIC Physics Fellow,***
****3 Research Associate, *4 Special Postdoctoral Researcher,***
****5 RHIC visiting Fellow***

Sub Nuclear System Research Division
RIKEN-BNL Research Center
Experimental Group

1. Abstract

RIKEN BNL Research Center (RBRC) Experimental Group studies the strong interactions (QCD) using RHIC accelerator at Brookhaven National Laboratory, the world first heavy ion collider and polarized p+p collider. We have three major activities: Spin Physics at RHIC, Heavy ion physics at RHIC, and detector upgrades of PHENIX experiment at RHIC.

We study the spin structure of the proton using the polarized proton-proton collisions at RHIC. This program has been promoted by RIKEN's leadership. The first focus of the research is to measure the gluon spin contribution to the proton spin. Our recent data analysis has shown that the proton spin carried by the gluons is small, which is a very striking finding beyond our expectations.

The aim of Heavy ion physics at RHIC is to re-create Quark Gluon Plasma (QGP), the state of Universe just after the Big Bang. Two important discoveries, jet quenching effect and strong elliptic flows, have established that new state of dense matter is indeed produced in heavy ion collisions at RHIC. We are proceeding to understand the nature of the matter. Recently, we have measured direct photons in Au+Au collisions for $1<p_T<3$ GeV/c , where thermal radiation from hot QGP is expected to dominate. The comparison between the data and theory calculations indicates that the initial temperature of 300 MeV to 600 MeV is achieved. These values are well above the transition temperature to QGP, which is calculated to be approximately 170 MeV by lattice QCD calculations.

We has major roles in detector upgrades of PHENIX experiment, namely, the silicon vertex tracker (VTX) and muon trigger upgrades. Both of these two upgrade projects have been completed recently and we took the first data using the upgrade detectors.

2. Major Research Subjects

(1) Experimental Studies of the Spin Structure of the Nucleon
(2) Study of Quark-Gluon Plasma at RHIC
(3) PHENIX detector upgrades

3. Summary of Research Activity

The RIKEN-BNL Research Center was established in 1997 to support the RIKEN activities at RHIC in BNL, and also to promote theoretical studies related to RHIC, i.e. theories of strong interaction. The center's first director was T. D. Lee (Columbia University), and in October 2003, the former director of BNL, N.P. Samios, succeeded to the post of the director. The center consists of a theory group lead by L. McLerran, a computing group lead by T. Izubuchi, and an experimental group lead by Y. Akiba, a vice chief scientist of RIKEN in Wako.

We study the strong interactions (QCD) using the RHIC accelerator at Brookhaven National Laboratory, the world first heavy ion collider and polarized p+p collider. We have three major activities: Spin Physics at RHIC, Heavy ion physics at RHIC, and detector upgrades of PHENIX experiment.

(1) Experimental study of spin structure of proton using RHIC polarized proton collider

How is the spin of proton formed with 3 quarks and gluons? This is a very fundamental question in Quantum Chromodynamics (QCD), the theory of the strong nuclear forces. The RHIC Spin Project has been established as an international collaboration between RIKEN and Brookhaven National Laboratory (BNL) to solve this problem by colliding two polarized protons for the first time in history. This project also has extended the physics capabilities of RHIC.

The first goal of the RHIC spin physics program is to elucidate a contribution of the gluon spin in the proton spin. We have measured double-helicity asymmetries of neutral pions to study gluon polarization in proton. Our most recent publication from 2006 run have shown that the gluon polarization in the proton is small, and only about half of proton spin can be accounted by gluon spin in the measured region of gluon momentum in proton. The remaining part must be carried by gluons in lower momentum region where the measurement is not sensitive, and/or reside in the orbital-angular momentum of quarks and gluons.

To finalize the smallness of the gluon-spin contribution, we need to measure double helicitiy asymmetry in direct photon production. This process is dominated by a single and the simplest process, gluon Compton scattering, in perturbative QCD, and is the golden channel to determine the gluon density and the gluon polarization in the proton. We published a paper on direct photon cross section in p+p collisions at RHIC. Preliminary results on double-helicity asymmetry of direct photon from the 2006 run have been obtained.

We have also accumulating transversely-polarized proton collision data to measure single transverse-spin asymmetries of processes which are predicted to be sensitive to the orbital-angular momentum of quarks and gluons. In 2006, 2008, and 2012 PHENIX recorded 2.7/pb, 4.5/pb, and 9.2/pb respectively, of transversely-polarized proton collisions data at 200 GeV to investigate single transverse-spin asymmetries. Several transverse spin analyses of these high statistics data are on going.

The 2009 run of RHIC is a major spin run. We had the first 500 GeV p+p run and a long p+p run at 200 GeV. The main purpose of the 500 GeV run is to measure anit-quark polarization from the single longitudinal asymmetry A_L in the W boson production. Approximately 14/pb of data were recorded in PHENIX in the 5 weeks of 500 GeV data taking period. From this data we have observed the first signal of W→e decays in p+p collisions in PHENIX central arm. We measured the production cross section of the W boson and a large spin asymmetry A_L in the W production. These results have been recently published in Physical Review Letters.

We have the second 500 GeV polarized p+p run in 2011. New steel absorber and new muon trigger system have been installed in PHENIX before the run to improve our capability to measure muons from the W decays. Approximately 25/pb of data were recorded during the run. Recently we had preliminary results of single spin asymmetry A_L of $W\rightarrow\mu$ in the 2011 run.

In addition to the study of polarized p+p collisions at RHIC, we study quark fragmentation function. With collaboration with the BELLE experiment at High Energy Accelerator Research Organization (KEK), we discovered that the spin direction of a quark can be determined from its hadronic fragments. Precise data of the quark fragmentation function can be used to understand the cross sections and the spin dependences of particle production in polarized p+p collisions at RHIC. We continue the study of the quark fragmentation function at BELLE.

(2) Experimental study of Quark-Gluon Plasma using RHIC heavy-ion collider

The goal of high energy heavy ion physics at RHIC is study of QCD in extreme conditions i.e. at very high temperature and at very high energy density. Experimental results from RHIC have established that dense partonic matter is formed in Au+Au collisions at RHIC. The matter is very dense and opaque, and it has almost no viscosity and behaves like a perfect fluid. These conclusions are primarily based on the following two discoveries:

- Strong suppression of high transverse momentum hadrons in central Au+Au collisions (jet quenching)
- Strong elliptic flow

The focus of the research in heavy ion physics at RHIC is now to investigate the properties of the matter. RBRC have played the leading roles in some of the most important results from PHENIX in the study of the matter properties. These include (1) measurements of heavy quark production from the single electrons from heavy flavor decay (2) measurements of J/y production (3) measurements of di-electron continuum and (4) measurements of direct photons.

The most important recent result is the measurement of direct photons for $1<p_T<5$ GeV/c in p+p and Au+Au through their internal conversion to e^+e^- pairs. If the dense partonic matter formed at RHIC is thermalized, it should emit thermal photons. Observation of thermal photon is direct evidence of early thermalization, and we can determine the initial temperature of the matter. It is predicted that thermal photons from QGP phase is the dominant source of direct photons for $1<p_T<3$ GeV/c at the RHIC energy. We measured the direct photon in this pT region from measurements of quasi-real virtual photons that decays into low-mass e^+e^- pairs. Strong enhancement of direct photon yield in Au+Au over the scaled p+p data has been observed. Several hydrodynamical models can reproduce the central Au+A data within a factor of two. These models assume formation of a hot system with initial temperature of T_{init} = 300 MeV to 600 MeV. This is the first measurement of initial temperature of quark gluon plasma formed at RHIC. These results are recently published in Physical Review Letters. Y. Akiba received 2011 Nishina Memorial Prize for this work.

Recently, we have constructed and installed a silicon vertex tracker VTX as written in the next section. Measurements of heavy quark production in p+p and A+A collisions using the new detector is the main focus of the group in the coming years. First VTX data is obtained in 2011 Au+Au run. More data in p+p, Cu+Au and U+U were obtained in 2012 run. We are working on the analysis of these data sets.

(3) PHENIX detector upgrade

The group has major roles in several PHENIX detector upgrades, namely, the silicon vertex tracker (VTX) and muon trigger upgrades.

VTX is 4 layers of silicon tracker, jointly funded by RIKEN and the US DOE. The inner two layers are silicon pixel detectors and the outer two layers are silicon strip detectors. The detector has been completed in November 2010 and has been installed in PHENIX IR. With this new detector we can measure heavy quark (charm and bottom) production in p+p and heavy ion collisions. We took the first data with the new detector in 2011.

Muon trigger upgrades are needed for W→ mu measurement at 500 GeV. New trigger electronics (Muon Trigger FEE) have been installed in the muon arms. New muon trigger detectors based on RPC technology have been also installed. With these new trigger-systems, we started measuring the W production in forward and backward direction in 2011 and recorded approximately 25/pb of polarized p+p collision data. Approximately twice of the data was obtained in 2012 run.

Group Leader

Yasuyuki AKIBA

Deputy Group Leader

Abhay DESHPANDE

Members

Yuji GOTO
Itaru NAKAGAWA
Takashi ICHIHARA
Atsushi TAKETANI
Yasushi WATANABE
Satoru YOKKAICHI
Ralf-Christian SEIDL
Kensuke OKADA *1
Kieran BOYLE *1
Josef SEELE *1
Stefan BATHE *2
Xiaorong WANG *2
John KOSTER *3 (RIKEN FPR)
Chin-Hao CHEN *3
Maki KUROSAWA *4

Visiting Members

Naohito SAITO (KEK)
Zheng LEE (BNL)
Kiyoshi TANIDA (Seoul Univ.)
Akio OGAWA (BNL)
Masahiro OKAMURA (BNL)
Rachid NOUICER (BNL)
Kotaro KONDO (BNL)
Ady HERSHCOVITCH (BNL)

****1RIKEN BNL Fellow, *2 RHIC Physics Fellow,***
****3 Research Associate, *4 Special Postdoctoral Researcher,***

RIBF Research Division
Radioactive Isotope Physics Laboratory

1. Abstract

This laboratory explores exotic nuclear structures and dynamics in exotic nuclei that have never been investigated before, such as those with highly unbalanced proton and neutron numbers. Our aim is to discover new phenomena and properties in exotic nuclei by developing new experimental techniques using fast radioisotope beams. Another important subject is the equation of state (EOS) in asymmetric nuclear matter and its association with the origin of elements and with neutron stars. For instance, we are attempting to better understand the underlying mechanism for exotic stability enhancements of very neutron-rich fluorine isotopes, the large deformation of the nucleus of Mg-34 with $N = 22$ despite its closeness to the $N = 20$ magic neutron number, and anomalous collectivity in ^{16}C. We are further extending these studies to medium- and heavy-mass regions by developing facilities, detectors, and unique methods at the Radioisotope Beam Factory (RIBF), thereby leading the challenging task of finding new exotic phenomena.

2. Major Research Subjects

(1) Study of structure and dynamics of exotic nuclei through development of new tools in terms of reaction- and technique-based methodology
(2) Research on EOS in asymmetric nuclear matter via heavy-ion-induced reactions
(3) Detector development for spectroscopy and reaction studies

3. Summary of Research Activity

(1) Missing mass method

The missing mass technique is promising for programs at the RIBF. Detection of recoil particles from a target is essential in determining the excitation energy of particle unbound states assuming no particle and gamma decay processes, and also obtaining the transfer angular momentum from the angular distribution measurement. We developed a solid hydrogen target as well as a detector system called ESPRI for proton (in)elastic scattering. In 2010, the first missing mass spectroscopy was performed at the RIBF, where the state-of-art detector MUST2 was solicited from France to investigate the matter distributions and unbound excited states of ^{24}O and its neighboring nuclei via proton elastic and inelastic scattering. The data are now being analyzed.

At the RIPS facility, a missing mass program under the PKU-RIKEN collaboration was conducted in 2009. In this program, the (p,p alpha) reaction was employed to investigate molecular structure in ^{6}He and ^{8}He, as well as the ^{7}H structure.

(2) In-beam gamma spectroscopy

In the medium- and heavy-mass region explored at the RIBF, the collective natures of nuclei are an important subject; they are obtained through the production and observation of high-excitation and high-spin states. To populate these states, heavy-ion-induced reactions such as fragmentation and fission are useful. To date, we have developed a two-step fragmentation technique as an efficient method of identifying and populating excited states, and lifetime measurements to deduce the transition strength. At the end of 2008, the first spectroscopy on the nuclei island-of-inversion region was performed, and the resulting data for the first excited state in ^{32}Ne were published in PRL in 2009. At the end of 2009, the second in-beam gamma spectroscopy campaign was organized, and backgrounds originating from atomic processes in heavy targets were investigated. At the end of 2010, the island-of-inversion region was revisited, and the region at $N = 28$ was also investigated. A multitude of data were obtained via the inelastic, nucleon knock-out, and fragmentation channels.

In 2011, preliminary results obtained from the 2010 data were presented at the ARIS11 conference. In October and November, in-beam gamma spectroscopy for a ^{78}Ni region and the vicinity of ^{132}Sn was conducted. In 2012, Coulomb excitation of ^{104}Sn was conducted, and excited states in ^{53}Ca and ^{54}Ca were observed.

(3) Decay spectroscopy

Beta and isomer spectroscopy are among the most efficient methods of studying nuclear structure, especially at non-yrast levels. We accumulated experimental techniques at the RIPS facility to investigate nuclear structure in the light-mass region via beta–gamma and beta–p coincidence. Concerning the medium- and heavy-mass region available at the RIBF, we developed two position-sensitive active stoppers to achieve low background via position correlation: strip-silicon detectors and a cylindrical active stopper called CAITEN. At the end of 2009, the first decay spectroscopy on neutron-rich nuclei with $A \sim 100$ was performed at the new RIBF facility. The half-lives of 18 neutron-rich nuclei were determined for the first time, and the results were published in PRL, where we discussed them in comparison with theoretical predictions as well as in terms of the r-process path. The 2009 data set produced two more letters on a new deformed magic number, $N = 64$, in the Zr isotopes (PRL) and development of axial symmetry in ^{110}Mo (PLB). At the same time, the CAITEN detector was successfully tested with fragments produced with a ^{48}Ca beam.

To further promote decay spectroscopy, the EUroball-RIKEN Cluster Array (EURICA) collaboration has begun. A few workshops were organized to discuss physics cases. Under the EU-RIKEN collaboration, 12 Euro Cluster Arrays have been installed at the RIBF. At the end of March 2012, the EURICA was commissioned and found to have the expected performances. Since June 2012, the EURICA setup has produced a multitude of data at the RIBF. In 2013, the EURICA setup was strengthened by the addition of Surry and Brighton $LaBr_3$ detectors solicited to measure the lifetime of excited states.

(4) Equation of state via heavy-ion central collisions

The EOS in asymmetric nuclear matter is a major subject in the physics of exotic nuclei. Concerning RIBF programs, a detector for pions produced in heavy-ion collisions is being tested at the HIMAC. A time projection chamber (TPC) for the SAMURAI spectrometer (SAMURAI-TPC) is being constructed under a collaboration with MSU and will be installed in 2014. The first EOS experiment is scheduled for fall of 2014.

(5) Nucleon correlations and cluster states in exotic nuclei

Nucleon correlations and cluster in nuclei are the central focus in a “beyond mean-field” picture. The relevant programs with in-beam gamma and invariant-mass techniques will depict nucleon condensations and correlations in nuclear media as a function of the density and temperature. Neutron halos and skin nuclei are laboratories for examining dilute neutron matter at the surface. By changing the excitation energies in neutron-rich nuclei, clustering phenomena and the role of neutrons will be investigated. In spring 2013, cluster states in ^{16}C have been sought via inelastic alpha scattering at the SAMURAI spectrometer, and benchmark data on the proton–neutron correlation in ^{12}C have been obtained via nucleon knock-out reactions with a C target.

Head

Hiroyoshi SAKURAI

Members

Takashi ICHIHARA
Takashi KISHIDA
Yukari MATSUO
Shunji NISHIMURA
Hideaki OTSU
Yoichi NAKAI
Pieter DOORNENBAL from Apr. 01
Hiu Ching LEE
Tadaaki ISOBE

Research Associates

Mizuki NISHIMURA
Hiroshi WATANABE until Aug. 30
Satoshi TAKEUCHI

Contract Researcher

Taro NAKAO until Mar. 31

Special Postdoctoral Researchers

Daiki NISHIMURA until Mar. 31
Juzo ZENIHIRO until Mar. 31

Foreign Postdoctoral Researchers

Pieter DOORNENBAL until Mar. 31
Zhihuan LI
Giuseppe LORUSSO from Sept. 19
David STEPPENBECK until Feb. 15

Senior Visiting Scientists

Shigeru KUBONO (University of Tokyo)
Kengo OGAWA (Chiba Univ.)

Visiting Scientists

Dam BINH (Institute of Physics, Vietnam Academy of Science and Technology,)
Silvio CHERUBINI (University of Catania, Italy)
Adrian GELBERG (Universitat zu Koeln, Germany)
Chuangye HE (China Institute of Atomic Energy)
Hyo Soon JUNG (Seoul National University)
Le KHIEM (Institute of Physics, Vietnam Academy of Science and Technology,)
Nikolaus KURZ (GSI, Germany)
Indranil MAZUMDAR (Tata Institute)
Evgueni NIKOLSKII (RRC Kurchatov Institute, Institute of General and Nuclear Physics, Russia)
Hooi Jin ONG (RCNP, Osaka Univ.)
Xiaolong WANG (Kyoto Univ.)
Kazuo IEKI (Rikkyo Univ.)
Yosuke KONDO (Tokyo Institute of Technology)
Kimiko SAKAGUCHI (Tohoku Univ.)
Megumi NIIKURA (University of Tokyo)
Daiki NISHIMURA (Tokyo University of Science) from Apr. 01
Nori AOI (RCNP, Osaka Univ.)
Naohiko OTSUKA (International Atomic Energy Agency, Austria)
Toshiyuki SUMIKAMA (Tohoku Univ.)
Takashi NAKAMURA (Tokyo Institute of Technology)
Hiroshi WATANABE (Beihang University) from Sept.
Atsushi HATAKEYAMA (Tokyo University of Agriculture and Technology)
Takamasa MOMOSE (The University of British Columbia, Canada)
Maya TAKECHI (GSI, Germany)
Mitsunori FUKUDA (Osaka Univ.)

Research Consultants

Yasuyuki GONO
Harutaka SAKAGUCHI
Yasuo AOKI
Tateaki TORII

Junior Research Associates

Kenta YOSHINAGA
Shintaro GO
Masami SAKO until Mar. 31
Masafumi MATSUSHITA
David STEPPENBECK from Feb. 16

Student Trainees

Yifan FANG (Osaka Univ.)
Jongwon HWANG (Seoul National University)
Duy NGUYEN (Institute of Physics, Vietnam Academy of Science and Technology)

Kosuke ABE (Nigata Univ.)
Takeshi ITO (Nigata Univ.)
Masaharu IZAWA (Meiji Univ.)
Takumi USUKURA (Rikkyo Univ.)
Yuuta SHIOKAWA (Rikkyo Univ.)
Yuki KATO (Meiji Univ.)
Daiki KANNO (Tokyo Institute of Technology)
Koudai IWAMOTO (Osaka Univ.)
Kouki KAMEI (Tohoku Univ.)
Takamasa YOSHIDA (Rikkyo Univ.)
Hiroyuki MIYASAKO (Miyazaki Univ.)
Syuu MIYAZAWA (Saitama Univ.)
Junpei MIYAZAKI (Tohoku Univ.)
Sunji KIM (Seoul National University)
Shumpei KINNO (Tokyo University of Science)
Sho KUBOTA (Tokyo University of Agriculture and Technology)
Yo KENMOKU (Osaka Univ.)
Hirotaka FURUKI (Osaka Univ.)
Yuta EBARA (Tokyo Gakugei Univ.)
Kento TAKAHASHI (Tohoku Univ.)
Jun TAKATSU (Osaka Univ.)
Kei IMAMURA (Meiji Univ.)
Takayuki SAKO (Tokyo Institute of Technology)
Kanae SATO (Saitama Univ.)
Yousuke MITSUYA (Meiji Univ.)
Yasuhiro YAMAGUCHI (Meiji Univ.)
Tetsuya YAMAMOTO (Osaka Univ.)
Naotaka ICHIHASHI (Saitama Univ.)
Yoshiaki SHIGA (Rikkyo Univ.)
Masaru WAKABAYASHI (Osaka Univ.)
Hiroki TETSUKA (Tokyo Gakugei Univ.)
Yifan ZHU (Tokyo University of Science)
Taku SAKAI (Nigata Univ.)
Masami SAKO (Kyoto Univ.) from Apr. 01
Fumi SUZAKI (Saitama Univ.)
Zheng Yu XU (University of Tokyo)
Toshiyuki OGURA (Nigata Univ.)
Kota KOBAYASHI (Rikkyo Univ.)
Nobuyuki KOBAYASHI (Tokyo Institute of Technology)
Keishi MATSUI (University of Tokyo)
Yasuto KAMISHOU (Osaka Univ.)
Hidekazu UENISHI (Osaka Univ.)
Shino ARAI (Meiji Univ.)
Yuusuke MORITA (Tokyo University of Science)
Kenichi SUGIMOTO (Osaka Univ.)
Daishiro SERA (Nigata Univ.)
Shun OGOSHI (Tokyo Institute of Technology)
Seijiro NISHI (Tokyo Institute of Technology)

Hiroki NISHIBATA (Osaka Univ.)
Tomoki ASAKA (Tohoku Univ.)
Miki HAYASAKA (Tokyo Gakugei Univ.)
Takahiro MASHIKO (Tohoku Univ.)
Sosuke MURAMOTO (Meiji Univ.)
Junichi OHNO (Osaka Univ.)
Ryo TANIUCHI (University of Tokyo)
Takahiro NIWA (Tsukuba Univ.)
Yoshihiro NAKAMURA (Nigata Univ.)
Tomohiro NAKASHIMA (Tokyo Institute of Technology)
Masayuki NAGASHIMA (Nigata Univ.)
Takahiro TAGUCHI (Tohoku Univ.)
Kunihiko TAJIRI (Osaka Univ.)
Ryuki TANAKA (Tokyo Institute of Technology)
Daisuke WATANABE (Tokyo University of Science)
Yoshiki TSUTSUI (Meiji Univ.)
Tomomi FUJITA (Meiji Univ.)
Ryogo MINAKATA (Tokyo Institute of Technology)
Ayumi YAGI (Osaka Univ.)
Daiki TOMITA (Rikkyo Univ.)
Kotomi MUTO (Tohoku Univ.)
Shota HIRASAWA (Tokyo University of Science)
Hisaya HOTAKA (Tokyo University of Science)
Masaki YAGUCHI (Osaka Univ.)
Giseung LEE (Tokyo Institute of Technology)
Shinji SUZUKI (Nigata Univ.)
Yasunori WADA (Tohoku Univ.)
Sijie DAI (Nishina School Peking Univ.)
Lijian GE (Nishina School Peking Univ.)
Fengyun LI (Nishina School Peking Univ.)
Jing LI (Nishina School Peking Univ.)
Tiantian WANG (Nishina School Peking Univ.)
Qiang WU (Nishina School Peking Univ.)
Hao XIE (Nishina School Peking Univ.)
Jinmin YANG (Nishina School Peking Univ.)
Daneng YANG (Nishina School Peking Univ.)
Hiroyuki OOTAGURO (Tokyo Metropolitan College of Industrial Technology)
Kazuya YORIMOTO (Tokyo Metropolitan College of Industrial Technology)

International Program Associates

Frank BROWNE
Ruijiu CHEN
Guillaume GEY
Hongna LIU
Kevin MOSCHNER
Jan TAPROGGE
Zsolt VAJTA
He WANG

Jin WU
Xiaofei YANG

Visiting Researchers
Didier BEAUMEL
Umesh GARG
Giuseppe LORUSSO until Sept. 18
Paer-Anders SOEDERSTROEM

Visiting Technicians
Ivan KOJOUHAROV
Henning SCHAFFNER

Secretaries
Yu NAYA
Tomoko FUJII

RIBF Research Division
Spin isospin Laboratory

1. Abstract

A nucleus is a finite-body quantum system of hadrons and is a self-organizing system governed by the strong interaction. How do "variety" and "regularity" develop and coexist in the nuclear world? We are aiming at clarifying its mechanism through experimental studies of radio-active nuclei produced at the RI Beam Factory.
In particular, the Spin-Isospin Laboratory pursues research activities putting focus on interplay of spin and isospin which are manifestations of symmetry of nature.
We are, at present, performing experiments with spin-polarized protons to solve the magicity-loss problem appearing far from the beta-stability line.

2. Major Research Subjects

(1) Experimental studies of radioactive nuclei via direct reactions
(2) Search for undiscovered states through RI-beam induced reactions
(3) Production of spin-polarized nuclei
(4) Study of nucleo-systhesis with heavy-ion storage ring

3. Summary of Research Activity

(1) Experimental studies of radioactive nuclei via direct reactions

Direct reactions induced by light-ions serve as powerful spectroscopic tools to investigate various aspects of nuclei. We are advancing experimental programs with the light-ion induced reactions with RI-beams in inverse kinematics, by developing new detector systems and advanced target systems. Spin asymmetry measurements for the proton elastic scattering from neutron-rich ^{6,8}He nuclei were performed at 71 MeV/u with a spin-polarized solid proton target. Results of the experiment indicate drastic weakening of the spin-orbit coupling in ^{6,8}He. In 2011, a missing-mass technique was brought into the (p,n) reaction studies in the inverse-kinematics with a newly-developed neutron detector array WINDS. The first experiment for ^{12}Be at 200 MeV/u was highly successful and provided us with rich information on Gamow-Teller strength in the nucleus.

(2) Search for yet-to-be-discovered states through RI-beam induced reactions

RI-beam induced charge exchange reactions have unique properties which are missing in stable-beam induced reactions and can be used to reach yet-to-be-discovered states. The capabilities of RI-beam induced charge exchange reactions are based on availabilities of

- A variety of selectivities in transferred quantum numbers, ΔS, ΔT, $\Delta T\mathbf{z}$, ΔL etc, and
- Kinematical conditions which can not be reached via the stable-beam induced reactions.

Several experiments have been done or are planned with the SHARAQ spectrometer at RIBF. In 2009, the first (t, ^{3}He) experiment with the SHARAQ spectrometer was performed for ^{90}Zr and ^{208}Pb targets and the results clearly shows a bump structure identified to be β^{+}-type isovector spin monopole resonances. A series of experiments to search for other isovector monopole resonances were conducted in 2010.

(3) Production of spin-polarized nuclei

A spin-polarized solid proton target is developed for use in RI-beam experiments. The polarization principle based on electron spin alignment in photo-excited triplet states in aromatic molecule enables the target operation in a low magnetic field of 0.1 T, which makes the polarized target unique for use in RI-beam experiments.

(4) Study of nucleo-systhesis with heavy-ion storage ring

The r-process of nucleo-synthesis is essentially important in accounting abundances of elements heavier than iron. Despite of its importance, not so much is known about the r-process. Determination of masses of neutron-rich nuclei with mass numbers of 60 or higher is crucial in pinning down the r-process path, which in turn lead us to a deeper understanding of the nucleo-sythesis. A new isochronous storage ring, called “Rare RI ring” is planned to be constructed to determine masses of very rare isotopes with a precision of $\Delta m/m = 10^{-6}$.

Head
Tomohiro UESAKA

Members
Masaki SASANO
Juzo ZENIHIRO

Contract Researcher
Masanori DOZONO

Special Postdoctoral Researcher
Hiroaki MATSUBARA

Senior Visiting Scientists
Hiroyuki SAGAWA (Aizu University)

Visiting Scientists
Takashi WAKUI (Tohoku University)
Satoshi SAKAGUCHI (Kyusyu University)
Kenjiro MIKI (Osaka University)
Yohei MATSUDA (Kyoto University)

Student Trainees
Tomomi KAWAHARA (Toho University)
Tatsuo BABA (Kyoto University)
Taku FUKUNAGA (Kyusyu University)
Tomosuke KADOYA (Kyoto University)
Megumi TAKAHASHI (Tohoku University)
Miho TSUMURA (Kyoto University)
Hidetomo WATANABE (Kyoto University)
Junpei YASUDA (Kyusyu University)
Syuhei GOTANDA (Miyazaki University)

Secretary
Tomoko FUJII
Yu NAYA

Part-timer
Reiko KOJIMA

RIBF Research Division
Superheavy Element Laboratory

1. Abstract

The elements with their atomic number Z>103 are called as trans-actinide or superheavy elements. The chemical properties of those elements have not yet been studied in detail. Those elements does not exist in nature therefore, they must be produced artificially for scientific studies. In our laboratory, we have been studying the physical and chemical properties of the superheavy elements utilizing the accelerators in RIKEN and various methods of efficient production for the superheavy elements.

2. Major Research Subjects

(1) Search for new superheavy elements
(2) Decay spectroscopy of the heaviest nuclei
(3) Study of the chemical properties of the heaviest elements
(4) Study of the reaction mechanism of the fusion process
(5) Development and maintenance of devices related to study of the superheavy elements

3. Summary of Research Activity

(1) Searching for new elements
To expand the periodic table of elements and the nuclear chart, we will search for new elements.

(2) Spectroscopic study of the nucleus of heavy elements
Using the high sensitivity system for detecting the heaviest element, we plan to perform a spectroscopic study of nuclei of the heavy elements.

(3) Chemistry of superheavy elements
Study of chemistry of the trans-actinide (superheavy element) has just started world-wide, making it a new frontier in the field of chemistry. Relativistic effects in chemical property are predicted by many theoretical studies. We will try to develop this new field.

(4) Study of a reaction mechanism for fusion process
Superheavy elements have been produced by complete fusion reaction of two heavy nuclei. However, the reaction mechanism of the fusion process is still not well understood. When we design an experiment to synthesize nuclei of the superheavy elements, we need to determine a beam-target combination and the most appropriate reaction energy. This is when assists of the theory become important. We will try to develop a reaction theory useful in designing an experiment by collaborating with the theorists.

(5) Development and maintenance of devices related to study of the superheavy elements
Gas-filled recoil separator has been used as the main experimental device for the study of superheavy elements. We are developing and maintaining the related devices including detectors for physical and chemical study. We will also offer user support if a researcher wishes to use the devices for his/her own research program.

Head
Kosuke MORITA

Member
Kouji MORIMOTO

Nishina Center Research Scientist
Daiya KAJI

Nishina Center Technical Scientist
Akira YONEDA

Postdoctoral Researcher
Yasuo WAKABAYASHI

Visiting Scientists

Fuyuki TOKANAI (Dept. Phys., Yamagata Univ.)

Research Consultants

Kenji KATORI

Students

Junior Research Associate

Mirei TAKEYAMA (Yamagata Univ.)

Student Trainees

Sayaka YAMAKI(Saitama Univ.)

Kengo TANAKA(Tokyo Univ. of Science)

RIBF Research Division
High Energy Astrophysics Laboratory

1. Abstract

In the immediate aftermath of the Big Bang, the beginning of the universe, only hydrogen and helium existed. However, nuclear fusion in the interior of stars and the explosion of supernovae in the universe over the course of 13.8 billion years led to the evolution of a world brimming with the many different elements we have today. By using man-made satellites to observe X-rays and gamma-rays emitted from celestial objects, we are observing the synthesis of the elements at their actual source. Our goal is to comprehensively elucidate the scenarios for the formation of the elements in the universe, together with our research on sub-atomic physics through the use of an accelerator.

2. Major Research Subjects

(1) Nucleosynthesis in Stars and Supernovae
(2) Particle Acceleration Mechanism in Astronomical Objects
(3) Physics in Extremely Strong Magnetism and Gravity
(4) Research and Development of Innovative X-ray and Gamma-ray detectors

3. Summary of Research Activity

High Energy Astrophysics Laboratory started in April 2010. The goal of our research is to reveal the mechanism of nucleosynthesis in the universe, and to observe exotic physical phenomena in extremely strong magnetic and/or gravitational field. We have observed supernova remnants, strongly magnetized neutron stars, pulsars, black holes and galaxies with X-ray astronomical satellites.

Dr. Satoru Katsuda won the Young Scientist Award of the Physical Society of Japan in the study of expansion dynamics of supernova remnants. We have measured the supernova remnant SN1006 with the Chandra satellite, and compared the image taken in 2012 with one taken in 2001. The comparison revealed that the northwest rim of the supernova remnant was expanding with the velocity of 3000 km/s. We observed the Pup A supernova remnant with the X-ray grating optics onboard the XMM-Newton satellite, and found that a fragment of ejecta showed the Doppler shift with a velocity of 1500 km/s toward us. The observed width of an oxygen line indicated that the ion temperature of plasma was about 30 eV. Measuring the ion temperature is an important breakthrough to know the acceleration efficiency of cosmic-rays at the supernova remnant.

We, Dr. Shin'ya Yamada et al., conducted unified X-ray spectral and timing studies of Cygnus X-1 in the low/hard and hard intermediate state using broadband Suzaku data. The 0.5-300 keV source luminosity changed over 1-5% of the Eddington limit for 15 solar masses. Variations on short (1-2 seconds) and long (days to months) time scales require at least three separate components: a constant component localized below ~ 2 keV, a broad soft one dominating in the 2-10 keV range, and a hard one mostly seen in 10-300 keV range. In view of the truncated disk/hot inner flow picture, these are respectively interpreted as emission from the truncated cool disk, a soft Compton component, and a hard Compton component.

We (Dr. Takao Kitaguchi, Dr. Asami Hayato and Dr. Teruaki Enoto et al.) continue to construct the Gravity and Extreme Magnetism Small Explorer (GEMS) under the collaboration with NASA Goddard Space Flight Center (USA). GEMS is the first dedicated satellite for the X-ray polarimetry, which is opening a new field in Astrophysics and Astronomy. In this fiscal year, we have done: a) polarization measurements and calibrations for the engineering test units of the X-ray polarimeter, b) a lifetime test of the detector, a measurement of a relationship between the basic performance (e.g., gas gain and energy resolution) and the outgassing from the materials inside detector, c) a performance test of the Modulated X-ray Source, the small X-ray generator for the calibration in space, and d) the performance test of the flight-designed Gas Electron Multiplier, which is a key device to multiply electron signals, developed by RIKEN. We developed a Monte-Carlo simulation to calculate the polarimeter response function to X-rays as well as to estimate the background spectrum produced by cosmic radiation. The predicted polarization capability to 4.5 keV X-rays agrees well with that with actual data. Besides, the in-orbit background rate is estimated to be lower than the count rate produced by observation targets. Unfortunately, the project was in the pending state due to the cost overrun on the US side. We are trying to resume the project.

We (Dr. Teruaki Enoto et al.) have tried to reveal the nature of a mysterious subclass of neutron stars, magnetars. We analyzed the Suzaku X-ray observation of an activated magnetar 1E 1547.0-5408, and found that accumulated spectrum of weak short bursts resembles the persistent emission of this source.

Head

Toru TAMAGAWA

Special Postdoctoral Researchers

Satoru KATSUDA
Shin'ya YAMADA
Asami HAYATO

Postdoctral Researchers

Takao KITAGUCHI

JSPS Researcher

Teruaki ENOTO

Visiting Scientists

Yukikatsu TERADA (Saitama Univ.)
Yujin NAKAGAWA (Waseda Univ.)
Madoka KAWAHARADA (ISAS/JAXA)
Aya BAMBA (ISAS/JAXA)
Asami HAYATO (NASA/GSFC)
Atsushi SENDA (JST)
Poshak GANDHI (ISAS/JAXA)
Ken OHSUGA (NAOJ)
Naohisa INADA (Univ. of Tokyo)
Rohta TAKAHASHI (Tomakomai Nat'l College of Tech.)
Toru MISAWA (Shinshu Univ.)
Hiroya YAMAGUCHI (CfA/Harvard Univ.)

Support Scientist / Technical Support Staff

Hiroshi KATO

Students

Junior Research Associates

Atsushi HARAYAMA (Saitama Univ.)

Student Trainees

Takanori IWAHASHI (Tokyo Univ. of Science)
Saori KONAMI (Tokyo Univ. of Science)
Wataru IWAKIRI (Saitama Univ.)
Fumi ASAMI (Tokyo Univ. of Science)
Rie YOSHII (Tokyo Univ. of Science)
Akifumi YOSHIKAWA (Tokyo Univ. of Science)
Yoko TAKEUCHI (Tokyo Univ. of Science)
Kenichi IWATA (Shibaura Institute of Technology)
Kenta KANEKO (Kogakuin Univ.)

Secretary

Yu NAYA

RIBF Research Division
Astro-Glaciology Research Unit

Our Astro-Glaciology Research Unit, organized in July 2011, promotes both theoretical and experimental studies to open up a new interdisciplinary research field between astrophysics and glaciology. On the theoretical side, we numerically simulate:

(1) Changes in the chemical composition of the stratosphere induced by high-energy photons and/or particles emitted from explosive astronomical phenomena, such as solar proton events and galactic supernovae, and

(2) The explosive nucleosynthesis, including the rapid neutron capture process (the r-process) for the creation of the elements heavier than iron, arising in the environment of core-collapse supernova explosions.

Subjects (1) and (2) themselves are very important in solar–terrestrial research and nuclear astrophysics, respectively; furthermore, the items (1) and (2) are intended to be coupled with experimental studies described below.

On the experimental side, we analyze the ice cores drilled at the Dome Fuji station in Antarctica in collaboration with the National Institute of Polar Research, Tokyo. These ice cores correspond to time capsules of the past. In particular, the ice cores obtained at Dome Fuji are known to be unique because they contain much more information on conditions in the stratosphere than any other ice cores recovered from other locations in either hemisphere. This means that the Dome Fuji ice cores may have an original advantage to study astronomical phenomena of the past, since γ-rays and high-energy protons emitted from astronomical events affect the chemical and isotopic compositions in the stratosphere and not those in the troposphere. Accordingly, we measure:

(3) Variations in the nitrate ion (NO_3^-) concentrations in the ice cores, in order to seek the proxy of past solar activity and the footprints of supernovae in our galaxy,

(4) Variations in the water isotopes (^{18}O and ^{2}H) in the ice cores, in order to reconstruct past temperature changes on the earth, and

(5) Variations in the nitrate isotope (^{15}N) in the ice cores, in order to investigate the possibility of this isotope becoming a new and a more stable proxy for solar activity and/or galactic supernovae.

Items (3), (4), and (5) have been analyzed with Dome Fuji ice cores with a temporal resolution of about 1 year. By comparing the results for items (3) and (4), we aim to understand the correlation between solar activity and climate changes in the past on the millennium scale. The basis for item (4) is already established in glaciology. Item (5) will be the one of very first measurements taken in ice cores. The theoretical studies related to items (1) and (2) will provide a background for distinguishing the characteristics of the astronomical events from meteorological noise that usually appears in the ice core data. Finally, we note that the supernova rate in our galaxy is crucial to understand the r-process nucleosynthesis but yet remains unknown. Our item (3) is also intended to diagnose the galactic supernova rate ultimately.

Head

Yuko MOTIZUKI

Members

Kazuya TAKAHASHI (Concurrent)
Yoichi NAKAI (Concurrent)

Contract Researcher

Kentaro SEKIGUCHI
Sachiko OKAMOTO

Visiting Scientists

Bradley MEYER (Clemson Univ., USA)
Sachiko AMARI (Washington Univ.,USA)
Akira HORI (Kitami Institute of Technology)
Hiroyuki KOURA (Japan Atomic Energy Agency)
Hideki MADOKORO (Mitsubishi Heavy Industries, Ltd.)
Takahiro TACHIBANA (Waseda High Sch., Waseda Univ.)
Kohji TAKAHASHI (Universite Libre de Bruxelles)
Hideharu AKIYOSHI (National Institute for Environmental Studies)

Makoto INOUE (National Institute for Environmental Studies)

Graduate Research Associate

Satomi KIKUCHI (Saitama Univ.)

Part-time Staff

Ai SHIMADA

Keiko FUKUSHIMA

Secretary

Yu KAWAMURA

Manami MARUYAMA

Yuri TSUBURAI

Yoko FUJITA

RIBF Research Division
Accelerator Group

1. Abstract

The accelerator group, consisting of seven teams, pursues various upgrades programs involving the new-generation heavy-ion accelerator facility, the Radioisotope Beam Factory (RIBF), to improve the accelerator performance and operation efficiency. The programs include research and development of a superconducting electron cyclotron resonance ion source, charge stripping systems, beam diagnostic devices, radiofrequency systems, control systems, and beam simulation studies. We also maintain the large infrastructure necessary to realize effective operation of the RIBF and are actively promoting the application of the facility to a variety of research fields.

Our primary mission is to supply intense, stable heavy-ion beams to users through effective operation, maintenance, and upgrading of the RIBF accelerators and related infrastructure. The director members listed below govern the development programs that are not dealt with by a single group, such as intensity upgrades and effective operation. They, along with other laboratories belonging to the RIBF research division, also explore future plans for the RIBF accelerators.

2. Major Research Subjects

(1) Intensity upgrade of RIBF accelerators (Okuno)
(2) Effective and stable operation of RIBF accelerators (Fukunishi)
(3) Investigation of future projects (Kamigaito, Fukunishi, Okuno)

3. Summary of Activity

(1) A new gas stripper system based on helium gas has been successfully commissioned.
(2) The bending power of the fRC cyclotron has been upgraded from K570 to K700 to accomodate the gas stripping scheme.
(3) High-intensity ^{238}U beam (max. 15 pnA) was supplied to users with high reliability (> 90 % in December).
(4) Deuterons, ^{18}O, ^{48}Ca, ^{124}Xe, and ^{70}Zn beams were also supplied to users with high intensities and reliabilities.
(5) Possible future plans were explored by considering the potential performance of RIBF accelerators and activities at rare-isotope beam facilities worldwide.

Group Director
Osamu KAMIGAITO

Deputy Group Director
Hiroki OKUNO (Intensity Upgrade)
Nobuhisa FUKUNISHI (Stable and Efficient Operation)

Members
Masayuki KASE

Secretary
Karen SAKUMA

RIBF Research Division
Accelerator Group
Accelerator R&D Team

1. Abstract

We are developing the key hardware in the upgrade of the Radioisotope Beam Factory (RIBF) accelerator complex. Our primary focus is the charge stripper, which plays an essential role in the complex. Charge strippers remove many electrons from ions and realize efficient acceleration of heavy ions by greatly enhancing the charge state. The intensity of uranium beams is limited by the lifetime of the carbon foil stripper conventionally installed in the acceleration chain. Improving the stripper lifetime is essential to increasing the beam power toward the final goal of the RIBF in the future. We are developing a low-Z gas stripper. Gas strippers are generally free from lifetime-related problems but produce a low equilibrium charge state because of the absence of density effects. A low-Z gas stripper, however, can produce an equilibrium charge state as high as that in carbon foil because the electron capture process is suppressed. Another focus is the upgrade of the world's first superconducting ring cyclotron.

2. Major Research Subjects

(1) Development of charge strippers for high-power beams (foil, low-Z gas)
(2) Upgrade of the superconducting ring cyclotron
(3) Maintenance and R&D of the electrostatic deflection/inflection channels for beam extraction/injection

3. Summary of Research Activity

(1) Development of charge strippers for high-power beams (foil, low-Z gas)
Okuno, H., Imao, H., Hasebe, H., Kuboki, H.
(2) Upgrade of the superconducting ring cyclotron
Okuno, H., Ohnishi, J.
(3) Maintenance and R&D of the electrostatic deflection/inflection channels for beam extraction/injection
Okuno, H., Ohnishi, J.

Team Leader
Hiroki OKUNO

Members
Jun-ichi OHNISHI
Hiroshi IMAO

Nishina Center Engineer
Hiroo HASEBE

Special Postdoctoral Researcher
Hironori KUBOKI

Visiting Scientists
Noriyosu HAYASHIZAKI (Tokyo Institute of Technology)
Mitsuhiro FUKUDA (RCNP, Osaka Univ.)
Andreas ADELMANN (PSI, Switzerland)

Research Consultants
Yoshiaki CHIBA
Isao YAMANE

RIBF Research Division
Accelerator Group
Ion Source Team

1. Abstract
Our aim is to operate and develop the ECR ion sources for the accelerator-complex system of the RI Beam Factory. We focus on further upgrading the performance of the RI Beam Factory through the design and fabrication of a superconducting ECR heavy-ion source for production of high-intensity uranium ions.

2. Major Research Subjects
(1) Operation and development of the ECR ion sources
(2) Development of a superconducting ECR heavy-ion source for production of high-intensity uranium ions

3. Summary of Research Activity
(1) Operation and development of ECR ion sources

T. Nakagawa, M. Kidera, Y. Higurashi, T. Ozeki, H. Haba, T. Urabe, and T. Kageyama

We routinely produce and supply various kinds of heavy ions such as zinc and neon ions for the super-heavy element serach experiment as well as uranium ions for RIBF experiments. We also perform R&D's to meet the requirements for stable supply of high-intensity heavy ion beams.

(2) Development of a superconducting ECR ion source for use in production of a high-intensity uranium beam

T. Nakagawa, J. Ohnishi, M. Kidera, Y. Higurashi, T. Ozeki, and H. Haba

The RIBF is required to supply uranium beams with very high intensity so as to produce RI's. We have designed and are fabricating an ECR ion source with high magnetic field and high microwave-frequency, since the existing ECR ion sources have their limits in beam intensity. The coils of this ion source are designed to be superconducting for the production of high magnetic field. We are also designing the low-energy beam transport line of the superconducting ECR ion source.

Team Leader
Takahide NAKAGAWA

Nishina center csientist
Masanori KIDERA
Yoshihide HIGURASHI

Special temporary employee
Tadashi KAGEYAMA

Special postdoctral reseracher
Takakazu OHZEKI
Tatsuya URABE

RIBF Research Division
Accelerator Group
RILAC Team

1. Abstract

The operation and maintenance of the RIKEN Heavy-ion Linac (RILAC) have been carried out. There are two operation modes: one is the stand-alone mode operation and the other is the injection mode operation. The RILAC has been used especially as an injector for the RIKEN RI- Beam Factory accelerator complex. The RILAC is composed of the ECR ion source, the frequency-variable RFQ linac, six frequency-variable main linac cavities, and six energy booster cavities (CSM).

2. Major Research Subjects

(1) The long term high stability of the RILAC operation.
(2) Improvement of high efficiency of the RILAC operation.

3. Summary of Research Activity

The RILAC was started to supply ion beams for experiments in 1981. Thousands hours are spent in a year for delivering many kinds of heavy-ion beams to various experiments.

The RILAC has two operation modes: one is the stand-alone mode operation delivering low-energy beams directly to experiments and the other is the injection mode operation injecting beams into the RRC. In the first mode, the RILAC supplies a very important beam to the nuclear physics experiment of "the research of super heavy elements". In the second mode, the RILAC plays a very important role as upstream end of the RIBF accelerator complex.

The maintenance of these devices is extremely important in order to keep the log-term high stability and high efficiency of the RILAC beams. Therefore, improvements are always carried out for the purpose of more stable and more efficient operation.

Team Leader
Eiji IKEZAWA

Member
Yutaka WATANABE

Research Consultants
Toshiya CHIBA
Masatake HEMMI
Yoshitoshi MIYAZAWA

RIBF Research Division
Accelerator Group
Cyclotron Team

1. Abstract

Together with other teams of Nishina Center accelerator division, maintaining and improving the RIBF cyclotron complex. The accelerator provides high intensity heavy ions. Our mission is to have stable operation of cyclotrons for high power beam operation. Recently stabilization of the rf system is a key issue to provide 10 kW heavy ion beam.

2. Major Research Subjects

(1) RF technology for Cyclotrons
(2) Operation of RIBF cyclotron complex
(3) Maintenance and improvement of RIBF cyclotrons
(4) Single turn operation for polarized deuteron beams
(5) Development of superconducting cavity for the rebuncher system

3. Summary of Research Activity

Development of the rf system for a reliable operation
Development of highly stabilized low level rf system
Development of superconducting rebuncher cavity
Development of the intermediate-energy polarized deuteron beams.

Team Leader
Naruhiko SAKAMOTO

Nishina Center Research Scientist
Kenji SUDA

Foreign Postdoctoral Researcher
Lu LIANG

RIBF Research Division
Accelerator Group
Beam Dynamics and Diagnostics Team

1. Abstract

In order to operate RIBF accelerator complex with the world-highest-intensity beams more efficiently, upgrades of beam diagnosis, computer control and power supplies are now in progress.

2. Major Research Subjects

(1) Stable and efficient operations of RIBF accelerator complex.
(2) Beam diagnostics.
(3) Accelerator control system.
(4) Stabilization of all the power supplies used in RIBF.

3. Summary of Research Activity

(1) Beam diagnosis
Two kinds of non-destructive beam current monitors including the world first HTc-SQUID monitor have been developed.
(2) Accelerator control system
EPICS-based control system and a homemade beam interlock system have been stably operated. A Java-based data archive system has been also developed.
(3) Bending-power upgrade of RIKEN fixed-frequency Ring Cyclotron (fRC)
RIKEN fRC has been successfully upgraded in its bending power (K = 700 MeV) to accept $^{238}U^{64+}$ ions obtained by the helium gas stripper launched recently.
(4) Upgrade of aging power supplies used for Riken Ring Cyclotron (RRC)
New power supplies having higher stabilities will be installed to further stabilize our old injector cyclotron RRC.

Team Leader
Nobuhisa FUKUNISHI

Members
Masaki FUJIMAKI
Keiko KUMAGAI
Tamaki WATANABE
Kazunari YAMADA

Contract Technical Scientist
Misaki KOBAYASHI-KOMIYAMA
Hiroshi WATANABE
Makoto NAGASE

Postdoctral Researcher
Takuya MAEYAMA

Visiting Scientists
Hiromichi RYUTO (Photonics and Electronics Science and Engineering Center, Kyoto University)
Jun-ichi ODAGIRI (Accelerator Laboratory, High Energy Accelerator Research Organization (KEK))

Research Consultants
Jiro FUJITA

RIBF Research Division
Accelerator Group
Cryogenic Technology Team

1. Abstract
We operate the cryogenic system for the superconducting ring cyclotron at the Radioisotope Beam Factory (RIBF). We also operate the helium cryogenic system in the southern part of the RIKEN Wako campus and deliver liquid helium to users at RIKEN. Our goal is to collect 100% of the helium gas after liquid helium usage on the Wako campus.

2. Major Research Subjects
(1) Operation of the cryogenic system for the superconducting ring cyclotron at the RIBF
(2) Operation of the helium cryogenic plant in the southern part of the Wako campus and delivering liquid helium to users on the Wako campus

3. Summary of Research Activity
(1) Operation of the cryogenic system for the superconducting ring cyclotron at the RIBF
Okuno, H., Dantsuka, T.
(2) Operation of the helium cryogenic plant in the southern part of the Wako campus and delivering liquid helium to users on the Wako campus
Dantsuka, T., Nakamura, M., Maie, T., Ikegami, K., Tsuruma, S., Okuno, H.

Team Leader
Hiroki OKUNO

Members
Masato NAKAMURA

Nishina Center Engineer
Takeshi MAIE

Technical Staff-I
Tomoyuki DANTSUKA

Research Consultant
Kumio IKEGAMI

Part-Time Staff
Shizuho TSURUMA

RIBF Research Division
Accelerator Group
Infrastructure Management Team

1. Abstract

The RIBF accelerators are an incomparable multi-stage accelerator complex. For the long and stable operations of these accelerators, their infrastructures become very important. Our team supports their infrastructure; buildings, electric facilities, cooling system, vacuum system and so on. It also concerns the regular operation and maintenance of all the accelerators, and improves or renews the old parts of the accelerators.

2. Major Research Subjects

Management of the RIBF accelerator infrastructure; buildings, electric facilities, cooling system, vacuum system and so on.

3. Summary of Research Activity

The current research subjects are summarized as follows:
(1) Operation and maintenance of infrastructure for RIBF accelerators.
(2) Improvement or renewal of the, especially old, accelerators.
(3) Support of accelerator operations.

Team Leader
Masayuki KASE

Members
Hiromi YAMASAWA

Temporary Employee
Tadashi FUJINAWA

Visiting Scientists
Hideshi MUTO (Tokyo Univ. of Sci. Suwa)

RIBF Research Division
Instrumentations Development Group

1. Abstract

This group develops experimental installations for the RI Beam factory. Experimental installations currently planned include designs containing common elements enabling multiple use, as well as others that are highly program specific. All are designed to maximize the research potential of the world's most intense RI beams, made possible by the exclusive equipment available at the RI Beam Factory.

2. Major Research Subjects

(1) SCRIT Project
(2) SLOWRI Project
(3) Rear RI Ring Project

3. Summary of Research Activity

We are developing beam manipulation technology in carrying out above listed project. They are the high-quality slow RI beam production (SCRIT and SLOWRI), the beam cooling and stopping (SCRIT and SLOWRI), and the beam accumulation technology (Rare RI Ring). The technological knowhow accumulated in our projects will play a significant role in the next generation RIBF. Future Plan for each project is described in subsections. SCRIT is now under construction and partially tested using stable isotopes, and RI production, for instance 132Sn, has already been succeeded. Rare RI Ring construction has been started in last year. Construction of SLOWRI facility is scheduled to be started in this year. They will be powerful tool for nuclear structure study for short-lived unstable nuclei.

Group Leader
Masanori WAKASUGI

Secretary
Minami IMANISHI

RIBF Research Division
Instrumentation Development Group
SLOWRI Team

1. Abstract

A next-generation slow radioactive nuclear ion beam facility (SLOWRI), providing high-purity, low-energy, small emittance ion beams for all elements, is being built as one of the principal facilities at the RIKEN RI-beam factory (RIBF). High-energy radioactive ion beams from the projectile fragment separator BigRIPS are thermalized in a large gas catcher cell. The thermalized ions in the gas cell are guided and extracted to a vacuum environment by a combination of dc electric fields and inhomogeneous rf fields (rf carpet ion guide). From there the slow ion beam is delivered via a mass separator and a switchyard to various devices: such as an ion trap, a collinear fast beam apparatus, and a multi-reflection time of flight mass spectrometer. In preliminary R&D work at the prototype SLOWRI facility, an overall efficiency of 5% for a 100A MeV ^{8}Li ion beam was achieved at the projectile fragment separator RIPS and the dependence of the efficiency on the ion beam intensity was investigated.

First optical spectroscopy experiments at the prototype SLOWRI were performed on Be isotopes. Energetic ions of ^{7,10,11}Be from RIPS were trapped and laser cooled in a linear rf trap after being extracted from a prototype gas cell; precision spectroscopy was performed. The evaluated ion temperature of <10 mK demonstrates that a reduction of more than 15 orders of magnitude for the kinetic energy of radioactive Be was achieved online. Precise investigation of the hyperfine structure could be used to confirm the anomalous mean radius of the valence neutron of the so-called neutron halo nucleus.

First online mass measurement with a multi-reflection time-of-flight mass spectrograph (MRTOF-MS) was also performed at the prototype SLOWRI setup. A slow continuous beam of ^{8}Li+ ions from the gas cell was bunched and cooled in two rf quadrupole ion traps and injected into an electrostatic multi-reflection mirror pair and ejected after several hundred revolutions. The time-of-flight, defined by the trap-ejection pulse and an ion's arrival on a micro channel plate detector, was measured precisely and compared with reference ions. A high mass resolving power of 160,000 was achieved with 5 ms TOF and the mass of ^{8}Li was determined with an uncertainty of 6.6×10^{-7} with 150 total ions. This new mass spectrograph is best suited for very heavy ions such as super heavy elements. Using a compact rf-carpet gas catcher at the GARIS facility, we will perform direct mass measurements of nuclei heavier than uranium with the MRTOF-MS.

The construction of SLOWRI has started and will be completed by the end of FY2013. The new facility will consist of two gas catcher cells: one a large He gas cell with rf-carpet ion guide for use with the main beam from BigRIPS, while the other is a small Ar gas cell which will be located in the vicinity of F2 slits of BigRIPS for parasitic production of slow RI-beams. Ions that would usually be abandoned in the slits can be caught in the cell and neutralized; RI will be selectively re-ionized by resonant ionization lasers in the vicinity of the exit of the cell. The beams from these two gas catchers will be mass separated by electro-magnetic isotope separators and merged into one beam transport line. They can each then be transported to the experimental room where various precision spectroscopy experiments will be performed. The commissioning is scheduled in FY2014 and the first experiment at the new facility will be performed by the end of FY2014.

2. Major Research Subjects

(1) Development and construction of the next-generation slow RI-beam facility
(2) Laser spectroscopy of trapped radioactive Beryllium isotopes.
(3) Development of a multi-reflection time-of-flight mass spectrograph for precision mass measurements of short-lived nuclei.
(4) Development of parasitic slow RI-beam production method using resonant laser ionization.

3. Summary of Research Activity

(1) Development of universal slow RI-beam facility

WADA, Michiharu, SONODA, Tetsu, SCHURY Peter, ITO, Yuta, NAIMI, Sarah, MITA, Hiroki, ARAI Fumiya, KUBO, Toshiyuki, KUSAKA Kensuke, Fujinawa Tadashi, MAIE Takeshi, YAMASAA Hideyuki, WOLLNIK, Hermann, KATAYAMA Ichiro, TAKAMINE, Aiko, OKADA, Kunihiro,

A next-generation slow radioactive nuclear ion beam facility (SLOWRI) which provides low-energy, high-purity, small emittance ion beams for all elements is being built as one of the principal facilities at the RIKEN RI-beam factory (RIBF). High-energy radioactive ion beams from the projectile fragment separator BigRIPS will be thermalized in a large gas catcher cell. The thermalized ions in the gas cell are guided and extracted to a vacuum environment by a combination of dc electric fields and inhomogeneous rf fields (rf carpet ion guide). From there the low-energy ion beam is delivered via a mass separator and switchyard to various devices, *e.g.* an ion trap, a collinear fast beam apparatus, and a multi-reflection time-of-flight mass spectrograph. In R&D work at the prototype SLOWRI setup, an overall efficiency of

5% for a 100*A* MeV ^{8}Li ion beam from the projectile fragment separator RIPS was achieved, and the dependence of the efficiency on the ion beam intensity was investigated.

A new mode of ion transport on the rf-carpet, the so-called ion surfing mode, was investigated with a coaxial circular rf-carpet for the first time. In addition to the ion-barrier rf signal, a four-phase audio frequency traveling wave signal was superimposed on the rf-carpet. Depending on the direction of the traveling wave, ions were transported to either the outermost electrode or the central exit with almost unity efficiency. This new mode can transport ions without need for a dc potential gradient along the carpet, allowing us to achieve a drift velocity of 100 m/s using a large size carpet without discharge problems.

(2) Laser spectroscopy of trapped radioactive beryllium isotope ions
WADA, Michiharu, TAKAMINE, Aiko, SCHURY Peter, SONODA Tetsu, OKADA, Kunihiro, KANAI, Yasuyuki, YOSHIDA, Atsushi, KUBO, Toshiyuki, YAMAZAKI, Yasunori, WOLLNIK, Hermann, SCHUESSLER, Hans, NODA, Koji, OHTANI, Shunsuke, KATAYAMA Ichiro

As a first application of the prototype SLOWRI setup, we applied hyperfine structure spectroscopy to Beryllium isotopes to determine, in particular, the anomalous radius of the valence neutron of the neutron halo nucleus ^{11}Be, and to determine the charge radii of these beryllium isotopes through laser-laser double resonance spectroscopy of laser-cooled ions. Laser cooling was an essential prerequisite for these experiments. The first laser spectroscopy experiments for Beryllium isotopes were performed to measure the resonance frequencies of the 2s $^{2}S_{1/2}$ - 2p $^{2}P_{3/2}$ transition of $^{7}Be^{+}$, ^{9}Be+, $^{10}Be^{+}$ and $^{10}Be^{+}$ ions; the nuclear charge radii of these isotopes were determined. The hyperfine structure of $^{11}Be^{+}$ and $^{7}Be^{+}$ ions using the laser-microwave double resonance spectroscopy were also performed and the magnetic hyperfine constants of $^{7}Be^{+}$ and $^{11}Be^{+}$ ions were determined with a relative accuracy of 10^{-7}. A measurement of Zeeman splitting in high magnetic fields, which is required to precisely determine the nuclear g-factor, is under preparation.

(3) Development of a multi-reflection TOF mass spectrograph for short-lived nuclei
SCHURY Peter, WADA, Michiharu, ITO, Yuta, NAIMI, Sarah, NAKAMURA, Sousuke, TAKAMINE, Aiko, SONODA Tetsu, MITA, Hiroki, ARAI Humiya, OKADA, Kunihiro, WOLLNIK, Hermann,

The atomic mass is one of the most important quantities of a nucleus and has been studied by various methods since the early days of physics. From among many methods we have chosen to implement a multi-reflection time-of-flight (MR-TOF) mass spectrograph. Slow RI beams extracted from the RF ion-guide are bunched and injected into the spectrometer with a repetition rate up to ~500 Hz. The spectrometer consists of two electrostatic mirrors between which the ions travel back and forth repeatedly. These mirrors are designed such that energy-isochronicity in the flight time is guaranteed during the multiple reflections while the flight time varies with the masses of ions. A mass-resolving power of 160,000 has been obtained with a 2.3 ms flight time for $^{40}K^{+}$ and $^{40}Ca^{+}$ isotopes. It is equivalent to using a 180 T magnet for a Penning trap mass spectrometer. This mass-resolving power should allow us to determine ion masses with a relative accuracy of 10^{-7}. The advantages of the MR-TOF spectrometer are: 1) short measurement periods, typically <5 ms, which allows all neutron rich nuclei to be investigated, 2) the device is compact and its operation is simple, especially, it is independent from the all upstream devices, accelerators and fragment separators, 3) ions of multiple isobars can be measured simultaneously, so that mass reference can easily be established in the mass spectra. In total, the number of measurable nuclides within a limited beam time would be larger than that can be achieved by other methods. It should be noted here also that this method could be used even during a low-duty parasitic beam time.

Online mass measurements of the short-lived lithium isotope ^{8}Li ($T_{1/2}$ = 840 ms) have been performed in FY2012. A low energy continuous $^{8}Li^{+}$ beam from the prototype SLOWRI was accumulated in a tapered linear rf quadrupole ion trap and stored in a flat rf quadrupole ion trap for further cooling and bunching. The ion bunch was injected into the MRTOF-MS and after several hundreds revolutions (a few milliseconds), the ions were ejected and detected by a micro-channel plate detector. The total TOF was compared with that of reference ions to determine the mass of ^{8}Li with a relative uncertainty of 6.6x10^{-7}. We found that a single reference ion is sufficient to determine the mass of unknown ions by the square of the TOF ratio. In the ^{8}Li measurement, $^{12}C^{+}$ --- the atomic mass standard --- was used for the reference. Even though the masses differ by 50%, the systematic uncertainty due to a possible TOF offset of 10 ns is still within the present accuracy.

This new mass spectrograph is best suited for direct mass measurements of very heavy nuclei, such as super heavy elements. We have started a project, SHE-MASS, aiming to comprehensively measure masses of nuclei heavier than uranium at the GARIS facility. For any time-of-flight mass spectrometers, mass references are indispensable. We developed an electro-spray ion source for molecular ions, which can produce a variety of molecular ions in a wide mass range. We used a compact rf-carpet for accumulating molecular ions with low abundant isotopes and found that there are isobaric molecules in many mass numbers. We have also confirmed that the accuracy of mass determination is always within the precision of the mass measurements in tests with isobaric triplets

(4) Development of parasitic slow RI-beam production scheme using resonance laser ionization

SONODA Tetsu, WADA, Michiharu, MITA, Hiroki, TOMITA, Hideki, SAKAMOTO, Chika, TAKATSUKA Takaaki, MATSUO Yukari, FURUKAWA, Takeshi, MIYATAKE Hiroari, JEONG, Sun Chan, ISHIYAMA, Hironobu, IMAI, Nobuaki, HIRAYAMA Yoshikazu, KATAYAMA Ichiro, IIMURA, Hideki, SHINOZUKA Tsutomu, WAKUI, Takashi, HUYSE, Mark, VAN DUPPEN, Piet, KUDRYAVTSEV, Yuri

More than 99.9% of RI ions produced in projectile fission or fragmentation are simply dumped in the first dipole magnet and the slits. A new scheme, named PALIS, to rescue such precious RI using a compact gas catcher cell and resonant laser ionization has been proposed. The thermalized RI ions in a cell filled with Ar gas can be quickly neutralized and transported to the exit of the cell by gas flow. Irradiation of resonance lasers at the exit selectively ionizes neutral RI atoms efficiently. The ionized RI ions can be further purified by a magnetic mass separator and transported to the SLOWRI experimental area for spectroscopy experiments. The resonant ionization scheme itself can also be a useful method to perform precision optical spectroscopy on RI of many elements.

An off-line setup for resonant ionization in a gas cell has been prepared. Extraction from a 500 mbar Ar gas cell by resonant ionization method for Ni, Cu, Ti, Nb, Co, Fe and In ions was demonstrated. Differential pumping from 500 mbar to 10^{-5} mbar using multiple small pumps and an rf sextupole ion beam guide (SPIG) has been achieved. Construction of a new gas cell to be placed at the second focal plane (F2) of BigRIPS is scheduled in FY2013.

An electrostatic lens made by a surface current on a uniform resistive material coated on a ceramic plate was also investigated. Such a lens can be placed at the exit of the cell to quickly and efficiently transport ions from the cell even at atmospheric pressure.

Head

Michiharu WADA

Members

Tetsu SONODA
Peter SCHURY
Sarah NAIMI
Yuta ITO
Sousuke NAKAMURA
Hiroki MITA
Shigeaki ARAI
Kensuke KUSAKA
Tadashi FUJINAWA
Takeshi MAIE
Hideyuki YAMASAWA
Humiya ARAI
Takaaki TAKATSUKA
Yoshitaka ADACHI
Aiko TAKAMINE
Kunihiro OKADA
Ichiro KATAYAMA
Hideki IIMURA
Hideki TOMITA
Hans SCHUESSLER
Hermann WOLLNIK
Hirokane KAWAKAMI

RIBF Research Division
Instrumentation Development Group
Polarized RI Beam Team

1. Abstract

The team conducts research and development studies of a technique for the production of spin-oriented radioactive-isotope beams (RIBs) and applies it to research in nuclear physics, fundamental physics, and materials science. Microscopic investigation of physical and chemical processes is performed on the basis of nuclear physics techniques that take advantage of intrinsic nuclear properties and phenomena (e.g., spins, electromagnetic nuclear moments, decay modes). In particular, the precession/resonance of an oriented nuclear spin under an external field is observed via a change in the angular distribution of radiation in the study of nuclear structures through nuclear moments. Experimental methods and devices for fundamental physics research with polarized nuclei have also been developed. The same methods are used to investigate condensed matter, such as semiconductors, ferromagnets, fullerenes, and systems with dilute magnetic impurities, by exploiting radioactive nuclei as microscopic probes into them. All these research activities are to be extended to a wide variety of unstable nuclei provided by the Radioisotope Beam Factory (RIBF). A method of producing beams of highly polarized radioactive nuclei, taking full advantage of the RIBF, is being developed.

2. Major Research Subjects

(1) Nuclear moment measurements of unstable nuclei utilizing fragmentation-induced spin-oriented RI beams
(2) RIKEN Projectile Fragment Separator (RIPS) upgrade and the development of highly polarized slow RI beams
(3) Fundamental physics: Study of symmetry
(4) Condensed matter studies using radioactive nuclear probes

3. Summary of Research Activity

(1) Nuclear-moment measurements of unstable nuclei utilizing fragmentation-induced spin-oriented RI beams

Our earlier work revealed that spin-oriented RIBs can be produced as a function of their outgoing momenta and emission angles in the projectile fragmentation reaction. With the obtained spin-polarized nuclei, ground- and excited-state nuclear moments can be determined by means of the β-ray-detected nuclear magnetic resonance (β-NMR) and time differential perturbed angular distribution (TDPAD) methods, respectively. The sub-themes are the following:

– Development of a new method of producing highly spin-aligned RIBs by two-step projectile fragmentation combined with the momentum dispersion matching technique and the magnetic moment measurement of isomeric states in ^{32}Al by the TDPAD method
– Nuclear structure study of neutron-rich aluminum isotopes $^{30\text{–}32}$Al on the border of the *island of inversion* and $^{33\text{–}34}$Al on/beyond it
– Investigation of a new *island of inversion* around $N = 28$ and nuclear moment measurements of neutron-rich isotopes
– Ground-state electric quadrupole moment measurements of ^{23}Al for the study of the $T = 3/2$ mirror symmetry
– Study of nuclei around the Fe region: isospin symmetry study by means of the magnetic moment of the 10^+ isomer in ^{54}Ni, and study of magicity in the vicinity of ^{68}Ni through the quadrupole moment of the $13/2^+$ isomeric state in ^{69}Cu and the isomeric state in ^{65}Fe

(2) RIPS upgrade and the development of highly polarized slow RI beams

The upgrade of the RIPS was proposed in the phase II programs. In the cyclotron-cascade acceleration scheme, beams are accelerated to an energy of E/A = 115 MeV by an intermediate-stage ring cyclotron (IRC). In this upgrade, the former fragment separator RIPS was equipped with a new beam line that delivers beams of heavy ions of E/A = 115 MeV from the IRC cyclotron. RI beams produced by the primary beams at this intermediate energy are energetic enough to produce RIBs via projectile fragmentation reactions and suitably low in energy to be stopped in a sample material of limited thickness. Compared with the production yield of RIBs in the present azimuthally varying field (AVF) Riken Ring Accelerator (RRC) acceleration scheme, the yield is dramatically increased. Our team is conducting a design study of the upgrade program. We noted that RIBs produced at E/A = 115 MeV can be spin-oriented so that further nuclear moment measurements can be conducted. Further, the addition of a new atomic beam resonance method combined with fragmentation-based RIBs to this program, which is under development, will enable the production of highly spin-polarized RIBs in a low beam energy region. Thus, they could be useful not only for nuclear moment measurements but also for spin-related subjects in nuclear physics, fundamental physics, and materials science.

(3) Fundamental physics: Study of symmetry

The nuclear spins of stable and unstable isotopes sometimes play important roles in fundamental physics research. New experimental methods and devices have been developed for studies of the violation of time reversal symmetry (T-violation) using spin-polarized nuclei. These experiments aim to detect the small frequency shift in the spin precession or measure the *T*-odd angular correlation in β decay as *T*-violating signals arising from new mechanisms beyond the Standard Model. The sub-themes are the following:

– Precise measurement of spin-precession frequency with a new type of nuclear spin maser for atomic electric dipole moment (EDM) search
– Development of highly sensitive atomic magnetometer for EDM experiments
– Development of a new Mott polarimeter for *T*-violation experiment using β decay of polarized unstable nuclei

(4) Condensed matter studies using radioactive nuclear probes
Online time differential perturbed angular correlation experiments have been conducted through γ-ray measurements by using RIBs as a probe. The microscopic structures and dynamics of ferromagnets and the properties of semiconductors have been investigated using the deduced internal local fields and the spin relaxation of the probe in materials. The β-NMR/nuclear quadrupole resonance (NQR) method is also used for these condensed matter studies. The methods and apparatus for these studies have been developed. In addition, basic studies of the probe nuclei have been conducted. The sub-themes are the following:

– Study of Fe impurities in silicon solar cells with online Mössbauer spectroscopy of implanted ^{57}Fe
– Development of an on-line perturbed angular-correlation method with ^{19}O beams as a new probe
– Study of the fast diffusion of Cu impurity atoms in Si through β-NMR/NQR with implanted ^{58}Cu
– Study of the superconductivity of diamond by heavy ion implantation

Team Leader
Hideki UENO

Member
Yoshio KOBAYASHI

Research Consultant
Takuya OKADA

Visiting Scientists
Hisazumi AKAI (Osaka Univ.)
Koichiro ASAHI (Tokyo Tech)
Dimiter BALABANSKI (Bulgarian Academy of Sciences)
Takeshi FURUKAWA (Tokyo Metropolitan Univ.)
Yuichi ICHIKAWA (Tokyo Tech)
Radomira LOZEVA (CNRS/IN2P3)
Kensaku MATSUTA (Osaka Univ.)
Jiro MURATA (Rikkyo Univ.)
Akihiro YOSHIMI (Okayama Univ.)
Makoto UCHIDA (Tokyo Tech)

Junior Research Associate
Yoko ISHIBASHI (Univ. of Tsukuba)

Student Trainees
Masatoshi CHIKAMORI (Tokyo Tech)
Hironori HAYASHI (Tokyo Tech)
Eri HIKOTA (Tokyo Tech)
Takeshi INOUE (Tokyo Tech)
Yuji ISHII (Tokyo Tech)

Xing LI (Tokyo Tech)
Ryousuke KANBE (Osaka Univ.)
Hirokazu MIYATAKE (Tokyo Tech)
Tsubasa NANAO (Tokyo Tech)
Yuichi OHTOMO (Tokyo Tech)
Yu SAKAMOTO (Tokyo Tech)
Shinichi SHINOZAKI (Osaka Univ.)
Hazuki SHIRAI (Tokyo Tech)
Takahiro SUZUKI (Tokyo Tech)
Masaomi TANAKA (Osaka Univ.)
Masato TSUCHIYA (Tokyo Tech)
Keisyun YAMAMURA (Fukui Univ. of Tech.)
Naoki YOSHIDA (Tokyo Tech)

RIBF Research Division
Instrumentation Development Group
Rare RI-ring Team

1. Abstract

We are developing the isochronous storage ring to precisely measure the mass for rare radioactive isotopes (Rare RI ring). It is assumed that uranium is synthesized by neutron capture process after the supernovae explosion (r-process). To prove r-process, mass measurements for the rare RI are indispensable. To deduce the mass, we measure the circulation time (cyclotron frequency) for the rare RI inside the ring. RI beams produce in RIBF have some energy spread. To compensate the spread, isochronicity inside the ring is indispensable (isochronous storage ring). We will inject the rare RI one by one to the ring (individual injection) to identify the RI event-by-event.

2. Major Research Subjects

Developments of isochronous storage ring to measure mass of rare RI.

3. Summary of Research Activity

Developments of isochronous storage ring to measure mass of rare RI.
Construction of Rare-RI Ring has been started in last year, and major components including infrastructure of the ring were already completed. To minimize construction cost, we re-used TARN-II bending magnets with additional trim coils as main components of the ring. A quick activated kicker magnet system required for one by one injection was also installed. In this year, we will make all instrumentations ready for commissioning of the ring.

Team Leader
Masanori WAKASUGI

Nishina Center Research Scientist
Yoshitaka YAMAGUCHI

Visiting Scientists
Akira OZAWA (Inst. Phys., Univ.of Tsukuba)
Takeshi SUZUKI (Saitama University)
Takayuki YAMAGUCHI (Saitama University)
Takashi KIKUCHI (Nagaoka University of Technology)
Daisuke NAGAE (Inst. Phys., Univ.of Tsukuba)

Junior Research Associate
Yasushi ABE (University of Tsukuba)

RIBF Research Division
Instrumentation Development Group
SCRIT Team

1. Abstract

We aim at the investigation of internal nuclear structure of short-lived radioactive nuclei (RI) by means of electron scattering. Electron scattering for RI's has never been performed duo to inability to make target of these nuclei. An electron-RI collider system, which requires a huge accelerator complex, has so far been unique solution to overcome the difficulty. We have developed a novel internal target system named SCRIT (Self-Confining RI Ion Target) in an electron storage ring to make the experiment easier with much compact experimental system.

2. Major Research Subjects

Development of the SCRIT technology and electron scattering for unstable nuclei.

3. Summary of Research Activity

Development of a novel internal target of unstable nuclei (SCRIT) in an electron storage ring for electron scattering experiment.
(Wakasugi, Ohnishi, Ichikawa, Kurita, Suda, Tamae, Wang, Hori, Hara)
We have almost completed the construction of the SCRIT electron scattering facility, while some components are still under construction. We succeeded in test experiment of SCRIT electron scattering using stable Cs and Xe isotopes supplied from an ISOL system named ERIS. The collision luminosity between electron beam and target ions trapped in the SCRIT device exceeds 10^{27} /(cm^{2}s) at the electron beam current of 200 mA. We succeeded in RI beam extraction from ERIS. RIs were produced by photo-fission of UCx target with an electron beam irradiation. We plan to start electron scattering experiment for RI supplied from ERIS in 2013.

Team Leader
Masanori WAKASUGI

Technical Researcher
Tetsuya OHNISHI

Research Consultant
Shin-ichi ICHIKAWA
Masahiro HARA
Toshitada HORI

Visiting Scientists
Toshimi SUDA (Research Center of Electron Photon Science, Tohoku Univ.)
Tadaaki TAMAE (Research Center of Electron Photon Science, Tohoku Univ.)
Kazuyoshi KURITA (Inst. Phys., Rikkyo Univ.)
Shuo WANG (Research Center of Electron Photon Science, Tohoku Univ.)

RIBF Research Division
Research Instruments Group

1. Abstract

The research instruments group is the driving force at RI Beam Factory (RIBF) for continuous enhancement of activities and competitiveness of experimental research. Consisting of five teams, we are in charge of the design, construction, operation and improvement of the core research instruments at RIBF, such as BigRIPS separator, ZeroDegree spectrometer, GARIS spectrometer and SAMURAI spectrometer, and the related infrastructure and equipments. The group also conducts related experimental research as well as R&D studies on the research instruments.

2. Major Research Subjects

Design, construction, operation and improvement of the core research instruments at RIBF and related R&D studies. Experimental studies on exotic nuclei.

3. Summary of Research Activity

The current research subjects are summarized as follows:
(1) Production and delivery of RI beams and related research
(2) Design, construction, operation, and improvement of the core research instruments at RIBF and their related infrastructure and equipments for continuous enhancement of activities and competitiveness of experimental research
(3) R&D studies on technical issues of the core research instruments and related equipments at RIBF
(4) Experimental research on exotic nuclei using the core research instruments at RIBF

Group Director
Toshiyuki KUBO

Senior Visiting Scientist
Toshio KOBAYASHI (Tohoku University)

Part-time Staff supporting research
Meiko Kurokawa

RIBF Research Division
Research Instruments Group
GARIS Team

1. Abstract

Development and maintenance of devices related to the study of superheavy elements

2. Major Research Subjects

(1) Maintenance and development of a recoil separator and related devices
(2) Development of rapid chemistry devices

3. Summary of Research Activity

(1) Maintenance and development of recoil separator

A gas-filled recoil separator has been used as the main experimental device for the study of superheavy elements. We will develop and maintain the related devices. We will also offer user support if a researcher wishes to use the devices for his/her own research program.

(2) Development of devices for fast chemistry

We research and develop devices for fast chemistry of superheavy elements. We also offer user support to potential users.

Team Leader
Kouji MORIMOTO

Nishina Center Research Scientist
Daiya KAJI

Nishina Center Technical Scientist
Akira YONEDA

RIBF Research Division
Research Instruments Group
BigRIPS Team

1. Abstract

This team is in charge of design, construction, development and operation of BigRIPS in-flight separator and its related research instruments at RI beam factory (RIBF). They are employed not only for the production of RI beams but also the experimental studies using RI beams.

2. Major Research Subjects

Design, construction, development and operation of BigRIPS in-flight separator, RI-beam transport lines, and their related research instruments

3. Summary of Research Activity

This team is in charge of design, construction, development and operation of BigRIPS in-flight separator, RI-beam transport lines, and their related research instruments such as ZeroDegree spectrometer at RI beam factory (RIBF). They are employed not only for the production of RI beams but also various kinds of experimental studies using RI beams.

The research subjects may be summarized as follows:

(1) General studies on RI-beam production using in-flight scheme.
(2) Studies on ion-optics of in-flight separators, including particle identification of RI beams
(3) Simulation and optimization of RI-beam production.
(4) Development of beam-line detectors and their data acquisition system.
(5) Experimental studies on production reactions and unstable nuclei.
(6) Experimental studies of the limits of nuclear binding.
(7) Development of superconducting magnets and their helium cryogenic systems.
(8) Development of a high-power production target system.
(9) Development of a high-power beam dump system.
(10) Development of a remote maintenance and remote handling systems.
(11) Operation, maintenance and improvement of BigRIPS separator system, RI-beam transport lines, and their related research instruments such as ZeroDegree spectrometer and so on.
(12) Experimental research using RI beams.

Team Leader
Koichi YOSHIDA

Members
Naohito INABE
Masao OHTAKE
Yoshiyuki YANAGISAWA

Contract Researchers
Kensuke KUSAKA
Naoki FUKUDA
Hiroyuki TAKEDA

Research Associates
Daisuke KAMEDA
Kanenobu TANAKA
Hiroshi SUZUKI

Part-time Staff
Hidekazu KUMAGAI

Visiting Scientist

Bradley SHERRILL (NSCL, Michigan State Univ., USA)
Daniel BAZIN (NSCL, Michigan State Univ., USA)
Laura BANDURA (NSCL, Michigan State Univ., USA)
Oleg TARASOV (NSCL, Michigan State Univ., USA)
David MORRISSEY (NSCL, Michigan State Univ., USA)
Maurico Portillo (FRIB, Michigan State Univ.,USA)
Hans GEISSEL (GSI, Germany)
Martin WINKLER (GSI, Germany)
Michael FAMIANO (Western Michigan Univ., USA)
Jerry NOLEN (Argonne National Lab., USA)
Shashikant MANIKONDA (Argonne National Lab., USA)
Yutaka MIZOI (Osaka Electro-Commnication Univ.)
Kazuo IEKI (Rikkyo Univ.)
Naohito IWASA (Tohoku Univ.)
Sadao MOMOTA (Kochi University of Technology)
Le Hong KHIEM (IOP, Vietnamese Academy for Science and Technology)
Viet Cuong PHAN (IOP, Vietnamese Academy for Science and Technology)
Jong Won KIM (Institute for Basic Science, Korea)
Myongjin KIM(Insutitute for Basic Science, Korea)

Students

Student Trainees

Daichi MURAI (Rikkyo Univ.)
Ayuko CHIBA (Tohoku Univ.)
Yohei OKODA (Tohoku Univ.)

RIBF Research Division
Research Instruments Group
SAMURAI Team

1. Abstract
In collaboration with research groups in and outside RIKEN, the team designs, develops and constructs the SAMURAI spectrometer and relevant equipment that are and will be used for reaction experiments using RI beams at RI Beam Factory. The SAMURAI spectrometer consists of a large superconducting dipole magnet and a variety of detectors to measure charged particles and neutrons. After the commissioning experiment in March 2012, the team prepared and conducted, in collaboration with researchers in individual experimental groups, the first series of experiments with SAMURAI in May 2012. The team also provides basis for research activities by, for example, organizing collaboration workshops by researchers who are interested in studies or plan to perform experiments with the SAMURAI spectrometer.

2. Major Research Subjects
Design, development, construction and maintenance of the SAMURAI spectrometer and its related research instruments. Help and management for SAMURAI-based research programs.

3. Summary of Research Activity
The current research activities are summarized as follows:

(1) Operation, maintenance and improvement of a large superconducting dipole magnet that is the main component of the SAMURAI spectrometer.
(2) Design, development and construction of various detectors that are used for nuclear reaction experiments at SAMURAI.
(3) Preparation for planning experiments using SAMURAI spectrometer.
(4) Maintenance and improvement of the SAMURAI beam line
(5) Formation of a collaboration platform called “SAMURAI collaboration”.

Team Leader
Tohru MOTOBAYASHI

Members
Hiromi SATO
Ken-ichiro YONEDA
Yohei SIMIZU

Senior Visiting Scientist
Toshio KOBAYASHI (Tohoku University)

Visiting Scientist
Bertis Charles RASCO (Louisiana State University, USA)
Julien Didier GIBELIN (LPC-Caen, France)
Nobuyuki CHIGA (Tohoku University)
Piotr BEDNARCZYK (IFJ PAN, Krakow, Poland)
Yasuhiro TOGANO (Tokyo Institute of Technology)

RIBF Research Division
Research Instruments Group
Computing and Network Team

1. Abstract

This team is in charge of development, management and operation of the computing and network environment, mail and information servers and data acquisition system and management of the information security of the RIKEN Nishina Center.

2. Major Research Subjects

(1) Development, management and operation of the general computing servers
(2) Development, management and operation of the mail and information servers
(3) Development, management and operation of the data acquisition system
(4) Development, management and operation of the network environment
(5) Management of the information security

3. Summary of Research Activity

This team is in charge of development, management and operation of the computing and network environment, mail and information servers and data acquisition system and management of the information security. The details are described elsewhere in this progress report.

(1) Development, management and operation of the general computing servers

We are operating Linux/Unix NIS/NFS cluster system for the data analysis of the experiments and general computing. This cluster system consists of eight computing servers with 28 CPU cores and totally 160 TB RAID of highly-reliable Fibre-channel HDD. Approximately 600 user accounts are registered on this cluster system. We have replaced the data analyses servers and RAID file systems for the experimental data in the spring of 2012. Details are described elsewhere in this volume. We are adopting the latest version of the Scientific Linux (X86_64) as the primary operating system, which is widely used in the accelerator research facilities, nuclear physics and high-energy physics communities in the world.

(2) Development, management and operation of the mail and information servers

We are operating RIBF.RIKEN.JP server as a mail/NFS/NIS server. This server is a core server of RIBF Linux/Unix cluster system. Postfix is used for mail transport software and dovecot is used for imap and pop mail services. These software packages enable secure and reliable mail delivery. Sophos Email protection advanced (PMX) installed on the mail front-end servers tags spam mails and isolates virus-infected mails. The probability to identify the spam is approximately 95-99%. We are operating several information servers such as WWW servers, Wiki servers, Groupware servers, Windows-Media and Quick-Time streaming servers, and an anonymous FTP server (FTP.RIKEN.JP).

(3) Development, management and operation of the data acquisition system

We are developing a data-acquisition system for the RIBF. This system has functions of network-distributed data processing, hierarchical event building and parallel readout. To get better readout speed, we have developed the tiny VME readout system based on FPGA. It can achieve the best readout speed of the VME bus. In collaboration with CEA Saclay and GANIL, the development of the multi-detector data base system is in progress. This system merges data taken by different DAQ systems based on the time stamp.

(4) Development, management and operation of the network environment

We have been managing the network environment collaborating with Advanced Center for Computing and Communications (ACCC). All the Ethernet ports of the information wall sockets are capable of the Gigabit Ethernet connection (10/100/1000BT). Many wireless LAN access points have been installed to cover the almost entire area of Nishina Center including the radiation control area.

(5) Management of the information security

It is essential to take proper information security measures for information assets.
We are managing the information security of Nishina Center collaborating with ACCC.

Team Leader
Takashi ICHIHARA

Member
Yasushi WATANABE
Hidetada BABA

RIBF Research Division
Research Instruments Group
Detector Team

1. Abstract

This team is in charge of development, fabrication, and operation of various detector for nuclear physics experiment in RIKEN Nishina center. Also the team organizes collaboration work for detector technology among related research groups in order to improve mutual share of knowledge and experience.

2. Major Research Subjects

(1) Improvement of beam line detectors
(2) Development of high dynamic range preamplifier for silicon strip detector
(3) Development of time projection chamber
(4) Construction and maintenance of silicon pixel detector.
(5) Search for extra dimensions by measuring short-range gravity
(6) Radiation detector for education

3. Summary of Research Activity

(1) Improvement of beam line detectors
BigRIPS has various beam line detector. Parallel Plate Avalanche Chamber (PPAC) and Ionization chamber (IC) are most popular detectors. We fabricated a PPAC from scratch as succession of technology. We tried to improve it by considering its elementary process as well as the IC. The discharge process of the PPAC under the high beam rate environment is analyzed and we proposed to introduce the high speed high voltage switching in order to reduce the damage from discharge. The factors which determine delta-E resolution of the IC were considered. The delta-E affects it with major fraction. The horizontally striped pads should be suitable for better delta-E resolution.

(2) Development of high dynamic range preamplifier
Coulomb break up experiment at RIBF needs high dynamic range silicon strip detector in order to identify the charged particle from proton to Sn. We have two solutions for analog amplifiers. One is dual gain preamplifier and other is square root response amplifier. Dual hybrid preamplifiers of application specific integrated circuit has been designed and fabricated by collaboration with KEK. The new chips were tested at test beam experiment with readout electronics made by Washington University and Texas A&M. and confirmed the performance. Also other square ROOT type amplifier was fabricated as a ASIC and achieved design performance by charge injection test.

(3) Development of time projection chamber
A time projection chamber will be used for SAMURAI spectrometer. RIKEN, Kyoto, Rikkyo and MSU are building TPC. For the electronics development, we developed 1st prototype board for monitoring of timing synchronization among. The board satisfies the basic requirements.

(4) Development of silicon pixel detector.
RIKEN, Rikkyo, KEK, and JAEA group is responsible for the pixel ladder fabrications for the RHIC PHENIX detector upgrade. The ladder is a module which is composed of pixel sensor modules, support frame, and readout bus. We completed the fabrication of ladders and installed them into the PHENIX apparatus in December 2010 and started operation successfully. Due to differences in CTE between the pixel stave and the silicone encapsulant, thermal cycling promoted the breaking of wire bonds during 2011 operation. The malfunctioned ladders have been repaired and spare ladder fabrication is ongoing.

(5) Search for extra dimensions by measuring short-range gravity
Short range gravity force is measured by using torsion pendulum. If the gravity force is deviated from the inverse square law, it will be the indication of the new physics. We are measuring the movement of the torsion pendulum by using CCD with online fashion analysis tools.

(6) Radiation detector for education
After Fukushima reactor accident, people are so worried about the radiation. The detector team has collaboration with University professors and high school teaches, for developing an educational system for knowledge of radiation. We concluded it is necessary to have radiation detector assemble kit with reasonable price. Our team developed the prototype detectors with spectrum display.

Team Leader

Atsushi TAKETANI

Post Doctoral Fellow

Yuki Sato

Visiting Scientist

Meiko UESAKA (Rikkyo University)
Kohei FUJIWARA (Tokyo Metropolitan Industrial Tehcnology Research Institute)

Research Consultant

Hiroyuki MURAKAMI

Students

Junior Research Associate

Kazufumi NINOMIYA
Hiroyuki MIYA

Student Trainees

Akira TAKUMA (Fac. of Sci., Rikkyo Univ.)
Tomoyuki Suzuki (Fac. of Sci., Rikkyo Univ.)
Kyousule URANO (Fac. of Sci., Rikkyo Univ.)
Yuji Furuya (Fac. of Sci., Rikkyo Univ.)

RIBF Research Division
Accelerator Applications Research Group

1. Abstract
Accelerator Applications Research Group promotes various applications of ion beams from RI Beam Factory. Radiation Biology Team studies biological effects of fast heavy ions and develops heavy-ion breeding. RI Applications Team studies production and application of radioisotopes and develops new technologies of accelerator mass spectrometry for the trace-element analyses. Details of these activities are described by each team elsewhere.

2. Major Research Subjects
Research and development in biology and chemistry utilizing heavy-ion beams from RI Beam Factory.

3. Summary of Research Activity
(1) Biological effects of fast heavy ions.
(2) Development of heavy-ion breeding.
(3) Production and application of radioisotopes.
(4) Developments of trace elements analyses.

Group Director
Tomoko ABE

Secretary
Yoshiko SAKATA

RIBF Research Division
Accelerator Applications Research Group
Radiation Biology Team

1. Abstract

The radiation biology team conducts studies of various biological effects of fast heavy ions. It is also involved in the development of a new technique for breeding plants by heavy-ion irradiation. Fast heavy ions can cause dense, localized ionization of matter along their tracks, in contrast to photons (e.g., X-rays and g-rays), which cause randomly distributed isolated ionization. The localized, dense ionization can cause double-strand DNA breaks in cells induced by; these breaks are not easily repaired, and they are more effective at inducing mutations than single-strand DNA breaks. A unique feature of our experimental facility at the RIKEN Ring Cyclotron (RRC) is that living bodies in helps them the atmosphere or bottles can be irradiated because the delivered heavy-ion beams have sufficiently high energy to penetrate matter to a significant depth. The radiation biology team uses a dedicated beam line (E5B) of the RRC to irradiate microbes, plants, and animals with a wide variety of ion beams, ranging from C to Fe. The research subjects include physiological studies of DNA repair, genome analyses of mutation, and mutation breeding of plants by heavy-ion irradiation. Some new cultivars have already been introduced to the market.

2. Major Research Subjects

(1) Biological effects of heavy-ion irradiation
(2) Ion-beam breeding and genome analysis
(3) Innovative applications of heavy-ion beams

3. Summary of Research Activity

The radiation biology team focuses on the biological effects of fast heavy ions from the RRC by using 135 MeV/u C, N, and Ne ions, 95 MeV/u Ar ions, and 90 MeV/u Fe ions. It is also involved in the development of a breeding technique for microbes and plants. The main topics covered are as follows:

(1) Biological effects of heavy-ion irradiation

A uniform dose distribution is the key to systematic studies and thus to improvement of the mutation efficiency. Therefore, plants and microbes are treated using ions with a stable linear energy transfer (LET). The deletion size appears to depend on the LET: Almost 90% of deletions are less than 53 bp in *Arabidopsis* when using C ions (22.5~30 keV/μm). This type of irradiation is suitable for examining breeding and reverse genetics systems in conjunction with single-nucleotide polymorphism detection systems, for example, targeting induced local lesions in genomes. Among the deletions, the proportion of large deletions (>100 bp) was about 54% for Ar-ion irradiation and about 64% for C-ion irradiation. Heavy-ion beams of 290 keV/μm are efficient inducers of large deletions.

(2) Ion-beam breeding and genome analysis

An LET of 30 keV/μm with C and N ions is the most effective for inducing mutations in *Arabidopsis*. In rice, the highest number of mutations is observed with C and Ne ions in the LET range of 61 to 74 keV/μm. Thus, the LET of the ion beam is an important factor affecting mutagenesis. Many types of mutations that produce variegated, dwarf, early- or late-flowering, high-yielding, and salt-tolerant phenotypes are found in M_2 plants. Over the last decade, molecular biology has made great advances through technological innovation. We use high-throughput DNA sequencing techniques such as next-generation sequencing instruments and microarray technologies to analyze gene mutations. Mutants have become more and more useful and important in modern genetic studies, enabling the discovery of genes that control important traits, and revealing the functions and mechanisms underlying their operations. The discovery of genes using mutants may lead to the emergence of a new field in biology, 'mutagenomics'.

(3) Innovative applications of heavy-ion beams

An international heavy-ion breeding research consortium has been organized, with 156 national user groups and 15 international institutes in 2011. The consortium includes agricultural experimental stations, universities, and seed and horticulture companies. The radiation biology team irradiated about 2200 different samples for a total beam time of 40 hours in one year. The advantages of heavy-ion mutagenesis include, a low dose with high survival rates, induction of high mutation rates, and a wide range of variation. The ion beam used often changes only a single characteristic. Thus, a new variety can be obtained by selecting a mutant that exhibits modification to a target trait while retaining the existing valuable traits. This approach has been particularly successful in flower breeding. The consortium has introduced 22 new cultivars of plants and 2 of microbes to the market in Japan, the USA, Canada, and the EU since 2001. The development period for these new varieties was only three years.

Team Leader
Tomoko ABE

Members
Katunori ICHINOSE
Koutaro ISHII
Masako IZUMI
Ryouhei MORITA
Teruyo TSUKADA
Kazuhide TSUNEIZUMI

Special Postdoctoral Researcher
Yusuke KAZAMA

Technical Staff I
Yoriko HAYASHI
Sachiko KOGURE

Technical Staff II
Sumie OHBU

Part-time Staffs
Yuko HAYASHI
Yuki SHIRAKAWA
Hideo TOKAIRIN
Satoko YASUDA
Taeko WAKANA

Visiting Scientists
Ryutaro AIDA (Natl. Inst. Floricult. Sci.)
Mari AMINO (Tokai University Hospital)
Chang-Hyu BAE (Sunchon Natl. Univ., Korea)
Hiroyuki DAIMON (Osaka Pref. Univ.)
Ali FERJANI (Tokyo Gakugei Univ.)
Makoto FUJIWARA (Grad. Sch., Col. Arts Sci., Univ. of Tokyo)
Eitaro FUKATSU (Forest tree beeding Cet.)
Yoshiya FURUSAWA (Natl. Inst. Radiol. Sci.)
Toshinari GODO (Botanic Gardens Toyama)
Misako HAMATANI (Hiroshima City Agric. Forest. Promot. Cen.)
Yasuhide HARA (Kanagawa Inst. Agric. Sci.)
Masanori HATASHITA (Wakasa Wan Energy Res. Cen.)
Atsushi HIGASHITANI (Grad. Sch. Life Sci., Tohoku Univ.)
Ryoichi HIRAYAMA (Natl. Inst. Radiol. Sci.)
Akiko HOKURA (Tokyo Denki Univ.)
Ichiro HONDA (Natl. Agric. Res. Cen.)
Mitsugu HORITA (Hokuren Agri. Res. Inst.)
Hiroyuki ICHIDA (Meiji Univ.)
Yuji ITO (Natl. Agric. Res. Cen., Hokkaido Region)

Akihiro IWASE (Grad. Sch. Engin., Osaka Pref. Univ.)
Hiroshi KAGAMI (Shizuoka Citrus Exp. Station)
Tetsuya KAKO (Suntory Flowers, Ltd.)
Si-Yong KANG (Dep. Rad. Plant Breed. Genet., KAERI, Korea)
Tomojirou KOIDE (Riken Vitamin Co., Ltd.)
Tsutomu KUBOYAMA (Ibaraki Univ.)
Norihiko MISHIMA (Fukuda Denshi Co., Ltd.)
Yutaka MIYAZAWA (Grad. Sch. Life Sci., Tohoku Univ.)
Kazumitsu MIYOSHI (Fac. Bioresour. Sci., Akita Pref. Univ.)
Toshikazu MORISHITA (Inst. Rad. Breeding, Natl. Inst. Agric. Res.)
Koji MURAI (Fukui Pref. Univ.)
Francesco MUSUMECI (Catania Univ.)
Daisuke NAKADA (Ela Medical Japan Co., Ltd.)
Koichiro NISHIKAWA (FLORSAIKA CIA. LTDA.)
Norihiro OHTSUBO (Natl. Inst. Floricult. Sci.)
Tomo OOMIYA (Hokkaido Ornamental Plants Veg. Res. Cen.)
Kenji OSAWA (Nagano Agric. Res. Cen.)
Masaya SAKAI (Fukuda Denshi Co., Ltd.)
Kouichi SAKAMOTO (YUKIGUNI AGURI Co., Ltd.)
Tadashi SATO (Grad. Sch. Life Sci., Tohoku Univ.)
Yoichi SATO (Riken Food Co., Ltd.)
Mikio SHIMADA (Kyoto Univ.)
Fumio SUGAWARA (Tokyo Univ. of Sci.)
Masao SUGIYAMA (Hokko Chem. Ind. Co., Ltd.)
Keita SUGIYAMA (Nat. Inst. Veg.Tea Sci.)
Ryuji SUGIYAMA (Ajinomoto, Co., INC.)
Kazunori SUZUKI (Plant Biotech. Inst. Ibaraki Agric. Cen.)
Masao SUZUKI (Natl. Inst. Radiol. Sci.)
Kenichi SUZUKI (Suntory Flowers, Ltd.)
Kunio SUZUKI (Technoflora, Co., Ltd.)
Hinako TAKEHISA (Natl. Inst. Agric. Sci.)
Sachie TANAKA (Tokai Univ.)
Teruhiko TERAKAWA (Hokko Chem. Ind. Co., Ltd.)
Ken TOKUHARA (Dogashima Orchid Cen.)
Masanori TOMITA (CRIEPI)
Hisashi TSUJIMOTO (Fac. Agri., Tottori Univ.)
Kozo TSUKADA (Nippon Veterinary and Life-sci. Univ.)
Makoto UBUKATA (Hokkaido Univ.)
Masao WATANABE (Fac. Agri., Tohoku Univ.)
Takuji YOSHIDA (Takii Seed Co., Ltd.)
Yasuko YOSHIHARA(Japan Atomic Energy Agency)
Koichiro YOSHIOKA (Tokai University Hospital)

Research Fellows

Hideki ASAUMI (Ehime Agricultural Experiment Station)
Masataka CHAYA (Nagasaki Agr. Forest. Exp. Station)
Fumiko HIDAKA (Kagoshima Pref. Inst. for Agric. Dev.)
Shunsuke IMANISHI (Natl. Inst.Veg. and Tea Sci.)

Hiroaki KISAKA (Ajinomoto, Co., INC.)
Yuri KURUMATANI (Chiba Pref. Agr. Res. Cent.)
Chikara KUWATA (Chiba Pref. Agr. Res. Cent.)
Tadanori MINO (Wadomari Cho Agr. Exp. Station)
Miyuki NISHI (Saga Agricultural Experiment Station)
Kyousuke NIWA (Hyogo Pref. Res. Inst.)
Tadahito OOTUBO (Wadomari Cho Agr. Exp. Station)
Eikou OOYABU (Saga Pref. Agr. Res. Cen.)
Takenori SAITO (Shizuoka Tea Exp. Station)
Yoshihide SAKITA (Wadomari Cho Agr. Exp. Station)
Tsukasa SHIRAO (Kagoshima Biotechnology Inst.)
Keiichi TAKAGI (Wakasa-wan Energy Research Center)
Kei-ichiro UENO (Kagoshima Biotechnology Inst.)
Naoji WAKITA (Wadomari Cho Agr. Exp. Station)

Consultant
Hiroyuki SAITO

Students
Junior Research Associate
Liqiu MA (Grad. Sch. Sci. & Engin., Saitama Univ.)

Student trainees
Hiroki HANASHIMA (Tokyo Denki Univ.)
Fumihiro MASUYAMA (Tokyo Denki Univ.)
Takuma NAGANO (Tokyo Denki Univ.)
Naoko ODA (Fac. Sci., Tokyo Univ. of Sci.)
Tetsuya OKABE (Fac. Sci., Tokyo Univ. of Sci.)
Hiroki TAOKA (Fac. Sci., Tokyo Univ. of Sci.)

RIBF Research Division
Accelerator Applications Research Group
RI Applications Team

1. Abstract

The RI Applications Team develops production technologies for radioisotopes (RIs) at the RIKEN RI Beam Factory (RIBF) for application studies in physics, chemistry, biology, medicine, and pharmaceutical and environmental sciences. Purified RIs such as ^{65}Zn and ^{109}Cd are delivered to universities and institutes for fee-based distribution through the Japan Radioisotope Association. Furthermore, we develop new mass spectrometry technologies for trace element analyses using accelerator technology and apply them to scientific research fields such as cosmochemistry, environmental science, and archaeology. We also develop chemical materials for electron cyclotron resonance (ECR) ion sources for acceleration of heavy ion such as ^{48}Ca, ^{70}Zn, and ^{238}U at the RIBF.

2. Major Research Subjects

(1) Research and development of RI production technology at the RIBF
(2) RI application research
(3) Development of trace element analysis using accelerator techniques and its application to geoscience and environmental science
(4) Research and development of chemical materials for ECR ion sources at the RIBF

3. Summary of Research Activity

(1) Research and development of RI production technology at the RIBF

Using heavy-ion accelerators at the RIBF, we are developing RI production technologies for application studies in physics, chemistry, biology, medicine, and pharmaceutical and environmental sciences. With proton and deuteron beams from the azimuthally varying field cyclotron (AVF), we produce about 30 radiotracers. Among them, ^{65}Zn, ^{109}Cd, and ^{88}Y are delivered to the Japan Radioisotope Association for fee-based distribution to the general public in Japan. Since 2007, we have accepted 65 orders for ^{65}Zn with a total activity of 363.5 MBq and 23 orders for ^{109}Cd with 164.0 MBq of activity. On the other hand, radionuclides of a large number of elements are simultaneously produced from metallic targets such as ^{nat}Ti, ^{nat}Ag, ^{nat}Hf, and ^{197}Au irradiated with a 135 MeV nucl.$^{-1}$ ^{14}N beam from the RIKEN Ring Cyclotron (RRC). This multitracer is also provided to universities and institutes for collaborative research.

(2) RI application research

The chemistry of newly discovered superheavy elements (SHEs, atomic numbers $Z \geq 104$) is an interesting and challenging research subject in nuclear and radiochemistry. We are developing SHE production systems as well as rapid chemistry apparatuses at the RIKEN Linear Accelerator (RILAC) and AVF. At the RILAC, a gas-jet transport system has been coupled to the gas-filled recoil ion separator (GARIS). We are developing a gas chromatograph apparatus directly coupled to the GARIS that enables in-situ complexation and gas chromatographic separation of a large variety of volatile SHE compounds. We have also installed a gas-jet-coupled SHE production system on the AVF beam line. Aqueous chemistry apparatuses for ion exchange and solvent extraction are under development together with automated rapid α particle and spontaneous fission detection systems. Using intense heavy-ion beams from the RILAC and AVF, SHEs such as ^{261}Rf, ^{262}Db, and ^{265}Sg are produced, and their chemical properties are investigated on a single-atom scale.

(3) Development of trace element analysis using accelerator techniques and its application to geoscience and environmental science

We developed two new mass spectrometry technologies for trace element analyses as an application of accelerator technology to various fields such as cosmochemistry, environmental science, and archaeology. One is a new type of accelerator mass spectrometry at the RILAC equipped with an ECR ion source. This system is available for measuring trace elements (10^{-14}–10^{-15} level) and is expected to be especially effective for measurements of low-electron-affinity elements such as ^{26}Al, ^{41}Ca, and ^{53}Mn. As a preliminary study, the ECR ion source system was evaluated and the basic data were obtained for the detection and quantitative analysis of trace nuclides in archaeological samples (cinnabar) and functional metals. We attempted to develop another technology by customizing a mass spectrometer equipped with a stand-alone ECR ion source for analyses of elemental and isotopic abundances. In 2012, we examined the Mo isotope measurements of metal samples using sputtering methods. Furthermore, we analyzed lead isotope ratios for vermilion (cinnabar) found in grave burials to examine their origins.

(4) Research and development of chemical materials for ECR ion sources at the RIBF

We prepared CaO, ZnO, and metallic U for ECR ion sources at the RIBF for acceleration of ^{48}Ca, ^{70}Zn, and ^{238}U ions, respectively, in collaboration with Ion Source Team at the RIKEN Nishina Center.

Team Leader
Hiromitsu HABA

Senior Research Scientist
Kazuya TAKAHASHI

Postdoctoral Researcher
Minghui HUANG

Technical Staff I
Jumpei KANAYA

Visiting Researcher
Suparna SODAYE (JSPS)

Part-timer2
Mika MAKITA

Visiting Scientists
Hiroshi HIDAKA (Fac. Sci., Hiroshima Univ.)
Mayeen Uddin KHANDAKER (Dep. Phys., Univ. Malaya)
Hidetoshi KIKUNAGA (Res. Center Elec. Photon Sci., Tohoku Univ.)
Tatsuo OKANO (Inst. Industrial Sci., Univ. Tokyo)
Hiroshi SHIMIZU (Fac. Sci., Hiroshima Univ.)
Miho TAKAHASHI (Tokyo Univ. Marine Sci. and Tech.)
Masayoshi TODA (Tokyo Univ. Marine Sci. and Tech.)
Tokuko WATANABE (Aoyama Gakuin Women's Junior College)
Shigekazu YONEDA (Natl. Sci. Museum)

Visiting Technicians
Ai OHTSUBO (Japan Radiation Association)
Yuichiro WAKITANI (Japan Radiation Association)
Shinichi YAMAMOTO (Japan Radiation Association)

Student Trainees
Junichi HIRATA (Tokyo Univ. Marine Sci. and Tech.)
Hajime KIMURA (Kanazawa Univ.)
Yuta KITAYAMA (Kanazawa Univ.)
Kouhei NAKAMURA (Osaka Univ.)
Eita MAEDA (Kanazawa Univ.)
Yuki SHIGEYOSHI (Kanazawa Univ.)
Keigo TOYOMURA (Osaka Univ.)

RIBF Research Division
User Liaison and Industrial Cooperation Group

Abstract

The essential mission of the "User Liaison and Industrial Cooperation (ULIC) Group" is to maximize the research activities of RIBF by attracting users in various fields with a wide scope.
The ULIC Group consists of two teams.
RIBF User Liaison Team provides various supports to visiting RIBF users through the RIBF Users Office. Managing RIBF beam time and organizing the Program Advisory Committee Meetings to review RIBF experimental proposals are also important mission of the Team in order to enhance common use of the RIBF. The Industrial Cooperation Team supports potential users in industries who use the beams for application purposes or for accelerator related technologies other than basic research. Production of various radioisotopes by the AVF cyclotron is also one of the important mission. The produced radioisotopes are distributed to researchers in Japan for a charge through the Japan Radioisotope Association.

Group Director
Hideyuki SAKAI

Deputy Group Director
Hideki UENO (Synergetic Common Use)

Members
Aiko NAKAO
Mieko KOGURE

Special Temporary Employee
Tadashi KAMBARA

Senior Visiting Scientists
Ikuko HAMAMOTO
Munetake ICHIMURA

Visiting Scientist
Byung-taik KIM

Assistants
Yoshiko SAKATA
Tomoko IWANAMI
Emiko ISOGAI
Katsura IWAI

RIBF Research Division
User Liaison and Industrial Cooperation Group
RIBF User Liaison Team

1. Abstract

To enhance synergetic common use of the world-class accelerator facility, the Radioactive-Isotope Beam Factory (RIBF), it is necessary to promote a broad range of applications and to maximize the facility's importance. The facilitation and promotion of the RIBF, as well as public relations activities on the RIBF, are important missions charged to the team. Important operational activities of the team include: i) the organization of international Program Advisory Committee (PAC) meetings to review experimental proposals submitted by RIBF users, ii) RIBF beam-time operation management, and iii) promotion of facility use by hosting outside users through the RIBF Independent Users program, which is a new-user registration program begun in FY2010 at the RIKEN Nishina Center (RNC) to enhance the synergetic common use of the RIBF. The team opened the RIBF Users Office in the RIBF building in 2010, which is the main point of contact for Independent Users and provides a wide range of services and information.

2. Major Research Subjects

(1) Promotion of the use of the RIBF
(2) Facilitation of the use of the RIBF
(3) Public relations activities of the RIBF

3. Summary of Research Activity

(1) Promotion of the use of RIBF
- The team has organized an international PAC for RIBF experiments; it consists of leading scientists worldwide and reviews proposals in the field of nuclear physics (NP) purely on the basis of their scientific merit and feasibility. The team also assists another PAC meeting for material and life sciences (ML) organized by the RNC Advanced Meson Laboratory. The NP and ML PAC meetings are organized twice a year.
- The team coordinates beam times for PAC-approved experiments and other development activities. It manages the operating schedule of the RIBF accelerator complex according to the decisions arrived at by the RIBF Machine Time Committee.
- To enhance collaborative use of the RIBF by researchers outside of RIKEN, the team has been developing research envelopments of RIBF Independent Users and the members of the Partner Institutions.
- To promote research activities at RIBF, proposals for User Liaison and Industrial Cooperation Group symposia/mini-workshops are solicited broadly both inside and outside of the RNC. The RIBF Users Office assists in the related paperwork.
- The team is the point of contact for the RIBF users' association. It arranges meetings at RNC headquarters for the RIBF User Executive Committee of the users' association, and supports their activities.

(2) Facilitation of the use of the RIBF

The RIBF Users Office, formed by the team in 2010, is a point of contact for user registration through the RIBF Independent User program. This activity includes:
- registration of users as RIBF Independent Users,
- registration of radiation workers at the RIKEN Wako Institute,
- provision of an RIBF User Card (a regular entry permit) and an optically stimulated luminescence dosimeter for each RIBF Independent User, and
- provision of safety training for new registrants regarding working around radiation, accelerator use at the RIBF facility, and information security, which must be completed before they begin RIBF research.

The RIBF Users Office is also a point of contact for users regarding RIBF beam-time-related paperwork, which includes:
- contact for beam-time scheduling and safety review of experiments by the In-House Safety Committee,
- preparation of annual Accelerator Progress Reports, and
- maintaining the above information in a beam-time record database.

In addition, the RIBF Users Office assists RIBF Independent Users with matters related to their visit, such as invitation procedures, visa applications, and the reservation of on-campus accommodation.

(3) Public relations activities of the RIBF
- The team conducts publicity activities, such as arranging for RIBF tours, development and improvement of the RNC official web site, and delivery of RNC news via email and the web.
- The team participates in exhibitions for public.

Team Leader

Hideki UENO

Vice Team Leader

Yasushi WATANABE

Technical Staff I

Narumasa MIYAUCHI

Visiting Scientist

Toshimi SUDA
Nori AOI
Yoshiteru SATO
Yutaka UTSUNO
Masayuki YAMAGAMI

RIBF Research Division
User Liaison and Industrial Cooperation Group
Industrial Cooperation Team

1. Abstract

The scope of the industrial cooperation team includes industrial application of RIBF facility and research and development for industrial application of accelerator associated technologies.

2. Major Subjects

Investigation of novel industrial applications of the accelerator beam and its related technologies.
Development of wear diagnostics for industrial parts implanting RI beams.
Distribution of radioisotopes Zn-65, Cd-109 and Y-88 produced at RIKEN AVF Cyclotron.

3. Summary of Research Activity

(1) Industrial application of RIBF

This team manages and supports the non-academic applications of heavy ion and RI beams at the RIBF facility. Until 2012, three private companies utilized the heavy-ion and RI beams. A development of a wear analysis technique using RI-beam, a heavy-ion irradiation test for semi-conductors of space use was carried out.

(2) Fee-based distribution of radioisotopes

At RIBF, various specific radioisotopes for research have been produced with the cyclotrons and used for research projects. This team handles fee-based distribution of radioisotopes Zn-65, Y-88 and Cd-109, which are produced by the RI application team at the AVF cyclotron, to non-affiliated users under a Material Transfer Agreement between Japan Radioisotope Association and RIKEN. In 2012, total amount of 58MBq of Zn-65 and 20MBq of Cd-109 were distributed. In addition, we started distribution of Y-88 in February 2010.

Team Leader
Atsushi YOSHIDA

Members
Aiko NAKAO
Hiroshige TAKEICHI

Visiting Scientists
Shuhei TATEMICHI (Fuji Electric Systems)
Masanori INOUE (Fuji Electric Systems)

RIBF Research Division
Safety Management Group

1. Abstract

The RIKEN Nishina Center for Accelerator-Based Science possesses one of the largest accelerator facilities in the world, which consists of two heavy-ion linear accelerators and five cyclotrons, and a proton linac. This is the only site in Japan where uranium ions are accelerated. The center also has electron accelerators of microtron and synchrotron storage ring. Our function is to keep the radiation level in and around the facility below the allowable limit and to keep the exposure of workers as low as reasonably achievable. We are also involved in the safety management of the Radioisotope Center, where many types of experiments are performed with sealed and unsealed radioisotopes.

2. Major Research Subjects

（１） Safety management at radiation facilities of Nishina Center for Accelerator-Based Science
（２） Safety management at Radioisotope Center
（３） Radiation shielding design and development of accelerator safety systems

3. Summary of Research Activity

Our most important task is to keep the personnel exposure as low as reasonably achievable and to prevent accidents. Therefore, we patrol the facility daily; measure the ambient dose rates; maintain the survey meters, shield doors, and exhaust air and wastewater facilities; replenish the protective supplies; and manage radioactive waste. We also provide advice, supervision, and assistance for major accelerator maintenance work.
The radiation safety interlock system of the RIBF building has been modified in conjunction with the construction of the EURICA detector. The access control system, which is a part of the Nishina safety interlock system, was extended to the gate of the RIBF building. The SCTIT interlock system was modified to meet the start of the experiment with unstable nuclides. A new interlock system was installed at the compact neutron source with a proton linac.

Head
Yoshitomo UWAMINO

Members
Hisao SAKAMOTO
Rieko HIGURASHI HIRUNUMA
Kanenobu TANAKA

Technical Staff I
Atsuko AKASHIO

Assistant
Tomomi OKAYASU

Contract Officer
Satoshi HASHIGUCHI (Daiwa Atomic Engineering Corp.)
Hiroyuki FUKUDA
Hiroki MUKAI (Japan Environment Research Corp.)
Mamoru TAKEKOSHI (Daiwa Atomic Engineering Corp.)

Temporary Employee
Masaharu OKANO

Visiting Scientists

Takashi NAKAMURA (Tohoku Univ.)
Koji OHISHI (Shimizu Corp.)
Noriaki NAKAO (Shimizu Corp.)

Secretary

Tsutomu YAMAKI
Kazushiro NAKANO
Hiroshi KATO
Shin FUJITA
Hiroko AISO
Kimie IGARASHI
Satomi IIZUKA

Center for Nuclear Study, Graduate School of Science, University of Tokyo.

1. Abstract

The Center for Nuclear Study (CNS) aims to elucidate the nature of nuclear system by producing the characteristic states where the Isospin, Spin and Quark degrees of freedom play central roles. These researches in CNS lead to the understanding of the matter based on common natures of many-body systems in various phases. We also aim at elucidating the explosion phenomena and the evolution of the universe by the direct measurements simulating nuclear reactions in the universe. In order to advance the nuclear science with heavy-ion reactions, we develop AVF upgrade, CRIB and SHARAQ facilities in the large-scale accelerators laboratories RIBF. We promote collaboration programs at RIBF as well as RHIC-PHENIX and LHC-ALICE with scientists in the world, and host international meetings and conferences. We also provide educational opportunities to young scientists in the heavy-ion science through the graduate course as a member of the department of physics in the University of Tokyo and through hosting the international summer school.

2. Major Research Subjects

(1) Accelerator Physics
(2) Nuclear Astrophysics
(3) Nuclear spectroscopy of exotic nuclei
(4) Quark physics
(5) Nuclear Theory
(6) SHARAQ project
(7) Active Target Development

3. Summary of Research Activity

(1) Accelerator Physics

One of the Major tasks of the accelerator group is the AVF upgrade project that includes development of ion sources, upgrading the AVF cyclotron of RIKEN and the beam line to CRIB. Development of ECR heavy ion sources is to provide a new HI beams, higher and stable beams of metallic ions, and to improve the control system. Two ECR sources now provide all the beams for the AVF cyclotron and support not only CRIB experiments but also a large number of RIBF experiments. One of the major developments performed for upgrading the AVF cyclotron is the increase of the energy up to K78 by the installation of a new central module. New beam monitors at the ion sources, the beam line, and the AVF were installed and used for diagnose various beams in order to improve the transmission efficiency.

(2) Nuclear Astrophysics

The nuclear astrophysics group is studying relevant astrophysical reactions and special nuclear structures using a low-energy RI beam separator, CRIB. Our main interest is on stellar thermonuclear reaction processes at high temperatures, such as hot p-p chain, hot CNO cycle, rp-process, and αp-process.

In 2012, proton resonant scattering measurement of ^{22}Na+p and ^{17}F+p were carried out in collaboration with Chinese groups (CIAE and IMP), and we observed resonances in the compound nuclei. We can evaluate resonant reaction rates using the resonant parameters we obtained. A production test of ^{44}Ti beam was also performed with KEK group, and we gained a prospect of producing a ^{44}Ti beam of 10^4 per second. We planned to use the beam for a measurement of ^{44}Ti(α,p) reaction cross section, which provide us a precise evaluation of the production rate of cosmic gamma ray from ^{44}Ti. We are also working for the development of the active target with GEM (GEM-MSTPC), to use it for decay detection measurements in the future. As an industrial application, it was proposed that the intense ^{7}Be beam at CRIB should be used for diagnostics of industrial materials. This project was proposed by RIKEN group, and an irradiation test was successfully performed in 2012.

(3) Nuclear structure of exotic nuclei

The NUSPEQ (NUclear SPectroscopy for Extreme Quantum system) group studies exotic structures in high-isospin and/or high-spin states in nuclei. The CNS GRAPE (Gamma-Ray detector Array with Position and Energy sensitivity) is a major apparatus for high-resolution in-beam gamma-ray spectroscopy. Missing mass spectroscopy using the SHARAQ is going to start as another approach on exotic nuclei. In 2012, the following progress has been made.

Analysis of α inelastic scattering data from nuclei in the island of inversion, which was taken by using GRAPE, has progressed, which gives information of the border of the island-of-inversion in the nuclear chart. Experiments of searching new isomers by using ^{238}U and ^{124}Xe primary beams from SRC were performed and 19 new isomers were found by the analysis of the obtained data.

A plunger system for recoil distance method was developed for the approved experiments of the lifetime measurements of neutron-rich fp-shell nuclei. The readout system of 12 detectors of the CNS GRAPE was upgraded, where digital pulse data taken by sampling ADCs are analyzed by FPGAs on boards.

The double-charge exchange reaction ^{4}He(^{8}He,^{8}Be)4n was measured at 200 A MeV for studying tetra neutron system, whose analysis is now in progress. Gamma-ray spectroscopy of neutron-rich Ca isotopes was performed, which shows low-lying spectra of the ^{53,54}Ca nuclei.

(4) Quark Physics

Main goal of the quark physics group is to understand the properties of hot and dense nuclear matter created by colliding heavy nuclei at relativistic energies. The group has been involved in the PHENIX experiment at Relativistic Heavy Ion Collider (RHIC) at Brookhaven National Laboratory, and the ALICE experiment at Large Hadron Collider (LHC) at CERN.

As for PHENIX, the group has been concentrating on the physics analysis involving leptons and photons; direct photon production at low transverse momentum using the virtual-gamma method, J/ψ production in ultra-peripheral Au+Au collisions, and electron measurement from semi-leptonic decay of heavy flavor mesons which uses the Si VTX detector subsystem.

As for ALICE, the group has involved in the data analyses, which include production of multi-particle correlation in Pb+Pb collisions, nuclear modification of energetic neutral pions in Pb+Pb collisions, and measurement of low-mass lepton pairs. The group has also been playing a leading role in the development of forward calorimeter for future upgrade. In 2012, the group started to involve in the ALICE-TPC upgrade using a Gas Electron Multiplier (GEM). Systematic studies of gain stability, ion back flow, and energy resolutions with various field configurations are underway at CNS and at CERN.

R&D of GEM and related techniques has been continuing. Development of resistive GEM with resistive anodes and GEM with glass insulator have been progressing in collaboration with the Tamagawa group of RIKEN.

(5) Nuclear Theory

The nuclear theory group has been promoting the RIKEN-CNS collaboration project on large-scale nuclear structure calculations since 2001 and maintaining its PC cluster. Based on this experience and its achievements, we participated in activities of HPCI Strategic Programs for Innovative Research (SPIRE) Field 5 "The origin of matter and the universe" in 2011. The SPIRE project aims at an integral understanding of the origin and structure of matter and the Universe utilizing the K computer, which was the world's fastest supercomputer in 2011.

In the SPIRE project, we are in charge of the elucidation of nuclear properties using ultra large-scale simulations of quantum many-body systems and its applications. In order to perform large-scale shell-model calculations, we developed an efficient computer program of the Monte Carlo Shell Model (MCSM) method for massive parallel computation, and performed benchmark calculations at K computer. We have been performing production runs at the K computer since September 2012. In parallel, we studied the effective interaction of medium-heavy nuclei which is essential for the large-scale shell-model calculations.

(6) SHARAQ project

A main subject of the SHARAQ program is charge-exchange reactions induced by heavy-ion beams, with which a variety of selectivities in transferred quantum numbers, ΔS, ΔT, ΔT_z, ΔL etc, are available. This year, the SHARAQ group carried out the measurement of the exothermic double-charge exchange (^{8}He,^{8}Be) reaction on liquid ^{4}He target to study the tetra-neutron system. Here the exothermicity of the (^{8}He, ^{8}Be) reaction is advantageous in populating the fragile tetra-neutron states from ^{4}He since the energy needed in the target excitation is almost completely compensated by the positive Q-value in the projectile. The missing mass was obtained successfully by simultaneously detecting two α particles produced by the decay of residual ^{8}Be nucleus.

The other research subject is directed toward the study of the structure of unstable nuclei. The polarized proton target was introduced for the first time at SHARAQ and the (pol-p,2p)/(pol-p,pn) reaction on unstable oxygen isotopes ^{14,22,24}O were performed (See article of Spin Isospin Lab of RIBF Research Division).

The dispersion-matching ion optics of SHARAQ was reexamined by using fragments of A/Z = 2 nuclei and the beam tuning procedure was simplified for rapid tuning. Also the time-of-flight components of transport matrix were measured by CVD diamond detectors. To achieve high momentum resolution in the system, event-by-event correction of beam trajectory was made by examining the hit positions at foci. A momentum resolution of 1/8100 (FWHM) was successfully obtained.

(7) Active Target Development

The aim of the active target project is to utilize the missing-mass spectroscopy in inverse kinematics by developing the active targets. We have developed two types of gaseous active targets, which are GEM-based TPCs, for high-energy (100-300MeV/u) beam experiments, where β+-type Gamow-Teller transition and inelastic scattering are studied, and for low-energy (a few MeV/u) beam experiments, where the (α,p) reactions are studied from the viewpoint of astrophysical interest.
A pilot experiment of the active target for high-energy beam (CAT) was performed at HIMAC. Secondary beam of 14O at 100 MeV/u was produced and bombarded the CAT, which was operated with three GEMs and 1-atm deuterium gas. The property of thick GEMs with low-pressure deuterium was studied for the low-pressure operation of the CAT.
As for the other type of the active target of CNS (GEM-MSTPC), we made a development for a pulsing operation of GEM with an external gate signal. GEM-MSTPC is going to be used in a beta delayed alpha particle decay measurement with a high-intensity beam.

Director

Takaharu OTSUKA

Scientific Staff

Susumu SHIMOURA (Professor)
Hideki HAMAGAKI (Professor)
Kentaro Yako (Associate Professor)
Noritak SHIMIZU (Project Associate Professor)
Hidetoshi YAMAGUCHI (Lecture)
Shin'ichiro MICHIMASA (Research Associate)
Taku GUNJI (Research Associate)
Shinsuke OTA (Research Associate)

Guest Scientists

Hiroaki Utsunomiya (Guest Professor)
Yutaka Utsuno (Guest Associate Professor)

Technical Staff

Norio YAMAZAKI
Yukimitsu OHSHIRO

Techinical Assistants

Shin-ichi WATANABE
Hiroshi KUREI
Takehiko SENOO
Akira YOSHINO
Shoichi YAMAKA
Kazuyuki YOSHIMURA
Masahiko TANAKA

Project Research Associates

Hisayuki TORII
Tooru YOSHIDA
Yoritaka Iwata

Post Doctoral Associates

Shuichiro EBATA
Yorito YAMAGUCHI
Taro NANAO
David, STEPPENBECK
Tomoaki TOGASHI

Graduate Students

David. M KAHL
Masashi, MATSUSHITA
Akihisa TAKAHARA
Hiroyuki MIYA
Ryoji AKIMOTO
Yasuto HORI
Hiroshi TOKIEDA
Tomoya TSUJI
Shintaro GO
Shoichiro KAWASE
ShinIchi HAYASHI
KeiIchi KISAMORI
Motonobu TAKAKI
Tang T. LEUNG
Yuko SEKIGUCHI
Toshihiko FUJII
Rin YOKOYAMA
Yuki KUBOTA
CheongSoo LEE
Kohei TERASAKI
Motoki KOBAYASHI

Administration Staff

Hiroshi YOSHIMURA
Yuko ASAKAWA
Ikuko YAMAMOTO
Takako ENDO
Yukino KISHI
Toshiko ITAGAKI
Yuko SOMA

RNB (Radioactive Nuclear Beam) group, IPNS (Institute for Particle and Nuclear Studies), KEK (High Energy Accelerator Research Organization)

1. Abstract

We have been developing an element-selective isotope separator, KISS (KEK Isotope Separation System) at RIKEN to investigate the β-decay properties of heavy neutron-rich nuclei with neutron numbers of N = 126 relevant to the r-process of heavy element nucleosynthesis in cosmos. The main components of the KISS installed in FY 2011 are now under on-line test to confirm the performance (efficiency and selectivity for isotopes of interest). Some other activities are also included.

2. Major Research Subjects

(1) Radioactive isotope beam production and manipulation for nuclear experiments.
(2) Explosive nucleosynthesis (rp- and r-process).
(3) Heavy ion reaction mechanism for producing heavy neutron-rich nuclei.
(4) Single particle states of neutron-rich nuclei by isobaric analog resonances.
(5) Development of RNB probes for materials science applications.

3. Summary of Research Activity

For the on-line test of the KISS, where will be confirmed the full processes in the KISS for stopping (thermalization and neutralization) and transporting by buffer gas (argon gas-flow of ~50 kPa in a gas-cell), and re-ionizing by laser irradiation energetic heavy ions, a stable ^{56}Fe beam from the RRC was directly injected into the gas-cell. Before the beam experiment, we firstly performed an off-line test to search for an efficient ionization scheme for Fe atom evaporated from a heated filament in the gas-cell. We have found a new ionization scheme, whose transitions are two steps for resonant excitation and ionization from the ground state of neutral Fe atom; $3d^6\,4s^2$ (J = 4) → $3d^6\,4s4p$ (J = 5) (λ_1 = 248.402 nm) → auto ionization state (λ_2 = 423.784 nm). The saturation power of the 1st step laser (λ_1) irradiation was 15 μJ/pulse, which is available in our present laser system. Secondly, we investigated the mass-distribution of ions extracted from the gas-cell of the KISS. Those ions primarily produced by α-particle irradiation from Am α-source (~40 kBeq), are supposed to be transformed to molecular side bands via associative chemical reactions with impurities existing in the gas cell. Therefore, the pattern of the mass distribution could be a good indicator of how much and many impurities exist in the gas cell. Indeed, we have watched how the mass distribution is evolved during our purification processes, i.e. such as baking, activation of the gas purifiers etc. In this way, we can check the impurity compositions in the gas cell; it is more or less qualitative at this moment, but, we are sure, accessible down to the level of impurity compositions of sub ppb. We have performed on-line test two times so far, but unfortunately could not succeed to confirm Fe ions that are resonantly ionized after all physical processes in the gas cell as mentioned above. After comprehensive discussions about possible reasons for our failure and continuous efforts, we have improved some critical problem points: purity in the gas-cell as well as the argon-gas supply system, and injection condition of the primary beam into the gas cell (so far, the Fe beam of 95 MeV/u was energy-degraded to ~0.5 MeV/u by a thick Al plate located about 2 m upstream of the gas cell. Now the main degradation will be conducted just in front of the gas-cell.) Another on-test will be performed soon with the improved conditions.
As an effort for developing resonant laser ionization system, the alpha decays of neutron-deficient gold and astatine isotopes were measured at CERN/ISOLDE. The isotopes were resonantly ionized by using three color lasers. For the astatine, Rydberg states were successfully measured, allowing us to determine the ionization potential for the first time.

In order to investigate the feasibility of the multi-nucleon transfer (MNT) in the reaction system of ^{136}Xe on ^{198}Pt for producing heavy neutron-rich isotopes around the mass number of 200 with the neutron magic number of 126, measurements of the MNT reaction cross sections with the large acceptance magnetic spectrometer VAMOS++ and the high efficiency gamma detector array EXOGAM were performed at GANIL in March 2012. The complete identification of the projectile-like fragments (PLFs) detected by the spectrometer was achieved. And it makes possible the comparison of the isotope distributions of the PLFs for different proton transfer channels, which shows a comparable strength of the proton pick-up and proton stripping channels. It is the first time to be experimentally measured and very much different from the case of the MNT reactions with light collision partners (up to Zr), where the neutron pick-up channels and proton stripping channels dominate. Compared with GRAZING calculations, the measured isotopic distributions of the PLFs show much enhanced cross sections in pick-up channels of more than one proton, correspondingly higher production of target-like fragments of our present interests could be anticipated. The analysis will be continued for the determination of the absolute cross sections of the PLFs production and identification of the target-like fragments (TLFs) with the gamma-rays detected by the EXOGAM array, which allows us to estimate the cross sections (presumably their lower limit) of TLFs.

For direct measurements of the reaction cross section of ^{44}Ti (α, p) ^{47}V, which is one of key reactions to evaluate ^{44}Ti yield in supernova nucleosynthesis, we performed the ^{44}Ti beam development at CRIB in FY2012. Using the production reaction of ^{3}He (^{42}Ca, ^{44}Ti), the intensity for ^{44}Ti was observed to be 130 - 350 pps with the ^{42}Ca beam of 1 pnA, corresponding to 0.9 – 2 * 10^4 pps when an available beam current of ^{42}Ca (70 pnA) at AVF cyclotron was assumed. As a first usage of the beam, an experiment searching for three-cluster states (^{40}Ca + α + α) among excited states of the compound system ^{48}Cr is considered by using ^{44}Ti (α, α) resonant elastic scatterings.

We performed experiments of the proton resonance elastic scatterings of ^{30}Mg and ^{20}Na which were accelerated by the REX-ISOLDE, as our continuing effort for investigating the nature of the single particle states of light neutron-rich or -deficient nuclei by using the thick target inverse kinematics (TTIK) method. With the ^{30}Mg beam of 2.92 MeV/u, we observed the isobaric analog resonances of the low-lying bound state in ^{31}Mg, giving us the information on the spectroscopic factors of the these states. Analysis is underway.

Group Leader

Hiroari MIYATAKE

Member

Yoshikazu HIRAYAMA
Nobuaki IMAI
Yutaka WATANABE
Hironobu ISHIYAMA
Sunchan JEONG
Michihiro OYAIZU
Yung-Hee KIM (PhD. student, Seoul National university)
Momo Mukai (M. student, Tsukuba University)

TORIJIN (Todai-RIKEN Joint International Program for Nuclear Physics)

1. Abstract

University of Tokyo and RIKEN have agreed to corporate with each other in the field of nuclear physics and have established Todai-RIKEN Joint International Program for Nuclear Physics (TORIJIN) in June 2006. The aim of this organization is to promote the international collaborations, such as JUSTIPEN (Japan-US Theory Institute for Physics with Exotic Nuclei). JUSTIPEN was launched in June 2006 in order to facilitate collaborations between U.S. and Japanese scientists whose main research thrust is in the area of the physics of exotic nuclei.

2. Main activities

Promote the international collaborations of both theoretical and experimental nuclear physicists under JUSTIPEN.

3. Summary of Research Activity

Under the JUSTIPEN program, 10 nuclear scientists in the U.S. have visited Japan in this fiscal year (Apr. 2012--Mar. 2013). Theoretical Nuclear Physics Laboratory and User Liaison and Industrial Cooperation Group were mainly responsible for the US visitors' accommodation and other arrangements. Under this project, a number of collaborations have been established. We also organized the 6th LACM-TORIJIN-JUSTIPEN workshop at Oak Ridge National Laboratory from Oct. 31 to Nov. 2, 2012 in Oak Ridge. Fifteen Japanese scientists attended the workshop and we had fruitful discussions. Also "JUSTIPEN workshop on supercomputing at CCP2012" was held on Oct. 15--16, at the "Conference on Computational Physics (CCP2012)" in Kobe, Japan.

The 11th CNS international summer school was organized from Aug. 29 to Sep. 4, 2012, for which we invited 9 lecturers, 4 of them from abroad.

Chair

Takaharu OTSUKA (University of Tokyo)

Vice chair

Hiroyoshi SAKURAI (University of Tokyo/RIKEN)

Steering board members

Susumu SHIMOURA (University of Tokyo)
Takashi NAKATSUKASA (RIKEN)
Tohru MOTOBAYASHI (RIKEN)

Events from April 2012 to March 2013

2012	Apr. 18	Opening Seremony of Renewed RIBF Garaly
	Apr. 20	RIKEN Wako Institute's Open House
	Apr. 23	The paper published in 2010 on "Identification of 45 New Neutron-Rich Isotopes Produced by In-Flight Fission of a 238U Beam at 345 MeV/nucleon", J. Phys. Soc. Jpn. 79, 073201(2010) was chosen as one of the "Most Cited Articles in 2011" by Journal of the Physical Society of Japan
	Apr. 24	Newcomers of Nishina Center2012
	May. 01	The SAMURAI experiment using beam commenced
	May. 29	RIKEN and BNL Sign extension of RIKEN-BNL MoU on spin physics projects
	May. 29	18th Meeting of the Managing and Steering Committee
	Jun. 18-19	The 11th Program Advisory Committee for Nuclear Physcis Experiments at RI Beam Factroy
	Jun. 26	Temperature at RHIC is recognized by Guinness World Records as the "Hightest Man-made temperature"
	Jul. 05	"Element Genesis: RIKEN RI Beam Factory", a video introducing RIKEN, was shown at the opening ceremony of Synradome, the dome projection theater in the Science Museum
	Aug. 6-10	Seoul National University-Nishina School
	Sep. 04-05	The 9th Program Advisory Committee for Materials and Life Science Experimets at RIKEN Nishina Center
	Sep. 27	Search for element 113 concluded at last! prove third time's a charm
	Oct. 02-12	Peking University-Nishina School
	Oct. 22	RIKEN and Tokyo Institute of Technology issued a joint press release on the research result obtained by using the RIBF facility for "A new method for producing highly spin-aligned RI beams by employing a two-step projectile-fragmentation process in combination with the momentum-dispersion matching technique"
	Nov. 07-08	Scientific Review Committee at RIKEN BNL Ceter
	Nov. 08	A paper on the discovery of 18 new isomers via research performed at RIBF was accepted by "Physical Review C"
	Nov. 10-11	Science Agora in Odaiba
	Nov. 22	Press release for Discovery of 18 new nuclear isomers
2013	Jan. 08	Signing of the MoU on the collaboration between RIKEN Nishina Center and the European Centre for Theoretical Studies in Nuclear Physics and Related Areas (ECT*)
	Jan. 22	Interim Review of Radioactive Isotope Physics Labratory
	Feb. 19	Interim Review of Instrumentation Development Group

2013	Feb. 19	Interim Review of Research Instruments Group
	Feb. 22	Interim Review of Accelerator Applications Research Group
	Mar. 05	Interim Review of Safety Management Group
	Mar. 07	Interim Review of Theoretical Nuclear Physics Laboratory

CNS

Aug. 29 - Sep. 04	The 10th CNS Summer School (CNSSS11)

Awards From April 2012 to March 2013

Awardee & Laboratory	Masaharu Okano (Safety Management Group)
Name of Award	The Yoshikawa Eiji Cultural Prize
Sponsoring organization	Yoshikawa Eiji Cultural Foundation
Date of award	Apr. 11, 2012

Awardee & Laboratory	Ryouhei Morita (Ion Beam Breeding Laboratory)
Name of Award	Outstanding Presentation Award
Sponsoring organization	Japanese Society of Breeding
Date of award	May 15, 2012

Awardee & Laboratory	Masako Yamada (Radiation Laboratory)
Name of Award	Takegoshi Award
Sponsoring organization	Graduate School of Science/ Faculty of Science, Kyoto University
Date of award	Jun. 26, 2012

Awardee & Laboratory	Taku Izubuchi (RIKEN BNL Research Center, Theory Group), Christoph Lehner (RIKEN BNL Research Center, Computing Group), Thomas Blum (RIKEN BNL Research Center, Computing Group)
Name of Award	Ken Wilson Lattice Award
Sponsoring organization	International Symposium on Lattice Field Theory
Date of award	Jun. 29, 2012

Awardee & Laboratory	Yoshihide Higurashi (Accelerator Group, Ion Source Team), Jun-ichi Onishi (Accelerator Group, Accelerator R&D Team), Tsuneaki Minato (Mitsubishi Electric)
Name of Award	PASJ Award for Technical Contributions
Sponsoring organization	Particle Accelerator Society of Japan
Date of award	Aug. 09, 2012

Awardee & Laboratory	Hiroshi Imao (Accelerator R&D Team)
Name of Award	Oral Presentation Award
Sponsoring organization	Particle Accelerator Society of Japan
Date of award	Aug. 10, 2012

Awardee & Laboratory	Masanori Dozono (Spin Isospin Laboratory)
Name of Award	Award of outstanding young physicists ---Experimental Nuclear Physics---
Sponsoring organization	Nuclear Experimental Physics Forum (Kakudan)
Date of award	Sep. 13, 2012

Awardee & Laboratory	Hiroaki Matsubara (Spin Isospin Laboratory)
Name of Award	Award of outstanding young physicists ---Experimental Nuclear Physics---
Sponsoring organization	Nuclear Experimental Physics Forum (Kakudan)
Date of award	Sep. 13, 2012

Awardee & Laboratory	Kenjiro Miki (Spin Isospin Laboratory)
Name of Award	Award of outstanding young physicists ---Experimental Nuclear Physics---
Sponsoring organization	Nuclear Experimental Physics Forum (Kakudan)
Date of award	Sep. 13, 2012

Awardee & Laboratory	Tetsuo Hatsuda (Quantum Hadron Physics Laboratory), Shinya Aoki (Quantum Hadron Physics Laboratory), Noriyoshi Ishii (Radiation Laboratory),
Name of Award	Tsukuba Prize
Sponsoring organization	The Science and Technology Promotion Foundation of Ibaraki
Date of award	Oct. 17, 2012

Awardee & Laboratory	RIKEN Nishina Center
Name of Award	Science Agora Prize
Sponsoring organization	Japan Science and Technology Agency
Date of award	Nov 20, 2012

Awardee & Laboratory	Tadashi Fujinawa (Accelerator Group)
Name of Award	Special award at the 45th annual meeting of the College of Industrial Technology, Nihon University, for giving lectures at many of the college's annual meetings
Sponsoring organization	College of Industrial Technology, Nihon University
Date of award	Dec. 01, 2012

Awardee & Laboratory	Tetsuo Hatsuda (Quantum Hadron Physics Laboratory), Shinya Aoki (Quantum Hadron Physics Laboratory), Noriyoshi Ishii (Radiation Laboratory),
Name of Award	Nishina Memorial Award
Sponsoring organization	Nishina Memorial Foundation
Date of award	Dec 06, 2012

Awardee & Laboratory	Kosuke Morita (Superheavy Element Laboratory)
Name of Award	NISTEP Award
Sponsoring organization	National Institute of Science and Technology
Date of award	Dec 20, 2012

Awardee & Laboratory	Masaki Sasano (Spin Isospin Laboratory)
Name of Award	Young Scientist Award
Sponsoring organization	The Physical Society of Japan
Date of award	Mar 26, 2013

Awardee & Laboratory	Tetsuya Onishi (Instrumentation Development Group), Toshiyuki Kubo (Research Instruments Group) et, al.
Name of Award	Award for Academic Papers on Physics
Sponsoring organization	The Physical Society of Japan
Date of award	Mar 28, 2013

Awardee & Laboratory	Satoru Katsuta (High Energy Astrophysics Laboratory)
Name of Award	Young Scientist Award
Sponsoring organization	The Physical Society of Japan
Date of award	Mar 28, 2013

VI. LIST OF PUBLICATIONS & PRESENTATIONS

RIKEN Nishina Center for Accelerator-Based Science

Publications

[Journal]

(Original Papers) *Subject to Peer Review

Higurashi Y., Nakagawa T., Kidera M., Aihara T., Kase M., and Yano Y.: "Enhancement of Ar8+ Current Extracted from RIKEN 18 GHz Electron Cyclotron Resonance Ion Source by Moving the Plasma Electrode toward the Resonance Zone", Jpn. J. Appl. Phys. **40**, 5134–5135 (2001). *

Higurashi Y., Nakagawa T., Kidera M., Kageyama T., Kase M., Goto A., and Yano Y.: "Production of Highly Charged Ga Ions from Organic Metal Comppound Using the Liquid-He-Free Superconducting Electron Cyclotron Resonance Ion Source at RIKEN", Jpn. J. Appl. Phys. **41**, 5442–5443 (2002). *

Higurashi Y., Nakagawa T., Kidera M., Aihara T., Kase M., and Yano Y.: "Enhancement of Ar8+ Ion Beam Intensity from RIKEN 18 GHz Electron Cyclotron Resonance Ion Source by Optimizing the Magnetic Field Configuration", Jpn. J. Appl. Phys. **42**, 3656–3657 (2003). *

Higurashi Y., Nakagawa T., Kidera M., Kageyama T., Aihara T., Kase M., and Yano Y.: "Optimization of magnetic field configuration for the roduction of Ar ions from RIKEN 18 GHz ECR ion source", Nucl. Instrum. Methods Phys. Res. A **510**, No. 2, pp. 206–210 (2003). *

Higurashi Y., Kidera M., Kase M., Nakagawa T., and Yano Y.: "Emittance measurement for intense beam of heavy ions from RIKEN 18 GHz ECRIS", Rev. Sci. Instrum. **75**, 1467 (2004). *

Higurashi Y., Kidera M., Nakagawa T., Aihara T., Kase M., and Yano Y.: "Effect of Plasma Electrode Position of RIKEN 18 GHz Electron Cyclotron Resonance Ion Source on Beam Intensity of Highly Charged Ar Ions", Jpn. J. Appl. Phys. **44**, 5216–5218 (2005). *

Higurashi Y., Kidera M., Nakagawa T., Aihara T., Kase M., Goto A., and Yano Y.: "Production of 70Zn Beam from RIKEN 18 GHz Electron Cyclotron Resonance Ion Source", Jpn. J. Appl. Phys. **44**, 8138–8140 (2005). *

Higurashi Y., Nakagawa T., Kidera M., Aihara T., Kobayashi K., Kase M., Goto A., and Yano Y.: "Effect of the plasma electrode position and shape on the beam intensity of the highly charged ions from RIKEN 18 GHz electron cyclotoron resonanse ion source", Rev. Sci. Instrum. **77**, No. 2, p. 03A329 (2006). *

Higurashi Y., Nakagawa T., Kidera M., Haba H., Aihara T., Kase M., Goto A., and Yano Y.: "Production of U beam from RIKEN 18 GHz electron cyclotron resonance ion source", Rev. Sci. Instrum. **79**, No. 2, p. 02C714 (2008). *

Chevrier R., Daugas J., Gaudefroy L., Ichikawa Y., Ueno H., Hass M., Cottenier S., Aoi N., Asahi K., Balabanski D. L., Fukuda N., Furukawa T., Georgiev G., Hayashi H., Iijima H., Inabe N., Inoue T., Ishihara M., Ishii Y., Kameda D., Kubo T., Nanao T., Neyens G., Ohnishi T., Rajabali M. M., Suzuki K., Takeda H., Tsuchiya M., Vermeulen N., Watanabe H., and Yoshimi A.: "Is the $7/21^-$ isomer state of ^{43}S spherical?", Phys. Rev. Lett. **108**, 162501-1–162501-5 (2012). *

Hatsuda T.: "Application of Fixed Scale Approach to Static Quark Free Energies in Quenched and 2 + 1 Flavor Lattice QCD with Improved Wilson Quark Action", Prog. Theor. Phys. **128**, No. 5, pp. 955–970 (2012). *

Sato H., Kubo T., Yano Y., Kusaka K., Ohnishi J., Yoneda K., Shimizu Y., Motobayashi T., Otsu H., Isobe T., Kobayashi T., Sekiguchi K., Nakamura T., Kondo Y., Togano Y., Murakami T., Tsuchihashi T., Orikasa T., and Maeta K.: "Superconducting dipole magnet for SAMURAI spectrometer", IEEE Trans. Appl. Supercond. **23**, No. 3, pp. 4500308-1–4500308-8 (2013). *

[Book · Proceedings]

(Original Papers) *Subject to Peer Review

Yamada K., Arai S., Fujimaki M., Fujinawa T., Fujisawa H., Fukunishi N., Goto A., Higurashi Y., Ikezawa E., Kase M., Komiyama M., Kumagai K., Maie T., Nakagawa T., Ohnishi J., Okuno H., Sakamoto N., Sato Y., Suda K., Watanabe H., Watanabe T., Watanabe Y., Yano Y., Yokouchi S., and Kamigaito O.: "Construction of new injector linac at RIBF", CYCLOTRONS'10, Lanzhou, 2010–9, JaCoW, Lanzhou, pp. 1–3 (2010).

Yamada K., Arai S., Fujimaki M., Fujinawa T., Fujisawa H., Fukunishi N., Goto A., Higurashi Y., Ikezawa E., Kamigaito O., Kase M., Komiyama M., Kumagai K., Maie T., Nakagawa T., Ohnishi J., Okuno H., Sakamoto N., Sato Y., Suda K., Watanabe H., Watanabe Y., Yano Y., and Yokouchi S.: "Construction of new injector linac for RI Beam Factory at RIKEN Nishina Center", Proceedings of of the 1st International Particle Accelerator Conference (IPAC'10), Kyoto, 2010–5, JaCoW, Kyoto, pp. 789–791 (2010).

(Others)

Yamaguchi Y., Wakasugi M., Suzuki H., Fujinawa T., Uesaka T., Yano Y., Ozawa A., Nagae D., Yamaguchi T., Suzuki T., Kikuchi T., Jiang W., Sasaki T., and Tokuchi A.: "Present status of Rare-RI Ring project in RIKEN RI Beam Factory", Proceedings of Science (PoS), Frascati, Italy, 2011–10, SISSA, Fascati, p. 070 (2012).

Oral Presentations

(International Conference etc.)

Higurashi Y., Nakagawa T., Kidera M., Aihara T., Kase M., and Yano Y.: "Effect of plasma electrode position on the beam intensity and emittance of RIKEN 18 GHz ECRIS", 16th International Conference on ECR Ion Sources (ECRIS 04), (Lawrence Berkeley National Laboratory), Berkeley, USA, Sept. (2004).

Yamada K., Okuno H., Fujimaki M., Fukunishi N., Goto

A., Hasebe H., Ikegami K., Kamigaito O., Kase M., Kumagai K., Maie T., Nagase M., Ohnishi J., Sakamoto N., Yokouchi S., and Yano Y.: "Status of the Superconducting Ring Cyclotron at RIKEN RI Beam Factory", 11th European Particle Accelerator Conference (EPAC 2008), (INFN-LNF), Genoa, Italy, June (2008).

Yamada K., Dantsuka T., Fujimaki M., Fujinawa T., Fukunishi N., Goto A., Hasebe H., Higurashi Y., Ikezawa E., Kamigaito O., Kase M., Komiyama M., Kuboki H., Kumagai K., Maie T., Nagase M., Nakagawa T., Ohnishi J., Okuno H., Sakamoto N., Sato Y., Suda K., Wakasugi M., Watanabe H., Watanabe T., Watanabe Y., Yano Y., and Yokouchi S.: "Progress on the commissioning of Radioactive Isotope Beam Factory at RIKEN Nishina Center", 11th International Conference on HEAVY ION ACCELERATOR TECHNOLOGY (HIAT09), (INFN-LNL), Venezia, Italy, June (2009).

Yamada K., Arai S., Fujimaki M., Fujinawa T., Fujisawa H., Fukunishi N., Goto A., Higurashi Y., Ikezawa E., Kamigaito O., Kase M., Komiyama M., Kumagai K., Maie T., Nakagawa T., Ohnishi J., Okuno H., Sakamoto N., Sato Y., Suda K., Watanabe H., Watanabe Y., Yano Y., and Yokouchi S.: "Construction of New Injector Linac for RI Beam Factory at RIKEN Nishina Center", 1st International Particle Accelerator Conference (IPAC'10), (High Energy Accelerator Research Organization), Kyoto, May (2010).

Yamada K., Arai S., Fujimaki M., Fujinawa T., Fujisawa H., Fukunishi N., Goto A., Higurashi Y., Ikezawa E., Kase M., Komiyama M., Kumagai K., Maie T., Nakagawa T., Ohnishi J., Okuno H., Sakamoto N., Sato Y., Suda K., Watanabe H., Watanabe T., Watanabe Y., Yano Y., Yokouchi S., and Kamigaito O.: "Construction of New Injector LINAC at RIBF", 19th International Conference on Cyclotrons and their Applications (CYCLOTRONS 2010), (IMP), Lanzhou, China, Sept. (2010).

Kuboki H., Okuno H., Hershcovitch A., Dantsuka T., Hasebe H., Ikegami K., Imao H., Kamigaito O., Kase M., Maie T., Nakagawa T., and Yano Y.: "Development of Plasma Window for gas charge strippers at RIKEN RIBF", 26th World Conference of the International Nuclear Target Development Society, (Johannes Gutenberg-Universitat and GSI), Mainz, Germany, Aug. (2012).

Enyo H.: "Nuclear Physics in Japan, Prospects being engaged in RIBF, J-PARC and other facilities -", 2012 Fall Meeting of the APS Division of Nuclear Physics, (American Physical Society), Newport Beach, CA, USA, Oct. (2012).

Sato H., Kubo T., Yano Y., Kusaka K., Ohnishi J., Yoneda K., Shimizu Y., Motobayashi T., Otsu H., Isobe T., Kobayashi T., Sekiguchi K., Nakamura T., Kondo Y., Togano Y., Murakami T., Tsuchihashi T., Orikasa T., and Maeta K.: "Superconducting dipole magnet for SAMURAI spectrometer", Applied Superconductivity Conference (ASC2012), (ASC), Portland, USA, Oct. (2012).

Enyo H.: "Prospect of RIKEN RI Beam Factory for Coming 5 Years", EXON2012(International Symposium on Exotic Nuclei), (EXON2012 Organizing Commetee), Vladivostok, Russia, Oct. (2012).

Yamaguchi Y., Wakasugi M., Ozawa A., Uesaka T., Yano Y., Fujinawa T., Fukunishi N., Inabe N., Kamigaito O., Kase M., Kikuchi T., Komiyama M., Kubo T., Kumagai K., Maie T., Ohnishi J., Tokuchi A., Yoshida K., Yamaguchi T., Nagae D., Zenihiro J., Suzuki T., Abe Y., and Suzaki F.: "Construction of Rare-RI Ring at RIKEN RI Beam Factory", 16th International Conference on Electromagnetic Isotope Separators and Techniques Related to their Applications (EMIS2012), (RIKEN KEK IMP), Matsue, Dec. (2012).

Quantum Hadron Physics Laboratory

Publications

[Journal]

(Original Papers) *Subject to Peer Review

Hatsuda T.: "Numerical study of QCD phase diagram at high temperature and density by a histogram method", Central European Journal of Physics **10**, 1322–1325 (2012). *

Hama Y., Hidaka Y., Tsitsishvili G., and Ezawa J.: "The study of Goldstone modes in $\nu = 2$ bilayer quantum Hall systems", Eur. Phys. J. B **85**, No. 368, pp. 1–13 (2012). *

Inoue T., Aoki S., Doi T., Hatsuda T., Ikeda Y., Ishii N., Murano K., Nemura H., and Sasaki K.: "Two-Baryon Potentials and H-Dibaryon from 3-flavor Lattice QCD Simulations", Nucl. Phys. A **881**, 28–43 (2012). *

Suzuki H.: " Supersymmetry, chiral symmetry and the generalized BRS transformation in lattice formulations of 4D $\mathcal{N} = 1$ SYM", Nucl. Phys. B **861**, No. 3, pp. 290–320 (2012). *

Ishii N., Aoki S., Doi T., Hatsuda T., Ikeda Y., Inoue T., Murano K., Nemura H., and Sasaki K.: "Hadron-Hadron Interactions from Imaginary-time Nambu-Bethe-Salpeter Wave Function on the Lattice", Phys. Lett. B **712**, 437–441 (2012). *

Endres M. G.: "Lattice theory for nonrelativistic fermions in one spatial dimension", Phys. Rev. A **85**, 063624-1–063624-9 (2012). *

Naidon P., Hiyama E., and Ueda M.: "Universality and the three-body parameter of ^{4}He trimers", Phys. Rev. A **86**, No. 012502, pp. 012502-1–012502-7 (2012). *

Yamamoto A. and Hatsuda T.: "Quantum Monte Carlo simulation of three-dimensional Bose-Fermi mixtures", Phys. Rev. A **86**, No. 043627, (2012). *

Endo S., Naidon P., and Ueda M.: "Crossover trimers connecting continuous and discrete scaling regimes", Phys. Rev. A **86**, No. 062703, pp. 062703-1–062703-14 (2012). *

Hatsuda T.: "Low-mass dilepton production through transport process in quark-gluon plasma", Phys. Rev. C **85**, 054903 (2012). *

Monnai A.: "Dissipative hydrodynamic effects on baryon stopping", Phys. Rev. C **86**, No. 1, pp. 014908:1–014908:9 (2012). *

Kawanai T. and Sasaki S.: "Charmonium potential from full lattice QCD", Phys. Rev. D **85**, No. 9, pp. 091503-1–091503-6 (2012). *

Sano T. and Yamazaki K.: "Random matrix model for chiral and color-flavor locking condensates", Phys. Rev. D **85**, No. 094032, pp. 094032-1–094032-10 (2012). *

Satow D. and Hidaka Y.: "Off-diagonal kinetic theory in ultrasoft momentum region at high temperature", Phys. Rev. D **85**, No. 116009, (2012). *

Aoyama T., Hayakawa M., Kinoshita T., and Nio M.: "Tenth-order QED contribution to lepton anomalous magnetic moment – sixth-order vertices containing an internal light-by-light scattering subdiagram", Phys. Rev. D **85**, 093013-1–093013-12 (2012). *

Hatsuda T.: "Equation of state in 2+1 flavor QCD with improved Wilson quarks by the fixed scale approach", Phys. Rev. D **85**, 094508 (2012). *

Dumitru A., Guo Y., Hidaka Y., Korthals Altes C. P., and Pisarski R. D.: "Effective matrix model for deconfinement in pure gauge theories", Phys. Rev. D **86**, No. 10, pp. 105017-1–105017-35 (2012). *

Hatsuda T.: "Complex Heavy-Quark Potential at Finite Temperature from Lattice QCD", Phys. Rev. Lett. **108**, 162001 (2012). *

Aoyama T., Hayakawa M., Kinoshita T., and Nio M.: "Tenth-order QED contribution to the electron g-2 and an improved value of the fine structure constant", Phys. Rev. Lett. **109**, No. 11, pp. 111807-1–111807-4 (2012). *

Aoyama T., Hayakawa M., Kinoshita T., and Nio M.: "Complete tenth-order QED contribution to the muon g-2", Phys. Rev. Lett. **109**, No. 11, pp. 111808-1–111808-4 (2012). *

Endres M. G.: "Transdimensional equivalence of universal constants for Fermi gases at unitarity", Phys. Rev. Lett. **109**, 250403 (2012). *

Naidon P., Hiyama E., and Ueda M.: "Universality and the three-body parameter of ^{4}He trimers", Physical Review A **86**, 012502–012508 (2012). *

Hatsuda T.: "Hadron interactions from lattice QCD", Prog. Part. Nucl. Phys. **67**, 122–129 (2012). *

Ikeda Y. and Iida H.: "Quark-anti-quark potentials from Nambu-Bethe-Salpeter amplitudes on lattice", Prog. Theor. Phys. **128**, 941–954 (2012). *

Aoki S., Doi T., Hatsuda T., Ikeda Y., Inoue T., Ishii N., Murano K., Nemura H., and Sasaki K.: "Lattice quantum chromodynamical approach to nuclear physics", Progress of Theoretical and Experimental Physics **2012**, No. 01A105, (2012). *

Hatsuda T. and Doi T.: "Lattice QCD approach to Nuclear Physics", Progress of Theoretical and Experimental Physics **2012**, 01A105 (2012). *

Hatsuda T.: "Hadron-Quark Crossover and Massive Hybrid Stars with Strangeness", Astrophysical Journal **764**, 12 (2013). *

Doi T. and Endres M. G.: "Unified contraction algorithm for multi-baryon correlators on the lattice", Comput. Phys. Commun. **184**, 117–123 (2013). *

Zhu C., Endo S., Naidon P., and Zhang P.: "Scattering and Bound States of two Polaritons in an Array of Coupled Cavities", Few Body Syst. **DOI 10.1007/s00601-012-0562-4**, 1–10 (2013). *

Suzuki H.: "Ferrara–Zumino supermultiplet and the energy-momentum tensor in the lattice formulation of 4D $\mathcal{N} = 1$ SYM", Nucl. Phys. B **868**, 459–475 (2013).

∗

Hatsuda T.: "Role of Vector Interaction and Axial Anomaly in the PNJL Modeling of the QCD Phase Diagram", Phys. Lett. B **719**, 131 (2013). ∗

Hatsuda T.: "Antiferrosmectic ground state of two-component dipolar Fermi gases: An analog of meson condensation in nuclear matter", Phys. Rev. A **87**, 021604 (2013). ∗

Endres M. G., Kaplan D. B., Lee J., and Nicholson A. N.: "Lattice Monte Carlo calculations for unitary fermions in a finite box", Phys. Rev. A **87**, 023615-1–023615-17 (2013). ∗

Fejoes G. P.: "Chiral symmetry breaking patterns in the $U_L(n) \times U_R(n)$ meson model", Phys. Rev. D **87**, No. 056006, (2013). ∗

Minami Y. and Hidaka Y.: "Relativistic hydrodynamics from projection operator method", Phys. Rev. E **87**, No. 023007, (2013). ∗

Fukushima K. and Hidaka Y.: "Magnetic Catalysis vs Magnetic Inhibition", Phys. Rev. Lett. **110**, No. 031601, (2013). ∗

Yamamoto A.: "Lattice QCD with strong external electric fields", Phys. Rev. Lett. **110**, 112001 (2013). ∗

Suzuki H.: "Remark on the energy-momentum tensor in the lattice formulation of 4D $\mathcal{N} = 1$ SYM", Physics Letter B **179**, 435–439 (2013). ∗

Hidaka Y., Hirono Y., Kimura T., and Minami Y.: "Viscoelastic-electromagnetism and Hall viscosity", Progress of Theoretical and Experimental Physics **2013**, No. 1, pp. 013A02-1–013A02-9 (2013). ∗

(Review)

Aoyama T., Hayakawa M., Kinoshita T., and Nio M.: "Quantum electrodynamics calculation of lepton anomalous magnetic moments: Numerical approach to the perturbation theory of QED", Progress of Theoretical and Experimental Physics **01A**, 107-1–107-36 (2012).

岡田信二, 早野龍五, 兵藤哲雄, 池田陽一: "K 中間子水素原子 X 線精密分光実験の拓く物理", 日本物理学会誌 **68**, No. 1, pp. 29–33 (2012).

[Book・Proceedings]

(Original Papers)　*Subject to Peer Review

Doi T. and HAL QCD C.: "Three-Nucleon Forces explored by Lattice QCD Simulations", PoS LAT2011, 2011–7, PoS, PoS, p. 151 (2011). ∗

Murano K., Ishii N., Aoki S., Hatsuda T., Doi T., Ikeda Y., Inoue T., and Sasaki k.: "Nuclear forces in the parity odd sector and the LS forces", Proceedings of Science, Lattice 2011, The Village at Squaw Valley, USA, 2011–6, Sissa, Italy, pp. 319–325 (2011).

Doi T. and HAL QCD C.: "The Lattice QCD Study of the Three-Nucleon Force", AIP Conf. Proc., Boston, USA, 2011– AIP, USA, pp. 399–401 (2012). ∗

Doi T. and HAL QCD C.: "Nuclear physics from lattice simulations", PoS LAT2012, 2012– PoS, PoS, p. 009 (2012). ∗

Charron B.: "Pion-pion interaction in the I=1 channel", PoS LAT2012, 2012– PoS, PoS, (2012). ∗

Yamamoto A.: "Lattice simulation of ultracold atomic Bose-Fermi mixtures", Proceedings of Science, Lattice 2012, sissa, Trieste, p. 049 (2012).

(Others)

Ohnishi S., Ikeda Y., Kamano H., and Sato T.: "Production Reaction of $\bar{K}NN$-πYN Resonance fromFaddeev Equations", Proceedings of the 20th International IUPAP Conference on Few-Body Problems in Physics(FB20), Fukuoka, 2012–8, Springer, Wien, p. DOI 10.1007/s00601-013-06 (2013).

Ohnishi S., Ikeda Y., Kamano H., and Sato T.: "Signature of strange dibaryon in kaon-induced reactions", Proceedings of The 5th Asia-Pacific Conference on Few-Body Problems in Physics 2011 (APFB2011), Seoul, Korea, 2011–8, Springer, Vienna, pp. 347–351 (2013).

Oral Presentations

(International Conference etc.)

Murano K., Ishii N., Aoki S., and Hatsuda T.: "LS force in NN system from Lattice QCD", YIPQS Symposium: Perspectives in Theoretical Physics–From Quark-Hadron Sciences to Unification of Theoretical Physics–, (Yukawa International Program for Quark-Hadron Sciences), Sakyo, Feb. (2011).

Hatsuda T.: "Recent results in particle and nuclear physics from lattice QCD", PANIC 2011, (MIT), Boston, USA, July (2011).

Murano K., Aoki S., Hatsuda T., and Ishii N.: "Nucleon-nucleon potential and its non-locality in lattice QCD", The fifth Asia-Pacific COnference on Few-Body Problems in Physics 2011, (SUNGKYUN KWAN UNIVERSITY), Seoul, Korea, Aug. (2011).

Endres M. G.: "Lattice study of unitary fermions: confined to a finite box and a trap", Seminar, (Syracuse University), Syracuse, USA, Feb. (2012).

Endres M. G.: "Unitary fermions and other strongly coupled systems: a lattice perspective", Seminar, (Syracuse University), Syracuse, USA, Feb. (2012).

Naidon P.: "Universal crossover of 2 heavy + 1 light particle trimers", ITAMP Research Frontiers in Ultra-Cold Atoms and Molecules: Unequal Mass Mixtures and Dipolar Molecules, (ITAMP), Cambridge, Boston, MA, USA, Apr. (2012).

Doi T. and HAL QCD C.: "Exploring Three-Nucleon Forces in Lattice QCD", New Horizons for Lattice Computations with Chiral Fermions, BNL, USA, May (2012).

Endres M. G.: "Four-component Fermi gas on the lattice", Seminar, (CASTS/LQCDHP), Taipei, Taiwan, May (2012).

Nio M., Aoyama T., Hayakawa M., and Kinoshita T.: "Tenth-order QED contribution to the lepton g-2", 43rd Annual Meeting of the APS, Division of Atomic, Molecular and Optical Physics, (American Physical Society), Anaheim, USA, June (2012).

Doi T. and HAL QCD C.: "Nuclear physics from lattice simulations", Lattice 2012, Cairns, Australia, June (2012).

Endres M. G.: "Universal four-component Fermi gas on the lattice", Lattice 2012, (University of Adelaide), Cairnes, Australia, June (2012).

Murano K., Ishii N., Aoki S., Hatsuda T., Doi T., Ikeda Y., Inoue T., Nemura H., and Sasaki K.: "First calculation of the spin-orbit force in the parity odd sector in NN system from Lattice QCD", The 30th International Symposium on Lattice Field Theory, (The University of Adelaide), Cairns, Australia, June (2012).

Yamamoto A.: "Lattice simulation of ultracold atomic Bose-Fermi mixtures", The 30th International Symposium on Lattice Field Theory, Cairns, Australia, June (2012).

Doi T. and HAL QCD C.: "Three-Nucleon Forces Explored on the Lattice", Crossover 2012, Nagoya, July (2012).

Naidon P.: "Universality of low-energy 3-atom systems", International Conference of Atomic Physics (ICAP), (ICAP), Ecole Polytechnique, Palaiseau, France, July (2012).

Doi T. and HAL QCD C.: "Three-Nucleon Forces Explored from Lattice QCD", Lattice Hadron Physics (LHP IV), Adelaide, Australia, July (2012).

Fejoes G. P.: "Phase transition in the $U_L(3)\times U_R(3)$ meson model from large-n approximation", Strong and Electroweak Matter 2012, (Swansea University), Swansea, Wales, United Kingdom, July (2012).

Hama Y., Hidaka Y., Tsitsishvili G., and Ezawa J.: "The study of Goldstone modes in $\nu = 2$ bilayer quantum Hall systems", HMF-20, (CNRS/UFJ/UPS/INSA Grenoble High Magnetic Field Laboratory), Chamonix, France, July–July (2012).

Monnai A.: "Dissipative hydrodynamic effects on the quark-gluon plasma at finite baryon density", Extreme QCD 2012, (George Washington University), Washington DC, USA, Aug. (2012).

Sakai Y., Sasaki T., Kouno H., and Yahiro M.: "Quark-gluon thermodynamics with Z_N symmetry", Extreme QCD 2013, (The George Washington University), Washington D.C., USA, Aug. (2012).

Doi T. and HAL QCD C.: "Few-baryon Interactions from Lattice QCD", Few-Body Problems in Physics, Fukuoka, Aug. (2012).

Hidaka Y. and Yamamoto N.: "A No-Go Theorem for Critical Phenomena in QCD at finite temperature and density", Quark matter 2012, Washington DC, USA, Aug. (2012).

Murano K., Ishii N., Aoki S., Hatsuda T., Doi T., Ikeda Y., Inoue T., and Sasaki k.: "Nuclear forces in the odd parity sector and the LS forces from Lattice QCD", The 20th International IUPAP Conference of Few-Body Problems in Physics, Fukuoka, Aug. (2012).

Ohnishi S., Ikeda Y., Kamano H., and Sato T.: "Production Reaction of $\bar{K}NN$-πYN Resonance from Faddeev Equations", The 20th International IUPAP Conference on Few-Body Problems in Physics (FB20), (IUPAP), Fukuoka, Aug. (2012).

Naidon P.: "Universality of the Efimov three-body parameter in atomic systems", The 20th International IUPAP Conference on Few-Body Problems in Physics (FB20), (Kyushu University and others), Fukuoka, Aug. (2012).

Monnai A.: "Dissipative hydrodynamic evolution of the QGP at finite baryon density", The 23rd International Conference on Ultrarelativistic Nucleus-Nucleus Collisions (Quark Matter 2012), Washington DC, USA, Aug. (2012).

Murano K., Ishii N., Aoki S., and Hatsuda T.: "Nuclear Forces from Lattice QCD toward LS-force", Korea-Japan workshop on nuclear and hadron physics at J-PARC, (Seoul National University), Seoul, Korea, Sept. (2012).

Hidaka Y.: "A No-Go Theorem for Critical Phenomena in QCD at finite temperature and density", NTERNATIONAL SCHOOL OF NUCLEAR PHYSICS 34th Course Probing the Extremes of Matter with Heavy Ions, Erice, Italy, Sept. (2012).

Suzuki H.: "Ferrara–Zumino supermultiplet and the energy-momentum tensor in the lattice formulation of 4D $\mathcal{N} = 1$ SYM", New frontiers in lattice gauge theory, (INFN), Florence, Italy, Sept.–Sept. (2012).

Yamamoto A.: "Chiral Magnetism", QCD Structure I, (Central China Normal University), Wuhan, China, Oct. (2012).

Doi T. and HAL QCD C.: "Exploring Three-Nucleon Forces on the Lattice", QCD Structure I, Wuhan, China, Oct. (2012).

Endres M. G.: "Universal Fermi gases on the lattice", Workshop on QCD Structure I, (CCNU), Wuhan, China, Oct. (2012).

Monnai A.: "Dissipative hydrodynamic evolution of hot quark matter at finite baryon density", Xth Quark Confinement and the Hadron Spectrum, (Technical University Munich), Garching, Germany, Oct. (2012).

Yamamoto A.: "Lattice QCD in strong magnetic and electric fields", QCD in strong magnetic fields, (ECT*), Trento, Italy, Nov. (2012).

Hidaka Y.: "Magnetic Inhibition, Vafa-Witten theorem, and Sign problem", Workshop on QCD in strong magnetic fields, (ECT*), Trento, Italy, Nov. (2012).

Doi T. and HAL QCD C.: "Hadron Interactions on the Lattice", Quarks to Universe in Computational Science (QUCS 2012), nara, Dec. (2012).

Ohnishi S., Ikeda Y., Kamano H., and Sato T.: "Production reaction of $\bar{K}NN$-πYN resonance and $\bar{K}N$ interaction", Quarks to Universe in Computational Science (QUCS 2012), (Grant-in-Aid for Scientific Research on

Innovative Areas Research on the Emergence of Hierarchical Structure of Matter by Bridging Particle, Nuclear and Astrophysics in Computational Science), Nara, Dec. (2012).

Doi T. and HAL QCD C.: "Nucleon-Nucleon Interactions from Lattice QCD", 2nd DST-SERC School on Nuclear Matter Under Extreme Conditions (NUMEC), Kolkata, India, Jan. (2013).

Naidon P.: "Origin of the universal three-body parameter in atomic Efimov physics", QS2C Theory Forum: International Symposium on Strongly Correlated Quantum Science, (The University of Tokyo, JSPS), Tokyo, Jan. (2013).

Endres M. G.: "Universal fermi gases on the lattice", Seminar, (NCTU), Hsinchu, Taiwan, Jan. (2013).

Endres M. G.: "Universal fermi gases on the lattice", Seminar, (NTU), Taipei, Taiwan, Jan. (2013).

Hama Y., Tsitsishvili G., and Ezawa J.: "Spin Josephson Supercurrent in the Canted Antiferromagnetic Phase", QS2C Theory Forum: International Symposium on "Strongly Correlated Quantum Science", (The University of Tokyo and RIKEN), Tokyo, Jan.–Jan. (2013).

Endres M. G.: "Unitary fermions on the lattice", Computation approaches to nuclear many-body problems and related quantum systems, Wako, Feb. (2013).

Hidaka Y.: "QCD in a strong magnetic field", Recent progress in hadron physics, (Yonsei University), Yonsei University, Korea, Feb. (2013).

Nio M., Aoyama T., Hayakawa M., and Kinoshita T.: "Tenth-order QED calculation of the lepton anomalous magnetic moments and precision determination of the fine-structure constant", The 5th GCOE International Symposium on "Weaving Science Web beyond Particle-Matter Hierarchy", (Tohoku University), Sendai, Mar. (2013).

(Domestic Conference)

村野啓子, 石井理修, 青木慎也, 初田哲男: Future Prospects of Hadron Physics at J-PARC and Large Scale Computational Physics, (J-PARC センター、計算基礎科学連携拠点), 東海村, 2 月 (2012).

Naidon P.: "Universality and the 3-body parameter of ^{4}He trimers", 日本物理学会, (日本物理学会), 大阪, 3 月 (2012).

門内晶彦: "相対論的散逸流体とクォークグルーオンプラズマ", 相対論的流体力学の理論と素粒子・原子核・宇宙物理への応用, 和光, 5 月 (2012).

門内晶彦: "有限密度における高温クォーク物質の相対論的散逸流体モデル", 東京大学駒場原子核理論研究室セミナー, (東京大学), 駒場, 6 月 (2012).

村野啓子, 青木慎也, 石井理修, 初田哲男, 土井琢身, 池田陽一, 井上貴史, 佐々木健志: "Spin-Orbit force in the NN system from Lattice QCD", 新学術領域「素核宇宙融合」×「新ハドロン」クロスオーバー研究会ー多様な手法でせまるハドロン物理への挑戦ー, (名古屋大学), 日本, 7 月 (2012).

佐野崇, 藤井宏次, 菊川芳夫: "有限密度ランダム行列模型に対する複素ランジュバン方程式", 京都大学基礎物理学研究所研究会「熱場の量子論とその応用」, (基礎物理学研究所), 京都, 8 月 (2012).

日高義将: "有限温度摂動論", 熱場の量子論とその応用, 京都, 8 月 (2012).

鈴木博: 離散的手法による場と時空のダイナミクス, 和光市, 8–8 月 (2012).

境祐二, Hong M., 初田哲男: 日本物理学会, (日本物理学会), 京都産業大学, 9 月 (2012).

日高義将, 福嶋健二: "Magnetic Catalysis vs Pions", 日本物理学会, (日本物理学会), 京都産業大, 9 月 (2012).

山本新: "Quantum Monte Carlo simulation of the (3+1)-dimensional Bose-Fermi mixtures", 日本物理学会, (日本物理学会), 横浜, 9 月 (2012).

門内晶彦: "Non-equilibrium QCD fluid at finite baryon chemical potential", Nagoya Mini-Workshop "Phenomenology and Experiments at RHIC and LHC", (Kobayashi-Maskawa Institute, Nagoya University), Nagoya, 9 月 (2012).

日高義将, 広野雄士, 木村太郎, 南佑樹: "カルタン形式によるトポロジカル粘性", 日本物理学会, (日本物理学会), 横浜国立大学, 9 月 (2012).

土井琢身, HAL QCD C.: "京コンピュータによるバリオン間相互作用の解明", 日本物理学会２０１２年秋季大会, 京都, 9 月 (2012).

大西祥太, 池田陽一, 鎌野寛之, 佐藤透: "チャンネル結合散乱方程式によるストレンジダイバリオン共鳴生成反応の解析", 日本物理学会２０１２年秋季大会, (日本物理学会), 京都, 9 月 (2012).

濱祐介, 日高義将, Tsitsishvili G., 江澤潤一: "2 層 $\nu = 2$ 量子ホール系におけるゴールドストーンモードの研究", 日本物理学会 2012 年秋季大会, (一般社団法人日本物理学会), 東京, 9–9 月 (2012).

大西祥太, 池田陽一, 鎌野寛之, 佐藤透: "3 体散乱方程式による $\bar{K}NN$-πYN 共鳴生成反応の研究", ELPH 研究会 C005「ダブルメソン生成とバリオン分光 〜LEPS/ELPH におけるハドロン光生成反応の最近の進展〜」, (東北大 ELPH), 仙台, 11 月 (2012).

木村太郎, 日高義将, 広野雄士, 南佑樹: "交差応答に対するトポロジカル有効理論", 第 6 回物性科学領域横断研究会, 東京大学本郷キャンパス, 11 月 (2012).

南佑樹, 日高義将: "森の射影演算子法による相対論的線形流体方程式の導出", 森肇先生記念研究集会　- 非線形・非平衡系の統計力学 - , (九州大学応用力学研究所), 九州大学, 11–11 月 (2012).

Fejoes G. P.: "Spontaneous symmetry breaking patterns in the $U_L(n) \times U_R(n)$ meson model", Future Prospects of Hadron Physics at J-PARC and Large Scale Computational Physics in 2013, (KEK), Tokai, Ibaraki, 2 月 (2013).

Theoretical Nuclear Physics Laboratory

Publications

[Journal]

(Original Papers) *Subject to Peer Review

Shen J., Zhao Y., Arima A., and Yoshinaga N.: "New extrapolation method for low-lying states of nuclei in the sd and the pf shells", Phys. Rev. C **83**, 044322-1–044322-8 (2011). *

Watanabe G., Yoon S., and Dalfovo F.: "Swallowtail Band Structure of the Superfluid Fermi Gas in an Optical Lattice", Phys. Rev. Lett. **107**, 270404-1– 270404-5 (2011). *

Guo L. and Nakatsukasa T.: "Time-dependent Hartree-Fock studies of the dynamical fusion threshold", EPJ Web Conf. **38**, 09003-1–09003-5 (2012).

Nguyen D. D.: "Viscosity of hot nuclei", J. Phys.: Conf. Ser. **366**, 01205-1–01205-5 (2012). *

Ebata S., Nakatsukasa T., and Inakura T.: "Study of pygmy dipole resonance with a new time-dependent mean field theory", J. Phys.: Conf. Ser. **381**, 012104-1–012104-6 (2012). *

Nakatsukasa T., Ebata S., Avogadro P., Guo L., Inakura T., and Yoshida K.: "Density functional approaches to nuclear dynamics", J. Phys.: Conf. Ser. **387**, 0120156-1–0120156-10 (2012). *

Nakatsukasa T.: "Real-time calculations of many-body dynamics in quantum systems", J. Phys.: Conf. Ser. **402**, No. 1, pp. 012032-1–012032-15 (2012). *

Shimada K., Ueno H., Neyens G., Asahi K., Balabanski D. L., Daugas J., Depuydt M., De Rydt M., Gaudefroy L., Grevy S., Hasama Y., Ichikawa Y., Kameda D., Morel P., Nagatomo T., Perrot L., Stodel C., Thomas J., Utsuno Y., Vanderheijden W., Vermeulen N., Vingerhoets P., Yagi E., Yoshida K., and Yoshimi A.: "Erosion of $N = 20$ shell in ^{33}Al investigated through the ground-state electric quadrupole moment", Phys. Lett. B **714**, 246–250 (2012). *

Nguyen D. D.: "Damping of giant dipole resonance in hot rotating nuclei", Phys. Rev. C **85**, No. 6, pp. 064323-1–064323-9 (2012). *

Nishimura S. and Kajino T.: "Impact of new β-decay half-lives on r-process nucleosynthesis", Phys. Rev. C **85**, No. 048801, pp. 1–4 (2012). *

Adachi T., Fujita Y., Bacher A. D., Berg G. P., Black T. C., De Frenne D., Foster ., Fujita H., Fujita K., Hatanaka K., Homma M., Jacobs E., Janecke J., Kanzaki Y., Katori K., Nakanishi K., Negret A., Otsuka T., Popescu L., Roberts D. A., Sakemi Y., Shimbara Y., Shimizu Y., Stephenson E. J., Tameshige Y., Tamii A., Uchida M., Ueno H., Yamanaka T., Yosoi M., and Zell K. O.: "High-resolution study of Gamow-Teller transitions via the ^{54}Fe(^{3}He,t)^{54}Co reaction", Phys. Rev. C **85**, 024308-1–024308-15 (2012). *

Tohyama M. and Nakatsukasa T.: "Fragmentation of electric dipole strength in $N = 82$ isotones", Phys. Rev. C **85**, 031302-1–031302-4 (2012). *

Nguyen H. Q. and Nguyen D. D.: "Specific shear viscosity in hot rotating systems of paired fermions", Phys. Rev. C **86**, No. 2, pp. 024302-1–024302-7 (2012). *

Sato K., Hinohara N., Yoshida K., Nakatsukasa T., Matsuo M., and Matuyanagi K.: "Shape transition and fluctuations in neutron-rich Cr isotopes around N=40", Phys. Rev. C **86**, No. 2, p. 024316 (2012). *

Nguyen D. D. and Nguyen H. Q.: "Giant dipole resonance in 201Tl at low temperature", Phys. Rev. C **86**, No. 4, pp. 044333-1–044333-7 (2012). *

Washiyama K., Bennaceur K., Avez B., Bender M., Heenen P., and Hellemans V.: "New parametrization of Skyrme's interaction for regularized multireference energy density functional calculations", Phys. Rev. C **86**, No. 5, pp. 054309-1–054309-14 (2012). *

Ward D., Macchiavelli A. O., Clark R. M., Cline D., Cromaz M., Deleplanque M. A., Diamond R. M., Fallon P., Goergen A., Hayes A. B., Lane G. J., Lee I. Y., Nakatsukasa T., Schmidt G., Stephens F. S., Svensso C. E., Teng R., Vetter K., and Wu C. Y.: "Band structure of ^{235}U", Phys. Rev. C **86**, 064319-1–064319-49 (2012). *

Ebata S., Nakatsukasa T., and Inakura T.: "Cb-TDHFB calculation for the low-lying $E1$ strength of heavy nuclei around the r-process path", Prog. Theor. Phys. Suppl. **196**, 316–321 (2012). *

Hinohara N., Sato K., Yoshida K., Nakatsukasa T., Matsuo M., and Matuyanagi K.: "Microscopic analysis of shape coexistence/mixing and shape phase transition in neutron-rich nuclei around ^{32}Mg", Prog. Theor. Phys. Suppl. **196**, 328–333 (2012). *

Inakura T., Nakatsukasa T., and Yabana K.: "Shell and neutron-skin effects on pygmy dipole resonances", Prog. Theor. Phys. Suppl. **196**, 365–370 (2012). *

Nakatsukasa T.: "Density functional approaches to collective phenomena in nuclei: Time-dependent density functional theory for perturbative and non-perturbative nuclear dynamics", Progress of Theoretical and Experimental Physics **2012**, 01A207-1–01A207-46 (2012). *

(Review)

中務孝: "原子核理論研究に横たわる多くの未解決問題", 化学 **66**, No. 11, pp. 39–42 (2011).

中務孝, 江幡修一郎: "正準基底表示の時間依存平均場理論と超流動原子核の線形応答", 日本物理学会誌 **67**, No. 4, pp. 243–246 (2012).

中務孝: "$N = Z$ 原子核の謎と新しい対凝縮相", パリティ **56**, No. 1, pp. 41–42 (2013).

(Others)

Kohama A., Iida K., and Oyamatsu K.: "Black-sphere approximation to nuclei and its application to reactions with neutron-rich nuclei,", Proceedings of French-Japanese Symposium on Nuclear Structure Problems, pp. 106–109 (2012).

[Book · Proceedings]

(Original Papers) *Subject to Peer Review

Fukuoka Y., Nakatsukasa T., Funaki Y., and Yabana K.: "Stochastic approach to correlations beyond the mean field with the Skyrme interaction", AIP Conference Proccedings 1491 "Nuclear Structure and Dynamics '12", Opatija, Croatioa, 2012–7, AIP, New York, pp. 222–225 (2012).

Nakatsukasa T., Inakura T., Avogadro P., Ebata S., Sato K., and Yabana K.: "Linear response calculation in the time-dependent density functional theory", AIP Conference Proceedings 1484 "Origin of Matter and Evolution of Galaxies 2011", Wako, 2011–11, AIP, New York, pp. 142–149 (2012).

Lacroix D., Ayik S., Yilmaz B., and Washiyama K.: "Large amplitude motion with a stochastic mean-field approach", EPJ Web of Conferences Vol. 38, NSRT12-International Conference on Nuclear Structure and Related Topics, Dubna, Russia, 2012–7, EDP Sciences, Les Ulis, pp. 06003-p.1–06003-p.5 (2012).

Hinohara N., Sato K., Matuyanagi K., Nakatsukasa T., Yoshida K., and Matsuo M.: "Large-amplitude quadrupole collective dynamics in neutron-rich Mg and Cr isotopes", French-Japanese Symposium on Nuclear Structure Problems, Wako, 2011–1, World Scientific, Singapore, pp. 122–125 (2012).

Sato K., Hinohara N., Matuyanagi K., Nakatsukasa T., and Matsuo M.: "Microscopic description of large-amplitude collective motions with local QRPA inertial masses", French-Japanese Symposium on Nuclear Structure Problems, Wako, 2011–1, World Scientific, Singapore, pp. 126–129 (2012).

Liang H., Meng J., Ring P., Roca-Maza X., and Zhao P.: "Local covariant density functional constrained by the relativistic Hartree-Fock theory", Nuclear Structure and Dynamics '12, Opatija, Croatia, 2012–7, AIP, New York, pp. 230–233 (2012). *

Sato K., Hinohara N., Nakatsukasa T., Matsuo M., and Matuyanagi K.: "Microscopic approach to large-amplitude deformation dynamics with local QRPA inertial masses", Rutherford Centennial Conference on Nuclear Physics, Manchester, UK, 2012–9, IOP Publishing, Bristol, p. 012103 (2012). *

Matuyanagi K., Hinohara N., and Sato K.: "BCS-pairing and nuclear vibrations", Fifty Years of Nuclear BCS: Pairing in Finite Systems, World Scientific, Singapore, pp. 111–124 (2013).

Oral Presentations

(International Conference etc.)

Nakatsukasa T.: "Microscopic approaches to large-amplitude collective motion", 5th ASRC International Workshop on Perspectives in Nuclear Fission, (JAEA), Tokai, Mar. (2012).

Nakatsukasa T.: "Time-dependent methods for quantum many-body dynamics", KITPC Program: From nucleon structure to nuclear structure and compact astrophysical objects, (KITPC), Beijing, China, June–July (2012).

Nakatsukasa T., Fukuoka Y., Funaki Y., and Yabana K.: "Stochastic approach to correlations beyond the mean field with the Skyrme interaction", 2nd International Conference on Nuclear Structure and Dynamics '12, (University of Zagreb), Opatija, Croatia, July (2012).

Liang H.: "Fine structure of spin-dipole excitations in covariant density functional theory", [RIBF-ULIC-Symposium-010] International Symposium on Perspective in Isospin Physics Role of non-central interactions in structure and dynamics of unstable nuclei , RIKEN, Aug. (2012).

Sato K.: "Mean-field calculation including proton-neutron mixing – toward proton-neutron pairing –", [RIBF-ULIC-Symposium-010]International Symposium on Perspective in Isospin Physics Role of non-central interactions in structure and dynamics of unstable nuclei , Wako, Aug. (2012).

Nguyen D. D.: "Description of giant dipole resonance's damping in highly excited nuclei", 47th Zakopane Conference on nuclear physics, (Institute of Nuclear Physics, Polish Academy of Sciences), Zakopane, Poland, Aug.–Sept. (2012).

Washiyama K., Heenen P., and Bender M.: "Regularized multi-reference energy density functional calculations for Mg isotopes", Collective Motion in Nuclei under Extreme Conditions (COMEX4), (University of Tokyo, Osaka University), Hayama, Oct. (2012).

Liang H.: "Self-consistent relativistic study of spin-isospin resonances", Collective Motion in Nuclei under Extreme Conditions (COMEX4), (Center for Nuclear Study (CNS) and Research Center for Nuclear Physics (RCNP)), RIKEN and Kanagawa, Oct. (2012).

Nakatsukasa T.: "Time-dependent density-functional calculation of nuclear response and collective motion", Collective Motion in Nuclei under Extreme Conditions (COMEX4), (Center of Nuclear Study, University of Tokyo), Hayama, Oct. (2012).

Sato K., Nakatsukasa T., Dobaczewski J., and Wojciech S.: "Mean-field calculation including proton-neutron mixing in atomic nuclei", Conference on Computational Physics 2012 (CCP2012), (Osaka University), Kobe, Oct. (2012).

Nakatsukasa T.: "Developments in finite amplitude method", 6th LACM-TORIJIN-JUSTIPEN workshop, (Oak Ridge National Laboratory), Oak Ridge, USA, Oct.–Nov. (2012).

Washiyama K., Heenen P., and Bender M.: "Multi-reference calculations with new regularizable Skyrme energy density functionals", The 6th LACM-TORIJIN-JUSTIPEN Workshop, (Oak Ridge National Laboratory, TORIJIN, JUSTIPEN), Oak Ridge, USA, Oct.–Nov. (2012).

Nakatsukasa T.: “Time-dependent density-functional studies on strength functions in neutron-rich nuclei”, 5th International Conference on Fission and properties of neutron-rich nuclei, (University of Vanderbilt), Sanibel Island, USA, Nov. (2012).

Sato K., Hinohara N., Yoshida K., Nakatsukasa T., Matsuo M., and Matuyanagi K.: “Microscopic approach to large-amplitude deformation dynamics with local QRPA”, 7th Italy-Japan Symposium on Nuclear Physics, (INFN), Milano, Italy, Nov. (2012).

Sato K., Nakatsukasa T., Satula W., and Dobaczewski J.: “Mean-field calculation including proton-neutron mixing in atomic nuclei –toward proton-neutron pairing–”, Quarks to Universe in Computational Science (QUCS 2012), Nara, Dec. (2012).

Liang H.: “Self-consistent study of spin-isospin resonances and a recent application in r-process calculations”, The 15th Mini-Workshop for Nuclear Physics and Nuclear Astrophysics, (Soongsil University), Seoul, Korea, Dec. (2012).

(Domestic Conference)

中務孝: “原子核物理入門”, KEK サマーチャレンジ, (KEK), つくば, 8 月 (2012).

近藤久直, 飯田圭, 小濱洋央, 親松和浩: “くろたまモデルによる安定核構造の系統的解析”, ミニワークショップ「不安定核と核データ」, 和光, 8–8 月 (2012).

小濱洋央, 飯田圭, 親松和浩: “中間エネルギーでの相互作用断面積データとくろたま断面積公式”, 日本物理学会 2012 年秋季大会, (日本物理学会), 京都, 9 月 (2012).

鷺山広平, Ayik S., Lacroix D.: “確率的平均場模型を用いた核子移行反応における質量分布幅の記述”, 日本物理学会, (日本物理学会), 京都, 9 月 (2012).

佐藤弘一, 中務孝, Satula W., Dobaczewski J.: “A=48 同重核における陽子—中性子混合を含んだ平均場計算”, 日本物理学会　2012 年秋季大会, (日本物理学会), 京都, 9 月 (2012).

Liang H.: “Nuclear charge-exchange excitations in a self-consistent covariant approach”, 千葉大学原子核理論セミナー, (Chiba University), Chiba, 11 月 (2012).

小濱洋央: “共同研究「RIBF 核反応データの高度利用研究」: 理研での取り組み”, RIBF-ULIC-miniWS019 「不安定核ビーム実験データベースの開発と利用」, 和光市, 11 月 (2012).

小濱洋央, 飯田圭, 親松和浩: “Nuclear sizes, total reaction cross sections, and nuclear symmetry energies”, RIBF ULIC mini-WS on ”Systematic study of nuclear radii -Theory and Experiment-”, 和光市, 12 月 (2012).

小濱洋央, 飯田圭, 親松和浩, 小浦寛之: “中間エネルギーでの不安定核全反応断面積と変形度”, 日本物理学会第 68 回年次大会, 東広島市, 3 月 (2013).

Liang H.: “Nuclear charge-exchange excitations in localized covariant density functional theory”, 仙台原子核科学コロキューム, (東北大学), 仙台, 3 月 (2013).

中務孝: “計算核物理のフロンティア”, 日本物理学会第 68 回年次大会, (日本物理学会), 東広島, 3 月 (2013).

鷺山広平, Heenen P., Bender M.: “正則化されたエネルギー密度汎関数を用いた生成座標法による Mg 同位体の記述”, 日本物理学会第 68 回年次大会, (日本物理学会), 東広島市, 3 月 (2013).

Strangeness Nuclear Physics Laboratory

Publications

[Journal]

(Original Papers) *Subject to Peer Review

Sakaguchi S., Iseri Y., Uesaka T., Tanifuji M., Amos K., Aoi N., Hashimoto Y., Hiyama E., Ichikawa M., Ichikawa Y., Ishikawa S., Itoh K., Itoh M., Iwasaki H., Karataglidis S., Kawabata T., Kawahara T., Kuboki H., Maeda Y., Matsuo R., Nakao T., Okamura H., Sakai H., Sasamoto Y., Sasano M., Sato Y., Sakaguchi-Sekiguchi K., Shinohara M., Suda K., Suzuki D., Takahashi Y., Tamii A., Wakui T., Yako K., Yamaguchi M., and Yamamoto Y.: "Analyzing power in elastic scattering of 6He from a polarized proton target at 71 MeV/nucleon", Phys. Rev. C **84**, No. 024604, pp. 024604-1–024604-17 (2011). *

Ohtani K., Gubler P., and Oka M.: "Parity projection of QCD sum rules for the nucleon", arXiv [**hep-ph**], No. 1209.1463, (2012). *

Fujiwara Y. and Fukukawa K.: "Off-shell effect of the quark-model NN interaction in the Nd scattering", Few Body Syst., pp. s00601-012-0501-4-1–s00601-012-0501-4-37 (2012). *

Koike T. and Harada T.: "Energy dependence of K^--"pp" effective potential derived from coupled-channel Green's function", Hyperfine Interact. **210**, No. 1-3, pp. 89–92 (2012). *

Inoue T., Aoki S., Doi T., Hatsuda T., Ikeda Y., Ishii N., Murano K., Nemura H., and Sasaki K.: "Two-Baryon Potentials and H-Dibaryon from 3-flavor Lattice QCD Simulations", Nucl. Phys. A **881**, 28–43 (2012). *

Ishii N., Aoki S., Doi T., Hatsuda T., Ikeda Y., Inoue T., Murano K., Nemura H., and Sasaki K.: "Hadron-Hadron Interactions from Imaginary-time Nambu-Bethe-Salpeter Wave Function on the Lattice", Phys. Lett. B **712**, 437–441 (2012). *

Naidon P., Hiyama E., and Ueda M.: "Universality and the three-body parameter of ^{4}He trimers", Phys. Rev. A **86**, No. 012502, pp. 012502-1–012502-7 (2012). *

Yamada T., Funaki Y., Myo T., Horiuchi H., Ikeda K., Roepke G., Schuck P., and Tohsaki A.: "Isoscalar monopole excitations in ^{16}O: α-cluster states at low energy and mean-field-type states at higher energy", Phys. Rev. C **85**, 034315-1–034315-14 (2012). *

Yabana K. and Funaki Y.: "Imaginary-time method for the radiative capture reaction rate", Phys. Rev. C **85**, 055803-1–055803-8 (2012). *

Zhou B., Ren Z., Xu C., Funaki Y., Yamada T., Tohsaki A., Horiuchi H., Schuck P., and Roepke G.: "New concept for the ground-state band in ^{20}Ne within a microscopic cluster model", Phys. Rev. C **86**, 014301-1–014301-8 (2012). *

Naidon P., Hiyama E., and Ueda M.: "Universality and the three-body parameter of ^{4}He trimers", Physical Review A **86**, 012502–012508 (2012). *

Hiyama E. and Kamimura M.: "Variational calculation of ^{4}He tetramer ground and excited states using a realistic pair potential", Physical Review A **85**, 022502–022516 (2012). *

Hiyama E. and Kamimura M.: "Linear correlations between ^{4}He trimer and tetramer energies calculated with various realistic ^{4}He potentials", Physical Review A **85**, 062505–062513 (2012). *

Fujiwara Y. and Fukukawa K.: "A practical method of solving cutoff coulomb problems in momentum space – application to the Lippmann-Schwinger resonating-group method and the pd elastic scattering", Prog. Theor. Phys. **128**, No. 2, pp. 301–347 (2012). *

Itahashi K., Fujioka H., Geissel H., Hirenzaki S., Itoh S., Jido D., Metag V., Nagahiro H., Nanova M., Nishi T., Okochi K., Outa H., Suzuki K., Tanaka Y., and Weick H.: "Feasibility Study of Observing eta' Mesic Nuclei with (p,d) Reaction", Prog. Theor. Phys. **128**, No. 3, pp. 601–613 (2012). *

Hiyama E. and Yamamoto Y.: "Structure of 10ΛBe and 10ΛB Hypernuclei Studied with the Four-Body Cluster Model", Prog. Theor. Phys. **128**, 105–124 (2012). *

Koike T. and Harada T.: "Formation of essential kaonic nuclei, "K^-pp"", Few Body Syst. **54**, No. 1-4, pp. 117–122 (2013).

Suzuki K., Gubler P., Morita K., and Oka M.: "Thermal modification of bottomonium spectra from QCD sum rules with the maximum entropy method", Nucl. Phys. A **897**, 28–41 (2013). *

Li A., Hiyama E., Zhou X. r., and Sagawa H.: "Tensor correlation, pairing interaction and deformation in Ne isotopes and Ne hypernuclei", Phys. Rev. C, (2013).

(Others)

Bhang H., Ajimura S., Aoki K., Banu A., Fukuda T., Hashimoto O., Hwang J. I., Kameoka S., Kang B. H., Kim E., Kim J., Kim M., Maruta T., Miura Y., Miyake Y., Nagae T., Nakamura M., Nakamura S. N., Noumi H., Okada S., Okayasu Y., Outa H., Park H., Saha P., Sato Y., Sekimoto M., Takahashi T., Tamura H., Tanida K., Toyoda A., Tshoo K., Tsukada K., Watanabe T., and Yim H.: "Three-Body $\Lambda NN \to nNN$ Nonmesonic Weak Decay Process of Λ Hypernuclei", Few Body Syst. **54**, No. 1-4, pp. 103–110 (2013).

[Book · Proceedings]

(Original Papers) *Subject to Peer Review

Murano K., Ishii N., Aoki S., Hatsuda T., Doi T., Ikeda Y., Inoue T., and Sasaki k.: "Nuclear forces in the parity odd sector and the LS forces", Proceedings of Science, Lattice 2011, The Village at Squaw Valley, USA, 2011–6, Sissa, Italy, pp. 319–325 (2011).

Fukuoka Y., Nakatsukasa T., Funaki Y., and Yabana K.: "Stochastic approach to correlations beyond the mean field with the Skyrme interaction", AIP Conference Proccedings 1491 "Nuclear Structure and Dynamics '12", Opatija, Croatioa, 2012–7, AIP, New York, pp. 222–225 (2012).

Fujiwara Y. and Fukukawa K.: "Deuteron breakup differential cross sections and analyzing powers of d+p scattering at $E_d = 16$ and 130 MeV", 20th International IUPAP Conference on Few-Body Problems in Physics, Fukuoka, 2012–8〜8, Springer Vienna, Vienna, pp. s00601-012-0551-7 -1–s00601-012-0551-7 -4 (2013). ∗

Fukukawa K. and Fujiwara Y.: "Coulomb effect in nucleon-deuteron elastic scattering", 20th International IUPAP Conference on Few-Body Problems in Physics, Fukuoka, 2012–8〜8, Springer Vienna, Vienna, pp. s00601-012-0594-9-1–s00601-012-0594-9-4 (2013). ∗

Li A.: "Neon Isotope and Lambda Hypernuclei with the Nijmegen Hyperon Interaction", 20th International IUPAP Conference on Few-Body Problems in Physics, Fukuoka, 2012–8〜8, Springer Vienna, Fukuoka, (2013).

Fukukawa K. and Fujiwara Y.: "Quark-model nucleon-nucleon interaction applied to nucleon-deuteron scattering", Few-Body Systems, Seoul, Republic of Korea, 2011–8〜8, Springer Vienna, Vienna, pp. 54(1-4), 489–54(1-4), 493 (2013).

Gubler P., Suzuki K., Morita K., and Oka M.: "Quarkonia at finite T: An approach based on QCD sum rules and the maximum entropy method", Few-Body Systems, Fukuoka, 2012–8, Springer Science+Business Media, Wien, pp. 1–4 (2013). ∗

Gubler P., Suzuki K., Morita K., and Oka M.: "Modification of hadronic spectral functions under extreme conditions: An approach based on QCD sum rules and the maximum entropy method", Nuclear Physics A, Barcelona, Spain, 2012–10, Elsevier, Amsterdam, pp. 1–4 (2013). ∗

(Review)

Gubler P.: "A Bayesian analysis of QCD sum rules", Springer Thesis, Springer Science+Business Media, Berlin, (2013).

(Others)

Funaki Y., Yamada T., Horiuchi H., Roepke G., Schuck P., and Tohsaki A.: "Alpha-clustering and condensation in nuclei", International Journal of Modern Physics E, Bruxelles, Belgium, 2010–5, P. Descouvemont, Bruxelles, pp. 874–879 (2011).

Yamada T. and Funaki Y.: "Cluster structures and single-cluster motions in ^{11}B and ^{13}C", International Journal of Modern Physics E, Bruxelles, Belgium, 2010–5, P. Descouvemont, Bruxelles, pp. 910–914 (2011).

Funaki Y., Yamada T., Horiuchi H., Roepke G., Schuck P., and Tohsaki A.: "Alpha clustering and condensation in nuclei", Journal of Physics: Conference Series, Paris, France, 2011–2, T. Otsuka, Paris, pp. 012033-1–012033-4 (2011).

Funaki Y., Yabana K., and Akahori T.: "A new theoretical approach to thermonuclear radiative-capture reaction rate", AIP Conference Proceedings, Wako, 2011–S. Kubono, Wako, pp. 457–459 (2012).

Yamada T. and Funaki Y.: "Three-body cluster structures and Hoyle-analogue states in ^{11}B", Progress of Theoretical Physics Supplement, Kyoto, Japna, 2011– K. Hagino, Kyoto, pp. 388–393 (2012).

Funaki Y., Yamada T., Horiuchi H., Roepke G., Schuck P., and Tohsaki A.: "Alpha Cluster States and Condensation in ^{16}O", Progress of Theoretical Physics Supplement, Kyoto, 2011– K. Hagino, Kyoto, pp. 439–444 (2012).

Fujiwara Y. and Fukukawa K.: "Nucleon-deuteron breakup differential cross sections derived from the quark-model NN interaction", Few-Body Systems, Seoul, Republic of Korea, 2011–8〜8, Springer Vienna, Vienna, pp. Vol. 54, Issue 1-4, 489–Vol. 54, Issue 1-4, 493 (2013).

Ohnishi S., Ikeda Y., Kamano H., and Sato T.: "Production Reaction of $\bar{K}NN$-πYN Resonance fromFaddeev Equations", Proceedings of the 20th International IUPAP Conference on Few-Body Problems in Physics(FB20), Fukuoka, 2012–8, Springer, Wien, p. DOI 10.1007/s00601-013-06 (2013).

Ohnishi S., Ikeda Y., Kamano H., and Sato T.: "Signature of strange dibaryon in kaon-induced reactions", Proceedings of The 5th Asia-Pacific Conference on Few-Body Problems in Physics 2011 (APFB2011), Seoul, Korea, 2011–8, Springer, Vienna, pp. 347–351 (2013).

Oral Presentations

(International Conference etc.)

Funaki Y.: "Alpha clustering and condensation in nuclei", EFES-IN2P3 Conference, "Many-body correlations from dilute to dense nuclear systems (MBC2011)", (Institut Henri Poincare), Paris, France, Feb. (2011).

Murano K., Ishii N., Aoki S., and Hatsuda T.: "LS force in NN system from Lattice QCD", YIPQS Symposium: Perspectives in Theoretical Physics–From Quark-Hadron Sciences to Unification of Theoretical Physics–, (Yukawa International Program for Quark-Hadron Sciences), Sakyo, Feb. (2011).

Funaki Y.: "Alpha particle condensates and cluster structures in nuclei", ECT* workshop on Clusters in Nuclei and Nuclear Matter, (ECT*), Trento, Italy, June (2011).

Murano K.: "Nuclear forces in the odd parity sector and the LS forces", the XXIX International Symposium on Lattice Field Theory, (Lawrence Livermore National Laboratory), The Village at Squaw Valley, USA, July–Oct. (2011).

Murano K., Aoki S., Hatsuda T., and Ishii N.: "Nucleon-nucleon potential and its non-locality in lattice QCD", The fifth Asia-Pacific COnference on Few-Body Problems in Physics 2011, (SUNGKYUN KWAN UNIVERSITY), Seoul, Korea, Aug. (2011).

Funaki Y.: "Resonance states and alpha particle condensation in ^{16}O", The fifth Asia-Pacific Conference on Few-Body Problems in Physics 2011, (Sungkyunkwan University), Seoul, Korea, Aug. (2011).

Funaki Y.: "'Resonances and alpha-particle condensate in ^{16}O studied with Complex Scaling Method", Dynamics and correlations in Exotic Nuclei (DCEN2011), (Yukawa Institute of Theoretical Physics), Kyoto, Sept. (2011).

Funaki Y.: "Resonances and alpha condensation in ^{16}O", Frontier Issues in Physics of Exotic Nuclei (YKIS2011), (Yukawa Institute of Theoretical Physics), Kyoto, Oct. (2011).

Funaki Y.: "A new theoretical approach to thermonuclear radiative-capture reaction rate", The 11th International Symposium on Origin of Matter and Evolution of Galaxies (OMEG11), Wako, Nov. (2011).

Hiyama E.: "Recent progress and future prospect of hypernuclear physic", HAPHY 2012-04: Theories for J-PARC Physics, (The Korean Hadron/Few-Body Physics Working Gorup), Pohang, Korea, Apr. (2012).

Gubler P.: "Bayesian approach to QCD sum rules", Seminar at TUM, (TUM), Munich, Germany, June (2012).

Murano K., Ishii N., Aoki S., Hatsuda T., Doi T., Ikeda Y., Inoue T., Nemura H., and Sasaki K.: "First calculation of the spin-orbit force in the parity odd sector in NN system from Lattice QCD", The 30th International Symposium on Lattice Field Theory, (The University of Adelaide), Cairns, Australia, June (2012).

Gubler P.: "Quarkonium at finite T: an approach based on QCD sum rules and the maximum entropy method", Workshop on hadron physics with strangeness and beyond, (Wien University), Wien, Austria, June (2012).

Nakatsukasa T., Fukuoka Y., Funaki Y., and Yabana K.: "Stochastic approach to correlations beyond the mean field with the Skyrme interaction", 2nd International Conference on Nuclear Structure and Dynamics '12, (University of Zagreb), Opatija, Croatia, July (2012).

Gubler P.: "Hot quarkonium spectral functions from QCD sum rules and the maximum entropy method", Quark Matter 2012 International Conference, (Brookhaven National Laboratory), Washington DC, USA, Aug. (2012).

Hiyama E.: "Structure of S=-1 and S=-2 hypernuclei", SNP12-International Workshop on Strangeness Nuclear Physics 2012, (Osaka Electro-Communication University), Neyagawa, Osaka, Aug. (2012).

Koike T. and Hiyama E.: "Formation of light p-shell Ξ^--hypernucleus via (K^-, K^+) reaction", The 20th International IUPAP Conference of Few-Body Problems in Physics, (International Union of Pure and Applied Physics (IUPAP)), Fukuoka, Aug. (2012).

Murano K., Ishii N., Aoki S., Hatsuda T., Doi T., Ikeda Y., Inoue T., and Sasaki k.: "Nuclear forces in the odd parity sector and the LS forces from Lattice QCD", The 20th International IUPAP Conference of Few-Body Problems in Physics, Fukuoka, Aug. (2012).

Gubler P.: "Quarkonia at finite T: An approach based on QCD sum rules and the maximum entropy method", The 20th International IUPAP Conference of Few-Body Problems in Physics, (Kyushu University, RCNP), Fukuoka, Aug. (2012).

Funaki Y.: "Gas-like states in finite nuclei", The 20th International IUPAP Conference on Few-Body Problems in Physics (FB20), (IUPAP), Fukuoka, Aug. (2012).

Ohnishi S., Ikeda Y., Kamano H., and Sato T.: "Production Reaction of $\bar{K}NN$-πYN Resonance from Faddeev Equations", The 20th International IUPAP Conference on Few-Body Problems in Physics (FB20), (IUPAP), Fukuoka, Aug. (2012).

Hiyama E.: "Varitation Calculation of 4He Tetramer Ground state and xcited states using a realistic 4He-4He potential", The 20th International IUPAP Conference on Few-Body Problems in Physics (FB20), (International Union of Pure and Applied Physics (IUPAP)), Fukuoka, Aug. (2012).

Suno H., Hiyama E., and Kamimura M.: "Theoretical study of triatomic systems involving helium atoms", Few-Body Problems in Physics, (International Union of Pure and Applied Physics), Fukuoka, Aug.–Aug. (2012).

Fukukawa K. and Fujiwara Y.: "Coulomb effect in the nucleon-deuteron elastic scattering", The 20th International IUPAP Conference on Few-Body Problems in Physics (FB20), (International Union of Pure and Applied Physics), Fukuoka, Aug.–Aug. (2012).

Hiyama E.: "Four- and five-body cluster structure of hypernuclei", 10th International Conference on Clustering Aspects of Nuclear Structure and Dynamics, (Institute of Nuclear Research of the Hungarian Academy of Sciences), Debrecen, Hungary, Sept. (2012).

Murano K., Ishii N., Aoki S., and Hatsuda T.: "Nuclear Forces from Lattice QCD toward LS-force", Korea-Japan workshop on nuclear and hadron physics at J-PARC, (Seoul National University), Seoul, Korea, Sept. (2012).

Funaki Y.: "Gas-like alpha cluster states and condensates in nuclei", The 10th International Conference on Clustering Aspects of Nuclear Structure and Dynamics (Cluster12), (Debrecen University), Debrecen, Hungary, Sept. (2012).

Koike T. and Hiyama E.: "Formation of light p-shell Ξ^--hypernucleus by (K^-, K^+) reaction", The 2nd Korea-Japan Workshop on Nuclear and Hadron Physics at J-PARC, (Pusan National University), Pusan, Korea, Sept. (2012).

Hiyama E.: "Few-body aspects of hypernuclear physics", VIII Tours Sysmposium on Nuclear Physics and astrophysics, (GANIL), Black Forest, Germany, Sept. (2012).

Hiyama E.: "Structure of Light Ξ hypernuclei", Second Korea-Japan workshop on nuclear and hadron physics at J-PARC, (Pusan National University), Busan, Korea, Sept.–Sept. (2012).

Ohnishi S., Hiyama E., and Kamimura M.: "Four-body calculation of ${}^{6}_{\Lambda}$H hypernucleus", 11th International Conference on Hypernuclear and Strange Particle Physics (HYP2012), (ICCUB), Barcelona, Spain, Oct. (2012).

Murano K.: "Nuclear force in the odd parity sector and the LS forces from Lattice QCD", 11th International Conference on Hypernuclear and Strange Particle Physics (HYP2012), (University of Barcelona), Barcelona, Spain, Oct. (2012).

Hiyama E.: "S=-1 and S=-2 light Hypernuclear structure", 11th International Conference on Hypernuclear and Strange Particle Physics (HYP2012), (The Institute of Cosmos Sciences (ICC) of the University of Barcelona), Barcelona, Spain, Oct. (2012).

Hiyama E.: "Few-body aspects of Hypernuclear physics", Autumn 2012 General Meeting of the Korean Physics Society, (Association of Asia Pacific Physical Societies), Pyungchang, Korea, Oct. (2012).

Hiyama E.: "Structure of S=-1 and S=-2 system", New trends in the low-energy QCD in the strangeness sector :experimental and theoretical aspects, (European Centre for Theoretical Studies in Nuclear Physics and Related Areas (ECT*)), Trento, Italy, Oct. (2012).

Hiyama E.: "Structure of nrutron-rich hypernuclei", Seminar of Department di Fisica, Universita di Torino, (Torino University), Torino, Italy, Oct. (2012).

Gubler P.: "Modification of hadronic spectral functions under extreme conditions: An approach based on QCD sum rules and the maximum entropy method", The 11th International Conference on Hypernuclear and Strange Particle Physics, (Universitat de Barcelona), Barcelona, Spain, Oct. (2012).

Hiyama E.: "Few-body structure of hypernuclei", The 8th China-Japan Joint Nuclear Physics Symposium, (China Institute of Atomic Energy), Beijing, China, Oct. (2012).

Funaki Y.: "New concept in clusterings and alpha-particle condensate in nuclei and hypernuclei", The 8th China-Japan Joint Nuclear Physics Symposium, (CIAE), Beijing, China, Oct. (2012).

Funaki Y.: "Alpha particle condensate in hypernuclei", The 8th JSPS Core-to-Core Symposium, (JSPS), Barcelona, Spain, Oct. (2012).

Funaki Y.: "Alpha-particle condensation in light hypernuclei", XI International Conference on Hypernuclear and Strange Particle Physics, (Barcelona University), Barcelona, Spain, Oct. (2012).

Gubler P.: "Recent results from QCD sum rule analyses based on the maximum entropy method", Xth Quark Confinement and the Hadron Spectrum, (TUM), Munich, Germany, Oct. (2012).

Hiyama E.: "Gaussian Expansion Method and application to Hypernuclear phtsics", Seminar at Beihang University, (Beihang University), Beihang, China, Nov. (2012).

Hiyama E.: "Few-body aspect of Hypernuclear physics", Seminar at Institute of High Energy Physics, (Institute of High Energy Physics), Beijing, China, Nov. (2012).

Hiyama E.: "Structure of S=-2 hypernuclei", Super FRS collaboration meeting, (GSI), Frankfurt, Germany, Nov. (2012).

Hiyama E.: "Study of S=-2 systems", Workshop on S= -2 and the related Nuclear Physics in HIDA-Takayama 2012, (Gifu University), Takayama, Nov. (2012).

Funaki Y.: "Gas-like alpha cluster states in excited states of light nuclei", Ab initio understanding of light nuclei workshop, (Birmingham University), Birmingham, United Kingdom, Dec. (2012).

Hiyama E.: "Recent progress of Hypernuclear physics", International Symposium "Nanoscience and Quantum Physics 2012", (Global COE Program), Tokyo, Dec. (2012).

Ohnishi S., Ikeda Y., Kamano H., and Sato T.: "Production reaction of $\bar{K}NN$-πYN resonance and $\bar{K}N$ interaction", Quarks to Universe in Computational Science (QUCS 2012), (Grant-in-Aid for Scientific Research on Innovative Areas Research on the Emergence of Hierarchical Structure of Matter by Bridging Particle, Nuclear and Astrophysics in Computational Science), Nara, Dec. (2012).

Murano K.: "Spin-Orbit force in the NN system from Lattice QCD", Quarks to Universe in Computational Science (QUCS 2012), (Joint Institute for Computational Fundamental Science), Nara, Dec. (2012).

Gubler P.: "Recent results from MEM analyses of QCD sum rules", Seminar at Yonsei University, (Yonsei University), Seoul, Korea, Dec. (2012).

Suno H.: "Efimov effect and resonances in atomic and molecular physics", Resonances and non-Hermitian systems in quantum mechanics, (Yukawa Institute for Theoretical Physics), Kyoto, Dec.–Dec. (2012).

Fukukawa K. and Hiyama E.: "Quark-model hyperon-hyperon interactions", YIPQS international molecule-type workshop on "Nuclear equation of state and hypernuclear physics", (Yukawa institute for theoretical physics), Kyoto, Jan.–Jan. (2013).

Hiyama E.: "Few-body calculation of light hypernuclei", Workshop on "Hypernuclear physics with Electromagnetic Probes", Wako, Feb. (2013).

Koike T. and Hiyama E.: "Formation of light Ξ^--hypernucleus by (K^-, K^+) reactions", Workshop on Future Prospects of Hadron Physics at J-PARC and Large Scale Computational Physics in 2013, (KEK theory center), Tokai, Feb. (2013).

Koike T. and Hiyama E.: "Ξ^--hypernuclear formation via (K^-, K^+) reaction", YIPQS international molecule-type workshop on "Nuclear equation of state and hypernuclear physics", (Yukawa Institute for Theoretical Physics, Kyoto University), Kyoto, Feb. (2013).

Fukukawa K.: "Hyperon-hyperon interaction based on quark-model baryon-baryon interactions", Second international school for strangeness nuclear physics (SNP2013), (School of Sci. Tohoku Univ. and Advanced sci. research center JAEA), Tokai and Sendai, Feb.–Feb. (2013).

Fukukawa K.: "Quark-model baryon-baryon interaction and its applications to nuclear many-body systems", Seminar in INFN, Sezione in Catania, (INFN), Catania, Italy, Mar.–Mar. (2013).

(Domestic Conference)

村野啓子, 石井理修, 青木慎也, 初田哲男: Future Prospects of Hadron Physics at J-PARC and Large Scale Computational Physics, (J-PARC センター、計算基礎科学連携拠点), 東海村, 2 月 (2012).

村野啓子: "格子 QCD によるテンソル力と短距離斥力", 日本物理学会第 67 回年次大会, (関西学院大学), 関西学院大学 西宮上ケ原キャンパス, 3 月 (2012).

肥山詠美子: "Baryon-baryon interaction and structure of few-body systems", 新学術領域「素核宇宙融合」×「新ハドロン」クロスオーバー研究会ー多様な手法でせまるハドロン物理への挑戦ー, (名古屋大学), 名古屋, 7 月 (2012).

村野 啓子, 青木 慎也, 石井 理修, 初田 哲男, 土井 琢身, 池田陽一, 井上貴史, 佐々木健志: "Spin-Orbit force in the NN system from Lattice QCD", 新学術領域「素核宇宙融合」×「新ハドロン」クロスオーバー研究会ー多様な手法でせまるハドロン物理への挑戦ー, (名古屋大学), 日本, 7 月 (2012).

福川 賢治: "Nucleon-deuteron scattering studied by a quark-model baryon-baryon interaction", 中務原子核物理学セミナー, (中務原子核物理学研究室), RIBF 棟 2 階 Conference room, 7–7 月 (2012).

村野啓子: "格子 QCD から求めるスピン軌道力", 日本物理学会 2012 年秋季大会, (京都産業大学), 京都, 9 月 (2012).

大西祥太, 池田陽一, 鎌野寛之, 佐藤透: "チャンネル結合散乱方程式によるストレンジダイバリオン共鳴生成反応の解析", 日本物理学会２０１２年秋季大会, (日本物理学会), 京都, 9 月 (2012).

福川賢治, 藤原義和: "クォーク模型非局所ガウス型相互作用による核子・重陽子散乱", 日本物理学会 2012 年秋季大会, (日本物理学会), 京都, 9–9 月 (2012).

大西祥太, 池田陽一, 鎌野寛之, 佐藤透: "3 体散乱方程式による $\bar{K}NN$-πYN 共鳴生成反応の研究", ELPH 研究会 C005「ダブルメソン生成とバリオン分光 ～LEPS/ELPH におけるハドロン光生成反応の最近の進展～」, (東北大 ELPH), 仙台, 11 月 (2012).

福川賢治, 藤原義和: "クォーク模型バリオン間相互作用による核子-重陽子弾性散乱", 「微視的有効相互作用の理論と核構造・核反応」, (基礎物理学研究所), 基礎物理学研究所, 2–2 月 (2013).

Mathematical Physics Laboratory

Publications

[Journal]

(Original Papers) *Subject to Peer Review

Hashimoto K. and Iizuka N.: "A Comment on Holographic Luttinger Theorem.", J. High Energy Phys. **1207**, 064 (2012). *

Higaki T., Kamada k., and Takahashi F.: "Higgs, moduli problem, baryogenesis and large volume compactifications.", J. High Energy Phys. **1209**, No. 043, (2012). *

Higaki T. and Takahashi F.: "Dark radiation and dark matter in large volume compactifications", J. High Energy Phys. **1211**, No. 125, (2012). *

Higaki T., Jeong K., and Takahashi F.: "Hybrid inflation in high-scale supersymmetry", J. High Energy Phys. **1212**, No. 111, (2012).

Fujimori T., Kimura T., Nitta M., and Ohashi K.: "Vortex counting from field theory", J. High Energy Phys. **2012**, No. 06, pp. 028-1–048-19 (2012). *

Fujikawa K.: "On neutrino masses via CPT violating Higgs interaction in the Standard Model", Phys. Lett. B **718**, 178–180 (2012). *

Fujikawa K.: "Universally valid Heisenberg uncertainty relation", Phys. Rev. A **A 85**, 062117 (2012). *

Aoyama T., Hayakawa M., Kinoshita T., and Nio M.: "Tenth-order QED contribution to lepton anomalous magnetic moment – sixth-order vertices containing an internal light-by-light scattering subdiagram", Phys. Rev. D **85**, 093013-1–093013-12 (2012). *

Hashimoto K., Maezawa Y., Eto M., Iida H., and Ishii T.: "Anomaly-induced charges in baryons", Phys. Rev. D **85**, 114038 (2012). *

Asano M. and Higaki T.: "Natural supersymmetric spectrum in mirage mediation", Phys. Rev. D **86**, No. 4, pp. 035020 - 1–035020 - 16 (2012). *

Misumi T., Nakano T., Kimura T., and Ohnishi A.: "Strong-coupling analysis of parity phase structure in staggered-Wilson fermions", Phys. Rev. D **D86**, No. 17, pp. 034501-1–034501-17 (2012). *

Ishikawa T., Blum T., Hayakawa M., Izubuchi T., Jung C., and Zhou R.: "Full QED+QCD Low-Energy Constants through Reweighting", Phys. Rev. Lett. **109**, No. 7, pp. 072002-1–072002-5 (2012). *

Aoyama T., Hayakawa M., Kinoshita T., and Nio M.: "Tenth-order QED contribution to the electron g-2 and an improved value of the fine structure constant", Phys. Rev. Lett. **109**, No. 11, pp. 111807-1–111807-4 (2012). *

Aoyama T., Hayakawa M., Kinoshita T., and Nio M.: "Complete tenth-order QED contribution to the muon g-2", Phys. Rev. Lett. **109**, No. 11, pp. 111808-1–111808-4 (2012). *

Misumi T., Kimura T., and Ohnishi A.: "QCD phase diagram with two-flavor lattice fermion formulations", Physical review **D86**, No. 9, pp. 094505-1–094505-12 (2012). *

Kimura T. and Nishioka T.: "The Chiral Heat Effect", Prog. Theor. Phys. **127**, No. 6, pp. 1009–1017 (2012). *

Fujikawa K.: "Does CHSH inequality test the model of local hidden variables?", Prog. Theor. Phys. **127**, 975–987 (2012). *

Fujikawa K.: "Conditional measurement in noncontextual hidden-variable models", Prog. Theor. Phys. **127**, 989–996 (2012). *

Kimura T.: "Spinless Basis for Spin-Singlet FQH States", Prog. Theor. Phys. **128**, No. 5, pp. 829–843 (2012). *

Eager R., Tachikawa Y., and Schmude J. W.: "Superconformal Indices, Sasaki-Einstein Manifolds, and Cyclic Homologies", Advances in Theoretical and Mathematical Physics **N/A**, No. N/A, (2013). *

Fujikawa K.: "Electromagnetic interaction in theory with Lorentz invariant CPT violation", Phys. Lett. B **718**, 1500–1504 (2013). *

Minami Y. and Hidaka Y.: "Relativistic hydrodynamics from projection operator method", Phys. Rev. E **87**, No. 023007, (2013). *

Higaki T., Jeong K., and Takahashi F.: "A Parallel World in the Dark", Preprint archive **1302.2516**, (2013).

Fujikawa K.: "Aspects of universally valid Heisenberg uncertainty relation", Progress of Theoretical and Experimental Physics **03A**, 03A03 (2013). *

Hidaka Y., Hirono Y., Kimura T., and Minami Y.: "Viscoelastic-electromagnetism and Hall viscosity", Progress of Theoretical and Experimental Physics **2013**, No. 1, pp. 013A02-1–013A02-9 (2013). *

(Review)

Aoyama T., Hayakawa M., Kinoshita T., and Nio M.: "Quantum electrodynamics calculation of lepton anomalous magnetic moments: Numerical approach to the perturbation theory of QED", Progress of Theoretical and Experimental Physics **01A**, 107-1–107-36 (2012).

[Book · Proceedings]

(Review)

Kimura T.: "Gauge Theory, Combinatorics, and Matrix Models", Linear Algebra - Theorems and Applications, InTech, Rijeka, pp. 75–98 (2012).

Oral Presentations

(International Conference etc.)

Hashimoto K.: "LANDSCAPE IN BOUNDARY STRING FIELD THEORY", MIT CTP seminar, (MIT), Boston, USA, Mar. (2012).

Hashimoto K.: "Holographic nuclei", Durham university seminar, (Durham university), Durham, UK, Apr. (2012).

Hashimoto K.: "Holographic nuclei", Mathematics and Applications of Branes in String and M-theory, (Cambridge university), Cambridge, UK, Apr. (2012).

Hashimoto K.: "Holographic Nuclei", Progress in Quantum Field Theory and String Theory, (Osaka city university), Osaka, Apr. (2012).

Kimura T.: "Spinless basis for spin-singlet FQH states", International Conference on Topological Quantum Phenomena, (Nagoya University), Nagoya, May (2012).

Fujikawa K.: "Second quantization, hidden gauge symmetry and geometric phases", Tonomura FIRST International Symposium on Electron Microscopy and Gauge Fields, (JST), Tokyo, May (2012).

Nio M., Aoyama T., Hayakawa M., and Kinoshita T.: "Tenth-order QED contribution to the lepton g-2", 43rd Annual Meeting of the APS, Division of Atomic, Molecular and Optical Physics, (American Physical Society), Anaheim, USA, June (2012).

Kimura T., Misumi T., and Ohnishi A.: "QCD Phase Diagram with Two-Flavor Fermion Discretizations", The 30th International Symposium on Lattice Field Theory, Cairns, Australia, June (2012).

Hashimoto K.: "FERROMAGNETIC NEUTRON STAR", CQuest seminar, (CQuest), Seoul, Korea, July (2012).

Hashimoto K.: "IMPURITIES IN ADS/CFT", CQuest seminar, (CQuest), Seoul, Korea, July (2012).

Taki M.: "Generalized Whittaker states and AGT correspondence", Geometric Correspondences of Gauge Theories, (SISSA), Italy, Italy, Sept. (2012).

Hashimoto K.: "Holographic magnetars", From Gravity to Strong Coupling Physics, (Kyoto university), Kyoto, Oct. (2012).

Hashimoto K.: "Superstring and hadron/nuclear physics", The 2nd OU-RuG Symposium on Particle-Nuclear and Condensed Matter Physics:New Challenges and Opportunities, (Osaka university, Groningen university), Osaka, Nov. (2012).

Fujikawa K.: " Quantum Discord, Hidden Variables and CHSH Inequality", Asia Pacific Conference and Workshop in Quantum Information Science 2012, (Univ. of Putra Malaysia), Putrajaya, Malaysia, Dec. (2012).

Hashimoto K.: "LANDSCAPE IN BOUNDARY STRING FIELD THEORY", KIAS (Korea Institute for Advanced Study) Seminar, (KIAS), Seoul, Korea, Feb. (2013).

Hashimoto K.: "ATOMIC NUCLEI AND MATRIX THEORY", Stanford High Energy Physics Colloquia, (Stanford university), Stanford, USA, Mar. (2013).

Nio M., Aoyama T., Hayakawa M., and Kinoshita T.: "Tenth-order QED calculation of the lepton anomalous magnetic moments and precision determination of the fine-structure constant", The 5th GCOE International Symposium on "Weaving Science Web beyond Particle-Matter Hierarchy", (Tohoku University), Sendai, Mar. (2013).

(Domestic Conference)

木村太郎: "組合せ論とランダム行列", 数理物理・物性基礎論セミナー, (お茶の水大学), お茶の水大学, 4 月 (2012).

檜垣 徹太郎: "Moduli stabilization and supersymmetry breaking for string phenomenology", 早稲田大学中里安倍研セミナー 2012, (早稲田大学), 早稲田大学, 4 月 (2012).

橋本幸士: 首都大学東京談話会, (首都大学東京), 東京, 5 月 (2012).

木村太郎: "Fractional quantum Hall effect, CFT, and symmetric polynomials", 名古屋大学数理物理セミナー, (名古屋大学大学院理学研究科), 名古屋大学, 5 月 (2012).

木村太郎: "Aoki phases in staggered-Wilson fermions", 筑波大学素粒子理論研究室セミナー, (筑波大学素粒子理論研究室), 筑波大学, 6 月 (2012).

瀧雅人: "Generalized Whittaker states for flavored AGT", 東京工業大学素粒子論研究室セミナー, (東京工業大学), 東京, 6 月 (2012).

瀧雅人: 東京大学駒場キャンパス素粒子論研究室セミナー, (東京大学), 東京, 6 月 (2012).

木村太郎: "Random matrix, zeta function, statistical mechanics", 東工大セミナー, (東京工業大学黒川研究室), 東京工業大学大岡山キャンパス, 6 月 (2012).

橋本幸士: "強相関系における不純物と重力理論", 物質科学の数学的手法と数理物理, 和光, 6 月 (2012).

木村 太郎: "Gauge theory and matrix models: β-deformation and orbifolding", 立教大学数理物理学研究センターセミナー, (立教大学数理物理学研究センター), 立教大学, 6 月 (2012).

藤森俊明, 木村太郎, 新田宗土, 大橋圭介: "Vortex counting and exact superpotential in two-dimensional $\mathcal{N} = (2, 2)$ theories", 場の理論と弦理論, (京都大学基礎物理学研究所), 京都大学, 7 月 (2012).

藤森俊明, 木村太郎, 新田宗土, 大橋圭介: "Vortex counting from field theory", 場の理論と弦理論, (京都大学基礎物理学研究所), 京都大学, 7 月 (2012).

瀧雅人: "Instantons and Whittaker states for CFT", 場の理論と弦理論, (京都大学基礎物理学研究所), 京都, 7 月 (2012).

浅野雅樹, 檜垣徹太郎: "Natural supersymmetric spectrum in mirage mediation", 素粒子物理学の進展 2012, (京都大学基礎物理学研究所), 京都大学基礎物理学研究所, 7 月 (2012).

木村太郎: "Vortex counting from field theory", 東京大学素粒子論研究室セミナー, (東京大学素粒子論研究室), 東京大学本郷キャンパス, 7 月 (2012).

橋本幸士: 北海道大学素粒子論セミナー, (北海道大学), 札幌, 7 月 (2012).

南佑樹: "Transport coefficients near QCD critical point", RHIC/LHC における量子・古典場のダイナミクス, 理化学研究所, 7–7 月 (2012).

木村太郎: "ゲージ理論とランダム行列", 日本物理学会, (日本物理学会), 横浜国立大学, 9 月 (2012).

藤森俊明, 木村太郎, 新田宗土, 大橋圭介: "2 次元 N=(2,2) 超対称ゲージ理論における superpotential と vortex counting

について", 日本物理学会, (日本物理学会), 京都産業大学, 9 月 (2012).

日高義将, 広野雄士, 木村太郎, 南佑樹: "カルタン形式によるトポロジカル粘性", 日本物理学会, (日本物理学会), 横浜国立大学, 9 月 (2012).

三角樹弘, 中野嵩士, 木村太郎, 大西明: "スタッガード・ウィルソンフェルミオンにおけるパリティ相構造の強結合解析", 日本物理学会, (日本物理学会), 京都産業大学, 9 月 (2012).

藤森俊明, 木村太郎, 新田宗士, 大橋圭介: "非可換渦分配関数の場の理論からの導出", 日本物理学会, (日本物理学会), 京都産業大学, 9 月 (2012).

檜垣徹太郎: "Cosmology in LARGE volume string models", 日本大学理工学部素粒子論コロキウム, (日本大学), 日本大学, 9 月 (2012).

浅野雅樹, 檜垣徹太郎: "Natural supersymmetric spectrum in mirage mediation", 日本物理学会　2012 年秋季大会, (京都産業大学), 京都産業大学, 9 月 (2012).

Schmude J. W.: "Superconformal gauge theories from a gravitational point of view", YITP workshop on gauge/gravity duality, (Yukawa Institute, University of Kyoto), 京都, 10 月 (2012).

橋本幸士: "超弦理論と D ブレーン", 山形大学集中講義, (山形大学), 山形, 10 月 (2012).

檜垣徹太郎: "Cosmology in LARGE volume string models", 首都大学東京素粒子論研究室セミナー, (首都大学東京), 首都大学東京, 10 月 (2012).

木村太郎: "ゼータ関数の統計力学とランダム行列", 中央大統計力学・確率論セミナー, (中央大学), 中央大学後楽園キャンパス, 10 月 (2012).

藤川和男: 日大理工・益川塾連携 素粒子物理学シンポジウム, (京都産業大学), 京都産業大学, 11 月 (2012).

橋本幸士: 京都大学素粒子論研究室セミナー, (京都大学), 京都, 11 月 (2012).

木村 太郎: "Transport phenomena and gauge theory of gravity", 京都大学凝縮系理論研究室セミナー, (京都大学凝縮系理論研究室), 京都大学, 11 月 (2012).

木村太郎: "Matrix models for Seiberg-Witten theory", 大阪大学素粒子論研究室セミナー, (大阪大学素粒子論研究室), 大阪大学豊中キャンパス, 11 月 (2012).

木村太郎: "Recent topics on lattice fermions", 大阪大学素粒子論研究室セミナー, (大阪大学素粒子論研究室), 大阪大学豊中キャンパス, 11 月 (2012).

木村太郎, 日高義将, 広野雄士, 南佑樹: "交差応答に対するトポロジカル有効理論", 第 6 回物性科学領域横断研究会, 東京大学本郷キャンパス, 11 月 (2012).

橋本幸士: 理研シンポジウム「宇宙線の発見から 100 年、X 線天体の発見から 50 年」, 和光, 11 月 (2012).

南佑樹, 日高義将: "森の射影演算子法による相対論的線形流体方程式の導出", 森肇先生記念研究集会　- 非線形・非平衡系の統計力学 -, (九州大学応用力学研究所), 九州大学, 11–11 月 (2012).

橋本 幸士: "LANDSCAPE IN BOUNDARY STRING FIELD THEORY", 大阪大学素粒子論研究室セミナー, (大阪大学), 大阪, 12 月 (2012).

Schmude J. W.: "SCFTs from gravity's point of view", Seminar at Osaka University, (大阪), 大阪, 1 月 (2013).

檜垣徹太郎: 山形大学理論量子グループセミナー, (山形大学理学部理論量子グループ), 山形大学理学部, 1 月 (2013).

檜垣徹太郎: "Cosmology in large volume string models", 大阪大学素粒子論研究室セミナー, (大阪大学理学研究科素粒子論研究室), 大阪大学理学研究科, 1 月 (2013).

瀧雅人: 立教大学数理物理学研究センターセミナー, (立教大学数理物理学研究センター), 立教大学池袋キャンパス, 1 月 (2013).

檜垣徹太郎: 立教大学理論物理コロキウム, (立教大学理学部理論物理学研究室), 立教大学理学部理論物理学研究室, 1 月 (2013).

瀧雅人: "フィンスラー幾何学と透明人間", エキゾチック時空幾何とその応用, 和光市, 2 月 (2013).

木村太郎: "輸送現象と時空", エキゾチック時空幾何とその応用, 理化学研究所　和光キャンパス, 2 月 (2013).

木村太郎: "トポロジカル物質相と格子フェルミオン", 理論計算分子科学研究領域オープンセミナー, (分子科学研究所), 分子科学研究所, 2 月 (2013).

木村太郎: "多成分分数量子ホール系における一重項状態と q 変形共形場理論", 日本物理学会, (日本物理学会), 東広島, 3 月 (2013).

檜垣徹太郎: LHC vs Beyond the Standard Model - 素粒子物理学の最先端 -, (京都大学基礎物理学研究所), 京都大学基礎物理学研究所, 3 月 (2013).

橋本幸士: "今後の展望", 日本物理学会 2013 年春季大会, (日本物理学会), 広島, 3 月 (2013).

Radiation Laboratory

Publications

[Journal]

(Original Papers) *Subject to Peer Review

Yoshioka T., Mishima K., Ino T., Taketani K., Mutou S., Morishima T., Shimizu H., Oku T., Suzuki J., Shinohara T., Sakai k., Sato H., Hirota K., Otake Y., Kitaguchi M., Hino M., Seki Y., Iwashita Y., Yamada M., Ichikawa M., Takanori S., Kawasaki S., Komamiya S., Kamiya Y., Otono H., Yamashita S., and Geltenbort P.: "Polarization of very cold neutron using a permanent magnet quadruple", Nucl. Instrum. Methods Phys. Res. A **634**, No. 1, pp. S17–S20 (2011). *

Taketani K., Ebisawa T., Hino M., Hirota K., Ino T., Kitaguchi M., Mishima K., Mutou S., Oide H., Oku T., Otono H., Sakai k., Shima T., Shimizu H., Yamashita T., and Yoshioka T.: "A high S/N ratio spin flip chopper system for a pulsed neutron source", Nucl. Instrum. Methods Phys. Res. A **634**, No. 1, pp. S134–S137 (2011). *

Yamada M., Iwashita Y., Kanaya T., Ichikawa M., Tongu H., Kennedy S. J., Shimizu H., Mishima K., Yamada N., Hirota K., Carpenter J. M., Lal J., Andersen K., Geltenbort P., Guerard B., Manzin G., Masahiro H., Kitaguchi M., and Bleuel M.: "The performance of magnetic lens for focusing VCN-SANS", Nucl. Instrum. Methods Phys. Res. A **634**, No. 1, pp. S156–S160 (2011). *

Richardson E., Akiba Y., Anderson N., Bickley A., Chujo T., Cole B. A., Esumi S., Haggerty J. S., Hanks J., Hemmick T., Hutchison M., Ikeda Y., Inaba M., Jia J., Lynch D., Miake Y., Mignerey A. C., Niida T., O'Brien E., Pak R., Shimomura M., Stankus P. W., Todoroki T., Watanabe K., Wei R., Xie W., Zajc W. A., and Zhang C.: "A reaction plane detector for PHENIX at RHIC", Nucl. Instrum. Methods Phys. Res. A **636**, No. 1, pp. 99–107 (2011). *

Ino T., Shinohara T., Adachi T., Hirota K., Hino M., Oku T., Taketani K., Mishima K., Yoshioka T., Arimoto y., Mutou S., Suzuki J., and Shimizu H.: "Development of thin film neutron focusing lenses", Nucl. Instrum. Methods Phys. Res. A, pp. S94–S96 (2011). *

Otake Y., OLBINADO M. P., Seki Y., Hirota K., Yamagata Y., Ju J., Adachi T., Morita S., IWASHITA Y., Hino M., Ichikawa M., Kitaguchi M., Takahashi T., YOSHIZAWS H., LEE S. W., YASHIRO W., and Momose A.: "Research toward the Development of Compact Neutron Interference Imaging Instrument with Gratings", J. Phys.: Conf. Ser. **340**, 012035-1–012035-6 (2012). *

Goto Y.: "Single transverse-spin asymmetry of very forward neutron production in polarized p + p collisions at PHENIX", J. Phys.: Conf. Ser. **389**, No. 1, pp. 012034–012034 (2012).

Inoue T., Aoki S., Doi T., Hatsuda T., Ikeda Y., Ishii N., Murano K., Nemura H., and Sasaki K.: "Two-Baryon Potentials and H-Dibaryon from 3-flavor Lattice QCD Simulations", Nucl. Phys. A **881**, 28–43 (2012). *

Albacete J. L., Dumitru A., Fujii H., and Nara Y.: "CGC predictions for p + Pb collisions at the LHC", Nucl. Phys. A **897**, No. 2013, pp. 1–27 (2012). *

Ishii N., Aoki S., Doi T., Hatsuda T., Ikeda Y., Inoue T., Murano K., Nemura H., and Sasaki K.: "Hadron-Hadron Interactions from Imaginary-time Nambu-Bethe-Salpeter Wave Function on the Lattice", Phys. Lett. B **712**, 437–441 (2012). *

Aoki K., Aramaki Y., Enyo H., Kanno K., Kawama D., Masumoto S., Nakai W., Ozawa K., Sekimoto M., Obara Y., Shibukawa T., Takahashi T., Watanabe Y., Komatsu Y., and Yokkaichi S.: "Development of GEM tracker for J-PARC E16 experiment", Nucl. Instrum. Methods Phys. Res. A, (2013). *

Fukushima K. and Hidaka Y.: "Magnetic Catalysis vs Magnetic Inhibition", Phys. Rev. Lett. **110**, No. 031601, (2013). *

(Review)

Akiba Y.: "Experimental Study of Quark Gluon Plasma at RHIC", Prog. Theor. Phys. Suppl., No. 187, pp. 55–67 (2011).

Akiba Y.: "ISMD2011: Experimental Conference Summary", Prog. Theor. Phys. Suppl., No. 193, pp. 340–347 (2012).

(Others)

Bhang H., Ajimura S., Aoki K., Banu A., Fukuda T., Hashimoto O., Hwang J. I., Kameoka S., Kang B. H., Kim E., Kim J., Kim M., Maruta T., Miura Y., Miyake Y., Nagae T., Nakamura M., Nakamura S. N., Noumi H., Okada S., Okayasu Y., Outa H., Park H., Saha P., Sato Y., Sekimoto M., Takahashi T., Tamura H., Tanida K., Toyoda A., Tshoo K., Tsukada K., Watanabe T., and Yim H.: "Three-Body $\Lambda NN \rightarrow nNN$ Nonmesonic Weak Decay Process of Λ Hypernuclei", Few Body Syst. **54**, No. 1-4, pp. 103–110 (2013).

[Book · Proceedings]

(Original Papers) *Subject to Peer Review

Murano K., Ishii N., Aoki S., Hatsuda T., Doi T., Ikeda Y., Inoue T., and Sasaki k.: "Nuclear forces in the parity odd sector and the LS forces", Proceedings of Science, Lattice 2011, The Village at Squaw Valley, USA, 2011–6, Sissa, Italy, pp. 319–325 (2011).

(Others)

Todoroki T. and PHENIX C.: "Two particle hadron correlations with higher harmonic flow in Au+Au 200 GeV collisions at RHIC-PHENIX", The Seventh Workshop on Particle Correlations and Femtoscopy, Tokyo, 2011–9, Proceedings of Science, Trieste, pp. 1–6 (2012).

Oral Presentations

(International Conference etc.)

Murano K., Ishii N., Aoki S., and Hatsuda T.: "LS force in NN system from Lattice QCD", YIPQS Symposium: Perspectives in Theoretical Physics–From Quark-Hadron Sciences to Unification of Theoretical Physics–, (Yukawa International Program for Quark-Hadron Sciences), Sakyo, Feb. (2011).

Murano K., Aoki S., Hatsuda T., and Ishii N.: "Nucleon-nucleon potential and its non-locality in lattice QCD", The fifth Asia-Pacific COnference on Few-Body Problems in Physics 2011, (SUNGKYUN KWAN UNIVERSITY), Seoul, Korea, Aug. (2011).

Todoroki T. and PHENIX Collaboratio .: "Two particle hadron correlations with higher harmonic reaction plane in Au+Au 200GeV collisions at RHIC-PHENIX", 7th Workshop on Particle Correlations and Femtoscopy(WPCF 2011), (University of Tokyo), Tokyo, Sept. (2011).

Goto Y.: "Single transverse-spin asymmetry of very forward neutron production in polarized pp collisions at PHENIX", 28th Winter Workshop on Nuclear Dynamics (WWND 2012), (Wayne State University), Dorado del Mar, Puerto Rico, USA, Apr. (2012).

Todoroki T.: "Two particle correlation measurements at PHENIX", Hard Probes 2012, (INFN, Universita di Cagliari), Cagliari , Italy, May–June (2012).

Murano K., Ishii N., Aoki S., Hatsuda T., Doi T., Ikeda Y., Inoue T., Nemura H., and Sasaki K.: "First calculation of the spin-orbit force in the parity odd sector in NN system from Lattice QCD", The 30th International Symposium on Lattice Field Theory, (The University of Adelaide), Cairns, Australia, June (2012).

Hachiya T.: "Event anisotropy of electrons from charm and bottom quark decays in 200GeV Au+Au collisions at RHIC-PHENIX", Quark Matter 2012 International Conference, (Brookhaven National Laboratory), Washington, USA, Aug. (2012).

Todoroki T. and PHENIX C.: "Two particle correlation measurements with respect to higher harmonic event planes at PHENIX", Quark Matter 2012 International Conference, (Brookhaven National Laboratory), Washington D.C., USA, Aug. (2012).

Murano K., Ishii N., Aoki S., Hatsuda T., Doi T., Ikeda Y., Inoue T., and Sasaki k.: "Nuclear forces in the odd parity sector and the LS forces from Lattice QCD", The 20th International IUPAP Conference of Few-Body Problems in Physics, Fukuoka, Aug. (2012).

Goto Y.: "Inclusive cross section and single transverse-spin asymmetry of very forward neutron production at PHENIX", 20th International Symposium on Spin Physics (SPIN 2012), (JINR (Joint Institute for Nuclear Research)), Dubna, Russia, Sept. (2012).

Murano K., Ishii N., Aoki S., and Hatsuda T.: "Nuclear Forces from Lattice QCD toward LS-force", Korea-Japan workshop on nuclear and hadron physics at J-PARC, (Seoul National University), Seoul, Korea, Sept. (2012).

Hachiya T.: "Heavy quark production at RHIC-PHENIX", 8th International Workshop on High pT Physics at LHC, (Central China National University), Wuhan, China, Oct. (2012).

Ralf S.: "spin dependent fragmentation function measurements in Belle", 3rd Workshop on the QCD Structure of the nucleon (QCD-N'12), (University of the Basque country), Bilbao, University of the Basque country, Spain, Oct.–Oct. (2012).

Aoki K.: "Mass modification of vector mesons", International Workshop on using Heavy Flavors to Probe New Hadron Spectroscopies / Dynamics, (Nagoya University), Haeundae, Busan, South Korea, Nov. (2012).

Tsuji T.: "Neutral pion measurements in Pb+Pb collisions at $\sqrt{S_{NN}} = 2.76$ TeV with ALICE at the LHC", The 4th Asian Triangle Heavy Ion conference (ATHIC 2012), (Pusan National University), Pusan, Korea, Nov. (2012).

Yokkaichi S.: "Experiment on meson-mass modifications at J-PARC", KEK theory workshop on Hadron physics with high-momentum hadron beams at J-PARC in 2013, (KEK), Tsukuba, Jan. (2013).

Komatsu Y., Aoki K., Enyo H., Aramaki Y., Kanno K., Kawama D., Masumoto S., Nakai W., Obara Y., Ozawa K., Sekimoto M., Shibukawa T., Takahashi T., Watanabe Y., and Yokkaichi S.: "Development of GEM Tracker for J-PARC E16 experiment", 13th Vienna conference of instrumentation, (Institute of High Energy Physics (HEPHY) of the Austrian Academy of Sciences), Vienna, Austria, Feb.–Feb. (2013).

(Domestic Conference)

大竹淑恵: "理研における中性子イメージングへの取り組み", H23 年度理研シンポジウム「理研から発信する中性子利用の新たな展開-ものづくり産業利用に向けた小型中性子源の開発-」, 埼玉県　和光市, 11 月 (2011).

大竹淑恵: "中性子干渉イメージング", 材料の異方性と強度・変形特性および中性子研究の新しい動き, (中性子産業利用推進協議会、　金属組織研究会、日本鉄鋼協会), 東京, 11 月 (2011).

村野啓子, 石井理修, 青木慎也, 初田哲男: Future Prospects of Hadron Physics at J-PARC and Large Scale Computational Physics, (J-PARC センター、計算基礎科学連携拠点), 東海村, 2 月 (2012).

青木和也: "Development of Hadron Blind Detector", 2011 年度「多彩なフレーバーで探る新しいハドロン存在形態の包括的研究」領域研究会, (RCNP), 大阪, 2 月 (2012).

轟木貴人: "Two particle correlations with respect to higher harmonic plane in Au+Au 200 GeV collisions at RHIC-PHENIX", 日本物理学会第 67 回年次大会, (日本物理学会), 西宮, 3 月 (2012).

四日市悟: "J-PARC E16 実験", J-PARC 高運動量ビームラインの物理, (高エネルギー加速器研究機構 素粒子原子核研究所), KEK, つくば市, 5 月 (2012).

村野 啓子, 青木 慎也, 石井 理修, 初田 哲男, 土井 琢身, 池田

陽一, 井上貴史, 佐々木健志: “Spin-Orbit force in the NN system from Lattice QCD”, 新学術領域「素核宇宙融合」×「新ハドロン」クロスオーバー研究会ー多様な手法でせまるハドロン物理への挑戦ー, (名古屋大学), 日本, 7 月 (2012).

四日市悟: “核物質中での質量の変化と QCD での質量獲得機構”, 日本物理学会 2012 年秋季大会, (日本物理学会), 京都, 9 月 (2012).

小松雄哉: “J-PARC E16 実験のための GEM を用いた飛跡検出器システムの設計と開発”, 日本物理学会, (日本物理学会), 京都, 9 月 (2012).

日高義将, 福嶋健二: “Magnetic Catalysis vs Pions”, 日本物理学会, (日本物理学会), 京都産業大, 9 月 (2012).

浅野秀光: “RHIC-PHENIX 実験における重クォーク由来の電子の方位角異方性測定”, 日本物理学会, (日本物理学会), 京都産業大学, 9 月 (2012).

轟木貴人: “Higher harmonic flow and two particle correlations at RHIC”, Phenomenology and Experiments at RHIC and LHC, (名古屋大学), 名古屋, 9 月 (2012).

辻智也: “Neutral pion measurements in Pb-Pb collisions at $\sqrt{}$ sNN = 2.76 TeV with ALICE at the LHC”, 日本物理学会, (日本物理学会), 京都, 9 月 (2012).

轟木貴人: “QM2012 ソフト物理における実験結果の報告”, 第 22 回 Haevy Ion Cafe + 第 15 回 Heavy Ion Pub 合同研究会, (名古屋大学), 名古屋, 9 月 (2012).

中村克朗: “RHIC PHENIX 実験における偏極陽子陽子衝突での単電子生成の二重スピン非対称度測定”, 日本物理学会, (日本物理学会), 京都府京都市, 9–9 月 (2012).

蜂谷崇, PHENIX collaboration .: “PHENIX-VTX を用いたチャーム及びボトム起源の電子測定”, 日本物理学会第 68 回年次大会, (日本物理学会), 広島, 3 月 (2013).

二橋 聖弥, The PHENIX C.: “Measurement of Ks in Au+Au collisions at $\sqrt{s_{NN}}$ = 200GeV at RHIC-PHENIX”, 日本物理学会, (一般社団法人　日本物理学会), 東広島市　広島大学　東広島キャンパス, 3 月 (2013).

高橋智則: “E16 readout system”, 2012 年度「多彩なフレーバーで探る新しいハドロン存在形態の包括的研究」領域研究会, (新学術領域「多彩なフレーバーで探る新しいハドロン存在形態の包括的研究」総括班), 大学共同利用機関法人 高エネルギー加速器研究機構, 3 月 (2013).

荒巻陽紀: “Lead-glass calorimeter preparation status for J-PARC E16”, 2012 年度「多彩なフレーバーで探る新しいハドロン存在形態の包括的研究」領域研究会, (新学術領域「多彩なフレーバーで探る新しいハドロン存在形態の包括的研究」総括班), 大学共同利用機関法人 高エネルギー加速器研究機構, 3 月 (2013).

四日市悟: “project C01 summary”, 2012 年度「多彩なフレーバーで探る新しいハドロン存在形態の包括的研究」領域研究会, (新学術領域 「多彩なフレーバーで探る新しいハドロン存在形態の包括的研究」総括班), KEK, つくば, 3 月 (2013).

Advanced Meson Science Laboratory

Publications

[Journal]

(Original Papers) *Subject to Peer Review

Yamazaki T. and Akaishi Y.: "Emission spectra and invariant masses of Λ and p in the stopped-K^-NN absorption process in ^{4}He and ^{6}Li", Nucl. Phys. A **792**, 229–248 (2007). *

Yamazaki T. and Akaishi Y.: "Basic $\overline{K}$ nuclear cluster, K^-pp, and its enhanced formation in the $p + p \rightarrow K^+ + X$ reaction", Phys. Rev. C **76**, 045201-1–045201-16 (2007). *

Yamazaki T. and Akaishi Y.: "Super strong nuclear force caused by migrating $\overline{K}$ mesons - Revival of the Heitler-London-Heisenberg scheme in kaonic nuclear clusters", Proc. Jpn. Acad., Ser. B **83**, 144–150 (2007). *

Yamazaki T. and Akaishi Y.: "The Fundamental Kaonic Nuclear Cluster K^-pp", Prog. Theor. Phys. Suppl., No. 168, pp. 581–588 (2007). *

Okada K., Wada M., Nakamura T., Takamine A., Lioubimov V., Schury P. H., Ishida Y., Sonoda T., Ogawa M., Yamazaki Y., Kanai Y., Kojima T., Yoshida A., Kubo T., Katayama I., Ohtani S., Wollnik H., and Schuessler H. A.: "A precision measurement of the hyperfine structure of laser-cooled $^7Be^+$ ions priduced by projectile fragmentation", Phys. Rev. Lett. **101**, No. 212502, pp. 212502-1–212502-4 (2008). *

Akaishi Y., Yamazaki T., and Myint K. S.: "Kaonic nuclear systems $\overline{K}N$ and $\overline{K}NN$ as decaying states", Proc. Jpn. Acad., Ser. B **84**, 264–273 (2008). *

Jafar E., Akaishi Y., and Yamazaki T.: "Experimental confirmation of the $\Lambda(1405)$ ansatz from resonant formation of a K^-p quasi-bound state in K^- absorption by ^{3}He and ^{4}He", Phys. Lett. B **686**, 23–28 (2010). *

Yamazaki T., Maggiora M., Kienle P., Suzuki K., Amoroso A., Alexeev M., Balestra F., Bedfer Y., Bertini R., Bland L. C., Brenschede A., Brochard F., Bussa M. P., Choi S., Colantoni M. L., Dressler R., Dzemidzic M., Faivre J. -., Ferrero A., Foryciarz J., Fŕohlich I., Frolov V., Garfagnini R., Grasso A., Heinz S., Jacobs W. W., Ḱuhn W., Panzieri D., Pfaff H. -., Pontecorvo G., Popov A., Ritman J., Tchalyshev V., Vigdor S. E., Salabura P., and Sosio S.: "Indication of a Deeply Bound and Compact K^- pp State Formed in the $pp \rightarrow p\Lambda K^+$ Reaction at 2.85GeV", Phys. Rev. Lett. **PRL 104**, No. 132502, pp. 132502-1–132502-5 (2010). *

Bazzi M., Beer G., Bombelli L., Bragadireanu M., Cargnelli M., Corradi G., Curceanu C. O., D'Uffizi A., Fiorini C., Frizzi T., Ghio F., Girolami B., Guaraldo C., Hayano R., Iliescu M., Ishiwatari T., Iwasaki M., Kienle P., Levi Sandri P., Longoni A., Lucherini V., Marton J., Okada S., Pietreanu D., Ponta T., Rizzo A., Romero Vidal A., Scordo A., Shi H., Sirghi D., Sirghi F., Tatsuno H., Tudorache A., Tudorache V., Vazquez Doce O., Widmann E., and Zmeskal J.: "A new measurement of kaonic hydrogen X-rays", Phys. Lett. B **704**, No. 3, pp. 113–117 (2011). *

Yamazaki T., Esmaili J., and Akaishi Y.: "Resonant formation of $\Lambda(1405)$ by stopped-K^- absorption in the deuteron", Phys. Rev. C **83**, No. 055207, pp. 055207-1–055207-8 (2011). *

Yamazaki T., Hassanvand M., and Akaishi Y.: "Theoretical investigation of the formation of K^-K^- pp in high-energy proton-proton collisions", Phys. Rev. C **84**, No. 015207, pp. 015207-1–015207-8 (2011). *

Yamazaki T., Akaishi Y., and Hassanvand M.: "New way to produce dense double-antikaonic dibaryon system, $\overline{K}$ $\overline{K}$ N N, through $\Lambda(1405)$-doorway sticking in p + p collisions", Proc. Jpn. Acad., Ser. B **87**, 362–370 (2011). *

Yamazaki T., Kienle P., Maggiora M., Suzuki K., Alexeev M. V., Balestra F., Bedfer Y., Bertini R., Bland L. C., Brenschede A., Brochard F., Bussa M. P., Chiosso M., Choi S., Colantoni M. L., Dressler R., Dzemidzic M., Faivre J. -., Ferrero A., Ferrero L., Foryciarz J., Fŕohlich I., Frolov V., Garfagnini R., Grasso A., Heinz S., Jacobs W. W., Ḱuhn W., Maggiora A., Panzieri D., Pfaff H. -., Pontecorvo G., Popov A., Ritman J., Tchalyshev V., Tosello F., Vigdor S. E., and Zosi G.: "Formation of the S=-1 resonance X(2265) in the reaction $pp \rightarrow X + K^+$ at 2.50 and 2.85GeV", Eur. Phys. J. A **48**, No. 183, (2012). *

Hama Y., Hidaka Y., Tsitsishvili G., and Ezawa J.: "The study of Goldstone modes in $\nu = 2$ bilayer quantum Hall systems", Eur. Phys. J. B **85**, No. 368, pp. 1–13 (2012). *

Yamazaki T.: "Toward cold and dense antikaonic nuclear clusters", Hyperfine Interact. **211**, No. 1-3, pp. 69–75 (2012). *

Yagi E., Hayashi T., Yoshida T., Koike S., Higami N., Hirabayashi K., Takebayashi A., Matsuba H., and Ogiwara K.: "Lattice location and density distribution of hydrogen in beta1-V2H", J. Phys. Soc. Jpn. **81**, No. 4, pp. 044602-1–044602-14 (2012). *

iio m., Iwasaki M., ishimoto s., satou m., enomoto s., hashimoto t., suzuki s., and hayano r. s.: "Development of liquid 3He target for experimental studies of antikaon-nucleon interaction at J-PARC", Nuclear Instruments and Methods in Physics Research Section A **687**, 1–6 (2012). *

Bazzi M., Beer G., Bombelli L., Bragadireanu M., Cargnelli M., Curceanu C. O., D'Uffizi A., Fiorini C., Frizzi T., Ghio F., Guaraldo C., Hayano R., Iliescu M., Ishiwatari T., Iwasaki M., Kienle P., Levi Sandri P., Longoni A., Marton J., Okada S., Pietreanu D., Ponta T., Rizzo A., Romero Vidal A., Emanuele S., Scordo A., Shi H., Sirghi D., Sirghi F., Tatsuno H., Tudorache A., Tudorache V., Vazquez Doce O., Wunschek B., Widmann E., and Zmeskal J.: "Measurements of the

strong-interaction widths of the kaonic ^{3}He and ^{4}He $2p$ levels", Phys. Lett. B **714**, No. 1, pp. 40–43 (2012). ∗

Shimada K., Ueno H., Neyens G., Asahi K., Balabanski D. L., Daugas J., Depuydt M., De Rydt M., Gaudefroy L., Grevy S., Hasama Y., Ichikawa Y., Kameda D., Morel P., Nagatomo T., Perrot L., Stodel C., Thomas J., Utsuno Y., Vanderheijden W., Vermeulen N., Vingerhoets P., Yagi E., Yoshida K., and Yoshimi A.: "Erosion of $N = 20$ shell in ^{33}Al investigated through the ground-state electric quadrupole moment", Phys. Lett. B **714**, 246–250 (2012). ∗

Adachi T., Fujita Y., Bacher A. D., Berg G. P., Black T. C., De Frenne D., Foster ., Fujita H., Fujita K., Hatanaka K., Homma M., Jacobs E., Janecke J., Kanzaki Y., Katori K., Nakanishi K., Negret A., Otsuka T., Popescu L., Roberts D. A., Sakemi Y., Shimbara Y., Shimizu Y., Stephenson E. J., Tameshige Y., Tamii A., Uchida M., Ueno H., Yamanaka T., Yosoi M., and Zell K. O.: "High-resolution study of Gamow-Teller transitions via the ^{54}Fe(^{3}He,t)^{54}Co reaction", Phys. Rev. C **85**, 024308-1–024308-15 (2012). ∗

Hiyama E. and Kamimura M.: "Variational calculation of ^{4}He tetramer ground and excited states using a realistic pair potential", Physical Review A **85**, 022502–022516 (2012). ∗

Hiyama E. and Kamimura M.: "Linear correlations between ^{4}He trimer and tetramer energies calculated with various realistic ^{4}He potentials", Physical Review A **85**, 062505–062513 (2012). ∗

Tada T.: "Matrix model criticality and resonant tunneling", Prog. Theor. Phys. **128**, No. 2, (2012). ∗

Itahashi K., Fujioka H., Geissel H., Hirenzaki S., Itoh S., Jido D., Metag V., Nagahiro H., Nanova M., Nishi T., Okochi K., Outa H., Suzuki K., Tanaka Y., and Weick H.: "Feasibility Study of Observing eta' Mesic Nuclei with (p,d) Reaction", Prog. Theor. Phys. **128**, No. 3, pp. 601–613 (2012). ∗

Sakuma F., Itahashi K., Iwasaki M., Ma Y., Onishi H., Okada S., Outa H., Tomono D., Yamazaki T., and E15 c.: "The K1.8BR spectrometer system at J-PARC", Progress of Theoretical and Experimental Physics, p. 02B011 (2012). ∗

(Review)

多田司: "ニュートリノ", Radioisotopes **62**, No. 1, pp. 39–52 (2013).

(Others)

Piscicchia K., Bazzi M., Berucci C., Bragadireanu M., Cargnelli M., Clozza A., Curceanu C. O., D'Uffizi A., Ghio F., Guaraldo C., Iliescu M., Ishiwatari T., Levi Sandri P., Marton J., Okada S., Pietreanu D., Poli Lener M., Rizzo A., Romero Vidal A., Sbardella E., Scordo A., Sirghi D., Sirghi F., Tatsuno H., Vazquez Doce O., Widmann E., and Zmeskal J.: "Kaon-nuclei interaction studies at low energies (the AMADEUS experiment)", Nuovo Cimento C **34**, No. 6, pp. 21–22 (2011).

Curceanu C. O., Bazzi M., Beer G., Berucci C., Bombelli L., Bragadireanu M., Cargnelli M., Clozza A., Corradi G., D'Uffizi A., Fiorini C., Frizzi T., Ghio F., Girolami B., Guaraldo C., Hayano R., Iliescu M., Ishiwatari T., Iwasaki M., Kienle P., Levi Sandri P., Longoni A., Lucherini V., Marton J., Okada S., Pietreanu D., Piscicchia K., Poli Lener M., Ponta T., Rizzo A., Romero Vidal A., Sbardella E., Scordo A., Shi H., Sirghi D., Sirghi F., Tatsuno H., Tudorache A., Tudorache V., Vazquez Doce O., Widmann E., Zmeskal J., and Wunschek B.: "Low-energy kaon-nucleon/nuclei interaction studies at DAΦNE (SIDDHARTA and AMADEUS experiments)", Nuovo Cimento C **34**, No. 6, pp. 23–27 (2011).

Bazzi M., Beer G., Bombelli L., Bragadireanu M., Cargnelli M., Corradi G., Curceanu C. O., D'Uffizi A., Fiorini C., Frizzi T., Ghio F., Guaraldo C., Hayano R., Iliescu M., Ishiwatari T., Iwasaki M., Kienle P., Levi Sandri P., Longoni A., Lucherini V., Marton J., Okada S., Pietreanu D., Ponta T., Rizzo A., Romero Vidal A., Scordo A., Shi H., Sirghi D., Sirghi F., Tatsuno H., Tudorache A., Tudorache V., Vazquez Doce O., Widmann E., and Zmeskal J.: "Kaonic hydrogen X-ray measurement in SIDDHARTA", Nucl. Phys. A **881**, No. 1, pp. 88–97 (2012).

Marton J., Bazzi M., Beer G., Berucci C., Bombelli L., Bragadireanu M., Cargnelli M., Curceanu C. O., D'Uffizi A., Fiorini C., Frizzi T., Ghio F., Guaraldo C., Hayano R., Iliescu M., Ishiwatari T., Iwasaki M., Kienle P., Levi Sandri P., Longoni A., Okada S., Pietreanu D., Ponta T., Rizzo A., Romero Vidal A., Sbardella E., Scordo A., Shi H., Sirghi D., Sirghi F., Tatsuno H., Tudorache A., Tudorache V., Vazquez Doce O., Wunschek B., Widmann E., and Zmeskal J.: "X-ray spectroscopy of light kaonic atoms – new results and perspectives", Nucl. Phys. B **233**, 173–178 (2012).

Bhang H., Ajimura S., Aoki K., Banu A., Fukuda T., Hashimoto O., Hwang J. I., Kameoka S., Kang B. H., Kim E., Kim J., Kim M., Maruta T., Miura Y., Miyake Y., Nagae T., Nakamura M., Nakamura S. N., Noumi H., Okada S., Okayasu Y., Outa H., Park H., Saha P., Sato Y., Sekimoto M., Takahashi T., Tamura H., Tanida K., Toyoda A., Tshoo K., Tsukada K., Watanabe T., and Yim H.: "Three-Body $\Lambda NN \to nNN$ Nonmesonic Weak Decay Process of Λ Hypernuclei", Few Body Syst. **54**, No. 1-4, pp. 103–110 (2013).

斎藤徳人, 宮 洸治, Loutchev O. A., 和田智之, 岡村幸太郎, 大石裕, 横山幸司, 石田勝彦, 岩崎雅彦: "超低速ミュオン源実現のための新レーザー開発現状", 日本中間子科学誌めそん **36**, 43–49 (2012).

[Book・Proceedings]

(Original Papers) *Subject to Peer Review

斎藤徳人, 和田智之, 岡村幸太郎, 岩崎雅彦: "超低速ミューオ

ン発生のための高出力ミューオン・ライマン α レーザーの開発", レーザー学会第 427 回研究会報告　高機能固体レーザーとその応用　No.RTM-12-15, 吹田市, 2012–7, レーザー学会, 日本, pp. 49–54 (2012).

大石裕, 岡村幸太郎, 宮　洸治, 斎藤徳人, 岩崎雅彦, 和田智之: "超低速ミュオン励起用 Lyman- α 光源", レーザー学会第 436 回研究会報告, 宮崎市, 2012–12, レーザー学会, 宮崎市, pp. 13–18 (2012).

Oral Presentations

(International Conference etc.)

Itahashi K.: "First precision spectroscopy of pionic atoms at RI beam factory", MESON 2012, (IUPAP), Cracow, Poland, May (2012).

Miyake Y., Ikedo Y., Shimomura K., Strasser P., Kawamura N., Nishiyama K., Koda A., Fujimori H., Makimura S., Nakamura J., Nagatomo T., Kadono R., Torikai E., Iwasaki M., Wada S., Saito N., Okamura K., Yokoyama K., Ito T., and Higemoto W.: "Ultra Slow Muon Microscopy by Laser Resonant Ionization at J-PARC, MUSE", 6th Internatinal Conference of Laser Probing (LAP2012), (Institute of Physique Nucleaire ORSAY), Paris, France, June (2012).

Hama Y., Hidaka Y., Tsitsishvili G., and Ezawa J.: "The study of Goldstone modes in $\nu = 2$ bilayer quantum Hall systems", HMF-20, (CNRS/UFJ/UPS/INSA Grenoble High Magnetic Field Laboratory), Chamonix, France, July–July (2012).

Iwasaki M., Itahashi K., Ma Y., Okada S., Onishi H., Outa H., Sakuma F., Tomono D., Yamazaki T., and E15 c.: "Overview of Kaonic nuclear state search based on E151st engineering run", International Workshop on Strangeness Nuclear Physics 2012 (SNP12), Osaka Electro-Communication University, Aug. (2012).

enomoto s., Itahashi K., Iwasaki M., Ma Y., Okada S., Onishi H., Outa H., Sakuma F., Tomono D., Yamazaki T., and E15 c.: "Study of Kaonic nuclear bound system and Lambda(1405) at J-PARC K1.8BR", International Workshop on Strangeness Nuclear Physics 2012 (SNP12), Osaka Electro-Communication University, japan, Aug. (2012).

Iwasaki M.: "Overview of kaonic nuclear state search based on e15-1st engineering run", SNP12-International Workshop on Strangeness Nuclear Physics 2012, (the Foundation for International Exchange in Academic Research and Education of Osaka Electro-Communication University and the Inoue Foundation for Science), Neyagawa, Aug. (2012).

tokuda m., Itahashi K., Iwasaki M., Ma Y., Okada S., Onishi H., Outa H., Sakuma F., Tomono D., Yamazaki T., and E15 c.: "A search for deeply bound kaonic nuclear states at J-PARC", The 20th International IUPAP Conference on Few-Body Problems in Physics (FB20), fukuoka, Aug. (2012).

Itahashi K.: "First precision spectroscopy of pionic toms at RI beam factory", The 20th International IUPAP Conference on Few-Body Problems in Physics (FB20), (IUPAP), Fukuoka, Aug. (2012).

Suno H., Hiyama E., and Kamimura M.: "Theoretical study of triatomic systems involving helium atoms", Few-Body Problems in Physics, (International Union of Pure and Applied Physics), Fukuoka, Aug.–Aug. (2012).

sada y., Itahashi K., Iwasaki M., Ma Y., Okada S., Onishi H., Outa H., Sakuma F., Tomono D., Yamazaki T., and E15 c.: "A search for deeply-bound kaonic nuclear states at the J-PARC E15 experiment", The 11th International Conference on Hypernuclear and Strange Particle Physics (HYP2012), Barcelona, Spain, Sept. (2012).

Iwasaki M.: "From strange to charm in nuclei based on J-PARC e15-1st", The 2nd Korea-Japan Workshop on Nuclear and Hadron Physics at J-PARC, (Center of Korean J-PARC Users), Pusan, Korea, Sept. (2012).

Ohnishi S., Hiyama E., and Kamimura M.: "Four-body calculation of ${}^{6}_{\Lambda}$H hypernucleus", 11th International Conference on Hypernuclear and Strange Particle Physics (HYP2012), (ICCUB), Barcelona, Spain, Oct. (2012).

Iwasaki M.: "A kaonic nuclear state search,e15-1st,engineering run", ECT*, (ECT*), Trento, Italy, Oct. (2012).

Sakuma F.: "Search for double anti-kaon nuclear bound states at J-PARC", ECT*, New trends in the low-energy QCD in the strangeness sector: experimental and theoretical aspects, (ECT*), Trent, Italy, Oct. (2012).

Yagi E., Mori K., Sugi C., and Koike S.: "Site change of hydrogen in Nb on alloying with Mo or Ta atoms", International Symposium on Metal-Hydrogen Systems-Fundamentals and Applications, (Organizing Committee of MH2012), Kyoto, Oct. (2012).

Okada S.: "Application of microcalorimeter for ultra-high precision kaonic-atom x-ray spectroscopy", New trends in the low-energy QCD in the strangeness sector :experimental and theoretical aspects, (European Centre for Theoretical Studies in Nuclear Physics and Related Areas (ECT*)), Trento, Italy, Oct. (2012).

Ishii Y., Watanabe I., Miyazaki T., Pratt F. L., and Kato R.: "μSR study of a quantum spin liquid, $EtMe_3Sb[Pd(dmit)_2]_2$", International Symposium on Material Science Opened by Molecular Degree of Freedom(MDF2012), Miyazaki, Dec. (2012).

Abdel Jawad M., Watanabe I., Tajima N., Ishii Y., and Kato R.: "Critical exponents of The Mott transition in $EtMe_3P[Pd(dmit)_2]_2$", International Symposium on Material Science Opened by Molecular Degree of Freedom(MDF2012), Miyazaki, Dec. (2012).

Hama Y., Tsitsishvili G., and Ezawa J.: "Spin Josephson Supercurrent in the Canted Antiferromagnetic Phase", QS2C Theory Forum: International Symposium on "Strongly Correlated Quantum Science", (The University of Tokyo and RIKEN), Tokyo, Jan.–Jan. (2013).

Tada T.: “Matrix model criticality and resonant tunneling”, Bangkok workshop on gravity, gauge theory, matrices and strings, (Chulalongkorn University), Bangkok, Thailand, Jan.–Feb. (2013).

(Domestic Conference)

中村惇平, 横山幸司, 斎藤徳人, 岡村幸太郎, 和田智之, 牧村俊助, 三宅康博, Patrick S., 池戸豊, 長友傑, 下村浩一郎, 西山樟生: “J-PARC・MLF ミュオン U ラインにおける超低速ミュオン顕微鏡計画のためのレーザー光輸送・診断系の設計・製作の現状”, 日本物理学会第 67 回年次大会, (日本物理学会), 西宮市, 3 月 (2012).

和田智之, 斎藤徳人, 岩崎雅彦, 岡村幸太郎: “超低速ミューオン発生のための高出力ミューオン・ライマン α レーザーの開発,”, レーザー学会第 427 回研究会高機能固体レーザーとその応用」, (一般社団法人レーザー学会), 吹田市, 7 月 (2012).

岡村幸太郎, 大石裕, 宮　洸治, 斎藤徳人, 和田智之, 岩崎雅彦: “ミュオニウム励起用 Lyman- α 光源の開発：1062 nm ファイバーレーザーおよび広帯域 821 nm 種光光源”, 新学術領域研究「超低速ミュオン顕微鏡が拓く物質・生命・素粒子科学のフロンティア」第 2 回領域会議, (北海道大学、北海道大学大学院), 札幌市, 8 月 (2012).

大石裕, 岡村幸太郎, 宮　洸治, 斎藤徳人, Loutchev O. A., 岩崎雅彦, 和田智之: “ミュオニウム励起用 Lyman- α 光源の開発：1062.78 nm 全固体増幅器および波長変換”, 新学術領域研究「超低速ミュオン顕微鏡が拓く物質・生命・素粒子科学のフロンティア」第 2 回領域会議, (北海道大学、北海道大学大学院), 札幌市, 8 月 (2012).

宮　洸治, 斎藤徳人, 岡村幸太郎, 大石裕, Loutchev O. A., 横山幸司, 岩崎雅彦, 和田智之: “ミュオニウム励起用ライマン α 光源の開発：波長可変 820.65nm システム (OMEGA2) &ライマン α シフター”, 新学術領域研究「超低速ミュオン顕微鏡が拓く物質・生命・素粒子科学のフロンティア」第 2 回領域会議, (北海道大学、北海道大学大学院), 札幌市, 8 月 (2012).

中村惇平, 横山幸司, 大石裕, 斎藤徳人, 岡村幸太郎, 牧村俊介, 三宅康博, Strasser P., 池戸豊, 長友傑, 下村浩一郎, 宮　洸治, 和田智之, 幸田章宏, 河村成肇, 西山樟生: “超低速ミュオン顕微鏡計画のためのレーザー輸送系の設計・製作の現状”, 新学術領域研究「超低速ミュオン顕微鏡が拓く物質・生命・素粒子科学のフロンティア」第 2 回領域会議, (北海道大学、北海道大学大学院), 札幌市, 8 月 (2012).

八木栄一, 森克仁, 杉千花, 小池茂年: “合金元素添加による Nb 中の水素の格子内位置の変化”, 日本物理学会 2012 年秋季大会, (日本物理学会), 横浜, 9 月 (2012).

八木栄一: “核反応チャネリング法で金属中の水素の存在状態を観る”, 第 22 回格子欠陥フォーラム・励起ナノプロセス研究会・理研シンポジウム合同研究会 「材料科学のための欠陥制御・評価」, (格子欠陥シンポジウム、励起ナノプロセス研究会), 三浦市, 9 月 (2012).

榎本瞬, 板橋健太, 岩崎雅彦, Ma Y., 岡田信二, 大西宏明, 應田治彦, 佐久間史典, 友野大, 山崎敏光, E15 c.: “J-PARC K1.8BR で用いる 前方中性子検出器の性能評価”, 日本物理学会, 京都産業大学, 9 月 (2012).

橋本直, 板橋健太, 岩崎雅彦, Ma Y., 岡田信二, 大西宏明, 應田治彦, 佐久間史典, 友野大, 山崎敏光, E15 c.: “J-PARC K1.8BR ビームラインスペクトロメータの性能評価”, 日本物理学会, 京都産業大学, 9 月 (2012).

佐田優太, 板橋健太, 岩崎雅彦, Ma Y., 岡田信二, 大西宏明, 應田治彦, 佐久間史典, 友野大, 山崎敏光, E15 c.: “PARC E15 実験に用いる円筒形検出器群の COMMISSIONING(5)”, 日本物理学会, 京都産業大学, 9 月 (2012).

大石裕, 斎藤徳人, 岡村幸太郎, 月花智博, 宮　洸治, 岩崎雅彦, 和田智之: “超低速ミュオン生成用高輝度 Lyman- α 光源の開発”, 秋季第 73 回応用物理学会学術講演会, (応用物理学会), 松山市, 9 月 (2012).

中村惇平, 横山幸司, 斎藤徳人, 岡村幸太郎, 牧村俊介, 三宅康博, Strasser P., 池戸豊, 長友傑, 下村浩一郎, 宮　洸治, 和田智之, 幸田章宏, 河村成肇, 西山樟生: “J-PARC・MLF・超低速ミュオン顕微鏡計画のためのレーザー輸送系の設計・製作の現状”, 日本物理学会 2012 年秋季大会, 京都市, 9 月 (2012).

多田司: “Matrix model criticality and resonant tunneling”, 日本物理学会２０１２年秋季大会, (日本物理学会), 京都産業大学, 9 月 (2012).

濱祐介, 日高義将, Tsitsishvili G., 江澤潤一: “2 層 $\nu = 2$ 量子ホール系におけるゴールドストーンモードの研究”, 日本物理学会 2012 年秋季大会, (一般社団法人日本物理学会), 東京, 9–9 月 (2012).

大石裕, 岡村幸太郎, 宮　洸治, 斎藤徳人, 岩崎雅彦, 和田智之: “超低速ミュオン励起用 Lyman- α 光源”, レーザー学会第 436 回研究会「短波長量子ビーム発生と応用」, 宮崎市, 12 月 (2012).

岩崎雅彦: 原子核の状態方程式とハイパー核物理, (HPCI 分野 5、新学術領域「中性子星核物質」), 京都, 1 月 (2013).

宮　洸治, 斎藤徳人, 岡村幸太郎, 大石裕, Loutchev O. A., 横山幸司, 岩崎雅彦, 和田智之: “ミュオニウム励起用 Lyman-α 光源の開発：光パラメトリック発振および増幅による 820.65nm 光源”, レーザー学会学術講演会第 33 回年次大会, (レーザー学会), 姫路市, 1 月 (2013).

大石裕, 岡村幸太郎, 斎藤徳人, 宮　洸治, Loutchev O. A., 横山幸司, 岩崎雅彦, 和田智之: “ミュオニウム励起用 Lyman- α 光源の開発：1062.78 nm 全個体増幅器および 212.55nm 波長変換”, レーザー学会学術講演会第 33 回年次大会, (一般社団法人レーザー学会), 姫路市, 1 月 (2013).

岡村幸太郎, 斎藤徳人, 大石裕, 宮　洸治, Loutchev O. A., 横山幸司, 岩崎雅彦, 和田智之: “ミュオニウム励起用 Lyman- α 光源の開発：1062nm 及び広帯域 821nm 種光光源”, レーザー学会学術講演会第 33 回年次大会, (一般社団法人レーザー学会), 姫路市, 1 月 (2013).

岡田信二: “DAFNE 加速器における K 中間子水素原子 X 線精密分光実験”, 第 9 回「ハドロン・スクエア」, 和光, 2 月 (2013).

岡田信二: “K 中間子原子 X 線超精密分光実験に向けたマイクロカロリメータの応用”, 日本物理学会第 68 回年次大会, (日本物理学会), 広島, 3 月 (2013).

佐田優太, 板橋健太, 岩崎雅彦, Ma Y., 岡田信二, 大西宏明, 應田治彦, 佐久間史典, 友野大, 山崎敏光, E15 c.: “J-PARC E15 実験における K 中間子原子核の探索”, 日本物理学会, 広島大学, 3 月 (2013).

中村 惇平, 横山 幸司, 大石 裕, 斎藤 徳人, 岡村 幸太郎, 牧村俊介, 三宅康博, 友野大, 長友傑, Strasser P., 池戸豊, 下村浩一郎, 宮　洸治, 和田智之, 河村成肇, 幸田章宏, 西山樟生: “J-PARC・MLF・超低速ミュオン顕微鏡計画のためのレーザー輸送系の完成”, 日本物理学会 2013 年春季大会, (日本物理学会), 東広島市, 3 月 (2013).

RIKEN BNL Research Center

Oral Presentations

(International Conference etc.)

Samios N. P.: "RBRC Scientific Review Committee Meeting", RIKEN BNL Research Center Workshop, (RBRC), BNL, Upton, New York, USA, Nov.–Nov. (2012).

Theory Group

Publications

[Journal]

(Original Papers) *Subject to Peer Review

Avsar E., Stasto A. M., Triantafyllopoulos D. N., and Zaslavsky D.: "Next-to-leading and resummed BFKL evolution with saturation boundary", J. High Energy Phys. **2011**, No. 10, pp. 138-1–138-36 (2011). *

Blaizot J., Gelis F., Liao J., McLerran L., and Venugopalan R.: "Bose-Einstein condensation and thermalization of the quark-gluon plasma", Nucl. Phys. A **873**, No. 1, pp. 68–80 (2011). *

D'Alesio U., Gamberg L., Kang Z., Murgia F., and Pisano C.: "Testing the Process Dependence of the Sivers Function Via Hadron Distributions Inside a Jet", Phys. Lett. B **704**, No. 5, pp. 637–640 (2011). *

Sun P., Xiao B., and Yuan F.: "Gluon Distribution Functions and Higgs Boson Production at Moderate Transverse Momentum", Phys. Rev. D **84**, No. 9, pp. 094005-1–094005-7 (2011). *

Berger J. and Stasto A. M.: "Small-x Nonlinear Evolution with Impact Parameter and the Structure Function Data", Phys. Rev. D **84**, No. 9, pp. 094022-1–094022-17 (2011). *

Kang Z., Xiao B., and Yuan F.: "QCD Resummation for Single Spin Asymmetries", Phys. Rev. Lett. **107**, No. 15, pp. 152002-1–152002-5 (2011). *

Bezrukov F., Kalmykov M. Y., Kniehl B. A., and Shaposhnikov M.: "Higgs boson mass and new physics", J. High Energy Phys. **2012**, No. 140, pp. 1–35 (2012). *

Lunardini C. and Tamborra I.: "Diffuse supernova neutrinos: oscillation effects, stellar cooling and progenitor mass dependence", Journal of Cosmology and Astroparticle Physics **2012**, No. 7, pp. 1–19 (2012). *

Dumitru A. and Petreska E.: "Initial conditions for dipole evolution beyond the McLerran-Venugopalan model", Nucl. Phys. A **879**, 59–76 (2012). *

Albacete J. L., Dumitru A., Fujii H., and Nara Y.: "CGC predictions for p + Pb collisions at the LHC", Nucl. Phys. A **897**, No. 2013, pp. 1–27 (2012). *

Kojo T.: "Chiral Symmetry in Quarkyonic Matter", Phys. At. Nucl. **75**, No. 5, pp. 632–636 (2012). *

Bzdak A. and Skokov V.: "Event-by-event fluctuations of magnetic and electric fields in heavy ion collisions", Phys. Lett. B **710**, No. 1, pp. 171–174 (2012). *

Bialas A., Bzdak A., and Zalewski K.: "Hidden asymmetry and long range rapidity correlations", Phys. Lett. B **710**, No. 2, pp. 332–334 (2012). *

Zhang X. and Liao J.: "Jet tomography of harmonic fluctuations in the initial condition of heavy ion collisions", Phys. Lett. B **713**, No. 1, pp. 35–40 (2012). *

McLerran L., Pisarski R. D., and Skokov V.: "Electroweak instantons, axions, and the cosmological constant", Phys. Lett. B **713**, No. 3, pp. 301–303 (2012). *

Bezrukov F. and Gorbunov D. S.: "Distinguishing between R2-inflation and Higgs-inflation", Phys. Lett. B **713**, No. 4-5, pp. 365–368 (2012). *

Stasto A. M., Xiao B., and Yuan F.: "Back-to-back correlations of di-hadrons in dAu collisions at RHIC", Phys. Lett. B **716**, No. 3-5, pp. 430–434 (2012). *

Bloczynski J., Huang X., Zhang X., and Liao J.: "Azimuthally fluctuating magnetic field and its impacts on observables in heavy-ion collisions", Phys. Lett. B **718**, No. 4-5, pp. 1529–1535 (2012). *

Dumitru A. and Nara Y.: "Scaling of fluctuations in pp and pA collisions, and eccentricities in relativistic heavy-ion collisions", Phys. Rev. C **85**, No. 3, pp. 034907-1–034907-5 (2012). *

Bzdak A.: "Suppression of elliptic-flow-induced correlations in an observable of possible local parity violation", Phys. Rev. C **85**, No. 4, pp. 044919-1–044919-4 (2012). *

Dumitru A., Kharzeev D. E., Levin E. M., and Nara Y.: "Gluon saturation in pA collisions at energies available at the CERN Large Hadron Collider: Predictions for hadron multiplicities", Phys. Rev. C **85**, No. 4, pp. 044920-1–044920-6 (2012). *

Bzdak A.: "Symmetric Correlations as seen in central Au + Au collisions at square-root S = 200A GeV", Phys. Rev. C **85**, No. 5, pp. 051901-1–051901-4 (2012). *

Bzdak A. and Koch V.: "Acceptance corrections to net baryon and net charge cumulants", Phys. Rev. C **86**, No. 4, pp. 044904-1–044904-7 (2012). *

Keehn J. G. and Lunardini C.: "Neutrinos from failed supernovae at future water and liquid argon detectors", Phys. Rev. D **85**, No. 4, pp. 043011-1–043011-16 (2012). *

Kang Z., Vitev I., and Xing H.: "Dihadron momentum imbalance and correlations in d+Au collisions", Phys. Rev. D **85**, No. 5, pp. 054024-1–054024-11 (2012). *

Kang Z. and Prokudin A.: "Global fitting of single spin asymmetry: An attempt", Phys. Rev. D **85**, No. 7, pp. 074008-1–074008-9 (2012). *

Kashiwa K., Pisarski R. D., and Skokov V. V.: "Critical endpoint for deconfinement in matrix and other effective models", Phys. Rev. D **85**, No. 11, pp. 114029-1–114029-7 (2012). *

Pisarski R. D. and Skokov V. V.: "Gross-Witten-Wadia transition in a matrix model of deconfinement", Phys. Rev. D **86**, No. 8, pp. 081701-1–081701-6 (2012). *

Lunardini C. and Sabancilar E.: "Cosmic strings as emitters of extremely high energy neutrinos", Phys. Rev. D **86**, No. 8, pp. 085008-1–085008-13 (2012). *

Alberte L. and Bezrukov F.: "Semiclassical calculation of multiparticle scattering cross sections in classicalizing theories", Phys. Rev. D **86**, No. 10, pp. 105008-1–105008-9 (2012). *

Dumitru A., Guo Y., Hidaka Y., Korthals Altes C. P., and Pisarski R. D.: "Effective matrix model for deconfinement in pure gauge theories", Phys. Rev. D **86**, No. 10, pp. 105017-1–105017-35 (2012). ∗

Kang Z., Mantry S., and Qiu J.: "N-jet event shapes as probes of nuclear dynamics", Phys. Rev. D **86**, No. 11, pp. 114011-1–114011-5 (2012). ∗

Lunardini C. and Razzaque S.: "High Energy Neutrinos from the Fermi Bubbles", Phys. Rev. Lett. **108**, No. 22, pp. 221102-1–221102-4 (2012). ∗

Liao J. and Shuryak E. V.: "Effect of Light Fermions on the Confinement Transition in QCD-Like Theories", Phys. Rev. Lett. **109**, No. 15, pp. 152001-1–152001-5 (2012). ∗

Dumitru A.: "Phenomenology of high gluon density QCD and heavy-ion physics at ISMD 2011: x smaller than ever!", Prog. Theor. Phys. **2012**, No. 193, pp. 348–357 (2012). ∗

Mocsy A.: "Viscosity versus Causality", Prog. Theor. Phys. Suppl. **2012**, No. 193, pp. 331–334 (2012). ∗

Bzdak A., Koch V., and Skokov V.: "Baryon number conservation and the cumulants of the net proton distribution", Phys. Rev. C **87**, No. 1, pp. 014901-1–014901-6 (2013). ∗

Kashiwa K., Sasaki T., Kouno H., and Yahiro M.: "Two-color QCD at imaginary chemical potential and its impact on real chemical potential", Phys. Rev. D **87**, No. 1, pp. 016015-1–016015-9 (2013). ∗

[Book · Proceedings]

(Original Papers) *Subject to Peer Review

Kojo T.: "INTERWEAVING CHIRAL SPIRALS AT FINITE QUARK DENSITY", Acta Physica Polonica B Proceedings Supplement, Wroclaw, Poland, 2011–5〜5, Jagiellonian University, Krakow, pp. 781–790 (2012). ∗

Oral Presentations

(International Conference etc.)

Kashiwa K.: "Extruction of nontrivial correlation between chiral and deconfinement transitions from two-color QCD at imaginary chemical potential", Quark Matter 2012, (Brookhaven National Laboratory), Washington, DC, USA, Aug. (2012).

Kashiwa K. and Fukushima K.: "Polyakov loop and QCD thermodynamics from the Landau gauge gluon and ghost propagators", Xth Quark Confinement and the Hadron Spectrum, Munich, Germany, Oct. (2012).

Computing Group

Publications

[Journal]

(Original Papers) *Subject to Peer Review

Namekawa Y., Aoki S., Ishikawa K., Ishizuka N., Izubuchi T., Kanaya K., Kuramashi Y., Okawa M., Taniguchi Y., Ukawa A., Ukita N., and Yoshie T.: "Charm Quark System at the Physical Point of 2+1 Flavor Lattice QCD", Phys. Rev. D **84**, No. 7, pp. 074505-1–074505-11 (2011). *

Blum T., Boyle P. A., Christ N. H., Garron N., Goode E., Izubuchi T., Lehner C., Liu Q., Mawhinney R. D., Sachrajda C. T., Soni A., Sturm C., Yin H., and Zhou R.: "K to pi pi decay amplitudes from lattice QCD", Phys. Rev. D **84**, No. 11, pp. 114503-1–114503-22 (2011). *

Lin C. D., Ogawa K., Ohki H., and Shintani E.: "Lattice study of infrared behaviour in SU(3) gauge theory with twelve massless flavours", J. High Energy Phys. **2012**, No. 096, pp. 1–37 (2012). *

Tiburzi B.: "Hadronic parity violation at next-to-leading order", Phys. Rev. D **85**, No. 5, pp. 054020-1–054020-16 (2012). *

Tiburzi B.: "Isotensor hadronic parity violation", Phys. Rev. D **86**, No. 9, pp. 097501-1–097501-5 (2012). *

Aoki Y., Christ N. H., Flynn J. M., Izubuchi T., Lehner C., Li M., Peng H., Soni A., Van de Water R. S., and Witzel O.: "Nonperturbative tuning of an improved relativistic heavy-quark action with application to bottom spectroscopy", Phys. Rev. D **86**, No. 11, pp. 116003-1–116003-28 (2012). *

Blum T., Boyle P. A., Christ N. H., Garron N., Goode E., Izubuchi T., Jung C., Kelly C., Lehner C., Lightman M., Liu Q., Lytle A. T., Mawhinney R. D., Sachrajda C. T., Soni A., and Sturm C.: "K to (pi pi)(I=2) Decay Amplitude from Lattice QCD", Phys. Rev. Lett. **108**, No. 14, pp. 141601-1–141601-5 (2012). *

Ishikawa T., Blum T., Hayakawa M., Izubuchi T., Jung C., and Zhou R.: "Full QED+QCD Low-Energy Constants through Reweighting", Phys. Rev. Lett. **109**, No. 7, pp. 072002-1–072002-5 (2012). *

Feng X., Aoki S., Fukaya H., Hashimoto S., Kaneko T., Noaki J., and Shintani E.: "Two-Photon Decay of the Neutral Pion in Lattice QCD", Phys. Rev. Lett. **109**, No. 18, pp. 182001-1–182001-5 (2012). *

Lin M. and Ohta S.: "Finite-size scaling in nucleon axial charge from 2+1-flavor DWF lattice QCD", Proceedings of Science **Lattice 2012**, No. 171, pp. 1–7 (2012). *

Experimental Group

Publications

[Journal]

(Original Papers) *Subject to Peer Review

Bathe S.: "PHENIX highlights", J. Phys. G **38, 2011**, No. 124001, pp. 1–7 (2011). *

Oral Presentations

(International Conference etc.)

Takahara A.: "J/psi Photoproduction in ultra-peripheral Au+Au collisions measured by RHIC-PHENIX", XX International Workshop on Deep-Inelastic Scattering and Related Subjects (DIS2012), (University of Bonn), Bonn, Germany, Mar. (2012).

Kuboki H., Okuno H., Hershcovitch A., Dantsuka T., Hasebe H., Ikegami K., Imao H., Kamigaito O., Kase M., Maie T., Nakagawa T., and Yano Y.: "Development of Plasma Window for gas charge strippers at RIKEN RIBF", 26th World Conference of the International Nuclear Target Development Society, (Johannes Gutenberg-Universitat and GSI), Mainz, Germany, Aug. (2012).

Komatsu Y., Aoki K., Enyo H., Aramaki Y., Kanno K., Kawama D., Masumoto S., Nakai W., Obara Y., Ozawa K., Sekimoto M., Shibukawa T., Takahashi T., Watanabe Y., and Yokkaichi S.: "Development of GEM Tracker for J-PARC E16 experiment", 13th Vienna conference of instrumentation, (Institute of High Energy Physics (HEPHY) of the Austrian Academy of Sciences), Vienna, Austria, Feb.–Feb. (2013).

Radioactive Isotope Physics Laboratory

Publications

[Journal]

(Original Papers) *Subject to Peer Review

Clark R. M., Kaji D., Morimoto K., and Watanabe H.: "High-K multi-quasiparticle states in ^{254}No", Phys. Lett. B **690**, 19 (2010). *

Sakaguchi S., Iseri Y., Uesaka T., Tanifuji M., Amos K., Aoi N., Hashimoto Y., Hiyama E., Ichikawa M., Ichikawa Y., Ishikawa S., Itoh K., Itoh M., Iwasaki H., Karataglidis S., Kawabata T., Kawahara T., Kuboki H., Maeda Y., Matsuo R., Nakao T., Okamura H., Sakai H., Sasamoto Y., Sasano M., Sato Y., Sakaguchi-Sekiguchi K., Shinohara M., Suda K., Suzuki D., Takahashi Y., Tamii A., Wakui T., Yako K., Yamaguchi M., and Yamamoto Y.: "Analyzing power in elastic scattering of 6He from a polarized proton target at 71 MeV/nucleon", Phys. Rev. C **84**, No. 024604, pp. 024604-1–024604-17 (2011). *

Nishimura S.: "Beta-gamma spectroscopy at RIBF", Progress of Theoretical and Experimental Physics **03**, No. 03C006, (2011). *

Ichikawa Y., Ueno H., Ishii Y., Furukawa T., Yoshimi A., Kameda D., Watanabe H., Aoi N., Asahi K., Balabanski D. L., Chevrier R., Daugas J., Fukuda N., Georgiev G., Hayashi H., Iijima H., Inabe N., Inoue T., Ishihara M., Kubo T., Nanao T., Ohnishi T., Suzuki K., Tsuchiya M., Takeda H., and Rajabali M. M.: "Production of spin-aligned RI beam via two-step fragmentation with dispersion matching", J. Phys.: Conf. Ser. **381**, 012090-1–012090-5 (2012). *

Ichikawa Y., Ueno H., Ishii Y., Furukawa T., Yoshimi A., Kameda D., Watanabe H., Aoi N., Asahi K., Balabanski D. L., Chevrier R., Daugas J., Fukuda N., Georgiev G., Hayashi H., Iijima H., Inabe N., Inoue T., Ishihara M., Kubo T., Nanao T., Ohnishi T., Suzuki K., Tsuchiya M., Takeda H., and Rajabali M. M.: "Production of spin-controlled rare isotope beams", Nat. Phys. **8**, No. 12, pp. 918–922 (2012). *

Sonoda T., Wada M., Tomita H., Sakamoto C., Takatsuka T., Furukawa T., Iimura H., Ito Y., Kubo T., Matsuo Y., Mita H., Naimi S., Nakamura S., Noto T., Schury P. H., Wakui T., Miyatake H., Jeong S., Watanabe Y., Isiyama H., Okada K., and Takamine A.: "Development of a resonant laser ionization gas cell for high-energy, short-lived nuclei", Nucl. Instrum. Methods Phys. Res. B **295**, No. 1, (2012). *

Nakano Y., Suda S., Hatakeyama A., Nakai Y., Komaki K., Takada E., Murakami T., and Azuma T.: "Selective production of the doubly excited 2 p2 (1D) state in He-like Ar16+ ions by esonant coherent excitation", Phys. Rev. A **85**, 020701-1–020701-4 (2012). *

Chevrier R., Daugas J., Gaudefroy L., Ichikawa Y., Ueno H., Hass M., Cottenier S., Aoi N., Asahi K., Balabanski D. L., Fukuda N., Furukawa T., Georgiev G., Hayashi H., Iijima H., Inabe N., Inoue T., Ishihara M., Ishii Y., Kameda D., Kubo T., Nanao T., Neyens G., Ohnishi T., Rajabali M. M., Suzuki K., Takeda H., Tsuchiya M., Vermeulen N., Watanabe H., and Yoshimi A.: "Is the $7/21^-$ isomer state of ^{43}S spherical?", Phys. Rev. Lett. **108**, 162501-1–162501-5 (2012). *

Inoue T., Nanao T., Chikamori M., Furukawa T., Yoshimi A., Ichikawa Y., Hayashi H., Tsuchiya M., Miyatake H., Ishii Y., Yoshida N., Shirai H., Uchida M., Ueno H., Matsuo Y., Fukuyama T., and Asahi K.: "^{129}Xe atomic EDM search with nuclear spin maser technique", Proceedings of 5th International Workshop on "Fundamental Physics Using Atoms 2011", pp. 64–68 (2012).

Sato H., Kubo T., Yano Y., Kusaka K., Ohnishi J., Yoneda K., Shimizu Y., Motobayashi T., Otsu H., Isobe T., Kobayashi T., Sekiguchi K., Nakamura T., Kondo Y., Togano Y., Murakami T., Tsuchihashi T., Orikasa T., and Maeta K.: "Superconducting dipole magnet for SAMURAI spectrometer", IEEE Trans. Appl. Supercond. **23**, No. 3, pp. 4500308-1–4500308-8 (2013). *

Oral Presentations

(International Conference etc.)

Sonoda T., Wada M., Tomita H., Sakamoto C., Ito Y., Schuessler H. A., Takamine A., Kubo T., Matsuo Y., Shinozuka T., Wakui T., Nakamura S., Furukawa T., Okada K., Kudryavtsev Y., Mark H., Van Duppen P., Miyatake H., Ishiyama H., Imai N., Watanabe Y., Hirayama Y., and Chon J.: "Development of the resonance ionization laser ion source for parasitic RI-beam production and in-gas-cell/jet laser spectroscopy at SLOWRI RIKEN", Advances in Radioactive Isotope Science (ARIS - 2011), (K.U.Leuven), Leuven, Belgium, May–May (2011).

Kobayashi T. and Matsuo Y.: "Production of metal cluster cations by femtosecond laser ablation of aluminum nitride", 28th Symposium on Chemical Kinetics and Dynamics, (Oraganizing committee of the Symposium on Chemical Kinetics and Dynamics), Kasuga, June (2012).

Ichikawa Y., Ueno H., Ishii Y., Furukawa T., Yoshimi A., Kameda D., Watanabe H., Aoi N., Asahi K., Balabanski D. L., Chevrier R., Daugas J., Fukuda N., Georgiev G., Hayashi H., Iijima H., Inabe N., Inoue T., Ishihara M., Kubo T., Nanao T., Ohnishi T., Suzuki K., Tsuchiya M., Takeda H., and Rajabali M. M.: "Spin-aligned RI beams and nuclear moment measurements at RIBF", RIBF Users Meeting 2012, Wako, Saitama, June (2012).

Nakai Y., Hidaka H., Watanabe N., and Kojima T.: "An equipment based on an ion drift-tube with selected-ion injection for studies of ionic cluster formation via thermochemical processes", 16th International Symposium on Small Particles and Inorganic Clusters (ISSPIC XVI), (Katholieke Universiteit Leuven), Leuven, Belgium, July (2012).

Ichikawa Y., Ueno H., Ishii Y., Furukawa T., Yoshimi A., Kameda D., Watanabe H., Aoi N., Asahi K., Balabanski D. L., Chevrier R., Daugas J., Fukuda N., Georgiev G., Hayashi H., Iijima H., Inabe N., Inoue T., Ishihara M., Kubo T., Nanao T., Ohnishi T., Suzuki K., Tsuchiya M., Takeda H., and Rajabali M. M.: "Spin manipulation of RI beams from two-stage projectile fragmentation reaction", Advanced Studies Institute on Symmetries and Spin (Spin-Praha-2012), (Charles University), Prague, Czech, July (2012).

Nakano Y., Hatakeyama A., Nakai Y., Komaki K., Takada E., Murakami T., and Azuma T.: "Anisotropy of Ly-a1 and Ly-a2 x-rays from H-like Ar17+, Fe25+, and Kr35+ associated with resonant coherent excitation", 16th International Conferences on the Physics of Highly Charged Ions, Heidelberg, Germany, Sept. (2012).

Ichikawa Y., Chikamori M., Inoue T., Furukawa T., Yoshimi A., Ohtomo Y., Hikota E., Suzuki T., Suzuki K., Nanao T., Miyatake H., Tsuchiya M., Yoshida N., Shirai H., Ino T., Ueno H., Matsuo Y., Fukuyama T., and Asahi K.: "Experimental study of EDM in ^{129}Xe atom using nuclear-spin maser", 6th International Workshop on Fundamental Physics Using Atoms 2012, (Tohoku Iniversity), Sendai, Sept. (2012).

Asahi K., Ichikawa Y., Chikamori M., Inoue T., Furukawa T., Yoshimi A., Ohtomo Y., Suzuki K., Nanao T., Miyatake H., Tsuchiya M., Yoshida N., Shirai H., Matsuo Y., Ueno H., and Fukuyama T.: "Experimental search for EDM in a diamagnetic atom ^{129}Xe with spin oscillator technics", Advanced Studies Institute on Symmetries and Spin (Spin-Praha-2012), (Charles University), Prague, Czech, Sept. (2012).

Asahi K., Ichikawa Y., Chikamori M., Inoue T., Furukawa T., Yoshimi A., Ohtomo Y., Suzuki K., Nanao T., Miyatake H., Tsuchiya M., Yoshida N., Shirai H., Matsuo Y., Ueno H., and Fukuyama T.: "Search for Electric Dipole Moment in ^{129}Xe Atom sing a Nuclear Spin Oscillator", The 20th International Symposium on Spin Physics (SPIN2012), (JINR, Dubna, Russia), Dubna, Russia, Sept. (2012).

Ichikawa Y., Ueno H., Ishii Y., Furukawa T., Yoshimi A., Kameda D., Watanabe H., Aoi N., Asahi K., Balabanski D. L., Chevrier R., Daugas J., Fukuda N., Georgiev G., Hayashi H., Iijima H., Inabe N., Inoue T., Ishihara M., Kubo T., Nanao T., Ohnishi T., Suzuki K., Tsuchiya M., Takeda H., and Rajabali M. M.: "Novel method for the production of spin-aligned RI beams in projectile fragmentation with the dispersion matching technique", The 4th Joint Meeting of the 16th International Conference on Hyperfine Interactions and the 20th International Symposium on Nuclear Quadrupole Interactions (HFI/NQI 2012), (China Institute of Atomic Energy), Beijing, China, Sept. (2012).

Inoue T., Furukawa T., Yoshimi A., Ichikawa Y., Chikamori M., Ohtomo Y., Tsuchiya M., Yoshida N., Shirai H., Uchida M., Suzuki K., Nanao T., Miyatake H., Ueno H., Matsuo Y., Fukuyama T., and Asahi K.: "Nuclear spin maser and experimental search for ^{129}Xe atomic EDM", The 4th Joint Meeting of the 16th International Conference on Hyperfine Interactions and the 20th International Symposium on Nuclear Quadrupole Interactions (HFI/NQI 2012), (China Institute of Atomic Energy), Beijing, China, Sept. (2012).

Sato H., Kubo T., Yano Y., Kusaka K., Ohnishi J., Yoneda K., Shimizu Y., Motobayashi T., Otsu H., Isobe T., Kobayashi T., Sekiguchi K., Nakamura T., Kondo Y., Togano Y., Murakami T., Tsuchihashi T., Orikasa T., and Maeta K.: "Superconducting dipole magnet for SAMURAI spectrometer", Applied Superconductivity Conference (ASC2012), (ASC), Portland, USA, Oct. (2012).

Furukawa T., Wakui T., Yang X., Fujita T., Imamura K., Yamaguchi Y., Tetsuka H., Tsutsui Y., Mitsuya Y., Ichikawa Y., Ishibashi Y., Yoshida N., Shirai H., Ebara Y., Hayasaka M., Arai S., Muramoto S., Hatakeyama A., Wada M., Sonoda T., Ito Y., Kobayashi T., Nishimura S., Nishimura M., Kondo Y., Yoneda K., Kubono S., Ohshiro Y., Ueno H., Shinozuka T., Shimoda T., Asahi K., and Matsuo Y.: "A Novel Nuclear Laser Spectroscopy Method using Superfluid Helium for the Measurement of Spins and Moments of Exotic Nuclei", 16th International Conference on Electromagnetic Isotope Separators and Techniques Related to their Applications (EMIS2012), Matsue, Dec. (2012).

Yang X., Furukawa T., Imamura K., Tetsuka H., Yamaguchi Y., Tsutsui Y., Fujita T., Mitsuya Y., Ichikawa Y., Ishibashi Y., Yoshida N., Shirai H., Wakui T., Kobayashi T., Hatakeyama A., Wada M., Ueno H., Shimoda T., Asahi K., and Matsuo Y.: "Control of the stopping position of unstable Rb beam in superfluid helium (He II) for nuclear laser spectroscopy of RI atoms", 16th International Conference on Electromagnetic Isotope Separators and Techniques Related to their Applications (EMIS2012), Matsue, Dec. (2012).

Imamura K., Furukawa T., Wakui T., Yang X., Yamaguchi Y., Tetsuka H., Mitsuya Y., Tsutsui Y., Fujita T., Ebara Y., Hayasaka M., Arai S., Muramoto S., Ichikawa Y., Ishibashi Y., Yoshida N., Shirai H., Hatakeyama A., Wada M., Sonoda T., Ito Y., Odashima H., Kobayashi T., Ueno H., Shimoda T., Asahi K., and Matsuo Y.: "Development of a helium cryostat for laser spectroscopy of atoms with unstable nuclei in superfluid helium", 16th International Conference on Electromagnetic Isotope Separators and Techniques Related to their Applications (EMIS2012), Matsue, Dec. (2012).

Ichikawa Y., Ueno H., Ishii Y., Furukawa T., Yoshimi A., Kameda D., Watanabe H., Aoi N., Asahi K., Balabanski D. L., Chevrier R., Daugas J., Fukuda N., Georgiev G., Hayashi H., Iijima H., Inabe N., Inoue T., Ishihara M., Kubo T., Nanao T., Ohnishi T., Suzuki K., Tsuchiya

M., Takeda H., and Rajabali M. M.: "Spin-aligned RI beams via two-step fragmentation reactions", 16th International Conference on Electromagnetic Isotope Separators and Techniques Related to their Applications (EMIS2012), (RIKEN Nishina Center, KEK, Institute of Modern Physics (China)), Matsue, Dec. (2012).

Yoshida N., Ueno H., Yoshimi A., Ishibashi Y., Ichikawa Y., Abe Y., Asahi K., Chikamori M., Fujita T., Furukawa T., Hikota E., Nagae D., Ohtomo Y., Saito Y., Shirai H., Suzuki T., and Yang X.: "Development of a new device control system for β-NMR experiments", The 16th IUPAP International Conference on Electromagnetic Isotope Separators and Techniques Related to Their Applications (EMIS2012), Matsue, Dec. (2012).

Ishibashi Y., Yoshida N., Ueno H., Yoshimi A., Ichikawa Y., Abe Y., Asahi K., Chikamori M., Fujita T., Furukawa T., Hikota E., Nagae D., Ohtomo Y., Saito Y., Shirai H., Suzuki T., Yang X., and Sakamoto N.: "Development of an adiabatic field rotation system to measure spin polarization of unstable nuclei", The 16th IUPAP International Conference on Electromagnetic Isotope Separators and Techniques Related to Their Applications (EMIS2012), Matsue, Dec. (2012).

Matsuo Y.: "Spin polarization of atoms produced by laser excitation and its applications to atomic and nuclear physics", Workshop on Low-Energy Radioactive Isotope Beam (RIB) Production by In-Gas Laser Ionization for Decay Spectroscopy at RIKEN, Wako, Dec. (2012).

Chikamori M., Ichikawa Y., Ohtomo Y., Hikota E., Sakamoto Y., Suzuki T., Bidinosti C. P., Inoue T., Furukawa T., Yoshimi A., Suzuki K., Nanao T., Miyatake H., Tsuchiya M., Yoshida N., Shirai H., Ino T., Ueno H., Matsuo Y., Fukuyama T., and Asahi K.: "^{3}He comagnetometer in ^{129}Xe active spin maser for EDM measurement", Program on CP violation in Elementary Particles and Composite Systems, (International CEntre for Theoretical Sciences), Mahabaleshwar, India, Feb. (2013).

Ichikawa Y., Chikamori M., Ohtomo Y., Hikota E., Sakamoto Y., Suzuki T., Bidinosti C. P., Inoue T., Furukawa T., Yoshimi A., Suzuki K., Nanao T., Miyatake H., Tsuchiya M., Yoshida N., Shirai H., Ino T., Ueno H., Matsuo Y., Fukuyama T., and Asahi K.: "Experimental search for atomic EDM in ^{129}Xe at Tokyo Tech.", Program on CP violation in Elementary Particles and Composite Systems, (International CEntre for Theoretical Sciences), Mahabaleshwar, India, Feb. (2013).

(Domestic Conference)

園田哲, 和田道治, 松尾由賀利, 久保敏幸, 富田英生, 坂本知佳, 能任琢真, 篠塚勉, 涌井崇志, 古川武, 伊藤由太, Schuessler H. A., 中村聡佑, 宮武宇也, 今井伸明, 石山博恒, 平山賀一, 渡辺 裕, 鄭 淳讃, 岡田 邦宏, 高峰 愛子, Kudryavtsev Y., Huyse M., Van Duppen P.: "ガスセル内レーザー共鳴イオン化法の開発とレーザー核分光への応用", 日本物理学会, (日本物理学会), 弘前, 9–9 月 (2011).

中井陽一, 日高宏, 渡部直樹, 小島隆夫: "イオン打ち込み型移動管を用いた水和クラスターイオンの生成実験の現状 2 - 水クラスターイオン生成実験", 日本物理学会第 67 回年次大会, (日本物理学会), 西宮, 3 月 (2012).

東俊行, 中野祐司, 中井陽一, 畠山温, 小牧研一郎, 高田栄一, 村上健: "コヒーレント共鳴励起による水素様重イオンから放出される Ly-α_1, Ly-α_2X 線強度の角度異方性観測", 日本物理学会第 67 回年次大会, (日本物理学会), 西宮, 3 月 (2012).

小林徹, 松尾由賀利: "フェムト秒レーザーアブレーションによるクラスターイオン生成", 第 9 回 AMO 討論会, (AMO 討論会実行委員会), 和光, 6 月 (2012).

岡野眞治, 加藤博, 上蓑義朋, 大津秀暁: "福島原子力発電所事故対応スペクトロメトリー (1) 測定システム", 日本原子力学会 2012 年 秋の大会, (日本原子力学会), 広島, 9 月 (2012).

上蓑義朋, 岡野眞治, 加藤博, 大津秀暁: "福島原子力発電所事故対応スペクトロメトリー（2）スペクトル解析", 日本原子力学会 2012 年 秋の大会, (日本原子力学会), 広島, 9 月 (2012).

佐藤優樹, 竹谷篤, 村上浩之, 西村太樹, 福田光順: "多重サンプリング型電離箱のパラメータ最適化に向けた考察", 日本物理学会, (日本物理学会), 京都, 9–9 月 (2012).

大友祐一, 市川雄一, 近森正敏, 彦田絵里, 鈴木貴大, Bidinosti C. P., 井上壮志, 古川武, 吉見彰洋, 鈴木都文, 七尾翼, 宮武裕和, 土屋真人, 吉田直貴, 白井葉月, 猪野隆, 松尾由賀利, 上野秀樹, 福山武志, 旭耕一郎: 中性子物理研究会, (名古屋大学), 名古屋, 11 月 (2012).

坂本雄, Bidinosti C. P., 市川雄一, 近森正敏, 大友祐一, 彦田絵里, 鈴木貴大, 井上壮志, 古川武, 吉見彰洋, 鈴木都文, 七尾翼, 宮武裕和, 土屋真人, 吉田直貴, 白井葉月, 猪野隆, 上野秀樹, 松尾由賀利, 福山武志, 旭耕一郎: "EDM 測定に向けた改良型磁場安定化システムの構築と性能評価", 日本物理学会第 68 回年次大会, (広島大学), 広島, 3 月 (2013).

近森正敏, 市川雄一, 大友祐一, 彦田絵里, 坂本雄, 鈴木貴大, Bidinosti C. P., 井上壮志, 古川武, 吉見彰洋, 鈴木都文, 七尾翼, 宮武裕和, 土屋真人, 吉田直貴, 白井葉月, 猪野隆, 上野秀樹, 松尾由賀利, 福山武志, 旭耕一郎: "^{3}He 共存磁力計の導入による ^{129}Xe 原子 EDM 測定実験", 日本物理学会第 68 回年次大会, (広島大学), 広島, 3 月 (2013).

鈴木貴大, 市川雄一, 近森正敏, 大友祐一, 彦田絵里, 坂本雄, Bidinosti C. P., 井上壮志, 古川武, 吉見彰洋, 鈴木都文, 七尾翼, 宮武裕和, 土屋真人, 吉田直貴, 白井葉月, 猪野隆, 上野秀樹, 松尾由賀利, 福山武志, 旭耕一郎: "^{129}Xe 原子 EDM 測定実験のための電場印加システム開発", 日本物理学会第 68 回年次大会, (広島大学), 広島, 3 月 (2013).

彦田絵里, 近森正敏, 市川雄一, 大友祐一, 坂本雄, 鈴木貴大, Bidinosti C. P., 井上壮志, 古川武, 吉見彰洋, 鈴木都文, 七尾翼, 宮武裕和, 土屋真人, 吉田直貴, 白井葉月, 猪野隆, 上野秀樹, 松尾由賀利, 福山武志, 旭耕一郎: "ダブルセルを用いた核スピンメーザー発振", 日本物理学会第 68 回年次大会, (広島大学), 広島, 3 月 (2013).

市川雄一, 近森正敏, 大友祐一, 彦田絵里, 坂本雄, 鈴木貴大, Bidinosti C. P., 井上壮志, 古川武, 吉見彰洋, 鈴木都文,

七尾翼, 宮武裕和, 土屋真人, 吉田直貴, 白井葉月, 猪野隆, 上野秀樹, 松尾由賀利, 福山武志, 旭耕一郎: “^{129}Xe 原子 EDM 測定実験のための ^{3}He 共存磁力計の性能評価”, 日本物理学会第 68 回年次大会, (広島大学), 広島, 3 月 (2013).

大友祐一, 市川雄一, 近森正敏, 彦田絵里, 坂本雄, 鈴木貴大, Bidinosti C. P., 井上壮志, 古川武, 吉見彰洋, 鈴木都文, 七尾翼, 宮武裕和, 土屋真人, 吉田直貴, 白井葉月, 猪野隆, 上野秀樹, 松尾由賀利, 福山武志, 旭耕一郎: “^{129}Xe/^{3}He 共存セルの偏極生成及び緩和機構”, 日本物理学会第 68 回年次大会, (広島大学), 広島, 3 月 (2013).

井上研二, 中野祐司, 東俊行, 増永拓也, 渡邊千嘉, 畠山温, 中井陽一, 小牧研一郎, 高田栄一, 村上健: “Ge 薄膜結晶中における 460MeV/u Fe^{25+} のコヒーレント 共鳴励起の観測”, 日本物理学会第 68 回年次大会, (一般社団法人日本物理学会), 広島大学, 3 月 (2013).

石橋陽子, 吉田直貴, 上野秀樹, 吉見彰洋, 市川雄一, 阿部康志, 旭耕一郎, 近森正敏, 藤田朋美, 古川武, 彦田絵里, 長江大輔, 大友祐一, 齋藤佑多, 白井葉月, 鈴木貴大, Yang X., 坂本成彦: “不安定核偏極度測定のための永久磁石を用いた断熱磁場回転装置の開発”, 日本物理学会第 68 回年次大会, (日本物理学会), 東広島, 3 月 (2013).

Yang X., 古川武, 今村慧, 手塚博紀, 山口康広, 筒井正機, 藤田朋美, 三津谷洋助, 江原悠太, 早坂美希, 新井信乃, 村本宗将, 市川雄一, 石橋陽子, 吉田直貴, 白井葉月, 涌井崇志, 小林徹, 園田哲, 伊藤由太, 西村俊二, 西村美月, 近藤洋介, 米田健一郎, 久保野茂, 大城幸光, 畠山温, 和田道治, 上野秀樹, 下田正, 旭 耕一郎, 松尾 由賀利: “Control the stopping position of 84,85Rb in He II for the laser spectroscopy in OROCHI experiment”, 日本物理学会第 68 回年次大会 , 東広島, 3 月 (2013).

手塚博紀, 涌井崇志, 古川武, Yang X., 今村慧, 山口康広, 筒井正機, 藤田朋美, 三津谷洋助, 早坂美希, 江原悠太, 新井信乃, 村本宗将, 市川雄一, 石橋陽子, 吉田直貴, 白井葉月, 和田道治, 上野秀樹, 下田正, 旭耕一郎, 小林徹, 畠山温, 植松晴子, 松尾由賀利: “超流動 He II 中 RI 原子のレーザー分光 OROCHI における蛍光検出系の高度化”, 日本物理学会第 68 回年次大会, 東広島, 3 月 (2013).

江原悠太, 三津谷洋助, 古川武, 今村慧, 筒井正機, 手塚博紀, 山口康広, Yang X., 加藤裕樹, 畠山温, 小林徹, 植松晴子, 松尾由賀利: “超流動 He 環境における Ga 原子の励起スペクトル測定”, 日本物理学会第 68 回年次大会, 東広島, 3 月 (2013).

今村慧, 古川武, Yang X., 山口康広, 手塚博紀, 筒井正機, 三津谷洋助, 小林徹, 畠山温, 小田島仁司, 松尾由賀利: “超流動ヘリウム環境おける Cs 原子の超微細構造間隔精密測定”, 日本物理学会第 68 回年次大会, 東広島, 3 月 (2013).

三津谷洋助, 古川武, 小林徹, Yang X., 加藤裕樹, 今村慧, 江原悠太, 山口康広, 手塚博紀, 筒井正機, 小田島仁司, 松尾由賀利: “超流動ヘリウム環境での 1 族、および 13 族原子の励起スペクトル”, 日本物理学会第 68 回年次大会, 東広島, 3 月 (2013).

Spin isospin Laboratory

Publications

[Journal]

(Original Papers) *Subject to Peer Review

Sakaguchi S., Iseri Y., Uesaka T., Tanifuji M., Amos K., Aoi N., Hashimoto Y., Hiyama E., Ichikawa M., Ichikawa Y., Ishikawa S., Itoh K., Itoh M., Iwasaki H., Karataglidis S., Kawabata T., Kawahara T., Kuboki H., Maeda Y., Matsuo R., Nakao T., Okamura H., Sakai H., Sasamoto Y., Sasano M., Sato Y., Sakaguchi-Sekiguchi K., Shinohara M., Suda K., Suzuki D., Takahashi Y., Tamii A., Wakui T., Yako K., Yamaguchi M., and Yamamoto Y.: "Analyzing power in elastic scattering of 6He from a polarized proton target at 71 MeV/nucleon", Phys. Rev. C **84**, No. 024604, pp. 024604-1–024604-17 (2011). *

Sonoda T., Wada M., Tomita H., Sakamoto C., Takatsuka T., Furukawa T., Iimura H., Ito Y., Kubo T., Matsuo Y., Mita H., Naimi S., Nakamura S., Noto T., Schury P. H., Wakui T., Miyatake H., Jeong S., Watanabe Y., Isiyama H., Okada K., and Takamine A.: "Development of a resonant laser ionization gas cell for high-energy, short-lived nuclei", Nucl. Instrum. Methods Phys. Res. B **295**, No. 1, (2012). *

(Review)

Obertelli A. and Uesaka T.: "Hydrogen targets for exotic-nuclei studies developed over the past 10 years", Eur. Phys. J. A **47**, 105–126 (2011).

[Book · Proceedings]

(Others)

Yamaguchi Y., Wakasugi M., Suzuki H., Fujinawa T., Uesaka T., Yano Y., Ozawa A., Nagae D., Yamaguchi T., Suzuki T., Kikuchi T., Jiang W., Sasaki T., and Tokuchi A.: "Present status of Rare-RI Ring project in RIKEN RI Beam Factory", Proceedings of Science (PoS), Frascati, Italy, 2011–10, SISSA, Fascati, p. 070 (2012).

Oral Presentations

(International Conference etc.)

Sonoda T., Wada M., Tomita H., Sakamoto C., Ito Y., Schuessler H. A., Takamine A., Kubo T., Matsuo Y., Shinozuka T., Wakui T., Nakamura S., Furukawa T., Okada K., Kudryavtsev Y., Mark H., Van Duppen P., Miyatake H., Ishiyama H., Imai N., Watanabe Y., Hirayama Y., and Chon J.: "Development of the resonance ionization laser ion source for parasitic RI-beam production and in-gas-cell/jet laser spectroscopy at SLOWRI RIKEN", Advances in Radioactive Isotope Science (ARIS - 2011), (K.U.Leuven), Leuven, Belgium, May–May (2011).

Uesaka T., Miki K., Sasamoto Y., and Noji S.: "Spin-isospin studies with RI-beam induced charge exchange reactions", ARIS 2011, (University of Leuven and University of Brussels), Leuven, Belgium, May–June (2011).

Uesaka T.: "Magnetic spectrometer at RIBF", Workshop on the high-rigidity spectrometer at FRIB, (NSCL, Michigan State University), East Lansing, USA, Aug. (2011).

Sasano M.: "Measurement of Gamow-Teller transitions from ^{56}Ni", 2011 Fall meeing of the American Physical Society Division of Nuclear Physics, (American Physical Society), Michigan State University, USA, Oct. (2011).

Uesaka T.: "RI-beam induced charge exchange reactions new usage of RI-beams ", Frontier Issues in Physics of Exotic Nuclei (YKIS2011), (Yukawa Institute for Theoretical Physics, Kyoto university), Kyoto, Oct. (2011).

Uesaka T.: "Spin in Isospin Physics", Korean Physical Society 2011 Fall Meeting, (Korean Physical Society), Busan, Korea, Oct. (2011).

Uesaka T.: "Spin-orbit splitting in oxygen isotopes", International symposium on frontiers in nuclear physics: Tensor interaction in nuclear and hadron physics, (Beihang University), Beijing, China, Nov. (2011).

Uesaka T.: "Reaction studies of exotic nuclei with Rare-RI ring", RIBF-ULIC-Symposium on Physics of Rare-RI Ring, Saitama, Nov. (2011).

Uesaka T.: "RI-beam induced charge exchange reactions as new probes to nuclei", The International Symposium on Physics of Unstable Nuclei 2011 (ISPUN11), (the Institute for Nuclear Science and Technique), Hanoi, Viet Nam, Nov. (2011).

Uesaka T.: "Reaction studies of exotic nuclei with polarized target and spectrometer", The 1st International Symposium on the Science with KoRIA, (KoRIA symposium organizing committee), Sejong, Korea, Dec. (2011).

Sasano M.: "Measurement of Gamow-Teller transitions from ^{56}Ni", Direct Reactions with Exotic Beams 2012, (Faculty of SMFN), Pisa, Italy, Mar. (2012).

Sasano M.: "Gamow-Teller transitions from ^{56}Ni", The 11th International Symposium on Origin of Matter and Evolution of Galaxies, (CNS, University of Tokyo), Wako, Nov. (2012).

Sasano M.: "Study of Gamow-Teller transitions from unstable nuclei via the (p,n) reaction in inverse kinematics", The 6th LACM-TORIJIN-JUSTIPEN Workshop, (ORNL), ORNL, USA, Nov. (2012).

Furukawa T., Wakui T., Yang X., Fujita T., Imamura K., Yamaguchi Y., Tetsuka H., Tsutsui Y., Mitsuya Y., Ichikawa Y., Ishibashi Y., Yoshida N., Shirai H., Ebara Y., Hayasaka M., Arai S., Muramoto S., Hatakeyama A., Wada M., Sonoda T., Ito Y., Kobayashi T., Nishimura S., Nishimura M., Kondo Y., Yoneda K., Kubono S., Ohshiro Y., Ueno H., Shinozuka T., Shimoda T., Asahi K., and Matsuo Y.: "A Novel Nuclear Laser Spectroscopy Method using Superfluid Helium for the Measurement of Spins and Moments of Exotic Nuclei", 16th International Conference on Electromagnetic Isotope Separators and Techniques Related to their Applications (EMIS2012), Matsue, Dec. (2012).

Yamaguchi Y., Wakasugi M., Ozawa A., Uesaka T., Yano Y., Fujinawa T., Fukunishi N., Inabe N., Kamigaito O., Kase M., Kikuchi T., Komiyama M., Kubo T., Kumagai K., Maie T., Ohnishi J., Tokuchi A., Yoshida K., Yamaguchi T., Nagae D., Zenihiro J., Suzuki T., Abe Y., and Suzaki F.: “Construction of Rare-RI Ring at RIKEN RI Beam Factory”, 16th International Conference on Electromagnetic Isotope Separators and Techniques Related to their Applications (EMIS2012), (RIKEN KEK IMP), Matsue, Dec. (2012).

Yang X., Furukawa T., Imamura K., Tetsuka H., Yamaguchi Y., Tsutsui Y., Fujita T., Mitsuya Y., Ichikawa Y., Ishibashi Y., Yoshida N., Shirai H., Wakui T., Kobayashi T., Hatakeyama A., Wada M., Ueno H., Shimoda T., Asahi K., and Matsuo Y.: “Control of the stopping position of unstable Rb beam in superfluid helium (He II) for nuclear laser spectroscopy of RI atoms”, 16th International Conference on Electromagnetic Isotope Separators and Techniques Related to their Applications (EMIS2012), Matsue, Dec. (2012).

Suzaki F., Zenihiro J., Yamaguchi T., Ozawa A., Uesaka T., Wakasugi M., Yamada K., and Yamaguchi Y.: “Design study of a resonant Schottky pick-up for Rare-RI Ring project”, 16th International Conference on Electromagnetic Isotope Separators and Techniques Related to their Applications (EMIS2012), (RIKEN KEK IMP), Matsue, Dec. (2012).

Imamura K., Furukawa T., Wakui T., Yang X., Yamaguchi Y., Tetsuka H., Mitsuya Y., Tsutsui Y., Fujita T., Ebara Y., Hayasaka M., Arai S., Muramoto S., Ichikawa Y., Ishibashi Y., Yoshida N., Shirai H., Hatakeyama A., Wada M., Sonoda T., Ito Y., Odashima H., Kobayashi T., Ueno H., Shimoda T., Asahi K., and Matsuo Y.: “Development of a helium cryostat for laser spectroscopy of atoms with unstable nuclei in superfluid helium”, 16th International Conference on Electromagnetic Isotope Separators and Techniques Related to their Applications (EMIS2012), Matsue, Dec. (2012).

Nagae D., Abe Y., Okada S., Ozawa A., Yamaguchi T., Suzuki H., Moriguchi T., Ishibashi Y., Fukuoka S., Nishikiori R., Suzuki T., Suzaki F., Yamaguchi Y., Uesaka T., and Wakasugi M.: “Time-of-flight detector applied to mass measurements in Rare-RI Ring”, 6th International Conference on Electromagnetic Isotope Separators and Techniques Related to their Applications (EMIS2012), (RIKEN KEK IMP), Matsue, Dec. (2012).

(Domestic Conference)

園田哲, 和田道治, 松尾由賀利, 久保敏幸, 富田英生, 坂本知佳, 能任琢真, 篠塚勉, 涌井崇志, 古川武, 伊藤由太, Schuessler H. A., 中村聡佑, 宮武宇也, 今井伸明, 石山博恒, 平山賀一, 渡辺裕, 鄭淳讃, 岡田邦宏, 高峰愛子, Kudryavtsev Y., Huyse M., Van Duppen P.: “ガスセル内レーザー共鳴イオン化法の開発とレーザー核分光への応用”, 日本物理学会, (日本物理学会), 弘前, 9–9 月 (2011).

Yang X., 古川武, 今村慧, 手塚博紀, 山口康広, 筒井正機, 藤田朋美, 三津谷洋助, 江原悠太, 早坂美希, 新井信乃, 村本宗将, 市川雄一, 石橋陽子, 吉田直貴, 白井葉月, 涌井崇志, 小林徹, 園田哲, 伊藤由太, 西村俊二, 西村美月, 近藤洋介, 米田健一郎, 久保野茂, 大城幸光, 畠山温, 和田道治, 上野秀樹, 下田正, 旭耕一郎, 松尾由賀利: “Control the stopping position of 84,85Rb in He II for the laser spectroscopy in OROCHI experiment”, 日本物理学会第 68 回年次大会, 東広島, 3 月 (2013).

手塚博紀, 涌井崇志, 古川武, Yang X., 今村慧, 山口康広, 筒井正機, 藤田朋美, 三津谷洋助, 早坂美希, 江原悠太, 新井信乃, 村本宗将, 市川雄一, 石橋陽子, 吉田直貴, 白井葉月, 和田道治, 上野秀樹, 下田正, 旭耕一郎, 小林徹, 畠山温, 植松晴子, 松尾由賀利: “超流動 He II 中 RI 原子のレーザー分光 OROCHI における蛍光検出系の高度化”, 日本物理学会第 68 回年次大会, 東広島, 3 月 (2013).

Superheavy Element Laboratory

Publications

[Journal]

(Original Papers) *Subject to Peer Review

Morimoto K., Morita K., Kaji D., Haba H., Katori K., Koura H., Ohnishi T., Ozawa A., Suda T., Sueki K., Tanihata I., Tokanai F., Yoneda A., and Yoshida A.: "Status of super heavy element research using GARIS at RIKEN", Nucl. Phys. A **738**, 129 (2004). *

Kaji D., Morimoto K., Morita K., Hasebe H., Yoshida A., Haba H., and Yoneda A.: "Target for the heaviest element production at RIKEN", Nucl. Instrum. Methods Phys. Res. A **590**, 198 (2007). *

Kaji D., Morimoto K., Sato N., Ichikawa T., Ohzeki K., Haba H., Koura H., Ozawa A., Sumita T., Yamaguchi T., Yoneda A., Yoshida A., and Morita K.: "Production and Decay Properties of ^{263}Hs", J. Phys. Soc. Jpn. **78**, No. 3, p. 035001 (2009). *

Clark R. M., Kaji D., Morimoto K., and Watanabe H.: "High-K multi-quasiparticle states in ^{254}No", Phys. Lett. B **690**, 19 (2010). *

Sato N., Haba H., Ichikawa T., Kaji D., Kudou Y., Morimoto K., Morita K., Ohzeki K., Sumita T., Yoneda A., Koura H., Ozawa A., Yamaguchi T., and Yoshida A.: "Production and Decay Properties of ^{264}Hs and ^{265}Hs", J. Phys. Soc. Jpn. **80**, 094201 (2011). *

Kaji D., Morita K., Morimoto K., Haba H., and Kudo H.: "Average charge of superheavy recoil ion in helium gas", Proc.Radiochim **1**, 105 (2011). *

Adachi T., Fujita Y., Bacher A. D., Berg G. P., Black T. C., De Frenne D., Foster ., Fujita H., Fujita K., Hatanaka K., Homma M., Jacobs E., Janecke J., Kanzaki Y., Katori K., Nakanishi K., Negret A., Otsuka T., Popescu L., Roberts D. A., Sakemi Y., Shimbara Y., Shimizu Y., Stephenson E. J., Tameshige Y., Tamii A., Uchida M., Ueno H., Yamanaka T., Yosoi M., and Zell K. O.: "High-resolution study of Gamow-Teller transitions via the ^{54}Fe(^{3}He,t)^{54}Co reaction", Phys. Rev. C **85**, 024308-1–024308-15 (2012). *

[Book・Proceedings]

(Technical Document)

加治大哉, 羽場宏光: "放射化学用語辞典", 放射化学用語辞典 , 2006– 日本放射化学会, 東京, (2006).

Oral Presentations

(International Conference etc.)

Kaji D.: "New separator GARIS-II at RIKEN", Gas-filled recoil separators: Present status and future outlook, (Jyvaskyla University), Jyvaskyla, Finland, May (2012).

Haba H., Kasamatsu Y., Kikunaga H., Yoneda A., Kanaya J., and Morita K.: "Automated rapid α/SF detection system for studying aqueous chemistry of superheavy elements at RIKEN", EuCheMS International Conference on Nuclear and Radiochemistry (NRC-8), (The European Association for Chemical and Molecular Sciences), Como, Italy, Sept. (2012).

Haba H., Kaji D., Kanaya J., Kasamatsu Y., Kikunaga H., Kikutani Y., Komori Y., Kudo H., Kudou Y., Morimoto K., Morita K., Murakami M., Nishio K., Ooe K., Ohzeki K., Sakai R., Sato N., Shinohara A., Sumita T., Toyoshima A., Tsukada K., and Yoneda A.: "RIKEN GARIS as a promising interface for superheavy element chemistry -Production of ^{261}Rf, ^{262}Db, and ^{265}Sg for chemical studies using the GARIS gas-jet system-", EuCheMS International Conference on Nuclear and Radiochemistry (NRC-8), (The European Association for Chemical and Molecular Sciences), Como, Italy, Sept. (2012).

Schury P. H., Jeong S., Haba H., Kaji D., Koura H., Ito Y., Mita H., Miyatake H., Morimoto K., Morita K., Naimi S., Nakamura S., Okada K., Ozawa A., Sonoda T., Takamine A., Wollnik H., and Wada M.: "A multi-reflection time of flight mass spectrograph for short-lived nuclei and heavy molecules", International Mass Spectrometry Conference, (Kyoto University), Kyoto, Sept. (2012).

Kaji D., Morimoto K., Sato N., Haba H., Kudou Y., Ohzeki K., Sumita T., Yoneda A., Wakabayashi Y., Murakami M., and Morita K.: "Gas-filled recoil ion separator GARIS-II", 16th International Conference on Electromagnetic Isotope Separators and Techniques Related to their Applications (EMIS2012), Matsue, Dec.– Dec. (2012).

(Domestic Conference)

加治大哉: "理研における重元素合成実験に関する準備状況", 「重元素の核化学」「核分裂の先端研究」専門研究会, (京都大学原子炉実験施設), 大阪, 1 月 (2002).

加治大哉, 森田浩介, 森本幸司, 米田晃, 須田利美, 吉田敦, 大西哲哉, 羽場宏光, 末木啓介, 鹿取謙二, 谷畑勇夫: "超重元素探索へ向けた理研－気体充填型反跳分離装置の性能評価", 日本物理学会, (立教大学), 東京, 9 月 (2002).

加治大哉, 森田浩介, 森本幸司, 米田晃, 須田利美, 吉田敦, 大西哲哉, 羽場宏光, 末木啓介, 鹿取謙二, 谷畑勇夫: "超重元素探索へ向けた理研－気体充填型反跳分離装置の性能評価", 放射化学討論会, (北海道大学), 北海道, 9 月 (2002).

加治大哉, 森田浩介, 森本幸司, 羽場宏光, 鹿取謙二, 小浦寛之, 大西哲哉, 小沢顕, 須田利美, 末木啓介, 谷畑勇夫, 米田晃, 吉田敦: "ヘリウムガス中における (超) 重元素の平衡電荷", 日本物理学会, (宮崎大学), 宮崎, 9 月 (2003).

加治大哉, 森田浩介, 森本幸司, 羽場宏光, 鹿取謙二, 小浦寛之, 大西哲哉, 小沢顕, 須田利美, 末木啓介, 谷畑勇夫, 米田晃, 吉田敦: "ヘリウムガス中における重い反跳原子の平衡電荷－理研における Z=111 番元素探索－", 放射化学討論会, (京都大学原子炉実験施設), 大阪, 10 月 (2003).

加治大哉, 森田浩介, 森本幸司: "気体充填型反跳分離装置を用いた (超) 重元素の平衡電荷測定", 重元素領域の核的・化学的性質　専門研究会, (京都大学原子炉実験施設), 大阪 , 1 月 (2004).

加治 大哉, 森田 浩介, 森本 幸司, 羽場 宏光, 小浦 寛之, 大西

哲哉, 小沢顕, 須田利美, 末木啓介, 山口貴之, 米田晃, 吉田敦: “209Bi+70Zn 反応を用いた 113 番元素探索”, 日本化学会, (神奈川大学), 神奈川, 3 月 (2005).

加治大哉, 森田浩介, 森本幸司, 羽場宏光, 小浦寛之, 大西哲哉, 小沢顕, 須田利美, 末木啓介, 山口貴之, 米田晃, 吉田敦: “209Bi(70Zn,n)278113 反応を用いた 113 番元素の合成”, 放射化学討論会, (金沢大学), 金沢, 9 月 (2005).

加治大哉: “ヘリウムガス中を運動する超重元素の平均平衡電荷に関する基礎研究—超重元素合成実験への寄与—”, 放射化学討論会, (金沢大学), 金沢, 9 月 (2005).

加治大哉, 羽場宏光, 森本幸司, 森田浩介, 佐藤望: “シーボギウム (Sg) の化学研究へ向けた 232Th+40Ar 反応による Sg 同位体の探索”, 日本化学会, (日本大学), 千葉, 3 月 (2006).

加治大哉: “IRRADIATION MONITOR @ GARIS”, Detector workshop @ RIKEN, 埼玉, 3 月 (2008).

加治大哉: “GARIS-II 開発の現状”, 超重元素化学ワークショップ 2008, 埼玉, 11 月 (2008).

加治大哉, 森本幸司, 佐藤望, 米田晃, 森田浩介: “新しい気体充填型反跳分離装置 GARIS-II の開発”, 放射化学討論会, (日本大学), 神奈川, 9 月 (2009).

加治大哉, 森本幸司, 羽場宏光, 市川隆敏, 小浦寛之, 工藤祐生, 小沢顕, 大関和貴, 住田貴之, 山口貴之, 米田晃, 吉田敦, 森田浩介: “新同位体 ^{263}Hs の生成および壊変特性”, 放射化学討論会, (日本大学), 神奈川, 9 月 (2009).

加治大哉, 羽場宏光, 笠松良崇, 工藤祐生, 森本幸司, 森田浩介, 大関和貴, 住田貴之, 米田晃, 佐藤望, 若林泰生, 村上昌史, 門叶冬樹, 生井沙織: “GARIS-II 開発の現状と初動試験”, 日本物理学会, (新潟大学), 新潟, 3 月 (2010).

加治大哉, 羽場宏光, 笠松良崇, 工藤祐生, 森本幸司, 森田浩介, 大関和貴, 住田貴之, 米田晃, 佐藤望, 若林泰生, 村上昌史, 門叶冬樹, 生井沙織: “GARIS-II commissioning 1”, 放射化学討論会, (大阪大学), 大阪, 9 月 (2010).

加治大哉, 羽場宏光, 笠松良崇, 工藤祐生, 森本幸司, 森田浩介, 大関和貴, 住田貴之, 米田晃, 小浦寛之, 佐藤望, 門叶冬樹: “中性子欠損領域の新アクチノイド核種 ^{234}Bk および ^{230}Am の観測”, 放射化学討論会, (大阪大学), 大阪, 9 月 (2010).

加治大哉: “新元素探索の最前線”, 放射化学討論会, (信州大学), 長野, 9 月 (2011).

羽場宏光, 笠松良崇, 菊永英寿, 金谷淳平, 米田晃, 森田浩介: “超重元素の溶液化学研究のための自動迅速放射線計測装置の開発”, 2012 日本放射化学会年会・第 56 回放射化学討論会, (日本放射化学会), 東京都目黒区, 10 月 (2012).

羽場宏光, 大関和貴, 笠松良崇, 加治大哉, 金谷淳平, 菊谷有希, 菊永英寿, 工藤久昭, 工藤祐生, 小森有希子, 酒井隆太郎, 篠原厚, 住田貴之, 豊嶋厚史, 西尾勝久, 村上昌史, 森田浩介, 森本幸司, 米田晃: “GARIS ガスジェット法によるドブニウムの化学実験対象核種 ^{262}Db の製造”, 2012 日本放射化学会年会・第 56 回放射化学討論会, (日本放射化学会), 東京都目黒区, 10 月 (2012).

花田貴寿, 福地知則, 神野伸一郎, 羽場宏光, 篠原厚, 渡辺恭良, 榎本秀一: “次世代 PET による複数分子同時イメージングの実証”, 第 52 回日本核医学会学術総会, (北海道大学大学院医学研究科　病態情報学講座　核医学分野), 札幌, 10 月 (2012).

加治大哉, 住田貴之, 長谷部裕雄, 田中謙伍, 羽場宏光, 森田浩介, 森本幸司, 若林泰生, 村上昌史, 武山美麗, 山木さやか: “超重元素生成のための新しい標的システム”, 2012 日本放射化学会年会・第 56 回放射化学討論会, (日本放射化学会), 東京工業大学, 10–10 月 (2012).

加治大哉, 住田貴之, 刈屋佳樹, 鹿取謙二, 工藤祐生, 森田浩介, 森谷透, 村上昌史, 武山美麗, 田中謙伍, 戸田光祐, 門叶冬樹, 若林泰生, 山木さやか, 米田晃, 大関和貴, 長谷部裕雄, 羽場宏光, 吉田敦, 山口貴之: “208Pb+70Zn 反応を用いた 277Cn の生成と壊変特性”, 2012 日本放射化学会年会・第 56 回放射化学討論会, (日本放射化学会), 東京工業大学, 10–10 月 (2012).

High Energy Astrophysics Laboratory

Publications

[Journal]

(Original Papers) *Subject to Peer Review

Nakagawa Y., Mihara T., Sugizaki M., Kohama M., Yamamoto T., Serino M., Matsuoka M., Kawai N., Morii M., Usui R., Sugimori K., Nakahira S., Negoro H., Nakajima M., Isobe N., and MAXI T.: "The First MAXI/GSC iew of Galactic Magnetars", "The First Year of MAXI: Monitoring Variable X-ray Sources", Poster Presentations, 4th International MAXI Workshop held November 30 - December 2, 2010 in Tokyo, Japan., p. (2010).

Kayo I., Inada N., Oguri M., Morokuma T., Hall P. B., Kochanek C. S., and Schneider D. P.: "Eight new quasar lenses from the Sloan Digital Sky Survey Quasar Lens Search", Astron. J. **139**, No. 4, pp. 1614–1621 (2010). *

Schneider D. P., Richards G. T., Hall P. B., Strauss M. A., Anderson S. F., Boroson T. A., Ross N. P., Shen Y., Brandt W. N., Fan X., Inada N., Jester S., Knapp G. R., Krawczyk C. M., Thakar A. R., Vanden Berk D. E., Voges W., Yanny B., York D. G., Bahcall N. A., Bizyaev D., Blanton M. R., Brewington H., Brinkmann J., Eisenstein D., Frieman J. A., Fukugita M., Gray J., Gunn J. E., Hibon P., Ivezic Z., Kent S. M., Kron R. G., Lee M. G., Lupton R. H., Malanushenko E., Malanushenko V., Oravetz D., Pan K., Pier J. R., Price T. N., Saxe D. H., Schlegel D. J., Simmons A., Snedden S. A., SubbaRao M. U., Szalay A. S., and Weinberg D. H.: "The Sloan Digital Sky Survey Quasar Catalog. V. Seventh Data Release", Astron. J. **139**, No. 6, pp. 2360–2373 (2010). *

McGreer I. D., Hall P. B., Fan X., Bian F., Inada N., Oguri M., Strauss M. A., Schneider D. P., and Farnsworth K.: "SDSS J094604.90+183541.8: A gravitationally lensed quasar at z = 4.8", Astron. J. **140**, No. 2, pp. 370–378 (2010). *

Inada N., Oguri M., Shin M., Kayo I., Strauss M. A., Hennawi J. F., Morokuma T., Becker R. H., White R. L., Kochanek C. S., Gregg M. D., Chiu K., Johnston D. E., Clocchiatti A., Richards G. T., Schneider D. P., Frieman J. A., Fukugita M., Gott R. J., Hall P. B., York D. G., Castander F. J., and Bahcall N. A.: "The Sloan Digital Sky Survey Quasar Lens Search. IV. Statistical Lens Sample from the fifth data release", Astron. J. **140**, No. 2, pp. 403–415 (2010). *

Yamaguchi H., Sawada M., and Bamba A.: "Searching for diffuse nonthermal X-rays from the Superbubbles N11 and N51D in the Large Magellanic Cloud", Astron. J. **715**, No. 1, pp. 412–420 (2010). *

Enoto T., Rea N., Nakagawa Y., Makishima K., Sakamoto T., Esposito P., G0tz D., Hurley K., Israel G. L., Kokubun M., Mereghetti S., Murakami H., Nakazawa K., Stella L., Tiengo A., Turolla R., Yamada S., Yamaoka K., and Zane S.: "Wide-band Suzaku Analysis of the Persistent Emission from SGR 0501+4516 During the 2008 Outburst", Astron. J. **715**, No. 1, pp. 665–670 (2010). *

Terada Y., Ishida M., Bamba A., Mukai K., Hayashi T., and Harayama A.: "X-ray Observation of AM Herculis in a Very Low State with Suzaku", Astron. J. **721**, No. 2, pp. 1908–1918 (2010). *

Hayato A., Yamaguchi H., Tamagawa T., Katsuda S., Hwang U., Hughes J. P., Ozawa M., Bamba A., Kinugasa K., Terada Y., Furuzawa A., Kunieda H., and Makishima K.: "Expansion Velocity of Ejecta in Tycho's Supernova Remnant Measured by Doppler Broadened X-ray Line Emission", Astron. J. **725**, No. 1, pp. 894–903 (2010). *

Takahashi R. and TAKAHASHI M.: "Anisotropic radiation field and trapped photons around the Kerr black hole", Astronomy and Astrophysics **513**, 7 (2010). *

Ota K., Iye M., Kashikawa N., Shimasaku K., Ouchi M., Totani T., Kobayashi M. A., Nagashima M., Harayama A., Kodaka N., Morokuma T., Furusawa H., Tajitsu A., and Hattori T.: "Lyα EMITTERS AT z = 7 IN THE SUBARU/XMM-NEWTON DEEP SURVEY FIELD: PHOTOMETRIC CANDIDATES AND LUMINOSITY FUNCTION", Astrophys. J. **722**, No. 803, pp. 803–811 (2010). *

Tomida K., Tomisaka K., Matsumoto T., Ohsuga K., Machida M. N., and Saigo K.: "Radiation magnetohydrodynamics simulation of proto-stellar collapse: two-component molecular outflow", Astrophys. J. Lett. **714**, No. 1, pp. L58–L63 (2010). *

TAKAHASHI M. and Takahashi R.: "Black Hole Aurora Powered by a Rotating Black Hole", Astrophys. J. Lett. **714**, No. 1, pp. L176–L180 (2010). *

Bamba A., Anada T., Dotani T., Mori K., Yamazaki R., Ebisawa K., and Vink J.: "X-ray Evolution of Pulsar Wind Nebulae", Astrophys. J. Lett. **719**, No. 2, pp. L116–L120 (2010). *

Jones T. M., Misawa T., Charlton J. C., Mshar A. C., and Ferland G. J.: "A Bare Molecular Cloud at z 0.45", Astrophysical Journal **715**, 1497–1507 (2010). *

Misawa T., Kawabata K. S., Eracleous E., Charlton J. C., and Kashikawa N.: "A Spectropolarimetric Test of the Structure of the Intrinsic Absorbers in the Quasar HS 1603+3820", Astrophysical Journal **719**, 1890–1895 (2010). *

Wu J., Charlton J. C., Misawa T., Eracleous M., and Ganguly R.: "The Physical Conditions of the Intrinsic N V Narrow Absorption Line Systems of Three Quasars", Astrophysical Journal **722**, 997–1012 (2010). *

Takahashi R. and Harada T.: "Observational testability of a Kerr bound in the x-ray spectrum of black hole candidates", Classical Quantum Gravity **27**, No. 7, p.

075003 (2010). ∗

Iwakiri W., Ohno M., Kamae T., Nakagawa Y., Terada Y., Tashiro M. S., Yoshida A., Yamaoka K., and Makishima K.: "Timing Analysis of Unusual GRB 090709A Observed by Suzaku Wide-band All sky Monitor", DECIPHERING THE ANCIENT UNIVERSE WITH GAMMA-RAY BURSTS. AIP Conference Proceedings **1279**, 89–92 (2010).

Bambi C., Harada T., Takahashi R., and Yoshida N.: "Outflows from accreting super-spinars", Phys. Rev. D **81**, No. 10, p. 104004-1 (2010). ∗

Caballero I., Terada Y., and Science T.: "Peculiar outburst of A 0535+26 observed with INTEGRAL, RXTE and Suzaku", Proc. of The Extreme sky: Sampling the Universe above 10 keV, (2010). ∗

Yamauchi S., Ueno M., Bamba A., and Koyama K.: "A New Candidate of a Cluster of Galaxies, 2XMM J045637.2+522411", Publ. Astron. Soc. Jpn. **62**, No. 2, pp. 219–224 (2010). ∗

Enoto T., Nakazawa K., Makishima K., Nakagawa Y., Sakamoto T., Ohno M., Takahashi T., Terada Y., Yamaoka K., Murakami T., and Takahashi H.: "Suzaku Discovery of a Hard X-Ray Tail in the Persistent Spectra from the Magnetar 1E 1547.0-5408 during its 2009 Activity", Publ. Astron. Soc. Jpn. **62**, No. 2, pp. 475–485 (2010). ∗

Arimoto M., Kawai N., Asano K., Hurley K., Serino M., Nakagawa Y., Shimokawabe T., Pazmino N. V., Sato R., Matsuoka M., Yoshida A., Tamagawa T., Shirasaki Y., Sugita S., Takahashi I., Atteia J., Pelangeon A., Vanderspek R., Graziani C., Prigozhin G., Villasenor J., Jernigan G. J., Crew G. B., Sakamoto T., Ricker G. R., Woosley S. E., Butler N., Levine A., Doty J. P., Donaghy T. Q., Lamb D. Q., Fenimore E., Galassi M., Boer M., Dezalay J., Olive J., Braga J., Manchanda R., and Pizzichini G.: "Spectral-Lag Relations in GRB Pulses Detected with HETE-2", Publ. Astron. Soc. Jpn. **62**, No. 2, pp. 487–499 (2010). ∗

Onda K., Tashiro M. S., Nakagawa Y., Yamaoka K., Terada Y., Ohno M., Sugita S., Sakamoto T., Toma K., Gandhi P., Kodaka N., Iwakiri W., Urata Y., Yamauchi M., and Fukazawa Y.: "Prompt MeV Emission from GRB070125 Observed by Suzaku/WAM", Publ. Astron. Soc. Jpn. **62**, No. 3, pp. 547–556 (2010). ∗

Someya K., Bamba A., and Ishida M.: "Suzaku observations of the Supernova Remnant N23 in the Large Magellanic Cloud", Publ. Astron. Soc. Jpn. **62**, No. 5, pp. 1301–1306 (2010). ∗

Endo A., Terada Y., and Science T.: "A Catalog of Suzaku/WAM Hard X-ray Solar Flares", Publ. Astron. Soc. Jpn. **62**, No. 5, pp. pp.1341–pp.1349 (2010). ∗

Sato K., Kawaharada M., Nakazawa K., Matsushita K., Ishisaki Y., Yamasaki N. Y., and Ohashi T.: "Metallicity of the Fossil Group NGC 1550 Observed with Suzaku", Publ. Astron. Soc. Jpn. **62**, No. 6, pp. 1423–1433 (2010). ∗

Konami S., Tamagawa T., Matsushita K., Tashiro M. S., Makishima K., and Nagino R.: "Abundance patterns in the interstellar medium of the S0 galaxy NGC 1316 (Fornax A) revealed with Suzaku", Publ. Astron. Soc. Jpn. **62**, No. 6, pp. 1435–1443 (2010). ∗

Morii M., Terada Y., and Suzaku T.: "Suzaku Observation of the Anomalous X-ray Pul sar 1E 1841-045", Publ. Astron. Soc. Jpn. **62**, pp.1249–1259 (2010). ∗

Onda K., Terada Y., and Science T.: "Time-Resolved Spectral Variability of the Prompt Emission from GRB 070125 Observed with Suzaku/WAM", Publ. Astron. Soc. Jpn. **62**, pp547–556 (2010). ∗

Sato T., Bamba A., Nakamura R., and Ishida M.: "Identification of CXOU J171405.7-381031 as a New Magnetar with XMM-Newton", Publications of the Astronomical Society of Japan Letters **62**, No. 5, pp. L33–L36 (2010). ∗

Takeuchi S., Ohsuga K., and Mineshige S.: "A novel jet model: Magnetically collimated, radiation-pressure driven Jet", Publications of the Astronomical Society of Japan Letters **62**, No. 5, pp. L43–L47 (2010). ∗

Terada Y., Ishida M., Bamba A., Mukai K., Makishima K., Hayashi T., Harayama A., and Morigami K.: "Discovery of possible non-thermal emission from AM Hercules in the very state with Suzaku-The second white dwarf pulsar?-", The Energetic Cosmos :from Suzaku to Astro-H Conference Proceeding **JAXA-SP-09-008E**, 200–201 (2010). ∗

Ishikawa M., Kawasaki K., Ueno S., Tomida H., Kohama M., Nakagawa Y., Sugizaki M., Serino M., Yamamoto T., Sootome T., Matsuoka M., Kawai N., Morii M., Sugimori K., Usui R., Yoshida A., Yamaoka K., Nakahira S., Tsunemi H., Kimura M., Negoro H., Nakajima M., Ozawa H., Suwa F., Ueda Y., Isobe N., Eguchi S., Hiroi K., Daikyuji A., Matsumura T., Yamazaki K., and MAXI T.: "The observation result of Galactic X-ray sources by MAXI", The First Year of MAXI: Monitoring Variable X-ray Sources, 4th International MAXI Workshop, p. 10-1 (2010).

Yasuda T., Iwakiri W., Terada Y., Tashiro M. S., Enoto T., Bamba A., Shibata S., Nakagawa Y., Makishima K., and Suzaku-Wam T.: "Discovery of MeV emission from a Magnetar, AXP 1E1547.0-5408, ith Suzaku / Wideband All-sky Monitor", The First Year of MAXI: Monitoring Variable X-ray Sources, 4th International MAXI Workshop, p. 31-1 (2010).

Uzawa A., Tsuboi Y., Morii M., Matsuoka M., Nakahira S., Matsumura T., Yamazaki K., Satoh R., Kawasaki K., Ueno S., Tomida H., Adachi Y., Kohama M., Mihara T., Sugizaki M., Serino M., Nakagawa Y., Kimura M., Kitayama H., Kawai N., Sugimori K., Usui R., Yoshida A., Yamaoka K., Kotani T., Hirose T., Negoro H., Nakajima M., Ozawa H., Sugawara A., Suwa F., Ueda Y., Isobe N., Eguchi S., Hiroi K., Yamauchi M., Daikyuji

A., and MAXI T.: "A giant flare from a weak-lined T Tauri Star TWA-7 detected with MAXI/GSC", The First Year of MAXI: Monitoring Variable X-ray Sources, 4th International MAXI Workshop, p. 34-1 (2010).

Ohno M., Kokubun M., Takahashi T., Yamaoka K., Serino M., Nakagawa Y., Tamagawa T., Fukazawa Y., Uehara T., Hanabata Y., Takahashi T., Sugita S., Vasquez N., Terada Y., Tashiro M. S., Iwakiri W., Takahara K., Yasuda T., Ohmori N., Daikyuji A., Nishioka Y., Yamauchi M., Urata Y., Tsai P. P., Nakazawa K., Makishima K., and Hong S.: "All-sky Observations with Suzaku Wide-band All-sky onitor and MAXI", The First Year of MAXI: Monitoring Variable X-ray Sources, 4th International MAXI Workshop, p. 53-1 (2010).

Negoro H., Miyoshi S., Ishiwata R., Nakajima N., Matsuoka M., Kawasaki K., Ueno M., Tomida H., Serino M., Ishikawa M., Mihara T., Kohama M., Sugizaki M., Nakagawa Y., Tsunemi H., Kawai N., Morii M., Yoshida A., Yamaoka K., Ueda Y., Isobe N., and Eguchi S.: "MAXI Nova Alert System and the Latest Scientific Results", X-RAY ASTRONOMY 2009; PRESENT STATUS, MULTI-WAVELENGTH APPROACH AND FUTURE PERSPECTIVES: Proceedings of the International Conference **1248**, 589–590 (2010).

Eisenstein D. J., Inada N., and The S.: "SDSS-III: Massive Spectroscopic Surveys of the Distant Universe, the Milky Way, and Extra-Solar Planetary Systems", Astron. J. **142**, No. 3, pp. 72-1–72-24 (2011). ∗

Rusu C. E., Oguri M., Inada N., Kayo I., Iye M., Hayano Y., Oya S., Hattori M., Saito Y., Ito M., Minowa Y., Pyo T., Terada H., Takami H., and Watanabe M.: "SDSS J133401.39+331534.3: A New Subarcsecond Gravitationally Lensed Quasar", Astron. J. **738**, No. 1, pp. 30-1–30-8 (2011). ∗

Nakamura R., Bamba A., Dotani T., Ishida M., Yamazaki R., and Kohri K.: "Evolution of Synchrotron X-Rays in Supernova Remnants", Astron. J. **746**, No. 2, pp. 134-1–134-5 (2011). ∗

Mineshige S. and Ohsuga K.: "Supercritical accretion and ULXs - what can we achieve?", Astronomische Nachrichten **332**, No. 4, p. 402 (2011). ∗

Takahashi R. and Mineshige S.: "Constraining the size of the dark region around the M87 black hole by space-VLBI observations", Astrophys. J. **729**, No. 2, p. 10 (2011). ∗

Suchy S., Terada Y., and Suzaku T.: "Suzaku Observations of the HMXB 1A 1118-61", Astrophys. J. **733**, No. 1, p. article id. 15 (2011). ∗

Kratzer R. M., Richards G. T., Goldberg D. M., Oguri M., Kochanek C. S., Hodge J. A., Becker R. H., and Inada N.: "Analyzing the Flux Anomalies of the Large-separation Lensed Quasar SDSS J1029+2623", Astrophys. J. Lett. **728**, No. 1, pp. L18–L22 (2011). ∗

Abadie J., Terada Y., and Science t.: "Search for Gravitational Wave Bursts from Six Magnetars", Astrophys. J. Lett. **734**, No. 2, p. L35 (2011). ∗

Gandhi P., Blain A. W., Russell D. M., Casella P., Malzac J., Corbel S., D'Avanzo P., Lewis F. W., Markoff S., Cadolle B. M., Goldoni P., Wachter S., Khangulyan D., and Mainzer A.: "A Variable Mid-infrared Synchrotron Break Associated with the Compact Jet in GX 339-4", Astrophys. J. Lett. **740**, No. 1, p. article id. L13, 7 pp. (2011). ∗

Vink J., Bamba A., and Yamazaki R.: "The Radiative X-ray and Gamma-ray Efficiencies of Rotation-powered Pulsars", Astrophysical Journal **727**, No. 2, pp. 131-1–131-5 (2011). ∗

Ohsuga K. and Mineshige S.: "Global Structure of Three Distinct Accretion Flows and Outflows around Black Holes from Two-dimensional Radiation-magnetohydrodynamic Simulations", Astrophysical Journal **736**, No. 1, p. 18 (2011). ∗

The CTA C. and Bamba A.: "Design concepts for the Cherenkov Telescope Array CTA: an advanced facility for ground-based high-energy gamma-ray astronomy", Experimental Astronomy **32**, No. 3, pp. 193–316 (2011). ∗

Actis M., Terada Y., and CTA t.: "Design concepts for the Cherenkov Telescope Array CTA: an advanced facility for ground-based high-energy gamma -ray astronomy", Experimental Astronomy **32**, 193–316 (2011). ∗

Ishikawa S., Saito S., Watanabe S., Odaka H., Fukuyama T., Sugimoto S., Kokubun M., Takahashi T., Terada Y., Tajima H., Tanaka T., Krucker S., Christe S., McBride S., and Glesener L.: "Fine-pitch semiconductor detector for the FOXSI mission", Institute of Electrical and Electronics Engineers Transactions on Nuclear Science **58**, pp2039–pp2046 (2011). ∗

Tsuchiya H., Enoto T., Yamada S., Yuasa T., Nakazawa K., Kitaguchi T., Kawaharada M., Kokubun M., Kato H., and Makishima K.: "Long-durationgamma-rayemissionsfrom2007and2008winterthunderstorms", J. Geophys. Res. **116**, No. D09113, pp. 1–14 (2011). ∗

Esposito P., Israel G. L., Turolla R., Mattana F., Tiengo A., Possenti A., Zane S., Rea N., Burgay M., G0tz D., Mereghetti S., Stella L., Wieringa M., Sarkissian J. M., Enoto T., Romano P., Sakamoto T., Nakagawa Y., Makishima K., Nakazawa K., Nishioka H., and Francois-Martin C.: "Long-term spectral and timing properties of the soft gamma-ray repeater SGR 1833-0832 and detection of extended X-ray emission around the radio pulsar PSR B1830-08", Mon. Not. R. Astron. Soc. **416**, No. 1, pp. 205–215 (2011). ∗

Kawakatu N. and Ohsuga K.: "New method for exploring super-Eddington active galactic nuclei by near-infrared observations", Mon. Not. R. Astron. Soc. **417**, No. 4, pp. 2562–2570 (2011). ∗

Miyoshi M., Shen Z., Oyama T., Takahashi R., and Kato Y.: "Oscillation Phenomena in the Disk around the Massive Black Hole Sagittarius A∗", Publ. Astron. Soc.

Jpn. **63**, No. 5, pp. 1093–1116 (2011). ∗

Gandhi P., Isobe N., Birkinshaw M., Worrall D. M., Sakon I., Iwasawa K., and Bamba A.: "Diffraction-Limited Subaru Imaging of M82: Sharp Mid-Infrared View of the Starburst Core", Publ. Astron. Soc. Jpn. **63**, No. SP2, p. S505S521 (2011). ∗

Katsuda S. and Yoshii R.: "Suzaku detection of diffuse hard X-ray emission outside Vela X", Publ. Astron. Soc. Jpn. **63**, No. SP3, pp. 827–836 (2011). ∗

Yamaguchi H., Koyama K., and Uchida H.: "Suzaku View of the Supernova Remnant RCW 86: X-Ray Studies of Newly-Discovered Fe-Rich Ejecta", Publ. Astron. Soc. Jpn. **63**, No. SP3, p. 837 (2011). ∗

Yamada S., Makishima K., Nakazawa K., Kokubun M., Kawaharada M., Kitaguchi T., Watanabe S., Takahashi H., Noda H., Nishioka h., Hiragi K., Hayashi K., Nakajima K., Tashio M., Sasano M., Nishino S., Torii S., Sakurai S., Takahashi T., Mizuno T., Enoto T., Yuasa T., Tanaka T., Kouzu T., Nakano T., Fukazawa Y., Terada Y., Uchiyama Y., Iwakiri W., and HXD t.: "Improvements in Calibration of GSO Scintillators in the Suzaku Hard X-Ray Detector", Publ. Astron. Soc. Jpn. **63**, No. SP3, pp. S645–S656 (2011). ∗

Hayashi T., Ishida M., Terada Y., Bamba A., and Shionome T.: "Suzaku Observation of the Intermediate Polar V1223 Sagittarii", Publ. Astron. Soc. Jpn. **63**, No. SP3, pp. S739–S750 (2011). ∗

Nakagawa Y., Makishima K., and Enoto T.: "The Suzaku Discovery of A Hard Power-Law Component in the Spectra of Short Bursts from SGR 0501+4516", Publ. Astron. Soc. Jpn. **63**, No. SP3, pp. S813–S820 (2011). ∗

Fujinaga T., Bamba A., Dotani T., Ozaki M., Puehlhofer G., Wagner S., Reimer O., Funk S., and Hinton J.: "Suzaku Observation of the Unidentified Very High Energy Gamma-Ray Source HESS J1702-420", Publ. Astron. Soc. Jpn. **63**, No. SP3, pp. S857–S864 (2011). ∗

Konami S., Tamagawa T., Matsushita K., Gandhi P., and Tsuru T. G.: "Suzaku metal abundance patterns in the outflow region of M82 and the importance of charge exchange", Publ. Astron. Soc. Jpn. **63**, No. SP3, pp. S913–S924 (2011). ∗

Yamauchi S., Bamba A., and Koyama K.: "A New Candidate of an X-Ray Luminous Cluster of Galaxies behind the Galactic Plane", Publ. Astron. Soc. Jpn. **63**, No. SP3, pp. S957–S961 (2011). ∗

Uchida H., Tsunemi H., Katsuda S., Mori K., Petre R., and Yamaguchi H.: "A Suzaku Study of Ejecta Structure and Origin of Hard X-Ray Emission in the Supernova Remnant G156.2+5.7", Publ. Astron. Soc. Jpn. **64**, No. 3, p. 61 (2011). ∗

Ohnishi T., Koyama K., Tsuru T. G., Masai K., Yamaguchi H., and Ozawa M.: "X-Ray Spectrum of a Peculiar Supernova Remnant, G359.1-0.5", Publications of the Astronomical Society of Japan **63**, 527 (2011). ∗

Yamaoka K., Yoshida A., Nonaka Y., Yoko S., Hara T., Yamamoto T., Mori K., Nakahira S., Kotani T., Nakagawa Y., Tomida H., Ueno S., Tamura T., and Torii S.: "The CALET Gamma-ray Burst Monitor (CGBM)", The 32nd nternational Cosmic Ray Conference, No. 0839, pp. 110–113 (2011). ∗

Aihara H., Inada N., and The S.: "The eighth data release of the Sloan Digital Sky Survey: First data from SDSS-III", The Astrophysical Journal Supplement **193**, No. 2, pp. 29-1–29-11 (2011). ∗

Hurley K., Terada Y., and HETE-2 T.: "The Interplanetary Netw ork Supplement to the HETE-2 Gamma-Ray Burst Catalog", The Astrophysical Journal Supplement **197**, No. 2, p. article id. 34 (2011). ∗

Yamaguchi H., Ozawa M., and Ohnishi T.: "New insights into SNR evolution revealed by the discovery of recombining plasmas", Advance in Space Research **49**, No. 3, p. 451 (2012). ∗

Lemoine-Goumard M., Renaud M., Vink J., Allen G. E., Bamba A., Giordano F., and Uchiyama Y.: "Constraints on cosmic-ray efficiency in the supernova remnant RCW 86 using multi-wavelength observations", Astron. Astrophys. **545**, A28-1–A28-9 (2012). ∗

Inada N., Oguri M., Shin M., Kayo I., Strauss M. A., Morokuma T., Rusu C. E., Fukugita M., Kochanek C. S., Richards G. T., Schneider D. P., York D. G., Bahcall N. A., Frieman J. A., Hall P. B., and White R. L.: "The Sloan Digital Sky Survey Quasar Lens Search. V. Final Catalog from the Seventh Data Release", Astron. J. **143**, No. 5, pp. 119-1–119-15 (2012). ∗

Oguri M., Inada N., Strauss M. A., Kochanek C. S., Kayo I., Shin M., Morokuma T., Richards G. T., Rusu C. E., Frieman J. A., Fukugita M., Schneider D. P., York D. G., Bahcall N. A., and White R. L.: "The Sloan Digital Sky Survey Quasar Lens Search. VI. Constraints on Dark Energy and the Evolution of Massive Galaxies", Astron. J. **143**, No. 5, pp. 120-1–120-14 (2012). ∗

Kishishita T., Bamba A., Uchiyama Y., Tanaka Y., and Takahashi T.: "X-Ray Investigation of the Diffuse Emission around Plausible γ-Ray Emitting Pulsar Wind Nebulae in Kookaburra Region", Astron. J. **750**, No. 2, pp. 162-1–162-8 (2012). ∗

Ota N., Oguri M., Dai X., Kochanek C. S., Richards G. T., Ofek E. O., Blandford R. D., Schrabback T., and Inada N.: "The Chandra View of the Largest Quasar Lens SDSS J1029+2623", Astron. J. **756**, No. 1, pp. 26-1–26-10 (2012). ∗

Paredes J. M. and Terada Y.: "Binaries with the eyes of CTA", Astroparticle, pp. 1–23 (2012). ∗

Yamaguchi H., Tanaka M., Maeda K., Slane P. O., Adam F., Smith R. K., Katsuda S., and Yoshii R.: "Elemental Abundances in the Possible Type Ia Supernova Remnant G344.7-0.1", Astrophys. J. **748**, No. 2, p. 137 (2012).

*

Margutti R., Soderberg A. M., Terada Y., and SNR C.: “Inverse Compton X-Ray Emission from Supernovae with Compact Progenitors: Application to SN2011fe”, Astrophys. J. **751**, No. 2, p. 134-10 (2012). *

Ichikawa K., Ueda Y., Terashima Y., Oyabu S., Gandhi P., Matsuta K., and Nakagawa T.: “Mid- and Far-infrared Properties of a Complete Sample of Local Active Galactic Nuclei”, Astrophys. J. **754**, No. 1, p. 14 (2012). *

Bamba A., Puehlhofer G., Acero F., Klochkov D., Tian W., Yamazaki R., Li Z., Horns D., Kosack K., and Komin N.: “Suzaku Observations of the Non-thermal Supernova Remnant HESS J1731-347”, Astrophys. J. **756**, No. 2, pp. 149-1–149-11 (2012). *

Katsuda S., Yamada S., and Tamagawa T.: “High-resolution X-ray Spectroscopy of the Galactic Supernova Remnant Puppis A with XMM-Newton RGS”, Astrophys. J. **756**, No. 49, pp. 49 - 1–49 - 7 (2012). *

Sanders N. E., Soderberg A. m., Valenti S., Foley R. J., Chornock R., Chomiuk L., Berger E., Smartt S., Hurley K., Barthelmy S. D., Levesque E. M., Narayan G., Botticella M. T., Briggs M. S., Connaughton V., Terada Y., Gehrels N., Golenetskii S., Mazets E., Cline T., Von Kienlin A., Boynton W., Chambers K. C., Grav T., Heasley J. N., Hodapp K. W., Jedicke R., Naiser N., Kirshner R. P., Kudritzki R. -., Luppino G. A., Lupton R. H., Magnier E. A., Moet D. G., Morgan J. S., Onaka P. M., Price P. A., Stubbs C. W., Tonry J. L., Wainscoat R. J., and Waterson M. F.: “SN 2010ay is a Luminous and Broad-lined Type Ic Supernova within a Low-metallicity Host Galaxy”, Astrophys. J. **756**, No. 184, pp. 1–19 (2012). *

Maeda K., Terada Y., Kasen D., Ropke F. K., Bamba A., Diehl R., Nomoto K., Kromer M., Seitenzahl I. R., Yamaguchi H., Tamagawa T., and Hillebrandt W.: “Prospect of Studying Hard X- and Gamma-Rays from Type Ia Supernovae”, Astrophys. J. **760**, No. 1, pp. 54-1–54-9 (2012). *

Iwakiri W., Terada Y., Mihara T., Angelini L., Tashiro M., Enoto T., Yamada S., Makishima K., Nakajima M., and Yoshida A.: “Possible Detection of an Emission Cyclotron Resonance Scattering Feature from the Accretion-powered Pulsar 4U 1626-67”, Astrophys. J. Lett. **751**, No. 1, pp. 35-1–35-11 (2012). *

Gandhi P., Yamamura I., and Takita S.: “Dramatic Infrared Variability of WISE J1810-3305: Catching Early-time Dust Ejection During the Thermal Pulse of an Asymptotic Giant Branch Star?”, Astrophys. J. Lett. **751**, No. 1, p. article id. L1, 6 pp. (2012). *

Katsuda S., Yamada S., and Tamagawa T.: “Discovery of a Pulsar Wind Nebula Candidate in the Cygnus Loop”, Astrophys. J. Lett. **754**, No. L7, pp. L7 - 1–L7 - 5 (2012). *

Liyi G., Haiguang X., Kawaharada M., Nakazawa K., Zhenzhen Q., Jingying W., Yu W., Zhongli Z., and Makishima K.: “Two-Phase ICM in the Central Region of the Rich Cluster of alaxies A1795: A Joint Chandra, XMM-Newton, and uzaku View”, Astrophysical Journal **749**, No. 2, p. 186 (2012). *

Kawashima T., Ohsuga K., Mineshige S., Yoshida T., Dominikus H., and Matsumoto R.: “Comptonized Photon Spectra of Supercritical Black Hole Accretion Flows with Application to Ultraluminous X-Ray Sources”, Astrophysical Journal **752**, No. 1, p. 12 (2012). *

Mitsuda K., Kelley R. L., and Terada Y.: “The High-Resolution X-Ray Microcalorimeter Spectrometer, SXS, on Astro-H”, J. Low Temp. Phys. **167**, No. 5-6, pp. 795–802 (2012). *

Asmus D., Honig S. F., Gandhi P., Smette A., and Duschl W. J.: “Nuclear mid-infrared properties of nearby low-luminosity AGN”, J. Phys.: Conf. Ser. **372**, No. 1, p. 012034 (2012). *

Enoto T., Nakagawa Y., Sakamoto T., and Makishima K.: “Spectral comparison of weak short bursts to the persistent X-rays from the magnetar 1E 1547.0-5408 in its 2009 outburst”, Mon. Not. R. Astron. Soc. **427**, No. 4, pp. 2824–2840 (2012). *

Tsuchiya H., Hibino K., Kawata K., Hotta N., Tateyama N., Ohnishi M., Takita M., Chen D., Huang J., H. L., J.L. Z., X.X. Y., Y.H T., S. M. N., Munakata K., Enoto T., and Makishima K.: “Observation of thundercloud-related gamma rays and neutrons in Tibet”, Phys. Rev. D **85**, No. 092006, pp. 1–35 (2012). *

Konno K. and Takahashi R.: “Spacetime rotation-induced Landau quantization”, Phys. Rev. D **856**, No. 6, p. 061502-1 (2012). *

Nakahira S., Terada Y., MAXI t., Suzaku t., and Swift t.: “A Spectral Study of the Black Hole Candidate XTE J1752-223 in the High/Soft State with MAXI, Suzaku, and Swift”, Publ. Astron. Soc. Jpn. **64**, No. 1, p. 13-12 (2012). *

Terada Y., Tashiro M. S., Bamba A., Yamazaki R., Kouzu T., Koyama S., and Seta H.: “Search for Diffuse X-Rays from the Bow Shock Region of Runaway Star BD +43 3654 with Suzaku”, Publ. Astron. Soc. Jpn. **64**, No. 6, pp. 138-1–138-7 (2012). *

Uchida H., Koyama K., Yamaguchi H., Sawada M., Ohnishi T., Tsuru T. G., Tanaka T., Yoshiike S., and Fukui Y.: “Recombining Plasma and Hard X-Ray Filament in the Mixed-Morphology Supernova Remnant W 44”, Publ. Astron. Soc. Jpn. **64**, No. 6, p. 141 (2012). *

Ichikawa K., Ueda Y., Terashima Y., Oyabu S., Gandhi P., Matsuta K., and Nakagawa T.: “Mid- and Far-infrared Properties of Local Active Galactic Nuclei”, Publications of The Korean Astronomical Society **27**, No. 4, pp. pp.275–279 (2012). *

Matsuta K., Gandhi P., Dotani T., Nakagawa T., Isobe N., Ueda Y., Ichikawa K., Terashima Y., Oyabu S., Tamamura I., and Stawarz L.: "Infrared and Hard X-Ray Diagnostics of AGN Identification from the Akari and Swift/bat All-Sky Surveys", Publications of The Korean Astronomical Society **27**, No. 4, pp. pp.285–pp.286 (2012). ∗

Enoto T., Nakagawa Y., Nakano T., Nishioka H., Yasuda T., Terada Y., Sakamoto T., Makishima K., and Suzaku Magnetar M.: "Recent Suzaku studies of the X-ray emission from magnetars", SUZAKU 2011: Exploring the X-ray Universe: Suzaku and Beyond. AIP Conference Proceedings **1427**, 68–75 (2012).

Ohno M., Hanabata Y., Uehara T., Takahashi T., Mizuno M., Fukazawa Y., Yamaoka K., Sugita S., Ohmori N., Akiyama M., Yamauchi M., Yasuda T., Terada Y., Iwakiri W., Takahara K., ASANIHA M., Kobayashi S., Tashiro M. S., Kokubun M., Takahashi T., Nakagawa Y., Urata Y., Tsai P. P., Chuang C., Nakazawa K., Murakami T., and Tajima H.: "The six year results of Suzaku Wide-band All-Sky monitor", SUZAKU 2011: Exploring the X-ray Universe: Suzaku and Beyond. AIP Conference Proceedings **1427**, 115–122 (2012).

Misawa T., Inada N., Ohsuga K., Gandhi P., Takahashi R., and Masamune O.: "Spectroscopy along multiple, lensed sight lines through outflowing winds in the Quasar SDSS J1029+2623", Astronomical Journal **145**, No. 2, p. 12 (2013). ∗

Acero F., Bamba A., Casanova S., de C. E., de Ona W. E., Gabici S., Gallant Y., Hadasch D., Marcowith A., Pedaletti G., Reimer O., Renaud M., Torres D. F., Volpe F., and the CTA c.: "Gamma-ray signatures of cosmic ray acceleration, propagation, and confinement in the era of CTA", Astroparticle Phys., p. (2013). ∗

Katsuda S.: "X-ray Proper Motions and Shock Speeds along the Northwestern Rim of SN 1006", Astrophys. J. **763**, No. 85, pp. 85 - 1–85 - 7 (2013). ∗

Takahashi H. R., Ohsuga K., Sekiguchi Y., Inoue T., and Tomida K.: "Explicit-Implicit Scheme for Relativistic Radiation Hydrodynamics", Astrophysical Journal **764**, No. 2, p. 13 (2013). ∗

Edeison R., Mushotzky R. F., Vaughan S., Scargle J., Gandhi P., Malkan M., and Baumgartner W. H.: "Kepler Observations of Rapid Optical Variability in the BL Lacertae Object W2R1926+42", Astrophysical Journal **766**, No. 1, p. article id. 16, 8 pp. (2013). ∗

Stawarz L., Tanaka Y. T., Madejski G., O'Sullivan S. P., Cheung C. C., Feain I. J., Fukuzawa Y., Gandhi P., Hardcastle M. J., Kataoka J., Ostriwski M., Reville B., Siemiginowska A., Simionescu A., Takahashi T., Takei Y., Takeuchi Y., and Werner N.: "Giant Lobes of Centaurus A Radio Galaxy Observed with the Suzaku X-Ray Satellite", Astrophysical Journal **766**, No. 1, p. article id. 48, 19 pp. (2013). ∗

Russell D. M., Markoff S., Casella P., Cantrell A. G., Chatterjec R., Fender R. P., Gallo E., Gandhi P., Homan J., Maitra D., Miller-Jones j. A., O'Brien K., and Shahbaz T.: "Jet spectral breaks in black hole X-ray binaries", Mon. Not. R. Astron. Soc. **429**, No. 1, pp. 815–832 (2013). ∗

Chiang C. -., Cackett E. M., Gandhi P., and Fabian A. C.: "Confirmation of the nature of the absorber in IRAS 09104+4109", Mon. Not. R. Astron. Soc. **Advance Access**, 8pp. (2013). ∗

Helder E. A., Vink J., Bamba A., Bleeker J. A., Burrows D. N., Ghavamian P., and Yamazaki R.: "Proper Motion of Halpha filaments in Supernova Remnant RCW86", Mon. Not. R. Astron. Soc., p. (2013). ∗

Harayama A., Terada Y., Ishida M., Hayashi T., Bamba A., and Tashiro M. S.: "Search for Non-Thermal Emissions from Isolated Magnetic White Dwarf EUVE J0317-855 with Suzaku", Publ. Astron. Soc. Jpn. **64**, No. 4, pp. – (2013). ∗

Nomura M., Ohsuga K., Wada K., Susa H., and Misawa T.: "Modeling line-driven disk wind for broad absorption lines of quasars", Publ. Astron. Soc. Jpn., p. (2013). ∗

Hanabata Y., Sawada M., Katagiri H., Bamba A., and Fukazawa Y.: "X-Ray Observations of the W51 Complex with Suzaku", Publ. Astron. Soc. Jpn., p. (2013). ∗

(Review)

Kawaharada M.: "Nearby 'hot spot' gives clues to growth of galaxy clusters", Cosmos Magazine online, pp. 1–2 (2010).

Kawaharada M.: "Suzaku witnessed the growth scene of the largest structure in space", JAXA Suzaku project topics, (2010).

Kawaharada M.: "A cosmic show-down", RIKEN RESEARCH, pp. 1–5 (2010).

Kawaharada M.: "Scholars unveil snapshot of galaxy cluster growth", The China Post, pp. 1–3 (2010).

Kawaharada M.: "Japanese Scientists measure growth in galaxy cluster", The Japan Times Online, pp. 1–5 (2010).

Kawaharada M.: "Astronomers study galaxy cluster growth", UPI.com, pp. 1–2 (2010).

川原田円: "アストロノミィ・ト ゥデイ、成長を続ける銀河団の姿をとらえた", ニュートン 7 月号, pp. 1–10 (2010).

川原田円: "宇宙の大規模構造の中で進化する銀河団", パリティ特集号, (2010).

川原田円: "理研ら、「すざく」の活用により銀河団 の成長方法を確認することに成功", マイコミジャーナルオンライン , (2010).

川原田円: "銀河団の成長確認", 日刊工業新聞, pp. 1–1 (2010).

川原田円: "銀河団、ガス流入で成長", 日経産業新聞, pp. 1–1 (2010).

川原田円: "すざく衛星で、宇宙最大の構造が成長する現場をとらえる", 理化学研究所と台湾中央研究院 (ASIAA) からの合同発表, (2010).

高橋労太: "ブラックホールを影絵としてとらえる", 科学, pp. 324–326 (2011).

川原田円, 岡部信広: "すざく衛星がとらえた銀河団外縁部ガスの特徴とそ の周辺の大規模構造との相関", 天文月報, No. 3, (2011).

勝田哲: "X 線で探る超新星残骸", ISAS ニュース **373**, 1–3 (2012).

(Others)

Amenomori M., Tsuchiya H., and Tibet AS g.: "Is the large-scale sidereal anisotropy of the galactic cosmic-ray intensity really instable at TeV energies?", Astropart Phys. **36**, No. 1, pp. 237–241 (2012).

Katsuda S.: "Violent Evolution of Supernova Remnants as Revealed by Chandra and XMM-Newton", Mem. Soc. Astron. Ital. **83**, No. 277, pp. 277 - 1–277 - 5 (2012).

Koizumi M., Kitatani F., Harada H., Takamine J., Kureta M., Seya M., Tsuchiya H., and Iimura H.: "ProposalofNeutronResonance Densitometry for Particle like debris of Melted Fuel using NRTA and NRCA", Proceedings of INMM 53rd Annual Meeting (Internet), pp. 1–8 (2012).

馬場彩: "cosmic wonder 超新星残がい - 恒星がつくる宇宙の花火", Newton, pp. 78–93 (2011).

馬場彩: "X 線で探る宇宙線加速源", 天文月報, pp. 634–640 (2011).

[Book · Proceedings]

(Original Papers) *Subject to Peer Review

Harayama A., Terada Y., Ishida M., Bamba A., Hayashi T., and Shionome T.: "Search for non-thermal emission from isolated magnetized white dwarfs with INTEGRAL", The Energetic Cosmos :from Suzaku to Astro-H, Otaru, 2010–6〜7, JAXA, Sagamihara, pp. 200–201 (2010).

Terada Y., Harayama A., Morigami K., Ishida M., Bamba A., Dotani T., Hayashi T., Okada S., Nakamura R., Makishima K., Mukai K., and Sachindra N.: "Systematic surveys of the non thermal emission from white dwarfs with Suzaku and INTEGRAL", X-Ray Astronomy 2009; Present Status, Multi-Wavelength Approach and Future Perspectives: Proceedings of the International Conference, Bologna, Italy, 2009–9, AIP Conference Proceedings,, Bologna, pp. 215–216 (2010).

Gandhi P., Russell D. M., Casella P., Malzac J., and Durant M.: "X-ray Binary Jets: New Constraints From Multi-wavelength Spectroscopy And Rapid Timing", American Astronomical Society,HEAD meeting 12, USA, 2011–9, AAS, Harbard, p. 44.04 (2011). ∗

Nakagawa Y., Enoto T., Makishima K., Yoshida A., Yamaoka K., Sakamoto T., Rea N., and Hurley K.: "Suzaku Detection of Hard X-ray Emission in SGR 0501+4516 Short Burst Spectrum", High-Energy Emission from Pulsars and their Systems, Astrophysics and Space Science Proceedings, Berlin, Springer-Verlag Berlin Heidelberg, Berlin, pp. 323–327 (2011). ∗

Enoto T., Makishima K., Rea N., Nakagawa Y., Nakazawa K., and Sakamoto T.: "Wide-band X-ray Studies of Magnetars with Suzaku", High-Energy Emission from Pulsars and their Systems, Astrophysics and Space Science Proceedings, 2011– Springer-Verlag Berlin Heidelberg, Berlin , pp. 275–278 (2011). ∗

Mason E. and Gandhi P.: "Interacting binaries: science cases where simultaneous multicolor medium resolution spectroscopy makes a difference", Proc. "First year of science with X-SHOOTER" Como., Italy, 2010–9, Astronomiche Nachrichten, Como, (2011). ∗

Gandhi P.: "Constraining accretion from coordinated multiwavelength rapid timing observations of X-ray binaries", The First Year of MAXI: Monitoring variable X-ray sources, Aoyama, 2010–11〜12, RIKEN, Wako, p. 75 (2011).

Gandhi P.: "Multiwavelength rapid timing & broad-band spectroscopy of X-ray binaries", The X-ray Universe 2011, Berlin, Germany, 2011–6, The X-ray Universe 2011, Harbard, (2011). ∗

Gandhi P., Asmus D., Hoenig S., and Smette A.: "Resolved mid-IR emission as an isotropic probe in AGN at high & low powers", The X-ray Universe 2011, Berlin, Germany, 2011–6, The X-ray Universe 2011, Berlin, (2011). ∗

Gandhi P.: "Multi-wavelength studies of accreting stellar mass black holes", 39th COSPAR Scientific Assembly, Mysore, India, 2012–7, ADS, Harbard, p. p.582 (2012). ∗

Gandhi P., Asmus D., Honig S. F., Smette A., Duschl W. J., Matsuta K., Ichikawa K., Ueda Y., Terashima Y., Gilli R., Comastri A., and Vagnali C.: "The high angular resolution view of local X-ray selected AGN in the mid-infrared", Half a Century of X-ray Astronomy, Proceedings of the conference, Mykonos island, Greece, 2012–9, HALF A CENTURY OF X-RAY ASTRONOMY, Mykonos island, pp. 1–18 (2012). ∗

Takeuchi Y., Tamagawa T., Asami F., Yoshikawa A., Iwahashi T., Konami S., and Iwakiri W.: "Signal shape and charge sharing between electrodes of GEM in dimethyl ether", Proceedings of 2nd International Conference on Micro Pattern Gaseous Detectors (MPGD2011), Kobe, 2011–8〜9, JINST, Bristol, pp. 2012 JINST 7 C03042 - 1–2012 JINST 7 C03042 - 12 (2012). ∗

Gendreau K., Asami F., Enoto T., Hayato A., Iwahashi T., Iwakiri W., Kaneko K., Kitaguchi T., Kohmura T., Takeuchi Y., Tamagawa T., Yamada S., Yoshikawa A., and XACT t.: "The x-ray advanced concepts testbed (XACT) sounding rocket payload", Proceedings of the SPIE, Volume 8443, Amsterdam, Netherlands, 2012–7, SPIE, Bellingham, pp. 84434V-1–84434V-7 (2012).

Gandhi P.: "Optical/IR - X-ray variability in X-ray binaries", X-ray Binaries. Celebrating 50 Years Since the Discovery of Sco X-1., Boston, USA, 2012–7, CXC, Harbard, pp. 1–19 (2012). ∗

Asmus D., Gandhi P., Hoenig S. F., and Smette A.: "The largest mid-infrared atlas of active galactic nuclei at sub-arcsecond spatial scales", Proceedings of the Torus Workshop 2012, Texas, USA, 2012–12, Cosmology and Extragalactic Astrophysics, Texas, pp. 1–8 (2013). *

(Review)

Terada Y. and Dotani T.: "The International X-ray Observatory and other X-r ay missions, expectations for pulsar physics", High-energy emission from pulsars and their systems, D. F. Torres and N. Rea, Berlin, (2011).

(Others)

大須賀健: "ゼロからわかるブラックホール", ゼロからわかるブラックホール, 講談社, , (2011).

Oral Presentations

(International Conference etc.)

Nakagawa Y., Enoto T., Makishima K., Yoshida A., Yamaoka K., Sakamoto T., Rea N., Hurley K., SUZAKU SGR 0501+4516 T., and HETE-2 T.: "Suzaku Detection of Hard X-ray Emission in SGR 0501+4516 Short Burst Spectrum", ICREA Workshop on The High-Energy Emission from Pulsars and their Systems, Barcelona, Spain, Apr. (2010).

Nakagawa Y., Tamagawa T., Yamaoka K., Sugita S., Yoshida A., Sato R., Ohno M., Nakazawa K., Tashiro M. S., Sugasahara T., Iwakiri W., Onda K., Urata Y., Yonetoku D., Murakami T., Kawai N., Usui R., Nakajima H., Endo A., Yamauchi M., Sonoda E., Ohmori N., Kohno K., Hayashi H., Daikyuji A., Noda K., Nishioka Y., Suzuki M., Tazaki F., Eguchi S., Kubota K., Ishino Y., Hiroi K., Ueda Y., and Suzaku GRB ToO T.: "Suzaku Observations of Long-Duration GRB 090709A X-ray Afterglow", The GRB Conference in Kyoto 2010, Kyoto, Apr. (2010).

Bamba A.: "Cosmic ray production in Supernovae and SNR", IXO Science Meeting, Paris, France, May (2010).

Ohsuga K.: "Radiation MHD Simulations of Black Hole Accretion Flow and Outflow", Relativistic Whirlwind, Trieste, Italy, May–June (2010).

Kawaharada M.: "Joint X-ray, lensing and optical study of Abell 1689: anisotropic gas temperature and entropy distributions associated with the large-scale structure", CL J2010: from Massive Galaxy Formation to Dark Energy, IPMU, June (2010).

Inada N.: "Probing Evolution of Hot Gas and Galaxy Distributions in Galaxy Cluster", Workshop "CL J2010+0628: from Massive Galaxy Formation to Dark Energy", (IPMU University of Tokyo), IPMU University of Tokyo, June (2010).

Nakagawa Y., Mihara T., Sugizaki M., Kohama M., Yamamoto T., Suzuki M., Matsuoka M., Kawai N., Morii M., Sugimori K., Yoshida A., Yamaoka K., Nakahira S., Negoro H., Nakajima M., Isobe N., and MAXI T.: "The First Results of Monitoring Galactic Magnetar Activities with MAXI/GSC", 38th COSPAR scientific assembly (COSPAR 2010), Bremen, Germany, July (2010).

Tsuchiya H., Enoto T., Torii T., Kato H., Okano M., and Makishima K.: "Electron Acceleration Induced by Cosmic Rays in Terrestrial Thunderstorm", AOGS (Asia Oceania Geoscience Society) 2010, (AOGS (Asia Oceania Geoscience Society) 2010), Hyderabad, India, July (2010).

Konami S., Tamagawa T., Gandhi P., Matsushita K., and Tsuru T. G.: "Metal abundances of the hot X-ray emitting ISM", The Infrared/X-ray Connection in Galaxy Evolution, (University College London), Surrey, UK, July (2010).

Inada N.: "Gravitationally lensed quasar survey using BOSS quasars", Sloan Digital Sky Survey III Collaboration Meeting, APC L'Universit'e Paris Diderot, France, Sept. (2010).

Ohsuga K.: "Radiation-magnetohydrodynamic simulations of black hole accretion flow and outflow", Accretion and Outflow in Black Hole Systems, Kathmandu, Nepal, Oct. (2010).

Bamba A.: "SNR study with CTA", CTA General Collaboration Meeting, Oxford, UK, Oct. (2010).

Inada N.: "Gravitationally lensed quasar survey using BOSS quasars", Workshop "Evolution of massive galaxies and their AGNs with the SDSS-III/BOSS survey", (IPMU University of Tokyo), IPMU University of Tokyo, Oct. (2010).

Kawaharada M.: "ICM up to the virial radius", ASTRO-H workshop, Tokyo, Dec. (2010).

Takahashi R.: "Constraining the size of the dark region around the M87 lack hole by space-VLBI observations", IPMU Workshop on Black Holes, (IPMU), Kashiwa, Feb. (2011).

Kawaharada M.: "ICM in cluster outskirts affected by large scale structure discovered by A1689", X-ray Universe 2011, Berlin, Germany, June (2011).

Ohsuga K.: "Radiation-HD/MHD simulations", BLACK HOLE SLIM DISK WORKSHOP, Warsaw, Poland, July (2011).

Yamaguchi H.: "Recombination X-rays from mixed-morphology SNRs", Exploring the X-ray Universe: Suzaku and Beyond, (Stanford), California, USA, July (2011).

Bamba A.: "Multi-wavelength Studies of PWNe", Suzaku 2011, Stanford, USA, July (2011).

Konami S., Tamagawa T., Gandhi P., Matsushita K., and Tsuru T. G.: "A comparison of X-ray emission mechanisms and inter-stellar metal abundances in starburst and non-starburst galaxies", Suzaku 2011: Exploring the X-ray universe: Suzaku and beyond, (SLAC National Accelerator Laboratory), Stanford, USA, July (2011).

Kawaharada M.: "Suzaku Discovery of A Hot Gas Region in A1689 Outskirts Connected to the Large Scale Structure", Suzaku conference 2011, California, USA, July (2011).

Yamaguchi H.: "Innershell Ionization & Fluorescence/Auger Yield: Need of a New Code, Required from Observations", AtomDB Symposium, Cambridge, USA, Aug. (2011).

Yoshikawa A., Tamagawa T., Asami F., Iwahashi T., Takeuchi Y., Hayato A., hamagaki h., ueno k., gunji t., akimoto r., hayashi s., Rui O., nukariya a., and ochi a.: "Development of Resistive Electrode Gas Electron Multiplifier (RE-GEM)", 2nd International Conference on Micro Pattern Gaseous Detectors, Kobe, Aug.–Sept. (2011).

Yamaguchi H.: "Elemental Abundances in the Supernova Remnant G344.7-0.1 Studied with Suzaku", American Astronomical Society, HEAD Meeting, Newport, USA, Sept. (2011).

Bamba A.: "Supernova Remnants as Chemical Element Distributors", Chemical Evolution of the Universe, Tokyo, Oct. (2011).

Kawaharada M.: "Japanese plans and technologies for future high-energy astrophysics", IAC2011, Cape Town, South Africa, Oct. (2011).

Konami S., Tamagawa T., Gandhi P., Matsushita K., and Tsuru T. G.: "A comparison of metal abundance patterns of inter-stellar medium in starburst and non-starburst galaxies", Workshop on Chemical Evolution of the Universe, (Tokyo Metropolitan University), Hachioji, Oct.–Nov. (2011).

Konami S., Tamagawa T., Gandhi P., Matsushita K., and Tsuru T. G.: "A comparison of metal abundance patterns of inter-stellar medium in starburst and non-starburst galaxies", 11th International Symposium on Origin of Matter and Evolution of Galaxies (OMEG11), Wako, Nov. (2011).

Konami S., Tamagawa T., and Matsushita K.: "A comparison of metal abundance patterns of inter-stellar medium in starburst and non-starburst galaxies with X-ray observation", INAF seminar, (INAF), Rome, Italy, Jan. (2012).

Konami S., Tamagawa T., and Matsushita K.: "The abundance pattern of O, Ne, Mg, and Fe in the X-ray emitting interstellar medium of a spiral and starburst galaxies", MAP seminar, (MPA), Garching, Germany, Feb. (2012).

Nakagawa Y., Makishima K., Enoto T., and Sakamoto T.: "Wide-Band Spectra of Magnetar Burst Emission", IAU Symposium 279, Nikko, Mar. (2012).

Nakagawa Y., Makishima K., Enoto T., Sakamoto T., Mihara T., Sugizaki M., Yamaoka K., Hurley K., Yoshida A., Gandhi P., Tashiro M. S., and Morii M.: "Wide-Band Spectra of Magnetar Burst Emission", Positrons in Astrophysics, Murren, Switzerland, May (2012).

Ohsuga K.: "Radiation-MHD simulations of accretion flows and outflows around Black Holes", ASTRONUM 2012, Big Island, Hawaii, , USA, June (2012).

Yamaguchi H.: "X-ray studies of Type Ia supernova remnants and prospect for future observations", Energetic Astronomy, Annapolis, USA, June (2012).

Terada Y.: "Review on High Energy observations in searches for Non-thermal emissions from Accelerated particles in Magnetic White Dwarfs", the 13th Marcel Grossmann Meeting, Stockholm Univ., Konungariket Sverige, June (2012).

Ohsuga K.: "Overview of recent advances in accretion disk theory", 2012 X-ray Binaries, Boston, MA, USA, July (2012).

Harayama A., Terada Y., Ishida M., Bamba A., and Hayashi T.: "Restrictions on non-thermal X-rays from isolated magnetic white dwarfs with Suzaku", Marcel Grossmann Meetings on general relativity, Stockholm,, Konungariket Sverige, July (2012).

Terada Y., Harayama A., Ishida M., Bamba A., Hayashi T., Dotani T., Mukai K., Yrata Y., Makishima K., Nitta A., and Jager O. d.: "Review on High Energy Observations in Search for non-thermal Emissions from Accelerated Particles in Magnetic White warfs", Marcel Grossmann Meetings on general relativity, (University of Rome), Stockholm, Konungariket Sverige, July (2012).

Hayashi T., Terada Y., Ishida M., and Harayama A.: "Suzaku searches for WD pulars with a spectral model of post-shock regions", Marcel Grossmann Meetings on general relativity, Stockholm, Konungariket Sverige, July (2012).

Kitaguchi T., Tamagawa T., Iwahashi T., Hayato A., and GEMS t.: "Monte-Carlo Estimation of In-orbit Background for X-ray Polarimeter onboard GEMS", The 39th COSPAR Scientific Assembly, (COSPAR), Mysor, India, July (2012).

Kitaguchi T., NuSTAR t., Tamagawa T., and GEMS t.: "Observation plans of X-rays from white dwarfs with NuSTAR and future polarimeters", The Thirteenth Marcel Grossmann Meeting, (ICRANet), Stockholm, Sweden, July (2012).

Yamaguchi H.: "NEI modeling What do we have? What do we need?", AtomDB Workshop, Cambridge, USA, Aug. (2012).

Nakagawa Y., Enoto T., Makishima K., Nakazawa K., Sakamoto T., Yoshida A., Yamaoka K., Hurley K., and Rea N.: "Wide-Band Spectra of Magnetar Emission", 8th INTEGRAL Workshop "The Restless Gamma-Ray Universe", Dublin, Ireland, Sept. (2012).

Ohsuga K.: "Simulations of the radiation-pressure instability of disk and outflow", Accretion flow instabilities, Warsaw, Poland, Sept. (2012).

Yamada S.: "Inhomogeneous coronae and a stable disk of Cyg X-1 revealed with Suzaku", HALF A CENTURY OF X-RAY ASTRONOMY, (ESA), MYKONOS, Greece, Sept. (2012).

Yamaguchi H.: "X-ray spectroscopy of young supernova remnants: revealing stellar nucleosynthesis their environment", Rutgers Univ., Rutgers Univ., USA, Sept. (2012).

Ohsuga K.: "Launching mechanisms", The Physics of Accretion onto Black Holes, Bern, Switzerland, Oct. (2012).

Terada Y., Harayama A., Hayashi T., Dotani T., Ishida M., Bamba A., Makishima K., Mukai K., Urata Y., Nitta A., Okkie d. J., Chadwick P., Wagner S., Buckley D., Tashiro M. S., Kozu T., Koyama S., and Yamazaki R.: "X-ray searches for new Galactic Particle-Acceleraration sites with Suzaku", X-ray astronomy towards the next 50 years, (INAF), MIlano, Italy, Oct. (2012).

Katsuda S., Yamada S., and Tamagawa T.: "Discovery of a Pulsar Wind Nebula Candidate in the Cygnus Loop", X-ray Astronomy: towards the next 50 years!, (Astronomical Observatory of Brera and the Istituto di Astrofisica Spaziale e Fisica Cosmica of INAF), Milan, Italy, Oct. (2012).

Yamaguchi H.: "Element Abundances in Supernova Remnants", X-ray Astronomy: towardsthe next 50 years!, Milano, Italy, Oct. (2012).

Nakagawa Y., Makishima K., Enoto T., Sakamoto T., Mihara T., Sugizaki M., Yamaoka K., Hurley K., Yoshida A., Gandhi P., Tashiro M. S., and Morii M.: "Wide-Band Spectra of Magnetar Persistent and Burst Emission", X-ray Astronomy: towardsthe next 50 years!, Milano, Italy, Oct. (2012).

Ohsuga K.: "Radiation Magnetohydrodynamics of Black Hole Accretion Flows and Outflows", East Asia Numerical Astrophysics Meeting, Kyoto, Oct.–Nov. (2012).

Yamaguchi H.: "X-ray Spectroscopy of Non-Equilibrium Plasmas in Supernova Remnants - Discoveries of new Spectral Features", Seminar, (NASA/GSFC), NASA/GSFC, USA, Dec. (2012).

An H., Kitaguchi T., and NuSTAR t.: "A magnetic white dwarf binary, AE Aquarii, in the 3–79 keV band with NuSTAR", 221th Meeting of the American Astronomical Society, (American Astronomical Society), Long Beach, USA, Jan. (2013).

Miyasaka H., Kitaguchi T., and NuSTAR t.: "Commissioning and in-flight calibration of the nuclear spectroscopic telescope array (NuSTAR)", 221th Meeting of the American Astronomical Society, (American Astronomical Society), Long Beach, USA, Jan. (2013).

Kaspi V., Kitaguchi T., and NuSTAR t.: "NuSTAR observations of magnetars and rotation-powered pulsars", 221th Meeting of the American Astronomical Society, (American Astronomical Society), Long Beach, USA, Jan. (2013).

Wik D., Kitaguchi T., and NuSTAR t.: "NuSTAR's hard look at clusters and relics: bullet cluster first results", 221th Meeting of the American Astronomical Society, (American Astronomical Society), Long Beach, USA, Jan. (2013).

Nynka M., Kitaguchi T., and NuSTAR t.: "NuSTAR's preliminary results of the pulsar wind nebula G21.5-0.9", 221th Meeting of the American Astronomical Society, (American Astronomical Society), Long Beach, USA, Jan. (2013).

Tomsick J., Kitaguchi T., and NuSTAR t.: "The NuSTAR program for galactic binaries", 221th Meeting of the American Astronomical Society, (American Astronomical Society), Long Beach, USA, Jan. (2013).

Madsen K., Kitaguchi T., and NuSTAR t.: "The NuSTAR program for pulsar-wind nebulae", 221th Meeting of the American Astronomical Society, (American Astronomical Society), Long Beach, USA, Jan. (2013).

Grefenstette B., Kitaguchi T., and NuSTAR t.: "The NuSTAR program for supernova remnants", 221th Meeting of the American Astronomical Society, (American Astronomical Society), Long Beach, USA, Jan. (2013).

(Domestic Conference)

馬場彩: "RCW86 逆行衝撃波での宇宙線加速の可能性", SNR 研究会, 名古屋, 4 月 (2010).

高橋労太: "『ブラックホール』は実在するのか?", ひらめき☆ときめきサイエンス, (独立行政法人 日本学術振興会), 愛知教育大学, 7 月 (2010).

大須賀健: "AGN の新理論", 『ALMA-近傍 AGN 観測』検討会, 国立天文台三鷹, 8 月 (2010).

小波さおり, 玉川徹, 松下恭子, 鶴剛: "「すざく」衛星によるスターバースト銀河 M82 の重元素組成比の決定", 日本天文学会 2010 年秋季年会, (社団法人　日本天文学会), 金沢, 9 月 (2010).

馬場彩: "「すざく」衛星による宇宙線加速超新星残骸 HESS J1731-347 の観測", 日本天文学会 2010 年秋季年会, 金沢市, 9 月 (2010).

中川友進, 榎戸輝揚, 牧島一夫, 中澤知洋, 坂本貴紀, 吉田篤正, 山岡和貴: "マグネターのバースト/X 線定常放射の広帯域スペクトルの研究", 日本天文学会 2010 年秋季年会, 石川, 9 月 (2010).

川原田円: "Abel 1689 銀河団周辺部の高温ガスの観測的研究", 日本物理学会, (日本物理学会), 九州工業大学, 9 月 (2010).

馬場彩: "次世代 X 線天文台と ALMA-Subaru で探る超新星での元素合成", ALMA-Subaru Workshop 2010, 東京, 9 月 (2010).

稲田直久: "HSC を用いた重力レンズクエーサーサーベイ、およびその『巨大ブラックホールと銀河の共進化』への寄与", 超広域サーベイで明かす巨大ブラックホールと銀河の共進化： 理論モデルと観測戦略, 東北大学, 9 月 (2010).

稲田 直久: "Evolution of Galaxy Light Distributions in Galaxy Clusters", 日本天文学会 2010 年秋季年会, 金沢大学, 9 月 (2010).

馬場彩: "CTA Japan が狙う SNR Science", 宇宙線研究所共同利用研究会「ガンマ線天文学　日本の戦略 」, 千葉, 10 月 (2010).

大須賀健: "放射磁気流体シミュレーションの拓く世界", 松山ブラックホールワークショッフ, 愛媛大学, 10 月 (2010).

川原田円: “X 線天文衛星 ASTRO-H”, JAXA 宇宙航空技術研究発表会, (JAXA), 東京, 11 月 (2010).

馬場彩: “超新星残骸プラズマとアバンダンス”, Astro-H に関するワークショッフ, 東京, 12 月 (2010).

馬場彩: “「すざく」衛星による宇宙線加速超新星残骸 HESS J1731-347 の観測 (II)：他波長との比較”, 日本天文学会 2011 年秋季年会, 鹿児島市, 3 月 (2011).

馬場彩: “「すざく」による TeV ガンマ線未同定天体 HESS J1507-582 の観測”, 日本天文学会 2011 年春季年会, 筑波大学, 3 月 (2011).

原山淳, 寺田幸功, 堂谷忠靖, 石田学, 馬場彩, 林多佳由, 浦田裕次, 玉川徹: “「すざく」による強磁場激変星 V2487 Oph と IGR J00234+6141 の観測”, 日本天文学会 2011 年春季年会, 筑波大学, 3 月 (2011).

中川友進, 三原建弘, 杉崎睦, 小浜光洋, 芹野素子, 松岡勝, 河合誠之, 森井幹雄, 薄井竜一, 杉森航介, 吉田篤正, 山岡和貴, 中平聡志, 根來均, 中島基樹, 磯辺直樹, 他 MAXI チーム: “全天 X 線監視装置 MAXI によるマグネターの観測”, 日本天文学会 2011 年春季年会, 茨城, 3 月 (2011).

馬場彩: “CTA 報告 9:CTA で狙う物理 SNR”, 日本物理学会第 66 回年次大会, 新潟大学, 3 月 (2011).

中川友進: “マグネターの X 線・γ 線による観測的研究”, コンパクト天体で探る極限物理, 京都, 3 月 (2011).

中川友進: “マグネターの X 線・γ 線による観測的研究”, 超新星からのマルチメッセンジャー, 三鷹, 3 月 (2011).

稲田直久: “Evolution of Galaxy Light Distributions in Galaxy Clusters. II.”, 日本天文学会 2011 年春季年会, 筑波大学, 3 月 (2011).

寺田幸功, 原山淳, 石田学, 堂谷忠靖, 馬場彩, 林多桂由, 浦田裕次, 林紅妙: “ハードな強磁場白色矮星からの非熱放射の探査”, 日本物理学会 2011 年春季大会, (日本物理学会), 新潟, 3 月 (2011).

大須賀健: “RHD/RMHD-Simulations of Super-Eddington Accretion Flows & Outflows; 超光度 X 線源は super-Eddington 天体か?”, 滞在型研究会「全天体形成」, 北海道大学, 8 月 (2011).

大須賀健: “ブラックホール降着円盤およびジェットの輻射磁気流体 シミュレーション”, 滞在型研究会「全天体形成」, 北海道大学, 8 月 (2011).

小波さおり, 玉川徹, 松下恭子: “X 線で探る天体の高エネルギー現象”, 奈良高専セミナー, (奈良高等工業専門学校), 大和郡山, 8 月 (2011).

金子健太, 幸村孝由, 玉川徹, 山田真也, 岩橋孝典, 阿佐美ふみ, 吉川瑛文, 武内陽子, 岩切渉, 早藤麻美: “X 線偏光観測衛星 GEMS 搭載のガス電子増幅器 (GEM) の電子増幅度の時間変動調査”, 日本天文学会 2011 年秋季年会, (鹿児島大学), 鹿児島県, 9 月 (2011).

中川 友進, 牧島 一夫, 榎戸 輝揚, 「すざく」衛星 SGR/AXP 観測チーム, HETE-2 T.: “マグネターのバースト/定常放射のスペクトルの研究”, 日本天文学会 2011 年秋季年会, 鹿児島, 9 月 (2011).

小波さおり, 玉川徹, 松下恭子: “温度の低い S0 銀河 NGC1553 と他の早期型銀河の重元素組成比の比較”, 日本天文学会 2011 年秋季年会, (社団法人　日本天文学会), 鹿児島, 9 月 (2011).

馬場彩: “ASTRO-H / CTA で探る Pulsar System”, High Energy Observation of Pulsar Systems for Future Missions, 埼玉, 9 月 (2011).

原山淳: “単独強磁場白色矮星の Suzaku, INTEGRAL, MAXI を使った探査”, Pulsar Systems 研究会, 埼玉, 9 月 (2011).

馬場彩: “SNR と CTA”, 宇宙線研究所共同利用研究会「マルチメッセンジャー宇宙物理学と CTA」, 千葉, 9 月 (2011).

勝田哲: “XMM-Newton RGS を用いた Puppis A 超新星残骸の X 線分散スペクトル解析”, 日本天文学会 2011 年秋季年会, (日本天文学会), 鹿児島大学, 9 月 (2011).

馬場彩: “X 線観測による銀河系内宇宙線加速源の研究”, 日本天文学会 2011 年秋季年会研究奨励賞受賞記念講演, 鹿児島市, 9 月 (2011).

阿佐美ふみ, 玉川徹, 飯高陽介, 宮川健太, 北口貴雄, 山田真也, 岩橋孝典, 吉川瑛文, 武内陽子, 小波さおり, 岩切渉, 金子健太, 幸村 (孝由), 早藤麻美: “ジメチルエーテル中での GEM の電子増幅度および放電特性”, 日本物理学会, (日本物理学会), 弘前大学, 9 月 (2011).

吉川瑛文, 玉川徹, 武内陽子, 阿佐美ふみ, 早藤麻美, 岩橋孝典, 浜垣秀樹, 上野一樹, 郡司卓, 秋元亮二, 林真一, Rui O., 越智敦彦, 忽滑谷淳史: “Resistive Electrode Gas Electron Multiplier (RE-GEM) の電子増幅度調査と開発状況”, 日本物理学会 2011 年秋季大会, (日本物理学会), 弘前大学, 9–9 月 (2011).

大須賀健: “ブラックホール降着・噴出流およびガス雲の形成について”, HSC 活動銀河核探査によるサイエンス, 京都大学, 11 月 (2011).

川原田円: “A1689 銀河団の外縁部プラズマの研究と今後の展望”, 銀河団 ワークショップ, 箱根, 12 月 (2011).

馬場彩: “すざくで観測した HESSJ1731-347”, ワークショップ「超新星残骸」, 名古屋, 1 月 (2012).

川原田円: “X 線で見る激動の宇宙-ASTRO-H の挑戦”, 宇宙学校せたがや, (宇宙航空研究開発機構), 東京, 1 月 (2012).

川原田円: “ASTRO-H で診る銀河団の進化に伴う銀河団ガスの加熱と粒子 加速”, 日本天文学会 2012 年春季年会, (日本天文学会), 京都市, 3 月 (2012).

小波さおり, 竹井洋, 大橋隆哉, 佐藤浩介, Irina Z., Eugene C., Rashid S.: “Astro-H で探る銀河団中心における共鳴散乱の直接観測”, 日本天文学会 2012 年春季年会, (社団法人　日本天文学会), 京都, 3 月 (2012).

勝田哲, 玉川徹: “Astro-H に向けて XMM-Newton RGS で試みる SNR のプラズマ診断”, 日本天文学会 2012 年春季年会, (日本天文学会), 龍谷大学, 3 月 (2012).

山口弘悦: “Development of Plasma Codes for High- Resolution X-Ray Spectroscopy and Prospects for Future Observations of Non-Equilibrium Plasma”, 日本天文学会 2012 年春季年会, (日本天文学会), 京都市, 3 月 (2012).

山口弘悦: “Establishing Type Iα Origins of RCW 86 and G334.7-0.1, Galactic Supernova Remnants Associated with Star Forming Regions”, 日本天文学会 2012 年春季年会, (日本天文学会), 京都市, 3 月 (2012).

中川友進, 牧島一夫, 榎戸輝揚, 坂本貴紀, 三原建弘, 杉崎睦, 山岡和貴, 吉田篤正, Gandhi P., 田代信, 森井幹雄, Hurley K., HETE-2 T.: “「すざく」衛星・HETE-2 衛星による

マグネターのバースト/定常放射の X 線スペクトルの研究", 日本天文学会 2012 年春季年会, 京都, 3 月 (2012).

北口貴雄, 玉川徹, 岩橋孝典, 山田真也, 阿佐美ふみ, 吉川瑛文, 武内陽子, 飯高陽介, 宮川健太, 岩切渉, 幸村孝由, 金子健太, 早藤麻美: “X線偏光観測衛星 GEMS に搭載するガス検出器の偏光応答モンテカルロシミュレータの開発”, 日本天文学会 2012 年春季年会, (日本天文学会), 京都, 3 月 (2012).

川原田円: “ASTRO-H 衛星搭載硬 X 線撮像検出器 (HXI) の開発の現状”, 日本物理学会, (日本物理学会), 関西学院大学, 3 月 (2012).

勝田哲, 玉川徹: “白鳥座ループ超新星残骸中のパルサー星雲候補の発見”, 日本天文学会, (日本天文学会), 龍谷大学, 3 月 (2012).

阿佐美ふみ, 玉川徹, 飯高陽介, 宮川健太, 北口貴雄, 山田真也, 岩橋孝典, 吉川瑛文, 武内陽子, 小波さおり, 岩切渉, 幸村孝由, 金子健太, 早藤麻美: “ジメチルエーテル中の不純物ガスによる電子吸着の GEM 動作への影響調査”, 日本物理学会, (日本物理学会), 関西学院大学, 3 月 (2012).

岩田憲一, 土屋晴文, 榎戸輝揚, 山田真也, 湯浅孝行, 川原田円, 北口貴雄, 中澤知洋, 国分紀秀, 加藤博, 岡野眞治, 牧島一夫: “2009 年および 2010 年における雷や雷雲からの放射線観測”, 日本物理学会　第 67 回年次大会, (日本物理学会), 西宮市, 3 月 (2012).

宮川健太, 飯高陽介, 玉川徹, 岩橋孝典, 阿佐美ふみ, 吉川瑛文, 武内陽子, 北口貴雄, 山田真也, 早藤麻美: “GEMS 衛星偏光計に使用するジメチルエーテル中の不純物ガスによるスペクトル変化の定量化”, 日本天文学会 2012 年春季年会, (日本天文学会), 京都市, 3–3 月 (2012).

岡本雄大, 勝田哲, 山田真也, 玉川徹: “X 線天文衛星 Suzaku による超新星残骸 RCW86 のマッピング観測”, 日本天文学会 2012 年春季年会, (社団法人日本天文学会), 龍谷大学, 3–3 月 (2012).

大須賀健: “輻射流体不安定による Clumpy な円盤風の形成について”, 松山ブラックホールワークショップ 2012, 愛媛大学, 6 月 (2012).

山田真也: “ASTRO-H 衛星で探るブラックホール連星の降着流”, 松山ブラックホールワークショップ 2012 — ASTRO-H 衛星で目指すブラックホール研究の新展開 —, (愛媛大学), 愛媛大学, 6 月 (2012).

武内陽子, 玉川徹, 勝田哲: “Ejecta Dynamics of Tycho's Supernova Remnant”, 3nd ASTRO-H Summer Schools, (ASTRO-H science tem), 京都, 8 月 (2012).

阿佐美ふみ, 榎戸輝揚, 山田真也, 玉川徹: “「すざく」衛星によるX線パルサー Hercules X-1 のスペクトル変動調査”, 日本天文学会, (日本天文学会), 大分大学, 9 月 (2012).

武内陽子, 玉川徹, 阿佐美ふみ, 吉川瑛文, 飯高陽介, 宮川健太, 早藤麻美, 北口貴雄, 榎戸輝揚, 山田真也, 幸村孝由, 金子健太, 岩橋孝典, 岩切渉: “宇宙 X 線偏光計に使用するジメチルエーテルと不純物ガスの電子吸着率の測定”, 日本天文学会, (大分大学), 大分, 9 月 (2012).

原山淳, 川原田円, 渡辺伸, 国分紀秀, 高橋忠幸, 田島宏康, 深沢泰司, 中澤知洋, 片岡淳, 寺田幸功, Team A.: “Astro-H HXI/SGD 検出器搭載の高電圧電源部の開発”, 日本天文学会 2012 年秋季年会, (日本天文学会), 鹿児島, 9 月 (2012).

林多佳由, 石田学, 寺田幸功, 原山淳: “Post-shock 領域の X 線スペクトルモデルによる白矮星からの非熱的放射の探査”, 日本天文学会 2012 年秋季年会, 大分, 9 月 (2012).

北口貴雄, 玉川徹, 早藤麻美, 榎戸輝揚, 山田真也, 岩橋孝典, 阿佐美ふみ, 吉川瑛文, 武内陽子, 岩切渉, 幸村孝由, 金子健太: “X線偏光観測衛星 GEMS に搭載するガス検出器の宇宙環境でのバックグラウンドの見積り”, 日本天文学会 2012 年秋季年会, (日本天文学会), 大分, 9 月 (2012).

岩橋孝典, 榎戸輝揚, 山田真也, 玉川徹, 牧島一夫, 西岡博之: “アウトバーストから 1 年半経過したマグネター 1E 1547.0-5408 の「すざく」衛星による追観測”, 日本天文学会 2012 年秋季年会, (日本天文学会), 大分大学, 9 月 (2012).

山口弘悦: 超新星と超新星残骸の融合研究会, (国立天文台), 三鷹市, 10 月 (2012).

馬場彩: “超新星残骸と高エネルギー観測”, 超新星と超新星残骸の融合研究会 - 較正進化・爆発メカニズムと元素合成 -, 東京, 10 月 (2012).

勝田哲: 超新星と超新星残骸の融合研究会—恒星進化・爆発メカニズムと元素合成—, (国立天文台), 国立天文台, 10 月 (2012).

山口弘悦: “Iα 超新星残骸の X 線観測から迫る親星の性質”, 東京大学でのセミナー公演, 東京大学本郷キャンパス, 10 月 (2012).

山田真也: “ブラックホールの不思議”, 複合的アプローチで探る宇宙の化学進化, (首都大学東京), 伊豆高原, 10 月 (2012).

勝田哲: “超新星残骸から探る超新星爆発メカニズムと元素合成”, 複合的アプローチで探る宇宙の化学進化, (首都大学東京), 静岡県・ホテル伊豆高原, 10 月 (2012).

北口貴雄, GEMS t.: “宇宙X線の偏光を測定する GEM-TPC の検出応答シミュレータの開発”, 第 9 回「マイクロパターンガス検出器 (MPGD) 研究会」, (長崎総合科学大学), 長崎, 12 月 (2012).

武内陽子: “低圧の純ジメチルエーテル中での GEM 動作特性”, 第 9 回 Micro-Pattern Gas Detector 研究会, (長崎総合科学大学), 長崎, 12 月 (2012).

大須賀健: “AGN の輻射磁気流体シミュレーション”, 25 回理論天文学懇談会シンポジウム, つくばエポカル, 12 月 (2012).

北口貴雄, 早藤麻美, 榎戸輝揚, 玉川徹, 山田真也, 岩橋孝典, 阿佐美ふみ, 吉川瑛文, 武内陽子, 岩切渉, 金子健太, 牧島一夫, GEMS t.: “X線偏光衛星 GEMS”, 第 13 回宇宙科学シンポジウム, (JAXA/ISAS), 相模原, 1 月 (2013).

北口貴雄, NuSTAR t.: 日本物理学会 2013 年春季大会, (日本物理学会), 東広島, 3 月 (2013).

Astro-Glaciology Research Unit

Publications

[Journal]

(Original Papers) *Subject to Peer Review

Morimoto K., Morita K., Kaji D., Haba H., Katori K., Koura H., Ohnishi T., Ozawa A., Suda T., Sueki K., Tanihata I., Tokanai F., Yoneda A., and Yoshida A.: "Status of super heavy element research using GARIS at RIKEN", Nucl. Phys. A **738**, 129 (2004). *

Kaji D., Morimoto K., Sato N., Ichikawa T., Ohzeki K., Haba H., Koura H., Ozawa A., Sumita T., Yamaguchi T., Yoneda A., Yoshida A., and Morita K.: "Production and Decay Properties of ^{263}Hs", J. Phys. Soc. Jpn. **78**, No. 3, p. 035001 (2009). *

Sato N., Haba H., Ichikawa T., Kaji D., Kudou Y., Morimoto K., Morita K., Ohzeki K., Sumita T., Yoneda A., Koura H., Ozawa A., Yamaguchi T., and Yoshida A.: "Production and Decay Properties of ^{264}Hs and ^{265}Hs", J. Phys. Soc. Jpn. **80**, 094201 (2011). *

望月優子, 高橋和也, 柴田一成: "地球上の物質からさぐる巨大太陽プロトン現象の発生頻度", ぶんせき **10**, 585–589 (2012). *

Oral Presentations

(International Conference etc.)

Motizuki Y.: "Supernova and Solar activity signatures from ice cores", IAU Symposium 288 Astrophysics from Antarctica, (IAU General Assembly XXVIII), Beijing, China, Aug. (2012).

Schury P. H., Jeong S., Haba H., Kaji D., Koura H., Ito Y., Mita H., Miyatake H., Morimoto K., Morita K., Naimi S., Nakamura S., Okada K., Ozawa A., Sonoda T., Takamine A., Wollnik H., and Wada M.: "A multi-reflection time of flight mass spectrograph for short-lived nuclei and heavy molecules", International Mass Spectrometry Conference, (Kyoto University), Kyoto, Sept. (2012).

Motizuki Y., Nakai Y., Takahashi K., Mototyama H., Suzuki K., Sekiguchi K., Akiyoshi H., Imamura T., and Tanabe K.: "Experimental and theoretical diagnoses of yearly-scale nitrate ion spikes observed in a Dome Fuji shallow ice core", The 3rd Int. Symposium on Polar Science, (National Institute of Polar Research), Tachikawa, Nov. (2012).

Takahashi K., Motizuki Y., Nakai Y., Suzuki K., Motoyama H., and Hori A.: "Chemical composition and their characteristics of shallow ice cores drilled at Dome Fuj, East Antarctica", The Third Symposium on Polar Science, (National Institute of Polar Research), Tachikawa, Nov. (2012).

Motizuki Y.: "Diagnosis of modulation in an Antarctic ice core oxygen isotope record", The annual meeting of Astronomical Soc. of Japan 2013 spring, (The Astronomical Society of Japan), Saitama, Mar. (2013).

(Domestic Conference)

加治大哉, 森田浩介, 森本幸司, 羽場宏光, 鹿取謙二, 小浦寛之, 大西哲哉, 小沢顕, 須田利美, 末木啓介, 谷畑勇夫, 米田晃, 吉田敦: "ヘリウムガス中における (超) 重元素の平衡電荷", 日本物理学会, (宮崎大学), 宮崎, 9 月 (2003).

加治大哉, 森田浩介, 森本幸司, 羽場宏光, 鹿取謙二, 小浦寛之, 大西哲哉, 小沢顕, 須田利美, 末木啓介, 谷畑勇夫, 米田晃, 吉田敦: "ヘリウムガス中における重い反跳原子の平衡電荷－理研における Z=111 番元素探索－", 放射化学討論会, (京都大学原子炉実験施設), 大阪, 10 月 (2003).

加治大哉, 森田浩介, 森本幸司, 羽場宏光, 小浦寛之, 大西哲哉, 小沢顕, 須田利美, 末木啓介, 山口貴之, 米田晃, 吉田敦: "209Bi+70Zn 反応を用いた 113 番元素探索", 日本化学会, (神奈川大学), 神奈川, 3 月 (2005).

加治大哉, 森田浩介, 森本幸司, 羽場宏光, 小浦寛之, 大西哲哉, 小沢顕, 須田利美, 末木啓介, 山口貴之, 米田晃, 吉田敦: "209Bi(70Zn,n)278113 反応を用いた 113 番元素の合成", 放射化学討論会, (金沢大学), 金沢, 9 月 (2005).

加治大哉, 森本幸司, 羽場宏光, 市川隆敏, 小浦寛之, 工藤祐生, 小沢顕, 大関和貴, 住田貴之, 山口貴之, 米田晃, 吉田敦, 森田浩介: "新同位体 ^{263}Hs の生成および壊変特性", 放射化学討論会, (日本大学), 神奈川, 9 月 (2009).

加治大哉, 羽場宏光, 笠松良崇, 工藤祐生, 森本幸司, 森田浩介, 大関和貴, 住田貴之, 米田晃, 小浦寛之, 佐藤望, 門叶冬樹: "中性子欠損領域の新アクチノイド核種 ^{234}Bk および ^{230}Am の観測", 放射化学討論会, (大阪大学), 大阪, 9 月 (2010).

堀彰, 望月優子, 中井陽一, 高橋和也, 本山秀明, 本堂武夫: "DF2001 浅層コアの高分解能密度測定と DFS1 年代を用いた年層解析の試行研究", 第 2 回極域科学シンポジウム, (国立極地研究所), 立川, 11 月 (2011).

堀彰, 望月優子, 中井陽一, 高橋和也, 本山秀明, 本堂武夫: "ドームふじ浅層コアの高分解能密度測定と年層解析", 北海道大学低温研究所シンポジウム「ドームふじコアを用いた新しい古環境復元法」, (北海道大学低温研究所), 札幌, 12 月 (2011).

望月優子: "南極氷床コアからさぐる過去の太陽活動周期", 太陽研究シンポジウム, (名古屋大学 STE 研共同研究集会及び宇宙科学研究所宇宙放射線シンポジウムの共催企画), 東京, 2 月 (2012).

高橋和也, 望月優子, 中井陽一: "DF01 浅層コア (7.7m-88.65m) の陽・陰イオン分析のまとめ ", 第 1 回 NEXT（最先端・次世代）合同ミーティング「南極氷床コアからさぐる過去２０００年の太陽活動に関する分野横断的研究」, 和光, 3 月 (2012).

島田藍, 望月優子: "DF2010 浅層コア陰イオン分析の現状", 第 1 回 NEXT（最先端・次世代）合同ミーティング「南極氷床コアからさぐる過去２０００年の太陽活動に関する分野横断的研究」, 和光, 3 月 (2012).

望月優子, 本山秀明, 飯塚芳徳, 藤田秀二, 藤田耕史, 保科優: "ドームふじ雪ピットの SEP 痕跡の一次探索とシグナルが見えない理由", 第 1 回 NEXT（最先端・次世代）合同ミーティング「南極氷床コアからさぐる過去２０００年の太陽活動に関する分野横断的研究」, 和光, 3 月 (2012).

望月優子: "プロジェクト全体像 (2):成層圏プロジェクト ",

第１回 NEXT（最先端・次世代）合同ミーティング「南極氷床コアからさぐる過去２０００年の太陽活動に関する分野横断的研究」, 和光, 3 月 (2012).

望月優子: “南極氷床コアからさぐる過去 2000 年の太陽活動に関する分野横断的研究 プロジェクト紹介と火山噴火年代 ”, 第 1 回 NEXT（最先端・次世代）合同ミーティング「南極氷床コアからさぐる過去２０００年の太陽活動に関する分野横断的研究」, 和光, 3 月 (2012).

関口健太郎, 中井陽一, 今村隆史, 秋吉英治, 望月優子: “爆発的天体イベントが引き起こす成層圏大気の化学組成変動について:ボックスモデルによる吟味の現状”, 第 1 回 NEXT（最先端・次世代）合同ミーティング「南極氷床コアからさぐる過去２０００年の太陽活動に関する分野横断的研究」, 和光, 3 月 (2012).

高橋和也, 望月優子: “氷床コア試料中の硝酸の同位体比測定への挑戦”, 第 1 回 NEXT（最先端・次世代）合同ミーティング「南極氷床コアからさぐる過去２０００年の太陽活動に関する分野横断的研究」, 和光, 3 月 (2012).

中井陽一, 望月優子: “放射線過程と大気中のエネルギー吸収”, 第 1 回 NEXT（最先端・次世代）合同ミーティング「南極氷床コアからさぐる過去２０００年の太陽活動に関する分野横断的研究」, 和光, 3 月 (2012).

堀彰, 望月優子, 中井陽一, 高橋和也, 本山秀明, 本堂武夫: “DF2010 浅層コアの密度測定の現状〜X 線透過法による密度測定とこれまでの研究〜”, 第 1 回 NEXT（最先端・次世代）合同ミーティング「南極氷床コアからさぐる過去２０００年の太陽活動に関する分野横断的研究」, 和光, 3 月 (2012).

熊谷紫麻見, 古宮尚, 望月優子: “超新星の X 線・ガンマ線放射（放射性元素起源）”, 第 1 回 NEXT（最先端・次世代）合同ミーティング「南極氷床コアからさぐる過去２０００年の太陽活動に関する分野横断的研究」, 和光, 3 月 (2012).

望月優子, 高橋和也, 中井陽一: “DF2010 浅層コアのトレンチ状況のまとめと水同位体比分析の現状報告”, 第 1 回 NEXT（最先端・次世代）合同ミーティング「南極氷床コアからさぐる過去２０００年の太陽活動に関する分野横断的研究」, 和光, 3 月 (2012).

関口健太郎, 中井陽一, 今村隆史, 秋吉英治, 望月優子: “高エネルギー粒子・光子が成層圏大気に引き起こす化学反応のシミュレーション”, 日本地球惑星科学連合 2012 年度大会, (日本地球惑星科学連合), 千葉, 5 月 (2012).

岡本祥子, 藤田耕史, 成田英器, Aizen V. A., 世良駿太郎, 竹内望, 植竹淳, 中澤文男, 三宅隆之, Nikitin S. A., 中尾正義: “シベリア・アルタイ山脈ベルーハアイスコアにおける結晶粒径と水安定同位体比の気候指標としての検証”, 日本地球惑星科学連合 2012 年度大会, (日本地球惑星科学連合), 千葉, 5 月 (2012).

脇谷雄一郎, 大坪亜衣, 山元真一, 山田崇裕, 神原正, 羽場宏光, 金谷淳平, 高橋和也: “理研 AVF サイクロトロンを用いた ^{109}Cd の製造に関する検討”, 第 49 回アイソトープ・放射線研究発表会, (日本アイソトープ協会), 東京大学弥生講堂, 7–7 月 (2012).

望月優子: “元素誕生〜私たちは星の子ども〜”, 2012 年度日本物理学会科学セミナー「元素誕生と周期表ー私たちを取り巻く原子核」, (日本物理学会), 東京, 8 月 (2012).

菊地里実: “Measurement of water isotopes in Dome Fuji ice cores for reconstruction of past air-temperature variation”, Noyori Summer School 2012, 松江, 9 月 (2012).

望月優子, 菊地里実, 岡本祥子, 高橋和也, 中井陽一, 本山秀明, 鈴木啓助, 堀彰, 植村立: “ドームふじ南 10km 地点掘削（2010 年）浅層コア中の水同位体比の測定”, 第 35 回極域気水圏シンポジウム, (国立極地研究所), 立川, 11 月 (2012).

岡本祥子, 望月優子, 本山秀明, 高橋和也, 眞壁明子, 木庭啓介: “南極ドームふじ南 10km 地点掘削（2010 年）の浅層コアにおける硝酸同位体比測定の試み”, 第 35 回極域気水圏シンポジウム, (国立極地研究所), 立川, 11 月 (2012).

望月優子: “氷床コアからさぐる過去の太陽活動と気温変動”, 第 819 回国立天文台談話会, (国立天文台), 三鷹, 1 月 (2013).

望月優子: “南極アイスコアから探る地球環境”, 第 1 回 NINS Colloquium「自然科学の将来像」, (自然科学研究機構), 箱根, 2 月 (2013).

岡本祥子, 高橋和也, 本山秀明, 真壁明子, 木庭啓介, 望月優子: “南極雪氷コアの硝酸塩同位体測定—太陽活動の代替指標としての検証に向けて”, 第 3 回 太陽活動と気候変動の関係に関する名古屋ワークショップ, (名古屋大学太陽地球環境研究所), 名古屋, 2 月 (2013).

望月優子: “ドームふじ南 2010 浅層コアのイオン・水同位体・硝酸塩同位体詳細分析の現状”, ドームふじアイスコアコンソーシアム（ICC）研究集会, (国立極地研究所氷床コア研究委員会), 立川, 3 月 (2013).

小濱洋央, 飯田圭, 親松和浩, 小浦寛之: “中間エネルギーでの不安定核全反応断面積と変形度”, 日本物理学会第 68 回年次大会, 東広島市, 3 月 (2013).

望月優子: “地球上の物質からさぐる太陽スーパーフレア痕跡と発生頻度”, 第 2 回スーパーフレア星研究ワークショップ, (京都大学), 佐用, 3 月 (2013).

Accelerator Group

Publications

[Journal]

(Original Papers) *Subject to Peer Review

Higurashi Y., Nakagawa T., Kidera M., Kageyama T., Kase M., Goto A., and Yano Y.: "Production of Highly Charged Ga Ions from Organic Metal Comppound Using the Liquid-He-Free Superconducting Electron Cyclotron Resonance Ion Source at RIKEN", Jpn. J. Appl. Phys. **41**, 5442–5443 (2002). *

Higurashi Y., Kidera M., Nakagawa T., Aihara T., Kase M., Goto A., and Yano Y.: "Production of 70Zn Beam from RIKEN 18 GHz Electron Cyclotron Resonance Ion Source", Jpn. J. Appl. Phys. **44**, 8138–8140 (2005). *

Higurashi Y., Nakagawa T., Kidera M., Aihara T., Kobayashi K., Kase M., Goto A., and Yano Y.: "Effect of the plasma electrode position and shape on the beam intensity of the highly charged ions from RIKEN 18 GHz electron cyclotoron resonanse ion source", Rev. Sci. Instrum. **77**, No. 2, p. 03A329 (2006). *

Higurashi Y., Nakagawa T., Kidera M., Haba H., Aihara T., Kase M., Goto A., and Yano Y.: "Production of U beam from RIKEN 18 GHz electron cyclotron resonance ion source", Rev. Sci. Instrum. **79**, No. 2, p. 02C714 (2008). *

Hasebe H., Kuboki H., Okuno H., Fukunishi N., Kamigaito O., Imao H., Goto A., and Kase M.: "Development of the carbon foils as charge strippers for high-intensity uranium ion beams", Nucl. Instrum. Methods Phys. Res. A **655**, No. 1, pp. 57–60 (2011). *

Haba H., Kanaya J., Mukai H., Kambara T., and Kase M.: "One-year monitoring of airborne radionuclides in Wako, Japan, after the Fukushima Dai-ichi nuclear power plant accident in 2011", Geochem. J. **46**, 271–278 (2012). *

Watanabe T., Fukunishi N., Kase M., Kamigaito O., Inamori S., and Kon K.: "Beam Current Monitor with a High-Tc Current Sensor and SQUID at the RIBF", J. Supercond. Nov. Magn., (2012). *

Imao H., Okuno H., Kuboki H., Yokouchi S., Fukunishi N., Kamigaito O., Hasebe H., Watanabe T., Kase M., and Yano Y.: "Charge stripping of 238U beam by helium gas stripper", Phys. Rev. Spec. Top.: Accel. Beams **15**, No. 123501, (2012). *

Okuno H., Fukunishi N., and Kamigaito O.: "Progress of RIBF Accelerators", Progress of Theoretical and Experimental Physics **2012**, No. 3, (2012). *

(Others)

Nakagawa T., Higurashi Y., Ohnishi J., Aihara T., Tamura M., Uchiyama A., Okuno H., Kusaka K., Kidera M., Komiyama M., Fujimaki M., Sato Y., Ikezawa E., Watanabe Y., Kase M., Goto A., Kamigaito O., and Yano Y.: "First results from the new RIKEN superconducting electron cyclotron resonance ion source", Rev. Sci. Instrum. **81**, No. 2, p. 02A320 (2010).

Imao H., Okuno H., Kuboki H., Yokouchi S., Fukunishi N., Kamigaito O., Hasebe H., Watanabe T., Kase M., and Yano Y.: "Charge stripping of Uranium-238 ion beam with low-Z gas stripper", Particle accelerator. Proceedings, 2nd International Conference, IPAC 2011 **C110904**, 1746–1748 (2011).

Okuno H., Fukunishi N., Hasebe H., Imao H., Kamigaito O., Kase M., and Kuboki H.: "New Developments in Low-Z Gas Stripper Sstem at RIKEN Radioactive Isotope Beam Factory (RIBF)", Proceedings of HIAT12 **1**, No. 1, p. 199 (2012).

Okuno H., Dantsuka T., Fujimaki M., Fujinawa T., Fukunishi N., Hasebe H., Higurashi Y., Ikegami K., Ikezawa E., Imao H., Kageyama T., Kamigaito O., Kase M., Kidera M., Komiyama M., Kuboki H., Kumagai K., Maie T., Nagase M., Nakagawa T., Nakamura M., Ohnishi J., Sakamoto N., Suda K., Watanabe H., Watanabe T., Watanabe Y., Yamada K., and Yamasawa H.: "Recent Achievements and Upgrade Programs at RIKEN Radioactive Isotope Beam Factory", Proceedings of IPAC12 **1**, No. 1, p. 430 (2012).

日暮祥英, 大西純一, 中川孝秀, 藍原利光, 田村匡史, 内山暁仁, 込山美咲, 藤巻正樹, 佐藤洋一, 池沢英二, 渡邉裕, 加瀬昌之, 後藤彰, 上垣外修一, 矢野安重: "理研における新しい超電導 ECR イオン源の開発", 加速器 **6**, No. 4, pp. 346–354 (2010).

[Book・Proceedings]

(Original Papers) *Subject to Peer Review

Yamada K., Arai S., Fujimaki M., Fujinawa T., Fujisawa H., Fukunishi N., Goto A., Higurashi Y., Ikezawa E., Kase M., Komiyama M., Kumagai K., Maie T., Nakagawa T., Ohnishi J., Okuno H., Sakamoto N., Sato Y., Suda K., Watanabe H., Watanabe T., Watanabe Y., Yano Y., Yokouchi S., and Kamigaito O.: "Construction of new injector linac at RIBF", CYCLOTRONS'10, Lanzhou, 2010–9, JaCoW, Lanzhou, pp. 1–3 (2010).

Yamada K., Arai S., Fujimaki M., Fujinawa T., Fujisawa H., Fukunishi N., Goto A., Higurashi Y., Ikezawa E., Kamigaito O., Kase M., Komiyama M., Kumagai K., Maie T., Nakagawa T., Ohnishi J., Okuno H., Sakamoto N., Sato Y., Suda K., Watanabe H., Watanabe Y., Yano Y., and Yokouchi S.: "Construction of new injector linac for RI Beam Factory at RIKEN Nishina Center", Proceedings of of the 1st International Particle Accelerator Conference (IPAC'10), Kyoto, 2010–5, JaCoW, Kyoto, pp. 789–791 (2010).

Yamada K., Arai S., Chiba Y., Fujisawa H., Ikezawa E., Kamigaito O., Kase M., Sakamoto N., Suda K., Watanabe Y., and Touchi Y.: "Rf-design and construction of new linac injector for RIKEN RI-Beam Factory", Proceedings of XXV Linear Accelerator Conference, Tsukuba, 2010–9, JaCoW, Tsukuba, pp. 572–574 (2010).

Kamigaito O.: "Rare-Isotope Beam Facilities in Asia", Proceedings of 12th Heavy Ion Accelerator Technology

Conference, Chicago, USA, 2012–6, Argonne National Laboratory , Chicago, pp. 28–32 (2012).

Watanabe Y., Fujimaki M., Fukunishi N., Hasebe H., Higurashi Y., Ikezawa E., Imao H., Kageyama T., Kamigaito O., Kase M., Kidera M., Komiyama M., Kuboki H., Kumagai K., Maie T., Nagase M., Nakagawa T., Ohnishi J., Okuno H., Sakamoto N., Suda K., Watanabe H., Watanabe T., Yamada K., Yokouchi S., Aihara T., Fukuzawa S., Hamanaka M., Ishikawa S., Kobayashi K., Kotaka Y., Koyama R., Nakamura T., Nishida M., Nishimura M., Ohki T., Oyamada K., Shibata J., Tamura M., Tsukiori N., Uchiyama A., Yadomi K., and Yamauchi H.: "Present status of RIKEN Ring Cyclotron Magnets", Proceedings of 3rd International Particle Accelerator Conference (IPAC 2012), New Orleans, USA, 2012–8, IPAC2012, IEEE, New Orleans, pp. 433–435 (2012). *

Lu L., Sakamoto N., Suda K., Yamada K., and Kamigaito O.: "Design Of A Spoke Cavity For RIKEN RI-Beam Factory", the International Particle Accelerator Conference IPAC'12, New Orleans, USA, 2012–5, JACoW, CERN, pp. 2245–2247 (2012).

山田一成, 池沢英二, 今尾浩士, 大西純一, 奥野広樹, 加瀬昌之, 熊谷桂子, 込山美咲, 後藤彰, 坂本成彦, 須田健嗣, 中川孝秀, 日暮祥英, 福西暢尚, 藤縄雅, 藤巻正樹, 眞家武士, 山澤秀行, 横内茂, 渡邉環, 渡辺博, 渡邉裕, 新井重昭, 藤澤博, 佐藤洋一, 上垣外修一: "理研 RIBF 用の新しい重イオン入射ライナック RILAC2 の製作", 第 7 回日本加速器学会年会プロシーディングス, 姫路市, 2010–8, 日本加速器学会, 東京, pp. 360–363 (2010).

(Others)

Yamada K., Suda K., Arai S., Fujimaki M., Fujinawa T., Fujisawa H., Fukunishi N., Higurashi Y., Ikezawa E., Imao H., Kamigaito O., Kase M., Komiyama M., Kumagai K., Maie T., Nakagawa T., Ohnishi J., Okuno H., Sakamoto N., Watanabe H., Watanabe T., Watanabe Y., Yamasawa H., Sato Y., and Goto A.: "Beam Commissioning and Operation of New Linac Injector for RIKEN RI Beam Factory", Proceedings of 3rd International Particle Accelerator Conference (IPAC 2012), New Orleans, USA, 2012–5, JACoW, New Orleans, pp. 1071–1073 (2012).

Oral Presentations

(International Conference etc.)

Yamada K., Okuno H., Fujimaki M., Fukunishi N., Goto A., Hasebe H., Ikegami K., Kamigaito O., Kase M., Kumagai K., Maie T., Nagase M., Ohnishi J., Sakamoto N., Yokouchi S., and Yano Y.: "Status of the Superconducting Ring Cyclotron at RIKEN RI Beam Factory", 11th European Particle Accelerator Conference (EPAC 2008), (INFN-LNF), Genoa, Italy, June (2008).

Yamada K., Dantsuka T., Fujimaki M., Fujinawa T., Fukunishi N., Goto A., Hasebe H., Higurashi Y., Ikezawa E., Kamigaito O., Kase M., Komiyama M., Kuboki H., Kumagai K., Maie T., Nagase M., Nakagawa T., Ohnishi J., Okuno H., Sakamoto N., Sato Y., Suda K., Wakasugi M., Watanabe H., Watanabe T., Watanabe Y., Yano Y., and Yokouchi S.: "Progress on the commissioning of Radioactive Isotope Beam Factory at RIKEN Nishina Center", 11th International Conference on HEAVY ION ACCELERATOR TECHNOLOGY (HIAT09), (INFN-LNL), Venezia, Italy, June (2009).

Yamada K., Arai S., Fujimaki M., Fujinawa T., Fujisawa H., Fukunishi N., Goto A., Higurashi Y., Ikezawa E., Kamigaito O., Kase M., Komiyama M., Kumagai K., Maie T., Nakagawa T., Ohnishi J., Okuno H., Sakamoto N., Sato Y., Suda K., Watanabe H., Watanabe Y., Yano Y., and Yokouchi S.: "Construction of New Injector Linac for RI Beam Factory at RIKEN Nishina Center", 1st International Particle Accelerator Conference (IPAC'10), (High Energy Accelerator Research Organization), Kyoto, May (2010).

Higurashi Y., Nakagawa T., Ohnishi J., Haba H., Ikezawa E., Fujimaki M., Watanabe Y., Kidera M., Komiyama M., Kase M., Goto A., Kamigaito O., Aihara T., Tamura M., and Uchiyama A.: "Production of U ion beam from RIKEN SC-ECRIS ith sputtering method", 19th International Workshop on ECR Ion Sources (ECRIS 2010), grenoble, France, Aug. (2010).

Yamada K., Arai S., Fujimaki M., Fujinawa T., Fujisawa H., Fukunishi N., Goto A., Higurashi Y., Ikezawa E., Kase M., Komiyama M., Kumagai K., Maie T., Nakagawa T., Ohnishi J., Okuno H., Sakamoto N., Sato Y., Suda K., Watanabe H., Watanabe T., Watanabe Y., Yano Y., Yokouchi S., and Kamigaito O.: "Construction of New Injector LINAC at RIBF", 19th International Conference on Cyclotrons and their Applications (CYCLOTRONS 2010), (IMP), Lanzhou, China, Sept. (2010).

Yamada K., Arai S., Chiba Y., Fujisawa H., Ikezawa E., Kamigaito O., Kase M., Sakamoto N., Suda K., Watanabe Y., and Touchi Y.: "RF-design and Construction of New Linac Injector for the RIKEN RI-Beam Factory", 25th Linear Accelerator Conference (LINAC10), (High Energy Accelerator Research Organization), Tsukuba, Sept. (2010).

Lu L., Sakamoto N., Suda K., Yamada K., and Kamigaito O.: "Design Of CW Superconducting Buncher For RIKEN RI-Beam Factory", 15th International Conference on RF Superconductivity, (SRF2011), Chicago, USA, July (2011).

Higurashi Y., Ohnishi J., Ohzeki K., Haba H., Fujimaki M., Komiyama M., Kamigaito O., Aihara T., Tamura M., and Uchiyama A.: "Production of highly charged uranium ion beam with RIKEN superconducting electron cyclotron resonance ion source", The 14th Int. Conf. on Ion Sources (ICIS11), (INFN-LNS, Italy), Giardini Naxos, Italy, Sept. (2011).

Higurashi Y., Ohnishi J., Ohzeki K., Haba H., Fujimaki

M., Komiyama M., Kamigaito O., Aihara T., Tamura M., and Uchiyama A.: "Results of RIKEN superconducting electron cyclotron resonance ion source with 28GHz", The 14th Int. Conf. on Ion Sources (ICIS11), (INFN-LNS, Italy), Giardini Naxos, Italy, Sept. (2011).

Kamigaito O.: "RIKEN Radioactive-Isotope Beam Factory", International Symposium on Vacuum Science and Technology and Its Application for Accelerators, (Variable Energy Cyclotron Center), India, Kolkata, Feb. (2012).

Watanabe T., Fukunishi N., Kase M., Kamigaito O., Inamori S., and Kon K.: "Beam Current Monitor with a High-Tc Current Sensor and SQUID at the RIBF", International Conference on Superconductivity and Magnetism (ICSM 2012), (Ankara University), Kumburgaz-Istanbul, Turkey, Apr.–May (2012).

Yamada K., Suda K., Arai S., Fujimaki M., Fujinawa T., Fujisawa H., Fukunishi N., Higurashi Y., Ikezawa E., Imao H., Kamigaito O., Kase M., Komiyama M., Kumagai K., Maie T., Nakagawa T., Ohnishi J., Okuno H., Sakamoto N., Watanabe H., Watanabe T., Watanabe Y., Yamasawa H., Sato Y., and Goto A.: "Beam Commissioning and Operation of New Linac Injector for RIKEN RI Beam Factory", 3rd International Particle Accelerator Conference (IPAC 2012), New Orleans, USA, May (2012).

Imao H., Okuno H., Kuboki H., Yokouchi S., Fukunishi N., Kamigaito O., Hasebe H., Watanabe T., Kase M., and Yano Y.: "Charge stripping of uranium-238 ion beam with helium gas stripper", IPAC12, (IEEE), New Orleans, USA, May (2012).

Okuno H., Dantsuka T., Fujimaki M., Fujinawa T., Fukunishi N., Hasebe H., Higurashi Y., Ikegami K., Ikezawa E., Imao H., Kageyama T., Kamigaito O., Kase M., Kidera M., Komiyama M., Kuboki H., Kumagai K., Maie T., Nagase M., Nakagawa T., Nakamura M., Ohnishi J., Sakamoto N., Suda K., Watanabe H., Watanabe T., Watanabe Y., Yamada K., and Yamasawa H.: "Recent Achievements and Upgrade Programs at RIKEN Radioactive Isotope Beam Factory", IPAC12, (IPAC12 International Organizing Committee), NewOrleans, USA, May–May (2012).

Kamigaito O.: "Rare-Isotope Beam Facilities in Asia", The 12th Heavy Ion Accelerator Technology Conference (HIAT2012), (Argonne National Laboratory), Chicago, USA, June (2012).

Okuno H., Fukunishi N., Hasebe H., Imao H., Kamigaito O., Kase M., and Kuboki H.: "New Developments in Low-Z Gas Stripper Sstem at RIKEN Radioactive Isotope Beam Factory (RIBF)", 12th International Conference on Heavy Ion Accelerator Technology, (Argonne National Laboratory), Chicago, IL, USA, June–June (2012).

Kuboki H., Okuno H., Hershcovitch A., Dantsuka T., Hasebe H., Ikegami K., Imao H., Kamigaito O., Kase M., Maie T., Nakagawa T., and Yano Y.: "Development of Plasma Window for gas charge strippers at RIKEN RIBF", 26th World Conference of the International Nuclear Target Development Society, (Johannes Gutenberg-Universitat and GSI), Mainz, Germany, Aug. (2012).

Watanabe Y., Fujimaki M., Fukunishi N., Hasebe H., Higurashi Y., Ikezawa E., Imao H., Kageyama T., Kamigaito O., Kase M., Kidera M., Komiyama M., Kuboki H., Kumagai K., Maie T., Nagase M., Nakagawa T., Ohnishi J., Okuno H., Sakamoto N., Suda K., Watanabe H., Watanabe T., Yamada K., Yokouchi S., Aihara T., Fukuzawa S., Hamanaka M., Ishikawa S., Kobayashi K., Kotaka Y., Koyama R., Nakamura T., Nishida M., Nishimura M., Ohki T., Oyamada K., Shibata J., Tamura M., Tsukiori N., Uchiyama A., Yadomi K., and Yamauchi H.: "Present status of RIKEN Ring Cyclotron Magnets", 3rd International Particle Accelerator Conference (IPAC 2012), (CAMD(Center for Advanced Microstructures and Devices, Louisiana State University)), New Orleans, USA, Aug. (2012).

Hasebe H., Kuboki H., Okuno H., Yamane I., Imao H., Fukunishi N., Kase M., and Kamigaito O.: "Development of new foil compounded from carbon nanotube and sputter-deposition carbon", INTDS 2012 (the 26th conference of the International Nuclear Target Development Society), (Univ-Mainz and GSI), Mainz, Germany, Aug. (2012).

Okuno H., Fukunishi N., Hasebe H., Imao H., Kamigaito O., Kase M., and Kuboki H.: "Charge Strippers for the RIKEN Radioisotope Beam Factory (RIBF)", INTDS2012, (INTDS), Mainz, Germany, Aug. (2012).

Imao H., Okuno H., Kamigaito O., Kuboki H., Hasebe H., Fukunishi N., Watanabe T., Fujimaki M., Watanabe Y., Maie T., Kase M., and Yano Y.: "Charge-stripping system for 238U ion beam with recirculating He gas", INTDS2012, (GSI), Mainz, Germany, Aug. (2012).

Higurashi Y., Ohnishi J., Ohzeki K., Haba H., Fujimaki M., Kidera M., Komiyama M., Kamigaito O., Aihara T., Tamura M., and Uchiyama A.: "RECENT DEVELOPMENTS OF THE RIKEN 28-GHZ SC-ECRIS", 20th International Workshop on Electron Cyclotron Resonance Ion Sources (ECRIS-2012), (Australian Nuclear Science and Technology Organisation), Sydney, Australia, Sept. (2012).

Suda K., Arai S., Chiba Y., Kamigaito O., Kase M., Sakamoto N., Watanabe Y., and Yamada K.: "Design of Coupler for Direct Coupled Amplifier to Drift Tube Linac Cavities of the Injector RILAC2 for RIKEN RI Beam Factory", 26th International Linear Accelerator Conference (LINAC12), (LINAC12 International Organizing Committee), Tel Aviv, Israel, Sept. (2012).

Sakamoto N., Fujimaki M., Higurashi Y., Hasebe H., Kamigaito O., Okuno H., Suda K., Watanabe T., Yamada K., and Koyama R.: "Commissioning of a New Injector for the RIKEN RI-Beam Factory", LINAC12, (Soreq Nuclear Research Center), Tel-Aviv, Israel, Sept. (2012).

Kamigaito O.: "Present Status of RIBF Accelerators at RIKEN", Science with Rare Ion Beams - SCRIBE-2012, (Variable Energy Cyclotron Center), Kolkata, India, Nov. (2012).

Yamaguchi Y., Wakasugi M., Ozawa A., Uesaka T., Yano Y., Fujinawa T., Fukunishi N., Inabe N., Kamigaito O., Kase M., Kikuchi T., Komiyama M., Kubo T., Kumagai K., Maie T., Ohnishi J., Tokuchi A., Yoshida K., Yamaguchi T., Nagae D., Zenihiro J., Suzuki T., Abe Y., and Suzaki F.: "Construction of Rare-RI Ring at RIKEN RI Beam Factory", 16th International Conference on Electromagnetic Isotope Separators and Techniques Related to their Applications (EMIS2012), (RIKEN KEK IMP), Matsue, Dec. (2012).

(Domestic Conference)

日暮祥英, 中川孝秀, 大西純一, 羽場宏光, 藤巻正樹, 池沢英二, 渡邉裕, 加瀬昌之, 後藤彰, 込山美咲, 上垣外修一, 田村匡史, 藍原利光, 内山暁仁: "理研新超電導 ECR イオン源の開発研究", 第 7 回日本加速器学会年会, (日本加速器学会), 姫路, 8 月 (2010).

池沢英二, 上垣外修一, 加瀬昌之, 渡邉裕, 大木智則, 藍原利光, 山内啓資, 内山暁仁, 小山田和幸, 田村匡史: "理研重イオンリニアックの現状報告", 第 8 回日本加速器学会年会, (日本加速器学会), 筑波, 8 月 (2011).

山田一成, 池沢英二, 今尾浩士, 大西純一, 奥野広樹, 加瀬昌之, 上垣外修一, 熊谷桂子, 込山美咲, 後藤彰, 坂本成彦, 須田健嗣, 中川孝秀, 日暮祥英, 福西暢尚, 藤縄雅, 藤巻正樹, 眞家武士, 山澤秀行, 横内茂, 渡邉環, 渡辺博, 渡邉裕, 新井重昭, 藤澤博, 佐藤洋一: "RIBF 用新入射器 RILAC2 のビームコミッショニング", 第 8 回加速器学会年会, (日本加速器学会), つくば市, 8 月 (2011).

寺岡毅, 神谷健太, 澤野郁夫, 中嶌輝子, 加々美裕, 神尾章子, 浜部直哉, 林依子, 龍頭啓充, 福西暢尚, 阿部知子: "重イオンビーム照射によるウンシュウミカン形態変異個体の果実品質の特徴", 園芸学会平成 23 年度秋季大会, (園芸学会), 岡山, 9 月 (2011).

今尾浩士, 奥野広樹, 久保木浩功, 横内茂, 福西暢尚, 上垣外修一, 長谷部裕雄, 渡邉環, 加瀬昌之, 後藤彰, 矢野安重: 日本物理学会第６７回年次大会, (大阪大学), 大阪, 3 月 (2012).

渡邉裕, 今尾浩士, 奥野広樹, 加瀬昌之, 上垣外修一, 熊谷桂子, 込山美咲, 坂本成彦, 須田健嗣, 長瀬誠, 福西暢尚, 藤巻正樹, 眞家武士, 山田一成, 渡邉環, 渡辺博, 石川盛, 小高康照, 小林清志, 小山亮, 柴田順翔, 月居憲俊, 仲村武志, 西田稔, 西村誠, 濱仲誠, 福澤聖児, 矢冨一慎: "理研リングサイクロトロン (RRC) の電磁石の老朽化", 第 9 回日本加速器学会年会, (日本加速器学会), 大阪, 8 月 (2012).

池沢英二, 上垣外修一, 加瀬昌之, 渡邉裕, 大木智則, 藍原利光, 山内啓資, 内山暁仁, 小山田和幸, 田村匡史: "理研重イオンリニアックの現状報告", 第 9 回日本加速器学会年会, (日本加速器学会), 大阪, 8 月 (2012).

渡邉環, 福西暢尚, 加瀬昌之, 上垣外修一, 稲森聡, 今康一: "高温超伝導電流センサーと SQUID を用いたビーム電流モニターの高感度化", 第 9 回日本加速器学会年会, (日本加速器学会), 大阪大学, 8 月 (2012).

今尾浩士, 奥野広樹, 久保木浩功, 上垣外修一, 長谷部裕雄, 福西暢尚, 渡邉環, 藤巻正樹, 渡邉裕, 眞家武士, 加瀬昌之, 矢野安重: 第 9 回日本加速器学会年会, (大阪大学), 大阪, 8 月 (2012).

坂本成彦, 段塚知志, 藤縄雅, 福西暢尚, 長谷部裕雄, 日暮祥英, 池上九三男, 池沢英二, 今尾浩士, 影山正, 上垣外修一, 加瀬昌之, 木寺正憲, 込山美咲, 久保木浩功, 熊谷桂子, 眞家武士, 長瀬誠, 中川孝秀, 中村仁音, 大西純一, 奥野広樹, 大関和貴, 須田健嗣, 渡辺博, 渡邉環, 渡邉裕, 山田一成, Lu L., 山澤秀行: "理研 RIBF における大強度重イオンビーム加速", 第 9 回日本加速器学会年会, 大阪, 8 月 (2012).

長谷部裕雄, 奥野広樹, 久保木浩功, 山根功, 今尾浩士, 福西暢尚, 加瀬昌之, 上垣外修一: "カーボンナノチューブ・カーボン蒸着膜の開発", 第 9 回　日本加速器学会, (日本加速器学会), 大阪大学, 8 月 (2012).

Accelerator R&D Team

Publications

[Journal]

(Original Papers) *Subject to Peer Review

Kaji D., Morimoto K., Morita K., Hasebe H., Yoshida A., Haba H., and Yoneda A.: "Target for the heaviest element production at RIKEN", Nucl. Instrum. Methods Phys. Res. A **590**, 198 (2007). *

Hasebe H., Kuboki H., Okuno H., Fukunishi N., Kamigaito O., Imao H., Goto A., and Kase M.: "Development of the carbon foils as charge strippers for high-intensity uranium ion beams", Nucl. Instrum. Methods Phys. Res. A **655**, No. 1, pp. 57–60 (2011). *

Sakaguchi S., Iseri Y., Uesaka T., Tanifuji M., Amos K., Aoi N., Hashimoto Y., Hiyama E., Ichikawa M., Ichikawa Y., Ishikawa S., Itoh K., Itoh M., Iwasaki H., Karataglidis S., Kawabata T., Kawahara T., Kuboki H., Maeda Y., Matsuo R., Nakao T., Okamura H., Sakai H., Sasamoto Y., Sasano M., Sato Y., Sakaguchi-Sekiguchi K., Shinohara M., Suda K., Suzuki D., Takahashi Y., Tamii A., Wakui T., Yako K., Yamaguchi M., and Yamamoto Y.: "Analyzing power in elastic scattering of 6He from a polarized proton target at 71 MeV/nucleon", Phys. Rev. C **84**, No. 024604, pp. 024604-1–024604-17 (2011). *

Yagi E., Hayashi T., Yoshida T., Koike S., Higami N., Hirabayashi K., Takebayashi A., Matsuba H., and Ogiwara K.: "Lattice location and density distribution of hydrogen in beta1-V2H", J. Phys. Soc. Jpn. **81**, No. 4, pp. 044602-1–044602-14 (2012). *

Imao H., Okuno H., Kuboki H., Yokouchi S., Fukunishi N., Kamigaito O., Hasebe H., Watanabe T., Kase M., and Yano Y.: "Charge stripping of 238U beam by helium gas stripper", Phys. Rev. Spec. Top.: Accel. Beams **15**, No. 123501, (2012). *

Higurashi Y., Nakagawa T., Ohnishi J., Haba H., Tamura M., Aihara T., Fujimaki M., Komiyama M., Uchiyama A., and Kamigaito O.: "Results of RIKEN superconducting electron cyclotron resonance ion source with 28GHz", Rev. Sci. Instrum. **83**, No. 2, p. 02A308 (2012). *

Higurashi Y., Nakagawa T., Ohnishi J., Haba H., Tamura M., Aihara T., Fujimaki M., Komiyama M., Uchiyama A., and Kamigaito O.: "Production of a highly charged uranium ion beam with RIKEN superconducting electron cyclotron resonance ion source", Rev. Sci. Instrum. **83**, No. 2, p. 02A333 (2012). *

Sato H., Kubo T., Yano Y., Kusaka K., Ohnishi J., Yoneda K., Shimizu Y., Motobayashi T., Otsu H., Isobe T., Kobayashi T., Sekiguchi K., Nakamura T., Kondo Y., Togano Y., Murakami T., Tsuchihashi T., Orikasa T., and Maeta K.: "Superconducting dipole magnet for SAMURAI spectrometer", IEEE Trans. Appl. Supercond. **23**, No. 3, pp. 4500308-1–4500308-8 (2013). *

(Others)

Nakagawa T., Higurashi Y., Ohnishi J., Aihara T., Tamura M., Uchiyama A., Okuno H., Kusaka K., Kidera M., Komiyama M., Fujimaki M., Sato Y., Ikezawa E., Watanabe Y., Kase M., Goto A., Kamigaito O., and Yano Y.: "First results from the new RIKEN superconducting electron cyclotron resonance ion source", Rev. Sci. Instrum. **81**, No. 2, p. 02A320 (2010).

Imao H., Okuno H., Kuboki H., Yokouchi S., Fukunishi N., Kamigaito O., Hasebe H., Watanabe T., Kase M., and Yano Y.: "Charge stripping of Uranium-238 ion beam with low-Z gas stripper", Particle accelerator. Proceedings, 2nd International Conference, IPAC 2011 **C110904**, 1746–1748 (2011).

Okuno H., Fukunishi N., Hasebe H., Imao H., Kamigaito O., Kase M., and Kuboki H.: "New Developments in Low-Z Gas Stripper Sstem at RIKEN Radioactive Isotope Beam Factory (RIBF)", Proceedings of HIAT12 **1**, No. 1, p. 199 (2012).

Okuno H., Dantsuka T., Fujimaki M., Fujinawa T., Fukunishi N., Hasebe H., Higurashi Y., Ikegami K., Ikezawa E., Imao H., Kageyama T., Kamigaito O., Kase M., Kidera M., Komiyama M., Kuboki H., Kumagai K., Maie T., Nagase M., Nakagawa T., Nakamura M., Ohnishi J., Sakamoto N., Suda K., Watanabe H., Watanabe T., Watanabe Y., Yamada K., and Yamasawa H.: "Recent Achievements and Upgrade Programs at RIKEN Radioactive Isotope Beam Factory", Proceedings of IPAC12 **1**, No. 1, p. 430 (2012).

日暮祥英, 大西純一, 中川孝秀, 藍原利光, 田村匡史, 内山暁仁, 込山美咲, 藤巻正樹, 佐藤洋一, 池沢英二, 渡邉裕, 加瀬昌之, 後藤彰, 上垣外修一, 矢野安重: "理研における新しい超電導 ECR イオン源の開発", 加速器 **6**, No. 4, pp. 346–354 (2010).

[Book・Proceedings]

(Original Papers) *Subject to Peer Review

Yamada K., Arai S., Fujimaki M., Fujinawa T., Fujisawa H., Fukunishi N., Goto A., Higurashi Y., Ikezawa E., Kase M., Komiyama M., Kumagai K., Maie T., Nakagawa T., Ohnishi J., Okuno H., Sakamoto N., Sato Y., Suda K., Watanabe H., Watanabe T., Watanabe Y., Yano Y., Yokouchi S., and Kamigaito O.: "Construction of new injector linac at RIBF", CYCLOTRONS'10, Lanzhou, 2010–9, JaCoW, Lanzhou, pp. 1–3 (2010).

Yamada K., Arai S., Fujimaki M., Fujinawa T., Fujisawa H., Fukunishi N., Goto A., Higurashi Y., Ikezawa E., Kamigaito O., Kase M., Komiyama M., Kumagai K., Maie T., Nakagawa T., Ohnishi J., Okuno H., Sakamoto N., Sato Y., Suda K., Watanabe H., Watanabe Y., Yano Y., and Yokouchi S.: "Construction of new injector linac for RI Beam Factory at RIKEN Nishina Center", Proceedings of of the 1st International Particle Accelerator Conference (IPAC'10), Kyoto, 2010–5, JaCoW, Kyoto, pp. 789–791 (2010).

Yamada K., Arai S., Chiba Y., Fujisawa H., Ikezawa

E., Kamigaito O., Kase M., Sakamoto N., Suda K., Watanabe Y., and Touchi Y.: "Rf-design and construction of new linac injector for RIKEN RI-Beam Factory", Proceedings of XXV Linear Accelerator Conference, Tsukuba, 2010–9, JaCoW, Tsukuba, pp. 572–574 (2010).

Watanabe Y., Fujimaki M., Fukunishi N., Hasebe H., Higurashi Y., Ikezawa E., Imao H., Kageyama T., Kamigaito O., Kase M., Kidera M., Komiyama M., Kuboki H., Kumagai K., Maie T., Nagase M., Nakagawa T., Ohnishi J., Okuno H., Sakamoto N., Suda K., Watanabe H., Watanabe T., Yamada K., Yokouchi S., Aihara T., Fukuzawa S., Hamanaka M., Ishikawa S., Kobayashi K., Kotaka Y., Koyama R., Nakamura T., Nishida M., Nishimura M., Ohki T., Oyamada K., Shibata J., Tamura M., Tsukiori N., Uchiyama A., Yadomi K., and Yamauchi H.: "Present status of RIKEN Ring Cyclotron Magnets", Proceedings of 3rd International Particle Accelerator Conference (IPAC 2012), New Orleans, USA, 2012–8, IPAC2012, IEEE, New Orleans, pp. 433–435 (2012). ＊

山田一成, 池沢英二, 今尾浩士, 大西純一, 奥野広樹, 加瀬昌之, 熊谷桂子, 込山美咲, 後藤彰, 坂本成彦, 須田健嗣, 中川孝秀, 日暮祥英, 福西暢尚, 藤縄雅, 藤巻正樹, 眞家武士, 山澤秀行, 横内茂, 渡邉環, 渡辺博, 渡邉裕, 新井重昭, 藤澤博, 佐藤洋一, 上垣外修一: "理研 RIBF 用の新しい重イオン入射ライナック RILAC2 の製作", 第 7 回日本加速器学会年会プロシーディングス, 姫路市, 2010–8, 日本加速器学会, 東京, pp. 360–363 (2010).

日暮祥英, 大西純一, 湊恒明: "28 GHz 超伝導 ECR イオン源の開発", 第 9 回日本加速器学会年会プロシーディングス, 豊中市, 2012–8, 日本加速器学会, 東京, p. 138 (2012).

大関和貴, 日暮祥英, 大西純一, 中川孝秀: "理研 28 GHz 超伝導 ECR イオン源のエミッタンス測定", 第 9 回日本加速器学会年会プロシーディングス, 豊中, 2012–8, 日本加速器学会, 東京, pp. 252–254 (2012).

(Others)

Yamada K., Suda K., Arai S., Fujimaki M., Fujinawa T., Fujisawa H., Fukunishi N., Higurashi Y., Ikezawa E., Imao H., Kamigaito O., Kase M., Komiyama M., Kumagai K., Maie T., Nakagawa T., Ohnishi J., Okuno H., Sakamoto N., Watanabe H., Watanabe T., Watanabe Y., Yamasawa H., Sato Y., and Goto A.: "Beam Commissioning and Operation of New Linac Injector for RIKEN RI Beam Factory", Proceedings of 3rd International Particle Accelerator Conference (IPAC 2012), New Orleans, USA, 2012–5, JACoW, New Orleans, pp. 1071–1073 (2012).

Oral Presentations

(International Conference etc.)

Yamada K., Okuno H., Fujimaki M., Fukunishi N., Goto A., Hasebe H., Ikegami K., Kamigaito O., Kase M., Kumagai K., Maie T., Nagase M., Ohnishi J., Sakamoto N., Yokouchi S., and Yano Y.: "Status of the Superconducting Ring Cyclotron at RIKEN RI Beam Factory", 11th European Particle Accelerator Conference (EPAC 2008), (INFN-LNF), Genoa, Italy, June (2008).

Yamada K., Dantsuka T., Fujimaki M., Fujinawa T., Fukunishi N., Goto A., Hasebe H., Higurashi Y., Ikezawa E., Kamigaito O., Kase M., Komiyama M., Kuboki H., Kumagai K., Maie T., Nagase M., Nakagawa T., Ohnishi J., Okuno H., Sakamoto N., Sato Y., Suda K., Wakasugi M., Watanabe H., Watanabe T., Watanabe Y., Yano Y., and Yokouchi S.: "Progress on the commissioning of Radioactive Isotope Beam Factory at RIKEN Nishina Center", 11th International Conference on HEAVY ION ACCELERATOR TECHNOLOGY (HIAT09), (INFN-LNL), Venezia, Italy, June (2009).

Yamada K., Arai S., Fujimaki M., Fujinawa T., Fujisawa H., Fukunishi N., Goto A., Higurashi Y., Ikezawa E., Kamigaito O., Kase M., Komiyama M., Kumagai K., Maie T., Nakagawa T., Ohnishi J., Okuno H., Sakamoto N., Sato Y., Suda K., Watanabe H., Watanabe Y., Yano Y., and Yokouchi S.: "Construction of New Injector Linac for RI Beam Factory at RIKEN Nishina Center", 1st International Particle Accelerator Conference (IPAC'10), (High Energy Accelerator Research Organization), Kyoto, May (2010).

Higurashi Y., Nakagawa T., Ohnishi J., Haba H., Tamura M., Aihara T., Fujimaki M., Komiyama M., Uchiyama A., and Kamigaito O.: "Developments of RIKEN New Superconducting ECR Ion Source", 1st International Particle Accelerator Conference (IPAC'10), Kyoto, May (2010).

Higurashi Y., Nakagawa T., Ohnishi J., Haba H., Ikezawa E., Fujimaki M., Watanabe Y., Kidera M., Komiyama M., Kase M., Goto A., Kamigaito O., Aihara T., Tamura M., and Uchiyama A.: "Production of U ion beam from RIKEN SC-ECRIS ith sputtering method", 19th International Workshop on ECR Ion Sources (ECRIS 2010), grenoble, France, Aug. (2010).

Yamada K., Arai S., Fujimaki M., Fujinawa T., Fujisawa H., Fukunishi N., Goto A., Higurashi Y., Ikezawa E., Kase M., Komiyama M., Kumagai K., Maie T., Nakagawa T., Ohnishi J., Okuno H., Sakamoto N., Sato Y., Suda K., Watanabe H., Watanabe T., Watanabe Y., Yano Y., Yokouchi S., and Kamigaito O.: "Construction of New Injector LINAC at RIBF", 19th International Conference on Cyclotrons and their Applications (CYCLOTRONS 2010), (IMP), Lanzhou, China, Sept. (2010).

Yamada K., Arai S., Chiba Y., Fujisawa H., Ikezawa E., Kamigaito O., Kase M., Sakamoto N., Suda K., Watanabe Y., and Touchi Y.: "RF-design and Construction of New Linac Injector for the RIKEN RI-Beam Factory", 25th Linear Accelerator Conference (LINAC10), (High Energy Accelerator Research Organization), Tsukuba, Sept. (2010).

Higurashi Y., Ohnishi J., Ohzeki K., Haba H., Fujimaki

M., Komiyama M., Kamigaito O., Aihara T., Tamura M., and Uchiyama A.: "Production of highly charged uranium ion beam with RIKEN superconducting electron cyclotron resonance ion source", The 14th Int. Conf. on Ion Sources (ICIS11), (INFN-LNS, Italy), Giardini Naxos, Italy, Sept. (2011).

Higurashi Y., Ohnishi J., Ohzeki K., Haba H., Fujimaki M., Komiyama M., Kamigaito O., Aihara T., Tamura M., and Uchiyama A.: "Results of RIKEN superconducting electron cyclotron resonance ion source with 28GHz", The 14th Int. Conf. on Ion Sources (ICIS11), (INFN-LNS, Italy), Giardini Naxos, Italy, Sept. (2011).

Yamada K., Suda K., Arai S., Fujimaki M., Fujinawa T., Fujisawa H., Fukunishi N., Higurashi Y., Ikezawa E., Imao H., Kamigaito O., Kase M., Komiyama M., Kumagai K., Maie T., Nakagawa T., Ohnishi J., Okuno H., Sakamoto N., Watanabe H., Watanabe T., Watanabe Y., Yamasawa H., Sato Y., and Goto A.: "Beam Commissioning and Operation of New Linac Injector for RIKEN RI Beam Factory", 3rd International Particle Accelerator Conference (IPAC 2012), New Orleans, USA, May (2012).

Imao H., Okuno H., Kuboki H., Yokouchi S., Fukunishi N., Kamigaito O., Hasebe H., Watanabe T., Kase M., and Yano Y.: "Charge stripping of uranium-238 ion beam with helium gas stripper", IPAC12, (IEEE), New Orleans, USA, May (2012).

Okuno H., Dantsuka T., Fujimaki M., Fujinawa T., Fukunishi N., Hasebe H., Higurashi Y., Ikegami K., Ikezawa E., Imao H., Kageyama T., Kamigaito O., Kase M., Kidera M., Komiyama M., Kuboki H., Kumagai K., Maie T., Nagase M., Nakagawa T., Nakamura M., Ohnishi J., Sakamoto N., Suda K., Watanabe H., Watanabe T., Watanabe Y., Yamada K., and Yamasawa H.: "Recent Achievements and Upgrade Programs at RIKEN Radioactive Isotope Beam Factory", IPAC12, (IPAC12 International Organizing Committee), NewOrleans, USA, May–May (2012).

Okuno H., Fukunishi N., Hasebe H., Imao H., Kamigaito O., Kase M., and Kuboki H.: "New Developments in Low-Z Gas Stripper Sstem at RIKEN Radioactive Isotope Beam Factory (RIBF)", 12th International Conference on Heavy Ion Accelerator Technology, (Argonne National Laboratory), Chicago, IL, USA, June–June (2012).

Kuboki H., Okuno H., Hershcovitch A., Dantsuka T., Hasebe H., Ikegami K., Imao H., Kamigaito O., Kase M., Maie T., Nakagawa T., and Yano Y.: "Development of Plasma Window for gas charge strippers at RIKEN RIBF", 26th World Conference of the International Nuclear Target Development Society, (Johannes Gutenberg-Universitat and GSI), Mainz, Germany, Aug. (2012).

Watanabe Y., Fujimaki M., Fukunishi N., Hasebe H., Higurashi Y., Ikezawa E., Imao H., Kageyama T., Kamigaito O., Kase M., Kidera M., Komiyama M., Kuboki H., Kumagai K., Maie T., Nagase M., Nakagawa T., Ohnishi J., Okuno H., Sakamoto N., Suda K., Watanabe H., Watanabe T., Yamada K., Yokouchi S., Aihara T., Fukuzawa S., Hamanaka M., Ishikawa S., Kobayashi K., Kotaka Y., Koyama R., Nakamura T., Nishida M., Nishimura M., Ohki T., Oyamada K., Shibata J., Tamura M., Tsukiori N., Uchiyama A., Yadomi K., and Yamauchi H.: "Present status of RIKEN Ring Cyclotron Magnets", 3rd International Particle Accelerator Conference (IPAC 2012), (CAMD(Center for Advanced Microstructures and Devices, Louisiana State University)), New Orleans, USA, Aug. (2012).

Hasebe H., Kuboki H., Okuno H., Yamane I., Imao H., Fukunishi N., Kase M., and Kamigaito O.: "Development of new foil compounded from carbon nanotube and sputter-deposition carbon", INTDS 2012 (the 26th conference of the International Nuclear Target Development Society), (Univ-Mainz and GSI), Mainz, Germany, Aug. (2012).

Okuno H., Fukunishi N., Hasebe H., Imao H., Kamigaito O., Kase M., and Kuboki H.: "Charge Strippers for the RIKEN Radioisotope Beam Factory (RIBF)", INTDS2012, (INTDS), Mainz, Germany, Aug. (2012).

Imao H., Okuno H., Kamigaito O., Kuboki H., Hasebe H., Fukunishi N., Watanabe T., Fujimaki M., Watanabe Y., Maie T., Kase M., and Yano Y.: "Charge-stripping system for 238U ion beam with recirculating He gas", INTDS2012, (GSI), Mainz, Germany, Aug. (2012).

Ohzeki K., Higurashi Y., Ohnishi J., and Nakagawa T.: "Design of new 18 GHz ECRIS for RIKEN RIBF", 20th International Workshop on Electron Cyclotron Resonance Ion Sources (ECRIS-2012), (Australian Nuclear Science and Technology Organisation), Sydney, Australia, Sept. (2012).

Ohzeki K., Higurashi Y., Nakagawa T., and Ohnishi J.: "Emittance measurement for U ion beams produced from RIKEN 28 GHz SC-ECRIS", 20th International Workshop on Electron Cyclotron Resonance Ion Sources (ECRIS-2012), (Australian Nuclear Science and Technology Organisation), Sydney, Australia, Sept. (2012).

Higurashi Y., Ohnishi J., Ohzeki K., Haba H., Fujimaki M., Kidera M., Komiyama M., Kamigaito O., Aihara T., Tamura M., and Uchiyama A.: "RECENT DEVELOPMENTS OF THE RIKEN 28-GHZ SC-ECRIS", 20th International Workshop on Electron Cyclotron Resonance Ion Sources (ECRIS-2012), (Australian Nuclear Science and Technology Organisation), Sydney, Australia, Sept. (2012).

Suda K., Arai S., Chiba Y., Kamigaito O., Kase M., Sakamoto N., Watanabe Y., and Yamada K.: "Design of Coupler for Direct Coupled Amplifier to Drift Tube Linac Cavities of the Injector RILAC2 for RIKEN RI Beam Factory", 26th International Linear Accelerator

Conference (LINAC12), (LINAC12 International Organizing Committee), Tel Aviv, Israel, Sept. (2012).

Sakamoto N., Fujimaki M., Higurashi Y., Hasebe H., Kamigaito O., Okuno H., Suda K., Watanabe T., Yamada K., and Koyama R.: "Commissioning of a New Injector for the RIKEN RI-Beam Factory", LINAC12, (Soreq Nuclear Research Center), Tel-Aviv, Israel, Sept. (2012).

Sato H., Kubo T., Yano Y., Kusaka K., Ohnishi J., Yoneda K., Shimizu Y., Motobayashi T., Otsu H., Isobe T., Kobayashi T., Sekiguchi K., Nakamura T., Kondo Y., Togano Y., Murakami T., Tsuchihashi T., Orikasa T., and Maeta K.: "Superconducting dipole magnet for SAMURAI spectrometer", Applied Superconductivity Conference (ASC2012), (ASC), Portland, USA, Oct. (2012).

Yamaguchi Y., Wakasugi M., Ozawa A., Uesaka T., Yano Y., Fujinawa T., Fukunishi N., Inabe N., Kamigaito O., Kase M., Kikuchi T., Komiyama M., Kubo T., Kumagai K., Maie T., Ohnishi J., Tokuchi A., Yoshida K., Yamaguchi T., Nagae D., Zenihiro J., Suzuki T., Abe Y., and Suzaki F.: "Construction of Rare-RI Ring at RIKEN RI Beam Factory", 16th International Conference on Electromagnetic Isotope Separators and Techniques Related to their Applications (EMIS2012), (RIKEN KEK IMP), Matsue, Dec. (2012).

(Domestic Conference)

日暮祥英, 中川孝秀, 大西純一, 羽場宏光, 藤巻正樹, 池沢英二, 渡邉裕, 加瀬昌之, 後藤彰, 込山美咲, 上垣外修一, 田村匡史, 藍原利光, 内山暁仁: "理研新超電導 ECR イオン源の開発研究", 第 7 回日本加速器学会年会, (日本加速器学会), 姫路, 8 月 (2010).

日暮祥英, 中川孝秀, 大西純一, 羽場宏光, 田村匡史, 藍原利光, 藤巻正樹, 込山美咲, 内山暁仁, 上垣外修一: "28GH z　超電導 ECR イオン源の開発", 第 8 回日本加速器学会年会, (日本加速器学会), 筑波, 8 月 (2011).

山田一成, 池沢英二, 今尾浩士, 大西純一, 奥野広樹, 加瀬昌之, 上垣外修一, 熊谷桂子, 込山美咲, 後藤彰, 坂本成彦, 須田健嗣, 中川孝秀, 日暮祥英, 福西暢尚, 藤縄雅, 藤巻正樹, 眞家武士, 山澤秀行, 横内茂, 渡邉環, 渡辺博, 渡邉裕, 新井重昭, 藤澤博, 佐藤洋一: "RIBF 用新入射器 RILAC2 のビームコミッショニング", 第 8 回加速器学会年会, (日本加速器学会), つくば市, 8 月 (2011).

今尾浩士, 奥野広樹, 久保木浩功, 横内茂, 福西暢尚, 上垣外修一, 長谷部裕雄, 渡邉環, 加瀬昌之, 後藤彰, 矢野安重: 日本物理学会第６７回年次大会, (大阪大学), 大阪, 3 月 (2012).

渡邉裕, 今尾浩士, 奥野広樹, 加瀬昌之, 上垣外修一, 熊谷桂子, 込山美咲, 坂本成彦, 須田健嗣, 長瀬誠, 福西暢尚, 藤巻正樹, 眞家武士, 山田一成, 渡邉環, 渡辺博, 石川盛, 小高康照, 小林清志, 小山亮, 柴田順翔, 月居憲俊, 仲村武志, 西田稔, 西村誠, 濱仲誠, 福澤聖児, 矢冨一慎: "理研リングサイクロトロン (RRC) の電磁石の老朽化", 第 9 回日本加速器学会年会, (日本加速器学会), 大阪, 8 月 (2012).

日暮祥英, 大西純一, 湊恒明: "28 GHz 超伝導 ECR イオン源の開発", 第 9 回日本加速器学会年会, (日本加速器学会), 豊中市, 8 月 (2012).

今尾浩士, 奥野広樹, 久保木浩功, 上垣外修一, 長谷部裕雄, 福西暢尚, 渡邉環, 藤巻正樹, 渡邉裕, 眞家武士, 加瀬昌之, 矢野安重: 第 9 回日本加速器学会年会, (大阪大学), 大阪, 8 月 (2012).

大関和貴, 日暮祥英, 大西純一, 中川孝秀: "理研 28 GHz 超伝導 ECR イオン源のエミッタンス測定", 第 9 回日本加速器学会年会, (日本加速器学会), 豊中, 8 月 (2012).

坂本成彦, 段塚知志, 藤縄雅, 福西暢尚, 長谷部裕雄, 日暮祥英, 池上九三男, 池沢英二, 今尾浩士, 影山正, 上垣外修一, 加瀬昌之, 木寺正憲, 込山美咲, 久保木浩功, 熊谷桂子, 眞家武士, 長瀬誠, 中川孝秀, 中村仁音, 大西純一, 奥野広樹, 大関和貴, 須田健嗣, 渡辺博, 渡邉環, 渡邉裕, 山田一成, Lu L., 山澤秀行: "理研 RIBF における大強度重イオンビーム加速", 第 9 回日本加速器学会年会, 大阪, 8 月 (2012).

長谷部裕雄, 奥野広樹, 久保木浩功, 山根功, 今尾浩士, 福西暢尚, 加瀬昌之, 上垣外修一: "カーボンナノチューブ・カーボン蒸着膜の開発", 第 9 回　日本加速器学会, (日本加速器学会), 大阪大学, 8 月 (2012).

加治大哉, 住田貴之, 長谷部裕雄, 田中謙伍, 羽場宏光, 森田浩介, 森本幸司, 若林泰生, 村上昌史, 武山美麗, 山木さやか: "超重元素生成のための新しい標的システム", 2012 日本放射化学会年会・第 56 回放射化学討論会, (日本放射化学会), 東京工業大学, 10–10 月 (2012).

加治大哉, 住田貴之, 刈屋佳樹, 鹿取謙二, 工藤祐生, 森田浩介, 森谷透, 村上昌史, 武山美麗, 田中謙伍, 戸田光祐, 門叶冬樹, 若林泰生, 山木さやか, 米田晃, 大関和貴, 長谷部裕雄, 羽場宏光, 吉田敦, 山口貴之: "208Pb+70Zn 反応を用いた 277Cn の生成と壊変特性", 2012 日本放射化学会年会・第 56 回放射化学討論会, (日本放射化学会), 東京工業大学, 10–10 月 (2012).

Ion Source Team

Publications

[Journal]

(Original Papers) *Subject to Peer Review

Higurashi Y., Nakagawa T., Kidera M., Aihara T., Kase M., and Yano Y.: "Enhancement of Ar8+ Current Extracted from RIKEN 18 GHz Electron Cyclotron Resonance Ion Source by Moving the Plasma Electrode toward the Resonance Zone", Jpn. J. Appl. Phys. **40**, 5134–5135 (2001). ∗

Higurashi Y., Nakagawa T., Kidera M., Kageyama T., Kase M., Goto A., and Yano Y.: "Production of Highly Charged Ga Ions from Organic Metal Comppound Using the Liquid-He-Free Superconducting Electron Cyclotron Resonance Ion Source at RIKEN", Jpn. J. Appl. Phys. **41**, 5442–5443 (2002). ∗

Higurashi Y., Nakagawa T., Kidera M., Aihara T., Kase M., and Yano Y.: "Effect of plasma electrode position on the beam intensity of heavy ions from a RIKEN 18 GHz electron cyclotron resonance ion source", Rev. Sci. Instrum. **73**, No. 2, p. 598 (2002). ∗

Higurashi Y., Nakagawa T., Kidera M., Aihara T., Kase M., and Yano Y.: "Enhancement of Ar8+ Ion Beam Intensity from RIKEN 18 GHz Electron Cyclotron Resonance Ion Source by Optimizing the Magnetic Field Configuration", Jpn. J. Appl. Phys. **42**, 3656–3657 (2003). ∗

Higurashi Y., Nakagawa T., Kidera M., Kageyama T., Aihara T., Kase M., and Yano Y.: "Optimization of magnetic field configuration for the roduction of Ar ions from RIKEN 18 GHz ECR ion source", Nucl. Instrum. Methods Phys. Res. A **510**, No. 2, pp. 206–210 (2003). ∗

Higurashi Y., Kidera M., Kase M., Nakagawa T., and Yano Y.: "Emittance measurement for intense beam of heavy ions from RIKEN 18 GHz ECRIS", Rev. Sci. Instrum. **75**, 1467 (2004). ∗

Higurashi Y., Kidera M., Nakagawa T., Aihara T., Kase M., and Yano Y.: "Effect of Plasma Electrode Position of RIKEN 18 GHz Electron Cyclotron Resonance Ion Source on Beam Intensity of Highly Charged Ar Ions", Jpn. J. Appl. Phys. **44**, 5216–5218 (2005). ∗

Higurashi Y., Kidera M., Nakagawa T., Aihara T., Kase M., Goto A., and Yano Y.: "Production of 70Zn Beam from RIKEN 18 GHz Electron Cyclotron Resonance Ion Source", Jpn. J. Appl. Phys. **44**, 8138–8140 (2005). ∗

Higurashi Y., Nakagawa T., Kidera M., Aihara T., Kobayashi K., Kase M., Goto A., and Yano Y.: "Effect of the plasma electrode position and shape on the beam intensity of the highly charged ions from RIKEN 18 GHz electron cyclotoron resonanse ion source", Rev. Sci. Instrum. **77**, No. 2, p. 03A329 (2006). ∗

Higurashi Y., Nakagawa T., Kidera M., Haba H., Aihara T., Kase M., Goto A., and Yano Y.: "Production of U beam from RIKEN 18 GHz electron cyclotron resonance ion source", Rev. Sci. Instrum. **79**, No. 2, p. 02C714 (2008). ∗

Kaji D., Morimoto K., Sato N., Ichikawa T., Ohzeki K., Haba H., Koura H., Ozawa A., Sumita T., Yamaguchi T., Yoneda A., Yoshida A., and Morita K.: "Production and Decay Properties of ^{263}Hs", J. Phys. Soc. Jpn. **78**, No. 3, p. 035001 (2009). ∗

Sato N., Haba H., Ichikawa T., Kaji D., Kudou Y., Morimoto K., Morita K., Ohzeki K., Sumita T., Yoneda A., Koura H., Ozawa A., Yamaguchi T., and Yoshida A.: "Production and Decay Properties of ^{264}Hs and ^{265}Hs", J. Phys. Soc. Jpn. **80**, 094201 (2011). ∗

Taniai T., Wakasugi S., Hashimoto S., Shimada A., Urabe T., Takahashi K., and Takahashi M.: "Elution Behavior and Environmental Impact of Heavy Metals and Rare-Earth Elements from Volcanic Ashes of Mt. Oyama, Miyake Island", International Journal of Environmental Analytical Chemistry **92**, 601–620 (2012). ∗

Higurashi Y., Nakagawa T., Ohnishi J., Haba H., Tamura M., Aihara T., Fujimaki M., Komiyama M., Uchiyama A., and Kamigaito O.: "Results of RIKEN superconducting electron cyclotron resonance ion source with 28GHz", Rev. Sci. Instrum. **83**, No. 2, p. 02A308 (2012). ∗

Higurashi Y., Nakagawa T., Ohnishi J., Haba H., Tamura M., Aihara T., Fujimaki M., Komiyama M., Uchiyama A., and Kamigaito O.: "Production of a highly charged uranium ion beam with RIKEN superconducting electron cyclotron resonance ion source", Rev. Sci. Instrum. **83**, No. 2, p. 02A333 (2012). ∗

木寺正憲: "電子サイクロトロン共鳴イオン源を用いた質量分析装置の開発", ぶんせき, No. 11, pp. 654–658 (2012). ∗

(Review)

木寺正憲: "電子サイクロトロン共鳴イオン源と重イオン線形加速器を用いた極微量多元素同時分析法", Isotope News, No. 701, pp. 6–10 (2012).

(Others)

Nakagawa T., Higurashi Y., Ohnishi J., Aihara T., Tamura M., Uchiyama A., Okuno H., Kusaka K., Kidera M., Komiyama M., Fujimaki M., Sato Y., Ikezawa E., Watanabe Y., Kase M., Goto A., Kamigaito O., and Yano Y.: "First results from the new RIKEN superconducting electron cyclotron resonance ion source", Rev. Sci. Instrum. **81**, No. 2, p. 02A320 (2010).

Okuno H., Dantsuka T., Fujimaki M., Fujinawa T., Fukunishi N., Hasebe H., Higurashi Y., Ikegami K., Ikezawa E., Imao H., Kageyama T., Kamigaito O., Kase M., Kidera M., Komiyama M., Kuboki H., Kumagai K., Maie T., Nagase M., Nakagawa T., Nakamura M., Ohnishi J., Sakamoto N., Suda K., Watanabe H., Watanabe T., Watanabe Y., Yamada K., and Yamasawa H.: "Recent Achievements and Upgrade Programs at RIKEN Radioactive Isotope Beam Factory", Proceedings of IPAC12 **1**, No. 1, p. 430 (2012).

日暮祥英, 大西純一, 中川孝秀, 藍原利光, 田村匡史, 内山暁仁, 込山美咲, 藤巻正樹, 佐藤洋一, 池沢英二, 渡邉裕, 加瀬昌之, 後藤彰, 上垣外修一, 矢野安重: "理研における新しい超電導 ECR イオン源の開発", 加速器 **6**, No. 4, pp. 346–354 (2010).

[Book・Proceedings]

(Original Papers) *Subject to Peer Review

Yamada K., Arai S., Fujimaki M., Fujinawa T., Fujisawa H., Fukunishi N., Goto A., Higurashi Y., Ikezawa E., Kase M., Komiyama M., Kumagai K., Maie T., Nakagawa T., Ohnishi J., Okuno H., Sakamoto N., Sato Y., Suda K., Watanabe H., Watanabe T., Watanabe Y., Yano Y., Yokouchi S., and Kamigaito O.: "Construction of new injector linac at RIBF", CYCLOTRONS'10, Lanzhou, 2010–9, JaCoW, Lanzhou, pp. 1–3 (2010).

Yamada K., Arai S., Fujimaki M., Fujinawa T., Fujisawa H., Fukunishi N., Goto A., Higurashi Y., Ikezawa E., Kamigaito O., Kase M., Komiyama M., Kumagai K., Maie T., Nakagawa T., Ohnishi J., Okuno H., Sakamoto N., Sato Y., Suda K., Watanabe H., Watanabe Y., Yano Y., and Yokouchi S.: "Construction of new injector linac for RI Beam Factory at RIKEN Nishina Center", Proceedings of of the 1st International Particle Accelerator Conference (IPAC'10), Kyoto, 2010–5, JaCoW, Kyoto, pp. 789–791 (2010).

Watanabe Y., Fujimaki M., Fukunishi N., Hasebe H., Higurashi Y., Ikezawa E., Imao H., Kageyama T., Kamigaito O., Kase M., Kidera M., Komiyama M., Kuboki H., Kumagai K., Maie T., Nagase M., Nakagawa T., Ohnishi J., Okuno H., Sakamoto N., Suda K., Watanabe H., Watanabe T., Yamada K., Yokouchi S., Aihara T., Fukuzawa S., Hamanaka M., Ishikawa S., Kobayashi K., Kotaka Y., Koyama R., Nakamura T., Nishida M., Nishimura M., Ohki T., Oyamada K., Shibata J., Tamura M., Tsukiori N., Uchiyama A., Yadomi K., and Yamauchi H.: "Present status of RIKEN Ring Cyclotron Magnets", Proceedings of 3rd International Particle Accelerator Conference (IPAC 2012), New Orleans, USA, 2012–8, IPAC2012, IEEE, New Orleans, pp. 433–435 (2012). *

山田一成, 池沢英二, 今尾浩士, 大西純一, 奥野広樹, 加瀬昌之, 熊谷桂子, 込山美咲, 後藤彰, 坂本成彦, 須田健嗣, 中川孝秀, 日暮祥英, 福西暢尚, 藤縄雅, 藤巻正樹, 眞家武士, 山澤秀行, 横内茂, 渡邉環, 渡辺博, 渡邉裕, 新井重昭, 藤澤博, 佐藤洋一, 上垣外修一: "理研 RIBF 用の新しい重イオン入射ライナック RILAC2 の製作", 第 7 回日本加速器学会年会プロシーディングス, 姫路市, 2010–8, 日本加速器学会, 東京, pp. 360–363 (2010).

日暮祥英, 大西純一, 湊恒明: "28 GHz 超伝導 ECR イオン源の開発", 第 9 回日本加速器学会年会プロシーディングス, 豊中市, 2012–8, 日本加速器学会, 東京, p. 138 (2012).

大関和貴, 日暮祥英, 大西純一, 中川孝秀: "理研 28 GHz 超伝導 ECR イオン源のエミッタンス測定", 第 9 回日本加速器学会年会プロシーディングス, 豊中, 2012–8, 日本加速器学会, 東京, pp. 252–254 (2012).

(Others)

Yamada K., Suda K., Arai S., Fujimaki M., Fujinawa T., Fujisawa H., Fukunishi N., Higurashi Y., Ikezawa E., Imao H., Kamigaito O., Kase M., Komiyama M., Kumagai K., Maie T., Nakagawa T., Ohnishi J., Okuno H., Sakamoto N., Watanabe H., Watanabe T., Watanabe Y., Yamasawa H., Sato Y., and Goto A.: "Beam Commissioning and Operation of New Linac Injector for RIKEN RI Beam Factory", Proceedings of 3rd International Particle Accelerator Conference (IPAC 2012), New Orleans, USA, 2012–5, JACoW, New Orleans, pp. 1071–1073 (2012).

Oral Presentations

(International Conference etc.)

Higurashi Y., Nakagawa T., Kidera M., Aihara T., Kase M., and Yano Y.: "Effect of plasma electrode position on the beam intensity and emittance of RIKEN 18 GHz ECRIS", 16th International Conference on ECR Ion Sources (ECRIS 04), (Lawrence Berkeley National Laboratory), Berkeley, USA, Sept. (2004).

Yamada K., Dantsuka T., Fujimaki M., Fujinawa T., Fukunishi N., Goto A., Hasebe H., Higurashi Y., Ikezawa E., Kamigaito O., Kase M., Komiyama M., Kuboki H., Kumagai K., Maie T., Nagase M., Nakagawa T., Ohnishi J., Okuno H., Sakamoto N., Sato Y., Suda K., Wakasugi M., Watanabe H., Watanabe T., Watanabe Y., Yano Y., and Yokouchi S.: "Progress on the commissioning of Radioactive Isotope Beam Factory at RIKEN Nishina Center", 11th International Conference on HEAVY ION ACCELERATOR TECHNOLOGY (HIAT09), (INFN-LNL), Venezia, Italy, June (2009).

Yamada K., Arai S., Fujimaki M., Fujinawa T., Fujisawa H., Fukunishi N., Goto A., Higurashi Y., Ikezawa E., Kamigaito O., Kase M., Komiyama M., Kumagai K., Maie T., Nakagawa T., Ohnishi J., Okuno H., Sakamoto N., Sato Y., Suda K., Watanabe H., Watanabe Y., Yano Y., and Yokouchi S.: "Construction of New Injector Linac for RI Beam Factory at RIKEN Nishina Center", 1st International Particle Accelerator Conference (IPAC'10), (High Energy Accelerator Research Organization), Kyoto, May (2010).

Higurashi Y., Nakagawa T., Ohnishi J., Haba H., Tamura M., Aihara T., Fujimaki M., Komiyama M., Uchiyama A., and Kamigaito O.: "Developments of RIKEN New Superconducting ECR Ion Source", 1st International Particle Accelerator Conference (IPAC'10), Kyoto, May (2010).

Higurashi Y., Nakagawa T., Ohnishi J., Haba H., Ikezawa E., Fujimaki M., Watanabe Y., Kidera M., Komiyama M., Kase M., Goto A., Kamigaito O., Aihara T., Tamura M., and Uchiyama A.: "Production of U ion beam from RIKEN SC-ECRIS ith sputtering method", 19th International Workshop on ECR Ion Sources (ECRIS 2010), grenoble, France, Aug. (2010).

Yamada K., Arai S., Fujimaki M., Fujinawa T., Fujisawa H., Fukunishi N., Goto A., Higurashi Y., Ikezawa E., Kase M., Komiyama M., Kumagai K., Maie T., Nakagawa T., Ohnishi J., Okuno H., Sakamoto N., Sato Y., Suda K., Watanabe H., Watanabe T., Watanabe Y., Yano Y., Yokouchi S., and Kamigaito O.: "Construction of New Injector LINAC at RIBF", 19th International Conference on Cyclotrons and their Applications (CYCLOTRONS 2010), (IMP), Lanzhou, China, Sept. (2010).

Higurashi Y., Ohnishi J., Ohzeki K., Haba H., Fujimaki M., Komiyama M., Kamigaito O., Aihara T., Tamura M., and Uchiyama A.: "Production of highly charged uranium ion beam with RIKEN superconducting electron cyclotron resonance ion source", The 14th Int. Conf. on Ion Sources (ICIS11), (INFN-LNS, Italy), Giardini Naxos, Italy, Sept. (2011).

Higurashi Y., Ohnishi J., Ohzeki K., Haba H., Fujimaki M., Komiyama M., Kamigaito O., Aihara T., Tamura M., and Uchiyama A.: "Results of RIKEN superconducting electron cyclotron resonance ion source with 28GHz", The 14th Int. Conf. on Ion Sources (ICIS11), (INFN-LNS, Italy), Giardini Naxos, Italy, Sept. (2011).

Yamada K., Suda K., Arai S., Fujimaki M., Fujinawa T., Fujisawa H., Fukunishi N., Higurashi Y., Ikezawa E., Imao H., Kamigaito O., Kase M., Komiyama M., Kumagai K., Maie T., Nakagawa T., Ohnishi J., Okuno H., Sakamoto N., Watanabe H., Watanabe T., Watanabe Y., Yamasawa H., Sato Y., and Goto A.: "Beam Commissioning and Operation of New Linac Injector for RIKEN RI Beam Factory", 3rd International Particle Accelerator Conference (IPAC 2012), New Orleans, USA, May (2012).

Okuno H., Dantsuka T., Fujimaki M., Fujinawa T., Fukunishi N., Hasebe H., Higurashi Y., Ikegami K., Ikezawa E., Imao H., Kageyama T., Kamigaito O., Kase M., Kidera M., Komiyama M., Kuboki H., Kumagai K., Maie T., Nagase M., Nakagawa T., Nakamura M., Ohnishi J., Sakamoto N., Suda K., Watanabe H., Watanabe T., Watanabe Y., Yamada K., and Yamasawa H.: "Recent Achievements and Upgrade Programs at RIKEN Radioactive Isotope Beam Factory", IPAC12, (IPAC12 International Organizing Committee), NewOrleans, USA, May–May (2012).

Kuboki H., Okuno H., Hershcovitch A., Dantsuka T., Hasebe H., Ikegami K., Imao H., Kamigaito O., Kase M., Maie T., Nakagawa T., and Yano Y.: "Development of Plasma Window for gas charge strippers at RIKEN RIBF", 26th World Conference of the International Nuclear Target Development Society, (Johannes Gutenberg-Universitat and GSI), Mainz, Germany, Aug. (2012).

Watanabe Y., Fujimaki M., Fukunishi N., Hasebe H., Higurashi Y., Ikezawa E., Imao H., Kageyama T., Kamigaito O., Kase M., Kidera M., Komiyama M., Kuboki H., Kumagai K., Maie T., Nagase M., Nakagawa T., Ohnishi J., Okuno H., Sakamoto N., Suda K., Watanabe H., Watanabe T., Yamada K., Yokouchi S., Aihara T., Fukuzawa S., Hamanaka M., Ishikawa S., Kobayashi K., Kotaka Y., Koyama R., Nakamura T., Nishida M., Nishimura M., Ohki T., Oyamada K., Shibata J., Tamura M., Tsukiori N., Uchiyama A., Yadomi K., and Yamauchi H.: "Present status of RIKEN Ring Cyclotron Magnets", 3rd International Particle Accelerator Conference (IPAC 2012), (CAMD(Center for Advanced Microstructures and Devices, Louisiana State University)), New Orleans, USA, Aug. (2012).

Ohzeki K., Higurashi Y., Ohnishi J., and Nakagawa T.: "Design of new 18 GHz ECRIS for RIKEN RIBF", 20th International Workshop on Electron Cyclotron Resonance Ion Sources (ECRIS-2012), (Australian Nuclear Science and Technology Organisation), Sydney, Australia, Sept. (2012).

Ohzeki K., Higurashi Y., Nakagawa T., and Ohnishi J.: "Emittance measurement for U ion beams produced from RIKEN 28 GHz SC-ECRIS", 20th International Workshop on Electron Cyclotron Resonance Ion Sources (ECRIS-2012), (Australian Nuclear Science and Technology Organisation), Sydney, Australia, Sept. (2012).

Higurashi Y., Ohnishi J., Ohzeki K., Haba H., Fujimaki M., Kidera M., Komiyama M., Kamigaito O., Aihara T., Tamura M., and Uchiyama A.: "RECENT DEVELOPMENTS OF THE RIKEN 28-GHZ SC-ECRIS", 20th International Workshop on Electron Cyclotron Resonance Ion Sources (ECRIS-2012), (Australian Nuclear Science and Technology Organisation), Sydney, Australia, Sept. (2012).

Haba H., Kaji D., Kanaya J., Kasamatsu Y., Kikunaga H., Kikutani Y., Komori Y., Kudo H., Kudou Y., Morimoto K., Morita K., Murakami M., Nishio K., Ooe K., Ohzeki K., Sakai R., Sato N., Shinohara A., Sumita T., Toyoshima A., Tsukada K., and Yoneda A.: "RIKEN GARIS as a promising interface for superheavy element chemistry -Production of ^{261}Rf, ^{262}Db, and ^{265}Sg for chemical studies using the GARIS gas-jet system-", EuCheMS International Conference on Nuclear and Radiochemistry (NRC-8), (The European Association for Chemical and Molecular Sciences), Como, Italy, Sept. (2012).

Sakamoto N., Fujimaki M., Higurashi Y., Hasebe H., Kamigaito O., Okuno H., Suda K., Watanabe T., Yamada K., and Koyama R.: "Commissioning of a New Injector for the RIKEN RI-Beam Factory", LINAC12, (Soreq Nuclear Research Center), Tel-Aviv, Israel, Sept. (2012).

Kaji D., Morimoto K., Sato N., Haba H., Kudou Y., Ohzeki K., Sumita T., Yoneda A., Wakabayashi Y., Murakami M., and Morita K.: "Gas-filled recoil ion separator GARIS-II", 16th International Conference on

Electromagnetic Isotope Separators and Techniques Related to their Applications (EMIS2012), Matsue, Dec.–Dec. (2012).

(Domestic Conference)

加治大哉, 森本幸司, 羽場宏光, 市川隆敏, 小浦寛之, 工藤祐生, 小沢顕, 大関和貴, 住田貴之, 山口貴之, 米田晃, 吉田敦, 森田浩介: “新同位体 ^{263}Hs の生成および壊変特性”, 放射化学討論会, (日本大学), 神奈川, 9 月 (2009).

加治大哉, 羽場宏光, 笠松良崇, 工藤祐生, 森本幸司, 森田浩介, 大関和貴, 住田貴之, 米田晃, 佐藤望, 若林泰生, 村上昌史, 門叶冬樹, 生井沙織: “GARIS-II 開発の現状と初動試験”, 日本物理学会, (新潟大学), 新潟, 3 月 (2010).

日暮祥英, 中川孝秀, 大西純一, 羽場宏光, 藤巻正樹, 池沢英二, 渡邉裕, 加瀬昌之, 後藤彰, 込山美咲, 上垣外修一, 田村匡史, 藍原利光, 内山暁仁: “理研新超電導 ECR イオン源の開発研究”, 第 7 回日本加速器学会年会, (日本加速器学会), 姫路, 8 月 (2010).

加治大哉, 羽場宏光, 笠松良崇, 工藤祐生, 森本幸司, 森田浩介, 大関和貴, 住田貴之, 米田晃, 佐藤望, 若林泰生, 村上昌史, 門叶冬樹, 生井沙織: “GARIS-II commissioning 1”, 放射化学討論会, (大阪大学), 大阪, 9 月 (2010).

加治大哉, 羽場宏光, 笠松良崇, 工藤祐生, 森本幸司, 森田浩介, 大関和貴, 住田貴之, 米田晃, 小浦寛之, 佐藤望, 門叶冬樹: “中性子欠損領域の新アクチノイド核種 ^{234}Bk および ^{230}Am の観測”, 放射化学討論会, (大阪大学), 大阪, 9 月 (2010).

日暮祥英, 中川孝秀, 大西純一, 羽場宏光, 田村匡史, 藍原利光, 藤巻正樹, 込山美咲, 内山暁仁, 上垣外修一: “28GH z 超電導 ECR イオン源の開発”, 第 8 回日本加速器学会年会, (日本加速器学会), 筑波, 8 月 (2011).

山田一成, 池沢英二, 今尾浩士, 大西純一, 奥野広樹, 加瀬昌之, 上垣外修一, 熊谷桂子, 込山美咲, 後藤彰, 坂本成彦, 須田健嗣, 中川孝秀, 日暮祥英, 福西暢尚, 藤縄雅, 藤巻正樹, 眞家武士, 山澤秀行, 横内茂, 渡邉環, 渡辺博, 渡邉裕, 新井重昭, 藤澤博, 佐藤洋一: “RIBF 用新入射器 RILAC2 のビームコミッショニング”, 第 8 回加速器学会年会, (日本加速器学会), つくば市, 8 月 (2011).

日暮祥英, 大西純一, 湊恒明: “28 GHz 超伝導 ECR イオン源の開発”, 第 9 回日本加速器学会年会, (日本加速器学会), 豊中市, 8 月 (2012).

大関和貴, 日暮祥英, 大西純一, 中川孝秀: “理研 28 GHz 超伝導 ECR イオン源のエミッタンス測定”, 第 9 回日本加速器学会年会, (日本加速器学会), 豊中, 8 月 (2012).

坂本成彦, 段塚知志, 藤縄雅, 福西暢尚, 長谷部裕雄, 日暮祥英, 池上九三男, 池沢英二, 今尾浩士, 影山正, 上垣外修一, 加瀬昌之, 木寺正憲, 込山美咲, 久保木浩功, 熊谷桂子, 眞家武士, 長瀬誠, 中川孝秀, 中村仁音, 大西純一, 奥野広樹, 大関和貴, 須田健嗣, 渡辺博, 渡邉環, 渡邉裕, 山田一成, Lu L., 山澤秀行: “理研 RIBF における大強度重イオンビーム加速”, 第 9 回日本加速器学会年会, 大阪, 8 月 (2012).

大関和貴, 日暮祥英, 中川孝秀: “ECR ion source for production of intense highly charged heavy ion beam”, 第 8 回異分野交流の夕べ, 和光, 8 月 (2012).

羽場宏光, 大関和貴, 笠松良崇, 加治大哉, 金谷淳平, 菊谷有希, 菊永英寿, 工藤久昭, 工藤祐生, 小森有希子, 酒井隆太郎, 篠原厚, 住田貴之, 豊嶋厚史, 西尾勝久, 村上昌史, 森田浩介, 森本幸司, 米田晃: “GARIS ガスジェット法によるドブニウムの化学実験対象核種 ^{262}Db の製造”, 2012 日本放射化学会年会・第 56 回放射化学討論会, (日本放射化学会), 東京都目黒区, 10 月 (2012).

加治大哉, 住田貴之, 刈屋佳樹, 鹿取謙二, 工藤祐生, 森田浩介, 森谷透, 村上昌史, 武山美麗, 田中謙伍, 戸田光祐, 門叶冬樹, 若林泰生, 山木さやか, 米田晃, 大関和貴, 長谷部裕雄, 羽場宏光, 吉田敦, 山口貴之: “208Pb+70Zn 反応を用いた 277Cn の生成と壊変特性”, 2012 日本放射化学会年会・第 56 回放射化学討論会, (日本放射化学会), 東京工業大学, 10–10 月 (2012).

RILAC Team

Publications

[Journal]

(Others)

Nakagawa T., Higurashi Y., Ohnishi J., Aihara T., Tamura M., Uchiyama A., Okuno H., Kusaka K., Kidera M., Komiyama M., Fujimaki M., Sato Y., Ikezawa E., Watanabe Y., Kase M., Goto A., Kamigaito O., and Yano Y.: "First results from the new RIKEN superconducting electron cyclotron resonance ion source", Rev. Sci. Instrum. **81**, No. 2, p. 02A320 (2010).

Okuno H., Dantsuka T., Fujimaki M., Fujinawa T., Fukunishi N., Hasebe H., Higurashi Y., Ikegami K., Ikezawa E., Imao H., Kageyama T., Kamigaito O., Kase M., Kidera M., Komiyama M., Kuboki H., Kumagai K., Maie T., Nagase M., Nakagawa T., Nakamura M., Ohnishi J., Sakamoto N., Suda K., Watanabe H., Watanabe T., Watanabe Y., Yamada K., and Yamasawa H.: "Recent Achievements and Upgrade Programs at RIKEN Radioactive Isotope Beam Factory", Proceedings of IPAC12 **1**, No. 1, p. 430 (2012).

日暮祥英, 大西純一, 中川孝秀, 藍原利光, 田村匡史, 内山暁仁, 込山美咲, 藤巻正樹, 佐藤洋一, 池沢英二, 渡邉裕, 加瀬昌之, 後藤彰, 上垣外修一, 矢野安重: "理研における新しい超電導 ECR イオン源の開発", 加速器 **6**, No. 4, pp. 346–354 (2010).

[Book・Proceedings]

(Original Papers) *Subject to Peer Review

Yamada K., Arai S., Fujimaki M., Fujinawa T., Fujisawa H., Fukunishi N., Goto A., Higurashi Y., Ikezawa E., Kase M., Komiyama M., Kumagai K., Maie T., Nakagawa T., Ohnishi J., Okuno H., Sakamoto N., Sato Y., Suda K., Watanabe H., Watanabe T., Watanabe Y., Yano Y., Yokouchi S., and Kamigaito O.: "Construction of new injector linac at RIBF", CYCLOTRONS'10, Lanzhou, 2010–9, JaCoW, Lanzhou, pp. 1–3 (2010).

Yamada K., Arai S., Fujimaki M., Fujinawa T., Fujisawa H., Fukunishi N., Goto A., Higurashi Y., Ikezawa E., Kamigaito O., Kase M., Komiyama M., Kumagai K., Maie T., Nakagawa T., Ohnishi J., Okuno H., Sakamoto N., Sato Y., Suda K., Watanabe H., Watanabe Y., Yano Y., and Yokouchi S.: "Construction of new injector linac for RI Beam Factory at RIKEN Nishina Center", Proceedings of of the 1st International Particle Accelerator Conference (IPAC'10), Kyoto, 2010–5, JaCoW, Kyoto, pp. 789–791 (2010).

Yamada K., Arai S., Chiba Y., Fujisawa H., Ikezawa E., Kamigaito O., Kase M., Sakamoto N., Suda K., Watanabe Y., and Touchi Y.: "Rf-design and construction of new linac injector for RIKEN RI-Beam Factory", Proceedings of XXV Linear Accelerator Conference, Tsukuba, 2010–9, JaCoW, Tsukuba, pp. 572–574 (2010).

Watanabe Y., Fujimaki M., Fukunishi N., Hasebe H., Higurashi Y., Ikezawa E., Imao H., Kageyama T., Kamigaito O., Kase M., Kidera M., Komiyama M., Kuboki H., Kumagai K., Maie T., Nagase M., Nakagawa T., Ohnishi J., Okuno H., Sakamoto N., Suda K., Watanabe H., Watanabe T., Yamada K., Yokouchi S., Aihara T., Fukuzawa S., Hamanaka M., Ishikawa S., Kobayashi K., Kotaka Y., Koyama R., Nakamura T., Nishida M., Nishimura M., Ohki T., Oyamada K., Shibata J., Tamura M., Tsukiori N., Uchiyama A., Yadomi K., and Yamauchi H.: "Present status of RIKEN Ring Cyclotron Magnets", Proceedings of 3rd International Particle Accelerator Conference (IPAC 2012), New Orleans, USA, 2012–8, IPAC2012, IEEE, New Orleans, pp. 433–435 (2012). ∗

山田一成, 池沢英二, 今尾浩士, 大西純一, 奥野広樹, 加瀬昌之, 熊谷桂子, 込山美咲, 後藤彰, 坂本成彦, 須田健嗣, 中川孝秀, 日暮祥英, 福西暢尚, 藤縄雅, 藤巻正樹, 眞家武士, 山澤秀行, 横内茂, 渡邉環, 渡辺博, 渡邉裕, 新井重昭, 藤澤博, 佐藤洋一, 上垣外修一: "理研 RIBF 用の新しい重イオン入射ライナック RILAC2 の製作", 第 7 回日本加速器学会年会プロシーディングス, 姫路市, 2010–8, 日本加速器学会, 東京, pp. 360–363 (2010).

(Others)

Yamada K., Suda K., Arai S., Fujimaki M., Fujinawa T., Fujisawa H., Fukunishi N., Higurashi Y., Ikezawa E., Imao H., Kamigaito O., Kase M., Komiyama M., Kumagai K., Maie T., Nakagawa T., Ohnishi J., Okuno H., Sakamoto N., Watanabe H., Watanabe T., Watanabe Y., Yamasawa H., Sato Y., and Goto A.: "Beam Commissioning and Operation of New Linac Injector for RIKEN RI Beam Factory", Proceedings of 3rd International Particle Accelerator Conference (IPAC 2012), New Orleans, USA, 2012–5, JACoW, New Orleans, pp. 1071–1073 (2012).

Oral Presentations

(International Conference etc.)

Yamada K., Dantsuka T., Fujimaki M., Fujinawa T., Fukunishi N., Goto A., Hasebe H., Higurashi Y., Ikezawa E., Kamigaito O., Kase M., Komiyama M., Kuboki H., Kumagai K., Maie T., Nagase M., Nakagawa T., Ohnishi J., Okuno H., Sakamoto N., Sato Y., Suda K., Wakasugi M., Watanabe H., Watanabe T., Watanabe Y., Yano Y., and Yokouchi S.: "Progress on the commissioning of Radioactive Isotope Beam Factory at RIKEN Nishina Center", 11th International Conference on HEAVY ION ACCELERATOR TECHNOLOGY (HIAT09), (INFN-LNL), Venezia, Italy, June (2009).

Yamada K., Arai S., Fujimaki M., Fujinawa T., Fujisawa H., Fukunishi N., Goto A., Higurashi Y., Ikezawa E., Kamigaito O., Kase M., Komiyama M., Kumagai K., Maie T., Nakagawa T., Ohnishi J., Okuno H., Sakamoto N., Sato Y., Suda K., Watanabe H., Watanabe Y., Yano Y., and Yokouchi S.: "Construction of New Injector Linac for RI Beam Factory at RIKEN Nishina Center", 1st International Particle Accelerator Conference (IPAC'10), (High Energy Accelerator Research Organization), Kyoto, May (2010).

Higurashi Y., Nakagawa T., Ohnishi J., Haba H., Ikezawa E., Fujimaki M., Watanabe Y., Kidera M., Komiyama M., Kase M., Goto A., Kamigaito O., Aihara T., Tamura M., and Uchiyama A.: "Production of U ion beam from RIKEN SC-ECRIS ith sputtering method", 19th International Workshop on ECR Ion Sources (ECRIS 2010), grenoble, France, Aug. (2010).

Yamada K., Arai S., Fujimaki M., Fujinawa T., Fujisawa H., Fukunishi N., Goto A., Higurashi Y., Ikezawa E., Kase M., Komiyama M., Kumagai K., Maie T., Nakagawa T., Ohnishi J., Okuno H., Sakamoto N., Sato Y., Suda K., Watanabe H., Watanabe T., Watanabe Y., Yano Y., Yokouchi S., and Kamigaito O.: "Construction of New Injector LINAC at RIBF", 19th International Conference on Cyclotrons and their Applications (CYCLOTRONS 2010), (IMP), Lanzhou, China, Sept. (2010).

Yamada K., Arai S., Chiba Y., Fujisawa H., Ikezawa E., Kamigaito O., Kase M., Sakamoto N., Suda K., Watanabe Y., and Touchi Y.: "RF-design and Construction of New Linac Injector for the RIKEN RI-Beam Factory", 25th Linear Accelerator Conference (LINAC10), (High Energy Accelerator Research Organization), Tsukuba, Sept. (2010).

Yamada K., Suda K., Arai S., Fujimaki M., Fujinawa T., Fujisawa H., Fukunishi N., Higurashi Y., Ikezawa E., Imao H., Kamigaito O., Kase M., Komiyama M., Kumagai K., Maie T., Nakagawa T., Ohnishi J., Okuno H., Sakamoto N., Watanabe H., Watanabe T., Watanabe Y., Yamasawa H., Sato Y., and Goto A.: "Beam Commissioning and Operation of New Linac Injector for RIKEN RI Beam Factory", 3rd International Particle Accelerator Conference (IPAC 2012), New Orleans, USA, May (2012).

Okuno H., Dantsuka T., Fujimaki M., Fujinawa T., Fukunishi N., Hasebe H., Higurashi Y., Ikegami K., Ikezawa E., Imao H., Kageyama T., Kamigaito O., Kase M., Kidera M., Komiyama M., Kuboki H., Kumagai K., Maie T., Nagase M., Nakagawa T., Nakamura M., Ohnishi J., Sakamoto N., Suda K., Watanabe H., Watanabe T., Watanabe Y., Yamada K., and Yamasawa H.: "Recent Achievements and Upgrade Programs at RIKEN Radioactive Isotope Beam Factory", IPAC12, (IPAC12 International Organizing Committee), NewOrleans, USA, May–May (2012).

Watanabe Y., Fujimaki M., Fukunishi N., Hasebe H., Higurashi Y., Ikezawa E., Imao H., Kageyama T., Kamigaito O., Kase M., Kidera M., Komiyama M., Kuboki H., Kumagai K., Maie T., Nagase M., Nakagawa T., Ohnishi J., Okuno H., Sakamoto N., Suda K., Watanabe H., Watanabe T., Yamada K., Yokouchi S., Aihara T., Fukuzawa S., Hamanaka M., Ishikawa S., Kobayashi K., Kotaka Y., Koyama R., Nakamura T., Nishida M., Nishimura M., Ohki T., Oyamada K., Shibata J., Tamura M., Tsukiori N., Uchiyama A., Yadomi K., and Yamauchi H.: "Present status of RIKEN Ring Cyclotron Magnets", 3rd International Particle Accelerator Conference (IPAC 2012), (CAMD(Center for Advanced Microstructures and Devices, Louisiana State University)), New Orleans, USA, Aug. (2012).

Imao H., Okuno H., Kamigaito O., Kuboki H., Hasebe H., Fukunishi N., Watanabe T., Fujimaki M., Watanabe Y., Maie T., Kase M., and Yano Y.: "Charge-stripping system for 238U ion beam with recirculating He gas", INTDS2012, (GSI), Mainz, Germany, Aug. (2012).

Suda K., Arai S., Chiba Y., Kamigaito O., Kase M., Sakamoto N., Watanabe Y., and Yamada K.: "Design of Coupler for Direct Coupled Amplifier to Drift Tube Linac Cavities of the Injector RILAC2 for RIKEN RI Beam Factory", 26th International Linear Accelerator Conference (LINAC12), (LINAC12 International Organizing Committee), Tel Aviv, Israel, Sept. (2012).

(Domestic Conference)

日暮祥英, 中川孝秀, 大西純一, 羽場宏光, 藤巻正樹, 池沢英二, 渡邉裕, 加瀬昌之, 後藤彰, 込山美咲, 上垣外修一, 田村匡史, 藍原利光, 内山暁仁: "理研新超電導 ECR イオン源の開発研究", 第 7 回日本加速器学会年会, (日本加速器学会), 姫路, 8 月 (2010).

池沢英二, 上垣外修一, 加瀬昌之, 渡邉裕, 大木智則, 藍原利光, 山内啓資, 内山暁仁, 小山田和幸, 田村匡史: "理研重イオンリニアックの現状報告", 第 8 回日本加速器学会年会, (日本加速器学会), 筑波, 8 月 (2011).

山田一成, 池沢英二, 今尾浩士, 大西純一, 奥野広樹, 加瀬昌之, 上垣外修一, 熊谷桂子, 込山美咲, 後藤彰, 坂本成彦, 須田健嗣, 中川孝秀, 日暮祥英, 福西暢尚, 藤縄雅, 藤巻正樹, 眞家武士, 山澤秀行, 横内茂, 渡邉環, 渡辺博, 渡邉裕, 新井重昭, 藤澤博, 佐藤洋一: "RIBF 用新入射器 RILAC2 のビームコミッショニング", 第 8 回加速器学会年会, (日本加速器学会), つくば市, 8 月 (2011).

渡邉裕, 今尾浩士, 奥野広樹, 加瀬昌之, 上垣外修一, 熊谷桂子, 込山美咲, 坂本成彦, 須田健嗣, 長瀬誠, 福西暢尚, 藤巻正樹, 眞家武士, 山田一成, 渡邉環, 渡辺博, 石川盛, 小高康照, 小林清志, 小山亮, 柴田順翔, 月居憲俊, 仲村武志, 西田稔, 西村誠, 濱仲誠, 福澤聖児, 矢冨一慎: "理研リングサイクロトロン (RRC) の電磁石の老朽化", 第 9 回日本加速器学会年会, (日本加速器学会), 大阪, 8 月 (2012).

池沢英二, 上垣外修一, 加瀬昌之, 渡邉裕, 大木智則, 藍原利光, 山内啓資, 内山暁仁, 小山田和幸, 田村匡史: "理研重イオンリニアックの現状報告", 第 9 回日本加速器学会年会, (日本加速器学会), 大阪, 8 月 (2012).

今尾浩士, 奥野広樹, 久保木浩功, 上垣外修一, 長谷部裕雄, 福西暢尚, 渡邉環, 藤巻正樹, 渡邉裕, 眞家武士, 加瀬昌之, 矢野安重: 第 9 回日本加速器学会年会, (大阪大学), 大阪, 8 月 (2012).

坂本成彦, 段塚知志, 藤縄雅, 福西暢尚, 長谷部裕雄, 日暮祥英, 池上九三男, 池沢英二, 今尾浩士, 影山正, 上垣外修一, 加瀬

昌之, 木寺正憲, 込山美咲, 久保木浩功, 熊谷桂子, 眞家武士, 長瀬誠, 中川孝秀, 中村仁音, 大西純一, 奥野広樹, 大関和貴, 須田健嗣, 渡辺博, 渡邉環, 渡邉裕, 山田一成, Lu L., 山澤秀行: "理研 RIBF における大強度重イオンビーム加速", 第 9 回日本加速器学会年会, 大阪, 8 月 (2012).

Cyclotron Team

Publications

[Journal]

(Original Papers) *Subject to Peer Review

Sakaguchi S., Iseri Y., Uesaka T., Tanifuji M., Amos K., Aoi N., Hashimoto Y., Hiyama E., Ichikawa M., Ichikawa Y., Ishikawa S., Itoh K., Itoh M., Iwasaki H., Karataglidis S., Kawabata T., Kawahara T., Kuboki H., Maeda Y., Matsuo R., Nakao T., Okamura H., Sakai H., Sasamoto Y., Sasano M., Sato Y., Sakaguchi-Sekiguchi K., Shinohara M., Suda K., Suzuki D., Takahashi Y., Tamii A., Wakui T., Yako K., Yamaguchi M., and Yamamoto Y.: "Analyzing power in elastic scattering of 6He from a polarized proton target at 71 MeV/nucleon", Phys. Rev. C **84**, No. 024604, pp. 024604-1–024604-17 (2011). *

(Others)

Okuno H., Dantsuka T., Fujimaki M., Fujinawa T., Fukunishi N., Hasebe H., Higurashi Y., Ikegami K., Ikezawa E., Imao H., Kageyama T., Kamigaito O., Kase M., Kidera M., Komiyama M., Kuboki H., Kumagai K., Maie T., Nagase M., Nakagawa T., Nakamura M., Ohnishi J., Sakamoto N., Suda K., Watanabe H., Watanabe T., Watanabe Y., Yamada K., and Yamasawa H.: "Recent Achievements and Upgrade Programs at RIKEN Radioactive Isotope Beam Factory", Proceedings of IPAC12 **1**, No. 1, p. 430 (2012).

[Book・Proceedings]

(Original Papers) *Subject to Peer Review

Yamada K., Arai S., Fujimaki M., Fujinawa T., Fujisawa H., Fukunishi N., Goto A., Higurashi Y., Ikezawa E., Kase M., Komiyama M., Kumagai K., Maie T., Nakagawa T., Ohnishi J., Okuno H., Sakamoto N., Sato Y., Suda K., Watanabe H., Watanabe T., Watanabe Y., Yano Y., Yokouchi S., and Kamigaito O.: "Construction of new injector linac at RIBF", CYCLOTRONS'10, Lanzhou, 2010–9, JaCoW, Lanzhou, pp. 1–3 (2010).

Yamada K., Arai S., Fujimaki M., Fujinawa T., Fujisawa H., Fukunishi N., Goto A., Higurashi Y., Ikezawa E., Kamigaito O., Kase M., Komiyama M., Kumagai K., Maie T., Nakagawa T., Ohnishi J., Okuno H., Sakamoto N., Sato Y., Suda K., Watanabe H., Watanabe Y., Yano Y., and Yokouchi S.: "Construction of new injector linac for RI Beam Factory at RIKEN Nishina Center", Proceedings of of the 1st International Particle Accelerator Conference (IPAC'10), Kyoto, 2010–5, JaCoW, Kyoto, pp. 789–791 (2010).

Yamada K., Arai S., Chiba Y., Fujisawa H., Ikezawa E., Kamigaito O., Kase M., Sakamoto N., Suda K., Watanabe Y., and Touchi Y.: "Rf-design and construction of new linac injector for RIKEN RI-Beam Factory", Proceedings of XXV Linear Accelerator Conference, Tsukuba, 2010–9, JaCoW, Tsukuba, pp. 572–574 (2010).

Watanabe Y., Fujimaki M., Fukunishi N., Hasebe H., Higurashi Y., Ikezawa E., Imao H., Kageyama T., Kamigaito O., Kase M., Kidera M., Komiyama M., Kuboki H., Kumagai K., Maie T., Nagase M., Nakagawa T., Ohnishi J., Okuno H., Sakamoto N., Suda K., Watanabe H., Watanabe T., Yamada K., Yokouchi S., Aihara T., Fukuzawa S., Hamanaka M., Ishikawa S., Kobayashi K., Kotaka Y., Koyama R., Nakamura T., Nishida M., Nishimura M., Ohki T., Oyamada K., Shibata J., Tamura M., Tsukiori N., Uchiyama A., Yadomi K., and Yamauchi H.: "Present status of RIKEN Ring Cyclotron Magnets", Proceedings of 3rd International Particle Accelerator Conference (IPAC 2012), New Orleans, USA, 2012–8, IPAC2012, IEEE, New Orleans, pp. 433–435 (2012). *

Lu L., Sakamoto N., Suda K., Yamada K., and Kamigaito O.: "Design Of A Spoke Cavity For RIKEN RI-Beam Factory", the International Particle Accelerator Conference IPAC'12, New Orleans, USA, 2012–5, JACoW, CERN, pp. 2245–2247 (2012).

山田一成, 池沢英二, 今尾浩士, 大西純一, 奥野広樹, 加瀬昌之, 熊谷桂子, 込山美咲, 後藤彰, 坂本成彦, 須田健嗣, 中川孝秀, 日暮祥英, 福西暢尚, 藤縄雅, 藤巻正樹, 眞家武士, 山澤秀行, 横内茂, 渡邉環, 渡辺博, 渡邉裕, 新井重昭, 藤澤博, 佐藤洋一, 上垣外修一: "理研 RIBF 用の新しい重イオン入射ライナック RILAC2 の製作", 第 7 回日本加速器学会年会プロシーディングス, 姫路市, 2010–8, 日本加速器学会, 東京, pp. 360–363 (2010).

(Others)

Yamada K., Suda K., Arai S., Fujimaki M., Fujinawa T., Fujisawa H., Fukunishi N., Higurashi Y., Ikezawa E., Imao H., Kamigaito O., Kase M., Komiyama M., Kumagai K., Maie T., Nakagawa T., Ohnishi J., Okuno H., Sakamoto N., Watanabe H., Watanabe T., Watanabe Y., Yamasawa H., Sato Y., and Goto A.: "Beam Commissioning and Operation of New Linac Injector for RIKEN RI Beam Factory", Proceedings of 3rd International Particle Accelerator Conference (IPAC 2012), New Orleans, USA, 2012–5, JACoW, New Orleans, pp. 1071–1073 (2012).

Oral Presentations

(International Conference etc.)

Yamada K., Okuno H., Fujimaki M., Fukunishi N., Goto A., Hasebe H., Ikegami K., Kamigaito O., Kase M., Kumagai K., Maie T., Nagase M., Ohnishi J., Sakamoto N., Yokouchi S., and Yano Y.: "Status of the Superconducting Ring Cyclotron at RIKEN RI Beam Factory", 11th European Particle Accelerator Conference (EPAC 2008), (INFN-LNF), Genoa, Italy, June (2008).

Yamada K., Dantsuka T., Fujimaki M., Fujinawa T., Fukunishi N., Goto A., Hasebe H., Higurashi Y., Ikezawa E., Kamigaito O., Kase M., Komiyama M., Kuboki H., Kumagai K., Maie T., Nagase M., Nakagawa T., Ohnishi J., Okuno H., Sakamoto N., Sato Y., Suda K., Wakasugi

M., Watanabe H., Watanabe T., Watanabe Y., Yano Y., and Yokouchi S.: "Progress on the commissioning of Radioactive Isotope Beam Factory at RIKEN Nishina Center", 11th International Conference on HEAVY ION ACCELERATOR TECHNOLOGY (HIAT09), (INFN-LNL), Venezia, Italy, June (2009).

Yamada K., Arai S., Fujimaki M., Fujinawa T., Fujisawa H., Fukunishi N., Goto A., Higurashi Y., Ikezawa E., Kamigaito O., Kase M., Komiyama M., Kumagai K., Maie T., Nakagawa T., Ohnishi J., Okuno H., Sakamoto N., Sato Y., Suda K., Watanabe H., Watanabe Y., Yano Y., and Yokouchi S.: "Construction of New Injector Linac for RI Beam Factory at RIKEN Nishina Center", 1st International Particle Accelerator Conference (IPAC'10), (High Energy Accelerator Research Organization), Kyoto, May (2010).

Yamada K., Arai S., Fujimaki M., Fujinawa T., Fujisawa H., Fukunishi N., Goto A., Higurashi Y., Ikezawa E., Kase M., Komiyama M., Kumagai K., Maie T., Nakagawa T., Ohnishi J., Okuno H., Sakamoto N., Sato Y., Suda K., Watanabe H., Watanabe T., Watanabe Y., Yano Y., Yokouchi S., and Kamigaito O.: "Construction of New Injector LINAC at RIBF", 19th International Conference on Cyclotrons and their Applications (CYCLOTRONS 2010), (IMP), Lanzhou, China, Sept. (2010).

Yamada K., Arai S., Chiba Y., Fujisawa H., Ikezawa E., Kamigaito O., Kase M., Sakamoto N., Suda K., Watanabe Y., and Touchi Y.: "RF-design and Construction of New Linac Injector for the RIKEN RI-Beam Factory", 25th Linear Accelerator Conference (LINAC10), (High Energy Accelerator Research Organization), Tsukuba, Sept. (2010).

Lu L., Sakamoto N., Suda K., Yamada K., and Kamigaito O.: "Design Of CW Superconducting Buncher For RIKEN RI-Beam Factory", 15th International Conference on RF Superconductivity, (SRF2011), Chicago, USA, July (2011).

Yamada K., Suda K., Arai S., Fujimaki M., Fujinawa T., Fujisawa H., Fukunishi N., Higurashi Y., Ikezawa E., Imao H., Kamigaito O., Kase M., Komiyama M., Kumagai K., Maie T., Nakagawa T., Ohnishi J., Okuno H., Sakamoto N., Watanabe H., Watanabe T., Watanabe Y., Yamasawa H., Sato Y., and Goto A.: "Beam Commissioning and Operation of New Linac Injector for RIKEN RI Beam Factory", 3rd International Particle Accelerator Conference (IPAC 2012), New Orleans, USA, May (2012).

Okuno H., Dantsuka T., Fujimaki M., Fujinawa T., Fukunishi N., Hasebe H., Higurashi Y., Ikegami K., Ikezawa E., Imao H., Kageyama T., Kamigaito O., Kase M., Kidera M., Komiyama M., Kuboki H., Kumagai K., Maie T., Nagase M., Nakagawa T., Nakamura M., Ohnishi J., Sakamoto N., Suda K., Watanabe H., Watanabe T., Watanabe Y., Yamada K., and Yamasawa H.: "Recent Achievements and Upgrade Programs at RIKEN Radioactive Isotope Beam Factory", IPAC12, (IPAC12 International Organizing Committee), NewOrleans, USA, May–May (2012).

Watanabe Y., Fujimaki M., Fukunishi N., Hasebe H., Higurashi Y., Ikezawa E., Imao H., Kageyama T., Kamigaito O., Kase M., Kidera M., Komiyama M., Kuboki H., Kumagai K., Maie T., Nagase M., Nakagawa T., Ohnishi J., Okuno H., Sakamoto N., Suda K., Watanabe H., Watanabe T., Yamada K., Yokouchi S., Aihara T., Fukuzawa S., Hamanaka M., Ishikawa S., Kobayashi K., Kotaka Y., Koyama R., Nakamura T., Nishida M., Nishimura M., Ohki T., Oyamada K., Shibata J., Tamura M., Tsukiori N., Uchiyama A., Yadomi K., and Yamauchi H.: "Present status of RIKEN Ring Cyclotron Magnets", 3rd International Particle Accelerator Conference (IPAC 2012), (CAMD(Center for Advanced Microstructures and Devices, Louisiana State University)), New Orleans, USA, Aug. (2012).

Suda K., Arai S., Chiba Y., Kamigaito O., Kase M., Sakamoto N., Watanabe Y., and Yamada K.: "Design of Coupler for Direct Coupled Amplifier to Drift Tube Linac Cavities of the Injector RILAC2 for RIKEN RI Beam Factory", 26th International Linear Accelerator Conference (LINAC12), (LINAC12 International Organizing Committee), Tel Aviv, Israel, Sept. (2012).

Sakamoto N., Fujimaki M., Higurashi Y., Hasebe H., Kamigaito O., Okuno H., Suda K., Watanabe T., Yamada K., and Koyama R.: "Commissioning of a New Injector for the RIKEN RI-Beam Factory", LINAC12, (Soreq Nuclear Research Center), Tel-Aviv, Israel, Sept. (2012).

Ishibashi Y., Yoshida N., Ueno H., Yoshimi A., Ichikawa Y., Abe Y., Asahi K., Chikamori M., Fujita T., Furukawa T., Hikota E., Nagae D., Ohtomo Y., Saito Y., Shirai H., Suzuki T., Yang X., and Sakamoto N.: "Development of an adiabatic field rotation system to measure spin polarization of unstable nuclei", The 16th IUPAP International Conference on Electromagnetic Isotope Separators and Techniques Related to Their Applications (EMIS2012), Matsue, Dec. (2012).

(Domestic Conference)

山田一成, 池沢英二, 今尾浩士, 大西純一, 奥野広樹, 加瀬昌之, 上垣外修一, 熊谷桂子, 込山美咲, 後藤彰, 坂本成彦, 須田健嗣, 中川孝秀, 日暮祥英, 福西暢尚, 藤縄雅, 藤巻正樹, 眞家武士, 山澤秀行, 横内茂, 渡邉環, 渡辺博, 渡邉裕, 新井重昭, 藤澤博, 佐藤洋一: "RIBF 用新入射器 RILAC2 のビームコミッショニング", 第 8 回加速器学会年会, (日本加速器学会), つくば市, 8 月 (2011).

渡邉裕, 今尾浩士, 奥野広樹, 加瀬昌之, 上垣外修一, 熊谷桂子, 込山美咲, 坂本成彦, 須田健嗣, 長瀬誠, 福西暢尚, 藤巻正樹, 眞家武士, 山田一成, 渡邉環, 渡辺博, 石川盛, 小高康照, 小林清志, 小山亮, 柴田順翔, 月居憲俊, 仲村武志, 西田稔, 西村誠, 濱仲誠, 福澤聖児, 矢冨一慎: "理研

リングサイクロトロン (RRC) の電磁石の老朽化", 第 9 回日本加速器学会年会, (日本加速器学会), 大阪, 8 月 (2012).

坂本成彦, 段塚知志, 藤縄雅, 福西暢尚, 長谷部裕雄, 日暮祥英, 池上九三男, 池沢英二, 今尾浩士, 影山正, 上垣外修一, 加瀬昌之, 木寺正憲, 込山美咲, 久保木浩功, 熊谷桂子, 眞家武士, 長瀬誠, 中川孝秀, 中村仁音, 大西純一, 奥野広樹, 大関和貴, 須田健嗣, 渡辺博, 渡邉環, 渡邉裕, 山田一成, Lu L., 山澤秀行: "理研 RIBF における大強度重イオンビーム加速", 第 9 回日本加速器学会年会, 大阪, 8 月 (2012).

石橋陽子, 吉田直貴, 上野秀樹, 吉見彰洋, 市川雄一, 阿部康志, 旭耕一郎, 近森正敏, 藤田朋美, 古川武, 彦田絵里, 長江大輔, 大友祐一, 齋藤佑多, 白井葉月, 鈴木貴大, Yang X., 坂本成彦: "不安定核偏極度測定のための永久磁石を用いた断熱磁場回転装置の開発", 日本物理学会第 68 回年次大会, (日本物理学会), 東広島, 3 月 (2013).

Beam Dynamics & Diagnostics Team

Publications

[Journal]

(Original Papers) *Subject to Peer Review

Watanabe T., Fukunishi N., Kase M., Kamigaito O., Inamori S., and Kon K.: "Beam Current Monitor with a High-Tc Current Sensor and SQUID at the RIBF", J. Supercond. Nov. Magn., (2012). *

Hirano T., Kazama Y., Ohbu S., Shirakawa Y., Liu Y., Kambara T., Fukunishi N., and Abe T.: "Molecular nature of mutations induced by high-LET irradiation with argon and carbon ions in *Arabidopsis thaliana*", Muta. Res./Fund. Mol. Mech. Mutagen. **735**, No. 1-2, pp. 19–31 (2012). *

Imao H., Okuno H., Kuboki H., Yokouchi S., Fukunishi N., Kamigaito O., Hasebe H., Watanabe T., Kase M., and Yano Y.: "Charge stripping of 238U beam by helium gas stripper", Phys. Rev. Spec. Top.: Accel. Beams **15**, No. 123501, (2012). *

Higurashi Y., Nakagawa T., Ohnishi J., Haba H., Tamura M., Aihara T., Fujimaki M., Komiyama M., Uchiyama A., and Kamigaito O.: "Results of RIKEN superconducting electron cyclotron resonance ion source with 28GHz", Rev. Sci. Instrum. **83**, No. 2, p. 02A308 (2012). *

Higurashi Y., Nakagawa T., Ohnishi J., Haba H., Tamura M., Aihara T., Fujimaki M., Komiyama M., Uchiyama A., and Kamigaito O.: "Production of a highly charged uranium ion beam with RIKEN superconducting electron cyclotron resonance ion source", Rev. Sci. Instrum. **83**, No. 2, p. 02A333 (2012). *

(Others)

Nakagawa T., Higurashi Y., Ohnishi J., Aihara T., Tamura M., Uchiyama A., Okuno H., Kusaka K., Kidera M., Komiyama M., Fujimaki M., Sato Y., Ikezawa E., Watanabe Y., Kase M., Goto A., Kamigaito O., and Yano Y.: "First results from the new RIKEN superconducting electron cyclotron resonance ion source", Rev. Sci. Instrum. **81**, No. 2, p. 02A320 (2010).

Imao H., Okuno H., Kuboki H., Yokouchi S., Fukunishi N., Kamigaito O., Hasebe H., Watanabe T., Kase M., and Yano Y.: "Charge stripping of Uranium-238 ion beam with low-Z gas stripper", Particle accelerator. Proceedings, 2nd International Conference, IPAC 2011 **C110904**, 1746–1748 (2011).

Okuno H., Dantsuka T., Fujimaki M., Fujinawa T., Fukunishi N., Hasebe H., Higurashi Y., Ikegami K., Ikezawa E., Imao H., Kageyama T., Kamigaito O., Kase M., Kidera M., Komiyama M., Kuboki H., Kumagai K., Maie T., Nagase M., Nakagawa T., Nakamura M., Ohnishi J., Sakamoto N., Suda K., Watanabe H., Watanabe T., Watanabe Y., Yamada K., and Yamasawa H.: "Recent Achievements and Upgrade Programs at RIKEN Radioactive Isotope Beam Factory", Proceedings of IPAC12 **1**, No. 1, p. 430 (2012).

日暮祥英, 大西純一, 中川孝秀, 藍原利光, 田村匡史, 内山暁仁, 込山美咲, 藤巻正樹, 佐藤洋一, 池沢英二, 渡邉裕, 加瀬昌之, 後藤彰, 上垣外修一, 矢野安重: "理研における新しい超電導 ECR イオン源の開発", 加速器 **6**, No. 4, pp. 346–354 (2010).

[Book・Proceedings]

(Original Papers) *Subject to Peer Review

Yamada K., Arai S., Fujimaki M., Fujinawa T., Fujisawa H., Fukunishi N., Goto A., Higurashi Y., Ikezawa E., Kase M., Komiyama M., Kumagai K., Maie T., Nakagawa T., Ohnishi J., Okuno H., Sakamoto N., Sato Y., Suda K., Watanabe H., Watanabe T., Watanabe Y., Yano Y., Yokouchi S., and Kamigaito O.: "Construction of new injector linac at RIBF", CYCLOTRONS'10, Lanzhou, 2010–9, JaCoW, Lanzhou, pp. 1–3 (2010).

Yamada K., Arai S., Fujimaki M., Fujinawa T., Fujisawa H., Fukunishi N., Goto A., Higurashi Y., Ikezawa E., Kamigaito O., Kase M., Komiyama M., Kumagai K., Maie T., Nakagawa T., Ohnishi J., Okuno H., Sakamoto N., Sato Y., Suda K., Watanabe H., Watanabe Y., Yano Y., and Yokouchi S.: "Construction of new injector linac for RI Beam Factory at RIKEN Nishina Center", Proceedings of of the 1st International Particle Accelerator Conference (IPAC'10), Kyoto, 2010–5, JaCoW, Kyoto, pp. 789–791 (2010).

Yamada K., Arai S., Chiba Y., Fujisawa H., Ikezawa E., Kamigaito O., Kase M., Sakamoto N., Suda K., Watanabe Y., and Touchi Y.: "Rf-design and construction of new linac injector for RIKEN RI-Beam Factory", Proceedings of XXV Linear Accelerator Conference, Tsukuba, 2010–9, JaCoW, Tsukuba, pp. 572–574 (2010).

Watanabe Y., Fujimaki M., Fukunishi N., Hasebe H., Higurashi Y., Ikezawa E., Imao H., Kageyama T., Kamigaito O., Kase M., Kidera M., Komiyama M., Kuboki H., Kumagai K., Maie T., Nagase M., Nakagawa T., Ohnishi J., Okuno H., Sakamoto N., Suda K., Watanabe H., Watanabe T., Yamada K., Yokouchi S., Aihara T., Fukuzawa S., Hamanaka M., Ishikawa S., Kobayashi K., Kotaka Y., Koyama R., Nakamura T., Nishida M., Nishimura M., Ohki T., Oyamada K., Shibata J., Tamura M., Tsukiori N., Uchiyama A., Yadomi K., and Yamauchi H.: "Present status of RIKEN Ring Cyclotron Magnets", Proceedings of 3rd International Particle Accelerator Conference (IPAC 2012), New Orleans, USA, 2012–8, IPAC2012, IEEE, New Orleans, pp. 433–435 (2012). *

Lu L., Sakamoto N., Suda K., Yamada K., and Kamigaito O.: "Design Of A Spoke Cavity For RIKEN RI-Beam Factory", the International Particle Accelerator Conference IPAC'12, New Orleans, USA, 2012–5, JACoW, CERN, pp. 2245–2247 (2012).

Furuta T., Ishikawa K., Fukunishi N., Noda S., Takagi S., Maeyama T., Fukasaku K., and Himeno R.: "Implementation of OpenMP and MPI hybrid parallelization to Monte Carlo dose simulation for particle therapy", IFMBE Proceedings, Beijing, China, 2012–6, Springer, Heidelberg, pp. 2099–2102 (2013). ＊

山田一成, 池沢英二, 今尾浩士, 大西純一, 奥野広樹, 加瀬昌之, 熊谷桂子, 込山美咲, 後藤彰, 坂本成彦, 須田健嗣, 中川孝秀, 日暮祥英, 福西暢尚, 藤縄雅, 藤巻正樹, 眞家武士, 山澤秀行, 横内茂, 渡邉環, 渡辺博, 渡邉裕, 新井重昭, 藤澤博, 佐藤洋一, 上垣外修一: "理研 RIBF 用の新しい重イオン入射ライナック RILAC2 の製作", 第 7 回日本加速器学会年会プロシーディングス, 姫路市, 2010–8, 日本加速器学会, 東京, pp. 360–363 (2010).

(Review)

Ohtsubo N., Sasaki K., Aida R., Ryuto H., Ichida H., Hayashi Y., and Abe T.: "Efficient modification of floral traits by heavy-ion beam irradiation on transgenic Torenia", Methods in Molecular Biology Vol. 847: Transgenic Plants, Humana Press, New York, p. 275-289 (2012).

Abe T., Ryuto H., and Fukunishi N.: "Ion Beam Radiation Mutagenesis", Plant mutation breeding and biotechnology, Vienna, Austria, 2012–11, CABI, Oxfordshire, pp. 99–106 (2012).

(Others)

Yamada K., Suda K., Arai S., Fujimaki M., Fujinawa T., Fujisawa H., Fukunishi N., Higurashi Y., Ikezawa E., Imao H., Kamigaito O., Kase M., Komiyama M., Kumagai K., Maie T., Nakagawa T., Ohnishi J., Okuno H., Sakamoto N., Watanabe H., Watanabe T., Watanabe Y., Yamasawa H., Sato Y., and Goto A.: "Beam Commissioning and Operation of New Linac Injector for RIKEN RI Beam Factory", Proceedings of 3rd International Particle Accelerator Conference (IPAC 2012), New Orleans, USA, 2012–5, JACoW, New Orleans, pp. 1071–1073 (2012).

Oral Presentations

(International Conference etc.)

Yamada K., Okuno H., Fujimaki M., Fukunishi N., Goto A., Hasebe H., Ikegami K., Kamigaito O., Kase M., Kumagai K., Maie T., Nagase M., Ohnishi J., Sakamoto N., Yokouchi S., and Yano Y.: "Status of the Superconducting Ring Cyclotron at RIKEN RI Beam Factory", 11th European Particle Accelerator Conference (EPAC 2008), (INFN-LNF), Genoa, Italy, June (2008).

Yamada K., Dantsuka T., Fujimaki M., Fujinawa T., Fukunishi N., Goto A., Hasebe H., Higurashi Y., Ikezawa E., Kamigaito O., Kase M., Komiyama M., Kuboki H., Kumagai K., Maie T., Nagase M., Nakagawa T., Ohnishi J., Okuno H., Sakamoto N., Sato Y., Suda K., Wakasugi M., Watanabe H., Watanabe T., Watanabe Y., Yano Y., and Yokouchi S.: "Progress on the commissioning of Radioactive Isotope Beam Factory at RIKEN Nishina Center", 11th International Conference on HEAVY ION ACCELERATOR TECHNOLOGY (HIAT09), (INFN-LNL), Venezia, Italy, June (2009).

Yamada K., Arai S., Fujimaki M., Fujinawa T., Fujisawa H., Fukunishi N., Goto A., Higurashi Y., Ikezawa E., Kamigaito O., Kase M., Komiyama M., Kumagai K., Maie T., Nakagawa T., Ohnishi J., Okuno H., Sakamoto N., Sato Y., Suda K., Watanabe H., Watanabe Y., Yano Y., and Yokouchi S.: "Construction of New Injector Linac for RI Beam Factory at RIKEN Nishina Center", 1st International Particle Accelerator Conference (IPAC'10), (High Energy Accelerator Research Organization), Kyoto, May (2010).

Higurashi Y., Nakagawa T., Ohnishi J., Haba H., Tamura M., Aihara T., Fujimaki M., Komiyama M., Uchiyama A., and Kamigaito O.: "Developments of RIKEN New Superconducting ECR Ion Source", 1st International Particle Accelerator Conference (IPAC'10), Kyoto, May (2010).

Higurashi Y., Nakagawa T., Ohnishi J., Haba H., Ikezawa E., Fujimaki M., Watanabe Y., Kidera M., Komiyama M., Kase M., Goto A., Kamigaito O., Aihara T., Tamura M., and Uchiyama A.: "Production of U ion beam from RIKEN SC-ECRIS ith sputtering method", 19th International Workshop on ECR Ion Sources (ECRIS 2010), grenoble, France, Aug. (2010).

Yamada K., Arai S., Fujimaki M., Fujinawa T., Fujisawa H., Fukunishi N., Goto A., Higurashi Y., Ikezawa E., Kase M., Komiyama M., Kumagai K., Maie T., Nakagawa T., Ohnishi J., Okuno H., Sakamoto N., Sato Y., Suda K., Watanabe H., Watanabe T., Watanabe Y., Yano Y., Yokouchi S., and Kamigaito O.: "Construction of New Injector LINAC at RIBF", 19th International Conference on Cyclotrons and their Applications (CYCLOTRONS 2010), (IMP), Lanzhou, China, Sept. (2010).

Yamada K., Arai S., Chiba Y., Fujisawa H., Ikezawa E., Kamigaito O., Kase M., Sakamoto N., Suda K., Watanabe Y., and Touchi Y.: "RF-design and Construction of New Linac Injector for the RIKEN RI-Beam Factory", 25th Linear Accelerator Conference (LINAC10), (High Energy Accelerator Research Organization), Tsukuba, Sept. (2010).

Lu L., Sakamoto N., Suda K., Yamada K., and Kamigaito O.: "Design Of CW Superconducting Buncher For RIKEN RI-Beam Factory", 15th International Conference on RF Superconductivity, (SRF2011), Chicago, USA, July (2011).

Higurashi Y., Ohnishi J., Ohzeki K., Haba H., Fujimaki M., Komiyama M., Kamigaito O., Aihara T., Tamura M., and Uchiyama A.: "Production of highly charged uranium ion beam with RIKEN superconducting electron cyclotron resonance ion source", The 14th Int. Conf. on Ion Sources (ICIS11), (INFN-LNS, Italy), Giardini Naxos, Italy, Sept. (2011).

Higurashi Y., Ohnishi J., Ohzeki K., Haba H., Fujimaki M., Komiyama M., Kamigaito O., Aihara T., Tamura

M., and Uchiyama A.: "Results of RIKEN superconducting electron cyclotron resonance ion source with 28GHz", The 14th Int. Conf. on Ion Sources (ICIS11), (INFN-LNS, Italy), Giardini Naxos, Italy, Sept. (2011).

Watanabe T., Fukunishi N., Kase M., Kamigaito O., Inamori S., and Kon K.: "Beam Current Monitor with a High-Tc Current Sensor and SQUID at the RIBF", International Conference on Superconductivity and Magnetism (ICSM 2012), (Ankara University), Kumburgaz-Istanbul, Turkey, Apr.–May (2012).

Yamada K., Suda K., Arai S., Fujimaki M., Fujinawa T., Fujisawa H., Fukunishi N., Higurashi Y., Ikezawa E., Imao H., Kamigaito O., Kase M., Komiyama M., Kumagai K., Maie T., Nakagawa T., Ohnishi J., Okuno H., Sakamoto N., Watanabe H., Watanabe T., Watanabe Y., Yamasawa H., Sato Y., and Goto A.: "Beam Commissioning and Operation of New Linac Injector for RIKEN RI Beam Factory", 3rd International Particle Accelerator Conference (IPAC 2012), New Orleans, USA, May (2012).

Imao H., Okuno H., Kuboki H., Yokouchi S., Fukunishi N., Kamigaito O., Hasebe H., Watanabe T., Kase M., and Yano Y.: "Charge stripping of uranium-238 ion beam with helium gas stripper", IPAC12, (IEEE), New Orleans, USA, May (2012).

Furuta T., Ishikawa K., Fukunishi N., Noda S., Takagi S., Maeyama T., Fukasaku K., and Himeno R.: "Implementation of OpenMP and MPI hybrid parallelization to Monte Carlo dose simulation for particle therapy", World congress on medical physics and biomedical engineering, (Asia-Oceania Federation of Organiztions for Medical Physics), Beijing, China, May (2012).

Okuno H., Dantsuka T., Fujimaki M., Fujinawa T., Fukunishi N., Hasebe H., Higurashi Y., Ikegami K., Ikezawa E., Imao H., Kageyama T., Kamigaito O., Kase M., Kidera M., Komiyama M., Kuboki H., Kumagai K., Maie T., Nagase M., Nakagawa T., Nakamura M., Ohnishi J., Sakamoto N., Suda K., Watanabe H., Watanabe T., Watanabe Y., Yamada K., and Yamasawa H.: "Recent Achievements and Upgrade Programs at RIKEN Radioactive Isotope Beam Factory", IPAC12, (IPAC12 International Organizing Committee), NewOrleans, USA, May–May (2012).

Furuta T., Ishikawa K., Fukunishi N., Noda S., Takagi S., Maeyama T., Fukasaku K., and Himeno R.: "Toward whole-body dose simulation for particle therapy using K computer", World Congress on Computational Mechanics, Sao Paulo, Brazil, July (2012).

Watanabe Y., Fujimaki M., Fukunishi N., Hasebe H., Higurashi Y., Ikezawa E., Imao H., Kageyama T., Kamigaito O., Kase M., Kidera M., Komiyama M., Kuboki H., Kumagai K., Maie T., Nagase M., Nakagawa T., Ohnishi J., Okuno H., Sakamoto N., Suda K., Watanabe H., Watanabe T., Yamada K., Yokouchi S., Aihara T., Fukuzawa S., Hamanaka M., Ishikawa S., Kobayashi K., Kotaka Y., Koyama R., Nakamura T., Nishida M., Nishimura M., Ohki T., Oyamada K., Shibata J., Tamura M., Tsukiori N., Uchiyama A., Yadomi K., and Yamauchi H.: "Present status of RIKEN Ring Cyclotron Magnets", 3rd International Particle Accelerator Conference (IPAC 2012), (CAMD(Center for Advanced Microstructures and Devices, Louisiana State University)), New Orleans, USA, Aug. (2012).

Imao H., Okuno H., Kamigaito O., Kuboki H., Hasebe H., Fukunishi N., Watanabe T., Fujimaki M., Watanabe Y., Maie T., Kase M., and Yano Y.: "Charge-stripping system for 238U ion beam with recirculating He gas", INTDS2012, (GSI), Mainz, Germany, Aug. (2012).

Higurashi Y., Ohnishi J., Ohzeki K., Haba H., Fujimaki M., Kidera M., Komiyama M., Kamigaito O., Aihara T., Tamura M., and Uchiyama A.: "RECENT DEVELOPMENTS OF THE RIKEN 28-GHZ SC-ECRIS", 20th International Workshop on Electron Cyclotron Resonance Ion Sources (ECRIS-2012), (Australian Nuclear Science and Technology Organisation), Sydney, Australia, Sept. (2012).

Suda K., Arai S., Chiba Y., Kamigaito O., Kase M., Sakamoto N., Watanabe Y., and Yamada K.: "Design of Coupler for Direct Coupled Amplifier to Drift Tube Linac Cavities of the Injector RILAC2 for RIKEN RI Beam Factory", 26th International Linear Accelerator Conference (LINAC12), (LINAC12 International Organizing Committee), Tel Aviv, Israel, Sept. (2012).

Sakamoto N., Fujimaki M., Higurashi Y., Hasebe H., Kamigaito O., Okuno H., Suda K., Watanabe T., Yamada K., and Koyama R.: "Commissioning of a New Injector for the RIKEN RI-Beam Factory", LINAC12, (Soreq Nuclear Research Center), Tel-Aviv, Israel, Sept. (2012).

Yamaguchi Y., Wakasugi M., Ozawa A., Uesaka T., Yano Y., Fujinawa T., Fukunishi N., Inabe N., Kamigaito O., Kase M., Kikuchi T., Komiyama M., Kubo T., Kumagai K., Maie T., Ohnishi J., Tokuchi A., Yoshida K., Yamaguchi T., Nagae D., Zenihiro J., Suzuki T., Abe Y., and Suzaki F.: "Construction of Rare-RI Ring at RIKEN RI Beam Factory", 16th International Conference on Electromagnetic Isotope Separators and Techniques Related to their Applications (EMIS2012), (RIKEN KEK IMP), Matsue, Dec. (2012).

Suzaki F., Zenihiro J., Yamaguchi T., Ozawa A., Uesaka T., Wakasugi M., Yamada K., and Yamaguchi Y.: "Design study of a resonant Schottky pick-up for Rare-RI Ring project", 16th International Conference on Electromagnetic Isotope Separators and Techniques Related to their Applications (EMIS2012), (RIKEN KEK IMP), Matsue, Dec. (2012).

(Domestic Conference)

日暮祥英, 中川孝秀, 大西純一, 羽場宏光, 藤巻正樹, 池沢英二, 渡邉裕, 加瀬昌之, 後藤彰, 込山美咲, 上垣外修一, 田村匡史,

藍原利光, 内山暁仁: “理研新超電導 ECR イオン源の開発研究”, 第 7 回日本加速器学会年会, (日本加速器学会), 姫路, 8 月 (2010).

日暮祥英, 中川孝秀, 大西純一, 羽場宏光, 田村匡史, 藍原利光, 藤巻正樹, 込山美咲, 内山暁仁, 上垣外修一: “28GH z 超電導 ECR イオン源の開発”, 第 8 回日本加速器学会年会, (日本加速器学会), 筑波, 8 月 (2011).

山田一成, 池沢英二, 今尾浩士, 大西純一, 奥野広樹, 加瀬昌之, 上垣外修一, 熊谷桂子, 込山美咲, 後藤彰, 坂本成彦, 須田健嗣, 中川孝秀, 日暮祥英, 福西暢尚, 藤縄雅, 藤巻正樹, 眞家武士, 山澤秀行, 横内茂, 渡邉環, 渡辺博, 渡邉裕, 新井重昭, 藤澤博, 佐藤洋一: “RIBF 用新入射器 RILAC2 のビームコミッショニング”, 第 8 回加速器学会年会, (日本加速器学会), つくば市, 8 月 (2011).

寺岡毅, 神谷健太, 澤野郁夫, 中嶌輝子, 加々美裕, 神尾章子, 浜部直哉, 林依子, 龍頭啓充, 福西暢尚, 阿部知子: “重イオンビーム照射によるウンシュウミカン形態変異個体の果実品質の特徴”, 園芸学会平成 23 年度秋季大会, (園芸学会), 岡山, 9 月 (2011).

今尾浩士, 奥野広樹, 久保木浩功, 横内茂, 福西暢尚, 上垣外修一, 長谷部裕雄, 渡邉環, 加瀬昌之, 後藤彰, 矢野安重: 日本物理学会第６７回年次大会, (大阪大学), 大阪, 3 月 (2012).

渡邉裕, 今尾浩士, 奥野広樹, 加瀬昌之, 上垣外修一, 熊谷桂子, 込山美咲, 坂本成彦, 須田健嗣, 長瀬誠, 福西暢尚, 藤巻正樹, 眞家武士, 山田一成, 渡邉環, 渡辺博, 石川盛, 小高康照, 小林清志, 小山亮, 柴田順翔, 月居憲俊, 仲村武志, 西田稔, 西村誠, 濱仲誠, 福澤聖児, 矢冨一慎: “理研リングサイクロトロン (RRC) の電磁石の老朽化”, 第 9 回日本加速器学会年会, (日本加速器学会), 大阪, 8 月 (2012).

渡邉環, 福西暢尚, 加瀬昌之, 上垣外修一, 稲森聡, 今康一: “高温超伝導電流センサーと SQUID を用いたビーム電流モニターの高感度化”, 第 9 回日本加速器学会年会, (日本加速器学会), 大阪大学, 8 月 (2012).

今尾浩士, 奥野広樹, 久保木浩功, 上垣外修一, 長谷部裕雄, 福西暢尚, 渡邉環, 藤巻正樹, 渡邉裕, 眞家武士, 加瀬昌之, 矢野安重: 第 9 回日本加速器学会年会, (大阪大学), 大阪, 8 月 (2012).

坂本成彦, 段塚知志, 藤縄雅, 福西暢尚, 長谷部裕雄, 日暮祥英, 池上九三男, 池沢英二, 今尾浩士, 影山正, 上垣外修一, 加瀬昌之, 木寺正憲, 込山美咲, 久保木浩功, 熊谷桂子, 眞家武士, 長瀬誠, 中川孝秀, 中村仁音, 大西純一, 奥野広樹, 大関和貴, 須田健嗣, 渡辺博, 渡邉環, 渡邉裕, 山田一成, Lu L., 山澤秀行: “理研 RIBF における大強度重イオンビーム加速”, 第 9 回日本加速器学会年会, 大阪, 8 月 (2012).

古田琢哉, 石川顕一, 福西暢尚, 野田茂穂, 高木周, 前山拓哉, 深作和明, 姫野龍太郎: “OpenMP-MPI ハイブリッド並列導入によるモンテカルロシミュレーションコード PHITS の改良”, 第１０４回日本医学物理学会学術大会, (日本医学物理学会), つくば, 9 月 (2012).

古田琢哉, 前山拓哉, 石川顕一, 福西暢尚, 深作和明, 野田茂穂, 高木周, 姫野龍太郎: “高精度粒子線治療シミュレータ開発に向けたモンテカルロ輸送計算コードの精度検証”, 日本物理学会, (日本物理学会), 東広島, 3 月 (2013).

Cryogenic Technology Team

Publications

[Journal]

(Others)

Okuno H., Dantsuka T., Fujimaki M., Fujinawa T., Fukunishi N., Hasebe H., Higurashi Y., Ikegami K., Ikezawa E., Imao H., Kageyama T., Kamigaito O., Kase M., Kidera M., Komiyama M., Kuboki H., Kumagai K., Maie T., Nagase M., Nakagawa T., Nakamura M., Ohnishi J., Sakamoto N., Suda K., Watanabe H., Watanabe T., Watanabe Y., Yamada K., and Yamasawa H.: "Recent Achievements and Upgrade Programs at RIKEN Radioactive Isotope Beam Factory", Proceedings of IPAC12 **1**, No. 1, p. 430 (2012).

[Book・Proceedings]

(Original Papers) *Subject to Peer Review

Yamada K., Arai S., Fujimaki M., Fujinawa T., Fujisawa H., Fukunishi N., Goto A., Higurashi Y., Ikezawa E., Kase M., Komiyama M., Kumagai K., Maie T., Nakagawa T., Ohnishi J., Okuno H., Sakamoto N., Sato Y., Suda K., Watanabe H., Watanabe T., Watanabe Y., Yano Y., Yokouchi S., and Kamigaito O.: "Construction of new injector linac at RIBF", CYCLOTRONS'10, Lanzhou, 2010–9, JaCoW, Lanzhou, pp. 1–3 (2010).

Yamada K., Arai S., Fujimaki M., Fujinawa T., Fujisawa H., Fukunishi N., Goto A., Higurashi Y., Ikezawa E., Kamigaito O., Kase M., Komiyama M., Kumagai K., Maie T., Nakagawa T., Ohnishi J., Okuno H., Sakamoto N., Sato Y., Suda K., Watanabe H., Watanabe Y., Yano Y., and Yokouchi S.: "Construction of new injector linac for RI Beam Factory at RIKEN Nishina Center", Proceedings of of the 1st International Particle Accelerator Conference (IPAC'10), Kyoto, 2010–5, JaCoW, Kyoto, pp. 789–791 (2010).

Watanabe Y., Fujimaki M., Fukunishi N., Hasebe H., Higurashi Y., Ikezawa E., Imao H., Kageyama T., Kamigaito O., Kase M., Kidera M., Komiyama M., Kuboki H., Kumagai K., Maie T., Nagase M., Nakagawa T., Ohnishi J., Okuno H., Sakamoto N., Suda K., Watanabe H., Watanabe T., Yamada K., Yokouchi S., Aihara T., Fukuzawa S., Hamanaka M., Ishikawa S., Kobayashi K., Kotaka Y., Koyama R., Nakamura T., Nishida M., Nishimura M., Ohki T., Oyamada K., Shibata J., Tamura M., Tsukiori N., Uchiyama A., Yadomi K., and Yamauchi H.: "Present status of RIKEN Ring Cyclotron Magnets", Proceedings of 3rd International Particle Accelerator Conference (IPAC 2012), New Orleans, USA, 2012–8, IPAC2012, IEEE, New Orleans, pp. 433–435 (2012). *

山田一成, 池沢英二, 今尾浩士, 大西純一, 奥野広樹, 加瀬昌之, 熊谷桂子, 込山美咲, 後藤彰, 坂本成彦, 須田健嗣, 中川孝秀, 日暮祥英, 福西暢尚, 藤縄雅, 藤巻正樹, 眞家武士, 山澤秀行, 横内茂, 渡邉環, 渡辺博, 渡邉裕, 新井重昭, 藤澤博, 佐藤洋一, 上垣外修一: "理研 RIBF 用の新しい重イオン入射ライナック RILAC2 の製作", 第 7 回日本加速器学会年会プロシーディングス, 姫路市, 2010–8, 日本加速器学会, 東京, pp. 360–363 (2010).

(Others)

Yamada K., Suda K., Arai S., Fujimaki M., Fujinawa T., Fujisawa H., Fukunishi N., Higurashi Y., Ikezawa E., Imao H., Kamigaito O., Kase M., Komiyama M., Kumagai K., Maie T., Nakagawa T., Ohnishi J., Okuno H., Sakamoto N., Watanabe H., Watanabe T., Watanabe Y., Yamasawa H., Sato Y., and Goto A.: "Beam Commissioning and Operation of New Linac Injector for RIKEN RI Beam Factory", Proceedings of 3rd International Particle Accelerator Conference (IPAC 2012), New Orleans, USA, 2012–5, JACoW, New Orleans, pp. 1071–1073 (2012).

Oral Presentations

(International Conference etc.)

Yamada K., Okuno H., Fujimaki M., Fukunishi N., Goto A., Hasebe H., Ikegami K., Kamigaito O., Kase M., Kumagai K., Maie T., Nagase M., Ohnishi J., Sakamoto N., Yokouchi S., and Yano Y.: "Status of the Superconducting Ring Cyclotron at RIKEN RI Beam Factory", 11th European Particle Accelerator Conference (EPAC 2008), (INFN-LNF), Genoa, Italy, June (2008).

Yamada K., Dantsuka T., Fujimaki M., Fujinawa T., Fukunishi N., Goto A., Hasebe H., Higurashi Y., Ikezawa E., Kamigaito O., Kase M., Komiyama M., Kuboki H., Kumagai K., Maie T., Nagase M., Nakagawa T., Ohnishi J., Okuno H., Sakamoto N., Sato Y., Suda K., Wakasugi M., Watanabe H., Watanabe T., Watanabe Y., Yano Y., and Yokouchi S.: "Progress on the commissioning of Radioactive Isotope Beam Factory at RIKEN Nishina Center", 11th International Conference on HEAVY ION ACCELERATOR TECHNOLOGY (HIAT09), (INFN-LNL), Venezia, Italy, June (2009).

Yamada K., Arai S., Fujimaki M., Fujinawa T., Fujisawa H., Fukunishi N., Goto A., Higurashi Y., Ikezawa E., Kamigaito O., Kase M., Komiyama M., Kumagai K., Maie T., Nakagawa T., Ohnishi J., Okuno H., Sakamoto N., Sato Y., Suda K., Watanabe H., Watanabe Y., Yano Y., and Yokouchi S.: "Construction of New Injector Linac for RI Beam Factory at RIKEN Nishina Center", 1st International Particle Accelerator Conference (IPAC'10), (High Energy Accelerator Research Organization), Kyoto, May (2010).

Yamada K., Arai S., Fujimaki M., Fujinawa T., Fujisawa H., Fukunishi N., Goto A., Higurashi Y., Ikezawa E., Kase M., Komiyama M., Kumagai K., Maie T., Nakagawa T., Ohnishi J., Okuno H., Sakamoto N., Sato Y., Suda K., Watanabe H., Watanabe T., Watanabe Y., Yano Y., Yokouchi S., and Kamigaito O.: "Construction of New Injector LINAC at RIBF", 19th International Conference on Cyclotrons and their Applications (CYCLOTRONS 2010), (IMP), Lanzhou, China, Sept.

(2010).

Yamada K., Suda K., Arai S., Fujimaki M., Fujinawa T., Fujisawa H., Fukunishi N., Higurashi Y., Ikezawa E., Imao H., Kamigaito O., Kase M., Komiyama M., Kumagai K., Maie T., Nakagawa T., Ohnishi J., Okuno H., Sakamoto N., Watanabe H., Watanabe T., Watanabe Y., Yamasawa H., Sato Y., and Goto A.: "Beam Commissioning and Operation of New Linac Injector for RIKEN RI Beam Factory", 3rd International Particle Accelerator Conference (IPAC 2012), New Orleans, USA, May (2012).

Okuno H., Dantsuka T., Fujimaki M., Fujinawa T., Fukunishi N., Hasebe H., Higurashi Y., Ikegami K., Ikezawa E., Imao H., Kageyama T., Kamigaito O., Kase M., Kidera M., Komiyama M., Kuboki H., Kumagai K., Maie T., Nagase M., Nakagawa T., Nakamura M., Ohnishi J., Sakamoto N., Suda K., Watanabe H., Watanabe T., Watanabe Y., Yamada K., and Yamasawa H.: "Recent Achievements and Upgrade Programs at RIKEN Radioactive Isotope Beam Factory", IPAC12, (IPAC12 International Organizing Committee), NewOrleans, USA, May–May (2012).

Kuboki H., Okuno H., Hershcovitch A., Dantsuka T., Hasebe H., Ikegami K., Imao H., Kamigaito O., Kase M., Maie T., Nakagawa T., and Yano Y.: "Development of Plasma Window for gas charge strippers at RIKEN RIBF", 26th World Conference of the International Nuclear Target Development Society, (Johannes Gutenberg-Universitat and GSI), Mainz, Germany, Aug. (2012).

Watanabe Y., Fujimaki M., Fukunishi N., Hasebe H., Higurashi Y., Ikezawa E., Imao H., Kageyama T., Kamigaito O., Kase M., Kidera M., Komiyama M., Kuboki H., Kumagai K., Maie T., Nagase M., Nakagawa T., Ohnishi J., Okuno H., Sakamoto N., Suda K., Watanabe H., Watanabe T., Yamada K., Yokouchi S., Aihara T., Fukuzawa S., Hamanaka M., Ishikawa S., Kobayashi K., Kotaka Y., Koyama R., Nakamura T., Nishida M., Nishimura M., Ohki T., Oyamada K., Shibata J., Tamura M., Tsukiori N., Uchiyama A., Yadomi K., and Yamauchi H.: "Present status of RIKEN Ring Cyclotron Magnets", 3rd International Particle Accelerator Conference (IPAC 2012), (CAMD(Center for Advanced Microstructures and Devices, Louisiana State University)), New Orleans, USA, Aug. (2012).

Imao H., Okuno H., Kamigaito O., Kuboki H., Hasebe H., Fukunishi N., Watanabe T., Fujimaki M., Watanabe Y., Maie T., Kase M., and Yano Y.: "Charge-stripping system for 238U ion beam with recirculating He gas", INTDS2012, (GSI), Mainz, Germany, Aug. (2012).

(Domestic Conference)

山田一成, 池沢英二, 今尾浩士, 大西純一, 奥野広樹, 加瀬昌之, 上垣外修一, 熊谷桂子, 込山美咲, 後藤彰, 坂本成彦, 須田健嗣, 中川孝秀, 日暮祥英, 福西暢尚, 藤縄雅, 藤巻正樹, 眞家武士, 山澤秀行, 横内茂, 渡邉環, 渡辺博, 渡邉裕, 新井重昭, 藤澤博, 佐藤洋一: "RIBF 用新入射器 RILAC2 のビームコミッショニング", 第 8 回加速器学会年会, (日本加速器学会), つくば市, 8 月 (2011).

渡邉裕, 今尾浩士, 奥野広樹, 加瀬昌之, 上垣外修一, 熊谷桂子, 込山美咲, 坂本成彦, 須田健嗣, 長瀬誠, 福西暢尚, 藤巻正樹, 眞家武士, 山田一成, 渡邉環, 渡辺博, 石川盛, 小高康照, 小林清志, 小山亮, 柴田順翔, 月居憲俊, 仲村武志, 西田稔, 西村誠, 濱仲誠, 福澤聖児, 矢冨一慎: "理研リングサイクロトロン (RRC) の電磁石の老朽化", 第 9 回日本加速器学会年会, (日本加速器学会), 大阪, 8 月 (2012).

今尾浩士, 奥野広樹, 久保木浩功, 上垣外修一, 長谷部裕雄, 福西暢尚, 渡邉環, 藤巻正樹, 渡邉裕, 眞家武士, 加瀬昌之, 矢野安重: 第 9 回日本加速器学会年会, (大阪大学), 大阪, 8 月 (2012).

坂本成彦, 段塚知志, 藤縄雅, 福西暢尚, 長谷部裕雄, 日暮祥英, 池上九三男, 池沢英二, 今尾浩士, 影山正, 上垣外修一, 加瀬昌之, 木寺正憲, 込山美咲, 久保木浩功, 熊谷桂子, 眞家武士, 長瀬誠, 中川孝秀, 中村仁音, 大西純一, 奥野広樹, 大関和貴, 須田健嗣, 渡辺博, 渡邉環, 渡邉裕, 山田一成, Lu L., 山澤秀行: "理研 RIBF における大強度重イオンビーム加速", 第 9 回日本加速器学会年会, 大阪, 8 月 (2012).

Infrastructure Management Team

Publications

[Journal]

(Original Papers) *Subject to Peer Review

Higurashi Y., Nakagawa T., Kidera M., Aihara T., Kase M., and Yano Y.: "Enhancement of Ar8+ Current Extracted from RIKEN 18 GHz Electron Cyclotron Resonance Ion Source by Moving the Plasma Electrode toward the Resonance Zone", Jpn. J. Appl. Phys. **40**, 5134–5135 (2001). *

Higurashi Y., Nakagawa T., Kidera M., Kageyama T., Kase M., Goto A., and Yano Y.: "Production of Highly Charged Ga Ions from Organic Metal Comppound Using the Liquid-He-Free Superconducting Electron Cyclotron Resonance Ion Source at RIKEN", Jpn. J. Appl. Phys. **41**, 5442–5443 (2002). *

Higurashi Y., Nakagawa T., Kidera M., Aihara T., Kase M., and Yano Y.: "Effect of plasma electrode position on the beam intensity of heavy ions from a RIKEN 18 GHz electron cyclotron resonance ion source", Rev. Sci. Instrum. **73**, No. 2, p. 598 (2002). *

Higurashi Y., Nakagawa T., Kidera M., Aihara T., Kase M., and Yano Y.: "Enhancement of Ar8+ Ion Beam Intensity from RIKEN 18 GHz Electron Cyclotron Resonance Ion Source by Optimizing the Magnetic Field Configuration", Jpn. J. Appl. Phys. **42**, 3656–3657 (2003). *

Higurashi Y., Nakagawa T., Kidera M., Kageyama T., Aihara T., Kase M., and Yano Y.: "Optimization of magnetic field configuration for the roduction of Ar ions from RIKEN 18 GHz ECR ion source", Nucl. Instrum. Methods Phys. Res. A **510**, No. 2, pp. 206–210 (2003). *

Higurashi Y., Kidera M., Kase M., Nakagawa T., and Yano Y.: "Emittance measurement for intense beam of heavy ions from RIKEN 18 GHz ECRIS", Rev. Sci. Instrum. **75**, 1467 (2004). *

Higurashi Y., Kidera M., Nakagawa T., Aihara T., Kase M., and Yano Y.: "Effect of Plasma Electrode Position of RIKEN 18 GHz Electron Cyclotron Resonance Ion Source on Beam Intensity of Highly Charged Ar Ions", Jpn. J. Appl. Phys. **44**, 5216–5218 (2005). *

Higurashi Y., Kidera M., Nakagawa T., Aihara T., Kase M., Goto A., and Yano Y.: "Production of 70Zn Beam from RIKEN 18 GHz Electron Cyclotron Resonance Ion Source", Jpn. J. Appl. Phys. **44**, 8138–8140 (2005). *

Higurashi Y., Nakagawa T., Kidera M., Aihara T., Kobayashi K., Kase M., Goto A., and Yano Y.: "Effect of the plasma electrode position and shape on the beam intensity of the highly charged ions from RIKEN 18 GHz electron cyclotoron resonanse ion source", Rev. Sci. Instrum. **77**, No. 2, p. 03A329 (2006). *

Higurashi Y., Nakagawa T., Kidera M., Haba H., Aihara T., Kase M., Goto A., and Yano Y.: "Production of U beam from RIKEN 18 GHz electron cyclotron resonance ion source", Rev. Sci. Instrum. **79**, No. 2, p. 02C714 (2008). *

(Others)

Nakagawa T., Higurashi Y., Ohnishi J., Aihara T., Tamura M., Uchiyama A., Okuno H., Kusaka K., Kidera M., Komiyama M., Fujimaki M., Sato Y., Ikezawa E., Watanabe Y., Kase M., Goto A., Kamigaito O., and Yano Y.: "First results from the new RIKEN superconducting electron cyclotron resonance ion source", Rev. Sci. Instrum. **81**, No. 2, p. 02A320 (2010).

Okuno H., Fukunishi N., Hasebe H., Imao H., Kamigaito O., Kase M., and Kuboki H.: "New Developments in Low-Z Gas Stripper Sstem at RIKEN Radioactive Isotope Beam Factory (RIBF)", Proceedings of HIAT12 **1**, No. 1, p. 199 (2012).

Okuno H., Dantsuka T., Fujimaki M., Fujinawa T., Fukunishi N., Hasebe H., Higurashi Y., Ikegami K., Ikezawa E., Imao H., Kageyama T., Kamigaito O., Kase M., Kidera M., Komiyama M., Kuboki H., Kumagai K., Maie T., Nagase M., Nakagawa T., Nakamura M., Ohnishi J., Sakamoto N., Suda K., Watanabe H., Watanabe T., Watanabe Y., Yamada K., and Yamasawa H.: "Recent Achievements and Upgrade Programs at RIKEN Radioactive Isotope Beam Factory", Proceedings of IPAC12 **1**, No. 1, p. 430 (2012).

日暮祥英, 大西純一, 中川孝秀, 藍原利光, 田村匡史, 内山暁仁, 込山美咲, 藤巻正樹, 佐藤洋一, 池沢英二, 渡邉裕, 加瀬昌之, 後藤彰, 上垣外修一, 矢野安重: "理研における新しい超電導 ECR イオン源の開発", 加速器 **6**, No. 4, pp. 346–354 (2010).

[Book・Proceedings]

(Original Papers) *Subject to Peer Review

Yamada K., Arai S., Fujimaki M., Fujinawa T., Fujisawa H., Fukunishi N., Goto A., Higurashi Y., Ikezawa E., Kase M., Komiyama M., Kumagai K., Maie T., Nakagawa T., Ohnishi J., Okuno H., Sakamoto N., Sato Y., Suda K., Watanabe H., Watanabe T., Watanabe Y., Yano Y., Yokouchi S., and Kamigaito O.: "Construction of new injector linac at RIBF", CYCLOTRONS'10, Lanzhou, 2010–9, JaCoW, Lanzhou, pp. 1–3 (2010).

Yamada K., Arai S., Fujimaki M., Fujinawa T., Fujisawa H., Fukunishi N., Goto A., Higurashi Y., Ikezawa E., Kamigaito O., Kase M., Komiyama M., Kumagai K., Maie T., Nakagawa T., Ohnishi J., Okuno H., Sakamoto N., Sato Y., Suda K., Watanabe H., Watanabe Y., Yano Y., and Yokouchi S.: "Construction of new injector linac for RI Beam Factory at RIKEN Nishina Center", Proceedings of of the 1st International Particle Accelerator Conference (IPAC'10), Kyoto, 2010–5, JaCoW, Kyoto, pp. 789–791 (2010).

Watanabe Y., Fujimaki M., Fukunishi N., Hasebe H., Higurashi Y., Ikezawa E., Imao H., Kageyama T., Kamigaito O., Kase M., Kidera M., Komiyama M., Kuboki H., Kumagai K., Maie T., Nagase M., Nakagawa

T., Ohnishi J., Okuno H., Sakamoto N., Suda K., Watanabe H., Watanabe T., Yamada K., Yokouchi S., Aihara T., Fukuzawa S., Hamanaka M., Ishikawa S., Kobayashi K., Kotaka Y., Koyama R., Nakamura T., Nishida M., Nishimura M., Ohki T., Oyamada K., Shibata J., Tamura M., Tsukiori N., Uchiyama A., Yadomi K., and Yamauchi H.: "Present status of RIKEN Ring Cyclotron Magnets", Proceedings of 3rd International Particle Accelerator Conference (IPAC 2012), New Orleans, USA, 2012–8, IPAC2012, IEEE, New Orleans, pp. 433–435 (2012). ＊

山田一成, 池沢英二, 今尾浩士, 大西純一, 奥野広樹, 加瀬昌之, 熊谷桂子, 込山美咲, 後藤彰, 坂本成彦, 須田健嗣, 中川孝秀, 日暮祥英, 福西暢尚, 藤縄雅, 藤巻正樹, 眞家武士, 山澤秀行, 横内茂, 渡邉環, 渡辺博, 渡邉裕, 新井重昭, 藤澤博, 佐藤洋一, 上垣外修一: "理研 RIBF 用の新しい重イオン入射ライナック RILAC2 の製作", 第 7 回日本加速器学会年会プロシーディングス, 姫路市, 2010–8, 日本加速器学会, 東京, pp. 360–363 (2010).

(Others)

Yamada K., Suda K., Arai S., Fujimaki M., Fujinawa T., Fujisawa H., Fukunishi N., Higurashi Y., Ikezawa E., Imao H., Kamigaito O., Kase M., Komiyama M., Kumagai K., Maie T., Nakagawa T., Ohnishi J., Okuno H., Sakamoto N., Watanabe H., Watanabe T., Watanabe Y., Yamasawa H., Sato Y., and Goto A.: "Beam Commissioning and Operation of New Linac Injector for RIKEN RI Beam Factory", Proceedings of 3rd International Particle Accelerator Conference (IPAC 2012), New Orleans, USA, 2012–5, JACoW, New Orleans, pp. 1071–1073 (2012).

Oral Presentations

(International Conference etc.)

Higurashi Y., Nakagawa T., Kidera M., Aihara T., Kase M., and Yano Y.: "Effect of plasma electrode position on the beam intensity and emittance of RIKEN 18 GHz ECRIS", 16th International Conference on ECR Ion Sources (ECRIS 04), (Lawrence Berkeley National Laboratory), Berkeley, USA, Sept. (2004).

Yamada K., Arai S., Fujimaki M., Fujinawa T., Fujisawa H., Fukunishi N., Goto A., Higurashi Y., Ikezawa E., Kamigaito O., Kase M., Komiyama M., Kumagai K., Maie T., Nakagawa T., Ohnishi J., Okuno H., Sakamoto N., Sato Y., Suda K., Watanabe H., Watanabe Y., Yano Y., and Yokouchi S.: "Construction of New Injector Linac for RI Beam Factory at RIKEN Nishina Center", 1st International Particle Accelerator Conference (IPAC'10), (High Energy Accelerator Research Organization), Kyoto, May (2010).

Higurashi Y., Nakagawa T., Ohnishi J., Haba H., Ikezawa E., Fujimaki M., Watanabe Y., Kidera M., Komiyama M., Kase M., Goto A., Kamigaito O., Aihara T., Tamura M., and Uchiyama A.: "Production of U ion beam from RIKEN SC-ECRIS ith sputtering method", 19th International Workshop on ECR Ion Sources (ECRIS 2010), grenoble, France, Aug. (2010).

Yamada K., Arai S., Fujimaki M., Fujinawa T., Fujisawa H., Fukunishi N., Goto A., Higurashi Y., Ikezawa E., Kase M., Komiyama M., Kumagai K., Maie T., Nakagawa T., Ohnishi J., Okuno H., Sakamoto N., Sato Y., Suda K., Watanabe H., Watanabe T., Watanabe Y., Yano Y., Yokouchi S., and Kamigaito O.: "Construction of New Injector LINAC at RIBF", 19th International Conference on Cyclotrons and their Applications (CYCLOTRONS 2010), (IMP), Lanzhou, China, Sept. (2010).

Yamada K., Suda K., Arai S., Fujimaki M., Fujinawa T., Fujisawa H., Fukunishi N., Higurashi Y., Ikezawa E., Imao H., Kamigaito O., Kase M., Komiyama M., Kumagai K., Maie T., Nakagawa T., Ohnishi J., Okuno H., Sakamoto N., Watanabe H., Watanabe T., Watanabe Y., Yamasawa H., Sato Y., and Goto A.: "Beam Commissioning and Operation of New Linac Injector for RIKEN RI Beam Factory", 3rd International Particle Accelerator Conference (IPAC 2012), New Orleans, USA, May (2012).

Okuno H., Dantsuka T., Fujimaki M., Fujinawa T., Fukunishi N., Hasebe H., Higurashi Y., Ikegami K., Ikezawa E., Imao H., Kageyama T., Kamigaito O., Kase M., Kidera M., Komiyama M., Kuboki H., Kumagai K., Maie T., Nagase M., Nakagawa T., Nakamura M., Ohnishi J., Sakamoto N., Suda K., Watanabe H., Watanabe T., Watanabe Y., Yamada K., and Yamasawa H.: "Recent Achievements and Upgrade Programs at RIKEN Radioactive Isotope Beam Factory", IPAC12, (IPAC12 International Organizing Committee), NewOrleans, USA, May–May (2012).

Okuno H., Fukunishi N., Hasebe H., Imao H., Kamigaito O., Kase M., and Kuboki H.: "New Developments in Low-Z Gas Stripper Sstem at RIKEN Radioactive Isotope Beam Factory (RIBF)", 12th International Conference on Heavy Ion Accelerator Technology, (Argonne National Laboratory), Chicago, IL, USA, June–June (2012).

Watanabe Y., Fujimaki M., Fukunishi N., Hasebe H., Higurashi Y., Ikezawa E., Imao H., Kageyama T., Kamigaito O., Kase M., Kidera M., Komiyama M., Kuboki H., Kumagai K., Maie T., Nagase M., Nakagawa T., Ohnishi J., Okuno H., Sakamoto N., Suda K., Watanabe H., Watanabe T., Yamada K., Yokouchi S., Aihara T., Fukuzawa S., Hamanaka M., Ishikawa S., Kobayashi K., Kotaka Y., Koyama R., Nakamura T., Nishida M., Nishimura M., Ohki T., Oyamada K., Shibata J., Tamura M., Tsukiori N., Uchiyama A., Yadomi K., and Yamauchi H.: "Present status of RIKEN Ring Cyclotron Magnets", 3rd International Particle Accelerator Conference (IPAC 2012), (CAMD(Center for Advanced Microstructures and Devices, Louisiana State University)), New Orleans, USA, Aug. (2012).

Okuno H., Fukunishi N., Hasebe H., Imao H., Kamigaito O., Kase M., and Kuboki H.: "Charge Strippers for the RIKEN Radioisotope Beam Factory (RIBF)", INTDS2012, (INTDS), Mainz, Germany, Aug. (2012).

Fujinawa T.: "Development of Cranes at the RIKEN RI Beam Factory", Asia-Pacific Conference on Electrical Installation, (The institute of Electrical lInstallation Engineers of Japan), Nagoya, Aug.–Aug. (2012).

Fujinawa T.: "RIKEN Nishina Center's Response to Fukushima Daiichi Nuclear", Internatinal Workshop on Accelerator Operation 2012, (SLAC), SLAC, USA, Aug.–Aug. (2012).

Kanaya J., Haba H., Mukai H., Kambara T., and Kase M.: "Airborne radionuclides measured in Wako, Japan, after the Fukushima Dai-ichi nuclear power plant accident in 2011", EuCheMS International Conference on Nuclear and Radiochemistry (NRC-8), (European Association for Chemical and Molecular Sciences (EuCheMS)), Como, Italy, Sept.–Sept. (2012).

Yamaguchi Y., Wakasugi M., Ozawa A., Uesaka T., Yano Y., Fujinawa T., Fukunishi N., Inabe N., Kamigaito O., Kase M., Kikuchi T., Komiyama M., Kubo T., Kumagai K., Maie T., Ohnishi J., Tokuchi A., Yoshida K., Yamaguchi T., Nagae D., Zenihiro J., Suzuki T., Abe Y., and Suzaki F.: "Construction of Rare-RI Ring at RIKEN RI Beam Factory", 16th International Conference on Electromagnetic Isotope Separators and Techniques Related to their Applications (EMIS2012), (RIKEN KEK IMP), Matsue, Dec. (2012).

(Domestic Conference)

日暮祥英, 中川孝秀, 大西純一, 羽場宏光, 藤巻正樹, 池沢英二, 渡邉裕, 加瀬昌之, 後藤彰, 込山美咲, 上垣外修一, 田村匡史, 藍原利光, 内山暁仁: "理研新超電導 ECR イオン源の開発研究", 第 7 回日本加速器学会年会, (日本加速器学会), 姫路, 8 月 (2010).

山田一成, 池沢英二, 今尾浩士, 大西純一, 奥野広樹, 加瀬昌之, 上垣外修一, 熊谷桂子, 込山美咲, 後藤彰, 坂本成彦, 須田健嗣, 中川孝秀, 日暮祥英, 福西暢尚, 藤縄雅, 藤巻正樹, 眞家武士, 山澤秀行, 横内茂, 渡邉環, 渡辺博, 渡邉裕, 新井重昭, 藤澤博, 佐藤洋一: "RIBF 用新入射器 RILAC2 のビームコミッショニング", 第 8 回加速器学会年会, (日本加速器学会), つくば市, 8 月 (2011).

渡邉裕, 今尾浩士, 奥野広樹, 加瀬昌之, 上垣外修一, 熊谷桂子, 込山美咲, 坂本成彦, 須田健嗣, 長瀬誠, 福西暢尚, 藤巻正樹, 眞家武士, 山田一成, 渡邉環, 渡辺博, 石川盛, 小高康照, 小林清志, 小山亮, 柴田順翔, 月居憲俊, 仲村武志, 西田稔, 西村誠, 濱仲誠, 福澤聖児, 矢冨一慎: "理研リングサイクロトロン (RRC) の電磁石の老朽化", 第 9 回日本加速器学会年会, (日本加速器学会), 大阪, 8 月 (2012).

坂本成彦, 段塚知志, 藤縄雅, 福西暢尚, 長谷部裕雄, 日暮祥英, 池上九三男, 池沢英二, 今尾浩士, 影山正, 上垣外修一, 加瀬昌之, 木寺正憲, 込山美咲, 久保木浩功, 熊谷桂子, 眞家武士, 長瀬誠, 中川孝秀, 中村仁音, 大西純一, 奥野広樹, 大関和貴, 須田健嗣, 渡辺博, 渡邉環, 渡邉裕, 山田一成, Lu L., 山澤秀行: "理研 RIBF における大強度重イオンビーム加速", 第 9 回日本加速器学会年会, 大阪, 8 月 (2012).

金谷淳平, 羽場宏光, 向井弘樹, 神原正, 加瀬昌之: "理研和光研究所において観測された福島第一原子力発電所事故由来の放射性核種—事故後 1 年間の大気中放射能濃度変化—", 2012 日本放射化学会年会・第 56 回放射化学討論会, (日本放射化学会), 東京都目黒区, 10–10 月 (2012).

藤縄雅: "福島第一原発事故と理研仁科センター", 日本大学生産工学部第 45 回学術講演会, (日本大学生産工学部), 千葉県習志野市, 12–12 月 (2012).

Instrumentation Development Group

Publications

[Journal]

(Original Papers) *Subject to Peer Review

Morimoto K., Morita K., Kaji D., Haba H., Katori K., Koura H., Ohnishi T., Ozawa A., Suda T., Sueki K., Tanihata I., Tokanai F., Yoneda A., and Yoshida A.: "Status of super heavy element research using GARIS at RIKEN", Nucl. Phys. A **738**, 129 (2004). *

Kaji D., Morimoto K., Sato N., Ichikawa T., Ohzeki K., Haba H., Koura H., Ozawa A., Sumita T., Yamaguchi T., Yoneda A., Yoshida A., and Morita K.: "Production and Decay Properties of ^{263}Hs", J. Phys. Soc. Jpn. **78**, No. 3, p. 035001 (2009). *

Sato N., Haba H., Ichikawa T., Kaji D., Kudou Y., Morimoto K., Morita K., Ohzeki K., Sumita T., Yoneda A., Koura H., Ozawa A., Yamaguchi T., and Yoshida A.: "Production and Decay Properties of ^{264}Hs and ^{265}Hs", J. Phys. Soc. Jpn. **80**, 094201 (2011). *

Naimi S., Nakamura S., Ito Y., Mita H., Okada K., Schury P. H., Sonoda T., Takamine A., Wada M., Wollnik H., and Ozawa A.: "An rf-carpet electrospray ion source to provide isobaric mass calibrants for trans-uranium elements", Int. J. Mass Spectrom. **337**, No. 24, pp. 24–28 (2013). *

[Book · Proceedings]

(Others)

Yamaguchi Y., Wakasugi M., Suzuki H., Fujinawa T., Uesaka T., Yano Y., Ozawa A., Nagae D., Yamaguchi T., Suzuki T., Kikuchi T., Jiang W., Sasaki T., and Tokuchi A.: "Present status of Rare-RI Ring project in RIKEN RI Beam Factory", Proceedings of Science (PoS), Frascati, Italy, 2011–10, SISSA, Fascati, p. 070 (2012).

Oral Presentations

(International Conference etc.)

Schury P. H., Jeong S., Haba H., Kaji D., Koura H., Ito Y., Mita H., Miyatake H., Morimoto K., Morita K., Naimi S., Nakamura S., Okada K., Ozawa A., Sonoda T., Takamine A., Wollnik H., and Wada M.: "A multi-reflection time of flight mass spectrograph for short-lived nuclei and heavy molecules", International Mass Spectrometry Conference, (Kyoto University), Kyoto, Sept. (2012).

Ozawa A.: "Nuclear mass measurements for the r-process in Rare-RI Ring", 1st Visiting NAOJ Fellow Workshop, Element Genesis and Cosmic Chemical Evolution: r-process perspective, (NAOJ RIKEN CNS KEK), Wako, Oct. (2012).

Ozawa A.: "Rare-RI Ring for mass measurements of exotic nuclei", A workshop on Science with Rare Ion Beams SCRIBE-2012, (Variable Energy Cyclotron Centre), Kolkata, India, Nov. (2012).

Yamaguchi Y., Wakasugi M., Ozawa A., Uesaka T., Yano Y., Fujinawa T., Fukunishi N., Inabe N., Kamigaito O., Kase M., Kikuchi T., Komiyama M., Kubo T., Kumagai K., Maie T., Ohnishi J., Tokuchi A., Yoshida K., Yamaguchi T., Nagae D., Zenihiro J., Suzuki T., Abe Y., and Suzaki F.: "Construction of Rare-RI Ring at RIKEN RI Beam Factory", 16th International Conference on Electromagnetic Isotope Separators and Techniques Related to their Applications (EMIS2012), (RIKEN KEK IMP), Matsue, Dec. (2012).

Suzaki F., Zenihiro J., Yamaguchi T., Ozawa A., Uesaka T., Wakasugi M., Yamada K., and Yamaguchi Y.: "Design study of a resonant Schottky pick-up for Rare-RI Ring project", 16th International Conference on Electromagnetic Isotope Separators and Techniques Related to their Applications (EMIS2012), (RIKEN KEK IMP), Matsue, Dec. (2012).

Nagae D., Abe Y., Okada S., Ozawa A., Yamaguchi T., Suzuki H., Moriguchi T., Ishibashi Y., Fukuoka S., Nishikiori R., Suzuki T., Suzaki F., Yamaguchi Y., Uesaka T., and Wakasugi M.: "Time-of-flight detector applied to mass measurements in Rare-RI Ring", 6th International Conference on Electromagnetic Isotope Separators and Techniques Related to their Applications (EMIS2012), (RIKEN KEK IMP), Matsue, Dec. (2012).

Naimi S., Nakamura S., Ito Y., Mita H., Okada K., Ozawa A., Takamine A., Wada M., and Wollnik H.: "ESI for mass calibration of MR-TOF mass spectrograph", The 16th International Conference on Electromagnetic Isotope Separators and their Applications (EMIS-2012), (RIKEN, KEK), Matsue, Dec. (2012).

(Domestic Conference)

加治大哉, 森田浩介, 森本幸司, 羽場宏光, 鹿取謙二, 小浦寛之, 大西哲哉, 小沢顕, 須田利美, 末木啓介, 谷畑勇夫, 米田晃, 吉田敦: "ヘリウムガス中における (超) 重元素の平衡電荷", 日本物理学会, (宮崎大学), 宮崎, 9 月 (2003).

加治大哉, 森田浩介, 森本幸司, 羽場宏光, 鹿取謙二, 小浦寛之, 大西哲哉, 小沢顕, 須田利美, 末木啓介, 谷畑勇夫, 米田晃, 吉田敦: "ヘリウムガス中における重い反跳原子の平衡電荷－理研における Z=111 番元素探索－", 放射化学討論会, (京都大学原子炉実験施設), 大阪, 10 月 (2003).

加治大哉, 森田浩介, 森本幸司, 羽場宏光, 小浦寛之, 大西哲哉, 小沢顕, 須田利美, 末木啓介, 山口貴之, 米田晃, 吉田敦: "209Bi+70Zn 反応を用いた 113 番元素探索", 日本化学会, (神奈川大学), 神奈川, 3 月 (2005).

加治大哉, 森田浩介, 森本幸司, 羽場宏光, 小浦寛之, 大西哲哉, 小沢顕, 須田利美, 末木啓介, 山口貴之, 米田晃, 吉田敦: "209Bi(70Zn,n)278113 反応を用いた 113 番元素の合成", 放射化学討論会, (金沢大学), 金沢, 9 月 (2005).

加治大哉, 森本幸司, 羽場宏光, 市川隆敏, 小浦寛之, 工藤祐生, 小沢顕, 大関和貴, 住田貴之, 山口貴之, 米田晃, 吉田敦, 森田浩介: "新同位体 ^{263}Hs の生成および壊変特性", 放射化学討論会, (日本大学), 神奈川, 9 月 (2009).

伊藤由太, 和田道治, Schury P. H., 園田哲, 高峰愛子, 岡田邦宏, Wollnik H., Shchepunov V., 小沢顕, 中村聡佑, Christian S.: "Development of MR-TOF Mass spectrograph for short-lived nuclei -II", 日本物理学会, (九州工業大学), 福岡, 9 月 (2010).

Schury P. H., 和田道治, 伊藤由太, 三田浩希, Naimi S., 中村聡佑, 岡田邦宏, 小沢顕, Viatcheslav S., 園田哲, 高峰愛子, Wollnik H.: "Development of Multi-Reflection Time-of-Flight Mass Spectrograph for short-lived nuclei V", 日本物理学会, (九州工業大学), 福岡, 9 月 (2010).

Naimi S., 中村 聡佑, 和田 道治, 伊藤 由太, Schury P. H., Wollnik H., 園田 哲, 小沢 顕, 三田 浩希, 高峰 愛子, 岡田邦宏: 日本物理学会, (九州工業大学), 福岡, 9 月 (2010).

中村聡佑, 和田道治, Schury P. H., 園田哲, 伊藤由太, Naimi S., 三田浩希, 高峰愛子, 小沢顕: "質量校正のための RF カーペットを用いた高効率 ESI の開発", 日本物理学会, (弘前大学), 青森, 9 月 (2011).

小沢顕: "稀少 RI リングプロジェクト　—R プロセス解明に向けて—", 第３１回不安定核セミナー, (筑波大学), つくば, 5 月 (2012).

伊藤由太, 和田道治, Schury P. H., Naimi S., 園田哲, 高峰愛子, 岡田邦宏, 中村聡佑, 三田浩希, Wollnik H., 小沢顕: 日本物理学会, (京都産業大学), 京都, 9 月 (2012).

Naimi S., 中村 聡佑, 和田 道治, 伊藤 由太, Schury P. H., Wollnik H., 園田 哲, 小沢 顕, 三田 浩希, 高峰 愛子, 岡田邦宏: "ElectroSpray ion source for mass calibration of MR-TOF mass spectrograph used in superheavy element mass measurement", 日本物理学会, (京都産業大学), 京都, 9 月 (2012).

Schury P. H., 和田 道治, 伊藤 由太, 三田 浩希, Naimi S., 中村聡佑, 岡田邦宏, 小沢顕, Viatcheslav S., 園田哲, 高峰愛子, Wollnik H.: "Multi-Reflection Time-of-Flight Mass Spectrograph for Heavy Ion Mass Measurements", 日本物理学会, (京都産業大学), 京都, 9 月 (2012).

SLOWRI Team

Publications

[Journal]

(Original Papers) *Subject to Peer Review

Okada K., Wada M., Nakamura T., Takamine A., Lioubimov V., Schury P. H., Ishida Y., Sonoda T., Ogawa M., Yamazaki Y., Kanai Y., Kojima T., Yoshida A., Kubo T., Katayama I., Ohtani S., Wollnik H., and Schuessler H. A.: "A precision measurement of the hyperfine structure of laser-cooled $^{7}Be^{+}$ ions priduced by projectile fragmentation", Phys. Rev. Lett. **101**, No. 212502, pp. 212502-1–212502-4 (2008). *

Wada M., Takamine A., Sonoda T., Okada K., and Schury P. H.: "Developments at the SLOWRI facility at RIKEN: precision optical spectroscopy of $^{7,9,10,11}Be^{+}$ ions", Hyperfine Interact. **199**, No. 269, pp. 269–277 (2011). *

Kimura N., Okada K., Schuessler H. A., Wada M., Takayanagi T., and Ohtani S.: "Sympathetic crystallization of CaH+ produced by a laser-induced reaction", Phys. Rev. A **83**, No. 033422, pp. 033422-1–033422-6 (2011). *

Ferrer R., Sonnenschein V., Beyhan B., Franchoo S., Huyse M., Kudryavtsev Y., Kron T., Lecesne N., Moore I., Pauwels D., Rens L., Reponen M., Rossnagel J., Savajols H., Sonoda T., Van den Bergh P., Van Duppen P., Wendt K., Radulov D., Osmond B., Raeder S., and Thomas J.: "Performance of a high repetition pulse rate laser system for in-gas-jet laser ionization studies with the Leuven laser ion source @ LISOL", Nucl. Instrum. Methods Phys. Res. B **291**, 29–37 (2012). *

Sonoda T., Wada M., Tomita H., Sakamoto C., Takatsuka T., Furukawa T., Iimura H., Ito Y., Kubo T., Matsuo Y., Mita H., Naimi S., Nakamura S., Noto T., Schury P. H., Wakui T., Miyatake H., Jeong S., Watanabe Y., Isiyama H., Okada K., and Takamine A.: "Development of a resonant laser ionization gas cell for high-energy, short-lived nuclei", Nucl. Instrum. Methods Phys. Res. B **295**, No. 1, (2012). *

Naimi S., Nakamura S., Ito Y., Mita H., Okada K., Schury P. H., Sonoda T., Takamine A., Wada M., Wollnik H., and Ozawa A.: "An rf-carpet electrospray ion source to provide isobaric mass calibrants for trans-uranium elements", Int. J. Mass Spectrom. **337**, No. 24, pp. 24–28 (2013). *

[Book · Proceedings]

(Others)

Yamada K., Suda K., Arai S., Fujimaki M., Fujinawa T., Fujisawa H., Fukunishi N., Higurashi Y., Ikezawa E., Imao H., Kamigaito O., Kase M., Komiyama M., Kumagai K., Maie T., Nakagawa T., Ohnishi J., Okuno H., Sakamoto N., Watanabe H., Watanabe T., Watanabe Y., Yamasawa H., Sato Y., and Goto A.: "Beam Commissioning and Operation of New Linac Injector for RIKEN RI Beam Factory", Proceedings of 3rd International Particle Accelerator Conference (IPAC 2012), New Orleans, USA, 2012–5, JACoW, New Orleans, pp. 1071–1073 (2012).

Oral Presentations

(International Conference etc.)

Wada M.: "Non-destructive beam current monitor using FCT", Second expert meeting on critical issues of next-generation high-intensity fragment separators, (RIKEN), Saitama, May (2006).

Wada M.: "Precision Spectroscopy with Slow RI Beams", INTERNATIONAL SUMMER SCHOOL ON SUBATOMIC PHYSICS, (Beijing University), Beijing, China, Aug. (2006).

Wada M.: "Laser spectroscopy of ^{7}Be and ^{10}Be at a prototype SLOWRI facility of RIKEN", 4th International Conference on Trapped Charged Particles and Fundamental Physics, (TRIUMF), Parksville, Canada, Sept. (2006).

Wada M.: "Laser spectroscopy of trapped Be isotopes at a prototype slow RI-beam facility of RIKEN", the 23rd International Nuclear Physics Conference, INPC2007, (J-PARC, RIKEN), Tokyo, June (2007).

Wada M.: "News from the RIKEN RI-beam factory", ISOLDE Workshop and Users meeting 2007/2008, (CERN), CERN, Switzerland, Dec. (2007).

Schury P. H., Okada K., Sonoda T., Takamine A., Wada M., Wollnik H., and Yamazaki Y.: "A Portable Multi-Reflection Time-of-Flight Mass Spectrograph for Rare Isotopes", International Workshop XXXVI on Gross Properties of Nuclei and Nuclear Excitations, Kleinwalsertal, Austria, Jan. (2008).

Wada M.: "Spectroscopy of Be isotopes at Prototype SLOWRI", 1st International Conference on Exotic Nuclei and Atomic Masses (ENAM08), Mazurian Lakes, Poland, Sept. (2008).

Schury P. H., Okada K., Sonoda T., Takamine A., Wada M., Yamazaki Y., and Wollnik H.: "Progress of the RIKEN MR-TOF", Fifth International Conference on Exotic Nuclei and Atomic Masses, Ryn, Poland, Sept. (2008).

Wada M.: "Precision hyperfine structure spectroscopy of Be isotopes at SLOWRI prototype and prospects of SLOWRI at RIKEN RIBF", 6th Japan-Italy Symposium on Heavy-Ion Physics, (JAEA), Tokai, Nov. (2008).

Wada M.: "SLOWRI Overview", JUSEIPEN Workshop to Promote and help Establish US-Japan: Experimental Collaborations using Rare Isotope Beams., (LBL), Berkely, USA, Sept. (2009).

Schury P. H.: "An Overview of Past, Present and Future Atomic Mass Measurement Techniques", Stanford High Energy Physics Colloquia, (Stanford University), Stanford, USA, Sept. (2010).

Sonoda T., Wada M., Tomita H., Sakamoto C., Ito Y., Schuessler H. A., Takamine A., Kubo T., Matsuo Y., Shinozuka T., Wakui T., Nakamura S., Furukawa T., Okada K., Kudryavtsev Y., Mark H., Van Duppen P., Miyatake H., Ishiyama H., Imai N., Watanabe Y., Hirayama Y., and Chon J.: "Development of the resonance ionization laser ion source for parasitic RI-beam production and in-gas-cell/jet laser spectroscopy at SLOWRI RIKEN", Advances in Radioactive Isotope Science (ARIS - 2011), (K.U.Leuven), Leuven, Belgium, May–May (2011).

Wada M.: "Precision spectroscopy of short-lived nuclei in ion traps", Cold Antimatter and High Precision Physics (Pbar11), Matsue, Nov. (2011).

Wada M.: "Ion trap laser spectroscopy of radioactive Beryllium isotopes and future of SLOWRI", 501. Wilhelm und Else Heraeus-Seminar: Nuclear Ground-State Properties of the Lightest Elements: Status and Perspectives, (University of Mainz), Physikzentrum Bad Honnef, Germany, Mar. (2012).

Yamada K., Suda K., Arai S., Fujimaki M., Fujinawa T., Fujisawa H., Fukunishi N., Higurashi Y., Ikezawa E., Imao H., Kamigaito O., Kase M., Komiyama M., Kumagai K., Maie T., Nakagawa T., Ohnishi J., Okuno H., Sakamoto N., Watanabe H., Watanabe T., Watanabe Y., Yamasawa H., Sato Y., and Goto A.: "Beam Commissioning and Operation of New Linac Injector for RIKEN RI Beam Factory", 3rd International Particle Accelerator Conference (IPAC 2012), New Orleans, USA, May (2012).

Suda K., Arai S., Chiba Y., Kamigaito O., Kase M., Sakamoto N., Watanabe Y., and Yamada K.: "Design of Coupler for Direct Coupled Amplifier to Drift Tube Linac Cavities of the Injector RILAC2 for RIKEN RI Beam Factory", 26th International Linear Accelerator Conference (LINAC12), (LINAC12 International Organizing Committee), Tel Aviv, Israel, Sept. (2012).

Schury P. H., Jeong S., Haba H., Kaji D., Koura H., Ito Y., Mita H., Miyatake H., Morimoto K., Morita K., Naimi S., Nakamura S., Okada K., Ozawa A., Sonoda T., Takamine A., Wollnik H., and Wada M.: "A multi-reflection time of flight mass spectrograph for short-lived nuclei and heavy molecules", International Mass Spectrometry Conference, (Kyoto University), Kyoto, Sept. (2012).

Furukawa T., Wakui T., Yang X., Fujita T., Imamura K., Yamaguchi Y., Tetsuka H., Tsutsui Y., Mitsuya Y., Ichikawa Y., Ishibashi Y., Yoshida N., Shirai H., Ebara Y., Hayasaka M., Arai S., Muramoto S., Hatakeyama A., Wada M., Sonoda T., Ito Y., Kobayashi T., Nishimura S., Nishimura M., Kondo Y., Yoneda K., Kubono S., Ohshiro Y., Ueno H., Shinozuka T., Shimoda T., Asahi K., and Matsuo Y.: "A Novel Nuclear Laser Spectroscopy Method using Superfluid Helium for the Measurement of Spins and Moments of Exotic Nuclei", 16th International Conference on Electromagnetic Isotope Separators and Techniques Related to their Applications (EMIS2012), Matsue, Dec. (2012).

Yang X., Furukawa T., Imamura K., Tetsuka H., Yamaguchi Y., Tsutsui Y., Fujita T., Mitsuya Y., Ichikawa Y., Ishibashi Y., Yoshida N., Shirai H., Wakui T., Kobayashi T., Hatakeyama A., Wada M., Ueno H., Shimoda T., Asahi K., and Matsuo Y.: "Control of the stopping position of unstable Rb beam in superfluid helium (He II) for nuclear laser spectroscopy of RI atoms", 16th International Conference on Electromagnetic Isotope Separators and Techniques Related to their Applications (EMIS2012), Matsue, Dec. (2012).

Imamura K., Furukawa T., Wakui T., Yang X., Yamaguchi Y., Tetsuka H., Mitsuya Y., Tsutsui Y., Fujita T., Ebara Y., Hayasaka M., Arai S., Muramoto S., Ichikawa Y., Ishibashi Y., Yoshida N., Shirai H., Hatakeyama A., Wada M., Sonoda T., Ito Y., Odashima H., Kobayashi T., Ueno H., Shimoda T., Asahi K., and Matsuo Y.: "Development of a helium cryostat for laser spectroscopy of atoms with unstable nuclei in superfluid helium", 16th International Conference on Electromagnetic Isotope Separators and Techniques Related to their Applications (EMIS2012), Matsue, Dec. (2012).

Wada M.: "Low Energy RI-Beams: Production and Applications", Korea Particle Accelerator School (KOPAS), (Institute for Basic Science), Sejong, Korea, Dec. (2012).

Naimi S., Nakamura S., Ito Y., Mita H., Okada K., Ozawa A., Takamine A., Wada M., and Wollnik H.: "ESI for mass calibration of MR-TOF mass spectrograph", The 16th International Conference on Electromagnetic Isotope Separators and their Applications (EMIS-2012), (RIKEN, KEK), Matsue, Dec. (2012).

Wada M.: "Geneology of Gas Cells for Low-Energy RI-beams", The 16th International Conference on Electromagnetic Isotope Separators and their Applications (EMIS-2012), Matsue, Dec. (2012).

Schury P. H., Mita H., Sonoda T., Ito Y., Naimi S., Nakamura S., Wollnik H., Wada M., and Takamine A.: "Multi-Reflection Time-of-Flight Mass Spectrograph for Short-Lived and Super-Heavy Nuclei", The 16th International Conference on Electromagnetic Isotope Separators and their Applications (EMIS-2012), (RIKEN, KEK), Matsue, Dec. (2012).

(Domestic Conference)

岩井良夫, 池田時浩, 小島隆夫, 金井保之, 和田道治, 前島一博, 今本尚子, 小林知洋, 萩原清, 成沢忠, Pokhil G. P., 山崎泰規: "蓋つきキャピラリーを用いた理研マイクロビーム細胞照射装置の開発", 日本物理学会, (北海道大学), 北海道, 9 月 (2007).

岡田 邦宏, 安田 和弘, 高柳 俊暢, 和田 道治, 大谷 俊介, Schuessler H. A.: "高周波八重極線形イオントラップにおける新しいタイプのクーロン結晶の生成", 日本物理学会, (北海道大学), 北海道, 9 月 (2007).

岡田邦宏, 高柳俊暢, 和田道治, 大谷俊介, Schuessler H. A.: “高周波八重極線形イオントラップにおけるクーロン結晶の生成と画像観測”, 日本物理学会, (山形大学), 山形, 9 月 (2008).

和田道治: “光学的分光による原子核構造の研究”, エクストリームフォトニクスシンポジウム「光で繋ぐ理研の基礎科学」, 理研, 5 月 (2009).

岡田邦宏, 木村直樹, 菅沼拓也, 高柳俊暢, 和田道治, 大谷俊介, Schuessler H. A.: “極低温イオン−極性分子衝突反応実験のためのクーロン結晶の分子動力学シミュレーション”, 日本物理学会, (大阪府立大学), 大阪, 9 月 (2009).

平山賀一, 今井伸明, 石山博恒, Jeong S., 宮武宇也, 仁木和昭, 岡田雅之, 小柳津充広, 渡辺裕, 和田道治, 高峰愛子: “Spectroscopy around N = 126 nuclei produced by multi-nucleon transfer reaction”, 日本物理学会 (日米合同開催), Hawaii, 10 月 (2009).

Schury P. H., 和田道治, 園田哲, 高峰愛子, 山崎泰規, Wollnik H.: “Status of Multi-Reflection Time-of-Flight Spectrometer for Radio-Isotopes at RIKEN”, 日本物理学会 (日米合同開催), Hawaii, 10 月 (2009).

高峰愛子, 和田道治, 岡田邦宏, 山崎泰規, 金井保之, 小島隆夫, 久保敏幸, 片山一郎, 大谷俊介, Wollnik H., Schuessler H. A.: “Be 同位体の荷電半径と超微細構造定数の測定”, 日本物理学会, (岡山大学), 岡山, 3 月 (2010).

和田道治: “ガスストッパーによる停止低速ビーム活用の現状と展望”, 日本物理学会, (岡山大学), 岡山, 3 月 (2010).

木村直樹, 菅沼拓也, 岡田邦宏, 高柳俊暢, 和田道治, Schuessler H. A.: “レーザー誘起反応により生成した分子イオンのクーロン結晶化の観測”, 日本物理学会, (岡山大学), 岡山, 3 月 (2010).

岡田邦宏, 木村直樹, 菅沼拓也, 高柳俊暢, 和田道治, Schuessler H. A.: “極低温イオン−極性分子衝突反応実験のためのシュタルク速度選別器の開発”, 日本物理学会, (岡山大学), 岡山, 3 月 (2010).

菅原拓也, 木村直樹, 岡田邦宏, 高柳俊暢, 和田道治, Schuessler H. A.: “高周波 6 重極線形イオントラップを用いた円筒形クーロン結晶の観測”, 日本物理学会, (岡山大学), 岡山, 3 月 (2010).

和田道治: “精密光学分光による原子核の研究”, 原子衝突研究協会　第３５回年会, (奈良女子大学), 奈良, 8 月 (2010).

伊藤由太, 和田道治, Schury P. H., 園田哲, 高峰愛子, 岡田邦宏, Wollnik H., Shchepunov V., 小沢顕, 中村聡佑, Christian S.: “Development of MR-TOF Mass spectrograph for short-lived nuclei -II”, 日本物理学会, (九州工業大学), 福岡, 9 月 (2010).

Schury P. H., 和田道治, 伊藤由太, 三田浩希, Naimi S., 中村聡佑, 岡田邦宏, 小沢顕, Viatcheslav S., 園田哲, 高峰愛子, Wollnik H.: “Development of Multi-Reflection Time-of-Flight Mass Spectrograph for short-lived nuclei V”, 日本物理学会, (九州工業大学), 福岡, 9 月 (2010).

Naimi S., 中村聡佑, 和田道治, 伊藤由太, Schury P. H., Wollnik H., 園田哲, 小沢顕, 三田浩希, 高峰愛子, 岡田邦宏: 日本物理学会, (九州工業大学), 福岡, 9 月 (2010).

木村直樹, 椎名皓一, 菅沼拓也, 高柳俊暢, 和田道治, Schuessler H. A., 岡田邦宏: “共同冷却法による CaH+のクーロン結晶化の観測とその生成速度”, 日本物理学会, (大阪府立大学), 大阪, 9 月 (2010).

菅沼拓也, 木村直樹, 高柳俊暢, 和田道治, Schuessler H. A., 岡田邦宏: “極低温イオン−極性分子衝突反応実験のためのシュタルク速度選別器の開発 II”, 日本物理学会, (大阪府立大学), 大阪, 9 月 (2010).

山田一成, 池沢英二, 今尾浩士, 大西純一, 奥野広樹, 加瀬昌之, 上垣外修一, 熊谷桂子, 込山美咲, 後藤彰, 坂本成彦, 須田健嗣, 中川孝秀, 日暮祥英, 福西暢尚, 藤縄雅, 藤巻正樹, 眞家武士, 山澤秀行, 横内茂, 渡邉環, 渡辺博, 渡邉裕, 新井重昭, 藤澤博, 佐藤洋一: “RIBF 用新入射器 RILAC2 のビームコミッショニング”, 第 8 回加速器学会年会, (日本加速器学会), つくば市, 8 月 (2011).

木村直樹, 椎名皓一, 高柳俊暢, 和田道治, Schuessler H. A., 岡田邦宏: “Ca+クーロン結晶と極性分子のレーザー誘起反応の測定”, 日本物理学会, (富山大学), 富山, 9 月 (2011).

古川貴浩, 菅沼拓也, 岡田邦宏, 和田道治, Schuessler H. A.: “シュタルク分子速度フィルターを用いた低速極性分子と Ca+クーロン結晶の反応測定”, 日本物理学会, (富山大学), 富山, 9 月 (2011).

中村聡佑, 和田道治, Schury P. H., 園田哲, 伊藤由太, Naimi S., 三田浩希, 高峰愛子, 小沢顕: “質量校正のための RF カーペットを用いた高効率 ESI の開発”, 日本物理学会, (弘前大学), 青森, 9 月 (2011).

園田哲, 和田道治, 松尾由賀利, 久保敏幸, 富田英生, 坂本知佳, 能任琢真, 篠塚勉, 涌井崇志, 古川武, 伊藤由太, Schuessler H. A., 中村聡佑, 宮武宇也, 今井伸明, 石山博恒, 平山賀一, 渡辺裕, 鄭淳讚, 岡田邦宏, 高峰愛子, Kudryavtsev Y., Huyse M., Van Duppen P.: “ガスセル内レーザー共鳴イオン化法の開発とレーザー核分光への応用”, 日本物理学会, (日本物理学会), 弘前, 9–9 月 (2011).

和田道治: “Direct mass measurements of SHE with MRTOF mass spectrograph”, RIBF ULIC min-WS on Possibility of Direct Mass Measurements of Super Heavy Elements, 理研, 10 月 (2011).

和田道治: “SLOWRI and GARIS -other mass measurements possibilities -”, RIBF-ULIC-Symposium: Physics of Rare-RI Ring, 理研, 11 月 (2011).

古川貴浩, 菅沼拓也, 木村直樹, 和田道治, Schuessler H. A., 岡田邦宏: “低速極性分子と共同冷却分子イオンの反応速度測定”, 日本物理学会, (関西学院大学), 大阪, 3 月 (2012).

伊藤由太, 和田道治, Schury P. H., Naimi S., 園田哲, 高峰愛子, 岡田邦宏, 中村聡佑, 三田浩希, Wollnik H., 小沢顕: 日本物理学会, (京都産業大学), 京都, 9 月 (2012).

Naimi S., 中村聡佑, 和田道治, 伊藤由太, Schury P. H., Wollnik H., 園田哲, 小沢顕, 三田浩希, 高峰愛子, 岡田邦宏: “ElectroSpray ion source for mass calibration of MR-TOF mass spectrograph used in superheavy element mass measurement”, 日本物理学会, (京都産業大学), 京都, 9 月 (2012).

Schury P. H., 和田道治, 伊藤由太, 三田浩希, Naimi S., 中村聡佑, 岡田邦宏, 小沢顕, Viatcheslav S., 園田哲, 高峰愛子, Wollnik H.: “Multi-Reflection Time-of-Flight Mass Spectrograph for Heavy Ion Mass Measurements”, 日本物理学会, (京都産業大学), 京都, 9 月 (2012).

三田浩希, 園田哲, 和田道治, 富田英生, 坂本知佳, 塚卓旦, 能任琢真, 飯村秀紀, Schury P. H., Naimi S., 伊藤由太, Wollnik H.: "理研レーザー共鳴イオン化ガスセルにおける引出効率の改良およびイオンビームのバンチ化テスト", 日本物理学会, (京都産業大学), 京都, 9 月 (2012).

Yang X., 古川武, 今村慧, 手塚博紀, 山口康広, 筒井正機, 藤田朋美, 三津谷洋助, 江原悠太, 早坂美希, 新井信乃, 村本宗将, 市川雄一, 石橋陽子, 吉田直貴, 白井葉月, 涌井崇志, 小林徹, 園田哲, 伊藤由太, 西村俊二, 西村美月, 近藤洋介, 米田健一郎, 久保野茂, 大城幸光, 畠山温, 和田道治, 上野秀樹, 下田 正, 旭 耕一郎, 松尾 由賀利: "Control the stopping position of 84,85Rb in He II for the laser spectroscopy in OROCHI experiment", 日本物理学会第 68 回年次大会, 東広島, 3 月 (2013).

手塚博紀, 涌井崇志, 古川武, Yang X., 今村慧, 山口康広, 筒井正機, 藤田朋美, 三津谷洋助, 早坂美希, 江原悠太, 新井信乃, 村本宗将, 市川雄一, 石橋陽子, 吉田直貴, 白井葉月, 和田道治, 上野秀樹, 下田正, 旭耕一郎, 小林徹, 畠山温, 植松晴子, 松尾由賀利: "超流動 He II 中 RI 原子のレーザー分光 OROCHI における蛍光検出系の高度化", 日本物理学会第 68 回年次大会, 東広島, 3 月 (2013).

Polarized RI Beam Team

Publications

[Journal]

(Original Papers) *Subject to Peer Review

Sakaguchi S., Iseri Y., Uesaka T., Tanifuji M., Amos K., Aoi N., Hashimoto Y., Hiyama E., Ichikawa M., Ichikawa Y., Ishikawa S., Itoh K., Itoh M., Iwasaki H., Karataglidis S., Kawabata T., Kawahara T., Kuboki H., Maeda Y., Matsuo R., Nakao T., Okamura H., Sakai H., Sasamoto Y., Sasano M., Sato Y., Sakaguchi-Sekiguchi K., Shinohara M., Suda K., Suzuki D., Takahashi Y., Tamii A., Wakui T., Yako K., Yamaguchi M., and Yamamoto Y.: "Analyzing power in elastic scattering of 6He from a polarized proton target at 71 MeV/nucleon", Phys. Rev. C **84**, No. 024604, pp. 024604-1–024604-17 (2011). *

Ichikawa Y., Ueno H., Ishii Y., Furukawa T., Yoshimi A., Kameda D., Watanabe H., Aoi N., Asahi K., Balabanski D. L., Chevrier R., Daugas J., Fukuda N., Georgiev G., Hayashi H., Iijima H., Inabe N., Inoue T., Ishihara M., Kubo T., Nanao T., Ohnishi T., Suzuki K., Tsuchiya M., Takeda H., and Rajabali M. M.: "Production of spin-aligned RI beam via two-step fragmentation with dispersion matching", J. Phys.: Conf. Ser. **381**, 012090-1–012090-5 (2012). *

Ichikawa Y., Ueno H., Ishii Y., Furukawa T., Yoshimi A., Kameda D., Watanabe H., Aoi N., Asahi K., Balabanski D. L., Chevrier R., Daugas J., Fukuda N., Georgiev G., Hayashi H., Iijima H., Inabe N., Inoue T., Ishihara M., Kubo T., Nanao T., Ohnishi T., Suzuki K., Tsuchiya M., Takeda H., and Rajabali M. M.: "Production of spin-controlled rare isotope beams", Nat. Phys. **8**, No. 12, pp. 918–922 (2012). *

Yoshimi A., Inoue T., Furukawa T., Nanao T., Suzuki K., Chikamori M., Tsuchiya M., Hayashi H., Uchida M., Hatakeyama N., Kagami S., Ichikawa Y., Miyatake H., and Asahi K.: "Low-frequency nuclear spin oscillator of ^{129}Xe with optical spin detector", Phys. Lett. A **376**, No. 24-25, pp. 1924–1929 (2012). *

Shimada K., Ueno H., Neyens G., Asahi K., Balabanski D. L., Daugas J., Depuydt M., De Rydt M., Gaudefroy L., Grevy S., Hasama Y., Ichikawa Y., Kameda D., Morel P., Nagatomo T., Perrot L., Stodel C., Thomas J., Utsuno Y., Vanderheijden W., Vermeulen N., Vingerhoets P., Yagi E., Yoshida K., and Yoshimi A.: "Erosion of $N = 20$ shell in ^{33}Al investigated through the ground-state electric quadrupole moment", Phys. Lett. B **714**, 246–250 (2012). *

Adachi T., Fujita Y., Bacher A. D., Berg G. P., Black T. C., De Frenne D., Foster ., Fujita H., Fujita K., Hatanaka K., Homma M., Jacobs E., Janecke J., Kanzaki Y., Katori K., Nakanishi K., Negret A., Otsuka T., Popescu L., Roberts D. A., Sakemi Y., Shimbara Y., Shimizu Y., Stephenson E. J., Tameshige Y., Tamii A., Uchida M., Ueno H., Yamanaka T., Yosoi M., and Zell K. O.: "High-resolution study of Gamow-Teller transitions via the ^{54}Fe(^{3}He,t)^{54}Co reaction", Phys. Rev. C **85**, 024308-1–024308-15 (2012). *

Imai N., Hirayama Y., Watanabe Y. X., Teranishi T., Hashimoto T., Hayakawa S., Ichikawa Y., Jeong S., Kahl D., Kubono S., Miyatake H., Ueno H., Yamaguchi H., Yoneda K., and Yoshimi A.: "Isobaric analog resonances of the $N = 21$ nucleus ^{35}Si", Phys. Rev. C **85**, 034313-1–034313-5 (2012). *

Chevrier R., Daugas J., Gaudefroy L., Ichikawa Y., Ueno H., Hass M., Cottenier S., Aoi N., Asahi K., Balabanski D. L., Fukuda N., Furukawa T., Georgiev G., Hayashi H., Iijima H., Inabe N., Inoue T., Ishihara M., Ishii Y., Kameda D., Kubo T., Nanao T., Neyens G., Ohnishi T., Rajabali M. M., Suzuki K., Takeda H., Tsuchiya M., Vermeulen N., Watanabe H., and Yoshimi A.: "Is the $7/21^{-}$ isomer state of ^{43}S spherical?", Phys. Rev. Lett. **108**, 162501-1–162501-5 (2012). *

Inoue T., Nanao T., Chikamori M., Furukawa T., Yoshimi A., Ichikawa Y., Hayashi H., Tsuchiya M., Miyatake H., Ishii Y., Yoshida N., Shirai H., Uchida M., Ueno H., Matsuo Y., Fukuyama T., and Asahi K.: "^{129}Xe atomic EDM search with nuclear spin maser technique", Proceedings of 5th International Workshop on "Fundamental Physics Using Atoms 2011", pp. 64–68 (2012).

Yoshimi A., Nanao T., Inoue T., Furukawa T., Chikamori M., Tsuchiya M., Hayashi H., Miyatake H., Ichikawa Y., Uchida M., Ueno H., and Asahi K.: "Development of high-sensitivity magnetometer for EDM experiment with ^{129}Xe spin ocsillator", Proceedings of 5th International Workshop on "Fundamental Physics Using Atoms 2011", pp. 69–73 (2012).

Oral Presentations

(International Conference etc.)

Ichikawa Y., Ueno H., Ishii Y., Furukawa T., Yoshimi A., Kameda D., Watanabe H., Aoi N., Asahi K., Balabanski D. L., Chevrier R., Daugas J., Fukuda N., Georgiev G., Hayashi H., Iijima H., Inabe N., Inoue T., Ishihara M., Kubo T., Nanao T., Ohnishi T., Suzuki K., Tsuchiya M., Takeda H., and Rajabali M. M.: "Spin-aligned RI beams and nuclear moment measurements at RIBF", RIBF Users Meeting 2012, Wako, Saitama, June (2012).

Ichikawa Y., Ueno H., Ishii Y., Furukawa T., Yoshimi A., Kameda D., Watanabe H., Aoi N., Asahi K., Balabanski D. L., Chevrier R., Daugas J., Fukuda N., Georgiev G., Hayashi H., Iijima H., Inabe N., Inoue T., Ishihara M., Kubo T., Nanao T., Ohnishi T., Suzuki K., Tsuchiya M., Takeda H., and Rajabali M. M.: "Spin manipulation of RI beams from two-stage projectile fragmentation reaction", Advanced Studies Institute on Symmetries and Spin (Spin-Praha-2012), (Charles University), Prague, Czech, July (2012).

Chikamori M., Ichikawa Y., Ohtomo Y., Hikota E., Suzuki

T., Inoue T., Furukawa T., Yoshimi A., Miyatake H., Nanao T., Tsuchiya M., Yoshida N., Shirai H., Ino T., and Asahi K.: "Development of ^{3}He co-magnetometer toward the experiment searching for an atomic EDM in ^{129}Xe", 6th International Workshop on Fundamental Physics Using Atoms 2012, (Tohoku Iniversity), Sendai, Sept. (2012).

Ichikawa Y., Chikamori M., Inoue T., Furukawa T., Yoshimi A., Ohtomo Y., Hikota E., Suzuki T., Suzuki K., Nanao T., Miyatake H., Tsuchiya M., Yoshida N., Shirai H., Ino T., Ueno H., Matsuo Y., Fukuyama T., and Asahi K.: "Experimental study of EDM in ^{129}Xe atom using nuclear-spin maser", 6th International Workshop on Fundamental Physics Using Atoms 2012, (Tohoku Iniversity), Sendai, Sept. (2012).

Ohtomo Y., Ichikawa Y., Chikamori M., Inoue T., Furukawa T., Yoshimi A., Miyatake H., Nanao T., Tsuchiya M., Yoshida N., Shirai H., Hikota E., Suzuki T., Ino T., and Asahi K.: "Production of nuclear-spin polarization and measurement of its relaxation time in ^{129}Xe/^{3}He gas cells", 6th International Workshop on Fundamental Physics Using Atoms 2012, (Tohoku Iniversity), Sendai, Sept. (2012).

Asahi K., Ichikawa Y., Chikamori M., Inoue T., Furukawa T., Yoshimi A., Ohtomo Y., Suzuki K., Nanao T., Miyatake H., Tsuchiya M., Yoshida N., Shirai H., Matsuo Y., Ueno H., and Fukuyama T.: "Experimental search for EDM in a diamagnetic atom ^{129}Xe with spin oscillator technics", Advanced Studies Institute on Symmetries and Spin (Spin-Praha-2012), (Charles University), Prague, Czech, Sept. (2012).

Asahi K., Ichikawa Y., Chikamori M., Inoue T., Furukawa T., Yoshimi A., Ohtomo Y., Suzuki K., Nanao T., Miyatake H., Tsuchiya M., Yoshida N., Shirai H., Matsuo Y., Ueno H., and Fukuyama T.: "Search for Electric Dipole Moment in ^{129}Xe Atom sing a Nuclear Spin Oscillator", The 20th International Symposium on Spin Physics (SPIN2012), (JINR, Dubna, Russia), Dubna, Russia, Sept. (2012).

Ichikawa Y., Ueno H., Ishii Y., Furukawa T., Yoshimi A., Kameda D., Watanabe H., Aoi N., Asahi K., Balabanski D. L., Chevrier R., Daugas J., Fukuda N., Georgiev G., Hayashi H., Iijima H., Inabe N., Inoue T., Ishihara M., Kubo T., Nanao T., Ohnishi T., Suzuki K., Tsuchiya M., Takeda H., and Rajabali M. M.: "Novel method for the production of spin-aligned RI beams in projectile fragmentation with the dispersion matching technique", The 4th Joint Meeting of the 16th International Conference on Hyperfine Interactions and the 20th International Symposium on Nuclear Quadrupole Interactions (HFI/NQI 2012), (China Institute of Atomic Energy), Beijing, China, Sept. (2012).

Inoue T., Furukawa T., Yoshimi A., Ichikawa Y., Chikamori M., Ohtomo Y., Tsuchiya M., Yoshida N., Shirai H., Uchida M., Suzuki K., Nanao T., Miyatake H., Ueno H., Matsuo Y., Fukuyama T., and Asahi K.: "Nuclear spin maser and experimental search for ^{129}Xe atomic EDM", The 4th Joint Meeting of the 16th International Conference on Hyperfine Interactions and the 20th International Symposium on Nuclear Quadrupole Interactions (HFI/NQI 2012), (China Institute of Atomic Energy), Beijing, China, Sept. (2012).

Furukawa T., Wakui T., Yang X., Fujita T., Imamura K., Yamaguchi Y., Tetsuka H., Tsutsui Y., Mitsuya Y., Ichikawa Y., Ishibashi Y., Yoshida N., Shirai H., Ebara Y., Hayasaka M., Arai S., Muramoto S., Hatakeyama A., Wada M., Sonoda T., Ito Y., Kobayashi T., Nishimura S., Nishimura M., Kondo Y., Yoneda K., Kubono S., Ohshiro Y., Ueno H., Shinozuka T., Shimoda T., Asahi K., and Matsuo Y.: "A Novel Nuclear Laser Spectroscopy Method using Superfluid Helium for the Measurement of Spins and Moments of Exotic Nuclei", 16th International Conference on Electromagnetic Isotope Separators and Techniques Related to their Applications (EMIS2012), Matsue, Dec. (2012).

Yang X., Furukawa T., Imamura K., Tetsuka H., Yamaguchi Y., Tsutsui Y., Fujita T., Mitsuya Y., Ichikawa Y., Ishibashi Y., Yoshida N., Shirai H., Wakui T., Kobayashi T., Hatakeyama A., Wada M., Ueno H., Shimoda T., Asahi K., and Matsuo Y.: "Control of the stopping position of unstable Rb beam in superfluid helium (He II) for nuclear laser spectroscopy of RI atoms", 16th International Conference on Electromagnetic Isotope Separators and Techniques Related to their Applications (EMIS2012), Matsue, Dec. (2012).

Imamura K., Furukawa T., Wakui T., Yang X., Yamaguchi Y., Tetsuka H., Mitsuya Y., Tsutsui Y., Fujita T., Ebara Y., Hayasaka M., Arai S., Muramoto S., Ichikawa Y., Ishibashi Y., Yoshida N., Shirai H., Hatakeyama A., Wada M., Sonoda T., Ito Y., Odashima H., Kobayashi T., Ueno H., Shimoda T., Asahi K., and Matsuo Y.: "Development of a helium cryostat for laser spectroscopy of atoms with unstable nuclei in superfluid helium", 16th International Conference on Electromagnetic Isotope Separators and Techniques Related to their Applications (EMIS2012), Matsue, Dec. (2012).

Ichikawa Y., Ueno H., Ishii Y., Furukawa T., Yoshimi A., Kameda D., Watanabe H., Aoi N., Asahi K., Balabanski D. L., Chevrier R., Daugas J., Fukuda N., Georgiev G., Hayashi H., Iijima H., Inabe N., Inoue T., Ishihara M., Kubo T., Nanao T., Ohnishi T., Suzuki K., Tsuchiya M., Takeda H., and Rajabali M. M.: "Spin-aligned RI beams via two-step fragmentation reactions", 16th International Conference on Electromagnetic Isotope Separators and Techniques Related to their Applications (EMIS2012), (RIKEN Nishina Center, KEK, Institute of Modern Physics (China)), Matsue, Dec. (2012).

Nagae D., Abe Y., Okada S., Ozawa A., Yamaguchi T., Suzuki H., Moriguchi T., Ishibashi Y., Fukuoka S., Nishikiori R., Suzuki T., Suzaki F., Yamaguchi Y., Uesaka T., and Wakasugi M.: "Time-of-flight detector applied to mass measurements in Rare-RI Ring", 6th International Conference on Electromagnetic Isotope Separators and Techniques Related to their Applications (EMIS2012), (RIKEN KEK IMP), Matsue, Dec. (2012).

Yoshida N., Ueno H., Yoshimi A., Ishibashi Y., Ichikawa Y., Abe Y., Asahi K., Chikamori M., Fujita T., Furukawa T., Hikota E., Nagae D., Ohtomo Y., Saito Y., Shirai H., Suzuki T., and Yang X.: "Development of a new device control system for β-NMR experiments", The 16th IUPAP International Conference on Electromagnetic Isotope Separators and Techniques Related to Their Applications (EMIS2012), Matsue, Dec. (2012).

Ishibashi Y., Yoshida N., Ueno H., Yoshimi A., Ichikawa Y., Abe Y., Asahi K., Chikamori M., Fujita T., Furukawa T., Hikota E., Nagae D., Ohtomo Y., Saito Y., Shirai H., Suzuki T., Yang X., and Sakamoto N.: "Development of an adiabatic field rotation system to measure spin polarization of unstable nuclei", The 16th IUPAP International Conference on Electromagnetic Isotope Separators and Techniques Related to Their Applications (EMIS2012), Matsue, Dec. (2012).

Chikamori M., Ichikawa Y., Ohtomo Y., Hikota E., Sakamoto Y., Suzuki T., Bidinosti C. P., Inoue T., Furukawa T., Yoshimi A., Suzuki K., Nanao T., Miyatake H., Tsuchiya M., Yoshida N., Shirai H., Ino T., Ueno H., Matsuo Y., Fukuyama T., and Asahi K.: "^{3}He comagnetometer in ^{129}Xe active spin maser for EDM measurement", Program on CP violation in Elementary Particles and Composite Systems, (International CEntre for Theoretical Sciences), Mahabaleshwar, India, Feb. (2013).

Ichikawa Y., Chikamori M., Ohtomo Y., Hikota E., Sakamoto Y., Suzuki T., Bidinosti C. P., Inoue T., Furukawa T., Yoshimi A., Suzuki K., Nanao T., Miyatake H., Tsuchiya M., Yoshida N., Shirai H., Ino T., Ueno H., Matsuo Y., Fukuyama T., and Asahi K.: "Experimental search for atomic EDM in ^{129}Xe at Tokyo Tech.", Program on CP violation in Elementary Particles and Composite Systems, (International CEntre for Theoretical Sciences), Mahabaleshwar, India, Feb. (2013).

(Domestic Conference)

近森正敏, 市川雄一, 大友祐一, 井上壮志, 古川武, 吉見彰洋, 土屋真人, 吉田直貴, 白井葉月, 猪野隆, 内田誠, 旭耕一郎: "^{129}Xe 原子 EDM 測定に向けた ^{3}He 共存磁力計の開発", 第 9 回原子・分子・光科学（AMO）討論会, 和光, 6 月 (2012).

近森正敏, 市川雄一, 井上壮志, 古川武, 吉見彰洋, 大友祐一, 土屋真人, 吉田直貴, 白井葉月, 猪野隆, 内田誠, 旭耕一郎: "^{129}Xe 原子 EDM 測定にむけた ^{3}He 共存磁力計の開発", 日本物理学会 2012 年秋季大会, (京都産業大学), 京都, 9 月 (2012).

市川雄一, 近森正敏, 井上壮志, 古川武, 吉見彰洋, 大友祐一, 土屋真人, 吉田直貴, 白井葉月, 猪野隆, 内田誠, 旭耕一郎: "^{3}He 共存磁力計を導入した ^{129}Xe 核スピンメーザーによる EDM 測定系の開発", 日本物理学会 2012 年秋季大会, (京都産業大学), 京都, 9 月 (2012).

大友祐一, 近森正敏, 市川雄一, 井上壮志, 古川武, 吉見彰洋, 土屋真人, 吉田直貴, 白井葉月, 猪野隆, 内田誠, 旭耕一郎: "^{3}He 共存磁力計の導入に向けた ^{3}He の核スピン偏極生成とその緩和時間測定", 日本物理学会 2012 年秋季大会, (京都産業大学), 京都, 9 月 (2012).

大友祐一, 市川雄一, 近森正敏, 彦田絵里, 鈴木貴大, Bidinosti C. P., 井上壮志, 古川武, 吉見彰洋, 鈴木都文, 七尾翼, 宮武裕和, 土屋真人, 吉田直貴, 白井葉月, 猪野隆, 松尾由賀利, 上野秀樹, 福山武志, 旭耕一郎: 中性子物理研究会, (名古屋大学), 名古屋, 11 月 (2012).

坂本雄, Bidinosti C. P., 市川雄一, 近森正敏, 大友祐一, 彦田絵里, 鈴木貴大, 井上壮志, 古川武, 吉見彰洋, 鈴木都文, 七尾翼, 宮武裕和, 土屋真人, 吉田直貴, 白井葉月, 猪野隆, 上野秀樹, 松尾由賀利, 福山武志, 旭耕一郎: "EDM 測定に向けた改良型磁場安定化システムの構築と性能評価", 日本物理学会第 68 回年次大会, (広島大学), 広島, 3 月 (2013).

近森正敏, 市川雄一, 大友祐一, 彦田絵里, 坂本雄, 鈴木貴大, Bidinosti C. P., 井上壮志, 古川武, 吉見彰洋, 鈴木都文, 七尾翼, 宮武裕和, 土屋真人, 吉田直貴, 白井葉月, 猪野隆, 上野秀樹, 松尾由賀利, 福山武志, 旭耕一郎: "^{3}He 共存磁力計の導入による ^{129}Xe 原子 EDM 測定実験", 日本物理学会第 68 回年次大会, (広島大学), 広島, 3 月 (2013).

鈴木貴大, 市川雄一, 近森正敏, 大友祐一, 彦田絵里, 坂本雄, Bidinosti C. P., 井上壮志, 古川武, 吉見彰洋, 鈴木都文, 七尾翼, 宮武裕和, 土屋真人, 吉田直貴, 白井葉月, 猪野隆, 上野秀樹, 松尾由賀利, 福山武志, 旭耕一郎: "^{129}Xe 原子 EDM 測定実験のための電場印加システム開発", 日本物理学会第 68 回年次大会, (広島大学), 広島, 3 月 (2013).

彦田絵里, 近森正敏, 市川雄一, 大友祐一, 坂本雄, 鈴木貴大, Bidinosti C. P., 井上壮志, 古川武, 吉見彰洋, 鈴木都文, 七尾翼, 宮武裕和, 土屋真人, 吉田直貴, 白井葉月, 猪野隆, 上野秀樹, 松尾由賀利, 福山武志, 旭耕一郎: "ダブルセルを用いた核スピンメーザー発振", 日本物理学会第 68 回年次大会, (広島大学), 広島, 3 月 (2013).

市川雄一, 近森正敏, 大友祐一, 彦田絵里, 坂本雄, 鈴木貴大, Bidinosti C. P., 井上壮志, 古川武, 吉見彰洋, 鈴木都文, 七尾翼, 宮武裕和, 土屋真人, 吉田直貴, 白井葉月, 猪野隆, 上野秀樹, 松尾由賀利, 福山武志, 旭耕一郎: "^{129}Xe 原子 EDM 測定実験のための ^{3}He 共存磁力計の性能評価", 日本物理学会第 68 回年次大会, (広島大学), 広島, 3 月 (2013).

大友祐一, 市川雄一, 近森正敏, 彦田絵里, 坂本雄, 鈴木貴大, Bidinosti C. P., 井上壮志, 古川武, 吉見彰洋, 鈴木都文, 七尾翼, 宮武裕和, 土屋真人, 吉田直貴, 白井葉月, 猪野隆, 上野秀樹, 松尾由賀利, 福山武志, 旭耕一郎: "^{129}Xe/^{3}He 共存セルの偏極生成及び緩和機構", 日本物理学会第 68 回年次大会, (広島大学), 広島, 3 月 (2013).

石橋陽子, 吉田直貴, 上野秀樹, 吉見彰洋, 市川雄一, 阿部康志, 旭耕一郎, 近森正敏, 藤田朋美, 古川武, 彦田絵里, 長江大輔, 大友祐一, 齋藤佑多, 白井葉月, 鈴木貴大, Yang X., 坂本成彦: "不安定核偏極度測定のための永久磁石を用いた断熱磁場回転装置の開発", 日本物理学会第 68 回年次大会, (日本物理学会), 東広島, 3 月 (2013).

Yang X., 古川武, 今村慧, 手塚博紀, 山口康広, 筒井正機, 藤田朋美, 三津谷洋助, 江原悠太, 早坂美希, 新井信乃, 村本宗将, 市川雄一, 石橋陽子, 吉田直貴, 白井葉月, 涌井崇志, 小林徹, 園田哲, 伊藤由太, 西村俊二, 西村美月, 近藤洋介, 米田健一郎, 久保野茂, 大城幸光, 畠山温, 和田道治, 上野秀樹, 下田正, 旭耕一郎, 松尾由賀利: "Control the stopping position of 84,85Rb in He II for the laser spectroscopy in OROCHI experiment", 日本物理学会第 68 回年次大会, 東広島, 3 月 (2013).

手塚博紀, 涌井崇志, 古川武, Yang X., 今村慧, 山口康広, 筒井正機, 藤田朋美, 三津谷洋助, 早坂美希, 江原悠太, 新井信乃, 村本宗将, 市川雄一, 石橋陽子, 吉田直貴, 白井葉月, 和田道治, 上野秀樹, 下田正, 旭耕一郎, 小林徹, 畠山温, 植松晴子, 松尾由賀利: "超流動 He II 中 RI 原子のレーザー分光 OROCHI における蛍光検出系の高度化", 日本物理学会第 68 回年次大会, 東広島, 3 月 (2013).

江原悠太, 三津谷洋助, 古川武, 今村慧, 筒井正機, 手塚博紀, 山口康広, Yang X., 加藤裕樹, 畠山温, 小林徹, 植松晴子, 松尾由賀利: "超流動 He 環境における Ga 原子の励起スペクトル測定", 日本物理学会第 68 回年次大会, 東広島, 3 月 (2013).

今村慧, 古川武, Yang X., 山口康広, 手塚博紀, 筒井正機, 三津谷洋助, 小林徹, 畠山温, 小田島仁司, 松尾由賀利: "超流動ヘリウム環境おける Cs 原子の超微細構造間隔精密測定", 日本物理学会第 68 回年次大会, 東広島, 3 月 (2013).

三津谷洋助, 古川武, 小林徹, Yang X., 加藤裕樹, 今村慧, 江原悠太, 山口康広, 手塚博紀, 筒井正機, 小田島仁司, 松尾由賀利: "超流動ヘリウム環境での 1 族、および 13 族原子の励起スペクトル", 日本物理学会第 68 回年次大会, 東広島, 3 月 (2013).

Rare RI-ring Team

Publications

[Journal]

(Original Papers) *Subject to Peer Review

Ichikawa Y., Ueno H., Ishii Y., Furukawa T., Yoshimi A., Kameda D., Watanabe H., Aoi N., Asahi K., Balabanski D. L., Chevrier R., Daugas J., Fukuda N., Georgiev G., Hayashi H., Iijima H., Inabe N., Inoue T., Ishihara M., Kubo T., Nanao T., Ohnishi T., Suzuki K., Tsuchiya M., Takeda H., and Rajabali M. M.: "Production of spin-aligned RI beam via two-step fragmentation with dispersion matching", J. Phys.: Conf. Ser. **381**, 012090-1–012090-5 (2012). *

Ichikawa Y., Ueno H., Ishii Y., Furukawa T., Yoshimi A., Kameda D., Watanabe H., Aoi N., Asahi K., Balabanski D. L., Chevrier R., Daugas J., Fukuda N., Georgiev G., Hayashi H., Iijima H., Inabe N., Inoue T., Ishihara M., Kubo T., Nanao T., Ohnishi T., Suzuki K., Tsuchiya M., Takeda H., and Rajabali M. M.: "Production of spin-controlled rare isotope beams", Nat. Phys. **8**, No. 12, pp. 918–922 (2012). *

[Book · Proceedings]

(Others)

Yamaguchi Y., Wakasugi M., Suzuki H., Fujinawa T., Uesaka T., Yano Y., Ozawa A., Nagae D., Yamaguchi T., Suzuki T., Kikuchi T., Jiang W., Sasaki T., and Tokuchi A.: "Present status of Rare-RI Ring project in RIKEN RI Beam Factory", Proceedings of Science (PoS), Frascati, Italy, 2011–10, SISSA, Fascati, p. 070 (2012).

Oral Presentations

(International Conference etc.)

Ichikawa Y., Ueno H., Ishii Y., Furukawa T., Yoshimi A., Kameda D., Watanabe H., Aoi N., Asahi K., Balabanski D. L., Chevrier R., Daugas J., Fukuda N., Georgiev G., Hayashi H., Iijima H., Inabe N., Inoue T., Ishihara M., Kubo T., Nanao T., Ohnishi T., Suzuki K., Tsuchiya M., Takeda H., and Rajabali M. M.: "Spin-aligned RI beams and nuclear moment measurements at RIBF", RIBF Users Meeting 2012, Wako, Saitama, June (2012).

Ichikawa Y., Ueno H., Ishii Y., Furukawa T., Yoshimi A., Kameda D., Watanabe H., Aoi N., Asahi K., Balabanski D. L., Chevrier R., Daugas J., Fukuda N., Georgiev G., Hayashi H., Iijima H., Inabe N., Inoue T., Ishihara M., Kubo T., Nanao T., Ohnishi T., Suzuki K., Tsuchiya M., Takeda H., and Rajabali M. M.: "Spin manipulation of RI beams from two-stage projectile fragmentation reaction", Advanced Studies Institute on Symmetries and Spin (Spin-Praha-2012), (Charles University), Prague, Czech, July (2012).

Ichikawa Y., Ueno H., Ishii Y., Furukawa T., Yoshimi A., Kameda D., Watanabe H., Aoi N., Asahi K., Balabanski D. L., Chevrier R., Daugas J., Fukuda N., Georgiev G., Hayashi H., Iijima H., Inabe N., Inoue T., Ishihara M., Kubo T., Nanao T., Ohnishi T., Suzuki K., Tsuchiya M., Takeda H., and Rajabali M. M.: "Novel method for the production of spin-aligned RI beams in projectile fragmentation with the dispersion matching technique", The 4th Joint Meeting of the 16th International Conference on Hyperfine Interactions and the 20th International Symposium on Nuclear Quadrupole Interactions (HFI/NQI 2012), (China Institute of Atomic Energy), Beijing, China, Sept. (2012).

Yamaguchi T.: "Detector developments for storage ring experiments", TSR-ISOLDE Workshop, (CERN), Meyrin, Switzerland, Oct. (2012).

Yamaguchi Y., Wakasugi M., Ozawa A., Uesaka T., Yano Y., Fujinawa T., Fukunishi N., Inabe N., Kamigaito O., Kase M., Kikuchi T., Komiyama M., Kubo T., Kumagai K., Maie T., Ohnishi J., Tokuchi A., Yoshida K., Yamaguchi T., Nagae D., Zenihiro J., Suzuki T., Abe Y., and Suzaki F.: "Construction of Rare-RI Ring at RIKEN RI Beam Factory", 16th International Conference on Electromagnetic Isotope Separators and Techniques Related to their Applications (EMIS2012), (RIKEN KEK IMP), Matsue, Dec. (2012).

Suzaki F., Zenihiro J., Yamaguchi T., Ozawa A., Uesaka T., Wakasugi M., Yamada K., and Yamaguchi Y.: "Design study of a resonant Schottky pick-up for Rare-RI Ring project", 16th International Conference on Electromagnetic Isotope Separators and Techniques Related to their Applications (EMIS2012), (RIKEN KEK IMP), Matsue, Dec. (2012).

Ichikawa Y., Ueno H., Ishii Y., Furukawa T., Yoshimi A., Kameda D., Watanabe H., Aoi N., Asahi K., Balabanski D. L., Chevrier R., Daugas J., Fukuda N., Georgiev G., Hayashi H., Iijima H., Inabe N., Inoue T., Ishihara M., Kubo T., Nanao T., Ohnishi T., Suzuki K., Tsuchiya M., Takeda H., and Rajabali M. M.: "Spin-aligned RI beams via two-step fragmentation reactions", 16th International Conference on Electromagnetic Isotope Separators and Techniques Related to their Applications (EMIS2012), (RIKEN Nishina Center, KEK, Institute of Modern Physics (China)), Matsue, Dec. (2012).

Nagae D., Abe Y., Okada S., Ozawa A., Yamaguchi T., Suzuki H., Moriguchi T., Ishibashi Y., Fukuoka S., Nishikiori R., Suzuki T., Suzaki F., Yamaguchi Y., Uesaka T., and Wakasugi M.: "Time-of-flight detector applied to mass measurements in Rare-RI Ring", 6th International Conference on Electromagnetic Isotope Separators and Techniques Related to their Applications (EMIS2012), (RIKEN KEK IMP), Matsue, Dec. (2012).

Yoshida N., Ueno H., Yoshimi A., Ishibashi Y., Ichikawa Y., Abe Y., Asahi K., Chikamori M., Fujita T., Furukawa T., Hikota E., Nagae D., Ohtomo Y., Saito Y., Shirai H., Suzuki T., and Yang X.: "Development of a new device control system for β-NMR experiments", The 16th IUPAP International Conference on Electromagnetic Isotope Separators and Techniques Related to

Their Applications (EMIS2012), Matsue, Dec. (2012).

Ishibashi Y., Yoshida N., Ueno H., Yoshimi A., Ichikawa Y., Abe Y., Asahi K., Chikamori M., Fujita T., Furukawa T., Hikota E., Nagae D., Ohtomo Y., Saito Y., Shirai H., Suzuki T., Yang X., and Sakamoto N.: "Development of an adiabatic field rotation system to measure spin polarization of unstable nuclei", The 16th IUPAP International Conference on Electromagnetic Isotope Separators and Techniques Related to Their Applications (EMIS2012), Matsue, Dec. (2012).

(Domestic Conference)

加治大哉, 住田貴之, 刈屋佳樹, 鹿取謙二, 工藤祐生, 森田浩介, 森谷透, 村上昌史, 武山美麗, 田中謙伍, 戸田光祐, 門叶冬樹, 若林泰生, 山木さやか, 米田晃, 大関和貴, 長谷部裕雄, 羽場宏光, 吉田敦, 山口貴之: "208Pb+70Zn 反応を用いた 277Cn の生成と壊変特性", 2012 日本放射化学会年会・第 56 回放射化学討論会, (日本放射化学会), 東京工業大学, 10–10 月 (2012).

石橋陽子, 吉田直貴, 上野秀樹, 吉見彰洋, 市川雄一, 阿部康志, 旭耕一郎, 近森正敏, 藤田朋美, 古川武, 彦田絵里, 長江大輔, 大友祐一, 齋藤佑多, 白井葉月, 鈴木貴大, Yang X., 坂本成彦: "不安定核偏極度測定のための永久磁石を用いた断熱磁場回転装置の開発", 日本物理学会第 68 回年次大会, (日本物理学会), 東広島, 3 月 (2013).

SCRIT Team

Publications

[Journal]

(Original Papers) *Subject to Peer Review

Morimoto K., Morita K., Kaji D., Haba H., Katori K., Koura H., Ohnishi T., Ozawa A., Suda T., Sueki K., Tanihata I., Tokanai F., Yoneda A., and Yoshida A.: "Status of super heavy element research using GARIS at RIKEN", Nucl. Phys. A **738**, 129 (2004). *

Ichikawa Y., Ueno H., Ishii Y., Furukawa T., Yoshimi A., Kameda D., Watanabe H., Aoi N., Asahi K., Balabanski D. L., Chevrier R., Daugas J., Fukuda N., Georgiev G., Hayashi H., Iijima H., Inabe N., Inoue T., Ishihara M., Kubo T., Nanao T., Ohnishi T., Suzuki K., Tsuchiya M., Takeda H., and Rajabali M. M.: "Production of spin-aligned RI beam via two-step fragmentation with dispersion matching", J. Phys.: Conf. Ser. **381**, 012090-1–012090-5 (2012). *

Ichikawa Y., Ueno H., Ishii Y., Furukawa T., Yoshimi A., Kameda D., Watanabe H., Aoi N., Asahi K., Balabanski D. L., Chevrier R., Daugas J., Fukuda N., Georgiev G., Hayashi H., Iijima H., Inabe N., Inoue T., Ishihara M., Kubo T., Nanao T., Ohnishi T., Suzuki K., Tsuchiya M., Takeda H., and Rajabali M. M.: "Production of spin-controlled rare isotope beams", Nat. Phys. **8**, No. 12, pp. 918–922 (2012). *

Adachi T., Fujita Y., Bacher A. D., Berg G. P., Black T. C., De Frenne D., Foster ., Fujita H., Fujita K., Hatanaka K., Homma M., Jacobs E., Janecke J., Kanzaki Y., Katori K., Nakanishi K., Negret A., Otsuka T., Popescu L., Roberts D. A., Sakemi Y., Shimbara Y., Shimizu Y., Stephenson E. J., Tameshige Y., Tamii A., Uchida M., Ueno H., Yamanaka T., Yosoi M., and Zell K. O.: "High-resolution study of Gamow-Teller transitions via the ^{54}Fe(^{3}He,t)^{54}Co reaction", Phys. Rev. C **85**, 024308-1–024308-15 (2012). *

Chevrier R., Daugas J., Gaudefroy L., Ichikawa Y., Ueno H., Hass M., Cottenier S., Aoi N., Asahi K., Balabanski D. L., Fukuda N., Furukawa T., Georgiev G., Hayashi H., Iijima H., Inabe N., Inoue T., Ishihara M., Ishii Y., Kameda D., Kubo T., Nanao T., Neyens G., Ohnishi T., Rajabali M. M., Suzuki K., Takeda H., Tsuchiya M., Vermeulen N., Watanabe H., and Yoshimi A.: "Is the $7/21^{-}$ isomer state of ^{43}S spherical?", Phys. Rev. Lett. **108**, 162501-1–162501-5 (2012). *

Oral Presentations

(International Conference etc.)

Ichikawa Y., Ueno H., Ishii Y., Furukawa T., Yoshimi A., Kameda D., Watanabe H., Aoi N., Asahi K., Balabanski D. L., Chevrier R., Daugas J., Fukuda N., Georgiev G., Hayashi H., Iijima H., Inabe N., Inoue T., Ishihara M., Kubo T., Nanao T., Ohnishi T., Suzuki K., Tsuchiya M., Takeda H., and Rajabali M. M.: "Spin-aligned RI beams and nuclear moment measurements at RIBF", RIBF Users Meeting 2012, Wako, Saitama, June (2012).

Ichikawa Y., Ueno H., Ishii Y., Furukawa T., Yoshimi A., Kameda D., Watanabe H., Aoi N., Asahi K., Balabanski D. L., Chevrier R., Daugas J., Fukuda N., Georgiev G., Hayashi H., Iijima H., Inabe N., Inoue T., Ishihara M., Kubo T., Nanao T., Ohnishi T., Suzuki K., Tsuchiya M., Takeda H., and Rajabali M. M.: "Spin manipulation of RI beams from two-stage projectile fragmentation reaction", Advanced Studies Institute on Symmetries and Spin (Spin-Praha-2012), (Charles University), Prague, Czech, July (2012).

Ichikawa Y., Ueno H., Ishii Y., Furukawa T., Yoshimi A., Kameda D., Watanabe H., Aoi N., Asahi K., Balabanski D. L., Chevrier R., Daugas J., Fukuda N., Georgiev G., Hayashi H., Iijima H., Inabe N., Inoue T., Ishihara M., Kubo T., Nanao T., Ohnishi T., Suzuki K., Tsuchiya M., Takeda H., and Rajabali M. M.: "Novel method for the production of spin-aligned RI beams in projectile fragmentation with the dispersion matching technique", The 4th Joint Meeting of the 16th International Conference on Hyperfine Interactions and the 20th International Symposium on Nuclear Quadrupole Interactions (HFI/NQI 2012), (China Institute of Atomic Energy), Beijing, China, Sept. (2012).

Ichikawa Y., Ueno H., Ishii Y., Furukawa T., Yoshimi A., Kameda D., Watanabe H., Aoi N., Asahi K., Balabanski D. L., Chevrier R., Daugas J., Fukuda N., Georgiev G., Hayashi H., Iijima H., Inabe N., Inoue T., Ishihara M., Kubo T., Nanao T., Ohnishi T., Suzuki K., Tsuchiya M., Takeda H., and Rajabali M. M.: "Spin-aligned RI beams via two-step fragmentation reactions", 16th International Conference on Electromagnetic Isotope Separators and Techniques Related to their Applications (EMIS2012), (RIKEN Nishina Center, KEK, Institute of Modern Physics (China)), Matsue, Dec. (2012).

(Domestic Conference)

加治大哉, 森田浩介, 森本幸司, 米田晃, 須田利美, 吉田敦, 大西哲哉, 羽場宏光, 末木啓介, 鹿取謙二, 谷畑勇夫: "超重元素探索へ向けた理研ー気体充填型反跳分離装置の性能評価", 日本物理学会, (立教大学), 東京, 9 月 (2002).

加治大哉, 森田浩介, 森本幸司, 米田晃, 須田利美, 吉田敦, 大西哲哉, 羽場宏光, 末木啓介, 鹿取謙二, 谷畑勇夫: "超重元素探索へ向けた理研ー気体充填型反跳分離装置の性能評価", 放射化学討論会, (北海道大学), 北海道, 9 月 (2002).

加治大哉, 森田浩介, 森本幸司, 羽場宏光, 鹿取謙二, 小浦寛之, 大西哲哉, 小沢顕, 須田利美, 末木啓介, 谷畑勇夫, 米田晃, 吉田敦: "ヘリウムガス中における (超) 重元素の平衡電荷", 日本物理学会, (宮崎大学), 宮崎, 9 月 (2003).

加治大哉, 森田浩介, 森本幸司, 羽場宏光, 鹿取謙二, 小浦寛之, 大西哲哉, 小沢顕, 須田利美, 末木啓介, 谷畑勇夫, 米田晃, 吉田敦: "ヘリウムガス中における重い反跳原子の平衡電荷ー理研における Z=111 番元素探索ー", 放射化学討論会, (京都大学原子炉実験施設), 大阪, 10 月 (2003).

加治大哉, 森田浩介, 森本幸司, 羽場宏光, 小浦寛之, 大西

哲哉, 小沢顕, 須田利美, 末木啓介, 山口貴之, 米田晃, 吉田敦: “209Bi+70Zn 反応を用いた 113 番元素探索”, 日本化学会, (神奈川大学), 神奈川, 3 月 (2005).

加治大哉, 森田浩介, 森本幸司, 羽場宏光, 小浦寛之, 大西哲哉, 小沢顕, 須田利美, 末木啓介, 山口貴之, 米田晃, 吉田敦: “209Bi(70Zn,n)278113 反応を用いた 113 番元素の合成”, 放射化学討論会, (金沢大学), 金沢, 9 月 (2005).

Research Instruments Group

Publications

[Journal]

(Original Papers) *Subject to Peer Review

Okada K., Wada M., Nakamura T., Takamine A., Lioubimov V., Schury P. H., Ishida Y., Sonoda T., Ogawa M., Yamazaki Y., Kanai Y., Kojima T., Yoshida A., Kubo T., Katayama I., Ohtani S., Wollnik H., and Schuessler H. A.: "A precision measurement of the hyperfine structure of laser-cooled $^{7}Be^{+}$ ions priduced by projectile fragmentation", Phys. Rev. Lett. **101**, No. 212502, pp. 212502-1–212502-4 (2008). *

Ichikawa Y., Ueno H., Ishii Y., Furukawa T., Yoshimi A., Kameda D., Watanabe H., Aoi N., Asahi K., Balabanski D. L., Chevrier R., Daugas J., Fukuda N., Georgiev G., Hayashi H., Iijima H., Inabe N., Inoue T., Ishihara M., Kubo T., Nanao T., Ohnishi T., Suzuki K., Tsuchiya M., Takeda H., and Rajabali M. M.: "Production of spin-aligned RI beam via two-step fragmentation with dispersion matching", J. Phys.: Conf. Ser. **381**, 012090-1–012090-5 (2012). *

Ichikawa Y., Ueno H., Ishii Y., Furukawa T., Yoshimi A., Kameda D., Watanabe H., Aoi N., Asahi K., Balabanski D. L., Chevrier R., Daugas J., Fukuda N., Georgiev G., Hayashi H., Iijima H., Inabe N., Inoue T., Ishihara M., Kubo T., Nanao T., Ohnishi T., Suzuki K., Tsuchiya M., Takeda H., and Rajabali M. M.: "Production of spin-controlled rare isotope beams", Nat. Phys. **8**, No. 12, pp. 918–922 (2012). *

Sonoda T., Wada M., Tomita H., Sakamoto C., Takatsuka T., Furukawa T., Iimura H., Ito Y., Kubo T., Matsuo Y., Mita H., Naimi S., Nakamura S., Noto T., Schury P. H., Wakui T., Miyatake H., Jeong S., Watanabe Y., Isiyama H., Okada K., and Takamine A.: "Development of a resonant laser ionization gas cell for high-energy, short-lived nuclei", Nucl. Instrum. Methods Phys. Res. B **295**, No. 1, (2012). *

Chevrier R., Daugas J., Gaudefroy L., Ichikawa Y., Ueno H., Hass M., Cottenier S., Aoi N., Asahi K., Balabanski D. L., Fukuda N., Furukawa T., Georgiev G., Hayashi H., Iijima H., Inabe N., Inoue T., Ishihara M., Ishii Y., Kameda D., Kubo T., Nanao T., Neyens G., Ohnishi T., Rajabali M. M., Suzuki K., Takeda H., Tsuchiya M., Vermeulen N., Watanabe H., and Yoshimi A.: "Is the $7/21^{-}$ isomer state of ^{43}S spherical?", Phys. Rev. Lett. **108**, 162501-1–162501-5 (2012). *

Sato H., Kubo T., Yano Y., Kusaka K., Ohnishi J., Yoneda K., Shimizu Y., Motobayashi T., Otsu H., Isobe T., Kobayashi T., Sekiguchi K., Nakamura T., Kondo Y., Togano Y., Murakami T., Tsuchihashi T., Orikasa T., and Maeta K.: "Superconducting dipole magnet for SAMURAI spectrometer", IEEE Trans. Appl. Supercond. **23**, No. 3, pp. 4500308-1–4500308-8 (2013). *

[Book · Proceedings]

(Original Papers) *Subject to Peer Review

Tanaka K., Inabe N., Ohnishi T., and Kubo T.: "Radiation Transport Calculation Using PHITS Code for the Activation of BigRIPS Separator at RIKEN Radioactive Isotope Beam Factory and Comparison with the Measurement", PROGRESS IN NUCLEAR SCIENCE TECHNOLOGY volume 2, Tokyo, 2010–10, Atomic Energy Society of Japan, Tokyo, pp. 955–959 (2011). *

Oral Presentations

(International Conference etc.)

Sonoda T., Wada M., Tomita H., Sakamoto C., Ito Y., Schuessler H. A., Takamine A., Kubo T., Matsuo Y., Shinozuka T., Wakui T., Nakamura S., Furukawa T., Okada K., Kudryavtsev Y., Mark H., Van Duppen P., Miyatake H., Ishiyama H., Imai N., Watanabe Y., Hirayama Y., and Chon J.: "Development of the resonance ionization laser ion source for parasitic RI-beam production and in-gas-cell/jet laser spectroscopy at SLOWRI RIKEN", Advances in Radioactive Isotope Science (ARIS - 2011), (K.U.Leuven), Leuven, Belgium, May–May (2011).

Ichikawa Y., Ueno H., Ishii Y., Furukawa T., Yoshimi A., Kameda D., Watanabe H., Aoi N., Asahi K., Balabanski D. L., Chevrier R., Daugas J., Fukuda N., Georgiev G., Hayashi H., Iijima H., Inabe N., Inoue T., Ishihara M., Kubo T., Nanao T., Ohnishi T., Suzuki K., Tsuchiya M., Takeda H., and Rajabali M. M.: "Spin-aligned RI beams and nuclear moment measurements at RIBF", RIBF Users Meeting 2012, Wako, Saitama, June (2012).

Ichikawa Y., Ueno H., Ishii Y., Furukawa T., Yoshimi A., Kameda D., Watanabe H., Aoi N., Asahi K., Balabanski D. L., Chevrier R., Daugas J., Fukuda N., Georgiev G., Hayashi H., Iijima H., Inabe N., Inoue T., Ishihara M., Kubo T., Nanao T., Ohnishi T., Suzuki K., Tsuchiya M., Takeda H., and Rajabali M. M.: "Spin manipulation of RI beams from two-stage projectile fragmentation reaction", Advanced Studies Institute on Symmetries and Spin (Spin-Praha-2012), (Charles University), Prague, Czech, July (2012).

Ichikawa Y., Ueno H., Ishii Y., Furukawa T., Yoshimi A., Kameda D., Watanabe H., Aoi N., Asahi K., Balabanski D. L., Chevrier R., Daugas J., Fukuda N., Georgiev G., Hayashi H., Iijima H., Inabe N., Inoue T., Ishihara M., Kubo T., Nanao T., Ohnishi T., Suzuki K., Tsuchiya M., Takeda H., and Rajabali M. M.: "Novel method for the production of spin-aligned RI beams in projectile fragmentation with the dispersion matching technique", The 4th Joint Meeting of the 16th International Conference on Hyperfine Interactions and the 20th International Symposium on Nuclear Quadrupole Interactions (HFI/NQI 2012), (China Institute of Atomic Energy), Beijing, China, Sept. (2012).

Tanaka K., Inabe N., Yoshida K., and Kubo T.: "Evaluation of radiation level and comparison with PHITS calculations for BigRIPS separator in RIBF", 12th International Conference on Radiation Shielding(ICRS-12) & 17th Topical Meeting of the Radiation Protection and Shielding Division of the American Nuclear Society (RPSD-2012), (Atomic Energy Society of Japan.), Nara, Sept.–Sept. (2012).

Sato H., Kubo T., Yano Y., Kusaka K., Ohnishi J., Yoneda K., Shimizu Y., Motobayashi T., Otsu H., Isobe T., Kobayashi T., Sekiguchi K., Nakamura T., Kondo Y., Togano Y., Murakami T., Tsuchihashi T., Orikasa T., and Maeta K.: "Superconducting dipole magnet for SAMURAI spectrometer", Applied Superconductivity Conference (ASC2012), (ASC), Portland, USA, Oct. (2012).

Yamaguchi Y., Wakasugi M., Ozawa A., Uesaka T., Yano Y., Fujinawa T., Fukunishi N., Inabe N., Kamigaito O., Kase M., Kikuchi T., Komiyama M., Kubo T., Kumagai K., Maie T., Ohnishi J., Tokuchi A., Yoshida K., Yamaguchi T., Nagae D., Zenihiro J., Suzuki T., Abe Y., and Suzaki F.: "Construction of Rare-RI Ring at RIKEN RI Beam Factory", 16th International Conference on Electromagnetic Isotope Separators and Techniques Related to their Applications (EMIS2012), (RIKEN KEK IMP), Matsue, Dec. (2012).

Ichikawa Y., Ueno H., Ishii Y., Furukawa T., Yoshimi A., Kameda D., Watanabe H., Aoi N., Asahi K., Balabanski D. L., Chevrier R., Daugas J., Fukuda N., Georgiev G., Hayashi H., Iijima H., Inabe N., Inoue T., Ishihara M., Kubo T., Nanao T., Ohnishi T., Suzuki K., Tsuchiya M., Takeda H., and Rajabali M. M.: "Spin-aligned RI beams via two-step fragmentation reactions", 16th International Conference on Electromagnetic Isotope Separators and Techniques Related to their Applications (EMIS2012), (RIKEN Nishina Center, KEK, Institute of Modern Physics (China)), Matsue, Dec. (2012).

(Domestic Conference)

高峰愛子, 和田道治, 岡田邦宏, 山崎泰規, 金井保之, 小島隆夫, 久保敏幸, 片山一郎, 大谷俊介, Wollnik H., Schuessler H. A.: "Be 同位体の荷電半径と超微細構造定数の測定", 日本物理学会, (岡山大学), 岡山, 3 月 (2010).

園田哲, 和田道治, 松尾由賀利, 久保敏幸, 富田英生, 坂本知佳, 能任琢真, 篠塚勉, 涌井崇志, 古川武, 伊藤由太, Schuessler H. A., 中村聡佑, 宮武宇也, 今井伸明, 石山博恒, 平山賀一, 渡辺裕, 鄭淳讃, 岡田邦宏, 高峰愛子, Kudryavtsev Y., Huyse M., Van Duppen P.: "ガスセル内レーザー共鳴イオン化法の開発とレーザー核分光への応用", 日本物理学会, (日本物理学会), 弘前, 9–9 月 (2011).

GARIS Team

Publications

[Journal]

(Original Papers) *Subject to Peer Review

Morimoto K., Morita K., Kaji D., Haba H., Katori K., Koura H., Ohnishi T., Ozawa A., Suda T., Sueki K., Tanihata I., Tokanai F., Yoneda A., and Yoshida A.: "Status of super heavy element research using GARIS at RIKEN", Nucl. Phys. A **738**, 129 (2004). *

Kaji D., Morimoto K., Morita K., Hasebe H., Yoshida A., Haba H., and Yoneda A.: "Target for the heaviest element production at RIKEN", Nucl. Instrum. Methods Phys. Res. A **590**, 198 (2007). *

Kaji D., Morimoto K., Sato N., Ichikawa T., Ohzeki K., Haba H., Koura H., Ozawa A., Sumita T., Yamaguchi T., Yoneda A., Yoshida A., and Morita K.: "Production and Decay Properties of ^{263}Hs", J. Phys. Soc. Jpn. **78**, No. 3, p. 035001 (2009). *

Clark R. M., Kaji D., Morimoto K., and Watanabe H.: "High-K multi-quasiparticle states in ^{254}No", Phys. Lett. B **690**, 19 (2010). *

Sato N., Haba H., Ichikawa T., Kaji D., Kudou Y., Morimoto K., Morita K., Ohzeki K., Sumita T., Yoneda A., Koura H., Ozawa A., Yamaguchi T., and Yoshida A.: "Production and Decay Properties of ^{264}Hs and ^{265}Hs", J. Phys. Soc. Jpn. **80**, 094201 (2011). *

Kaji D., Morita K., Morimoto K., Haba H., and Kudo H.: "Average charge of superheavy recoil ion in helium gas", Proc.Radiochim **1**, 105 (2011). *

Oral Presentations

(International Conference etc.)

Morimoto K.: "Decay Properties of SHE", 11th International conference on nucleus-nucleus collisions (NN2012), San Antonio, USA, May–June (2012).

Kaji D., Morimoto K., Sato N., Haba H., Kudou Y., Ohzeki K., Sumita T., Yoneda A., Wakabayashi Y., Murakami M., and Morita K.: "Gas-filled recoil ion separator GARIS-II", 16th International Conference on Electromagnetic Isotope Separators and Techniques Related to their Applications (EMIS2012), Matsue, Dec.–Dec. (2012).

Morimoto K.: "Status of GARIS and GARIS-II", 9th ASRC International Workshop "Chemistry of the Superheavy Elements", (Advanced Science Research Center , Japan Atomic Energy Agency), Wako, Mar.–Aug. (2013).

(Domestic Conference)

加治大哉, 森田浩介, 森本幸司, 米田晃, 須田利美, 吉田敦, 大西哲哉, 羽場宏光, 末木啓介, 鹿取謙二, 谷畑勇夫: "超重元素探索へ向けた理研－気体充填型反跳分離装置の性能評価", 日本物理学会, (立教大学), 東京, 9 月 (2002).

加治大哉, 森田浩介, 森本幸司, 米田晃, 須田利美, 吉田敦, 大西哲哉, 羽場宏光, 末木啓介, 鹿取謙二, 谷畑勇夫: "超重元素探索へ向けた理研－気体充填型反跳分離装置の性能評価", 放射化学討論会, (北海道大学), 北海道, 9 月 (2002).

加治大哉, 森田浩介, 森本幸司, 羽場宏光, 鹿取謙二, 小浦寛之, 大西哲哉, 小沢顕, 須田利美, 末木啓介, 谷畑勇夫, 米田晃, 吉田敦: "ヘリウムガス中における (超) 重元素の平衡電荷", 日本物理学会, (宮崎大学), 宮崎, 9 月 (2003).

加治大哉, 森田浩介, 森本幸司, 羽場宏光, 鹿取謙二, 小浦寛之, 大西哲哉, 小沢顕, 須田利美, 末木啓介, 谷畑勇夫, 米田晃, 吉田敦: "ヘリウムガス中における重い反跳原子の平衡電荷－理研における Z=111 番元素探索－", 放射化学討論会, (京都大学原子炉実験施設), 大阪, 10 月 (2003).

加治大哉, 森田浩介, 森本幸司: "気体充填型反跳分離装置を用いた (超) 重元素の平衡電荷測定", 重元素領域の核的・化学的性質　専門研究会, (京都大学原子炉実験施設), 大阪 , 1 月 (2004).

加治大哉, 森田浩介, 森本幸司, 羽場宏光, 小浦寛之, 大西哲哉, 小沢顕, 須田利美, 末木啓介, 山口貴之, 米田晃, 吉田敦: "209Bi+70Zn 反応を用いた 113 番元素探索", 日本化学会, (神奈川大学), 神奈川, 3 月 (2005).

加治大哉, 森田浩介, 森本幸司, 羽場宏光, 小浦寛之, 大西哲哉, 小沢顕, 須田利美, 末木啓介, 山口貴之, 米田晃, 吉田敦: "209Bi(70Zn,n)278113 反応を用いた 113 番元素の合成", 放射化学討論会, (金沢大学), 金沢, 9 月 (2005).

加治大哉, 羽場宏光, 森本幸司, 森田浩介, 佐藤望: "シーボギウム (Sg) の化学研究へ向けた 232Th+40Ar 反応による Sg 同位体の探索", 日本化学会, (日本大学), 千葉, 3 月 (2006).

加治大哉, 森本幸司, 佐藤望, 米田晃, 森田浩介: "新しい気体充填型反跳分離装置 GARIS-II の開発", 放射化学討論会, (日本大学), 神奈川, 9 月 (2009).

加治大哉, 森本幸司, 羽場宏光, 市川隆敏, 小浦寛之, 工藤祐生, 小沢顕, 大関和貴, 住田貴之, 山口貴之, 米田晃, 吉田敦, 森田浩介: "新同位体 ^{263}Hs の生成および壊変特性", 放射化学討論会, (日本大学), 神奈川, 9 月 (2009).

加治大哉, 羽場宏光, 笠松良崇, 工藤祐生, 森本幸司, 森田浩介, 大関和貴, 住田貴之, 米田晃, 佐藤望, 若林泰生, 村上昌史, 門叶冬樹, 生井沙織: "GARIS-II 開発の現状と初動試験", 日本物理学会, (新潟大学), 新潟, 3 月 (2010).

加治大哉, 羽場宏光, 笠松良崇, 工藤祐生, 森本幸司, 森田浩介, 大関和貴, 住田貴之, 米田晃, 佐藤望, 若林泰生, 村上昌史, 門叶冬樹, 生井沙織: "GARIS-II commissioning 1", 放射化学討論会, (大阪大学), 大阪, 9 月 (2010).

加治大哉, 羽場宏光, 笠松良崇, 工藤祐生, 森本幸司, 森田浩介, 大関和貴, 住田貴之, 米田晃, 小浦寛之, 佐藤望, 門叶冬樹: "中性子欠損領域の新アクチノイド核種 ^{234}Bk および ^{230}Am の観測", 放射化学討論会, (大阪大学), 大阪, 9 月 (2010).

加治大哉, 住田貴之, 長谷部裕雄, 田中謙伍, 羽場宏光, 森田浩介, 森本幸司, 若林泰生, 村上昌史, 武山美麗, 山木さやか: "超重元素生成のための新しい標的システム", 2012 日本放射化学会年会・第 56 回放射化学討論会, (日本放射化学会), 東京工業大学, 10–10 月 (2012).

BigRIPS Team

Publications

[Journal]

(Original Papers) *Subject to Peer Review

Ichikawa Y., Ueno H., Ishii Y., Furukawa T., Yoshimi A., Kameda D., Watanabe H., Aoi N., Asahi K., Balabanski D. L., Chevrier R., Daugas J., Fukuda N., Georgiev G., Hayashi H., Iijima H., Inabe N., Inoue T., Ishihara M., Kubo T., Nanao T., Ohnishi T., Suzuki K., Tsuchiya M., Takeda H., and Rajabali M. M.: "Production of spin-aligned RI beam via two-step fragmentation with dispersion matching", J. Phys.: Conf. Ser. **381**, 012090-1–012090-5 (2012). *

Ichikawa Y., Ueno H., Ishii Y., Furukawa T., Yoshimi A., Kameda D., Watanabe H., Aoi N., Asahi K., Balabanski D. L., Chevrier R., Daugas J., Fukuda N., Georgiev G., Hayashi H., Iijima H., Inabe N., Inoue T., Ishihara M., Kubo T., Nanao T., Ohnishi T., Suzuki K., Tsuchiya M., Takeda H., and Rajabali M. M.: "Production of spin-controlled rare isotope beams", Nat. Phys. **8**, No. 12, pp. 918–922 (2012). *

Shimada K., Ueno H., Neyens G., Asahi K., Balabanski D. L., Daugas J., Depuydt M., De Rydt M., Gaudefroy L., Grevy S., Hasama Y., Ichikawa Y., Kameda D., Morel P., Nagatomo T., Perrot L., Stodel C., Thomas J., Utsuno Y., Vanderheijden W., Vermeulen N., Vingerhoets P., Yagi E., Yoshida K., and Yoshimi A.: "Erosion of $N = 20$ shell in ^{33}Al investigated through the ground-state electric quadrupole moment", Phys. Lett. B **714**, 246–250 (2012). *

Chevrier R., Daugas J., Gaudefroy L., Ichikawa Y., Ueno H., Hass M., Cottenier S., Aoi N., Asahi K., Balabanski D. L., Fukuda N., Furukawa T., Georgiev G., Hayashi H., Iijima H., Inabe N., Inoue T., Ishihara M., Ishii Y., Kameda D., Kubo T., Nanao T., Neyens G., Ohnishi T., Rajabali M. M., Suzuki K., Takeda H., Tsuchiya M., Vermeulen N., Watanabe H., and Yoshimi A.: "Is the $7/21^-$ isomer state of ^{43}S spherical?", Phys. Rev. Lett. **108**, 162501-1–162501-5 (2012). *

Itahashi K., Fujioka H., Geissel H., Hirenzaki S., Itoh S., Jido D., Metag V., Nagahiro H., Nanova M., Nishi T., Okochi K., Outa H., Suzuki K., Tanaka Y., and Weick H.: "Feasibility Study of Observing eta' Mesic Nuclei with (p,d) Reaction", Prog. Theor. Phys. **128**, No. 3, pp. 601–613 (2012). *

Sato H., Kubo T., Yano Y., Kusaka K., Ohnishi J., Yoneda K., Shimizu Y., Motobayashi T., Otsu H., Isobe T., Kobayashi T., Sekiguchi K., Nakamura T., Kondo Y., Togano Y., Murakami T., Tsuchihashi T., Orikasa T., and Maeta K.: "Superconducting dipole magnet for SAMURAI spectrometer", IEEE Trans. Appl. Supercond. **23**, No. 3, pp. 4500308-1–4500308-8 (2013). *

(Others)

Nakagawa T., Higurashi Y., Ohnishi J., Aihara T., Tamura M., Uchiyama A., Okuno H., Kusaka K., Kidera M., Komiyama M., Fujimaki M., Sato Y., Ikezawa E., Watanabe Y., Kase M., Goto A., Kamigaito O., and Yano Y.: "First results from the new RIKEN superconducting electron cyclotron resonance ion source", Rev. Sci. Instrum. **81**, No. 2, p. 02A320 (2010).

[Book · Proceedings]

(Original Papers) *Subject to Peer Review

Tanaka K., Inabe N., Ohnishi T., and Kubo T.: "Radiation Transport Calculation Using PHITS Code for the Activation of BigRIPS Separator at RIKEN Radioactive Isotope Beam Factory and Comparison with the Measurement", PROGRESS IN NUCLEAR SCIENCE TECHNOLOGY volume 2, Tokyo, 2010–10, Atomic Energy Society of Japan, Tokyo, pp. 955–959 (2011). *

(Others)

Yamaguchi Y., Wakasugi M., Suzuki H., Fujinawa T., Uesaka T., Yano Y., Ozawa A., Nagae D., Yamaguchi T., Suzuki T., Kikuchi T., Jiang W., Sasaki T., and Tokuchi A.: "Present status of Rare-RI Ring project in RIKEN RI Beam Factory", Proceedings of Science (PoS), Frascati, Italy, 2011–10, SISSA, Fascati, p. 070 (2012).

Oral Presentations

(International Conference etc.)

Ichikawa Y., Ueno H., Ishii Y., Furukawa T., Yoshimi A., Kameda D., Watanabe H., Aoi N., Asahi K., Balabanski D. L., Chevrier R., Daugas J., Fukuda N., Georgiev G., Hayashi H., Iijima H., Inabe N., Inoue T., Ishihara M., Kubo T., Nanao T., Ohnishi T., Suzuki K., Tsuchiya M., Takeda H., and Rajabali M. M.: "Spin-aligned RI beams and nuclear moment measurements at RIBF", RIBF Users Meeting 2012, Wako, Saitama, June (2012).

Ichikawa Y., Ueno H., Ishii Y., Furukawa T., Yoshimi A., Kameda D., Watanabe H., Aoi N., Asahi K., Balabanski D. L., Chevrier R., Daugas J., Fukuda N., Georgiev G., Hayashi H., Iijima H., Inabe N., Inoue T., Ishihara M., Kubo T., Nanao T., Ohnishi T., Suzuki K., Tsuchiya M., Takeda H., and Rajabali M. M.: "Spin manipulation of RI beams from two-stage projectile fragmentation reaction", Advanced Studies Institute on Symmetries and Spin (Spin-Praha-2012), (Charles University), Prague, Czech, July (2012).

Ichikawa Y., Ueno H., Ishii Y., Furukawa T., Yoshimi A., Kameda D., Watanabe H., Aoi N., Asahi K., Balabanski D. L., Chevrier R., Daugas J., Fukuda N., Georgiev G., Hayashi H., Iijima H., Inabe N., Inoue T., Ishihara M., Kubo T., Nanao T., Ohnishi T., Suzuki K., Tsuchiya M., Takeda H., and Rajabali M. M.: "Novel method for the production of spin-aligned RI beams in projectile fragmentation with the dispersion matching technique", The 4th Joint Meeting of the 16th International Conference on Hyperfine Interactions and the 20th International Symposium on Nuclear Quadrupole Interactions (HFI/NQI 2012), (China Institute of Atomic Energy), Beijing, China, Sept. (2012).

Tanaka K., Inabe N., Yoshida K., and Kubo T.: "Evaluation of radiation level and comparison with PHITS calculations for BigRIPS separator in RIBF", 12th International Conference on Radiation Shielding(ICRS-12) & 17th Topical Meeting of the Radiation Protection and Shielding Division of the American Nuclear Society (RPSD-2012), (Atomic Energy Society of Japan.), Nara, Sept.–Sept. (2012).

Sato H., Kubo T., Yano Y., Kusaka K., Ohnishi J., Yoneda K., Shimizu Y., Motobayashi T., Otsu H., Isobe T., Kobayashi T., Sekiguchi K., Nakamura T., Kondo Y., Togano Y., Murakami T., Tsuchihashi T., Orikasa T., and Maeta K.: "Superconducting dipole magnet for SAMURAI spectrometer", Applied Superconductivity Conference (ASC2012), (ASC), Portland, USA, Oct. (2012).

Yamaguchi Y., Wakasugi M., Ozawa A., Uesaka T., Yano Y., Fujinawa T., Fukunishi N., Inabe N., Kamigaito O., Kase M., Kikuchi T., Komiyama M., Kubo T., Kumagai K., Maie T., Ohnishi J., Tokuchi A., Yoshida K., Yamaguchi T., Nagae D., Zenihiro J., Suzuki T., Abe Y., and Suzaki F.: "Construction of Rare-RI Ring at RIKEN RI Beam Factory", 16th International Conference on Electromagnetic Isotope Separators and Techniques Related to their Applications (EMIS2012), (RIKEN KEK IMP), Matsue, Dec. (2012).

Ichikawa Y., Ueno H., Ishii Y., Furukawa T., Yoshimi A., Kameda D., Watanabe H., Aoi N., Asahi K., Balabanski D. L., Chevrier R., Daugas J., Fukuda N., Georgiev G., Hayashi H., Iijima H., Inabe N., Inoue T., Ishihara M., Kubo T., Nanao T., Ohnishi T., Suzuki K., Tsuchiya M., Takeda H., and Rajabali M. M.: "Spin-aligned RI beams via two-step fragmentation reactions", 16th International Conference on Electromagnetic Isotope Separators and Techniques Related to their Applications (EMIS2012), (RIKEN Nishina Center, KEK, Institute of Modern Physics (China)), Matsue, Dec. (2012).

Nagae D., Abe Y., Okada S., Ozawa A., Yamaguchi T., Suzuki H., Moriguchi T., Ishibashi Y., Fukuoka S., Nishikiori R., Suzuki T., Suzaki F., Yamaguchi Y., Uesaka T., and Wakasugi M.: "Time-of-flight detector applied to mass measurements in Rare-RI Ring", 6th International Conference on Electromagnetic Isotope Separators and Techniques Related to their Applications (EMIS2012), (RIKEN KEK IMP), Matsue, Dec. (2012).

SAMURAI Team

Publications

[Journal]

(Original Papers) *Subject to Peer Review

Yoshioka T., Mishima K., Ino T., Taketani K., Mutou S., Morishima T., Shimizu H., Oku T., Suzuki J., Shinohara T., Sakai k., Sato H., Hirota K., Otake Y., Kitaguchi M., Hino M., Seki Y., Iwashita Y., Yamada M., Ichikawa M., Takanori S., Kawasaki S., Komamiya S., Kamiya Y., Otono H., Yamashita S., and Geltenbort P.: "Polarization of very cold neutron using a permanent magnet quadruple", Nucl. Instrum. Methods Phys. Res. A **634**, No. 1, pp. S17–S20 (2011). ∗

Adachi T., Fujita Y., Bacher A. D., Berg G. P., Black T. C., De Frenne D., Foster ., Fujita H., Fujita K., Hatanaka K., Homma M., Jacobs E., Janecke J., Kanzaki Y., Katori K., Nakanishi K., Negret A., Otsuka T., Popescu L., Roberts D. A., Sakemi Y., Shimbara Y., Shimizu Y., Stephenson E. J., Tameshige Y., Tamii A., Uchida M., Ueno H., Yamanaka T., Yosoi M., and Zell K. O.: "High-resolution study of Gamow-Teller transitions via the ^{54}Fe(^{3}He,t)^{54}Co reaction", Phys. Rev. C **85**, 024308-1–024308-15 (2012). ∗

Imai N., Hirayama Y., Watanabe Y. X., Teranishi T., Hashimoto T., Hayakawa S., Ichikawa Y., Jeong S., Kahl D., Kubono S., Miyatake H., Ueno H., Yamaguchi H., Yoneda K., and Yoshimi A.: "Isobaric analog resonances of the $N = 21$ nucleus ^{35}Si", Phys. Rev. C **85**, 034313-1–034313-5 (2012). ∗

Sato H., Kubo T., Yano Y., Kusaka K., Ohnishi J., Yoneda K., Shimizu Y., Motobayashi T., Otsu H., Isobe T., Kobayashi T., Sekiguchi K., Nakamura T., Kondo Y., Togano Y., Murakami T., Tsuchihashi T., Orikasa T., and Maeta K.: "Superconducting dipole magnet for SAMURAI spectrometer", IEEE Trans. Appl. Supercond. **23**, No. 3, pp. 4500308-1–4500308-8 (2013). ∗

Oral Presentations

(International Conference etc.)

Sato H., Kubo T., Yano Y., Kusaka K., Ohnishi J., Yoneda K., Shimizu Y., Motobayashi T., Otsu H., Isobe T., Kobayashi T., Sekiguchi K., Nakamura T., Kondo Y., Togano Y., Murakami T., Tsuchihashi T., Orikasa T., and Maeta K.: "Superconducting dipole magnet for SAMURAI spectrometer", Applied Superconductivity Conference (ASC2012), (ASC), Portland, USA, Oct. (2012).

Furukawa T., Wakui T., Yang X., Fujita T., Imamura K., Yamaguchi Y., Tetsuka H., Tsutsui Y., Mitsuya Y., Ichikawa Y., Ishibashi Y., Yoshida N., Shirai H., Ebara Y., Hayasaka M., Arai S., Muramoto S., Hatakeyama A., Wada M., Sonoda T., Ito Y., Kobayashi T., Nishimura S., Nishimura M., Kondo Y., Yoneda K., Kubono S., Ohshiro Y., Ueno H., Shinozuka T., Shimoda T., Asahi K., and Matsuo Y.: "A Novel Nuclear Laser Spectroscopy Method using Superfluid Helium for the Measurement of Spins and Moments of Exotic Nuclei", 16th International Conference on Electromagnetic Isotope Separators and Techniques Related to their Applications (EMIS2012), Matsue, Dec. (2012).

(Domestic Conference)

Yang X., 古川武, 今村慧, 手塚博紀, 山口康広, 筒井正機, 藤田朋美, 三津谷洋助, 江原悠太, 早坂美希, 新井信乃, 村本宗将, 市川雄一, 石橋陽子, 吉田直貴, 白井葉月, 涌井崇志, 小林徹, 園田哲, 伊藤由太, 西村俊二, 西村美月, 近藤洋介, 米田健一郎, 久保野茂, 大城幸光, 畠山温, 和田道治, 上野秀樹, 下田 正, 旭 耕一郎, 松尾 由賀利: "Control the stopping position of 84,85Rb in He II for the laser spectroscopy in OROCHI experiment", 日本物理学会第 68 回年次大会, 東広島, 3 月 (2013).

Detector Team

Oral Presentations

(Domestic Conference)

佐藤優樹, 竹谷篤, 村上浩之, 西村太樹, 福田光順: “多重サンプリング型電離箱のパラメータ最適化に向けた考察”, 日本物理学会, (日本物理学会), 京都, 9–9 月 (2012).

Accelerator Applications Research Group

Publications

[Journal]

(Original Papers) *Subject to Peer Review

Kazama Y., Nishihara K., Bergero R., Fujiwara M., Abe T., Charlesworth D., and Kawano S.: "*SlWUS1*; An X-linked Gene Having No Homologous Y-Linked Copy in *Silene latifolia*", G3: Genes, Genomes, Genetics **2**, 1269–1278 (2012). ∗

Niwa K. and Abe T.: "Chimeras with mosaic pattern in archeospore germlings of Pyropia Yesoensis Ueda (Bangiales, Rhodophyta)", J. Phycol. **48**, No. 3, pp. 706–709 (2012). ∗

Cabanos C., Katayama H., Urabe H., Kuwata C., Murota Y., Abe T., Okumoto Y., and maruyama N.: "Heavy-ion beam irradiation is an effective technique for reducing major allergens in peanut seeds", Mol. Breed. **30**, 1037–1044 (2012). ∗

Kazama Y., Ma L., Hirano T., Ohbu S., Shirakawa Y., Hatakeyama S., Tanaka S., and Abe T.: "Rapid evaluation of effective linear energy transfer in heavy ion utagenesis of *Arabidopsis thaliana*", Plant Biotechnol. **29**, No. 5, pp. 440–444 (2012). ∗

Yasui Y., Mori M., Aii J., Abe T., Matsumoto D., Sato S., Hayashi Y., Ohnishi O., and Ota T.: "S-LOCUS EARLY FLOWERING 3 Is Exclusively Present in he Genomes of Short-Styled Buckwheat Plants that xhibit Heteromorphic Self-Incompatibility", PLoS One **7**, No. 2, p. e31264 (2012). ∗

Shirao T., Ueno K., Abe T., and Matsuyama T.: "Development of DNA markers for identifying chrysanthemum cultivars generated by ion-beam irradiation", Mol. Breed. **31**, No. 3, pp. 729–735 (2013). ∗

Kazama Y., Fujiwara M., Takehisa H., Ohbu S., Saito H., Ichida H., Hayashi Y., and Abe T.: "Characterization of a heavy-ion induced white flower mutant of allotetraploid *Nicotiana tabacum*", Plant Cell Rep. **32**, No. 1, pp. 11–19 (2013). ∗

(Review)

横堀正敏, 阿部知子: "重イオンビーム照射を利用した吟醸酒用の新しい酵母の開発", ブレインテクノニュース **148**, 29–33 (2011).

(Others)

阿部知子: "ユーザーの夢を叶える", NL だより **416**, 1 (2012).

[Book · Proceedings]

(Review)

Ohtsubo N., Sasaki K., Aida R., Ryuto H., Ichida H., Hayashi Y., and Abe T.: "Efficient modification of floral traits by heavy-ion beam irradiation on transgenic Torenia", Methods in Molecular Biology Vol. 847: Transgenic Plants, Humana Press, New York, p. 275-289 (2012).

Niwa K. and Abe T.: "Heavy-ion beam mutagenesis in Porphyra yezoensis", Porphyra yezoensis:Frontiers in physiological and molecular biological research, Nova Science Publishers, Inc., New York, pp. 119–132 (2012).

Oral Presentations

(International Conference etc.)

Hokura A., Yamaoka W., Hayashi Y., Terada Y., Abe T., and Nakai I.: "Micro-XRF imaging and X-ray absorption fine structure analysis utilizing high-energy synchrotron radiation to investigate the accumulation mechanism of Cd in plants", METALLOMICS 2011, (European Virtual Institute for Speciation Analysis), Munster, Germany, June (2011).

Hokura A., Yoshii Y., Nakai I., Abe T., Itouga M., Sakakibara H., and Tarada Y.: "Chemical speciation of copper, lead and gold accumulated in moss by X-ray analyses using synchrotron radiation", The 7th international conference on instrumental methods of analysis modern trends and applications, Chania Crete, Greece, Sept. (2011).

Imanishi S., Noguchi A., Kazama Y., Hirano T., Hayashi Y., Abe T., Matsuo S., and Kikuchi K.: "Analysis of gene expression levels in tomato mutants induced by heavy-ion-beams irradiation", 8th Solanaceae and 2nd Cucurbitaceae Genome Joint Conference, Kobe, Nov.–Dec. (2011).

Nishiura A., Kazama Y., Abe T., Nitta M., Nasuda S., and Murai K.: "A large scale mutant panel of einkorn wheat developed by heavy-ion beam mutagenesis and its application for flowering-time mutant screening", Joint 22nd international Triticeae mapping initiative workshop and 4th U.S.National wheat genomics workshop, North Dakota, USA, June (2012).

Abe T.: "Recent progress of mutation breeding in modern genome science era", Innovative Biothechnological tools for plant breeding, (The Korean Society of breeding Science), Daegu, Korea, July (2012).

Murai K., Kazama Y., and Abe T.: "A large scale mutant panel of wheat developed by heavy-ion beam mutagenesis and its application for genetic research", 8th International Symposium on Swift Heavy Ions in Matter (SHIM 2012), (SHIM2012 Organizing Committee), Kyoto, Oct. (2012).

Kazama Y., Hirano T., Ohbu S., Shirakawa Y., and Abe T.: "LET-dependent effects of heavy-ion irradiation on mutation induction in *Arabidopsis thaliana*", 8th International Symposium on Swift Heavy Ions in Matter (SHIM 2012), (SHIM2012 Organizing Committee), Kyoto, Oct. (2012).

Abe T.: "Ion beam mutagenesis and mutagenomics", 16th International Conference on Electromagnetic Isotope Separators and Techniques Related to their Applications (EMIS2012), Matsue, Dec. (2012).

(Domestic Conference)

高原学, 蝦名真澄, 飯村敬二, 森田竜平, 風間裕介, 阿部知子,

高溝正, 中川仁: “アポミクシス遺伝子単離に向けたイオンビームの利用”, 日本育種学会第 119 回講演会, (日本育種学会), 横浜, 3 月 (2011).

寺岡毅, 神谷健太, 澤野郁夫, 中嶌輝子, 加々美裕, 神尾章子, 浜部直哉, 林依子, 龍頭啓充, 福西暢尚, 阿部知子: “重イオンビーム照射によるウンシュウミカン形態変異個体の果実品質の特徴”, 園芸学会平成 23 年度秋季大会, (園芸学会), 岡山, 9 月 (2011).

田岡裕規, 保倉明子, 後藤文之, 吉原利一, 阿部知子, 寺田靖子, 中井泉: “放射光高エネルギー μ-XRF 分析を用いた Cd 超集積シダ植物ヘビノネゴザにおける Cd の蓄積機構の解明”, 第 47 回 X 線分析討論会, (日本分析化学会 X 線分析研究懇談会), 福岡, 10 月 (2011).

林依子, 森田竜平, 永野拓馬, 半澤栄子, 東海林英夫, 小暮祥子, 若菜妙子, 白川侑希, 保倉明子, 高橋和也, 佐藤雅志, 阿部知子: “重イオンビーム照射によって誘発したイネ耐塩性突然変異系統の特性比較 2”, 日本育種学会第 121 回講演会, (日本育種学会), 宇都宮, 3 月 (2012).

高原学, 蝦名真澄, 森田竜平, 風間裕介, 阿部知子, 高溝正, 中川仁: “重イオンビーム照射によるアポミクシス遺伝子領域での欠失変異誘発と線量・LET の影響”, 日本育種学会第 121 回講演会, (日本育種学会), 宇都宮, 3 月 (2012).

佐々木克友, 山口博康, 間竜太郎, 四方康範, 阿部知子, 大坪憲弘: “トレニア TfUFO 変異体の花芽発達に関する解析”, 第 53 回日本植物生理学会年会, (日本植物生理学会), 京都, 3 月 (2012).

阿部知子, 平野智也, 風間裕介: “重イオンビームによる品種改良技術の開発から遺伝子機能解明へ”, 佐賀県試験研究機関　シンクロトロン放射光利活用発表会, (九州シンクロトロン光研究センター), 鳥栖, 3 月 (2012).

横堀正敏, 南澤賢, 高橋友哉, 増田こずえ, 林依子, 阿部知子: “清酒酵母の開発”, 第 8 回イオンビーム育種研究会大会, (イオンビーム育種研究会), 高崎, 5 月 (2012).

玉木克知, 山中正仁, 小山佳彦, 林依子, 阿部知子: “イオンビーム照射によるキクの花色変異について”, 第 8 回イオンビーム育種研究会大会, (イオンビーム育種研究会), 高崎, 5 月 (2012).

佐々木克友, 阿部知子, 大坪憲弘: “重イオンビーム照射による有用形質トレニアの作出と原因遺伝子の解明”, 第 51 回ガンマーフィールドシンポジウム, 水戸, 7 月 (2012).

二羽恭介, 阿部知子: “重イオンビーム照射で誘発されたスサビノリ葉状体のモザイク状キメラ”, 日本藻類学会第 36 回大会, (日本藻類学会), 札幌, 7 月 (2012).

大田修平, 松田尚大, 竹下毅, 渡邉光一, 風間裕介, 阿部知子, 河野重行: “単細胞緑藻 Parachlorella kessleri における高増殖能有する重イオン照射株のスクリーニング”, 日本藻類学会第 36 回大会, (日本藻類学会), 札幌, 7 月 (2012).

風間裕介, 石井公太郎, 平野智也, 阿部知子: “重イオンビーム誘発性転換変異体を用いた植物 Y 染色体性決定領域の解析”, 新学術領域「ゲノム支援」２０１２年度 拡大班会議, (文部科学省科学研究費新学術領域研究（研究領域提案型）『生命科学系３分野支援活動』), 御殿場, 8 月 (2012).

安井康夫, 森正之, 相井城太郎, 阿部知子, 佐藤信吾, 田中宥司, 松本大生, 林依子, 大西近江, 大田竜也: “ソバ属の自殖性植物における S-LOCUS EARLY FLOWERING 3 遺伝子の崩壊”, 日本育種学会第 122 回講演会, (日本育種学会), 京都, 9 月 (2012).

相井城太郎, 安井康夫, 森正之, 阿部知子, 佐藤信吾, 田中宥司, 松本大生, 林依子, 大西近江, 大田竜也: “ソバの二花柱性関連遺伝子 S-LOCUS EARLY FLOWERING 3 の同定”, 日本育種学会第 122 回講演会, (日本育種学会), 京都, 9 月 (2012).

西美友紀, 石地耕太朗, 伊東寛史, 阿部知子, 岡和彦: “シンクロトロン光および重イオンビーム照射したイチゴ‘さがほのか’における突然変異率の比較”, 園芸学会平成 24 年度秋季大会, 福井, 9 月 (2012).

石井公太郎, 風間裕介, 青沼航, 川元　章, 阿部知子, 河野重行: “雌雄異株植物ヒロハノマンテマの効率的な染色体標本の作製”, 日本植物形態学会第 24 回総会・大会, (日本植物形態学会), 姫路, 9 月 (2012).

片野真奈, 風間裕介, 平野智也, 阿部知子, 塚谷裕一, Ferjani A.: “*fugu5* 変異体に見られる補償作用の背景には独自の細胞伸長制御系が存在する”, 日本植物学会第 76 回大会, (日本植物学会), 姫路, 9 月 (2012).

青沼航, 川元　章, 石井公太郎, 風間裕介, 阿部知子, 河野重行: “ヒロハノマンテマの *SlAP3* 欠損変異体を含む Y 染色体部分欠損変異体の網羅的単離”, 日本植物学会第 76 回大会, (日本植物学会), 姫路, 9 月 (2012).

大田修平, 松田尚大, 竹下毅, 水野雄介, 渡邉光一, 平田愛子, 風間裕介, 阿部知子, 河野重行: “クロレラにおけるデンプン・オイル蓄積の動態解析と物質生産変異株の単離ストラテジー”, 日本植物学会第 76 回大会, (日本植物学会), 姫路, 9 月 (2012).

石井公太郎, 青沼航, 西山りゑ, 風間裕介, 阿部知子, 河野重行: “ヒロハノマンテマ性染色体の組換え抑制によって生じた *SlAP3X/Y* 周辺の構造変化”, 日本植物学会第 76 回大会, (日本植物学会), 姫路, 9 月 (2012).

和山真里奈, 松浦葉月, 大田修平, 渡邉光一, 平田愛子, 風間裕介, 阿部知子, 河野重行: “ヘマトコッカスにおけるアスタキサンチン蓄積の電顕三次元動態解析と突然変異体の単離”, 日本植物学会第 76 回大会, (日本植物学会), 姫路, 9 月 (2012).

風間裕介, 石井公太郎, 青沼航, 阿部知子, 河野重行: “ヒロハノマンテマの 2 つのホモログ遺伝子 *SlSUP* と *SlWUS* の発現と性染色体座乗”, 日本植物学会第 76 回大会, (日本植物学会), 姫路, 9 月 (2012).

馬立秋, 風間裕介, 阿部知子, 田中秀逸, 畠山晋: “鉄イオンビーム照射によって生じた DNA 二本鎖切断の修復機構と変異生成”, 日本遺伝学会第 84 回大会, (日本遺伝学会), 福岡, 9 月 (2012).

松山知樹, 白尾吏, 上野敬一郎, 古川浩二, 岩澤洋樹, 阿部知子, 田畑哲之: “イオンビーム照射したキクとシンビジウムでのゲノム DNA 変異検出”, 園芸学会平成 24 年度秋季大会, (園芸学会), 福井, 9 月 (2012).

古川浩二, 岩澤洋樹, 阿部知子, 田畑哲之, 松山知樹: “DNA マーキングによるシンビジウムの品種判別技術の開発”, 日本育種学会第 122 回講演会, (日本育種学会), 京都, 9 月 (2012).

古川浩二, 岩澤洋樹, 阿部知子, 田畑哲之, 松山知樹: “シンビジウム品種内系統判別のための DNA マークのメリクロン

増殖系統での保存性確認", 日本 DNA 多型学会第 21 回学術集会, (日本 DNA 多型学会), 京都, 11 月 (2012).

風間裕介, 平野智也, 石井公太郎, 大部澄江, 阿部知子: "重イオンビーム突然変異誘発における LET 効果の解析と雌雄異種植物ヒロハノマンテマの性転換変異体ラインの構築", 木原生物学研究所植物遺伝資源科学研究室プログレスセミナー, (木原生物学研究所植物遺伝資源科学研究室), 横浜, 11 月 (2012).

石井公太郎, 森田竜平, 小暮祥子, 一瀬勝紀, 林依子, 阿部知子: "イネの重イオンビーム照射応答遺伝子の解析", 東京大学植物生存システム研究室秋学期セミナー, (東京大学植物生存システム研究室), 柏, 12 月 (2012).

佐藤陽一, 平野智也, 阿部知子: "大型褐藻類の育種技術の開発—国内初の品種登録を目指して—", 東京大学植物生存システム研究室秋学期セミナー, (東京大学植物生存システム研究室), 柏, 12 月 (2012).

風間裕介, 平野智也, 石井公太郎, 大部澄江, 白川侑希, 林祐子, 阿部知子: "重イオンビームによるオンデマンド変異誘発", 東京大学植物生存システム研究室秋学期セミナー, (東京大学植物生存システム研究室), 柏, 12 月 (2012).

阿部知子: "品種改良技術開発から Mutagenomics へ", 島根県農業技術センター　セミナー「重イオンビームを利用した育種の最先端」, (島根県農業技術センター), 松江, 12 月 (2012).

佐藤雅志, 遠藤貴司, 阿部知子: "塩害耐性イネ作出に向けて", 共同利用・共同研究「植物遺伝資源・ストレス科学研究拠点」シンポジウム 物による東日本大震災被災農地の修復, (岡山大学資源植物科学研究所), 倉敷, 2 月 (2013).

阿部知子: "世界に一つだけの花", 全複工・(社) 全肥商連合合同特別講演会, (全複工・(社) 全肥商連合), 東京, 2 月 (2013).

石井公太郎, 森田竜平, 小暮祥子, 林依子, 平野智也, 渋川登美子, 長村吉晃, 阿部知子: "重イオンビーム照射によって誘導されるイネ遺伝子の網羅的解析", 日本育種学会第 123 回講演会, (日本育種学会), 東京, 3 月 (2013).

風間裕介, 平野智也, 石井公太郎, 大部澄江, 白川侑希, 林祐子, 阿部知子: "重イオンビームを用いたシロイヌナズナタンデム遺伝子破壊ラインの構築", 日本育種学会第 123 回講演会, (日本育種学会), 東京, 3 月 (2013).

西浦愛子, 風間裕介, 阿部知子, 新田みゆき, 那須田周平, 村井耕二: "一粒系コムギの極早生突然変異体 (*extra early-flowering*) における花成形質と花成関連遺伝子の発現パターンの解析", 日本育種学会第 123 回講演会, (日本育種学会), 東京, 3 月 (2013).

三橋進也, 風間裕介, 阿部知子, 生方信: "重 イオンビームによる担子菌の変異株作製に関する研究", 日本農芸化学会 2013 年度大会, (日本農芸化学会), 仙台, 3 月 (2013).

風間裕介, 平野智也, 石井公太郎, 大部澄江, 白川侑希, 林祐子, 阿部知子: "重イオンビームによるオンデマンド変異誘発法の開発とタンデム遺伝子破壊ラインの構築", 第 54 回日本植物生理学会年会, (日本植物生理学会), 岡山, 3 月 (2013).

Radiation Biology Team

Publications　Publications

[Journal]

(Original Papers)　*Subject to Peer Review

Lee J. M., Hull J. J., Kawai T., Tsuneizumi K., Kurihara M., Tanokura M., Nagata K., Nagasawa H., and Matsumoto S.: "Establishment of Sf9 transformants constitutively expressing PBAN receptor variants: application to functional evaluation.", Frontiers in Endocrinology **3**, 56-1–56-8 (2012). *

Kazama Y., Nishihara K., Bergero R., Fujiwara M., Abe T., Charlesworth D., and Kawano S.: "*SlWUS1*; An X-linked Gene Having No Homologous Y-Linked Copy in *Silene latifolia*", G3: Genes, Genomes, Genetics **2**, 1269–1278 (2012). *

Niwa K. and Abe T.: "Chimeras with mosaic pattern in archeospore germlings of Pyropia Yesoensis Ueda (Bangiales, Rhodophyta)", J. Phycol. **48**, No. 3, pp. 706–709 (2012). *

Cabanos C., Katayama H., Urabe H., Kuwata C., Murota Y., Abe T., Okumoto Y., and maruyama N.: "Heavy-ion beam irradiation is an effective technique for reducing major allergens in peanut seeds", Mol. Breed. **30**, 1037–1044 (2012). *

Hirano T., Kazama Y., Ohbu S., Shirakawa Y., Liu Y., Kambara T., Fukunishi N., and Abe T.: "Molecular nature of mutations induced by high-LET irradiation with argon and carbon ions in *Arabidopsis thaliana*", Muta. Res./Fund. Mol. Mech. Mutagen. **735**, No. 1-2, pp. 19–31 (2012). *

Kazama Y., Ma L., Hirano T., Ohbu S., Shirakawa Y., Hatakeyama S., Tanaka S., and Abe T.: "Rapid evaluation of effective linear energy transfer in heavy ion utagenesis of *Arabidopsis thaliana*", Plant Biotechnol. **29**, No. 5, pp. 440–444 (2012). *

Fujiwara M., Yoshioka Y., Hirano T., Kazama Y., Abe T., Hayashi K., and Itoh R.: "Visualization of plastid movement in the pollen tube of *Arabidopsis thaliana*", Plant Signaling Behav. **7**, No. 1, pp. 34–37 (2012). *

Yasui Y., Mori M., Aii J., Abe T., Matsumoto D., Sato S., Hayashi Y., Ohnishi O., and Ota T.: "S-LOCUS EARLY FLOWERING 3 Is Exclusively Present in he Genomes of Short-Styled Buckwheat Plants that xhibit Heteromorphic Self-Incompatibility", PLoS One **7**, No. 2, p. e31264 (2012). *

Hirano T., Takagi K., Hoshino Y., and Abe T.: "DNA damage response in male gametes of *Cyrtanthus mackenii* during pollen tube growth", AoB PLANTS **5**, No. plt004, pp. 1–10 (2013). *

Kazama Y., Fujiwara M., Takehisa H., Ohbu S., Saito H., Ichida H., Hayashi Y., and Abe T.: "Characterization of a heavy-ion induced white flower mutant of allotetraploid *Nicotiana tabacum*", Plant Cell Rep. **32**, No. 1, pp. 11–19 (2013). *

古川浩二, 岩澤洋樹, 阿部知子, 田畑哲之, 松山知樹: "シンビジウム品種内系統判別のための DNA マーク作出と増殖個体での保存性の確認", DNA 多型 **20**, 91–93 (2012). *

田岡裕規, 保倉明子, 後藤文之, 吉原利一, 阿部知子, 寺田靖子, 中井泉: "放射光蛍光 X 線分析を用いる重金属超蓄積シダ植物ヘビノネゴザ（Athyrium yokoscense) における Cd 蓄積機構の研究", X 線分析の進歩 **43**, 1–14 (2012). *

(Review)

横堀正敏, 阿部知子: "重イオンビーム照射を利用した吟醸酒用の新しい酵母の開発", ブレインテクノニュース **148**, 29–33 (2011).

泉雅子: "放射線の人体への影響", 日本物理学会誌 **68**, No. 3, pp. 141–148 (2013).

(Others)

阿部知子: "ユーザーの夢を叶える", NL だより **416**, 1 (2012).

[Book・Proceedings]

(Review)

Ohtsubo N., Sasaki K., Aida R., Ryuto H., Ichida H., Hayashi Y., and Abe T.: "Efficient modification of floral traits by heavy-ion beam irradiation on transgenic Torenia", Methods in Molecular Biology Vol. 847: Transgenic Plants, Humana Press, New York, p. 275-289 (2012).

Abe T., Ryuto H., and Fukunishi N.: "Ion Beam Radiation Mutagenesis", Plant mutation breeding and biotechnology, Vienna, Austria, 2012–11, CABI, Oxfordshire, pp. 99–106 (2012).

Niwa K. and Abe T.: "Heavy-ion beam mutagenesis in Porphyra yezoensis", Porphyra yezoensis:Frontiers in physiological and molecular biological research, Nova Science Publishers, Inc., New York, pp. 119–132 (2012).

Oral Presentations　Oral Presentations

(International Conference etc.)

Hokura A., Yamaoka W., Hayashi Y., Terada Y., Abe T., and Nakai I.: "Micro-XRF imaging and X-ray absorption fine structure analysis utilizing high-energy synchrotron radiation to investigate the accumulation mechanism of Cd in plants", METALLOMICS 2011, (European Virtual Institute for Speciation Analysis), Munster, Germany, June (2011).

Hokura A., Yoshii Y., Nakai I., Abe T., Itouga M., Sakakibara H., and Tarada Y.: "Chemical speciation of copper, lead and gold accumulated in moss by X-ray analyses using synchrotron radiation", The 7th international conference on instrumental methods of analysis modern trends and applications, Chania Crete, Greece, Sept. (2011).

Imanishi S., Noguchi A., Kazama Y., Hirano T., Hayashi Y., Abe T., Matsuo S., and Kikuchi K.: "Analysis of gene expression levels in tomato mutants induced by heavy-ion-beams irradiation", 8th Solanaceae and 2nd Cucurbitaceae Genome Joint Conference, Kobe, Nov.–Dec. (2011).

Hirano T., Kazama Y., Ohbu S., Shirakawa Y., and Abe T.: "Molecular nature of mutations induced by heavy-ion beam in *Arabidopsis thaliana*", EMBO Workshop: Genetic stability and change: Genome maintenance mechanisms in plants, (The Organising Committee of Genetic stability and change: Genome maintenance mechanisms in plants), Roscoff, France, May (2012).

Kazama Y., Hirano T., Ohbu S., Shirakawa Y., and Abe T.: "Optimization of ion-beam irradiation for highly efficient mutagenesis using a rapid detection method of mutation.", EMBO Workshop: Genetic stability and change: Genome maintenance mechanisms in plants, (The Organising Committee of Genetic stability and change: Genome maintenance mechanisms in plants), Roscoff, France, May (2012).

Nishiura A., Kazama Y., Abe T., Nitta M., Nasuda S., and Murai K.: "A large scale mutant panel of einkorn wheat developed by heavy-ion beam mutagenesis and its application for flowering-time mutant screening", Joint 22nd international Triticeae mapping initiative workshop and 4th U.S.National wheat genomics workshop, North Dakota, USA, June (2012).

Abe T.: "Recent progress of mutation breeding in modern genome science era", Innovative Biothechnological tools for plant breeding, (The Korean Society of breeding Science), Daegu, Korea, July (2012).

Ferjani A., Katano M., Kazama Y., Hirano T., Abe T., and Tsukaya H.: "Compensated cell enlargement in *fugu5* mutant occurs through a unique pathway", 10th International Congress on Plant Molecular Biology, (International Society for Plant Molecular Biology), Jeju, Korea, Oct. (2012).

Murai K., Kazama Y., and Abe T.: "A large scale mutant panel of wheat developed by heavy-ion beam mutagenesis and its application for genetic research", 8th International Symposium on Swift Heavy Ions in Matter (SHIM 2012), (SHIM2012 Organizing Committee), Kyoto, Oct. (2012).

Takagi K., Hirano T., Kazama Y., Tsukada T., Hayashi Y., and Abe T.: "Distribution of gamma-H2AX in Interphase Nuclei of *Arabidopsis* Root Tips", 8th International Symposium on Swift Heavy Ions in Matter (SHIM 2012), (SHIM2012 Organizing Committee), Kyoto, Oct. (2012).

Suzuki K. and Abe T.: "Innovative technology in flower breeding using heavy-ion beams", 8th International Symposium on Swift Heavy Ions in Matter (SHIM 2012), Kyoto, Oct. (2012).

Kazama Y., Hirano T., Ohbu S., Shirakawa Y., and Abe T.: "LET-dependent effects of heavy-ion irradiation on mutation induction in *Arabidopsis thaliana*", 8th International Symposium on Swift Heavy Ions in Matter (SHIM 2012), (SHIM2012 Organizing Committee), Kyoto, Oct. (2012).

Mizuno T., Miyazawa S., Izumi M., Hanaoka F., Imamoto N., and Torigoe H.: "Intrinsically disordered amino-terminal region of DNA polymerase alpha catalytic subunit is interactive region for other replicative factors", the 8th 3r symposium, Awajishima , Nov. (2012).

Furukawa K., Iwasawa H., Abe T., Tabata S., and Matsuyama T.: "Heavy ion-beam breeding and cultivar identification by 'DNA Marking' in Cymbidium", The 11th Asia Pacific Orchid Conference, (Asia Pacific Orchid Conference), Okinawa, Jan. (2013).

(Domestic Conference)

岩井良夫, 池田時浩, 小島隆夫, 金井保之, 和田道治, 前島一博, 今本尚子, 小林知洋, 萩原清, 成沢忠, Pokhil G. P., 山崎泰規: "蓋つきキャピラリーを用いた理研マイクロビーム細胞照射装置の開発", 日本物理学会, (北海道大学), 北海道, 9 月 (2007).

高城啓一, 畑下昌範, 久米恭, 塚田晃代, 泉雅子, 風間裕介, 林依子, 阿部知子: "γ - H2AX フォーカスのイオンビームトラックに沿った形態変化", 日本放射線影響学会第 52 回大会, (日本放射線影響学会), 広島, 11 月 (2009).

高原学, 蝦名真澄, 飯村敬二, 森田竜平, 風間裕介, 阿部知子, 高溝正, 中川仁: "アポミクシス遺伝子単離に向けたイオンビームの利用", 日本育種学会第 119 回講演会, (日本育種学会), 横浜, 3 月 (2011).

Cabanos C., Katayama H., Urabe H., 桑田主税, Murota Y., 阿部知子, Okumoto Y., maruyama N.: "Screening of peanut lines lacking a major allergen induced by heavy-ion beam irradiation", 日本育種学会第 120 回講演会, (日本育種学会), 福井, 9 月 (2011).

寺岡毅, 神谷健太, 澤野郁夫, 中嶌輝子, 加々美裕, 神尾章子, 浜部直哉, 林依子, 龍頭啓充, 福西暢尚, 阿部知子: "重イオンビーム照射によるウンシュウミカン形態変異個体の果実品質の特徴", 園芸学会平成 23 年度秋季大会, (園芸学会), 岡山, 9 月 (2011).

田岡裕規, 保倉明子, 後藤文之, 吉原利一, 阿部知子, 寺田靖子, 中井泉: "放射光高エネルギー μ-XRF 分析を用いた Cd 超集積シダ植物ヘビノネゴザにおける Cd の蓄積機構の解明", 第 47 回 X 線分析討論会, (日本分析化学会 X 線分析研究懇談会), 福岡, 10 月 (2011).

林依子, 森田竜平, 永野拓馬, 半澤栄子, 東海林英夫, 小暮祥子, 若菜妙子, 白川侑希, 保倉明子, 高橋和也, 佐藤雅志, 阿部知子: "重イオンビーム照射によって誘発したイネ耐塩性突然変異系統の特性比較 2", 日本育種学会第 121 回講演会, (日本育種学会), 宇都宮, 3 月 (2012).

高原学, 蝦名真澄, 森田竜平, 風間裕介, 阿部知子, 高溝正, 中川仁: "重イオンビーム照射によるアポミクシス遺伝子領域での欠失変異誘発と線量・LET の影響", 日本育種学会第 121 回講演会, (日本育種学会), 宇都宮, 3 月 (2012).

山谷浩史, 佐藤豊, 増田優, 森田竜平, 西村実, 草場信: "イネ stay-green 遺伝子 NYC4 の単離と機能解析", 日本育種学会第 121 回講演会, (日本育種学会), 宇都宮, 3 月 (2012).

古川浩二, 岩澤洋樹, 阿部知子, 田畑哲之, 松山知樹: "DNA マーキングによるシンビジウムの品種内判別（第 6 報）", 園芸学会平成 24 年春季大会, (園芸学会), 堺, 3 月 (2012).

佐々木克友, 山口博康, 間竜太郎, 四方康範, 阿部知子, 大坪憲弘: "トレニア TfUFO 変異体の花芽発達に関する解析",

第 53 回日本植物生理学会年会, (日本植物生理学会), 京都, 3 月 (2012).

阿部知子, 平野智也, 風間裕介: “重イオンビームによる品種改良技術の開発から遺伝子機能解明へ”, 佐賀県試験研究機関　シンクロトロン放射光利活用発表会, (九州シンクロトロン光研究センター), 鳥栖, 3 月 (2012).

増山文博, 保倉明子, 阿部知子, 平野智也, 寺田靖子, 佐野俊夫: “放射光蛍光Ｘ線分析によるタバコ BY-2 培養細胞における Cd 蓄積機構の解明”, 第 72 回分析化学討論会, (日本分析化学会), 鹿児島大学, 5 月 (2012).

西村実, 森田竜平, 山口博康, 長谷純宏: “イネ品種「ひとめぼれ」のイオンビームおよびガンマ線照射による胚乳アミロースライブラリー育成”, 第８回イオンビーム育種研究会大会, (イオンビーム育種研究会), 高崎, 5 月 (2012).

横堀正敏, 南澤賢, 高橋友哉, 増田こずえ, 林依子, 阿部知子: “清酒酵母の開発”, 第８回イオンビーム育種研究会大会, (イオンビーム育種研究会), 高崎, 5 月 (2012).

高城啓一, 平野智也, 風間裕介, 塚田晃代, 林依子, 阿部知子: “シロイヌナズナ照射根端におけるγ-AtH2AX 分布”, 第８回イオンビーム育種研究会大会, (イオンビーム育種研究会), 群馬県高崎市, 5 月 (2012).

玉木克知, 山中正仁, 小山佳彦, 林依子, 阿部知子: “イオンビーム照射によるキクの花色変異について”, 第８回イオンビーム育種研究会大会, (イオンビーム育種研究会), 高崎, 5 月 (2012).

佐々木克友, 阿部知子, 大坪憲弘: “重イオンビーム照射による有用形質トレニアの作出と原因遺伝子の解明”, 第 51 回ガンマーフィールドシンポジウム, 水戸, 7 月 (2012).

二羽恭介, 阿部知子: “重イオンビーム照射で誘発されたスサビノリ葉状体のモザイク状キメラ”, 日本藻類学会第 36 回大会, (日本藻類学会), 札幌, 7 月 (2012).

大田修平, 松田尚大, 竹下毅, 渡邉光一, 風間裕介, 阿部知子, 河野重行: “単細胞緑藻 Parachlorella kessleri における高増殖能有する重イオン照射株のスクリーニング”, 日本藻類学会第 36 回大会, (日本藻類学会), 札幌, 7 月 (2012).

風間裕介, 石井公太郎, 平野智也, 阿部知子: “重イオンビーム誘発性転換変異体を用いた植物 Y 染色体性決定領域の解析”, 新学術領域「ゲノム支援」２０１２年度 拡大班会議, (文部科学省科学研究費新学術領域研究（研究領域提案型）『生命科学系３分野支援活動』), 御殿場, 8 月 (2012).

平松紘実, 坪内文音, カバノスセローン, 桑田主税, 平野智也, 阿部知子, 奥本裕, 裏出令子, 丸山伸之: “落花生種子貯蔵タンパク質 Ara h 3 の分子構造と特性の解析”, 日本育種学会第 122 回講演会, (日本育種学会), 京都, 9 月 (2012).

安井康夫, 森正之, 相井城太郎, 阿部知子, 佐藤信吾, 田中宥司, 松本大生, 林依子, 大西近江, 大田竜也: “ソバ属の自殖性植物における S-LOCUS EARLY FLOWERING 3 遺伝子の崩壊”, 日本育種学会第 122 回講演会, (日本育種学会), 京都, 9 月 (2012).

相井城太郎, 安井康夫, 森正之, 阿部知子, 佐藤信吾, 田中宥司, 松本大生, 林依子, 大西近江, 大田竜也: “ソバの二花柱性関連遺伝子 S-LOCUS EARLY FLOWERING 3 の同定”, 日本育種学会第 122 回講演会, (日本育種学会), 京都, 9 月 (2012).

西美友紀, 石地耕太朗, 伊東寛史, 阿部知子, 岡和彦: “シンクロトロン光および重イオンビーム照射したイチゴ‘さがほのか’における突然変異率の比較”, 園芸学会平成 24 年度秋季大会, 福井, 9 月 (2012).

石井公太郎, 風間裕介, 青沼航, 川元　章, 阿部知子, 河野重行: “雌雄異株植物ヒロハノマンテマの効率的な染色体標本の作製”, 日本植物形態学会第 24 回総会・大会, (日本植物形態学会), 姫路, 9 月 (2012).

高城啓一, 平野智也, 風間裕介, 林依子, 塚田晃代, 阿部知子: “シロイヌナズナ幼苗根端における放射線照射後の AtH2AX リン酸化”, 日本放射線影響学会第 55 回大会, (日本放射線影響学会), 東北大学, 9 月 (2012).

片野真奈, 風間裕介, 平野智也, 阿部知子, 塚谷裕一, Ferjani A.: “*fugu5* 変異体に見られる補償作用の背景には独自の細胞伸長制御系が存在する”, 日本植物学会第 76 回大会, (日本植物学会), 姫路, 9 月 (2012).

青沼航, 川元　章, 石井公太郎, 風間裕介, 阿部知子, 河野重行: “ヒロハノマンテマの *SlAP3* 欠損変異体を含む Y 染色体部分欠損変異体の網羅的単離”, 日本植物学会第 76 回大会, (日本植物学会), 姫路, 9 月 (2012).

大田修平, 松田尚大, 竹下毅, 水野雄介, 渡邉光一, 平田愛子, 風間裕介, 阿部知子, 河野重行: “クロレラにおけるデンプン・オイル蓄積の動態解析と物質生産変異株の単離ストラテジー”, 日本植物学会第 76 回大会, (日本植物学会), 姫路, 9 月 (2012).

石井公太郎, 青沼航, 西山りゑ, 風間裕介, 阿部知子, 河野重行: “ヒロハノマンテマ性染色体の組換え抑制によって生じた *SlAP3X/Y* 周辺の構造変化”, 日本植物学会第 76 回大会, (日本植物学会), 姫路, 9 月 (2012).

和山真里奈, 松浦葉月, 大田修平, 渡邉光一, 平田愛子, 風間裕介, 阿部知子, 河野重行: “ヘマトコッカスにおけるアスタキサンチン蓄積の電顕三次元動態解析と突然変異体の単離”, 日本植物学会第 76 回大会, (日本植物学会), 姫路, 9 月 (2012).

風間裕介, 石井公太郎, 青沼航, 阿部知子, 河野重行: “ヒロハノマンテマの２つのホモログ遺伝子 *SlSUP* と *SlWUS* の発現と性染色体座乗”, 日本植物学会第 76 回大会, (日本植物学会), 姫路, 9 月 (2012).

馬立秋, 風間裕介, 阿部知子, 田中秀逸, 畠山晋: “鉄イオンビーム照射によって生じた DNA 二本鎖切断の修復機構と変異生成”, 日本遺伝学会第 84 回大会, (日本遺伝学会), 福岡, 9 月 (2012).

風間裕介, 平野智也, 石井公太郎, 大部澄江, 阿部知子: “重イオンビーム突然変異誘発における LET 効果の解析と雌雄異種植物ヒロハノマンテマの性転換変異体ラインの構築”, 木原生物学研究所植物遺伝資源科学研究室プログレスセミナー, (木原生物学研究所植物遺伝資源科学研究室), 横浜, 11 月 (2012).

石井公太郎, 森田竜平, 小暮祥子, 一瀬勝紀, 林依子, 阿部知子: “イネの重イオンビーム照射応答遺伝子の解析”, 東京大学植物生存システム研究室秋学期セミナー, (東京大学植物生存システム研究室), 柏, 12 月 (2012).

佐藤陽一, 平野智也, 阿部知子: “大型褐藻類の育種技術の開発—国内初の品種登録を目指して—”, 東京大学植物生存システム研究室秋学期セミナー, (東京大学植物生存システム研究室), 柏, 12 月 (2012).

風間裕介, 平野智也, 石井公太郎, 大部澄江, 白川侑希, 林祐子, 阿部知子: “重イオンビームによるオンデマンド変異誘発”, 東京大学植物生存システム研究室秋学期セミナー, (東京大学植物生存システム研究室), 柏, 12 月 (2012).

石井公太郎, 森田竜平, 小暮祥子, 林依子, 平野智也, 渋川登美子, 長村吉晃, 阿部知子: “重イオンビーム照射によって誘導されるイネ遺伝子の網羅的解析”, 日本育種学会第 123 回講演会, (日本育種学会), 東京, 3 月 (2013).

風間裕介, 平野智也, 石井公太郎, 大部澄江, 白川侑希, 林祐子, 阿部知子: “重イオンビームを用いたシロイヌナズナタンデム遺伝子破壊ラインの構築”, 日本育種学会第 123 回講演会 , (日本育種学会), 東京, 3 月 (2013).

西浦愛子, 風間裕介, 阿部知子, 新田みゆき, 那須田周平, 村井耕二: “一粒系コムギの極早生突然変異体（*extra early-flowering*）における花成形質と花成関連遺伝子の発現パターンの解析”, 日本育種学会第 123 回講演会, (日本育種学会), 東京, 3 月 (2013).

三橋進也, 風間裕介, 阿部知子, 生方信: “重 イオンビームによる担子菌の変異株作製に関する研究”, 日本農芸化学会 2013 年度大会, (日本農芸化学会), 仙台, 3 月 (2013).

風間裕介, 平野智也, 石井公太郎, 大部澄江, 白川侑希, 林祐子, 阿部知子: “重イオンビームによるオンデマンド変異誘発法の開発とタンデム遺伝子破壊ラインの構築”, 第 54 回日本植物生理学会年会, (日本植物生理学会), 岡山, 3 月 (2013).

本橋健次, 池田時浩, 小島隆夫, 小山貴宏, 鈴木優紀: “低速 Ar^{8+} イオンの ZnO 表面散乱における面極性依存性”, 日本物理学会第 68 回年次大会, (日本物理学), 広島, 3 月 (2013).

加藤恭平, 金衛国, 関口達也, 高木あゆみ, 藤原智, 萱場千尋, 箕輪達哉, 池田時浩, 小林知洋: “マイクロ光ビームの生成に向けたガラスキャピラリーにおける光の透過特性：テーパー角の影響”, 日本物理学会第 68 回年次大会, (日本物理学会), 広島, 3 月 (2013).

平野智也, 風間裕介, 石井公太郎, 大部澄江, 白川侑希, 林祐子, 阿部知子: “重イオンビームにより誘発したシロイヌナズナ変異体の全ゲノム解析”, 日本育種学会第 123 回講演会, (日本育種学会), 東京, 3 月 (2013).

森田竜平, 中川繭, 小暮祥子, 林依子, 東海林英夫, 竹久妃奈子, 佐藤雅志, 阿部知子: “イネ温度感受性 virescent 変異体の解析２”, 日本育種学会第 123 回講演会, (日本育種学会), 東京, 3–3 月 (2013).

RI Applications Team

Publications

[Journal]

(Original Papers) *Subject to Peer Review

Morimoto K., Morita K., Kaji D., Haba H., Katori K., Koura H., Ohnishi T., Ozawa A., Suda T., Sueki K., Tanihata I., Tokanai F., Yoneda A., and Yoshida A.: "Status of super heavy element research using GARIS at RIKEN", Nucl. Phys. A **738**, 129 (2004). *

Kaji D., Morimoto K., Morita K., Hasebe H., Yoshida A., Haba H., and Yoneda A.: "Target for the heaviest element production at RIKEN", Nucl. Instrum. Methods Phys. Res. A **590**, 198 (2007). *

Higurashi Y., Nakagawa T., Kidera M., Haba H., Aihara T., Kase M., Goto A., and Yano Y.: "Production of U beam from RIKEN 18 GHz electron cyclotron resonance ion source", Rev. Sci. Instrum. **79**, No. 2, p. 02C714 (2008). *

Kaji D., Morimoto K., Sato N., Ichikawa T., Ohzeki K., Haba H., Koura H., Ozawa A., Sumita T., Yamaguchi T., Yoneda A., Yoshida A., and Morita K.: "Production and Decay Properties of ^{263}Hs", J. Phys. Soc. Jpn. **78**, No. 3, p. 035001 (2009). *

Sato N., Haba H., Ichikawa T., Kaji D., Kudou Y., Morimoto K., Morita K., Ohzeki K., Sumita T., Yoneda A., Koura H., Ozawa A., Yamaguchi T., and Yoshida A.: "Production and Decay Properties of ^{264}Hs and ^{265}Hs", J. Phys. Soc. Jpn. **80**, 094201 (2011). *

Kaji D., Morita K., Morimoto K., Haba H., and Kudo H.: "Average charge of superheavy recoil ion in helium gas", Proc.Radiochim **1**, 105 (2011). *

Haba H., Kanaya J., Mukai H., Kambara T., and Kase M.: "One-year monitoring of airborne radionuclides in Wako, Japan, after the Fukushima Dai-ichi nuclear power plant accident in 2011", Geochem. J. **46**, 271–278 (2012). *

Taniai T., Wakasugi S., Hashimoto S., Shimada A., Urabe T., Takahashi K., and Takahashi M.: "Elution Behavior and Environmental Impact of Heavy Metals and Rare-Earth Elements from Volcanic Ashes of Mt. Oyama, Miyake Island", International Journal of Environmental Analytical Chemistry **92**, 601–620 (2012). *

Li Z., Toyoshima A., Asai M., Tsukada K., Sato T., Sato N., Kikuchi T., Nagame Y., Schaedel M., Pershina V., Liang X., Kasamatsu Y., Komori Y., Ooe K., Shinohara A., Goto S., Murayama H., Murakami M., Kudo H., Haba H., Takeda Y., Nishikawa M., Yokoyama A., Ikarashi S., Sueki K., Akiyama K., and Kratz J. V.: "Sulfate complexation of element 104, Rf, in H2SO4/HNO3 mixed solution", Radiochim. Acta **100**, 157–164 (2012). *

Higurashi Y., Nakagawa T., Ohnishi J., Haba H., Tamura M., Aihara T., Fujimaki M., Komiyama M., Uchiyama A., and Kamigaito O.: "Results of RIKEN superconducting electron cyclotron resonance ion source with 28GHz", Rev. Sci. Instrum. **83**, No. 2, p. 02A308 (2012). *

Higurashi Y., Nakagawa T., Ohnishi J., Haba H., Tamura M., Aihara T., Fujimaki M., Komiyama M., Uchiyama A., and Kamigaito O.: "Production of a highly charged uranium ion beam with RIKEN superconducting electron cyclotron resonance ion source", Rev. Sci. Instrum. **83**, No. 2, p. 02A333 (2012). *

Hirata J., Takahashi K., and Takahashi M.: "Determination method of multi elements in ferromanganese samples by LA-ICP-MS", Anal. Sci. **29**, 151–155 (2013). *

Asai M., Tsukada K., Sakama M., Haba H., Ichikawa T., Ishii Y., Toyoshima A., Ishii T., Nishinaka I., Nagame Y., Kasamatsu Y., Shibata M., Kojima Y., and Hayashi H.: "Ground-state configuration of the N = 157 nucleus 259No", Phys. Rev. C **87**, No. 014332, pp. 1–6 (2013). *

寺沢薫, 南武志, 武内章記, 高橋和也, 東影悠: "同位体分析法を用いた桜井茶臼山古墳出土朱の産地推定の試み", 奈良県立橿原考古学研究所彙報　青陵 **136**, 1–4 (2012). *

(Review)

羽場宏光: "反跳核分離装置が拓く新元素の化学", Isotope News, No. 702, pp. 2–7 (2012).

羽場宏光: "新元素の化学ー気体充填型反跳核分離装置を用いた新展開ー", 放射線 **38**, No. 2, pp. 73–78 (2012).

[Book・Proceedings]

(Others)

桜井弘, 荒野泰, 上山憲一, 小谷明, 高妻孝光, 佐治英郎, 鈴木晋一郎, 寺嶋孝仁, 中山祐正, 根谷三郎, 羽場宏光, 廣田俊, 藤井敏司, 吉村哲彦: 元素１１１の新知識　第２版増補版, 鈴木　哲, 東京都, (2013).

(Technical Document)

加治大哉, 羽場宏光: "放射化学用語辞典", 放射化学用語辞典, 2006– 日本放射化学会, 東京, (2006).

Oral Presentations

(International Conference etc.)

Higurashi Y., Nakagawa T., Ohnishi J., Haba H., Tamura M., Aihara T., Fujimaki M., Komiyama M., Uchiyama A., and Kamigaito O.: "Developments of RIKEN New Superconducting ECR Ion Source", 1st International Particle Accelerator Conference (IPAC'10), Kyoto, May (2010).

Higurashi Y., Nakagawa T., Ohnishi J., Haba H., Ikezawa E., Fujimaki M., Watanabe Y., Kidera M., Komiyama M., Kase M., Goto A., Kamigaito O., Aihara T., Tamura M., and Uchiyama A.: "Production of U ion beam from RIKEN SC-ECRIS ith sputtering method", 19th International Workshop on ECR Ion Sources (ECRIS 2010), grenoble, France, Aug. (2010).

Higurashi Y., Ohnishi J., Ohzeki K., Haba H., Fujimaki M., Komiyama M., Kamigaito O., Aihara T., Tamura M., and Uchiyama A.: "Production of highly charged uranium ion beam with RIKEN superconducting electron cyclotron resonance ion source", The 14th Int. Conf. on Ion Sources (ICIS11), (INFN-LNS, Italy), Giardini Naxos, Italy, Sept. (2011).

Higurashi Y., Ohnishi J., Ohzeki K., Haba H., Fujimaki M., Komiyama M., Kamigaito O., Aihara T., Tamura M., and Uchiyama A.: "Results of RIKEN superconducting electron cyclotron resonance ion source with 28GHz", The 14th Int. Conf. on Ion Sources (ICIS11), (INFN-LNS, Italy), Giardini Naxos, Italy, Sept. (2011).

Higurashi Y., Ohnishi J., Ohzeki K., Haba H., Fujimaki M., Kidera M., Komiyama M., Kamigaito O., Aihara T., Tamura M., and Uchiyama A.: "RECENT DEVELOPMENTS OF THE RIKEN 28-GHZ SC-ECRIS", 20th International Workshop on Electron Cyclotron Resonance Ion Sources (ECRIS-2012), (Australian Nuclear Science and Technology Organisation), Sydney, Australia, Sept. (2012).

Haba H., Kasamatsu Y., Kikunaga H., Yoneda A., Kanaya J., and Morita K.: "Automated rapid α/SF detection system for studying aqueous chemistry of superheavy elements at RIKEN", EuCheMS International Conference on Nuclear and Radiochemistry (NRC-8), (The European Association for Chemical and Molecular Sciences), Como, Italy, Sept. (2012).

Omtvedt P. J., Ooe K., Schaedel M., Lerum H. V., Toyoshima A., Haba H., Nagame Y., Tsukada K., and Kratz J. V.: "Liquid-phase Studies of Seaborgium using the Automated Liquid-liquid Extraction system SISAK", EuCheMS International Conference on Nuclear and Radiochemistry (NRC-8), (The European Association for Chemical and Molecular Sciences), Como, Italy, Sept. (2012).

Toyoshima A., Ooe K., Asai M., Miyashita S., Sato T., Sato N., Kaneya Y., Kitatsuji Y., Tsukada K., Nagame Y., Schaedel M., Kasamatsu Y., Shinohara A., Haba H., Even J., Omtvedt P. J., and Kratz J. V.: "Redox studies of the heaviest elements using an electrolytic column apparatus", EuCheMS International Conference on Nuclear and Radiochemistry (NRC-8), (The European Association for Chemical and Molecular Sciences), Como, Italy, Sept. (2012).

Haba H., Kaji D., Kanaya J., Kasamatsu Y., Kikunaga H., Kikutani Y., Komori Y., Kudo H., Kudou Y., Morimoto K., Morita K., Murakami M., Nishio K., Ooe K., Ohzeki K., Sakai R., Sato N., Shinohara A., Sumita T., Toyoshima A., Tsukada K., and Yoneda A.: "RIKEN GARIS as a promising interface for superheavy element chemistry -Production of ^{261}Rf, ^{262}Db, and ^{265}Sg for chemical studies using the GARIS gas-jet system-", EuCheMS International Conference on Nuclear and Radiochemistry (NRC-8), (The European Association for Chemical and Molecular Sciences), Como, Italy, Sept. (2012).

Yokoyama A., Shigeyoshi Y., Takeda Y., Araki M., Toyoshima A., Tsukada K., Kasamatsu Y., Kikunaga H., Haba H., and Kanaya J.: "Study on Quadrivalent Chemical Species of Rutherfordium in Aqueous Solution by Means of TTA resin", EuCheMS International Conference on Nuclear and Radiochemistry (NRC-8), (The European Association for Chemical and Molecular Sciences), Como, Italy, Sept. (2012).

Schury P. H., Jeong S., Haba H., Kaji D., Koura H., Ito Y., Mita H., Miyatake H., Morimoto K., Morita K., Naimi S., Nakamura S., Okada K., Ozawa A., Sonoda T., Takamine A., Wollnik H., and Wada M.: "A multi-reflection time of flight mass spectrograph for short-lived nuclei and heavy molecules", International Mass Spectrometry Conference, (Kyoto University), Kyoto, Sept. (2012).

Kanaya J., Haba H., Mukai H., Kambara T., and Kase M.: "Airborne radionuclides measured in Wako, Japan, after the Fukushima Dai-ichi nuclear power plant accident in 2011", EuCheMS International Conference on Nuclear and Radiochemistry (NRC-8), (European Association for Chemical and Molecular Sciences (EuCheMS)), Como, Italy, Sept.–Sept. (2012).

Khandaker M. U., Haba H., Kanaya J., Otuka N., and Mohd H. A.: "Investigations of the ^{nat}Ti(d,x)^{48}V nuclear reactions for beam monitoring purposes", Perfik 2012 - 2012 National Conference on Physics - UKM, (Universiti Kebangsaan Malaysia), Pahang, Malaysia, Nov.–Nov. (2012).

Kaji D., Morimoto K., Sato N., Haba H., Kudou Y., Ohzeki K., Sumita T., Yoneda A., Wakabayashi Y., Murakami M., and Morita K.: "Gas-filled recoil ion separator GARIS-II", 16th International Conference on Electromagnetic Isotope Separators and Techniques Related to their Applications (EMIS2012), Matsue, Dec.–Dec. (2012).

Haba H.: "Experiments on 265Sg at GARIS", 9th ASRC International Workshop "Chemistry of the Superheavy Elements", (Japan Atomic Energy Agency), Wako, Mar. (2013).

(Domestic Conference)

加治大哉, 森田浩介, 森本幸司, 米田晃, 須田利美, 吉田敦, 大西哲哉, 羽場宏光, 末木啓介, 鹿取謙二, 谷畑勇夫: "超重元素探索へ向けた理研ー気体充填型反跳分離装置の性能評価", 日本物理学会, (立教大学), 東京, 9 月 (2002).

加治大哉, 森田浩介, 森本幸司, 米田晃, 須田利美, 吉田敦, 大西哲哉, 羽場宏光, 末木啓介, 鹿取謙二, 谷畑勇夫: "超重元素探索へ向けた理研ー気体充填型反跳分離装置の性能評価", 放射化学討論会, (北海道大学), 北海道, 9 月 (2002).

加治大哉, 森田浩介, 森本幸司, 羽場宏光, 鹿取謙二, 小浦寛之, 大西哲哉, 小沢顕, 須田利美, 末木啓介, 谷畑勇夫, 米田晃, 吉田敦: "ヘリウムガス中における (超) 重元素の平衡電荷", 日本物理学会, (宮崎大学), 宮崎, 9 月 (2003).

加治大哉, 森田浩介, 森本幸司, 羽場宏光, 鹿取謙二, 小浦寛之, 大西哲哉, 小沢顕, 須田利美, 末木啓介, 谷畑勇夫, 米田晃, 吉田敦: "ヘリウムガス中における重い反跳原子の平衡電荷ー理研における Z=111 番元素探索ー", 放射化学討論会,

(京都大学原子炉実験施設), 大阪, 10 月 (2003).

加治大哉, 森田浩介, 森本幸司, 羽場宏光, 小浦寛之, 大西哲哉, 小沢顕, 須田利美, 末木啓介, 山口貴之, 米田晃, 吉田敦: "209Bi+70Zn 反応を用いた 113 番元素探索", 日本化学会, (神奈川大学), 神奈川, 3 月 (2005).

加治大哉, 森田浩介, 森本幸司, 羽場宏光, 小浦寛之, 大西哲哉, 小沢顕, 須田利美, 末木啓介, 山口貴之, 米田晃, 吉田敦: "209Bi(70Zn,n)278113 反応を用いた 113 番元素の合成", 放射化学討論会, (金沢大学), 金沢, 9 月 (2005).

加治大哉, 羽場宏光, 森本幸司, 森田浩介, 佐藤望: "シーボギウム (Sg) の化学研究へ向けた 232Th+40Ar 反応による Sg 同位体の探索", 日本化学会, (日本大学), 千葉, 3 月 (2006).

加治大哉, 森本幸司, 羽場宏光, 市川隆敏, 小浦寛之, 工藤祐生, 小沢顕, 大関和貴, 住田貴之, 山口貴之, 米田晃, 吉田敦, 森田浩介: "新同位体 ^{263}Hs の生成および壊変特性", 放射化学討論会, (日本大学), 神奈川, 9 月 (2009).

加治大哉, 羽場宏光, 笠松良崇, 工藤祐生, 森本幸司, 森田浩介, 大関和貴, 住田貴之, 米田晃, 佐藤望, 若林泰生, 村上昌史, 門叶冬樹, 生井沙織: "GARIS-II 開発の現状と初動試験", 日本物理学会, (新潟大学), 新潟, 3 月 (2010).

日暮祥英, 中川孝秀, 大西純一, 羽場宏光, 藤巻正樹, 池沢英二, 渡邉裕, 加瀬昌之, 後藤彰, 込山美咲, 上垣外修一, 田村匡史, 藍原利光, 内山暁仁: "理研新超電導 ECR イオン源の開発研究", 第 7 回日本加速器学会年会, (日本加速器学会), 姫路, 8 月 (2010).

加治大哉, 羽場宏光, 笠松良崇, 工藤祐生, 森本幸司, 森田浩介, 大関和貴, 住田貴之, 米田晃, 佐藤望, 若林泰生, 村上昌史, 門叶冬樹, 生井沙織: "GARIS-II commissioning 1", 放射化学討論会, (大阪大学), 大阪, 9 月 (2010).

加治大哉, 羽場宏光, 笠松良崇, 工藤祐生, 森本幸司, 森田浩介, 大関和貴, 住田貴之, 米田晃, 小浦寛之, 佐藤望, 門叶冬樹: "中性子欠損領域の新アクチノイド核種 ^{234}Bk および ^{230}Am の観測", 放射化学討論会, (大阪大学), 大阪, 9 月 (2010).

日暮祥英, 中川孝秀, 大西純一, 羽場宏光, 田村匡史, 藍原利光, 藤巻正樹, 込山美咲, 内山暁仁, 上垣外修一: "28GH z　超電導 ECR イオン源の開発", 第 8 回日本加速器学会年会, (日本加速器学会), 筑波, 8 月 (2011).

林依子, 森田竜平, 永野拓馬, 半澤栄子, 東海林英夫, 小暮祥子, 若菜妙子, 白川侑希, 保倉明子, 高橋和也, 佐藤雅志, 阿部知子: "重イオンビーム照射によって誘発したイネ耐塩性突然変異系統の特性比較 2", 日本育種学会第 121 回講演会, (日本育種学会), 宇都宮, 3 月 (2012).

豊嶋厚史, Li Z., 浅井雅人, 佐藤望, 佐藤哲也, 金谷佑亮, 北辻章浩, 大江一弘, 塚田和明, 永目諭一郎, Schaedel M., 笠松良崇, 篠原厚, 羽場宏光, Even J.: "101 番元素メンデレビウム (Md) の酸化還元電位測定", 日本化学会第 92 春季年会, (日本化学会), 横浜, 3 月 (2012).

笠松良崇, 塩原直也, 小森有希子, 菊谷有希, 横北卓也, 木野愛子, 吉村崇, 高橋成人, 菊永英寿, 大槻勤, 三頭聰明, 羽場宏光, 高宮幸一, 篠原厚: "104 番元素 Rf の水酸化物沈殿作成に向けた基礎研究", 日本化学会第 92 春季年会, (日本化学会), 横浜, 3 月 (2012).

脇谷雄一郎, 大坪亜衣, 山元真一, 山田崇裕, 神原正, 羽場宏光, 金谷淳平, 高橋和也: "理研 AVF サイクロトロンを用いた ^{109}Cd の製造に関する検討", 第 49 回アイソトープ・放射線研究発表会, (日本アイソトープ協会), 東京大学弥生講堂, 7–7 月 (2012).

羽場宏光, 笠松良崇, 菊永英寿, 金谷淳平, 米田晃, 森田浩介: "超重元素の溶液化学研究のための自動迅速放射線計測装置の開発", 2012 日本放射化学会年会・第 56 回放射化学討論会, (日本放射化学会), 東京都目黒区, 10 月 (2012).

豊嶋厚史, 宮下直, 大江一弘, 浅井雅人, 佐藤哲也, 塚田和明, 北辻章浩, 永目諭一郎, Schaedel M., Omtvedt P. J., Kratz J. V., 羽場宏光, 笠松良崇, 篠原厚, 和田彩佳, 秋山和彦, 大浦泰嗣, 横山明彦, 末木啓介: "シーボーギウム（Sg）の酸化還元研究にむけた同族元素 Mo と W の電解還元", 2012 日本放射化学会年会・第 56 回放射化学討論会, (日本放射化学会), 東京都目黒区, 10 月 (2012).

大江一弘, 塚田和明, 浅井雅人, 佐藤哲也, 豊嶋厚史, 宮下直, 永目諭一郎, Schaedel M., 金谷佑亮, Lerum H. V., Omtvedt P. J., Kratz J. V., 羽場宏光, 笠松良崇, 篠原厚, 秋山和彦, 大浦泰嗣, 横山明彦, 末木啓介: "Sg の酸化還元研究に向けた迅速溶媒抽出装置 SISAK の改良", 2012 日本放射化学会年会・第 56 回放射化学討論会, (日本放射化学会), 東京都目黒区, 10 月 (2012).

村上昌史, 後藤真一, 羽場宏光, 金谷淳平, 工藤久昭: "^{nat}Zr + p, ^{nat}Hf + p 反応の励起関数測定", 2012 日本放射化学会年会・第 56 回放射化学討論会, (日本放射化学会), 東京都目黒区, 10 月 (2012).

羽場宏光, 大関和貴, 笠松良崇, 加治大哉, 金谷淳平, 菊谷有希, 菊永英寿, 工藤久昭, 工藤祐生, 小森有希子, 酒井隆太郎, 篠原厚, 住田貴之, 豊嶋厚史, 西尾勝久, 村上昌史, 森田浩介, 森本幸司, 米田晃: "GARIS ガスジェット法によるドブニウムの化学実験対象核種 ^{262}Db の製造", 2012 日本放射化学会年会・第 56 回放射化学討論会, (日本放射化学会), 東京都目黒区, 10 月 (2012).

宮下直, 豊嶋厚史, 大江一弘, 浅井雅人, 佐藤哲也, 北辻章浩, 塚田和明, 永目諭一郎, Schaedel M., Omtvedt P. J., Kratz J. V., 羽場宏光, 笠松良崇, 篠原厚, 秋山和彦, 大浦泰嗣, 横山明彦, 末木啓介: "Sg の酸化還元研究に向けた Mo と W の溶媒抽出", 2012 日本放射化学会年会・第 56 回放射化学討論会, (日本放射化学会), 東京都目黒区, 10 月 (2012).

花田貴寿, 福地知則, 神野伸一郎, 羽場宏光, 篠原厚, 渡辺恭良, 榎本秀一: "次世代 PET による複数分子同時イメージングの実証", 第 52 回日本核医学会学術総会, (北海道大学大学院医学研究科　病態情報学講座　核医学分野), 札幌, 10 月 (2012).

加治大哉, 住田貴之, 長谷部裕雄, 田中謙伍, 羽場宏光, 森田浩介, 森本幸司, 若林泰生, 村上昌史, 武山美麗, 山木さやか: "超重元素生成のための新しい標的システム", 2012 日本放射化学会年会・第 56 回放射化学討論会, (日本放射化学会), 東京工業大学, 10–10 月 (2012).

加治大哉, 住田貴之, 刈屋佳樹, 鹿取謙二, 工藤祐生, 森田浩介, 森谷透, 村上昌史, 武山美麗, 田中謙伍, 戸田光祐, 門叶冬樹, 若林泰生, 山木さやか, 米田晃, 大関和貴, 長谷部裕雄, 羽場宏光, 吉田敦, 山口貴之: "208Pb+70Zn 反応を用いた 277Cn の生成と壊変特性", 2012 日本放射化学会年会・第 56 回放射化学討論会, (日本放射化学会), 東京工業大学, 10–10 月 (2012).

金谷淳平, 羽場宏光, 高橋和也, 神原正, 脇谷雄一郎, 山元真一, 大坪亜衣: "理研 AVF サイクロトロンを用いた頒布用 Cd-109 の製造", 2012 日本放射化学会年会・第 56 回放射化学討論会, (日本放射化学会), 東京都目黒区, 10–10 月 (2012).

金谷淳平, 羽場宏光, 向井弘樹, 神原正, 加瀬昌之: "理研和光研究所において観測された福島第一原子力発電所事故由来の放射性核種—事故後 1 年間の大気中放射能濃度変化—", 2012 日本放射化学会年会・第 56 回放射化学討論会, (日本放射化学会), 東京都目黒区, 10–10 月 (2012).

福林新, 竹中文章, 佐々木崇了, 松浦栄次, 神野伸一郎, 羽場宏光, 榎本秀一: "医学応用に向けたジルコニウム-89 の製造及び精製法の確立", 日本薬学会第 133 年会, (日本薬学会), 横浜, 3 月 (2013).

花田貴寿, 福地知則, 神野伸一郎, 篠原厚, 羽場宏光, 渡辺恭良, 榎本秀一: "複数分子同時イメージングが可能な PET 開発とその実証", 日本薬学会第 133 年会, (日本薬学会), 横浜, 3 月 (2013).

User Liaison and Industrial Cooperation Group

Publications Publications

[Journal]

(Original Papers) *Subject to Peer Review

Sakaguchi S., Iseri Y., Uesaka T., Tanifuji M., Amos K., Aoi N., Hashimoto Y., Hiyama E., Ichikawa M., Ichikawa Y., Ishikawa S., Itoh K., Itoh M., Iwasaki H., Karataglidis S., Kawabata T., Kawahara T., Kuboki H., Maeda Y., Matsuo R., Nakao T., Okamura H., Sakai H., Sasamoto Y., Sasano M., Sato Y., Sakaguchi-Sekiguchi K., Shinohara M., Suda K., Suzuki D., Takahashi Y., Tamii A., Wakui T., Yako K., Yamaguchi M., and Yamamoto Y.: "Analyzing power in elastic scattering of 6He from a polarized proton target at 71 MeV/nucleon", Phys. Rev. C **84**, No. 024604, pp. 024604-1–024604-17 (2011). ∗

Tamegai T., Taen T., Yagyuda H., Nakajima Y., Okayasu S., Sasase M., Kitamura H., Murakami T., Kambara T., and Kanai Y.: "Low-field anomaly of vortex dynamics in iron-pnictide superconductors", Physica C **471**, 777–780 (2011). ∗

Yagyuda H., Nakajima Y., Tamegai T., Kanai Y., and Kambara T.: "Critical current density and vortex dynamics in uranium irradiated Co-doped $BaFe_2As_2$", Physica C **471**, 790–793 (2011). ∗

Haba H., Kanaya J., Mukai H., Kambara T., and Kase M.: "One-year monitoring of airborne radionuclides in Wako, Japan, after the Fukushima Dai-ichi nuclear power plant accident in 2011", Geochem. J. **46**, 271–278 (2012). ∗

Hirano T., Kazama Y., Ohbu S., Shirakawa Y., Liu Y., Kambara T., Fukunishi N., and Abe T.: "Molecular nature of mutations induced by high-LET irradiation with argon and carbon ions in *Arabidopsis thaliana*", Muta. Res./Fund. Mol. Mech. Mutagen. **735**, No. 1-2, pp. 19–31 (2012). ∗

Tamegai T., Taen T., Yagyuda H., Tsuchiya Y., Mohan S., Taniguchi T., Nakajima Y., Okayasu S., Sasase M., Kitamura H., Murakami T., Kambara T., and Kanai Y.: "Effects of particle irradiations on vortex states in iron-based superconductors", Supercond. Sci. Technol. **25**, 084008 (2012). ∗

Oral Presentations Oral Presentations

(International Conference etc.)

Ribierre J., Fujihara T., Watanabe S., Matsumoto M., Takaishi K., Muto T., Nakao A., Hashizume D., Muranaka A., Uchiyama M., and Aoyama T.: "Quinoidal oligothiophene derivatives for flexible organic electronic applications", E-MRS 2012 Spring Meeting, (European Materials Research Society), Strasbourg, France, May (2012).

Kanaya J., Haba H., Mukai H., Kambara T., and Kase M.: "Airborne radionuclides measured in Wako, Japan, after the Fukushima Dai-ichi nuclear power plant accident in 2011", EuCheMS International Conference on Nuclear and Radiochemistry (NRC-8), (European Association for Chemical and Molecular Sciences (EuCheMS)), Como, Italy, Sept.–Sept. (2012).

Lin H., Zhu B., Sekine J., Nakao A., Wu Y., Luo S., Yamashita Y., and Yu H.: "Electrically responsive conducting polymer with dynamic coupling to neuron for noninvasively removable bionic devices", 2nd International Conference on Biomaterials Science in Tsukuba (ICBS2013), Tsukuba, Mar. (2013).

(Domestic Conference)

神原正: "理研 RIBF における応用研究と産業利用", 筑波大学複合タンデム加速器施設の新展開 ‐タンデム加速器更新計画と今後の研究展望‐, (筑波大学研究基盤総合センター応用加速器部門), 筑波, 3 月 (2012).

脇谷雄一郎, 大坪亜衣, 山元真一, 山田崇裕, 神原正, 羽場宏光, 金谷淳平, 高橋和也: "理研 AVF サイクロトロンを用いた ^{109}Cd の製造に関する検討", 第 49 回アイソトープ・放射線研究発表会, (日本アイソトープ協会), 東京大学弥生講堂, 7–7 月 (2012).

金谷淳平, 羽場宏光, 高橋和也, 神原正, 脇谷雄一郎, 山元真一, 大坪亜衣: "理研 AVF サイクロトロンを用いた頒布用 Cd-109 の製造", 2012 日本放射化学会年会・第 56 回放射化学討論会, (日本放射化学会), 東京都目黒区, 10–10 月 (2012).

金谷淳平, 羽場宏光, 向井弘樹, 神原正, 加瀬昌之: "理研和光研究所において観測された福島第一原子力発電所事故由来の放射性核種—事故後 1 年間の大気中放射能濃度変化—", 2012 日本放射化学会年会・第 56 回放射化学討論会, (日本放射化学会), 東京都目黒区, 10–10 月 (2012).

林興安, 朱波, 関根淳, 中尾愛子, Wu Y., 羅世強, Yamashita Y., Yu H.: "An Electrochemically Switchable Organic Conducting Biomaterial toward Dynamic Coupling with Cells and Tissues", 日本化学会第 93 春季年会 (2013), (日本化学会), 滋賀県草津市, 3 月 (2013).

User Support Office

Publications

[Journal]

(Original Papers) *Subject to Peer Review

Morimoto K., Morita K., Kaji D., Haba H., Katori K., Koura H., Ohnishi T., Ozawa A., Suda T., Sueki K., Tanihata I., Tokanai F., Yoneda A., and Yoshida A.: "Status of super heavy element research using GARIS at RIKEN", Nucl. Phys. A **738**, 129 (2004). *

Kaji D., Morimoto K., Sato N., Ichikawa T., Ohzeki K., Haba H., Koura H., Ozawa A., Sumita T., Yamaguchi T., Yoneda A., Yoshida A., and Morita K.: "Production and Decay Properties of ^{263}Hs", J. Phys. Soc. Jpn. **78**, No. 3, p. 035001 (2009). *

Sato N., Haba H., Ichikawa T., Kaji D., Kudou Y., Morimoto K., Morita K., Ohzeki K., Sumita T., Yoneda A., Koura H., Ozawa A., Yamaguchi T., and Yoshida A.: "Production and Decay Properties of ^{264}Hs and ^{265}Hs", J. Phys. Soc. Jpn. **80**, 094201 (2011). *

Sakaguchi S., Iseri Y., Uesaka T., Tanifuji M., Amos K., Aoi N., Hashimoto Y., Hiyama E., Ichikawa M., Ichikawa Y., Ishikawa S., Itoh K., Itoh M., Iwasaki H., Karataglidis S., Kawabata T., Kawahara T., Kuboki H., Maeda Y., Matsuo R., Nakao T., Okamura H., Sakai H., Sasamoto Y., Sasano M., Sato Y., Sakaguchi-Sekiguchi K., Shinohara M., Suda K., Suzuki D., Takahashi Y., Tamii A., Wakui T., Yako K., Yamaguchi M., and Yamamoto Y.: "Analyzing power in elastic scattering of 6He from a polarized proton target at 71 MeV/nucleon", Phys. Rev. C **84**, No. 024604, pp. 024604-1–024604-17 (2011). *

Ichikawa Y., Ueno H., Ishii Y., Furukawa T., Yoshimi A., Kameda D., Watanabe H., Aoi N., Asahi K., Balabanski D. L., Chevrier R., Daugas J., Fukuda N., Georgiev G., Hayashi H., Iijima H., Inabe N., Inoue T., Ishihara M., Kubo T., Nanao T., Ohnishi T., Suzuki K., Tsuchiya M., Takeda H., and Rajabali M. M.: "Production of spin-aligned RI beam via two-step fragmentation with dispersion matching", J. Phys.: Conf. Ser. **381**, 012090-1–012090-5 (2012). *

Ichikawa Y., Ueno H., Ishii Y., Furukawa T., Yoshimi A., Kameda D., Watanabe H., Aoi N., Asahi K., Balabanski D. L., Chevrier R., Daugas J., Fukuda N., Georgiev G., Hayashi H., Iijima H., Inabe N., Inoue T., Ishihara M., Kubo T., Nanao T., Ohnishi T., Suzuki K., Tsuchiya M., Takeda H., and Rajabali M. M.: "Production of spin-controlled rare isotope beams", Nat. Phys. **8**, No. 12, pp. 918–922 (2012). *

Sonoda T., Wada M., Tomita H., Sakamoto C., Takatsuka T., Furukawa T., Iimura H., Ito Y., Kubo T., Matsuo Y., Mita H., Naimi S., Nakamura S., Noto T., Schury P. H., Wakui T., Miyatake H., Jeong S., Watanabe Y., Isiyama H., Okada K., and Takamine A.: "Development of a resonant laser ionization gas cell for high-energy, short-lived nuclei", Nucl. Instrum. Methods Phys. Res. B **295**, No. 1, (2012). *

Yoshimi A., Inoue T., Furukawa T., Nanao T., Suzuki K., Chikamori M., Tsuchiya M., Hayashi H., Uchida M., Hatakeyama N., Kagami S., Ichikawa Y., Miyatake H., and Asahi K.: "Low-frequency nuclear spin oscillator of ^{129}Xe with optical spin detector", Phys. Lett. A **376**, No. 24-25, pp. 1924–1929 (2012). *

[Book · Proceedings]

(Others)

Yamaguchi Y., Wakasugi M., Suzuki H., Fujinawa T., Uesaka T., Yano Y., Ozawa A., Nagae D., Yamaguchi T., Suzuki T., Kikuchi T., Jiang W., Sasaki T., and Tokuchi A.: "Present status of Rare-RI Ring project in RIKEN RI Beam Factory", Proceedings of Science (PoS), Frascati, Italy, 2011–10, SISSA, Fascati, p. 070 (2012).

Oral Presentations

(International Conference etc.)

Ichikawa Y., Ueno H., Ishii Y., Furukawa T., Yoshimi A., Kameda D., Watanabe H., Aoi N., Asahi K., Balabanski D. L., Chevrier R., Daugas J., Fukuda N., Georgiev G., Hayashi H., Iijima H., Inabe N., Inoue T., Ishihara M., Kubo T., Nanao T., Ohnishi T., Suzuki K., Tsuchiya M., Takeda H., and Rajabali M. M.: "Spin-aligned RI beams and nuclear moment measurements at RIBF", RIBF Users Meeting 2012, Wako, Saitama, June (2012).

Ichikawa Y., Ueno H., Ishii Y., Furukawa T., Yoshimi A., Kameda D., Watanabe H., Aoi N., Asahi K., Balabanski D. L., Chevrier R., Daugas J., Fukuda N., Georgiev G., Hayashi H., Iijima H., Inabe N., Inoue T., Ishihara M., Kubo T., Nanao T., Ohnishi T., Suzuki K., Tsuchiya M., Takeda H., and Rajabali M. M.: "Spin manipulation of RI beams from two-stage projectile fragmentation reaction", Advanced Studies Institute on Symmetries and Spin (Spin-Praha-2012), (Charles University), Prague, Czech, July (2012).

Ichikawa Y., Chikamori M., Inoue T., Furukawa T., Yoshimi A., Ohtomo Y., Hikota E., Suzuki T., Suzuki K., Nanao T., Miyatake H., Tsuchiya M., Yoshida N., Shirai H., Ino T., Ueno H., Matsuo Y., Fukuyama T., and Asahi K.: "Experimental study of EDM in ^{129}Xe atom using nuclear-spin maser", 6th International Workshop on Fundamental Physics Using Atoms 2012, (Tohoku Iniversity), Sendai, Sept. (2012).

Asahi K., Ichikawa Y., Chikamori M., Inoue T., Furukawa T., Yoshimi A., Ohtomo Y., Suzuki K., Nanao T., Miyatake H., Tsuchiya M., Yoshida N., Shirai H., Matsuo Y., Ueno H., and Fukuyama T.: "Experimental search for EDM in a diamagnetic atom ^{129}Xe with spin oscillator technics", Advanced Studies Institute on Symmetries and Spin (Spin-Praha-2012), (Charles University), Prague, Czech, Sept. (2012).

Asahi K., Ichikawa Y., Chikamori M., Inoue T., Furukawa T., Yoshimi A., Ohtomo Y., Suzuki K., Nanao T., Miyatake H., Tsuchiya M., Yoshida N., Shirai H., Matsuo Y., Ueno H., and Fukuyama T.: "Search for Electric Dipole Moment in ^{129}Xe Atom sing a Nuclear Spin Oscillator", The 20th International Symposium on Spin Physics (SPIN2012), (JINR, Dubna, Russia), Dubna, Russia, Sept. (2012).

Ichikawa Y., Ueno H., Ishii Y., Furukawa T., Yoshimi A., Kameda D., Watanabe H., Aoi N., Asahi K., Balabanski D. L., Chevrier R., Daugas J., Fukuda N., Georgiev G., Hayashi H., Iijima H., Inabe N., Inoue T., Ishihara M., Kubo T., Nanao T., Ohnishi T., Suzuki K., Tsuchiya M., Takeda H., and Rajabali M. M.: "Novel method for the production of spin-aligned RI beams in projectile fragmentation with the dispersion matching technique", The 4th Joint Meeting of the 16th International Conference on Hyperfine Interactions and the 20th International Symposium on Nuclear Quadrupole Interactions (HFI/NQI 2012), (China Institute of Atomic Energy), Beijing, China, Sept. (2012).

Inoue T., Furukawa T., Yoshimi A., Ichikawa Y., Chikamori M., Ohtomo Y., Tsuchiya M., Yoshida N., Shirai H., Uchida M., Suzuki K., Nanao T., Miyatake H., Ueno H., Matsuo Y., Fukuyama T., and Asahi K.: "Nuclear spin maser and experimental search for ^{129}Xe atomic EDM", The 4th Joint Meeting of the 16th International Conference on Hyperfine Interactions and the 20th International Symposium on Nuclear Quadrupole Interactions (HFI/NQI 2012), (China Institute of Atomic Energy), Beijing, China, Sept. (2012).

Yamaguchi Y., Wakasugi M., Ozawa A., Uesaka T., Yano Y., Fujinawa T., Fukunishi N., Inabe N., Kamigaito O., Kase M., Kikuchi T., Komiyama M., Kubo T., Kumagai K., Maie T., Ohnishi J., Tokuchi A., Yoshida K., Yamaguchi T., Nagae D., Zenihiro J., Suzuki T., Abe Y., and Suzaki F.: "Construction of Rare-RI Ring at RIKEN RI Beam Factory", 16th International Conference on Electromagnetic Isotope Separators and Techniques Related to their Applications (EMIS2012), (RIKEN KEK IMP), Matsue, Dec. (2012).

Ichikawa Y., Ueno H., Ishii Y., Furukawa T., Yoshimi A., Kameda D., Watanabe H., Aoi N., Asahi K., Balabanski D. L., Chevrier R., Daugas J., Fukuda N., Georgiev G., Hayashi H., Iijima H., Inabe N., Inoue T., Ishihara M., Kubo T., Nanao T., Ohnishi T., Suzuki K., Tsuchiya M., Takeda H., and Rajabali M. M.: "Spin-aligned RI beams via two-step fragmentation reactions", 16th International Conference on Electromagnetic Isotope Separators and Techniques Related to their Applications (EMIS2012), (RIKEN Nishina Center, KEK, Institute of Modern Physics (China)), Matsue, Dec. (2012).

Nagae D., Abe Y., Okada S., Ozawa A., Yamaguchi T., Suzuki H., Moriguchi T., Ishibashi Y., Fukuoka S., Nishikiori R., Suzuki T., Suzaki F., Yamaguchi Y., Uesaka T., and Wakasugi M.: "Time-of-flight detector applied to mass measurements in Rare-RI Ring", 6th International Conference on Electromagnetic Isotope Separators and Techniques Related to their Applications (EMIS2012), (RIKEN KEK IMP), Matsue, Dec. (2012).

Chikamori M., Ichikawa Y., Ohtomo Y., Hikota E., Sakamoto Y., Suzuki T., Bidinosti C. P., Inoue T., Furukawa T., Yoshimi A., Suzuki K., Nanao T., Miyatake H., Tsuchiya M., Yoshida N., Shirai H., Ino T., Ueno H., Matsuo Y., Fukuyama T., and Asahi K.: "^{3}He comagnetometer in ^{129}Xe active spin maser for EDM measurement", Program on CP violation in Elementary Particles and Composite Systems, (International CEntre for Theoretical Sciences), Mahabaleshwar, India, Feb. (2013).

Ichikawa Y., Chikamori M., Ohtomo Y., Hikota E., Sakamoto Y., Suzuki T., Bidinosti C. P., Inoue T., Furukawa T., Yoshimi A., Suzuki K., Nanao T., Miyatake H., Tsuchiya M., Yoshida N., Shirai H., Ino T., Ueno H., Matsuo Y., Fukuyama T., and Asahi K.: "Experimental search for atomic EDM in ^{129}Xe at Tokyo Tech.", Program on CP violation in Elementary Particles and Composite Systems, (International CEntre for Theoretical Sciences), Mahabaleshwar, India, Feb. (2013).

(Domestic Conference)

加治大哉, 森田浩介, 森本幸司, 米田晃, 須田利美, 吉田敦, 大西哲哉, 羽場宏光, 末木啓介, 鹿取謙二, 谷畑勇夫: "超重元素探索へ向けた理研－気体充填型反跳分離装置の性能評価", 日本物理学会, (立教大学), 東京, 9 月 (2002).

加治大哉, 森田浩介, 森本幸司, 米田晃, 須田利美, 吉田敦, 大西哲哉, 羽場宏光, 末木啓介, 鹿取謙二, 谷畑勇夫: "超重元素探索へ向けた理研－気体充填型反跳分離装置の性能評価", 放射化学討論会, (北海道大学), 北海道, 9 月 (2002).

加治大哉, 森田浩介, 森本幸司, 羽場宏光, 鹿取謙二, 小浦寛之, 大西哲哉, 小沢顕, 須田利美, 末木啓介, 谷畑勇夫, 米田晃, 吉田敦: "ヘリウムガス中における (超) 重元素の平衡電荷", 日本物理学会, (宮崎大学), 宮崎, 9 月 (2003).

加治大哉, 森田浩介, 森本幸司, 羽場宏光, 鹿取謙二, 小浦寛之, 大西哲哉, 小沢顕, 須田利美, 末木啓介, 谷畑勇夫, 米田晃, 吉田敦: "ヘリウムガス中における重い反跳原子の平衡電荷－理研における Z=111 番元素探索－", 放射化学討論会, (京都大学原子炉実験施設), 大阪, 10 月 (2003).

加治大哉, 森田浩介, 森本幸司, 羽場宏光, 小浦寛之, 大西哲哉, 小沢顕, 須田利美, 末木啓介, 山口貴之, 米田晃, 吉田敦: "209Bi+70Zn 反応を用いた 113 番元素探索", 日本化学会, (神奈川大学), 神奈川, 3 月 (2005).

加治大哉, 森田浩介, 森本幸司, 羽場宏光, 小浦寛之, 大西哲哉, 小沢顕, 須田利美, 末木啓介, 山口貴之, 米田晃, 吉田敦: "209Bi(70Zn,n)278113 反応を用いた 113 番元素の合成", 放射化学討論会, (金沢大学), 金沢, 9 月 (2005).

加治大哉, 森本幸司, 羽場宏光, 市川隆敏, 小浦寛之, 工藤祐生, 小沢顕, 大関和貴, 住田貴之, 山口貴之, 米田晃, 吉田敦, 森田浩介: "新同位体 ^{263}Hs の生成および壊変特性", 放射化学討論会, (日本大学), 神奈川, 9 月 (2009).

大友祐一, 市川雄一, 近森正敏, 彦田絵里, 鈴木貴大, Bidinosti C. P., 井上壮志, 古川武, 吉見彰洋, 鈴木都文, 七尾翼, 宮武

裕和, 土屋真人, 吉田直貴, 白井葉月, 猪野隆, 松尾由賀利, 上野秀樹, 福山武志, 旭耕一郎: 中性子物理研究会, (名古屋大学), 名古屋, 11 月 (2012).

坂本雄, Bidinosti C. P., 市川雄一, 近森正敏, 大友祐一, 彦田絵里, 鈴木貴大, 井上壮志, 古川武, 吉見彰洋, 鈴木都文, 七尾翼, 宮武裕和, 土屋真人, 吉田直貴, 白井葉月, 猪野隆, 上野秀樹, 松尾由賀利, 福山武志, 旭耕一郎: "EDM 測定に向けた改良型磁場安定化システムの構築と性能評価", 日本物理学会第 68 回年次大会, (広島大学), 広島, 3 月 (2013).

近森正敏, 市川雄一, 大友祐一, 彦田絵里, 坂本雄, 鈴木貴大, Bidinosti C. P., 井上壮志, 古川武, 吉見彰洋, 鈴木都文, 七尾翼, 宮武裕和, 土屋真人, 吉田直貴, 白井葉月, 猪野隆, 上野秀樹, 松尾由賀利, 福山武志, 旭耕一郎: "^{3}He 共存磁力計の導入による ^{129}Xe 原子 EDM 測定実験", 日本物理学会第 68 回年次大会, (広島大学), 広島, 3 月 (2013).

鈴木貴大, 市川雄一, 近森正敏, 大友祐一, 彦田絵里, 坂本雄, Bidinosti C. P., 井上壮志, 古川武, 吉見彰洋, 鈴木都文, 七尾翼, 宮武裕和, 土屋真人, 吉田直貴, 白井葉月, 猪野隆, 上野秀樹, 松尾由賀利, 福山武志, 旭耕一郎: "^{129}Xe 原子 EDM 測定実験のための電場印加システム開発", 日本物理学会第 68 回年次大会, (広島大学), 広島, 3 月 (2013).

彦田絵里, 近森正敏, 市川雄一, 大友祐一, 坂本雄, 鈴木貴大, Bidinosti C. P., 井上壮志, 古川武, 吉見彰洋, 鈴木都文, 七尾翼, 宮武裕和, 土屋真人, 吉田直貴, 白井葉月, 猪野隆, 上野秀樹, 松尾由賀利, 福山武志, 旭耕一郎: "ダブルセルを用いた核スピンメーザー発振", 日本物理学会第 68 回年次大会, (広島大学), 広島, 3 月 (2013).

市川雄一, 近森正敏, 大友祐一, 彦田絵里, 坂本雄, 鈴木貴大, Bidinosti C. P., 井上壮志, 古川武, 吉見彰洋, 鈴木都文, 七尾翼, 宮武裕和, 土屋真人, 吉田直貴, 白井葉月, 猪野隆, 上野秀樹, 松尾由賀利, 福山武志, 旭耕一郎: "^{129}Xe 原子 EDM 測定実験のための ^{3}He 共存磁力計の性能評価", 日本物理学会第 68 回年次大会, (広島大学), 広島, 3 月 (2013).

大友祐一, 市川雄一, 近森正敏, 彦田絵里, 坂本雄, 鈴木貴大, Bidinosti C. P., 井上壮志, 古川武, 吉見彰洋, 鈴木都文, 七尾翼, 宮武裕和, 土屋真人, 吉田直貴, 白井葉月, 猪野隆, 上野秀樹, 松尾由賀利, 福山武志, 旭耕一郎: "^{129}Xe/^{3}He 共存セルの偏極生成及び緩和機構", 日本物理学会第 68 回年次大会, (広島大学), 広島, 3 月 (2013).

Industrial Cooperation Team

Publications

[Journal]

(Original Papers) *Subject to Peer Review

Morimoto K., Morita K., Kaji D., Haba H., Katori K., Koura H., Ohnishi T., Ozawa A., Suda T., Sueki K., Tanihata I., Tokanai F., Yoneda A., and Yoshida A.: "Status of super heavy element research using GARIS at RIKEN", Nucl. Phys. A **738**, 129 (2004). *

Kaji D., Morimoto K., Morita K., Hasebe H., Yoshida A., Haba H., and Yoneda A.: "Target for the heaviest element production at RIKEN", Nucl. Instrum. Methods Phys. Res. A **590**, 198 (2007). *

Okada K., Wada M., Nakamura T., Takamine A., Lioubimov V., Schury P. H., Ishida Y., Sonoda T., Ogawa M., Yamazaki Y., Kanai Y., Kojima T., Yoshida A., Kubo T., Katayama I., Ohtani S., Wollnik H., and Schuessler H. A.: "A precision measurement of the hyperfine structure of laser-cooled $^{7}Be^{+}$ ions priduced by projectile fragmentation", Phys. Rev. Lett. **101**, No. 212502, pp. 212502-1–212502-4 (2008). *

Kaji D., Morimoto K., Sato N., Ichikawa T., Ohzeki K., Haba H., Koura H., Ozawa A., Sumita T., Yamaguchi T., Yoneda A., Yoshida A., and Morita K.: "Production and Decay Properties of ^{263}Hs", J. Phys. Soc. Jpn. **78**, No. 3, p. 035001 (2009). *

Sato N., Haba H., Ichikawa T., Kaji D., Kudou Y., Morimoto K., Morita K., Ohzeki K., Sumita T., Yoneda A., Koura H., Ozawa A., Yamaguchi T., and Yoshida A.: "Production and Decay Properties of ^{264}Hs and ^{265}Hs", J. Phys. Soc. Jpn. **80**, 094201 (2011). *

Tamura T., Gunji A., Takeichi H., Shigemasu H., Inagaki M., Kaga M., and Kitazaki M.: "Audio-vocal monitoring system revealed by mu-rhythm activity", Front. Psychol. Lang. Sci. **3**, No. 225, (2012). *

Oral Presentations

(International Conference etc.)

Takeichi H., Mitsudo T., Nakajima Y., and Tobimatsu S.: "Electrophysiological correlates of subjective equality and inequality between neighboring time intervals", 12th International Conference on Music Perception and Cognition, Thessaloniki, Greece, July (2012).

Mitsudo T., Nakajima Y., Remijn G. B., Takeichi H., Goto Y., and Tobimatsu S.: "Electrophysiological substrates of auditory temporal assimilation between two neighboring time intervals", 12th International Conference on Music Perception and Cognition, Thessaloniki, Greece, July (2012).

Nakajima Y., Takeichi H., Kidera S., and Ueda K.: "Multivariate analyses of speech signals in singing and nonsinging voices", 12th International Conference on Music Perception and Cognition, Thessaloniki, Greece, July (2012).

Gunji A., Takeichi H., and Inagaki M.: "Voice-specific brain responses: a NIRS study", 30th International Congress of Psychology, (International Union of Psychological Science), Cape Town, South Africa, July (2012).

(Domestic Conference)

加治大哉, 森田浩介, 森本幸司, 米田晃, 須田利美, 吉田敦, 大西哲哉, 羽場宏光, 末木啓介, 鹿取謙二, 谷畑勇夫: "超重元素探索へ向けた理研ー気体充填型反跳分離装置の性能評価", 日本物理学会, (立教大学), 東京, 9 月 (2002).

加治大哉, 森田浩介, 森本幸司, 米田晃, 須田利美, 吉田敦, 大西哲哉, 羽場宏光, 末木啓介, 鹿取謙二, 谷畑勇夫: "超重元素探索へ向けた理研ー気体充填型反跳分離装置の性能評価", 放射化学討論会, (北海道大学), 北海道, 9 月 (2002).

加治大哉, 森田浩介, 森本幸司, 羽場宏光, 鹿取謙二, 小浦寛之, 大西哲哉, 小沢顕, 須田利美, 末木啓介, 谷畑勇夫, 米田晃, 吉田敦: "ヘリウムガス中における (超) 重元素の平衡電荷", 日本物理学会, (宮崎大学), 宮崎, 9 月 (2003).

加治大哉, 森田浩介, 森本幸司, 羽場宏光, 鹿取謙二, 小浦寛之, 大西哲哉, 小沢顕, 須田利美, 末木啓介, 谷畑勇夫, 米田晃, 吉田敦: "ヘリウムガス中における重い反跳原子の平衡電荷ー理研における Z=111 番元素探索ー", 放射化学討論会, (京都大学原子炉実験施設), 大阪, 10 月 (2003).

加治大哉, 森田浩介, 森本幸司, 羽場宏光, 小浦寛之, 大西哲哉, 小沢顕, 須田利美, 末木啓介, 山口貴之, 米田晃, 吉田敦: "209Bi+70Zn 反応を用いた 113 番元素探索", 日本化学会, (神奈川大学), 神奈川, 3 月 (2005).

加治大哉, 森田浩介, 森本幸司, 羽場宏光, 小浦寛之, 大西哲哉, 小沢顕, 須田利美, 末木啓介, 山口貴之, 米田晃, 吉田敦: "209Bi(70Zn,n)278113 反応を用いた 113 番元素の合成", 放射化学討論会, (金沢大学), 金沢, 9 月 (2005).

加治大哉, 森本幸司, 羽場宏光, 市川隆敏, 小浦寛之, 工藤祐生, 小沢顕, 大関和貴, 住田貴之, 山口貴之, 米田晃, 吉田敦, 森田浩介: "新同位体 ^{263}Hs の生成および壊変特性", 放射化学討論会, (日本大学), 神奈川, 9 月 (2009).

竹市博臣, 光藤崇子, 中島祥好, 飛松省三: "多変量解析による時間知覚の脳内機序の解明：時間同化現象の分析", 第 27 回日本生体磁気学会大会, 東京, 5–6 月 (2012).

加治大哉, 住田貴之, 刈屋佳樹, 鹿取謙二, 工藤祐生, 森田浩介, 森谷透, 村上昌史, 武山美麗, 田中謙伍, 戸田光祐, 門叶冬樹, 若林泰生, 山木さやか, 米田晃, 大関和貴, 長谷部裕雄, 羽場宏光, 吉田敦, 山口貴之: "208Pb+70Zn 反応を用いた 277Cn の生成と壊変特性", 2012 日本放射化学会年会・第 56 回放射化学討論会, (日本放射化学会), 東京工業大学, 10–10 月 (2012).

竹市博臣, 中島祥好, 光藤崇子, 飛松省三: "Bhattacharyya 距離を用いた時間知覚に関連する脳磁場の分析", 日本基礎心理学会第 31 回大会, 福岡, 11–11 月 (2012).

光藤崇子, 中島祥好, 廣永成人, 竹市博臣, 飛松省三: "リズム判断時の脳活動：脳磁図による検討", 日本基礎心理学会第 31 回大会, 福岡, 11–11 月 (2012).

中島祥好, 竹市博臣, 木寺沙紀, 上田和夫, 岸田拓也: "朗読音声と歌唱音声との因子分析", 日本基礎心理学会第 31 回大会, 福岡, 11–11 月 (2012).

Safety Management Group

Publications

[Journal]

(Original Papers) *Subject to Peer Review

Tsuchiya H., Enoto T., Yamada S., Yuasa T., Nakazawa K., Kitaguchi T., Kawaharada M., Kokubun M., Kato H., and Makishima K.: "Long-durationgamma-rayemissionsfrom2007and2008winterthunderstorms", J. Geophys. Res. **116**, No. D09113, pp. 1–14 (2011). *

Haba H., Kanaya J., Mukai H., Kambara T., and Kase M.: "One-year monitoring of airborne radionuclides in Wako, Japan, after the Fukushima Dai-ichi nuclear power plant accident in 2011", Geochem. J. **46**, 271–278 (2012). *

Uwamino Y., Sakamoto H., Higurashi R., Mukai H., Fukuda H., and Akashio A.: "A state of the RIKEN radioisotope beam factory", Indian Journal of Pure and Applied Physics **50**, No. 7, pp. 442–445 (2012). *

[Book · Proceedings]

(Original Papers) *Subject to Peer Review

Hagiwara M., Sanami T., Iwamoto Y., Matsuda N., Sakamoto Y., Nakane Y., Nakashima H., Masumoto K., and Uwamino Y.: "Measurement of neutron and gamma-ray yields on thick targets bombarded with 12 MeV protons", Proceedings of the 2011 Symposium on Nuclear Data, JAEA-Conf 2012-001, INDC(JPN)-197, Tokai, 2011–11, Japan Atomic Energy Agency, Tokai, pp. 111–116 (2012). *

(Review)

中村尚司, 飯本武志, 上蓑義朋, 黒澤忠弘, 鈴木敏和, 柚木彰: "はじめての放射線測定 — 正しく理解し、正しく測ろう放射線 —", はじめての放射線測定 — 正しく理解し、正しく測ろう放射線 —, 公益社団法人 日本アイソトープ協会, 東京都, (2012).

Oral Presentations

(International Conference etc.)

Tsuchiya H., Enoto T., Torii T., Kato H., Okano M., and Makishima K.: "Electron Acceleration Induced by Cosmic Rays in Terrestrial Thunderstorm", AOGS (Asia Oceania Geoscience Society) 2010, (AOGS (Asia Oceania Geoscience Society) 2010), Hyderabad, India, July (2010).

Kanaya J., Haba H., Mukai H., Kambara T., and Kase M.: "Airborne radionuclides measured in Wako, Japan, after the Fukushima Dai-ichi nuclear power plant accident in 2011", EuCheMS International Conference on Nuclear and Radiochemistry (NRC-8), (European Association for Chemical and Molecular Sciences (EuCheMS)), Como, Italy, Sept.–Sept. (2012).

(Domestic Conference)

岩田憲一, 土屋晴文, 榎戸輝揚, 山田真也, 湯浅孝行, 川原田円, 北口貴雄, 中澤知洋, 国分紀秀, 加藤博, 岡野眞治, 牧島一夫: "2009 年および 2010 年における雷や雷雲からの放射線観測", 日本物理学会 第 67 回年次大会, (日本物理学会), 西宮市, 3 月 (2012).

岡野眞治, 加藤博, 上蓑義朋, 大津秀暁: "福島原子力発電所事故対応スペクトロメトリー (1) 測定システム", 日本原子力学会 2012 年 秋の大会, (日本原子力学会), 広島, 9 月 (2012).

上蓑義朋, 岡野眞治, 加藤博, 大津秀暁: "福島原子力発電所事故対応スペクトロメトリー（２）スペクトル解析", 日本原子力学会 2012 年 秋の大会, (日本原子力学会), 広島, 9 月 (2012).

金谷淳平, 羽場宏光, 向井弘樹, 神原正, 加瀬昌之: "理研和光研究所において観測された福島第一原子力発電所事故由来の放射性核種—事故後 1 年間の大気中放射能濃度変化—", 2012 日本放射化学会年会・第 56 回放射化学討論会, (日本放射化学会), 東京都目黒区, 10–10 月 (2012).

CNS (Center for Nuclear Study, Graduate School of Science, University of Tokyo)

Publications

[Journal]

(Original Papars) *Subject to Peer Review

Chen J., Chen A.A., Amadio G., Cherubini S., Fujikawa H., Hayakawa S., He J.J., Iwasa N., Kahl D., Khiem L.H., Kubono S., Kurihara S., Kwon Y.K., Cognata M. La., Moon J.Y., Niikura M., Nishimura S., Pearson J., Pizzone R.G., Teranishi T., Togano Y., Wakabayashi Y., Yamaguchi H.: "Strong ^{25}Al+p resonances via elastic proton scattering with a radioactive ^{25}Al beam " Phys. Rev. C **85** (2012) 015805.

Imai N., Hirayama Y., Watanabe Y.X., Teranishi T., Hashimoto T., Hayakawa S., Ichikawa Y., Ishiyama H., Jeong S.C., Kahl D., Kubono S., Miyatake H., Ueno H., Yamaguchi H., Yoneda K., Yoshimi A.: "Isobaric analog resonances of the $N = 21$ nucleus ^{35}Si", Phys. Rev. C **85** (2012) 034313.

Jung H.S., Lee C.S., Kwon Y.K., Moon J.Y., Lee J.H., Yun C.C., Kubono S., Yamaguchi H., Hashimoto T., Kahl D., Hayakawa S., Seonho Choi, Kim M.J., Kim Y.H., Kim Y.K., Park J.S., Kim E.J., Moon C.B., Teranishi T., Wakabayashi Y., Iwasa N., Yamada N.T., Togano Y., Kato S., Cherubini S., Rapisarda: G.G.: "Experimental study of resonant states in ^{27}P via elastic scattering of ^{26}Si+p", Phys. Rev. C **85** (2012) 045802.

Abelev B., *et al.* for the ALICE Collaboration: "Heavy flavour decay muon production at forward rapidity in proton-proton collisions at $\sqrt{s} = 7$ TeV", Phys. Lett. B **708** (2012) 265.

Abelev B., *et al.* for the ALICE Collaboration: "Measurement of Event Background Fluctuations for Charged Particle Jet Reconstruction in Pb-Pb collisions at $\sqrt{s_{NN}} = 2.76$ TeV", JHEP **03** (2012) 053.

Admodt K., *et al.* for the ALICE Collaboration: "Femtoscopy of pp collisions at $\sqrt{s} = 0.9$ and 7 TeV at the LHC with two-pion Bose-Einstein correlations", Phys. Rev. D **84** (2011) 112004.

Abelev B., *et al.* for the ALICE Collaboration: "Measurement of charm production at central rapidity in proton-proton collisions at $\sqrt{s} = 7$ TeV", JHEP **01** (2012) 128.

Abelev B., *et al.* for the ALICE Collaboration: "J/ψ polarization in pp collisions at $\sqrt{s}$=7 TeV", Phys. Rev. Lett. **108** (2012) 082001.

Admodt K., *et al.* for the ALICE Collaboration: "Particle-Yield Modification in Jetlike Azimuthal Dihadron Correlations in Pb-Pb Collisions at $\sqrt{s_{NN}} = 2.76$ TeV", Phys. Rev. Lett. **108** (2012) 092301.

Admodt K., *et al.* for the ALICE Collaboration: "Harmonic decomposition of two particle angular correlations in Pb-Pb collisions at $\sqrt{s_{NN}} = 2.7$ TeV", Phys. Lett. B **708** (2012) 249–264.

Mizusaki T., Shimizu N.: "New variational Monte Carlo method with energy variance extrapolation for large-scale shell-model calculations", Phys. Rev. C **85** (2012) 021301(R).

Doi T., Aoki S., Hatsuda T., Ikeda Y., Inoue T., Ishii N., Murano K., Nemura H., Sasaki K., "Exploring Three-Nucleon Forces in Lattice QCD", Prog. Theor. Phys. **127** (2012) 723.

Doi T., Aoki S., Hatsuda T., Ikeda Y., Inoue T., Ishii N., Murano K., Nemura H., Sasaki K., for the HAL QCD Collaboration: "Two-Baryon Potentials and H-Dibaryon from 3-flavor Lattice QCD Simulations", Nucl. Phys. A **881** (2012) 28.

Chen J., Chen A.A., Amthor A.M., Bazin D., Becerril A.D., Gade A., Galaviz D., Glasmacher T., Kahl D., Lorusso G., Matos M., Ouellet C.V., Pereira J., Schatz H., Smith K., Wales B., Weisshaar D., Zegers R.G.T.: "^{26}Si excited states via one-neutron removal from a ^{27}Si radioactive ion beam", Phys. Rev. C **85** (2012) 045809.

Zhang G.L., Zhang C.L., Zhang H.Q., Lin C.J., Pang D.Y., Wu X.K., Jia H.M., An G.P., Wu Z.D., Xu X.X., Yang F., Liu Z.H., Kubono S., Yamaguchi H., Hayakawa S., Binh D.N., Kwon Y.K., Iwasa N., Mazzocco M., La Commara M., Romoli M., Signorini C.: "Quasi-elastic scattering of the proton drip line nucleus ^{17}F on ^{12}C at 60 MeV", Eur. Phys. J. A **48** (2012) 65.

Kurilkin P.K., Ladygin V.P., Uesaka T., Suda K., Gurchin Uy.V., Isupov A.Yu., Itoh K., Janek M., Karachuk J.T., Kawabata T., Khrenov A.N., Kiselev A.S., Kizka V.A., Krasnov V.A., Ladygina N.B., Livanov A.N., Maeda Y., Malakhov A.I., Piradin S.M., Rezunikov S.G., Sakaguchi S., Sakai H., Sasamoto Y., Sekiguchi K., Shikhale M.A., Vasilie T.A., Witala H.: "Measurement of the vector and tensor analyzing powers for the *dp*-elastic scattering at 880 MeV", Phys. Lett. B **715** (2012) 61–65.

Miki K., Sakai H., Uesaka T., Baba H., Bai C.L., Berg G.P.A., Fukuda N., Kameda D., Kawabata T., Kawase S., Kubo T., Michimasa S., Miya H., Noji S., Ohnishi T., Ota S., Saito A., Sasamoto Y., Sagawa H., Sasano M., Shimoura S., Takeda H., Tokieda H., Yako K., Yanagisawa Y., Zegers R.G.T.: "Identification of the β^+ Isovector Spin Monopole Resonance via the ^{208}Pb and ^{90}Zr(t,^{3}He) Reactions at 300 MeV/u", Phys. Rev. Lett. **108** (2012) 262503.

Sasano M., Sakai H., Yako K., Wakasa T., Dozono M., Rodin V., Faessler A., Fujita K., Greenfield M.B., Hatanaka K., Itoh K., Kawabata T., Kuboki H., Maeda Y., Miki K., Muto K., Noji S., Okamura H., Sakemi Y., Sekiguchi K., Shimizu Y., Sasamoto Y., Tameshige Y., Tamii A., Uesaka T.: "Gamow-Teller transition strengths in the intermediate nucleus of the ^{116}Cd double-β decay by the ^{116}Cd$(p,n)^{116}$In and ^{116}Sn$(n,p)^{116}$In reactions at 300 MeV", Phys. Rev. C **85** (2012) 061301(R).

Uesaka T., Shimoura S., Sakai H.: "The SHARAQ spectrometer", Prog. of Theor. and Exp. Phys. (2012)

03C007.

Takeuchi S., Matsushita M., Aoi N., Doornenbal P., Li K., Motobayashi T., Scheit H., Steppenbeck D., Wang H., Baba H., Bazin D., Caceres L., Crawford H., Fallon P., Gernhauser R., Gibelin J., Go S., Grevy S., Hinke C., Hoffman C.R., Hughes R., Ideguchi E., Jenkins D., Kobayashi N., Kondo Y., Krucken R., Bleis T.Le, Lee J., Lee G., Matta A., Michimasa S., Nakamura T., Ota S., Petri M., Sako T., Sakurai H., Shimoura S., Steiger K., Takahashi K., Takechi M., Togano Y., Winkler R., Yoneda K.: "Well Developed Deformation in ^{42}Si", Phys. Rev. Lett. **109** (2012) 182501.

Togano Y., Yamada Y., Iwasa N., Yamada K., Motobayashi T., Aoi N., Baba H., Bishop S., Cai X., Doornenbal P., Fang D., Furukawa T., Ieki K., Kawabata T., Kanno S., Kobayashi N., Kondo Y., Kuboki T., Kume N., Kurita K., Kurokawa M., Ma Y.G., Matsuo Y., Murakami H., Matsushita M., Nakamura T., Okada K., Ota S., Satou Y., Shimoura S., Shioda R., N. Tanaka K., Takeuchi S., Tian W., Wang H., Wang J., Yoneda K.: "Hindered Proton Collectivity in $^{28}_{16}$S$_{12}$: Possible Magic Number at $Z = 16$", Phys. Rev. Lett. **108** (2012) 222501.

Tshoo K., Satou Y., Bhang H., Choi S., Nakamura T., Kondo Y., Deguchi S., Kawada Y., Kobayashi N., Nakayama Y., Tanaka K.N., Tanaka N., Aoi N., Ishihara M., Motobayashi T., Otsu H., Sakurai H., Takeuchi S., Togano Y., Yoneda K., Li Z.H., Delaunay F., Gibelin J., Marques F.M., Orr N.A., Honda T., Matsushita M., Kobayashi T., Miyashita Y., Sumikama T., Yoshinaga K., Shimoura S., Sohler D., Zheng T., Cao Z.X.: "N=16 Spherical Shell Closure in ^{24}O", Phys. Rev. Lett. **102** (2012) 022501.

Steppenbeck D., Janssens R.V.F., Freeman S.J., Carpenter M.P., Chowdhury P., Deacon A.N., Honma M., Jin H., Lauritsen T., Lister C.J., Meng J., Peng J., Seweryniak D., Smith J.F., Sun Y., Tabor S.L., Varley B.J., Yang Y.-C., Zhang S.Q., Zhao P.W., Zhu S.: "Magnetic rotation and quasicollective structures in ^{58}Fe: Influence of the $\nu g_{9/2}$ orbital", Phys. Rev. C **85** (2012) 044316.

Akamatsu Y., Hamagaki H., Hatsuda T., Hirano T.: "Low-mass dilepton production through transport process in quark-gluon plasma", Phys. Rev. C **85** (2012) 054903.

Abelev B., *et al.* for the ALICE Collaboration: = 7 TeV", Phys. Lett. B **708** (2012) 265.

Abelev B., *et al.* for the ALICE Collaboration: "Measurement of Event Background Fluctuations for Charged Particle Jet Reconstruction in Pb-Pb collisions at $\sqrt{s_{NN}}$ = 2.76 TeV", JHEP **03** (2012) 053.

Abelev B., *et al.* for the ALICE Collaboration: "Light vector meson production in pp collisions at $\sqrt{s} = 7$ TeV", Phys. Lett. B **710** (2012) 557–568.

Abelev B., *et al.* for the ALICE Collaboration: "Multi-strange baryon production in pp collisions at $\sqrt{s} =$ 7 TeV with ALICE", Phys. Lett. B **712** (2012) 309.

Abelev B., *et al.* for the ALICE Collaboration: "Underlying Event measurements in pp collisions at $\sqrt{s} = 0.9$ and 7 TeV with the ALICE experiment at the LHC", JHEP **1207** (2012) 116.

Abelev B., *et al.* for the ALICE Collaboration: "Measurement of charm production at central rapidity in proton proton collisions at $\sqrt{s} = 2.76$ TeV", JHEP **1207** (2012) 191.

Abelev B., *et al.* for the ALICE Collaboration: "J/ψ suppression at forward rapidity in Pb-Pb collisions at $\sqrt{s_{NN}}$ = 2.76 TeV", Phys. Rev. Lett. **109** (2012) 072301.

Abelev B., *et al.* for the ALICE Collaboration: "Transverse sphericity of primary charged particles in minimum bias proton-proton collisions at $\sqrt{s} = 0.9$, 2.76 and 7 TeV", Eur. Phys. J. C **72** (2012) 2124.

Abelev B., *et al.* for the ALICE Collaboration: "Production of muons from heavy flavour decays at forward rapidity in pp and Pb–Pb collisions a t $\sqrt{s_{\rm NN}} = 2.76$ TeV", Phys. Rev. Lett. **109** (2012) 112301.

Abelev B., *et al.* for the ALICE Collaboration: "Suppression of high transverse momentum prompt D mesons in central Pb–Pb collisions at $\sqrt{s_{NN}} = 2.76$ TeV", JHEP **9** (2012) 112.

Abelev B., *et al.* for the ALICE Collaboration: "Neutral pion and eta meson production in proton-proton collisions at $\sqrt{s} = 0.9$ TeV and 7 TeV", Phys. Lett. B **717** (2012) 162–172.

Abelev B., *et al.* for the ALICE Collaboration: "K0s-K0s correlations in 7 TeV pp collisions from the LHC ALICE experiment", Phys. Lett. B **717** (2012) 151–161.

Abelev B., *et al.* for the ALICE Collaboration: "Production of K*(892)0 and phi(1020) in pp collisions at $\sqrt{s} = 7$ TeV", Eur. Phys. J. C **72** (2012) 2183.

Abelev B., *et al.* for the ALICE Collaboration: "Rapidity and transverse momentum dependence of inclusive J/ψ production in pp collisions at $\sqrt{s} = 7$ TeV", Phys. Lett. B **718** (2012) 692698.

Abelev B., *et al.* for the ALICE Collaboration: "Ds meson production at central rapidity in proton–proton collisions at $\sqrt{s} = 7$ TeV", Phys. Lett. B **718** (2012) 279–294.

Adare A., *et al.* for the PHENIX Collaboration: "Cold-nuclear-matter effcts on heavy-quark production in d+Au collisions at $\sqrt{s_{NN}} = 200$ GeV", Phys. Rev. Lett. **109** (2012) 242301.

Adare A., *et al.* for the PHENIX Collaboration: "Measurement of Transverse Single-Spin Asymmetries for J/psi Production in Polarized p+p Collisions at $\sqrt{s} =$ 200 GeV (and Erratum)" , Phys. Rev. D **86** (2012) 099904.

Adare A., *et al.* for the PHENIX Collaboration: "Measurement of Direct Photons in Au+Au Collisions at $\sqrt{s_{NN}} = 200$ GeV", Phys. Rev. Lett. **109** (2012) 152302.

Adare A., *et al.* for the PHENIX Collaboration: "Evolution of π^0 suppression in Au+Au collisions from $\sqrt{s_{NN}}$ = 39 to 200 GeV", Phys. Rev. Lett. **109** (2012) 152301.

Adare A., *et al.* for the PHENIX Collaboration: "Observation of direct-photon collective flow in Au+Au collisions at $\sqrt{s_{NN}}$ = 200GeV", Phys. Rev. Lett. 109, 122302 (2012)

Adare A., *et al.* for the PHENIX Collaboration: "Nuclear-Modification Factor for Open-Heavy-Flavor Production at Forward Rapidity in Cu+Cu Collisions at $\sqrt{s_{NN}}$ =200 GeV", Phys. Rev. C 86, 024909 (2012)

Adare A., *et al.* for the PHENIX Collaboration: "Deviation from quark-number scaling of the anisotropy parameter v_2 of pions, kaons, and protons in Au+Au collisions at $\sqrt{s_{NN}}$ = 200 GeV", Phys. Rev. C 85, 064914 (2012)

Adare A., *et al.* for the PHENIX Collaboration: "Ground and excited charmonium state production in p+p collisions at $\sqrt{s}$ =200 GeV", Phys. Rev. D 85, 092004 (2012)

Holt J.D., Otsuka T., Schwenk A., Suzuki T.: "Three-body forces and shell structure in calcium isotopes", J. Phys. G **39** (2012) 085111.

Suzuki T., Yoshida T., Kajino T., Otsuka T.: "Beta Decays of isotones with neutron magic number of N=126 and r-process nucleosynthesis", Phys. Rev. C **85** (2012) 015802.

Diffenderfer E.S., Baby L.T., Santiago-Gonzalez D., Ahsan N., Rojas A., Volya A., Wiedenhover I., Wuosmaa A.H., Carpenter M.P., Janssens R.V.F., Lister C.J., Devlin M., Sarantites D.G., Sobotka L.G., Utsuno Y., Horoi M.: "High-spin spectrum of 24Mg studied through multiparticle angular correlations", Phys. Rev. C **85** (2912) 034311.

Kotila J., Nomura K., Guo L., Shimizu N., Otsuka T.: "Shape phase transitions in the interacting boson model: Phenomenological versus microscopic descriptions", Phys. Rev. C **85** (2012) 054309.

Shimizu N., Utsuno Y., Mizusaki T., Honma M., Tsunoda Y., Otsuka T.: "Variational procedure for nuclear shell-model calculations and energy-variance extrapolation", Phys. Rev. C **85** (2012) 054301.

Utsuno Y., Mizusaki T., Brown B.A., Honma M., Mizusaki T., Shimizu N.: "Shape transitions in exotic Si and S isotopes and tensor-force-driven Jahn-Teller effect", Phys. Rev. C **86** (2012) 051301(R).

Lang L., Otsuka T., Shimizu N., Utsuno Y., Roth R.: "No-core Monte Carlo shell model calculation for ^{10}Be and ^{12}Be low-lying spectra", Phys. Rev. C **86** (2012) 014302.

Bauer C., Behrens T., Bildstein V., Blazhev A., Bruyneel B., Butterworth J., Clement E., Coquard L., Egido J.L., Ekstrom A., Fitzpatrick C.R., Fransen C., Gernhauser R., Habs D., Hess H., Leske J., Kroll T., Krucken R., Lutter R., Marley P., Moller T., Otsuka T., Patronis N., Petts A., Pietralla N., Rodriguez T.R., Shimizu N., Stahl C., Stefanescu I., Stora T., Thirolf P.G., Voulot D., Walle J. van de, Warr N., Wenander F., Wiens A.: "Prolate shape of ^{140}Ba from a first combined Doppler-shift and Coulomb-excitation measurement at the REX-ISOLDE facility", Phys. Rev. C **86** (2012) 034310.

Nomura K., Rodriguez-Guzman R., Robledo L.M., Shimizu N.: "Shape coexistence in Lead isotopes in the interacting boson model with Gogny energy density functional", Phys. Rev. C **86** (2012) 034322.

Abe T., Maris P., Otsuka T., Shimizu N., Utsuno Y., Vary J.P.: "Benchmarks of the ab initio FCI, MCSM and NCFC methods", Phys. Rev. C **86** (2012) 054301.

Shimizu N., Abe T., Tsunoda Y., Utsuno Y., Yoshida T., Mizusaki T., Honma M., Otsuka T.: "New generation of the Monte Carlo shell model for the K computer era", Prog. Theor. Exp. Phys. bf 2012(1) (2012) 01A205.

Nomura K., Shimizu N., Vretenar D., Niksic T., Otsuka T.: "Robust regularity in γ-soft nuclei and its microscopic realization", Phys. Rev. Lett. **108** (2012) 132501.

Shimada K., Ueno H., Neyens G., Asahi K., Balabanski D.L., Daugas J.M., Depuydt M., Rydt M.De, Gaudefroy L., Grevy S., Hasama Y., Ichikawa Y., Kameda D., Morel P., Nagatomo T., Perrot L., Stodel Ch., Thomas J.-C., Utsuno Y., Vanderheijden W., Vermeulen N., Vingerhoets P., Yagi E., Yoshida K., Yoshimi A.: "Erosion of N=20 shell in ^{33}Al investigated through the ground-state electric quadrupole moment", Phys. Lett. B **714** (2012) 246–250.

[Book Proceedings]

(Original Papars) *Subject to Peer Review

Doi T., for HAL QCD Collaboration: "The Lattice QCD Study of the Three-Nucleon Force", Proc. 19th Particles and Nuclei Int. Conf. (PANIC11), AIP Conf. Proc. **1441** (2012) 399–401.

Itahashi K., Berg G.P.A., Fujioka H., Geissel H., Hayano R.S., Hirenzaki S., Ikeno N., Inabe N., Itoh S., Kameda D., Kubo T., Matsubara H., Michimasa S., Miki K., Miya H., Nakamura M., Nishi T., Noji S., Ota S., Suzuki K., Takeda H., Todoroki K., Tsukada K., Uesaka T., Weick H., Yoshida K., "Measurement of Pionic ^{121}Sn atoms at the RI beam factory", Hyperfine Interact. **209** (2012) 51–56.

Hamagaki H.,: "High Energy Density QCD – Experimental Overview –", Proc. of the 41th Int. Symp. on Multiparticle Dynamics (ISMD 2011), Sep. 26–30, 2011, Miyajima, Hiroshima, Japan, Prog. Theor. Phys. Suppl. **193** (2012) 79–88.

Uesaka T., Matsubara H., Miki K., Noji S., Sakai H., Sasamoto Y., Shimoura S., Takaki M., Yako K.: for the SHARAQ Collaboration: "New Experimental Studies of Nuclear Spin-Isospin Responses", Proc. of Frontier Issues in Physics of Exotic Nuclei (YKIS2011), Prog. Theor. Phys. Suppl. **196** (2012) 150–157.

Ebata S., Nakatsukasa T., Inakura T.,: "Cb-TDHFB calculation for the low-lying E1 strength of heavy nuclei

around the r-process path", Proc. of Frontier Issues in Physics of Exotic Nuclei (YKIS2011), Prog. Theor. Phys. Suppl. **196** (2012) 316–321.

Ideguchi E., Ota S., Morikawa T., Oshima M., Koizumi M., Toh Y., Kimura A., Harada H., Furutaka K., Nakamura S., Kitatani F., Hatsukawa Y., Shizuma T., Sugawara M., Watanabe Y.X., Hirayama Y., Oi M.: "Superdeformed Band in Asymmetric $N > Z$ Nucleus, Ar-40 and High-Spin States in A=30 similar to 40 Nuclei", Proc. of Frontier Issues in Physics of Exotic Nuclei (YKIS2011), Prog. Theor. Phys. Suppl. **196** (2012) 427–432.

Utsuno Y., Otsuka T., Brown B.A., Honma M., Mizusaki T., Shimizu N.: "Shell evolution around and beyond N=28 studied with large-scale shell- model calculations", Proc. of Frontier Issues in Physics of Exotic Nuclei (YKIS2011), Prog. Theor. Phys. Suppl. **196** (2012) 304–309.

Wang Y.B., Guo B., Jin S.J., Li Z.H., Binh D.N., Hashimoto H., Hayakawa S., He J.J., Hu J., Iwasa N., Kahl D.M., Kubono S., Kume N., Li E.T., Li Y.J., Liu X., Su J., Xu S.W., Yamaguchi H., Yan S.Q., Zeng S., Bai X.X., Lian G., Wang B.X., Liu W.P.: "Indirect measurements of reactions in hot p-p chain and CNO cycles", The 11th Int. Symp. on Origin of Matter and Evolution of Galaxies (OMEG2011), AIP Conf. Proc. **1484** (2012) 19–24.

Binh D.N., Kubono S., Yamaguchi H., Hayakawa S., Hashimoto T., Kahl D., Teranishi T., Iwasa N., Kato S., Khiem L.H., Tho N.T., Wakabayashi Y.: "Measurement of ^{21}Na(α, p)^{24}Mg stellar reaction using a ^{21}Na RI-beam", The 11th Int. Symp. on Origin of Matter and Evolution of Galaxies (OMEG2011), AIP Conf. Proc. **1484** (2012) 25–30.

Otsuka T., Suzuki T.: "Nuclear forces, exotic nuclei and stellar evolution", The 11th Int. Symp. on Origin of Matter and Evolution of Galaxies (OMEG2011), AIP Conf. Proc. **1484** (2012) 45–46.

Nakatsukasa T., Inakura T., Avogadro P., Ebata S., Sato K., Yabana K.: "Linear-response calculation in the time-dependent density functional theory ", The 11th Int. Symp. on Origin of Matter and Evolution of Galaxies (OMEG2011), AIP Conf. Proc. **1484** (2012) 142–149.

Sumikama T., Yoshinaga K., Watanabe H., Nishimura S., Miyashita Y., Yamaguchi K., Sugimoto K., Chiba J., Li Z., Baba H., Berryman J.S., Blasi N., Bracco A., Camera F., Doornenbal P., Go S., Hashimoto T., Hayakawa S., Hinke C., Ideguchi E., Isobe T., Ito Y., Jenkins D.G., Kawada Y., Kobayashi N., Kondo Y., Krucken R., Kubono S., Lorusso G., Nakano T., Kurata-Nishimura M., Odahara A., Ong H.J., Ota S., Podolyak Z., Sakurai H., Scheit H., Steiger K., Steppenbeck D., Takano S., Takashima A., Tajiri K., Teranishi T., Wakabayashi Y., Walker P.M., Wieland O., Yamaguchi H.: "Search for spin-orbit-force reduction at ^{106,108}Zr around r-process path", The 11th Int. Symp. on Origin of Matter and Evolution of Galaxies (OMEG2011), AIP Conf. Proc. **1484** (2012) 156–160.

Kubono S., Binh D.N., Hayakawa S., Hashimoto T., Kahl D.M., Yamaguchi H., Wakabayashi Y., Teranishi T., Iwasa N., Komatsubara T., Kato S., Chen A., Cherubini S., Choi S.H., Hahn I.S., He J.J., Khiem L.H., Lee C.S., Kwon Y.K., Wanajo S., Janka H.T.: "Experimental challenge to nuclear physics problems in the nu p-process", The 11th Int. Symp. on Origin of Matter and Evolution of Galaxies (OMEG2011), AIP Conf. Proc. **1484** (2012) 189–196.

Nishimura S., for the RIBF Decay Collaboration: "Beta-decay spectroscopy relevant to the r-process nucleosynthesis", The 11th Int. Symp. on Origin of Matter and Evolution of Galaxies (OMEG2011), AIP Conf. Proc. **1484** (2012) 209–216.

Yamaguchi H., Kahl D., Hu J., Kubono S., Hayakawa S., Hashimoto T.: "Alpha-induced reaction studies using low-energy RI beams at CRIB", The 11th Int. Symp. on Origin of Matter and Evolution of Galaxies (OMEG2011), AIP Conf. Proc. **1484** (2012) 225–231.

Shimoura S.: "Spin-Isospin responses via charge exchange reactions of RI beams at SHARAQ", The 11th Int. Symp. on Origin of Matter and Evolution of Galaxies (OMEG2011), AIP Conf. Proc. **1484** (2012) 253–256.

Cherubini S., Gulino M., Rapisarda G.G., Spitaleri C., Cognata M.L., Lamia L., Kubono S., Yamaguchi H., Hayakawa S., Wakabayashi Y., Iwasa N., Kato S., Komatsubara H., Teranishi T., Coc A., Sereville N.D., Hammache F.: "Trojan Horse Method and RIBs: The ^{18}F(p, α)^{15}O reaction at astrophysical energies" The 11th Int. Symp. on Origin of Matter and Evolution of Galaxies (OMEG2011), AIP Conf. Proc. **1484** (2012) 293–300.

Suzuki T., Yoshida T., Kajino T., Otsuka T.: "First-forbidden transitions in N=126 isotones and r-process nucleosynthesis ", The 11th Int. Symp. on Origin of Matter and Evolution of Galaxies (OMEG2011), AIP Conf. Proc. **1484** (2012) 363–364.

Yoshida T., Itagaki N., and Katö K.: "Symplectic structure and transition properties of ^{12}C", The 11th Int. Symp. on Origin of Matter and Evolution of Galaxies (OMEG2011), AIP Conf. Proc. **1484** (2012) 424–426.

Ebata S., Nakatsukasa T., Inakura T.: "Systematic study of low-lying E1 strength using the time-dependent mean field theory", The 11th Int. Symp. on Origin of Matter and Evolution of Galaxies (OMEG2011), AIP Conf. Proc. **1484** (2012) 427–429.

Hayakawa S., Kubono S., Kahl D., Yamaguchi H., Binh D.N., Hashimoto T., Wakabayashi Y., He J.J., Iwasa N., Kato S., Komatsubara T., Kwon Y.K., Teranishi T.: "Direct measurement of the breakout reaction ^{11}C(α, p)^{14}N in explosive hydrogen-burning process", The 11th Int. Symp. on Origin of Matter and Evolution of Galaxies (OMEG2011), AIP Conf. Proc. **1484** (2012) 445–447.

Hashimoto T., Kubono S., Yamaguchi H., Hayakawa S., Kahl D.M., Ota S., Michimasa S., Tokieda H., Ishiyama H., Watanabe Y.X., Hirayama Y., Imai N., Miyatake H., Jeong S.C., Yamaguchi K., Arai I., Komatsubara T., Fukuda T., Mizoi Y., Das S.K., Iwasa N., Yamada T., Chen A.A., He J.J.: "Direct measurement of the ^{18}Ne(α, p)^{21}Na reaction", The 11th Int. Symp. on Origin of Matter and Evolution of Galaxies (OMEG2011), AIP Conf. Proc. **1484** (2012) 454–456.

Otsuka T.: "Interacting boson model and nucleons ", of his 70th birthday, AIP Conf. Proc. **1488** 445 (2012).

Nakatsukasa T., Ebata S., Avogadro P., Guo L., Inakura T., Yoshida K.: "Density functional approaches to nuclear dynamics", Proc. XXXVth Symp. on Nucl. Phys., J. Phys. Conf. Ser. **387** (2012) 012015.

Yoshikawa A., Tamagawa T., Iwahashi T., Asami F., Takeuchi Y., Hayato A., Hamagaki H., Gunji T., Akimoto R., Nukariya A., Hayashi S., Ueno K., Ochi A., Oliveira R.: "Development of Resistive Electrode Gas Electron Multiplier (RE-GEM)", 2nd Int. Conf. on Micro Pattern Gaseous Detectors (MPGD2011), Aug. 29–Sep. 1, 2011, Maiko, Kobe, Japan, JINST **7** (2012) C06006.

Hayashi S., Hamagaki H., Gunji T., Tanaka M., Ikeda H.: "Development of a Wide-Dynamic Range Front-End ASIC for W + Si calorimeter", Proceedings of the 2012 IEEE Nuclear Science Symp. and Medical Imaging Conf. Oct. 29–Nov. 3, 2012, Disneyland Hotel, Anaheim, USA, Conf. Record (2012) 576–580.

Sekiguchi Y., Tokieda H., Ota S., Michimasa S., Dozono M., Tamagawa T., Gunji T., Yamaguchi H., Hamagaki H., Tamagawa T., Uesaka T.: "Performance of GEM with Deuterium Gas and GEM with Glass Insulator", at the 2012 IEEE Nuclear Science Symp. and Medical Imaging Conf., Oct. 29–Nov. 3, 2012, Disneyland Hotel, Anaheim, USA, Conf. Record (2012) 1772–1774.

Sekiguchi Y., Gunji T., Hamagaki H., Hayashi S., Hori Y.: "Development of W+Si Based Electromagnetic Calorimeter for the Upgrade of the LHC-ALICE Experiment", at the 2012 IEEE Nuclear Science Symp. and Medical Imaging Conf., Oct. 29–Nov. 3, 2012, Disneyland Hotel, Anaheim, USA, Conf. Record (2012) 1854–1856.

Itahashi K., Berg G.P.A., Fujioka H., Geissel H., Hayano R.S., Hirenzaki S., Ikeno N., Inabe K., Itoh S., Kameda D., Kubo T., Matsubara H., Michimasa S., Miki K., Miya H., Nakamura M., Nishi T., Noji S., Ota S., Suzuki K., Takeda H., Todoroki K., Tsukada K., Uesaka T., Weick H., Yoshida K.: "First pionic atom spectroscopy at RIBF", Proc. 12th Int. Workshop on Production, Properties and Interactions of MESONS (MESON2012), Eur. Phys. J. Web Conf. **37** (2012) 01013.

Oral Presentations

(International Conference etc.)

Yamaguchi H. (Poster): "Recent astrophysical studies at the low-energy RI beam separator CRIB", XII International Symposium on Nuclei in the Cosmos (NIC-XII), Aug. 6–11, 2012, Cairns Convention Centre, Cairns, Australia.

Kahl D. (Poster): "Measurement of the ^{30}S+α System for Type-I X-ray Bursts", XII International Symposium on Nuclei in the Cosmos (NIC-XII), Aug. 6–11, 2012, Cairns Convention Centre, Cairns, Australia.

Yamaguchi H. (Oral): "Experimental studies on supernova nucleosynthesis in low-mass and proton-rich region", 1st Visiting NAOJ Fellow Workshop Element Genesis and Cosmic Chemical Evolution: r-process perspective, Oct. 17–19, 2012, RIKEN, Wako, Saitama, Japan.

Yamaguchi H. (Oral): "Studying alpha-cluster structure using low-energy RI beams at CRIB", RIKEN HPCI workshop on alpha-particle condensation, Nov. 13–19, 2012, RIKEN, Wako, Saitama, Japan.

Yamaguchi H. (Oral): "Studying nuclear reactions with the low-energy RI beam separator CRIB", 7th Italy-Japan symposium on Nuclear Physics, Nov. 20–23, 2012, University of Milano, Milano, Italy.

Yamaguchi H. (Oral): "Recent developments and reseach projects at the low-energy RI beam facility CRIB", 16th International Conference on Electromagnetic Isotope Separators and Techniques Related to their Applications (EMIS2012), Dec. 2–7, 2012, Matsue, Shimane, Japan.

Nakao T. (Poster): "Measurement of the ^{30}S+α System Using an Active Target", Applications (EMIS2012), Dec. 2–7, Matsue, Shimane, Japan.

Yamaguchi H. (Oral): "CRIB – a low energy RI beam facility of CNS", RIBF Users Meeting 2012, Jun 20–21, 2012, RIKEN, Wako, Saitama, Japan.

Ota S. (Oral): "Capability of cns active target for the (d,p) reactions in inversekinematics", RIBF ULIC mini-workshop on radiative neutron capture reactions for r-process, Jul. 26, 2012, RIKEN.

Ota S. (Oral): "Possibility of forward angle measurement in use of cns active target", Towards forward angle inelastic scattering experiments at RIBF, Apr. 4, 2012, RIKEN, Saitama, Japan.

Ota S. (Oral): "Charge exchange reactions, hadronic probe for neutrino-nucleus interactions," 6th meeting of OMEG Institute on Element Genesis and Neutrinos, 25, Jul., 2012, RIKEN, Saitama, Japan.

Shimoura S. (Oral): "Physics opportunities using double-charge exchange reactions", Exotic Nuclear Structure From Nucleons (ENSFN 2012), Oct. 10–12, 2012, University of Tokyo, Tokyo, Japan.

Steppenbeck D., Takeuchi S., Aoi N., Baba H., Fukuda N., Go S., Doornenbal P., Honma M., Lee J., Matsui K., Matsushita M., Michimasa S., Motobayashi T., Otsuka T., Shiga Y., Söderström P.-A., Sumikama T., H.Suzuki, Taniuchi R., Valiente-Dobón J.J., Wang H., Yoneda K. (Oral): "Investigating the strength of the $N = 34$ subshell closure in ^{54}Ca", Exotic Nuclear Structure From Nucleons (ENSFN 2012), Oct. 10–12, 2012, University of Tokyo, Tokyo, Japan.

Yako K., Sakai H., Kubota Y., Matsubara H., Michimasa S., Miki K., Miya H., Kurata-Nishimura M., Noji S., Lee C.S., Ohnishi T., Ota S., Baba H., Sasano M., Shimizu Y., Shimoura S., Takaki M., Takeda H., Tang T.L., Tokieda H., Uesaka T., Xu Z.Y., Yokoyama R., Zegers R.G.T., Fujii T., Inabe N., Kawase S., Kikuchi Y., Kisamori K., Kubo T. (Oral): "Measurement of ^{12}Be(p,n)^{12}B reaction at 200A MeV in inverse kinematics", Collective Motions in nuclei under EXtreme conditions (COMEX4), Oct. 22–26, 2012, Shonan Village Center, Hayama, Kanagawa, Japan.

Kisamori K. (Poster): "Missing-mass spectroscopy of the 4n system by exothermic double-charge exchange reaction ^{4}He(^{8}He,^{8}Be)4n",): Collective Motions in nuclei under EXtreme conditions (COMEX4), Oct. 22–26, 2012, Shonan Village Center, Hayama, Kanagawa, Japan.

Takaki M., Matsubara H., Uesaka T., Shimoura S., Aoi N., Dozono M., Fujii T., Hashimoto T., Hatanaka K, Kawabata T., Kawase S., Kisamori K., Lee C.S., Lee J., Tang T.L., Maeda Y., Michimasa S., Miki K., Miya H., Noji S., Ota S., Sakaguchi S., Sasano M., Suzuki T., Takahisa K., Tamii A., Tokieda H., Yako K., Yokota N., Yokoyama R., Zenihiro J. (Poster): "Study of the ^{12}Be nucleus via the heavy-ion double-charge exchange ^{12}C(^{18}O,^{18}Ne) reaction", Collective Motions in nuclei under EXtreme conditions (COMEX4), Oct. 22–26, 2012, Shonan Village Center, Hayama, Kanagawa, Japan.

Miya H., Shimoura S., Kisamori K., Baba H., Baba T., Dozono M., Fukuda N., Fujii T., Go S., Ideguchi E., Inabe N., Ito M., Kameda D., Kawabata T., Kawase S., Kikuchi Y., Kubo T., Kubota Y., Kobayashi M., Kondo Y., Lee C.S., Maeda Y., Matsubara H., Miki K., Michimasa S., Nishi T., Nishimura M., Noji S., Ota S., Sakaguchi S., Sakai H., Sasamoto Y., Sasano M., Sato H., Shimizu Y., Suzuki H., Takaki M., Takeda H., Takeuchi S., Tamii A., Tokieda H., Tsumura M., Uesaka T., Yanagisawa Y., Yako K., Yokoyama R., Yoshida K., Assie M., Beaumel D., Fariouz H., Stolz A. (Poster): "Study of spin-isospin response via exothermic charge exchange (^{8}He, ^{8}Liγ)", Collective Motions in nuclei under EXtreme conditions (COMEX4), Oct. 22–26, 2012, Shonan Village Center, Hayama, Kanagawa, Japan.

Michimasa S., Uesaka T., Ota S., Shimoura S., Sasamoto Y., Miki K., Noji S., Miya H., Tokieda H., Kawase S., Kisamori K., Takaki M., Dozono M., Kawabata T., Kikuchi Y., Kubota Y., Kurei H., Lee C.S., Matsubara H., Yako K., Nishi T., Yamazaki N., Yoshino A., Sakai H., Kubo T., Yanagisawaa Y., Baba H., Berg G.P., Roussel-Chomaz P., Bazin D. for the SHARAQ collaboration (Oral): " SHARAQ spectrometer for high-resolution studies of RI-induced reactions" 16th International Conference on Electromagnetic Isotope Separators and Techniques Related to their Applications (EMIS2012), Dec. 2–7, 2012, Kunibiki-Messe, Matsue, Japan.

Yako K., Kobayashi M., Shimoura S., Dozono M., Fujii T., Kawase S., Kikuchi Y., Kisamori K., Kubota Y., Matsubara H., Michimasa S., Miki K., Miya H., Noji S., Lee C.S., Ohnishi T., Ota S., Sakai H., Sasamoto Y., Sasano M., Takaki M., Tokieda H., Uesaka T., Xu Z.Y., Yokoyama R. (Oral): "Development of WINDS for (p,n) measurements in inverse kinematics" 16th International Conference on Electromagnetic Isotope Separators and Techniques Related to their Applications (EMIS2012), Dec. 2–7, 2012, Kunibiki-Messe, Matsue, Japan.

Michimasa S., Takaki M., Dozono M., Go S., Baba H., Ideguchi E., Kisamori K., Matsubara H., Miya H., Ota S., Sakai H., Shimoura S., Stolz A., Tang T.L., Tokieda H., Uesaka T., Zegers R.G.T. (Poster): "Development of CVD diamond detector for time-of-flight measurements", 16th International Conference on Electromagnetic Isotope Separators and Techniques Related to their Applications (EMIS2012), Dec. 2–7th, 2012, Kunibiki-Messe, Matsue, Japan.

Miya H., Shimoura S., Ota S., Matsubara H., Miki K., Kawase S., Fujii T., Kubota Y., Lee C.S., Michimasa S., Uesaka T. (Poster): "Performance of Low-Pressure Multi-Wire Drift Chamber for High-Intensity RI Beams", 16th International Conference on Electromagnetic Isotope Separators and Techniques Related to their Applications (EMIS2012), Dec. 2–7, 2012, Kunibiki-Messe, Matsue, Japan.

Gunji T. for the ALICE Collaboration (Poster): "A GEM-based Continuous Readout Scheme for the ALICE-TPC", XXIII International Conference on Ultrarelativistic Nucleus-Nucleus collisions (QM2012), Aug. 13–18, 2012, Washington, D.C., USA.

Gunji T. for the ALICE Collaboration (Poster): "Development of W+Si-Pad/Micro-Pad based ElectroMagnetic Calormeter for the ALICE upgrade", XXIII International Conference on Ultrarelativistic Nucleus-Nucleus collisions (QM2012), Aug. 13–18, 2012, Washington, D.C., USA.

Gunji T. for the ALICE Collaboration (Poster): "FoCAL - a high granurality electromagnetic calorimeter for forward direct photon measurements as an upgrade of ALICE", XXIII International Conference on Ultrarelativistic Nucleus-Nucleus collisions (QM2012), Aug. 13–18, 2012, Washington, D.C., USA.

Gunji T. for the ALICE Collaboration (Oral): "Future Perspectives of the ALICE Experiment and ALICE detector upgrades", 4th Asian Triangle Heavy Ion conference (ATHIC2012), Nov. 14–17, 2012, Grand Hotel, Pusan, South Korea.

Nagaoka T., Gunji T., Hamagaki H., Hatsuda T., Hirano

T. (Oral): "Sequential melting of quarkonia in quark-gluon fluid at RHIC and LHC", 4th Asian Triangle Heavy Ion conference (ATHIC2012), Nov. 14–17, 2012, Grand Hotel, Pusan, South Korea.

Hori Y. for the ALICE collaboration (Oral): "Mixed harmonic azimuthal correlations in $\sqrt{s_{NN}} = 2.76$ TeV Pb-Pb collisions measured with the ALICE experiment at the LHC", 23rd International conference on ultrarelativistic nucleus-nucleus collisions, Aug. 13–18, 2012, Washington D.C., USA.

Hori Y. for the ALICE collaboration (Oral): "Mixed harmonic azimuthal correlations in $\sqrt{s_{NN}} = 2.76$ TeV Pb-Pb collisions measured with the ALICE experiment at the LHC", International Symposium on Multiparticle Dynamics 2012, Sep. 16–21, 2012, Kielce, Poland.

Akimoto R. for the PHENIX Collaboration (Poster): "Measurement of charm and bottom yields in Au+Au collisions at RHIC-PHENIX experiment", 23rd International conference on ultrarelativistic nucleus-nucleus collisions, Aug. 13–18, 2012, Washington D.C., USA.

Tsuji T. for the ALICE Collaboration (Oral): "Neutral pion measurements in Pb-Pb Collisions at $\sqrt{s_{NN}} = 2.76$ TeV with ALICE at the LHC", The 4th Asian Triangle Heavy Ion Conference (ATHIC 2012), Nov. 14–17, 2012, Grand Hotel, Pusan, South Korea.

Hayashi S., Hamagaki H., Gunji T., Tanaka M., Ikeda H. (Oral): "Development of a Wide-Dynamic Range Front-End ASIC for W + Si calorimeter", 2012 IEEE Nuclear Science Symposium and Medical Imaging Conference, Oct. 29–Nov. 3, 2012, Disneyland Hotel, Anaheim, USA.

Sekiguchi Y., Tokieda H., Ota S., Michimasa S., Dozono M., Tamagawa T., Gunji T., Yamaguchi H., Hamagaki H., Tamagawa T., Uesaka T. (Oral): "Performance of GEM with Deuterium Gas and GEM with Glass Insulator", 2012 IEEE Nuclear Science Symposium and Medical Imaging Conference, Oct. 29–Nov. 3, 2012, Disneyland Hotel, Anaheim, USA.

Sekiguchi Y., Gunji T., Hamagaki H., Hayashi S., Hori Y. (Oral): "Development of W+Si Based Electromagnetic Calorimeter for the Upgrade of the LHC-ALICE Experiment", 2012 IEEE Nuclear Science Symposium and Medical Imaging Conference, Oct. 29–Nov. 3, 2012, Disneyland Hotel, Anaheim, USA.

Sekiguchi Y., Hamagaki H., Gunji T., Arai Y., Imamura T., Ohmoto T., Iwata A. (Poster): "Development of SOI Pixel Sensor for Environmental Radiation Monitor", 2012 IEEE Nuclear Science Symposium and Medical Imaging Conference, Oct. 29–Nov. 3, 2012, Disneyland Hotel, Anaheim, USA.

Gunji T. (Oral): "Simulation Study of Ion Back Flow for the GEM-TPC upgrade for ALICE", RD51 Mini-workshop, June 13–15, 2012, CERN, Switzerland.

Akimoto R. for the PHENIX Collaboration (Oral): "Measurement of charm and bottom contributions to electrons from heavy quark decay at RHIC-PHENIX experiment", 5th International workshop on heavy quark production in heavy-ion collisions, Nov. 14–17, 2012, Utrecht University, Netherland.

Shimizu N. (Oral): "Recent deveploments toward large-scale shell-model calculcations", International Molecule "Nuclear forces and neutron-rich matter", Mar. 15, 2012, YITP, Kyoto, Japan.

Otsuka T. (Oral, Invited): "Novel structure of exotic nuclei and nuclear forces", 14th National Conference on Nuclear Structure in China, Apr. 12 (12–14), 2012, Huzhou, China.

Otsuka T. (Oral, Invited): "Shell evolution in exotic nuclei", Symposium for the 40th Anniversary of DNP of KPS, Apr. 26 (24–27), 2012, Daejeon, Korea.

Otsuka T. (Oral, Invited): "Spin properties of effective two-body interaction extracted from three-body forces", EMMI Program The extreme matter physics of nuclei: from universal properties to neutron-rich extremens, May 3 (Apr. 16–May 11), 2011, GSI, Darmstadt, Germany.

Otsuka T. (Oral, Invited): "Shell evolution in exotic nuclei", Workshop on RI Physics Theory, May 11–12, 2012, Riviera Hotel, Daejeon, Korea.

Otsuka T. (Oral, Invited): "Shell evolution with tensor and three-body forces", 11th International Conference on Nucleus-Nucleus Collision, May 27-June 1, 2012, San Antonio, Texas, USA.

Otsuka T. (Oral, Invited): "Exotic nuclei and nuclear forces", Nobel Symposium on Physics with Radioactive Beams, June 10–15, 2012, Goteborg, Sweden.

Utsuno Y. (Oral, Invited): "Monte Carlo shell model and its applications to exotic nuclei", International Workshop "Nuclear Theory in the Supercomputing Era", June 18–22, 2012, Khabarovsk, Russia.

Otsuka T. (Oral, Invited): "Rotating around atomic nuclei and my cup of models", Gelberg 90 Colloqium, June 28, 2012, IKP, Koeln, Germany.

Otsuka T. (Oral, Invited): "Perspectives of Monte Carlo Shell Model", International Symposium Nuclear Structure and Dynamics II, July 9–13, 2012, Opatija, Croatia.

Utsuno Y. (Oral, Invited): "Tensor-force driven shell evolution in correlated nuclei", International Symposium on Perspective in Isospin Physics - Role of non- central interactions in structure and dynamics of unstable nuclei, Aug. 27–28, 2012, Wako, Japan.

Otsuka T. (Oral, Invited): "Three-body forces and neutron-rich exotic nuclei", 20th International IUPAP Few-Body Conference Aug. 20–25, 2012, Fukuoka international Congress Center, Japan.

Yoshida T., Shimizu N., Abe T., Otsuka T. (Oral): "Intrinsic structure of light nuclei in Monte Carlo Shell model calculation, The 20th Internatinal IUPAP Conference on Few-Body Problems in Physics (FB20)" Aug. 20–25, 2012, Fukuoka international Congress Center, Japan.

Otsuka T. (Oral, Invited): "Nuclear Structure towards the driplines: understanding many-body forces and correlations", Zakopane Conference on Nuclear Physics Extremes of the Nuclear Landscape, 47th in the series of Zakopane Schools of Physics, Aug. 27–Sep. 1, 2012, Zakopane, Poland.

Yoshida T., Itagaki N., Katō K. (Oral): "Algebraic approach for cluster structure in 12C and 16O", 10th International Conference on Clustering Aspects of Nuclear Structure and Dynamics, Sep. 25 (24–28), 2012, Debrecen, Hungary.

Utsuno Y. (Oral, Invited): "Recent shell model results for exotic nuclei", VIII Tours Symposium on Nuclear Physics and Astrophysics, Sep. 2–7, 2012, Lenzkirch-Saig, Germany.

Otsuka T. (Oral, Invited): "Perspectives of Physics of Exotic Nuclei", APCTP mini-workshop on nuclear structure, APCTP headquarter, Sep. 21–22, 2012, Pohang, Korea.

Utsuno Y. (Oral, Invited): "Evolution of the shell structure probed by energy levels of exotic nuclei", 3rd RIBF discussion on "Gamma-Ray Spectroscopy of Medium-Mass Neutron-Rich Nuclei," Sep. 24, 2012, Sendai, Japan.

Ebata S., Nakatsukasa T., Inakura T. (Oral): "Systematic study of low-lying E1 strength from light to heavy nuclei", Collective Motions in nuclei under EXtreme conditions (COMEX4), Oct. 22–26, 2012, Shonan Village Center, Hayama, Kanagawa, Japan.

Otsuka T. (Oral, Invited): "New horizon of computational nuclear structure physics in the K computer era – A shell-model perspective –", International Conference on Computational Physics, Oct. 15–18, 2012, Kobe, Japan.

Ebata S. (Oral): "Simulation of heavy ion collision using time-dependent density functional theory including nuclear superfluidty", Conference on Computational Physics (CCP2012), Oct. 14–18, 2012, Nichii Gakkan Kobe Port Island Center, Hyogo, Japan.

Yoshida T., Shimizu N., Abe T., Otsuka T. (Oral): "Cluster structure obtained from Monte Carlo shell model calculation", Conference on Computational Physics (CCP2012), Oct. 14–18, 2012, Nichii Gakkan Kobe Port Island Center, Hyogo, Japan.

Utsuno Y. (Oral, Invited): "Towards unified description of the shell evolution", International Symposium "Exotic Nuclear Structure From Nucleons", Oct. 10–12, 2012, University of Tokyo, Japan.

Shimizu N., Abe T., Tsunoda Y., Utsuno Y., Yoshida T., Mizusaki T., Honma M., Otsuka T. (Oral, Invited): "History and future perspectives of the Monte Carlo shell model", International symposium "Exotic Nuclear Structure from Nucleons", Oct. 10–12, 2012, University of Tokyo, Japan.

Ebata S., Nakatsukasa T., Inakura T. (Oral): "Systematic investigation of E1 strength for the isotopes from Z = 28 to 50", International symposium "Exotic Nuclear Structure from Nucleons", Oct. 10–12, 2012, University of Tokyo, Japan.

Yoshida T., Shimizu N., Abe T., Otsuka T. (Oral): "Density profiles in the intrinsic frame of light nuclei obtained from Monte Carlo shell model calculation", International symposium "Exotic Nuclear Structure from Nucleons", Oct. 10–12, 2012, University of Tokyo, Japan.

Otsuka T. (Oral, Invited): "Advanced Monte Carlo Shell Model calculations and exotic nuclei around Z=28", LACM-TORIJIN-JUSTIPEN workshop, Oct. 31–Nov. 2, 2012, Oak Ridge, USA.

Yoshida T., Shimizu N., Abe T., Otsuka T. (Oral): "Study of intrinsic states for light nuclei in Monte Carlo shell model calculation", The 6th LACM-TORIJIN-JUSTIPEN Workshop, Oct. 31–Nov. 2, 2012, Oak Ridge, USA.

Otsuka T. (Oral, Invited): "An Overview of Exotic Nuclei and Nuclear Forces, and Monte Carlo Shell Model", 7th Italy-Japan Symposium, Nov. 20–23, 2012, Milano, Italy.

Utsuno Y. (Oral, Invited): "Shell evolution in neutron-rich calcium isotopes", 7th Italy-Japan Symposium on Nuclear Physics, Nov. 20–23, 2012, Milan, Italy.

Utsuno Y. (Oral, Invited): "Manifestation of the shell evolution in energy levels of exotic nuclei", RCNP International Workshop on Physics Opportunities Using Compton Suppressed Ge Clover Array (Clover12), Dec. 7–8, 2012, Osaka, Japan.

Shimizu N. (Oral): "New Generation of the Monte Carlo Shell Model for the K-Computer Era", one-day workshop on "ab initio study of nuclear structure and reaction", Dec. 11, 2012, RCNP, Osaka Univ. Japan.

Otsuka T. (Oral, Invited): "Low-lying continuum states of drip-line Oxygen isotopes", Resonance workshop, Dec. 13 (12–13), 2012, RIFP, Kyoto, Japan.

(Domestic Conference)

Ota S. (Oral): "Development of ActiveTarget GEM-TPC using Deuterium Gas", 9th MPGD workshop, Dec. 7–8, 2012, Nagasaki Institute of Applied Science, Nagasaki, Japan.

Hamagaki H. (Oral): "LHC ALICE 実験における GEMTPC 計画について "、第 9 回 Micro-Pattern Gas Detector 研究会、2012 年 12 月 7 日.8 日、長崎総合科学大学，長崎.

Hori Y. (Oral): "Mixed harmonic charge dependent azimuthal correlations in relativistic HIC", 14th Heavy Ion Pub, May 5, 2012, the University of Hiroshima, Hiroshima, Japan.

Yamaguchi Y.L (Oral): "Direct Photons at RHIC", Dynamics of Classical and Quantum Fields at RHIC/LHC, July 7th, 2012, RIKEN, Saitama, Japan.

Torii H. (Oral): "Photon at LHC", Dynamics of Classical and Quantum Fields at RHIC/LHC, July 7th, 2012, RIKEN, Saitama, Japan.

Torii H. (Oral): "Hard Probe" 22th Heavy Ion Cafe and

15th Heavy Ion Pub, September 6th, 2012, Nagoya University, Nagoya

川瀬頌一郎，上坂友洋，下浦享，矢向謙太郎，大田晋輔，道正新一郎，時枝紘史，宮裕之，Tang Tsz Leung，木佐森慶一，高木基伸，久保田悠樹，李清秀，横山輪，藤井俊彦，小林幹，笹野匡紀，銭廣十三，松原礼明，堂園昌伯，Jenny Lee，酒井英行，久保敏幸，吉田光一，稲辺尚人，柳澤善行，竹田浩之，日下健祐，福田直樹，亀田大輔，鈴木宏，河原朋美，涌井崇志，坂口聡志，野呂哲夫，若狭智嗣，安田淳平，福永拓，前田幸重，Wooyoung Kim，Sanghoon Hwang，Samvel Stepanyan，Alexandre Obertelli，Alfredo Galindo-Uribarri，Elizabeth Padilla-Rodal、“偏極陽子標的を用いた陽子ノックアウト反応による 14,22,24O のスピン軌道分離の研究”、日本物理学会 2012 年秋期大会、2012 年 9 月 11 日.9 月 14 日、京都産業大学、京都.

李清秀，大田晋輔，時枝紘史，松原礼明，堂園昌伯，川瀬頌一郎，道正新一郎，久保田悠樹，山口英斉，酒向正己，大津秀暁，浜垣秀樹，上坂友洋，川畑貴裕，久保野茂，前田幸重，“アクティブターゲットにおける高エネルギー反跳粒子の測定”, 日本物理学会 2012 年秋期大会、2012 年 9 月 11 日.14 日、京都産業大学、京都.

Miya H., Shimoura S., Kisamori K., Baba H., Baba T., Dozono M., Fukuda N., Fujii T., Go S., Ideguchi E., Inabe N., Ito M., Kameda D., Kawabata T., Kawase S., Kikuchi Y., Kubo T., Kubota Y., Kobayashi M., Kondo Y., Lee C.S., Maeda Y., Matsubara H., Miki K., Michimasa S., Nishi T., Nishimura M., Noji S., Ota S., Sakaguchi S., Sakai H., Sasamoto Y., Sasano M., Sato H., Shimizu Y., Suzuki H., Takaki M., Takeda H., Takeuchi S., Tamii A., Tokieda H., Tsumura M., Uesaka T., Yanagisawa Y., Yako K., Yokoyama R., Yoshida K., Assie M., Beaumel D., Fariouz H., Stolz A.: “Study of spin-isospin response via exothermic charge exchange (^{8}He, ^{8}Liγ)”, JPS Autumn meeting , Sep. 11–14, 2012, Kyoto Sangyo University, Miura-gun, Kyoto, Japan.

Kobayashi M., Shimoura S., Yako K., Ota S., Kawase S., Kisamori K., Kubota Y., Sasano M., Takaki M., Dozono M., Michimasa S., Miya H., Lee C.S. (Oral): “Development of a system for (p, n) measurements in inverse kinematics”, at the JPS Autumn meeting, Sep. 11–14, 2012, Kyoto Sangyo University, Kyoto, Japan.

Kisamori K., Shimoura S., Lee C., Ideguchi E., Inabe N., Ito M., Uesaka T., Ota S., Kameda D., Kawabata T., Kawase S., Kikuchi Y., Kubo T., Kubota Y., Go S., Kobayashi M., Kondo Y., Sakaguchi S., Sakai H., Sasamoto Y., Sasano M., Sato H., Shimizu Y., Suzuki H., Takaki M., Tamii A., Takeda H., Takeuchi S., Tumura M., Tokieda H., Nishi T., Nishimura M., Noji S., Baba H., Baba T., Dozono M., Fukuda N., Fujii T., Maeda Y., Matsubara H., Miki K., Michimasa S., Miya H., Yanagisawa Y., Yako K., Yokoyama R., Yoshida K., Assie M., Beaumel D., Fariouz H., Stolz A. (Oral): “Missing mass spectroscopy of 4n system by exothermic double-charge exchange reaction ^{4}He(^{8}He,^{8}Be)4n”, at the JPS Autumn meeting, Sep. 11–14, 2012, Kyoto Sangyo University, Kyoto, Japan.

Go S., Kameda D., Kubo T., Inabe N., Fukuda N., Takeda H., Suzuki H., Yoshida K., Kusaka K., Tanaka K., Yanagisawa Y., Ohtake M., Ohnishi T., Sato H., Shimizu Y., Baba H., Kurokawa M., Nishimura D., Iwasa N., Chiba A., Yamada H., Ieki K., Murai D., Ideguchi E., Yokoyama R., Fujii T., Nishibata H., Momota S., Sato Y., Hwang J., Kim S., Tarasov O.B., Morrissey D.J., Sherrill B.M., Simpson G.: “Isomers at N=100 in neutron rich region”, JPS Autumn meeting, Sep. 11–14, 2012, Kyoto Sangyo University, Kyoto, Japan.

横山輪，久保敏幸，稲辺尚人，福田直樹，竹田浩之，亀田大輔，鈴木宏，吉田光一，日下健祐，田中鐘信，柳沢善行，大竹政雄，大西哲哉，佐藤広海，清水陽平，馬場秀忠，黒川明子，西村太樹，家城和夫，村井大地，井手口栄治，郷慎太郎，藤井俊彦，岩佐直仁，山田拓，千葉鮎子，百田佐多生，西畑洸希，O.B. Tarasov，D.J. Morrissey，B.M. Sherrill，佐藤義輝，Kim Sunji，Hwnag Jongwon，G. Simpson (Oral): “中性子過剰 Z=60 近傍のアイソマー探索”, 日本物理学会 2012 年秋期大会、2012 年 9 月 11 日.14 日、京都産業大学、京都.

Yamaguchi Y.L for the ALICE Collaboration (Oral, Invited): “LHC-ALIC 実験の初期成果から将来展望まで”, JPS Autumn Meeting, Sept. 11–14, 2012, Kyoto-Sangyo University, Kyoto, Japan.

Akimoto R. for the PHENIX Collaboration (Oral): “Measurement of electrons from charms and bottoms created in Au+Au collisions at $\sqrt{s_{NN}} = 200$ GeV at the RHIC-PHENIX experiment”, JPS Autumn meeting, Sep. 11–14, 2012, Kyoto Sangyo University, Kyoto, Japan.

Tsuji T. for the ALICE Collaboration (Oral): “π 0 measurements on Pb-Pb collisions at $\sqrt{s_{NN}} = 2.76$ TeV with ALICE at the LHC”, JPS Autumn Meeting, Sep. 11–14, 2012, Kyoto-Sangyo university, Kyoto, Japan.

Sekiguchi Y., Hamagaki H., Gunji T., Arai Y., Imamura T., Ohmoto T., Iwata A. (Oral): “環境放射線センサーのための SOI ピクセル検出器の開発”, JPS Autumn Meeting, Sep. 11–14, 2012, Kyoto-Sangyo University, Kyoto, Japan.

Utsuno Y., Shimizu N., Honma M., Mizusaki T., Otsuka T. (Oral): “Shell evolution in antimony isotopes”, JPS 2012 Autumn Meeting, Sep. 11–14, 2012, Kyoto Sangyo Univ, Kyoto, Japan.

Ebata S. (Oral): “Application of Cb-TDHFB to nuclear collision II”, JPS 2012 Autumn Meeting, Sep. 11–14, 2012, Kyoto Sangyo Univ, Kyoto, Japan.

Shimizu N., Mizusaki T., Kaneko K. (Oral): “Extension of Monte Carlo method on nuclear shell model diagonalization”, JPS 2012 Autumn Meeting, Sep.11–14, 2012, Kyoto Sangyo Univ, Kyoto, Japan.

Shimizu N. (Oral): “Nuclear structure calculations aimed at K computer”, JPS 2012 Autumn Meeting, Sep.11–14, 2012, Kyoto Sangyo Univ, Kyoto, Japan.

Yoshida T., Itagaki N., Katö (Oral) K.: “Study of linear-chain structure of ^{16}O in alpha cluster model", JPS 2012 Autumn Meeting, Sep.11–14, 2012, Kyoto Sangyo Univ, Kyoto, Japan.

Radioactive nuclear beam group IPNS (Institute for Particle and Nuclear Studies) KEK (High Energy Accelerator Research Organization)

Publications

[Journal]

(Original Papers) *Subject to Peer Review

Ishiyama H., Jeong S.C., Watanabe Y.X., Hirayama Y., Imai N., Miyatake H., Oyaizu M., Katayama I., Sataka M., Osa A., Otokawa Y., Matsuda M., Makii H., "Toward Online Nanoscale Diffusion Measurements Using Radioactive ^{8}Li Tracer", Jpn. J. Appl. Phys **52** (2013) 010205,*

Das S.K., Ishiyama H., Watanabe Y.X., Miyatake H., Hirayama Y., Jeong S.C., Yamaguchi K., "Energy resolution and gas gain study of GEM-MSTPC for measurement of ^{44}Ti$(\alpha, \mathrm{p})^{47}$V reaction", Bangladish Journal of Physics **12** (2012) 1-7,*

Sonoda T., Wada M., Tomita H., Sakamoto C., Takatsukasa T., Noto T., Matsuo Y., Iimura H., Shinozuka T., Wakui T., Kubo T., Schury P., Ito Y., Naimi S., Nakamura S., Mita H., Furukawa T., Miyatake H., Jeong S.C., Ishiyama H., Imai N., Watanabe Y.X., Hirayama Y., "Development of a resonant laser ionization gas cell for high–energy, short,ived nuclei", Nucl. Instrum. meth. B. **295** (2013) 1-10,*

Ueno H., Miyatake H., Yamamoto Y., Tanimoto S., Shimoda T., Aoi N., Asahi K., Ideguchi E., Ishihara M., Izumi H., Kishida T., Kubo T., Mitsuoka S., Mizoi Y., Notani N., Ogawa H., Ozawa A., Sakai M., Shirakura T., Takahashi N., Yoneda K., "β–delayed neutron and γ–ray spectroscopy of 17C utilizing spin–polarized 17B", Phys. Rev. C **C87** (2013)034316.,*

[Book・ Proceedings]

(Original Papers) *Subject to Peer Review

Shimoda T., Tajiri K., Odahara A., Suga M., Hamatani N., Nishibata H., Takatsu J., Yokoyama J., Hirayama Y., Imai N., Miyatake H., Person M.C., Levy C.D.P., Jackson K.P., Leguillon R.D., Petrache "Structure of mg isotope studied by β–decay spectroscopy of spin–polarized na isotopes: Shape coexistence in 30mg", Prog. of Theor. Phys. Suppl. **196** (2012) 310-315; Frontier Issues in Physics of Exotic Nuclei of the Yukawa Interneational Seminar 2011 (YKIS2011) and Long–Term Workshop on Dynamics and Correlations in Exotic Nuclei DCEN2011). ,*

Ideguchi E., Ota S., Morikawa T., Oshima M., Koizumi M., Toh Y., Kimura A., Harada H., Furutaka K., Nakamura S., Kitatani F., Hatsukawa Y., Shizuma T., Sugawara M., Watanabe Y.X., Hirayama Y., Oi M., "Superdeformed Band in Asymmetric $N > Z$ Nuceus, 40Ar and High–Spin States in $A = 30 \sim 40$ Nuclei", Prog. of Theor. Phys. Suppl. Issue **196** (2012) 427-432; Frontier Issues in Physics of Exotic Nuclei of the Yukawa Interneational Seminar 2011 (YKIS2011) and Long–Term Workshop on Dynamics and Correlations in Exotic Nuclei DCEN2011). ,*

Hashimoto T., Kubono S., Yamaguchi H., Hayakawa S., Kahl D. M., Ota S., Michimasa S., Tokieda S., Ishiyama H., Watanabe Y.X., Hirayama H., Imai N., Miyatake H., Jeong S.C., Yamaguchi K., Arai I., Komatsubara T., Fukuda T., Mizoi Y., Das S.K., Iwasa N., Yamada T., Chen A. A., He J. J., "Direct measurement of the 18Ne(α, p)21Na reaction", AIP Conference Proceedings **1484** (2012) 454-456.

Makii H., Miyatake H., Wakabayashi Y., ishiyama H., Niki K., Okada M., Imai N., Watanabe Y.X., Hirayama Y., Jeong S.C., Shima T., Nishinaka I., Mitsuoka S., Nishio K., Chiba S., Arai I.,
"Measurement of the 12C(α, γ)16 reaction at TRIAC", AIP Conference Proceedings **1484** (2012) 269-274.

Oral Presentations

(International Conference etc.)

Watanabe Y.X.,: Hirayama Y.,: Imai N.,: Ishiyama H.,: Imai N.,: Jeong S.C.,: Miyatake H.,: Oyaizu M.,: Okada M.,: Matsuo Y.,: Sonoda T.,: Wada M.,: Huyse M.,: Kudryavtsev Yu.,: Van Duppen P.,: "KEK Isotope Separation System(KISS) at RIKEN", Workshop on Low-Energy Radioactive Isotope Beam (RIB) Production By In–Gas Lazer Ionization for Decay Spectroscopy at RIKEN, 10–11 December, 2012, RIKEN

Hirayama Y.,: Jeong S.C,: Miyatake H.,: Ishiyama H.,: Watanabe Y.X.,: Imai N.,: Oyaizu M.,: Wada M.,: Sonoda T.,: Matsuo Y.,: Van Duppen P.,: Kudryavtsev Yu.,: Huyse M.,: "On and Off–line test results of the KISS gas cell ", Workshop on Low-Energy Radioactive Isotope Beam (RIB) Production By In–Gas Lazer Ionization for Decay Spectroscopy at RIKEN, 10–11 December, 2012, RIKEN

Watanabe Y.X.,: Hirayama Y.,: Imai N.,: Ishiyama H.,: Imai N.,: Jeong S.C.,: Miyatake H.,: Clement E.,: France G. de,: Navin A.,: Rejmund M.,: Schmitt C.,: Pollarolo G.,: Corradi L.,: Fioretto E.,: Montanari D.,: Choi S.H.,: Kim Y.H.,: Song J.S.,: Niikura M.,: Suzuki D.,: Nishibata H.,: Takatsu J.,: "Study of collisions of $^{136}\mathrm{Xe} + {}^{198}\mathrm{Pt}$ for the KEK isotope separation system", XVI International Conference on Electromagnetic Isotope Separators and Techniques Related to their Applications (EMIS2012), 2–7 December, 2012, Matsue, Japan

Ishiyama H., "Current Status of KISS project to study $\beta-$decay properties of N = 126 neutron–rich nuclei ", The 1st NAOJ Visiting Fellow Workshop Program Element Genesis and Cosmic Chemical Evolution: r–process perspective, 17–19 October, 2012, RIKEN

Miyatake H., "KEK Isotope Separation System (KISS), Present and Future", RISP W.S., 7-9th May, 2012, Daejeon, Korea.

Miyatake H., "Nuclear astrophysics in KEK RNB group", Workshop on Low–Energy RI Beams and the Physics, 14th Oct., 2012, Beijing, China.

Miyatake H., "Present status of the Kiss project", The 8th China–Japan Joint Nuclear Physics Symposium (CJJNPS 2012), 15-19th Oct., 2012, Beijing, China.

Imai N., "Nuclear structure around 32Mg via proton resonance elastic scattering", The 8th China–Japan Joint Nuclear Physics Symposium (CJJNPS 2012), 15-19th Oct., 2012, Beijing, China.

Miyatake H., "Present status of the Kiss project", Symposium Italy–Japan 2012 on Nuclear Physics, 20-23rd Nov. 2012, Milano, Italy.

Imai N., "A single shot experiment: proton resonance elastic scattering for single particle structures of neutron–rich nuclei", RIBF users meeting 2012, 20-21th June, 2012, RIKEN.

Hirayama Y., "Present status of KEK KISS project at RIKEN", RIBF users meeting 2012, 20-21th June, 2012, RIKEN.

Hirayama Y., "Spectroscopy of r–process nuclei with N = 126 by KISS (KEK Isotope Separation System", Gas–Cell–based laser Ionization Spectroscopy Development, 31th May - 1st June, 2012, Leuven, Belgium.

TORIJIN (Todai-RIKEN Joint International Program for Nuclear Physics)

Publications

[Journal]

Original Papers *Subject to Peer Review

Bertulani C.A., Liu Hongliang, Sagawa H.: "Global investigation of odd-even mass differences and radii with isospin-dependent pairing interactions", Phys. Rev. C **85**, 014321 (2012).

Möller P., Myers W.D., Sagawa H., Yoshida S.: "New Finite-Range Droplet Mass Model and Equation-of-State Parameters", Phys. Rev. Lett. **108**, 052501 (2012).

Möller P., Randrup J., Sierk A.J.: "Calculated fission yields of neutron-deficient mercury isotopes", Phys. Rev. C **85**, 024396 (2012).

Abusara H., Afanasjev A.V., Ring P.: "Fission barriers in covariant density functional theory: Extrapolation to superheavy nuclei", Phys. Rev. C **85**, 024314 (2012).

Ichikawa T., Iwamoto A., Moller P., Sierk A.J.: "Effect of Pairing Correlations on Incompressibility and Symmetry Energy in Nuclear Matter and Finite Nuclei", Phys. Rev. C. **86**, 024610 (2012).

Abe T., Maris P., Otsuka T., Shimizu N., Utsuno Y., Vary J.P.: "Benchmarks of the full configuration interaction, Monte Carlo shell model, and no-core full configuration methods", Phys. Rev. C. **86**, 054301 (2012).

Avogadro P., Nakatsukasa T.: "Efficient calculation for the quasiparticle random-phase approximation matrix", Phys. Rev. C **87**, 014331 (2013).

VII. LIST OF PREPRINTS

(2012 April ～2013 March)

RIKEN-MP

40 Adrian Dumitru, Yun Guo et al. "Effective matrix model for deconfinement in pure gauge theories" May, 2012

44 Daisuke Satow, Yoshimasa Hidaka "Off-diagonal kinetic theory in ultrasoft momentum region at high temperature" Apr, 2012

45 Yoshimasa Hidaka, Yuji Hirono et al. "Viscoelastic-electromagnetism and Hall viscosity" June, 2012

46 Toshiaki Fujimori, Taro Kimura et al. "Vortex counting from field theory" Apr, 2012

47 Masaki Asano, Tetsutaro Higaki "Natural supersymmetric spectrum in mirage mediation" Apr, 2012

48 Tatsuhiro Misumi, Taro Kimura et al. "QCD phase diagram with 2-flavor fermion formulations" June, 2012

49 Tatsuhiro Misumi, Takashi Z. Nakano et al. "Strong-coupling Analysis of Parity Phase Structure in Staggered-Wilson Fermions" May, 2012

52 Minoru Eto, Koji Hashimoto et al. "Ferromagnetic neutron stars: axial anomaly, dense neutron matter, and pionic wall" Aug, 2012

53 Tetsutaro Higaki, Fuminobu Takahashi "Dark Radiation and Dark Matter in Large Volume Compactifications" Aug, 2012

54 Taro Kimura, Shin-ya Koyama et al. "Euler Products beyond the Boundary" Sep, 2012

55 Yuki Minami and Yoshimasa Hidaka "Relativistic hydrodynamics from projection operator method" Oct, 2012

56 Takashi Z. Nakano, Tatsuhiro Misumi et al. "Strong coupling analysis of Aoki phase in Staggered-Wilosn fermions" Oct, 2012

57 Taro Kimura, Tatsuhiro Misumi et al. "QCD Phase Diagram with 2-flavor Lattice Fermion Formulations" Oct, 2012

58 Taro Kimura "Hofstadter problem in higher dimensions" Oct, 2012

59 Tetsutaro Higaki, Kwang Sik Jeong et al. "Hybrid inflation in high-scale supersymmetry" Nov, 2012

60 Koji Hashimoto, Masaki Murata "A Landscape in Boundary String Field Theory: New Class of Solutions with Massive State Condensation" Nov, 2012

61 Tomohiro Amemiya, Daisuke Nishiyama et al. "Asymmetric Cloaking Theory Based on Finsler Geometry ~ How to design Harry Potter's invisibility cloak with a scientific method ~" Nov, 2012

62 Kazuo Fujikawa "Universally valid Heisenberg uncertainty relation" Dec, 2012

63 M. Chaichian, K. Fujikawa and A. Tureanu "On neutrino masses via CPT violating Higgs interaction in the Standard Model" Dec, 2012

64 M. Chaichian, K. Fujikawa and A. Tureanu "Electromagnetic interaction in theory with Lorentz invariant CPT violationl" Dec, 2012

65 K. Fujikawa and K. Umetsu "Aspects of universally valid Heisenberg uncertainty relation" Dec, 2012

66 Hiroaki Kanno, Kazunobu Maruyoshi et al. "W3 irregular states and isolated N = 2 superconformal field theories" Jan, 2013

67 Tetsutaro Higaki, Kwang Sik Jeong et al. "A Parallel World in the Dark" Feb, 2013

68 Yasufumi Araki, Taro Kimura "Phase structure of 2-dimensional topological insulators by lattice strong coupling expansion" Mar, 2013

69 Koji Hashioto, Norihiro Iizuka et al. "Towards Holographic Spintronics" Mar, 2013

70 Masato Taki "Holomorphic Blocks for 3d Non-abelian Partition Functions" Mar, 2013

71 Richard Eager, Johannes Schmude "Superconformal Indices and M2 Branes" Mar, 2013

72 Richard Eager, Johannes Schmude et al. "Superconformal Indices, Sasaki-Einstein Manifolds, and Cyclic Homologies" Oct, 2012

RIKEN-QHP

17 Shigehiro Yasui, Yuji Hirono et al. "Non-Abelian statistics of vortices with non-Abelian Dirac fermions" Apr, 2012

18 Takumi Doi, Michael G. Endres "Unified contraction algorithm for multi-baryon correlators on the lattice" May, 2012

19 Y. Araki, G.W. Semenoff "Spin versus charge density wave order in graphene-like systems" Apr, 2012

20 Adrian Dumitru, Yun Guo et al. "Effective matrix model for deconfinement in pure gauge theories" May, 2012

21 Michael G. Endres "Lattice theory for nonrelativistic fermions in one spatial dimension" Apr, 2012

22 Akihiko Monnai "Dissipative hydrodynamic effects on baryon stopping" Apr, 2012

23 Daisuke Satow, Yoshimasa Hidaka "Off-diagonal kinetic theory in ultrasoft momentum region at high temperature" Apr, 2012

24 Yoshimasa Hidaka, Yuji Hirono et al. "Viscoelastic-electromagnetism and Hall viscosity" June, 2012

25 Tatsumi Aoyama, Masashi Hayakawa et al. "Tenth-order QED contribution to the electron g-2 and an improved value of the fine structure constant" May, 2012

26 Tatsumi Aoyama, Masashi Hayakawa et al. "Complete tenth-order QED contribution to the muon g-2" May, 2012

27 Y. Hama, Y. Hidaka et al. "The study of Goldstone modes in ν=2 bilayer quantum Hall systems" July, 2012

28 Arata Yamamoto "Chiral magnetic effect on the lattice" July, 2012

29 Arata Yamamoto "Lattice simulation of ultracold atomic Bose-Fermi mixtures" July, 2012

30 Yoshiko Kanada-En'yo and Yoshimasa Hidaka "alpha-cluster correlations and symmetry breaking in light nuclei" Aug, 2012

31 Minoru Eto, Koji Hashimoto et al. "Ferromagnetic neutron stars: axial anomaly, dense neutron matter, and pionic wall" Sep, 2012

32 Sinya Aoki, Takumi Doi et al. "Lattice QCD approach to Nuclear Physics" June, 2012

38 Nino M. Bratovic, Tetsuo Hatsuda et al. "Role of Vector Interaction and Axial Anomaly in the PNJL Modeling of the QCD Phase Diagram" Apr, 2012

39 Kenji Maeda, Tetsuo Hatsuda et al. "Antiferrosmectic ground state of two-component dipolar Fermi gases: An analog of meson condensation in nuclear matter" May, 2012

40 Kota Masuda, Tetsuo Hatsuda et al. "Hadron-Quark Crossover and Massive Hybrid Stars with Strangeness" May, 2012

43 Kenji Fukushima and Yoshimasa Hidaka "Magnetic Catalysis vs Magnetic Inhibition" Sep, 2012

44 Yoshimasa Hidaka and Arata Yamamoto "Charged vector mesons in a strong magnetic field" Sep, 2012

45 Yuki Minami and Yoshimasa Hidaka "Relativistic hydrodynamics from projection operator method" Oct, 2012

46 Arata Yamamoto and Tetsuo Hatsuda "Quantum Monte Carlo Simulation of three-dimensional Bose-Fermi mixtures" Sep, 2012

47 Hiroshi Suzuki "Ferrara-Zumino supermultiplet and the energy-momentum tensor in the lattice formulation of 4D N=1 SYM" Sep, 2012

48 Hiroshi Suzuki "Remark on the energy-momentum tensor in the lattice formulation of 4D N=1 SYM" Sep, 2012

49 Michael G. Endres "Transdimensional Equivalence of Universal Constants for Fermi Gases at Unitarity" Oct, 2012

51 Yusuke Hama, George Tsitsishvili et al. "Spin Josephson Supercurrent in the Canted Antiferromagnetic Phase" Nov, 2012

52 Arata Yamamoto "Lattice QCD with strong external electric fields" Oct, 2012

53 Yuji Sakai, Hiroaki Kouno et al. "The quarkyonic phase and the ZNc symmetry" May, 2012

54 Yuji Hirono, Masaru Hongo et al. "Estimation of electric conductivity of the quark gluon plasma via asymmetric heavy-ion collisions" Nov, 2012

55 Sinya Aoki, Bruno Charron et al. "Construction of energy-independent potentials above inelastic thresholds in quantum field theories" Dec, 2012

56 Tomoya Hayata, Kanabu Nawa and Tetsuo Hatsuda "Time-dependent Heavy-Quark Potential at Finite Temperature from Gauge/Gravity Duality" Nov, 2012

57 Yoshimasa Hidaka, Naoki Yamamoto "Some exact results on the QCD critical point" Dec, 2012

58 Takumi Doi [HAL QCD Collaboration] "Few-baryon interactions from lattice QCD" Nov, 2012

59 Takumi Doi [HAL QCD Collaboration] "Nuclear physics from lattice simulations" Dec, 2012

60 G. Fejos "Chiral symmetry breaking patterns in the U_L(n)xU_R(n) meson model" Dec, 2012

61 Bruno Charron [HAL QCD Collaboration] "Pion-pion interaction in the I=1 channel" Dec, 2012

64 Sinya Aoki, Janos Balog et al. "Short Distance Repulsion Among Baryons" Feb, 2013

65 Michael G. Endres "Numerical study of unitary fermions in one spatial dimension" Mar, 2013

66 Y.Maezawa, T.Umeda et al. "Application of fixed scale approach to static quark free energies in quenched and 2+1 flavor lattice QCD with improved Wilson quark action" Feb, 2013

67 T. Inoue et al. [HAL QCD Collaboration] "Two-Baryon Potentials and H-Dibaryon from 3-flavor Lattice QCD Simulations" Feb, 2013

68 T. Hatsuda "Nuclear force and nuclear physics from lattice quantum chromodynamics" Feb, 2013

69 S.Ejiri et al. [WHOT-QCD Collaboration] "Probability distribution functions in the finite density lattice QCD" Feb, 2013

70 Y.Nakagawa et al. [WHOT-QCD Collaboration] "Phase structure of finite density QCD with a histogram method" Feb, 2013

71 T. Umeda et al. [WHOT-QCD Collaboration] "Thermodynamics in 2+1 flavor QCD with improved Wilson quarks by the fixed scale approach" Feb, 2013

72 K.Masuda, T.Hatsuda and T.Takatsuka "Hadron-Quark Crossover and Massive Hybrid Stars" Feb, 2013

75 Chuan-zhou Zhu, Shimpei Endo et al. "Scattering and Bound States of two Polaritons in an Array of Coupled Cavities" Oct, 2012

76 Pascal Naidon, Shimpei Endo et al. "Physical Origin of the Universal Three-body Parameter in Atomic Efimov Physics" Aug, 2012

78 Yasufumi Araki, Taro Kimura "Phase structure of 2-dimensional topological insulators by lattice strong coupling expansion" Mar, 2013

79 S. Aoki, N. Ishii et al. "Asymptotic behavior of Nambu-Bethe-Salpeter wave functions for multi-particles in quantum field theories" Mar, 2013

80 Arata Yamamoto and Yuji Hirono "Lattice QCD in rotating frames" Mar, 2013

85 Akihiko Sekine, Takashi Z. Nakano et al. "Strong Coupling Expansion in a Correlated Three-Dimensional Topological Insulator" Jan, 2013

RIKEN-NC-NP

62 Kenichi Matsuyanagi, Nobuo Hinohara et al. "BCS-pairing and nuclear vibrations" May, 2012

65 M. Sasano, H. Sakai et al. "Gamow-Teller transition strengths in the intermediate nucleus of the 116Cd double-β decay by the 116Cd(p, n)116In and 116Sn(n, p)116In reactions at 300 MeV" Apr, 2012

68 N. Quang Hung and N. Dinh Dang "Specific shear viscosity in hot rotating systems of paired fermions" June, 2012

69 RIBF理論研究推進会議メンバー "RIBFの物理" ("Physics in RIBF" by RIBF clear Theory Forum, in Japansese) May, 2012

70 W. Horiuchi, T. Inakura et al. "Glauber-model analysis of total reaction cross sections for Ne, Mg, Si, and S isotopes with Skyrme-Hartree-Fock densities" July, 2012

72 Kosuke Morita, Kouji Morimoto et al. "New Result in the Production and Decay of an Isotope, 278[113], of the 113th Element" Sep, 2012

73 S. Takeuchi, M. Matsushita et al. "Well-developed deformation in 42Si" July, 2012

77 T. Nakatsukasa, S. Ebata et al. "Density functional approaches to nuclear dynamics" May, 2012

78 Takashi Nakatsukasa "Density functional approaches to collective phenomena in nuclei: Time-dependent density-functional theory for perturbative and non-perturbative nuclear dynamics" May, 2012

79 Y. Fukuoka, T. Nakatsukasa et al. "Stochastic approach to correlations beyond the mean field with the Skyrme interaction" Sep, 2012

84 Ikuko Hamamoto "Neutron shell structure and deformation in neutron-drip-line nuclei" May, 2012

85 Huai-Qiang Gu, Haozhao Liang et al. "The Slater approximation for Coulomb exchange effects in nuclear covariant density functional theory" Oct, 2012

86 Z. M. Niu, Y. F. Niu et al. "β-decay half-lives of neutron-rich nuclei and matter flow in the r-process" Oct, 2012

87 Nguyen Dinh Dang "Damping of giant dipole resonance in highly excited nuclei" Sep, 2012

88 Nguyen Dinh Dang and Nguyen Quang Hung "Giant dipole resonance in 201-Tl at low temperature" Aug, 2012

89 Nguyen Quang Hung and Nguyen Dinh Dang "Specific shear viscosity in hot rotating systems of paired fermions" June, 2012

90 T. Sonoda, M.Wada et al. "Development of a resonant laser ionization gas cell for high-energy, short-lived nuclei" Aug, 2012

91 D. Kameda, T. Kubo, T. Ohnishi et al. "Observation of new microsecond isomers among fission products of 345 MeV/nucleon 238U" Aug, 2012

92 Koichi Sato, Nobuo Hinohara et al. "Shape transition and fluctuation in neutron-rich Cr isotopes around N = 40" June, 2012

93 T. Ichikawa, J.A. Maruhn et al. "Existence of exotic torus configuration in high-spin excited states of 40Ca" July, 2012

94 Y. Ichikawa, H. Ueno et al. "Production of spin-controlled rare isotope beams" June, 2012

95 H. Z. Liang, J. Meng et al. "Local covariant density functional constrained by the relativistic Hartree-Fock theory" Aug, 2012

97 T. Nakatsukasa "N=Z原子核の謎と新しい対凝縮相" ("Mysteries in N=Z nuclei and new phases of pair condensation", in Japanese) Sep, 2012

98 D. Ward, A. O. Macchiavelli et al. "Band structure of 235U" June, 2012

99 Paolo Avogadro, Takashi Nakatsukasa "Efficient calculation for the quasiparticle random-phase approximation matrix" Oct, 2012

100 Shuichiro Ebata, Tsunenori Inakura et al. "Time-dependent density-functional studies on strength functions in neutron-rich nuclei" Feb, 2013

103 Takatoshi Ichikawa and Kenichi Matsuyanagi "Damping of Quantum Vibrations Revealed in Deep Sub-barrier Fusion" Feb, 2013

CNS-REP

87 H. Yamaguchi, T. Hashimoto, S. Hayakawa, D.N. Binh, D. Kahl, S. Kubono, Y. Wakabayashi, T. Kawabata and T Teranishi, "Alpha resonance structure in ^{11}B studied via resonant scattering of ^{7}Li+α" CNS-REP 87 Feb. 2011

88 T. Gunji "CNS Annual Report 2010" CNS-REP 88 Feb. 2012

VIII. LIST OF SYMPOSIA & WORKSHOPS

April 2012 ~ March 2013

1 "The 6th OMEG Institute meeting-Element Genesis and Neutrinos-" RNC Apr. 25

2 "The 1st RIBF Debate Session =r-process=" RNC May. 25

3 "New mathematical methods in material science and mathematical science" RNC June 15-18

4 "RIBF Users Meeting 2012" RNC June 20-21

5 "The 3rd Program Advisory Committee meeting for Industrial Experiments at RI Beam Factory (IN-PAC)" RNC Jul. 02

6 "The 2nd RIBF Debate Session =deformed halo=" RNC Jul. 25

7 "RIKEN friends in Industry" Lectur and Excursion Jul. 30

8 "Seoul National University-Nishina School" RNC Aug. 06-10

9 "The 9th Program Advisory Committee Meeting for Materials and Life Science at RIKEN Nishina Center (ML-PAC)" RNC Sept. 04-05

10 "The 3rd RIBF Debate Session =gamma-ray spectroscopy in medium-heacy neutron-rich nucle=" Tohoku University Sept. 24

11 "SAMURAI International Workshop 2012" Kyoto University Sep. 10

12 "Peking University- Nishina School" RNC Oct. 02-12

13 "The 1st NAOJ Visiting Fellow Workshop Program Element Genesis and Cosmic Chemical Evolution : r-process perspective" RNC Oct. 17-19

14 "COMEX4 Preschool" RNC Oct. 22

15 "Workshop on Fragmentation Functions and QCD 2012 (Fragmentation 2012)" RNC Nov. 09-11

16 "Science Agora" Odaiba area in Tokyo Nov. 10-11

17 "Japan-Korea PHENIX collaboration workshop" Ewha Womens University Nov. 27

18 "16th International Conference on Electromagnetic Isotope Separators and Techniques Related to their Applications (EMIS 2012)" Matsue in Shimane Dec. 02-07

19 "The 4th RIBF Debate Session =Fission in heavy nuclei=" Tohoku University Dec. 28

20 "The 5th RIBF Debate Session =Neutron skin and photonuclear reaction=" RNC Feb. 21

21 "Hypernuclear physics with Electromagnetic Probes" RNC Feb. 22-28

22 "Relativistic viscoelastic fluid mechanics " RNC Feb. 23

CNS

1 "Exotic Nuclear Structure From Nucleons (ENSFN2012)" University of Tokyo Oct. 10-12

2 "Collective Motion in Nuclei under Extreme Conditions (COMEX4)" Hayama, Japan Oct. 22-26

3 "Review Meeting on CRIB Activities." CNS Wako Campus Jun. 21-22

4 "The 11th International Symposium on Origin of Matter and Evolution of Galaxies" RNC Nov. 14-17

TORIJIN

1 "The 6th LACM-TORIJIN-JUSTIPEN Workshop" Oak Ridge National Laboratory, U.S. Oct. 31-Nov. 02

2 "JUSTIPEN workshop on supercomputing at CCP2012" Kobe, Japan Oct. 15-16

KEK

1 "XVI International Conferece on Electromagnetic Isotope Separators and Techniques Related to their Applications" Matsue Japan Dec. 02-07

2 "Workshop on Low-Energy Radioactive Isotope Beam (RIB) Production by In-Gas Laser Ionization for Decay Spectroscopy at RIKEN" RIKEN Dec. 10-11

IX. LIST OF SEMINARS

(2012 April ~2013 March)

Theoretical Research Division

1 Hiroya Suno (RNC) "A diabatic hyperspherical study of traiatomic helium systems" Apr. 09

2 Ryuichiro Kitano (Tohoku University) "Higgs mechanism and confinement" Apr. 16

3 Ryosuke Sato (The University of Tokyo) "125 GeV Higgs in Supersymmetry" Apr. 16

4 Koike Takahisa (RNC) "Formation of light Xi^- hypernuclei via (K^-, K^+) reaction" Apr. 16

5 Masuo Suzuki (Nishina Memorial Foundation) "Nature hates waste --New principle of minimum entropy production" Apr. 17

6 Noyuki Sakumichi (The University of Tokyo) "Criteria of off-diagonal long-range order based on the Lee-Yang cluster expansion method" Apr. 17

7 Naoki Yamamoto (Yukawa Instiute for Theoretical Physics, Kyoto University & Institute for Nuclear Theory, University of Washington, USA) "Holography and anomaly matching for resonances" Apr. 23

8 Lie Ang (RNC) "Massive neutron stars and the equation of state of matter at high densities" Apr. 23

9 Kenji Morita (Kyoto University) "Baryon number probability distribution in the presence of second order phase transition" May 07

10 Tetsuji Kimura (Rikkyo University) "Flux Compactifications and Gauged Supergravities" May 07

11 Atsushi Mochizuki (RIKEN) "A mathematical study for dynamics of complex biological networks" May 11

12 Akira Furusaki (RIKEN) "Topological insulators and superconductors" May 14

13 Yusuke Namekawa (University of Tsukuba) "Charm quark physics from lattice QCD" May 14

14 Nan Su (Bielefeld University) "QCD thermodynamics at intermediate coupling" May 15

15 Takeshi Yamazaki (Nagoya University) "Calculation of lighter nuclei from Quenched lattice QCD" May 19

16 Hiroyuki Fuji (Nagoya University) "Volume Conjecture, QFT, and Strings" May 21

17 Atsushi Tamii (RCNP) "Tensor Correlation in the Ground States of N=Z Nuclei" May 23

18 Masahiro Isaka (Hokkaido University) "Structure study of p-sd shell and neutron-rich Λ hypernuclei by using AMD" May 28

19 Kei Iida (Kochi University) "Physics of Neutron Stars" May 29-30

20 Kazuo Fujikawa (RNC) "Lorentz invariant CPT violation: Particle and antiparticle mass splitting" Jun. 08

21 Hideo Aoki (The University of Tokyo) "Non-equilibrium phenomena in strongly correlated systems and topological systems" Jun. 20

22 Hirokazu Tamura (Tohoku University) "Development of hypernuclear physics at J-PARC" Jun. 25

23 Yasuko Urata (Tohoku University) "Resonant Microwave Interactions with Antihydrogen" Jun. 29

24 Anyi Li (University of Washington) "Fermion bag solutions to some sign problems in four-fermion field theories" Jul. 02

25 Shotaro Imai (Osaka University) "Thermodynamics for two color quark-hadron system at finite density" Jul. 02

26 Hiromitsu Takeuchi (Hiroshima University) "Tachyon condensation and brane annihilation in Bose-Einstein condensates" Jul. 06

27 Zhou Bo (RCNP) "New concept for the ground-state band in 20Ne within a microscopic cluster model" Jul. 09

28 Andreas Ipp (Vienna University of Technology) "HBT correlations of photons from an anisotropic quark-gluon plasma" Jul. 09

29 Kenji Fukukawa (RNC) "Nucleon-deuteron scattering studied by a quark-model baryon-baryon interaction" Jul. 18

30 N. Yasutake (Chiba Inst. Tech.) "Thermodynamical description of hadron-quark phase transition and its implications on compact-star phenomena" Jul. 23

31 Tomoki Fukai (RIKEN BNL) "Highly non-random network design for brain computation" Jul. 23

32 Nobutoshi Yasutake (Chiba Institute of Technology) "Thermodynamical description of hadron-quark phase transition and its implications on compact-star phenomena" Jul. 23

33 Syoko Okamoto (RNC) "Ranges of moisture-source temperature estimated from Antarctic ice cores stable isotope records over glacial–interglacial cycles" Jul. 31

34 Kenji Morita (KEK) "New States of Gauge Theories on a Circle Through Stochastic Evolutions" Aug.01

35 Yosuke Sumitomo (HonKong Institute of Technology) "A Stringy Mechanism for a Small Cosmological Constant" Aug.01

36 Keiichiro Hara (Fukuoka Univ.) "stratospheric circulation of nitric acid in Antarctica from aerosol studies" Aug. 07

37 Motoi Tachibana (Saga University) "Holographic cold nuclear matter as dilute instanton gas" Sep. 24

38 Hidetoshi Katori (RIKEN) "Optical lattice clocks and newer roles for clocks" Sep. 25

39 Hiroaki Utsunomiya (Konan University/CNS) "Photonuclear reactions and related topics - from PDR to nucleosynthesis" Sep. 26

40 Tsunenori Inakura (RNC) "Shell effect on pygmy dipole resonances" Sep. 26

41 Sho Ozaki (RNC) "Low energy charmonium-hadron scattering from lattice QCD" Sep. 26

42 Bernold Fiedler (Free University of Berlin) "Structured hybrid models and Hilbert's thirteenth problem" Oct. 04

43 Toru Kojo (University of Bielefeld) "Can the nucleon axial charge be O(Nc^0)?" Oct. 04

44 Kazuo Fujikawa (The University of Tokyo) "Various Phases and Interference in Quantum Mechanics: In memory of late Dr. Akira Tonomura" Oct. 09

45 Bjarke Gudnason (The Hebrew University of Jerusalem) "High Q monopoles and dwarf galaxy sized solitonic dark matter" Oct. 15

46 Takuya Shibata (Osaka University) "Particle production in an intense electromagnetic field" Oct. 22

47 Carlo Barbieri (University of Surrey) "Toward ab-initio description of open-shells in neutron rich nuclei" Oct. 29

48 Johannes Schmude (IPMU, The University of Tokyo) "On the gravity duals of superconformal gauge theories" Oct. 29

49 Chiho Nonaka (Nagoya University) "Dynamical model based on relativistic hydrodynamics for relativistic heavy ion collisions" Oct. 29

50 Satomi Kikuchi (RNC) "Seasonal variations in oxygen isotope ratios of daily collected precipitation and wind drift sales and in the final snow cover at Dome Fuji Station, Antarctica" Oct. 30

51 Minoru Eto (Yamagata University) "Knot Walls" Nov. 12

52 Daisuke Satow (Kyoto University) "Ultrasoft Fermion Mode in Hot or Dense Boson-Fermion System" Nov. 12

53 Syoko Okamoto (RNC) "Sulphate–climate coupling over the past 300,000 years in inland Antarctica" Nov. 13

54 James S. M. Anderson (University of Tokyo) "GKCI Approach for Solving the Electronic and Nuclear Schroedinger Equation" Nov. 13

55 Yusuke Nishida (Los Alamos National Laboratory) "New analogies between extreme QCD and cold atoms" Nov. 19

56 Koichiro Asahi (Tokyo Institute of Technology) "Search for Electric Dipole Moment in 129Xe Atom Using a Nuclear Spin Oscillator" Nov. 20

57 Frieder Lenz (University of Erlangen-Nuernberg) "Thermodynamics properties of quantum fields close to horizons" Nov. 28

58 Toichiro Kinoshita (Cornell University) "Tenth-Order Lepton Anomalous Magnetic Moments and High Precision Determination of Fine Structure Constant" Dec. 05

59 Yoichi Ikeda (RNC) "Antikaon-nucleon interactions and kaonic dibaryons in chiral unitary model" Dec. 03

60 Naoto Saito (KEK) "Muon g-2 and EDM measurement at J-PARC" Dec. 05

61 Kazumitsu Sakai (The University of Tokyo) "Multiple Schramm-Loewner evolutions for conformal field theories with Lie algebra symmetries" Dec. 10

62 S.X. Nakamura (YITP) "Dynamical coupled-channels model for meson productions and application to strange nuclear physics" Dec. 10

63 Kenji Morita (Kyoto university) "Net baryon number probability distribution near chiral transition" Dec. 17

64 Yoshinori Tokura (RIKEN) "Science of Magnetic Skyrmions" Dec. 18

65 Shin Muroya (Matsumoto University) "Stochastic quantization of a finite temperature lattice field theory in the real time formula" Dec. 26

66 Hidehiko Shimada (Okayama Institute for Quantum Physics) "Test of M-theoretic AdS4/CFT3 for states with large angular momentum" Jan. 07

67 Yoshiyuki Miyamoto (AIST) "First principles simulation for photo-excitation and carrier splitting in condensed matters" Jan. 07

68 Naoki Yoshida (The University of Tokyo/IPMU) "The first light and the first heavy elements in the universe" Jan. 08

69 Christoph Lehner (RIKEN BNL) "Precise constraints on CP violation from lattice QCD" Jan. 28

70 Hsiang-nan Li (Institute of Physics, Academia Sinica) "Glauber gluons in pion-proton Drell-Yan process" Jan. 28

71 Yutaka Ookouchi (Kyoto University) "Cosmic R-tube, Vacuum Instability and R-axion Cosmology" Jan. 28

72 Antonio Miguel Garcia-Garcia (The University of Cambridge) "Smaller is different and more: an excursion in modern nanoscale superconductivity" Jan. 29

73 Kyogo Kawaguchi (The University of Tokyo) "Energetics and efficiency of molecular motors " Feb. 04

74 Yongseok Oh (Kyungpook National University) "Properties of hyperons with multi strangeness" Feb. 05

75 Leonid Glozman (University of Graz) "Confinement, chiral symmetry breaking and the mass generation of hadrons" Feb.18

76 Yutaka Ookouchi (Kyoto University) "Cosmic R-tube, Vacuum Instability and R-axion Cosmology" Feb. 25

77 Shinji Okada (RNC) "Precision X-ray spectroscopy of kaonic hydrogen atom at DAFNE" Feb. 25

78 Tetsuo Hyodo (Tokyo Institute of Technology) "Kbar-N interaction and Lambda(1405)" Feb. 25

79 Yusuke Tanimura (Tohoku University) "Application of the Inverse Hamiltonian Method to Relativistic Mean Field Calculations on 3-dimensional Cartesian Mesh" Feb. 27

80 Masaki Murata (Institute of Physics ASCR) "Relationship between Marginal Deformation Parameters in Boundary CFT and Cubic SFT " Mar. 04

Sub Nuclear Research Division

1 Brian Tiburzi (City College of New York and RBRC) "A saga of the weak and the strong: hadronic parity violation" Apr. 05

2 Eigo Shintani (RBRC) "Chiral symmetry breaking in lattice QED model with fermion brane" Apr. 26

3 Larry McLerran (BNL) "Electroweak Axions, Instantons and the Cosmological Constant" May 03

4 Kimmo Tuominen (University of Jyvaskyla & Helsinki Institute of Physics) "Flavors in dynamical electroweak symmetry breaking" May 10

5 Charlotte Van Hulse (University of the Basque Country) "Hadronization studies at HERMES" May 14

6 Alexei Bazavov (BNL) "The transition temperature in QCD" May 24-29

7 Elina Seel (University of Frankfurt) "The thermodynamics of the 2-dimensional O(N) model" May 31

8 Mara Grahl (University of Frankfurt) "Two-flavor linear sigma model in presence of axial anomaly from Functional Renormalization Group" May 31

9 Shigemi Ohta (KEK) "Nucleon structure from 2+1-flavor dynamical DWF QCD at nearly physical pion mass" Jun. 07

10 Art Olin (TRIUMF/University of Victoria) "Coulomb Breakup and Reaction Cross Sections for Deformed Halo Nucleus 31Ne" Jul. 02

11 Shu Lin (RBRC) "Evolution of singularities in unequal time correlator in thermalization of strongly coupled gauge theory" Jul. 12

12 Koji Kashiwa (RBRC) "Critical endpoint for deconfinement in matrix and other effective models" Jun. 21

13 Yoshio Kobayashi (RNC) "In-Beam Mössbauer Spectroscopy using RI Beam and nuclear reactions" Jul. 23

14 Jinfeng Liao (Indiana University / RBRC) "The QCD Plasma Near Tc: An Update" Jul. 26

15 Kirill Tuchin (Iowa State University) "Hard Probes of QGP in strong magnetic field" Aug. 02

16 Fedor Bezrukov (University of Connecticut / RBRC) "The Higgs boson mass – what it means for Standard Model?" Aug. 16

17 Robert Lang (Technical University Munich) "Transport phenomena in NJL-type models" Aug. 23

18 Matthias Drews (Technical University Munich) "Neutron Stars and Functional Renormalization Group" Aug. 23

19 Kazuhiro Watanabe (The University of Tokyo) "Heavy quark production in pA collision with rcBK evolution" Aug. 30

20 Tatsuhiro Misumi (BNL) "Novel phase structure for lattice flavored chemical potential" Sep. 06

21 Vladimir Skokov (BNL) "Making sense of the photon azimuthal anisotropy" Sep. 13

22 Li Yan(Stony Brook) "Non-linear flow response in hydrodynamics and plane correlations" Sep. 20

23 Yue Ma (RNC) "Hyperon, proton and anti-proton:a short summary of research experience" Sep. 27

24 Giuseppe Mussardo (SISSA, Trieste) "Non abelian anyons and the art of computing with knots" Nov. 01

25 Jacqueline Bonnet (Universitat Giessen) "Effects of strong magnetic fields in QCD - First results from a Dyson-Schwinger perspective" Dec. 20

26 Daniel Pitonyak (Temple University) "Single- and double-spin asymmetries in inelastic proton-proton collisions" Jan. 10

27 Lea Santos (Yeshiva University) "Thermalization and entropy of isolated quantum many-body systems" Jan 17

28 Etsuko Itou (KEK) "Recent study on the conformal fixed point in the SU(3) gauge theory" Feb. 07

29 Tatsuhiro Misumi (BNL) "Phase structure in gauge theory with compacted dimensions" Feb. 28

30 Radoslaw Kycia (Cracow University of Technology) "On blowup in semilinear wave equations" Mar. 07

31 Eiji Nakano (Kochi Univ.) "Non-Abelian Vortex in Dense QCD --- orientational moduli dynamics ---" Mar. 14

32 Xu Feng (KEK) "The neutral pion decay and the chiral anomaly on the lattice" Mar. 28

RIBF Research Division

1 Stephan Ulmer (RIKEN) "The Magnet in the (Anti) proton - Quantum jump spectroscopy with antimatter" Apr. 03

2 Stephan Ulmer (RIKEN) "Nuclear Incompressibility, the Asymmetry Term, and the MEM Effect" Apr. 04

3 Kenta Itahashi (RNC) "First precision spectroscopy of pionic atoms at RIBF" May 22

4 Syunji Nishimura (RNC) "r-process nucleosynthesis" May 24

5 Kajino Toshikata (National Astromomical Observatory of Japan) "R-process; Astro.+Theory side" May 24

6 Michiharu Wada (RNC) "An advanced universal slow RI beam facility and its applications" May 29

7 Masaomi Tanaka (National Astronomical Observatory of Japan) "Optical Observations of Supernova Explosions" May 31

8 Nobuya Nishimura (University of Basel) "Current Status of r-process studies in Core-Collapse Supernovae Explosions" Jun. 05

9 Pascal Naidon (RNC) "Universal few-body physics with atoms" Jun. 08

10 Pieter Doornenbal (RNC) "Morphometrical studies on the Island of Inversion" Jun. 10

11 Charlie Rasco (Louisiana State University) "Beta Decay Measurements of Neutron-Rich Nuclei at the RIBF" Jun. 12

12 Janet M. Conrad (Massachusetts Institute of Technology) "Cyclotrons -- New Sources for Neutrino Physics" Jun. 14

13 Kenji Saito (MSU-NSCL) "Heavy-ion superconductive accelerator in MSU-FRIB" Jul. 03

14 Juzo Zenihiro (RNC) "Nucleon density distributions extracted from proton elastic scattering at intermediate energies" Jul. 17

15 Taiichi Yamada (Kanto Gakuin University) "Cluster structure and isoscalar monopole excitation in light nuclei" Jul. 24

16 Ken’ichiro Nakazato (Tokyo University of Science) "Probe into nuclear matter with compact astrophysical objects" Jul. 26

17 Hajime Kawahara (Tokyo Metropolitan University) "How to know the surface world of exoplanets" Sep. 06

18 Didier Beaumel (Institut de physique Nucleaire) "Direct reactions studies using the MUST2 array" Sep. 18

19 Hiroya Yamaguchi (Harvard-Smithsonian Center for Astrophysics High Energy Astrophysics Division) "Nucleosynthesis in Type Ia Supernovae and Their Environment" Oct. 18

20 Hideki Uchiyama (The University of Tokyo) "Suzaku study of the Galactic Ridge X-ray Emission -It’s NOT a big fat duh YET!-" Oct. 25

21 Takeuchi Satoshi (RNC) "Well-developed deformation in 42Si" Oct. 30

22 Lee G. Sobotka (Washington University in St.Louis) "Continuum spectroscopy of light nuclei studied by high-order correlation experiments" Nov. 09

23 Peter Schuck (Institute Nuclear Physics, Orsay) "Quartet condensation in infinite matter" Nov. 15

24 Patrick Hautle (Paul Scherrer Institut) "Dynamic Nuclear Polarization - from Polarized Targets to Metabolic Imaging" Nov. 19

25 Akira Ozawa (Tsukuba University) "Present status of Rare-RI Ring and mass measurements for R-process" Nov. 27

26 H.-J. Kluge (GSI) "High-Precision Experiments Using Radioactive Ions, Lasers and/or Storage Devices" Nov. 30

27 Nabhiraj Yalagoud (VECC) "Recent R&D of ion sources at VECC" Dec. 14

28 Yuichi Ichikawa (Tokyo Institute of Technology) "Production of spin-controlled RI beams" Dec. 25

29 Kosuke Morita (RNC) "New Result in the Production and Decay of an Isotope, (^278) 113, of the 113th Element" Jan.15

30 Takashi Nakano (RCNP) "New Theta+ result from LEPS." Jan. 25

31 Takumi Doi (RNC) "Lattice QCD studies for two- and three-nucleon forces" Jan. 29

32 In-Ja Song (Jeju National University) "Utilization of transgenic technique and mutation for generating new varieties of grass" Jan. 29

33 Masao Watanabe (Tohoku University) "Molecular mechanism of self/non-self recognition in Brassica self-incompatibility " Feb. 05

34 Daisuke Kameda (RNC) "Observation of 18 new microsecond isomers among fission products from in-flight fission of 345 MeV/nucleon 238U" Feb. 26

KEK

1 Ozawa Akira (Univ. of Tsukuba) "rare-RI ring at RIBF" May 14

AUTHOR INDEX

L

N

O

P

R

S

Z

RIKEN Accelerator Progress Report *vol.* **46**

独立行政法人理化学研究所加速器年次報告　第46巻 (2013)

印　刷　平成25年（2013）　9月26日
発　行　平成25年（2013）　10月31日

発行者　独立行政法人理化学研究所　仁科加速器研究センター
代表者　延　與　秀　人
〒351-0198　埼玉県和光市広沢2番1号
progress@ribf.riken.jp

編集者　独立行政法人理化学研究所　仁科加速器研究センター
加速器年次報告編集委員会

印刷所　松枝印刷株式会社
〒303-0034　茨城県常総市水海道天満町2438